CHM 321: INORGANIC CHEMISTRY



Bryan P. Nell
Ripon College



CHM 321 Inorganic Chemistry

This text is disseminated via the Open Education Resource (OER) LibreTexts Project (https://LibreTexts.org) and like the thousands of other texts available within this powerful platform, it is freely available for reading, printing, and "consuming."

The LibreTexts mission is to bring together students, faculty, and scholars in a collaborative effort to provide an accessible, and comprehensive platform that empowers our community to develop, curate, adapt, and adopt openly licensed resources and technologies; through these efforts we can reduce the financial burden born from traditional educational resource costs, ensuring education is more accessible for students and communities worldwide.

Most, but not all, pages in the library have licenses that may allow individuals to make changes, save, and print this book. Carefully consult the applicable license(s) before pursuing such effects. Instructors can adopt existing LibreTexts texts or Remix them to quickly build course-specific resources to meet the needs of their students. Unlike traditional textbooks, LibreTexts' web based origins allow powerful integration of advanced features and new technologies to support learning.



LibreTexts is the adaptable, user-friendly non-profit open education resource platform that educators trust for creating, customizing, and sharing accessible, interactive textbooks, adaptive homework, and ancillary materials. We collaborate with individuals and organizations to champion open education initiatives, support institutional publishing programs, drive curriculum development projects, and more.

The LibreTexts libraries are Powered by NICE CXone Expert and was supported by the Department of Education Open Textbook Pilot Project, the California Education Learning Lab, the UC Davis Office of the Provost, the UC Davis Library, the California State University Affordable Learning Solutions Program, and Merlot. This material is based upon work supported by the National Science Foundation under Grant No. 1246120, 1525057, and 1413739.

Any opinions, findings, and conclusions or recommendations expressed in this material are those of the author(s) and do not necessarily reflect the views of the National Science Foundation nor the US Department of Education.

Have questions or comments? For information about adoptions or adaptions contact info@LibreTexts.org or visit our main website at https://LibreTexts.org.

This text was compiled on 01/12/2026

TABLE OF CONTENTS

Licensing

1: Atomic Structure, Molecular Structure, and Bonding

- 1.1: Introduction to Inorganic Chemistry
  - 1.1.1: What is Inorganic Chemistry?
  - 1.1.2: Inorganic vs Organic Chemistry
  - 1.1.3: History of Inorganic Chemistry
- 1.2: Atomic Structure
  - 1.2.1: Historical Development of Atomic Theory
    - 1.2.1.1: The Periodic Table
    - 1.2.1.2: Discovery of Subatomic Particles and the Bohr Atom
  - 1.2.2: The Schrödinger equation, particle in a box, and atomic wavefunctions
    - 1.2.2.1: Particle in a Box
    - 1.2.2.2: Quantum Numbers and Atomic Wave Functions
    - 1.2.2.3: Aufbau Principle
    - 1.2.2.4: Shielding
  - 1.2.3: Periodic Properties of Atoms
    - 1.2.3.1: Ionization energy
    - 1.2.3.2: Electron Affinity
    - 1.2.3.3: Covalent and Ionic Radii
- 1.3: Rutherford's Atom
- 1.4: Bohr's Atom
- 1.5: Simple Bonding Theory
  - 1.5.1: Lewis Electron-Dot Diagrams
    - 1.5.1.1: Resonance
    - 1.5.1.2: Breaking the octet rule with higher electron counts (hypervalent atoms)
    - 1.5.1.3: Formal Charge
    - 1.5.1.4: Lewis fails to predict unusual cases- Boron and Beryllium
  - 1.5.2: Valence Shell Electron-Pair Repulsion
    - 1.5.2.1: Lone Pair Repulsion
    - 1.5.2.2: Multiple Bonds
    - 1.5.2.3: Electronegativity and Atomic Size Effects
  - 1.5.3: Molecular Polarity
  - 1.5.4: Hydrogen Bonding
  - 1.5.5: Valence Bond Theory
  - 1.5.6: Hybrid Atomic Orbitals
- 1.6: Molecular Orbital Theory
  - 1.6.1: Prelude to Molecular Orbital Theory
  - 1.6.2: Formation of Molecular Orbitals from Atomic Orbitals
    - 1.6.2.1: Molecular Orbitals from s Orbitals
    - 1.6.2.2: Molecular Orbitals from p Orbitals
    - 1.6.2.3: Molecular orbitals from d orbitals

- 1.6.2.4: Nonbonding Orbitals and Other Factors
- 1.6.3: Homonuclear Diatomic Molecules
  - 1.6.3.1: Molecular Orbitals
  - 1.6.3.2: Orbital Mixing
  - 1.6.3.3: Diatomic Molecules of the First and Second Periods
  - 1.6.3.4: Photoelectron Spectroscopy
- 1.6.4: Heteronuclear Diatomic Molecules
  - 1.6.4.1: Polar bonds
  - 1.6.4.2: Ionic Compounds and Molecular Orbitals

2: Molecular Symmetry and Group Theory

- 2.1: Symmetry Elements and Operations
- 2.2: Point Groups
  - 2.2.1: Groups of Low and High Symmetry
  - 2.2.2: Other Groups
- 2.3: Properties and Representations of Groups
  - 2.3.1: Matrices
  - 2.3.2: Representations of Point Groups
  - 2.3.3: Character Tables
- 2.4: Examples and Applications of Symmetry
  - 2.4.1: Molecular Vibrations
  - 2.4.2: Chirality
- 2.5: Generating SALCs for Polyatomic Molecules
  - 2.5.1: Bifluoride anion
  - 2.5.2: Carbon Dioxide
  - 2.5.3: H_2O
  - 2.5.4: NH_3
  - 2.5.5: CO_2 (Revisted with Projection Operators)
  - 2.5.6: BF_3

3: Acid-Base Chemistry and an Introduction to Coordination Compounds

- 3.1: Bronsted-Lowry acids and bases
- 3.2: Lewis Acids and Bases
- 3.3: Acidity of the Hexaaqua Ions
- 3.4: Hard/Soft Acids and Bases
- 3.5: Quantitative Measures of Hardness and Softness
- 3.6: Coordination Chemistry- Structure and Isomers
  - 3.6.1: History
  - 3.6.2: Nomenclature and Ligands
  - 3.6.3: Acid-Base and Donor-Acceptor Chemistry
    - 3.6.3.1: Acid-Base Models as Organizing Concepts
    - 3.6.3.2: Lewis Concept and Frontier Orbitals
      - 3.6.3.2.1: The frontier orbital approach considers Lewis acid-base reactions in terms of the donation of electrons from the base's highest occupied orbital into the acid's lowest unoccupied orbital.
      - 3.6.3.2.2: All other things being equal, electron withdrawing groups tend to make Lewis acids stronger and bases weaker while electron donating groups tend to make Lewis bases stronger and acids weaker

- 3.6.3.2.3: The electronic spectra of charge transfer complexes illustrate the impact of frontier orbital interactions on the electronic structure of Lewis acid-base adducts
- 3.6.3.2.4: Substances' solution phase Lewis basicity towards a given acid may be estimated using the enthalphy change for dissociation of its adduct with a reference acid of similar hardness.
- 3.6.3.2.5: In the boron trifluoride affinity scale, the enthalphy change on formation of an adduct between the base and boron trifluoride is taken as a measure of Lewis basicity.
- 3.6.3.2.6: Lewis base strength may also be estimated by measuring structural or energy changes upon formation of a Lewis acid-base complex, as illustrated by efforts to spectroscopically assess the strengths of halogen bonds
- 3.6.3.2.7: Bulky groups weaken the strength of Lewis acids and bases because they introduce steric strain into the resulting acid-base adduct.
- 3.6.3.2.8: Frustrated Lewis pair chemistry uses Lewis acid and base sites within a molecule that are sterically restricted from forming an adduct with each other.

- 3.6.3.3: Hard and Soft Acids and Bases
  - 3.6.3.3.1: Hard-Hard and Soft-Soft preferences may be explained and quantified in terms of electrostatic and covalent and electronic stabilization on the stability of Lewis acid-base adducts
  - 3.6.3.3.2: Quantitative Measures of Hardness, Softness, and Acid-Base Interactions from a Hard Soft Acid-Base Principle Perspective Involve Orbital Energies and/or Apportioning Acid-Base Bonding in Terms of Electrostatic and Covalent Factors
- 3.6.3.4: Problems

- 3.6.4: Coordination Numbers and Structures
- 3.6.5: Isomerism

- 3.7: Coordination Chemistry- Bonding
  - 3.7.1: Crystal Field Theory
  - 3.7.2: Crystal Field Stabilization Energy
  - 3.7.3: Factors That Affect Crystal Field Splitting
  - 3.7.4: Ligand Field Theory
  - 3.7.5: Metal-Metal Bonds
    - 3.7.5.1: Metal-Metal Multiple Bonds
  - 3.7.6: Jahn-Teller Distortions

4: Electronic Structure and Spectra of d-Metal Complexes

- 4.1: Absorption of Light
  - 4.1.1: Beer-Lambert Absorption Law
- 4.2: Quantum Numbers of Multielectron Atoms
  - 4.2.1: Finding Microstates and Term Symbols
  - 4.2.2: Spin-Orbit Coupling
- 4.3: Electronic Spectra of Coordination Compounds
  - 4.3.1: Symmetry labels for split terms
  - 4.3.2: Correlation Diagrams
  - 4.3.3: Tanabe-Sugano Diagrams
  - 4.3.4: Applications of Tanabe-Sugano Diagrams
  - 4.3.5: Tetrahedral Complexes
  - 4.3.6: Selection Rules
  - 4.3.7: Charge-Transfer Spectra
  - 4.3.8: Applications of Charge-Transfer

5: Reactions of d-Metal Complexes

- 5.1: Thermodynamic Stability of Metal Complexes
- 5.2: Trends in Kinetic Lability
- 5.3: Ligand Substitution Mechanisms
- 5.4: Substitutions in Square Planar Complexes
  - 5.4.1: Kinetics and Stereochemistry of Square Planar Reactions
  - 5.4.2: Evidence for Associative Reactions
- 5.5: The Trans Effect Observation
- 5.6: The Trans Effect Explanation
- 5.7: Redox Mechanisms
  - 5.7.1: Outer Sphere Electron Transfer
  - 5.7.2: Inner Sphere Electron Transfer

6: Organometallic Chemistry

- 6.1: Introduction to Organometallic Chemistry
- 6.2: Nomenclature, Ligands, and Classification
- 6.3: Electron Counting in Organometallic Complexes
  - 6.3.1: The 18 Electron Rule
  - 6.3.2: Simplifying the Organometallic Complex by Deconstruction
- 6.4: Survey of Organometallic Ligands
  - 6.4.1: Carbon Monoxide (Carbonyl Complexes)
  - 6.4.2: Ligands similar to CO
  - 6.4.3: Hydrides and Dihydrogen Complexes
- 6.5: Bonding between Metal Atoms and Organic Pi Systems
  - 6.5.1: Linear π Systems
  - 6.5.2: Cyclic π systems
  - 6.5.3: Odd-numbered π Systems
  - 6.5.4: Fullerene Complexes
- 6.6: Metal-Carbon Bonds
  - 6.6.1: Metal Alkyls
  - 6.6.2: Carbenes
  - 6.6.3: Carbyne (Alkylidyne) Complexes
  - 6.6.4: Carbido and Cumulene Complexes
  - 6.6.5: Carbon Wires- Polyyne and Polyene Bridges
- 6.7: Characterization of Organometallic Complexes

7: Organometallic Reactions and Catalysis

- 7.1: Reactions Involving Gain or Loss of Ligands
  - 7.1.1: Ligand Dissociation and Substitution
  - 7.1.2: Oxidative Addition
  - 7.1.3: Reductive Elimination
  - 7.1.4: Sigma Bond Metathasis
  - 7.1.5: Application of Pincer Ligands
- 7.2: Reactions Invloving Modification of Unsaturated Ligands
  - 7.2.1: Introduction to Insertion
  - 7.2.2: CO Insertions (Alkyl Migration)

- 7.2.3: Migratory Insertion-1,2-Insertions
- 7.2.4: β-Elimination Reactions
- 7.2.5: Abstraction and Addition
- 7.3: Organometallic Catalysts
  - 7.3.1: Catalytic Deuteration
  - 7.3.2: Hydroformylation
  - 7.3.3: Monsanto Acetic Acid Process
  - 7.3.4: Wacker (Smidt) Process
  - 7.3.5: Hydrogenation by Wilkinson's Catalyst
  - 7.3.6: Olefin Metathesis
- 7.4: Heterogeneous Catalysts
  - 7.4.1: Ziegler-Natta Polymerizations
  - 7.4.2: Water-Gas Shift Reaction
- 7.5: Problems
  - 7.5.1: Concept Review Questions Chapter 12
  - 7.5.2: Homework Problems Chapter 12

8: Solid State Chemistry

- 8.1: Prelude to Metals and Alloys
- 8.2: Unit Cells and Crystal Structures
- 8.3: Crystal Structures of Metals
- 8.4: Conduction in Metals
- 8.5: Atomic Orbitals and Magnetism
- 8.6: Ferro-, Ferri- and Antiferromagnetism
- 8.7: Hard and Soft Magnets
- 8.8: Defects in Metallic Crystals
- 8.9: X-ray Crystallography
- 8.10: Miller Indices (hkl)
- 8.11: Powder X-ray Diffraction
- 8.12: Prelude to Ionic and Covalent Solids - Structures
- 8.13: Close-packing and Interstitial Sites
- 8.14: Structures Related to NaCl and NiAs
- 8.15: Tetrahedral Structures
- 8.16: Layered Structures and Intercalation Reactions
- 8.17: Ionic Radii and Radius Ratios
- 8.18: Structure Maps
- 8.19: Energetics of Crystalline Solids- The Ionic Model
- 8.20: Born-Haber Cycles for NaCl and Silver Halides
- 8.21: Lattice Energies and Solubility
- 8.22: Spinel, Perovskite, and Rutile Structures
- 8.23: Kapustinskii Equation
- 8.24: New Page

9: Bioinorganic Chemistry

- 9.1: Biological Significance of Iron, Zinc, Copper, Molybdenum, Cobalt, Chromium, Vanadium, and Nickel
- 9.2: Introduction to Amino Acids and Proteins
- 9.3: Overview of Hemoglobin and Myoglobin
  - 9.3.1: Myoglobin, Hemoglobin, and their Ligands

- 9.3.2: Oxygen Transport by the Proteins Myoglobin and Hemoglobin
- 9.4: Ferrodoxins, Hydrogenases, and Nitrogenases - Metal-Sulfide Proteins
  - 9.4.1: Iron-sulfur Proteins and Models
  - 9.4.2: Iron-sulfur Proteins and Models (Part 2)
  - 9.4.3: Iron-sulfur Proteins and Models (Part 3)
  - 9.4.4: Iron-sulfur Proteins and Models (Part 4)
- 9.5: The Reaction Pathways of Zinc Enzymes and Related Biological Catalysts
  - 9.5.1: About Carbonic Anhydrase
  - 9.5.2: Catalytic Mechanism
  - 9.5.3: Metal Substitution
- 9.6: Metals in Medicine
  - 9.6.1: Metal Deficiency and Disease
  - 9.6.2: Toxic Effects of Metals
  - 9.6.3: Aspects of Platinum Binding to DNA
  - 9.6.4: Survey of Metals Used for Diagnosis and Chemotherapy
  - 9.6.5: Platinum Anticancer Drugs- A Case Study
  - 9.6.6: Mapping the Major Adducts of cis- and trans-DDP on DNA; Sequence Specificity
  - 9.6.7: Structure of Platinum-DNA Complexes
  - 9.6.8: Site-specifically Platinated DNA \(\;^{154}\)
  - 9.6.9: Bioinorganic Chemistry of Platinum Anticancer Drugs- How Might They Work?
  - 9.6.10: Bioinorganic Chemistry of Platinum Anticancer Drugs; How Might They Work? (Part 2)
  - 9.6.11: Design of New Inorganic Anticancer Drugs
- 9.7: Electron Transfer

10: Special Topics

- 10.1: f-Block Metals- Lanthanides and Actinides
  - 10.1.1: Introduction
  - 10.1.2: f-Orbitals and Oxidation States
  - 10.1.3: Atoms and Ion Sizes
    - 10.1.3A: The Lanthanoid Contraction
    - 10.1.3B: Coordination Numbers
  - 10.1.4: Spectroscopic and Magnetic Properties
    - 10.1.4A: Electronic Spectra and Magnetic Moments - Lanthanoids
    - 10.1.4B: Luminescence of Lanthanoid Complexes
    - 10.1.4C: Electronic Spectra and Magnetic Moments - Actinoids
  - 10.1.5: Sources of the Lanthanoids and Actinoids
    - 10.1.5A: Occurrence and Separation of the Lanthanoids
    - 10.1.5B: The Actinoids
  - 10.1.6: Lanthanoid Metals
  - 10.1.7: Inorganic Compounds and Coordination Complexes of the Lanthanoids
    - 10.1.7A: Halides
    - 10.1.7B: Hydroxides and Oxides
    - 10.1.7C: Complexes of Ln(III)
  - 10.1.8: Organometallic Complexes of the Lanthanoids
    - 10.1.8A: \(\sigma\)-Bonded Complexes
    - 10.1.8B: Cyclopentadienyl Complexes

- 10.1.8C: Bis(arene) Derivatives
- 10.1.8D: Complexes Containing the \(\eta^8\)-cyclooctatetraenyl Ligand
- 10.1.9: The Actinoid Metals
- 10.1.10: Inorganic Compounds and Coordination Complexes of Thorium, Uranium, and Plutonium
  - 10.1.10A: Thorium
  - 10.1.10B: Uranium
  - 10.1.10C: Plutonium
- 10.1.11: Organometallic Complexes of Thorium and Uranium
  - 10.1.11A: (\sigma\)-Bonded Complexes
  - 10.1.11B: Cyclopentadienyl Derivatives
  - 10.1.11C: Complexes Containing the \(\eta^8\)-cyclooctatetraenyl Ligand

- 10.2: Physical Inorganic Techniques
  - 10.2.1: Electronic Spectroscopy
    - 10.2.1A: UV-VIS Absorption Spectroscopy
    - 10.2.1B: Types of Absorption
    - 10.2.1C: Absorbance and the Beer-Lambert Law
    - 10.2.1D: Emission Spectroscopy
  - 10.2.2: Nuclear Magnetic Resonance (NMR) Spectroscopy
  - 10.2.3: Electron Paramagnetic Resonance (EPR) Spectroscopy
    - 10.2.3A: What is EPR Spectroscopy?
    - 10.2.3B: The Zeeman Electronic Effect
    - 10.2.3C: EPR Spectra
  - 10.2.4: Mossbauer Spectroscopy
    - 10.2.4A: The Technique of Mossbauer Spectroscopy
    - 10.2.4B: What Can Isomer Shift Data Tell Us?
  - 10.2.5: Structure Determination - Diffraction Methods
    - 10.2.5A: X-Ray Diffraction (XRD)
    - 10.2.5B: Single Crystal X-Ray Diffraction
    - 10.2.5C: Powder X-Ray Diffraction
    - 10.2.5D: Single Crystal Neutron Diffraction
    - 10.2.5E: Electron Diffraction
    - 10.2.5F: Low-Energy Electron Diffraction (LEED)
    - 10.2.5G: Structural Databases
  - 10.2.6: Photoelectron Spectroscopy (PES, UPS, XPS, ESCA)
  - 10.2.7: Mass Spectrometry
    - 10.2.7A: Electron Ionization (EI)
    - 10.2.7B: Fast Atom Bombardment (FAB)
    - 10.2.7C: Matrix-Assisted Laser Desorption Ionization Time-of-Flight (MALDI-TOF)
    - 10.2.7D: Electrospray Ionization (ESI)
- 10.3: Fluxional Behavior
  - 10.3.1: Determination of Energetics of Fluxional Molecules by NMR

Index

Glossary

Detailed Licensing

Detailed Licensing

Licensing

*A detailed breakdown of this resource's licensing can be found in **Back Matter/Detailed Licensing**.*

1: Atomic Structure, Molecular Structure, and Bonding

1.1: Introduction to Inorganic Chemistry

1.2: Atomic Structure

1.3: Rutherford's Atom

1.4: Bohr's Atom

1.5: Simple Bonding Theory

1.6: Molecular Orbital Theory

1: Atomic Structure, Molecular Structure, and Bonding is shared under a CC BY-NC-SA 4.0 license and was authored, remixed, and/or curated by LibreTexts.

SECTION OVERVIEW

1.1: Introduction to Inorganic Chemistry

This chapter introduces some history and context about the field of Inorganic Chemistry.

1.1.1: What is Inorganic Chemistry?

1.1.2: Inorganic vs Organic Chemistry

1.1.3: History of Inorganic Chemistry

1.1: Introduction to Inorganic Chemistry is shared under a CC BY-NC-SA 4.0 license and was authored, remixed, and/or curated by LibreTexts.

1.1.1: What is Inorganic Chemistry?

Where did the name "Inorganic Chemistry" come from? Well, the term "Organic Chemistry" literally means the *chemistry of life*. Organic chemistry is the study of carbon-based molecules because the first molecules that were isolated from living organisms contained carbon. On the other hand, minerals and other non-living things seemed to be made of other elements. For some time in our history, scientists believed that the chemical difference between living and non-living things was carbon. So, if "organic" molecules are the molecules of life, then is "inorganic chemistry" the "chemistry of death"? Almost? "Inorganic" chemistry historically meant the chemistry of "non-living" things; and these were non-carbon based molecules and ions.

The names "organic" and "inorganic" come from science history, and still today a generally-accepted definition of *Inorganic Chemistry is the study of non-carbon molecules, or all the elements on the periodic table except carbon (*Figure **1.1.1.1**. But, this definition is not completely correct because the field of Inorganic Chemistry also includes organometallic compounds and the study of some carbon-based molecules that have properties that are familiar to metals (like conduction of electricity). This makes the field of inorganic chemistry very broad, and practically limitless. A great way to understand the breadth of the field is to take a look at the abstracts in the latest article of Inorganic Chemistry. Or, check out the 20 most-read articles from this past year using the links below.

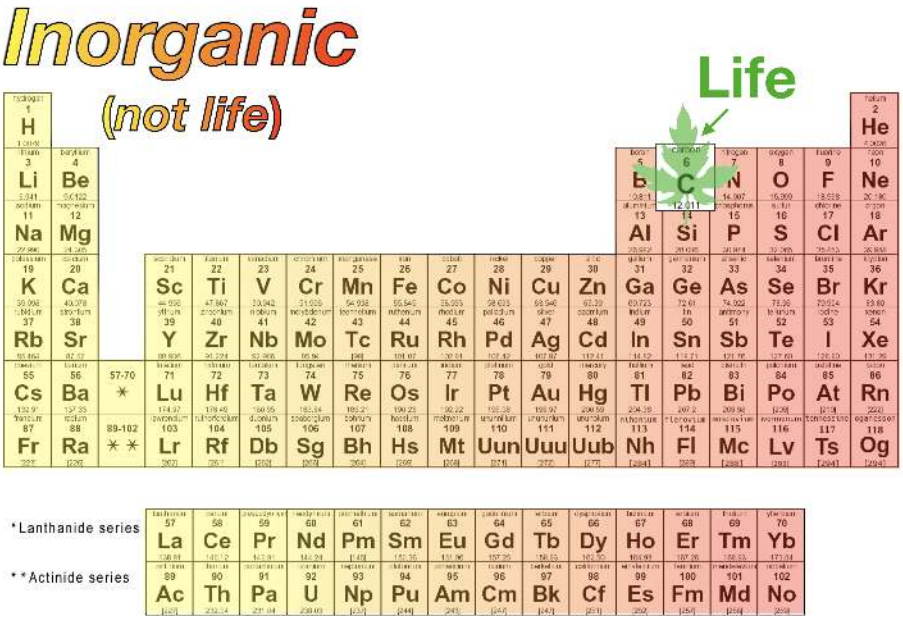


Figure **1.1.1.1**. An illustration of the historic meaning of "organic" and "inorganic". The modern understanding of organic and inorganic chemistry is not consistent with these historical meanings. (Kathryn Haas; CC-NC-BY-SA)

External links:

- The journal, Inorganic Chemistry: https://pubs.acs.org/journal/inocaj
- The latest issue of Inorganic chemistry: https://pubs.acs.org/toc/inocaj/current
- The most popular Inorganic Chemistry articles from the past month and the past year: https://pubs.acs.org/action/showMostReadArticles?journalCode=inocaj

Practice

? What are the Sub-Fields of Inorganic Chemistry?

To appreciate the breadth of Inorganic Chemistry, go to the most recent issue of Inorganic Chemistry and look at the titles and visual abstracts. Identify at least 4 sub-fields of Inorganic Chemistry.

Answer

There are a lot of correct answers here! The point here is that you notice that Inorganic Chemistry is a very broad field. It has something for almost everyone because many other fields overlap with Inorganic Chemistry. You might notice that some of the sub-fields you identified are also interdisciplinary fields between inorganic chemistry and another discipline. For a list of some of the subfields of Inorganic Chemistry, check this Wikipedia article.

1.1.1: What is Inorganic Chemistry? is shared under a CC BY-NC-SA 4.0 license and was authored, remixed, and/or curated by LibreTexts.

- **1.1: What is Inorganic Chemistry?** by Kathryn Haas is licensed CC BY-NC-SA 4.0.

1.1.2: Inorganic vs Organic Chemistry

The division between the fields of Inorganic and Organic chemistry has become blurred. For example, let's look at one of the major classes of catalysts used for organic synthesis reactions: organometalic catalysts (Figure **1.1.2.1**). Organometallic catalysts like these, and all organometallic compounds, contain metals that are bonded to carbon or carbon-containing molecules. So, are they "inorganic" because they contain metals, or "organic" because they contain carbon? These illustrate that clear divisions between organic and inorganic chemistry do not exist. Further, metal ions are common in biology and so the idea that metals are "inorganic" and thus classed as "non-living or non-biological" is incorrect. A canonical example is the organometallic catalyst adenosylcobalbumin, which is an important biological cofactor containing a cobalt (Co) ion (Figure **1.1.2.1**, right) and a cobalt-carbon bond.

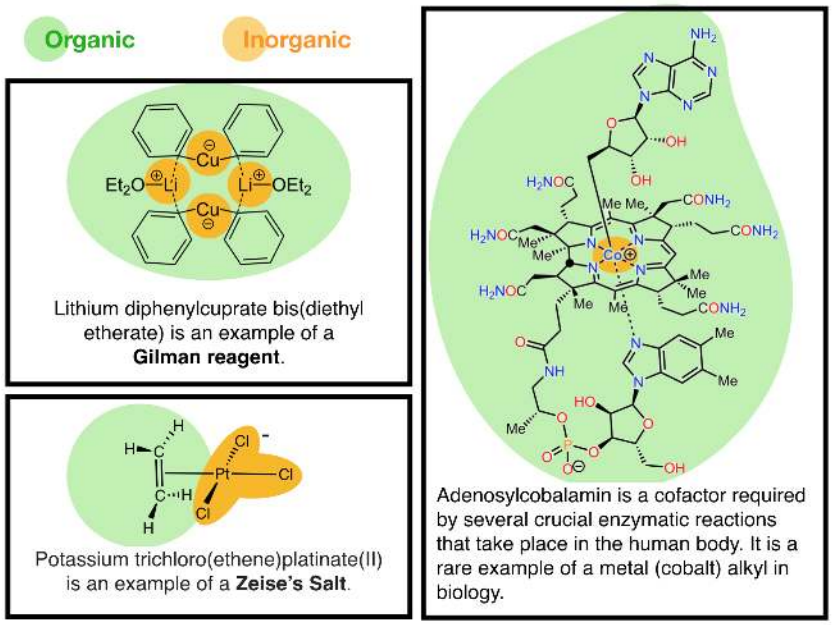
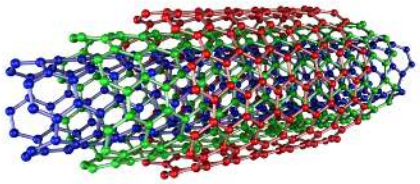


Figure **1.1.2.1**: Some examples of organometallic catalysts. These compounds catalyze organic reactions or biochemical reactions and they are compounds that contain both carbon and metals. These compounds are examples of molecules that cannot be defined only as organic molecules or only as inorganic molecules. Adenosylcobalbumin is an example of an organometallic catalyst that is present in biology, further illustrating that "inorganic" metals are important cofactors in biology. This image is based on information on the Wikipedia article on Organometallic Chemistry and is created from images found there; attribution to images created by Alsosaid1987, AdoCbl-ColorCoded, CC BY-SA 4.0 and Smokefoot, Zeise'sSalt, CC BY-SA 3.0. (Kathryn Haas; CC-BY-SA)

Some of the subfields of Inorganic Chemistry focus on electrical conductivity of inorganic materials (i.e., conduction, superconduction, and semiconduction) and on the study of optical and electronic properties of inorganic nanomaterials. Electrical conductivity is a canonical property of metals, but carbon-based materials also demonstrate electrical conductivity. For example, carbon nanotubes conduct electricity through their extended conjugated π systems. Fullerenes, of which the most famous is Buckminsterfullerene, or Buckeyball (C_{60}), demonstrate interesting properties that are similar to nanoparticles, and when combined with metals and crystallized can demonstrate superconductivity.



Buckminsterfullerene is a type of fullerene with the formula C_{60}



Triple-walled armchair **carbon nanotube**

Figure 1.1.2.2: This figure is created from information found on the Wikipedia articles for Buckmisterfullerene and carbon nanotubes. Attribution Eric Wieser, Multi-walled Carbon Nanotube, CC BY-SA 3.0. (Kathryn Haas; CC-BY-SA)

Although carbon nanotubes and fullerenes are allotropes of carbon, their material properties are somewhat foreign to many organic chemists, who traditionally have focused on smaller organic molecules having very different properties. However, these properties are familiar to inorganic chemists. Thus, inorganic chemists have embraced these molecules as "inorganic" due to the fact that they behave more like inorganic materials than smaller organic molecules. This class of carbon-based molecules serves as another example of molecules that are not perfectly matched to the traditional definitions of "organic" and "inorganic" chemistry. Certainly, the future will hold more and more examples of molecules that do not fit into the traditional disciplines of chemistry.

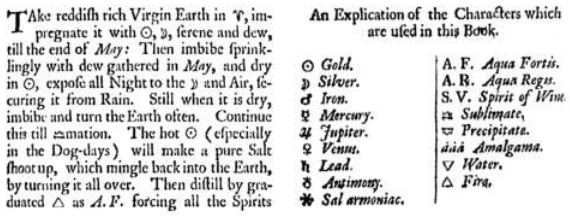
This page titled 1.1.2: Inorganic vs Organic Chemistry is shared under a CC BY-NC-SA 4.0 license and was authored, remixed, and/or curated by Kathryn Haas.

- **1.2: Inorganic vs Organic Chemistry** by Kathryn Haas is licensed CC BY-NC-SA 4.0.

1.1.3: History of Inorganic Chemistry

Metals serve an essential role in many aspects of human civilization and have defined ages of human history. The period of time from about 3300 BC to 1200 BC is often referred to as the Bronze Age. During this period our ancestors first started using metal and learned to mix various elements with copper to make a strong alloy, called bronze. This age yielded significant advancement in the crafting of sharper knives and stronger weapons out of metal instead of rock, wood and bone. Around 1200 BC the human race found an even harder metal and discovered a much stronger alloy called steel. This period is known as the Iron Age. More recently, periods of time known as Gold Rushes have caused huge changes in population distributions and wealth in some countries. Metal has obvious importance in our modern way of life. Today, iron and steel are used for making buildings, machines, automobiles, jewelry, cooking pots, tools, weapons, vehicles, electronics, surgical instruments and symbolic structures like the Eiffel Tower and the Statue of Liberty. Gold, silver, and copper still serve as currency for trade and exchange of goods and services.

The existence of chemistry as a field of study owes much to the fact that gold was a valuable commodity throughout our history. In both the ancient Egyptian society and during the Roman Empire, gold mines were the property of the state, not an individual or group. So there were few ways for most people to legally get any gold for themselves. The Alchemists were a varied group of scholars and charlatans who aimed to solve this problem by creating the **Philosopher's Stone** (which caused the transmutation of lead into gold). Three major streams of alchemy are known: Chinese, Indian, and European, with all three streams having some factors in common. Techniques developed in the European stream ultimately influenced the development of the science of chemistry.


TAke reddiſh rich Virgin Earth in ♈, impregnate it with ☉, ☽, ſerene and dew, till the end of *May*: Then imbibe ſprinklingly with dew gathered in *May*, and dry in ☉, expoſe all Night to the ☽ and Air, ſecuring it from Rain. Still when it is dry, imbibe and turn the Earth often. Continue this till ≏mation. The hot ☉ (eſpecially in the Dog-days) will make a pure Salt ſhoot up, which mingle back into the Earth, by turning it all over. Then diſtill by graduated △ as *A. F.* forcing all the Spirits

An Explication of the Characters which are uſed in this Book.

☉ *Gold.*
☽ *Silver.*
♂ *Iron.*
☿ *Mercury.*
♃ *Jupiter.*
♀ *Venus.*
♄ *Lead.*
♁ *Antimony.*
❋ *Sal armoniac.*

A. F. *Aqua Fortis.*
A. R. *Aqua Regis.*
S. V. *Spirit of Wine.*
♎ *Sublimate.*
♉ *Precipitate.*
äää Amalgama.
▽ *Water.*
△ *Fire.*

Figure 1.1.3.1. Alchemist recipe. Many of the specific approaches that alchemists used when they tried changing lead into gold are vague and unclear. Each alchemist had his own code for recording his data. The processes were kept secret so others could not profit from them. Different scholars developed their own set of symbols as they recorded the information they came up with. Many alchemists were not very honest, taking money from a nobleman by claiming to be able to make gold from lead, then leaving town in the middle of the night. Sometimes the nobleman would detect the fraud and have the alchemist hung. By the 1300's, several European rules had declared alchemy to be illegal and set out strict punishments for those practicing the alchemical arts.

Although alchemists were never successful in changing lead into gold, they made several contributions to modern-day chemistry. Strong acids and bases were discovered, including nitric acid (*ce*$HNO3$), sulfuric acid (H_2SO_4), and hydrochloric acid (HCl), as well as sodium hydroxide ($NaOH$). Glassware for running chemical reactions was developed, as were methods for distillation, crystallization, and sublimation. Alchemy helped improve the study of metallurgy and the extraction of metals from ores. More systematic approaches to research were developed that allowed the discovery of atoms and laid the groundwork for development of the periodic table. For more about the History of Chemistry in general, try the LibreText page A Brief History of Chemistry.

Inorganic compounds have been known and used since antiquity; probably the oldest is the deep blue pigment called Prussian blue ($Fe_4[Fe(CN)_6]_3$). However, the chemical nature of these substances was unknown until the late nineteenth and early twentieth century when the modern field of coordination chemistry emerged. Much of what we know about inorganic chemistry is based largely on the work of and debates between Alfred Werner (1866–1919; Nobel Prize in Chemistry in 1913) and Sophus Mads Jørgensen (1837 –1914). After Werner succeeded in these debates, the field of inorganic chemistry declined in popularity until the mid-twentieth century, when the second world war stimulated renewed interest. During the post-war era, several important discoveries and theories were developed. For example, important theories of bonding in coordination compounds were developed.

Soon after World War II, Crystal Field Theory (CFT) and Ligand Field Theory (LFT) were developed. These are two critical and complimentary theories that provide explanations of spectroscopic, chemical, and structural properties of inorganic coordination compounds, CFT being more simple, and LFT more accurate. In the 1950's, organometallic catalysts were discovered that catalyzed important organic reactions and the Haber-Bosch Process was discovered. The Haber-Bosch Process is catalyzed by an inorganic oxide catalyst and is one of the world's most important industrial reactions. It provides for the synthesis of ammonia directly from elemental nitrogen, N_2, and hydrogen, H_2.

$$N_2(g) + 3H_2(g) \rightleftharpoons 2NH_3(g) \quad (1.1.3.1)$$

Since its development in the early twentieth century, it has led to the production of an enormous quantity of fertilizer, vastly increasing global food production. As a result, it is estimated that a significant fraction of the nitrogen content in the typical human body is ultimately derived from this process. Yet while the reaction must be run at high temperatures and pressures in the industrial setting, the nitrogenase enzyme in the roots of plants can carry out this reaction at the mild conditions within the soil. Intense investigations were then aimed at improving inorganic catalysts through understanding the metal cofactors in enzymes. The link between the Haber-Bosch industrial process and the nitrogenase enzyme was an early bridge between the fields of organometallic chemistry and biochemistry.

Contributions

Part of this page is adapted from K.Haas Ph.D. dissertation

Part of this page is adapted from the following LibreTexts pages

- Alchemy contributed by CK-12 Foundation by Sharon Bewick, Richard Parsons, Therese Forsythe, Shonna Robinson, and Jean Dupon.
- Werner's Theory of Coordination Compounds
- The Haber-Bosch Process Worksheet

1.1.3: History of Inorganic Chemistry is shared under a CC BY-NC-SA 4.0 license and was authored, remixed, and/or curated by LibreTexts.

- **1.3: History of Inorganic Chemistry** by Kathryn Haas is licensed CC BY-NC-SA 4.0.

SECTION OVERVIEW

1.2: Atomic Structure

1.2.1: Historical Development of Atomic Theory

- 1.2.1.1: The Periodic Table
- 1.2.1.2: Discovery of Subatomic Particles and the Bohr Atom

1.2.2: The Schrödinger equation, particle in a box, and atomic wavefunctions

- 1.2.2.1: Particle in a Box
- 1.2.2.2: Quantum Numbers and Atomic Wave Functions
- 1.2.2.3: Aufbau Principle
- 1.2.2.4: Shielding

1.2.3: Periodic Properties of Atoms

- 1.2.3.1: Ionization energy
- 1.2.3.2: Electron Affinity
- 1.2.3.3: Covalent and Ionic Radii

1.2: Atomic Structure is shared under a CC BY-NC-SA 4.0 license and was authored, remixed, and/or curated by LibreTexts.

1.2.1: Historical Development of Atomic Theory

Notes about this page

The page below is a brief overview on the history of atomic theory. It contains lots of video media. Use this page as a review from earlier in your chemistry journey!

Alternatives pages on the history of atomic theory are:

- A more detailed overview that includes practice problems is here (click).
- Another brief overview is here (click).

Learning Objectives

By the end of this section, you will be able to:

- State the postulates of Dalton's atomic theory
- Use postulates of Dalton's atomic theory to explain the laws of definite and multiple proportions
- Outline milestones in the development of modern atomic theory
- Summarize and interpret the results of the experiments of Thomson, Millikan, and Rutherford

A Video Introduction to Atomic Theory through the Nineteenth Century From Crash Course Chemistry



***Video* 1.2.1.1*:* Lavoisier's discovery of The Law of Conservation of Matter led to the Laws of Definite and Multiple Proportions and eventually Dalton's Atomic Theory.**

Atomic Theory through the Nineteenth Century

The earliest recorded discussion of the basic structure of matter comes from ancient Greek philosophers, the scientists of their day. In the fifth century BC, Leucippus and Democritus argued that all matter was composed of small, finite particles that they called *atomos*, a term derived from the Greek word for "indivisible." They thought of atoms as moving particles that differed in shape and size, and which could join together. Later, Aristotle and others came to the conclusion that matter consisted of various combinations of the four "elements"—fire, earth, air, and water—and could be infinitely divided. Interestingly, these philosophers thought about atoms and "elements" as philosophical concepts, but apparently never considered performing experiments to test their ideas.

The Aristotelian view of the composition of matter held sway for over two thousand years, until English schoolteacher John Dalton helped to revolutionize chemistry with his hypothesis that the behavior of matter could be explained using an atomic theory. First published in 1807, many of Dalton's hypotheses about the microscopic features of matter are still valid in modern atomic theory. Here are the postulates of Dalton's atomic theory.

1. Matter is composed of exceedingly small particles called atoms. An atom is the smallest unit of an element that can participate in a chemical change.
2. An element consists of only one type of atom, which has a mass that is characteristic of the element and is the same for all atoms of that element (Figure **1.2.1.1**). A macroscopic sample of an element contains an incredibly large number of atoms, all of which have identical chemical properties.
3. Atoms of one element differ in properties from atoms of all other elements.
4. A compound consists of atoms of two or more elements combined in a small, whole-number ratio. In a given compound, the numbers of atoms of each of its elements are always present in the same ratio (Figure **1.2.1.2**).
5. Atoms are neither created nor destroyed during a chemical change, but are instead rearranged to yield substances that are different from those present before the change (Figure **1.2.1.3**).

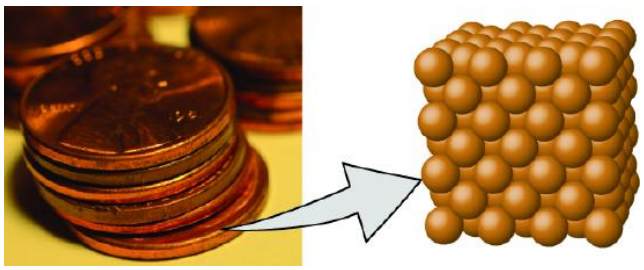


Figure* 1.2.1.1*: *A pre-1982 copper penny (left) contains approximately 3 × 10^{22} copper atoms (several dozen are represented as brown spheres at the right), each of which has the same chemical properties. (credit: modification of work by "slgckgc"/Flickr)*

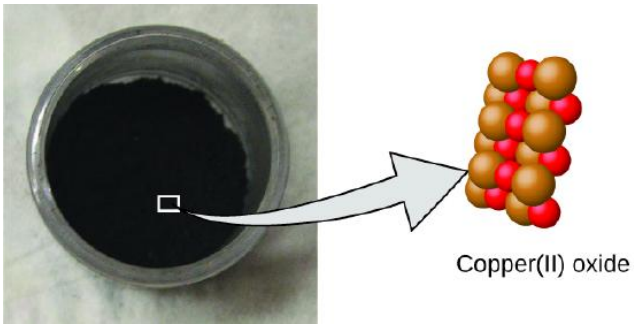


Figure* 1.2.1.2*: *Copper(II) oxide, a powdery, black compound, results from the combination of two types of atoms—copper (brown spheres) and oxygen (red spheres)—in a 1:1 ratio. (credit: modification of work by "Chemicalinterest"/Wikimedia Commons)*

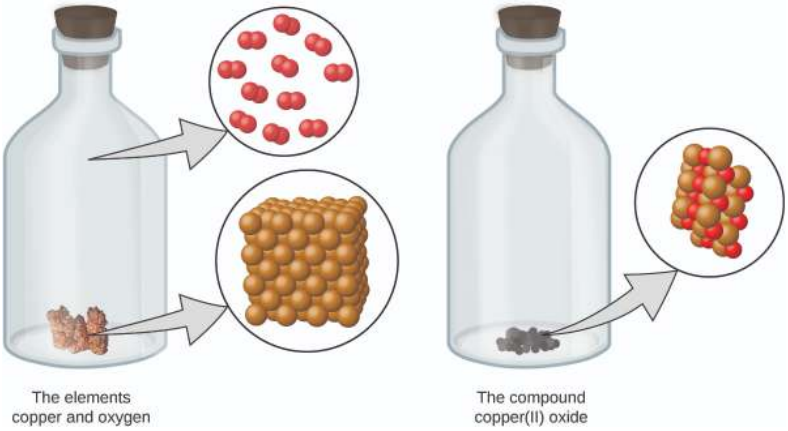


Figure* 1.2.1.3*: *When the elements copper (a shiny, red-brown solid, shown here as brown spheres) and oxygen (a clear and colorless gas, shown here as red spheres) react, their atoms rearrange to form a compound containing copper and oxygen (a powdery, black solid). (credit copper: modification of work by http://images-of-elements.com/copper.php).*

Dalton's atomic theory provides a microscopic explanation of the many macroscopic properties of matter that you've learned about. For example, if an element such as copper consists of only one kind of atom, then it cannot be broken down into simpler substances, that is, into substances composed of fewer types of atoms. And if atoms are neither created nor destroyed during a chemical change, then the total mass of matter present when matter changes from one type to another will remain constant (the law of conservation of matter (or mass)).

Want to learn more about the Law of Conservation of Mass?



Video* 1.2.1.2*: "We are made of star stuff" - Carl Sagan.

Example 1.2.1.1: Testing Dalton's Atomic Theory

In the following drawing, the green spheres represent atoms of a certain element. The purple spheres represent atoms of another element. If the spheres touch, they are part of a single unit of a compound. Does the following chemical change represented by these symbols violate any of the ideas of Dalton's atomic theory? If so, which one?

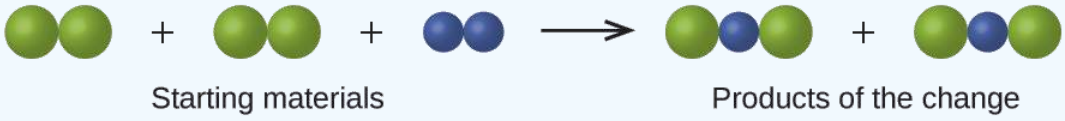


Solution

The starting materials consist of two green spheres and two purple spheres. The products consist of only one green sphere and one purple sphere. This violates Dalton's postulate that atoms are neither created nor destroyed during a chemical change, but are merely redistributed. (In this case, atoms appear to have been destroyed.)

Exercise 1.2.1.1

In the following drawing, the green spheres represent atoms of a certain element. The purple spheres represent atoms of another element. If the spheres touch, they are part of a single unit of a compound. Does the following chemical change represented by these symbols violate any of the ideas of Dalton's atomic theory? If so, which one



Answer

> The starting materials consist of four green spheres and two purple spheres. The products consist of four green spheres and two purple spheres. This does not violate any of Dalton's postulates: Atoms are neither created nor destroyed, but are redistributed in small, whole-number ratios.

Dalton knew of the experiments of French chemist Joseph Proust, who demonstrated that *all samples of a pure compound contain the same elements in the same proportion by mass*. This statement is known as the law of definite proportions or the law of constant composition. The suggestion that the numbers of atoms of the elements in a given compound always exist in the same ratio is consistent with these observations. For example, when different samples of isooctane (a component of gasoline and one of the standards used in the octane rating system) are analyzed, they are found to have a carbon-to-hydrogen mass ratio of 5.33:1, as shown in Table **1.2.1.1**.

Table 1.2.1.1: Constant Composition of Isooctane

Sample	Carbon	Hydrogen	Mass Ratio
A	14.82 g	2.78 g	$\frac{14.82\ \text{g carbon}}{2.78\ \text{g hydrogen}} = \frac{5.33\ \text{g carbon}}{1.00\ \text{g hydrogen}}$
B	22.33 g	4.19 g	$\frac{22.33\ \text{g carbon}}{4.19\ \text{g hydrogen}} = \frac{5.33\ \text{g carbon}}{1.00\ \text{g hydrogen}}$
C	19.40 g	3.64 g	$\frac{19.40\ \text{g carbon}}{3.63\ \text{g hydrogen}} = \frac{5.33\ \text{g carbon}}{1.00\ \text{g hydrogen}}$

It is worth noting that although all samples of a particular compound have the same mass ratio, the converse is not true in general. That is, samples that have the same mass ratio are not necessarily the same substance. For example, there are many compounds other than isooctane that also have a carbon-to-hydrogen mass ratio of 5.33:1.00.

Dalton also used data from Proust, as well as results from his own experiments, to formulate another interesting law. The law of multiple proportions states that *when two elements react to form more than one compound, a fixed mass of one element will react with masses of the other element in a ratio of small, whole numbers*. For example, copper and chlorine can form a green, crystalline solid with a mass ratio of 0.558 g chlorine to 1 g copper, as well as a brown crystalline solid with a mass ratio of 1.116 g chlorine to 1 g copper. These ratios by themselves may not seem particularly interesting or informative; however, if we take a ratio of these ratios, we obtain a useful and possibly surprising result: a small, whole-number ratio.

$$\frac{\frac{1.116\ \text{g Cl}}{1\ \text{g Cu}}}{\frac{0.558\ \text{g Cl}}{1\ \text{g Cu}}} = \frac{2}{1} \tag{1.2.1.1}$$

This 2-to-1 ratio means that the brown compound has twice the amount of chlorine per amount of copper as the green compound.

This can be explained by atomic theory if the copper-to-chlorine ratio in the brown compound is 1 copper atom to 2 chlorine atoms, and the ratio in the green compound is 1 copper atom to 1 chlorine atom. The ratio of chlorine atoms (and thus the ratio of their masses) is therefore 2 to 1 (Figure **1.2.1.4**).

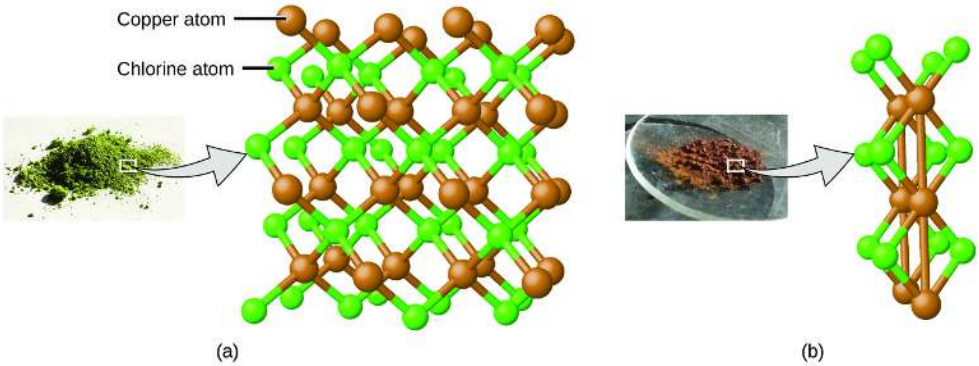


***Figure 1.2.1.4**: Compared to the copper chlorine compound in (a), where copper is represented by brown spheres and chlorine by green spheres, the copper chlorine compound in (b) has twice as many chlorine atoms per copper atom. (credit a: modification of*

work by "Benjah-bmm27"/Wikimedia Commons; credit b: modification of work by "Walkerma"/Wikimedia Commons)

Example 1.2.1.2: Laws of Definite and Multiple Proportions

A sample of compound A (a clear, colorless gas) is analyzed and found to contain 4.27 g carbon and 5.69 g oxygen. A sample of compound B (also a clear, colorless gas) is analyzed and found to contain 5.19 g carbon and 13.84 g oxygen. Are these data an example of the law of definite proportions, the law of multiple proportions, or neither? What do these data tell you about substances A and B?

Solution

In compound A, the mass ratio of carbon to oxygen is:

$$\frac{1.33\text{ g O}}{1\text{ g C}}$$

In compound B, the mass ratio of carbon to oxygen is:

$$\frac{2.67\text{ g O}}{1\text{ g C}}$$

The ratio of these ratios is:

$$\frac{\frac{1.33\text{ g O}}{1\text{ g C}}}{\frac{2.67\text{ g O}}{1\text{ g C}}} = \frac{1}{2}$$

This supports the law of multiple proportions. This means that A and B are different compounds, with A having one-half as much carbon per amount of oxygen (or twice as much oxygen per amount of carbon) as B. A possible pair of compounds that would fit this relationship would be A = CO_2 and B = CO.

Exercise 1.2.1.2

A sample of compound X (a clear, colorless, combustible liquid with a noticeable odor) is analyzed and found to contain 14.13 g carbon and 2.96 g hydrogen. A sample of compound Y (a clear, colorless, combustible liquid with a noticeable odor that is slightly different from X's odor) is analyzed and found to contain 19.91 g carbon and 3.34 g hydrogen. Are these data an example of the law of definite proportions, the law of multiple proportions, or neither? What do these data tell you about substances X and Y?

Answer

In compound X, the mass ratio of carbon to hydrogen is $\frac{14.13\text{ g C}}{2.96\text{ g H}}$.

In compound Y, the mass ratio of carbon to oxygen is $\frac{19.91\text{ g C}}{3.34\text{ g H}}$.

The ratio of these ratios is

$$\frac{\frac{14.13\text{ g C}}{2.96\text{ g H}}}{\frac{19.91\text{ g C}}{3.34\text{ g H}}} = \frac{4.77\text{ g C/g H}}{5.96\text{ g C/g H}} = 0.800 = \frac{4}{5}.$$

This small, whole-number ratio supports the law of multiple proportions. This means that X and Y are different compounds.

In the two centuries since Dalton developed his ideas, scientists have made significant progress in furthering our understanding of atomic theory. Much of this came from the results of several seminal experiments that revealed the details of the internal structure of atoms. Here, we will discuss some of those key developments, with an emphasis on application of the scientific method, as well

as understanding how the experimental evidence was analyzed. While the historical persons and dates behind these experiments can be quite interesting, it is most important to understand the concepts resulting from their work.

Atomic Theory After the Nineteenth Century

If matter were composed of atoms, what were atoms composed of? Were they the smallest particles, or was there something smaller? In the late 1800s, a number of scientists interested in questions like these investigated the electrical discharges that could be produced in low-pressure gases, with the most significant discovery made by English physicist J. J. Thomson using a cathode ray tube. This apparatus consisted of a sealed glass tube from which almost all the air had been removed; the tube contained two metal electrodes. When high voltage was applied across the electrodes, a visible beam called a cathode ray appeared between them. This beam was deflected toward the positive charge and away from the negative charge, and was produced in the same way with identical properties when different metals were used for the electrodes. In similar experiments, the ray was simultaneously deflected by an applied magnetic field, and measurements of the extent of deflection and the magnetic field strength allowed Thomson to calculate the charge-to-mass ratio of the cathode ray particles. The results of these measurements indicated that these particles were much lighter than atoms (Figure **1.2.1.1**).

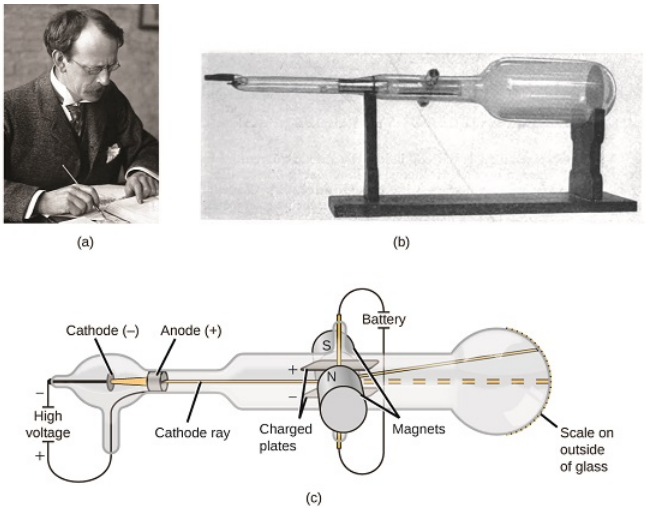
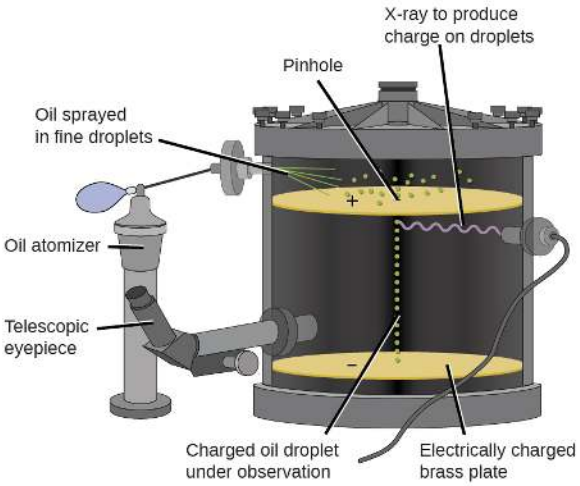


Figure* 1.2.1.5: (a) J. J. Thomson produced a visible beam in a cathode ray tube. (b) This is an early cathode ray tube, invented in 1897 by Ferdinand Braun. (c) In the cathode ray, the beam (shown in yellow) comes from the cathode and is accelerated past the anode toward a fluorescent scale at the end of the tube. Simultaneous deflections by applied electric and magnetic fields permitted Thomson to calculate the mass-to-charge ratio of the particles composing the cathode ray. (credit a: modification of work by Nobel Foundation; credit b: modification of work by Eugen Nesper; credit c: modification of work by "Kurzon"/Wikimedia Commons).*

Based on his observations, here is what Thomson proposed and why: The particles are attracted by positive (+) charges and repelled by negative (−) charges, so they must be negatively charged (like charges repel and unlike charges attract); they are less massive than atoms and indistinguishable, regardless of the source material, so they must be fundamental, subatomic constituents of all atoms. Although controversial at the time, Thomson's idea was gradually accepted, and his cathode ray particle is what we now call an electron, a negatively charged, subatomic particle with a mass more than one thousand-times less that of an atom. The term "electron" was coined in 1891 by Irish physicist George Stoney, from "*electr*ic i*on*."

In 1909, more information about the electron was uncovered by American physicist Robert A. Millikan via his "oil drop" experiments. Millikan created microscopic oil droplets, which could be electrically charged by friction as they formed or by using X-rays. These droplets initially fell due to gravity, but their downward progress could be slowed or even reversed by an electric field lower in the apparatus. By adjusting the electric field strength and making careful measurements and appropriate calculations, Millikan was able to determine the charge on individual drops (Figure **1.2.1.2**).



Oil drop	Charge in coulombs (C)
A	4.8×10^{-19} C
B	3.2×10^{-19} C
C	6.4×10^{-19} C
D	1.6×10^{-19} C
E	4.8×10^{-19} C

***Figure* 1.2.1.6:** *Millikan's experiment measured the charge of individual oil drops. The tabulated data are examples of a few possible values.*

Looking at the charge data that Millikan gathered, you may have recognized that the charge of an oil droplet is always a multiple of a specific charge, 1.6×10^{-19} C. Millikan concluded that this value must therefore be a fundamental charge—the charge of a single electron—with his measured charges due to an excess of one electron (1 times 1.6×10^{-19} C), two electrons (2 times 1.6×10^{-19} C), three electrons (3 times 1.6×10^{-19} C), and so on, on a given oil droplet. Since the charge of an electron was now known due to Millikan's research, and the charge-to-mass ratio was already known due to Thomson's research (1.759×10^{11} C/kg), it only required a simple calculation to determine the mass of the electron as well.

$$\text{Mass of electron} = 1.602 \times 10^{-19} \cancel{\text{C}} \times \frac{1 \text{ kg}}{1.759 \times 10^{11} \cancel{\text{C}}} = 9.107 \times 10^{-31} \text{ kg} \tag{2.3.1}$$

Scientists had now established that the atom was not indivisible as Dalton had believed, and due to the work of Thomson, Millikan, and others, the charge and mass of the negative, subatomic particles—the electrons—were known. However, the positively charged part of an atom was not yet well understood. In 1904, Thomson proposed the "plum pudding" model of atoms, which described a positively charged mass with an equal amount of negative charge in the form of electrons embedded in it, since all atoms are electrically neutral. A competing model had been proposed in 1903 by Hantaro Nagaoka, who postulated a Saturn-like atom, consisting of a positively charged sphere surrounded by a halo of electrons (Figure 1.2.1.3).

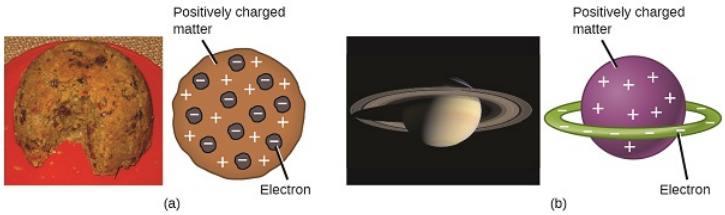


***Figure* 1.2.1.7**: *(a) Thomson suggested that atoms resembled plum pudding, an English dessert consisting of moist cake with embedded raisins ("plums"). (b) Nagaoka proposed that atoms resembled the planet Saturn, with a ring of electrons surrounding a positive "planet." (credit a: modification of work by "Man vyi"/Wikimedia Commons; credit b: modification of work by "NASA"/Wikimedia Commons).*

The next major development in understanding the atom came from Ernest Rutherford, a physicist from New Zealand who largely spent his scientific career in Canada and England. He performed a series of experiments using a beam of high-speed, positively charged alpha particles (α particles) that were produced by the radioactive decay of radium; α particles consist of two protons and two neutrons (you will learn more about radioactive decay in the chapter on nuclear chemistry). Rutherford and his colleagues Hans Geiger (later famous for the Geiger counter) and Ernest Marsden aimed a beam of α particles, the source of which was

embedded in a lead block to absorb most of the radiation, at a very thin piece of gold foil and examined the resultant scattering of the α particles using a luminescent screen that glowed briefly where hit by an α particle.

What did they discover? Most particles passed right through the foil without being deflected at all. However, some were diverted slightly, and a very small number were deflected almost straight back toward the source (Figure **1.2.1.4**). Rutherford described finding these results: “It was quite the most incredible event that has ever happened to me in my life. It was almost as incredible as if you fired a 15-inch shell at a piece of tissue paper and it came back and hit you”[1] (p. 68).

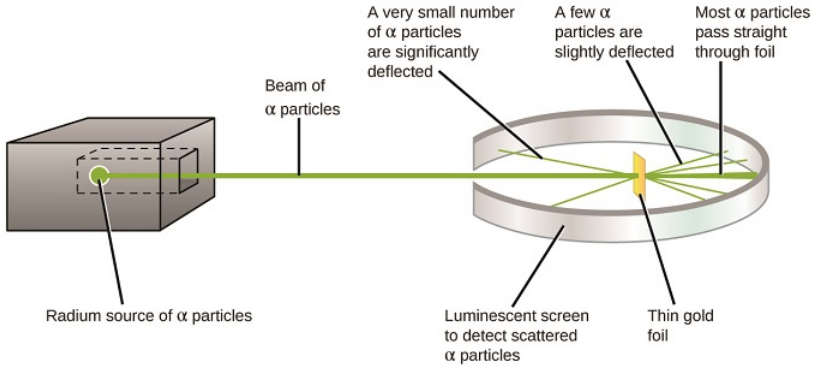


Figure* 1.2.1.8*: *Geiger and Rutherford fired α particles at a piece of gold foil and detected where those particles went, as shown in this schematic diagram of their experiment. Most of the particles passed straight through the foil, but a few were deflected slightly and a very small number were significantly deflected.*

Here is what Rutherford deduced: Because most of the fast-moving α particles passed through the gold atoms undeflected, they must have traveled through essentially empty space inside the atom. Alpha particles are positively charged, so deflections arose when they encountered another positive charge (like charges repel each other). Since like charges repel one another, the few positively charged α particles that changed paths abruptly must have hit, or closely approached, another body that also had a highly concentrated, positive charge. Since the deflections occurred a small fraction of the time, this charge only occupied a small amount of the space in the gold foil. Analyzing a series of such experiments in detail, Rutherford drew two conclusions:

1. The volume occupied by an atom must consist of a large amount of empty space.
2. A small, relatively heavy, positively charged body, the nucleus, must be at the center of each atom.

This analysis led Rutherford to propose a model in which an atom consists of a very small, positively charged nucleus, in which most of the mass of the atom is concentrated, surrounded by the negatively charged electrons, so that the atom is electrically neutral (Figure **1.2.1.5**).

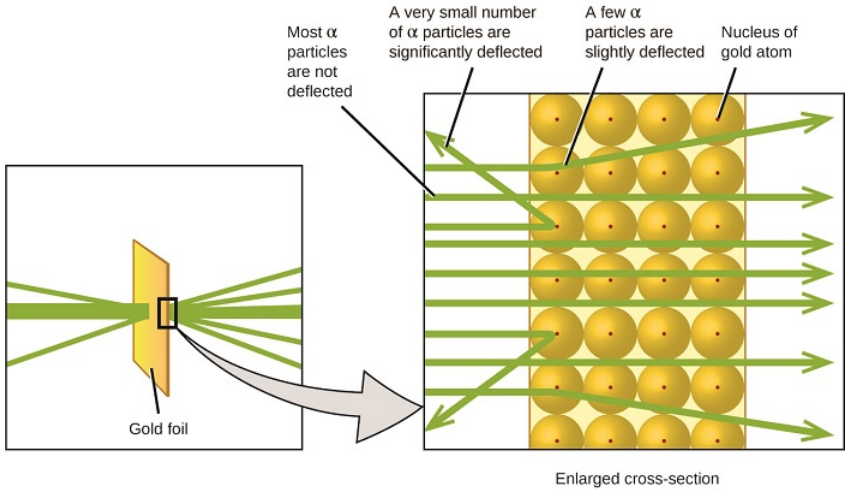
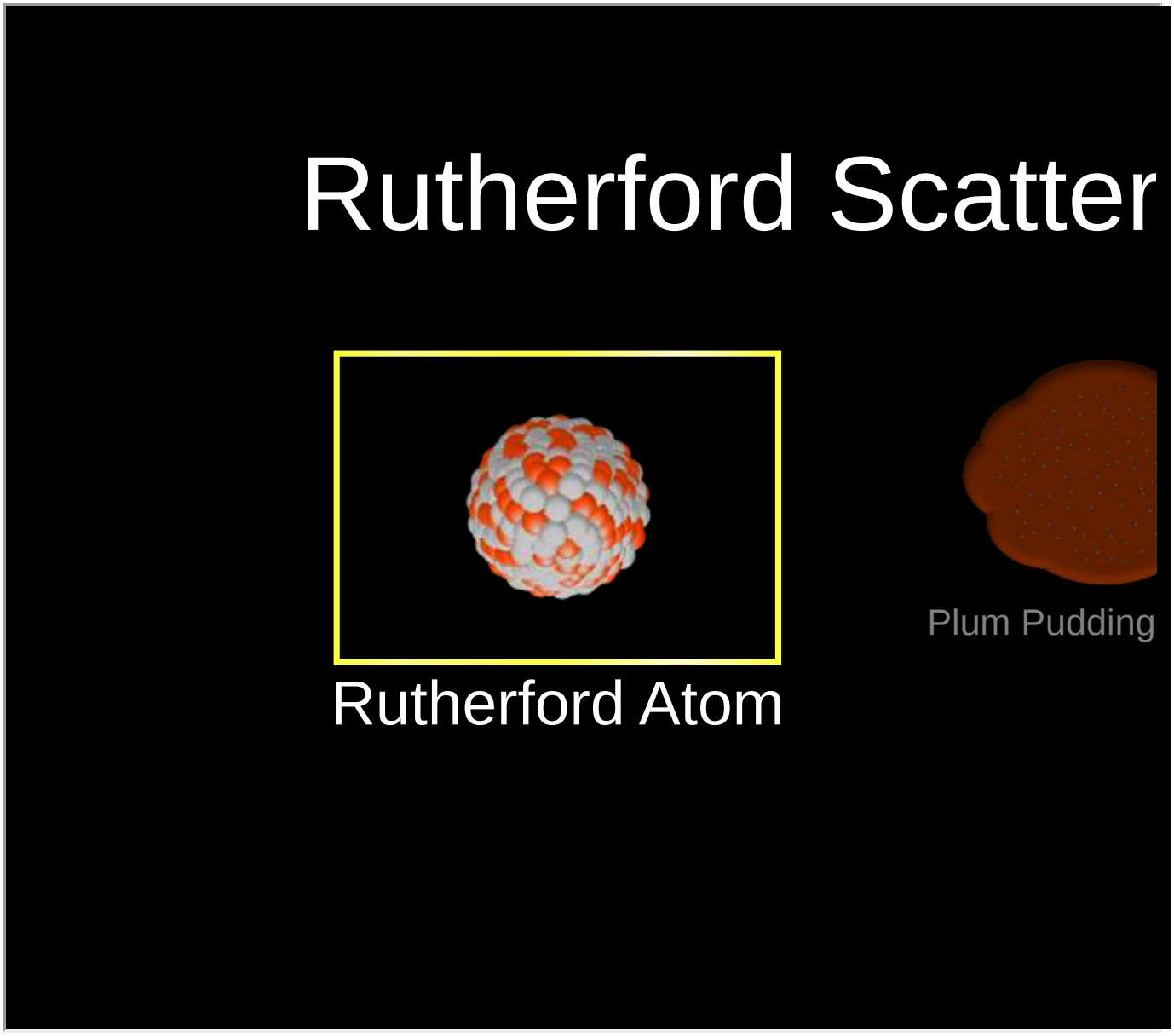


Figure* 1.2.1.9*: *The α particles are deflected only when they collide with or pass close to the much heavier, positively charged gold nucleus. Because the nucleus is very small compared to the size of an atom, very few α particles are deflected. Most pass through*

the relatively large region occupied by electrons, which are too light to deflect the rapidly moving particles.

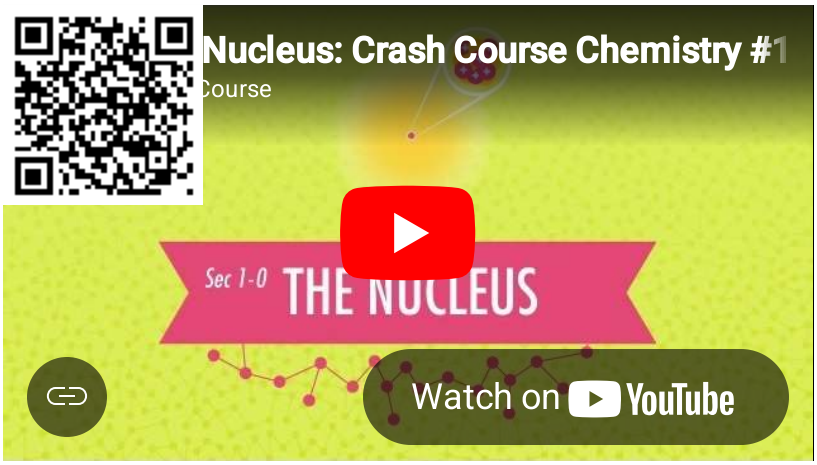
After many more experiments, Rutherford also discovered that the nuclei of other elements contain the hydrogen nucleus as a "building block," and he named this more fundamental particle the proton, the positively charged, subatomic particle found in the nucleus. With one addition, which you will learn next, this nuclear model of the atom, proposed over a century ago, is still used today.



Another important finding was the discovery of isotopes. During the early 1900s, scientists identified several substances that appeared to be new elements, isolating them from radioactive ores. For example, a "new element" produced by the radioactive decay of thorium was initially given the name mesothorium. However, a more detailed analysis showed that mesothorium was chemically identical to radium (another decay product), despite having a different atomic mass. This result, along with similar findings for other elements, led the English chemist Frederick Soddy to realize that an element could have types of atoms with different masses that were chemically indistinguishable. These different types are called isotopes—atoms of the same element that differ in mass. Soddy was awarded the Nobel Prize in Chemistry in 1921 for this discovery.

One puzzle remained: The nucleus was known to contain almost all of the mass of an atom, with the number of protons only providing half, or less, of that mass. Different proposals were made to explain what constituted the remaining mass, including the

existence of neutral particles in the nucleus. As you might expect, detecting uncharged particles is very challenging, and it was not until 1932 that James Chadwick found evidence of neutrons, uncharged, subatomic particles with a mass approximately the same as that of protons. The existence of the neutron also explained isotopes: They differ in mass because they have different numbers of neutrons, but they are chemically identical because they have the same number of protons. This will be explained in more detail later in this unit.



Video* 1.2.1.2*: An Introduction to Subatomic Particles

Summary



***Video* 1.2.1.3*:** A summary of discoveries in atomic theory.*



***Video* 1.2.1.4*:** A different summary of discoveries in atomic theory.*

The ancient Greeks proposed that matter consists of extremely small particles called atoms. Dalton postulated that each element has a characteristic type of atom that differs in properties from atoms of all other elements, and that atoms of different elements can combine in fixed, small, whole-number ratios to form compounds. Samples of a particular compound all have the same elemental proportions by mass. When two elements form different compounds, a given mass of one element will combine with masses of the other element in a small, whole-number ratio. During any chemical change, atoms are neither created nor destroyed.

Although no one has actually seen the inside of an atom, experiments have demonstrated much about atomic structure. Thomson's cathode ray tube showed that atoms contain small, negatively charged particles called electrons. Millikan discovered that there is a fundamental electric charge—the charge of an electron. Rutherford's gold foil experiment showed that atoms have a small, dense, positively charged nucleus; the positively charged particles within the nucleus are called protons. Chadwick discovered that the nucleus also contains neutral particles called neutrons. Soddy demonstrated that atoms of the same element can differ in mass; these are called isotopes.

Footnotes

1. Ernest Rutherford, "The Development of the Theory of Atomic Structure," ed. J. A. Ratcliffe, in *Background to Modern Science*, eds. Joseph Needham and Walter Pagel, (Cambridge, UK: Cambridge University Press, 1938), 61–74. Accessed September 22, 2014, https://ia600508.us.archive.org/3/it...e032734mbp.pdf.

Glossary

Dalton's atomic theory
: set of postulates that established the fundamental properties of atoms

law of constant composition
: (also, law of definite proportions) all samples of a pure compound contain the same elements in the same proportions by mass

law of multiple proportions
: when two elements react to form more than one compound, a fixed mass of one element will react with masses of the other element in a ratio of small whole numbers

law of definite proportions
: (also, law of constant composition) all samples of a pure compound contain the same elements in the same proportions by mass

alpha particle (α particle)
: positively charged particle consisting of two protons and two neutrons

electron
: negatively charged, subatomic particle of relatively low mass located outside the nucleus

isotopes
: atoms that contain the same number of protons but different numbers of neutrons

neutron
: uncharged, subatomic particle located in the nucleus

proton
: positively charged, subatomic particle located in the nucleus

nucleus
: massive, positively charged center of an atom made up of protons and neutrons

Contributors

- Paul Flowers (University of North Carolina - Pembroke), Klaus Theopold (University of Delaware) and Richard Langley (Stephen F. Austin State University) with contributing authors. Textbook content produced by OpenStax College is licensed under a Creative Commons Attribution License 4.0 license. Download for free at http://cnx.org/contents/85abf193-2bd...a7ac8df6@9.110).
- Adelaide Clark, Oregon Institute of Technology
- Crash Course Chemistry: Crash Course is a division of Complexly and videos are free to stream for educational purposes.
- TED-Ed's commitment to creating lessons worth sharing is an extension of TED's mission of spreading great ideas. Within TED-Ed's growing library of TED-Ed animations, you will find carefully curated educational videos, many of which represent collaborations between talented educators and animators nominated through the TED-Ed website.

1.2.1: Historical Development of Atomic Theory is shared under a CC BY-NC-SA 4.0 license and was authored, remixed, and/or curated by LibreTexts.

- **2.1: Historical Development of Atomic Theory** is licensed CC BY-NC-SA 4.0.

1.2.1.1: The Periodic Table

Learning Objectives

- To become familiar with the history of the periodic table.

The modern periodic table has evolved through a long history of attempts by chemists to arrange the elements according to their reactivity and other properties as an aid in predicting chemical behavior. Now that we have arranged the table according to electronic structure, it makes sense to go back and look at earlier efforts in the light of what we know about electronic structure.

One of the first to suggest such an arrangement was the German chemist Johannes Dobereiner (1780–1849), who noticed that many of the known elements could be grouped in triads, sets of three elements that have similar properties—for example, chlorine, bromine, and iodine; or copper, silver, and gold. Dobereiner proposed that all elements could be grouped in such triads, but subsequent attempts to expand his concept were unsuccessful. We now know that portions of the periodic table—the *d* block in particular—contain triads of elements with substantial similarities. The middle three members of most of the other columns, such as sulfur, selenium, and tellurium in group 16 or aluminum, gallium, and indium in group 13, also have remarkably similar chemistry.

By the mid-19th century, the atomic masses of many of the elements had been determined. The English chemist John Newlands (1838–1898), hypothesizing that the chemistry of the elements might be related to their masses, arranged the known elements in order of increasing atomic mass and discovered that every seventh element had similar properties (Figure 3.4.1). Newlands therefore suggested that the elements could be classified into octaves: a group of seven elements (not counting the noble gases, which were unknown at the time) that correspond to the *horizontal* rows in the main group elements. Unfortunately, Newlands's "law of octaves" did not seem to work for elements heavier than calcium, and his idea was publicly ridiculed. At one scientific meeting, Newlands was asked why he didn't arrange the elements in alphabetical order instead of by atomic mass, since that would make just as much sense! Actually, Newlands was on the right track—with only a few exceptions, atomic mass does increase with atomic number, and similar properties occur every time a set of ns^2np^6 subshells is filled. Despite the fact that Newlands's table had no logical place for the *d*-block elements, he was honored for his idea by the Royal Society of London in 1887.

John Newlands (1838–1898)

Newlands noticed that elemental properties repeated every seventh (or multiple of seven) element, as musical notes repeat every eighth note.

No.	No.	No.	No.	No.	No.	No.	No.
H 1	F 8	Cl 15	Co & Ni 22	Br 29	Pd 36	I 42	Pt & Ir 50
Li 2	Na 9	K 16	Cu 23	Rb 30	Ag 37	Cs 44	Tl 51
G 3	Mg 10	Ca 17	Zn 25	Sr 31	Bd [sic-Cd] 38	Ba & V 45	Pb 54
Bo 4	Al 11	Cr 19	Y 24	Ce & La 33	U 40	Ta 46	Th 56
C 5	Si 12	Ti 18	In 26	Zr 32	Sn 39	W 47	Hg 52
N 6	**P 13**	Mn 20	**As 27**	Di & Mo 34	**Sb 41**	Nb 48	**Bi 55**
O 7	S 14	Fe 21	Se 28	Ro & Ru 35	Te 43	Au 49	Os 51

NOTE. Where two elements happen to have the same equivalent, both are designated by the same number.

Figure 3.4.1 The arrangement of the elements into octaves as proposed by **Newlands:** *The table shown here accompanied a letter from a 27-year-old Newlands to the editor of the journal Chemical News in which he wrote: "If the elements are arranged in the order of their equivalents, with a few slight transpositions, as in the accompanying table, it will be observed that elements belonging to the same group usually appear on the same horizontal line. It will also be seen that the numbers of analogous elements generally differ either by 7 or by some multiple of seven; in other words, members of the same group stand to each other in the same relation as the extremities of one or more octaves in music. Thus, in the nitrogen group, between nitrogen and phosphorus there are 7 elements; between phosphorus and arsenic, 14; between arsenic and antimony, 14; and lastly, between antimony and bismuth, 14 also. This peculiar relationship I propose to provisionally term the Law of Octaves. I am, &c. John A. R. Newlands, F.C.S. Laboratory, 19, Great St. Helen's, E.C., August 8, 1865."*

The periodic table achieved its modern form through the work of the German chemist Julius Lothar Meyer (1830–1895) and the Russian chemist Dimitri Mendeleev (1834–1907), both of whom focused on the relationships between atomic mass and various physical and chemical properties. In 1869, they independently proposed essentially identical arrangements of the elements. Meyer aligned the elements in his table according to periodic variations in simple atomic properties, such as "atomic volume" (Figure

3.4.2), which he obtained by dividing the atomic mass (molar mass) in grams per mole by the density of the element in grams per cubic centimeter. This property is equivalent to what is today defined as molar volume, the molar mass of an element divided by its density (measured in cubic centimeters per mole):

$$\frac{molar\ mass\ \left(g/mol\right)}{density\ \left(g/cm^3\right)} = molar\ volume\ \left(cm^3/mol\right)$$

As shown in Figure 3.4.2 , the alkali metals have the highest molar volumes of the solid elements. In Meyer's plot of atomic volume versus atomic mass, the nonmetals occur on the rising portion of the graph, and metals occur at the peaks, in the valleys, and on the down slopes.

Dimitri Mendeleev (1834–1907)

When his family's glass factory was destroyed by fire, Mendeleev moved to St. Petersburg, Russia, to study science. He became ill and was not expected to recover, but he finished his PhD with the help of his professors and fellow students. In addition to the periodic table, another of Mendeleev's contributions to science was an outstanding textbook, *The Principles of Chemistry*, which was used for many years.

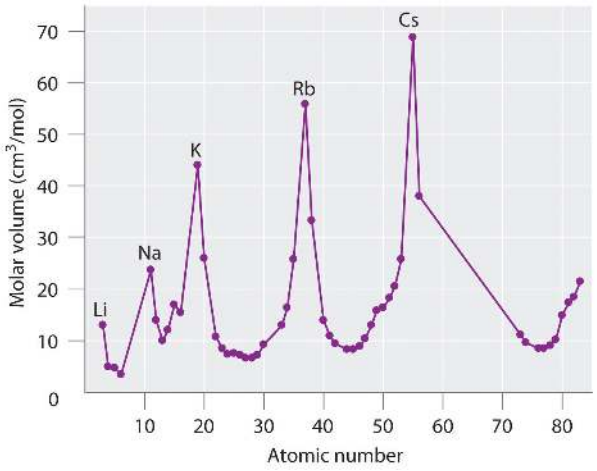


Figure 3.4.2 Variation of atomic volume with atomic number, adapted from Meyer's plot of **1870:** *Note the periodic increase and decrease in atomic volume. Because the noble gases had not yet been discovered at the time this graph was formulated, the peaks correspond to the alkali metals (group 1).*

Mendeleev's Periodic Table

Mendeleev, who first published his periodic table in 1869 (Figure 3.4.3), is usually credited with the origin of the modern periodic table. The key difference between his arrangement of the elements and that of Meyer and others is that Mendeleev did not assume that all the elements had been discovered (actually, only about two-thirds of the naturally occurring elements were known at the time). Instead, he deliberately left blanks in his table at atomic masses 44, 68, 72, and 100, in the expectation that elements with those atomic masses would be discovered. Those blanks correspond to the elements we now know as scandium, gallium, germanium, and technetium.

Reihen	Gruppe I. — R^2O	Gruppe II. — RO	Gruppe III. — R^2O^3	Gruppe IV. RH^4 RO^2	Gruppe V. RH^3 R^2O^5	Gruppe VI. RH^2 RO^3	Gruppe VII. RH R^2O^7	Gruppe VIII. — RO^4
1	H=1							
2	Li=7	Be=9,4	B=11	C=12	N=14	O=16	F=19	
3	Na=23	Mg=24	Al=27,3	Si=28	P=31	S=32	Cl=35,5	
4	K=39	Ca=40	—=44	Ti=48	V=51	Cr=52	Mn=55	Fe=56, Co=59, Ni=59, Cu=63.
5	(Cu=63)	Zn=65	—=68	—=72	As=75	Se=78	Br=80	
6	Rb=85	Sr=87	?Yt=88	Zr=90	Nb=94	Mo=96	—=100	Ru=104, Rh=104, Pd=106, Ag=108.
7	(Ag=108)	Cd=112	In=113	Sn=118	Sb=122	Te=125	J=127	
8	Cs=133	Ba=137	?Di=138	?Ce=140	—	—	—	— — — —
9	(—)	—				—	—	
10	—	—	?Er=178	?La=180	Ta=182	W=184	—	Os=195, Ir=197, Pt=198, Au=199.
11	(Au=199)	Hg=200	Tl=204	Pb=207	Bi=208	—	—	
12	—	—	—	Th=231	—	U=240	—	— — — —

Figure 3.4.3 Mendeleev's periodic table, as published in the German journal *Annalen der Chemie und Pharmacie* in 1872: *The column headings "Reihen" and "Gruppe" are German for "row" and "group." Formulas indicate the type of compounds formed by each group, with "R" standing for "any element" and superscripts used where we now use subscripts. Atomic masses are shown after equal signs and increase across each row from left to right.*

The groups in Mendeleev's table are determined by how many oxygen or hydrogen atoms are needed to form compounds with each element. For example, in Group I, two atoms of hydrogen (H), lithium (Li), sodium (Na), and potassium (K) form compounds with one atom of oxygen. In Group VII, one atom of fluorine (F), chlorine (Cl), and bromine (Br), reacts with one atom of hydrogen. Notice how this approach has trouble with the transition metals. Until roughly 1960, a rectangular table developed from Mendeleev's table and based on reactivity was standard at the front of chemistry lecture halls.

The most convincing evidence in support of Mendeleev's arrangement of the elements was the discovery of two previously unknown elements whose properties closely corresponded with his predictions (Table 3.4.1). Two of the blanks Mendeleev had left in his original table were below aluminum and silicon, awaiting the discovery of two as-yet-unknown elements, *eka*-aluminum and *eka*-silicon (from the Sanskrit *eka*, meaning "one," as in "one beyond aluminum"). The observed properties of gallium and germanium matched those of *eka*-aluminum and *eka*-silicon so well that once they were discovered, Mendeleev's periodic table rapidly gained acceptance.



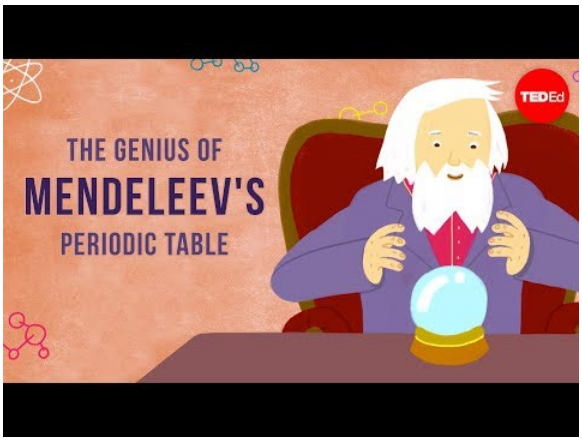


Table 3.4.1 Comparison of the properties predicted by Mendeleev in 1869 for *eka*-aluminum and *eka*-silicon with the properties of gallium (discovered in 1875) and germanium (discovered in 1886)

Property	*eka*-Aluminum (predicted)	Gallium (observed)	*eka*-Silicon (predicted)	Germanium (observed)
atomic mass	68	69.723	72	72.64
element	metal	metal	dirty-gray metal	gray-white metal
	low mp*	mp = 29.8°C	high mp	mp = 938°C
	d = 5.9 g/cm^3	d = 5.91 g/cm^3	d = 5.5 g/cm^3	d = 5.323 g/cm^3
oxide	E_2O_3	Ga_2O_3	EO_2	GeO_2
	d = 5.5 g/cm^3	d = 6.0 g/cm^3	d = 4.7 g/cm^3	d = 4.25 g/cm^3
chloride	ECl_3	$GaCl_3$	ECl_4	$GeCl_4$
	volatile	mp = 78°C bp* = 201°C	bp < 100°C	bp = 87°C

*mp = melting point; bp = boiling point.

When the chemical properties of an element suggested that it might have been assigned the wrong place in earlier tables, Mendeleev carefully reexamined its atomic mass. He discovered, for example, that the atomic masses previously reported for beryllium, indium, and uranium were incorrect. The atomic mass of indium had originally been reported as 75.6, based on an assumed stoichiometry of InO for its oxide. If this atomic mass were correct, then indium would have to be placed in the middle of the nonmetals, between arsenic (atomic mass 75) and selenium (atomic mass 78). Because elemental indium is a silvery-white *metal*, however, Mendeleev postulated that the stoichiometry of its oxide was really In_2O_3 rather than InO. This would mean that indium's atomic mass was actually 113, placing the element between two other metals, cadmium and tin.

One group of elements absent from Mendeleev's table was the noble gases, all of which were discovered more than 20 years later, between 1894 and 1898, by Sir William Ramsay (1852–1916; Nobel Prize in Chemistry 1904). Initially, Ramsay did not know where to place these elements in the periodic table. Argon, the first to be discovered, had an atomic mass of 40. This was greater than chlorine's and comparable to that of potassium; so Ramsay, using the same kind of reasoning as Mendeleev, decided to place the noble gases between the halogens and the alkali metals.

The Role of the Atomic Number in the Periodic Table

Despite its usefulness, Mendeleev's periodic table was based entirely on empirical observation supported by very little understanding. It was not until 1913, when a young British physicist, H. G. J. Moseley (1887–1915), while analyzing the frequencies of x-rays emitted by the elements, discovered that the underlying foundation of the order of the elements was the

atomic number, not the atomic mass. Moseley hypothesized that the placement of each element in his series corresponded to its atomic number *Z*, which is the number of positive charges (protons) in its nucleus. Argon, for example, although having an atomic mass greater than that of potassium (39.9 amu versus 39.1 amu, respectively), was placed *before* potassium in the periodic table. While analyzing the frequencies of the emitted x-rays, Moseley noticed that the atomic number of argon is 18, whereas that of potassium is 19, which indicated that they were indeed placed correctly. Moseley also noticed three gaps in his table of x-ray frequencies, so he predicted the existence of three unknown elements: technetium (Z = 43), discovered in 1937; promethium (Z = 61), discovered in 1945; and rhenium (Z = 75), discovered in 1925.

H. G. J. Moseley (1887–1915)

Moseley left his research work at the University of Oxford to join the British army as a telecommunications officer during World War I. He was killed during the Battle of Gallipoli in Turkey.

Example 3.4.1

Before its discovery in 1999, some theoreticians believed that an element with a Z of 114 existed in nature. Use Mendeleev's reasoning to name element 114 as *eka*-_____; then identify the known element whose chemistry you predict would be most similar to that of element 114.

Given: atomic number

Asked for: name using prefix *eka*-

Strategy:

A Using the periodic table locate the n = 7 row. Identify the location of the unknown element with Z = 114; then identify the known element that is directly above this location.

B Name the unknown element by using the prefix *eka*- before the name of the known element.

Solution:

A The n = 7 row can be filled in by assuming the existence of elements with atomic numbers greater than 112, which is underneath mercury (Hg). Counting three boxes to the right gives element 114, which lies directly below lead (Pb). **B** If Mendeleev were alive today, he would call element 114 *eka*-lead.

Exercise

Use Mendeleev's reasoning to name element 112 as *eka*-_____; then identify the known element whose chemistry you predict would be most similar to that of element 112.

Answer: *eka*-mercury

Summary

The periodic table arranges the elements according to their electron configurations, such that elements in the same column have the same valence electron configurations. Periodic variations in size and chemical properties are important factors in dictating the types of chemical reactions the elements undergo and the kinds of chemical compounds they form. The modern periodic table was based on empirical correlations of properties such as atomic mass; early models using limited data noted the existence of **triads** and **octaves** of elements with similar properties. The periodic table achieved its current form through the work of Dimitri Mendeleev and Julius Lothar Meyer, who both focused on the relationship between atomic mass and chemical properties. Meyer arranged the elements by their atomic volume, which today is equivalent to the **molar volume**, defined as molar mass divided by molar density. The correlation with the electronic structure of atoms was made when H. G. J. Moseley showed that the periodic arrangement of the elements was determined by atomic number, not atomic mass.

Key Takeaways

- The elements in the periodic table are arranged according to their properties, and the periodic table serves as an aid in predicting chemical behavior.

Conceptual Problems

1. Johannes Dobereiner is credited with developing the concept of chemical triads. Which of the group 15 elements would you expect to compose a triad? Would you expect B, Al, and Ga to act as a triad? Justify your answers.
2. Despite the fact that Dobereiner, Newlands, Meyer, and Mendeleev all contributed to the development of the modern periodic table, Mendeleev is credited with its origin. Why was Mendeleev's periodic table accepted so rapidly?
3. How did Moseley's contribution to the development of the periodic table explain the location of the noble gases?
4. The *eka*- naming scheme devised by Mendeleev was used to describe undiscovered elements.
    1. Use this naming method to predict the atomic number of *eka*-mercury, *eka*-astatine, *eka*-thallium, and *eka*-hafnium.
    2. Using the *eka*-prefix, identify the elements with these atomic numbers: 79, 40, 51, 117, and 121.

Numerical Problem

1. Based on the data given, complete the table.

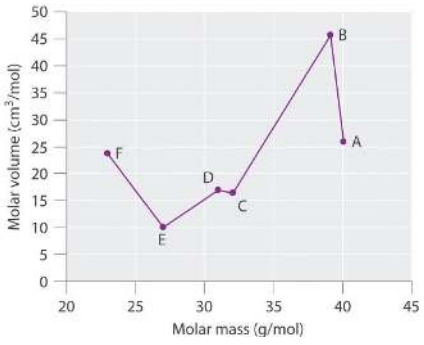
Species	Molar Mass (g/mol)	Density (g/cm^3)	Molar Volume (cm^3/mol)
A	40.078		25.85
B	39.09	0.856	
C	32.065		16.35
D		1.823	16.98
E	26.98		9.992
F	22.98	0.968	

Plot molar volume versus molar mass for these substances. According to Meyer, which would be considered metals and which would be considered nonmetals?

Answer

1.

Species	Molar Mass (g/mol)	Density (g/cm^3)	Molar Volume (cm^3/mol)
A	**40.078**	1.550	**25.85**
B	**39.09**	**0.856**	45.67
C	**32.065**	1.961	**16.35**
D	30.95	**1.823**	**16.98**
E	**26.98**	2.700	**9.992**
F	**22.98**	**0.968**	23.7



Meyer found that the alkali metals had the highest molar volumes, and that molar volumes decreased steadily with increasing atomic mass, then leveled off, and finally rose again. The elements located on the rising portion of a plot of molar volume versus molar mass were typically nonmetals. If we look at the plot of the data in the table, we can immediately identify those elements with the largest molar volumes (A, B, F) as metals located on the left side of the periodic table. The element with the smallest molar volume (E) is aluminum. The plot shows that the subsequent elements (C, D) have molar volumes that are larger than that of E, but smaller than those of A and B. Thus, C and D are most likely to be nonmetals (which is the case: C = sulfur, D = phosphorus).

Contributors and Attributions

- Anonymous

Modified by Joshua Halpern

Video from TED-Ed Lou Serocp

1.2.1.1: The Periodic Table is shared under a CC BY-NC-SA 4.0 license and was authored, remixed, and/or curated by LibreTexts.

- **2.1.1: The Periodic Table** is licensed CC BY-NC-SA 4.0.

1.2.1.2: Discovery of Subatomic Particles and the Bohr Atom

Hydrogen Absorption and Emission Spectra

When a high-voltage electrical discharge is passed through a sample of hydrogen gas (H_2) at low pressure, the result is individual isolated hydrogen atoms that emit a red light. Unlike blackbody radiation, the color of the light emitted by the hydrogen atoms does not depend greatly on the temperature of the gas in the tube. When the emitted light is passed through a prism, only a few narrow lines of particular wavelengths, called a line spectrum, are observed rather than a continuous range of wavelengths (Figure **1.2.1.2.1**). The light emitted by hydrogen atoms is red because, of its four characteristic lines, the most intense line in its spectrum is in the red portion of the visible spectrum, at 656 nm.

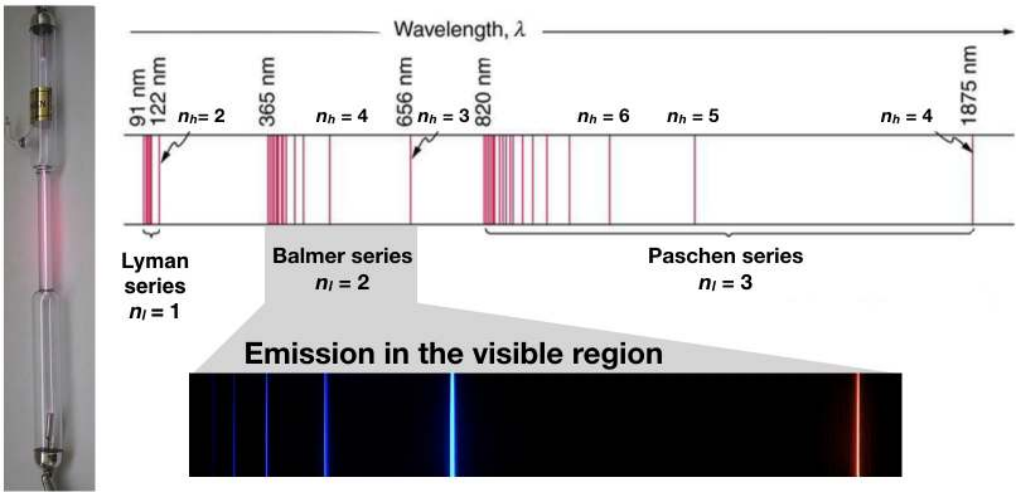


Figure **1.2.1.2.1**: The emission of light by hydrogen atoms. (left) A sample of excited hydrogen atoms emits a characteristic red light. (bottom) When the light emitted by a sample of excited hydrogen atoms is split into its component wavelengths by a prism, four characteristic violet, blue, green, and red emission lines can be observed, with the most intense at 656 nm. (top) A diagram showing extended regions of the electromagnetic spectrum and the hydrogen line spectra that are observed. (Kathryn Haas; CC-BY-SA)

The Balmer Series

In 1885, a Swiss mathematics teacher, Johann Balmer (1825–1898), showed that the frequencies of the lines observed in the visible region of the hydrogen line spectrum fit a simple equation that can be expressed as follows:

$$u = constant\left(\frac{1}{2^2} - \frac{1}{n^2}\right) \tag{1.2.1.2.1}$$

where n = 3, 4, 5, 6. As a result, these lines are known as the *Balmer series*. The Swedish physicist Johannes Rydberg (1854–1919) subsequently restated and expanded Balmer's result in the *Rydberg equation*:

$$\frac{1}{\lambda} = R_H\left(\frac{1}{n_l^2} - \frac{1}{n_h^2}\right) \tag{1.2.1.2.2}$$

,

where n_l and n_h are positive integers, $n_h > n_l$, and R_H, the *Rydberg constant*, has a value of 1.09737 × 10^7 m^{-1}. Like Balmer's equation, Rydberg's simple equation described the wavelengths of the visible lines in the emission spectrum of hydrogen (with $n_l = 2, n_h = 3, 4, 5, ...$). More importantly, Rydberg's equation also predicted the wavelengths of other series of lines that would be observed in the emission spectrum of hydrogen: one in the ultraviolet ($n_l = 1, n_h = 2, 3, 4, ...$) and one in the infrared ($n_l = 3, n_h = 4, 5, 6$).

Other Series

The results given by Balmer and Rydberg for the spectrum in the visible region of the electromagnetic spectrum start with $n_h = 3$, and $n_l = 2$.

Is there a different series with the following formula (e.g., $n_l = 1$)?

$$\frac{1}{\lambda} = R_H \left(\frac{1}{1^2} - \frac{1}{n^2} \right) \tag{1.2.1.2.3}$$

The values for n_h and wavenumber u for this series would be:

Table 1.2.1.2.1: The Lyman Series of Hydrogen Emission Lines ($n_l = 1$)

n_h	2	3	4	5
λ (nm)	121	102	97	94
$\tilde{u}$ (cm^{-1})	82,2291	97,530	102,864	105,332

Do you know what region of the electromagnetic radiation these lines are in? Of course, these lines are in the UV region, and they are not visible, but they are detected by instruments; these lines form a **Lyman series**. The existences of the Lyman series and Balmer's series suggest the existence of more series. For example, the series with $n_2^2 = 3$ and n_1^2 = 4, 5, 6, 7, ... is called the **Pashen series**.

Multiple series

The spectral lines are grouped into series according to n_1 values. Lines are named sequentially starting from the longest wavelength/lowest frequency of the series using Greek letters within each series. For example, the ($n_1 = 1/n_2 = 2$) line is called "Lyman-alpha" (Ly-α), while the ($n_1 = 3/n_2 = 7$) line is called "Paschen-delta" (Pa-δ). The first six series have specific names:

- Lyman series with $n_1 = 1$
- Balmer series with $n_1 = 2$
- Paschen series (or Bohr series) with $n_1 = 3$
- Brackett series with $n_1 = 4$
- Pfund series with $n_1 = 5$
- Humphreys series with $n_1 = 6$



The spectral series of hydrogen based on the Rydberg Equation (on a logarithmic scale).

Example 1.2.1.2.1: The Lyman Series

The so-called Lyman series of lines in the emission spectrum of hydrogen corresponds to transitions from various excited states to the *n* = 1 orbit. Calculate the wavelength of the lowest-energy line in the Lyman series to three significant figures. In what region of the electromagnetic spectrum does it occur?

Given: lowest-energy orbit in the Lyman series

Asked for: wavelength of the lowest-energy Lyman line and corresponding region of the spectrum

Strategy:

A. Substitute the appropriate values into Equation ***Ref*2.1.2.2** (the Rydberg equation) and solve for λ.
B. Locate the region of the electromagnetic spectrum corresponding to the calculated wavelength.

Solution:

We can use the Rydberg equation (Equation ***Ref*2.1.2.2** to calculate the wavelength:

$$\frac{1}{\lambda} = R_H \left(\frac{1}{n_l^2} - \frac{1}{n_h^2} \right)$$

A For the Lyman series, $n_1 = 1$.

$$\begin{aligned} \frac{1}{\lambda} &= R_H \left(\frac{1}{n_l^2} - \frac{1}{n_h^2} \right) \\ &= 1.097 \times m^{-1} \left(\frac{1}{1} - \frac{1}{4} \right) \\ &= 8.228 \times 10^6 \; m^{-1} \end{aligned}$$

Spectroscopists often talk about energy and frequency as equivalent. The cm^{-1} unit (wavenumbers) is particularly convenient. We can convert the answer in part A to cm^{-1}.

$$\begin{aligned} \tilde{u} &= \frac{1}{\lambda} \\ &= 8.228 \times 10^6 \cancel{m^{-1}} \left(\frac{\cancel{m}}{100 \; cm} \right) \\ &= 82,280 \; cm^{-1} \end{aligned}$$

and

$$\lambda = 1.215 \times 10^{-7} \; m = 122 \; nm$$

This emission line is called Lyman alpha and is the strongest atomic emission line from the sun; it drives the chemistry of the upper atmosphere of all the planets producing ions by stripping electrons from atoms and molecules. It is completely absorbed by oxygen in the upper stratosphere, dissociating O_2 molecules to O atoms, which react with other O_2 molecules to form stratospheric ozone (O_3).

B This wavelength is in the ultraviolet region of the spectrum.

? Exercise 1.2.1.2.1: The Pfund Series

The Pfund series of lines in the emission spectrum of hydrogen corresponds to transitions from higher excited states to $n_1 = 5$. Calculate the wavelength of the *second* line in the Pfund series to three significant figures. In which region of the spectrum does it lie?

Answer

$4.65 \times 10^3 \; nm$; infrared

The above discussion presents only a phenomenological description of hydrogen emission lines. Balmer and Rydberg could predict where emission lines could occur, but they could not explain why lines followed this pattern using any useful theory. For an explanation of why atoms demonstrate discrete emission spectra, quantum theories were developed.

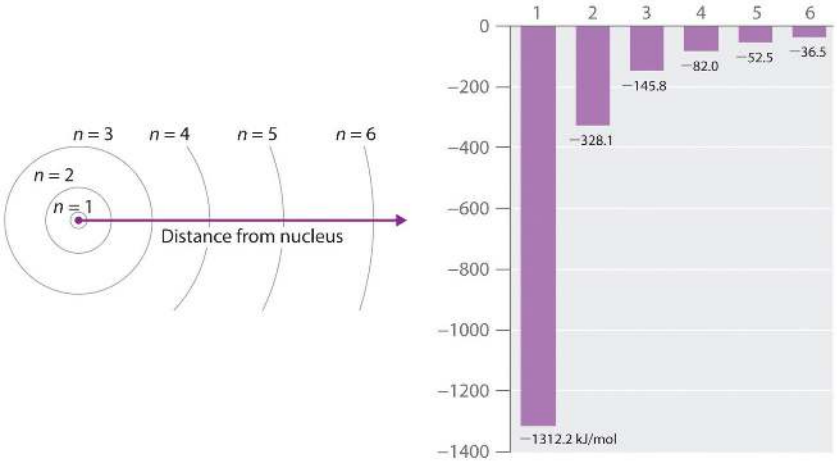
The Bohr Model

In 1913, a Danish physicist, Niels Bohr (1885–1962; Nobel Prize in Physics, 1922), proposed a theoretical model for the hydrogen atom that explained its emission spectrum. Bohr's model required only one assumption: *The electron moves around the nucleus in circular orbits that can have only certain allowed radii*. Rutherford's earlier model of the atom had also assumed that electrons moved in circular orbits around the nucleus and that the atom was held together by the electrostatic attraction between the positively charged nucleus and the negatively charged electron. Although we now know that the assumption of circular orbits was incorrect, Bohr's insight also posited that *the electron could occupy only certain regions of space*.

Using classical physics, Niels Bohr showed that the energy of an electron in a particular orbit is given by

$$E_n = \frac{-R_H hc}{n^2} \tag{1.2.1.2.4}$$

where R_H is the Rydberg constant, h is Planck's constant, c is the speed of light, and n is a positive integer corresponding to the number assigned to the orbit, with $n = 1$ corresponding to the orbit closest to the nucleus. In this model $n = \infty$ corresponds to the level where the energy holding the electron and the nucleus together is zero. In that level, the electron is unbound from the nucleus and the atom has been separated into a negatively charged (the electron) and a positively charged (the nucleus) ion. In this state the radius of the orbit is also infinite. The atom has been ionized.

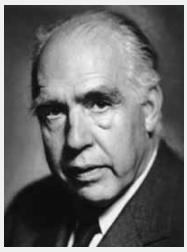


(a) Hydrogen orbits (Bohr model). Orbits are not drawn to scale. **(b) Hydrogen orbit energy (kJ/mol) vs. *n***

Figure **1.2.1.2.2**: *The Bohr Model of the hydrogen atom (a) The distance of the orbit from the nucleus increases with increasing n. (b) The energy of the orbit becomes increasingly less negative with increasing n.*

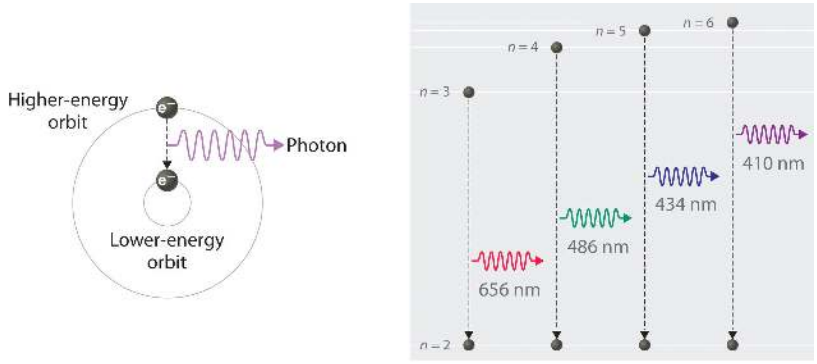
Niels Bohr (1885–1962)

During the Nazi occupation of Denmark in World War II, Bohr escaped to the United States, where he became associated with the Atomic Energy Project.



In his final years, he devoted himself to the peaceful application of atomic physics and to resolving political problems arising from the development of atomic weapons.

As n decreases, the energy holding the electron and the nucleus together becomes increasingly negative; the radius of the orbit shrinks and more energy is needed to ionize the atom. The orbit with n = 1 is the lowest lying and most tightly bound. The negative sign in Equation ??? indicates that the electron-nucleus pair is more tightly bound (i.e. at a lower potential energy) when they are near each other than when they are far apart. Because a hydrogen atom with its one electron in this orbit has the lowest possible energy, this is the **ground state** (the most stable arrangement of electrons for an element or a compound) for a hydrogen atom. As n increases, the radius of the orbit increases; the electron is farther from the proton, which results in a less stable arrangement with higher potential energy (Figure **1.2.1.2.2*a***). A hydrogen atom with an electron in an orbit with n > 1 is therefore in an **excited state**, defined as any arrangement of electrons that is higher in energy than the ground state. When an atom in an excited state undergoes a transition to the ground state in a process called decay, it loses energy by emitting a photon whose energy corresponds to the *difference* in energy between the two states (Figure **1.2.1.2.1**).



(a) Electronic emission transition (b) Balmer series transitions

Figure **1.2.1.2.3**: *The emission of light by a hydrogen atom in an excited state. (a) Light is emitted when the electron undergoes a transition from an orbit with a higher value of n (at a higher energy) to an orbit with a lower value of n (at lower energy). (b) The Balmer series of emission lines is due to transitions from orbits with n ≥ 3 to the orbit with n = 2. The differences in energy between these levels correspond to light in the visible portion of the electromagnetic spectrum.*

So the difference in energy (Δ*E*) between any two orbits or energy levels is given by $\Delta E = E_{n_l} - E_{n_h}$, where n_l is the final orbit and n_h the initial orbit. Substituting from Bohr's equation (Equation 2.1.2.4) for each energy value gives

$$\Delta E = E_{final} - E_{initial} = -\frac{R_H hc}{n_h^2} - \left(-\frac{R_H hc}{n_l^2}\right) = -R_H hc\left(\frac{1}{n_h^2} - \frac{1}{n_l^2}\right) \tag{1.2.1.2.5}$$

If $n_h > n_l$, the transition is from a higher energy state (larger-radius orbit) to a lower energy state (smaller-radius orbit), as shown by the dashed arrow in part (a) in Figure **1.2.1.2.3**. Substituting hc/λ for ΔE gives

$$\Delta E = \frac{hc}{\lambda} = -R_H hc\left(\frac{1}{n_h^2} - \frac{1}{n_l^2}\right) \tag{1.2.1.2.6}$$

Canceling *hc* on both sides gives

$$\frac{1}{\lambda} = -R_H\left(\frac{1}{n_h^2} - \frac{1}{n_l^2}\right) \tag{1.2.1.2.7}$$

Except for the negative sign, this is the same equation that Rydberg obtained experimentally. The negative sign in Equations 1.2.1.2.6 and 1.2.1.2.7 indicates that energy is released as the electron moves from orbit n_h to orbit n_l because orbit n_h is at a higher energy than orbit n_l. Bohr calculated the value of R_H from fundamental constants such as the charge and mass of the electron and Planck's constant and obtained a value of $1.0974 \times 10^7\ m^{-1}$, the same number Rydberg had obtained by analyzing the emission spectra.

We can now understand the physical basis for the Balmer series of lines in the emission spectrum of hydrogen (**1.2.1.2.3***b*); the lines in this series correspond to transitions from higher-energy orbits (n > 2) to the second orbit (n = 2). Thus, the hydrogen atoms in the sample have absorbed energy from the electrical discharge and decayed from a higher-energy excited state (n > 2) to a lower-energy state (n = 2) by emitting a photon of electromagnetic radiation whose energy corresponds exactly to the difference in energy between the two states (Figure **1.2.1.2.3***a*). The n = 3 to n = 2 transition gives rise to the line at 656 nm (red), the n = 4 to n = 2 transition to the line at 486 nm (green), the n = 5 to n = 2 transition to the line at 434 nm (blue), and the n = 6 to n = 2 transition to the line at 410 nm (violet). Because a sample of hydrogen contains a large number of atoms, the intensity of the various lines in a line spectrum depends on the number of atoms in each excited state. At the temperature in the gas discharge tube, more atoms are in the n = 3 than the n ≥ 4 levels. Consequently, the n = 3 to n = 2 transition is the most intense line, producing the characteristic red color of a hydrogen discharge (Figure **1.2.1.2.1***a*). Other families of lines are produced by transitions from excited states with n > 1 to the orbit with n = 1 or to orbits with n ≥ 3. These transitions are shown schematically in Figure **1.2.1.2.4** :

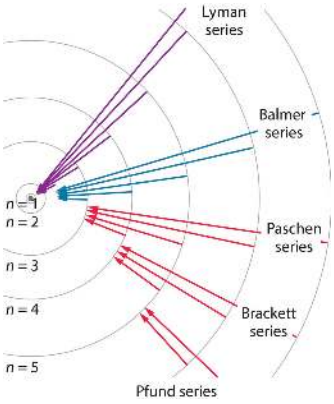


Figure 1.2.1.2.4: Electron transitions responsible for the various series of lines observed in the emission spectrum of hydrogen. The Lyman series of lines is due to transitions from higher-energy orbits to the lowest-energy orbit (n = 1); these transitions release a great deal of energy, corresponding to radiation in the ultraviolet portion of the electromagnetic spectrum. The Paschen, Brackett, and Pfund series of lines are due to transitions from higher-energy orbits to orbits with n = 3, 4, and 5, respectively; these transitions release substantially less energy, corresponding to infrared radiation. (Orbits are not drawn to scale.)

Using Atoms to Time

In contemporary applications, electron transitions are used in timekeeping that needs to be exact. Telecommunications systems, such as cell phones, depend on timing signals that are accurate within a millionth of a second per day; the same goes for the devices that control the US power grid. Global positioning system (GPS) signals must be accurate within a billionth of a second per day, which is equivalent to gaining or losing no more than one second in 1,400,000 years. Quantifying time requires finding an event with an interval that repeats on a regular basis.

To achieve the accuracy required for modern purposes, physicists have turned to the atom. The current standard used to calibrate clocks is the cesium atom. Supercooled cesium atoms are placed in a vacuum chamber and bombarded with microwaves whose frequencies are carefully controlled. When the frequency is exactly right, the atoms absorb enough energy to undergo an electronic transition to a higher-energy state. Decay to a lower-energy state emits radiation. The microwave frequency is continually adjusted, serving as the clock's pendulum.

In 1967, the second was defined as the duration of 9,192,631,770 oscillations of the resonant frequency of a cesium atom, called the *cesium clock*. Research is currently under way to develop the next generation of atomic clocks that promise to be even more accurate. Such devices would allow scientists to monitor vanishingly faint electromagnetic signals produced by nerve pathways in the brain and allow geologists to measure variations in gravitational fields, which cause fluctuations in time, that would aid in the discovery of oil or minerals.

Example 1.2.1.2.1: The Lyman Series

The so-called Lyman series of lines in the emission spectrum of hydrogen corresponds to transitions from various excited states to the n = 1 orbit. Calculate the wavelength of the lowest-energy line in the Lyman series to three significant figures. In what region of the electromagnetic spectrum does it occur?

Given: lowest-energy orbit in the Lyman series

Asked for: wavelength of the lowest-energy Lyman line and corresponding region of the spectrum

Strategy:

A. Substitute the appropriate values into Equation 2.1.2.4 (the Rydberg equation) and solve for λ.
B. Use Figure 2.2.1 to locate the region of the electromagnetic spectrum corresponding to the calculated wavelength.

Solution:

We can use the Rydberg equation to calculate the wavelength:

$$\frac{1}{\lambda} = -R_H \left(\frac{1}{n_h^2} - \frac{1}{n_l^2} \right)$$

A For the Lyman series, /(n_l = 1\). The lowest-energy line is due to a transition from the n = 2 to n = 1 orbit because they are the closest in energy.

$$\frac{1}{\lambda} = -R_H \left(\frac{1}{n_h^2} - \frac{1}{n_l^2} \right) = 1.097 \times m^{-1} \left(\frac{1}{1} - \frac{1}{4} \right) = 8.228 \times 10^6 \; m^{-1}$$

It turns out that spectroscopists (the people who study spectroscopy) use cm^{-1} rather than m^{-1} as a common unit. Wavelength is inversely proportional to energy but frequency is directly proportional as shown by Planck's formula, E=hu.

Spectroscopists often talk about energy and frequency as equivalent. The cm^{-1} unit is particularly convenient. The infrared range is roughly 200 - 5,000 cm^{-1}, the visible from 11,000 to 25,000 cm^{-1} and the UV between 25,000 and 100,000 cm^{-1}. The units of cm^{-1} are called wavenumbers, although people often refer to the unit as inverse centimeters. We can convert the answer in part A to cm^{-1}.

$$\tilde{u} = \frac{1}{\lambda} = 8.228 \times 10^6 \; \cancel{m^{-1}} \left(\frac{\cancel{m}}{100 \; cm} \right) = 82,280 \; cm^{-1}$$

and

$$\lambda = 1.215 \times 10^{-7} \; m = 122 \; nm$$

This emission line is called Lyman alpha. As the strongest atomic emission line from the sun, it drives the chemistry of the upper atmosphere of all the planets, producing ions by stripping electrons from atoms and molecules. It is completely absorbed by oxygen in the upper stratosphere, dissociating O_2 molecules to O atoms which react with other O_2 molecules to form stratospheric ozone.

B This wavelength is in the ultraviolet region of the spectrum.

? Exercise 1.2.1.2.1: The Pfund Series

The Pfund series of lines in the emission spectrum of hydrogen corresponds to transitions from higher excited states to the n = 5 orbit. Calculate the wavelength of the *second* line in the Pfund series to three significant figures. In which region of the spectrum does it lie?

Answer

4.65×10^3 nm; infrared

Bohr's model of the hydrogen atom gave an exact explanation for its observed emission spectrum. The following are his key contributions to our understanding of atomic structure:

- Electrons can occupy only certain regions of space, called *orbits*.
- Orbits closer to the nucleus are lower in energy.
- Electrons can move from one orbit to another by absorbing or emitting energy, giving rise to characteristic spectra.

Unfortunately, Bohr could not explain *why* the electron should be restricted to particular orbits. Also, despite a great deal of conjecturing, such as assuming that orbits could be ellipses rather than circles, his model could not quantitatively explain the emission spectra of any element other than hydrogen (Figure **1.2.1.2.5**). In fact, Bohr's model worked only for species that contained just one electron: H, He^+, Li^{2+}, and so forth. Scientists needed a fundamental change in their way of thinking about the electronic structure of atoms to advance beyond the Bohr model.

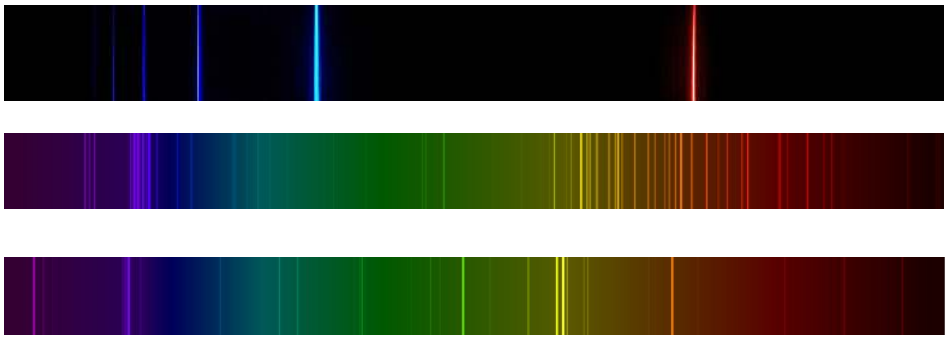


Figure 1.2.1.2.5: The emission spectra of elements compared to hydrogen. **Top:** hydrogen gas (atomized to hydrogen atoms in the discharge tube). **Middle:** neon. **Bottom:** mercury. The strongest lines in the hydrogen spectrum are in the far UV Lyman series starting at 124 nm and below. The strongest lines in the mercury spectrum are at 181 and 254 nm, also in the UV. These are not shown. Attribution: Hydrogen (Jan Homann / CC BY-SA); Neon (Teravolt at en.Wikipedia / Public domain); Mercury (Teravolt at en.Wikipedia / Public domain)

The Energy States of the Hydrogen Atom

Thus far, we have explicitly considered only the emission of light by atoms in excited states, which produces an emission spectrum (a spectrum produced by the emission of light by atoms in excited states). The converse, absorption of light by ground-state atoms to produce an excited state, can also occur, producing an absorption spectrum (a spectrum produced by the absorption of light by ground-state atoms).

> When an atom emits light, it decays to a lower energy state; when an atom absorbs light, it is excited to a higher energy state.

If white light is passed through a sample of hydrogen, hydrogen atoms absorb energy as an electron is excited to higher energy levels (orbits with $n \geq 2$). If the light that emerges is passed through a prism, it forms a continuous spectrum with *black* lines (corresponding to no light passing through the sample) at 656, 468, 434, and 410 nm. These wavelengths correspond to the $n = 2$ to $n = 3$, $n = 2$ to $n = 4$, $n = 2$ to $n = 5$, and $n = 2$ to $n = 6$ transitions. Any given element therefore has both a characteristic emission spectrum and a characteristic absorption spectrum, which are essentially complementary images.

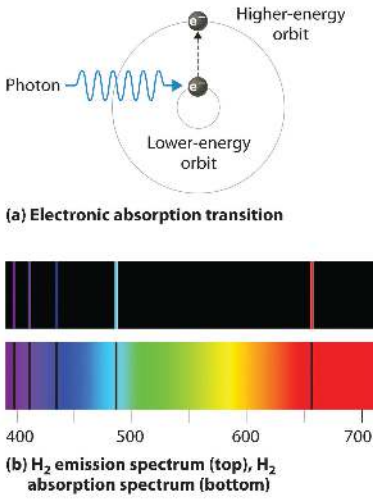


Figure 1.2.1.2.6: Absorption and emission spectra. Absorption of light by a hydrogen atom. (a) When a hydrogen atom absorbs a photon of light, an electron is excited to an orbit that has a higher energy and larger value of n. (b) Images of the emission and absorption spectra of hydrogen are shown here.

Emission and absorption spectra form the basis of *spectroscopy*, which uses spectra to provide information about the structure and the composition of a substance or an object. In particular, astronomers use emission and absorption spectra to determine the composition of stars and interstellar matter. As an example, consider the spectrum of sunlight shown in Figure 1.2.1.2.7. Since the sun is very hot, it emits light in the form of a continuous emission spectrum. Superimposed on the spectrum, however, is a series of

dark lines primarily resulting from the absorption of specific frequencies of light by cooler atoms in the outer atmosphere of the sun. By comparing these lines with the spectra of elements measured on Earth, we now know that the sun contains large amounts of hydrogen, iron, and carbon, along with smaller amounts of other elements. During the solar eclipse of 1868, the French astronomer Pierre Janssen (1824–1907) observed a set of lines that did not match those of any known element. He suggested that they were due to the presence of a new element, which he named *helium*, from the Greek *helios*, meaning "sun." Helium (He) was finally discovered in uranium ores on Earth in 1895. Alpha particles are helium nuclei. Alpha particles emitted by radioactive uranium nuclei pick up electrons from the rocks to form helium atoms.

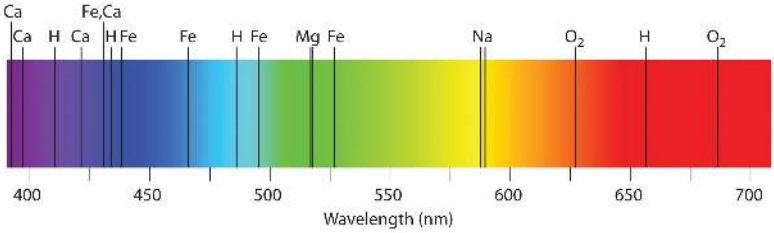


Figure **1.2.1.2.7**: *The visible spectrum of sunlight. The characteristic dark lines are mostly due to the absorption of light by elements that are present in the cooler outer part of the sun's atmosphere; specific elements are indicated by the labels. The lines at 628 and 687 nm, however, are due to the absorption of light by oxygen molecules in Earth's atmosphere.*

The familiar red color of neon signs used in advertising is due to the emission spectrum of neon shown in part (b) in Figure **1.2.1.2.5**. Similarly, the blue and yellow colors of certain street lights are caused, respectively, by mercury and sodium discharges. In all these cases, an electrical discharge excites neutral atoms to a higher energy state, and light is emitted when the atoms decay to the ground state. In the case of mercury, most of the emission lines are below 450 nm, which produces a blue light (part (c) in Figure **1.2.1.2.5**). In the case of sodium, the most intense emission lines are at 589 nm, which produces an intense yellow light.

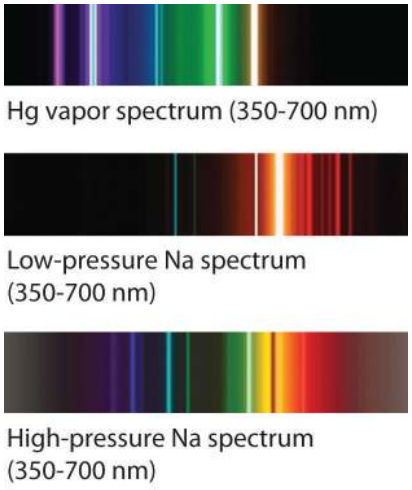


Figure **1.2.1.2.8**: *The emission spectra of sodium and mercury. Many street lights use bulbs that contain sodium or mercury vapor. Due to the very different emission spectra of these elements, they emit light of different colors. The lines in the sodium lamp are broadened by collisions. The dark line in the center of the high pressure sodium lamp where the low pressure lamp is strongest is caused by absorption of light in the cooler outer part of the lamp.*

Summary

There is an intimate connection between the atomic structure of an atom and its spectral characteristics. Atoms of individual elements emit light at only specific wavelengths, producing a **line spectrum** rather than the continuous spectrum of all wavelengths produced by a hot object. Niels Bohr explained the line spectrum of the hydrogen atom by assuming that the electron moved in circular orbits and that orbits with only certain radii were allowed. Lines in the spectrum were due to transitions in which an electron moved from a higher-energy orbit with a larger radius to a lower-energy orbit with smaller radius. The orbit closest to the nucleus represented the **ground state** of the atom and was most stable; orbits farther away were higher-energy **excited states**. Transitions from an excited state to a lower-energy state resulted in the emission of light with only a limited number of wavelengths. Atoms can also absorb light of certain energies, resulting in a transition from the ground state or a lower-energy

excited state to a higher-energy excited state. This produces an **absorption spectrum**, which has dark lines in the same position as the bright lines in the **emission spectrum** of an element. Bohr's model revolutionized the understanding of the atom but could not explain the spectra of atoms heavier than hydrogen.

Contributors and Attributions

- Modified by Joshua Halpern (Howard University)

1.2.1.2: Discovery of Subatomic Particles and the Bohr Atom is shared under a CC BY-NC-SA 4.0 license and was authored, remixed, and/or curated by LibreTexts.

- **2.1.2: Discovery of Subatomic Particles and the Bohr Atom** is licensed CC BY-NC-SA 3.0.

1.2.2: The Schrödinger equation, particle in a box, and atomic wavefunctions

2.02: The Schrödinger equation particle in a box and atomic wavefunctions

This page titled 1.2.2: The Schrödinger equation, particle in a box, and atomic wavefunctions is shared under a CC BY-NC-SA 4.0 license and was authored, remixed, and/or curated by Kathryn Haas.

1.2.2.1: Particle in a Box

2.2.01: Particle in a Box

This page titled 1.2.2.1: Particle in a Box is shared under a CC BY-NC-SA 4.0 license and was authored, remixed, and/or curated by Kathryn Haas.

1.2.2.2: Quantum Numbers and Atomic Wave Functions

2.2.02: Quantum Numbers and Atomic Wave Functions

This page titled 1.2.2.2: Quantum Numbers and Atomic Wave Functions is shared under a CC BY-NC-SA 4.0 license and was authored, remixed, and/or curated by Kathryn Haas.

1.2.2.3: Aufbau Principle

2.2.03: Aufbau Principle

This page titled 1.2.2.3: Aufbau Principle is shared under a CC BY-NC-SA 4.0 license and was authored, remixed, and/or curated by Kathryn Haas.

1.2.2.4: Shielding

2.2.04: Shielding

This page titled 1.2.2.4: Shielding is shared under a CC BY-NC-SA 4.0 license and was authored, remixed, and/or curated by Kathryn Haas.

SECTION OVERVIEW

1.2.3: Periodic Properties of Atoms

General periodic trends are specific patterns that are present within the periodic table; these are patterns in properties like electronegativity, ionization energy, electron affinity, atomic radius, melting point, and metallic character. General periodic trends provide chemists with an invaluable tool to quickly predict an element's properties. These trends exist because of the similar atomic structure of the elements within their respective group families or periods, and because of the periodic nature of the elements. Some of the general periodic trends are described in this section.

1.2.3.1: Ionization energy

1.2.3.2: Electron Affinity

1.2.3.3: Covalent and Ionic Radii

References

1. Russo, Steve, and Mike Silver. Introductory Chemistry. San Francisco: Pearson, 2007.
2. Petrucci, Ralph H, et al. General Chemistry: Principles and Modern Applications. 9th Ed. New Jersey: Pearson, 2007.
3. Atkins, Peter et. al, *Physical Chemistry*, 7th Edition, 2002, W.H Freeman and Company, New York, pg. 390.
4. Alberty, Robert A. et. al, *Physical Chemistry*, 3rd Edition, 2001, John Wiley & Sons, Inc, pg. 380.
5. Kots, John C. et. al, *Chemistry & Chemical Reactivity*, 5th Edition, 2003, Thomson Learning Inc, pg. 305-309.

1.2.3: Periodic Properties of Atoms is shared under a CC BY-NC-SA 4.0 license and was authored, remixed, and/or curated by LibreTexts.

1.2.3.1: Ionization energy

Ionization energy (IE) is the energy required to **remove an electron from a neutral atom or cation in its gaseous phase**. IE is also known as *ionization potential*.

$$A^{n+}_{(g)} \longrightarrow A^{(n+1)+}_{(g)} + e^- \qquad IE = \Delta U$$

Conceptually, ionization energy is the affinity of an element for its outermost electron (an electron it already has in its valence shell).

1st, 2nd, and 3rd Ionization Energies

The symbol I_1 stands for the ***first ionization energy*** (energy required to take away an electron from a neutral atom, where $n = 0$). The symbol I_2 stands for the ***second ionization energy*** (energy required to take away an electron from an atom with a +1 charge, $n = 2$.)

- **First Ionization Energy,** I_1 (general element, A):

$$A_{(g)} \rightarrow A^{1+}_{(g)} + e^-$$

- **Second Ionization Energy,** I_2 (general element, A):

$$A^{1+}_{(g)} \rightarrow A^{2+}_{(g)} + e^-$$

- **Third Ionization Energy,** I_3 (general element, A):

$$A^{2+}_{(g)} \rightarrow A^{3+}_{(g)} + e^-$$

Each succeeding ionization energy is larger than the preceding energy. This means that $I_1 < I_2 < I_3 < ... < I_n$ will always be true. For example, ionization energy increases as succeeding electrons are taken away from **Mg**.

$$Mg_{\,(g)} \rightarrow Mg^{+}{}_{(g)} + e^- \quad I_1 = 738\,kJ/mol$$

$$Mg^{+}{}_{(g)} \rightarrow Mg^{2+}{}_{(g)} + e^- \quad I_2 = 1451\,kJ/mol$$

Ionization energy is correlated with the strength of attraction between the positively-charged nucleus and the negatively-charged valence electrons. The higher the ionization energy, the stronger the attractive force between nucleus and valence electrons, and the more energy is required to remove a valence electron. The lower the ionization energy, the weaker the attractive force between nucleus and valence electrons, and the less energy required to remove a valence electron.

General periodic trends in electron affinity

In general, ionization energies increase from left to right and decrease down a group; however, there are variations in these trends that would be expected from the effects of penetration and shielding. The trends in **first ionization energy** are shown in Figure 1.2.3.1.1 and are summarized below.

- **Across a period:** As Z* increases across a period, the ionization energy of the elements generally increases from left to right. However there are breaks or variation in the trends in the following cases:
  - IE is especially low when removal of an electron creates a newly empty p subshell (examples include I_1 of B, Al, Sc)
  - IE energy is especially low where removal of an electron results in a half-filled p or d subshell (examples include I_1 of O, S)
  - IE increases more gradually across the d- and f-subshells compared to s- and p- subshells. This is because d- and f- electrons are weakly penetrating and experience especially low Z*.
- **From one period to the next:** There is an especially large decrease in IE with the start of every new period (from He to Li or from Ne to Na for example). This is consistent with the idea that IE is especially low when removal of an electron creates a newly empty s-subshell.
- **Noble gases:** The noble gases posses very high ionization energies. Note that helium has the highest ionization energy of all the elements.

- **Down a group:** Although Z* increases going down a group, there is no reliable trend in IE going down any group; in some cases IE increases going down a group, while in other cases IE decreases going down a group.

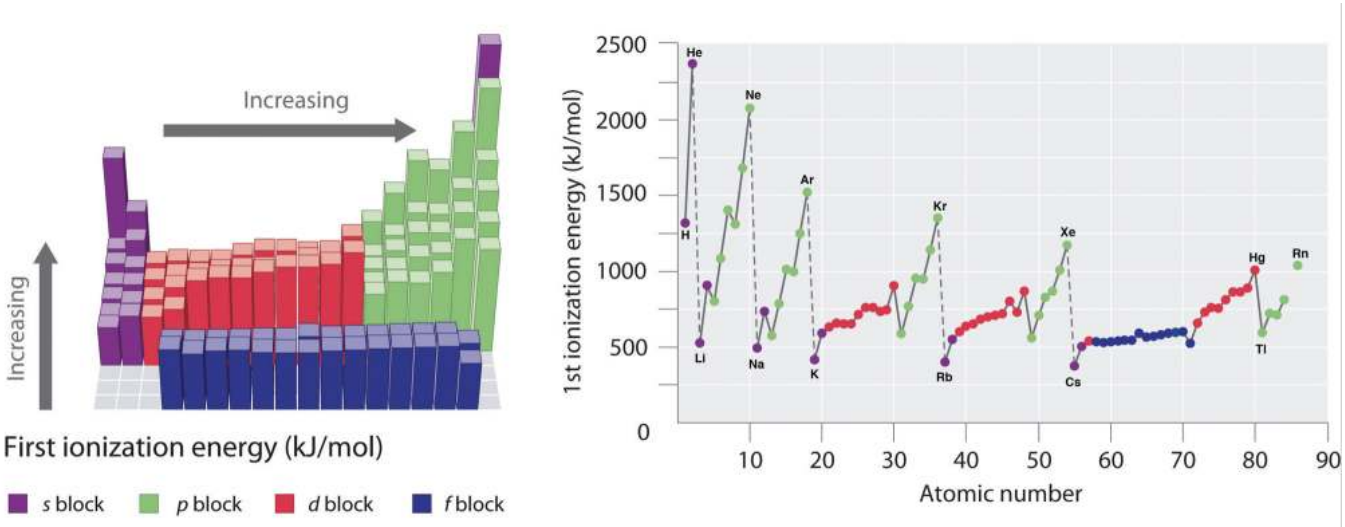


Figure 1.2.3.1.1: Graph showing the First Ionization Energy of the Elements. Left: ionization energies are mapped onto the periodic table, where the magnitude of ionization energy is depicted as a bar graph. Right: the first ionization energy is plotted against atomic number. In both panels the elements of the s-block are shown in purple, p-block are shown in green, d-block are shown in red, and f-block are shown in blue. (CC BY-NC-SA 3.0; anonymous)

Plots of the I_1, I_2, and I_3 of elements from hydrogen to krypton (first four periods) are shown in Figure 1.2.3.1.2. Notice that $I_3 > I_2 > I_1$. Also notice that trends mentioned above for I_1 hold true for subsequent ionizations when electron configurations are considered!

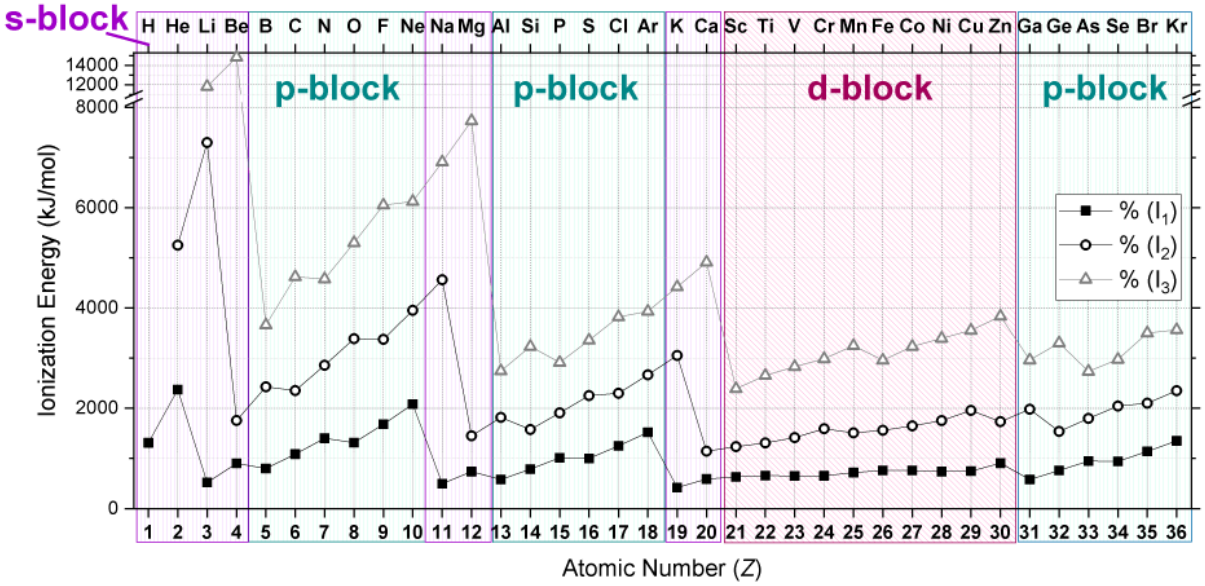


Figure 1.2.3.1.2. The first (I_1), second (I_2), and third (I_3) ionization energies plotted for elements with Z = 1 to 36 (H to Kr). The position of each element in its atomic form is indicated as s- p- or d-block. (CC-BY-NC-SA; Kathryn Haas)

1.2.3.1: Ionization energy is shared under a CC BY-NC-SA 4.0 license and was authored, remixed, and/or curated by LibreTexts.

- **2.3.1: Ionization energy** by Bingyao Zheng, Emily Nguyen, Kathryn Haas, Swetha Ramireddy is licensed CC BY-NC-SA 3.0.

1.2.3.2: Electron Affinity

Definitions of Electron Affinity

According to IUPAC, there are two different, but equivalent, definitions of **electron affinity (EA)**.[1]

Definition: Electron Affinity defined as removal of an electron

Electron affinity can be defined as the energy *required* when an electron is removed from a gaseous anion. The reaction as shown in equation 1.2.3.2.1 is *endothermic* (positive ΔU) for elements except noble gases and alkaline earth metals. Under this definition, the more positive the EA value, the higher an atom's affinity for electrons.

$$A^-_{(g)} \longrightarrow A_{(g)} + e^- \qquad EA = \Delta U \tag{1.2.3.2.1}$$

The reaction shown in Equation 1.2.3.2.1 is similar those that define ionization energy. For this reason, the EA is also described as the *zeroth ionization energy*.

Definition: Electron Affinity defined as addition of an electron

An alternate and more common definition is the microscopic reverse of Equation 1.2.3.2.1. This more common definition states that electron affinity is the energy *released* when an electron is added to a gaseous atom, as shown in Equation 1.2.3.2.2. The reaction as shown in equation 1.2.3.2.2 is *exothermic* (negative ΔU) for elements except noble gases and alkaline earth metals. The more negative this EA value, the higher an atom's affinity for electrons.

$$A_{(g)} + e^- \longrightarrow A^-_{(g)} \qquad EA = \Delta U \tag{1.2.3.2.2}$$

Conceptually, this second definition is quite similar to the concept of electronegativity; but unlike electronegativity, EA is a well-defined quantitative measurement.

Trends in Electron Affinity

For this discussion, we will use the definition of EA that is consistent with it being a *zeroth ionization energy:* a more positive (larger) value means that the EA is higher (meaning stronger affinity toward an electron).

- **Across a period**: Similar to ionization energy, EA generally increases across a row of the periodic table; this observation is consistent with the increase in effective nuclear charge (Z*) from left to right across a period. However, there are variations across a period that are similar to variations in ionization energy and that can be explained by shielding, penetration, and electron configuration.
- **Down a group**: Like the case of ionization energy trends, EA does not consistently decrease going down a column of the periodic table despite the fact that Z^* increases down a group.

The trend in EA follows a zig-zag pattern similar to the one seen with ionization energies, except that it is displaced by one unit from the trend in I_1, two units from I_2, and so on. For example, EA peaks at F, while I_1 peaks at Ne, I_2 peaks at Na, and I_3 peaks at Mg. A plot of EA for the first 13 elements is shown overlaid on plots of I_1, I_2 and I_3 in Figure 1.2.3.2.1., where the shifts in the peaks and valleys within each zig-zag trend are indicated.

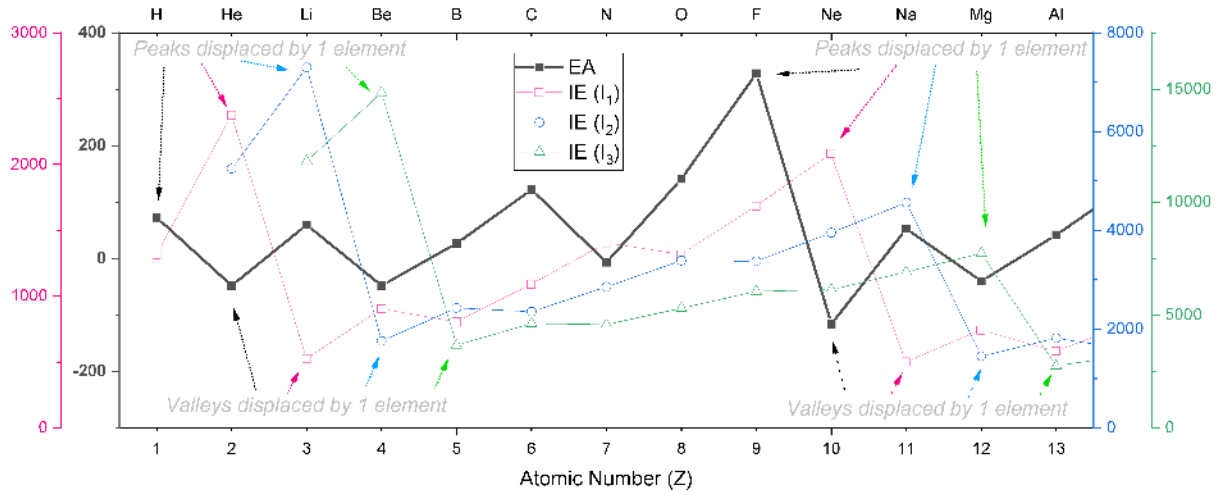


Figure **1.2.3.2.1**. A plot of electron affinity (the zeroth ionization energy) is overlaid on plots of the first (I_1), second (I_2), and third (I_3) ionization energies. Each plot is shown using separate y-axes. Trends in EA are similar to those in ionization energies, except that the peaks and valleys of the trends are shifted by one unit, as indicated. These plots are shown in units of kJ/mole. (CC-BY-NC-SA; Kathryn Haas)

Sources

1. IUPAC. Compendium of Chemical Terminology, 2nd ed. (the "Gold Book"). Compiled by A. D. McNaught and A. Wilkinson. Blackwell Scientific Publications, Oxford (1997). Online version (2019-) created by S. J. Chalk. ISBN 0-9678550-9-8. doi.org/10.1351/goldbook.
2. Electron Affinity (data page), Wikipedia. en.Wikipedia.org/wiki/Electron_affinity_(data_page) Accessed 12/3/19.

1.2.3.2: Electron Affinity is shared under a CC BY-NC-SA 4.0 license and was authored, remixed, and/or curated by LibreTexts.

- **2.3.2: Electron Affinity** by Kathryn Haas is licensed CC BY-NC-SA 4.0.

1.2.3.3: Covalent and Ionic Radii

Measurement of Radius

There are several methods that can be used to determine radii of atoms and ions:

- **Nonpolar atomic radii:** The radius of an atom is derived from the bond lengths within nonpolar molecules; one-half the distance between the nuclei of two atoms within a covalent bond.
- **van der Waals radius:** The radius of an atom is determined by collision with other atoms.
- **Crystal radii**: The atomic or ionic radius is determined using electron density maps from X-ray data.

The measurement of atomic or ionic size will depend on a number of factors, including the covalent character of bonding in any particular molecule, coordination number, physical state (liquid, solid, gas), the identity of nearby atoms/ions, variation in crystal structure, and distortions within regular crystal structures. You should keep in mind that the size of an atom or ion is a "fuzzy" measure, and the radius under a different set of conditions will probably change slightly.

Regardless, measured atomic and ionic radii reveal obvious trends across the periodic table and between atoms and ions. The relative atomic sizes shown in Figure **1.2.3.3.1** were derived from crystallographic data.[1]

Trends in Atomic Radius

Atomic size generally decreases gradually from left to right across a period of elements. As nuclear charge (Z) increases, we expect the effective nuclear charge (Z*) of the valence electrons to also increase. Increasing Z pulls electrons closer to the nucleus. However, with each additional unit of Z, there is also an additional electron. The change in size is a balance of a compression caused by increasing Z and an expansion in the number of electrons. As a result, the atomic radius decreases *gradually* across a period.

Atomic size generally increases going down a group. As valence electrons occupy higher level shells due to the increasing quantum number (n), size increases despite the fact that Z and Z* are increasing going down the group.

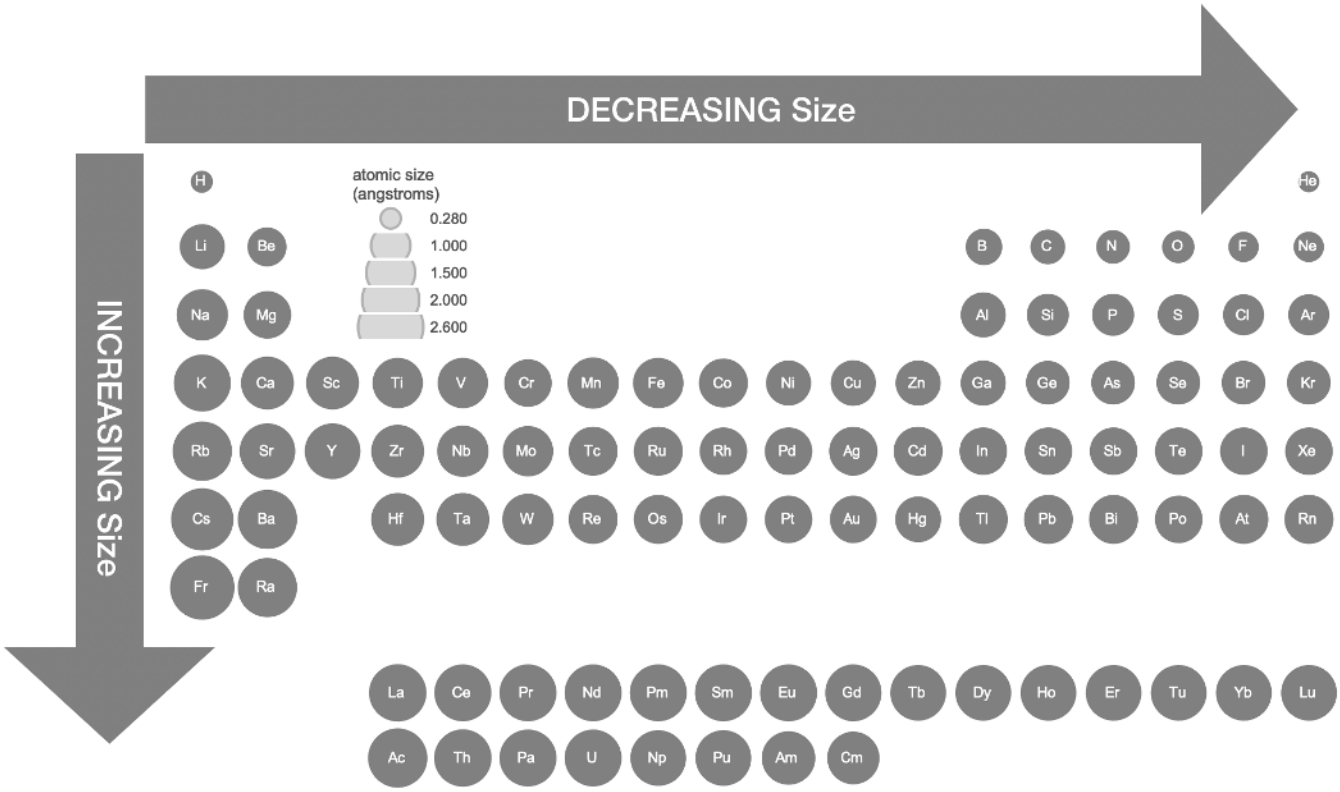


Figure **1.2.3.3.1**. *Atomic Radii Calculated from Crystalographic Data. Data from Cordero, Beatriz, Veronica Gomez, Ana E. Platero-Prats, Marc Reves, Jorge Echeverria, Eduard Cremades, Flavia Barragan, and Santiago Alvarez. "Covalent Radii Revisited." Dalton Transactions, no. 21 (2008): 2832–38. doi:10.1039/b801115j.* (Kathryn Haas; CC-NC-BY-SA)

Trends in Ionic Radius

Trends in ionic radius follow general trends in atomic radius for ions of the same charge. Ionic radius varies with the charge of the ion (and number of electrons) and the electron configuration (e.g. high spin or low spin).

Cations

Compared to their atoms, cations have the same Z but fewer electrons. Removal of electrons from an atom to form a cation results in a significant increase in effective nuclear charge, resulting in all other electrons being more strongly attracted to the nucleus, and having a lower energy level. The result is a contraction in size from the atom to cation. Figure **1.2.3.3.2** visually illustrates the relative size of atoms and some cations of the first four periods; the data is available in tabular format in Figure **1.2.3.3.3**.

Anions

Compared to their atoms, anions have the same Z but more electrons. Addition of electrons to an atom to form an anion results in a decrease in effective nuclear charge, which corresponds to a decrease in attractive force between the nucleus and electrons. Lower attractive force leads to expansion, where the size of the atom becomes larger in the formation of an anion. Figure **1.2.3.3.2** visually illustrates the relative size of atoms and some anions of the first four periods, while the data is available in tabular format in Figure **1.2.3.3.3**.

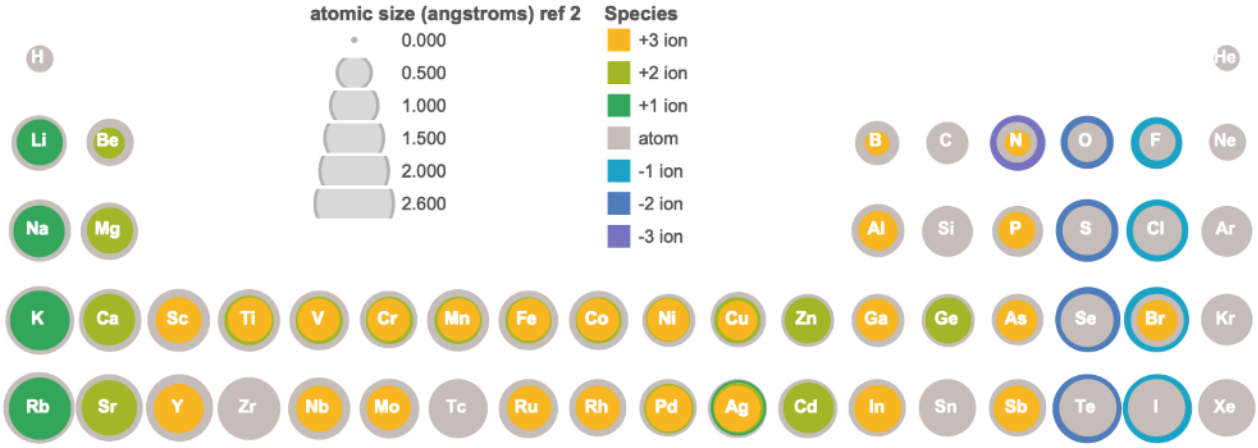


Figure **1.2.3.3.2**. This figure illustrates relative size of atoms and ions of the first four periods of the periodic table. Atomic radius is indicated by grey circles. Radius of cations is shown in green (+1), lime (+2), and yellow (+3) circles. Radius of anions are shown as aqua (-1), blue (-2), and purple (-3) circles. Data from sources 1-3. (Kathryn Haas; CC-NC-BY-SA)

H 0.31 (atom) 0 (+1)																	He 0.28 (atom)
Li 1.28 (atom) 0.9 (+1) - -	Be 0.96 (atom) 0.41 (+2) - -											B 0.84 (atom) 0.25 (+1)	C 0.76 (atom) 0.29 (+4)	N 1.32 (-3) 0.71 (atom) 0.3 (+3) 0.27 (+5)	O 1.21 (-2) 0.66 (atom)	F 1.145 (-1) 0.57 (atom)	Ne 0.58 (atom)
Na 1.66 (atom) 1.16 (+1)	Mg 1.41 (atom) 0.86 (+2)											Al 1.21 (atom) 0.675 (+3)	Si 1.11 (atom) 0.4 (+4)	P 1.07 (atom) 0.58 (+3) 0.31 (+5)	S 1.7 (-2) 1.05 (atom) 0.51 (+4) 0.26 (+6)	Cl 1.67 (-1) 1.02 (atom)	Ar 1.06 (atom)
K 2.03 (atom) 1.52 (+1)	Ca 1.76 (atom) 1.14 (+2)	Sc 1.7 (atom) 0.885 (+3)	Ti 1.6 (atom) 1 (+2) 0.81 (+3) 0.745 (+4)	V 1.53 (atom) 0.93 (+2) 0.78 (+3) 0.72 (+4)	Cr 1.39 (atom) 0.94 (+2 hs) 0.87 (+2 ls) 0.7555 (+3) 0.69 (+4) 0.63 (+5) 0.58 (+6)	Mn 1.61 (atom) 0.97 (+2 hs) 0.81 (+2 ls) 0.785 (+3 hs) 0.72 (+3 ls) 0.67 (+4) 0.47 (+5) 0.395 (+6) 0.39 (+7)	Fe 1.52 (atom) 0.92 (+2 hs) 0.765 (+3 hs) 0.75 (+2 ls) 0.725 (+4) 0.69 (+3 ls) 0.39 (+6)	Co 1.5 (atom) 0.885 (+2 hs) 0.79 (+2 ls) 0.75 (+3 hs) 0.685 (+3 ls) 0.67 (+4 hs)	Ni 1.24 (atom) 0.83 (+2) 0.74 (+3 hs) 0.7 (+3 ls) 0.62 (+4)	Cu 1.32 (atom) 0.91 (+1, cn6) 0.87 (+2, cn6) 0.68 (+3, cn6)	Zn 1.22 (atom) 0.88 (+2)	Ga 1.22 (atom) 0.76 (+3)	Ge 1.2 (atom) 0.87 (+2) 0.67 (+4)	As 1.19 (atom) 0.72 (+3) 0.6 (+5)	Se 1.84 (-2) 1.2 (atom) 0.64 (+4) 0.56 (+6)	Br 1.82 (-1) 1.2 (atom) 0.73 (+3) 0.53 (+7) 0.45 (+5)	Kr 1.16 (atom)
Rb 2.2 (atom) 1.66 (+1)	Sr 1.95 (atom) 1.32 (+2)	Y 1.9 (atom) 1.04 (+3)	Zr 1.75 (atom) 0.86 (+4)	Nb 1.64 (atom) 0.86 (+3) 0.82 (+4) 0.78 (+5)	Mo 1.54 (atom) 0.83 (+3) 0.79 (+4) 0.75 (+5) 0.73 (+6)	Tc 1.47 (atom) 0.785 (+4) 0.74 (+5) 0.7 (+7)	Ru 1.46 (atom) 0.82 (+3) 0.76 (+4) 0.705 (+5) 0.52 (+7) 0.5 (+8)	Rh 1.42 (atom) 0.805 (+3) 0.74 (+4) 0.69 (+5)	Pd 1.39 (atom) 0.73 (+1) 1 (+2) 0.9 (+3) 0.755 (+4)	Ag 1.45 (atom) 1.29 (+1) 1.08 (+2) 0.89 (+3)	Cd 1.44 (atom) 1.09 (+2)	In 1.42 (atom) 0.94 (+3)	Sn 1.39 (atom) 0.83 (+4)	Sb 1.39 (atom) 0.9 (+3) 0.74 (+5)	Te 2.07 (-2) 1.38 (atom) 1.1 (+4) 0.7 (+6)	I 2.06 (-1) 1.39 (atom) 1.09 (+5) 0.67 (+7)	Xe 1.4 (atom) 0.62 (+8)

Figure 1.2.3.3.3.

This figure shows radii (in Angstroms) of atoms and ions of the first four periods of the periodic table. Radii from each element are listed from largest to smallest, ionic charge indicated in parentheses (); hs = high spin, ls = low spin, cn6 = coordination number is 6. Data from sources 1-3. (Kathryn Haas; CC-NC-BY-SA)

References

1. Cordero, Beatriz, Veronica Gomez, Ana E. Platero-Prats, Marc Reves, Jorge Echeverria, Eduard Cremades, Flavia Barragan, and Santiago Alvarez. *"Covalent Radii Revisited." Dalton Transactions, no. 21 (2008): 2832–38. doi:10.1039/b801115j.*
2. R. D. Shannon (1976). "Revised effective ionic radii and systematic studies of interatomic distances in halides and chalcogenides". *Acta Crystallogr A.* **32** (5): 751–767. Bibcode:1976AcCrA..32..751S. doi:10.1107/S0567739476001551.
3. Wikipedia articles on Atomic Radius and Ionic Radius.

1.2.3.3: Covalent and Ionic Radii is shared under a CC BY-NC-SA 4.0 license and was authored, remixed, and/or curated by LibreTexts.

- **2.3.3: Covalent and Ionic Radii** by Bingyao Zheng, Emily Nguyen, Kathryn Haas, Swetha Ramireddy is licensed CC BY-NC-SA 4.0.

1.3: Rutherford's Atom

Learning Objectives

- Introduce the initial attempts to explain the structure of atoms.

The Gold Foil Experiment

In 1911, Rutherford and coworkers Hans Geiger and Ernest Marsden initiated a series of groundbreaking experiments that would completely change the accepted model of the atom. They bombarded very thin sheets of gold foil with fast moving **alpha particles**. Alpha particles, a type of natural radioactive particle, are positively charged particles with a mass about four times that of a hydrogen atom.

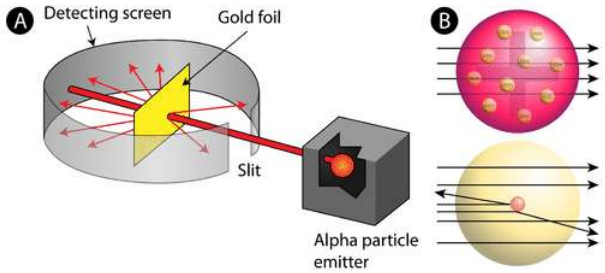


Figure **1.3.1**: *(A) The experimental setup for Rutherford's gold foil experiment: A radioactive element that emitted alpha particles was directed toward a thin sheet of gold foil that was surrounded by a screen which would allow detection of the deflected particles. (B) According to the plum pudding model (top) all of the alpha particles should have passed through the gold foil with little or no deflection. Rutherford found that a small percentage of alpha particles were deflected at large angles, which could be explained by an atom with a very small, dense, positively-charged nucleus at its center (bottom).*

According to the accepted atomic model, in which an atom's mass and charge are uniformly distributed throughout the atom, the scientists expected that all of the alpha particles would pass through the gold foil with only a slight deflection or none at all. Surprisingly, while most of the alpha particles were indeed undeflected, a very small percentage (about 1 in 8000 particles) bounced off the gold foil at very large angles. Some were even redirected back toward the source. No prior knowledge had prepared them for this discovery. In a famous quote, Rutherford exclaimed that it was "as if you had fired a 15-inch [artillery] shell at a piece of tissue and it came back and hit you."

Rutherford needed to come up with an entirely new model of the atom in order to explain his results. Because the vast majority of the alpha particles had passed through the gold, he reasoned that most of the atom was empty space. In contrast, the particles that were highly deflected must have experienced a tremendously powerful force within the atom. He concluded that all of the positive charge and the majority of the mass of the atom must be concentrated in a very small space in the atom's interior, which he called the nucleus. The **nucleus** is the tiny, dense, central core of the atom and is composed of protons and neutrons.

Rutherford's atomic model became known as the **nuclear model**. Most of the α-particles were not scattered; they passed unchanged through the thin metal foil. Some of the few that were scattered were scattered in the backward direction; i.e. they recoiled. This backward scattering requires that the foil contain heavy particles. When an α-particle hits one of these heavy particles it simply recoils backward, just like a ball thrown at a brick wall. Since most of the α-particles don’t get scattered, the heavy particles (the nuclei of the atoms) must occupy only a very small region of the total space of the atom. Most of the space must be empty or occupied by very low-mass particles. These low-mass particles are the electrons that surround the nucleus. It is worth emphasizing just how small the nucleus is compared to the rest of the atom. If we could blow up an atom to be the size of a large professional football stadium, the nucleus would be about the size of a marble.

Rutherford's Failed Planetary Atom

There are some basic problems with the Rutherford model. The Coulomb force that exists between oppositely charge particles means that a positive nucleus and negative electrons should attract each other, and the atom should collapse. To prevent the collapse, the electron was postulated to be orbiting the positive nucleus. The Coulomb force (discussed below) is used to change the direction of the velocity, just as a string pulls a ball in a circular orbit around your head or the gravitational force holds the

moon in orbit around the Earth. The origin for this hypothesis that suggests this perspective is plausible is the similarity of gravity and Coulombic interactions. The expression for the force of gravity between two masses (Newton's Law of gravity) is

$$F_{gravity} \propto \frac{m_1 m_2}{r^2} \tag{1.3.1}$$

with m_1 and m_2 representing the **mass** of object 1 and 2, respectively and r representing the distance between the objects centers

The expression for the Coulomb force between two charged species is

$$F_{Coulomb} \propto \frac{Q_1 Q_2}{r^2} \tag{1.3.2}$$

with Q_1 and Q_2 representing the **charge** of object 1 and 2, respectively and r representing the distance between the objects centers.

However, this analogy has a problem too. An electron going around in a circle is constantly being accelerated because its velocity vector is changing. A charged particle that is being accelerated emits radiation. This property is essentially how a radio transmitter works. A power supply drives electrons up and down a wire and thus transmits energy (electromagnetic radiation) that your radio receiver picks up. The radio then plays the music for you that is encoded in the waveform of the radiated energy.

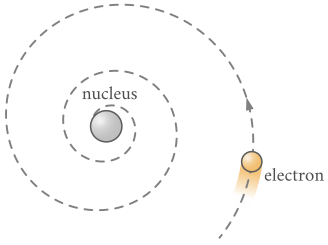


Figure **1.3.2**: The classical death spiral of an electron around a nucleus. (CC BY-NC; Ümit Kaya)

If the orbiting electron is generating radiation, it is losing energy. If an orbiting particle loses energy, the radius of the orbit decreases. To conserve angular momentum, the frequency of the orbiting electron increases. The frequency increases continuously as the electron collapses toward the nucleus. Since the frequency of the rotating electron and the frequency of the radiation that is emitted are the same, both change continuously to produce a continuous spectrum and not the observed discrete lines. Furthermore, if one calculates how long it takes for this collapse to occur, one finds that it takes about 10^{-11} seconds. This means that nothing in the world based on the structure of atoms could exist for longer than about 10^{-11} seconds. Clearly something is terribly wrong with this classical picture, which means that something was missing at that time from the known laws of physics.

Conservative Forces can be explained with Potentials

A conservative force is dependent only on the position of the object. If a force is conservative, it is possible to assign a numerical value for the potential at any point. When an object moves from one location to another, the force changes the potential energy of the object by an amount that does not depend on the path taken. The potential can be constructed as simple derivatives for 1-D forces:

$$F = -\frac{dV}{dx}$$

or as gradients in 3-D forces

$$F = -\nabla V$$

where ∇ is the vector of partial derivatives

$$\nabla = \left(\frac{\partial}{\partial x}, \frac{\partial}{\partial y}, \frac{\partial}{\partial z}\right)$$

The most familiar conservative forces are gravity and Coloumbic forces.

The Coulomb force law (Equation 1.3.2) comes from the corresponding Coulomb potential (sometimes call electrostatic potential)

$$V(r) = \frac{kQ_1Q_2}{r} \tag{1.3.3}$$

and it can be easily verified that the Coulombic force from this interaction ($F(r)$ is

$$F(r) = -\frac{dV}{dr} \tag{1.3.4}$$

As r is varied, the energy will change, so that we have an example of a potential energy curve $V(r)$ (Figure 1.3.2;). If Q_1 and Q_2 are the same sign, then the curve which is a purely **repulsive potential**, i.e., the energy increases monotonically as the charges are brought together and decreases monotonically as they are separated. From this, it is easy to see that like charges (charges of the same sign) repel each other.

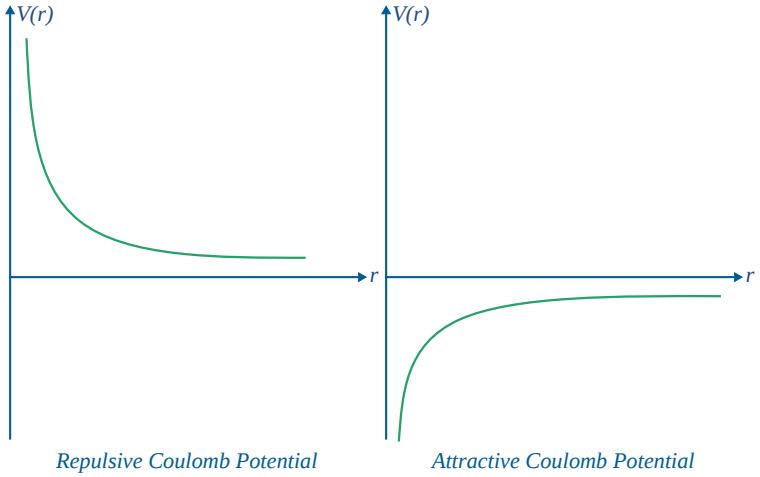


Figure 1.3.3: Potential energy curve for the Coulomb interactions between two charges of same sign (left) and opposite signs (right). (CC BY-NC; Ümit Kaya)

If the charges are of opposite sign, then the curve appears roughly Figure 1.3.2; and this is a purely **attractive potential**. Thus, the energy decreases as the charges are brought together, implying that opposite charges attract.

Contributors and Attributions

- CK-12 Foundation by Sharon Bewick, Richard Parsons, Therese Forsythe, Shonna Robinson, and Jean Dupon.
- Mark Tuckerman (New York University)
- David M. Hanson, Erica Harvey, Robert Sweeney, Theresa Julia Zielinski ("Quantum States of Atoms and Molecules")
- Template:Contriboundless

1.3: Rutherford's Atom is shared under a CC BY-NC-SA 4.0 license and was authored, remixed, and/or curated by LibreTexts.

1.4: Bohr's Atom

Review Necessary Skills

- Relate the wavelength (λ) and frequency (ν) of light to the velocity of light (c) ($c = \lambda\nu$) and to the energy of a photon (E) ($E = h\nu = hc/\lambda$).
  - Find help using $c = \lambda\nu$ and lots of problems here on ChemTeam.
  - Find help using $E = h\nu = hc/\lambda$ and lots of problems here on ChemTeam.
- Relate charge, distance, and electrostatic potential energy using Coulomb's law ($U = k\ q_1 \times q_2/r$) qualitatively.
  - Here is an interactive simulation.
  - Coulomb's law
  - Here is a review in the context of atoms with some problems.
- Describe what happens to molecules when they interact with electromagnetic radiation.
  - What happens to molecules at different wavelengths? See NO_2 in this simulation. Don't worry if this doesn't look familiar, it is just a reminder that IR, microwave, and UV light all interact with molecules differently.

Experiments that can't be explained without quantization of energy or position

Photoelectric effect
(see demo below or go to PheT)



Click to Run or Download (Needs Java!)

Atomic line spectra
(see demo below or go to PheT)



Click to Run or Download (Needs Java!)

Electron diffraction
(see demo below or go to PheT)



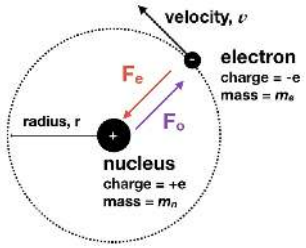
Click to Run

Double-slit experiment
(see demo or go to PheT)



Click to Run or Download (Needs Java!)

Bohr's Model of the Hydrogen Atom



The Danish scientist, Niels Bohr, introduced the first theory that quantized the energy of electrons in atoms. Although Bohr's reasoning relies on classical concepts and hence, is not a correct explanation, the reasoning is interesting, and so we examine this model for its historical significance. This is now referred to as "Old Quantum Theory", while the "New Quantum Theory" is that described by the Schrodinger equation, and that will be described a bit later. Below, the story of Bohr's model will be described. Another way to tell the story is here.

Bohr's Condition of a Stable Orbit: Bohr imagined that electrons were in circular orbit around a nucleus. He applied classical mechanics to rationalize that if the electron of charge, $-e$, were to be in a stable orbit around a nucleus of opposite charge, $+e$, then the electrostatic attractive force (F_e) between the electron and nucleus must be exactly opposed by the outward centripetal force (F_o) created by the electron's circular orbit. (We can ignore any gravitational force because it is relatively weak.)

Where the electrostatic attractive force F_e and centripetal force F_o are,

$$F_e = \frac{(+e)(-e)}{r^2} = -\frac{e^2}{r^2} \tag{1.4.1}$$

$$F_o = \frac{m_e v^2}{r} \tag{1.4.2}$$

For a stable orbit to exist $F_e + F_o = 0$, or,

$$F_o = -F_e \tag{1.4.3}$$

$$\frac{m_e v^2}{r} = \frac{e^2}{r^2} \tag{1.4.4}$$

Bohr's Calculation of the Electron's Energy: Bohr could calculate the total energy of the electron, again using classical mechanics. The total energy of a system is the sum of the kinetic energy (KE, energy of motion of the electron) and the potential energy (PE, from the electrostatic attraction, F_e and the distance, r).

$$KE = \frac{1}{2} m_e v^2 \tag{1.4.5}$$

$$PE = rF_e = r\left(-\frac{e^2}{r^2}\right) = -\frac{e^2}{r} \tag{1.4.6}$$

If total Energy (E) is equal to the sum of KE and PE,

$$E = KE + PE = \frac{1}{2} m_e v^2 - \frac{e^2}{r} \tag{1.4.7}$$

This expression can be simplified by first solving equation (4) for $m_e v^2 = \frac{e^2}{r}$ and substituting into equation 7.

$$E = \frac{1}{2}\left(\frac{e^2}{r}\right) - \frac{2}{2}\left(\frac{e^2}{r}\right) = -\frac{1}{2}\left(\frac{e^2}{r}\right) = -\frac{e^2}{2r} \tag{1.4.8}$$

Now we see that energy of the electron, E, can be calculated if we know the distance, r, at which the electron is orbiting. This is a good time to remind ourselves that we also know, from Planck's work, that $E = h\nu$. This reminds us that the electron is a wave with frequency, ν, in units of sec^{-1}. So, we could also write,

$$E = -\frac{e^2}{2r} = h\nu \tag{1.4.9}$$

Bohr's Quantization, and Equations for Radius, r, and Velocity, v: Bohr knew that electrons must have stable orbits, otherwise the electrons would fall into the nucleus. Bohr was familiar with Maxwell's theory of classical electromagnetism and knew that in a classical theory, the orbiting electron should radiate energy away and eventually collapse into the nucleus (E is given off as r decreases). He circumvented this problem by following Planck's idea underlying blackbody radiation and positing that the orbital angular momentum $p = m_e v r$ of the electron could only take on specific values. He proposed those values to be units of $\frac{h}{2\pi}$, where h is Planck's constant. Bohr's proposal was,

$$m_e v r = n\frac{h}{2\pi} \tag{1.4.10}$$

where n is the first quantum number and can have values of any integer ($n = 1, 2, 3...$). This relationship can be rearranged to find the velocity, v,

$$v = n\frac{h}{m_e r 2\pi} \tag{1.4.11}$$

This implies that only certain velocities are allowed, since only certain values of n are allowed. This expression for v can be substituted into the condition of a stable orbit (using a rearranged version of equation 4, ($m_e v^2 = \frac{e^2}{r}$) to give equation 12. Ultimately, this allows us to find how the radius, r, depends on the the quantum number, n, as shown in equation 13.

$$\frac{m_e\left(n\frac{h}{m_e r 2\pi}\right)^2}{r} = \frac{m_e n^2 h^2}{4m_e^2 r^2 \pi^2} = \frac{n^2 h^2}{4m_e r^2 \pi^2} = \frac{e^2}{r} \tag{1.4.12}$$

This expression can be rearranged to solve for r,

$$r = \frac{n^2 h^2}{4\pi^2 m_e e^2 K} \tag{1.4.13}$$

K is the Coulomb constant which is needed for unit conversion and has a value of

$K = 8.9875517923x10^9 \frac{Nm^2}{C^2}$

This expression shows Bohr's assumption that there are discrete distances where the electron can orbit, as the values or r are restricted by the integer values of n. The relationship between n and E is found by substitution of the equation for r into equation 8 or 9.

$$E = -\frac{e^2 K}{2\left(\frac{n^2 h^2}{4\pi^2 m_e e^2 K}\right)} = -\frac{e^2 K 4\pi^2 m_e e^2 K}{2n^2 h^2} = -\frac{2\pi^2 m_e e^4 2K^2}{n^2 h^2} \tag{1.4.14}$$

This expression shows that energy is quantized, as like values of v and r, the energy depends on the integer value, n.

Exercise 1.4.1

Show how you would find the Bohr radius, velocity, and energy of an electron in the first shell of a hydrogen atom.

Answer

$r = \frac{n^2 h^2}{4\pi^2 m_e e^2 K}$

$r = \frac{1^2(6.626070x10^{-34})^2}{4(3.141592654)^2(9.10938356x10^{-31})(1.602176634x10^{-19})^2(8.9875517923x10^9)}$

$r = \frac{(4.390480364x10^{-67})J^2s^2}{(8.296805693x10^{-67})kgNm^2}$

$r = 5.292x10^{-11}m$

$v = n\frac{h}{m_e r 2\pi}$

$v = 1\frac{6.626070x10^{-34}}{(9.10938356x10^{-31})(5.292x10^{-11})2(3.141592654)}$

$v = \frac{6.626070x10^{-34}Js}{3.028926207x10^{-40}kgm}$

$v = 2.19x10^6 m/s$

$E = -\frac{2\pi^2 m_e e^4 2K^2}{n^2 h^2}$

$E = -\frac{2(3.141592654)^2(9.10938356x10^{-31})(1.602176634x10^{-19})^4(8.9875517923x10^9)^2}{1^2(6.626070x10^{-34})^2}$

$E = -\frac{9.570687085x10^{-85}kgN^4m^4}{4.390480367x10^{-67}J^2s^2}$

$E = -2.1799x10^{-18}J$

Hydrogen Absorption and Emission Spectra

When a high-voltage electrical discharge is passed through a sample of hydrogen gas (H_2) at low pressure, the result is individual isolated hydrogen atoms that emit a red light. Unlike blackbody radiation, the color of the light emitted by the hydrogen atoms does not depend greatly on the temperature of the gas in the tube. When the emitted light is passed through a prism, only a few narrow lines of particular wavelengths,

called a line spectrum, are observed rather than a continuous range of wavelengths (Figure **1.4.1**). The light emitted by hydrogen atoms is red because, of its four characteristic lines, the most intense line in its spectrum is in the red portion of the visible spectrum, at 656 nm.

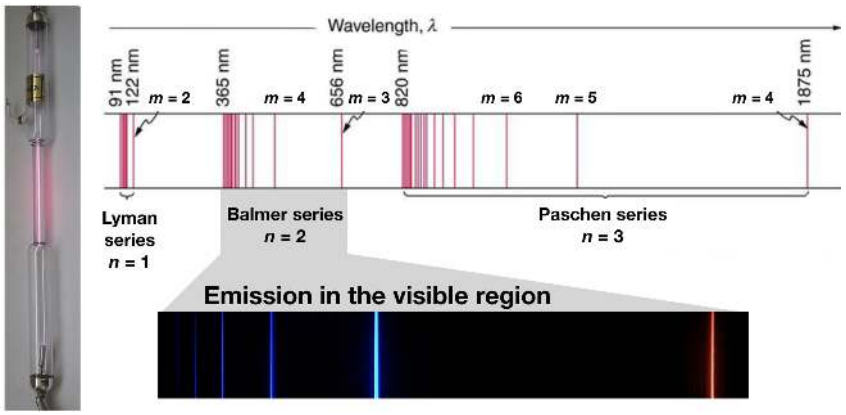


Figure* 1.4.1*: *The Emission of Light by Hydrogen Atoms. (left) A sample of excited hydrogen atoms emits a characteristic red light. (bottom) When the light emitted by a sample of excited hydrogen atoms is split into its component wavelengths by a prism, four characteristic violet, blue, green, and red emission lines can be observed, the most intense of which is at 656 nm. (top) An diagram showing extended regions of the electromagnetic spectrum and the hydrogen line spectra that are observed.*

In 1885, a Swiss mathematics teacher, Johann Balmer (1825–1898), showed that the frequencies of the lines observed in the visible region of the hydrogen line spectrum fit a simple equation that can be expressed as follows:

$$\nu = constant\left(\frac{1}{2^2} - \frac{1}{n^2}\right) \tag{1.4.15}$$

where n = 3, 4, 5, 6. As a result, these lines are known as the *Balmer series*. The Swedish physicist Johannes Rydberg (1854–1919) subsequently restated and expanded Balmer's result in the *Rydberg equation*:

$$\frac{1}{\lambda} = R_h\left(\frac{1}{n^2} - \frac{1}{m^2}\right) \tag{1.4.16}$$

where n and m are positive integers, $m > n$, and R_h the *Rydberg constant*, has a value of 1.09737 × 10^7 m^{-1}. Like Balmer's equation, Rydberg's simple equation described the wavelengths of the visible lines in the emission spectrum of hydrogen (with n = 2, m = 3, 4, 5,…). More important, Rydberg's equation also predicted the wavelengths of other series of lines that would be observed in the emission spectrum of hydrogen: one in the ultraviolet (n = 1, m = 2, 3, 4,…) and one in the infrared (n = 3, m = 4, 5, 6).

Exercise 1.4.2

Solve the Rydberg Equation for a line where $m = 3$ and $n = 1$. In what region of the electromagnetic spectrum does this appear, and which series is this?

Answer

$\frac{1}{\lambda} = R_h\left(\frac{1}{n^2} - \frac{1}{m^2}\right)$

$\frac{1}{\lambda} = 1.09737x10^7 m^{-1}\left(\frac{1}{1^2} - \frac{1}{3^2}\right)$

$\frac{1}{\lambda} = 9754400m^{-1}$

$\lambda = 1.03x10^{-7}m = 102.5nm$

This is in the Ultra-violet region.

Sources

The Bohr Theory of the Hydrogen Atom

Line Spectra and the Bohr Model

1.4: Bohr's Atom is shared under a CC BY-NC-SA 4.0 license and was authored, remixed, and/or curated by LibreTexts.

SECTION OVERVIEW

1.5: Simple Bonding Theory

1.5.1: Lewis Electron-Dot Diagrams

1.5.1.1: Resonance

1.5.1.2: Breaking the octet rule with higher electron counts (hypervalent atoms)

1.5.1.3: Formal Charge

1.5.1.4: Lewis fails to predict unusual cases- Boron and Beryllium

1.5.2: Valence Shell Electron-Pair Repulsion

1.5.2.1: Lone Pair Repulsion

1.5.2.2: Multiple Bonds

1.5.2.3: Electronegativity and Atomic Size Effects

1.5.3: Molecular Polarity

1.5.4: Hydrogen Bonding

1.5.5: Valence Bond Theory

1.5.6: Hybrid Atomic Orbitals

1.5: Simple Bonding Theory is shared under a CC BY-NC-SA 4.0 license and was authored, remixed, and/or curated by LibreTexts.

1.5.1: Lewis Electron-Dot Diagrams

In 1916, Gilbert Lewis Newton introduced a simple way to show the bonding between atoms in a molecule though Lewis electron dot diagrams. Creating Lewis diagrams is rather simple and requires only a few steps and some accounting of the valence electrons on each atom. Valence electrons are represented as dots. When two electrons are paired (lone pairs), they are represented by two adjacent dots located on an atom, and when two paired electrons are shared between atoms (bonds), they are shown as lines. For example, below are the electron dot structures of atoms and the Lewis electron dot structures of the molecules.

These diagrams are helpful because they allow us to show how atoms are connected, and when coupled with Valence Shell Electron Repulsion Theory (VSEPR), we can use Lewis structures to predict the shape of the molecule.

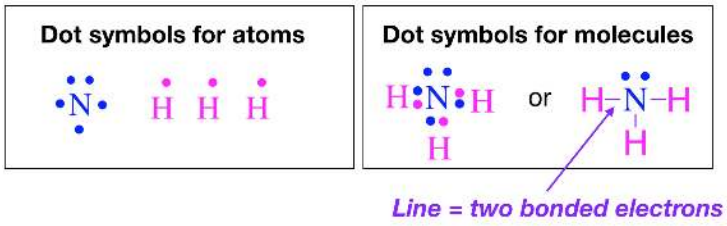


Figure 1.5.1.1: Lewis dot structure of atoms comprising ammonia and the dot structure of the molecule. (Kathryn Haas; CC-NC-BY-SA)

The drawing of Lewis electron-dot structures is guided largely by the **octet rule**: that atoms form bonds to achieve eight electrons in their valence shell. For many elements, a full valence shell has an electron configuration of s^2p^6, or eight electrons. A common exception to this rule is the first row elements, H and He. These two elements have $n = 1$ as their valence shell, and so they have only two electrons in a full valence shell ($1s^2$ electron configuration). Although H and He are exceptions to the "octet rule", they still form bonds to achieve a full valence shell. It may be better to think of this as the "full valence" rule of bonding. We will see many more violations to the "octet" rule as we progress through this course. In the case of metals and metalloids, breaking of the rules is particularly common. (CC-BY-NC-SA; Kathryn Haas)

Common violations of the octet rule

- **Less than eight electrons (hypovalency)**: H and He are examples of elements that cannot have more than two electrons in their full valence shell. Additionally, there are cases where a valid Lewis structure contains atoms with ***hypovalency:*** *partially-filled valence shells*. An example of this is a *carbocation, a positively charged carbon with only six electrons in its valence shell.* Carbocations are important intermediates in organic chemistry, and they are highly reactive (unstable) Lewis acids (electrophiles). Another example of hypovalency is the Lewis structure for BH_3, which shows boron with three bonds, and only six electrons in its valence shell. Boron hydride is a strong Lewis Acid. (Side note: the actual chemical form of BH_3 is not well-predicted by the Lewis structure and we'll see more about this in Section 3.1.4.)
- **More than eight electrons (hypervalency)**: This is a case where an element has more than eight electrons in its valence shell. It is common for larger atoms ($n \geq 3$), and it is discussed further in Section 3.1.2.

Pitfall alert! There are different rules for counting electrons depending on the purpose of the counting. These are the rules for counting for "octets". The rules for counting for calculation of an atom's formal charge are !!different!! and are described in Section 3.1.1. When an atom is part of a molecule, all electrons that are associated with the atom are counted as contributing to the atom's valence. This includes electrons that are lone pairs on the atoms, and *all* electrons that are shared in bonds. If four electrons are shared between two atoms, it is a double bond. If six electrons are shared between atoms, it is a triple bond.

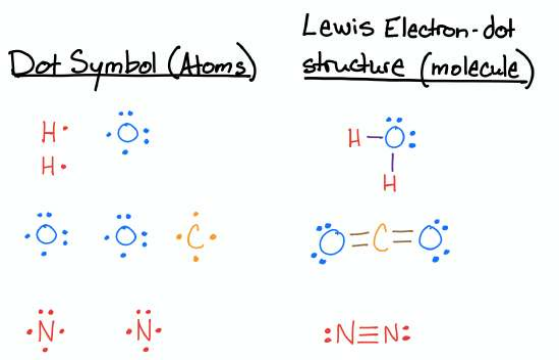
Electrons in valence (octet) = total unbonded electrons on the atom + total bonded electrons (2 electrons per bond)

Even if you're an old pro at drawing Lewis structures, it's a good idea to polish up. Please complete the practice exercises below. You should get out an actual piece of paper (I know...just do it. It's good for you.) and a writing tool and try to complete each problem before checking the answer.

? Exercise 1.5.1.1

Draw the Lewis structures for H_2O, CO_2, and N_2.

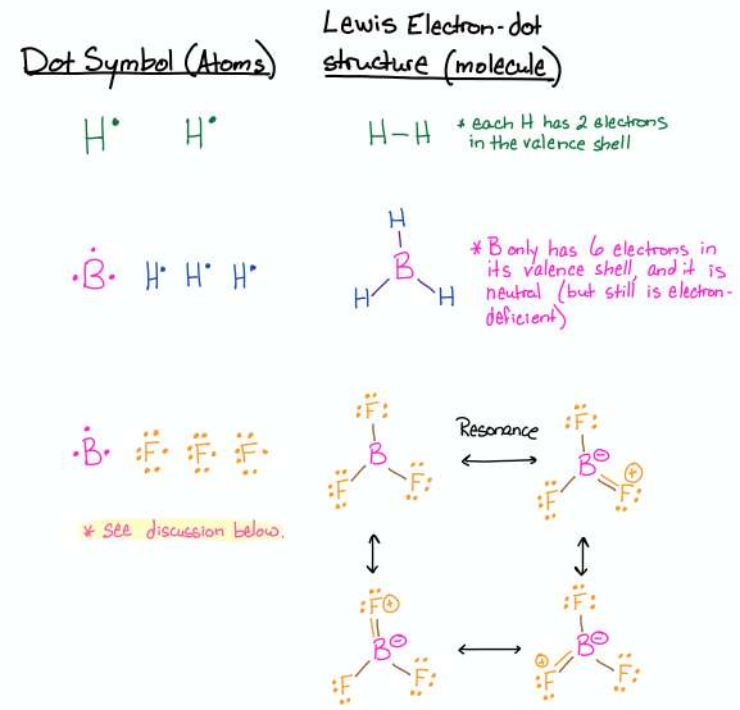
Answer



? Exercise 1.5.1.2

Draw the Lewis structures for H_2, BH_3 and BF_3.

Answer



These three examples include atoms that have less than eight electrons in their valence shell. In the case of H, it is satisfied with only two electrons in its valence, as was discussed earlier in this section. The case of BH_3 was also discussed above. In the Lewis structure of BH_3, the boron can only have six electrons in its octet and it is neutral in charge. The boron is electron deficient even though it has neutral charge.

The case of BF_3 deserves a discussion: If you are unfamiliar with resonance and formal charge, see Sections 3.1.1 (Resonance) and 3.1.3 (Formal Charge) first and come back to this afterward. You might have drawn the BF_3 structure similar to the one that is drawn for BH_3, where boron has three bonds and only six electrons in its valence shell. If you did that, then you are correct; but if you only gave this structure, then your answer is not complete. There are three other correct

ways to draw the structure. Since F has lone pairs of electrons, other valid Lewis structures would each have a double bond to one of the fluorines (three total). All of these structures are called resonance structures, and based on the four of them, we could predict that BF_3 would have B-F bonds that have some double-bond character. If fact, this is the case for BF_3; it has bond lengths that are shorter than single bonds, but longer than double bonds. Read more about it on its Wikipedia page here (click).

Outside Links

- en.Wikipedia.org/wiki/Lewis_structures
- http://www.ausetute.com.au/lewisstr.html
- cost.georgiasouthern.edu/chem...cule/lewis.htm

This page titled 1.5.1: Lewis Electron-Dot Diagrams is shared under a CC BY-NC-SA 4.0 license and was authored, remixed, and/or curated by Kathryn Haas.

- **3.1: Lewis Electron-Dot Diagrams** by Kathryn Haas is licensed CC BY-NC-SA 4.0.
- **2.1B: Lewis Structures** by Andrew Iskandar is licensed CC BY 4.0.

1.5.1.1: Resonance

Learning Objectives

- To understand the concept of resonance.

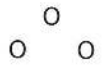
Resonance structures are a set of two or more Lewis Structures that collectively describe the electronic bonding of a single polyatomic species including fractional bonds and fractional charges. Resonance structures are capable of describing delocalized electrons that cannot be expressed by a single Lewis formula with an integral number of covalent bonds.

Sometimes one Lewis Structure is not Enough

Sometimes, even when formal charges are considered, the bonding in some molecules or ions cannot be described by a single Lewis structure. Resonance is a way of describing delocalized electrons within certain molecules or polyatomic ions where the bonding cannot be expressed by a single Lewis formula. A molecule or ion with such delocalized electrons is represented by several contributing structures (also called resonance structures or canonical forms). Such is the case for ozone ($\mathbf{O_3}$), an allotrope of oxygen with a V-shaped structure and an O–O–O angle of 117.5°.

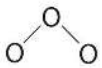
Ozone (O_3)

1. We know that ozone has a V-shaped structure, so one O atom is central:



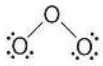
2. Each O atom has 6 valence electrons, for a total of 18 valence electrons.

3. Assigning one bonding pair of electrons to each oxygen–oxygen bond gives



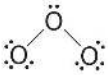
with 14 electrons left over.

4. If we place three lone pairs of electrons on each terminal oxygen, we obtain

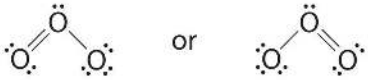


and have 2 electrons left over.

5. At this point, both terminal oxygen atoms have octets of electrons. We therefore place the last 2 electrons on the central atom:

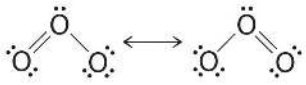


6. The central oxygen has only 6 electrons. We must convert one lone pair on a terminal oxygen atom to a bonding pair of electrons —but which one? Depending on which one we choose, we obtain either



Which is correct? In fact, neither is correct. Both predict one O–O single bond and one O=O double bond. As you will learn, if the bonds were of different types (one single and one double, for example), they would have different lengths. It turns out, however, that both O–O bond distances are identical, 127.2 pm, which is shorter than a typical O–O single bond (148 pm) and longer than the O=O double bond in O_2 (120.7 pm).

Equivalent Lewis dot structures, such as those of ozone, are called **resonance structures**. The position of the *atoms* is the same in the various resonance structures of a compound, but the position of the *electrons* is different. Double-headed arrows link the different resonance structures of a compound:



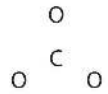
The double-headed arrow indicates that the actual electronic structure is an *average* of those shown, not that the molecule oscillates between the two structures.

> *When it is possible to write more than one equivalent resonance structure for a molecule or ion, the actual structure is the average of the resonance structures.*

The Carbonate (CO_3^{2-}) Ion

Like ozone, the electronic structure of the carbonate ion cannot be described by a single Lewis electron structure. Unlike O_3, though, the actual structure of CO_3^{2-} is an average of *three* resonance structures.

1. Because carbon is the least electronegative element, we place it in the central position:



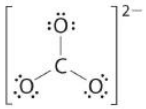
The three oxygens are drawn in the shape of a triangle with the carbon at the center of the triangle.

2. Carbon has 4 valence electrons, each oxygen has 6 valence electrons, and there are 2 more for the −2 charge. This gives 4 + (3 × 6) + 2 = 24 valence electrons.

3. Six electrons are used to form three bonding pairs between the oxygen atoms and the carbon:



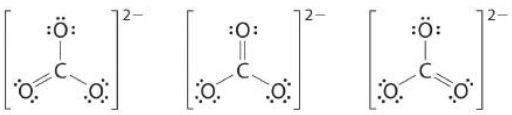
4. We divide the remaining 18 electrons equally among the three oxygen atoms by placing three lone pairs on each and indicating the −2 charge:



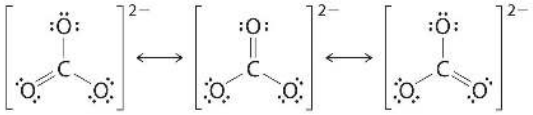
The Lewis dot structure has a central carbon that is bonded to 3 oxygens. Each oxygen has 3 lone pairs. The molecule is inside square brackets and has a charge of minus 2.

5. No electrons are left for the central atom.

6. At this point, the carbon atom has only 6 valence electrons, so we must take one lone pair from an oxygen and use it to form a carbon–oxygen double bond. In this case, however, there are *three* possible choices:



As with ozone, none of these structures describes the bonding exactly. Each predicts one carbon–oxygen double bond and two carbon–oxygen single bonds, but experimentally all C–O bond lengths are identical. We can write resonance structures (in this case, three of them) for the carbonate ion:



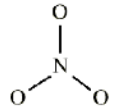
The resonance structure includes all three Lewis dot structures with double headed arrows between them.

The actual structure is an average of these three resonance structures.

The Nitrate (NO_3^-) ion

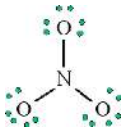
1. Count up the valence electrons: (1*5) + (3*6) + 1(ion) = **24** electrons

2. Draw the bond connectivities:

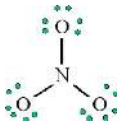


The three oxygens are drawn in the shape of a triangle with the nitrogen at the center of the triangle.

3. Add octet electrons to the atoms bonded to the center atom:

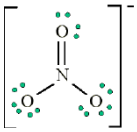


4. Place any leftover electrons (24-24 = **0**) on the center atom:



5. Does the central atom have an octet?

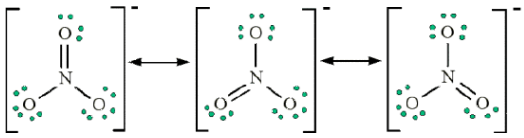
- **NO**, it has 6 electrons
- Add a multiple bond (first try a double bond) to see if the central atom can achieve an octet:



A double bond is added between one oxygen and the central nitrogen. The molecule has a negative charge.

6. Does the central atom have an octet?

- YES
- Are there possible resonance structures? YES



Note: We would expect that the bond lengths in the $\mathbf{NO_3^-}$ ion to be somewhat shorter than a single bond.



Example 1.5.1.1.1: Benzene

Benzene is a common organic solvent that was previously used in gasoline; it is no longer used for this purpose, however, because it is now known to be a carcinogen. The benzene molecule (C_6H_6) consists of a regular hexagon of carbon atoms, each of which is also bonded to a hydrogen atom. Use resonance structures to describe the bonding in benzene.

Given: molecular formula and molecular geometry

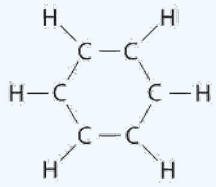
Asked for: resonance structures

Strategy:

A. Draw a structure for benzene illustrating the bonded atoms. Then calculate the number of valence electrons used in this drawing.
B. Subtract this number from the total number of valence electrons in benzene and then locate the remaining electrons such that each atom in the structure reaches an octet.
C. Draw the resonance structures for benzene.

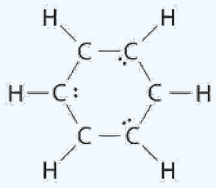
Solution:

A Each hydrogen atom contributes 1 valence electron, and each carbon atom contributes 4 valence electrons, for a total of (6 × 1) + (6 × 4) = 30 valence electrons. If we place a single bonding electron pair between each pair of carbon atoms and between each carbon and a hydrogen atom, we obtain the following:



Each carbon atom in this structure has only 6 electrons and has a formal charge of +1, but we have used only 24 of the 30 valence electrons.

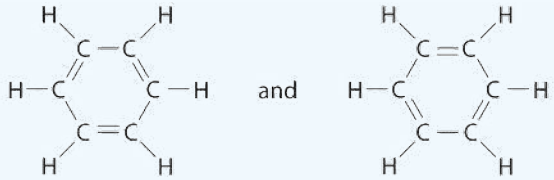
B If the 6 remaining electrons are uniformly distributed pairwise on alternate carbon atoms, we obtain the following:



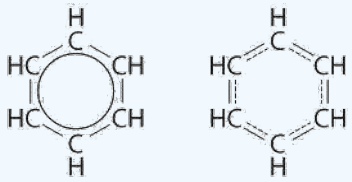
Three carbon atoms now have an octet configuration and a formal charge of −1, while three carbon atoms have only 6 electrons and a formal charge of +1. We can convert each lone pair to a bonding electron pair, which gives each atom an octet of

electrons and a formal charge of 0, by making three C=C double bonds.

C There are, however, two ways to do this:



Each structure has alternating double and single bonds, but experimentation shows that each carbon–carbon bond in benzene is identical, with bond lengths (139.9 pm) intermediate between those typically found for a C–C single bond (154 pm) and a C=C double bond (134 pm). We can describe the bonding in benzene using the two resonance structures, but the actual electronic structure is an average of the two. The existence of multiple resonance structures for aromatic hydrocarbons like benzene is often indicated by drawing either a circle or dashed lines inside the hexagon:

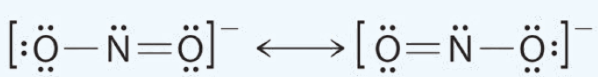


Benzene

? Exercise 1.5.1.1.1: Nitrite Ion

The sodium salt of nitrite is used to relieve muscle spasms. Draw two resonance structures for the nitrite ion (NO_2^-).

Answer



There is a double bond between one oxygen and the nitrogen, It can be found on the left oxygen or the right oxygen.

Resonance structures are particularly common in oxoanions of the *p*-block elements, such as sulfate and phosphate, and in aromatic hydrocarbons, such as benzene and naphthalene.

Warning

If several reasonable resonance forms for a molecule exists, the "actual electronic structure" of the molecule will probably be intermediate between all the forms that you can draw. The classic example is benzene in Example **1.5.1.1.1**. One would expect the double bonds to be shorter than the single bonds, but if one overlays the two structures, you see that one structure has a single bond where the other structure has a double bond. The best measurements that we can make of benzene do not show two bond lengths - instead, they show that the bond length is intermediate between the two resonance structures.

Resonance structures is a mechanism that allows us to use all of the possible resonance structures to try to predict what the actual form of the molecule would be. Single bonds, double bonds, triple bonds, +1 charges, -1 charges, these are our limitations in explaining the structures, and the true forms can be in between - a carbon-carbon bond could be mostly single bond with a little bit of double bond character and a partial negative charge, for example.

Summary

Some molecules have two or more chemically equivalent Lewis electron structures, called resonance structures. Resonance is a mental exercise and method within the Valence Bond Theory of bonding that describes the delocalization of electrons within molecules. These structures are written with a **double-headed arrow** between them, indicating that none of the Lewis structures accurately describes the bonding but that the actual structure is an average of the individual resonance structures. Resonance

structures are used when one Lewis structure for a single molecule cannot fully describe the bonding that takes place between neighboring atoms relative to the empirical data for the actual bond lengths between those atoms. The net sum of valid resonance structures is defined as a resonance hybrid, which represents the overall delocalization of electrons within the molecule. A molecule that has several resonance structures is more stable than one with fewer. Some resonance structures are more favorable than others.

1.5.1.1: Resonance is shared under a CC BY-NC-SA 4.0 license and was authored, remixed, and/or curated by LibreTexts.

- **8.6: Resonance Structures** is licensed CC BY-NC-SA 3.0.

1.5.1.2: Breaking the octet rule with higher electron counts (hypervalent atoms)

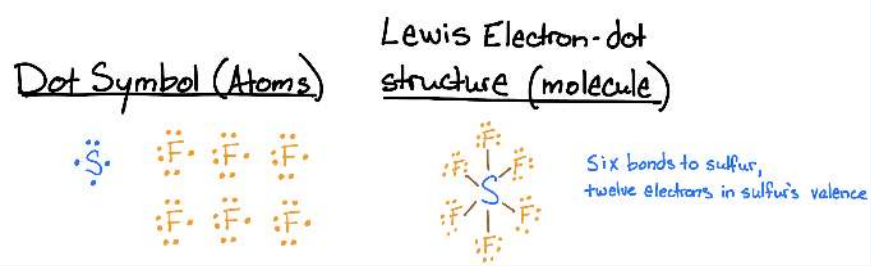
The octet rule applies well to atoms in the second row of the periodic table, where a full valence shell includes eight electrons with an electron configuration of s^2p^6. Even elements in the third and fourth row are known to follow this rule *sometimes*, but not always. In larger atoms, where $n \geq 3$ the valence shell contains additional subshells: the $d, f, g...$ subshells. Therefore, atoms with $n \geq 3$ can have higher valence shell counts by "expanding" into these additional subshells. When atoms contain more than eight electrons in their valence shell, they are said to be **hypervalent**. Hypervalency allows atoms with $n \geq 3$ to break the octet rule by having more than eight electrons. This also means they can have five or more bonds; something that is nearly unheard of for atoms with $n \leq 2$. Complete the exercises below to see examples of molecules containing hypervalent atoms.

? Exercise 1.5.1.2.1

Draw the Lewis structures for sulfur hexafluoride (SF_6).

Answer

Each fluorine atom has one valence electron and will make one bond each. The sulfur has six valence electrons, and must make six bonds to form a molecule with the six fluorine atoms. The molecular structure has six bonds to sulfur, with twelve valence electrons. The sulfur is hypervalent.

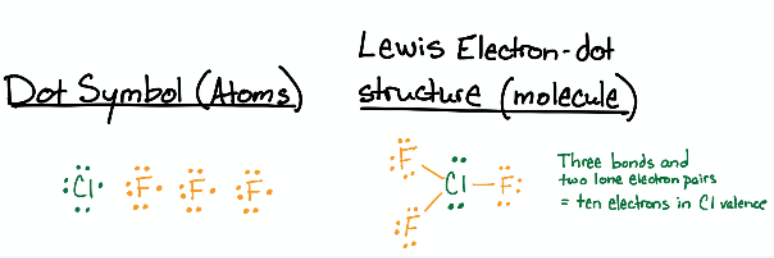


? Exercise 1.5.1.2.1

Draw the Lewis structure for chlorine trifluoride (ClF_3.

Answer

All atoms are halogens and each has seven valence electrons. Chlorine is capable of hypervalency because it is in the third row of the periodic table; however fluorine cannot have more than eight valence electrons in its valence because it is in the second row. The structure has the three fluorine atoms bonded to a central chlorine atom. The chlorine has a valence of ten electrons due to its three bonds and two lone pairs.



Is hypervalency real? Not exactly. Hypervalency is a concept associated with hybrid orbital theory and Lewis theory. It's useful for some simple things, like predicting how atoms are connected and predicting molecular shape. But the idea that the d-orbitals are involved in bonding isn't accurate according to wave mechanics.

For main group molecules, chemists (like Pauling) thought a long time ago that hypervalence is due to expanded s^2p^6 octets. The consensus is now clear that d orbitals are NOT involved in bonding in molecules like SF_6 any more than they are in SF_4 and SF_2. In all three cases, there is a small and roughly identical participation of d-orbitals in the wavefunctions. This has been established in both MO and VB theory. However, using hybrid orbitals with d-orbital contributions equips us with a language which can pragmatically describe the geometries of highly coordinated substances.

While hybrid orbitals are a powerful tool to describe the geometries and shape of molecules and metal complexes, in "real" molecules their significance may be debated. Often a more realistic molecular orbitals approach is needed. However, from an epistemologically simple point of view, bonding theories can only be judged by their predictions. To the extent that hybridization can explain the shapes of PF_5 and SF_6, valence bond theory is a perfectly good theory. To the extent that if you write out the valence bond wavefunction using hybridized orbitals and calculate energies and other properties à la Pauling (i.e., ionization energy and electron affinities) and find them to be off from experimental results (by tens of kcals/mol), then valence bond theory is not accurate.

> *Bonding theories can only be judged by their predictions.*

A simple explanation that can be given is that molecular wavefunctions constructed out of hybridized atomic orbitals are accurate enough to predict some things, but not others. Predictions of any theory must be compared with empirical evidence to assess when they work and when they fail. When a theory gives the wrong answer, at least one assumption must not hold. In this case, the valence bond wavefunction is not accurate enough to capture some important features of a system's electronic structure. It may not be the most intellectually satisfying answer, but to say more would result in a much more complicated answer and certainly far beyond the level reasonably expected from general chemistry discussions.

This page titled 1.5.1.2: Breaking the octet rule with higher electron counts (hypervalent atoms) is shared under a CC BY-NC-SA 4.0 license and was authored, remixed, and/or curated by Kathryn Haas.

- **3.1.2: Breaking the octet rule with higher electron counts (hypervalent atoms)** by Kathryn Haas is licensed CC BY-NC-SA 4.0.

1.5.1.3: Formal Charge

The formal charge of an atom in a molecule is the *hypothetical* charge the atom would have if we could redistribute the electrons in the bonds evenly between the atoms. Another way of saying this is that formal charge results when we take the number of valence electrons of a neutral atom, subtract the nonbonding electrons, and then subtract the number of bonds connected to that atom in the Lewis structure.

Calculating Formal Charges

We calculate the formal charge of an atom in a molecule or polyatomic ions as follows:

Formal Charge = (valence electrons of the "free" element) - (unshared electrons) - (bonds).

We can double-check formal charge calculations by determining the sum of the formal charges for the whole structure. The sum of the formal charges of all atoms in a molecule must be zero; the sum of the formal charges in an ion should equal the charge of the ion.

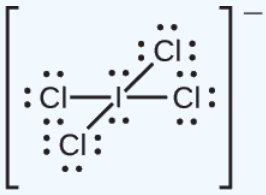
We must remember that the formal charge calculated for an atom is not the *actual* charge of the atom in the molecule. Formal charge is only a useful bookkeeping procedure; it does not indicate the presence of actual charges.

Calculating Formal Charge from Lewis Structures

Assign formal charges to each atom in the interhalogen ion ICl_4^-.

Solution

We divide the bonding electron pairs equally for all I–Cl bonds:



We assign lone pairs of electrons to their atoms. Each Cl atom now has seven electrons assigned to it, and the I atom has eight.

Subtract this number from the number of valence electrons for the neutral atom:

- I: 7 – 8 = –1
- Cl: 7 – 7 = 0

The sum of the formal charges of all the atoms equals –1, which is identical to the charge of the ion (–1).

Exercise 1.5.1.3.1

Calculate the formal charge for each atom in the carbon monoxide molecule:



Answer

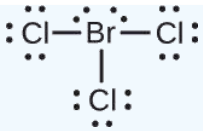
C −1, O +1

Example: Calculating Formal Charge from Lewis Structures

Assign formal charges to each atom in the interhalogen molecule $BrCl_3$.

Solution

Assign one of the electrons in each Br–Cl bond to the Br atom and one to the Cl atom in that bond:



Assign the lone pairs to their atom. Now each Cl atom has seven electrons and the Br atom has seven electrons.

Subtract this number from the number of valence electrons for the neutral atom. This gives the formal charge:

- Br: 7 – 7 = 0
- Cl: 7 – 7 = 0

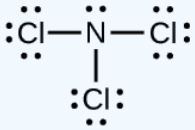
All atoms in $\mathbf{BrCl_3}$ have a formal charge of zero, and the sum of the formal charges totals zero, as it must in a neutral molecule.

? Exercise 1.5.1.3.2

Determine the formal charge for each atom in $\mathbf{NCl_3}$.

Answer

N: 0; all three Cl atoms: 0



1.5.1.3: Formal Charge is shared under a CC BY-NC-SA 4.0 license and was authored, remixed, and/or curated by LibreTexts.

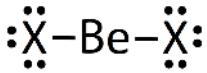
- **7.5: Formal Charges and Resonance** by OpenStax is licensed CC BY 4.0. Original source: https://openstax.org/details/books/chemistry-2e.

1.5.1.4: Lewis fails to predict unusual cases- Boron and Beryllium

Two notable cases where Lewis theory fails to predict structure are the cases of beryllium (**Be**) and boron (**B**). These two atoms are in period 2 ($n = 2$) of the periodic table and their atoms have the valence electron configurations of $2s^2$ and $2s^2 2p^1$, respectively.

Beryllium

The Lewis electron dot structures are shown below for BeX_2, where **X** is one of the halogens, **F** or **Cl**.



Each of the structures above would predict a linear geometry for the BeX_2 molecule. Together the three resonance structures suggest partial double-bond character in the Be-X bond, which results in an intermediate bond length between a single and double bond.

There are issues with each of these resonance structures. The structure on the left would predict only four electrons around **Be**; thus, the atom does not fulfill the octet rule. The structure on the left suggests multiple bonds for the halogen (**X**) and high separation of charge with formal charge on each atom. The structure in the middle is a mix of these problems. None of these situations is ideal according to Lewis theory. Further, experimental data is not consistent with any of these structures or their resonance hybrid (except in the case of $BeCl_2$ at very high temperatures).

It turns out that the monomer of BeX_2 does exist, but only at very high temperatures and low pressures. Even under extreme conditions, the monomer is not particularly stable due to the electron deficiency around **Be**.

BeF_2

At ambient temperature and pressure, BeF_2 is a solid that looks similar to quartz (Figure **1.5.1.4.1**) The Be is four-coordinate with tetrahedral geometry; each F is two-coordinate and the Be-F bond length is 1.54 Å. This structure is possible due to an extended 3-dimensional network in the solid where adjacent BeF_2 units are bonded to one another, as shown in Figure **1.5.1.4.1**.

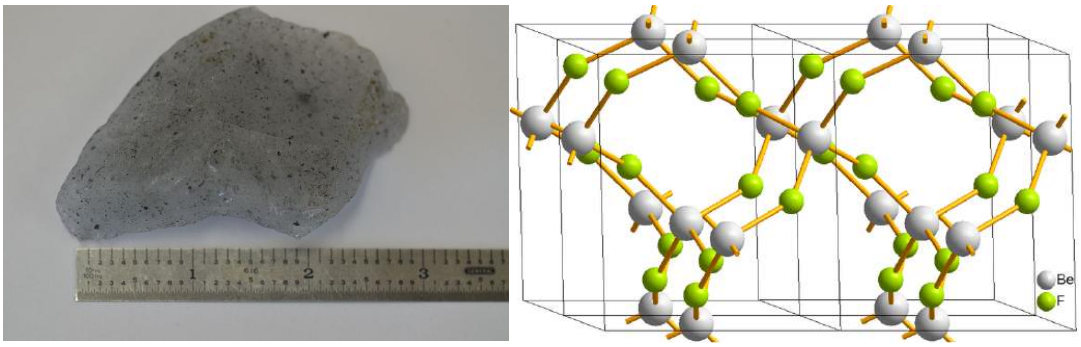


Figure **1.5.1.4.1**: (left) A nugget of beryllium fluoride obtained from Materion. Black spots are carbon (CC BY-SA 3.0; Bckelleher via Wikipedia). (right) BeF2 structure (CC BY-SA 3.0 Unported; Materialscientist via Wikipedia)

In the liquid phase, BeF_2 has a fluctuating tetrahedral structure where Be and F ions exchange. The vapor phase is reached at temperatures higher than 1000 °C (at ~ 1 atm). In the vapor phase, BeF_2 exists as a monomer with linear geometry and a bond length of 1.43 Å, consistent with a double bond between **Be** and **F**.

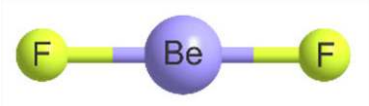


Figure **1.5.1.4.2**: Geometries of BeF_2. (CC BY; Ibon Alkorta and Anthony C. Legoe via Inorganics)

$BeCl_2$

At ambient temperature and pressure, $BeCl_2$ is a solid. As in BeF_2 described above, $BeCl_2$ has four-coordinate, tetrahedral Be and two-coordinate Cl. In contrast to BeF_2, solid $BeCl_2$ is a 1-dimensional polymer consisting of edge-shared tetrahedral.

In the gas phase, $BeCl_2$ exists as a dimer with two chlorine atoms bridging two Be atoms. In the dimer, the Be atoms are 3-coordinate. Bridging Cl atoms are two-coordinate, while terminal Cl atoms are one-coordinate. At higher temperatures in the vapor phase, the linear monomer also exists.

Boron ($2s^2 2p^1$)

Prediction based on Lewis structures:

Lewis structures of $\mathbf{BH_3}$ and $\mathbf{BF_3}$ were described in Exercise 3.1.2, and are drawn again below for convenience.

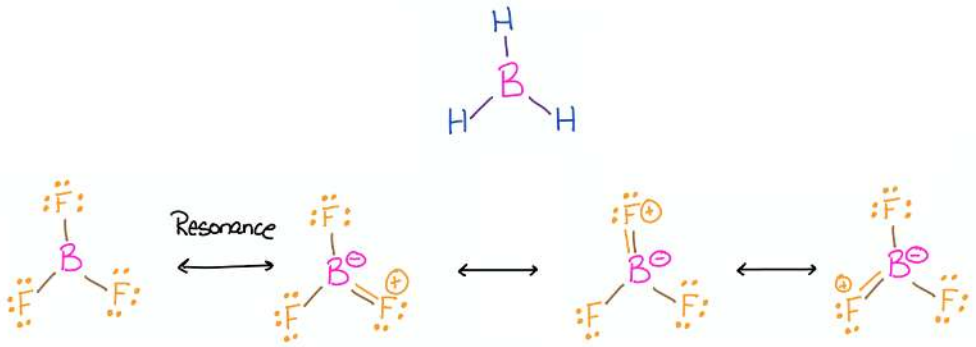


Figure 1.5.1.4.2: Lewis structures of $\mathbf{BH_3}$ and $\mathbf{BF_3}$. (Kathryn Haas; CC-NC-BY-SA)

Boron trihalides

Boron trihalides, like $\mathbf{BF_3}$, have properties that are largely predicted by Lewis structures and VSEPR theory. The Lewis structure for $\mathbf{BF_3}$ includes several resonance structures. The structure with only single bonds is the most common representation for this molecule because the charge separation shown in the other structures is considered to be unfavorable. The highly polarized B-F bond has a dipole moment that lies opposite to the indicated formal charges shown in the resonance structures with double bonds between boron and fluorine.

The resonance hybrid of $\mathbf{BF_3}$ predicts partial double bond character between boron and fluorine, thus a bond length shorter than a single bond. Using the Lewis structures and VSEPR theory, we would predict a trigonal planar geometry around boron. In fact, the actual structure of $\mathbf{BF_3}$ is a monomer with trigonal planar geometry and with bond length that is shorter than a single bond. The case is similar to structures of other boron trihalides as well.

Boron trihalides are electron deficient at the boron center and react readily with Lewis bases. In other words they are strong Lewis acids (electrophiles).

Boron trihydride (BH_3 is really B_2H_6)

The properties of boron trihydride ($\mathbf{BH_3}$) are not predicted by the simple predictions made through Lewis structures and VSEPR. The monomer, BH_3, is not stable, but when dissolved in the presence of a Lewis base, BH_3 can form a stable acid-base adduct. In its pure form, the compound actually exists as a dimeric gas with a molecular unit of B_2H_6 (try drawing a valid Lewis structure for that!). Its unexpected structure includes two H's that bridge the two boron atoms in 3-center-2-electron bonds. You can read more about B_2H_6 on the Wikipedia page for Diborane(6). The unique bonding observed for boron is described more in Chapter 8 and Chapter 15.

This page titled 1.5.1.4: Lewis fails to predict unusual cases- Boron and Beryllium is shared under a CC BY-NC-SA 4.0 license and was authored, remixed, and/or curated by Kathryn Haas.

- **3.1.4: Lewis Fails to Predict Unusual Cases - Boron and Beryllium** by Kathryn Haas is licensed CC BY-NC-SA 4.0.

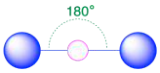
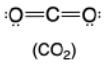
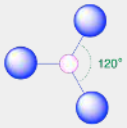
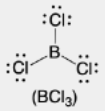
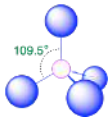
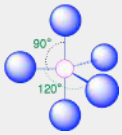
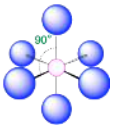
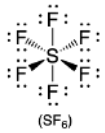
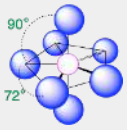
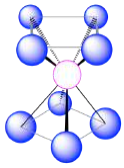
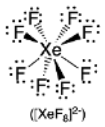
1.5.2: Valence Shell Electron-Pair Repulsion

Introduction to VSEPR

The **Valence Shell Electron Repulsion (VSEPR)** model can predict the structure of most molecules and polyatomic ions in which the central atom is a nonmetal; it also works for some structures in which the central atom is a metal. VSEPR builds on Lewis electron dot structures (discussed in Section 3.1); Lewis structures alone predict only connectivity while the Lewis structure and VSEPR together can predict the geometry of each atom in a molecule. The main idea of VSEPR theory is that pairs of electrons (in bonds and in lone pairs) repel each other. The pairs of electrons (in bonds and in lone pairs) are called "groups". Because electrons repel each other electrostatically, the most stable arrangement of electron groups (i.e., the one with the lowest energy) is the one that minimizes repulsion. Groups are positioned around the central atom in a way that produces the molecular structure with the lowest energy. In other words, the repulsion between groups around an atom favors a geometry in which the groups are as far apart from each other as possible. Although VSEPR is simplistic because it does not account for the subtleties of orbital interactions that influence molecular shapes, it accurately predicts the three-dimensional structures of a large number of compounds.

We can use the VSEPR model to predict the geometry around the atoms in a polyatomic molecule or ion by focusing on the number of electron pairs (groups) around a *central atom* of interest. Groups include bonded and unbonded electrons; a single bond, a double bond, a triple bond, a lone pair of electrons, or even a single unpaired electron each count as one group. The molecule or polyatomic ion is given an AX_mE_n designation, where **A is the central atom**, **X is a bonded atom**, **E is a nonbonding** valence electron group (usually a lone pair of electrons), and m and n are integers. The number of groups is equal to the sum of m and n. Using this information, we can describe the molecular geometry around a central atom, that is, the arrangement of the *bonded atoms* in a molecule or polyatomic ion. The geometries that are predicted from VSEPR when a central atom has only bonded groups ($n = 0$) are listed below in Table **1.5.2.1**. The cases where lone pairs contribute to the total groups ($n \geq 1$) are discussed in the next section about lone pair repulsion.

Table **1.5.2.1**. Geometries predicted using VSEPR theory (bonded groups only).

Groups around central atom (m + n)	Geometry Name	Geometry Sketch	Predicted bond Angle	Example
2	linear		180°	
3	trigonal plane		120°	
4	tetrahedron		109.5°	
5	trigonal bipyramid		90° and 120°	
6	octahedron		90°	
7	pentagonal bipyramid		90° and 72°	
8	square antiprism		70.5°, 99.6° and 109.5°	

Practice

VSEPR to predict Molecular Geometry

You can follow these four steps to predict the geometry around an atom using VSEPR:

1. Draw the Lewis electron structure of the molecule or polyatomic ion.
2. For the central atom of interest, assign the AX_mE_n designation and the total number of groups (m+n).
3. Determine the electron group arrangement around the central atom that minimizes repulsions.
4. Describe the molecular geometry.

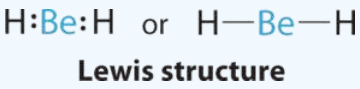
Use the procedure above to complete the exercises below

Exercise 1.5.2.1

Predict the geometry around the central atom in BeH_2 and CO_2.

Answer BeH_2

1. The central atom, beryllium, contributes two valence electrons, and each hydrogen atom contributes one. The Lewis electron structure is



Lewis structure

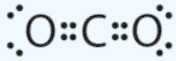
2. There are two groups around the central atom, and both groups are single bonds. Thus BeH_2 is designated as AX_2.

3. We see from Table **1.5.2.1** that the arrangement that minimizes repulsions places the groups 180° apart.

4. From Table **1.5.2.1** we see that with two bonding pairs, the molecular geometry that minimizes repulsions in BeH_2 is *linear.*

Answer CO_2

1. The central atom, carbon, contributes four valence electrons, and each oxygen atom contributes six. The Lewis electron structure is



2. The carbon atom forms two double bonds. Each double bond is counted as one group, so there are two groups around the central atom. Once again, both groups around the central atom are bonds, so CO_2 is designated as AX_2.

3. Like BeH_2, the arrangement that minimizes repulsions places the groups 180° apart.

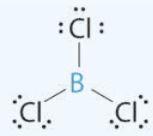
4. VSEPR only recognizes groups around the *central* atom (the carbon). Thus the lone pairs on the oxygen atoms do not influence the molecular geometry. With two bonded groups on the central atom and no lone pairs, the molecular geometry of CO_2 is linear (Table **1.5.2.1**). The structure of CO_2 is shown in Table **1.5.2.1**.

? Exercise 1.5.2.2

Predict the geometry around the central atom in BCl_3 and CO_3^{2-}.

Answer BCl_3

1. The central atom, boron, contributes three valence electrons, and each chlorine atom contributes seven valence electrons. The Lewis electron structure is



Lewis structure

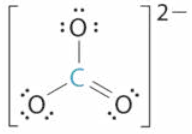
2. There are three groups around the central atom and all are single bonds. The structure is designated as AX_3.

3. To minimize repulsions, the groups are placed 120° apart (Table **1.5.2.1**).

4. From Table **1.5.2.1** we see that with three bonding pairs around the central atom, the molecular geometry of BCl_3 is *trigonal planar*.

Answer CO_3^{2-}

1. The central atom, carbon, has four valence electrons, and each oxygen atom has six valence electrons. The Lewis electron structure of one of three resonance forms is represented as

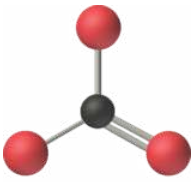


Lewis structure

2. The structure of CO_3^{2-} is a resonance hybrid. It has three identical bonds, each with a bond order of $1\frac{1}{3}$. All electron groups are bonds. With three bonding groups around the central atom, the structure is designated as AX_3.

3. We minimize repulsions by placing the three groups 120° apart (Table **1.5.2.1**).

4. We see from Table **1.5.2.1** that the molecular geometry of CO_3^{2-} is trigonal planar with bond angles of 120°.



Molecular geometry
(trigonal planar)

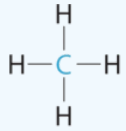
In our next example we encounter the effects of lone pairs and multiple bonds on molecular geometry for the first time.

? Exercise 1.5.2.3

Predict the geometry around the central atom in CH_4, PCl_5 and SF_6.

Answer CH_4

1. The central atom, carbon, contributes four valence electrons, and each hydrogen atom has one valence electron, so the full Lewis electron structure is

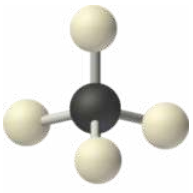


Lewis structure

2. There are four electron groups around the central atom. All electron groups are bonding pairs, so the structure is designated as AX_4.

3. As shown in Table **1.5.2.1**, repulsions are minimized by placing the groups in the corners of a tetrahedron with bond angles of 109.5°.

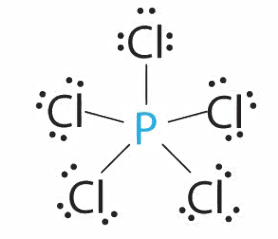
4. With four bonding pairs, the molecular geometry of methane is *tetrahedral* (Table **1.5.2.1**).



Molecular geometry
(tetrahedral)

Answer PCl_5

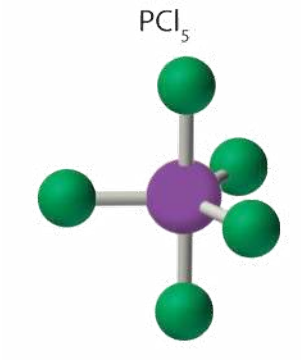
1. Phosphorus has five valence electrons and each chlorine has seven valence electrons, so the Lewis electron structure of PCl_5 is



2. There are five bonding groups around phosphorus, the central atom. All electron groups are bonds, so the structure is designated as AX_5.

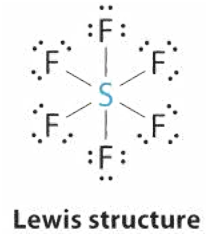
3. The structure that minimizes repulsions is a *trigonal bipyramid*, which consists of two trigonal pyramids that share a base (Table 1.5.2.1).

4. The molecular geometry of PCl_5 is *trigonal bipyramidal*, as shown below. The molecule has three atoms in a plane in *equatorial* positions and two atoms above and below the plane in *axial* positions. The three equatorial positions are separated by 120° from one another, and the two axial positions are at 90° to the equatorial plane. The axial and equatorial positions are not chemically equivalent.



Answer SF_6

1. The central atom, sulfur, contributes six valence electrons, and each fluorine atom has seven valence electrons, so the Lewis electron structure is

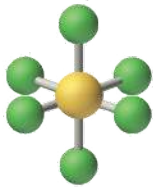


With an expanded valence, this species is an exception to the octet rule.

2. There are six electron groups around the central atom, each a bonding pair. We see from Figure 1.5.2.2 that the geometry that minimizes repulsions is *octahedral*.

3. With only bonding pairs, SF_6 is designated as AX_6. All positions are chemically equivalent, so all electronic interactions are equivalent.

4. There are six nuclei, so the molecular geometry of SF_6 is octahedral.



Molecular geometry
(octahedral)

This page titled 1.5.2: Valence Shell Electron-Pair Repulsion is shared under a CC BY-NC-SA 4.0 license and was authored, remixed, and/or curated by Kathryn Haas.

- **3.2: Valence Shell Electron-Pair Repulsion** by Kathryn Haas is licensed CC BY-NC-SA 4.0.

1.5.2.1: Lone Pair Repulsion

In the previous section, we saw how to use VSEPR to predict the geometry around a central atom based on the number of groups attached to a central atom. However, our previous discussion was limited to the simple cases where all of the groups were bonded groups (i.e., in the designation AX_mE_n , n=0). When all of the groups are bonds, the geometries can be predicted using information in Table 3.2.1 in the previous section. Now we will consider cases where one or more of these groups are lone pairs.

Lone pairs have stronger repulsive forces than bonded groups.

When one or more of the groups is a lone pair of electrons (non-bonded electrons), the experimentally-observed geometry around an atom is slightly different than in the case where all groups are bonds. The actual bond angles are similar, but not exactly the same, as those predicted based on the *total number of groups* (the "parent" geometry). When there is a mixture of group types (**lone pairs (E)** ***and*** **bonded groups (X)**) there are three different types of angles to consider: bond angles between two bonded atoms (**X-X** angles), angles between a bonded atom and a lone pair (**X-E** angles), and angles between two lone pairs (**E-E** angles). Empirical evidence shows the following trend in the degree of bond angles around atoms with a mixture of group types:

Trend in bond angles:

E-E >**X-E** >**X-X**

Using empirical evidence as a guide, we can predict that lone pairs repel other electron groups more strongly than bonded pairs. The molecular geometry of molecules with lone pairs of electrons is better predicted when we consider that electronic repulsion created by lone pairs is stronger than the repulsion from bonded groups. It is difficult to predict the exact bond angle based on this principle, but we can predict approximate angles, as described and summarized below in Table **1.5.2.1.1**.

Table **1.5.2.1.1**: Predictions of molecular geometry and bond angles around atoms with a mixture of bonded (X) and unbonded (E) electron groups.

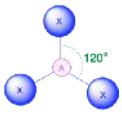
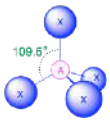
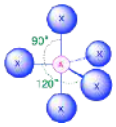
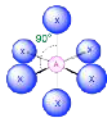
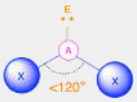
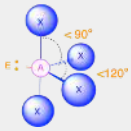
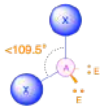
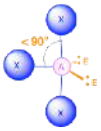
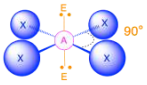
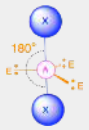
Electron Groups (*m* + *n*)					
	2 (steric number = 2)	**3** (steric number = 3)	**4** (steric number = 4)	**5** (steric number = 5)	**6** (steric number = 6)
Parent Geometry (0 lone pairs) AX_m	 AX_2, linear 180°	 AX_3, trig. plane 120°	 $AX4$, tetrahedron 109.5°	 AX_5, trig. bipyramid 90°, 120°	 AX_6, octahedron 90°
1 lone pair AX_mE_1		 $AX2E_1$, bent <120°	 AX_3E_1, trig. pyramid <109.5°	 AX_4E_1, see-saw <90°, <120°	 AX_5E_1, square pyramid 90°, <90°
2 lone pairs AX_mE_2			 AX_2E_2, bent <109.5°	 AX_3E_2, T-shape <90°	 AX_4E_2, square plane 90°
3 lone pairs AX_mE_3				 AX_2E_3, linear 180°	

Table **1.5.2.1.1** summarizes the geometries and bond angles predicted for nearest-neighbor bonded groups on central atoms with a mixture of lone pairs and bonded groups. The table does not cover all possible situations; it only includes cases where there are two bonded groups in which an X-X angle is measurable between nearest-neighbors. A more detailed description of some selected cases is given below.

Two Electron Groups (m + n = 2)

(Steric number = 2) In the case that there are only two electron groups around a central atom, those groups will lie 180° from one another. This results in a linear molecular geometry with 180° bond angles.

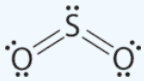
Three Electron Groups (m + n = 3)

(Steric number = 3) In the case that there are three electron groups around a central atom, those groups will lie approximately 120° from one another in space. This results in an electronic geometry that is approximately **trigonal planar**. There are two different molecular geometries that are possible in this category:

- When all of the electron groups are bonds (m = 3 or AX_3), the molecular geometry is a ***trigonal plane*** with **120°** bond angles.
- When there is one lone pair (m=2, n=1 or AX_2E_1), the molecular geometry is ***bent*** with a bond angle that is slightly **less than 120°**.

✔ AX_2E Molecules: Example SO_2

1. The central atom, sulfur, has 6 valence electrons, as does each oxygen atom. With 18 valence electrons, the Lewis electron structure is shown below.



2. There are three electron groups around the central atom: two double bonds and one lone pair. We initially place the groups in a trigonal planar arrangement to minimize repulsions (Table **1.5.2.1.1**).

3. With two bonding pairs and one lone pair, the structure is designated as AX_2E. This designation has a total of three electron pairs, two X and one E. The lone pair occupies more space around the central atom than a bonding pair (even double bonds!). Bonding pairs and lone pairs repel each other electrostatically in the order BP–BP < LP–BP < LP–LP. In SO_2, we have one BP–BP interaction and two LP–BP interactions.

4. The molecular geometry is described only by the positions of the nuclei, *not* by the positions of the lone pairs. Thus, with two nuclei and one lone pair the shape is *bent*, or *V shaped*, which can be viewed as a trigonal planar arrangement with a missing vertex. The O-S-O bond angle is expected to be *less than* 120° because of the extra space taken up by the lone pair.

Four Electron Groups (m + n = 4)

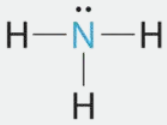
(Steric number = 4) In the case that there are four electron groups around a central atom, those groups will lie approximately 109.5° from one another in space. This results in an electronic geometry that is approximately **tetrahedral**. There are three different molecular geometries that are possible in this category:

- When all electron groups are bonds (m=4 or AX_4), the molecular geometry is a ***tetrahedron*** with bond angles of **109.5°**.
- When there is one lone pair (m=3, n=1 or AX_3E_1), the molecular geometry is a ***trigonal pyramid*** with bond angles of **slightly less than 109.5°**.
- When there are two lone pairs (m=2, n=2 or AX_2E_2), the molecular geometry is ***bent*** with bond angles of **slightly less than 109.5°**.

📌 AX_3E Molecules: Example NH_3

One of the limitations of Lewis structures is that they depict molecules and ions in only two dimensions. With four electron groups, we must learn to show molecules and ions in three dimensions.

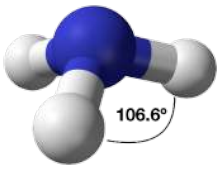
1. In ammonia, the central atom, nitrogen, has five valence electrons and each hydrogen donates one valence electron, producing the Lewis electron structure



Lewis structure

2. There are four electron groups around nitrogen, three bonding pairs and one lone pair. Repulsions are minimized by directing each hydrogen atom and the lone pair to the corners of a tetrahedron.

3. With three bonding pairs and one lone pair, the structure is designated as AX_3E. This designation has a total of four electron pairs, three X and one E. We expect the LP–BP interactions to cause the bonding pair angles to deviate significantly from the angles of a perfect tetrahedron.



The Difference in the Space Occupied by a Lone Pair of Electrons and by a Bonding Pair

As with SO_2, this composite model of electron distribution and negative electrostatic potential in ammonia shows that a lone pair of electrons occupies a larger region of space around the nitrogen atom than does a bonding pair of electrons that is shared with a hydrogen atom.

4. There are three nuclei and one lone pair, so the molecular geometry is *trigonal pyramidal*. In essence, this is a tetrahedron with a vertex missing. However, the H–N–H bond angles are less than the ideal angle of 109.5° because of LP–BP repulsion. The bond angles in ammonia are 106.6°.

AX_2E_2 Molecules: Example H_2O

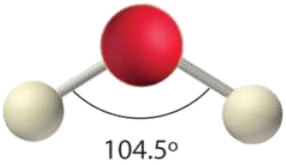
1. Oxygen has six valence electrons and each hydrogen has one valence electron, producing the Lewis electron structure



2. There are four groups around the central oxygen atom, two bonding pairs and two lone pairs. Repulsions are minimized by directing the bonding pairs and the lone pairs to the corners of a tetrahedron.

3. With two bonding pairs and two lone pairs, the structure is designated as AX_2E_2 with a total of four electron pairs. Due to LP–LP, LP–BP, and BP–BP interactions, we expect a significant deviation from idealized tetrahedral angles.

4. With two hydrogen atoms and two lone pairs of electrons, the structure has significant lone pair interactions. There are two nuclei about the central atom, so the molecular shape is *bent*, or *V shaped*, with an H–O–H angle that is even less than the H–N–H angles in NH_3, as we would expect because of the presence of two lone pairs of electrons on the central atom rather than one. This molecular shape is essentially a tetrahedron with two missing vertices.



Five Electron Groups (m + n = 5)

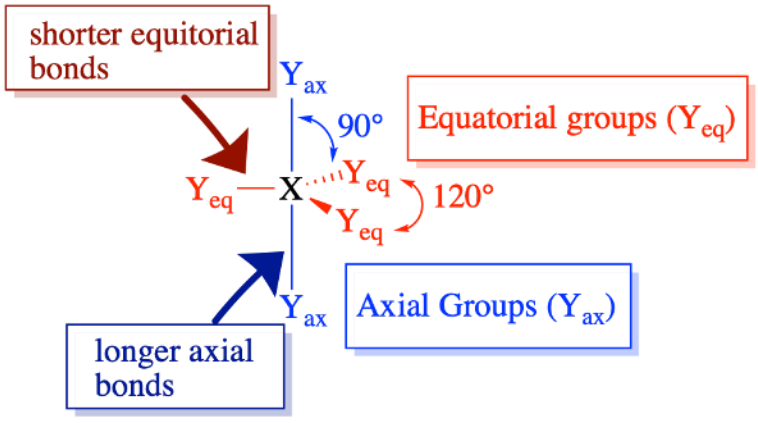


Figure: Trigonal pyramidal molecules (steric number 5) possess different bond angles and lengths for axial (ax) and equatorial (eq) pendant atoms. (CC-BY-NC-SA; Kathryn Haas).

(Steric number = 5) In the case that there are five electron groups around a central atom, there are two different types of positions around the central atom: equatorial positions and axial positions. The three equatorial ligands are 120° from one another and are 90° from each of the two axial ligands. The axial positions have three adjacent groups oriented 90° away in space. Axial groups are thus more crowded than the equatorial positions with only two adjacent groups at 90°. The crowding of axial positions results in slight differences in bond distances; crowded axial groups have longer bonds than the less crowded equatorial groups. Lone pairs of electrons generally prefer to occupy equatorial positions rather than axial positions. The justification for this preference, according to VSEPR theory, is that the lone electron pairs are more repulsive than bonding electron pairs, and thus the lone pairs prefer the less crowded equatorial positions.

The arrangement of five groups around a central atom results in a **trigonal bipyramidal** electronic geometry. There are four different molecular geometries that are possible in this category, depending upon the number of bonded groups and lone pairs of electrons:

- When all electron groups are bonds (m=5 or AX_5), the molecular geometry is a ***trigonal bipyramid*** with bond angles of **120°** and **90°** between adjacent ligands.
- When there is one lone pair (m=4, n=1 or AX_4E_1), the lone pair occupies one of the equatorial positions. The molecular geometry is called a ***see saw*** with bond angles of **slightly less than 120°** and **slightly less than 90°**.
- When there are two lone pairs (m=3, n=2 or AX_3E_2), each lone pair occupies one of the three equatorial positions. The molecular geometry is ***T-shaped*** with bond angles of **slightly less than 120°** and **slightly less than 90°**.
- When there are three lone pairs (m=1, n=3 or AX_3E_2), the lone pairs occupy the three equatorial positions. The molecular geometry is ***linear*** with bond angles of **180°**.

AX_4E Molecules: SF_4

1. The sulfur atom has six valence electrons and each fluorine has seven valence electrons, so the Lewis electron structure is



Lewis structure

With an expanded valence, this species is an exception to the octet rule.

2. There are five groups around sulfur, four bonding pairs and one lone pair. With five electron groups, the lowest energy arrangement is a trigonal bipyramid.

3. We designate SF_4 as AX_4E; it has a total of five electron pairs. However, because the axial and equatorial positions are not chemically equivalent, where do we place the lone pair? If we place the lone pair in the axial position, we have three LP–BP repulsions at 90°. If we place it in the equatorial position, we have two 90° LP–BP repulsions at 90°. With fewer 90° LP–BP repulsions, we can predict that the structure with the lone pair of electrons in the *equatorial position is more stable than the one with the lone pair in the axial position*. We also expect a deviation from ideal geometry because a lone pair of electrons occupies more space than a bonding pair.

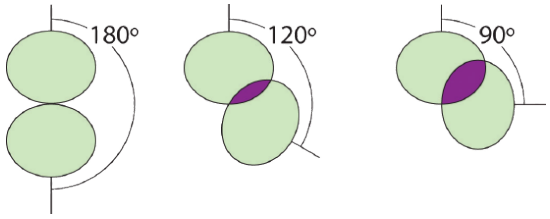
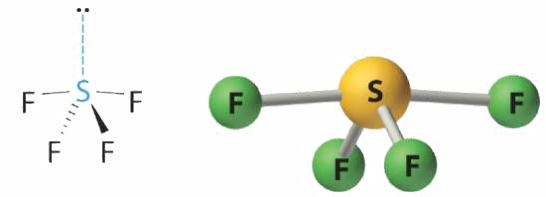


Illustration of the Area Shared by Two Electron Pairs versus the Angle between Them

At 90°, the two electron pairs share a relatively large region of space, which leads to strong repulsive electron–electron interactions.

4. With four nuclei and one lone pair of electrons, the molecular structure is based on a trigonal bipyramid with a missing equatorial vertex; it is described as a *seesaw*. The F_{axial}–S–F_{axial} angle is 173° rather than 180° because of the lone pair of electrons

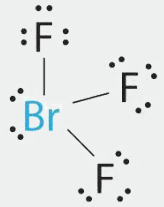
in the equatorial plane.



Molecular geometry (seesaw)

AX_3E_2 Molecules: BrF_3

1. The bromine atom has seven valence electrons, and each fluorine has seven valence electrons, so the Lewis electron structure is

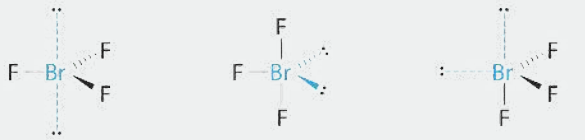


Lewis structure

Once again, we have a compound that is an exception to the octet rule.

2. There are five groups around the central atom, three bonding pairs and two lone pairs. We again direct the groups toward the vertices of a trigonal bipyramid.

3. With three bonding pairs and two lone pairs, the structural designation is AX_3E_2 with a total of five electron pairs. Because the axial and equatorial positions are not equivalent, we must decide how to arrange the groups to minimize repulsions. If we place both lone pairs in the axial positions, we have six LP–BP repulsions at 90°. If both are in the equatorial positions, we have four LP–BP repulsions at 90°. If one lone pair is axial and the other equatorial, we have one LP–LP repulsion at 90° and three LP–BP repulsions at 90°:



Lone pairs axial (a) | Lone pairs equatorial (b) | Lone pairs axial and equatorial (c)

Interactions	(a)	(b)	(c)
90° LP–LP	0	0	1
90° LP–BP	6	4	3

Structure (c) can be eliminated because it has a LP–LP interaction at 90°. Structure (b), with fewer LP–BP repulsions at 90° than (a), is lower in energy. However, we predict a deviation in bond angles because of the presence of the two lone pairs of electrons.

4. The three nuclei in BrF_3 determine its molecular structure, which is described as *T shaped*. This is essentially a trigonal bipyramid that is missing two equatorial vertices. The F_{axial}–Br–F_{axial} angle is 172°, less than 180° because of LP–BP repulsions.

Because lone pairs occupy more space around the central atom than bonding pairs, electrostatic repulsions are more important for lone pairs than for bonding pairs.

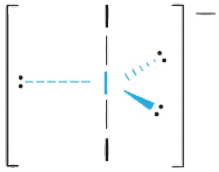
AX_2E_3 Molecules: I_3^-

1. Each iodine atom contributes seven electrons and the negative charge one, so the Lewis electron structure is



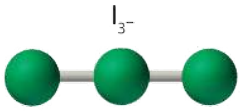
2. There are five electron groups about the central atom in I_3^-, two bonding pairs and three lone pairs. To minimize repulsions, the groups are directed to the corners of a trigonal bipyramid.

3. With two bonding pairs and three lone pairs, I_3^- has a total of five electron pairs and is designated as AX_2E_3. We must now decide how to arrange the lone pairs of electrons in a trigonal bipyramid in a way that minimizes repulsions. Placing them in the equatorial positions eliminates 90° LP–LP repulsions and minimizes the number of 90° LP–BP repulsions.



The three lone pairs of electrons have equivalent interactions with the three iodine atoms, so we do not expect any deviations in bonding angles.

4. With three nuclei and three lone pairs of electrons, the molecular geometry of I_3^- is linear. This can be described as a trigonal bipyramid with three equatorial vertices missing. The ion has an I–I–I angle of 180°, as expected.



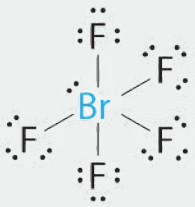
Six Electron Groups (m + n = 6)

(Steric number = 6) In the case that there are six electron groups around a central atom, the nearest groups will lie approximately 90° from one another in space. This results in an electronic geometry that is approximately **octahedral**. There are three relevant molecular geometries in this category:

- When all electron groups are bonds (m=6 or AX_6), the molecular geometry is an ***octahedron*** with bond angles of **90°** between adjacent bonds.
- When there is one lone pair (m=5, n=1 or AX_5E_1) we now distinguish between the axial and equitorial positions; the lone pair is considered to be in one of the axial positions, while the bond directly opposite of the lone pair is the axial bond. The molecular geometry is a ***square pyramid*** with bond angles of **90°** between adjacent equatorial bonds and **slightly less than 90°** between the axial bond and equatorial groups.
- When there are two lone pairs (m=4, n=2 or AX_4E_2), the lone pairs are opposite of one another and each occupy an axial position. The molecular geometry is ***square planar*** with bond angles of **90°**.

AX_5E Molecules: BrF_5

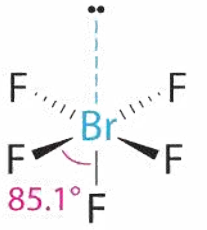
1. The central atom, bromine, has seven valence electrons, as does each fluorine, so the Lewis electron structure is



Lewis structure

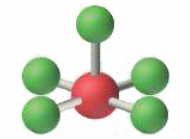
With its expanded valence, this species is an exception to the octet rule.

2. There are six electron groups around the Br, five bonding pairs and one lone pair. Placing five F atoms around Br while minimizing BP–BP and LP–BP repulsions gives the following structure:



3. With five bonding pairs and one lone pair, BrF_5 is designated as AX_5E; it has a total of six electron pairs. The BrF_5 structure has four fluorine atoms in a plane in an equatorial position and one fluorine atom and the lone pair of electrons in the axial positions. We expect all F_{axial}–Br–$F_{equatorial}$ angles to be less than 90° because of the lone pair of electrons, which occupies more space than the bonding electron pairs.

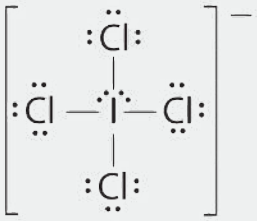
4. With five nuclei surrounding the central atom, the molecular structure is based on an octahedron with a vertex missing. This molecular structure is *square pyramidal*. The F_{axial}–B–$F_{equatorial}$ angles are 85.1°, less than 90° because of LP–BP repulsions.



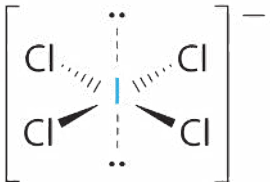
Molecular geometry
(square pyramidal)

AX_4E_2 Molecules: ICl_4^-

1. The central atom, iodine, contributes seven electrons. Each chlorine contributes seven, and there is a single negative charge. The Lewis electron structure is

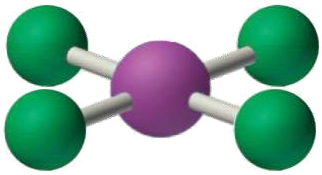


2. There are six electron groups around the central atom, four bonding pairs and two lone pairs. The structure that minimizes LP–LP, LP–BP, and BP–BP repulsions is



3. ICl_4^- is designated as AX_4E_2 and has a total of six electron pairs. Although there are lone pairs of electrons, with four bonding electron pairs in the equatorial plane and the lone pairs of electrons in the axial positions, all LP–BP repulsions are the same. Therefore, we do not expect any deviation in the Cl–I–Cl bond angles.

4. With five nuclei, the ICl4− ion forms a molecular structure that is *square planar*, an octahedron with two opposite vertices missing.



Summary

The arrangement of bonded atoms in a molecule or polyatomic ion is crucial to understanding the chemistry of a molecule, but Lewis electron structures give no information about **molecular geometry**. The **valence-shell electron-pair repulsion (VSEPR) model** allows us to predict which of the possible structures is actually observed in most cases. VSEPR is based on the assumption that pairs of electrons occupy space, and the lowest-energy structure is the one that minimizes repulsions between electron pairs. In the VSEPR model, the molecule or polyatomic ion is given an AX_mE_n designation, where A is the central atom, X is a bonded atom, E is a nonbonding valence electron group (usually a lone pair of electrons), and *m* and *n* are integers. Each group around the central atom is designated as a bonding pair (BP) or lone (nonbonding) pair (LP). From the BP and LP interactions we can predict both the relative positions of the atoms and the angles between the bonds, called the **bond angles**. From this we can describe the **molecular geometry**. The VSEPR model can be used to predict the shapes of many molecules and polyatomic ions, but it gives no information about bond lengths and the presence of multiple bonds. A combination of VSEPR and a bonding model, such as Lewis electron structures, is necessary to understand the presence of multiple bonds.

The relationship between the number of electron groups around a central atom, the number of lone pairs of electrons, and the molecular geometry is summarized in Table **1.5.2.1.1**.

Example Excercises

✔ Example 1.5.2.1.1

Using the VSEPR model, predict the molecular geometry of each molecule or ion.

1. PF_5 (phosphorus pentafluoride, a catalyst used in certain organic reactions)
2. H_3O^+ (hydronium ion)

Given: two chemical species

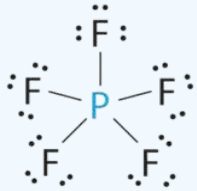
Asked for: molecular geometry

Strategy:

A. Draw the Lewis electron structure of the molecule or polyatomic ion.
B. Determine the electron group arrangement around the central atom that minimizes repulsions.
C. Assign an AX_mE_n designation; then identify the LP–LP, LP–BP, or BP–BP interactions and predict deviations in bond angles.
D. Describe the molecular geometry.

Solution:

1. **A** The central atom, P, has five valence electrons and each fluorine has seven valence electrons, so the Lewis structure of PF_5 is



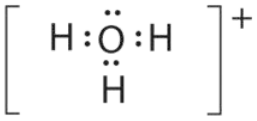
B There are five bonding groups about phosphorus. The structure that minimizes repulsions is a trigonal bipyramid.

C All electron groups are bonding pairs, so PF_5 is designated as AX_5. Notice that this gives a total of five electron pairs. With no lone pair repulsions, we do not expect any bond angles to deviate from the ideal.

D The PF_5 molecule has five nuclei and no lone pairs of electrons, so its molecular geometry is trigonal bipyramidal.



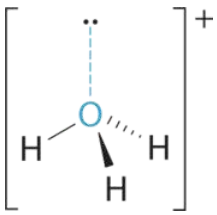
- **A** The central atom, O, has six valence electrons, and each H atom contributes one valence electron. Subtracting one electron for the positive charge gives a total of eight valence electrons, so the Lewis electron structure is



B There are four electron groups around oxygen, three bonding pairs and one lone pair. Like NH_3, repulsions are minimized by directing each hydrogen atom and the lone pair to the corners of a tetrahedron.

C With three bonding pairs and one lone pair, the structure is designated as AX_3E and has a total of four electron pairs (three X and one E). We expect the LP–BP interactions to cause the bonding pair angles to deviate significantly from the angles of a perfect tetrahedron.

D There are three nuclei and one lone pair, so the molecular geometry is *trigonal pyramidal*, in essence a tetrahedron missing a vertex. However, the H–O–H bond angles are less than the ideal angle of 109.5° because of LP–BP repulsions:



? Exercise 1.5.2.1.1

Using the VSEPR model, predict the molecular geometry of each molecule or ion.

a. XeO_3
b. PF_6^-
c. NO_2^+

Answer a

trigonal pyramidal

Answer b

octahedral

Answer c

linear

Example 1.5.2.1.2

Predict the molecular geometry of each molecule.

1. XeF_2
2. $SnCl_2$

Given: two chemical compounds

Asked for: molecular geometry

Strategy:

Use the strategy given in Example 1.5.2.1.1.

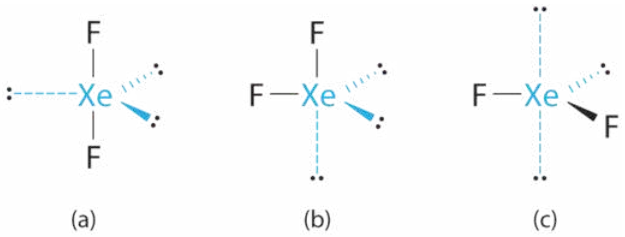
Solution:

1. **A** Xenon contributes eight electrons and each fluorine seven valence electrons, so the Lewis electron structure is



B There are five electron groups around the central atom, two bonding pairs and three lone pairs. Repulsions are minimized by placing the groups in the corners of a trigonal bipyramid.

C From B, XeF_2 is designated as AX_2E_3 and has a total of five electron pairs (two X and three E). With three lone pairs about the central atom, we can arrange the two F atoms in three possible ways: both F atoms can be axial, one can be axial and one equatorial, or both can be equatorial:

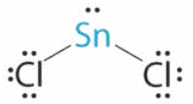


Interactions			
90 LP–LP	0	2	2

The structure with the lowest energy is the one that minimizes LP–LP repulsions. Both (b) and (c) have two 90° LP–LP interactions, whereas structure (a) has none. Thus both F atoms are in the axial positions, like the two iodine atoms around the central iodine in I_3^-. All LP–BP interactions are equivalent, so we do not expect a deviation from an ideal 180° in the F–Xe–F bond angle.

D With two nuclei about the central atom, the molecular geometry of XeF_2 is linear. It is a trigonal bipyramid with three missing equatorial vertices.

- **A** The tin atom donates 4 valence electrons and each chlorine atom donates 7 valence electrons. With 18 valence electrons, the Lewis electron structure is



B There are three electron groups around the central atom, two bonding groups and one lone pair of electrons. To minimize repulsions the three groups are initially placed at 120° angles from each other.

C From B we designate $SnCl_2$ as AX_2E. It has a total of three electron pairs, two X and one E. Because the lone pair of electrons occupies more space than the bonding pairs, we expect a decrease in the Cl–Sn–Cl bond angle due to increased LP–BP repulsions.

D With two nuclei around the central atom and one lone pair of electrons, the molecular geometry of $SnCl_2$ is bent, like SO_2, but with a Cl–Sn–Cl bond angle of 95°. The molecular geometry can be described as a trigonal planar arrangement with one vertex missing.

? Exercise 1.5.2.1.2

Predict the molecular geometry of each molecule.

a. SO_3
b. XeF_4

Answer a

trigonal planar

Answer b

square planar

This page titled 1.5.2.1: Lone Pair Repulsion is shared under a CC BY-NC-SA 4.0 license and was authored, remixed, and/or curated by Kathryn Haas.

- **3.2.1: Lone Pair Repulsion** by Kathryn Haas is licensed CC BY-NC-SA 4.0.
- **3.2.2: Multiple Bonds** by Kathryn Haas is licensed CC BY-NC-SA 4.0.

1.5.2.2: Multiple Bonds

In the previous sections, we saw how to predict the approximate geometry around an atom using VSEPR theory, and we learned that lone pairs of electrons slightly distort bond angles from the "parent" geometry. This page discusses the effect of multiple (double and triple) bonds between bonded atoms.

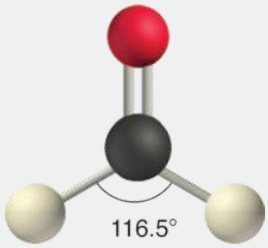
Double and triple bonds are more repulsive than single bonds

VSEPR theory predicts that double and triple bonds have stronger repulsive forces than single bonds. Like lone pairs of electrons, multiple bonds occupy more space around the central atom than a single bond. The result is that bond angles are slightly distorted compared to the parent geometry. Since a multiple bond has a higher electron density than a single bond, its electrons occupy more space than those of a single bond. Double and triple bonds distort bond angles in a way similar to what lone pairs do. Due to the stronger repulsion, double and triple bonds occupy positions similar to those of lone pairs in groups with 5 and 6 electron groups.

Examples 1.5.2.2.1

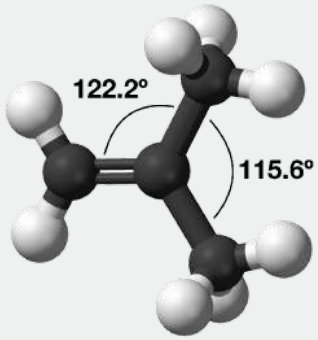
CH_2O

In a molecule such as CH_2O (AX_3), whose structure is shown below, the double bond repels the single bonds more strongly than the single bonds repel each other. This causes a deviation from ideal geometry (an H–C–H bond angle of 116.5° rather than 120°).



2-methybutene

In the molecule, $CH_2C(CH_3)_2$, the methyl—C—methyl bond angle is 115.6°, which is less than the 120° bond angle that would be expected of the parent geometry. On the other hand, the acetyl—C—methyl bond angle is greater than 120°, with an actual bond angle of 122.2°.



Atoms with both lone pairs and multiple bonds

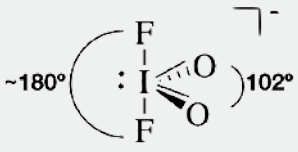
In general, we expect that a lone pair has slightly greater repulsive force than a multiple bond, and that a multiple bond has slightly greater repulsive force than a single bond. The **order of expected repulsive force** is:

$$\text{lone pair} > \text{double or triple bond} > \text{single bond}$$

Examples1.5.2.2.1

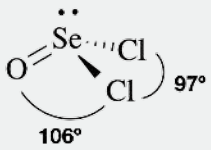
$IO_2F_2^-$

With five electron groups, the IO_2F_2 molecule has an approximately trigonal bipyramidal electronic (parent) geometry. The central iodine atom has a single bond to each of the fluorine atoms, a double bond to each oxygen, and a lone pair. The lone pair and the double bonds will occupy more space around iodine than each of the single bonds. Thus, we expect the lone pair and double bonds to occupy equatorial positions around the central iodine. The O=I=O bond angle is 102° (*much* smaller than the 120° angle expected from the parent geometry). This dramatically smaller angle is a result of the increased repulsion between the lone pair and the double bond.



$SeOCl_2$

With four electron groups, the $SeOCl_2$ molecule has four electron groups and approximately tetrahedral electronic (parent) geometry. It has both a lone pair and a double bond on the central selenium atom. The two chlorine atoms are singly bonded to selenium, while the oxygen is double bonded. The lone pair is most repulsive, followed by the double bonded oxygen, and then the chlorine bonds. This gives a Cl—Se—Cl bond angle of 97° and a Cl—Se—O bond angle of 106°; both angles are less than the 109.5° angles expected for the ideal tetrahedral geometry.



Practice

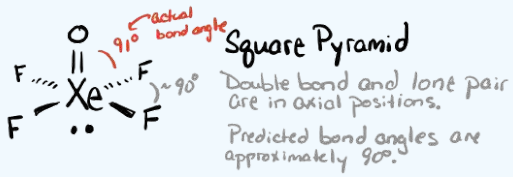
Exercise 1.5.2.2.1

Use VSEPR theory to predict the geometries and draw the structures of the following.

a. $XeOF_4$
b. NO_2^-
c. $SOCl_2$
d. IOF_3^-

Answer a

This molecule has six electron groups around the central Xe atom (steric number 6), and thus has an approximately octahdral electronic (parent) geometry. There is a double bond to O and a lone pair, both of which are more strongly repulsive than the single bonds to F. The double bond and lone pair will be directly opposite to each other, designated as axial positions. The result is a square pyramidal molecular geometry. VSEPR theory predicts F—Xe—F bond angles of 90°. As a general rule, lone pairs are slightly more repulsive than multiple bonds, and so we might expect the O—Xe—F bond angles to be <90°; *however in this case the actual O—Xe—F bond angle is observed to be 91°* (you could not have predicted the latter).



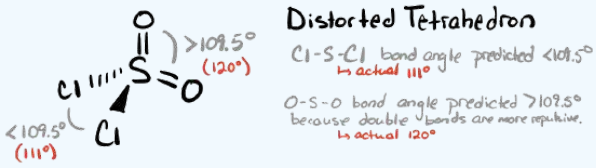
Answer b

This molecule has three electron groups around the central atom: one lone pair and two double bonds to oxygen atoms. This results in an approximately trigonal planar electronic (parent geometry). We expect the lone pair to be slightly more repulsive than double bonds, and so we expect the O—N—O bond angle to be slightly less than 120°. *The actual O—N—O angle is 115°.*



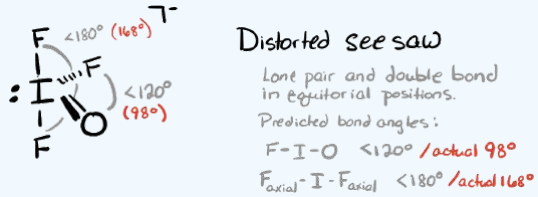
Answer c

This molecule has four electron groups (steric number 4) with an approximately tetrahedral electronic (parent) geometry. Each double bonded oxygen will take up more space around the central S than the single bonded Cl atoms. We should expect the double bonds to repel each other more strongly than they repel each single bond, with the least repulsive interaction being between the two single bonds. The bond angle for Cl—S—Cl is expected to be <109.5° according to VSEPR theory (however, it is actually 111°). We would expect the bond angle for O—S—O to be larger than the angle for Cl—S—Cl and for Cl—S—O. The O—S—O bond angle is predicted to be >109.5° (and the actual bond angle is 120°). The molecular geometry is a distorted tetrahedron.



Answer d

This molecule has five electron groups (steric number 5) with an approximately trigonal bipyramidal electronic (parent) geometry. There is one lone pair, a double bond to O, and three single bonds to F atoms around the central I atom. The lone pair and double bond are most repulsive, and should occupy the less crowded equatorial positions rather than the more crowded axial positions. This results in a seesaw molecular geometry. With the more repulsive lone pair and the strongest equatorial repulsive force being between the double bond and lone pair, we should expect the $F_{equatorial}$—I—O bond angle to be less than the 120° angle expected for the parent geometry (*it is actually much less, at 98°*). Due to repulsion between the axial F atoms and both the lone pair and double bond, we should expect the F—S—F bond angles to be compressed. The F_{axial}—I—F_{axial} is actually 168°.



References

- Miessler, G.; Fischer, P.J.; Tarr, D. (2014). Inorganic Chemistry. New Jersey: Prentice-Hall. pp. 55

This page titled 1.5.2.2: Multiple Bonds is shared under a CC BY-NC-SA 4.0 license and was authored, remixed, and/or curated by Kathryn Haas.

- **3.2.2: Multiple Bonds** by Kathryn Haas is licensed CC BY-NC-SA 4.0.

1.5.2.3: Electronegativity and Atomic Size Effects

Introduction

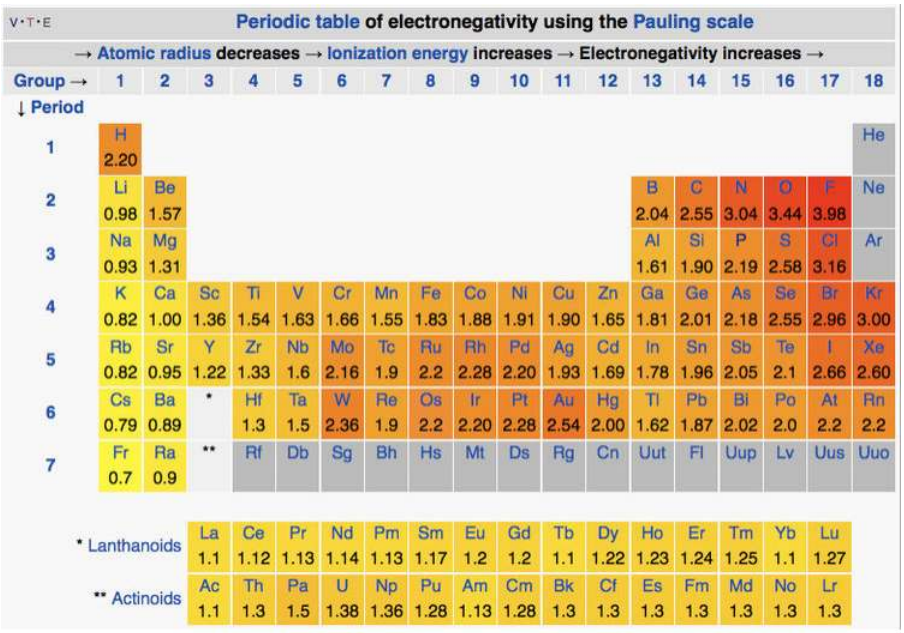
We saw in previous sections how lone pairs of electrons and multiple bonds distort bond angles between non-central atoms (ligands) around a central atom. This section describes how ligand **electronegativity and size also influence bond angles and molecular geometry**. Electronegativity is generally correlated with atomic size going down any group of the periodic table. There are some cases where bond angles can be predicted by these correlations. However, size and electronegativity can also work as competing factors in determining bond angles.

Definitions of Electronegativity

Linus Pauling introduced the first electronegativity scale in 1932 in order to explain the extra stability of molecules with polar bonds.[1] The electronegativity of an atom, represented by the Greek letter χ (chi), can be defined as the tendency of an atom to draw electrons to itself in a chemical bond. On the Pauling scale, the electronegativity difference between two atoms A and B was defined in terms of the dissociation energies E_d of the A-A, B-B, and A-B bonds:

$$\chi_A - \chi_B = \sqrt{E_d(AB) - [E_d(AA) + E_d(BB)]/2}$$

where the energies are expressed in electron volts. Pauling's scale of electronegativity ranges from Fluorine (most electronegative = 4.0) to Francium (least electronegative = 0.7). [2,3] The polarity of bonds and assignment of formal charges is predicted by electronegativity differences.



Periodic table of electronegativity using the Pauling scale

→ Atomic radius decreases → Ionization energy increases → Electronegativity increases →

Group →	1	2	3	4	5	6	7	8	9	10	11	12	13	14	15	16	17	18
↓ Period																		
1	H 2.20																	He
2	Li 0.98	Be 1.57											B 2.04	C 2.55	N 3.04	O 3.44	F 3.98	Ne
3	Na 0.93	Mg 1.31											Al 1.61	Si 1.90	P 2.19	S 2.58	Cl 3.16	Ar
4	K 0.82	Ca 1.00	Sc 1.36	Ti 1.54	V 1.63	Cr 1.66	Mn 1.55	Fe 1.83	Co 1.88	Ni 1.91	Cu 1.90	Zn 1.65	Ga 1.81	Ge 2.01	As 2.18	Se 2.55	Br 2.96	Kr 3.00
5	Rb 0.82	Sr 0.95	Y 1.22	Zr 1.33	Nb 1.6	Mo 2.16	Tc 1.9	Ru 2.2	Rh 2.28	Pd 2.20	Ag 1.93	Cd 1.69	In 1.78	Sn 1.96	Sb 2.05	Te 2.1	I 2.66	Xe 2.60
6	Cs 0.79	Ba 0.89	*	Hf 1.3	Ta 1.5	W 2.36	Re 1.9	Os 2.2	Ir 2.20	Pt 2.28	Au 2.54	Hg 2.00	Tl 1.62	Pb 1.87	Bi 2.02	Po 2.0	At 2.2	Rn 2.2
7	Fr 0.7	Ra 0.9	**	Rf	Db	Sg	Bh	Hs	Mt	Ds	Rg	Cn	Uut	Fl	Uup	Lv	Uus	Uuo

* Lanthanoids	La 1.1	Ce 1.12	Pr 1.13	Nd 1.14	Pm 1.13	Sm 1.17	Eu 1.2	Gd 1.2	Tb 1.1	Dy 1.22	Ho 1.23	Er 1.24	Tm 1.25	Yb 1.1	Lu 1.27
** Actinoids	Ac 1.1	Th 1.3	Pa 1.5	U 1.38	Np 1.36	Pu 1.28	Am 1.13	Cm 1.28	Bk 1.3	Cf 1.3	Es 1.3	Fm 1.3	Md 1.3	No 1.3	Lr 1.3

Figure 1.5.2.3.1: Table of Pauling electronegativities from Wikipedia's Electronegativity page (click).

While directly relevant to the strength of chemical bonds, the Pauling definition of electronegativity has a significant limitation: calculating each value requires data from several compounds in which specific atoms are bonded. This means that the scale cannot be successfully applied to all situations. To overcome this limitation, alternative electronegativity scales were developed based on different thermochemical measurements or calculations. These other scales are listed in the table below. More thorough descriptions of how values in each scale are calculated are described on Wikipedia's Electronegativity page (click) and a concise history of electronegativity scales is summarized in ref 4.

Scale Developer	Year first described	Characteristics
Linus Pauling[1]	1932	Based on bond energies
Robert S. Mulliken[5,6]	1934	Based on valence electron properties of atoms (electron affinity and ionization energy)
Louis Allred & Eugene G. Rochow[7]	1958	Based on electrostatic force (effective nuclear charge)
Robert T. Sanderson[8]	1983	Based on atomic electron density
Ralph G. Pearson[9]	1985	Related to Hard-Soft Acid-Based theory
Leland C. Allen, Joseph Mann, Terry L. Meek[10,11,12]	1989, 2000	Average ionization energies of valence shell electrons, configuration energies (CE) $$\mathrm{CE} = \frac{n\varepsilon_s + m\varepsilon_p}{n+m}$$ n = number of s electrons m = number of p electrons $\varepsilon_s, \varepsilon_p$ = experimental 1-electron s and p energies

The primary advantage to this scale developed by Mann, Meek, and Allen[12] is that it is based on configuration energy (CE), the average ionization energies of valence electrons in ground state free atoms. A scale based on ionization energies can be calculated more directly for any element. However, a critique of all electronegativity scales, including this one, is that they are all based on assumptions that fail in some cases.

There is a relationship between electronegativity and atomic size because both are related to ionization energy. Like ionization energy, there is a general trend across the periodic table for both electronegativity and atomic size; in general, smaller atoms toward the top right-hand side of the periodic table have greater electronegativity values and smaller atomic size. We will see below that both electronegativity and atomic size influence bond angles and absolute molecular geometry around a central atom. In some cases, the size and electronegativity affects are aligned; in some cases these effects compete.

Electronegativity and Size Influence Bond Angles

Let's begin by examining the bond angles of several trigonal pyramidal molecules. The molecules shown in Figure **1.5.2.3.2** each have three identical "pendant groups" on the central atom (Figure **1.5.2.3.2**). *Pendant atoms* or *pendant groups* are the atoms, or groups of atoms, that are bonded directly to the central atom. The molecules shown here are arranged according to the size of the central and pendant atoms. Central atoms increase in size going down this figure, and pendant atoms increase in size going across from left to right. The bond angles and bond lengths are labeled in each case.

What trends can you identify?

Trends in Size

First, let's examine how the size of the central and pendant groups might influence bond angle. In VSEPR theory, **the size of atoms (or groups of atoms) will affect bond angles due to changes in steric interactions between pendant groups.**

Size of the central atom

Examine the relationship between the size of the central atom and the bond angles in Figure **1.5.2.3.2** (go down any column in the figure). For example, compare NH_3, PH_3, AsH_3, and SbH_3, with bond angles 106.6°, 93.2°, 92.1°, and 91.6°, respectively. In this series, the size of the central atom increases from N to Sb while the size of the pendant atom (hydrogen) remains constant. *As the size of the central atom increases, the bond angles decrease; thus, we observe a negative relationship between size of the central atom and the bond angle in these molecules*. This relationship is explained by sterics. As the central atom increases in size, the

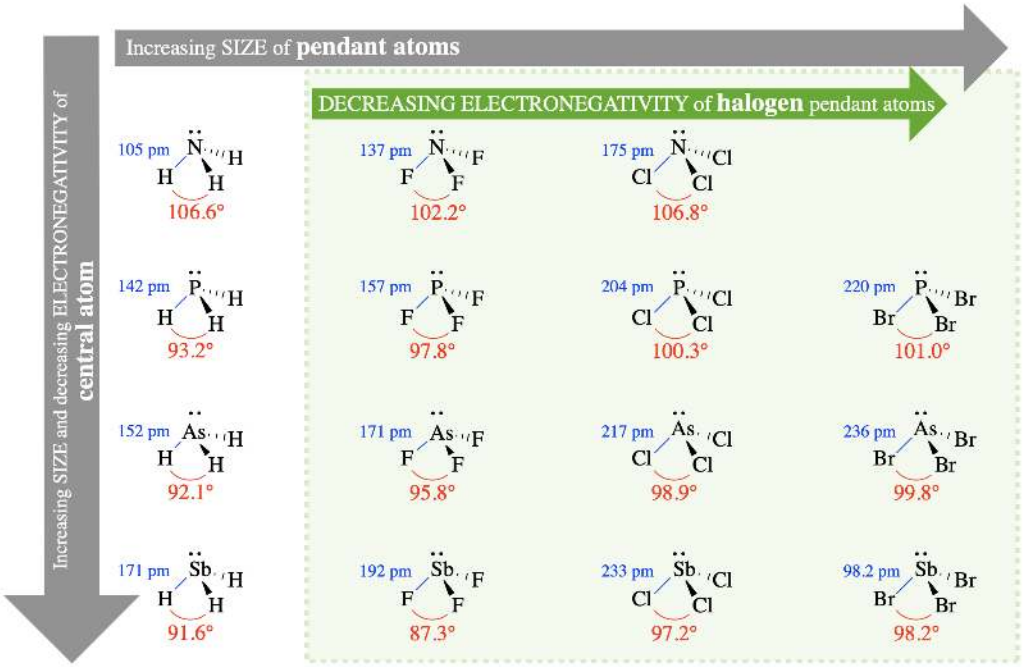


Figure 1.5.2.3.2: Several molecules with trigonal pyramidal electronic geometry are shown arranged according to size of the central atom (increasing size of central atom from top to bottom) and pendant atom (increasing size of pendant atoms from left to right). Bond angles and bond lengths are indicated. (Kathryn Haas; CC-NC-BY-SA)

bond lengths also increase and the pendant atoms are farther from each other in space. In VSEPR theory, this will reduce steric interactions between the pendant groups. Since the lone pair on these molecules is more repulsive than bonded groups, the decrease in steric interactions between bonded groups results in a decrease in bond angles.

Size of the pendant atoms (or groups)

Examine the relationships between size of the halogen pendant atoms and bond angle in Figure 1.5.2.3.2 (go across any row within the shaded region). For example, compare PF_3, PCl_3, and PBr_3, with bond angles 97.8°, 100.3°, and 101.0°, respectively. In this series, the size of the pendant atom increases from F to Br while the central atom remains constant (phosphorous). *As the size of pendant atoms increases, the bond angle increases; thus, we observe a direct relationship between size of the pendant group and the bond angle in these molecules*. Again, we can explain this using sterics. As the size of the pendant atoms increases, sterics between the pendant groups will increase (despite small changes in bond length). Increased steric interactions between pendant groups will prefer larger bond angles between the groups.

This trend fails, however, if we consider the molecules with hydrogen as the pendant atoms. Notice, for example, that H is the smallest pendant atom. If we consider the trend described above, we should assume that XH_3 (where X is a variable atom) would have the smallest bond angle in the series of XH_3, XF_3, XCl_3, and XBr_3. However this is not the case of NH_3, NF_3, and NCl_3, with bond angles 106.6°, 102.2°, and 106.8°, respectively. To explain the variation in these bond angles, we need to consider electronegativity.

Trends in Electronegativity

Now let's examine how electronegativity influences bond angles around a central atom. In VSEPR theory, **electronegativity of atoms/groups will affect bond angles due to changes in the distribution of electron pairs around the central atom (and thus changes in the severity of electron pair repulsion).** This really comes down to bond polarity caused by the difference in electronegativity between the central atom and pendant groups (bond polarity in the context of valence bond theory). In a polar bond, the more electronegative atom will pull electron density towards itself. When a pendant atom is more electronegative, it will pull the bonded electron pair towards itself and away from the central atom; this will reduce the electron pair repulsion between bonded electron pairs on the central atom. A decrease in electron pair repulsion on the central atom should decrease bond angles between the groups (Figure 1.5.2.3.3).

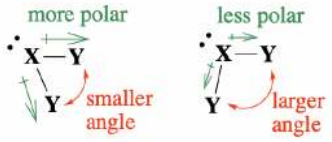


Figure **1.5.2.3.3**. When electron pairs are distributed away from the central atom, repulsions are decreased, allowing smaller bond angles. (Kathryn Haas; CC-NC-BY-SA)

Electronegativity is an alternative explanation to the trends we already examined above in Figure **1.5.2.3.2** . For example, when we compare the halogen pendant atoms (shaded region in Figure **1.5.2.3.2**) , the electronegativity of pendant groups decreases, bond polarity of the bonds decreases, and bond angles increase going from left to right and from F to Br. As more electron density remains on the central atom, electron repulsion between the bonded pairs increases and bond angles increase.

The electronegativity argument can also be used to explain the fact that NH_3 (106.6°) has a larger bond angle than NF_3 (102.2°). This particular case illustrates how electronegativity and size can be competing factors. While electronegativity differences seem to dominate in the case of NH_3 (106.6°) compared to NF_3 (102.2°), size differences still dominate in the cases of other XH_3 and XF_3 examples in Figure **1.5.2.3.2**).

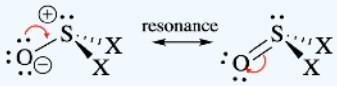
? Exercise 1.5.2.3.1

Predict the geometry and approximate bond angles. Then put the molecules in each series in order of smallest to largest bond angle. Defend your answer.

a. The X-S-X bond angle in OSF_2, $OSCl_2$, $OSBr_2$
b. H_2O, H_2S, H_2Se, H_2Te
c. H_2O, OF_2, OCl_2

Answer (a)

Geometry and predicted bond angles: These are molecules with steric number 4. They can be written as two different resonance structures, and the resonance hybrid would have double bond character between S and O.



We would expect a trigonal pyramidal geometry with all bond angles <109.5° because the lone pair is more repulsive than bonds. Because the double bond is more repulsive than single bonds, we should also expect the O-S-X bond angles to be greater than the X-S-X bond angles.

Trend: This is a series of molecules that varies in the identity of the pendant atoms; the variation is within the halogens. The size of the halogens increases, and the electronegativity decreases in the order F, Cl, Br. Both size and electronegativity would lead us to conclude that the X-S-X bond angles would increase in the order $OSF_2 < OSCl_2 < OSBr_2$

Explanation: (1) Increasing electonegativity of the pendant atom (F > Cl > Br) increases the polarity of the bond and reduces the electron density of the bonded pair on the central atom. This reduces the e-e repulsions of adjacent bonded electron pairs on S, allowing the halogens to become closer. The more electronegative pendant atoms can have smaller bond angles. (2) Increasing size of pendant atoms (F < Cl < Br) increases steric repulsions and increases bond angle. Both explanations lead to the same predicted trend.

The actual measured X-S-X bond angles are OSF_2 (92.3°) / $OSCl_2$ (96.2°) / $OSBr_2$ (98.2°). The trend in these bond angles is consistent with the prediction.

Answer (b)

Geometry and predicted bond angles: These are molecules with steric number 4, bent molecular geometry, with predicted bond angles <109.5° because the two lone pairs are each more repulsive than the bonds. There are two lone pairs and two single bonds to H around each central atom.

Trend: This is a series of molecules that varies in the identity of the central atom. The central atom increases in the order O < S < Se < Te, where Te is the largest element and O is the smallest. Arguments based on size would lead us to predict that the pendant groups of H_2Te would be less sterically crowded and thus have a smaller bond angle than the pendant groups of H_2O. The electronegativity decreases in the order O > S > Se > Te, where O is the most electronegative element and Te is the least. Thus, we expect the bonding electro pairs to be closer to the central atom on O than they would be on Te; we should expect H_2Te to have the least electron pair repulsions and thus smallest bond angle in this series, while H_2O would have the strongest electron pair repulsions and largest bond angles.

Both arguments lead to the same conclusion, that the order of increasing bond angle is $H_2Te < H_2Se < H_2S < H_2O$.

The actual measured bond angles are H_2Te (90.2°) / H_2Se (90.6°) / H_2S (92.1°) / H_2O (104.5). The trend in these bond angles is consistent with prediction.

Answer (c)

Geometry and predicted bond angles: These are molecules with steric number 4, bent molecular geometry, with predicted bond angles <109.5° because the two lone pairs are each more repulsive than the bonds. There are two lone pairs and two single bonds to H around each central atom. (This is similar to the case in (b)).

Trend: This is a series of molecules that varies in the identity of the pendant atoms; two of the molecules have halogens, and the other has hydrogen pendant atoms. This is a case where size and electronegativity will be conflicting factors because trends in electronegativity do not mirror the trend in size.

- *Size:* The size of pendant atoms increases in the order H < F < Cl where H is smallest and Cl is largest. Prediction of bond angles based on size alone would lead to the predicted order of increasing bond angle $H_2O < OF_2 < OCl_2$.
- *Electronegativity*: The electronegativity decreases in the order F > Cl > H where F has the greatest electronegativity and H has the least. Since we expect the most electronegative pendant atoms to have the smallest bond angles, prediction based on electronegativity alone would lead to the predicted order of increasing bond angle $OF_2 < OCl_2 < H_2O$.

The points above illustrate how the two different arguments would lead to different predictions about the trend in bond angle. This makes it difficult to predict the actual order of increasing bond angle. However, we saw above in the example of NH_3 vs NF_3 that electronegativity is more important than size; yet in the case of NH_3 vs NCl_3, the much larger size of the pendant atom is more important. If we apply this lesson to the current problem, we might predict the order $OF_2 < H_2O < OCl_2$, and in fact this more nuanced prediction, based on a similar case, matches the actual order for measured bond angles: OF_2 (103.3°) < H_2O (104.5°) < OCl_2 (110.9°).

Group Electronegativities

You probably heard the terms "electron donating group" and "electron withdrawing group" from your coursework in Organic Chemistry. For example, the acid trifluoroacetic acid (TFA) is more acidic than acetic acid due to the electron withdrawing effects of the CF_3 group compared to CH_3. CF_3 is an electron withdrawing group, while CH_3 is an electron donating group. In other words, CF_3 is more electronegative than CH_3.

The electron withdrawing ability (electronegativity) of groups can be estimated and compared, just as they are with atoms. Although there is no one scale that is used for group electronegativities, and published values even for the same groups vary widely, there are reliable trends within similar groups. The same size and electronegativity factors discussed above that affect bond angles for *pendant atoms*, also can be used to rationalize distorted bond angles for *pendant groups* around a central atom.

? Exercise 1.5.2.3.2

Consider the relative electronegativities and sizes of the pendant atoms/groups in the following examples. Is the trend in bond angles what you would expect from the relative group electronegativities and relative sizes? What, if any, is the more dominant factor in determining the trend?

a. $N(CH_3)_3$ has an C-N-C bond angle of 110.9°, while $N(CF_3)_3$ has a bond angle of 117.9°.
b. The X-S-X bond angles in molecules of the form $SO_2(X)_2$ are: $SO_2(OH)_2$ 101.3°; $SO_2(CF_3)_2$ 102.0°; $SO_2(CH_3)_2$ 102.6°.

Answer (a)

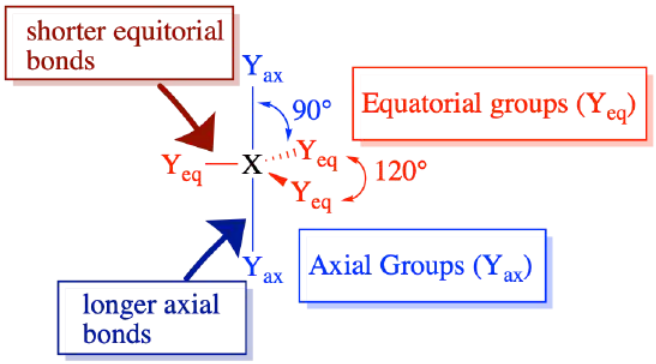
Add texts here. Do not delete this text first.

Answer (b)

Add texts here. Do not delete this text first.

Special case of electronegativity and size in steric number 5 (trigonal bypyramid)

Molecules with steric number 5 are interesting because they posses two different types of positions (equatorial and axial). These positions have unique bond angles and bond lengths. Pendant atoms/groups have different preferences for the axial and equatorial positions that depend somewhat on their electronegativity.



Molecules with steric number 5 possess different bond angles and lengths for axial (ax) and equatorial (eq) pendant atoms. (CC-BY-NC-SA; Kathryn Haas)

In a previous section, we discussed the preference of lone pairs and multiple bonds for the equatorial positions in trigonal bipyramidal molecules. VSEPR theory rationalizes this by assuming that lone pairs and multiple bonds are more repulsive than the electron pairs in single bonds. Equatorial positions are less crowded (with only two closest neighbors at 90°, and two farther neighbors at 120°) compared to axial positions (with three closest neighbors at 90°), thus the more repulsive groups prefer the less crowded equatorial positions.

Pendant groups that are more electronegative result in weaker electron pair repulsion around the central atom, while groups that are less electronegative result in stronger electron-pair repulsion around the central atom (as described above). The result for steric number 5: **bonding pairs to *less electronegative elements* are *more repulsive,* and *generally prefer equatorial* positions.** Still, lone pairs and multiple bonds are more repulsive than single bonds and would show a stronger preference for equatorial positions.

Examples and Nuances

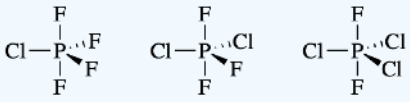
? Exercise 1.5.2.3.3

Some examples of molecule that demonstrate the equatorial preference of less electronegative groups are below. Predict (draw) their structures.

a. PF_4Cl, PF_3Cl_2, and PF_2Cl_3
b. $PF_4(CH_3)$ $PF_3(CH_3)_2$, and $PF_2(CH_3)_3$

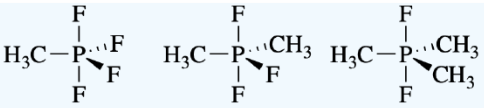
Answer (a)

Cl is less electronegative than F; thus we expect Cl to have stronger preference for the equatorial positions.

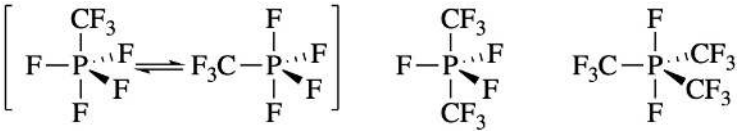


Answer (b)

CH_3, an electron donating group, is less electronegative than F. We expect CH_3 to have a stronger preference for the equatorial positions.



In the exercise above, the structures can be explained by the electronegativity of the pendant groups; less electronegative groups prefer the equatorial positions. There are other similar molecules for which explanations (or predictions) are difficult. For example, the series of molecules below seems to have completely random placement of F and CF_3 groups. **These structures could not be predicted based on VSEPR theory.** It seems that in this case, the more symmetrical arrangements of pendant groups is preferred.



References and resources

1. Pauling, L. (1932). "The Nature of the Chemical Bond. IV. The Energy of Single Bonds and the Relative Electronegativity of Atoms". *J. Am. Chem. Soc.* **54**(9): 3570–3582. doi:10.1021/ja01348a011.
2. Housecroft, Catherine E. et. al. "Inorganic Chemistry" 3rd Edition. Pearson Education Limited 2008. Chapter 2.5 "Electronegativity Values" pgs. 42-44
3. International Union of Pure and Applied Chemistry. "Electronegativity". goldbook.iupac.org/E01990.html.
4. Pearson, R.G. *Acc. Chem. Res.* 1990, 23, 1, 1–2. https://doi.org/10.1021/ar00169a001
5. Mulliken, R. S. (1934). "A New Electroaffinity Scale; Together with Data on Valence States and on Valence Ionization Potentials and Electron Affinities". *J. Chem. Phys.***2** (11): 782–793. doi:10.1063/1.1749394.
6. Mulliken, R. S. (1935). "Electronic Structures of Molecules XI. Electroaffinity, Molecular Orbitals and Dipole Moments". J. Chem. Phys. **3** (9): 573–585. doi:10.1063/1.1749731.
7. Allred, A. L.; Rochow, E. G. (1958). "A scale of electronegativity based on electrostatic force". *Journal of Inorganic and Nuclear Chemistry*. **5** (4): 264–268. doi:10.1016/0022-1902(58)80003-2
8. Sanderson, R. T. (1983). "Electronegativity and bond energy". *Journal of the American Chemical Society*. **105** (8): 2259–2261. doi:10.1021/ja00346a026
9. Pearson, R. G. (1985). "Absolute electronegativity and absolute hardness of Lewis acids and bases". J. Am. Chem. Soc. 107 (24): 6801. doi:10.1021/ja00310a009.
10. Allen, Leland C. (1989). "Electronegativity is the average one-electron energy of the valence-shell electrons in ground-state free atoms". Journal of the American Chemical Society. 111 (25): 9003–9014. doi:10.1021/ja00207a003.
11. Mann, Joseph B.; Meek, Terry L.; Allen, Leland C. (2000). "Configuration Energies of the Main Group Elements". Journal of the American Chemical Society. 122 (12): 2780–2783. doi:10.1021/ja992866e.
12. Mann, Joseph B.; Meek, Terry L.; Knight, Eugene T.; Capitani, Joseph F.; Allen, Leland C. (2000). "Configuration energies of the d-block elements". Journal of the American Chemical Society. 122 (21): 5132–5137. doi:10.1021/ja9928677

Acknowledgment

- Matthew Salem (UC Davis) (Pauling Electronegativity)
- Introduction to Inorganic Chemistry Wikibook (https://chem.libretexts.org/Bookshel..._Bond_Strength)
- Curated or created by Kathryn Haas

This page titled 1.5.2.3: Electronegativity and Atomic Size Effects is shared under a CC BY-NC-SA 4.0 license and was authored, remixed, and/or curated by Kathryn Haas.

- **3.2.3: Electronegativity and Atomic Size Effects** by Kathryn Haas is licensed CC BY-NC-SA 4.0.

1.5.3: Molecular Polarity

Dipole moments occur when there is a separation of charge. They can occur between two ions in an ionic bond or between atoms in a covalent bond; dipole moments arise from differences in electronegativity. The larger the difference in electronegativity, the larger the dipole moment. The distance between the charge separation is also a deciding factor in the size of the dipole moment. The dipole moment is a measure of the polarity of the molecule.

Introduction

When atoms in a molecule share electrons unequally, they create what is called a dipole moment. This occurs when one atom is more electronegative than another, resulting in that atom pulling more tightly on the shared pair of electrons, or when one atom has a lone pair of electrons and the difference of electronegativity vector points in the same way. One of the most common examples is the water molecule, made up of one oxygen atom and two hydrogen atoms. The differences in electronegativity and lone electrons give oxygen a partial negative charge and each hydrogen a partial positive charge.

Dipole Moment

When two electrical charges, of opposite sign and equal magnitude, are separated by a distance, an electric dipole is established. The size of a dipole is measured by its dipole moment (μ). Dipole moment is measured in Debye units, which is equal to the distance between the charges multiplied by the charge (1 Debye equals $3.34 \times 10^{-30}\ C\,m$). The dipole moment of a molecule can be calculated by Equation 1.5.3.1:

$$\vec{\mu} = \sum_i q_i \vec{r}_i \tag{1.5.3.1}$$

where

- $\vec{\mu}$ is the dipole moment vector
- q_i is the magnitude of the i^{th} charge, and
- $\vec{r}_i$ is the vector representing the position of i^{th} charge.

The dipole moment acts in the direction of the vector quantity. An example of a polar molecule is $\mathbf{H_2O}$. Because of the lone pair on oxygen, the structure of $\mathbf{H_2O}$ is bent (via VSEPR theory), which means that the vectors representing the dipole moment of each bond do not cancel each other out. Hence, water is polar.

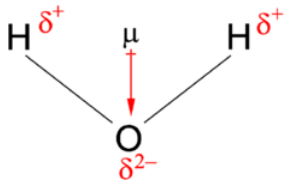


Figure 1.5.3.1: Dipole moment of water. The convention in chemistry is that the arrow representing the dipole moment goes from positive to negative. Physicist tend to use the opposite orientation.

The vector points from positive to negative, on both the molecular (net) dipole moment and the individual bond dipoles. Table A2 shows the electronegativity of some of the common elements. The larger the difference in electronegativity between the two atoms, the more electronegative that bond is. To be considered a polar bond, the difference in electronegativity must be large. The dipole moment points in the direction of the vector quantity of each of the bond electronegativities added together.

It is relatively easy to measure dipole moments: just place a substance between charged plates (Figure 1.5.3.2); polar molecules increase the charge stored on the plates, and the dipole moment can be obtained (i.e., via the capacitance of the system). Nonpolar $\mathbf{CCl_4}$ is not deflected; moderately polar acetone deflects slightly; highly polar water deflects strongly. In general, polar molecules will align themselves: (1) in an electric field, (2) with respect to one another, or (3) with respect to ions (Figure 1.5.3.2).

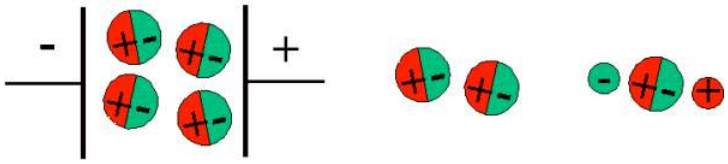


Figure 1.5.3.2: Polar molecules align themselves in an electric field (left), with respect to one another (middle), and with respect to ions (right)

Equation 1.5.3.1 can be simplified for a simple separated two-charge system like diatomic molecules or when considering a bond dipole within a molecule

$$\mu_{diatomic} = Q \times r \tag{1.5.3.2}$$

This bond dipole is interpreted as the dipole from a charge separation over a distance r between the partial charges Q^+ and Q^- (or the more commonly used terms δ^+ - δ^-); the orientation of the dipole is along the axis of the bond. Consider a simple system of a single electron and proton separated by a fixed distance. When the proton and electron are close together, the dipole moment (degree of polarity) decreases. However, as the proton and electron get farther apart, the dipole moment increases. In this case, the dipole moment is calculated as (via Equation 1.5.3.2):

$$\begin{aligned} \mu &= Qr \\ &= (1.60 \times 10^{-19}\, C)(1.00 \times 10^{-10}\, m) \\ &= 1.60 \times 10^{-29}\, C \cdot m \end{aligned}$$

The Debye characterizes the size of the dipole moment. When a proton and electron are 100 pm apart, the dipole moment is $4.80\ D$:

$$\begin{aligned} \mu &= (1.60 \times 10^{-29}\, C \cdot m)\left(\frac{1\ D}{3.336 \times 10^{-30}\, C \cdot m}\right) \\ &= 4.80\ D \end{aligned}$$

$4.80\ D$ is a key reference value and represents a pure charge of +1 and -1 separated by 100 pm. If the charge separation is increased then the dipole moment increases (linearly):

- If the proton and electron are separated by 120 pm:

$$\mu = \frac{120}{100}(4.80\ D) = 5.76\ D \tag{1.5.3.3}$$

- If the proton and electron are separated by 150 pm:

$$\mu = \frac{150}{100}(4.80\ D) = 7.20\ D \tag{1.5.3.4}$$

- If the proton and electron are separated by 200 pm:

$$\mu = \frac{200}{100}(4.80\ D) = 9.60\ D \tag{1.5.3.5}$$

Example 1.5.3.1: Water

The water molecule in Figure 1.5.3.1 can be used to determine the direction and magnitude of the dipole moment. From the electronegativities of oxygen and hydrogen, the difference in electronegativity is 1.2e for each of the hydrogen-oxygen bonds. Next, because the oxygen is the more electronegative atom, it exerts a greater pull on the shared electrons; it also has two lone pairs of electrons. From this, it can be concluded that the dipole moment points from between the two hydrogen atoms toward the oxygen atom. Using the equation above, the dipole moment is calculated to be 1.85 D by multiplying the distance between the oxygen and hydrogen atoms by the charge difference between them and then finding the components of each that point in the direction of the net dipole moment (the angle of the molecule is 104.5˚).

The bond moment of the O-H bond =1.5 D, so the net dipole moment is

$$\mu = 2(1.5)\cos\left(\frac{104.5^\circ}{2}\right) = 1.84\ D$$

Polarity and Structure of Molecules

The shape of a molecule and the polarity of its bonds determine the OVERALL POLARITY of that molecule. A molecule that contains polar bonds might not have any overall polarity, depending upon its shape. The simple definition of whether a complex molecule is polar or not depends upon whether its overall centers of positive and negative charges overlap. If these centers lie at the same point in space, then the molecule has no overall polarity (and is non polar). If a molecule is completely symmetric, then the dipole moment vectors on each molecule will cancel each other out, making the molecule nonpolar. A molecule can only be polar if the structure of that molecule is not symmetric.

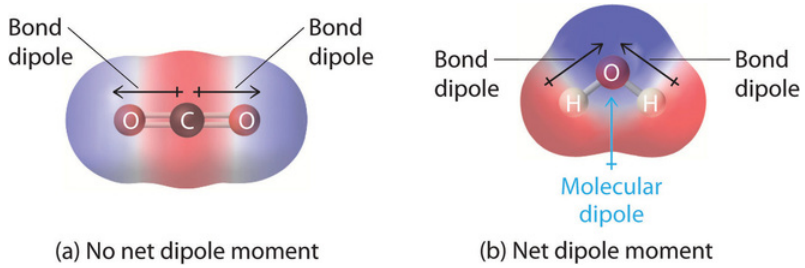


Figure 1.5.3.3: Charge distributions of CO_2 and H_2O\). Blue and red colored regions are negatively and positively signed regions, respectively. (CC BY-SA-NC 3.0; anonymous)

A good example of a nonpolar molecule that contains polar bonds is carbon dioxide (Figure 1.5.3.3*a*). This is a linear molecule and each C=O bond is, in fact, polar. The central carbon will have a net positive charge, and the two outer oxygen atoms a net negative charge. However, since the molecule is linear, these two bond dipoles cancel each other out (i.e. the vector addition of the dipoles equals zero) and the overall molecule has a zero dipole moment ($\mu = 0$).

> *Although a polar bond is a prerequisite for a molecule to have a dipole, not all molecules with polar bonds exhibit dipoles*

For AB_n molecules, where A is the central atom and B are all the same types of atoms, there are certain molecular geometries which are symmetric. Therefore, they will have no dipole even if the bonds are polar. These geometries include linear, trigonal planar, tetrahedral, octahedral and trigonal bipyramid.

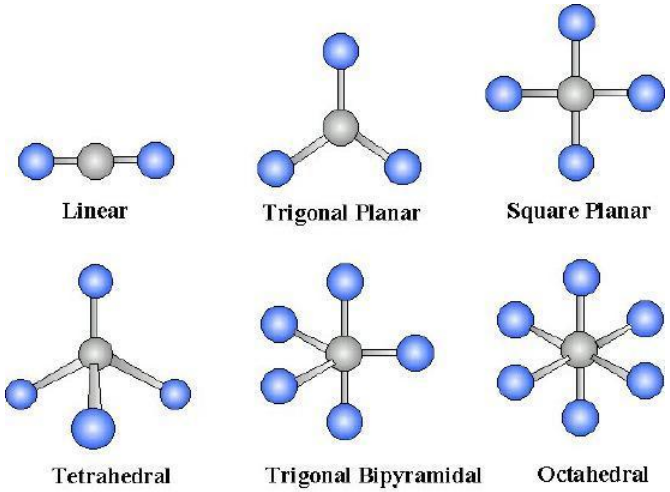
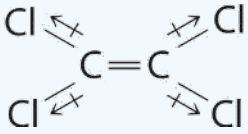


Figure 1.5.3.4: Molecular geometries with exact cancellation of polar bonding to generate a non-polar molecule ($\mu = 0$)

Example 1.5.3.3: C_2Cl_4

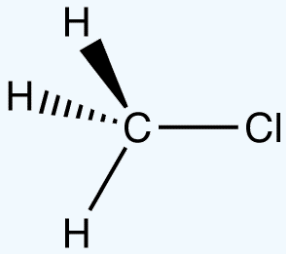
Although the C–Cl bonds are rather polar, the individual bond dipoles cancel one another in this symmetrical structure, and $Cl_2C{=}CCl_2$ does not have a net dipole moment.



Example 1.5.3.3: CH_3Cl

C-Cl, the key polar bond, is 178 pm. Measurement reveals 1.87 D. From this data, % ionic character can be computed. If this bond were 100% ionic (based on proton & electron),

$$\mu = \frac{178}{100}(4.80\ D)$$
$$= 8.54\ D$$



Although the bond length is ***increasing***, the dipole is ***decreasing*** as you move down the halogen group. The electronegativity decreases as we move down the group. Thus, the greater influence is the electronegativity of the two atoms (which influences the ***charge*** at the ends of the dipole).

Table **1.5.3.1**: Relationship between Bond length, Electronegativity and Dipole moments in simple Diatomics

Compound	Bond Length (Å)	Electronegativity Difference	Dipole Moment (D)
HF	0.92	1.9	1.82
HCl	1.27	0.9	1.08
HBr	1.41	0.7	0.82
HI	1.61	0.4	0.44

References

1. *Housecroft, Catherine E. and Alan G. Sharpe. Inorganic Chemistry. 3rd ed. Harlow: Pearson Education, 2008. Print. (Pages 44-46)*
2. *Tro, Nivaldo J. Chemistry: A Molecular Approach. Upper Saddle River: Pearson Education, 2008. Print. (Pages 379-386)*

1.5.3: Molecular Polarity is shared under a CC BY-NC-SA 4.0 license and was authored, remixed, and/or curated by LibreTexts.

- **Dipole Moments** by Delmar Larsen, Mike Blaber is licensed CC BY 4.0.

1.5.4: Hydrogen Bonding

A hydrogen bond is an intermolecular force (IMF) that forms a special type of dipole-dipole attraction when a hydrogen atom bonded to a strongly electronegative atom exists in the vicinity of another electronegative atom with a lone pair of electrons. Intermolecular forces (IMFs) occur between molecules. Other examples include ordinary dipole-dipole interactions and dispersion forces. Hydrogen bonds are are generally stronger than ordinary dipole-dipole and dispersion forces, but weaker than true covalent and ionic bonds.

The evidence for hydrogen bonding

Many elements form compounds with hydrogen. If you plot the boiling points of the compounds of the group 14 elements with hydrogen, you find that the boiling points increase as you go down the group.

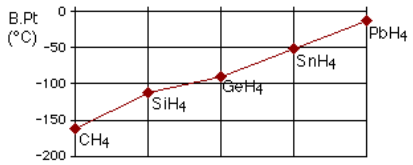


Figure 1: Boiling points of group 14 elemental halides.

The increase in boiling point happens because the molecules are getting larger with more electrons, and so van der Waals dispersion forces become greater. If you repeat this exercise with the compounds of the elements in groups 15, 16, and 17 with hydrogen, something odd happens.

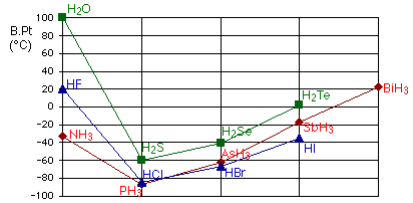


Figure 2: Boiling points of group 15-17 elemental halides.

Although the same reasoning applies for group 4 of the periodic table, the boiling point of the compound of hydrogen with the first element in each group is abnormally high. In the cases of NH_3, H_2O and HF there must be some additional intermolecular forces of attraction, requiring significantly more heat energy to break the IMFs. These relatively powerful intermolecular forces are described as hydrogen bonds.

Origin of Hydrogen Bonding

The molecules capable of hydrogen bonding include the following:

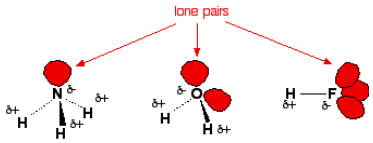


Figure 3: The lone pairs responsible for hydrogen bonding in NH_3, H_2O, and HF. The solid line represents a bond in the plane of the screen or paper. Dotted bonds are going back into the screen or paper away from you, and wedge-shaped ones are coming out towards you.

Notice that in each of these molecules:

- The hydrogen is attached directly to a highly electronegative atoms, causing the hydrogen to acquire a highly positive charge.
- Each of the highly electronegative atoms attains a high negative charge and has at least one "active" lone pair. Lone pairs at the 2-level have electrons contained in a relatively small volume of space, resulting in a high negative charge density. Lone pairs at higher levels are more diffuse and, resulting in a lower charge density and lower affinity for positive charge.

> *If you are not familiar with electronegativity, you should follow this link before you go on.*

Consider two water molecules coming close together.

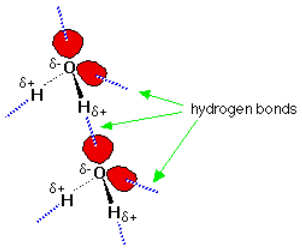


Figure 4: Hydrogen bonding in water

The δ^+ hydrogen is so strongly attracted to the lone pair that it is almost as if you were beginning to form a co-ordinate (dative covalent) bond. It doesn't go that far, but the attraction is significantly stronger than an ordinary dipole-dipole interaction. Hydrogen bonds have about a tenth of the strength of an average covalent bond, and are constantly broken and reformed in liquid water. If you liken the covalent bond between the oxygen and hydrogen to a stable marriage, the hydrogen bond has "just good friends" status.

Water is an ideal example of hydrogen bonding. Notice that each water molecule can potentially form four hydrogen bonds with surrounding water molecules: two with the hydrogen atoms and two with the with the oxygen atoms. There are exactly the right numbers of δ^+ hydrogens and lone pairs for every one of them to be involved in hydrogen bonding.

This is why the boiling point of water is higher than that of ammonia or hydrogen fluoride. In the case of ammonia, the amount of hydrogen bonding is limited by the fact that each nitrogen only has one lone pair. In a group of ammonia molecules, there are not enough lone pairs to go around to satisfy all the hydrogens. In hydrogen fluoride, the problem is a shortage of hydrogens. In water, two hydrogen bonds and two lone pairs allow formation of hydrogen bond interactions in a lattice of water molecules. Water is thus considered an ideal hydrogen bonded system.

More complex examples of hydrogen bonding

The hydration of negative ions

When an ionic substance dissolves in water, water molecules cluster around the separated ions. This process is called hydration. Water frequently attaches to positive ions by co-ordinate (dative covalent) bonds. It bonds to negative ions using hydrogen bonds.

> *If you are interested in the bonding in hydrated positive ions, you could follow this link to co-ordinate (dative covalent) bonding.*

The diagram shows the potential hydrogen bonds formed with a chloride ion, Cl-. Although the lone pairs in the chloride ion are at the 3-level and would not normally be active enough to form hydrogen bonds, they are made more attractive by the full negative charge on the chlorine in this case.

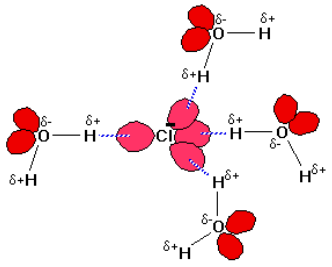


Figure 5: Hydrogen bonding between chloride ions and water.

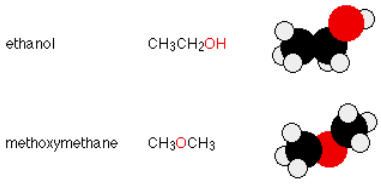
However complicated the negative ion, there will always be lone pairs that the hydrogen atoms from the water molecules can hydrogen bond to.

Hydrogen bonding in alcohols

An alcohol is an organic molecule containing an -OH group. Any molecule which has a hydrogen atom attached directly to an oxygen or a nitrogen is capable of hydrogen bonding. Hydrogen bonds also occur when hydrogen is bonded to fluorine, but the HF

group does not appear in other molecules. Molecules with hydrogen bonds will always have higher boiling points than similarly sized molecules which don't have an -O-H or an -N-H group. The hydrogen bonding makes the molecules "stickier," such that more heat (energy) is required to separate them. This phenomenon can be used to analyze boiling point of different molecules, defined as the temperature at which a phase change from liquid to gas occurs.

Ethanol, $\mathbf{CH_3CH_2{-}O{-}H}$, and methoxymethane, $\mathbf{CH_3{-}O{-}CH_3}$, both have the same molecular formula, $\mathbf{C_2H_6O}$.

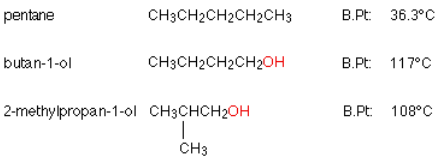


They have the same number of electrons, and a similar length. The van der Waals attractions (both dispersion forces and dipole-dipole attractions) in each will be similar. However, ethanol has a hydrogen atom attached directly to an oxygen; here the oxygen still has two lone pairs like a water molecule. Hydrogen bonding can occur between ethanol molecules, although not as effectively as in water. The hydrogen bonding is limited by the fact that there is only one hydrogen in each ethanol molecule with sufficient $\delta+$ charge.

In methoxymethane, the lone pairs on the oxygen are still there, but the hydrogens are not sufficiently $\delta+$ for hydrogen bonds to form. Except in some rather unusual cases, the hydrogen atom has to be attached directly to the very electronegative element for hydrogen bonding to occur. The boiling points of ethanol and methoxymethane show the dramatic effect that the hydrogen bonding has on the stickiness of the ethanol molecules:

ethanol (with hydrogen bonding)	78.5°C
methoxymethane (without hydrogen bonding)	-24.8°C

The hydrogen bonding in the ethanol has lifted its boiling point about 100°C. It is important to realize that hydrogen bonding exists in addition to van der Waals attractions. For example, all the following molecules contain the same number of electrons, and the first two have similar chain lengths. The higher boiling point of the butan-1-ol is due to the additional hydrogen bonding.



Comparing the two alcohols (containing -OH groups), both boiling points are high because of the additional hydrogen bonding; however, the values are not the same. The boiling point of the 2-methylpropan-1-ol isn't as high as the butan-1-ol because the branching in the molecule makes the van der Waals attractions less effective than in the longer butan-1-ol.

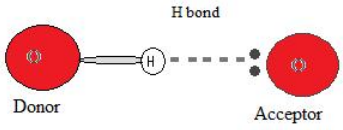
Hydrogen bonding in organic molecules containing nitrogen

Hydrogen bonding also occurs in organic molecules containing N-H groups; recall the hydrogen bonds that occur with ammonia. Examples range from simple molecules like CH_3NH_2 (methylamine) to large molecules like proteins and DNA. The two strands of the famous double helix in DNA are held together by hydrogen bonds between hydrogen atoms attached to nitrogen on one strand, and lone pairs on another nitrogen or an oxygen on the other one.

Donors and Acceptors

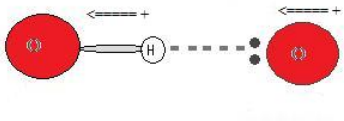
In order for a hydrogen bond to occur there must be both a hydrogen donor and an acceptor present. The donor in a hydrogen bond is usually a strongly electronegative atom such as N, O, or F that is covalently bonded to a hydrogen bond.

The hydrogen acceptor is an electronegative atom of a neighboring molecule or ion that contains a lone pair that participates in the hydrogen bond.



Why does a hydrogen bond occur?

Since the hydrogen donor (N, O, or F) is strongly electronegative, it pulls the covalently bonded electron pair closer to its nucleus, and away from the hydrogen atom. The hydrogen atom is then left with a partial positive charge, creating a dipole-dipole attraction between the hydrogen atom bonded to the donor and the lone electron pair of the acceptor. This results in a hydrogen bond.(see Interactions Between Molecules With Permanent Dipoles)

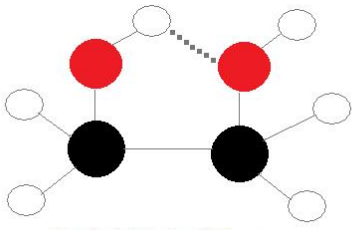


Types of hydrogen bonds

Although hydrogen bonds are well-known as a type of IMF, these bonds can also occur within a single molecule, between two identical molecules, or between two dissimilar molecules.

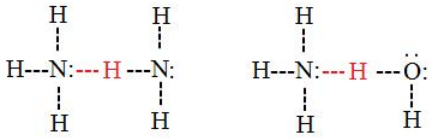
Intramolecular hydrogen bonds

Intramolecular hydrogen bonds are those which occur *within* one single molecule. This occurs when two functional groups of a molecule can form hydrogen bonds with each other. In order for this to happen, both a hydrogen donor a hydrogen acceptor must be present within one molecule, and they must be within close proximity of each other in the molecule. For example, intramolecular hydrogen bonding occurs in ethylene glycol ($C_2H_4(OH)_2$) between its two hydroxyl groups due to the molecular geometry.


Intramolecular h-bonding in Ethylene Glycol molecule

Intermolecular hydrogen bonds

Intermolecular hydrogen bonds occur *between* separate molecules in a substance. They can occur between any number of like or unlike molecules as long as hydrogen donors and acceptors are present in positions where they can interact with one another. For example, intermolecular hydrogen bonds can occur between NH_3 molecules alone, between H_2O molecules alone, or between NH_3 and H_2O molecules.



Properties and effects of hydrogen bonds

On Boiling Point

When we consider the boiling points of molecules, we usually expect molecules with larger molar masses to have higher normal boiling points than molecules with smaller molar masses. This, without taking hydrogen bonds into account, is due to greater dispersion forces (see Interactions Between Nonpolar Molecules). Larger molecules have more space for electron distribution and thus more possibilities for an instantaneous dipole moment. However, when we consider the table below, we see that this is not always the case.

Compound	Molar Mass	Normal Boiling Point
H_2O	18 g/mol	373 K
HF	20 g/mol	292.5 K
NH_3	17 g/mol	239.8 K
H_2S	34 g/mol	212.9 K
HCl	36.4 g/mol	197.9 K
PH_3	34 g/mol	185.2 K

We see that H_2O, HF, and NH_3 each have higher boiling points than the same compound formed between hydrogen and the next element moving down its respective group, indicating that the former have greater intermolecular forces. This is because H_2O, HF, and NH_3 all exhibit hydrogen bonding, whereas the others do not. Furthermore, H_2O has a smaller molar mass than HF but partakes in more hydrogen bonds per molecule, so its boiling point is higher.

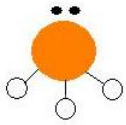
On Viscosity

The same effect that is seen on boiling point as a result of hydrogen bonding can also be observed in the viscosity of certain substances. Substances capable of forming hydrogen bonds tend to have a higher viscosity than those that do not form hydrogen bonds. Generally, substances that have the possibility for multiple hydrogen bonds exhibit even higher viscosities.

Factors preventing Hydrogen bonding

Electronegativity

Hydrogen bonding cannot occur without significant electronegativity differences between hydrogen and the atom it is bonded to. Thus, we see molecules such as PH_3, which do not participate in hydrogen bonding. PH_3 exhibits a trigonal pyramidal molecular geometry like that of ammonia, but unlike NH_3 it cannot hydrogen bond. This is due to the similarity in the electronegativities of phosphorous and hydrogen. Both atoms have an electronegativity of 2.1, and thus, there is no dipole moment. This prevents the hydrogen atom from acquiring the partial positive charge needed to hydrogen bond with the lone electron pair in another molecule. (see Polarizability)



Atom Size

The size of donors and acceptors can also affect the ability to hydrogen bond. This can account for the relatively low ability of Cl to form hydrogen bonds. When the radii of two atoms differ greatly or are large, their nuclei cannot achieve close proximity when they interact, resulting in a weak interaction.

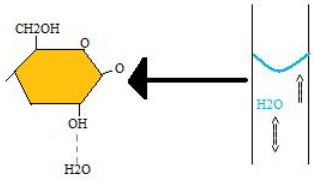


Hydrogen Bonding in Nature

Hydrogen bonding plays a crucial role in many biological processes and can account for many natural phenomena such as the Unusual properties of Water. In addition to being present in water, hydrogen bonding is also important in the water transport system of plants, secondary and tertiary protein structure, and DNA base pairing.

Plants

The cohesion-adhesion theory of transport in vascular plants uses hydrogen bonding to explain many key components of water movement through the plant's xylem and other vessels. Within a vessel, water molecules hydrogen bond not only to each other, but also to the cellulose chain that comprises the wall of plant cells. Since the vessel is relatively small, the attraction of the water to the cellulose wall creates a sort of capillary tube that allows for capillary action. This mechanism allows plants to pull water up into their roots. Furthermore, hydrogen bonding can create a long chain of water molecules, which can overcome the force of gravity and travel up to the high altitudes of leaves.



Proteins

Hydrogen bonding is present abundantly in the secondary structure of proteins, and also sparingly in tertiary conformation. The secondary structure of a protein involves interactions (mainly hydrogen bonds) between neighboring polypeptide backbones which contain nitrogen-hydrogen bonded pairs and oxygen atoms. Since both N and O are strongly electronegative, the hydrogen atoms bonded to nitrogen in one polypeptide backbone can hydrogen bond to the oxygen atoms in another chain and vice-versa. Though they are relatively weak, these bonds offer substantial stability to secondary protein structure because they repeat many times and work collectively.

In tertiary protein structure, interactions are primarily between functional R groups of a polypeptide chain; one such interaction is called a hydrophobic interaction. These interactions occur because of hydrogen bonding between water molecules around the hydrophobe that further reinforces protein conformation.

References

1. Brown, et al. Chemistry:The Central Science. 11th ed. Upper Saddle River, New Jersey: Pearson/Prentice Hall, 2008.
2. Chang, Raymond. General Chemistry:The Essential Concepts. 3rd ed. New York: Mcgraw Hill, 2003
3. Petrucci, et al. General Chemistry: Principles & Modern Applications. 9th ed. Upper Saddle River, New Jersey: Pearson/Prentice Hall, 2007.

1.5.4: Hydrogen Bonding is shared under a CC BY-NC-SA 4.0 license and was authored, remixed, and/or curated by LibreTexts.

- **Hydrogen Bonding** by Jim Clark, Jose Pietri is licensed CC BY-NC-SA 4.0.

1.5.5: Valence Bond Theory

Learning Objectives

- Describe the formation of covalent bonds in terms of atomic orbital overlap
- Define and give examples of σ and π bonds

As we know, a scientific theory is a strongly supported explanation for observed natural laws or large bodies of experimental data. For a theory to be accepted, it must explain experimental data and be able to predict behavior. For example, VSEPR theory has gained widespread acceptance because it predicts three-dimensional molecular shapes that are consistent with experimental data collected for thousands of different molecules. However, VSEPR theory does not provide an explanation of chemical bonding.

There are successful theories that describe the electronic structure of atoms. We can use quantum mechanics to predict the specific regions around an atom where electrons are likely to be located: A spherical shape for an *s* orbital, a dumbbell shape for a *p* orbital, and so forth. However, these predictions only describe the orbitals around free atoms. When atoms bond to form molecules, atomic orbitals are not sufficient to describe the regions where electrons will be located in the molecule. A more complete understanding of electron distributions requires a model that can account for the electronic structure of molecules. One popular theory holds that a covalent bond forms when a pair of electrons is shared by two atoms and is simultaneously attracted by the nuclei of both atoms. In the following sections, we will discuss how such bonds are described by valence bond theory and hybridization.

Valence bond theory describes a covalent bond as the overlap of half-filled atomic orbitals (each containing a single electron) that yield a pair of electrons shared between the two bonded atoms. We say that orbitals on two different atoms overlap when a portion of one orbital and a portion of a second orbital occupy the same region of space. According to valence bond theory, a covalent bond results when two conditions are met:

1. an orbital on one atom overlaps an orbital on a second atom and
2. the single electrons in each orbital combine to form an electron pair.

The mutual attraction between this negatively charged electron pair and the two atoms' positively charged nuclei serves to physically link the two atoms through a force we define as a covalent bond. The strength of a covalent bond depends on the extent of overlap of the orbitals involved. Orbitals that overlap extensively form bonds that are stronger than those that have less overlap.

The energy of the system depends on how much the orbitals overlap. Figure **1.5.5.1** illustrates how the sum of the energies of two hydrogen atoms (the colored curve) changes as they approach each other. When the atoms are far apart there is no overlap, and by convention we set the sum of the energies at zero. As the atoms move together, their orbitals begin to overlap. Each electron begins to feel the attraction of the nucleus in the other atom. In addition, the electrons begin to repel each other, as do the nuclei. While the atoms are still widely separated, the attractions are slightly stronger than the repulsions, and the energy of the system decreases. (A bond begins to form.) As the atoms move closer together, the overlap increases, so the attraction of the nuclei for the electrons continues to increase (as do the repulsions among electrons and between the nuclei). At some specific distance between the atoms, which varies depending on the atoms involved, the energy reaches its lowest (most stable) value. This optimum distance between the two bonded nuclei is the bond distance between the two atoms. The bond is stable because at this point, the attractive and repulsive forces combine to create the lowest possible energy configuration. If the distance between the nuclei were to decrease further, the repulsions between nuclei and the repulsions as electrons are confined in closer proximity to each other would become stronger than the attractive forces. The energy of the system would then rise (making the system destabilized), as shown at the far left of Figure **1.5.5.1**.

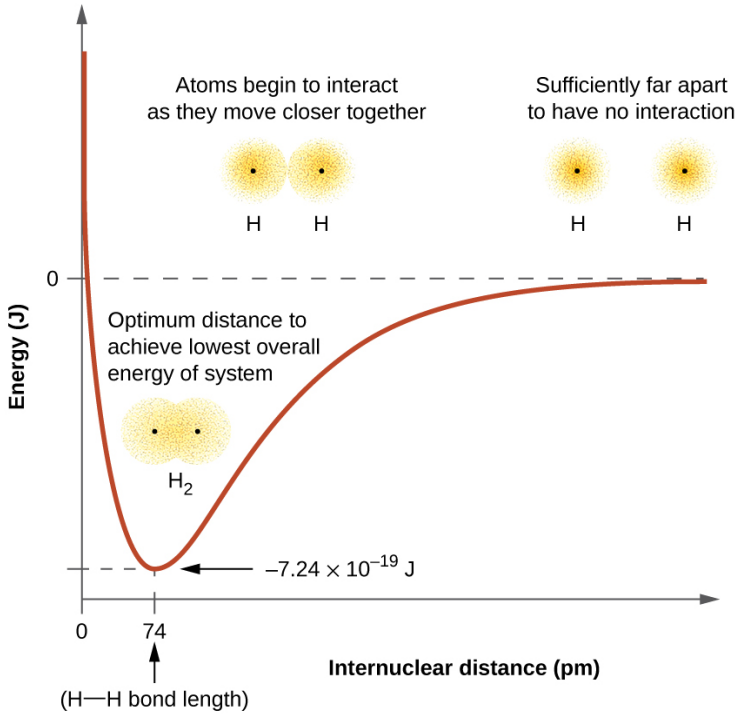


Figure 1.5.5.1: The interaction of two hydrogen atoms changes as a function of distance. The energy of the system changes as the atoms interact. The lowest (most stable) energy occurs at a distance of 74 pm, which is the bond length observed for the H_2 molecule.

A pair of diagrams are shown and labeled “a” and “b”. Diagram a shows three consecutive images. The first image depicts two separated blurry circles, each labeled with a positive sign and the term “H atom.” The phrase written under them reads, “Sufficiently far apart to have no interaction.” The second image shows the same two circles, but this time they are much closer together and are labeled, “Atoms begin to interact as they move closer together.” The third image shows the two circles overlapping, labeled, “H subscript 2,” and, “Optimum distance to achieve lowest overall energy of system.” Diagram b shows a graph on which the y-axis is labeled “Energy (J),” and the x-axis is labeled, “Internuclear distance (p m).” The midpoint of the y-axis is labeled as zero. The curve on the graph begins at zero p m and high on the y-axis. The graph slopes downward steeply to a point far below the zero joule line on the y-axis and the lowest point reads “0.74 p m” and “H bonded to H bond length.” It is also labeled “ negative 7.24 times 10 superscript negative 19 J.” The graph then rises again to zero J. The graph is accompanied by the same images from diagram a; the first image correlates to the point in the graph where it crosses the zero point on the y-axis, the third image where the graph is lowest.

The bond energy is the difference between the energy minimum (which occurs at the bond distance) and the energy of the two separated atoms. This is the quantity of energy released when the bond is formed. Conversely, the same amount of energy is required to break the bond. For the H_2 molecule shown in Figure 1.5.5.1, at the bond distance of 74 pm the system is $7.24 \times 10^{-19}\ J$ lower in energy than the two separated hydrogen atoms. This may seem like a small number. However, we know from our earlier description of thermochemistry that bond energies are often discussed on a per-mole basis. For example, it requires $7.24 \times 10^{-19}\ J$ to break one H–H bond, but it takes $4.36 \times 10^{5}\ J$ to break 1 mole of H–H bonds. A comparison of some bond lengths and energies is shown in Table 1.5.5.1. We can find many of these bonds in a variety of molecules, and this table provides average values. For example, breaking the first C–H bond in CH4 requires 439.3 kJ/mol, while breaking the first C–H bond in $H{-}CH_2C_6H_5$ (a common paint thinner) requires 375.5 kJ/mol.

Table 1.5.5.1: Representative Bond Energies and Lengths

Bond	Length (pm)	Energy (kJ/mol)		Bond	Length (pm)	Energy (kJ/mol)
H–H	74	436		C–O	140.1	358
H–C	106.8	413		C = O	119.7	745
H–N	101.5	391		C ≡ O	113.7	1072
H–O	97.5	467		H–Cl	127.5	431
C–C	150.6	347		H–Br	141.4	366
C = C	133.5	614		H–I	160.9	298
C ≡ C	120.8	839		O–O	148	146
C–N	142.1	305		O = O	120.8	498
C = N	130.0	615		F–F	141.2	159
C ≡ N	116.1	891		Cl–Cl	198.8	243

In addition to the distance between two orbitals, the orientation of orbitals also affects their overlap (other than for two *s* orbitals, which are spherically symmetric). Greater overlap is possible when orbitals are oriented such that they overlap on a direct line between the two nuclei. Figure **1.5.5.2** illustrates this for two *p* orbitals from different atoms; the overlap is greater when the orbitals overlap end to end rather than at an angle.

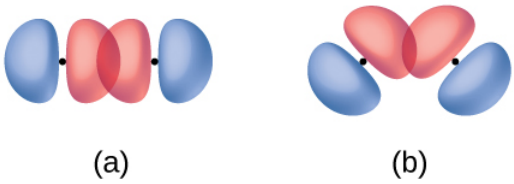


Figure **1.5.5.2**: (a) The overlap of two p orbitals is greatest when the orbitals are directed end to end. (b) Any other arrangement results in less overlap. The dots indicate the locations of the nuclei.

The overlap of two *s* orbitals (as in H_2), the overlap of an *s* orbital and a *p* orbital (as in HCl), and the end-to-end overlap of two *p* orbitals (as in Cl_2) all produce sigma bonds (σ bonds), as illustrated in Figure **1.5.5.3**. A σ bond is a covalent bond in which the electron density is concentrated in the region along the internuclear axis; that is, a line between the nuclei would pass through the center of the overlap region. Single bonds in Lewis structures are described as σ bonds in valence bond theory.

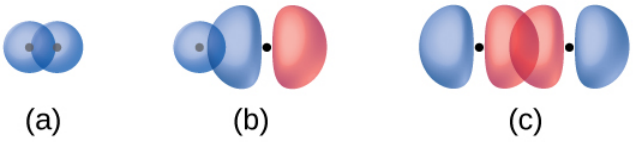


Figure **1.5.5.3**: Sigma (σ) bonds form from the overlap of the following: (a) two s orbitals, (b) an s orbital and a p orbital, and (c) two p orbitals. The dots indicate the locations of the nuclei.

Three diagrams are shown and labeled “a,” “b,” and “c.” Diagram a shows two spherical orbitals lying side by side and overlapping. Diagram b shows one spherical and one peanut-shaped orbital lying near one another so that the spherical orbital overlaps with one end of the peanut-shaped orbital. Diagram c shows two peanut-shaped orbitals lying end to end so that one end of each orbital overlaps the other.

A pi bond (π bond) is a type of covalent bond that results from the side-by-side overlap of two *p* orbitals, as illustrated in Figure **1.5.5.4**. In a π bond, the regions of orbital overlap lie on opposite sides of the internuclear axis. Along the axis itself, there is a node, that is, a plane with no probability of finding an electron.

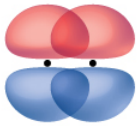
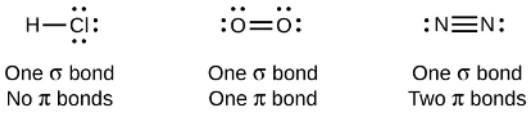


Figure 1.5.5.4: Pi (π) bonds form from the side-by-side overlap of two p orbitals. The dots indicate the location of the nuclei.

While all single bonds are σ bonds, multiple bonds consist of both σ and π bonds. As the Lewis structures suggest, O_2 contains a double bond, and N_2 contains a triple bond. The double bond consists of one σ bond and one π bond, and the triple bond consists of one σ bond and two π bonds. Between any two atoms, the first bond formed will always be a σ bond, but there can only be one σ bond in any one location. In any multiple bond, there will be one σ bond, and the remaining one or two bonds will be π bonds. These bonds are described in more detail later in this chapter.

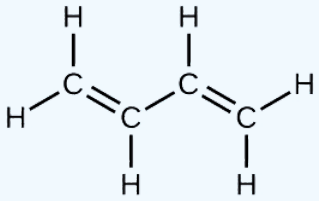


A diagram contains three Lewis structures. The left most structure shows an H atom bonded to a C l atom by a single bond. The C l atom has three lone pairs of electrons. The phrase “One sigma bond No pi bonds” is written below the drawing. The center structure shows two O atoms bonded by a double bond. The O atoms each have two lone pairs of electrons. The phrase “One sigma bond One pi bond” is written below the drawing. The right most structure shows two N atoms bonded by a triple bond. Each N atom has a lone pairs of electrons. The phrase “One sigma bond Two pi bonds” is written below the drawing.

As seen in Table 1.5.5.1, an average carbon-carbon single bond is 347 kJ/mol, while in a carbon-carbon double bond, the π bond increases the bond strength by 267 kJ/mol. Adding an additional π bond causes a further increase of 225 kJ/mol. We can see a similar pattern when we compare other σ and π bonds. Thus, each individual π bond is generally weaker than a corresponding σ bond between the same two atoms. In a σ bond, there is a greater degree of orbital overlap than in a π bond.

✔ Example 1.5.5.1: Counting σ and π Bonds

Butadiene, C_4H_6, is used to make synthetic rubber. Identify the number of σ and π bonds contained in this molecule.



Butadiene

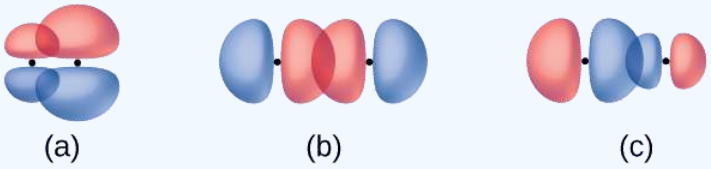
Solution

There are six σ C–H bonds and one σ C–C bond, for a total of seven from the single bonds. There are two double bonds that each have a π bond in addition to the σ bond. This gives a total nine σ and two π bonds overall.

? Exercise 1.5.5.1

Identify each illustration as depicting a σ or π bond:

a. side-by-side overlap of a 4*p* and a 2*p* orbital
b. end-to-end overlap of a 4*p* and 4*p* orbital
c. end-to-end overlap of a 4*p* and a 2*p* orbital



Answer

(a) is a π bond with a node along the axis connecting the nuclei while (b) and (c) are σ bonds that overlap along the axis.

Summary

Valence bond theory describes bonding as a consequence of the overlap of two separate atomic orbitals on different atoms that creates a region with one pair of electrons shared between the two atoms. When the orbitals overlap along an axis containing the nuclei, they form a σ bond. When they overlap in a fashion that creates a node along this axis, they form a π bond.

Glossary

overlap
coexistence of orbitals from two different atoms sharing the same region of space, leading to the formation of a covalent bond

node
plane separating different lobes of orbitals, where the probability of finding an electron is zero

pi bond (π bond)
covalent bond formed by side-by-side overlap of atomic orbitals; the electron density is found on opposite sides of the internuclear axis

sigma bond (σ bond)
covalent bond formed by overlap of atomic orbitals along the internuclear axis

valence bond theory
description of bonding that involves atomic orbitals overlapping to form σ or π bonds, within which pairs of electrons are shared

---

This page titled 1.5.5: Valence Bond Theory is shared under a CC BY-NC-SA 4.0 license and was authored, remixed, and/or curated by OpenStax.

- **8.2: Valence Bond Theory** by OpenStax is licensed CC BY 4.0. Original source: https://openstax.org/details/books/chemistry-2e.

1.5.6: Hybrid Atomic Orbitals

Learning Objectives

- Explain the concept of atomic orbital hybridization
- Determine the hybrid orbitals associated with various molecular geometries

Thinking in terms of overlapping atomic orbitals is one way for us to explain how chemical bonds form in diatomic molecules. However, to understand how molecules with more than two atoms form stable bonds, we require a more detailed model. As an example, let us consider the water molecule, in which we have one oxygen atom bonding to two hydrogen atoms. Oxygen has the electron configuration $1s^2 2s^2 2p^4$, with two unpaired electrons (one in each of the two 2*p* orbitals). Valence bond theory would predict that the two O–H bonds form from the overlap of these two 2*p* orbitals with the 1*s* orbitals of the hydrogen atoms. If this were the case, the bond angle would be 90°, as shown in Figure **1.5.6.1**, because *p* orbitals are perpendicular to each other. Experimental evidence shows that the bond angle is 104.5°, not 90°. The prediction of the valence bond theory model does not match the real-world observations of a water molecule; a different model is needed.

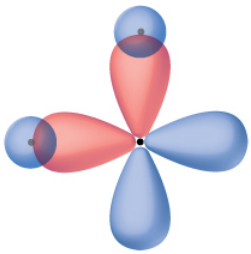


Figure **1.5.6.1**: The hypothetical overlap of two of the 2p orbitals on an oxygen atom (red) with the 1s orbitals of two hydrogen atoms (blue) would produce a bond angle of 90°. This is not consistent with experimental evidence.[1]

Two peanut-shaped orbitals lie perpendicular to one another. They overlap with spherical orbitals to the left and top of the diagram.

Quantum-mechanical calculations suggest why the observed bond angles in H_2O differ from those predicted by the overlap of the 1*s* orbital of the hydrogen atoms with the 2*p* orbitals of the oxygen atom. The mathematical expression known as the wave function, ψ, contains information about each orbital and the wavelike properties of electrons in an isolated atom. When atoms are bound together in a molecule, the wave functions combine to produce new mathematical descriptions that have different shapes. This process of combining the wave functions for atomic orbitals is called hybridization and is mathematically accomplished by the *linear combination of atomic orbitals*, LCAO, (a technique that we will encounter again later). The new orbitals that result are called hybrid orbitals. The valence orbitals in an *isolated* oxygen atom are a 2*s* orbital and three 2*p* orbitals. The valence orbitals in an oxygen atom in a water molecule differ; they consist of four equivalent hybrid orbitals that point approximately toward the corners of a tetrahedron (Figure **1.5.6.2**). Consequently, the overlap of the O and H orbitals should result in a tetrahedral bond angle (109.5°). The observed angle of 104.5° is experimental evidence for which quantum-mechanical calculations give a useful explanation: Valence bond theory must include a hybridization component to give accurate predictions.

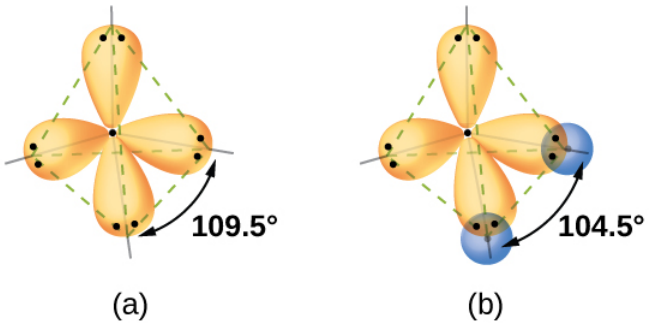


Figure **1.5.6.2**: (a) A water molecule has four regions of electron density, so VSEPR theory predicts a tetrahedral arrangement of hybrid orbitals. (b) Two of the hybrid orbitals on oxygen contain lone pairs, and the other two overlap with the 1s orbitals of hydrogen atoms to form the O–H bonds in H_2O. This description is more consistent with the experimental structure.

Two diagrams are shown and labeled “a” and “b.” Diagram a shows two peanut-shaped orbitals lying in a tetrahedral arrangement around the letter “O.” Diagram b shows the same two orbitals, but they now overlap to the top and to the left with two spherical orbitals, each labeled “H.” A pair of electrons occupies each lobe of the peanut-shaped orbitals.

The following ideas are important in understanding hybridization:

1. Hybrid orbitals do not exist in isolated atoms. They are formed only in covalently bonded atoms.
2. Hybrid orbitals have shapes and orientations that are very different from those of the atomic orbitals in isolated atoms.
3. A set of hybrid orbitals is generated by combining atomic orbitals. The number of hybrid orbitals in a set is equal to the number of atomic orbitals that were combined to produce the set.
4. All orbitals in a set of hybrid orbitals are equivalent in shape and energy.
5. The type of hybrid orbitals formed in a bonded atom depends on its electron-pair geometry as predicted by the VSEPR theory.
6. Hybrid orbitals overlap to form σ bonds. Unhybridized orbitals overlap to form π bonds.

In the following sections, we shall discuss the common types of hybrid orbitals.

1.5.6.1: sp Hybridization

The beryllium atom in a gaseous $BeCl_2$ molecule is an example of a central atom with no lone pairs of electrons in a linear arrangement of three atoms. There are two regions of valence electron density in the $BeCl_2$ molecule that correspond to the two covalent Be–Cl bonds. To accommodate these two electron domains, two of the Be atom’s four valence orbitals will mix to yield two hybrid orbitals. This hybridization process involves mixing of the valence *s* orbital with one of the valence *p* orbitals to yield two equivalent *sp* hybrid orbitals that are oriented in a linear geometry (Figure **1.5.6.3**). In this figure, the set of *sp* orbitals appears similar in shape to the original *p* orbital, but there is an important difference. The number of atomic orbitals combined always equals the number of hybrid orbitals formed. The *p* orbital is one orbital that can hold up to two electrons. The *sp* set is two equivalent orbitals that point 180° from each other. The two electrons that were originally in the *s* orbital are now distributed to the two *sp* orbitals, which are half filled. In gaseous $BeCl_2$, these half-filled hybrid orbitals will overlap with orbitals from the chlorine atoms to form two identical σ bonds.

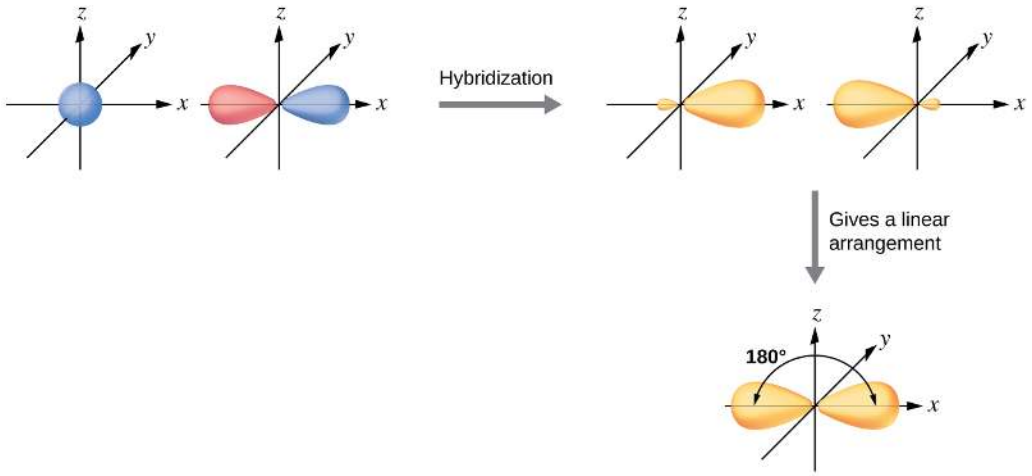


Figure **1.5.6.3**: Hybridization of an s orbital (blue) and a p orbital (red) of the same atom produces two sp hybrid orbitals (yellow). Each hybrid orbital is oriented primarily in just one direction. Note that each sp orbital contains one lobe that is significantly larger than the other. The set of two sp orbitals are oriented at 180°, which is consistent with the geometry for two domains.

A series of three diagrams connected by a right-facing arrow that is labeled, “Hybridization,” and a downward-facing arrow labeled, “Gives a linear arrangement,” are shown. The first diagram shows a blue spherical orbital and a red, peanut-shaped orbital, each placed on an X, Y, Z axis system. The second diagram shows the same two orbitals, but they are now purple and have one enlarged lobe and one smaller lobe. Each lies along the x-axis in the drawing. The third diagram shows the same two orbitals, but their smaller lobes now overlap along the x-axis while their larger lobes are located at and labeled as “180 degrees” from one another.

We illustrate the electronic differences in an isolated Be atom and in the bonded Be atom in the orbital energy-level diagram in Figure **1.5.6.4**. These diagrams represent each orbital by a horizontal line (indicating its energy) and each electron by an arrow. Energy increases toward the top of the diagram. We use one upward arrow to indicate one electron in an orbital and two arrows (up and down) to indicate two electrons of opposite spin.

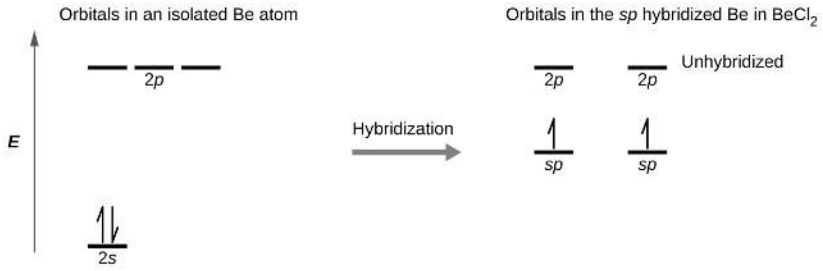


Figure **1.5.6.4**: This orbital energy-level diagram shows the sp hybridized orbitals on Be in the linear $BeCl_2$ molecule. Each of the two sp hybrid orbitals holds one electron and is thus half filled and available for bonding via overlap with a Cl 3p orbital.

A diagram is shown in two parts, connected by a right facing arrow labeled, “Hybridization.” The left diagram shows an up-facing arrow labeled, “E.” To the lower right of the arrow is a short, horizontal line labeled, “2 s,” that has two vertical half-arrows facing up and down on it. To the upper right of the arrow are a series of three short, horizontal lines labeled, “2 p.” Above these two sets of lines is the phrase, “Orbitals in an isolated B e atom.” The right side of the diagram shows two short, horizontal lines placed halfway up the space and each labeled, “s p.” An upward-facing half arrow is drawn vertically on each line. Above these lines are two other short, horizontal lines, each labeled, “2 p.” Above these two sets of lines is the phrase, “Orbitals in the s p hybridized B e in B e C l subscript 2.”

When atomic orbitals hybridize, the valence electrons occupy the newly created orbitals. The Be atom had two valence electrons, so each of the *sp* orbitals gets one of these electrons. Each of these electrons pairs up with the unpaired electron on a chlorine atom when a hybrid orbital and a chlorine orbital overlap during the formation of the Be–Cl bonds. Any central atom surrounded by just two regions of valence electron density in a molecule will exhibit *sp* hybridization. Other examples include the mercury atom in the linear $HgCl_2$ molecule, the zinc atom in $Zn(CH_3)_2$, which contains a linear C–Zn–C arrangement, and the carbon atoms in HCCH and CO_2.

1.5.6.2: sp^2 Hybridization

The valence orbitals of a central atom surrounded by three regions of electron density consist of a set of three sp^2 hybrid orbitals and one unhybridized p orbital. This arrangement results from sp^2 hybridization, the mixing of one s orbital and two p orbitals to produce three identical hybrid orbitals oriented in a trigonal planar geometry (Figure **1.5.6.5**).

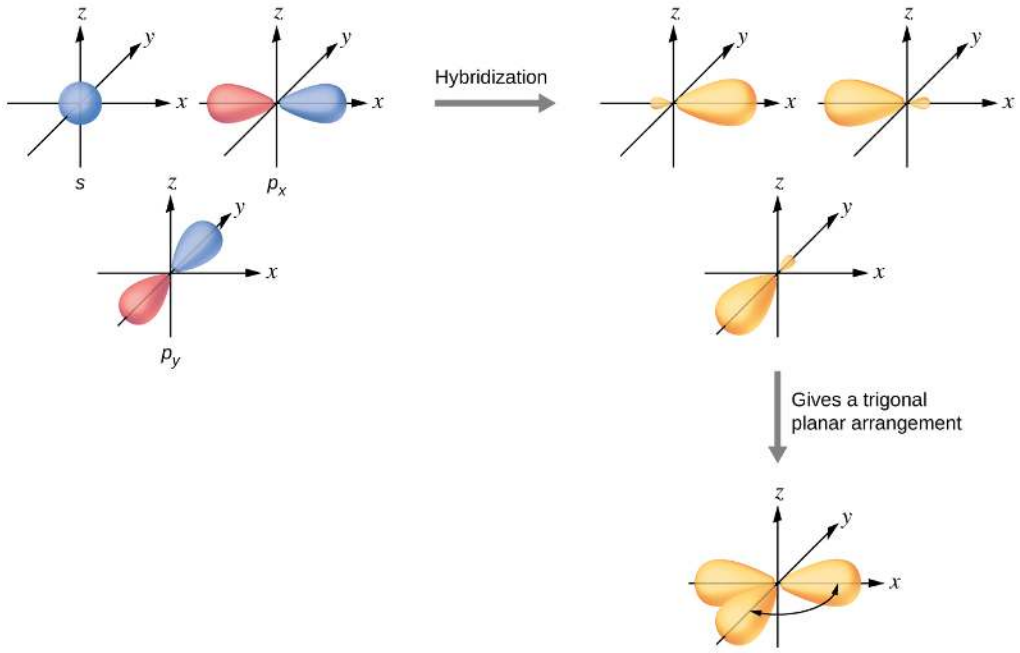


Figure **1.5.6.5**: The hybridization of an s orbital (blue) and two p orbitals (red) produces three equivalent sp^2 hybridized orbitals (yellow) oriented at 120° with respect to each other. The remaining unhybridized p orbital is not shown here, but is located along the z axis.

A series of three diagrams connected by a right-facing arrow that is labeled, “Hybridization,” and a downward-facing arrow labeled, “Gives a trigonal planar arrangement,” are shown. The first diagram shows a blue spherical orbital and two red, peanut-shaped orbitals, each placed on an X, Y, Z axis system. The two red orbitals are located on the x and z axes, respectively. The second diagram shows the same three orbitals, but they are now purple and have one enlarged lobe and one smaller lobe. Each lies in a different axis in the drawing. The third diagram shows the same three orbitals, but their smaller lobes now overlap while their larger lobes are located at and labeled as “120 degrees” from one another.

Although quantum mechanics yields the “plump” orbital lobes as depicted in Figure **1.5.6.5**, sometimes for clarity these orbitals are drawn thinner and without the minor lobes, as in Figure **1.5.6.6**, to avoid obscuring other features of a given illustration. We will use these “thinner” representations whenever the true view is too crowded to easily visualize.

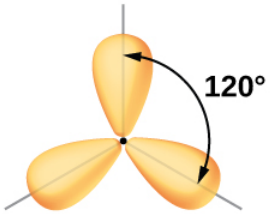


Figure **1.5.6.6**: This alternate way of drawing the trigonal planar sp^2 hybrid orbitals is sometimes used in more crowded figures.

Three balloon-like orbitals are shown, and connect together near their narrower ends in one plane. The angle between a pair of lobes is labeled, “120 degrees.”

The observed structure of the borane molecule, BH_3, suggests sp^2 hybridization for boron in this compound. The molecule is trigonal planar, and the boron atom is involved in three bonds to hydrogen atoms (Figure **1.5.6.7**).

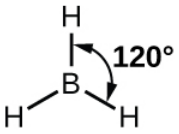


Figure **1.5.6.7**: BH_3 is an electron-deficient molecule with a trigonal planar structure.

A boron atom is shown connected to three hydrogen atoms, which are arranged around it like a pyramid. The angle from one line connecting the boron atom to a hydrogen atom to another line connecting the boron atom to a hydrogen atom is labeled, “120 degrees.”

We can illustrate the comparison of orbitals and electron distribution in an isolated boron atom and in the bonded atom in BH_3 as shown in the orbital energy level diagram in Figure **1.5.6.8**. We redistribute the three valence electrons of the boron atom in the three sp^2 hybrid orbitals, and each boron electron pairs with a hydrogen electron when B–H bonds form.

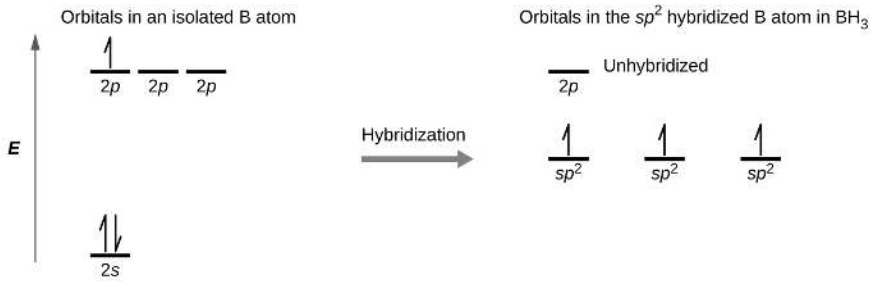


Figure **1.5.6.8**: In an isolated B atom, there are one 2s and three 2p valence orbitals. When boron is in a molecule with three regions of electron density, three of the orbitals hybridize and create a set of three sp^2 orbitals and one unhybridized 2p orbital. The three half-filled hybrid orbitals each overlap with an orbital from a hydrogen atom to form three σ bonds in BH_3.

A diagram is shown in two parts, connected by a right facing arrow labeled, “Hybridization.” The left diagram shows an up-facing arrow labeled “E.” To the lower right of the arrow is a short, horizontal line labeled, “2 s,” that has two vertical half-arrows facing up and down on it. To the upper right of the arrow are a series of three short, horizontal lines labeled, “2 p.” Above both sets of these lines is the phrase, “Orbitals in an isolated B atom.” One of the lines has a vertical, up-facing arrow drawn on it. The right side of the diagram shows three short, horizontal lines placed halfway up the space and each labeled, “s p superscript 2.” An upward-facing half arrow is drawn vertically on each line. Above these lines is one other short, horizontal line, labeled, “2 p.” Above both sets of lines is the phrase, “Orbitals in the s p superscript 2 hybridized B atom in B H subscript 3.”

Any central atom surrounded by three regions of electron density will exhibit sp^2 hybridization. This includes molecules with a lone pair on the central atom, such as ClNO (Figure **1.5.6.9**), or molecules with two single bonds and a double bond connected to the central atom, as in formaldehyde, CH_2O, and ethene, H_2CCH_2.

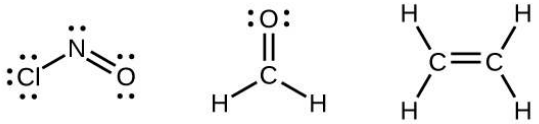


Figure **1.5.6.9**: The central atom(s) in each of the structures shown contain three regions of electron density and are sp^2 hybridized. As we know from the discussion of VSEPR theory, a region of electron density contains all of the electrons that point in one direction. A lone pair, an unpaired electron, a single bond, or a multiple bond would each count as one region of electron density.

Three Lewis structures are shown. The left-hand structure shows a chlorine atom surrounded by three lone pairs of electrons single bonded to a nitrogen atom with one lone pair of electrons and double bonded to an oxygen atom with two lone pairs of electrons. The middle structure shows a carbon atom single bonded to two hydrogen atoms and double bonded to an oxygen atom that has two lone pairs of electrons. The right-hand structure shows two carbon atoms, double bonded to one another and each single bonded to two hydrogen atoms.

1.5.6.3: sp^3 Hybridization

The valence orbitals of an atom surrounded by a tetrahedral arrangement of bonding pairs and lone pairs consist of a set of four sp^3 hybrid orbitals. The hybrids result from the mixing of one *s* orbital and all three *p* orbitals that produces four identical sp^3 hybrid orbitals (Figure **1.5.6.10**). Each of these hybrid orbitals points toward a different corner of a tetrahedron.

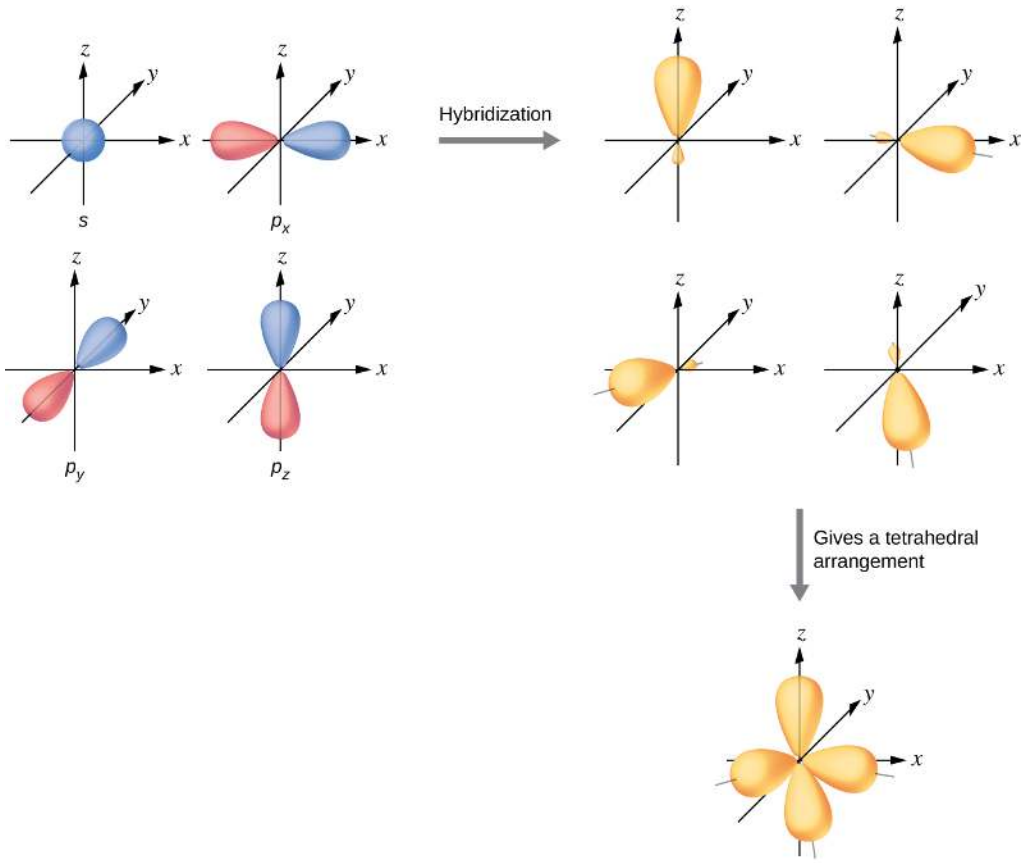


Figure **1.5.6.10**: The hybridization of an s orbital (blue) and three p orbitals (red) produces four equivalent sp^3 hybridized orbitals (yellow) oriented at 109.5° with respect to each other.

A series of three diagrams connected by a right-facing arrow that is labeled, “Hybridization,” and a downward-facing arrow labeled, “Gives a tetrahedral arrangement,” are shown. The first diagram shows a blue spherical orbital and three red, peanut-shaped orbitals, each placed on an x, y, z axis system. The three red orbitals are located on the x , y and z axes, respectively. The second diagram shows the same four orbitals, but they are now purple and have one enlarged lobe and one smaller lobe. Each lies in a different axis in the drawing. The third diagram shows the same four orbitals, but their smaller lobes now overlap to form a tetrahedral structure.

A molecule of methane, CH_4, consists of a carbon atom surrounded by four hydrogen atoms at the corners of a tetrahedron. The carbon atom in methane exhibits sp^3 hybridization. We illustrate the orbitals and electron distribution in an isolated carbon atom and in the bonded atom in CH_4 in Figure **1.5.6.11**. The four valence electrons of the carbon atom are distributed equally in the hybrid orbitals, and each carbon electron pairs with a hydrogen electron when the C–H bonds form.

https://chem.libretexts.org/@go/page/484684

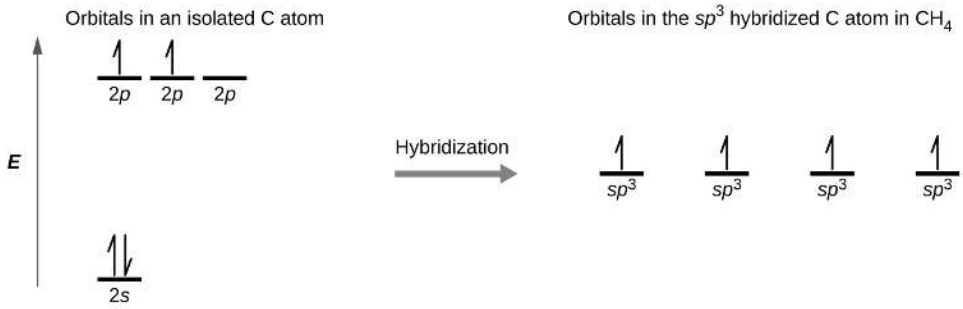


Figure **1.5.6.11**: The four valence atomic orbitals from an isolated carbon atom all hybridize when the carbon bonds in a molecule like CH_4 with four regions of electron density. This creates four equivalent sp^3 hybridized orbitals. Overlap of each of the hybrid orbitals with a hydrogen orbital creates a C–H σ bond.

A diagram is shown in two parts, connected by a right facing arrow labeled, “Hybridization.” The left diagram shows an up-facing arrow labeled “E.” To the lower right of the arrow is a short, horizontal line labeled, “2 s,” that has two vertical half-arrows facing up and down on it. To the upper right of the arrow are a series of three short, horizontal lines labeled, “2 p.” Two of the lines have a vertical, up-facing arrow drawn on them. Above both sets of lines is the phrase, “Orbitals in an isolated C atom.” The right side of the diagram shows four short, horizontal lines placed halfway up the space and each labeled, “s p superscript 3.” An upward-facing half arrow is drawn vertically on each line. Above these lines is the phrase, “Orbitals in the s p superscript 3 hybridized C atom in C H subscript 4.”

In a methane molecule, the 1*s* orbital of each of the four hydrogen atoms overlaps with one of the four sp^3 orbitals of the carbon atom to form a sigma (σ) bond. This results in the formation of four strong, equivalent covalent bonds between the carbon atom and each of the hydrogen atoms to produce the methane molecule, CH_4.

The structure of ethane, C_2H_6, is similar to that of methane in that each carbon in ethane has four neighboring atoms arranged at the corners of a tetrahedron—three hydrogen atoms and one carbon atom (Figure **1.5.6.10**). However, in ethane an sp^3 orbital of one carbon atom overlaps end to end with an sp^3 orbital of a second carbon atom to form a σ bond between the two carbon atoms. Each of the remaining sp^3 hybrid orbitals overlaps with an *s* orbital of a hydrogen atom to form carbon–hydrogen σ bonds. The structure and overall outline of the bonding orbitals of ethane are shown in Figure **1.5.6.12**. The orientation of the two CH_3 groups is not fixed relative to each other. Experimental evidence shows that rotation around σ bonds occurs easily.

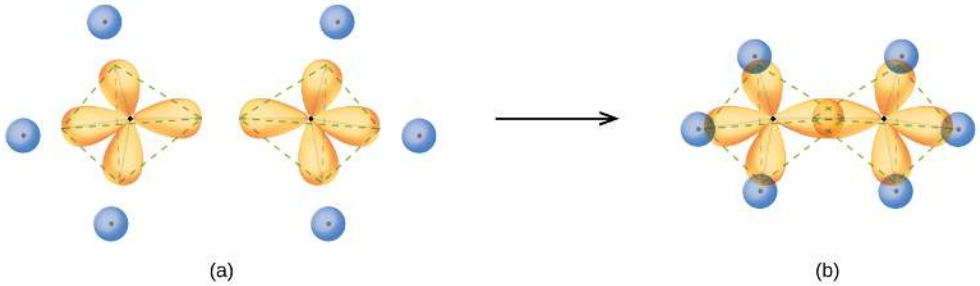


Figure **1.5.6.12**: (a) In the ethane molecule, C_2H_6, each carbon has four sp^3 orbitals. (b) These four orbitals overlap to form seven σ bonds.

Two diagrams are shown and labeled “a” and “b.” Diagram a shows two carbon atoms, each surrounded by their four s p subscript three hybridized orbitals in a three dimensional arrangement. Each of the orbitals is shown overlapping with a spherical hydrogen atom. Diagram b shows the same general arrangement, but the hydrogen atoms are just represented by an, “H” and their spherical orbitals are not shown.

An sp^3 hybrid orbital can also hold a lone pair of electrons. For example, the nitrogen atom in ammonia is surrounded by three bonding pairs and a lone pair of electrons directed to the four corners of a tetrahedron. The nitrogen atom is sp^3 hybridized with one hybrid orbital occupied by the lone pair.

The molecular structure of water is consistent with a tetrahedral arrangement of two lone pairs and two bonding pairs of electrons. Thus we say that the oxygen atom is sp^3 hybridized, with two of the hybrid orbitals occupied by lone pairs and two by bonding pairs. Since lone pairs occupy more space than bonding pairs, structures that contain lone pairs have bond angles slightly distorted from the ideal. Perfect tetrahedra have angles of 109.5°, but the observed angles in ammonia (107.3°) and water (104.5°) are slightly smaller. Other examples of sp^3 hybridization include CCl_4, PCl_3, and NCl_3.

1.5.6.4: sp^3d and sp^3d^2 Hybridization

To describe the five bonding orbitals in a trigonal bipyramidal arrangement, we must use five of the valence shell atomic orbitals (the *s* orbital, the three *p* orbitals, and one of the *d* orbitals), which gives five sp^3d hybrid orbitals. With an octahedral arrangement of six hybrid orbitals, we must use six valence shell atomic orbitals (the *s* orbital, the three *p* orbitals, and two of the *d* orbitals in its valence shell), which gives six sp^3d^2 hybrid orbitals. These hybridizations are only possible for atoms that have *d* orbitals in their valence subshells (that is, not those in the first or second period).

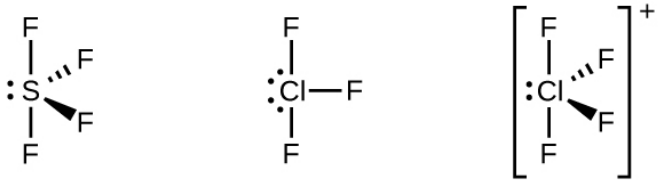


Figure **1.5.6.13**: The three compounds pictured exhibit sp^3d hybridization in the central atom and a trigonal bipyramid form. SF_4 and ClF_4^+ *have one lone pair of electrons on the central atom, and* ClF_3 *has two lone pairs giving it the T-shape shown.*

Three Lewis structures are shown along with designations of molecular shape. The left image shows a sulfur atom singly bonded to four fluorine atoms. The sulfur atom has one lone pair of electrons while each fluorine has three. Two fluorine atoms are drawn vertically up and down from the sulfur while the other two are shown going into and out of the page. The second structure shows one chlorine atom singly bonded to three fluorine atoms. The chlorine has two lone pairs of electrons while each fluorine has three. Two fluorine atoms are drawn vertically up and down from the sulfur while the other is shown horizontally. The right structure shows a chlorine atom singly bonded to four fluorine atoms. The chlorine atom has one lone pair of electrons and a superscript plus sign, while each fluorine has three lone pairs of electrons. Two fluorine atoms are drawn vertically up and down from the sulfur while the other two are shown going into and out of the page.

In a molecule of phosphorus pentachloride, PCl_5, there are five P–Cl bonds (thus five pairs of valence electrons around the phosphorus atom) directed toward the corners of a trigonal bipyramid. We use the 3*s* orbital, the three 3*p* orbitals, and one of the 3*d* orbitals to form the set of five sp^3d hybrid orbitals (Figure **1.5.6.13**) that are involved in the P–Cl bonds. Other atoms that exhibit sp^3d hybridization include the sulfur atom in SF_4 and the chlorine atoms in ClF_3 and in ClF_4^+. (The electrons on fluorine atoms are omitted for clarity.)

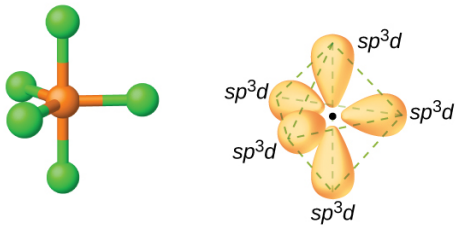


Figure **1.5.6.14**: (a) The five regions of electron density around phosphorus in PCl_5 require five hybrid sp^3d orbitals. (b) These orbitals combine to form a trigonal bipyramidal structure with each large lobe of the hybrid orbital pointing at a vertex. As before, there are also small lobes pointing in the opposite direction for each orbital (not shown for clarity).

Two images are shown and labeled “a” and “b.” Image a depicts a ball-and-stick model in a trigonal bipyramidal arrangement. Image b depicts the hybrid orbitals in the same arrangement and each is labeled, “s p superscript three d.”

The sulfur atom in sulfur hexafluoride, SF_6, exhibits sp^3d^2 hybridization. A molecule of sulfur hexafluoride has six bonding pairs of electrons connecting six fluorine atoms to a single sulfur atom. There are no lone pairs of electrons on the central atom. To bond six fluorine atoms, the 3*s* orbital, the three 3*p* orbitals, and two of the 3*d* orbitals form six equivalent sp^3d^2 hybrid orbitals, each directed toward a different corner of an octahedron. Other atoms that exhibit sp^3d^2 hybridization include the phosphorus atom in PCl_6^-, the iodine atom in the interhalogens IF_6^+, IF_5, ICl_4^-, IF_4^- and the xenon atom in XeF_4.

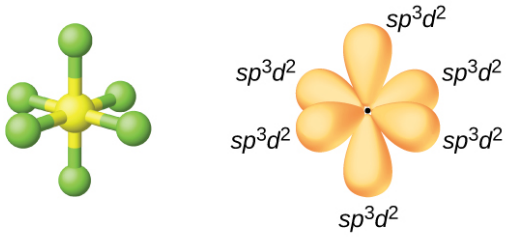


Figure **1.5.6.15**: (a) Sulfur hexafluoride, SF_6, has an octahedral structure that requires sp^3d^2 hybridization. (b) The six sp^3d^2 orbitals form an octahedral structure around sulfur. Again, the minor lobe of each orbital is not shown for clarity.

Two images are shown and labeled “a” and “b.” Image a depicts a ball-and-stick model in an octahedral arrangement. Image b depicts the hybrid orbitals in the same arrangement and each is labeled, “s p superscript three d superscript two.”

1.5.6.5: Assignment of Hybrid Orbitals to Central Atoms

The hybridization of an atom is determined based on the number of regions of electron density that surround it. The geometrical arrangements characteristic of the various sets of hybrid orbitals are shown in Figure **1.5.6.16**. These arrangements are identical to those of the electron-pair geometries predicted by VSEPR theory. VSEPR theory predicts the shapes of molecules, and hybrid orbital theory provides an explanation for how those shapes are formed. To find the hybridization of a central atom, we can use the following guidelines:

1. Determine the Lewis structure of the molecule.
2. Determine the number of regions of electron density around an atom using VSEPR theory, in which single bonds, multiple bonds, radicals, and lone pairs each count as one region.
3. Assign the set of hybridized orbitals from Figure **1.5.6.16** that corresponds to this geometry.

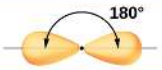
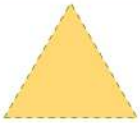
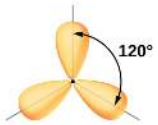
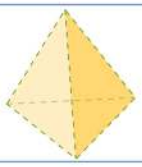
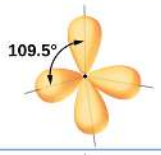
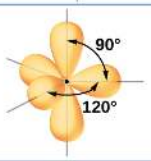
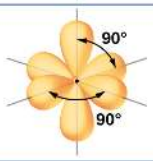
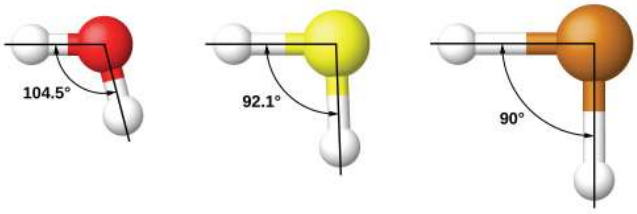
Regions of Electron Density	Arrangement		Hybridization	
2		linear	*sp*	
3		trigonal planar	sp^2	
4		tetrahedral	sp^3	
5		trigonal bipyramidal	sp^3d	
6		octahedral	sp^3d^2	

Figure **1.5.6.16**: The shapes of hybridized orbital sets are consistent with the electron-pair geometries. For example, an atom surrounded by three regions of electron density is sp^2 hybridized, and the three sp^2 orbitals are arranged in a trigonal planar fashion.

A table is shown that is composed of five columns and six rows. The header row contains the phrases, “Regions of electron density,” “Arrangement,” (which has two columns below it), and “Hybridization,” (which has two columns below it). The first column contains the numbers “2,” “3,” “4,” “5,” and “6.” The second column contains images of a line, a triangle, a three sided pyramid, a trigonal bipyramid, and an eight-faced ocatahedron. The third column contains the terms, “Linear,” “Trigonal planar,” “Tetrahedral,” “Trigonal bipyramidal,” and “Octahedral.” The fourth column contains the terms “s p,” “s p superscript 2,” “s p superscript 3,” “s p superscript 3 d,” and “s p superscript 3 d superscript 2.” The last column contains drawings of the molecules beginning with a peanut-shaped structure marked with an angle of “180 degrees.” The second structure is made up of three equal-sized, rounded structures connected at one point with an angle of “120 degrees,” while the third structure is a three-dimensional arrangement of four equal-sized, rounded structures labeled as “109.5 degrees.” The fourth structure is made up of five equal-sized, rounded structures connected at “120 and 90 degrees,” while the fifth structure has six equal-sized, rounded structures connected at “90 degrees.”

> *It is important to remember that hybridization was devised to rationalize experimentally observed molecular geometries, not the other way around.*

The model works well for molecules containing small central atoms, in which the valence electron pairs are close together in space. However, for larger central atoms, the valence-shell electron pairs are farther from the nucleus, and there are fewer repulsions. Their compounds exhibit structures that are often not consistent with VSEPR theory, and hybridized orbitals are not necessary to explain the observed data.



Three Lewis structures are shown. The left structure shows an oxygen atom with two lone pairs of electrons single bonded to two hydrogen atoms. The middle structure is made up of a sulfur atom with two lone pairs of electrons single bonded to two hydrogen atoms. The right structure is made up of a tellurium atom with two lone pairs of electrons single bonded to two hydrogen atoms. From left to right, the bond angles of each molecule decrease.

For example, we have discussed the H–O–H bond angle in H_2O, 104.5°, which is more consistent with sp^3 hybrid orbitals (109.5°) on the central atom than with 2*p* orbitals (90°). Sulfur is in the same group as oxygen, and H_2S has a similar Lewis structure. However, it has a much smaller bond angle (92.1°), which indicates much less hybridization on sulfur than oxygen. Continuing down the group, tellurium is even larger than sulfur, and for H_2Te, the observed bond angle (90°) is consistent with overlap of the 5*p* orbitals, without invoking hybridization. We invoke hybridization where it is necessary to explain the observed structures.

Example 1.5.6.1: Assigning Hybridization

Ammonium sulfate is important as a fertilizer. What is the hybridization of the sulfur atom in the sulfate ion, SO_4^{2-}?

Solution

The Lewis structure of sulfate shows there are four regions of electron density.

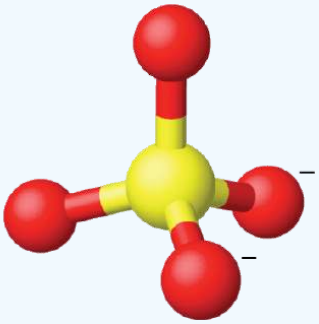
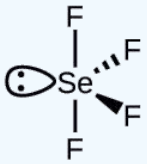


Figure 1.5.6.16).

A structure is shown in which a sulfur atom is bonded to four oxygen atoms in a tetrahedral arrangement. Two of the oxygen atoms have a negative charge.

Exercise 1.5.6.1

What is the hybridization of the selenium atom in SeF_4?



A Lewis structure is shown in which four fluorine atoms are each attached to one sulfur atom. Two of the attached fluorine atoms are vertically attached up and down, while two are attached into and out of the page to the right. The sulfur also has one lone pair of electrons attached to the left of the structure.

Answer

The selenium atom is sp^3d hybridized.

Example 1.5.6.2: Assigning Hybridization

Urea, $NH_2C(O)NH_2$, is sometimes used as a source of nitrogen in fertilizers. What is the hybridization of each nitrogen and carbon atom in urea?

Solution

The Lewis structure of urea is

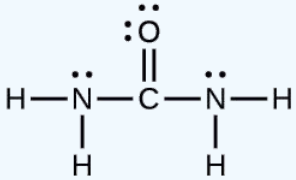


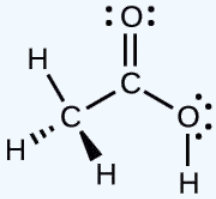
Figure 1.5.6.16). This is the hybridization of the nitrogen atoms in urea.

A Lewis structure is shown in which a carbon atom is double bonded to an oxygen atom that has two lone pairs of electrons. The carbon atom forms single bonds to two nitrogen atoms. Each nitrogen is single bonded to two hydrogen atoms, and each nitrogen atoms has one lone pair of electrons.

The carbon atom is surrounded by three regions of electron density, positioned in a trigonal planar arrangement. The hybridization in a trigonal planar electron pair geometry is sp^2 (Figure 1.5.6.16), which is the hybridization of the carbon atom in urea.

Exercise 1.5.6.1

Acetic acid, $H_3CC(O)OH$, is the molecule that gives vinegar its odor and sour taste. What is the hybridization of the two carbon atoms in acetic acid?



A Lewis structure is shown in which a carbon atom is double bonded to an oxygen atom that has two lone pairs of electrons and single bonded to another oxygen atom that is single boned to a hydrogen atom. This second oxygen atom has two lone pairs of electrons. The carbon is also single bonded to a carbon atom that is single bonded to three hydrogen atoms.

Answer

$H_3\underline{C}$, sp^3; $\underline{C}(O)OH$, sp^2

Summary

We can use hybrid orbitals, which are mathematical combinations of some or all of the valence atomic orbitals, to describe the electron density around covalently bonded atoms. These hybrid orbitals either form sigma (σ) bonds directed toward other atoms of the molecule or contain lone pairs of electrons. We can determine the type of hybridization around a central atom from the geometry of the regions of electron density about it. Two such regions imply *sp* hybridization; three, sp^2 hybridization; four, sp^3 hybridization; five, sp^3d hybridization; and six, sp^3d^2 hybridization. Pi (π) bonds are formed from unhybridized atomic orbitals (*p* or *d* orbitals).

1.5.6.5.1: Footnotes

1. Note that orbitals may sometimes be drawn in an elongated “balloon” shape rather than in a more realistic “plump” shape in order to make the geometry easier to visualize.

1.5.6.5.2: Glossary

hybrid orbital
orbital created by combining atomic orbitals on a central atom

hybridization
model that describes the changes in the atomic orbitals of an atom when it forms a covalent compound

***sp* hybrid orbital**
one of a set of two orbitals with a linear arrangement that results from combining one *s* and one *p* orbital

sp^2 hybrid orbital
one of a set of three orbitals with a trigonal planar arrangement that results from combining one *s* and two *p* orbitals

sp^3 hybrid orbital
one of a set of four orbitals with a tetrahedral arrangement that results from combining one *s* and three *p* orbitals

sp^3d hybrid orbital
one of a set of five orbitals with a trigonal bipyramidal arrangement that results from combining one *s*, three *p*, and one *d* orbital

sp^3d^2 hybrid orbital
one of a set of six orbitals with an octahedral arrangement that results from combining one *s*, three *p*, and two *d* orbitals

---

This page titled 1.5.6: Hybrid Atomic Orbitals is shared under a CC BY-NC-SA 4.0 license and was authored, remixed, and/or curated by OpenStax.

- **8.3: Hybrid Atomic Orbitals** by OpenStax is licensed CC BY 4.0. Original source: https://openstax.org/details/books/chemistry-2e.

SECTION OVERVIEW

1.6: Molecular Orbital Theory

1.6.1: Prelude to Molecular Orbital Theory

1.6.2: Formation of Molecular Orbitals from Atomic Orbitals

- 1.6.2.1: Molecular Orbitals from s Orbitals
- 1.6.2.2: Molecular Orbitals from p Orbitals
- 1.6.2.3: Molecular orbitals from d orbitals
- 1.6.2.4: Nonbonding Orbitals and Other Factors

1.6.3: Homonuclear Diatomic Molecules

- 1.6.3.1: Molecular Orbitals
- 1.6.3.2: Orbital Mixing
- 1.6.3.3: Diatomic Molecules of the First and Second Periods
- 1.6.3.4: Photoelectron Spectroscopy

1.6.4: Heteronuclear Diatomic Molecules

- 1.6.4.1: Polar bonds
- 1.6.4.2: Ionic Compounds and Molecular Orbitals

1.6: Molecular Orbital Theory is shared under a CC BY-NC-SA 4.0 license and was authored, remixed, and/or curated by LibreTexts.

1.6.1: Prelude to Molecular Orbital Theory

Valence bond (VB) theory gave us a qualitative picture of chemical bonding, which was useful for predicting the shapes of molecules, bond strengths, etc. It fails to describe some bonding situations accurately because it ignores the wave nature of the electrons. Molecular orbital (MO) theory has the potential to be more quantitative. With it we can also get a picture of where the electrons are in the molecule, as shown in the image at the right. This can help us understand patterns of bonding and reactivity that are otherwise difficult to explain.

Although MO theory in principle gives us a way to calculate the energies and wavefunctions of electrons in molecules very precisely, usually we settle for simplified models. These models do not give very accurate orbital and bond energies, but they do explain concepts such as resonance (e.g., in the ferrocene, $C_{10}H_{10}Fe$, molecule) that are hard to represent otherwise. We can get more accurate energies from MO theory using computational methods. While MO theory is more correct than VB theory and can be very accurate in predicting the properties of molecules, it is also rather complicated even for fairly simple molecules. For example, you should be able to draw the VB pictures for CO, NH_3, and benzene, but we will find that these are increasingly challenging with MO theory.

1.6.1: Prelude to Molecular Orbital Theory is shared under a CC BY-NC-SA 4.0 license and was authored, remixed, and/or curated by LibreTexts.

- **2.1: Prelude to Molecular Orbital Theory** by Chemistry 310 is licensed CC BY-SA 4.0. Original source: https://en.wikibooks.org/wiki/Introduction_to_Inorganic_Chemistry.

1.6.2: Formation of Molecular Orbitals from Atomic Orbitals

Molecular orbital theory extends from quantum theory and the atomic orbital wavefunctions (ψ) described by the Schrödinger equation. While the Schrödinger equation defines a Ψ for electrons in individual atoms, we can approximate the molecular wavefunction (what Ψ would look like if we combined the ψ of individual atoms). The addition or subtraction of wavefunctions is termed **linear combination of atomic orbitals** (LCAO). Molecular orbital theory is applied to LCAO to describe bonding.

The LCAO for the wavefunction of two atoms (ψ_a and ψ_b) is represented by the general expression below. The coefficients c_a and c_b quantify the contribution of each atomic ψ to the molecular Ψ.

$$\Psi = c_a\psi_a + c_b\psi_b$$

For two atomic ψs to form a bond, three conditions must be satisfied:

- First, the **distance between the atoms** must be small enough to provide good overlap. This is because the two orbitals must be able to overlap using regions of ψ^2 where the probability of finding electrons is significant. If atoms are not close enough, ψ_a and ψ_b cannot interact productively. At the same time, the atoms must be far enough apart that their nuclei do not repel each other.
- The **symmetry of the orbitals** must be compatible such that regions of ψ_a and ψ_b with the same sign constructively interfere more than regions with opposite sign destructively interfere. In other words, for a productive interaction, there must be a relatively high probability of finding an electron between the two nuclei, and this depends on the symmetry (and sign of the ψ) of the atomic orbitals.
- Third, the **energies of the atomic orbitals** must be similar. Orbitals with similar energy combine to make the most stable bonding molecular orbitals. Atomic orbitals with very different energies form less stable bonding interactions, and the larger the difference in the atomic orbitals, the weaker the bonding interaction will be.

Atomic orbitals combine to form molecular orbitals when these three conditions are met. The result is a set of bonding molecular orbitals that are lower in energy than the original atomic orbital energies.

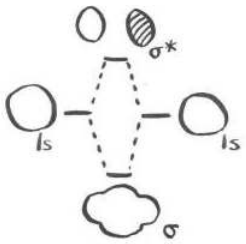
This page titled 1.6.2: Formation of Molecular Orbitals from Atomic Orbitals is shared under a CC BY-NC-SA 4.0 license and was authored, remixed, and/or curated by Kathryn Haas.

- **5.1: Formation of Molecular Orbitals from Atomic Orbitals** by Kathryn Haas is licensed CC BY-SA 4.0.

1.6.2.1: Molecular Orbitals from s Orbitals

In the case of the hydrogen molecule, we took two atomic orbitals and combined them to form two molecular orbitals. These new molecular orbitals had different wavelengths than the two atomic orbitals: one had a longer wavelength and was a little lower in energy, while the other had a shorter wavelength and was a little higher in energy. If we take into account the energy of the two original atomic wavefunctions, and compare them to the total energy of the two new molecular wavefunctions, there is no change overall.

We started with two atomic orbitals, and by combining them we produced two molecular orbitals. Both of these ideas are useful in considering the formation of more complex molecules from individual atoms.

- - The average energy of the orbitals has remained almost constant.
  - Also, the number of wavefunctions has remained constant.
  - 

Of course, from the point of view of the two real electrons, some remarkable changes have occurred. Both of these electrons have adopted a longer wavelength and a lower energy and that has made all the difference. There is an occupied molecular orbital and an unoccupied molecular orbital; only the occupied orbital makes a real energetic contribution to the overall stability of the molecule. The unoccupied orbital is completely imaginary.

A bonding picture of He_2 would look exactly the same, because it would also involve the overlap of 1s electrons on one atom with 1s electrons on the other atom. There would be a different electronic energy, however. That difference would affect the prospects of helium-helium bond formation.

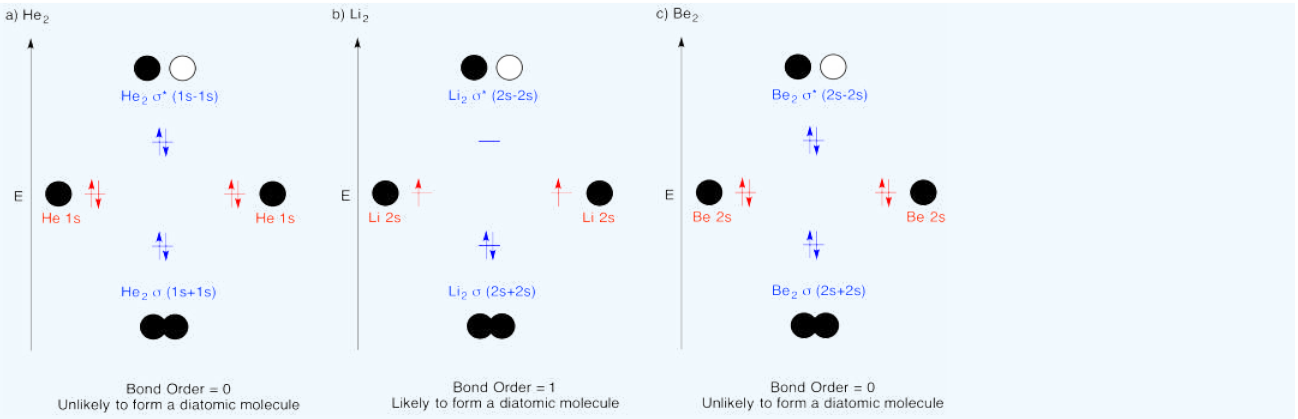
- The electrons have lower kinetic energy in the bond than they had before bonding.
- Electronic energy has decreased. A stable bond has formed.

? Exercise 1.6.2.1.1

Construct molecular orbital diagrams for the following diatomic species and discuss the likelihood of bond formation in each case.

a. He_2.
b. Li_2.
c. Be_2.

Answer



This page titled 1.6.2.1: Molecular Orbitals from s Orbitals is shared under a CC BY-NC-SA 4.0 license and was authored, remixed, and/or curated by Chris Schaller.

1.6.2.2: Molecular Orbitals from p Orbitals

Bonding with P-orbitals

Sigma bonding with p-orbitals

Other diatomic molecules in the upper right corner of the periodic table can be constructed in a similar way. Look at dinitrogen, N_2.

We can think about how dinitrogen would form if two nitrogen atoms were placed close enough together to share electrons. Nitrogen has more electrons than hydrogen, so this interaction is more complicated.

In our qualitative examination of bonding in main group diatomics, we will take the approach used in Lewis structures and just look at the valence electrons. A quantitative molecular orbital calculation with a computer would not take this shortcut, but would include all of the electrons in the atoms that are bonding together.

Nitrogen has five valence electrons, and these electrons are found in the 2s and 2p levels. There are three possible atomic orbitals in the 2p level where some of these electrons could be found: p_x, p_y and p_z. We need to look at the interaction between the s and p_x, p_y and p_z orbitals on one nitrogen atom with the s and p_x, p_y and p_z orbitals on the other nitrogen. That process could be extremely complicated, but:

- Orbital interactions are governed by symmetry.

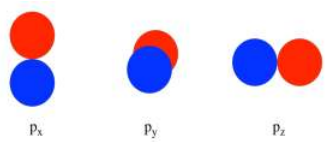
Orbitals interact most easily with other orbitals that have the same element of symmetry. For now, we can simplify and say that orbitals on one atom only interact with the same type of orbitals on the other atom.

- s orbitals interact with s orbitals. We can already see how that will work out in dinitrogen, because that is what happened in dihydrogen.
- p_x orbitals interact with p_x orbitals.
- p_y orbitals interact with p_y orbitals.
- p_z orbitals interact with p_z orbitals.

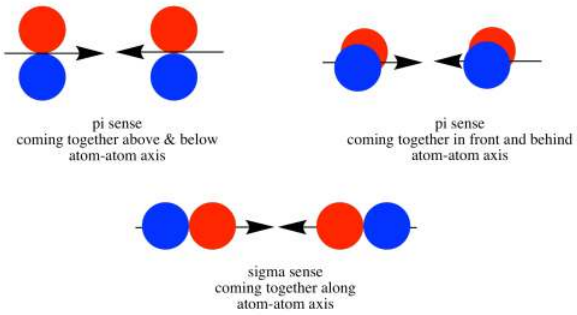
Another complication here is that the s and p orbitals do not start out at the same energy level. When the orbitals mix, one combination goes up in energy and one goes down. Does the s antibonding combination go higher in energy than the combinations from p orbitals? Do the p bonding combinations go lower in energy than the combinations from s orbitals? We will **simplify** and **assume** that the s and p levels remain completely separate from each other. This is not always true, but the situation varies depending on what atoms we are dealing with.

- The combination of one s orbital with another is just like in hydrogen. Two original orbitals will combine and rearrange to produce two new orbitals.
- There is a bonding combination in which the orbitals are in phase. The new orbital produced has a longer wavelength than the original orbital. It is lower in energy.
- There is an antibonding combination in which the orbitals are out of phase. The new orbital produced has a shorter wavelength than the original orbital. It is higher in energy.

In considering the interaction of two p orbitals, we have to keep in mind that p orbitals are directional. A p orbital lies along a particular axis: x, y or z. The three p orbitals on nitrogen are all mutually perpendicular (or orthogonal) to each other. That situation is in contrast to s orbitals, which are spherical and thus look the same from any direction.

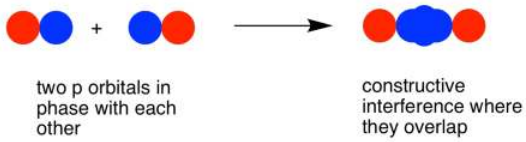


We first need to define one axis as lying along the N-N bond. It does not really matter which one. We arbitrarily say the N-N bond lies along the z axis. The p_z orbitals have a different spatial relationship to each other compared to the p_y and p_x. The p_z orbitals lie along the bond axis, whereas the p_y and p_x are orthogonal to it.

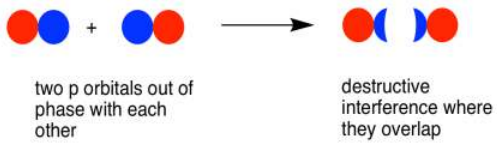


As the nitrogen atoms are brought together, one lobe on one p_z orbital overlaps strongly with one lobe on the other p_z orbital. The other lobes point away from each other and do not interact in any obvious way.

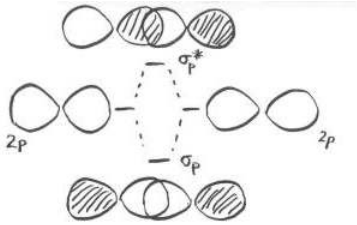
As with the s orbital, the p_z orbitals can be in-phase or out-of-phase. The in-phase combination results in constructive interference. (Here, "in-phase" means the lobes that overlap are in-phase; for that to happen the two p orbitals are actually completely out-of-phase with each other mathematically, so that one orbital is the mirror image of the other.) This combination is at a longer wavelength than the original orbital. It is a lower energy combination.



The out-of-phase combination (meaning in this case that the overlapping lobes are out-of-phase) results in destructive interference. This combination is at shorter wavelength than the original orbital. It is a higher energy combination.



As a result, we have two different combinations stemming from two different p orbitals coming together in two different ways. We get a low-energy, in-phase, bonding combination and a high-energy, out-of-phase, antibonding combination.

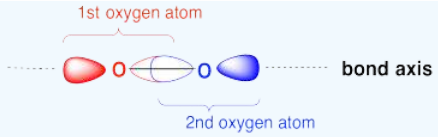


What about those other p orbitals, the ones that do not lie along the bond axis? We'll take a look at that problem on the next page.

? Exercise 1.6.2.2.2

Draw an MO cartoon of a sigma bonding orbital formed by the overlap of two p orbitals between two oxygen atoms. Label the positions of the oxygen nuclei with the symbol "O". Label the O-O bond axis.

Answer



Exercise 1.6.2.2.3

Chemical reactions can be described by MO diagrams too! Consider the following reaction in which a new sigma bond is formed.



Draw an MO diagram for the reaction above. In other words, start from the one frontier MO on each reactant to build the MO's of the new sigma bond in the product.

o Draw the orbital from the base (hydroxide) that is likely to donate its electrons.

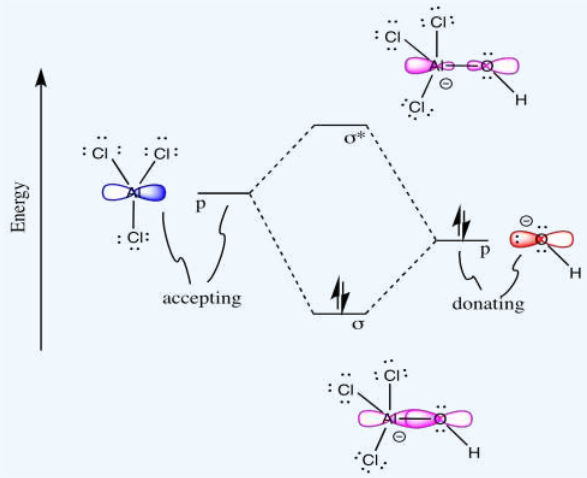
o Draw the orbital from the acid (aluminum chloride) that is likely to accept electrons.

o Complete the MO mixing diagram of these two orbitals:

- Label the electron donating orbital
- Label the electron accepting orbital
- Populate the MO mixing diagram with electrons

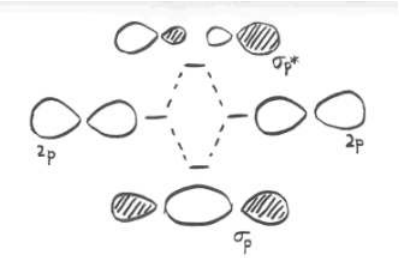
o Draw a cartoon showing each reactant and product MO that contributes to the bonding interaction.

Answer



Pi-bonding with p-orbitals

Earlier, we saw that p orbitals that lie along the same axis can interact to form bonds.



Parallel, but not collinear, p orbitals can also interact with each other. They would approach each other side by side, above and below the bond axis between the two atoms. They can be close enough to each other to overlap, although they do not overlap as strongly as orbitals lying along the bond axis. They can make an in-phase combination, as shown below.

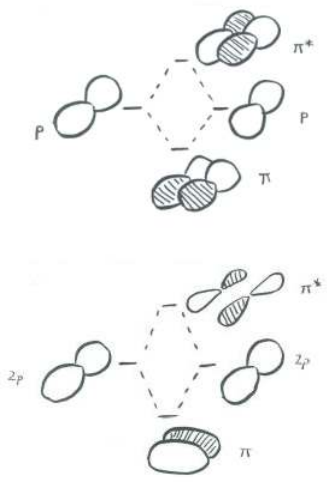


They could also make an out-of-phase combination, as shown below.



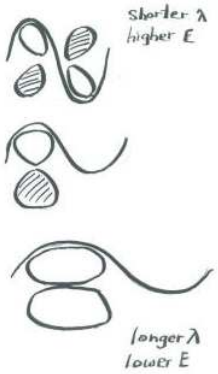
- parallel p orbitals can overlap to produce bonding and antibonding combinations.
- the resulting orbitals contain nodes along the bond axis.
- the electron density is found above and below the bond axis.
- this is called a p (pi) bond.

The illustration above is for one set of p orbitals that are orthogonal to the bond axis. The second picture shows the result of the constructive (or destructive) interference. A similar picture could be shown for the other set of p orbitals.

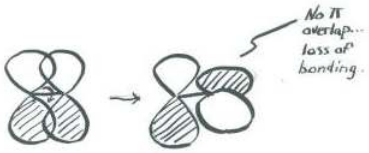


In a main group diatomic species like dinitrogen, one p orbital lying along the bond axis can engage in s bonding. The two p orbitals orthogonal to the bond axis can engage in p bonding. There will be both bonding and antibonding combinations.

Just as the sigma-bonding orbitals display progressively shorter wavelengths along the bonding axis as they go to higher energy, so do the pi bonding orbitals. In other words, there are more nodes in the higher-energy orbitals than in the lower-energy ones.



An important consequence of the spatial distribution or "shape" of a p orbital is that it is not symmetric with respect to the bond axis. An s orbital is not affected when the atom at one end of the bond is rotated with respect to the other. A p orbital is affected by such a rotation. If one atom turns with respect to the other, the p orbital would have to stretch to maintain the connection. The orbitals would not be able to overlap, so the connection between the atoms would be lost.



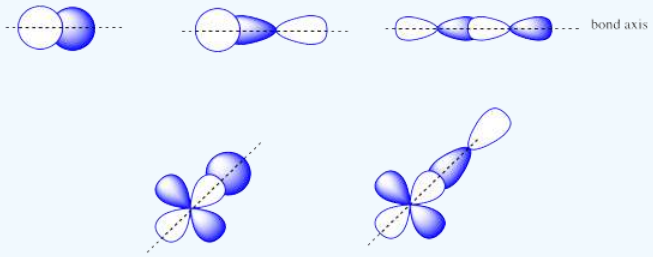
? Exercise 1.6.2.2.4

The combinations of _____ atomic orbitals leads to σ orbitals.

Draw pictures.

Answer

The combinations of ***s*** + ***s*** OR ***s*** + ***p*** OR ***p*** + ***p*** OR ***s*** + ***d*** OR ***p*** + ***d*** atomic orbitals can lead to σ orbitals.



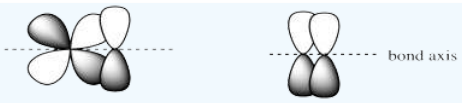
? Exercise 1.6.2.2.5

The combinations of _____ atomic orbitals leads to π orbitals.

Draw pictures.

Answer

The combinations of side by side p + p or p + d atomic orbitals leads to π orbitals.



Exercise 1.6.2.2.6

Which molecular orbital is typically the highest in energy?

a. p
b. σ
c. π*
d. π
e. σ*

Answer

e) σ*

Exercise 1.6.2.2.7

Why would a *core* 1s orbital not interact with a *valence* 2s orbital?

Hint: Why is a Li_2O bond stronger than a K_2O bond?

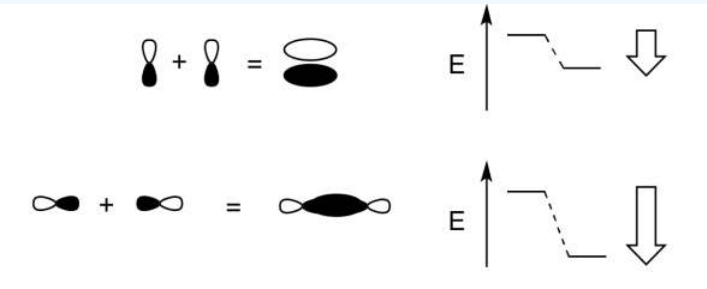
Answer

Li^+ and O^{2-} are more similar in size than K^+ and O^{2-}, so the bond between Li^+ and O^{2-} is stronger.

The energy difference between any core orbitals and valence orbitals is too large, so they cannot interact. In order for orbitals to interact, the orbitals need to have the same symmetry, be in the same plane, and be similar in energy.

Exercise 1.6.2.2.8

Add a few words to explain the ideas conveyed in these drawings.



Answer

When two parallel p orbitals combine out-of-phase, destructive interference occurs.

There is a node between the atoms.

The energy of the electrons increases.

When two parallel p orbitals combine in-phase, constructive interference occurs.

There is no node between the atoms; the electrons are found above and below the axis connecting the atoms.

The energy of the electrons decreases.

Attribution

Chris P Schaller, Ph.D., (College of Saint Benedict / Saint John's University)

Curated or created by Kathryn Haas

This page titled 1.6.2.2: Molecular Orbitals from p Orbitals is shared under a CC BY-NC-SA 4.0 license and was authored, remixed, and/or curated by Chris Schaller.

- **5.1.2: Molecular Orbitals from p Orbitals** by Chris Schaller is licensed CC BY-NC 3.0.

1.6.2.3: Molecular orbitals from d orbitals

In transition metals and other heavier elements, the d orbitals may combine with other orbitals of compatible symmetry (and energy) to form molecular orbitals. Generally, there are three types of bonding and antibonding interactions that may occur with d orbitals: sigma (σ), pi (π), and delta (δ) bonds.

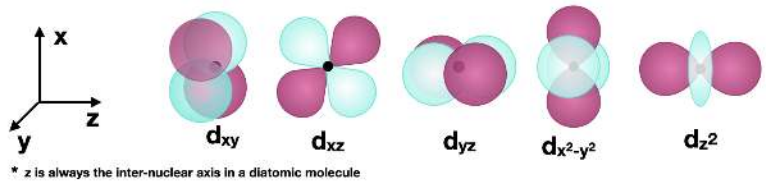


Figure 1.6.2.3.1: The five $3d$ orbitals are shown. The orientation of the axes is consistent and the z axis is horizontal for convenience in drawing bonding along the z axis (see examples below). (CC-BY-SA; Kathryn Haas)

Sigma (σ) bonding with d orbitals

σ bonds are symmetric with respect to the inter-nuclear axis (in a diatomic molecule, this is the z axis). An example of a σ bond formed by d orbitals is that of two d_{z^2} orbitals (see Figure 1.6.2.3.2). If a bonded atom is in a position other than on the z axis (in an octahedral geometry, for example), σ bonds can also form. For example, two $d_{x^2-y^2}$ orbitals on atoms bonded along the x or y axes could also form a σ bond.

d orbitals can also form σ bonds with other types of orbitals with the appropriate symmetry. Examples of orbitals with appropriate symmetry are the s orbital and certain p orbitals on another atom, as shown below in Figure 1.6.2.3.2.

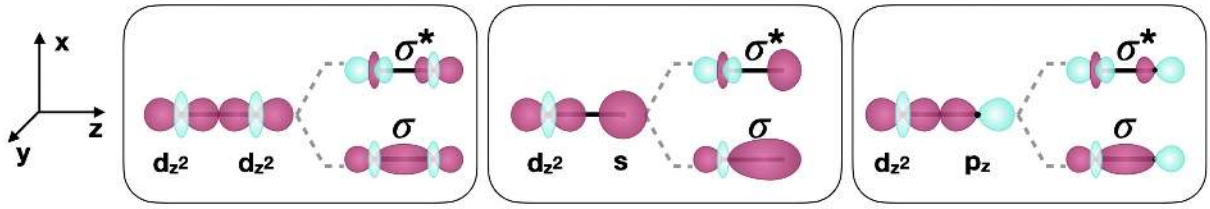


Figure 1.6.2.3.2: Selected examples of σ bonds involving d orbitals along the z internuclear axis (shown as a bold horizontal line) between two atoms. (CC-BY-SA; Kathryn Haas)

Pi (π) bonding with d orbitals

π bonds are those with one node that is in-plane with the internuclear axis. A π bond can form between two d orbitals or between d orbitals and other types of orbitals with comparable symmetry. An example of a π bond between two d orbitals is that formed by two d_{xz} orbitals along the z axis (shown in Figure 1.6.2.3.3). d orbitals can also form π bonds using p orbitals with compatible symmetry, as shown in Figure 1.6.2.3.3.

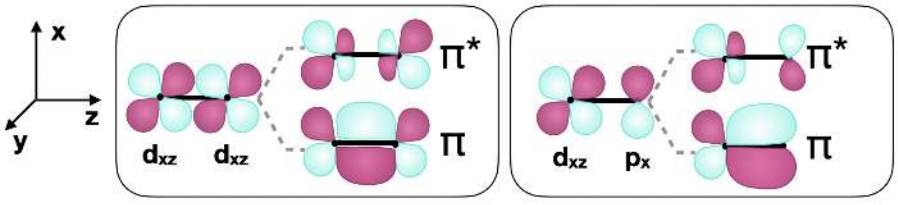


Figure 1.6.2.3.3: Selected examples of π bonds involving d orbitals along the z internuclear axis (shown as a bold horizontal line) between two atoms. (CC-BY-SA; Kathryn Haas)

Delta (δ) bonding with d orbitals

δ bonds are those with two nodes that are in-plane with the internuclear axis. δ bonds can form between two d orbitals with appropriate symmetry. For example, when two atoms bond along the z axis, the d_{xy} orbitals and the two $d_{x^2-y^2}$ orbitals can form δ bonds (Figure 1.6.2.3.4).

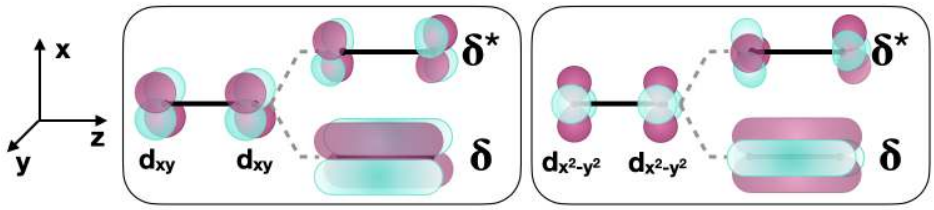


Figure **1.6.2.3.4**: Selected examples of δ bonds involving d orbitals along the z internuclear axis (shown in bold horizontal line) between two atoms. (CC-BY-SA; Kathryn Haas)

Incompatible orbitals

In the descriptions above, we focused on how bonds (and antibonds) can be formed with d orbitals. All bonding and non-bonding interactions require that orbitals have compatible symmetry to form productive interactions. It is worth mentioning that orbitals with symmetry that is incompatible with the d orbitals will not have bonding or antibonding interactions with d orbitals. The figure below shows several sets of orbitals that are incompatible for bonding.

Curated or created by Kathryn Haas

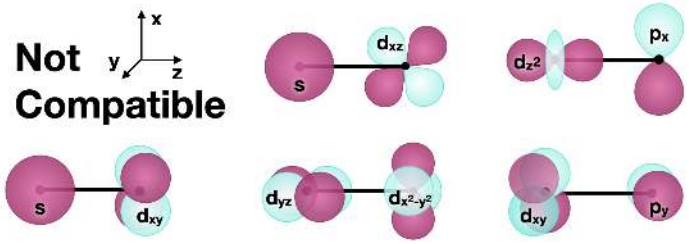


Figure **1.6.2.3.5**: Several incompatible pairs of orbitals. (CC-BY-SA; Kathryn Haas)

This page titled 1.6.2.3: Molecular orbitals from d orbitals is shared under a CC BY-NC-SA 4.0 license and was authored, remixed, and/or curated by Kathryn Haas.

- **5.1.3: Molecular orbitals from d orbitals** by Kathryn Haas is licensed CC BY-SA 4.0.

1.6.2.4: Nonbonding Orbitals and Other Factors

The simplest case is when there is an even number of atomic orbitals that all combine to form strong bonding and antibonding orbitals. But what if there is an uneven number of atomic orbitals? Or what if there are some orbitals that don't meet the criteria for bonding? Or what if the bonding interactions are weak? In these cases, there will be molecular orbitals on the molecule that have non-bonding character.

It is important to note that the bonding, non-bonding, and antibonding nature of orbitals exist on a spectrum. Some bonding and anti-bonding orbitals may have some non-bonding character depending on where their energies lie with respect to the original atomic orbital energies. When molecular orbitals have energies similar to their original atomic orbitals, they will have some non-bonding character. The closer the energies of atomic and molecular orbitals, the more non-bonding the molecular orbitals.

Two major factors to consider

Uneven number of atomic orbitals: In the case that there is an uneven number of atomic orbitals with compatible symmetry, orbitals with non-bonding character will form. For example, in the case where three atomic orbitals combine, the most common result is formation of a low-energy bonding orbital, a high energy antibonding orbital, and a non-bonding orbital of intermediate energy (Figure **1.6.2.4.1**).

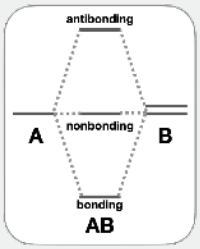


Figure **1.6.2.4.1**. This figure illustrates the most common case for three atomic orbitals that combine to form three molecular orbitals; formation of one low-energy bonding, one high-energy antibonding, and one intermediate energy non-bonding molecular orbital. (CC-BY-NC-SA, Kathryn Haas)

Differences in energy: Combination of orbitals with different energies may lead to orbitals with non-bonding character. Atomic orbitals that have similar energies will have the strongest interactions, and result in bonding molecular orbitals with much lower energies than the component atomic orbitals. On the other hand, atomic orbitals with very unequal energies have a weaker interaction because the molecular orbitals are closer in energy to the atomic orbital energies, thus there is less energy benefit to putting electrons in the bonding molecular orbitals (Figure **1.6.2.4.2**). When bonding or antibonding orbitals are close to the energies of the contributing atomic orbitals, those molecular orbitals may have some non-bonding character.

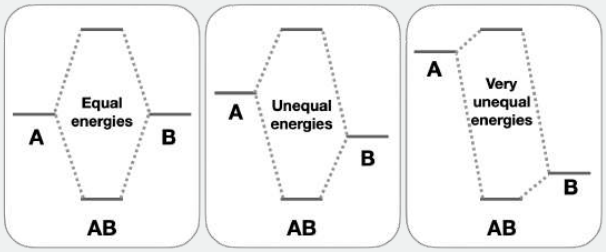


Figure **1.6.2.4.2**. This figure illustrates how relative energies of atomic orbitals result in molecular orbitals that are more or less favorable. The greater the energy difference between atomic orbitals and the bonding molecular orbital, the more eneretically favorable it is for bonding to occur. (CC-BY-NC-SA, Kathryn Haas)

This page titled 1.6.2.4: Nonbonding Orbitals and Other Factors is shared under a CC BY-NC-SA 4.0 license and was authored, remixed, and/or curated by Kathryn Haas.

- **5.1.4: Nonbonding Orbitals and Other Factors** by Kathryn Haas is licensed CC BY-SA 4.0.

SECTION OVERVIEW

1.6.3: Homonuclear Diatomic Molecules

In this section you will be introduced to the molecular orbital diagrams of several homonuclear diatomic molecules. Homonuclear diatomic molecules are molecules made of exactly two identical atoms, and they are relatively simple.

1.6.3.1: Molecular Orbitals

1.6.3.2: Orbital Mixing

1.6.3.3: Diatomic Molecules of the First and Second Periods

1.6.3.4: Photoelectron Spectroscopy

This page titled 1.6.3: Homonuclear Diatomic Molecules is shared under a CC BY-NC-SA 4.0 license and was authored, remixed, and/or curated by Kathryn Haas.

1.6.3.1: Molecular Orbitals

There are several cases where our more elementary models of bonding (like Lewis Theory and Valence Bond Theory) fail to predict the actual molecular properties and reactivity. A classic example is the case of O_2 and its magnetic properties. At very cold temperatures, O_2 is attracted to a magnetic field, and thus it must be paramagnetic (unpaired electrons give rise to magnetism). Watch the video below!



The magnetic properties of O_2 are easily rationalized by its **molecular orbital diagram**. A molecular orbital diagram is a diagram that shows the relative energies and identities of each molecular orbital in a molecule. Figure 1.6.3.1.1 shows a simplified and generic molecular orbital diagram for a second-row homonuclear diatomic molecule. The diagram is simplified in that it assumes that interactions are limited to degenerate orbitals from two atoms (see next section).

There are some things you should note as you inspect Figure 1.6.3.1.1 (and keep these in mind as you draw your own diagrams!). First, notice that there are the **same number of molecular orbitals as there are atomic orbitals**. Second, notice that **each orbital in the diagram is rigorously labeled** using labels (σ and π) that include the subscripts u and g. These labels and subscripts indicate the symmetry of the orbitals. The σ symbol indicates that the orbital is symmetric with respect to the internuclear axis, while the π label indicates that there is one node along that axis. The g and u stand for *gerade* and *ungerade*, the German words for *even* and *uneven*, respectively. The subscript g is given to orbitals that are *even*, or *symmetric*, with respect to an inversion center. The subscript u is given to orbitals that are *uneven*, or *antisymetric*, with respect to an inversion center. The pictures of calculated molecular orbitals are shown in Figure 1.6.3.1.1 to illustrate the symmetry of each orbital.

Another important thing to notice is that the diagram in Figure 1.6.3.1.1 lacks electrons (because it is generic for any second-row diatomic molecule). If this were a *complete* molecular orbital diagram it would **include the electrons for each atom and for the molecule**. Electrons in molecular orbitals are filled in the same way an atomic orbital diagram would be filled, where electrons occupy lower energy orbitals before higher energy orbitals, and electrons occupy empty degenerate orbitals before pairing. A complete molecular orbital diagram would show whether the molecule is diamagnetic or paramagnetic. It can also be used to calculate the bond order of the molecule (the number of bonds between atoms) using the formula below:

$$\text{Bond order } = \frac{1}{2}\left[\begin{pmatrix}\text{number of electrons}\\ \text{in bonding orbitals}\end{pmatrix} - \begin{pmatrix}\text{number of electrons}\\ \text{in antibonding orbitals}\end{pmatrix}\right]$$

In general, non-valence (core) electrons can be ignored because they contribute nothing to the bond order. In fact, many molecular orbital diagrams will ignore the core orbitals, as they are insignificant for bonding interactions and reactivity.

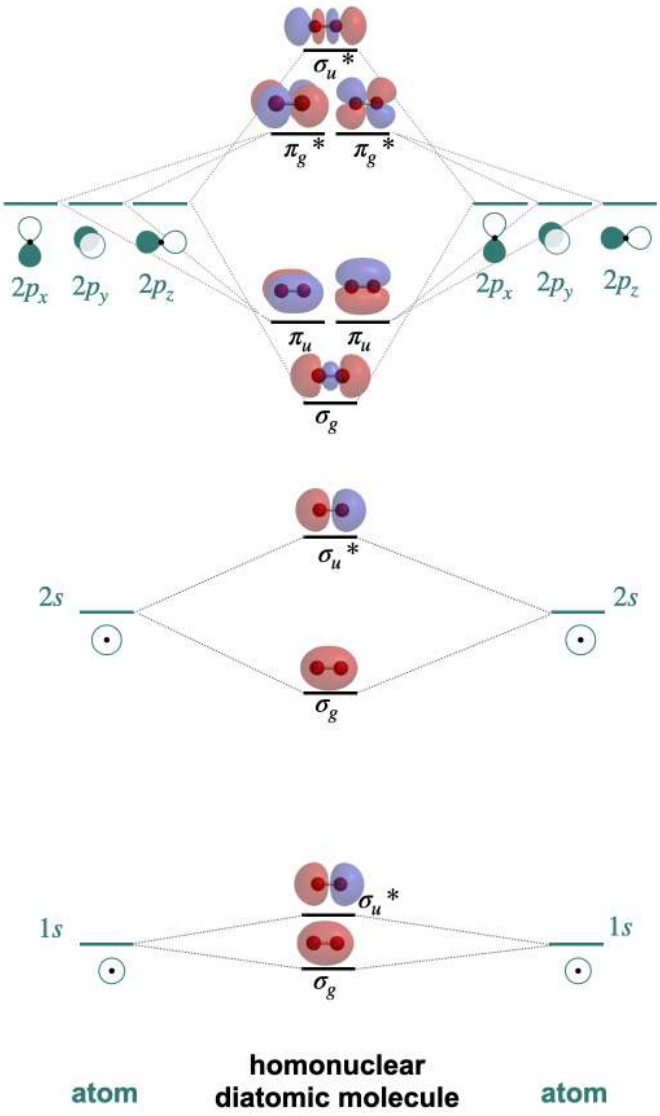


Figure **1.6.3.1.1**: A generic molecular orbital diagram for a homonuclear diatomic molecule of second-row elements assuming no orbital mixing (interactions are formed by orbitals of the same energy from each atom). (CC-BY-NC-SA, Kathryn Haas)

Now, to see how this molecular orbital diagram can explain the magnetic behaviour of O_2, complete the example below.

Example 1.6.3.1.1

Let's change Figure **1.6.3.1.1** to make it specific for O_2. Re-draw the MO diagram (no need to draw the shapes of orbitals). Fill in the correct number of electrons for each oxygen atom on either side of the diagram. Then, fill in the total molecular electrons in the center. Calculate the bond order and determine whether it is diamagnetic or paramagnetic.

Solution

The diagram in Figure **1.6.3.1.1** includes core orbitals (the 1s) and valence electrons (2s, 2p). Therefore, we will consider all the electrons in an oxygen atom and a dioxygen molecule. An oxygen atom has eight total electrons. So we fill eight electrons into the atomic orbitals for the oxygen atom on the right, and eight electrons into the atomic orbitals for oxygen on the left. The total number of electrons for the molecule is sixteen, so fill in 16 electrons into the molecular orbitals, being sure to apply Hund's rule and the Aufbau principle. The result is a diagram that looks like the one drawn below in Figure **1.6.3.1.2**.

The bond order is calculated using the molecular orbitals (we can ignore atomic orbitals). There are 10 electrons in binding orbitals and 6 electrons in antibonding orbitals). This gives a bond order of $\frac{1}{2}(10-6)=2$. This bond order is consistent with valence bond theory!

This diagram indicates that dioxygen is paramagnetic; it has two unpaired electrons in the π^* orbitals. This paramagnetic electron configuration explains why dioxygen is attacted to magnetic fields!

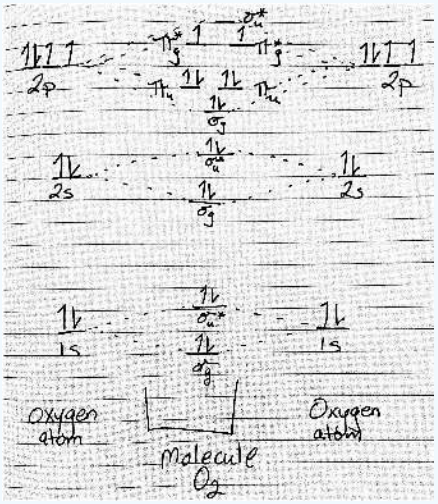


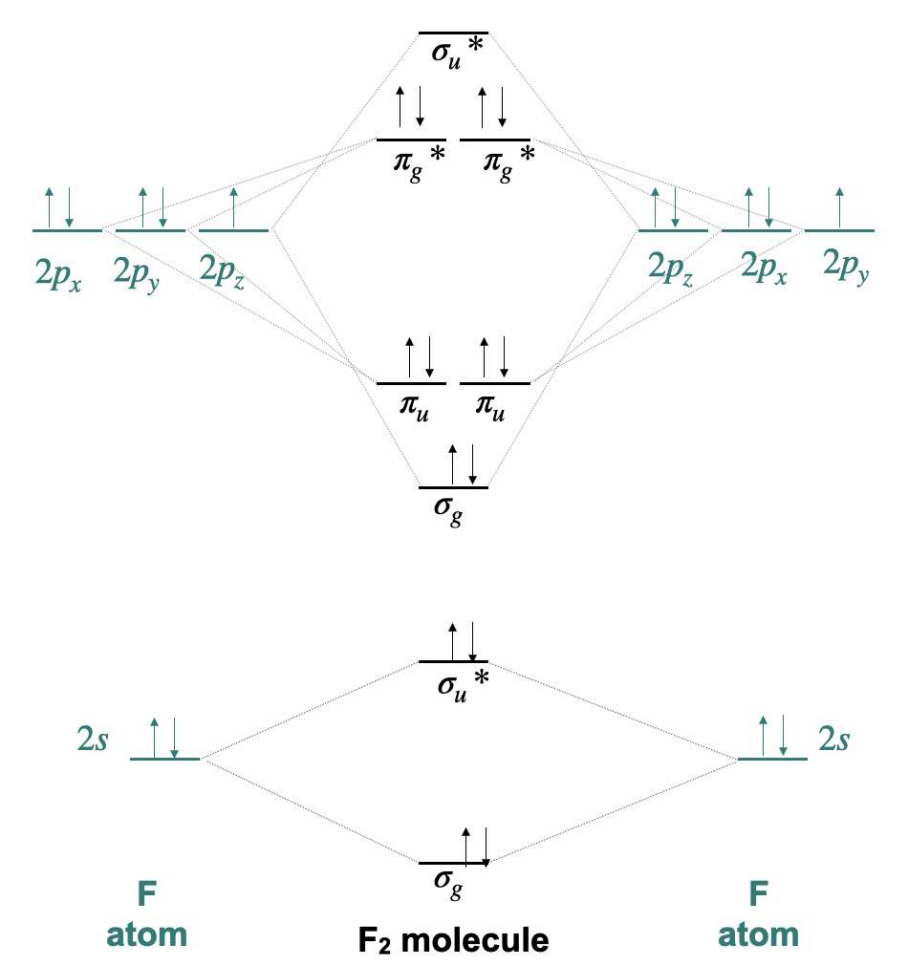
Figure 1.6.3.1.2: Hand-drawn molecular orbital diagram for dioxygen. (CC-BY-SA; Kathryn Haas)

? Exercise 1.6.3.1.1

Draw the molecular orbital diagram for $\mathbf{F_2}$; be sure to label your orbitals with the appropriate symmetry and count your orbitals to make sure that the total number of atomic orbitals and molecular orbitals is the same. As a shortcut, include only the valence orbitals and electrons. What is the bond order? Is the molecule diamagnetic or paramagnetic?

Answer

The valence orbitals on an F atom are 2s and 2p. And, there are seven valence electrons in F. This gives fourteen total valence electrons. The MO diagram of the valence molecular orbitals can be constructed by combining the valence 2s and valence 2p orbitals from each F atom. The bond order is 1 and the molecule is diamagnetic.



This page titled 1.6.3.1: Molecular Orbitals is shared under a CC BY-NC-SA 4.0 license and was authored, remixed, and/or curated by Kathryn Haas.

- **5.2.1: Molecular Orbitals** by Kathryn Haas is licensed CC BY-SA 4.0.

1.6.3.2: Orbital Mixing

In the previous section, we introduced a simplified molecular orbital (MO) diagram, assuming that interactions were limited to degenerate orbitals of compatible symmetry. A version of that *simplified* diagram for second-row homonuclear diatomics is shown on the left side of Figure **1.6.3.2.1** (only valence orbitals shown).

In reality, orbitals of compatible symmetry can combine, or mix, even when they have different energies. When sets of orbitals mix, it has the effect of decreasing the energy of the lower-energy set and increasing the energy of the higher-energy set. There are two ways to explain mixing, described in the points below. The diagram on the right of side of Figure **1.6.3.2.1** shows how energy levels are affected by orbital mixing.

- **Starting from the simplified MO diagram and mixing molecular orbitals of like symmetry**: If we start with the "no mixing" simplified diagram shown on the left, we can pick out the orbitals with like symmetry and consider what will happen if these molecular orbitals mix. For example, starting from the MO diagram on the left side of Figure **1.6.3.2.1**, we see that there are two σ_g orbitals that have identical symmetry (hence they have identical symmetry labels). Upon mixing, the lower-energy $\sigma_g(2s)$ will decrease in energy while the higher-energy $\sigma_g(2p)$ will increase in energy. Likewise, there are two σ_u^* orbitals that will mix, decreasing the energy of $\sigma_u^*(2s)$ while increasing the energy of $\sigma_u^*(2p)$.
- **Starting from and mixing atomic orbitals of compatible symmetry**: Starting from the atomic orbitals, we can select the orbitals that have compatible symmetry to make productive interactions, and combine them as a set to make molecular orbitals. From the two sets of atomic orbitals on the right panel in Figure **1.6.3.2.1**, there are two sets of four orbitals with compatable symmetry; one is the set of two $2s$ and two $2p_z$ orbitals. These four orbitals can combine to form molecular orbitals with σ symmetry. They combine to form one lowest-energy bonding σ_g, a highest-energy σ_u^*, and two orbitals with intermediate energy (σ_g, and σ_u^*). This treatment can be expressed as the linear combination of four atomic orbitals:

  $$\Psi = c_1\psi(2s_a) \pm c_2\psi(2s_b) \pm c_3\psi(2p_a) \pm c_4\psi(2p_b)$$

  where the coefficients $c_1 = c_2$ and $c_3 = c_4$ for homonuclear diatomic molecules.

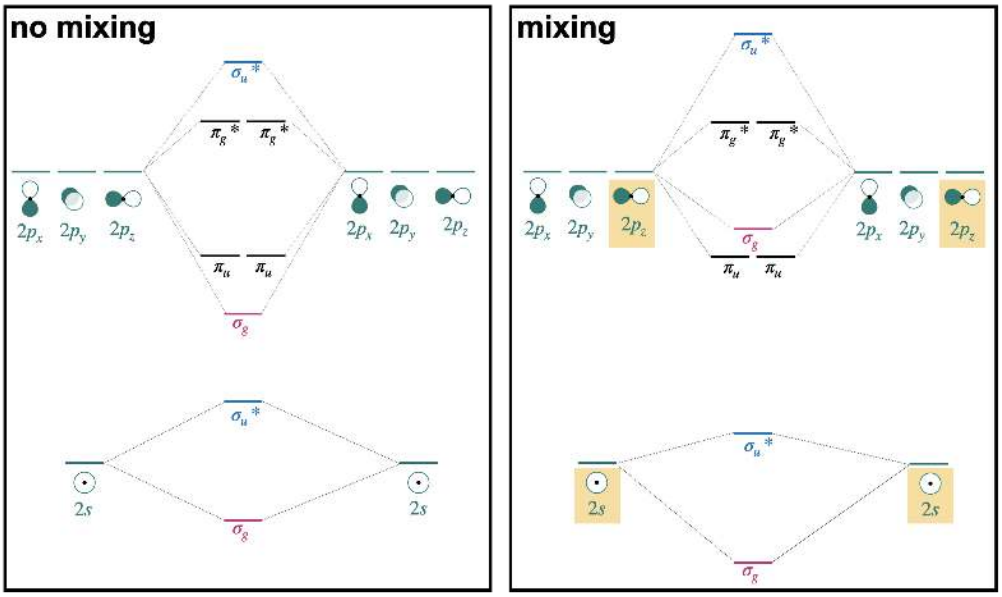


Figure **1.6.3.2.1**: Mixing of orbitals with like symmetry affects the energies of molecular orbitals. The simplified case where no mixing occurs is shown on the left. The effects of mixing are shown on the right. The σ_g orbitals of like symmetry are highlighted in fuschia and the σ_u^* orbitals of like symmetry are highlighted in blue. A group of atomic orbitals of similar symmetry are highlighted in yellow boxes; these atomic orbitals combine to give all σ molecular orbitals. (CC-BY-SA, Kathryn Haas)

In the case of homonuclear diatomic molecules of the second row, orbital mixing has important consequences for the energetic order of the $\sigma_g(2p)$ and $\pi_u(2p)$ orbitals. This will be discussed in the next section.

This page titled 1.6.3.2: Orbital Mixing is shared under a CC BY-NC-SA 4.0 license and was authored, remixed, and/or curated by Kathryn Haas.

- **5.2.2: Orbital Mixing** by Kathryn Haas is licensed CC BY-SA 4.0.

https://chem.libretexts.org/@go/page/484694

1.6.3.3: Diatomic Molecules of the First and Second Periods

First Period Homonuclear Diatomic Molecules

In the first row of the periodic table, the valence atomic orbitals are $1s$. There are two possible homonuclear diatomic molecules of the first period:

Dihydrogen, H_2 [$\sigma_g^2(1s)$]: This is the simplest diatomic molecule. It has only two molecular orbitals (σ_g and σ_u^*), two electrons, a bond order of 1, and is diamagnetic. Its bond length is 74 pm. MO theory would lead us to expect bond order to decrease and bond length to increase if we either add or subtract one electron. The calculated bond length for the H_2^+ ion is approximately 105 pm.[1]

Dihelium, He_2 [$\sigma_g^2\sigma_u^{*2}(1s)$]: This molecule has a bond order of zero due to equal number of electrons in bonding and antibonding orbitals. Like other nobel gases, He exists in the atomic form and does not form bonds at ordinary temperatures and pressures.

Exercise 1.6.3.3.1

Draw the complete molecular orbital diagrams for H_2 and for He_2. Include sketches of the atomic and molecular orbitals.

Answer

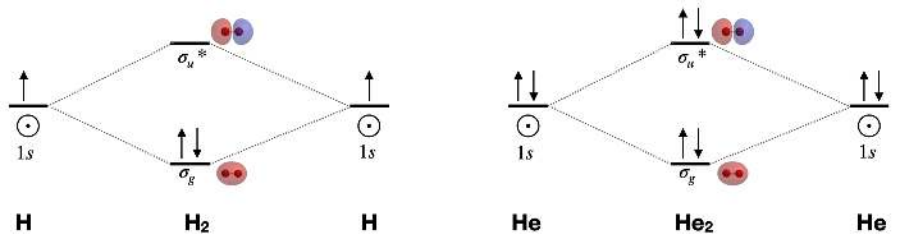


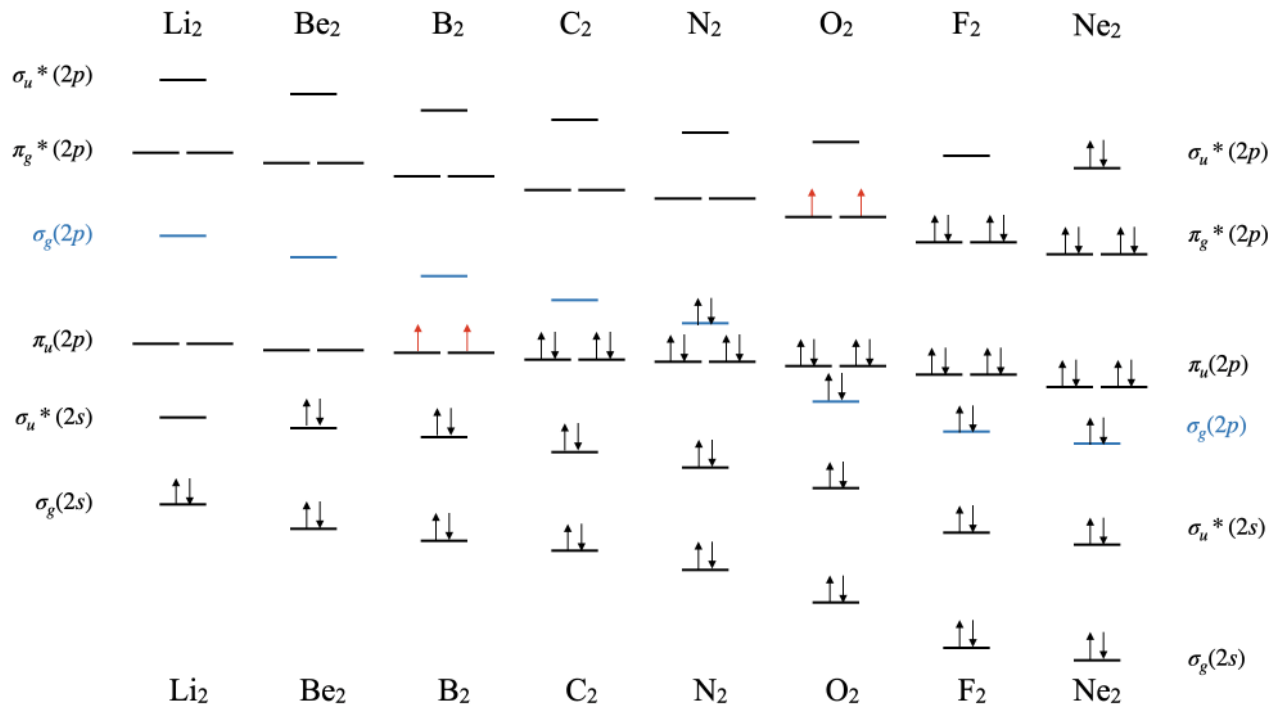
Figure for Exercise 1.6.3.3.1: Molecular orbital diagrams for dihydrogen and dihelium. Molecular orbital surfaces calculated using Spartan software. (CC-BY-NC-SA; Kathryn Haas)

A complete molecular orbital diagram includes all atomic orbitals and molecular orbitals, their symmetry labels, and electron filling.

Second Period Homonuclear Diatomic Molecules

The second period elements span from Li to Ne. The valence orbitals are 2s and 2p. In their molecular orbital diagrams, non-valence orbitals (1s in this case) are often disregarded in molecular orbital diagrams.

Orbital mixing has significant consequences for the magnetic and spectroscopic properties of second period homonuclear diatomic molecules because it affects the order of filling of the $\sigma_g(2p)$ and $\pi_u(2p)$ orbitals. Early in period 2 (up to and including nitrogen), the $\pi_u(2p)$ orbitals are lower in energy than the $\sigma_g(2p)$ (see Figure 1.6.3.3.1). However, later in period 2, the $\sigma_g(2p)$ orbitals are pulled to a lower energy. This lowering in energy of $\sigma_g(2p)$ is not unique; all of the σ orbitals in the molecule are pulled to lower energy due to the increasing positive charge of the nucleus. The π orbitals in the molecule are also affected, but to a much lesser extent than σ orbitals. The reason has to do with the high penetration of s atomic orbitals compared to p atomic orbitals (recall our previous discussion on penetration and shielding, and its effect on periodic trends). The σ molecular orbitals have more s character and thus their energy is more influenced by increasing nuclear charge. As nuclear charge increases, the energy of the $\sigma_g(2p)$ orbital is lowered significantly more than the energy of the $\pi_u(2p)$ orbitals (Figure 1.6.3.3.1).



	Li_2	Be_2	B_2	C_2	N_2	O_2	F_2	Ne_2
Unpaired e⁻	0	0	2	0	0	2	0	0
Bond Order	1	0	1	2	3	2	1	0
Experimental* Bond Length (pm)	267.3	246.0	159.0	124.3	109.8	120.8	141.2	310.0

*Experimental bond lengths from "List of Experimental Diatomic Bond Lengths", NIST, https://cccbdb.nist.gov/diatomicexpbondx.asp

Figure 1.6.3.3.1: Molecular orbital energy-level diagrams for the diatomic molecules of the period 2 elements. Unlike earlier diagrams, *only the valence molecular orbital energy levels for the **molecules** are shown here (atomic orbitals not shown for simplicity).* For Li_2 through N_2, the $\sigma_g(2p)$ orbital is higher in energy than the $\pi_u(2p)$ orbitals. In contrast, from O_2 onward, the $\sigma_g(2p)$ orbital is *lower* in energy than the $\pi_u(2p)$ orbitals because the nuclear charge increases across the row. The experimental bond lengths correlate with the calculated bond order. (CC-BY-NC-SA, Kathryn Haas)

Dilithium, Li_2 $[\sigma_g^2(2s)]$: This molecule has a bond order of one and is observed experimentally in the gas phase to have one Li-Li bond.

Diberylium, Be_2 $[\sigma_g^2\sigma_u^{*2}(2s)]$: This molecule has a bond order of zero due to the equal number of electrons in bonding and antibonding orbitals. Although Be_2 does not exist under ordinary conditions, it can be produced in a laboratory and its bond length measured (Figure 1.6.3.3.2). Although the bond is very weak, its bond length is surprisingly ordinary for a covalent bond of the second period elements.[2]

Diboron, B_2 $[\sigma_g^2\sigma_u^{*2}(2s)\pi_u^1\pi_u^1(2p)]$: The case of diboron is one that is much better described by molecular orbital theory than by Lewis structures or valence bond theory. This molecule has a bond order of one. The molecular orbital description of diboron also predicts, accurately, that diboron is paramagnetic. The paramagnetism is a consequence of orbital mixing, resulting in the σ_g orbital's being at a higher energy than the two degenerate π_u^* orbitals.

Dicarbon, C_2 $[\sigma_g^2\sigma_u^{*2}(2s)\pi_u^2\pi_u^2(2p)]$: This molecule has a bond order of two. Molecular orbital theory predicts two bonds with π symmetry, and no σ bonding. C_2 is rare in nature because its allotrope, diamond, is much more stable.

Dinitrogen, N_2 $[\sigma_g^2\sigma_u^{*2}(2s)\pi_u^2\pi_u^2\sigma_g^2(2p)]$: This molecule is predicted to have a triple bond. This prediction is consistent with its short bond length and bond dissociation energy. The energies of the $\sigma_g(2p)$ and $\pi_u(2p)$ orbitals are very close, and their relative energy levels have been a subject of some debate (see next section for discussion).

Dioxygen, O_2 $[\sigma_g^2\sigma_u^{*2}(2s)\sigma_g^2\pi_u^2\pi_u^2\pi_g^{*1}\pi_g^{*1}(2p)]$: This is another case where valence bond theory fails to predict actual properties. Molecular orbital theory correctly predicts that dioxygen is paramagnetic, with a bond order of two. Here, the molecular orbital diagram returns to its "normal" order of orbitals where orbital mixing could be somewhat ignored, and where $\sigma_g(2p)$ is lower in energy than $\pi_u(2p)$.

Difluorine, F_2 $[\sigma_g^2\sigma_u^{*2}(2s)\sigma_g^2\pi_u^2\pi_u^2\pi_g^{*2}\pi_g^{*2}(2p)]$: This molecule has a bond order of one and like oxygen, the $\sigma_g(2p)$ is lower in energy than $\pi_u(2p)$.

Dineon, Ne_2 $[\sigma_g^2\sigma_u^{*2}(2s)\sigma_g^2\pi_u^2\pi_u^2\pi_g^{*2}\pi_g^{*2}\sigma_u^{*2}(2p)]$: Like other noble gases, Ne exists in the atomic form and does not form bonds at ordinary temperatures and pressures. Like Be_2, Ne_2 is an unstable species that has been created in extreme laboratory conditions and its bond length has been measured (Figure **1.6.3.3.2**)

? Exercise 1.6.3.3.2

Draw the complete molecular orbital diagram for O_2. Show calculation of its bond order and tell whether it is diamagnetic or paramagnetic.

Answer

O_2 is paramagnetic with a bond order of 2. Its $\sigma_g(2p)$ molecular orbital is lower in energy that the set of $\pi_u(2p)$ orbitals.

$$\text{Bond order} = \frac{1}{2}\left[\left(\begin{array}{c}\textbf{8 electrons in}\\ \textbf{valence bonding orbitals}\end{array}\right) - \left(\begin{array}{c}\textbf{4 electrons in}\\ \textbf{valence antibonding orbitals}\end{array}\right)\right]$$

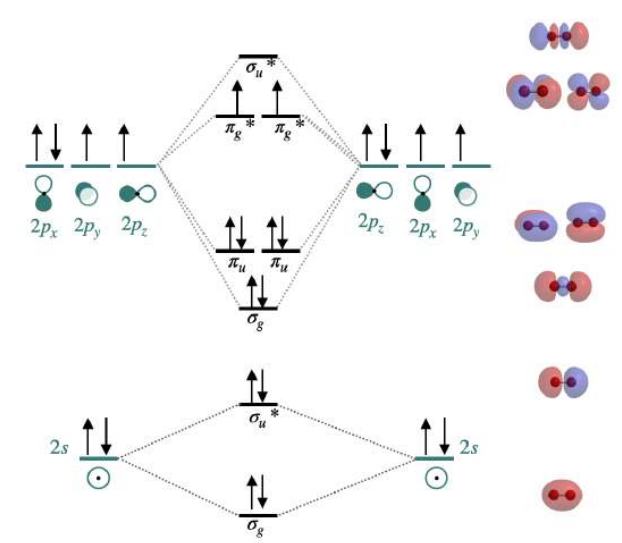


Figure for Exercise **1.6.3.3.2**. Molecular orbital diagram of O_2. (CC-BY-NC-SA, Kathryn Haas)

? Exercise 1.6.3.3.3: The Peroxide Ion

Use a qualitative molecular orbital energy-level diagram to predict the electron configuration, the bond order, and the number of unpaired electrons in the peroxide ion (O_2^{2-}).

Answer

This diagram looks similar to that of $\mathbf{O_2}$, except that there are two additional electrons.
$(\sigma_g(2s))^2\,(\sigma_u^*(2s))^2\,(\sigma_g(2p))^2\,(\pi_u(2p))^4\,(\pi_g(2p))^4$; bond order of 1; no unpaired electrons.

Bond Lengths in Homonuclear Diatomic Molecules

The trends in experimental bond lengths are predicted by molecular orbital theory, specifically by the calculated bond order. The values of bond order and experimental bond lengths for the second period diatomic molecules are given in Figure **1.6.3.3.1**, and

shown in graphical format on the plot in Figure **1.6.3.3.2**. From the plot, we can see that bond length correlates well with bond order, with a minimum bond length occurring where the bond order is greatest ($\mathbf{N_2}$). The shortest bond distance is at $\mathbf{N_2}$ due to its high bond order of 3. From $\mathbf{N_2}$ to $\mathbf{F_2}$ the bond distance increases despite the fact that atomic radius decreases.

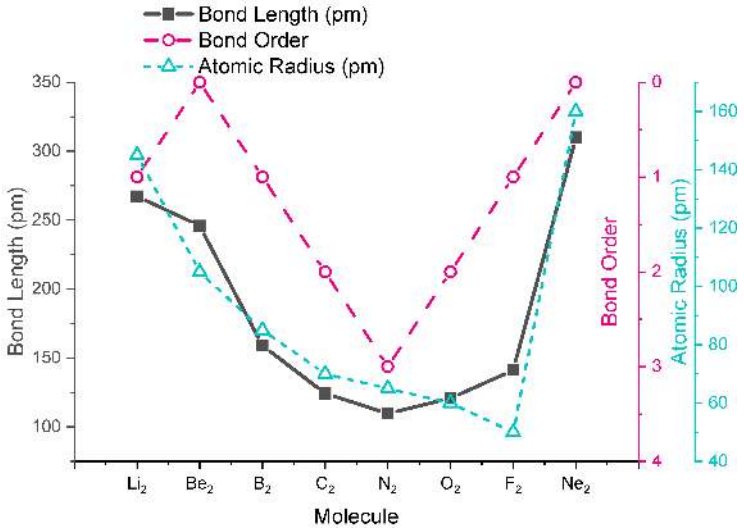


Figure **1.6.3.3.2**: Overlayed plots of bond length (black squares), bond order (pink circles), and atomic radius (teal triangles) versus atomic number for second period homonuclear diatomic molecules. (CC-BY-NC-SA; Kathryn Haas)

References

1. NIST, Calculated Geometries available for H_2^+ (Hydrogen cation) 2Σg+ D∞h, available at https://cccbdb.nist.gov/diatomicexpbondx.asp
2. Merritt, J. M.; Bondybey, V. E.; Heaven, M. C., Beryllium Dimer-Caught in the Act of Bonding. *Science* **2009,** *324* (5934), 1548-1551.

This page titled 1.6.3.3: Diatomic Molecules of the First and Second Periods is shared under a CC BY-NC-SA 4.0 license and was authored, remixed, and/or curated by Kathryn Haas.

- **5.2.3: Diatomic Molecules of the First and Second Periods** by Kathryn Haas is licensed CC BY-SA 4.0.
- **5.P: Problems** is licensed CC BY-SA 4.0.

1.6.3.4: Photoelectron Spectroscopy

A photoelectron spectrum can show the relative energies of occupied molecular orbitals by ionization. The *ionization energy* is a direct measure of the energy required to just remove the electron concerned from its initial level to the vacuum level (free electron). Photoelectron spectroscopy measures the relative energies of the ground and excited positive ion states that are obtained by removal of single electrons from the neutral molecule.

$$A + \text{photon} \rightarrow A^{+} + e^{-}$$

The information obtained from photoelectron spectroscopy is typically discussed in terms of the electronic structure and bonding in the ground states of neutral molecules, with ionization of electrons occurring from bonding molecular orbitals, lone pairs, antibonding molecular orbitals, or atomic cores. These descriptions reflect the relationship of ionization energies to the molecular orbital model of electronic structure.

Ionization energies are directly related to the energies of molecular orbitals (by Koopmans' theorem).

Example: Photoelectron spectrum of dihydrogen

The molecular orbital description of dihydrogen involves two $1s$ atomic orbitals generating two molecular orbitals: a bonding σ_g and an antibonding σ_u^*. The two electrons occupy the σ_g bonding orbital, leaving the molecule with a bond order of one (Figure **1.6.3.4.1**). The PES spectrum of dihydrogen (Figure **1.6.3.4.1**) has a single band that corresponds to the ionization of one electron from the σ_g. The multiple peaks are due to electrons ejecting from a range of stimulated vibrational energy levels. When extensive vibrational structure is resolved in a PES molecular orbital, then the removal of an electron from that molecular orbital induces a significant change in the bonding (in this case an increase in the bond length due to decrease in bond order).

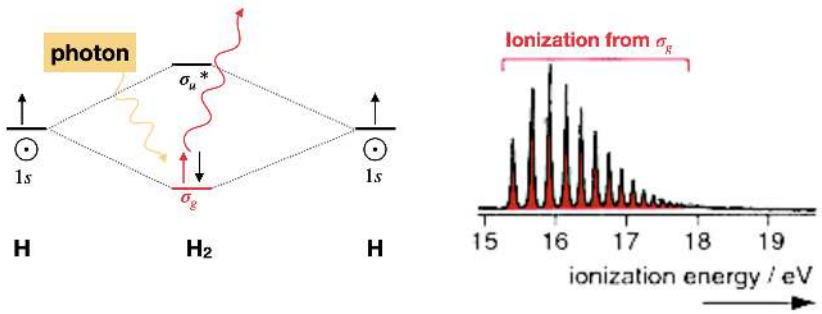


Figure **1.6.3.4.1**: The molecular orbital diagram and photoelectron spectrum of dihydrogen. (CC-BY-NC-SA; Libretexts)

Example: Photoelectron spectrum of dinitrogen

Diatomic nitrogen is more complex than hydrogen since multiple molecular orbitals are occupied. Five molecular orbitals are occupied; two of them are degenerate. Three bands in the photoelectron spectrum correspond to ionization of an electron in $\sigma_g(2p)$, $\pi_u(2p)$ and $\sigma_u^*(2s)$ molecular orbitals. Ionization of the fourth type of orbital, $\sigma_g(2s)$, does not appear in Figure **1.6.3.4.2** because it is either off scale or because the incident light $h\nu$ used did not have sufficient energy to ionize electrons in that deeply stabilized molecular orbital. Note that extensive vibrational structure for the $\pi_u(2p)$ band indicates that the removal of an electron from this molecular orbital causes a significant change in the bonding.

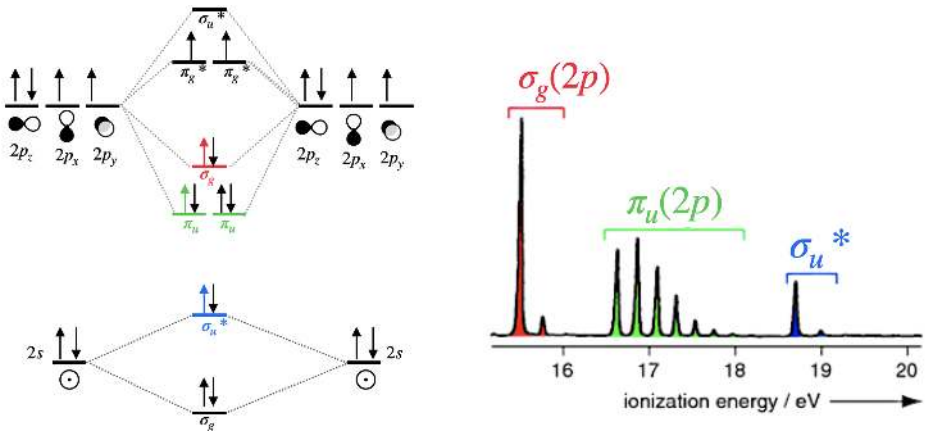


Figure **1.6.3.4.2**: The molecular orbital diagram and photoelectron spectrum of dinitrogen. (CC-BY-NC-SA; Libretexts)

From the photoelectron spectrum of dinitrogen, we can see that the electrons in the $\sigma_g(2p)$ orbital can be ionized using less energy than required to ionize electrons in the $\pi_u(2p)$ orbital. This is evidence for $\sigma_g(2p)$ existing at a higher energy than the $\pi_u(2p)$ orbitals.

This page titled 1.6.3.4: Photoelectron Spectroscopy is shared under a CC BY-NC-SA 4.0 license and was authored, remixed, and/or curated by Kathryn Haas.

- **10.4: Photoelectron Spectroscopy** by Roger Nix is licensed CC BY 4.0.

SECTION OVERVIEW

1.6.4: Heteronuclear Diatomic Molecules

Diatomic molecules with two non-identical atoms are called **heteronuclear** diatomic molecules. When atoms are not identical, the molecule forms by combining atomic orbitals of unequal energies. *The result is a polar bond in which atomic orbitals contribute unevenly to each molecular orbital*.

The application of molecular orbital theory to heteronuclear diatomic molecules is similar to the case of homonuclear diatomics, except that the atomic orbitals from each atom have different energies and contribute unequally to molecular orbitals. Recall that atomic orbitals must have compatible symmetry and similar energy to combine into molecular orbitals. In the case where atomic orbitals of like symmetry have different energies, they combine less favorably than orbitals that are closer to one another in energy. As a general rule, orbitals that have energy differences of greater than 10-14 eV do not combine favorably. In the molecular orbital diagram, the closer a molecular orbital is to an atomic orbital, the more that atomic orbital contributes to the molecular orbital. This last point is helpful for back-of-the napkin estimations of what the molecular orbitals "look" like.

In this section, you should learn how to generate molecular orbital diagrams of heteronuclear diatomic molecules. To approach such a problem, we must start with a knowledge of the relative energies of electrons in different atomic orbitals. In other words, we need knowledge of the orbital potential energies (or orbital ionization energies).

1.6.4.1: Polar bonds

1.6.4.2: Ionic Compounds and Molecular Orbitals

Sources:

- Gray, Harry. *Electrons and Chemical Bonding*, Benjamin, 1964.
- Miessler, Gary L, and Donald A. Tarr. *Inorganic Chemistry*. Upper Saddle River, N.J: Pearson Education, 2014. Print.

1.6.4: Heteronuclear Diatomic Molecules is shared under a CC BY-NC-SA 4.0 license and was authored, remixed, and/or curated by LibreTexts.

1.6.4.1: Polar bonds

Molecular orbital diagrams for heteronuclear diatomic molecules

The molecular orbital diagram of a heteronuclear diatomic molecule is approached in a way similar to that of a homonuclear diatomic molecule. The orbital diagrams may also look similar. A major difference is that the more electronegative atom will have orbitals at a lower energy level. Two examples of heteronuclear diatomic molecules will be explored below as illustrative examples.

Carbon monoxide MO diagram

Carbon monoxide is an example of a heteronuclear diatomic molecule where both atoms are second-row elements. The valence molecular orbitals in both atoms are the $2s$ and $2p$ orbitals. The molecular orbital diagram for carbon monoxide (Figure **1.6.4.1.1**) is constructed in a way similar to how you would construct dicarbon or dioxygen, except that the oxygen orbitals have a lower potential energy than analogous carbon orbitals. The labeling of molecular orbitals in this diagram follows a convention by which orbitals are given serial labels according to type of orbital (σ, π, etc.). The lowest energy orbitals of any type are assigned a value of 1 and higher energy orbitals of the same type are assigned by increasing intervals (..2, 3, 4...). The orbital labeling system described previously is inappropriate for heteronuclear diatomic molecules that cannot be assigned g and u subscripts.

A consequence of unequal atomic orbital energy levels is that orbital mixing is significant. Notice the order of the molecular orbitals labeled 1π and 3σ in Figure **1.6.4.1.1**. This is a similar order of π and σ orbitals to the one we saw in the case of the σ_g and π_u orbitals of N_2 and lighter diatomics of the second period. Because the oxygen $2p_z$ orbital is close in energy to both the carbon $2p_z$ and carbon $2s$, these three orbitals will have significant interaction (mixing). The result is an increase in the energy of the 3σ orbital and a decrease in energy of the $2\sigma^*$ orbital, resulting in the diagram shown in Figure **1.6.4.1.1**.

In the case of carbon monoxide (Figure **1.6.4.1.1**), atomic orbitals contribute unequally to each molecular orbital. For example, because the $2s$ orbital of oxygen is very close in energy to the 2σ moelcular orbital, it contributes to that molecular orbital more than the $2s$ orbital from carbon. Notice the shape of this 2σ orbital and how it is unevenly distributed over the two atoms; it is more heavily distributed on the oxygen because it is most like the oxygen $2s$. This is in line with the assumption that electron density is distributed more on oxygen because it is more electronegative than carbon. Likewise, the 1π orbitals are unevenly distributed, with more distribution close to the oxygen.

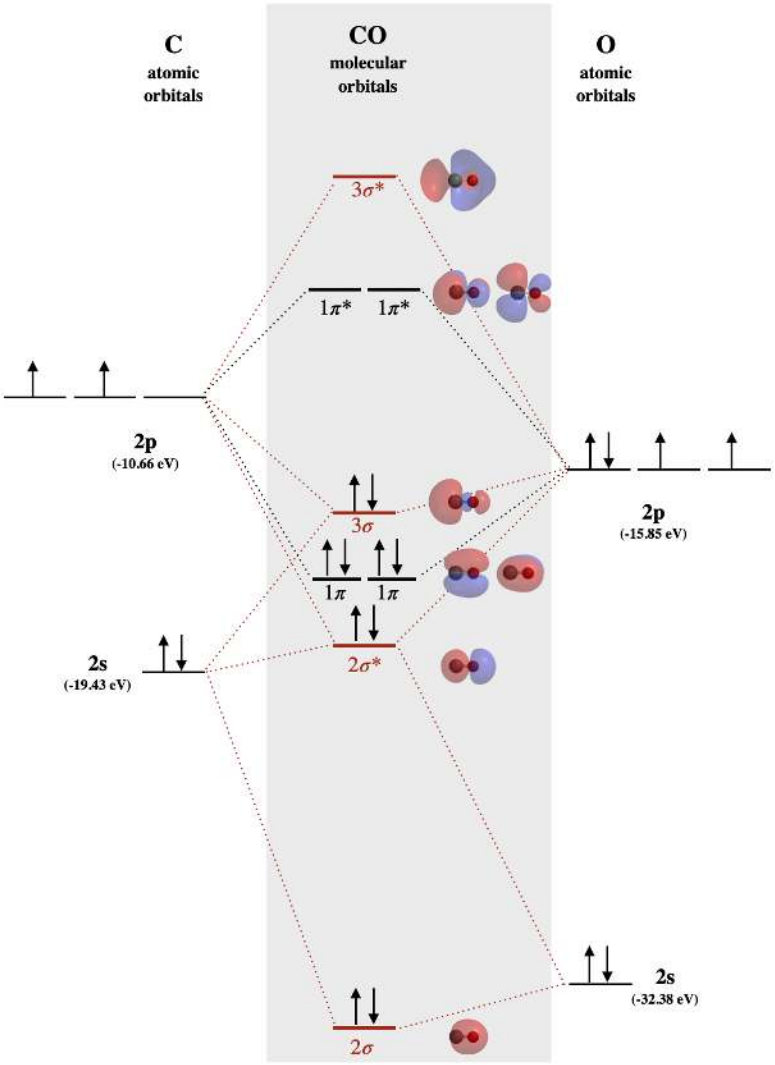
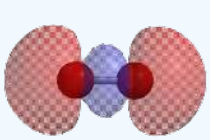


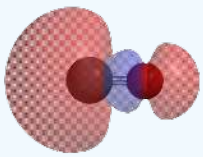
Figure 1.6.4.1.1: Molecular orbital diagram of carbon monoxide. The labeling of molecular orbitals in this diagram follows a convention by which orbitals are given serial names according to the type of orbital (σ, π, etc.). The lowest energy orbitals of any type are assigned a value of 1 and higher energy orbitals of the same type are assigned by increasing intervals (..2, 3, 4...). The orbital labeling system described previously is inappropriate for heteronuclear diatomic molecules that cannot be assigned g and u subscripts. Molecular orbital surfaces were calculated using Spartan software. (Kathryn Haas, CC-BY-NC-SA)

? Exercise 1.6.4.1.1

Examine the shape of the 3σ orbital of carbon monoxide in Figure 1.6.4.1.1. Describe what ways this shape is different from the shape of the σ_g orbitals from second period homonuclear diatomic molecules (see Fig. 5.2.1.1). Rationalize these differences. Both orbitals are re-created below for convenience.



σ_g of homonuclear diatomic



3σ of CO

Answer

https://chem.libretexts.org/@go/page/484698

The 3σ orbital is like the σ_g in that it has three lobes and two nodes distributed along the internuclear bond. They are different in their distribution. The two external lobes of σ_g are evenly distributed because they are an equal combination of two p_z orbitals (one from each atom). The 3σ orbital is more heavily distributed toward the carbon atom, the less electronegative atom, than toward the oxygen. The unequal distribution of 3σ is apparent in the unequal sizes of its exterior lobes and the uneven shape of the interior lobe. The heavier distribution within the exterior lobe on carbon is caused by the mixing of the carbon $2s$ orbital with carbon and oxygen $2p_z$ orbitals. The uneven shape of the interior lobe, where it leans toward oxygen, is best explained by the fact that the 3σ orbital is closer in energy to the oxygen $2p_z$ than the carbon $2p_z$.

Hydrogen fluoride MO diagram

Hydrogen fluoride is an example of a heteronuclear diatomic molecule in which the two atoms are from different periods. In this case, the valence orbital of H is $1s$ while those of F are $2s$ and $2p$. The molecular orbital diagram for HF is shown in Figure 1.6.4.1.2.

Three of these orbitals have compatible symmetry for mixing; these are the hydrogen $1s$, fluorine $2s$, and fluorine $2p$. However, the extent to which they will interact depends on their relative energies. Fluorine is more electronegative than H, and the fluorine atom has a higher first ionization energy than does hydrogen. From these trends, we can expect that the fluorine valence orbitals are lower in energy than that of hydrogen. From Table 5.3.1, we find that the 1s orbital of H (-13.6 eV) is higher in energy than both fluorine orbitals (-18.7 and -40.2 eV, respectively for $2p$ and $2s$). The energies of hydrogen $1s$ and fluorine $2p$ are a good match for combination; however, the fluorine $2s$ orbital is much too different to create a productive interaction. Therefore, we expect that the fluorine $2s$ will create a non-bonding molecular orbital, while the $1s$ and $2p_z$ orbitals combine to make σ bonding and σ^* antibonding molecular orbitals. The remaining $2p_x$ and $2p_y$ orbitals do not have compatible symmetry for bonding with hydrogen, and they will form non-bonding π molecular orbitals. The non-bonding orbitals will have similar energy and character as their component atomic orbitals.

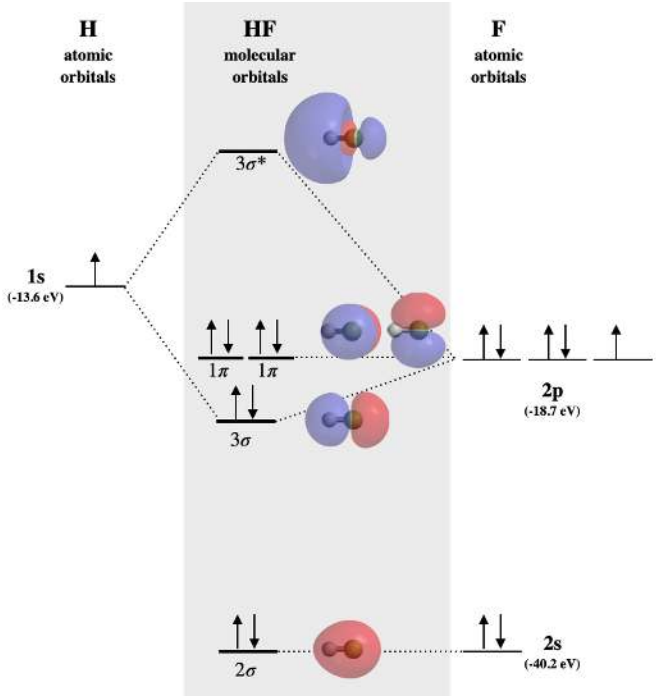


Figure 1.6.4.1.2: Molecular Orbital diagram of hydrogen fluoride. Molecular orbitals calculated using Spartan software. (Kathryn Haas, CC-BY-NC-SA)

Chemical reactions take place at the HOMO and LUMO orbitals

Knowledge of molecular orbital diagrams, and the shapes of molecular orbitals, can be used to accurately explain and predict chemical reactivity. Chemical reactions take place using the highest occupied molecular orbitals (HOMO) of a nucleophile or Lewis base, and the lowest unoccupied molecular orbital (LUMO) of an electrophile or Lewis acid.

> *Lewis bases react using electrons in the HOMO, while Lewis acids react using the empty LUMO.*

Example: Reactivity of CO with metal ions

CO is an excellent ligand for many metal ions. In fact, the strong affinity between CO and the heme iron (Fe) ions in hemoglobin can explain the mechanism of carbon monoxide poisoning. When CO binds in place of O_2 to hemoglobin, that hemoglobin can no longer carry O_2 to tissue cells. CO binding to hemoglobin is strong and practically irreversible. When CO binds to metal ions, it does so through the carbon atom. This is contrary to expectations based on the Lewis structure and the known bond polarity, where electron density is polarized toward oxygen. The distribution of the electron density of the HOMO of CO can explain this observation!

? Exercise 1.6.4.1.2

Refer to the MO diagram for CO. Identify the HOMO and explain why CO bonds to metal ions through the carbon atom rather than through the oxygen atom.

Answer

In the interaction between CO and a metal ion, CO would act as a Lewis base; thus it will react using electrons in its HOMO. The MO diagram for CO is shown in Figure 1.6.4.1.1: the HOMO is the 3σ orbital (also discussed in ? Exercise 1.6.4.1.1). The electron density of that MO is centered around the carbon atom, thus the carbon atom will be a better Lewis base than the O atom.

This page titled 1.6.4.1: Polar bonds is shared under a CC BY-NC-SA 4.0 license and was authored, remixed, and/or curated by Kathryn Haas.

- **5.3.2: Polar bonds** by Kathryn Haas is licensed CC BY-SA 4.0.

1.6.4.2: Ionic Compounds and Molecular Orbitals

Ionic interactions lie at one extreme on a spectrum of bonding. On the opposite end of the spectrum are the non-polar covalent bonds (e.g., homonuclear diatomics). In these molecules, molecular orbitals are formed by equal-energy atomic orbitals, resulting in electron density evenly distributed over the molecule. In the middle of the spectrum are the cases of polar covalent bonds (e.g., heteronuclear diatomics), in which atomic orbitals of unequal energies contribute unequally to molecular orbitals, resulting in uneven distribution of electron density across the molecule. In the case of polar bonds, the electron density is shifted toward the more electronegative atom since that atom contributes more to the lowest energy bonding molecular orbitals. Molecular orbital diagrams can be drawn for ionic compounds as if they are extremely polar bonds in which electrons are not only shifted toward, but are transferred completely to the more electronegative atom.

Example: NaCl

In **NaCl**, the sodium **3*s*** orbital (-5.2 eV) is significantly higher in energy than the chlorine valence orbitals. The chlorine **3*s*** and **3p_z** orbitals have compatible symmetry, yet only the **3p_z** orbital (-13.8 eV) is close enough in energy to interact with the Na **3*s***; still, the energy difference is large enough to make bonding weak. The Na **3*s*** orbital combines with Cl **3p_z** to form the molecular orbitals labeled **4σ** and **4σ*** in Figure **1.6.4.2.1**. The **4σ** orbital is weakly bonding, but is very close in energy to the Cl **3p_z** orbital, and is mostly Cl-like in character. Notice that all **σ** orbitals look very much like either **s** or **p** orbitals centered on the **Cl** atom, while the **4σ*** orbital is centered almost entirely on Na. The lack of molecular orbitals that are distributed over both atoms at once is consistent with a lack of significant covalent bond character in **NaCl**. The bonding here is characterized by transfer of one electron from **Na** to **Cl** and is almost entirely electrostatic. Bonding that is mostly electrostatic in character is non-directional, unlike true covalent bonding.

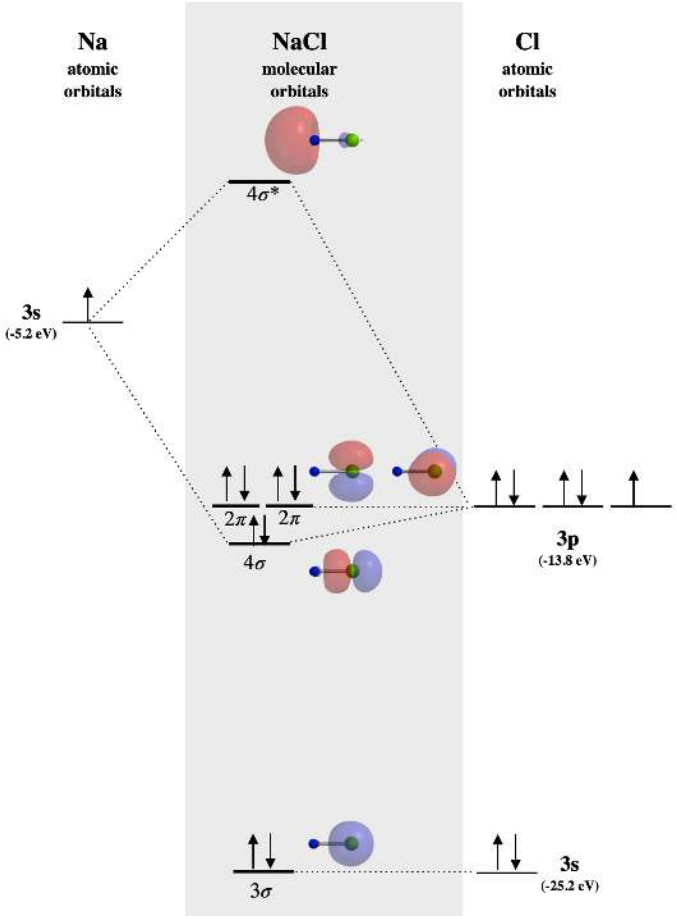


Figure **1.6.4.2.1**: The molecular orbital diagram for sodium chloride. Molecular orbital surfaces calculated using Spartan software indicate almost no covalent nature of bonding. (CC-BY-NC-SA, Kathryn Haas)

Exercise 1.6.4.2.1

Draw the molecular orbital diagram for **LiF**. Make sure to label all molecular orbitals appropriately, and specify whether they are mostly bonding, non-bonding, or antibonding. Identify the HOMO and LUMO. Sketch the approximate shapes of all orbitals.

Answer

We expect **LiF** to be an ionic compound because the energy difference in valence orbitals is at least 10-14 eV. (See Table 5.3.1) There are a variety of ways used to label molecular orbitals. In the figure below, we are using the convention of labeling each type of orbital with numbers starting from the lowest-energy orbitals. The 1σ orbital would be mostly F $1s$ in character and is not shown. The 2σ orbital is mostly non-bonding in nature, although it has a very small contribution from $2s$ of Li due to compatible symmetry. The 3σ orbital is slightly bonding but it is mostly F$2p$ in character. The two 1π orbitals are completely non-bonding. The $3\sigma^*$ orbital is antibonding.

- HOMO is 1π
- LUMO is $3\sigma^*$

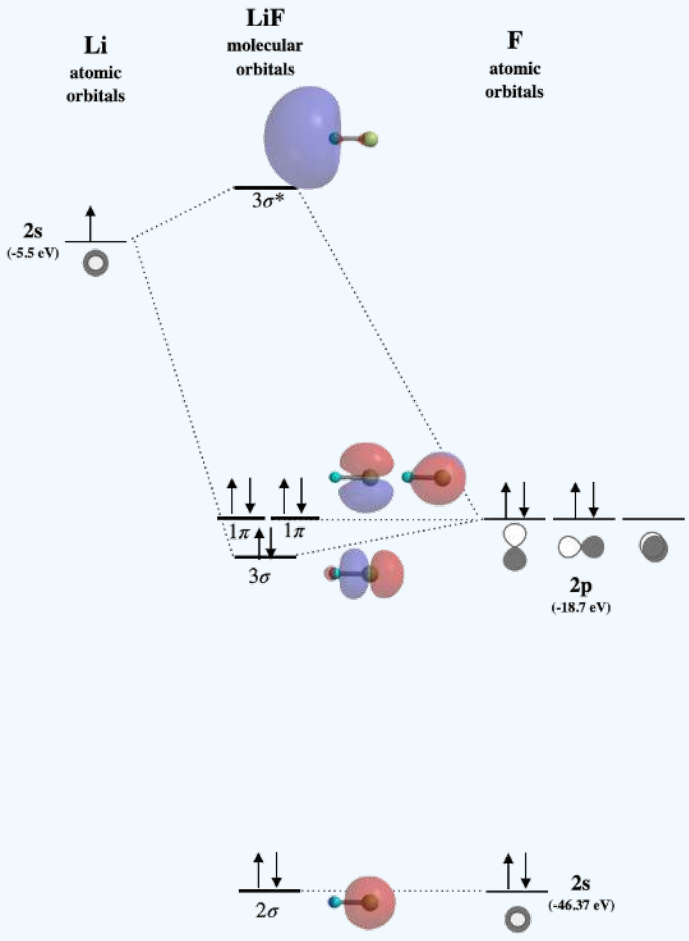


Figure for Exercise **1.6.4.2.1**: Molecular orbital diagram for the ionic compund, LiF. (CC-BY-NC-SA, Kathryn Haas)

This page titled 1.6.4.2: Ionic Compounds and Molecular Orbitals is shared under a CC BY-NC-SA 4.0 license and was authored, remixed, and/or curated by Kathryn Haas.

- **5.3.3: Ionic Compounds and Molecular Orbitals** by Kathryn Haas is licensed CC BY-SA 4.0.

CHAPTER OVERVIEW

2: Molecular Symmetry and Group Theory

2.1: Symmetry Elements and Operations

2.2: Point Groups

2.2.1: Groups of Low and High Symmetry

2.2.2: Other Groups

2.3: Properties and Representations of Groups

2.3.1: Matrices

2.3.2: Representations of Point Groups

2.3.3: Character Tables

2.4: Examples and Applications of Symmetry

2.4.1: Molecular Vibrations

2.4.2: Chirality

2.5: Generating SALCs for Polyatomic Molecules

2.5.1: Bifluoride anion

2.5.2: Carbon Dioxide

2.5.3: H_2O

2.5.4: NH_3

2.5.5: CO_2 (Revisted with Projection Operators)

2.5.6: BF_3

2: Molecular Symmetry and Group Theory is shared under a CC BY-NC-SA 4.0 license and was authored, remixed, and/or curated by LibreTexts.

2.1: Symmetry Elements and Operations

Introduction

The symmetry of a molecule consists of **symmetry operations** and **symmetry elements**. A symmetry operation is an operation that is performed to a molecule which leaves it indistinguishable and superimposable on the original position. Symmetry operations are performed with respect to symmetry elements (points, lines, or planes).

An example of a symmetry operation is a 180° rotation of a water molecule in which the resulting position of the molecule is indistinguishable from the original position (see Figure **2.1.1**). In this example, the symmetry operation is the rotation and the symmetry element is the axis of rotation.

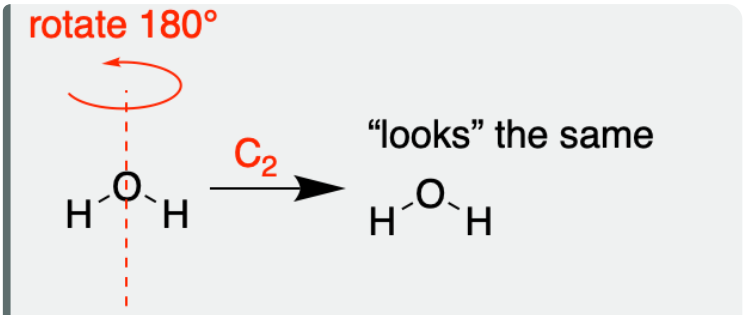


Figure 2.1.1: An example of a symmetry operation is a 180° rotation where the resulting position is indistinguishable from the original. A 180° rotation is called a C_2 operation; the axis of rotation is the symmetry element.

There are five types of symmetry operations: **identity**, **reflection**, **inversion**, **proper rotation**, and **improper rotation**. The symmetry elements that correspond to the five types of symmetry operations are listed in Table **2.1.1**.

Table **2.1.1***: Table of elements and operations*

Element	Operation	Symbol
Identity	identity	E
Proper rotation	rotation by (360/n)°	C_n
Reflection	reflection in a plane	σ
Inversion	inversion of a point at (x,y,z) to (-x,-y,-z)	*i*
Improper rotation	rotation by (360/n)°, followed by reflection in the plane perpendicular to the rotation axis	S_n

Symmetry Operations and Elements

Identity (E)

All molecules have the identity element. The identity operation is doing nothing to the molecule (it doesn't rotate, reflect, or invert...it just is).

Proper Rotation and Proper Axis (C_n)

A "proper" rotation is just a simple rotation operation about an axis. The symbol for any proper rotation or proper axis is $C_{(360/n)}$, where n is the degree of rotation. Thus, a 180° rotation is a C_2 rotation around a C_2 axis, and a 120° rotation is a C_3 rotation about a C_3 axis.

PRINCIPLE AXIS: The principle axis of a molecule is the highest order proper rotation axis, in other words, the largest value of n. For example, if a molecule had C_2 and C_4 axes, the C_4 is the principle axis.

Reflection and Symmetry Planes (σ)

Mirror planes are symmetry planes within the molecule. A reflection operation occurs with respect to a plane of symmetry. There are three classes of symmetry elements:

1. σ_h (horizontal): horizontal planes are perpendicular to principal axis
2. σ_v (vertical): vertical planes are parallel to the principal axis
3. σ_d (dihedral): dihedral planes are parallel to the principle axis and bisect two C_2 axes

Inversion and Inversion Center (i)

The inversion operation requires a point of symmetry (a center of symmetry within a molecule). In other words, a point at the center of the molecule that can transform (x,y,z) into (-x,-y,-z) coordinate. Structures of tetrahedron, triangles, and pentagons lack an inversion center.

Improper rotation (S_n)

Improper rotation is a combination of a rotation with respect to an axis of rotation (C_n), followed by a reflection through a plane perpendicular to that C_n axis. In short, an S_n operation is equivalent to C_n followed by σ_h.

References

1. Introduction to Molecular Symmetry by J. S Ogden
2. Inorganic Chemistry by Catherine Housecroft And Alan G. Sharpe.

2.1: Symmetry Elements and Operations is shared under a CC BY-NC-SA 4.0 license and was authored, remixed, and/or curated by LibreTexts.

SECTION OVERVIEW

2.2: Point Groups

Introduction

A **Point Group** describes all the symmetry operations that can be performed on a molecule that result in a conformation indistinguishable from the original. Point groups are used in Group Theory, the mathematical analysis of groups, to determine properties such as a molecule's molecular orbitals.

Assigning Point Groups

While a point group contains all of the symmetry operations that can be performed on a given molecule, it is not necessary to identify all of these operations to determine the molecule's overall point group. Instead, a molecule's point group can be determined by following a set of steps which analyze the presence (or absence) of particular symmetry elements.

Steps for assigning a molecule's point group:

1. Determine if the molecule has an infinite rotation axis.
2. If yes, determine if there is an inversion center. If no, find the highest order rotation axis, C_n, and continue.
3. If the molecule does not contain a rotation axis, look for either a mirror plane or an inversion center. If you find at least one rotation axis, look for multiple rotation axes where the n value is greater than 2.
4. Determine if the molecule has any C_2 axes perpendicular to the principal C_n axis. If so, then there are n such C_2 axes, and the molecule is in the D set of point groups. If not, it is in either the C or S set of point groups.
5. Determine if the molecule has a horizontal mirror plane (σ_h) perpendicular to the principal C_n axis. If so, the molecule is either in the C_{nh} or D_{nh} set of point groups.
6. Determine if the molecule has a vertical mirror plane (σ_v) containing the principal C_n axis. If so, the molecule is either in the C_{nv} or D_{nd} set of point groups. If not, and if the molecule has n perpendicular C_2 axes, then it is part of the D_n set of point groups.
7. Determine if there is an improper rotation axis, S_{2n}, collinear with the principal C_n axis. If so, the molecule is in the S_{2n} point group. The S_{2n} point group is extremely unlikely to appear in this course. If not, the molecule is in the C_n point group.

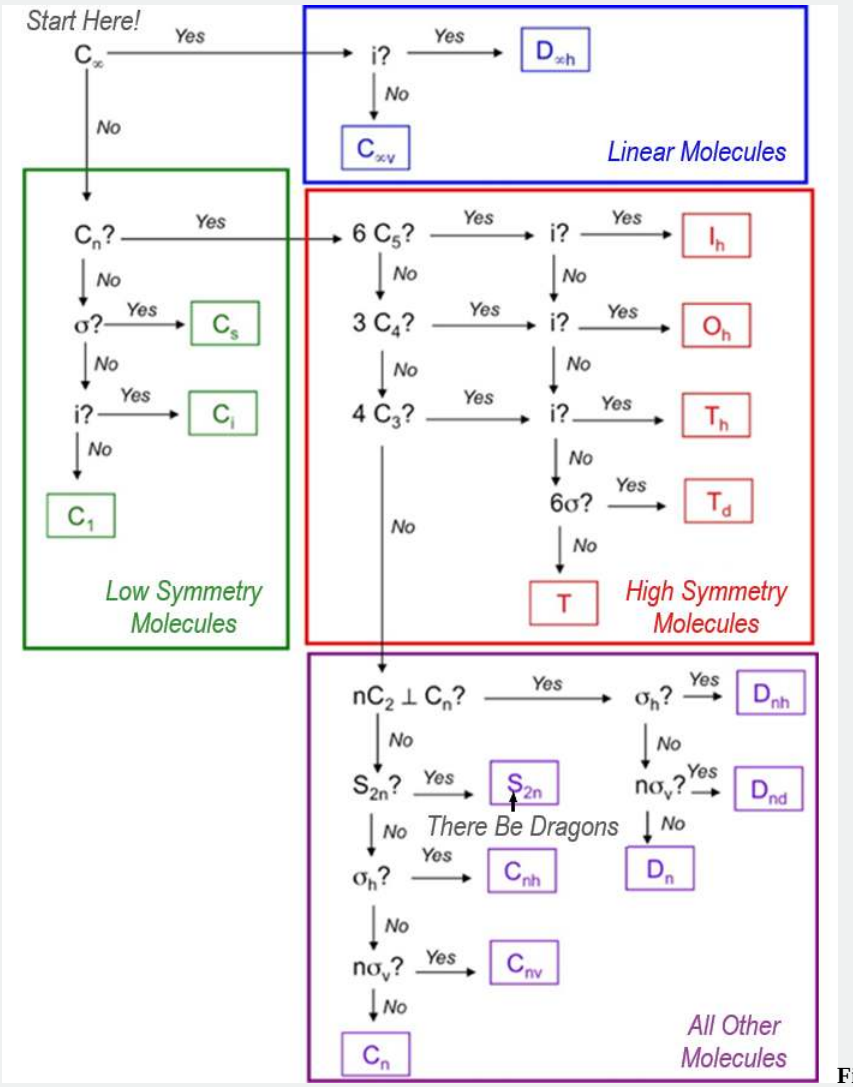


Figure 2.2.1: Decision tree for determining a molecule's point group (CC-BY-NC-SA; Chip Nataro)

Example 2.2.1

Find the point group of borane (BH3).

Answer

Solution

1. Borane does not have an infinite rotation axis.
2. Highest order rotation axis: C3
3. There are not multiple axes with n greater than 2.
4. There are 3 C_2 axes perpendicular to the principal axis
5. There is a horizontal mirror plane (σ_h)

Borane is in the D_{3h} point group.

See Also

Symmetry Challenge

2.2.1: Groups of Low and High Symmetry

2.2.2: Other Groups

2.2: Point Groups is shared under a CC BY-NC-SA 4.0 license and was authored, remixed, and/or curated by LibreTexts.

2.2.1: Groups of Low and High Symmetry

Low Symmetry Point Groups

Low symmetry point groups include the C_1, C_s, and C_i groups

Group	Description	Example
C_1	only the identity operation (E)	CHFClBr
C_s	only the identity operation (E) and one mirror plane	C_2H_2ClBr
C_i	only the identity operation (E) and a center of inversion (i)	$C_2H_2Cl_2Br$

High Symmetry Point Groups

High symmetry point groups include the T_d, O_h, I_h, $C_{\infty v}$, and $D_{\infty h}$ groups. The table below describes their characteristic symmetry operations. The full set of symmetry operations included in the point group is described in the corresponding character table.

Group	Description	Example
$C_{\infty v}$	linear molecule with an infinite number of rotation axes and vertical mirror planes (σ_v)	HBr
$D_{\infty h}$	linear molecule with an infinite number of rotation axes, vertical mirror planes (σ_v), perpendicular C_2 axes, a horizontal mirror plane (σ_h), and an inversion center (i)	CO_2
T_d	typically have tetrahedral geometry, with 4 C_4 axes, 3 C_2 axes, 3 S_4 axes, and 6 dihedral mirror planes (σ_d)	CH_4
O_h	typically have octahedral geometry, with 3 C_4 axes, 4 C_3 axes, and an inversion center (i) as characteristic symmetry operations	SF_6
I_h	typically have an icosahedral structure, with 6 C_5 axes as characteristic symmetry operations	$B_{12}H_{12}^{2-}$

2.2.1: Groups of Low and High Symmetry is shared under a CC BY-NC-SA 4.0 license and was authored, remixed, and/or curated by LibreTexts.

2.2.2: Other Groups

D Groups

The D set of point groups are classified as D_{nh}, D_{nd}, or D_n, where n refers to the principal axis of rotation. Overall, the D groups are characterized by the presence of n C_2 axes perpendicular to the principal C_n axis. Further classification of a molecule in the D groups depends on the presence of horizontal or vertical/dihedral mirror planes.

Group	Description	Example
D_{nh}	n perpendicular C_2 axes, and a horizontal mirror plane (σ_h)	benzene, C_6H_6 is D_{6h}
D_{nd}	n perpendicular C_2 axes, and a vertical mirror plane (σ_v)	propadiene, C_3H_4 is D_{2d}
D_n	n perpendicular C_2 axes, no mirror planes	$[Co(en)_3]^{3+}$ is D_3

C Groups

The C set of point groups are classified as C_{nh}, C_{nv}, or C_n, where n refers to the principal axis of rotation. The C set of groups are characterized by the absence of n C_2 axes perpendicular to the principal C_n axis. Further classification of a molecule in the C groups depends on the presence of horizontal or vertical/dihedral mirror planes.

Group	Description	Example
C_{nh}	horizontal mirror plane (σ_h) perpendicular to the principal C_n axis	boric acid, H_3BO_3 is C_{3h}
C_{nv}	vertical mirror plane (σ_v) containing the principal C_n axis	ammonia, NH_3 is C_{3v}
C_n	no mirror planes	$P(C_6H_5)_3$ is C_3

S Groups

The S set of point groups are classified as S_{2n}, where n refers to the principal axis of rotation. The S set of groups are characterized by the absence of n C_2 axes perpendicular to the principal C_n axis, as well as the absence of horizontal and vertical/dihedral mirror planes. However, there is an improper rotation (or a rotation-reflection) axis collinear with the principal C_n axis.

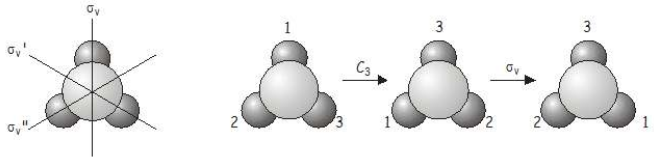
Group	Description	Example
S_{2n}	improper rotation (or a rotation-reflection) axis collinear with the principal C_n axis	12-crown-4 is S_4

2.2.2: Other Groups is shared under a CC BY-NC-SA 4.0 license and was authored, remixed, and/or curated by LibreTexts.

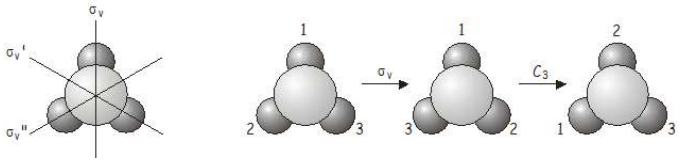
2.3: Properties and Representations of Groups

Group Multiplication

Now we will investigate what happens when we apply two symmetry operations in sequence. As an example, consider the NH_3 molecule, which belongs to the C_{3v} point group. Consider what happens if we apply a C_3rotation (120˚ counter-clockwise) followed by a σ_v reflection (reflection over the σ_v axis). We write this combined operation $\sigma_v C_3$ (when written, symmetry operations operate on the thing directly to their right, just as operators do in quantum mechanics – we therefore have to work backwards from right to left from the notation to get the correct order in which the operators are applied). As we shall soon see, the order in which the operations are applied is important.



The combined operation $\sigma_v C_3$ is equivalent to σ_v'' (note the double prime on σ_v''!), which is also a symmetry operation of the C_{3v} point group. Now let's see what happens if we apply the operators in the reverse order, i.e., $C_3\sigma_v$ is (σ_v followed by C_3).



Again, the combined operation $C_3\sigma_v$ is equivalent to another operation of the point group, this time σ_v' (note the single prime on σ_v'!).

There are two important points that are illustrated by this example:

1. The order in which two operations are applied is important. For two symmetry operations A and B, AB is not necessarily the same as BA, i.e. symmetry operations do not in general ***commute***. In some groups the symmetry elements do commute; such groups are said to be ***Abelian***.
2. If two operations from the same point group are applied in sequence, the result will be equivalent to another operation from the point group. Symmetry operations that are related to each other by other symmetry operations of the group are said to belong to the same ***class***. In NH_3, the three mirror planes σ_v, σ_v' and σ_v'' belong to the same class (related to each other through a C_3 rotation), as do the rotations C_3^+ and C_3^- (anticlockwise and clockwise rotations about the principal axis, related to each other by a vertical mirror plane).

Four Properties of Mathematical Groups

Now that we have explored some of the properties of symmetry operations and elements and their behavior within point groups, we are ready to introduce the formal mathematical definition of a group. The definitions below will be put into the context of *molecular* symmetry.

A mathematical group is defined as a set of elements (A_1, A_2, A_3...) together with a rule for forming combinations A_i,A_j... For our purposes, A_1, A_2, A_3, etc. are symmetry elements and A_i, A_j, etc. are symmetry operations described in a previous section. The elements of the group and the rule for combining them must satisfy the following four criteria.

1. The group must include the **identity** E, which commutes with other members of the group. In other terms, $EA_i = A_i$ for all the elements of the group. Application of the identity operation before or after another operation, A_i, results in the same outcome as A_i alone.
2. The elements must satisfy the group property that the combination of any pair of elements is also an element of the group. For example, in the C_{3v} point group, a C_3 rotation followed by a σ_v gives another operation that is already part of the group: a σ_v''.

3. Each symmetry operation A_i must have an inverse A_i^{-1}, which is also an element of the group, such that

$$A_i A_i^{-1} = A_i^{-1} A_i = E$$

   The inverse g_i^{-1} effectively 'undoes' the effect of the symmetry operation g_i. For example, in the C_{3v} point group, the inverse of C_3^+ is C_3^-.
4. The rule of combination must be associative

$$(A_i A_j)(A_k) = A_i(A_j A_k)$$

   Or $A(BC) = (AB)C$. In other words, the order of operations should not matter.

Group theory is an important area in mathematics, and luckily for chemists the mathematicians have already done most of the work for us. Along with the formal definition of a group comes a comprehensive mathematical framework that allows us to carry out a rigorous treatment of symmetry in molecular systems and learn about its consequences.

Many problems involving operators or operations (such as those found in quantum mechanics or group theory) may be reformulated in terms of matrices. Any of you who have come across transformation matrices before will know that symmetry operations such as rotations and reflections may be represented by matrices. It turns out that the set of matrices representing the symmetry operations in a group obey all the conditions laid out above in the mathematical definition of a group, and using matrix representations of symmetry operations simplifies carrying out calculations in group theory. Before we learn how to use matrices in group theory, it will probably be helpful to review some basic definitions and properties of matrices.

*This page was adapted from here (click).

Contributors and Attributions

- Claire Vallance (University of Oxford)
- Curated or created by Kathryn Haas

2.3: Properties and Representations of Groups is shared under a CC BY-NC-SA 4.0 license and was authored, remixed, and/or curated by LibreTexts.

- **4.3: Properties and Representations of Groups** by Kathryn Haas is licensed CC BY-NC-SA 4.0.

2.3.1: Matrices

The symmetry of molecules is essential for understanding the structures and properties of organic and inorganic compounds. The properties of chemical compounds are often easily explained by consideration of symmetry. For example, the symmetry of a molecule determines whether the molecule has a permanent dipole moment or not. The theories that describe optical activity, infrared and ultraviolet spectroscopy, and crystal structure involve the application of symmetry considerations. Matrix algebra is the most important mathematical tool in the description of symmetry.

The properties of symmetry groups are organized in character tables (discussed later in this chapter). Character tables are constructed based on matrices. This page is a brief description of matrices and matrix multiplication.

What is a matrix?

An $m \times n$ matrix $\mathbf{A}$ is a rectangular array of numbers with m rows and n columns. The numbers m and n are the dimensions of $\mathbf{A}$. The numbers in the matrix are called its entries. The entry in row i and column j is called a_{ij}.

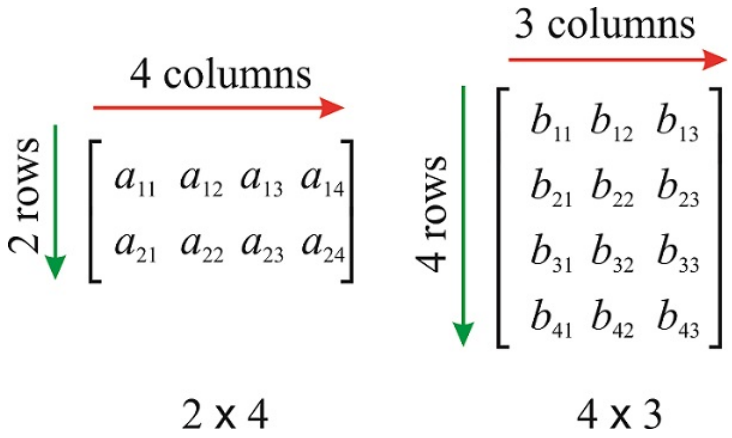


Figure **2.3.1.1**: Matrices of different dimensions

Some types of matrices have special names:

- A square matrix:

$$\begin{pmatrix} 3 & -2 & 4 \\ 5 & 3i & 3 \\ -i & 1/2 & 9 \end{pmatrix}$$

  with $m = n$
- A rectangular matrix:

$$\begin{pmatrix} 3 & -2 & 4 \\ 5 & 3i & 3 \end{pmatrix}$$

  with $m \neq n$
- A column vector:

$$\begin{pmatrix} 3 \\ 5 \\ -i \end{pmatrix}$$

  with $n = 1$
- A row vector:

$$\begin{pmatrix} 3 & -2 & 4 \end{pmatrix}$$

  with $m = 1$
- The identity matrix:

$$\begin{pmatrix} 1 & 0 & 0 \\ 0 & 1 & 0 \\ 0 & 0 & 1 \end{pmatrix}$$

with $a_{ij} = \delta_{i,j}$, where $\delta_{i,j}$ is a function defined as $\delta_{i,j} = 1$ if $i = j$ and $\delta_{i,j} = 0$ if $i \neq j$.

- A diagonal matrix:

$$\begin{pmatrix} a & 0 & 0 \\ 0 & b & 0 \\ 0 & 0 & c \end{pmatrix}$$

with $a_{ij} = c_i \delta_{i,j}$.

- An upper triangular matrix:

$$\begin{pmatrix} a & b & c \\ 0 & d & e \\ 0 & 0 & f \end{pmatrix}$$

All the entries below the main diagonal are zero.

- A lower triangular matrix:

$$\begin{pmatrix} a & 0 & 0 \\ b & c & 0 \\ d & e & f \end{pmatrix}$$

All the entries above the main diagonal are zero.

- A triangular matrix is one that is either lower triangular or upper triangular.

The Trace of a Matrix

The trace of an $n \times n$ square matrix $\mathbf{A}$ is the sum of the diagonal elements, and formally defined as $Tr(\mathbf{A}) = \sum_{i=1}^{n} a_{ii}$.

For example,

$$\mathbf{A} = \begin{pmatrix} 3 & -2 & 4 \\ 5 & 3i & 3 \\ -i & 1/2 & 9 \end{pmatrix} ; Tr(\mathbf{A}) = 12 + 3i$$

Singular and Nonsingular Matrices

A square matrix with nonzero determinant is called *nonsingular*. A matrix whose determinant is zero is called *singular*. (Note that you cannot calculate the determinant of a non-square matrix).

For a 2x2 matrix,

$$\mathbf{B} = \begin{pmatrix} a & b \\ c & d \end{pmatrix} ; det(\mathbf{B}) = ad - cb$$

For a 3x3 matrix,

$$\mathbf{C} = \begin{pmatrix} a & b & c \\ d & e & f \\ g & h & i \end{pmatrix}$$

$$det(\mathbf{C}) = a \begin{pmatrix} e & f \\ h & i \end{pmatrix} - b \begin{pmatrix} d & f \\ g & i \end{pmatrix} + c \begin{pmatrix} d & e \\ g & h \end{pmatrix}$$

$$det(\mathbf{C}) = aei - ahf - bdi + bgf + cdh - cge$$

The Matrix Transpose

The matrix transpose, most commonly written $\mathbf{A}^T$, is the matrix obtained by exchanging $\mathbf{A}$'s rows and columns. It is obtained by replacing all elements a_{ij} with a_{ji}. For example:

$$\mathbf{A} = \begin{pmatrix} 3 & -2 & 4 \\ 5 & 3i & 3 \end{pmatrix} \rightarrow \mathbf{A}^T = \begin{pmatrix} 3 & 5 \\ -2 & 3i \\ 4 & 3 \end{pmatrix}$$

Matrix Multiplication

To multiply two matrices, the number of vertical columns in the first matrix must be the same as the number of rows in the second matrix. If $\mathbf{A}$ has dimensions $m \times n$ and $\mathbf{B}$ has dimensions $n \times p$, then the product $\mathbf{AB}$ is defined, and has dimensions $m \times p$.

$$c_{ij} = \sum a_{ij} \times b_{ij}$$

The entry $a_{ij} \times b_{ij}$ is obtained by multiplying row i of $\mathbf{A}$ by column j of $\mathbf{B}$, which is done by multiplying corresponding entries together and then adding the results:

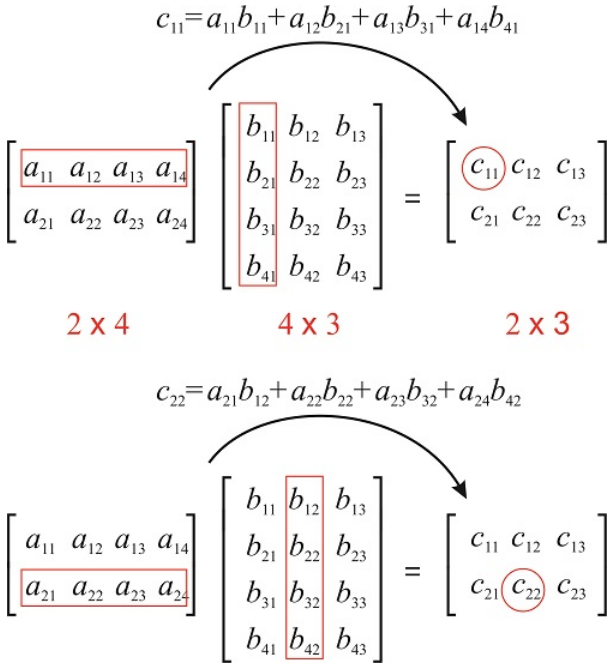


Figure 2.3.1.1: Matrix multiplication

Example 2.3.1.1

Calculate the product

$$\begin{pmatrix} 1 & -2 & 4 \\ 5 & 0 & 3 \\ 0 & 1/2 & 9 \end{pmatrix} \begin{pmatrix} 1 & 0 \\ 5 & 3 \\ -1 & 0 \end{pmatrix}$$

Solution

We need to multiply a 3×3 matrix by a 3×2 matrix, so we expect a 3×2 matrix as a result.

$$\begin{pmatrix} 1 & -2 & 4 \\ 5 & 0 & 3 \\ 0 & 1/2 & 9 \end{pmatrix} \begin{pmatrix} 1 & 0 \\ 5 & 3 \\ -1 & 0 \end{pmatrix} = \begin{pmatrix} a & b \\ c & d \\ e & f \end{pmatrix}$$

To calculate a, which is entry (1,1), we use row 1 of the matrix on the left and column 1 of the matrix on the right:

$$\begin{pmatrix} 1 & -2 & 4 \\ 5 & 0 & 3 \\ 0 & 1/2 & 9 \end{pmatrix} \begin{pmatrix} 1 & 0 \\ 5 & 3 \\ -1 & 0 \end{pmatrix} = \begin{pmatrix} a & b \\ c & d \\ e & f \end{pmatrix} \rightarrow a = 1 \times 1 + (-2) \times 5 + 4 \times (-1) = -13$$

To calculate b, which is entry (1,2), we use row 1 of the matrix on the left and column 2 of the matrix on the right:

$$\begin{pmatrix}1 & -2 & 4\\ 5 & 0 & 3\\ 0 & 1/2 & 9\end{pmatrix}\begin{pmatrix}1 & 0\\ 5 & 3\\ -1 & 0\end{pmatrix}=\begin{pmatrix}a & b\\ c & d\\ e & f\end{pmatrix}\rightarrow b=1\times 0+(-2)\times 3+4\times 0=-6$$

To calculate c, which is entry (2,1), we use row 2 of the matrix on the left and column 1 of the matrix on the right:

$$\begin{pmatrix}1 & -2 & 4\\ 5 & 0 & 3\\ 0 & 1/2 & 9\end{pmatrix}\begin{pmatrix}1 & 0\\ 5 & 3\\ -1 & 0\end{pmatrix}=\begin{pmatrix}a & b\\ c & d\\ e & f\end{pmatrix}\rightarrow c=5\times 1+0\times 5+3\times(-1)=2$$

To calculate d, which is entry (2,2), we use row 2 of the matrix on the left and column 2 of the matrix on the right:

$$\begin{pmatrix}1 & -2 & 4\\ 5 & 0 & 3\\ 0 & 1/2 & 9\end{pmatrix}\begin{pmatrix}1 & 0\\ 5 & 3\\ -1 & 0\end{pmatrix}=\begin{pmatrix}a & b\\ c & d\\ e & f\end{pmatrix}\rightarrow d=5\times 0+0\times 3+3\times 0=0$$

To calculate e, which is entry (3,1), we use row 3 of the matrix on the left and column 1 of the matrix on the right:

$$\begin{pmatrix}1 & -2 & 4\\ 5 & 0 & 3\\ 0 & 1/2 & 9\end{pmatrix}\begin{pmatrix}1 & 0\\ 5 & 3\\ -1 & 0\end{pmatrix}=\begin{pmatrix}a & b\\ c & d\\ e & f\end{pmatrix}\rightarrow e=0\times 1+1/2\times 5+9\times(-1)=-13/2$$

To calculate f, which is entry (3,2), we use row 3 of the matrix on the left and column 2 of the matrix on the right:

$$\begin{pmatrix}1 & -2 & 4\\ 5 & 0 & 3\\ 0 & 1/2 & 9\end{pmatrix}\begin{pmatrix}1 & 0\\ 5 & 3\\ -1 & 0\end{pmatrix}=\begin{pmatrix}a & b\\ c & d\\ e & f\end{pmatrix}\rightarrow f=0\times 0+1/2\times 3+9\times 0=3/2$$

The result is:

$$\begin{pmatrix}1 & -2 & 4\\ 5 & 0 & 3\\ 0 & 1/2 & 9\end{pmatrix}\begin{pmatrix}1 & 0\\ 5 & 3\\ -1 & 0\end{pmatrix}=\begin{pmatrix}-13 & -6\\ 2 & 0\\ -13/2 & 3/2\end{pmatrix}$$

Example 2.3.1.2

Calculate

$$\begin{pmatrix}1 & -2 & 4\\ 5 & 0 & 3\end{pmatrix}\begin{pmatrix}1\\ 5\\ -1\end{pmatrix}$$

Solution

We are asked to multiply a 2×3 matrix by a 3×1 matrix (a column vector). The result will be a 2×1 matrix (a vector).

$$\begin{pmatrix}1 & -2 & 4\\ 5 & 0 & 3\end{pmatrix}\begin{pmatrix}1\\ 5\\ -1\end{pmatrix}=\begin{pmatrix}a\\ b\end{pmatrix}$$

$$a=1\times 1+(-2)\times 5+4\times(-1)=-13$$

$$b=5\times 1+0\times 5+3\times(-1)=2$$

The solution is:

$$\begin{pmatrix}1 & -2 & 4\\ 5 & 0 & 3\end{pmatrix}\begin{pmatrix}1\\ 5\\ -1\end{pmatrix}=\begin{pmatrix}-13\\ 2\end{pmatrix}$$

Need help? The link below contains solved examples: Multiplying matrices of different shapes (three examples): http://tinyurl.com/kn8ysqq

External links:

- Multiplying matrices, example 1: http://patrickjmt.com/matrices-multiplying-a-matrix-by-another-matrix/
- Multiplying matrices, example 2: http://patrickjmt.com/multiplying-matrices-example-2/
- Multiplying matrices, example 3: http://patrickjmt.com/multiplying-matrices-example-3/

The Commutator

Matrix multiplication is not, in general, commutative. For example, we can perform

$$\begin{pmatrix} 1 & -2 & 4 \\ 5 & 0 & 3 \end{pmatrix} \begin{pmatrix} 1 \\ 5 \\ -1 \end{pmatrix} = \begin{pmatrix} -13 \\ 2 \end{pmatrix}$$

but cannot perform

$$\begin{pmatrix} 1 \\ 5 \\ -1 \end{pmatrix} \begin{pmatrix} 1 & -2 & 4 \\ 5 & 0 & 3 \end{pmatrix}$$

Even with square matrices, that can be multiplied both ways, multiplication is not commutative. In this case, it is useful to define the **commutator**, defined as:

$$[\mathbf{A}, \mathbf{B}] = \mathbf{AB} - \mathbf{BA}$$

Example 2.3.1.3

Given $\mathbf{A} = \begin{pmatrix} 3 & 1 \\ 2 & 0 \end{pmatrix}$ and $\mathbf{B} = \begin{pmatrix} 1 & 0 \\ -1 & 2 \end{pmatrix}$

Calculate the commutator $[\mathbf{A}, \mathbf{B}]$

Solution

$$[\mathbf{A}, \mathbf{B}] = \mathbf{AB} - \mathbf{BA}$$

$$\mathbf{AB} = \begin{pmatrix} 3 & 1 \\ 2 & 0 \end{pmatrix} \begin{pmatrix} 1 & 0 \\ -1 & 2 \end{pmatrix} = \begin{pmatrix} 3 \times 1 + 1 \times (-1) & 3 \times 0 + 1 \times 2 \\ 2 \times 1 + 0 \times (-1) & 2 \times 0 + 0 \times 2 \end{pmatrix} = \begin{pmatrix} 2 & 2 \\ 2 & 0 \end{pmatrix}$$

$$\mathbf{BA} = \begin{pmatrix} 1 & 0 \\ -1 & 2 \end{pmatrix} \begin{pmatrix} 3 & 1 \\ 2 & 0 \end{pmatrix} = \begin{pmatrix} 1 \times 3 + 0 \times 2 & 1 \times 1 + 0 \times 0 \\ -1 \times 3 + 2 \times 2 & -1 \times 1 + 2 \times 0 \end{pmatrix} = \begin{pmatrix} 3 & 1 \\ 1 & -1 \end{pmatrix}$$

$$[\mathbf{A}, \mathbf{B}] = \mathbf{AB} - \mathbf{BA} = \begin{pmatrix} 2 & 2 \\ 2 & 0 \end{pmatrix} - \begin{pmatrix} 3 & 1 \\ 1 & -1 \end{pmatrix} = \begin{pmatrix} -1 & 1 \\ 1 & 1 \end{pmatrix}$$

$$[\mathbf{A}, \mathbf{B}] = \begin{pmatrix} -1 & 1 \\ 1 & 1 \end{pmatrix}$$

Multiplication of a vector by a scalar

The multiplication of a vector $\vec{v}_1$ by a scalar n produces another vector of the same dimensions that lies in the same direction as $\vec{v}_1$;

$$n \begin{pmatrix} x \\ y \end{pmatrix} = \begin{pmatrix} nx \\ ny \end{pmatrix}$$

The scalar can stretch or compress the length of the vector, but cannot rotate it (figure [fig:vector_by_scalar]).

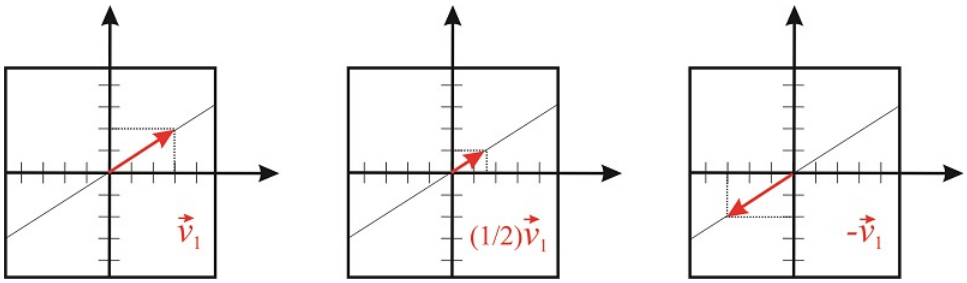


Figure **2.3.1.2**: Multiplication of a vector by a scalar

Multiplication of a square matrix by a vector

The multiplication of a vector $\vec{v_1}$ by a square matrix produces another vector of the same dimensions of $\vec{v_1}$. For example, we can multiply a 2×2 matrix and a 2-dimensional vector:

$$\begin{pmatrix} a & b \\ c & d \end{pmatrix} \begin{pmatrix} x \\ y \end{pmatrix} = \begin{pmatrix} ax + by \\ cx + dy \end{pmatrix}$$

For example, consider the matrix

$$\mathbf{A} = \begin{pmatrix} -2 & 0 \\ 0 & 1 \end{pmatrix}$$

The product

$$\begin{pmatrix} -2 & 0 \\ 0 & 1 \end{pmatrix} \begin{pmatrix} x \\ y \end{pmatrix}$$

is

$$\begin{pmatrix} -2x \\ y \end{pmatrix}$$

We see that 2×2 matrices act as operators that transform one 2-dimensional vector into another 2-dimensional vector. This particular matrix keeps the value of y constant and multiplies the value of x by -2 (Figure **2.3.1.3**).

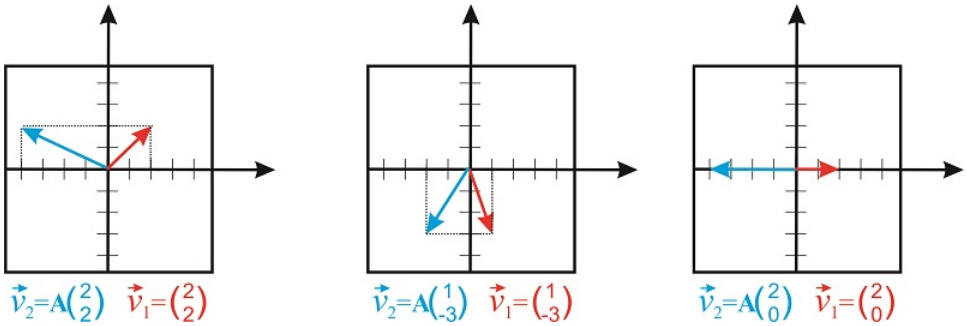


Figure **2.3.1.3**: Multiplication of a vector by a square matrix

Notice that matrices are useful ways of representing operators that change the orientation and size of a vector. An important class of operators that are of particular interest to chemists are the so-called symmetry operators.

Attribution

This page was adapted from Matrices (click here), contributed by Marcia Levitus, Associate Professor (Biodesign Institute) at Arizona State University.

Curated or created by Kathryn Haas

2.3.1: Matrices is shared under a CC BY-NC-SA 4.0 license and was authored, remixed, and/or curated by LibreTexts.

- **4.3.1: Matrices** by Kathryn Haas is licensed CC BY-NC-SA 4.0.

2.3.2: Representations of Point Groups

Symmetry Operations: Matrix Representations

A **symmetry operation**, such as a rotation around a symmetry axis or a reflection through a plane, is an operation that, when performed on an object, results in a new orientation of the object that is indistinguishable from the original. For example, if we rotate a square in the plane by $\pi/2$ or π, the new orientation of the square is superimposable on the original one (Figure **2.3.2.1**).

If rotation by an angle θ of a molecule (or object) about some axis results in an orientation of the molecule (or object) that is superimposable on the original, the axis is called a rotation axis. The molecule (or object) is said to have an n-fold rotational axis, where n is $2\pi/\theta$. The axis is denoted as C_n. The square of Figure **2.3.2.1** has a C_4 axis perpendicular to the plane because a $90°$ rotation leaves the figure indistinguishable from the initial orientation. This axis is also a C_2 axis because a $180°$ degree rotation leaves the square indistinguishable from the original square. In addition, the figure has several other C_2 axis that lie on the same plane as the square:

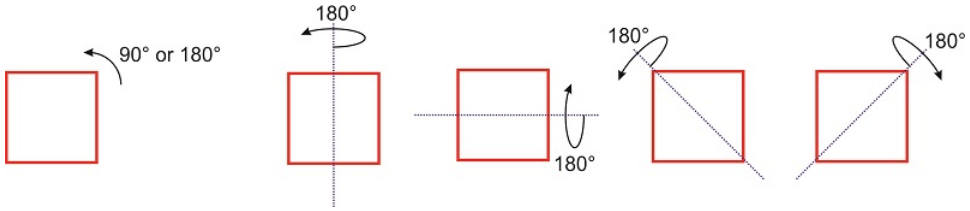


Figure **2.3.2.1**: Symmetry operations performed on a square

A symmetry operation moves all the points of the object from one initial position to a final position, and that means that symmetry operators are 3×3 square matrices (or 2×2 in two dimensions). Each symmetry operation can be expressed as a **transformation matrix** where the vector (x', y', z') represents the new coordinates of the point (x, y, z) after the symmetry operation.

$$[\text{New Coordinates}(x', y', z')] = [\text{Transformation Matrix}] \times [\text{Old Coordinates}(x, y, z)]$$

We will use the example of water, which is in the C_{2v} point group, to illustrate how transformation matrices can be used to represent the symmetry of a group.

Figure **2.3.2.2** shows the three symmetry elements of the molecule of water (H_2O). This molecule has only one rotation axis, which is 2-fold, and therefore we call it a "C_2 axis." It also has two mirror planes, one that contains the two hydrogen atoms (σ_{yz}), and another one perpendicular to it (σ_{xz}). Both planes contain the C_2 axis.

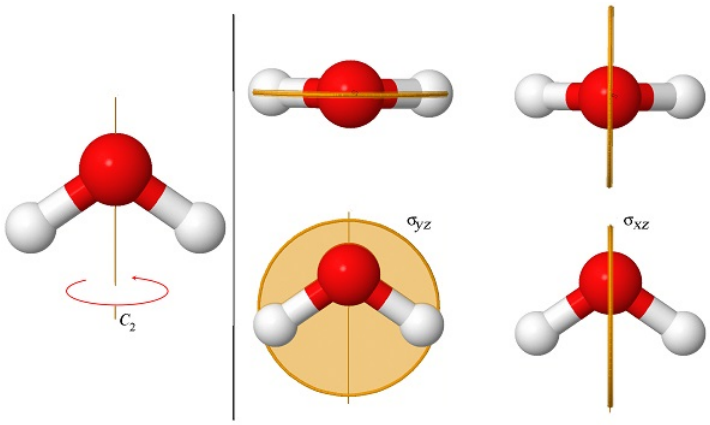


Figure **2.3.2.2**: The symmetry elements of the molecule of water

Transformation Matrix of C_2 rotation

A 2-fold rotation around the z−axis changes the location of a point (x, y, z) to $(-x, -y, z)$ (see Figure **2.3.2.3**). By convention, rotations are always taken in the counterclockwise direction.

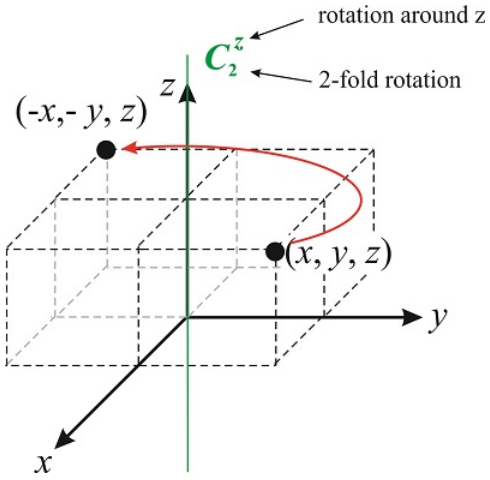


Figure 2.3.2.3: A 2-fold rotation around the z-axis

What is the matrix that represents the C_2 rotation? The matrix transforms the vector (x, y, z) into $(-x, -y, z)$, so

$$C_2(x, y, z) = (-x, -y, z)$$

$$\begin{pmatrix} a_{11} & a_{12} & a_{13} \\ a_{21} & a_{22} & a_{23} \\ a_{31} & a_{32} & a_{33} \end{pmatrix} \begin{pmatrix} x \\ y \\ z \end{pmatrix} = \begin{pmatrix} -x \\ -y \\ z \end{pmatrix}$$

We know the matrix is a 3×3 square matrix because it needs to multiply a 3-dimensional vector. In addition, we write the vector as a vertical column to satisfy the requirements of matrix multiplication.

$$\begin{pmatrix} a_{11} & a_{12} & a_{13} \\ a_{21} & a_{22} & a_{23} \\ a_{31} & a_{32} & a_{33} \end{pmatrix} \begin{pmatrix} x \\ y \\ z \end{pmatrix}$$

$$a_{11}x + a_{12}y + a_{13}z = -x$$

$$a_{21}x + a_{22}y + a_{23}z = -y$$

$$a_{31}x + a_{32}y + a_{33}z = z$$

and we conclude that $a_{11} = -1$, $a_{12} = a_{13} = 0$, $a_{22} = -1$, $a_{21} = a_{23} = 0$ and $a_{33} = 1$, $a_{31} = a_{32} = 0$. The transformation matrix of the C_2 operation of the C_{2v} point group is:

$$C_2 = \begin{pmatrix} -1 & 0 & 0 \\ 0 & -1 & 0 \\ 0 & 0 & 1 \end{pmatrix}$$

Transformation Matrix of σ_{xz} reflection

Rotations are not the only symmetry operations we can perform on a molecule. Figure 2.3.2.4 illustrates the reflection of a point through the xz plane. This operation transforms the vector (x, y, z) into the vector $(x, -y, z)$. Symmetry operators involving reflections through a plane are usually denoted with the letter σ, so the operator that reflects a point through the xz plane is $\hat{\sigma}_{xz}$:

$$\sigma_{xz}(x, y, z) = (x, -y, z)$$

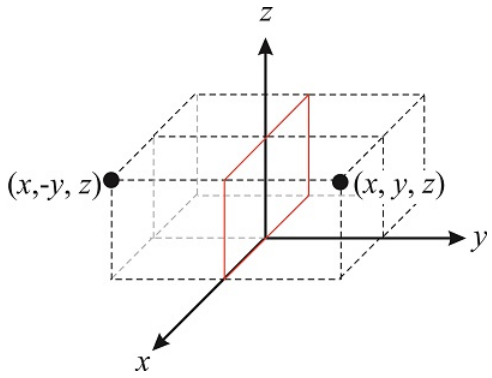


Figure **2.3.2.3**: A reflection through the xz plane

Following the same logic we used for the rotation matrix, we can write the σ_{xz} transformation matrix as:

$$\sigma_{x,z} = \begin{pmatrix} 1 & 0 & 0 \\ 0 & -1 & 0 \\ 0 & 0 & 1 \end{pmatrix}$$

This is true because

$$\begin{pmatrix} 1 & 0 & 0 \\ 0 & -1 & 0 \\ 0 & 0 & 1 \end{pmatrix} \begin{pmatrix} x \\ y \\ z \end{pmatrix} = \begin{pmatrix} x \\ -y \\ z \end{pmatrix}$$

? Exercise 2.3.2.1

Find the transformation matrix of the identity (E) and the $\sigma_{y,z}$ operations under the C_{2v} point group.

Answer

The transformation matrix for E is $\begin{pmatrix} 1 & 0 & 0 \\ 0 & 1 & 0 \\ 0 & 0 & 1 \end{pmatrix}$.

The transformation matrix for $\sigma_{v(yz)''}$ is $\begin{pmatrix} -1 & 0 & 0 \\ 0 & 1 & 0 \\ 0 & 0 & 1 \end{pmatrix}$.

Characters

For a square matrix, the ***character*** is the trace of the matrix. For the C_2 operation, with the transformation matrix

$$\begin{pmatrix} -1 & 0 & 0 \\ 0 & -1 & 0 \\ 0 & 0 & 1 \end{pmatrix},$$

the trace is $(-1) + (-1) + 1 = -1$.

The set of characters for a point group is called a **reducible representation (Γ)**. The reducible representation for the C_{2v} point group is:

C_{2v}	E	C_2	σ_v	σ'_v
Γ	3	−1	1	1

? Exercise 2.3.2.1

Prove that the characters in the reducible representation for C_{2v} are correct:

C_{2v}	E	C_2	σ_v	σ'_v
Γ	3	−1	1	1

Answer

For the E operation, with the transformation matrix $\begin{pmatrix}1&0&0\\0&1&0\\0&0&1\end{pmatrix}$, the trace is $1+1+1=3$.

For the C_2^z operation, with the transformation matrix $\begin{pmatrix}-1&0&0\\0&-1&0\\0&0&1\end{pmatrix}$, the trace is $(-1)+(-1)+1=-1$.

For the $\sigma_{v(xz)'}$ operation, with the transformation matrix $\begin{pmatrix}1&0&0\\0&-1&0\\0&0&1\end{pmatrix}$, the trace is $1+(-1)+1=1$.

For the $\sigma_{v(yz)''}$ operation, with the transformation matrix $\begin{pmatrix}-1&0&0\\0&1&0\\0&0&1\end{pmatrix}$, the trace is $-1+1+1=1$.

This gives the reducible representation

C_{2v}	E	C_2	σ_v	σ_v'
Γ	3	−1	1	1

Reducible and Irreducible Representations

Let us now go back and look in more detail at the transformation matrices of the C_{2v} point group that we derived above. If we look at the matrices carefully we see that they all take the same block diagonal form (a square matrix is said to be **block diagonal** if all the elements are zero except for a set of submatrices lying along the diagonal).

$$E=\begin{pmatrix}[1]&0&0\\0&[1]&0\\0&0&[1]\end{pmatrix},\ C_2=\begin{pmatrix}[-1]&0&0\\0&[-1]&0\\0&0&[1]\end{pmatrix},$$
$$\sigma'_{v(xz)}=\begin{pmatrix}[1]&0&0\\0&[-1]&0\\0&0&[1]\end{pmatrix},\ \sigma_{v(yz)''}=\begin{pmatrix}[-1]&0&0\\0&[1]&0\\0&0&[1]\end{pmatrix}$$

All the non-zero elements become 1x1 matrices that each represent individual x, y, z coordinates. In other words, the element a_{11} represents x, a_{22} represents y, and a_{33} represents z. The matrix elements for x from each transformation matrix combine to form an irreducible representation of the C_{2v} point group. Likewise, the matrix elements for y combine to form a second irreducible representation, and the same is true for z elements. These irreducible representations are shown below:

C_{2v}	E	C_2	σ_v	σ_v'	Coordinate Used
	1	−1	1	−1	x
	1	−1	−1	1	y
	1	1	1	1	z
Γ	3	−1	1	1	

The irreducible representations add to form the reducible representation, Γ. This Γ, which is the set of 3x3 matrices, can be reduced to the set of 1x1 matrices of the irreducible representations. The irreducible representations cannot be reduced further, hence their name.

Sources & Attribution

- Parts of this page was adapted from Matrices (click here) (Symmetry Operators), contributed by Marcia Levitus, Associate Professor (Biodesign Institute) at Arizona State University.
- Parts of this page were adapted from Reductions of Representations, contributed by

  Claire Vallance (University of Oxford)
- Curated or created by Kathryn Haas

2.3.2: Representations of Point Groups is shared under a CC BY-NC-SA 4.0 license and was authored, remixed, and/or curated by LibreTexts.

- **4.3.2: Representations of Point Groups** by Kathryn Haas is licensed CC BY-NC-SA 4.0.

2.3.3: Character Tables

Introduction to Character Tables, using C_{2v} as example

A character table is the complete set of irreducible representations of a symmetry group. In the previous section, we derived three of the four irreducible representations for the C_{2v} point group. These three irreducible representations are labeled A_1, B_1, and B_2. The fourth irreducible representation, A_2, can be derived using the properties (or "rules") for irreducible representations listed below.

Properties of Characters of Irreducible Representations in Point Groups

1. There is always a totally symmetric representation in which all the characters are 1.
   e.g. In C_{2v}, A_1 is totally symmetric.
2. The order of the group (h) is the total number of symmetry operations in the group.
   e.g. In C_{2v}, $h = 4$
3. Similar operations are listed as classes (R) and appear as columns in the table.
   e.g. In C_{2v}, there are four classes of operations, E, C_2, $\sigma_{v(xz)}$, and $\sigma'_{v(yz)}$
4. The number of irreducible representations (rows) must equal the number of classes (columns). This results in all character tables being square.
   e.g. In C_{2v}, there are four classes and four irreducible representations.
5. The sum of squares of all characters under E is equal to the order of the group: $h = \sum [\chi_i]^2$
   e.g. In C_{2v}, $h = 1^2 + 1^2 + 1^2 + 1^2 = 4$
6. For any irreducible representation (i), the sum of squares of its characters multiplied by the number of operations in the class is the order of the group: $h = \sum [\chi_i(R)]^2$
   e.g. For A_2 in C_{2v}, $h = (1 \times 1)^2 + (1 \times 1)^2 + (-1 \times 1)^2 + (-1 \times 1)^2 = 4$
7. Irreducible representations are orthogonal. For any two representations (i and j): $\sum [\chi_i * (R) \chi_j(R)] = 0$
   e.g. For B_1 and B_2 of C_{2v}, $[1 \times 1] + [-1 \times -1] + [1 \times -1] + [-1 \times 1] = 0$

The complete character table for C_{2v} is given below.

C_{2v}	E	C_2	σ_v	σ'_v	$h = 4$	
A_1	1	1	1	1	z	x^2, y^2, z^2
A_2	1	1	−1	−1	R_z	xy
B_1	1	−1	1	−1	x, R_y	xz
B_2	1	−1	−1	1	y, R_x	yz

The various sections of the table are as follows:

i. The first element in the table gives the name of the point group, usually in Schoenflies (C_{2v}) notation.
ii. Along the first row are the symmetry operations of the group, E, C_2, σ_v and σ_v'', followed by the order of the group, h.
iii. In the first column are the irreducible representations of the group, represented by Mulliken Labels. In C_{2v} the irreducible representations are A_1, A_2, B_1 and B_2. The Mulliken labels indicate the symmetry of each representation (explained further below).
iv. The characters (χ) of the irreducible representations under each symmetry operation are given in the bulk of the table.
v. The final column(s) of the table lists a number of functions that transform as the various irreducible representations of the group. These are the Cartesian axes (x, y, z), the Cartesian products ($z^2, x^2 + y^2, xy, xz, yz$), and the rotations ($R_x, R_y, R_z$) (explained further below).

Another example: C_{3v}

Th C_{3v} point group has three classes of operations: E, C_3, and $\sigma_{v(xz)}$. The derivation of transformation matrices for E and $\sigma_{v(xz)}$ is similar to the case for C_{2v}. However, the C_{3v} operation does not give simple 1 or -1 characters. If we carry out a rotation about z by an angle θ, our x and y axes are transformed onto new axes x' and y'. The new axes can each be written as a linear combination of our original x and y axes. The derivation of the rotation matrices will not be covered in this text, but is described elsewhere:

$$x' = x\cos\theta + y\sin\theta$$
$$y' = -x\sin\theta + y\cos\theta$$

For a C_3 rotation counterclockwise through 120° (or $\frac{2\pi}{3}$):

$$x' = x\cos(2\pi/3) + y\sin(2\pi/3) = -\tfrac{1}{2}x - \tfrac{\sqrt{3}}{2}y$$
$$y' = -x\sin(2\pi/3) + y\cos(2\pi/3) = \tfrac{\sqrt{3}}{2}x - \tfrac{1}{2}y$$

The transformation matrices for symmetry operations of C_{3v} are as follows:

$$E = \begin{pmatrix} 1 & 0 & 0 \\ 0 & 1 & 0 \\ 0 & 0 & 1 \end{pmatrix} \quad C_3 = \begin{pmatrix} -\frac{1}{2} & -\frac{\sqrt{3}}{2} & 0 \\ \frac{\sqrt{3}}{2} & -\frac{1}{2} & 0 \\ 0 & 0 & 1 \end{pmatrix} \quad \sigma'_{v(xz)} = \begin{pmatrix} 1 & 0 & 0 \\ 0 & -1 & 0 \\ 0 & 0 & 1 \end{pmatrix}$$

The C_3 transformation matrix contains off-diagonal entries, and therefore it cannot be block diagonalized as 1x1 matrices. However, the first two lines can be diagonalized as a 2x2 and the last line as a 1x1 matrix (Figure **2.3.3.1**):

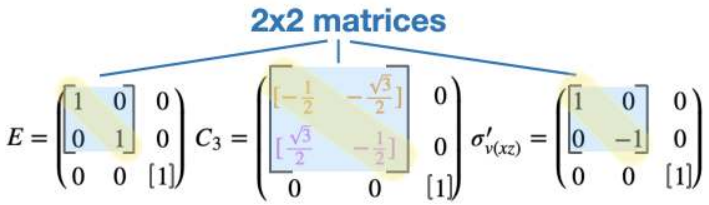


Figure **2.3.3.1**: The C_3 transformation matrix contains off-diagonal entries, and therefore it cannot be block diagonalized as 1x1 matrices. However, the first two lines can be diagonalized as a 2x2 and the last line as a 1x1 matrix. (CC-BY-NC-SA; Kathryn Haas)

The character from a 2x2 matrix is the sum of the trace of that matrix. So, for the C_3 operation, the 2x2 matrix gives the character -1 (from $-\frac{1}{2} + -\frac{1}{2}$).

The character table for C_{3v} is shown below.

C_{3v}	E	$2C_3$	$3\sigma_v$	$h = 6$
A_1	1	1	1	$z, z^2, x^2 + y^2$
A_2	1	1	−1	R_z
E	2	−1	0	$(x, y), (xy, x^2 + y^2), (xz, yz), (R_x, R_y)$

Additional features of character tables

Additional Features of Character Tables

1. Symmetry operations of the same class are grouped into the same column (class) in the character table and not listed separately.
   e.g. In the C_{3v} point group, there are four operations: E, C_3, C_3^2, and σ_v. The C_3 and C_3^2 operations are listed together in the character table as $2C_3$.
2. IF there are multiple C_2 axes (in a D group), the C_2 axes that are perpendicular to the principle axis are labeled with primes (e.g. C_2' and C_2''); when there are multiple types of perpendicular C_2 axes, one prime (C_2') means that it passes through more atoms, while a double prime (C_2'') means it goes between atoms.
3. Mirror planes that are perpendicular to the principle axis are "horizontal" mirror planes and are designated with an h subscript (σ_h). Mirror planes that are in-plane with the principle axis are "vertical" mirror planes, σ_v. When there are two types of vertical mirror planes, those that run through more atoms are σ_v while those that run between atoms are "dihedral", σ_d.
4. Matching the symmetry operations listed in the character table to the symmetry operations of a molecule can confirm its point group.

5. Irreducible representations are each assigned a Mulliken label, listed in the left-hand column, that indicates the symmetry of that representation as follows:

Mulliken Labels	**meaning**
A	singly degenerate (1x1), symmetric to principle axis
B	singly degenerate (1x1), antisymmetric to principle axis
E	doubly degenerate (2x2)
T	triply degenerate (3x3)
Subscripts and superscripts	**meaning**
1	symmetric to $\sigma_v$or perpendicular to C_2
2	anti-symmetric to $\sigma_v$or perpendicular to C_2
g	symmetric to inversion center
u	anti-symmetric to inversion center
$'$	symmetric to σ_h
$''$	anti-symmetric to σ_h

6. The right-hand columns of the character table list a number of functions that transform as the various irreducible representations of the group. These are the Cartesian axes (x, y, z), the Cartesian products $(z^2, x^2 + y^2, xy, xz, yz)$, and the rotations (R_x, R_y, R_z). These expressions indicate the properties of orbitals within the symmetry group. The s-orbital, which is totally symmetric, corresponds to the irreducible representation that possesses symmetry of x^2, y^2 and z^2 combined. The p -orbitals each possess the symmetry of the corresponding axis (e.g. p_x corresponds to the x axis). Each of the d-orbitals possess the symmetry of the corresponding binary product (e.g. d_{xy} corresponds to the binary product, xy, in the character table).

The functions listed in the final column of the table are important in many chemical applications of group theory, particularly in spectroscopy. For example, by looking at the transformation properties of x, y and z (sometimes given in character tables as T_x, T_y, T_z) we can discover the symmetry of translations along the x, y, and z axes. Similarly, R_x, R_y and R_z represent rotations about the three Cartesian axes. The transformation properties of x, y, and z can be used to determine whether or not a molecule is IR-active or whether or not it can absorb a photon of x-, y-, or z-polarized light and undergo a spectroscopic transition. The Cartesian products play a similar role in determining selection rules for Raman transitions, which involve two photons.

A visual summary of the sections and their significance is given in Figure **2.3.3.2**. Character tables for common point groups are given in the References section of LibreTexts Bookshelves.

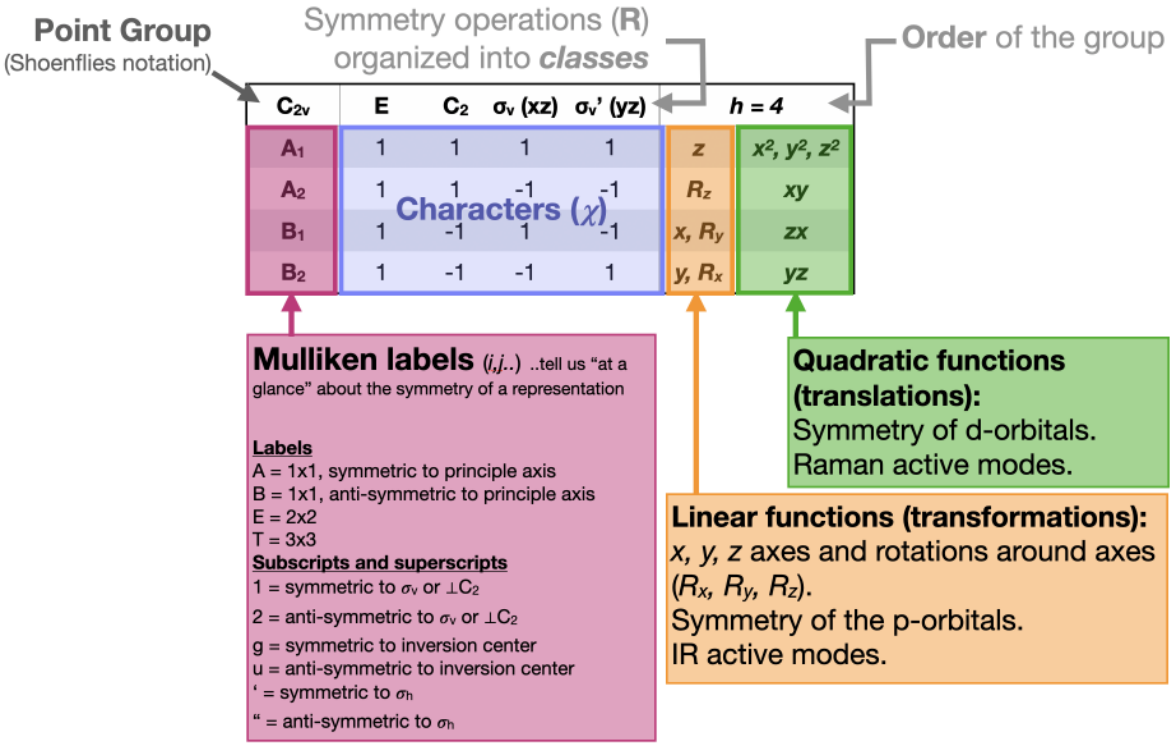


Figure **2.3.3.2**: Visual summary of the sections of a character table and their meaning. (CC-BY-NC-SA; Kathryn Haas)

Contributors and Attributions

- Curated or created by Kathryn Haas
- Claire Vallance (University of Oxford)

  adapted from Character Tables (click here)

This page titled 2.3.3: Character Tables is shared under a CC BY-NC-SA 4.0 license and was authored, remixed, and/or curated by Kathryn Haas.

- **4.3.3: Character Tables** by Kathryn Haas is licensed CC BY-NC-SA 4.0.

SECTION OVERVIEW

2.4: Examples and Applications of Symmetry

The purpose of learning group theory is that molecular symmetry can be applied to understand the properties of molecules. This chapter introduces two applications of symmetry: chirality and molecular vibrations (in the context of analyzing IR and Raman spectra). An additional application of symmetry, to understand molecular bonding, deserves its own chapter and will be explored in Chapter 5.

2.4.1: Molecular Vibrations

2.4.2: Chirality

2.4: Examples and Applications of Symmetry is shared under a CC BY-NC-SA 4.0 license and was authored, remixed, and/or curated by LibreTexts.

2.4.1: Molecular Vibrations

Symmetry and group theory can be applied to understand molecular vibrations. This is particularly useful in the context of predicting the number of peaks expected in the infrared (IR) and Raman spectra of a given compound.

We will use water as a case study to illustrate how group theory is used to predict the number of peaks in IR and Raman spectra.

How many IR and Raman peaks would we expect for H_2O?

To answer this question with group theory, a pre-requisite is that you **assign the molecule's point group and assign an axis system** to the entire molecule. By convention, the z axis is collinear with the principle axis, the x axis is in-plane with the molecule or the most number of atoms. It is a good idea to stick with this convention (see Figure 2.4.1.1).

What is the point group for H_2O? (click to see answer)

H_2O has the following operations: E, C_2, σ_v, σ_v'. The point group is C_{2v}.

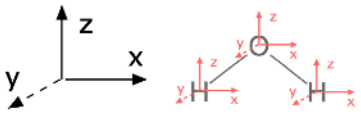


Figure 2.4.1.1: The first step to finding normal modes is to assign a consistent axis system to the entire molecule and to each atom. (CC-BY-SA; Kathryn Haas)

Now that we know the molecule's point group, we can use group theory to determine the symmetry of all motions in the molecule, or the symmetry of each of its degrees of freedom. Then we will subtract rotational and translational degrees of freedom to find the vibrational degrees of freedom. The number of degrees of freedom depends on the number of atoms (N) in a molecule. Each atom in the molecule can move in three dimensions (x, y, z), and so the number of degrees of freedom is three dimensions times N number of atoms, or $3N$. The total degrees of freedom include a number of vibrations, three translations (in x, y, and z), and either two or three rotations. Linear molecules have two rotational degrees of freedom, while non-linear molecules have three. The vibrational modes are represented by the following expressions:

$$\begin{aligned} \text{Linear Molecule Degrees of Freedom} &= 3N-5 \\ \text{Non-Linear Molecule Degrees of Freedom} &= 3N-6 \end{aligned}$$

Our goal is to find the symmetry of all degrees of freedom, and then determine which are vibrations that are IR- and Raman-active.

STEP 1: Find the reducible representation for all normal modes Γ_{modes}.

The first major step is to **find a reducible representation (Γ)** for the movement of all atoms in the molecule (including rotational, translational, and vibrational degrees of freedom). We'll refer to this as Γ_{modes}. To find normal modes using group theory, **assign an axis system** to each individual atom to represent the three dimensions in which each atom can move. Each axis on each atom should be consistent with the conventional axis system you previously assigned to the entire molecule (see Figure 2.4.1.1).

Γ_{modes} is the sum of the characters (trace) of the transformation matrix for the entire molecule (in the case of water, there are 9 degrees of freedom and this is now a 9x9 matrix). Let's walk through this step-by-step. The transformation matrix of E and C_2 are shown below:

$$E = \begin{pmatrix} 1 & 0 & 0 & 0 & 0 & 0 & 0 & 0 & 0 \\ 0 & 1 & 0 & 0 & 0 & 0 & 0 & 0 & 0 \\ 0 & 0 & 1 & 0 & 0 & 0 & 0 & 0 & 0 \\ 0 & 0 & 0 & 1 & 0 & 0 & 0 & 0 & 0 \\ 0 & 0 & 0 & 0 & 1 & 0 & 0 & 0 & 0 \\ 0 & 0 & 0 & 0 & 0 & 1 & 0 & 0 & 0 \\ 0 & 0 & 0 & 0 & 0 & 0 & 1 & 0 & 0 \\ 0 & 0 & 0 & 0 & 0 & 0 & 0 & 1 & 0 \\ 0 & 0 & 0 & 0 & 0 & 0 & 0 & 0 & 1 \end{pmatrix} \begin{pmatrix} x_{oxygen} \\ y_{oxygen} \\ z_{oxygen} \\ x_{hydrogen-a} \\ y_{hydrogen-a} \\ z_{hydrogen-a} \\ x_{hydrogen-b} \\ y_{hydrogen-b} \\ z_{hydrogen-b} \end{pmatrix} = \begin{pmatrix} x'_{oxygen} \\ y'_{oxygen} \\ z'_{oxygen} \\ x'_{hydrogen-a} \\ y'_{hydrogen-a} \\ z'_{hydrogen-a} \\ x'_{hydrogen-b} \\ y'_{hydrogen-b} \\ z'_{hydrogen-b} \end{pmatrix}, \chi = 9$$

$$C_2 = \begin{pmatrix} -1 & 0 & 0 & 0 & 0 & 0 & 0 & 0 & 0 \\ 0 & -1 & 0 & 0 & 0 & 0 & 0 & 0 & 0 \\ 0 & 0 & 1 & 0 & 0 & 0 & 0 & 0 & 0 \\ 0 & 0 & 0 & 0 & 0 & 0 & -1 & 0 & 0 \\ 0 & 0 & 0 & 0 & 0 & 0 & 0 & -1 & 0 \\ 0 & 0 & 0 & 0 & 0 & 0 & 0 & 0 & 1 \\ 0 & 0 & 0 & -1 & 0 & 0 & 0 & 0 & 0 \\ 0 & 0 & 0 & 0 & -1 & 0 & 0 & 0 & 0 \\ 0 & 0 & 0 & 0 & 0 & 1 & 0 & 0 & 0 \end{pmatrix} \begin{pmatrix} x_{oxygen} \\ y_{oxygen} \\ z_{oxygen} \\ x_{hydrogen-a} \\ y_{hydrogen-a} \\ z_{hydrogen-a} \\ x_{hydrogen-b} \\ y_{hydrogen-b} \\ z_{hydrogen-b} \end{pmatrix} = \begin{pmatrix} x'_{oxygen} \\ y'_{oxygen} \\ z'_{oxygen} \\ x'_{hydrogen-a} \\ y'_{hydrogen-a} \\ z'_{hydrogen-a} \\ x'_{hydrogen-b} \\ y'_{hydrogen-b} \\ z'_{hydrogen-b} \end{pmatrix}, \chi = 1$$

It is unnecessary to find the transformation matrix for each operation since it is only the TRACE that gives us the character, and any off-diagonal entries do not contribute to Γ_{modes}. The values that contribute to the trace can be found simply by performing each operation in the point group and assigning a value to each individual atom to represent how it is changed by that operation. If the atom moves away from itself, that atom gets a character of zero (this is because any non-zero characters of the transformation matrix are off of the diagonal). If the atom remains in place, each of its three dimensions is assigned a value of $\cos\theta$. For the example of H_2O under the C_{2v} point group, the axes that remain unchanged ($\theta = 0°$) are assigned a value of $\cos(0°) = 1$, while those that are moved into the negative of themselves (rotated or reflected to $\theta = 180°$) are assigned $\cos(180°) = -1$. The character for Γ is the sum of the values for each transformation.

Let's walk through the steps to assign characters of Γ_{modes} for H_2O to illustrate how this works:

For the operation E, performed on H_2O, all three atoms remain in place. The three axes x, y, z on each atom remain unchanged. Thus, each of the three axes on each of three atom (nine axes) is assigned the value $\cos(0°) = 1$, resulting in a sum of $\chi = 9$ for the Γ_{modes}.

For the operation C_2, the two hydrogen atoms are moved away from their original position, and so the hydrogens are assigned a value of zero. The oxygen remains in place; the z-axis on oxygen is unchanged ($\cos(0°) = 1$), while the x and y axes are inverted ($\cos(180°)$). The sum of these characters gives $\chi = -1$ in the Γ_{modes}.

Now you try! Find the characters of $\sigma_{v(xz)}$ and $\sigma_{v(yz)}$ under the C_{2v} point group. Compare what you find to the Γ_{modes} for all normal modes given below.

C_{2v}	E	C_2	σ_v	σ'_v
Γ_{modes}	9	−1	3	1

(2.4.1.1)

STEP 2: Break Γ_{modes} into its component irreducible representations.

Now that we've found the Γ_{modes} (2.4.1.1), we need to break it down into the individual irreducible representations ($i, j, k...$) for the point group. We can do this systematically using the following formula:

Misplaced '#'

In other words, the number of irreducible representations of type i is equal to the sum of the number of operations in the class × the character of the Γ_{modes} × the character of i, and that sum is divided by the order of the group (h).

Using equation ???, we find that for all normal modes of H_2O:

$$\Gamma_{modes} = 3A_1 + 1A_2 + 3B_1 + 2B_2 \tag{2.4.1.2}$$

.

Notice there are 9 irreducible representations in Equation 2.4.1.2. These irreducible representations represent the symmetries of all 9 motions of the molecule: vibrations, rotations, and translations.

? Exercise 2.4.1.1: Derive the irreducible representation in equation 2.4.1.2.

Derive the nine irreducible representations of Γ_{modes} for H_2O, expression 2.4.1.2.

Hint

To find the number of each kind of irreducible representation that combine to form the Γ_{modes}, we need the characters of Γ_{modes} that we found above (2.4.1.1), the C_{2v} character table (below), and equation ???.

C_{2v}	$1E$	$1C_2$	$1\sigma_v$	$1\sigma_v'$	$h=4$	
A_1	1	1	1	1	z	x^2, y^2, z^2
A_2	1	1	−1	−1	R_z	xy
B_1	1	−1	1	−1	x, R_y	xz
B_2	1	−1	−1	1	y, R_x	yz

In the C_{2v} point group, each class has only one operation, so the number of operations in each class (from equation ???) is 1 for each class. This has been explicitly added to the character table above for emphasis.

Answer

The number of $A_1 = \frac{1}{4}[(1\times 9\times 1) + (1\times(-1)\times 1) + (1\times 3\times 1) + (1\times 1\times 1)] = 3A_1$

The number of $A_2 = \frac{1}{4}[(1\times 9\times 1) + (1\times(-1)\times 1) + ((-1)\times 3\times 1) + ((-1)\times 1\times 1)] = 1A_2$

The number of $B_1 = \frac{1}{4}[(1\times 9\times 1) + ((-1)\times(-1)\times 1) + (1\times 3\times 1) + ((-1)\times 1\times 1)] = 3B_1$

The number of $B_2 = \frac{1}{4}[(1\times 9\times 1) + ((-1)\times(-1)\times 1) + ((-1)\times 3\times 1) + (1\times 1\times 1)] = 2B_2$

STEP 3: Subtract rotations and translations to find vibrational modes.

Because we are interested in molecular vibrations, we need to subtract the rotations and translations from the total degrees of freedom.

$$\text{Vibrations} = \Gamma_{modes} - \text{Rotations} - \text{Translations}$$

In the example of H_2O, the total degrees of freedom are given above in equation 2.4.1.2, and therefore the vibrational degrees of freedom can be found by:

$$H_2O \text{ vibrations} = (3A_1 + 1A_2 + 3B_1 + 2B_2) - \text{Rotations} - \text{Translations} \tag{2.4.1.3}$$

But which of the irreducible representations are ones that represent rotations and translations? The symmetry of rotational and translational degree modes can be found by inspecting the right-hand columns of any character table. Rotational modes correspond to irreducible representations that include R_x, R_y, and R_z in the table, while each of the three translational modes has the same symmetry as the x, y and z axes. For a non-linear molecule, subtract three rotational irreducible representations and three translational irreducible representations from the total Γ_{modes}.

In the specific case of water, we refer to the C_{2v} character table:

C_{2v}	E	C_2	σ_v	σ_v'	$h=4$	
A_1	1	1	1	1	z	x^2, y^2, z^2
A_2	1	1	−1	−1	R_z	xy
B_1	1	−1	1	−1	x, R_y	xz
B_2	1	−1	−1	1	y, R_x	yz

In C_{2v}, translations correspond to B_1, B_2, and A_1 (respectively for x, yz), and rotations correspond to B_2, B_1, and A_1 (respectively for R_x, R_y, R_z). Subtracting these six irreducible representations from Γ_{modes} will leave us with the irreducible representations for vibrations.

$$\begin{aligned} H_2O \text{ vibrations} &= \Gamma_{modes} - \text{Rotations} - \text{Translations} \\ &= (3A_1 + 1A_2 + 3B_1 + 2B_2) - (A_1 + B_1 + B_2) - (A_2 + B_1 + B_2) \\ &= 2A_1 + 1B_1 \end{aligned}$$

The three vibrational modes for H_2O are $2A_1 + 1B_1$. Note that we have the correct number of vibrational modes based on the expectation of $3N - 6$ vibrations for a non-linear molecule.

STEP 4: Determine which of the vibrational modes are IR-active and Raman-active.

The next step is to determine which of the vibrational modes is IR-active and Raman-active. To do this, we apply the IR and Raman Selection Rules below:

IR and Raman Selection Rules

Infrared selection rules:

If a vibration results in the change in the molecular dipole moment, it is IR-active. In the character table, we can recognize the vibrational modes that are IR-active by those with symmetry of the x, y, and z axes.

In C_{2v}, any vibrations with A_1, B_1 or B_2 symmetry would be IR-active.

Raman selection rules:

If a vibration results in a change in the molecular polarizability, it will be Raman-active. In the character table, we can recognize the vibrational modes that are Raman-active by those with symmetry of any of the binary products (xy, xz, yz, x^2, y^2, and z^2) or a linear combination of binary products (e.g. $x^2 - y^2$).

In C_{2v}, any vibrations with A_1, A_2, B_1 or B_2 symmetry would be Raman-active.

In our H_2O example, we found that of the three vibrational modes, two have A_1 and one has B_1 symmetry. Both A_1 and B_1 are IR-active, and both are also Raman-active. ***There are two possible IR peaks and three possible Raman peaks expected for water***.*

*It is important to note that this prediction tells only what is possible, but not what we might actually see in the IR and Raman spectra. For example, if the two IR peaks overlap, we might actually notice only one peak in the spectrum. Or, if one or more peaks is off-scale, we wouldn't see it in actual data. Group theory tells us what is *possible and allows us to make predictions or interpretations of spectra*.

Summary of Analysis for Water

Each molecular motion for water, or any molecule, can be assigned a symmetry under the molecule's point group. For water, we found that there are a total of 9 molecular motions; $3A_1 + A_2 + 3B_1 + 2B_2$. Six of these motions are not the translations and rotations. The remaining motions are vibrations; two with A_1 symmetry and one with B_1 symmetry.

We can tell what these vibrations would look like based on their symmetries. The two A_1 vibrations must be completely symmetric, while the B_1 vibration is antisymmetric with respect to the principal C_2 axis.

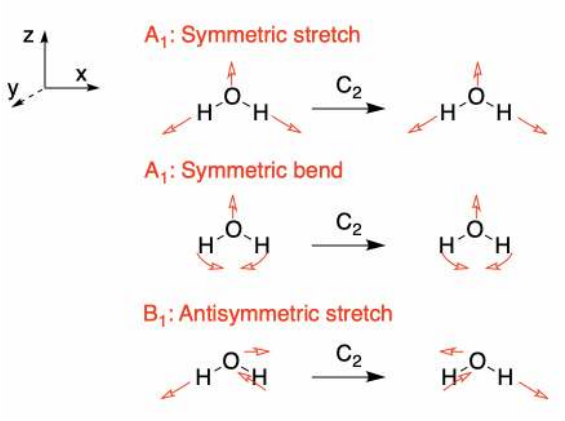


Figure 2.4.1.2: Illustration of the vibrational motions of water. The antisymmetric stretch has B_1 symmetry, while the symmetric stretch and symmetric bend both have A_1 symmetry. (Click here to see animation) (CC-BY-NC-SA; Kathryn Haas)

Table 2.4.1.1: Summary of the Symmetry of Molecular Motions for Water

All Motions (step 2 above)	Translations (x,y,z)	Rotations (R_x, R_y, R_z)	**Remaining Vibrations**	Description of Vibration
$3A_1$	$1A_1$		$2A_1$	One is a symmetric stretch. The other is a symmetric bend. Both are *IR-active* and *Raman-active*
A_2		$1A_2$		
$3B_1$	$1B_1$	$1B_1$	$1B_1$	Antisymmetric stretch that is *IR-active* and *Raman-active*.
$2B_2$	$1B_2$	$1B_2$		

? Exercise 2.4.1.2

Find the symmetries of all motions of the square planar complex, tetrachloroplatinate (II). Determine which are rotations, translations, and vibrations. Determine which vibrations are IR and Raman active.

Answer

The point group of $[PtCl_4]^{2-}$ is D_{4h} (refer to its character table). There are five atoms and 15 vectors (x, y, z for each atom × 5 atoms).

STEP 1: The first major step is to **find a reducible representation (Γ)** for the movement of all atoms in the molecule.

C_{2v}	E	$2C_4$	C_2	$2C_2'$	$2C_2''$	i	$2S_4$	σ_h	$2\sigma_v$	$2\sigma_d$
Γ_{modes}	15	1	−1	−3	−1	−3	−1	5	3	1

(2.4.1.4)

.

STEP 2: Break Γ_{modes} into its component irreducible representations.

Following the process described earlier, we come to $A_{1g} + A_{2g} + B_{1g} + B_{2g} + E_g + 2A_{2u} + B_{2u} + 3E_u$. This accounts for all modes of movement, including rotations and translations.

STEP 3: Subtract rotations and translations to find vibrational modes.

The translations are $A_{2u} + E_u$ and the rotations are $A_{2g} + E_g$.
The remaining normal modes are: $A_{1g} + B_{1g} + B_{2g} + A_{2u} + B_{2u} + 2E_u$

STEP 4: Determine which of the vibrational modes are IR-active and Raman-active:

$A_{2u} + E_u$ are IR-active. Since A_{2u} is singly degenerate and E_u is doubly degenerate, we expect three possible IR bands.
$A_{1g} + B_{1g} + B_{2g}$ are Raman-Active. Each of these is singly degenerate, so we expect three possible Raman bands.

Selected Vibrational Modes

The interpretation of CO stretching vibrations in an IR spectrum is particularly useful. Symmetry and group theory can be applied to predict the number of CO stretching bands that appear in a vibrational spectrum for a given metal coordination complex. A classic example of this application is in distinguishing isomers of metal-carbonyl complexes. For example, the *cis*- and *trans*-isomers of square planar metal dicarbonyl complexes ($ML_2(CO)_2$) have a different number of IR stretches that can be predicted and interpreted using symmetry and group theory. Another example is the case of *mer*- and *fac*- isomers of octahedral metal tricarbonyl complexes ($ML_3(CO)_3$). Structures of the two types of metal carbonyl configurations and their isomers are shown in Figure **2.4.1.1**. The isomers in each case can be distinguished using vibrational spectroscopy.

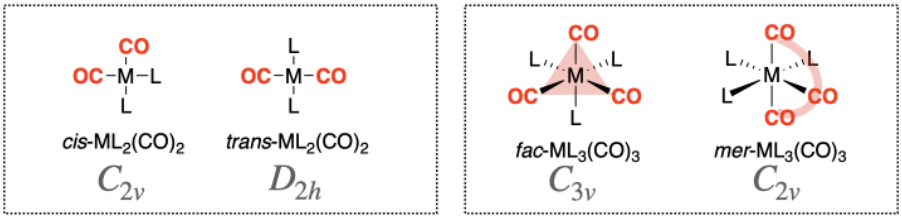


Figure **2.4.1.3**: Cis- and *trans*- isomers of square planar metal dicarbonyl complexes ($ML_2(CO)_2$) are shown in the left box. *Mer*- and *fac*- isomers of octahedral metal tricarbonyl complexes ($ML_3(CO)_3$) are shown in the right box. The point group for each of the general structures is also shown. (CC-BY-NC-SA; Kathryn Haas)

EXAMPLE 1: Distinguishing *cis*- and *trans*- isomers of square planar metal dicarbonyl complexes

General structures of the *cis*- and *trans*- isomers of square planar metal dicarbonyl complexes ($ML_2(CO)_2$) are shown in the left box in Figure **2.4.1.1**. We can use symmetry and group theory to predict how many carbonyl stretches we should expect for each isomer following the steps below.

Step 1: Assign the point group and Cartesian coordinates for each isomer.

The *cis*-isomer has C_{2v} symmetry and the *trans*-isomer has D_{2h} symmetry. We assign the Cartesian coordinates so that z is colinear with the principle axis in each case. For the D_2h isomer, there are several orientations of the z axis possible. The axes shown in Figure **2.4.1.2** will be used here.



Figure **2.4.1.4**: Cis- and *trans*- isomers of square planar metal dicarbonyl complexes ($ML_2(CO)_2$) are shown and oriented with respect to the Cartesian coordinates shown at the left so that the highest-order rotation axis is colinear with z and the molecule is co-planar with the xz plane. The vector along each C—O bond is shown using a red arrow (→). These vectors represent the direction of C—O stretching motions. (CC-BY-NC-SA; Kathryn Haas)

Step 2: Produce a reducible representation (Γ) for CO stretches in each isomer

First, assign a vector along each C—O bond in the molecule to represent the direction of C—O stretching motions, as shown in Figure **2.4.1.2** (red arrows →). These vectors are used to produce a reducible representation (**Γ**) for the C—O stretching motions in each molecule. Using the symmetry operations under the appropriate character table, assign a value of 1 to each vector that remains in place during the operation, and a value of 0 if the vector moves out of place. There will be no occasion where a vector remains in place but is inverted, so a value of -1 will not occur.

cis- $ML_2(CO)_2$:

For *cis*- $ML_2(CO)_2$, the point group is C_{2v} and so we use the operations under the C_{2v} character table to create the Γ_{cis-CO}.

C_{2v}	E	C_2	$\sigma_v(xz)$	$\sigma_v'(yz)$
Γ_{cis-CO}	2	0	2	0

trans- $ML_2(CO)_2$:

For trans- $ML_2(CO)_2$, the point group is D_{2h} and so we use the operations under the D_{2h} character table to create the $\Gamma_{trans-CO}$.

D_{2h}	E	$C_2(z)$	$C_2(y)$	$C_2(x)$	i	$\sigma(xy)$	$\sigma(xz)$	$\sigma(yz)$
$\Gamma_{trans-CO}$	2	0	0	2	0	2	2	0

Step 3: Break each Γ into its component irreducible representations

Each Γ can be reduced using inspection or by the systematic method described previously.

In the case of the *cis*- $ML_2(CO)_2$, the CO stretching vibrations are represented by A_1 and B_1 irreducible representations:

C_{2v}	E	C_2	$\sigma_v(xz)$	$\sigma_v'(yz)$		
Γ_{cis-CO}	2	0	2	0		
A_1	1	1	1	1	z	x^2, y^2, z^2
B_1	1	−1	1	−1	x, R_y	xz

(2.4.1.5)

In the case of *trans*- $ML_2(CO)_2$, the CO stretching vibrations are represented by A_1 and B_{3u} irreducible representations:

D_{2h}	E	$C_2(z)$	$C_2(y)$	$C_2(x)$	i	$\sigma(xy)$	$\sigma(xz)$	$\sigma(yz)$	
$\Gamma_{trans-CO}$	2	0	0	2	0	2	2	0	
A_g	1	1	1	1	1	1	1	1	$x^2,\ y^2,\ z^2$
B_{3u}	1	−1	−1	1	−1	1	1	−1	x

These irreducible representations correspond to the symmetries of only the selected C—O vibrations. Since these motions are isolated to the C—O group, they do not include any rotations or translations of the entire molecule, and so we do not need to find and subtract rotationals or translations (unlike the previous cases where all motions were considered).

Step 4: Determine which vibrational modes are IR-active and/or Raman-active

Apply the infrared selection rules described previously to determine which of the CO vibrational motions are IR-active and Raman-active. The two isomers of $ML_2(CO)_2$ are described below.

In the case of the *cis*- $ML_2(CO)_2$, the CO stretching vibrations are represented by A_1 and B_1 irreducible representations. The characters of both representations and their functions are shown above, in 2.4.1.5 (and can be found in the C_{2v} character table). Under C_{2v}, both the A_1 and B_1 CO vibrational modes are IR-active and Raman-active. Therefore, two bands in the IR spectrum and two bands in the Raman spectrum are possible.

In the case of the trans- $ML_2(CO)_2$, the CO stretching vibrations are represented by A_g and B_{3u} irreducible representations. The characters of both representations and their functions are shown above, in 2.4.1.5 (and can be found in the D_{2h} character table). Under D_{2h}, the A_g vibrational mode is is Raman-active only, while the B_{3u} vibrational mode is IR-active only. Therefore, only one IR band and one Raman band are possible for this isomer.

Summary

It is possible to distinguish between the two isomers of square planar $ML_2(CO)_2$ using either IR or Raman vibrational spectroscopy. The *cis*- $ML_2(CO)_2$ can produce two CO stretches in an IR or Raman spectrum, while the *trans*- $ML_2(CO)_2$ isomer can produce only one band in either type of vibrational spectrum. If a sample of $ML_2(CO)_2$ produced two CO stretching bands, we could rule out the possibility of a pure sample of *trans*-$ML_2(CO)_2$.

Exercise 2.4.1.3

Repeat the steps outlined above to determine how many CO vibrations are possible for *mer*-$ML_3(CO)_3$ and *fac*-$ML_3(CO)_3$ isomers (see Figure **2.4.1.1**) in both IR and Raman spectra. Could either of these vibrational spectroscopies be used to distinguish the two isomers?

Answer

Step 1: Assign the point group and Cartesian coordinates for each isomer.
The *fac*-isomer is C_{3v}. The *mer*-isomer is C_{2v}.

Step 2: Produce a reducible representation for CO stretches in each isomer.

Step 3: Break each into its component irreducible representations.

Step 4: Determine which vibrational modes are IR-active and/or Raman-active.

***For fac*-$ML_3(CO)_3$**, the point group is C_{3v} and so we use the operations under the C_{3v} character table to create the Γ_{fac-CO}. Then break it into its irreducible representations and determine which are IR and Raman active:

C_{3v}	E	$2C_2$	$3\sigma_v$
Γ_{fac-CO}	3	0	1

This reduces to $A_1 + E$. Both of these are IR active, and since one is singly degenerate while the other is doubly degenerate, we expect three possible IR bands from this isomer. Both vibrational modes are also Raman active, and again we would expect three possible bands in the Raman spectrum.

For mer-$ML_3(CO)_3$, the point group is C_{2v} and so we use the operations under the C_{2v} character table to create the Γ_{mer-CO}. Then break it into its irreducible representations and determine which are IR and Raman active:

C_{2v}	E	C_2	$\sigma_v(xz)$	$\sigma'_v(yz)$
Γ_{mer-CO}	3	1	3	1

This reduces to $2A_1 + B_1$; both A_1 and B_1 are IR and Raman active. So this isomer would have three possible IR bands and three possible Raman Bands.

These two isomers have the same number of possible bands in both IR and Raman spectroscopy. It would not be straightforward to distinguish them from each other based on the number of possible bands in the vibrational spectrum.

This page titled 2.4.1: Molecular Vibrations is shared under a CC BY-NC-SA 4.0 license and was authored, remixed, and/or curated by Kathryn Haas.

- **4.4.2: Molecular Vibrations** by Kathryn Haas is licensed CC BY-NC 4.0.

2.4.2: Chirality

Introduction

Around the year 1847, the French scientist Louis Pasteur provided an explanation for the optical activity of tartaric acid salts. When he carried out a particular reaction, Pasteur observed that two types of crystals precipitated. Patiently and carefully using tweezers, Pasteur was able to separate the two types of crystals. Pasteur noticed that the types rotated plane-polarized light by the same amount but in different directions. These two compounds are called enantiomers.

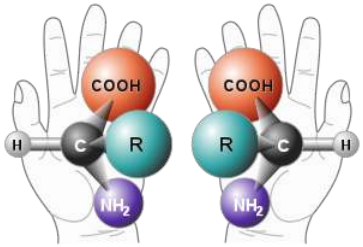


Figure 2.4.2.1: Two enantiomers of an amino acid (with side chain R).

What is chirality?

A molecule is **chiral** (or **dissymetric**) if it is non-superimposable on its mirror image. The two mirror images of a chiral molecule are called enantiomers. Enantiomers have the same physical properties (e.g., melting point, etc.). They differ in their ability to rotate plane polarized light and in their reactivity with other chiral molecules. Due to their ability to rotate plane polarized light, they are referred to as being *optically active*.

Using Symmetry to Determine Chirality

There are some general rules of thumb that help determine whether a molecule is chiral or achiral. The point group of the molecule, and the symmetry operations within that point group, can give clues as to whether the molecule is chiral.

Symmetry operations of chiral molecules

A chiral molecule cannot possess a plane of symmetry (σ), a center of inversion (i), or an improper rotation (S_n). Due to the fact that all groups that lack both σ and i also lack S_n, **a molecule that belongs to any group that lacks S_n is chiral**.

An example of an inorganic coordination complex is tris(ethylenediamine)cobalt(III) (Figure 2.4.2.1). Figure 2.4.2.1 shows the two enantiomers of tris(ethylenediamine)cobalt(III): the **Δ** and **Λ** isomers.

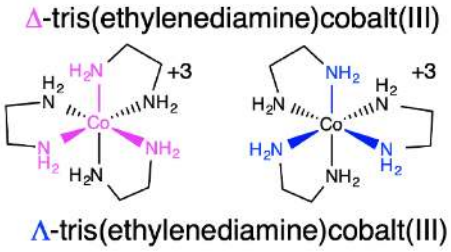


Figure 2.4.2.2: Two chiral enantiomers of tris(ethylenediamine)coalt(III).

You can visualize the **Λ** and **Δ** isomers by imagining that the ligands around the metal centers are blades of a fan. To push the air toward you, you would need to rotate the **Δ** isomer clockwise, and the **Λ** isomer counter-clockwise.

Exercise 2.4.2.1

Which point groups are possible for chiral molecules?

Answer

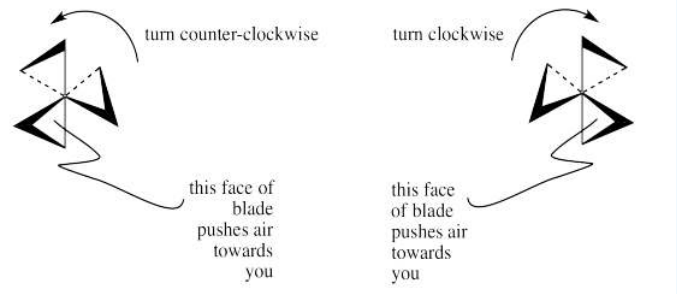


Figure **2.4.2.3**: Another way of thinking about the chirality of the two chiral enantiomers of tris(ethylenediamine)coalt(III) shown in Figure **2.4.2.2**. This figure was taken from Structure and Reactivity in Organic, Biological, and Inorganic Chemistry.

As a result of the previous discussion, there are a few classes of point groups that lack an improper axis. Those classes are C_1, C_n, and D_n.

2.4.2: Chirality is shared under a CC BY-NC-SA 4.0 license and was authored, remixed, and/or curated by LibreTexts.

- **4.4.1: Chirality** by Kathryn Haas is licensed CC BY-NC 4.0.

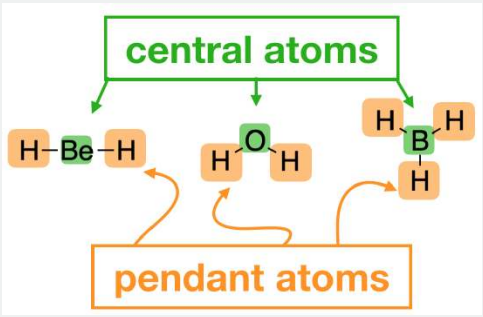
SECTION OVERVIEW

2.5: Generating SALCs for Polyatomic Molecules

We can extend the method we used for diatomic molecules to draw the molecular orbitals of more complicated, polyatomic molecules (molecules with more than two atoms). To combine several different atoms in a molecular orbital diagram, we will group orbitals from different atoms into sets that match the symmetry of a central atom. These **group orbitals** are also referred to as **symmetry adapted linear combinations (SALCs)**. We'll use a stepwise approach to do this as summarized below.

Symmetry adapted linear combinations (SALCs)

We need SALCs (aka group orbitals) to draw molecular orbital (MO) diagrams of *polyatomic* molecules. SALCs are groups of orbitals on **pendant atoms**. These groups of orbitals much match the symmetry of valence orbitals on the **central atom** in order to create a productive interaction. When we combine SALCs with the atomic orbitals on the central atom, we can generate an MO diagram that gives us information about the molecule's bonding and electronic states.



Below is a set of steps you can follow to find SALCs and draw an MO Diagram. Each step will be illustrated in detail through the examples in the subsections that follow this page.

1. Find the **point group** of the molecule and assign Cartesian coordinates so that z is the principal axis.
   Sometimes we can simplify things by looking only at the point group of the relevant orbitals. Only simplify when instructed to do so.*
2. Identify and count the pendant atoms' valence orbitals.
   Is there more than 1 type for each atom (ex. just s, or s and p?) We expect 1 SALC for each ligand orbital.
3. Generate a **reducible representation (Γ)** for the group of pendant atom orbitals using the appropriate character table.
   You have to do this for each set of orbital types. If you only have s orbitals for each ligand, you only need to generate 1 reducible representation. If you have p orbitals, you would generate additional Γ*'s for p_x, p_y, and p_z.*
4. Break the Γ into its component **irreducible representations** from the character table. Note the symmetry of each irreducible representation, its associated orbitals, and their degeneracy.
5. If you are asked to sketch the shapes of SALCs, determine what they "look like" using one of the following strategies.
   (a) Shortcut: if the reducible representations are listed with s, p, or d orbitals in the character table, just draw them (… and skip steps b-c)
   (b) Systematic (Projection Operator) method: Draw an expanded character table and draw your molecule with each ligand identified by letters or numbers (*a,b,c...* or *i,j,k...* or *1,2,3...*) Determine where each pendant atom/orbital ends up under each of the operations of your expanded table. Project the values for each irreducible representation onto the chart you created and then add up the values. Positive and negative values are opposite signed orbitals.
6. Draw the MO diagram by combining SALCs with AO's of like symmetry. When drawing SALC energy levels, remember that the more nodal planes in your SALC orbital drawing, the higher the energy for that SALC orbital.

** When we are focused on orbitals, as in the case for finding group orbitals and drawing molecular orbital diagrams, the symmetry of the orbitals is what we are interested in. In the case of high-symmetry point groups, like $D_{\infty h}$ and $C_{\infty v}$, even though the molecule may have a C_∞ axis, the orbitals do not necessarily retain this symmetry element. For example, the p_x orbital would not have a C_∞ axis, but rather a C_2 axis. It is sufficient and useful to substitute D_{2h} for $D_{\infty h}$ and C_{2v} for $C_{\infty v}$ to simplify the problem.*

2.5.1: Bifluoride anion

2.5.2: Carbon Dioxide

2.5.3: H_2O

2.5.4: NH_3

2.5.5: CO_2 (Revisted with Projection Operators)

2.5.6: BF_3

2.5: Generating SALCs for Polyatomic Molecules is shared under a CC BY-NC-SA 4.0 license and was authored, remixed, and/or curated by LibreTexts.

2.5.1: Bifluoride anion

Finding SALCs and drawing the MO diagram for [F-H-F]$^-$

The linear anion [F-H-F]$^-$ is a good place to start as an example to illustrate the process of generating pendant atom SALCs and then constructing a molecular orbital diagram for a polyatomic molecule. We will proceed using the steps outlined on the previous page for generating SALCs and a molecular orbital diagram.

Step 1. Find the point group of the molecule and assign Cartesian coordinates so that z is the principal axis.

We begin by assigning the appropriate point group for this molecule: $D_{\infty h}$ (Figure **2.5.1.1**). As mentioned in the previous page, it is useful to substitute D_{2h} for $D_{\infty h}$ when generating SALCs and molecular orbital diagrams. The z axis is assigned to be colinear with the principal axis, and in this case is the same as the C_∞ axis (Figure **2.5.1.1**).

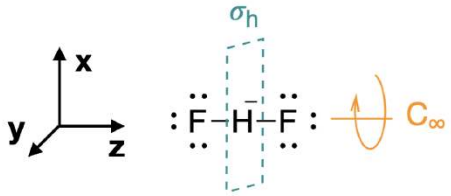


Figure **2.5.1.1**: The [FHF]$^-$ anion belongs to the $D\infty_h$ point group. (CC-BY-NC-SA; Kathryn Haas)

Step 2. Identify and count the pendant atoms' valence orbitals.

The next step is to identify the valence orbitals on the pendant F atoms that will form SALCs. In most cases, you should consider all of the valence orbitals. In this case, each of the fluorine atoms has four valence orbitals ($2s$, $2p_x$, $2p_y$, and $2p_z$). From these eight fluorine valence orbitals, we should expect eight group orbitals (SALCs).

3. - 5. Generate SALCS (shortcut)

To draw these SALCs for this molecule is rather simple, and we don't need to follow all the steps of finding the Γ's and reducing them. Rather, you can proceed as if you are creating bonding and antibonding molecular orbitals between the two F atoms, except that the F orbitals are separated by the H atom. Approximate sketches of the eight SALCs from F valence orbitals are shown in Figure **2.5.1.2**.

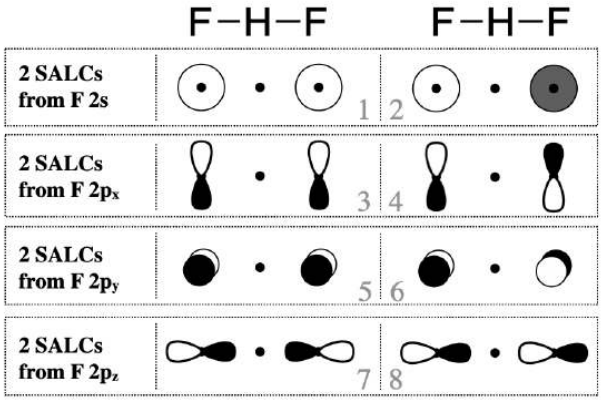


Figure **2.5.1.2**: Eight SALCs from the valence orbitals of two fluorine atoms. (CC-BY-NC-SA; Kathryn Haas)

6. Draw the MO diagram by combining SALCs with AO's of like symmetry.

SALCs can productively interact with the central atom only when symmetry is compatible. Just some of the groups of orbitals in Figure **2.5.1.2** possess appropriate symmetry to combine with the hydrogen atom valence orbital (the H $1s$). In this simple case, you can decide whether orbitals have compatible symmetry by visually inspecting the shapes of the group orbitals. The F $2p_y$ and $2p_x$ orbitals do not have appropriate symmetry to bond to the H $1s$ orbital because the nodes of these orbitals run through the center of the H $1s$ orbital, thus we can eliminate all SALCs composed from F $2p_x$ and $2p_y$ (*these are SALCs numbered 3-6 in Figure* **2.5.1.2**). On the other hand, the F $2s$ and $2p_z$ orbitals individually do have appropriate shape and direction in space for productive interaction

with an H $1s$ orbital. However only SALCs where the *entire group* has appropriate symmetry will combine with H $1s$ to produce bonding or antibonding molecular orbitals. Only the SALCs labeled with numbers 1 and 7 can combine with an s orbital in the center of the group. The ways in which these SALCs are able to combine with H $1s$ are illustrated in Figure **2.5.1.3**.

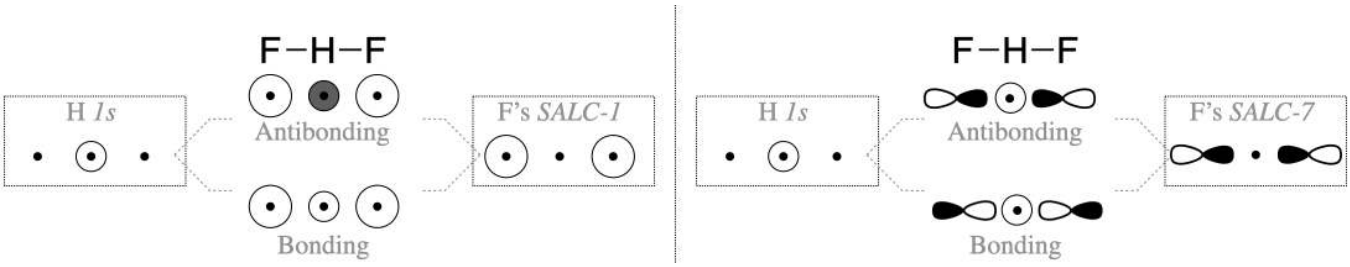
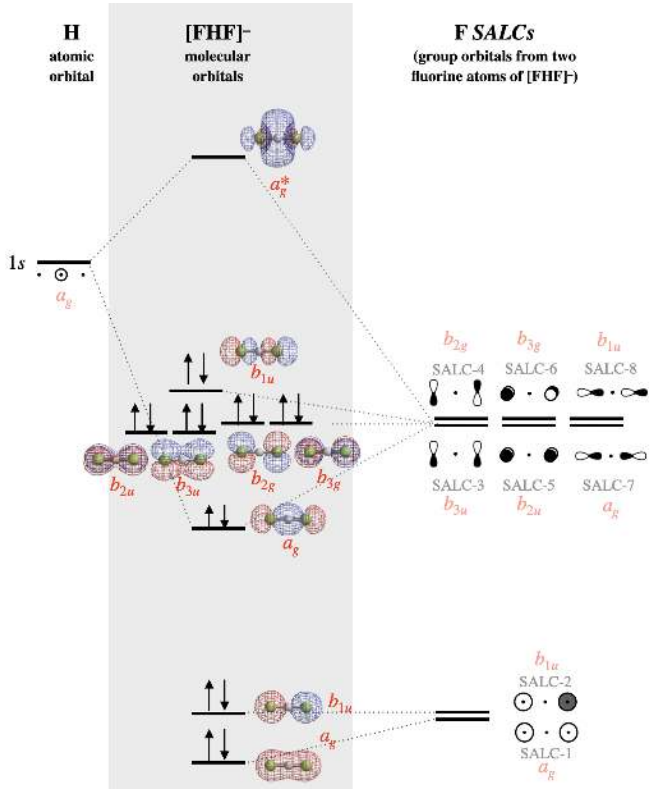


Figure **2.5.1.3**: Combinations of a central H $1s$ orbital with the group orbitals, SALC-1 and SALC-7 from Figure **2.5.1.2**, to create bonding and antibonding interactions. (CC-BY-NC-SA; Kathryn Haas)

Before we assume that both SALC-1 and SALC-7 will combine with the H $1s$ orbital, we must consider the energies of all atomic orbitals. The F $2p_z$ orbital has a potential energy of -18.7 eV (see Table 5.3.1). This is a good match for the H $1s$ orbital (-13.6 eV). However, the F $2s$ orbital has a much lower energy of -46.37 eV and would have weak interaction with the H $1s$.

The molecular orbital diagram for $[F\text{-}H\text{-}F]^-$ is shown in Figure **2.5.1.4**. Notice that all atomic orbitals, group orbitals (SALCs), and molecular orbitals in Figure **2.5.1.4** are assigned a symmetry label that corresponds to each element's symmetry under the D_{2h} point group. The molecular orbital labels correspond to **lower-case Mulliken Labels** of individual reducible representations from the D_{2h} character table. Upper-case symbols are used to indicate symmetry and irreducible representations, while lower-case symbols are used to indicate the identity of an orbital with that symmetry. The labeling methods described for simple diatomic linear molecules (σ, π) are not sufficient to indicate the more complex symmetries of the molecular orbitals in polyatomic molecules. The use of lower-case Mulliken symbols is the most rigorous way to label the orbitals. Refer to your instructor for how you should label orbitals for any graded work.

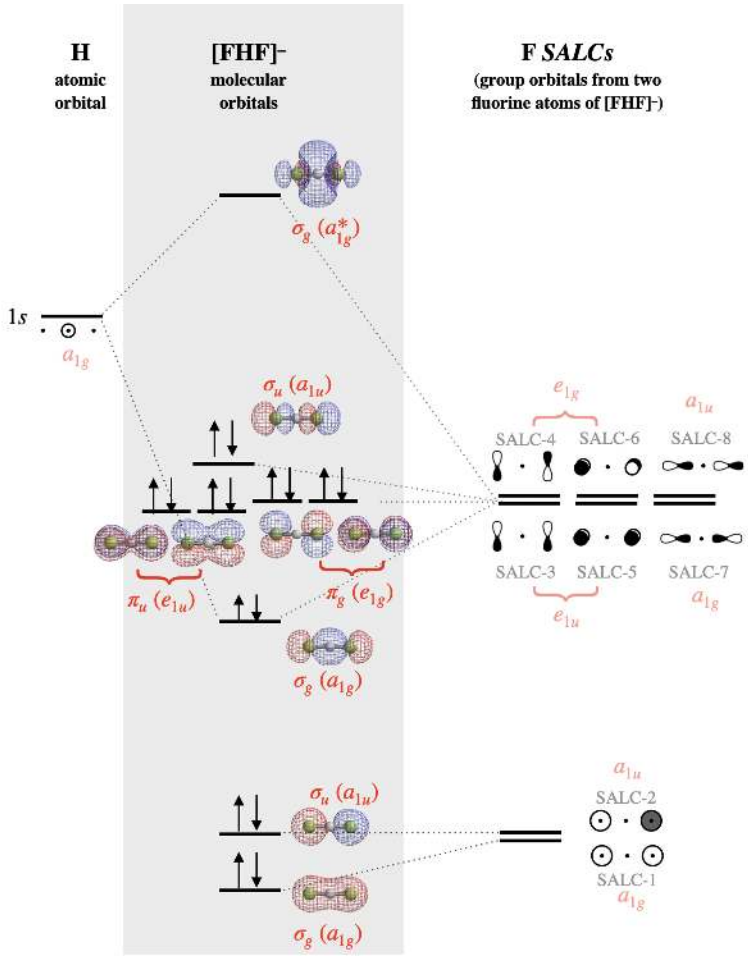


https://chem.libretexts.org/@go/page/484701

Figure **2.5.1.4**:The molecular orbital diagram for [F-H-F]⁻. The molecular orbital surfaces and relative energy levels were calculated using Spartan software. SALCs are labeled according to numbers assigned in Figure **2.5.1.2**. The symmetry of each SALC and orbital under the D_{2h} **point group** is shown in red font. (CC-BY-NC-SA; Kathryn Haas)

Click here for a version of Figure 2.5.1.4 using $D_{\infty h}$ labeling:

For high-symmetry groups, a shortcut is to use a lower-symmetry group that maintains the critical symmetry elements. In the case of the $D_{\infty h}$ point group, it is often sufficient to use the approximation of the D_{2h} point group and character table. This is the same MO diagram as shown above, but using the symmetry labels appropriate for the D_{2h} approximation.



Alternate Figure **2.5.1.4**: The molecular orbital diagram for [F-H-F]⁻. The molecular orbital surfaces and relative energy levels were calculated using Spartan software. SALCs are labeled according to numbers assigned in Figure **2.5.1.2**. The symmetry of each SALC and orbital under the D_{2h} **point group** is shown in red font. (CC-BY-NC-SA; Kathryn Haas)

Constructing the MO diagram

After identifying the atomic orbitals and constructing SALCs, place the atomic orbitals of H on one side of the diagram and all SALCs from F on the other side. Molecular orbitals are in the center.

The lowest-energy fluorine SALCs will be those composed of the lowest-energy atomic orbitals of fluorine; these would be SALC-1 (a_{1g}) and SALC-2 (a_{1u}) that are constructed from fluorine s atomic orbitals. Of these two orbitals, the one with zero nodes would be slightly lower in energy than the one with one node. When these two orbitals form molecular orbitals, the completely symmetric SALC-1 will be mostly non-bonding with slight bonding character from minor combination with the hydrogen $1s$ orbital. SALC-2, however is symmetrically incompatible with hydrogen $1s$ and will be a truly non-bonding orbital distributed over both F atoms.

The six SALCs constructed of fluorine p orbitals will have higher energy since the fluorine p atomic orbitals are higher in energy than the s orbitals (SALC-3 through SALC-8). Again, we expect SALCs with more nodes (SALC-4, -6, -8) to have slightly higher

energy than those with fewer nodes (SALC-3, -5, -7). SALC-7 will form a bonding and antibonding interaction with the hydrogen **1*s*** orbital. All other SALCS are truly non-bonding, but are non-degenerate non-bonding orbitals.

In bifluoride, there is an important distinction between the Lewis structure and molecular orbital description of lone pairs. In Lewis theory, the lone pairs are localized to individual fluorine atoms, while in the molecular orbital description each lone pair is distributed over both fluorine atoms at once (see surface depiction of each molecular orbital in Figure **2.5.1.4**).

2.5.1: Bifluoride anion is shared under a CC BY-NC-SA 4.0 license and was authored, remixed, and/or curated by LibreTexts.

- **5.4.1: Bifluoride anion** is licensed CC BY-SA 4.0.

2.5.2: Carbon Dioxide

Construct SALCs and the molecular orbital diagram for CO_2

Carbon dioxide is another linear molecule. This example is slightly more complex than the previous example of the bifluoride anion. While bifluoride had only one valence orbital to consider in its central H atom (the $1s$ orbital), carbon dioxide has a larger central atom, and thus more valence orbitals that will interact with SALCs.

Preliminary Steps

Step 1. Find the point group of the molecule and assign Cartesian coordinates so that z is the principal axis.

The CO_2 molecule is linear and its point group is $D_{\infty h}$. The z axis is collinear with the C_∞ axis. We will use the D_{2h} point group as a substitute since the orbital symmetries are retained in the D_{2h} point group.

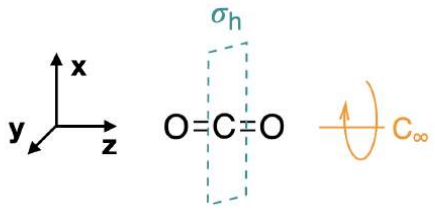


Figure 2.5.2.1: CO_2 belongs to the $D_{\infty h}$ point group. (CC_BY-NC-SA; Kathryn Haas)

Step 2. Identify and count the pendant atoms' valence orbitals.

Each of the two pendant oxygen atoms has four valence orbitals; $2s$, $2p_x$, $2p_y$, and $2p_z$. Thus, we can expect a total of eight SALCs.

Generate SALCs

The SALCs for CO_2 are identical in shape and symmetry to those described in the previous example for the bifluoride anion. But instead of cutting to the shortcut, we will systematically derive the SALCs here to demonstrate the process.

Step 3. Generate the Γ's

Use the D_{2h} character table to generate four reducible representations ($\Gamma's$); one for each of the four types of pendant atom orbitals (s, p_x, p_y, p_z). For each s orbital, assign a value of 1 if it remains in place during the operation or zero if it moves out of its original place. For each p orbital, assign 1 if there is no change, -1 if it remains in place but is inverted, and 0 if it moves out of its original position. The four Γ's are given below:

D_{2h}	E	$C_2(z)$	$C_2(y)$	$C_2(x)$	i	$\sigma(xy)$	$\sigma(xz)$	$\sigma(yz)$
Γ_{2s}	2	2	0	0	0	0	2	2
Γ_{2p_x}	2	−2	0	0	0	0	2	−2
Γ_{2p_y}	2	−2	0	0	0	0	−2	2
Γ_{2p_z}	2	2	0	0	0	0	2	2

Step 4. Break Γ's into irreducible representations for individual SALCs

Reduce each Γ into its component irreducible representations. There are two strategies that can be used to do this. The quick and easy way is to do it "by inspection", but this only works well for simple cases. The other is by using the systematic approach for breaking a Γ into reducible representations described previously in section 4.4.2 using the following formula:

$$\text{number of } i = \frac{1}{h}\sum(\text{number of operations in class}) \times (\chi_\Gamma) \times (\chi_i) \tag{2.5.2.1}$$

In other words, the number of irreducible representations of type i is equal to the sum of the number of operations in the class × the character of the Γ_{modes} × the character of i, and that sum is divided by the order of the group (h).

Using either approach results in the following eight irreducible representations ($2A_g + 2B_{1u} + B_{2g} + B_{3u} + B_{3g} + B_{2u}$):

$\mathbf{D_{2h}}$	E	$C_2(z)$	$C_2(y)$	$C_2(x)$	i	$\sigma(xy)$	$\sigma(xz)$	$\sigma(yz)$	
$\mathbf{\Gamma_{2s} = A_g + B_{1u}}$	$\mathbf{\Gamma_{2s}}$	**2**	**2**	**0**	**0**	**0**	**0**	**2**	**2**
	A_g	1	1	1	1	1	1	1	1
	B_{1u}	1	1	−1	−1	−1	−1	1	1
$\mathbf{\Gamma_{2p_x} = B_{2g} + B_{3u}}$	$\mathbf{\Gamma_{2p_x}}$	**2**	**−2**	**0**	**0**	**0**	**0**	**2**	**−2**
	B_{2g}	1	−1	1	−1	1	−1	1	−1
	B_{3u}	1	−1	−1	1	−1	1	1	−1
$\mathbf{\Gamma_{2p_y} = B_{3g} + B_{2u}}$	$\mathbf{\Gamma_{2p_y}}$	**2**	**−2**	**0**	**0**	**0**	**0**	**−2**	**2**
	B_{3g}	1	−1	−1	1	1	−1	−1	1
	B_{2u}	1	−1	1	−1	−1	1	−1	1
$\mathbf{\Gamma_{2p_z} = A_g + B_{1u}}$	$\mathbf{\Gamma_{2p_z}}$	**2**	**2**	**0**	**0**	**0**	**0**	**2**	**2**
	A_g	1	1	1	1	1	1	1	1
	B_{1u}	1	1	−1	−1	−1	−1	1	1

Step 5. Sketch the SALCs

From the systematic process above, you have found the symmetries (the irreducible representations) of all eight SALCs under the D_{2h} point group. To sketch the SALC that corresponds to each irreducible representation, again we use the D_{2h} character table, and specifically the functions listed on the right side columns of the table.

Two A_g SALCs (one from s and one from p_z): The A_g SALCs are each singly degenerate and symmetric with respect to both the principal axis (z) and the inversion center (i) (based on its Mulliken Label). We can look at the functions in the D_{2h} character table that correspond to A_g and see that it is completely symmetric under the group (because the combination of x^2, y^2, z^2 shows that it is totally symmetric). This would be the same symmetry as an s orbital on the central atom. From this information, we know that these SALCs must have symmetry compatible with an s orbital on the central atom, and we can draw the two A_g SALCs shown in Figure 2.5.2.2.

Two B_{1u} SALCs (one from s and one from p_z): The Mulliken Label tells us that the B_{1u} SALCs are each antisymmetric with respect to both the principal axis and the inversion center. The function, z, appearing with B_{1u} in the character table tells us that these SALCs have the same symmetry as the z axis, or a p_z orbital on the central atom. From this information, we know that these two SALCs should be compatible with a p_z orbital on the central atom, and we can draw the two B_{1u} SALCs shown in Figure 2.5.2.2.

All other SALCs shown below are derived using a strategy similar to the one in the two cases described above.

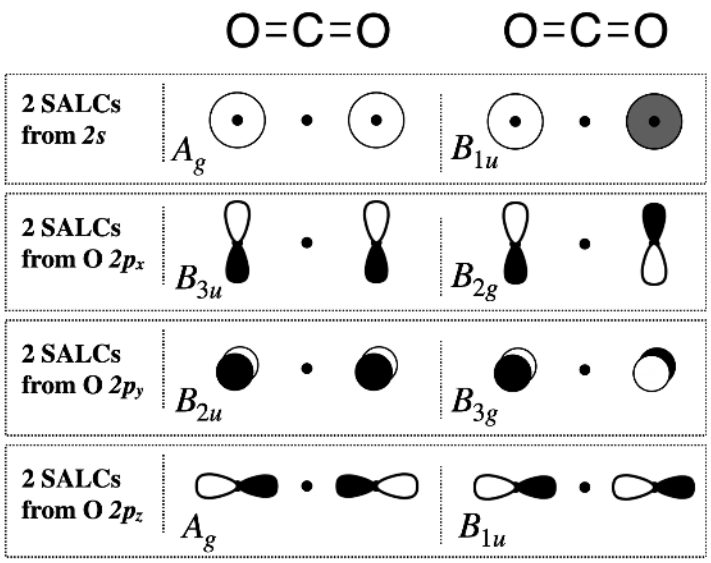


Figure 2.5.2.2: SALCs from the valence orbitals of oxygen atoms in CO_2. (CC-BY-NC-SA; Kathryn Haas)

Draw the MO diagram for CO_2

Step 6. Combine SALCs with AO's of like symmetry.

First we identify the valence orbitals on carbon: there are four including $2s$, $2p_x$, $2p_y$, and $2p_z$. Now we identify the symmetry of each using the D_{2h} character table. The symmetry of a central s orbital corresponds to the combination of functions x^2, y^2, and z^2 in the character table; this is A_g. The p_z orbital corresponds to the symmetry of the linear function z in the character table; this is B_{1u}. And so on... The symmetries of the C valence orbitals are listed below.

$$2s = A_g$$
$$2p_x = B_{3u}$$
$$2p_y = B_{2u}$$
$$2p_z = B_{1u}$$

Now that we have identified the symmetries of the eight oxygen SALCs and the four valence orbitals on carbon, we know which atomic orbitals and SALCs may combine based on compatible symmetries. We also need to know the relative orbital energy levels so that we can predict the relative strength of orbital interactions. The orbital ionization energies are listed in Section 5.3.

With knowledge of both orbital symmetries and energies, we can construct the molecular orbital diagram. The carbon atom goes on one side of the diagram while the oxygen SALCs are drawn on the opposite side. Molecular orbitals are drawn in the center column of the diagram:

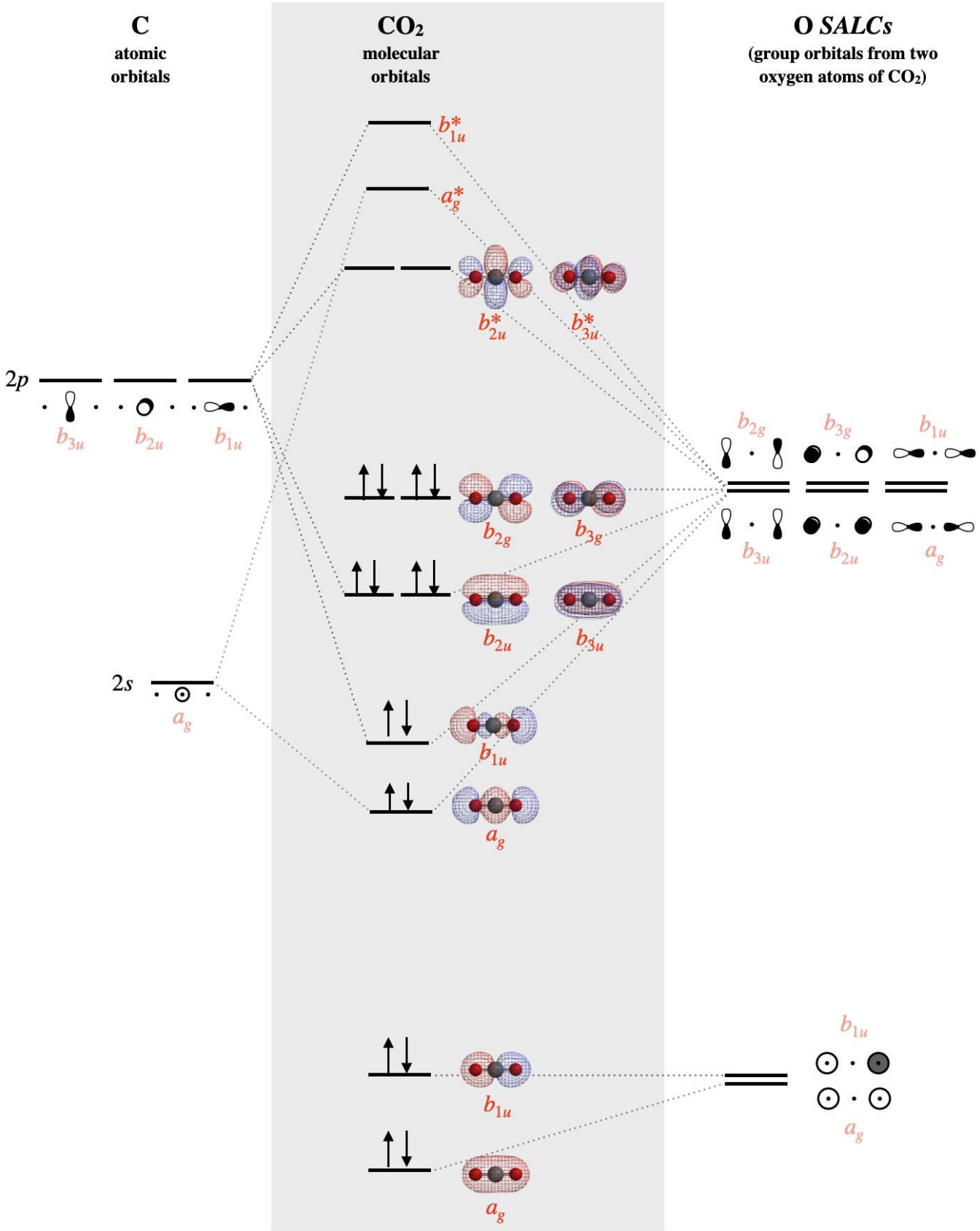


Figure 2.5.2.3: Molecular orbital diagram for carbon dioxide. (CC-BY-NC-SA; Kathryn Haas)

The SALCs on the right side of the diagram above are constructed from groups of either the $2s$ atomic orbitals of oxygen, or the $2p$ atomic orbitals of oxygen. Each SALC will combine with the atomic orbitals of carbon that have compatible symmetry; but the strength of the interaction depends on their relative energies. The individual valence atomic orbitals of oxygen have energies of $-32.36eV$ ($2s$) and $-15.87eV$ ($2p$), while the valence orbitals of carbon have energies of $-19.47eV$ ($2s$) and $-10.66eV$ ($2p$). The $2s$ orbitals of the oxygen are far lower in energy ($-32.36eV$) than all other valence orbitals, and so we should expect that molecular orbitals that are constructed from these oxygen $2s$ will be mostly non-bonding. These mostly non-bonding orbitals are the a_{1g} and b_{1g} orbitals shown at the bottom of Figure 2.5.2.3. The a_g orbital is lower in energy than the b_{1u} due to slight mixing with other orbitals of a_g symmetry.

The bonding orbitals of CO_2 include two $sigma$ molecular orbitals of a_g and b_{1u} symmetry and two π molecular orbitals of b_{2u} and b_{3u} symmetry. Each of these bonding molecular orbitals possesses a higher-energy antibonding partner. The b_{2g} and b_{3g} SALCs that are formed from oxygen $2p_x$ and $2p_y$ orbitals have no compatible match with carbon valence orbitals; thus they form two b_{2g} and b_{3g} molecular orbitals, which are truly non-bonding and mostly oxygen in character. Still, notice that each orbital is spread across both oxygen atoms at once, and again we see that each non-bonding electron pair in the HOMO is very different in molecular orbital theory compared to Lewis theory. Each non-bonding pair is distributed over both oxygen atoms at once in molecular orbital theory, while in Lewis theory each lone pair is isolated to one atom or to localized bonds attached to that atom.

This page titled 2.5.2: Carbon Dioxide is shared under a CC BY-NC-SA 4.0 license and was authored, remixed, and/or curated by Kathryn Haas.

- **5.4.2: Carbon Dioxide** by Kathryn Haas is licensed CC BY-SA 4.0.

2.5.3: H_2O

Construct SALCs and the molecular orbital diagram for H_2O.

This is the first example so far that is not a linear molecule. Water is a bent molecule, and so it is important to remember that interactions of pendant ligands are dependent on their positions in space. You should consider the positions of the three atoms in water to be essentially fixed in relation to each other. The process for constructing the molecular orbital diagram *for a non-linear molecule*, like water, is similar to the process for linear molecules. We will walk through the steps below to construct the molecular orbital diagram of water.

Preliminary Steps

Step 1. Find the point group of the molecule and assign Cartesian coordinates so that z is the principal axis.

The H_2O molecule is bent and its point group is C_{2v}. The z axis is collinear with the principal axis, the C_2 axis. There is no need to simplify this problem, as we had done for previous examples. The C_{2v} point group is simple enough.

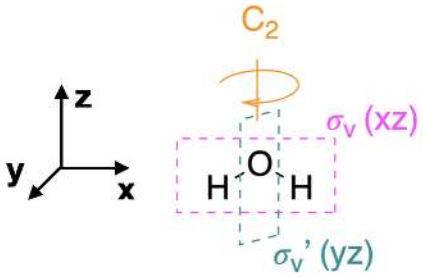


Figure **2.5.3.1**: The water molecular is in the C_{2v} point group. (CC-BY-NC-SA; Kathryn Haas)

Step 2. Identify and count the pendant atoms' valence orbitals.

Each of the two pendant hydrogen atoms has one valence orbital, the $1s$. Thus, we can expect a total of two SALCs from these two atoms.

Generate SALCs

The SALCs for H_2O are quite simple, yet we will systematically derive the SALCs here to demonstrate the process.

Step 3. Generate the Γ's

Use the C_{2v} character table to generate one reducible representation (Γ); in this case we need only one Γ because there is only one type of valence orbital (the $1s$). For each s orbital, assign a value of 1 if it remains in place during the operation or zero if it moves out of its original place. The Γ is given below:

C_{2v}	E	C_2	$\sigma_v(xz)$	$\sigma_v'(yz)$
Γ_{1s}	2	0	2	0

Step 4. Break Γ's into irreducible representations for individual SALCs

Reduce each Γ into its component irreducible representations. Using either of the processes described previously, we find that the Γ reduces to the two irreducible representations A_1 and B_1 under the C_{2v} point group.

C_{2v}	E	C_2	$\sigma_v(xz)$	$\sigma_v'(yz)$
Γ_{1s}	**2**	**0**	**2**	**0**
A_1	1	1	1	1
B_1	1	−1	1	−1

Step 5. Sketch the SALCs

From the systematic process above, you have found the symmetries (the irreducible representations) of both SALCs under the C_{2v} point group. To sketch the SALC that corresponds to each irreducible representation, again we use the C_{2v} character table, and

specifically the functions listed on the right side columns of the table.

One A_1 SALC: The A_1 SALC is singly degenerate and symmetric with respect to both the principle axis (z) and the inversion center (i) (based on its Mulliken Label). We can look at the functions in the C_{2v} character table that correspond to A_1 and see that it is completely symmetric under the group (because the combination of x^2, y^2, z^2 shows that it is totally symmetric). This would be the same symmetry as an s orbital on the central oxygen atom. From this information, we know that this SALC must have symmetry compatible with an s orbital on the central atom. We can also see from the character table that the z axis, and thus a p_z orbital on oxygen, also possesses A_1 symmetry. This tells us that in addition to being compatible with the oxygen s orbital, it should also be compatible with the oxygen p_z orbital. From this information we can draw the A_1 SALC shown in Figure **2.5.3.2**. *If it is not obvious how the A_1 sketch in Fig.* **2.5.3.2** *is compatible with the s and p_z orbitals of oxygen, inspect the drawings corresponding to molecular orbitals $2a_1$ and $3a_1$ in Fig.* **2.5.3.3**.

One B_1 SALC: The Mulliken Label tells us that the B_1 SALC is singly degenerate and antisymmetric with respect to both the principal axis and the inversion center. The function, x, appearing with B_1 in the character table tells us that this SALC has the same symmetry as the x axis, or a p_x orbital on the central oxygen atom. From this information, we know that this SALC should be compatible with a p_x orbital on the central atom, and we can draw the B_1 SALCs shown in Figure **2.5.3.2**. *If it is not obvious how the B_1 sketch in Fig.* **2.5.3.2** *is compatible with the p_x orbital of oxygen, inspect the drawing corresponding to molecular orbital $1b_1$ in Fig.* **2.5.3.3**.

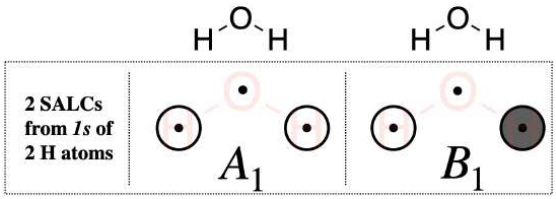


Figure **2.5.3.2**: Sketch of the A_1 and B_1 hydrogen SALCs of water. (CC-BY-NC-SA; Kathryn Haas)

Not convinced about the sketches of these SALCs? You can convince yourself by putting them to the test. Try the exercise below.

? Exercise 2.5.3.1

Perform all operations of the C_{2v} point group on the two sketches of H SALCs shown in Figure **2.5.3.2**, and convince yourself that each sketch does possess the A_1 and B_1 symmetries assigned to them, respectively, under the C_{2v} point group.

Answer

Add texts here. Do not delete this text first.

Draw the MO diagram for H_2O

Step 6. Combine SALCs with AO's of like symmetry.

First we must identify the valence orbitals on the central oxygen: there are four including $2s$, $2p_x$, $2p_y$, and $2p_z$. Now we identify the symmetry of each using the C_{2v} character table. The symmetry of a central $2s$ orbital corresponds to the combination of functions x^2, y^2, and z^2 in the character table; this is A_1. The p_z orbital also corresponds to A_1. And so on... The symmetries of oxygen valence orbitals are listed below.

$$2s = A_1$$
$$2p_x = B_1$$
$$2p_y = B_2$$
$$2p_z = A_1$$

Now that we have identified the symmetries of the two hydrogen SALCs and the four valence orbitals on oxygen, we know which atomic orbitals and SALCs may combine based on compatible symmetries. We also need to know the relative orbital energy levels so that we can predict the relative strength of orbital interactions. The orbital ionization energies are listed in Section 5.3.1.

With knowledge of both orbital symmetries and energies, we can construct the molecular orbital diagram. The valence orbitals of oxygen go on one side of the diagram while the hydrogen group orbitals are drawn on the opposite side. Molecular orbitals are

drawn in the center column of the diagram, as shown in Figure **2.5.3.3**:

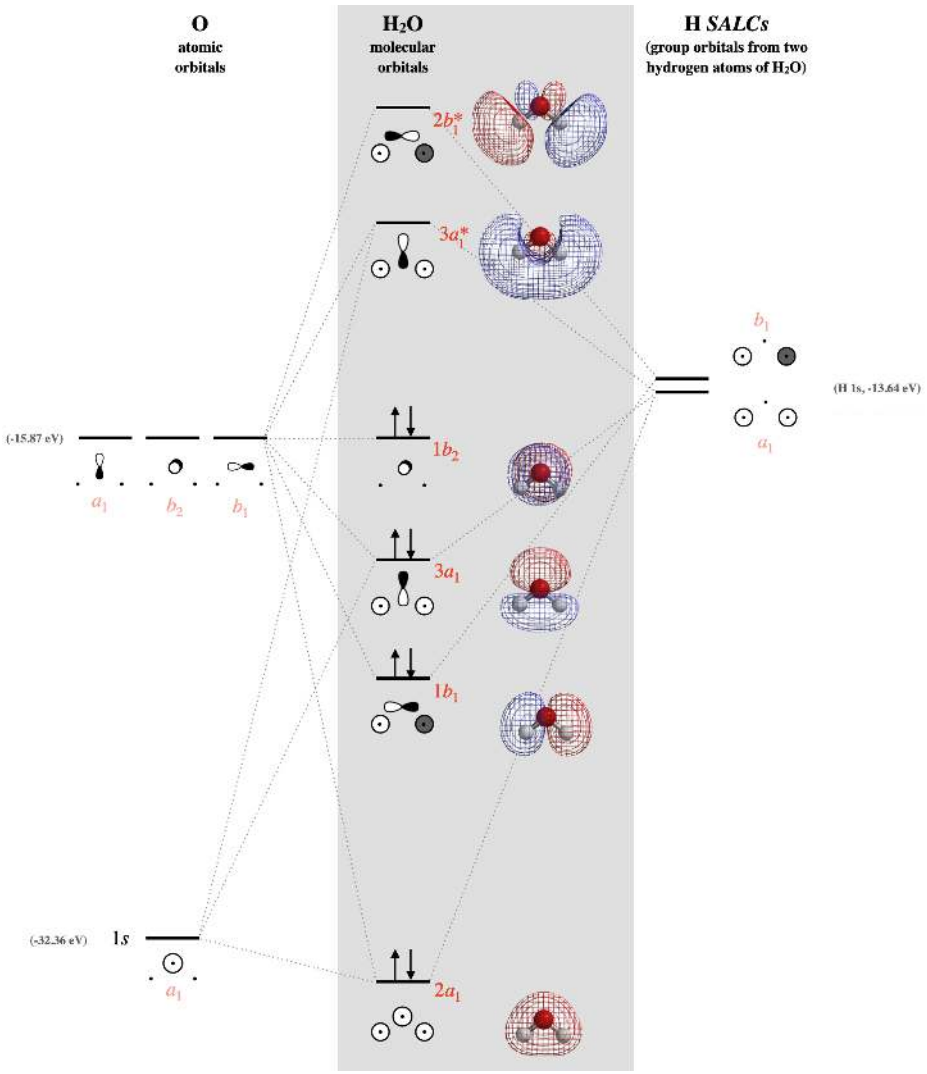


Figure **2.5.3.3**: The molecular orbital diagram of water. Molecular orbital surfaces calculated using Spartan software. The surface of the $3a_1^*$ orbital has been trimmed. (CC-BY-NC-SA; Kathryn Haas)

Example 2.5.3.1

In the previous examples shown for the molecular orbital diagrams of the bifluoride anion and carbon dioxide, we discussed differences in the understanding of those molecules from molecular orbital theory compared to Lewis structures. Water contains two lone pairs in its Lewis structure. Compare the predictions about water's lone pairs of electrons and its reactivity based on (1) the combination of elementary models (Lewis, Valence Bond, and Hybridized Orbital theories) and (2) Molecular Orbital theory. Specifically address and explain how the elementary models differ from molecular orbital theory in the following respects:

a. Where are the lone pairs in water?
b. Are the two lone pairs equivalent or are they different?
c. Where are sites on the molecule that will undergo reaction with electrophiles and nucleophiles?

Solution

1) Elementary models: The Lewis structure predicts that two lone pairs are (a) localized on the oxygen atom of water and that (b) both lone pairs are equivalent. The Lewis structure, combined with Valence Bond Theory, would predict that lone pairs occupy two equivalent hybridized sp^3 atomic orbitals on oxygen. (c) Lewis theory would predict that the oxygen lone pairs are

nucleophiles; thus an electrophile would react with the oxygen atom lone pairs. The polarized O-H bond leaves the H atoms as the most electrophilic locations on the water molecule; thus nucleophiles would react at the H atoms of water.

2) Molecular orbital theory: The molecular orbitals predict that (a) the two lone pairs of water are not equivalent, and that (b) each is distributed over the entire molecule. One lone pair is in the truly non-bonding $1b_2$ orbital (Figure **2.5.3.3**), which is also the HOMO. There is not another truly non-bonding orbital in the molecule, but the lowest-energy $2a_1$ orbital could be considered mostly non-bonding due to the large energy difference between it and other valence orbitals. (c) Although the $2a_1$ orbital can be considered mostly non-bonding, we cannot expect the electrons in $2a_1$ to react readily, as they are in the lowest-energy molecular orbital. Molecular orbital theory predicts that reactions occur at the HOMO and LUMO orbitals. The HOMO reacts with electrophiles, and in this case, the HOMO is distributed over the top and bottom faces of the molecule, and is centered on the oxygen atom. The LUMO would react with nucleophiles. The LUMO is the orbital labeled $3a_1^*$ in Figure **2.5.3.3**, and has a major lobe that is distributed more heavily over the H atoms, and from this we should predict H atoms to be the preferred site of reaction for nucleophiles.

Expressing molecular orbitals in terms of Ψ

The general expression for a molecular orbital, or the linear combination of atomic orbitals (LCAO), was given previously as $\Psi = c_a\psi_a + c_b\psi_b$. In this expression, the wavefunction of two atoms (ψ_a and ψ_b) is combined to form the wavefunction of the molecular orbital. The coefficients c_a and c_b quantify the contribution of each atomic ψ to the molecular Ψ.

$$\Psi = c_a\psi_a + c_b\psi_b$$

In the case of polyatomic orbitals, each LCAO is constructed of atomic orbitals from a central atom and group orbitals (SALCs) from the pendent atoms. In the case of water, the expression above could be modified to give the expression below.

$$\Psi = c_{oxygen}\,(\psi_{oxygen}) + c_{SALCs}\,(N(\psi_{H_a} \pm \psi_{H_b}))$$

N represents the normalizing requirement that was mentioned previously in reference to the requirements for electron wavefunctions and probability functions. The normalizing requirement simply stated is the requirement that the probability of finding the electron in any orbital, including group orbitals, is 1. In general, the value of N for a group orbital is...

$$N = \frac{1}{\sum c_i^2}$$

...where c_i is the coefficient of each unique atomic orbital that contributes to the group. For the hydrogen SALCs of water, there are two atomic orbitals that contribute to equally to each SALC, and so the coefficient on each of the two orbitals is 1. This gives $N = \left(\frac{1}{\sqrt{1^2+1^2}}\right) = \frac{1}{\sqrt{2}}$ for the H SALCs of water.

There are only two hydrogen SALCs: the one in which the hydrogen wavefunctions are added ($N(\psi_{H_a} + \psi_{H_b})$) has A_1 symmetry, and the one in which the hydrogen wavefunctions are subtracted ($N(\psi_{H_a} - \psi_{H_b})$) has B_1 symmetry.

The molecular orbitals from Figure **2.5.3.3** are expressed below in terms of their LCAO of individual wavefunctions. Yet, note that these expressions are simplifications that ignore orbital mixing. For example, as expressed below, they ignore contributions of oxygen $2s$ to the higher energy moelcular orbitals with A_1 symmetry (the $3a_1$ and $3a_1^*$ in Figure **2.5.3.3**).

MO		*OxygenAO*		*HydrogenSALC*	*Description*
Ψ_{2a_1}	=	$c_{(ox1)}\psi_{(2s)}$	+	$c_{(hy1)}[N(\psi_{H_a} + \psi_{H_b})]$	$c_{(hy1)}$ is positive; bonding, slightly nonbonding
Ψ_{1b_1}	=	$c_{(ox2)}\psi_{(2p_x)}$	+	$c_{(hy2)}[N(\psi_{H_a} - \psi_{H_b})]$	$c_{(hy2)}$ is positive; bonding
Ψ_{3a_1}	=	$c_{(ox3)}\psi_{(2p_z)}$	+	$c_{(hy3)}[N(\psi_{H_a} + \psi_{H_b})]$	$c_{(hy3)}$ is positive; bonding
Ψ_{1b_2}	=	$\psi_{(2p_y)}$			nonbonding
$\Psi^*_{3a_1}$	=	$c_{(ox4)}\psi_{(2p_z)}$	+	$c_{(hy4)}[N(\psi_{H_a} + \psi_{H_b})]$	$c_{(hy4)}$ is negative; antibonding
$\Psi^*_{1b_1}$	=	$c_{(ox5)}\psi_{(2p_x)}$	+	$c_{(hy5)}[N(\psi_{H_a} - \psi_{H_b})]$	$c_{(hy5)}$ is negative; antibonding

2.5.3: H_2O is shared under a CC BY-NC-SA 4.0 license and was authored, remixed, and/or curated by LibreTexts.

- **5.4.3: H_2O** is licensed CC BY-SA 4.0.

2.5.4: NH_3

Construct SALCs and the molecular orbital diagram for NH_3

This is the first example so far that has more than two pendant atoms and the first example in which the molecule has atoms that lie in three dimensions (i.e., it is not flat). Ammonia is a trigonal pyramidal molecule, with three pendant hydrogen atoms. The three-dimensional shape and the odd number of pendant atoms makes this example more complicated than the previous cases of water, carbon dioxide, and bifluoride. In this case, sketching the shapes (step 5) of pendant atom SALCs is less straightforward; rather, an alternative method, the **projection operator method**, is preferred for generating pictorial representations of the SALCs.

As in previous examples, it is important to remember that interactions of pendant ligands are dependent on their positions in three-dimensional space. You should consider the positions of the four atoms in ammonia to be essentially fixed in relation to each other. We will walk through the steps used to construct the molecular orbital diagram of ammonia. The first few steps are the same as you've seen before:

Step 1. Find the point group of the molecule and assign Cartesian coordinates so that z is the principal axis.

The NH_3 molecule is trigonal pyramidal and its point group is C_{3v}. The z axis is collinear with the principal axis, the C_3 axis.

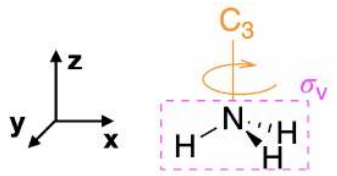


Figure **2.5.4.1**: The ammonia molecule is in the C_{3v} point group. (CC-BY-NC-SA; Kathryn Haas)

Step 2. Identify and count the pendant atoms' valence orbitals.

Each of the three pendant hydrogen atoms has one valence orbital; the $1s$. Thus, we can expect a total of three SALCs from these three atoms.

Step 3. Generate the Γ's

Use the C_{3v} character table to generate one reducible representation (Γ); in this case we need only one Γ because there is only one type of valence orbital (the $1s$). For each s orbital, assign a value of 1 if it remains in place during the operation or zero if it moves out of its original place. The Γ is given below:

C_{3v}	E	$2C_3$	$3\sigma_v$
Γ_{1s}	3	0	1

Step 4. Break Γ's into irreducible representations for individual SALCs

Reduce each Γ into its component irreducible representations. Using either of the processes described previously, we find that the Γ reduces to the two irreducible representations A_1 and E under the C_{3v} point group.

C_{3v}	E	$2C_3$	$3\sigma_v$
Γ_{1s}	3	0	2
A_1	1	1	1
E	2	−1	0

Notice that we only found TWO irreducible representations. But, in fact we have THREE different SALCs. The E irreducible representation is doubly degenerate, which in this context means that it corresponds to two degenerate SALCs. Thus, we have already found the symmetries of the three SALCs for ammonia: Two of the SALCs are degenerate with E symmetry under the C_{3v} point group, while the third SALC has A_1 symmetry.

Step 5. Sketch the SALCs using the PROJECTION OPERATOR METHOD

From the first four steps (described above), you have found the symmetries (the irreducible representations) of all three SALCs under the C_{3v} point group. To sketch the SALC that corresponds to each irreducible representation, again we use the C_{3v} character

table. But now we will introduce the **projection operator method** to derive the surface representation of each SALC.

Step 5.1: Label the pendent atoms

In the projection operator method, first **label each of the pendant atoms so that we can distinguish identical atoms from one another**; for example, identify the three hydrogen atoms on ammonia as H_a, H_b, and H_c (Figure 2.5.4.2).

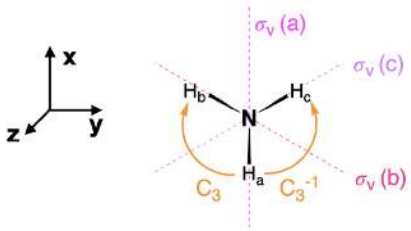


Figure 2.5.4.2: The three H's in NH_3 are chemically identical, but we can distinguish them using labels for the purpose of applying the projection operator method. In this figure, we have placed the z axis along the principal C_3 axis and placed the x axis colinear with one H. Each of the three H atoms has been labeled as H_a, H_b, or H_c. The σ_v that is coplanar with each H is labeled similarly (a, b, c) to keep account of each individual plane of symmetry. (CC-BY-NC-SA; Kathryn Haas)

Step 5.2: Create an expanded character table with one pendant atom's projected position after each operation

We will **perform each operation of the C_{3v} point group on this labeled molecule** and follow where one of the atoms is projected after the operation is complete. We will arbitrarily choose H_a. For example, upon performing the identity operation, E, the H_a atom is projected onto itself. On the other hand, H_a is projected onto H_b upon a clockwise C_3 rotation (as drawn in Figure 2.5.4.2). We take into account the result of each operation using an expanded character table (refer to the table below, 2.5.4.1). In the expanded character table, each operation within each class is written separately (i.e., $2C_3$ is accounted for separately as C_3 and C_3^{-1}).

Table 2.5.4.1: The expanded character table, and the projection of H_a by each operation is shown below.

C_{3v}	E	C_3	C_3^{-1}	$\sigma_v(a)$	$\sigma_v(b)$	$\sigma_v(c)$
Projection of H_a	H_a	H_b	H_c	H_a	H_c	H_b

(2.5.4.1)

Step 5.3: Find the contribution of each pendant atom to each SALC

Next, **create a linear combination of the projections for each of the SALCs** (the irreducible representations found in step 4). For each of the irreducible representations, multiply the projection by the respective character of the operation.

$$\text{Contribution of each atom to the SALC } = \sum(\text{Projection of } H_a \times \chi)$$

The linear combination for all irreducible representations of C_3v is shown below.

Table 2.5.4.2: The symmetry adapted linear combination (SALC) for each irreducible representation of C_3v is shown.

C_{3v}	E	C_3	C_3^{-1}	$\sigma_v(a)$	$\sigma_v(b)$	$\sigma_v(c)$	Linear Combination
Projection of H_a	H_a	H_b	H_c	H_a	H_c	H_b	
A_1	1	1	1	1	1	1	$= 2H_a + 2H_b + 2H_c$
A_2	1	1	1	−1	−1	−1	$= 0$
E	2	−1	−1	0	0	0	$= 2H_a - H_b - H_c$

(2.5.4.2)

Notice that there are only two irreducible representations that produce SALCs, and these are the same that were found in Step 4, above. This illustrates the fact that only the irreducible representations found through the reduction of the Γ will produce SALCs. We can ignore any irreducible representations that were not found in Step 4. Or, you can check your work in Step 4 by applying the projection operator to any irreducible representations not found in Step 4, and finding that they produce a sum of zero.

Step 5.4: Sketch the SALCs

The meaning of the linear combinations found in Table 2.5.4.2 is as follows:

- **Sketch the SALC with A_1 symmetry:** The linear combination $2H_a + 2H_b + 2H_c$ indicates all contributions to this SALC are of the same sign (of the wavefunction). Qualitatively, this means there is no node in this SALC. We can take this SALC almost literally to assume that all three H 1s wavefunctions contribute equally to the SALC. We can also use the fact that the A_1 representation possesses the full symmetry of the C_3v point group, is compatible with an s orbital on N, and thus is a totally symmetric SALC.

  Quantitatively, we can apply the normalizing factor, N, for this SALC. The linear combination for the A_1 SALC in Table 2.5.4.2 shows us that the coefficient for each orbital is 1. Thus, the normalizing factor for the A_1 SALC is $N = \left(\frac{1}{\sqrt{1^2+1^2+1^2}}\right) = \frac{1}{\sqrt{3}}$. This tells us that H_a, H_b, and H_c each contribute $\frac{1}{\sqrt{3}}$ to the normalized A_1 group orbital:

  $$A_1 \text{ group orbital } = \frac{1}{\sqrt{3}}\left[\psi_{H_a} + \psi_{H_b} + \psi_{H_c}\right]$$

  This is shown visually in Figure 2.5.4.3.
- **Sketch two SALCs with E symmetry:** The linear combination $2H_a - H_b - H_c$ indicates that there are contributions with both positive and negative sign to the wavefunction for each of the E group orbitals. Qualitatively, this tells us that there is a node within each of these two SALCs, and that the total contribution of the positive portion of the wavefunction is equal to the contribution of the negative portion.
  - **Finding the first E SALC:**
    For one of the SALCs, we can take the linear combination from Table 2.5.4.2 almost literally: The contribution from H_a is equal and opposite to the sum of the contributions from $H_b + H_c$. This would result in a SALC as shown in Figure 2.5.4.3 (E, left), that would have symmetry of the x axis and that would be compatible with the p_x orbital on N. The node exists in the yz plane and there is an equal contribution of positive and negative parts of the total wavefunction.

    We can also apply the normalizing factor, N, to find this SALC. The linear combination for the E SALC in Table 2.5.4.2 shows us that the coefficients for orbital contributions are 2, -1, and -1. Thus, the normalizing factor for the first E SALC is $N = \left(\frac{1}{\sqrt{2^2+(-1)^2+(-1)^2}}\right) = \frac{1}{\sqrt{6}}$. This normalized E group orbital is:

    $$\text{First } E \text{ group orbital } = \frac{1}{\sqrt{6}}\left[2\psi_{H_a} - \psi_{H_b} - \psi_{H_c}\right]$$

    This is shown visually in Figure 2.5.4.3 (E, left).
  - **Finding the second E SALC:**
    The second SALC is less obvious at first glance. We must use clues from the character table to help us determine what it should "look like". Since the E representation transforms as the group, (x, y), we know that one of the SALCs will have the symmetry of the x axis and p_x orbital on the central nitrogen atom, while the other should possess the symmetry of the y axis and be compatible with the p_y orbital on nitrogen. This alone could lead you to the sketch of the second SALC with E symmetry shown in Figure 2.5.4.3 (E, right). This second E SALC must have a node in the xz plane, and because H_a lies in this node, H_a cannot contribute to this group orbital. Retaining the fact that the positive and negative contributions of the linear combination must be equal, we can arrive at a SALC that has equal but opposite contributions of H_b and H_c, and no contribution by H_c (Figure 2.5.4.3, right).

    We can also apply the normalizing factor, N, to find this SALC. But we must apply the fact that H_a cannot contribute to the SALC with "y" symmetry. We remove the contribution of H_a, leaving us with coefficients of 0 for H_a and 1 for H_b and H_c. Thus, the normalizing factor for the second E SALC is $N = \left(\frac{1}{\sqrt{0^2+1^2+1^2}}\right) = \frac{1}{\sqrt{2}}$. To this, we must add positive and negative coefficients so that the entire wavefunction of this SALC is normalized. The result for this normalized E group orbital is:

    $$\text{Second } E \text{ group orbital } = \frac{1}{\sqrt{2}}\left[\psi_{H_b} - \psi_{H_c}\right]$$

    This is shown visually in Figure 2.5.4.3.

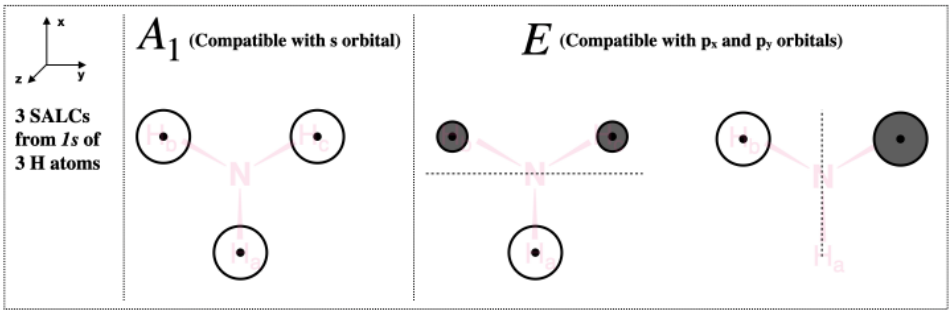


Figure 2.5.4.3: Sketches of H SALCs of ammonia from the perspective of the C_3 axiz (z axis). The A_1 SALC is shown at the left, while two degenerate SALCs with E symmetry are shown on the right. Nodes for E group orbitals are shown as dashed lines. (CC-BY-NC-SA; Kathryn Haas)

Step 6. Combine SALCs with AO's of like symmetry to draw the MO diagram for NH_3

First we must identify the valence orbitals on the central nitrogen: there are four including $2s$, $2p_x$, $2p_y$, and $2p_z$. Now we identify the symmetry of each using the C_{3v} character table. The symmetry of a central $2s$ orbital corresponds to the combination of functions x^2, y^2, and z^2 in the character table; this is A_1. The p_z orbital also corresponds to A_1. And so on... The symmetries of nitrogen valence orbitals are listed below.

$$2s = A_1$$
$$(2p_x,\ 2p_y) = E$$
$$2p_z = A_1$$

The next step is to get a sense of the relative energies of valence atomic orbitals for nitrogen and hydrogen, and then construct the molecular orbital diagram. The nitrogen $2s$ orbital is about 12 eV lower in energy than a H $1s$. This difference is an acceptable energy-match for the H orbitals to interact, but would not usually result in a strong interaction. On the other hand, the nitrogen 2p orbitals have an energy very close to the hydrogen 1s, different by only 0.5 eV. Knowledge of the relative energies of the atomic orbitals tells us that, when constructing a diagram, we can place the H SALCs at an energy similar to that of the N $2p$ orbitals, while the N $2s$ is much lower (Figure 2.5.4.4).

The $2s$ and $2p_z$ orbitals have A_1 symmetry and can combine with the A_1 SALC. These orbitals will give three molecular orbitals. The $2s$ orbital will not have strong interactions with the other orbitals of A_1 symmetry due to the large energy difference. The $2p_z$ orbital will not have good overlap with the wavefunctions for the three hydrogen orbitals due to their positions in space: The $2p_z$ orbital has half of its angular distribution pointed away from the hydrogen orbitals, and half pointed toward the center of a triangle formed by the three hydrogen atoms. The nitrogen $2s$ and $2p_z$ will combine with the hydrogen SALC of A_1 symmetry to give three molecular orbitals; one low-energy bonding orbital, one mid-energy non-bonding orbital, and one high-energy antibonding orbital. The mid-level non-bonding a_1 molecular orbital is close in energy to, and resembles, the nitrogen $2p_z$ orbital. The lowest energy a_1 molecular orbital will be lower in energy, but be similar to the nitrogen $2s$.

The remaining two $2p$ orbitals are degenerate and possess E symmetry under the C_{3v} point group. Although these orbitals are a good energy match, again, their orientation and positions in space do not allow for good orbital overlap, and their bonding and antibonding interactions are relatively weak compared to what we might otherwise expect from such a good energy match. The e atomic orbitals of nitrogen will combine with the e SALCs to give a set of two degenerate bonding molecular orbitals and a set of two degenerate antibonding orbitals (four total molecular orbitals of e symmetry). The MO diagram for NH_3 is shown in Figure 2.5.4.4, with calculated electron density surfaces of each MO shown.

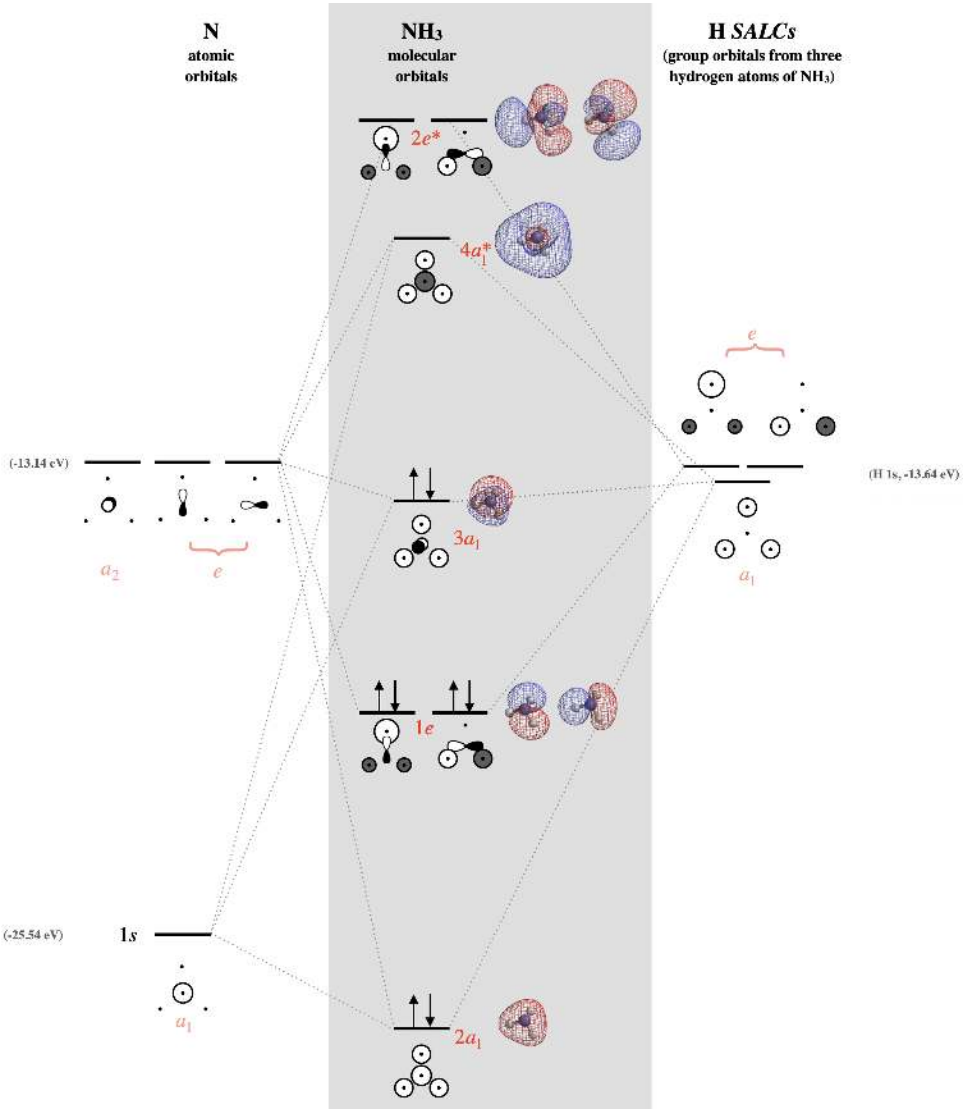


Figure **2.5.4.4**: The molecular orbital diagram of ammonia. Molecular orbitals surfaces calculated using Spartan software. (CC-BY-NC-SA; Kathryn Haas)

2.5.4: NH3 is shared under a CC BY-NC-SA 4.0 license and was authored, remixed, and/or curated by LibreTexts.

- **5.4.4: NH3** by Kathryn Haas is licensed CC BY-SA 4.0.

2.5.5: CO_2 (Revisted with Projection Operators)

The process for finding SALCs and constructing the molecular orbital diagram for carbon dioxide was described in a previous section (Section 5.4.2). However, we also just presented an alternative strategy, the projection operator method, to finding the shapes of SALCs in Section 5.4.4. Let's revisit carbon dioxide and demonstrate how you can use the projection operator method to find SALCs for carbon dioxide.

Just as before, we can simplify the problem by approximating the $D_{\infty h}$point group using D_{2h}. The first four steps for constructing the MO diagram would be the same as described in Section 5.4.2. and we will pick up from that point (with Step 5) to find what the SALCs look like using the projection operator method.

The projection operator method applied to CO_2

Step 5.1: Label the pendent atoms.

We can label the pendant atoms as O_a and O_b, as in Figure 2.5.5.1.

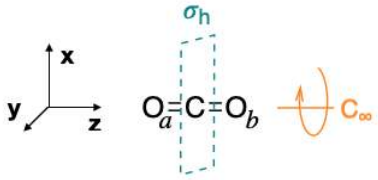


Figure 2.5.5.1: The structure of carbon dioxide with pendant oxygen atoms distinguished with labels a and b. Note that we will approximate the C_∞ axis as a C_2 axis to simplify the process of finding the SALCs. (CC-BY-SA; Kathryn Haas)

Step 5.2: Create an expanded character table with one pendant atom's projected position for each operation

The D_{2h} character table needs no expansion because each operation is in its own class. We will arbitrarily choose to determine the new position of O_a after each operation.

D_{2h}	E	$C_2(z)$	$C_2(y)$	$C_2(x)$	i	$\sigma(xy)$	$\sigma(xz)$	$\sigma(yz)$
Projection of O_a	O_a	O_a	O_b	O_b	O_b	O_b	O_a	O_a

Step 5.3: Find the contribution of each pendant atom to each SALC

Create a linear combination of the projections for each or the SALCs. The irreducible representations were found in step 4 in Section 5.4.2. Eight irreducible representations were found to be: $2A_g + 2B_{1u} + B_{2g} + B_{3u} + B_{3g} + B_{2u}$. For each of the irreducible representations, multiply the projection by the respective character of the operation.

$$\text{Contribution of each atom to the SALC } = \sum(\text{Projection of } H_a \times \chi)$$

The linear combination for all irreducible representations of D_{2h} are shown below.

Table 2.5.5.1: The symmetry adapted linear combination (SALC) for each irreducible representations of C_3v are shown.

D_{2h}	E	$C_2(z)$	$C_2(y)$	$C_2(x)$	i	$\sigma(xy)$	$\sigma(xz)$	$\sigma(yz)$	Linear Combination
Projection of O_a	O_a	O_a	O_b	O_b	O_b	O_b	O_a	O_a	
A_g	1	1	1	1	1	1	1	1	$= 4O_a + 4O_b$
B_{1u}	1	1	−1	−1	−1	−1	1	1	$= 4O_a - 4O_b$
B_{2g}	1	−1	1	−1	1	−1	1	−1	$= 0$
B_{3u}	1	−1	−1	1	−1	1	1	−1	$= 0$
B_{3g}	1	−1	−1	1	1	−1	−1	1	$= 0$
B_{2u}	1	−1	1	−1	−1	1	−1	1	$= 0$

(2.5.5.1)

Notice that there are only two irreducible representations that produce SALCs, the A_g and the B_{1u}. Since we found two of each ($2A_g + 2B_{1u}$) when we found the irreducible representations, we know that there will be two SALCs of A_g symmetry and two of B_{1u}

symmetry; that is four total SALCs from the pendant oxygens. This is the same as what we found in Section 5.4.2 using a different method.

Step 5.4: Sketch the SALCs

The SALCs with A_g symmetry: Quantitatively, we can apply the normalizing factor, N, for these SALCs. Each atom contributes equally to the SALCs, thus the normalizing factor for the A_g SALC is $N = \left(\frac{1}{\sqrt{1^2+1^2}}\right) = \frac{1}{\sqrt{2}}$. This tells us that each oxygen contributes $\frac{1}{\sqrt{2}}$ to each of the normalized A_g group orbitals:

$$A_g \text{ group orbital } = \frac{1}{\sqrt{2}}\left[\psi_{O_a} + \psi_{O_b}\right]$$

The linear combination $4O_a + 4O_b$ indicates that wavefunctions from each oxygen atom contribute equally to each of the two SALCs, with the same sign of the wavefunction for each. Because we know that A_g is totally symmetric (all 1's in the characters), we can assume that the SALC's will look like a symmetric arrangement of oxygen orbitals. But which orbitals contribute? We could peek at the character table to get a hint. But we'll treat this problem systematically.

The SALCs with B_{1u} symmetry: The linear combination $4O_a - 4O_b$ indicates that each oxygen atom contributes equally, but that they have opposite wavefunctions. Application of the normalizing factor would give us:

$$B_{1u} \text{ group orbital } = \frac{1}{\sqrt{2}}\left[\psi_{O_a} + \psi_{O_b}\right]$$

But how do we know what the SALCs look like? Again, the character table can give us some hints, but we'll use a systematic process, below.

What do the SALCs look like? One way to systematically derive the SALC shapes is to perform the projection (Step 5.3) on specific groups of orbitals on the oxygen atom. For example, if we replicate Table 2.5.5.1 using just the group of oxygen 2s orbitals and the A_g and B_{1u} representations, we get the following:

D_{2h}	E	$C_2(z)$	$C_2(y)$	$C_2(x)$	i	$\sigma(xy)$	$\sigma(xz)$	$\sigma(yz)$	Linear Combination
Projection of 2s orbital of O_a	$O1s_a$	$O1s_a$	$O1s_b$	$O1s_b$	$O1s_b$	$O1s_b$	$O1s_a$	$O1s_a$	
A_g	1	1	1	1	1	1	1	1	$= 4O1s_a + 4O1s_b$
B_{1u}	1	1	−1	−1	−1	−1	1	1	$= 4O1s_a - 4O1s_b$

(2.5.5.2)

This tells us that one of the A_g SALCs looks like two oxygen 1s orbitals with equal signs and contributions. It also tells us that one of the B_{1u} SALCs looks like two s orbitals with opposite signs and equal magnitudes. These two SALCs are shown in Figure 2.5.5.2.

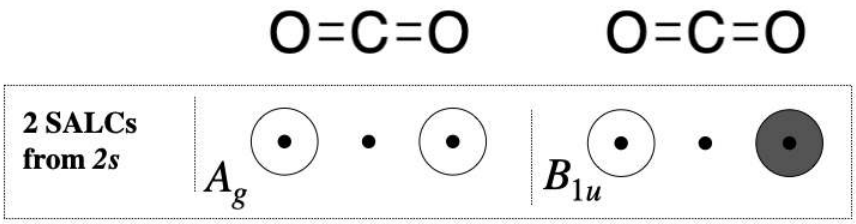


Figure 2.5.5.2: SALCs derived from two oxygen 2s orbitals from carbon dioxide. Compare to Section 5.4.2. (CC-BY-SA; Kathryn Haas)

If we do the same for the $2p_z$ orbitals, we need to pay attention to the orientation of the p orbital lobes. If the orbital is moved into the opposite orientation, it would get a negative sign in the projection (see below).

$\mathbf{D_{2h}}$	E	C_2 (z)	C_2 (y)	C_2 (x)	i	$\sigma(x$ $y)$	$\sigma(x$ $z)$	$\sigma(yz)$	Linear Combination
Projection of 2px orbital of O_a	$+O2$ pz_a	$+O2$ pz_a	$-O2$ pz_b	$+O2$ pz_b	$-O2$ pz_b	$-O2$ pz_b	$+O2$ pz_a	$+O2$ pz_a	
A_g	1	1	1	1	1	1	1	1	$= 4O2pz_a$ $- 4O2pz_b$
B_{1u}	1	1	−1	−1	−1	−1	1	1	$= 4O2pz_a$ $+ 4O2pz_b$

(2.5.5.3)

This tells us that one of the A_g SALCs is derived from two $2p_z$ orbitals of opposite sign but equal magnitude. In other words, the two p orbitals are pointing in opposite directions, but the lobes that are facing one another are of the same sign (see Figure **2.5.5.3**, left). This also tells us that one of the B_{1u} orbitals is derived from two p_z orbitals of equal magnitude and equal sign (pointing in the same directions, with lobes facing one another of opposite sign!) (see Figure **2.5.5.3**, right).

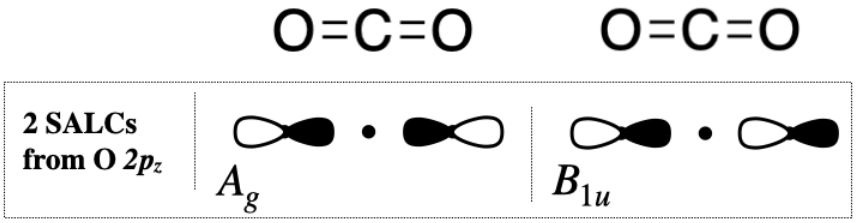


Figure **2.5.5.3**: SALCs derived from two oxygen $2p_z$ orbitals from carbon dioxide. Compare to Section 5.4.2. (CC-BY-SA; Kathryn Haas)

Now we have reached the same SALCs that we found previously in Section 5.4.2, but by an alternate method.

2.5.5: CO_2 (Revisted with Projection Operators) is shared under a CC BY-NC-SA 4.0 license and was authored, remixed, and/or curated by LibreTexts.

- **5.4.4: NH_3** by Kathryn Haas is licensed CC BY-SA 4.0.

2.5.6: BF_3

The case of boron trifluoride (BF_3) is an example of a molecule with one more layer of complexity than the other examples we have seen in previous sections in this chapter. (BF_3) is more complex than previous examples because it is the first case in which there are multiple types of valence orbitals on the pendant atoms. (BF_3) possesses s and p orbitals on *both* the central atom and all of the pendant atoms. We can follow the same steps that we have previously to derive other molecular orbital diagrams; however, there is one important difference: we will treat each type of pendant orbital as an individual set of SALCs.

Step 1. Find the point group of the molecule and assign Cartesian coordinates so that z is the principal axis.

The BH_3 molecule is trigonal planar, and its point group is D_{3h}. The z axis is colinear with the principle axis, the C_3 axis.

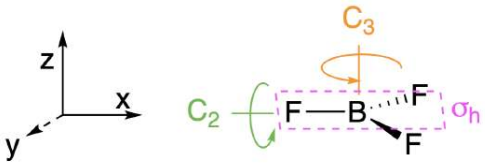


Figure 2.5.6.1: The molecule is in the D_{3h} point group. (CC-BY-NC-SA; Kathryn Haas)

Step 2. Identify and count the pendant atoms' valence orbitals.

Each of the three pendant fluorine atoms has four valence orbitals: one $2s$ and three $2p$ orbitals. Thus, we can expect a total of twelve SALCs from the three atoms. However, we will treat each type of orbital from the F atoms as its own set; each will have its own set of coordinates, with the y axis along the M-L bond. Thus we expect the following:

- One set of $2s$ SALCs: there is one 2s orbital on each of three atoms. This set will have three SALCs.
- One set of $2p_x$ SALCs: there is one $2p_x$ orbital on each of three atoms. Each of these individual orbitals is perpendicular to the M-L bond and coplanar with the molecule. This set will have three SALCs.
- One set of $2p_y$ SALCs: there is one $2p_y$ orbital on each of three atoms. Each of these individual orbitals is colinear with the M-L bond. This set will have three SALCs.
- One set of $2p_z$ SALCs: there is one $2p_z$ orbital on each of three atoms. Each of these individual orbitals is perpendicular to the M-L bond and parallel with the principal axis of the molecule. This set will have three SALCs.

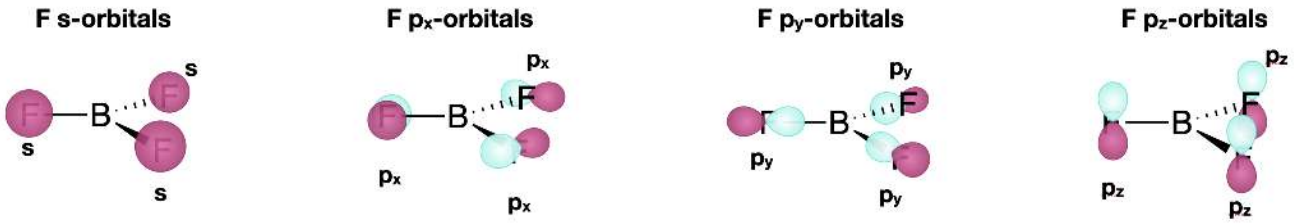


Figure 2.5.6.2: Individual sets of pendant fluorine atomic orbitals will create separate sets of SALCs. (CC-BY-SA; Kathryn Haas)

Step 3. Generate the Γ's for each set of SALCs

Use the D_{3h} character table to generate one reducible representation (Γ) for each of the four sets of pendant atomic orbitals shown in Figure 2.5.6.2; in this case we need four Γ because there are four types of valence orbital (the s, p_x, p_y, p_z).

- For the set of s orbitals: perform the operation for each class in the character table. Each s orbital is assigned a value depending on whether it moves or not: assign a value of 1 if it remains in place during the operation, or 0 (zero) if it moves out of its original place.
- for each set of p orbitals: Now there are phases (signs of the wavefunction), so a negative value is possible. Assign a value of 1 to each p orbital if it remains in place and in phase during the operation; assign a -1 if the atom's position remains, while the phase of the orbital is inverted (the positive lobe moves to the position of the negative lobe and vice versa); assign a 0 if it moves out of its original position.

The Γ for each type is given below:

$\mathbf{D_{3h}}$	E	$2C_3$	$3C_2$	σ_h	$2S_3$	$3\sigma_v$
$\mathbf{\Gamma_{2s}}$	3	0	1	3	0	1
$\mathbf{\Gamma_{2p_x}}$	3	0	−1	3	0	−1
$\mathbf{\Gamma_{2p_y}}$	3	0	1	3	0	1
$\mathbf{\Gamma_{2p_z}}$	3	0	−1	−3	0	1

Step 4. Break Γ's into irreducible representations for individual SALCs

Reduce each $\mathbf{\Gamma}$ into its component irreducible representations. Using either of the processes described previously, we find that each of the $\mathbf{\Gamma}$ reduces to two irreducible representations under the $\boldsymbol{D_{3h}}$ point group; in each case one is singly degenerate ($\boldsymbol{A}$) and the other doubly degenerate ($\boldsymbol{E}$). This equates to three SALCs for each $\mathbf{\Gamma}$ (orbital type) and a total of twelve SALCs. This should give us confidence! We were in fact expecting 12 SALCs because we found that there were twelve pendant atomic orbitals to start with.

D_{3h}	E	$2C_3$	$3C_2$	σ_h	$2S_3$	$3\sigma_v$
$\mathbf{\Gamma_{2s}}$	**3**	**0**	**1**	**3**	**0**	**1**
A_1'	1	1	1	1	1	1
E'	2	−1	0	2	−1	0

D_{3h}	E	$2C_3$	$3C_2$	σ_h	$2S_3$	$3\sigma_v$
$\mathbf{\Gamma_{2p_x}}$	**3**	**0**	**−1**	**3**	**0**	**−1**
A_2'	1	1	−1	1	1	−1
E'	2	−1	0	2	−1	0

D_{3h}	E	$2C_3$	$3C_2$	σ_h	$2S_3$	$3\sigma_v$
$\mathbf{\Gamma_{2p_y}}$	**3**	**0**	**1**	**3**	**0**	**1**
A_1'	1	1	1	1	1	1
E'	2	−1	0	2	−1	0

D_{3h}	E	$2C_3$	$3C_2$	σ_h	$2S_3$	$3\sigma_v$
$\mathbf{\Gamma_{2p_z}}$	**3**	**0**	**−1**	**−3**	**0**	**1**
A_2''	1	1	−1	−1	−1	1
E''	2	−1	0	−2	1	0

Step 5: Sketch the SALCs

We'll skip this step for now to make this problem simpler.

Step 6: Draw the MO diagram by combining SALCs with AO's of like symmetry.

We now know the symmetries of different pendant orbital SALCs - and it is helpful if we also know their relative energies, and the energies of the valence orbitals on the central boron atom. We can make predictions based on periodic trends, or we can use a table of ionization energies as a guide. The symmetries of the boron $\boldsymbol{2s}$ and $\boldsymbol{2p}$ orbitals can be found from the $\boldsymbol{D_{3h}}$ character table.

2.5.6: BF_3 is shared under a CC BY-NC-SA 4.0 license and was authored, remixed, and/or curated by LibreTexts.

- **5.4.4: NH_3** by Kathryn Haas is licensed CC BY-SA 4.0.

CHAPTER OVERVIEW

3: Acid-Base Chemistry and an Introduction to Coordination Compounds

- 3.1: Bronsted-Lowry acids and bases
- 3.2: Lewis Acids and Bases
- 3.3: Acidity of the Hexaaqua Ions
- 3.4: Hard/Soft Acids and Bases
- 3.5: Quantitative Measures of Hardness and Softness
- 3.6: Coordination Chemistry- Structure and Isomers
  - 3.6.1: History
  - 3.6.2: Nomenclature and Ligands
  - 3.6.3: Acid-Base and Donor-Acceptor Chemistry
    - 3.6.3.1: Acid-Base Models as Organizing Concepts
    - 3.6.3.2: Lewis Concept and Frontier Orbitals
      - 3.6.3.2.1: The frontier orbital approach considers Lewis acid-base reactions in terms of the donation of electrons from the base's highest occupied orbital into the acid's lowest unoccupied orbital.
      - 3.6.3.2.2: All other things being equal, electron withdrawing groups tend to make Lewis acids stronger and bases weaker while electron donating groups tend to make Lewis bases stronger and acids weaker
      - 3.6.3.2.3: The electronic spectra of charge transfer complexes illustrate the impact of frontier orbital interactions on the electronic structure of Lewis acid-base adducts
      - 3.6.3.2.4: Substances' solution phase Lewis basicity towards a given acid may be estimated using the enthalphy change for dissociation of its adduct with a reference acid of similar hardness.
      - 3.6.3.2.5: In the boron trifluoride affinity scale, the enthalphy change on formation of an adduct between the base and boron trifluoride is taken as a measure of Lewis basicity.
      - 3.6.3.2.6: Lewis base strength may also be estimated by measuring structural or energy changes upon formation of a Lewis acid-base complex, as illustrated by efforts to spectroscopically assess the strengths of halogen bonds
      - 3.6.3.2.7: Bulky groups weaken the strength of Lewis acids and bases because they introduce steric strain into the resulting acid-base adduct.
      - 3.6.3.2.8: Frustrated Lewis pair chemistry uses Lewis acid and base sites within a molecule that are sterically restricted from forming an adduct with each other.
    - 3.6.3.3: Hard and Soft Acids and Bases
      - 3.6.3.3.1: Hard-Hard and Soft-Soft preferences may be explained and quantified in terms of electrostatic and covalent and electronic stabilization on the stability of Lewis acid-base adducts
      - 3.6.3.3.2: Quantitative Measures of Hardness, Softness, and Acid-Base Interactions from a Hard Soft Acid-Base Principle Perspective Involve Orbital Energies and/or Apportioning Acid-Base Bonding in Terms of Electrostatic and Covalent Factors
    - 3.6.3.4: Problems
  - 3.6.4: Coordination Numbers and Structures
  - 3.6.5: Isomerism
- 3.7: Coordination Chemistry- Bonding
  - 3.7.1: Crystal Field Theory
  - 3.7.2: Crystal Field Stabilization Energy
  - 3.7.3: Factors That Affect Crystal Field Splitting
  - 3.7.4: Ligand Field Theory
  - 3.7.5: Metal-Metal Bonds

3.7.5.1: Metal-Metal Multiple Bonds
3.7.6: Jahn-Teller Distortions

3: Acid-Base Chemistry and an Introduction to Coordination Compounds is shared under a CC BY-NC-SA 4.0 license and was authored, remixed, and/or curated by LibreTexts.

3.1: Bronsted-Lowry acids and bases

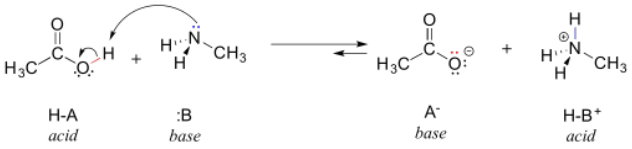
We'll begin our discussion of acid-base chemistry with a couple of essential definitions. The first of these was proposed in 1923 by the Danish chemist Johannes Brønsted and the English chemist Thomas Lowry, and has come to be known as the **Brønsted-Lowry definition of acidity and basicity**. An acid, by the Brønsted-Lowry definition, is a species which acts as a proton donor (i.e., it gives away an H^+), while a base is a proton (H^+) acceptor. One of the most familiar examples of a Brønsted-Lowry acid-base reaction is between hydrochloric acid and hydroxide ion:



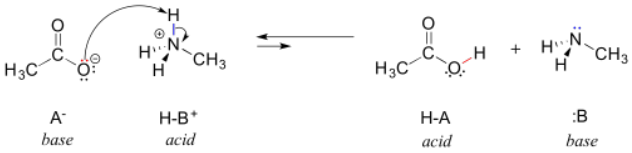
In this reaction, a proton is transferred from HCl (the acid, or proton *donor*) to hydroxide ion (the base, or proton *acceptor*). As we learned in the previous chapter, curved arrows depict the movement of electrons in this bond-breaking and bond-forming process.

After a Brønsted-Lowry acid donates a proton, what remains is called the **conjugate base**. Chloride ion is thus the conjugate base of hydrochloric acid. Conversely, when a Brønsted-Lowry base accepts a proton it is converted into its **conjugate acid** form: water is thus the conjugate acid of hydroxide ion.

Here is an organic acid-base reaction between acetic acid and methylamine:

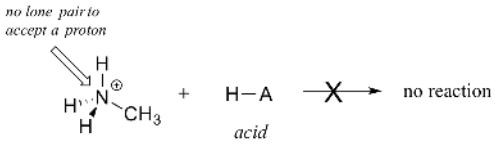


In the reverse of this reaction, acetate ion is the base and methylammonium ion (protonated methylamine) is the acid.



For now, let's just consider one common property of bases: *in order to act as a base, a molecule must have a reactive pair of electrons*. In all of the acid-base reactions we'll see in this chapter, the basic species has an atom with a lone pair of electrons. When methylamine acts as a base, for example, the lone pair of electrons on the nitrogen atom is used to form a new bond to a proton. A negative charge often (but not always!) indicates that a structure (in this case, an anion) is likely to act as a base.

Clearly, methylammonium ion cannot act as a base – it does not have a reactive pair of electrons with which to accept a proton.



In summary,

- A Brønsted-Lowry acid is a proton (hydrogen ion) donor.
- A Brønsted-Lowry base is a proton (hydrogen ion) acceptor.

When a Brønsted acid HA dissociates in water, it increases the concentration of hydrogen ions in the solution, H^+; conversely, Brønsted bases dissociate by taking a proton from the solvent (water) to generate OH^-.

- *Acid dissociation*

$$HA_{(aq)} \rightleftharpoons A^-_{(aq)} + H^+_{(aq)} \tag{3.1.1}$$

- *Acid Ionization Constant:*

$$K_a = \frac{[A^-][H^+]}{[HA]} \tag{3.1.2}$$

- *Base dissociation:*

$$B_{(aq)} + H_2O_{(l)} \rightleftharpoons HB^+_{(aq)} + OH^-_{(aq)} \tag{3.1.3}$$

- Base Ionization Constant

$$K_b = \frac{[HB^+][OH^-]}{[B]} \tag{3.1.4}$$

The determination of a substance as a Brønsted-Lowry acid or base can only be done by observing the reaction. In the case of the H_2O it is a base in the first case and an acid in the second case.

Water does not need to be involved in a Bronsted-Lowry reaction. In general, for an acid HA and a base Z, we have

$$HA + Z \rightleftharpoons A^- + HZ^+ \tag{3.1.5}$$

- A Donates H to form HZ^+.
- Z Accepts H from A which forms HZ^+
- A^- becomes conjugate base of HA and in the reverse reaction it accepts a H from HZ to recreate HA in order to remain in equilibrium
- HZ^+ becomes a conjugate acid of Z and in the reverse reaction it donates a H to A^- recreating Z in order to remain in equilibrium

3.1: Bronsted-Lowry acids and bases is shared under a CC BY-NC-SA 4.0 license and was authored, remixed, and/or curated by LibreTexts.

3.2: Lewis Acids and Bases

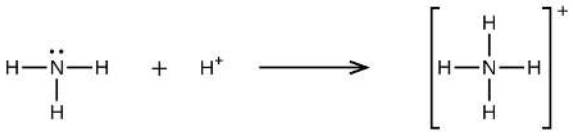
Learning Objectives

- Explain the Lewis model of acid-base chemistry
- Write equations for the formation of adducts and complex ions
- Perform equilibrium calculations involving formation constants

In 1923, G. N. Lewis proposed a generalized definition of acid-base behavior in which acids and bases are identified by their ability to accept or to donate a pair of electrons and form a coordinate covalent bond.

A coordinate covalent bond (or dative bond) occurs when one of the atoms in the bond provides both bonding electrons. For example, a coordinate covalent bond occurs when a water molecule combines with a hydrogen ion to form a hydronium ion. A coordinate covalent bond also results when an ammonia molecule combines with a hydrogen ion to form an ammonium ion. Both of these equations are shown here.

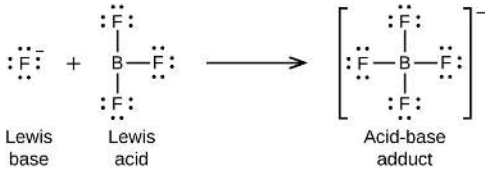




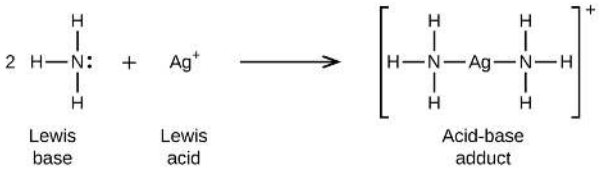
- A Lewis acid is any species (molecule or ion) that can *accept* a pair of electrons, and a Lewis base is any species (molecule or ion) that can *donate* a pair of electrons.

A Lewis acid-base reaction occurs when a base donates a pair of electrons to an acid. A **Lewis acid-base adduct**, a compound that contains a coordinate covalent bond between the Lewis acid and the Lewis base, is formed. The following equations illustrate the general application of the Lewis concept.

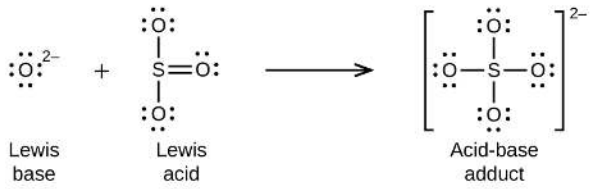
The boron atom in boron trifluoride, BF_3, has only six electrons in its valence shell. Being short of the preferred octet, BF_3 is a very good Lewis acid and reacts with many Lewis bases; a fluoride ion is the Lewis base in this reaction, donating one of its lone pairs:



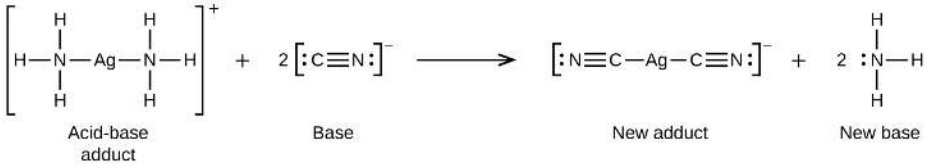
In the following reaction, each of two ammonia molecules, Lewis bases, donates a pair of electrons to a silver ion, the Lewis acid:

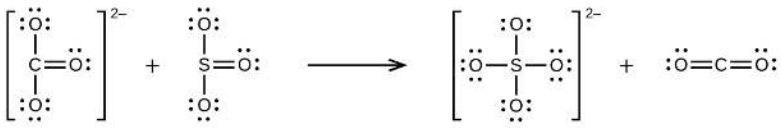


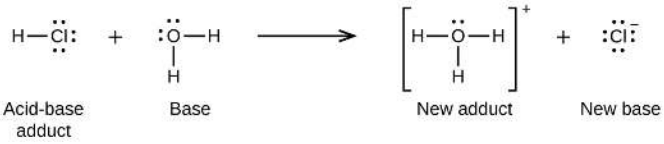
Nonmetal oxides act as Lewis acids and react with oxide ions, Lewis bases, to form oxyanions:



Many Lewis acid-base reactions are displacement reactions in which one Lewis base displaces another Lewis base from an acid-base adduct, or in which one Lewis acid displaces another Lewis acid:

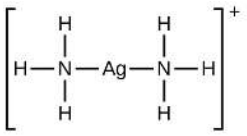






The last displacement reaction shows how the reaction of a Brønsted-Lowry acid with a base fits into the Lewis concept. A Brønsted-Lowry acid such as HCl is an acid-base adduct according to the Lewis concept, and proton transfer occurs because a more stable acid-base adduct is formed. Thus, although the definitions of acids and bases in the two theories are quite different, the theories overlap considerably.

Many slightly soluble ionic solids dissolve when the concentration of the metal ion in solution is decreased through the formation of complex (polyatomic) ions in a Lewis acid-base reaction. For example, silver chloride dissolves in a solution of ammonia because the silver ion reacts with ammonia to form the complex ion $[Ag(NH_3)_2]^+$. The Lewis structure of the $[Ag(NH_3)_2]^+$ ion is:



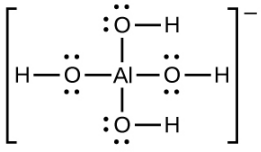
The equations for the dissolution of AgCl in a solution of NH_3 are:

$$\mathrm{AgCl}(s) \longrightarrow \mathrm{Ag^+}(aq) + \mathrm{Cl^-}(aq) \tag{3.2.1}$$

$$\mathrm{Ag^+}(aq) + 2\,\mathrm{NH_3}(aq) \longrightarrow [\mathrm{Ag(NH_3)_2}]^+(aq) \tag{3.2.2}$$

$$\text{Net: } \mathrm{AgCl}(s) + 2\,\mathrm{NH_3}(aq) \longrightarrow [\mathrm{Ag(NH_3)_2}]^+(aq) + \mathrm{Cl^-}(aq) \tag{3.2.3}$$

Aluminum hydroxide dissolves in a solution of sodium hydroxide or another strong base because of the formation of the complex ion $\mathrm{Al(OH)_4^-}$. The Lewis structure of the $\mathrm{Al(OH)_4^-}$ ion is:



The equations for the dissolution are:

$$[Al(OH)_3](s) \longrightarrow Al^{3+}(aq) + 3\,OH^-(aq) \tag{3.2.4}$$

$$Al^{3+}(aq) + 4\,OH^-(aq) \longrightarrow [Al(OH)_4]^-(aq) \tag{3.2.5}$$

$$\text{Net: } [Al(OH)_3](s) + OH^-(aq) \longrightarrow [Al(OH)_4]^-(aq) \tag{3.2.6}$$

Mercury(II) sulfide dissolves in a solution of sodium sulfide because HgS reacts with the S^{2-} ion:

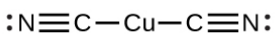
$$HgS(s) \longrightarrow Hg^{2+}(aq) + S^{2-}(aq) \tag{3.2.7}$$

$$Hg^{2+}(aq) + 2\,S^{2-}(aq) \longrightarrow [HgS_2]^{2-}(aq) \tag{3.2.8}$$

$$\text{Net: } HgS(s) + S^{2-}(aq) \longrightarrow [HgS_2]^{2-}(aq) \tag{3.2.9}$$

A complex ion consists of a central atom, typically a transition metal cation, surrounded by ions, or molecules called ligands. These ligands can be neutral molecules like H_2O or NH_3, or ions such as CN^- or OH^-. Often, the ligands act as Lewis bases, donating a pair of electrons to the central atom. The ligands aggregate themselves around the central atom, creating a new ion with a charge equal to the sum of the charges and, most often, a transitional metal ion. This more complex arrangement is why the resulting ion is called a *complex ion*. The complex ion formed in these reactions cannot be predicted; it must be determined experimentally. The types of bonds formed in complex ions are called coordinate covalent bonds, as electrons from the ligands are being shared with the central atom. Because of this, complex ions are sometimes referred to as coordination complexes. This will be studied further in upcoming chapters.

The equilibrium constant for the reaction of the components of a complex ion to form the complex ion in solution is called a formation constant (K_f) (sometimes called a stability constant). For example, the complex ion $[Cu(CN)_2]^-$ is shown here:



It forms by the reaction:

$$Cu^+(aq) + 2\,CN^-(aq) \rightleftharpoons [Cu(CN)_2]^-(aq) \tag{3.2.10}$$

At equilibrium:

$$K_f = Q = \frac{[Cu(CN)2-]}{[Cu+][CN-]^2} \tag{3.2.11}$$

The inverse of the formation constant is the dissociation constant (K_d), the equilibrium constant for the *decomposition* of a complex ion into its components in solution. We will work with dissociation constants further in the exercises for this section. Table E4 and Table 3.2.1 are tables of formation constants. In general, the larger the formation constant, the more stable the complex; however, as in the case of K_{sp} values, the stoichiometry of the compound must be considered.

Table 3.2.1: Common Complex Ions by Decreasing Formation Constants

Substance	K_f at 25 °C
$[Cd(CN)_4]^{2-}$	3×10^{18}
$[Ag(NH_3)_2]^+$	1.7×10^7
$[AlF_6]^{3-}$	7×10^{19}

As an example of dissolution by complex ion formation, let us consider what happens when we add aqueous ammonia to a mixture of silver chloride and water. Silver chloride dissolves slightly in water, giving a small concentration of Ag^+ ($[Ag^+] = 1.3 \times 10^{-5}\ M$):

$$AgCl(s) \rightleftharpoons Ag^+(aq) + Cl^-(aq) \tag{3.2.12}$$

However, if NH_3 is present in the water, the complex ion, $[Ag(NH_3)_2]^+$, can form according to the equation:

$$Ag^+(aq) + 2\,NH_3(aq) \rightleftharpoons [Ag(NH_3)_2]^+(aq) \tag{3.2.13}$$

with

$$K_f = \frac{[Ag(NH3)2+]}{[Ag+][NH3]^2} = 1.7 \times 10^7 \tag{3.2.14}$$

The large size of this formation constant indicates that most of the free silver ions produced by the dissolution of AgCl combine with NH_3 to form $[Ag(NH_3)_2]^+$. As a consequence, the concentration of silver ions, $[Ag^+]$, is reduced, and the reaction quotient for the dissolution of silver chloride, $[Ag^+][Cl^-]$, falls below the solubility product of AgCl:

$$Q = [Ag^+][Cl^-] < K_{sp} \tag{3.2.15}$$

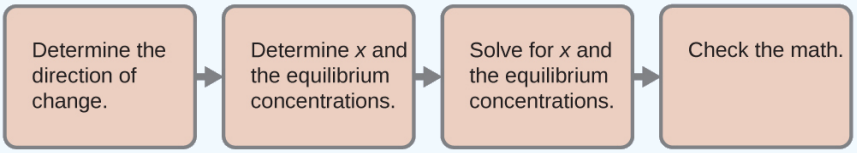
More silver chloride then dissolves. If the concentration of ammonia is great enough, all of the silver chloride dissolves.

Example 3.2.1: Dissociation of a Complex Ion

Calculate the concentration of the silver ion in a solution that initially is 0.10 *M* with respect to $[Ag(NH_3)_2]^+$.

Solution

We use the familiar path to solve this problem:



1. *Determine the direction of change.* The complex ion $[Ag(NH_3)_2]^+$ is in equilibrium with its components, as represented by the equation:

$$Ag^+(aq) + 2\,NH_3(aq) \rightleftharpoons [Ag(NH_3)_2]^+(aq) \tag{3.2.16}$$

We write the equilibrium as a formation reaction because Table **3.2.1** lists formation constants for complex ions. Before equilibrium, the reaction quotient is larger than the equilibrium constant (K_f = 1.7 x 10^7), and $Q = \frac{0.10}{0 \times 0} = \infty$ (it is infinitely large), so the reaction shifts to the left to reach equilibrium.

This page titled 3.2: Lewis Acids and Bases is shared under a CC BY-NC-SA 4.0 license and was authored, remixed, and/or curated by OpenStax.

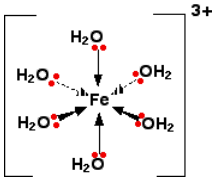
- **15.2: Lewis Acids and Bases** by OpenStax is licensed CC BY 4.0. Original source: https://openstax.org/details/books/chemistry-2e.

3.3: Acidity of the Hexaaqua Ions

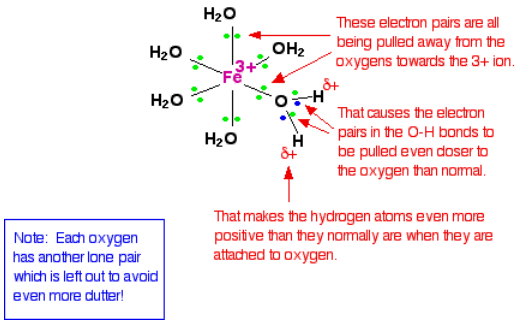
This page explains why complex ions of the type $[M(H_2O)_6]^{n+}$ are acidic.

The Charge Distribution within Complex Ion

The pH of solutions containing hexaaqua ions vary a lot from one metal to another (assuming you are comparing solutions of equal concentrations). However, the underlying explanation is the same for all of them. We'll take the hexaaquairon(III) ion, $[Fe(H_2O)_6]^{3+}$ as typical. The structure of the ion is:



Each of the six water molecules are attached to the central iron(III) ion via a coordinate bond using one of the lone pairs on the oxygen. We'll choose one of these water molecules at random (it doesn't make any difference which one!), and look at the bonding in a bit more detail - showing all the bonds around the oxygen. Imagine for the moment that the 3+ charge is located entirely on the iron.



When the lone pairs on the oxygen atoms form coordinate bonds with the iron, there is obviously a movement of electrons towards the iron. That has an effect on the electrons in the O-H bonds. These electrons, in turn, get pulled towards the oxygen even more than usual. That leaves the hydrogen nuclei more exposed than normal. The overall effect is that each of the hydrogen atoms is more positive than it is in ordinary water molecules. The 3+ charge is no longer located entirely on the iron but spread out over the whole ion - much of it on the hydrogen atoms.

The effect of dissolving this ion in water

The hydrogen atoms attached to the water ligands are sufficiently positive that they can be pulled off in a reaction involving water molecules in the solution. The first stage of this process is:

$$Fe(H_2O)_6^{3+} + H_2O \rightleftharpoons Fe(H_2O)_5(OH)^{2+} + H_3O^+ \tag{3.3.1}$$

The complex ion is acting as an (Arrhenius) acid by donating a hydrogen ion to water molecules in the solution. The water is, of course, acting as a (Arrhenius) base by accepting the hydrogen ion. Because of the confusing presence of water from two different sources (the ligands and the solution), it is easier to simplify Equation 3.3.1:

$$[Fe(H_2O)_6]^{3+}(aq) \rightleftharpoons [Fe(H_2O)_5(OH)]^{2+}(aq) + H^+(aq) \tag{3.3.2}$$

However, if you write it like this, remember that the hydrogen ion is not just falling off the complex ion. It is being pulled off by a water molecule in the solution. Whenever you write "$H^+(aq)$" what you really mean is a hydroxonium ion, H_3O^+.

The hexaaquairon(III) ion is quite strongly acidic giving solutions with a pH around 1.5, depending on concentration. You can get further loss of hydrogen ions as well, from a second and a third water molecule since the complex ion is a polyprotic acid.

Losing a second hydrogen ion:

$$[Fe(H_2O)_5(OH)]^{2+}(aq) \rightleftharpoons [Fe(H_2O)_4(OH)_2]^{+}(aq) + H^{+}(aq) \quad (3.3.3)$$

and a third one:

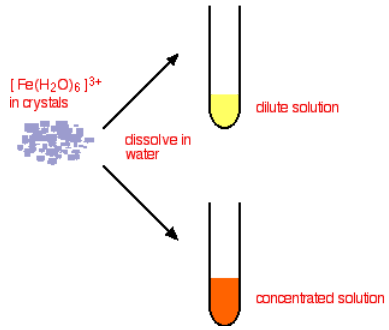
$$[\,Fe(H_2O)_4(OH)_2]^{+}(aq) \rightleftharpoons [\,Fe(H_2O)_3(OH)_4](s) + H^{+}(aq) \quad (3.3.4)$$

This time you end up with a neutral complex and because it has no charge, it does not dissolve to any extent in water, and a precipitate is formed.

In practice

What do you actually get in solution if you dissolve an iron(III) salt in water? In fact you get a mixture of all the complexes that you have seen in the equations above. These reactions are all equilibrium, so everything will be present. The proportions depend on how concentrated the solution is.

The color of the solution is very variable and depends in part on the concentration of the solution. Dilute solutions containing iron(III) ions can be pale yellow. More concentrated ones are much more orange, and may even produce some orange precipitate. None of these colors represents the true color of the $[Fe(H_2O)_6]^{3+}$ ion - which is a very pale lilac color and is only really easy to see in solids containing the ion.

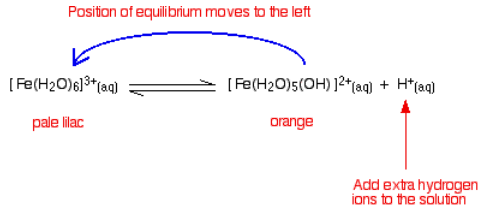


Looking at the equilibrium showing the loss of the first hydrogen ion:

$$\underbrace{Fe(H_2O)_6^{3+}}_{\text{pale lilac}} + H_2O \rightleftharpoons \underbrace{Fe(H_2O)_5(OH)^{2+}}_{\text{orange}} + H_3O^{+} \quad (3.3.5)$$

The color of the new complex ion on the right-hand side is so strong that it completely masks the color of the hexaaqua ion. In concentrated solutions, the equilibrium position will be even further to the right-hand side (Le Chatelier's Principle), and so the color darkens. You will also get significant loss of other hydrogen ions (Equation 3.3.3 and 3.3.4) leading to some formation of the neutral complex and thus some precipitate.

The position of this equilibrium can be shifted by adding extra hydrogen ions from a concentrated acid (e.g., by adding concentrated nitric acid to a solution of iron(III) nitrate). The new hydrogen ions push the position of the equilibrium to the left so that you can see the color of the hexaaqua ion. This is slightly easier to follow if you write the simplified version of the equilibrium (Equation 3.3.2).



3+ Ions are More Acidic than 2+ ions

Solutions containing 3+ hexaaqua ions tend to have pH in the range from 1 to 3. Solutions containing 2+ ions have higher pH - typically around 5 - 6, although they can go down to about 3. Remember that the reason that these ions are acidic is because of

the pull of the electrons towards the positive central ion. An ion with 3+ charges on it is going to pull the electrons more strongly than one with only 2+ charges.

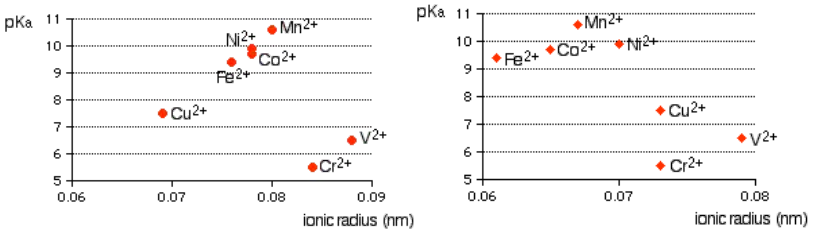
In 3+ ions, the electrons in the O-H bonds will be pulled further away from the hydrogen atoms than in 2+ ions. That means that the hydrogen atoms in the water ligands will have a greater positive charge in a 3+ ion, and so will be more attracted to water molecules in the solution. If they are more attracted, they will be more readily lost - and so the 3+ ions are more acidic.

The Effect of ionic radius on acidity

If you have ions of the same charge, it seems reasonable that the smaller the volume this charge is packed into, the greater the distorting effect on the electrons in the O-H bonds. Ions with the same charge but in a smaller volume (a higher charge density) would be expected to be more acidic. You would therefore expect to find that the smaller the radius of the metal ion, the stronger the acid. Unfortunately, it's not that simple!

Almost every data source that you refer to quotes different values for ionic radii. This is because the radius of a metal ion varies depending on what negative ion it is associated with. We are interested in what happens when the metal ion is bonded to water ligands. Whatever values we take are unlikely to represent the real situation. In the graphs which follow, values for ionic radii from two common sources were used so that you can see the difference it makes to the argument.

If it is true that the smaller the ionic radius, the stronger the acidity of the hexaaqua ion, you would expect some sort of regular increase in pK_a (showing weaker acids) as ionic radius increases. The following graphs plot pK_a against ionic radii for the 2+ ions of the elements in the first transition series from vanadium to copper. The first graph plots pK_a against ionic radii taken from Chemistry Data Book by Stark and Wallace.



There is a trend for several of the ions, but it is completely broken by vanadium and chromium. The second graph uses ionic radii taken from the Nuffield Advanced Science Book of Data.

There probably is a relationship between ionic radius and acid strength. The problem is that there are other more important effects operating as well (quite apart from differences in charge) that can completely swamp the effect of the changes in ionic radius. You have to look in far more detail at the bonding in the hexaaqua ions and the product ions.

Contributors and Attributions

- Jim Clark (Chemguide.co.uk)

This page titled 3.3: Acidity of the Hexaaqua Ions is shared under a CC BY-NC-SA 4.0 license and was authored, remixed, and/or curated by Jim Clark.

3.4: Hard/Soft Acids and Bases

The Hard Soft Acid Base Principle is a Conceptual Tool for Thinking About Patterns of Lewis acid base Reactivity

The explanation of the trends in metal distribution, halide salt solubility, and preferred metal coordination patterns is rooted in Arland, Chatt, and Davies' observation that *Lewis acids and bases could be classified into two groups based on their propensity to form stable compounds with one another* (*e.g.* acids in a class tend to form more stable adducts with bases in the same class than they did with bases in the other).[1] Arland, Chatt, and Davies somewhat boringly termed these groups class a and class b but today they are known by Ralph Pearson's name for them. Pearson called the class a acids and bases hard and class b acids and bases soft. These terms reflect how "soft" these substance's electron clouds are towards distortion or, in other words, their polarizability (Figure **3.4.1**). Pearson terms acids and bases which are relatively polarizable **soft** and those which are difficult to polarize **hard.**

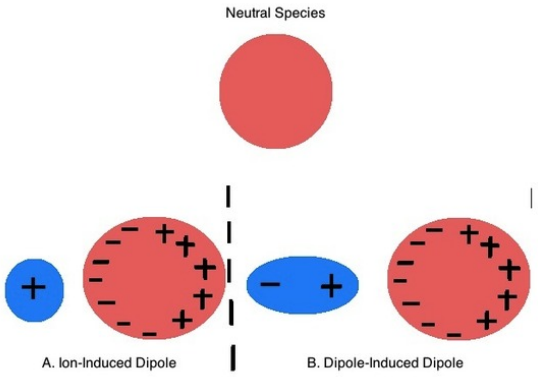


Figure **3.4.1**: Polarizability refers to the ease with which a substance's electron cloud may be distorted under the action of an electric field. An fragment's polarizability determines the degree to which its electron cloud is distorted by A.) an Ion and B.) a polar molecule to induce a dipole moment. The figure is taken from (and the caption expanded from) Cox, Kelly and Dana Reusser "Polarizability" in https://chem.libretexts.org/Bookshelves/Physical_and_Theoretical_Chemistry_Textbook_Maps/Supplemental_Modules_(Physical_and_Theoretical_Chemistry)/Physical_Properties_of_Matter/Atomic_and_Molecular_Properties/Intermolecular_Forces/Specific_Interactions/Polarizability

Recognizing Hard and Soft Acids and Bases

Hard acids and bases come in two varieties:

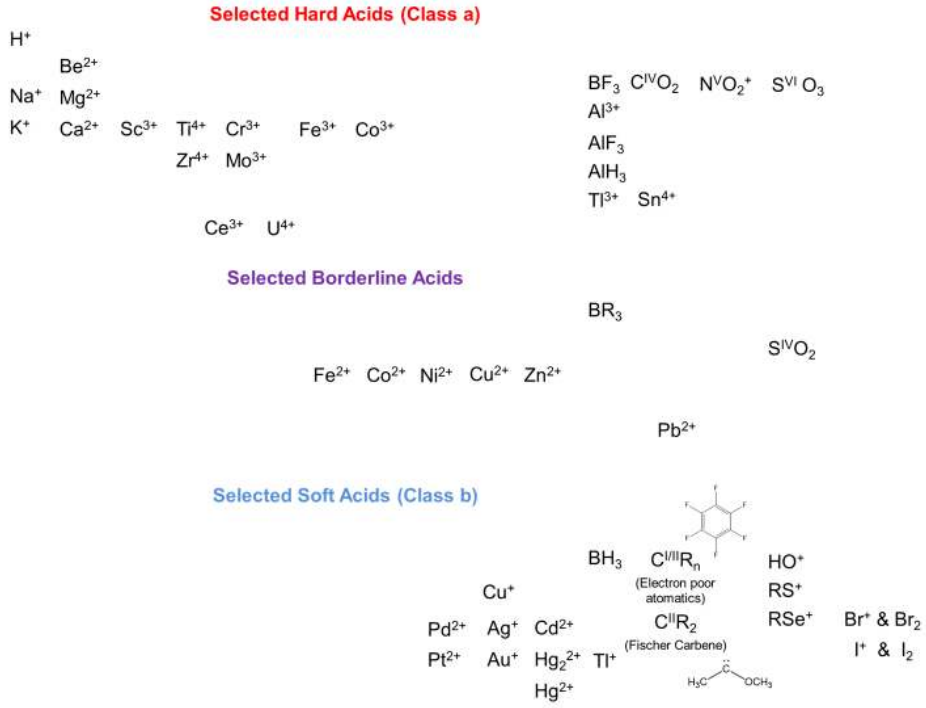
1. hard acid and base sites which possess few valence electrons and for which polarization therefore involves distorting core electrons, which are difficult to distort because they are close to the nucleus and experience a high nuclear charge. The most common examples of such substances are Lewis acids hard acids towards the left of the periodic table.
2. hard acids and base sites with a high charge density (highly charged relative to size) and/or which are electron deficient. In these cases polarization involves distorting electrons that already experience strong unshielded electrostatic interactions.

Soft acids and bases also come in two varieties

1. soft acids and bases which posses many valence electrons and so are more readily polarized. In consequence, all other tings being equal, soft acids and bases are more likely to be found towards the middle or right of the periodic table.
2. soft acids and bases with little charge density and/or which are relatively electron rich.

Note that the hard-soft classification should not be thought of as if all hard acids and bases are equally hard and all soft acids and bases equally soft. There is a graduation in hardness and softness and a number of intermediate acids and bases which do not fit

neatly in either category. With this caveat in mind, representative **hard, soft, and borderline acids** are given below. Notice how they illustrate the trends just outlined.



As expected, hard acids tend to be found towards the left side of the periodic table and involve higher oxidation states and/or electron donating substituents while soft acids are more common to the right of the periodic table and involve lower oxidation states and/or electron donating substituents.

Illustrative hard, soft, and borderline bases are given below. Again, notice how these substances illustrate the general trends.

Selected Hard Bases (Class a)

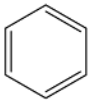
Nitrogen bases	Oxygen bases		small halides
NH_2^-	OH^-	CO_3^{2-}	F^-
NH_3	H_2O	RCO_2^-	Cl^-
RNH_2	ROH	NO_3^-	
NH_2NH_2	ROR	PO_4^{3-}	
		SO_4^{2-}	

Selected Borderline Bases

electron-poor Nitrogen bases		low oxidation state element oxyanions	intermediate halides
N_3^-		NO_2^-	
NO_2^-			Br^-
SCN^-		SO_3^{2-}	
N_2			

Selected Soft Bases (Class b)

Carbon bases	P and As bases	Sulfur bases	large halides & pseudohalides
R^-	PR_3	RS^-	H^-
CO	$P(OR)_3$	RSH	I^-
CN^-	AsR_3	RSR	
RNC		SCN^-	
$R_2C{=}CR_2$ (alkenes)			



(electron-rich aromatics)

Qualitative Estimation of the Relative Hardness and Softness of Lewis Acids and Bases

As can be seen from the examples above, **hard acids are relatively electron-poor and hard bases electron-rich** since they have comparatively

- small frontier orbitals, reflective of their relatively small atom/ion/fragment sizes
- high (for acids) or low (for bases) oxidation states on the base atom, reflected in a large positive formal charge (for acids) or negative formal charge (for bases)
- low polarizability, due to loss or gain of substantial numbers of electrons, or the localization of
  - positive charge on an electropositive element or an atom bearing electron-withdrawing substituents
  - negative charge on an electronegative element or an atom bearing electron-donating substituents

In contrast to hard acids and bases **soft acids are relatively electron-rich and soft bases larger and more electron poor** since they have comparatively

- large frontier orbitals, reflective of their relatively large atom/ion/fragment sizes
- low oxidation states, often resulting in small or nonexistent atomic charges
- high polarizability, as might be expected of species in which electron-electron repulsions are lower and electrons are spread over a large volume. Sometimes this is indicated by
  - positive charge on an electronegative element or an atom bearing electron-donating substituents
  - negative charge on an electropositive element or an atom bearing electron-withdrawing substituents

Exercise 3.4.1

Rank the acid or bases in each set in increasing order of expected hardness?

(a) Cr^{2+} and Cr^{3+}

(b) H^+, Cs^+, and Tl^+

(c) SCN^- (acting as a base at N) and SCN^- (acting as a base at S)

(d) AlF_3, AlH_3, $AlMe_3$

(e) The side chains of the following proteinogenic amino acids

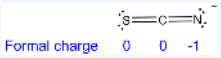


Answer

(a) $Cr^{2+} < Cr^{3+}$ All other things being equal, hardness increases with oxidation state.

(b) $Tl^+ < Cs^+ < H^+$ The order reflects Cs^+ and Tl^+'s larger size relative to H^+ (which doesn't possess any electrons that can be polarized anyway) and that Tl^+ still possesses two valence electrons while Cs^+ possesses none.

(c) SCN^- (acting as a base at S) < SCN^- (acting as a base at N) The order reflects that N is more elctronegative than S and possesses a more negative formal charge of -1.



(d) $AlH_3 < AlMe_3$, AlF_3 The hardness increases as the substituents on the Lewis acid Al center become less electron donating and more electron withdrawing (and, incidentally, harder bases) as their electronegativity increases in the order H^- < CH_3^- < F^-. Note that the order of electron donating ability for H^- and CH_3^- is the opposite observed for carbocations, for which hyperconjugation plays a larger role.

(e) Sec < Cys < Ser The hardness increases as the electronegativity of the Lewis base chalcogen increases on going from a selenol to a thiol to an alcohol.

The Hard-Soft Acid-Base Principle (HSAB Principle)

The **Hard-Soft acid-base principle (HSAB Principle) explains patterns in Lewis acid-base reactivity in terms of a *like reacts with like preference***. Both thermodynamically and kinetically hard acids prefer hard bases and soft acids soft bases. Specifically,

- Thermodynamically, hard acids form stronger acid-base complexes with hard bases while soft acids form stronger complexes with soft bases.
- Kinetically, hard acids/electrophiles react more quickly with hard bases/nucleophiles while soft acids/electrophiles react more quickly with soft bases/neucleophiles

Applications of the HSAB principle include

1. Predicting the equilibrium or speed of *Lewis acid-base metathesis and displacement reactions.* In a Lewis acid-base *metathesis reaction* the acids and bases swap partners

$$A_1{:}B_1 + A_2{:}B_2 \underset{}{\overset{k_1,\ K_{eq}}{\rightleftharpoons}} A_1B_2 + A_2{:}B_1 \tag{3.4.1}$$

For example, the equilibrium position of the metathesis reaction between TlF and K_2S favors the products:

$$2TlF + K_2S \rightleftharpoons Tl_2S + 2KF$$

(3.4.2)

consistent with the HSAB's hard-hard and soft-soft preference.

$$\underset{\text{soft hard}}{2\,Tl^{+}F^{-}} + \underset{\text{hard soft}}{(K^{+})_2S^{2-}} \rightleftharpoons \underset{\text{soft soft}}{(Tl^{+})_2\,S^{2-}} + \underset{\text{hard hard}}{2\,K^{+}F^{-}}$$

(3.4.3)

The HSAB principle also allows for prediction of the position of displacement reactions, in which a Lewis acid or base forms an adduct using a base or acid from an existing Lewis acid-base complex. In these reactions, the displacement of acid or base from the reactant complex to may be thought of as a sort of metathesis reaction, one in which in the unbound acid or base switches places with one in the complex. For example, the reaction between HI and methylmercury cation

$$HI + HgSCH_3^{+} \rightleftharpoons CH_3SHgI + H^{+}$$

(3.4.4)

involves displacement of an iodide from HI to give CH_3HgI. The position of the equilibrium favors CH_3HgI since both CH_3Hg^{+} and I^{-} are both soft, while H^{+} is a hard acid.

$$\underset{\text{hard-soft}}{H\text{-}I} + \underset{\text{soft}}{CH_3Hg^{+}} \rightleftharpoons \underset{\text{soft -soft}}{CH_3Hg\text{-}I} + \underset{\text{hard}}{H^{+}}$$

(3.4.5)

Exercise 3.4.2

Predict the position of equilibrium for the following reaction.

$$Fe_2O_3 + 3Ag_2S \rightleftharpoons Fe_2S_3 + 3Ag_2O$$

Answer

The equilibrium will favor the reactants (K<1) since the hard-hard and soft-soft interactions in the reactants are more stable than the hard-soft interactions in the products.

$$\underset{\text{hard hard}}{(Fe^{3+})_2\,(O^{2-})_3} + \underset{\text{soft soft}}{3\,(Ag^{+})_2S^{2-}} \rightleftharpoons \underset{\text{hard soft}}{(Fe^{3+})_2\,(S^{2-})_3} + \underset{\text{soft hard}}{3\,(Ag^{+})_2O^{2-}}$$

Exercise 3.4.3

Predict whether K for the following equilibria will be <<1, ~1, or >>1.

a. $2HF + (CH_3Hg)_2S \rightleftharpoons 2CH_3HgF + H_2S$

b. $Ag(NH_3)_2^{+} + 2PH_3 \rightleftharpoons Ag(PH_3)_2^{+} + 2NH_3$

c. $Ag(PH_3)_2^{+} + 2H_3B-SH_2 \rightleftharpoons 2H_3B-PH_3 + Ag(SH_2)_2^{+}$

d. $H_3B-NH_3 + F_3B-SH_2 \rightleftharpoons H_3B-SH_2 + F_3B-NH_3$

Answer

a. K< < 1 since the reactant adducts are hard-hard and soft-soft while the products involve hard-soft interactions

b. K>>1 since the reactant complex, diamine silver(I) is a complex of a hard base, NH_3, with the soft acid, Ag^+, while the product is a complex of the same soft acid with the soft base phosphine.

c. K~1 since all the adducts amongst the reactants and products involve soft acids and bases

d. K>>1 since BH_3 is a softer acid than BF_3 so it will form a stronger complex with the softer base H_2S while the harder BF_3 forms a stronger complex with the harder base NH_3.

2. Predicting the relative strengths of a given set of *Lewis acids or bases towards a particular substrate*. Consider, for example, the relative strengths of a BH_3, BMe_3, and BF_3 towards group 15 hydrides like NH_3, PH_3, and AsH_3. Of the boranes listed, the hardest acid BF_3 is the strongest acid towards the hard base NH_3 while BH_3 is the strongest towards AsH_3.[†]

Exercise 3.4.4

Which acid will form the most stable complex with CO - BH_3, BF_3, or BMe_3?

Answer

BH_3. Since CO forms complexes primarily through its carbon lone pair it is a soft base and so will form the strongest complex with the softest Lewis acid.

The Theoretical Interpretation of the Hard Soft Acid-Base Principle is that hard-hard preferences reflect superior electrostatic stabilization while soft-soft preferences reflect superior covalent stabilization.

The hard-hard and soft-soft preferences in Lewis acid-base interactions reflect that

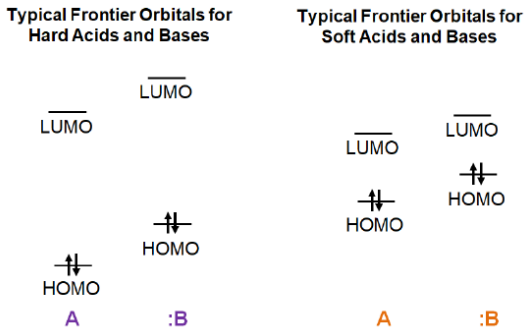
- The lone pair of a hard base is strongly stabilized electrostatically by a hard acid
- The lone pair of a soft base is strongly stabilized by forming a covalent bond with a soft acid
- The lone pair of a hard or soft base is comparatively weakly stabilized by an acid opposite to it in hardness or softness since the overall electrostatic and covalent stabilization of the adduct is comparatively weak.

To see why this is the case it is helpful to divide the contributions to the interaction energy between an acid and a base as follows:

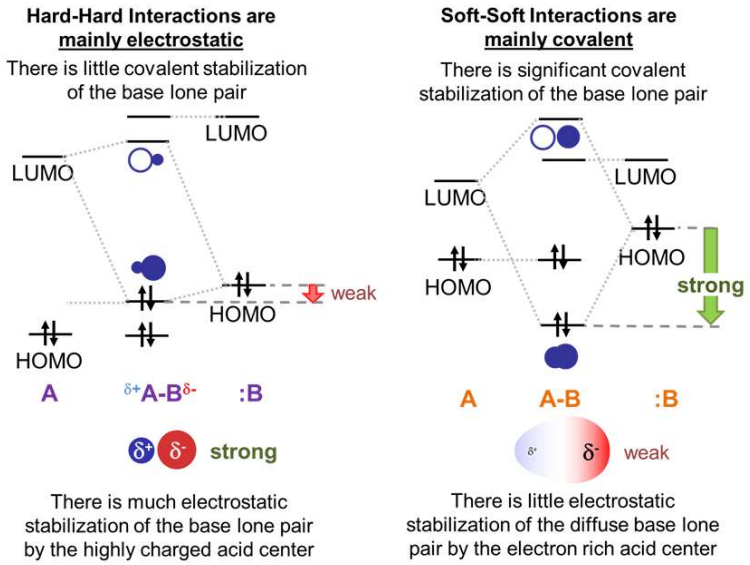
$$\text{Interaction Energy} = \underbrace{\text{Electrostatic attractions and repulsions of partial atomic charges}}_{\text{Ionic term}} + \underbrace{\text{Interactions between filled orbitals on one fragment and unfilled orbitals on the other}}_{\text{Covalent term}} + \underbrace{\text{Electrostatic repulsions between filled orbitals on the two fragments}}_{\text{Steric term}} \tag{3.4.6}$$

Of the three contributions to the interaction energy, only the ionic and covalent terms directly relate to the hardness of the interacting acid and base. One approach to thinking about how hardness influences the ionic and covalent contributions is to consider the frontier orbitals involved in the acid-base interaction. This is sometimes done through the use of the Salem-Klopman equation,[1,*] although in the treatment which follows a more qualitative approach will be employed.

Both hard acids and bases will have comparatively low energy HOMO levels and high energy LUMO levels, with a correspondingly high HOMO-LUMO gap. In contrast, soft acids and bases will have comparatively high-energy HOMO levels and low-energy LUMO levels, giving a comparatively smaller HOMO-LUMO gap.



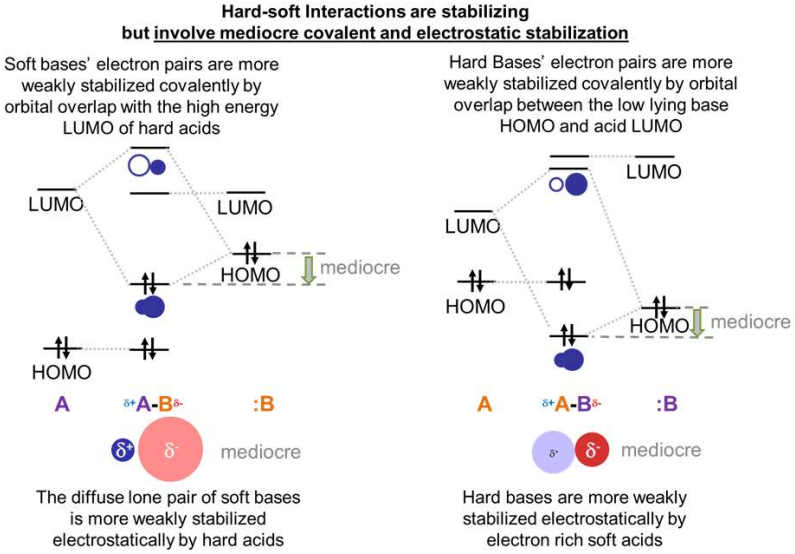
Given this, consider the frontier orbital interactions involved in the formation of an acid-base complex for the possible cases, as illustrated schematically below.



The large gap in energy between hard bases' highly stabilized HOMO lone pairs and the high energy LUMO of hard acids ensures that in **hard acid-hard base adducts the dominant stabilizing interaction will involve electrostatic attraction between the base lone pair and the electropositive Lewis acid center**. Fortunately, since the electron clouds in hard bases are relatively dense and electron rich while hard Lewis acids are highly charged and small these electrostatic interactions are strong.

In contrast, in **soft acid-soft base adducts the dominant stabilizing interaction will be covalent.** This is because the small gap in energy between a soft base HOMO and soft acid LUMO enables the formation of a well-stabilized bonding orbital with significant electron density between the acid and base.

The orbitals interactions between hard acids and soft bases and soft acids and hard bases are intermediate between the hard acid-hard base and soft acid-soft base cases.



This means that the adducts are stable relative to free acid and base – just not as well stabilized as in the hard acid and hard base case. In the case of hard acids and soft bases the hard acids are less able to stabilize the soft bases' relatively diffuse electron pair electrostatically and there isn't as much covalent stabilization as in adducts of soft acids and bases due to hard acid's high energy.

References

1. Ahrland, S.; Chatt, J.; Davies, N. R., The relative affinities of ligand atoms for acceptor molecules and ions. Quarterly Reviews, Chemical Society 1958, 12 (3), 265-276.

2. Pearson, R. G., Hard and Soft Acids and Bases. Journal of the American Chemical Society 1963, 85 (22), 3533-3539.

3. Fleming, I., Molecular orbitals and organic chemical reactions. Reference ed.; Wiley: Hoboken, N.J., 2010.

Notes

* Despite the fruitfulness of this observation, in general it is important to reduce the potential for observer bias by checking observations like these against compounds reported in the chemical literature and databases like the Inorganic Crystal Structure and Cambridge Crystallographic Databases.

** These are very soluble in water, to the point where some solutions are perhaps better described as solutions of water in the halide.

† This can be predicted based on the relative hardness of BF_3, BR_3, and BH_3 in the list of hard and soft acids. However, for those of you who may be confused as to why H is considered a better electron donor for the purposes of softening a Lewis acid center while alkyl groups are better electron donors for the purposes of stabilizing carbocations in organic chemistry, the dominant effect is the lower electronegativity of H relative to carbon (in CH_3). The effect of electron donation due to hyperconjugation isn't as great for thermodynamically stable bases like BX_3/BR_3.

†† For more on the Salem-Klopman equation see Fleming, I., Molecular orbitals and organic chemical reactions. Reference ed.; Wiley: Hoboken, N.J., 2010; pp. 138-143.

Contributors and Attributions

Stephen M. Contakes (Westmont College)

3.4: Hard/Soft Acids and Bases is shared under a CC BY-NC-SA 4.0 license and was authored, remixed, and/or curated by LibreTexts.

3.5: Quantitative Measures of Hardness and Softness

Pearson Absolute Hardness is a useful metric of hardness based on orbital energies

The recognition that hard acids and bases possess a large HOMO-LUMO gap suggests that the gap size itself might serve as a useful index of hardness. The basis for this idea may be found by considering Pearson's definition of absolute hardness, η.[1] **Pearson's absolute hardness, η**, is half the second derivative of a species energy with respect to changes in total number of electrons, N_{e^-}

$$Pearson's\ absolute\ hardness = \eta = \frac{1}{2}\frac{d^2E}{dN_{e^-}^2} \tag{3.5.1}$$

$$(in\ \ eV)$$

and, since acid and bases' hardness and softness are inversely related, Pearson's absolute softness, σ, is just the inverse of hardness

$$Pearson's\ \ softness = \frac{1}{\eta} \tag{3.5.2}$$

Of these, Pearson's absolute hardness is related to the **Mulliken definition of electronegativity** as the first derivative of a species energy with respect to changes in total number of electrons.

$$Mulliken\ electronegativity = \chi = \frac{dE}{dN_{e^-}} \tag{3.5.3}$$

$$(in\ \ eV)$$

Operationally, both the Pearson hardness and Mulliken electronegativity are approximated in terms of the energies associated with unit changes in the number of electrons – *i.e.* in terms of ionization energies and electronegativities. Specifically,

$$Pearson's\ absolute\ hardness = \eta \approx \frac{IE - EA}{2} \tag{3.5.4}$$

$$Mulliken\ \ electronegativity = \chi \approx \frac{IE + EA}{2} \tag{3.5.5}$$

$$where\ \ IE\ \ and\ \ EA\ \ are\ \ in\ \ eV$$

The connection between Pearson's absolute hardness/softness and the HOMO-LUMO gap then follows from Koopman's theorem, in which the ionization energy (IE) is just the opposite of the HOMO energy.

$$IE = -E_{HOMO} \tag{3.5.6}$$

Similarly, the electron affinity (EA), defined as the opposite of the energy released on absorption of an electron, may be taken as an approximation of the LUMO energy.

$$E_{LUMO} \approx -EA \tag{3.5.7}$$

So Pearson's absolute hardness is just half the HOMO-LUMO gap (band gap) size in electron volts

$$Pearson's\ absolute\ hardness, \eta \approx \frac{E_{LUMO} - E_{HOMO}}{2} \tag{3.5.8}$$

$$where\ all\ values\ are\ given\ in\ eV$$

and the Mulliken electronegativity is just the average of the HOMO and LUMO energies (~Fermi energy):

$$Mulliken\ electronegativity, \chi \approx -\frac{E_{LUMO} + E_{HOMO}}{2} \tag{3.5.9}$$

$$where\ all\ values\ are\ given\ in\ eV$$

The relationships between the Pearson absolute hardness, Mulliken electronegativity, and HOMO and LUMO energies are depicted schematically for the group 1A monocations in Figure **3.5.1**.

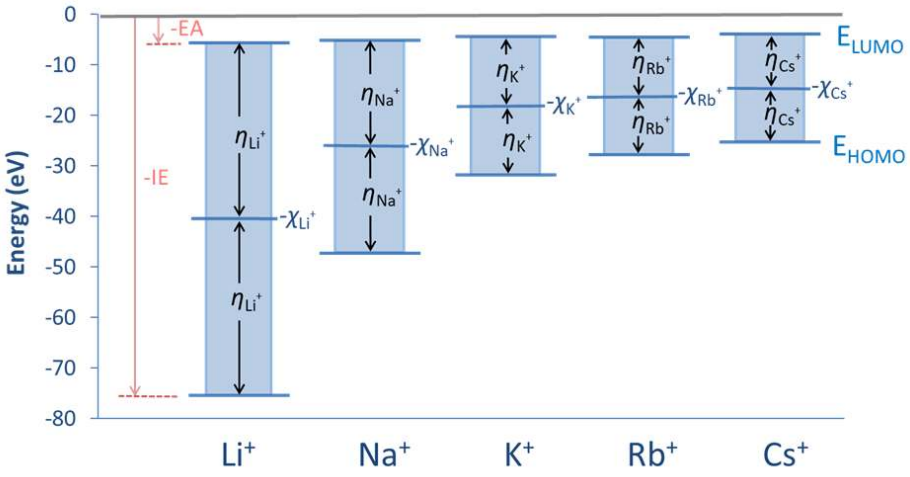


Figure **3.5.1**. Relationships between Pearson absolute hardness, Mulliken electronegativity, and HOMO and LUMO energies for the group 1A monocations.

Values of the Pearson hardness and Mulliken electronegativity for several acids and bases are given in Table **3.5.1**. The values in the table confirm the expected trends, showing an increase in hardness with size (down a group), with increasing charge, and as substituent electronegativity increases for a series of isolobal ions.

Table **3.5.1**: Pearson Absolute Hardness and Related Parameters for Selected Acids and Bases.[2] Taken from Pearson, R. G., Absolute electronegativity and hardness: application to inorganic chemistry. Inorganic Chemistry 1988, 27 (4), 734-740.

Species	Ionization Energy, IE or I (eV)	Electron Affinity, EA or A (eV)	Mulliken Electronegativity, χ (eV)	Pearson Absolute Hardness, η (eV)
Selected Acids				
Group 1A monocations				
Li^+	75.64	5.39	40.52	35.12
Na^+	47.29	5.14	26.21	21.08
K^+	31.63	4.34	17.99	13.64
Rb^+	27.28	4.18	15.77	11.55
Cs^+	25.1	3.89	14.5	10.6

Group 11 monocations				
Cu^{+}	20.29	7.73	14.01	6.28
Ag^{+}	21.49	7.58	14.53	6.96
Au^{+}	20.5	9.23	14.9	5.6
Isoelectronic Row 3 Metal Cations				
Na^{+}	47.29	5.14	26.21	21.08
Mg^{2+}	80.14	15.04	47.59	32.55
Al^{3+}	119.99	28.45	74.22	45.77
Changes with Transition Metal Ion Charge				
Fe^{2+}	30.65	16.18	23.42	7.24
Fe^{3+}	54.8	30.65	42.73	12.08
Co^{2+}	33.50	17.06	25.28	8.22
Co^{3+}	51.3	22	42.4	8.9

		.5		
Boron trihalides				
BF_3	15.81	-3.5	6.2	9.7
BCl_3	11.60	0.33	5.97	5.64
BBr_3	10.51	0.82	5.67	4.85
CO_2	13.8	-3.8	5.0	8.8
CS_2	10.08	0.62	5.35	5.56
Selected Bases				
Group 17 monoanions (taken to be identical to the free atom values; for arguments as to why this is reasonable see Pearson, R. G., Inorg. Chem. 1988, 27 (4), 734-740.)				
F^-	17.42	3.40	10.41	7.01
Cl^-	13.01	3.62	8.31	4.70
Br^-	11.84	3.36	7.60	4.24
I^-	10.45	3.06	6.76	3.70
Group 15 hydrides				
NH_3	10.7	-5	2.6	8.2

		.6		
PH_3	10.0	-1.9	4.1	6.0
Trimethylpnictides				
NMe_3	7.8	-4.8	1.5	6.3
PMe_3	8.6	-3.1	2.8	5.9
$AsMe_3$	8.7	-2.7	3.0	5.7
Group 16 hydrides				
H_2O	12.6	-6.4	3.1	9.5
H_2S	10.5	-2.1	4.2	6.2
Phosphorous trihalides				
PF_3	12.3	-1.0	5.7	6.7
$PC1_3$	10.2	0.8	5.5	4.7
PBr_3	9.9	1.6	5.6	4.2

Drago-Wayland Acid-Base Parameters allow for estimation of the electrostatic and covalent contributions to the enthalpy of formation of a Lewis acid-base adduct.

Although Pearson hardness values are a useful metric of acid and bases' hardness, they cannot easily be used to estimate the Lewis acid-base interaction energy. This is not the case for the EC model developed by Drago and Wayland.[3] In the **Drago and Wayland's EC Model** the enthalpy of formation of an acid base adduct, AB,

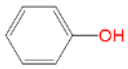
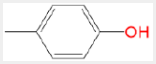
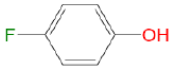
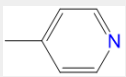
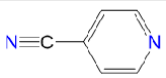
$$A + B \rightleftharpoons AB \qquad \Delta H_{AB\ adduct} \tag{3.5.10}$$

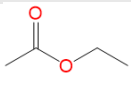
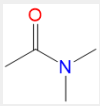
from the acid (A) and base (B) can be calculated as the sum of products of electrostatic (E) and covalent (C) factors that reflect the propensity of the acid and base to engage in strong electrostatic and covalent interactions with one another:

$$-\Delta H_{AB\ adduct} = E_A E_B + C_A C_B \tag{3.5.11}$$

where E_A and C_A are the electrostatic and covalent parameters for the acid and E_B and C_B the electrostatic and covalent parameters for the base given in units of $kcal^{½}$ $mol^{-½}$. E and C parameters for selected acids and bases are given in Table **3.5.2**.

Table **3.5.2**: E and C Parameters for selected Lewis acids and bases according to the ECW model.[4,5] Taken from Vogel, G. C.; Drago, R. S., The ECW Model. *Journal of Chemical Education* 1996, 73 (8), 701 and Drago, R. S. A modern approach to acid-base chemistry. *Journal of Chemical Education* 1974, 51 (5), 300 (for BF_3).

Species	E (kcal^{½} mol$^{-½}$)	C (kcal^{½} mol$^{-½}$)	W (kcal mol^{-1})	C/E
Acids				
I_2	0.5†	2†	0	4
ICl	2.92	1.66	0	0.57
H_2O	1.31	0.78	0	0.59
SO_2	0.51	1.56	0	3.1
$HCCl_3$ (chloroform)	1.56	0.44	0	0.28
$(CH_3)_3COH$	1.07	0.69	0	0.65
$(CF_3)_3COH$	3.06	1.88	-0.87	0.61
	2.27	1.07	0	0.47
	2.23	1.03	0	0.46
	2.30	1.11	0	0.48
	1.38	0.68	0	0.49
BF_3	1.62	9.88		6.10
$B(CH_3)_3$	2.90	3.60	0	1.2
$Al(CH_3)_3$	8.66	3.68	0	0.43
$Ga(C_2H_5)_3$	6.95	1.48	0	0.21
$In(CH_3)_3$	6.60	2.15	0	0.33
$Zn[N(Si(CH_3)_3)]_2$	2.75	2.32	0	0.84
$Cd[N(Si(CH_3)_3)]_2$	2.50	1.83	0	0.73
Bases				
NH_3	2.31	2.04		0.88
CH_3NH_2	2.16	3.13		1.4
$(CH_3)_2NH$	1.80	4.21		2.3
$(CH_3)_3N$	1.21	5.61		4.6
	1.78	3.54		2.0
	1.81	3.73		2.0
	1.53	2.94		1.9

Species	E (kcal^{½} mol$^{-½}$)	C (kcal^{½} mol$^{-½}$)	W (kcal mol^{-1})	C/E
CH_3CN	1.64	0.71		0.43
$ClCH_2CN$	1.67	0.33		0.20
$CH_3C(O)CH_3$	1.74	1.26		0.72
$(C_2H_5)_2O$	1.80	1.63		0.91
	1.64	2.18		1.3
 (EtOAc)	1.63	0.95		0.58
	2.35†	1.31		0.56
$(CH_3)_2S$	0.25	3.75		15
$(CH_3CH_2)_2S$	0.24	3.92†		15
	0.26	4.07		16
$(CH_3)_2Se$	0.05	4.24		83
$(CH_3)_2SO$	2.4	1.47		0.61
$(CH_3)_3P$	0.25	5.81		24
$(CH_3O)_3P$	0.13	4.83		37
$(C_6H_5)_3PO$	2.59	1.67		0.64
$(C_6H_5)_3PS$	0.35	3.65		10
C_6H_6	0.70	0.45		0.64

† These values were fixed to parameterize the rest of the E and C parameters.

Trends in the relative values of C and E for the acids and bases in Table **3.5.2** are very roughly consistent with the trends in hardness and softness outlined earlier. However, the parameters suggest that some trends in hardness reflect changes in species ability to engage in ionic interactions while others reflect changes in species ability to engage in strong covalent interactions. For example, C_B for the dimethylchalcogenides increases steadily from 1.5 to 4.25 kcal^{½} mol$^{-½}$ on going from Me_2O to Me_2Se while E_B decreases from 1.68 to 0.05 kcal^{½} mol$^{-½}$, suggesting that electrostatic and covalent factors are both involved in a decreases in base hardness down group 16. However, in the case of phosphines and amines it appears that electrostatic factors are primarily responsible for the decrease in hardness down group 15. On going from Me_3N to Me_3P, C_B only increases slighly from 5.61 to 5.81 kcal^{½} mol$^{-½}$while E_B decreases from 1.21 to 0.25 kcal^{½} mol$^{-½}$- *i.e.* to 20% of the Me_3N value.

However, some species tend to have very high values for both E and C, reflecting their ability to engage in strong electrostatic and covalent interactions while others have small values for both, reflecting their relative stability as free species in solution.

As can be seen by comparing the acids and bases listed in the absolute hardness table (Table **3.5.1**) and the EC parameters table (Table **3.5.2**) The EC model has primarily been applied to organic and main group organometallic acids and bases. However, a variety of extensions have been proposed that enable its wider applicability.

Since the simple EC model only includes electrostatic and covalent considerations and thus ignores steric, lattice energy, and other contributions to the interaction energy. Thus it is only useful for analyzing the interaction energies of sterically unhindered adducts in which solvation energy and other contributions to the overall interaction energy are insignificant. However, additional refinements of the model attempt to extend its usefulness by accomodating various factors, such as

- *Steric strain.* Specifically, Hancock and Martell[6] introduced a D parameter to account for any additional steric strain introduced on adduct formation,* giving

$$-\Delta H_{AB\ adduct} = E_A E_B + C_A C_B - D_A D_B \tag{3.5.12}$$

- *Charge transfer on adduct formation.* As discussed in section 6.4.2 the formation of a Lewis acid base complex results in a net transfer of electron density from the electron donor (base) to the acceptor (acid). Drago and Wong[7] extended the EC model to include that charge transfer by adding what they called receptance factors that account for the acid's ability to receive electron density (R_A) and transference factors that account for the base's ability to donate electron density (T_B), giving

$$-\Delta H_{AB\ adduct} = E_A E_B + C_A C_B + R_A T_B \tag{3.5.13}$$

  This extension of the EC model is called the **electrostatic-covalent-transfer or ECT model**. Notably, it has been applied successfully to adducts involving ions, for which the R_AT_B term can account for as much as 31% of the interaction energy.

- *Any constant energy term, such as the energy needed to cleave a dimer in order to make the Lewis acid (e.g. $Al_2Cl_6 \rightarrow 2AlCl_3$).* Drago and Vogel[4] extended the EC model to accommodate these constant energy terms, which they designated W. The resulting model is called the **ECW model** for which

$$-\Delta H_{AB\ adduct} = E_A E_B + C_A C_B + W \tag{3.5.14}$$

$$where\ \ W = W_A + W_B$$

A simple application of EC and extended EC models is that they allow the enthalpy of adduct formation to be calculated. These enthalpy calculations based on the EC model are consistent with the superior interaction energy of hard-hard and soft-soft interactions compared to hard-soft ones. Consider, for example, the transfer of I_2 between BF_3 and $InMe_3$. H_3N-BF_3 and H_3N-$InMe_3$.

$$H_3N - BF_3 + InMe_3 \rightleftharpoons BF_3 + H_3N - InMe_3 \tag{3.5.15}$$

Since H_3N is a hard base and BF_3 and $InMe_3$ harder and softer acids, respectively, the equilibrium us expected to favor the reactant, H_3N-BF_3. Assuming the equilbrium is enthalpically driven this qualitative analysis is consistent with the expected endothermic enthalpy of the reaction, as may be seen from the calculated enthalpies of adduct formation for both H_3N-BF_3 and H_3N-$InMe_3$.

For H_3N-BF_3:

$$-\Delta H_{H_3N-BF_3} = E_{BF_3} E_{NH_3} + C_{BF_3} C_{NH_3} \tag{3.5.16}$$

$$-\Delta H_{H_3N-BF_3} = (1.62)(2.31) + (9.88)(2.04) \tag{3.5.17}$$

$$-\Delta H_{H_3N-BF_3} = 3.74\ kcal/mol + 20.1\ kcal/mol = 23.8\ kcal/mol \tag{3.5.18}$$

$$\Delta H_{H_3N-BF_3} = -23.8\ kcal/mol \tag{3.5.19}$$

For H_3N-$InMe_3$:

$$-\Delta H_{H_3N-InMe_3} = E_{InMe_3} E_{NH_3} + C_{InMe_3} C_{NH_3} \tag{3.5.20}$$

$$-\Delta H_{H_3N-InMe_3} = (6.6)(2.31) + (2.15)(2.04) \tag{3.5.21}$$

$$-\Delta H_{H_3N-InMe_3} = 15.25\ kcal/mol + 4.39\ kcal/mol = 19.63\ kcal/mol \tag{3.5.22}$$

$$\Delta H_{H_3N-InMe_3} = -19.63\ kcal/mol \tag{3.5.23}$$

So H_3N-BF_3 is enthalpically favored by -4.2 kcal/mol [=-23.8 kcal/mol - (-19.63 kcal/mol) according to Hess' Law].

In addition to their utility for estimating enthalpies of Lewis acid-base complex formation, EC and related models serve as a useful tool for estimating the relative importance of ionic, covalent, and steric factors in complex formation. Specifically,

- The relative contributions of ionic and covalent factors can be calculated directly as from the E and C terms. This can provide insight into why some complexes are more stable than others. Such calculations reveal that the hard-hard adduct H_3N-BF_3 is favored over the hard-soft adduct H_3N-$InMe_3$ because of the strong covalent interaction holding together H_3N-BF_3. The covalent term accounts for 84% of energy of the H_3N-BF_3 interaction and is largely lost on formation of H_3N-$InMe_3$, for which it contributes only 22% of the interaction energy. When the electrostatic term is accounted for it can be seen that the formation of H_3N-$InMe_3$ from H_3N-BF_3 is disfavored since it would result in a loss of 15.7 kcal/mol of covalent stabilization that would be incompletely compensated for by a gain of 11.5 kcal/mol of electrostatic stabilization.
- The role of other contributions to the bonding in a Lewis acid-base complex may be estimated from the discrepancy between experimental and EC model calculated stabilization energies. This is because the EC parameters assume sigma bonding and so any deviation between the calculated and experimental enthalpies of complex formation can be attributed to non-sigma contributions.
    - This is done explicitly in extensions of the EC model. For instance, in the case of the Hancock and Martell, ECT, and ECW extensions of the EC model the contribution of the steric, charge transfer, and constant energy factors (like dimer dissociation) are directly computed in the model.
    - Comparisons of the difference between the energies calculated using ordinary EC parameters and the observed enthalpies has also been used as an estimate of the
        - steric strain energy in strained adducts, which exhibit a less exothermic heat of adduct formation than expected
        - π-backbonding energy in adducts which are capable of such interactions and exhibit a more exothermic heat of formation than expected.[8-10]
    - For examples see (a) Drago, R. S., The interpretation of reactivity in chemical and biological systems with the E and C model. Coordination Chemistry Reviews 1980, 33 (3), 251-277; (b) Drago, R. S.; Bilgrien, C. J., Inductive transfer and coordination of ligands in metal—metal bonded systems. Polyhedron 1988, 7 (16), 1453-1468; (c) Drago, R. S., The question of a synergistic metal-metal interaction leading to .pi.-back-bond stabilization in dirhodium tetrabutyrate adducts. Inorganic Chemistry 1982, 21 (4), 1697-1698.
- The role of electrostatic, covalent, and other contributions to the spectroscopic behavior of Lewis acid-base complexes can be assessed similarly using specialized versions of the ECW or ECT model that allow for calculation of changes in spectroscopic parameters on adduct formation - *e.g.* OH stretching frequencies. Details are beyond the scope of this text but may be found in the original literature;[11] for example Drago, R. S.; Vogel, G. C. *JACS* 1992, 114 (24), 9527-9532; Vogel, G. C.; Drago, R. S., *J. Chem. Educ.* 1996, 73 (8), 701; Drago, R. S.; Wong, N. M., *J. Chem. Educ.* 1996, 73 (2), 123.).

Pearson Softness Parameters have been proposed as a means of calculating the equilibrium constant for formation of a Lewis acid-base adduct, although they are more commonly used to estimate metal toxicity

Pearson also proposed a softness parameter that can be used to estimate the thermodynamics of Lewis acid base complex formation, this time in the form fo the equilibrium constant for

$$A + B \overset{K}{\rightleftharpoons} AB \tag{3.5.24}$$

for which Pearson proposed

$$logK = S_A S_B + \sigma_a \sigma_B \tag{3.5.25}$$

where S_A and S_B are acid and base parameters related to the strength of the acid-base interaction and σ_A and σ_B are acid and base parameters related to softness. This approach hasn't found as wide acceptance in studies of chemical reactivity as the Drago-Wayland and absolute hardness parameters. However, because the toxicity of metal ions' sometimes depends on their propensity to bind soft Lewis bases in living systems, the softness parameter's which Pearson and Mawby subsequently proposed based on the relative energies of metal flourine and metal iodine bonds[12] has been widely used as a tool for predicting metal ion toxicity.[13]

References

1. Pearson, R. G., Absolute electronegativity and absolute hardness of Lewis acids and bases. *Journal of the American Chemical Society* 1985, 107 (24), 6801-6806.

2. Pearson, R. G., Absolute electronegativity and hardness: application to inorganic chemistry. *Inorganic Chemistry* 1988, 27 (4), 734-740.

3. Drago, R. S.; Wayland, B. B., A Double-Scale Equation for Correlating Enthalpies of Lewis Acid-Base Interactions. *Journal of the American Chemical Society* 1965, 87 (16), 3571-3577.

4. Vogel, G. C.; Drago, R. S., The ECW Model. *Journal of Chemical Education* 1996, 73 (8), 701.

5. Drago, R. S. A modern approach to acid-base chemistry. *Journal of Chemical Education* 1974, 51 (5), 300

6. Hancock, R. D.; Martell, A. E., Hard and Soft Acid-Base Behavior in Aqueous Solution: Steric Effects Make Some Metal Ions Hard: A Quantitative Scale of Hardness-Softness for Acids and Bases. *Journal of Chemical Education* 1996, 73 (7), 654.

7. Drago, R. S.; Wong, N. M., The Role of Electron-Density Transfer and Electronegativity in Understanding Chemical Reactivity and Bonding. *Journal of Chemical Education* 1996, 73 (2), 123.

8. Drago, R. S., The interpretation of reactivity in chemical and biological systems with the E and C model. Coordination Chemistry Reviews 1980, 33 (3), 251-277.

9. Drago, R. S.; Bilgrien, C. J., Inductive transfer and coordination of ligands in metal—metal bonded systems. Polyhedron 1988, 7 (16), 1453-1468.

10. Drago, R. S., The question of a synergistic metal-metal interaction leading to .pi.-back-bond stabilization in dirhodium tetrabutyrate adducts. Inorganic Chemistry 1982, 21 (4), 1697-1698.

11. Drago, R. S.; Vogel, G. C., Interpretation of spectroscopic changes upon adduct formation and their use to determine electrostatic and covalent (E and C) parameters. *Journal of the American Chemical Society* 1992, 114 (24), 9527-9532.

12. Pearson, R. G.; Mawby, R. J. The Nature of Metal-Halogen Bonds in Gutmann, V. *Halogen Chemistry, vol. 3.* Academic Press: London, 1967, pp. 55-84.

13. Kinraide, T. B. Improved Scales for Metal Ion Softness and Toxicity *Environmental Toxicology and Chemistry* 2009, 28 (3), 525-533.

Notes

* More precisely, the D parameters account for the difference in steric strain in the adduct relative to a water adduct of the Lewis acid.

Contributors

Stephen Contakes (Westmont College, USA)

3.5: Quantitative Measures of Hardness and Softness is shared under a CC BY-NC-SA 4.0 license and was authored, remixed, and/or curated by LibreTexts.

SECTION OVERVIEW

3.6: Coordination Chemistry- Structure and Isomers

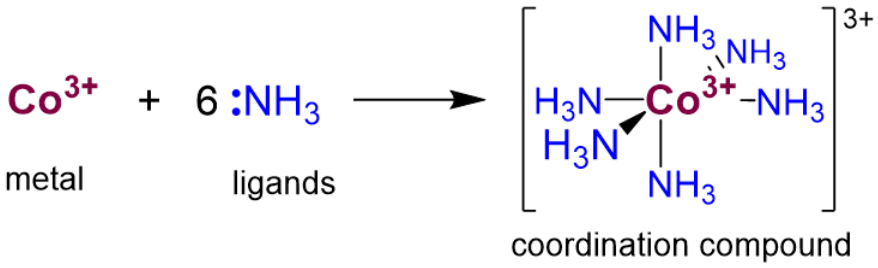
Introduction

Coordination compounds are important to all areas of chemistry, engineering, the life and environmental sciences, and beyond. In the synthetic laboratory catalytic amounts of coordination compounds enable organic chemists to synthesize new compounds selectively and in high yield under mild condition. Applied industrially, coordination compound catalysts serve as vital catalysts that facilitate the conversion of raw petrochemical or bio-derived feedstocks into useful industrial and consumer products. Without them life as we know it would be impossible as many biochemical systems are coordination complexes. Examples include the hemoglobin which transports oxygen around our bodies and the myoglobin which stores it, the photosystems which harvest light and use light energy in photosynthesis, the constituents of the respiratory chain, and many of the enzymes involved in the expression and transmission of genetic information. In studying coordination chemistry you are about to take your first steps into a vast and exciting world.

What is a Coordination Compound?

Coordination compounds consist of one or more metals bound to one or more Lewis base ligands. For example, hexaminechromium(III) ion is a coordination complex in which six ammonia ligands coordinate a Co^{3+} ion, as shown in Scheme **3.6.1**.

Scheme **3.6.1**: Formation of hexaminechromium(III) ion from Co^{3+} and NH_3.



(**3.6.1**)

Such complexes are called coordination compounds or complexes because the ligand-metal bond may be thought of as a coordinate covalent bond in which both of the bonding electrons come from the ligand, which is then said to coordinate the metal. This coordinate covalent model is a very useful formalism for understanding the basic features of coordination chemistry, although it does not always accurately reflect the actual details of the bonding in every coordination complex. Nevertheless, even in those cases where the simple coordinate covalent bond model breaks down the coordinate covalent bond concept supplies the language sophisticated models employ to describe the more complex bonding involved.

Additional Important Terms

Some of the common widely terms that follow from the coordinate covalent model of bonding in coordination complexes include

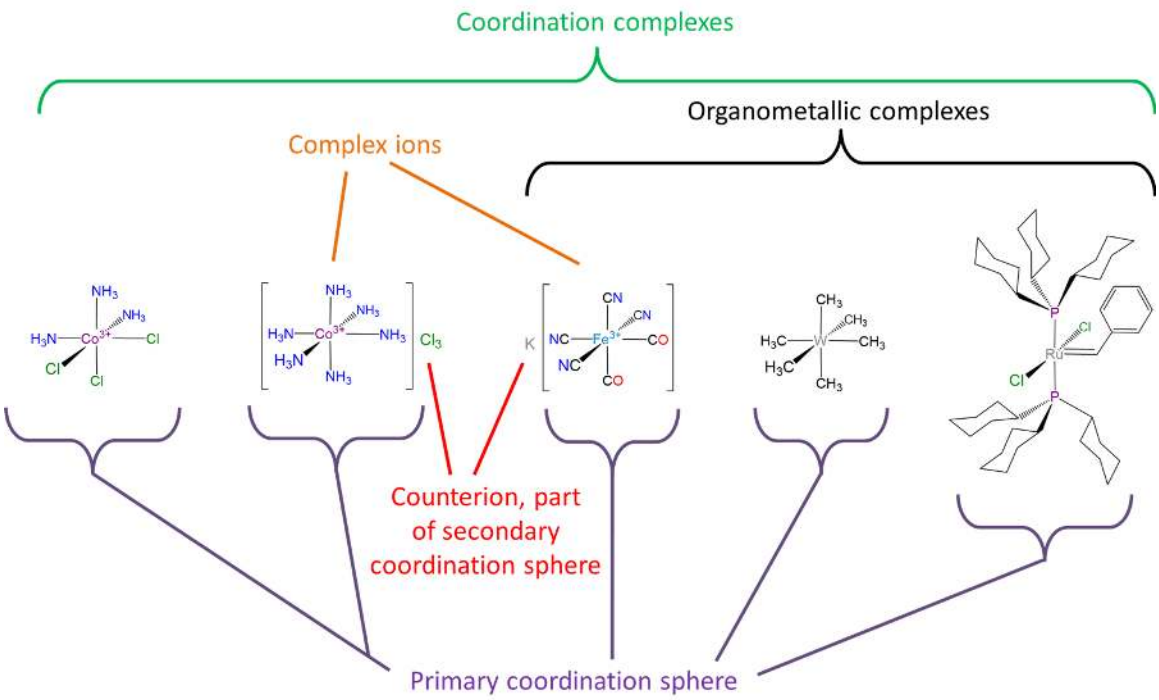
- Coordination compounds are also called **coordination complexes**, **metal complexes**, or just **complexes**. The term **complex** refers to coordination compounds' composite nature, in that they may be thought of as comprised of multiple ligand and metal ion parts that can be restored by breaking the coordinate covalent bonds holding the complex together. This is in contrast to inorganic or organic molecules which are more commonly thought about as whole molecules held together by the sharing of electrons contributed by all the atoms.
- Coordination complexes that are ions are called **complex ions.**
- Ligands bound to the coordination complex are said to reside in the **primary** or **inner coordination sphere**. These bound ligands are not readily exchangeable, in contrast to nearby counterions and solvent molecules, which are said to reside in the

secondary or **outer coordination sphere**.

- The portion of the complex contributing the electron pairs is said to be the **donor** and the portion which receives them the **acceptor**. In conventional coordination compounds the ligand is the donor and the metal the acceptor. In these cases it would be equally convenient to refer to the ligand donor as the Lewis base and the metal acceptor as the Lewis acid. However, in more complex bonding scenarios there may be multiple electron pair donation and acceptance interactions taking place between each pair of atoms and donor-acceptor language will be more convenient.
- The number of ligand sites donating lone pairs to the central atom is referred to as the **coordination number**. For most complexes this will just be equal to the number of ligand atoms bound to the metal. In simple complexes it is just equal to the number of ligands. For instance, the cobalt in Scheme **3.6.1** has a coordination number of six.
- Although technically compounds with metal-carbon bonds are coordination complexes term coordination complex is sometimes used to refer to complexes which do not possess metal-carbon bonds in their primary coordination sphere. Complexes which possess metal-carbon bonds are called organometallic compounds instead. The use of the terms organometallic and coordination to distinguish organometallic compounds from other types of coordination compounds is often convenient since many organometallic ligands engage in more than simple σ donor acceptor coordinate covalent bond formation with the metal center. However, this is true of some wholly inorganic ligands too so it should always be kept in mind that organometallic compounds are just a type of coordination compound and that inorganic ligands can in principle be tuned in interact with a metal center in much the same way an organic ligand does.

A summary of some of the concepts and terms used to describe coordination compounds is given in Scheme **3.6.2**.

Scheme **3.6.2**: Some terms used to describe coordination compounds. This work by Stephen Contakes is licensed under a Creative Commons Attribution 4.0 International License.



Contributors and Attributions

Stephen Contakes, Westmont College

Unless otherwise noted, all line drawings on this page are by Stephen Contakes and licensed under a Creative Commons Attribution 4.0 International License.

Learning Objectives

- Determine the correct name and chemical formula for a metal complex from its structure
- Identify the denticity of a ligand from its structure
- Recognize and name the different types of isomers in metal complexes

3.6.1: History

3.6.2: Nomenclature and Ligands

3.6.3: Acid-Base and Donor-Acceptor Chemistry

3.6.3.1: Acid-Base Models as Organizing Concepts

3.6.3.2: Lewis Concept and Frontier Orbitals

3.6.3.2.1: The frontier orbital approach considers Lewis acid-base reactions in terms of the donation of electrons from the base's highest occupied orbital into the acid's lowest unoccupied orbital.

3.6.3.2.2: All other things being equal, electron withdrawing groups tend to make Lewis acids stronger and bases weaker while electron donating groups tend to make Lewis bases stronger and acids weaker

3.6.3.2.3: The electronic spectra of charge transfer complexes illustrate the impact of frontier orbital interactions on the electronic structure of Lewis acid-base adducts

3.6.3.2.4: Substances' solution phase Lewis basicity towards a given acid may be estimated using the enthalphy change for dissociation of its adduct with a reference acid of similar hardness.

3.6.3.2.5: In the boron trifluoride affinity scale, the enthalphy change on formation of an adduct between the base and boron trifluoride is taken as a measure of Lewis basicity.

3.6.3.2.6: Lewis base strength may also be estimated by measuring structural or energy changes upon formation of a Lewis acid-base complex, as illustrated by efforts to spectroscopically assess the strengths of halogen bonds

3.6.3.2.7: Bulky groups weaken the strength of Lewis acids and bases because they introduce steric strain into the resulting acid-base adduct.

3.6.3.2.8: Frustrated Lewis pair chemistry uses Lewis acid and base sites within a molecule that are sterically restricted from forming an adduct with each other.

3.6.3.3: Hard and Soft Acids and Bases

3.6.3.3.1: Hard-Hard and Soft-Soft preferences may be explained and quantified in terms of electrostatic and covalent and electronic stabilization on the stability of Lewis acid-base adducts

3.6.3.3.2: Quantitative Measures of Hardness, Softness, and Acid-Base Interactions from a Hard Soft Acid-Base Principle Perspective Involve Orbital Energies and/or Apportioning Acid-Base Bonding in Terms of Electrostatic and Covalent Factors

3.6.3.4: Problems

3.6.4: Coordination Numbers and Structures

3.6.5: Isomerism

3.6: Coordination Chemistry- Structure and Isomers is shared under a CC BY-NC-SA 4.0 license and was authored, remixed, and/or curated by LibreTexts.

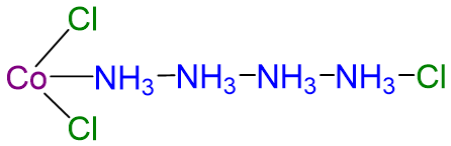
3.6.1: History

History of the Coordination Compounds

Coordination compounds have been known and used since antiquity; one of the oldest synthetic pigments is the blue pigment Egyptian blue, a copper complex of formula $CaCuSi_4O_{10}$ used by the Egyptians since the third Millenium B.C. (in ancient China the Ba analogue, Han blue, was discovered independently). The blue color of Egyptian blue is due to interlocked $Cu(Si_2O_7)_4$ units in which each copper is coordinated by four O atoms in a square planar arrangement. Later, in 1706, the Berlin painter Diesbach would discover another deep blue pigment, Prussian blue: $\mathbf{KFe_2(CN)_6}$.

Despite their long use, the chemical nature of coordination compounds was unclear for a number of reasons. For example, many compounds called “double salts” were known, such as $\mathbf{AlF_3 \cdot 3\,KF}$, $\mathbf{Fe(CN)_2 \cdot 4\,KCN}$, and $\mathbf{ZnCl_2 \cdot 2\,CsCl}$, which were combinations of simple salts in fixed and apparently arbitrary ratios. Why should $\mathbf{AlF_3 \cdot 3\,KF}$ exist but not $\mathbf{AlF_3 \cdot 4\,KF}$ or $\mathbf{AlF_3 \cdot 2\,KF}$? And why should a 3:1 KF:$\mathbf{AlF_3}$ mixture have different chemical and physical properties than either of its components? Similarly, adducts of metal salts with neutral molecules such as ammonia were also known—for example, $\mathbf{CoCl_3 \cdot 6\,NH_3}$, which was first prepared sometime before 1798. Like the double salts, the compositions of these adducts exhibited fixed and apparently arbitrary ratios of the components. For example, $\mathbf{CoCl_3 \cdot 6\,NH_3}$, $\mathbf{CoCl_3 \cdot 5\,NH_3}$, $\mathbf{CoCl_3 \cdot 4\,NH_3}$, and $\mathbf{CoCl_3 \cdot 3\,NH_3}$ were all known and had very different properties, but despite all attempts, chemists could not prepare $\mathbf{CoCl_3 \cdot 2\,NH_3}$ or $\mathbf{CoCl_3 \cdot NH_3}$.

Although the chemical composition of such compounds was readily established by existing analytical methods, their chemical nature was puzzling and highly controversial. The major problem was that what we now call valence (i.e., the oxidation state) and coordination number were thought to be identical. As a result, highly implausible (to modern eyes at least) structures were proposed for such compounds. Of these the most influential was the Blomstrand-Jørgensen chain theory of bonding in coordination compounds, which predicted the “Chattanooga choo-choo” model for $CoCl_3 \cdot 4NH_3$ shown in Scheme **3.6.1.I**.



Scheme **3.6.1.I**. Blomstrand-Jørgensen chain theory model of bonding in $CoCl_3 \cdot 4NH_3$.

Nevertheless, this theory was not wholly illogical and, in fact, explained much of the analytical data on coordination compounds available to chemists of the time. This data included the electrical conductivity of aqueous solutions of these compounds, which was roughly proportional to the number of ions formed per mole, and the number of free chloride ions present, which could be determined by precipitating them gravimetrically as AgCl. In the case of $CoCl_3 \cdot 4NH_3$, two ions and one chloride were produced when the compound was dissolved in water, which Jørgensen was able to explain using the chain structure shown above by postulating that chlorides attached to NH_3 could dissociate while those attached to Co could not. The modern theory of coordination chemistry, which overthrew the chain theory, is based largely on the work of Alfred Werner (1866–1919; Nobel Prize in Chemistry in 1913). In a series of careful experiments carried out in the late 1880s and early 1890s, he examined the properties of several series of metal halide complexes with ammonia. For example, five different “adducts” of ammonia with $PtCl_4$ were known at the time: $PtCl_4 \cdot nNH_3$ (n = 2–6). Some of Werner’s original data on these compounds are shown in Table **3.6.1.1**. Werner’s data on $PtCl_4 \cdot 6NH_3$ in Table **3.6.1.1** showed that all the chloride ions were present as free chloride. In contrast, $PtCl_4 \cdot 2NH_3$, was a neutral molecule that did not give free chloride ions when dissolved in water.

Alfred Werner (1866–1919)

Werner, the son of a factory worker, was born in Alsace. He developed an interest in chemistry at an early age, and he did his first independent research experiments at age 18. While doing his military service in southern Germany, he attended a series of chemistry lectures, and he subsequently received his PhD at the University of Zurich in Switzerland, where he was appointed professor of chemistry at age 29. He won the Nobel Prize in Chemistry in 1913 for his work on coordination compounds, which he performed as a graduate student and first presented at age 26. Apparently, Werner was so obsessed with solving the riddle of the structure of coordination compounds that his brain continued to work on the problem even while he was asleep. In

1891, when he was only 25, he woke up in the middle of the night and, in only a few hours, had laid the foundation for modern coordination chemistry.

Table **3.6.1.1**: Werner's Data on Complexes of Ammonia with $PtCl_4$

Complex	Conductivity (ohm^{-1})	Number of Ions per Formula Unit	Number of Cl^- Ions Precipitated by Ag^+
$PtCl_4 \cdot 6NH_3$	523	5	4
$PtCl_4 \cdot 5NH_3$	404	4	3
$PtCl_4 \cdot 4NH_3$	299	3	2
$PtCl_4 \cdot 3NH_3$	97	2	1
$PtCl_4 \cdot 2NH_3$	0	0	0

These data led Werner to postulate that metal ions have two different kinds of valence: (1) a primary valence (oxidation state) that corresponds to the positive charge on the metal ion and (2) a secondary valence (coordination number) that is the total number of ligands bound to the metal ion. If Pt had a primary valence of 4 and a secondary valence of 6, Werner could explain the properties of the $PtCl_4 \cdot NH_3$ adducts by the following reactions, where the metal complex is enclosed in square brackets:

$$[Pt(NH_3)_6]Cl_4 \rightarrow [Pt(NH_3)_6]^{4+}(aq) + 4Cl^-(aq) \quad (3.6.1.1)$$

$$[Pt(NH_3)_5Cl]Cl_3 \rightarrow [Pt(NH_3)_5Cl]^{3+}(aq) + 3Cl^-(aq) \quad (3.6.1.2)$$

$$[Pt(NH_3)_4Cl_2]Cl_2 \rightarrow [Pt(NH_3)_4Cl_2]^{2+}(aq) + 2Cl^-(aq) \quad (3.6.1.3)$$

$$[Pt(NH_3)_3Cl_3]Cl \rightarrow [Pt(NH_3)_3Cl_3]^{+}(aq) + Cl^-(aq) \quad (3.6.1.4)$$

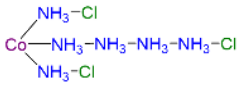
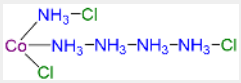
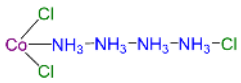
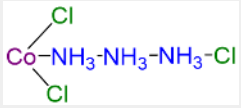
$$[Pt(NH_3)_2Cl_4] \rightarrow [Pt(NH_3)_2Cl_4]^{0}(aq) \quad (3.6.1.5)$$

Further work showed that the two missing members of the series—$[Pt(NH_3)Cl_5]^-$ and $[PtCl_6]^{2-}$—could be prepared as their mono- and dipotassium salts, respectively. Similar studies established coordination numbers of 6 for Co^{3+} and Cr^{3+} and 4 for Pt^{2+} and Pd^{2+}.

? Exercise 3.6.1.1. The $CoCl_3xNH_3$ series.

The series $CoCl_3 \cdot xNH_3$ was particularly important in establishing the correctness of Werner's coordination theory over the rival chain theory. By ~1900 conductivity measurements suggested that the members of the series gave the number of ions shown in Table **3.6.1.1**.

Table **3.6.1.1**. The CoCl3·xNH3 series according to coordination theory, chain theory, and experiment.

Compound	Color	Werner formulation	Blomstrand-Jørgensen chain theory formulation	Number of ions in solution
$CoCl_3 \cdot 6NH_3$	yellow	$[Co(NH_3)_6]Cl_3$		4
$CoCl_3 \cdot 5NH_3$	violet	$[Co(NH_3)_5Cl]Cl_2$		3
$CoCl_3 \cdot 4NH_3$	green	$[Co(NH_3)_4Cl_2]Cl$		2
$CoCl_3 \cdot 3NH_3$	orange	$[Co(NH_3)_4Cl_3]$		0

What does this data suggest about the relative explanatory power of Werner's coordination theory and chain theory? Explain.

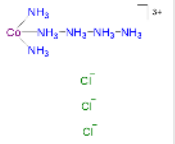
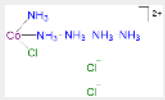
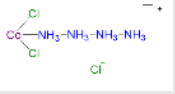
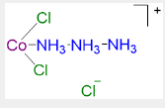
Answer

Remember that

- chain theory predicts that the number of ions is the number formed when the Cl atoms bound in a chain with NH_3 dissociate.
- coordination theory predicts the number of ions based on the number of complex ions and their counterions.

Based on this the predictions of coordination theory and chain theory can be compared with the experimental data, as is done in Table **3.6.1.2**.

Table **3.6.1.2**: Comparison of ions predicted for the $CoCl_3 \cdot xNH_3$ series by coordination theory and chain theory with the number observed experimentally.

Compound	Color	Ions predicted by Werner's coordination theory	Number of ions predicted by coordination theory	Ions predicted by Blomstrand-Jørgensen chain theory	Number of ions predicted by chain theory	Observed Number of ions in solution
$CoCl_3 \cdot 6NH_3$	yellow	$[Co(NH_3)_6]^{3+}$ Cl^- Cl^- Cl^-	4		4	4
$CoCl_3 \cdot 5NH_3$	violet	$[Co(NH_3)_5Cl]^{2+}$ Cl^- Cl^-	3		3	3
$CoCl_3 \cdot 4NH_3$	green	$[Co(NH_3)_4Cl_2]^+$ Cl^-	2		2	2
$CoCl_3 \cdot 3NH_3$	orange	None	0		2	0

As can be seen by comparing the number of ions predicted by coordination and chain theory in Table **3.6.1.2**, coordination theory successfully explains all the observed ion counts, while chain theory fails to explain the lack of ions observed for $CoCl_3 \cdot 3NH_3$.

Nevertheless, as is often the case when developing theoretical models using data from real experimental investigations, these observations did not convince Jørgensen, who could point to the experimental difficulty of determining the number of ions present from solution conductivity data.

What ultimately convinced Jørgensen of the correctness of Werner's coordination model over his own chain theory was how Werner's explanation of the structure of cobalt coordination complexes using an octahedral coordination geometry explained the existence of isomers in Co complexes containing Cl and NH_3 ligands. In the case of $[Co(NH_3)_4Cl_2]Cl$ two isomers were known: one red and the other green. Because both compounds had the same chemical composition and the same number of groups of the same kind attached to the same metal, there had to be something different about the arrangement of the ligands around the metal ion. Werner's key insight was that the six ligands in $[Co(NH_3)_4Cl_2]Cl$ had to be arranged at the vertices of an octahedron because that was the only structure consistent with the existence of two, and only two, stereoisomers (Figure **3.6.1.1**). His conclusion was also corroborated by the existence of two and only two stereoisomers of the next compound in the series: $Co(NH_3)_3Cl_3$.

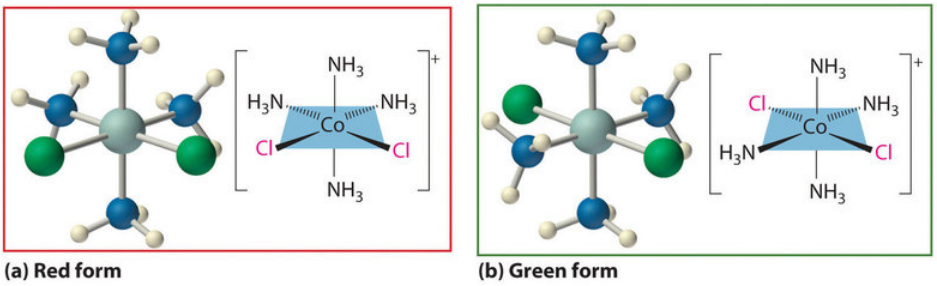


Figure **3.6.1.1**. The $[Co(NH_3)_4Cl_2]^+$ ion can have two different arrangements of the ligands, which results in different colors: if the two Cl^- ligands are next to each other (*cis*), the complex is red (a), but if they are opposite each other (*trans*), the complex is green (b).

✔ Example **3.6.1.1**: Why did Werner propose an octahedral geometry for 6-coordinate complexes?

In Werner's time, many complexes of the general formula MA_4B_2 were known, but no more than two different compounds with the same composition had been prepared for any metal. To confirm Werner's reasoning that this suggests these complexes possess an octahedral geometry, calculate the maximum number of different structures possible for six-coordinate MA_4B_2 complexes with each of the three most symmetrical possible structures the ligands will form about the central metal - a hexagon, a trigonal prism, and an octahedron.

Assuming that the absence of evidence for additional compounds in this case serves as reasonable circumstantial evidence for their absence, what does the fact that no more than two forms of any MA_4B_2 complex were known suggest about the three-dimensional structures of these complexes?

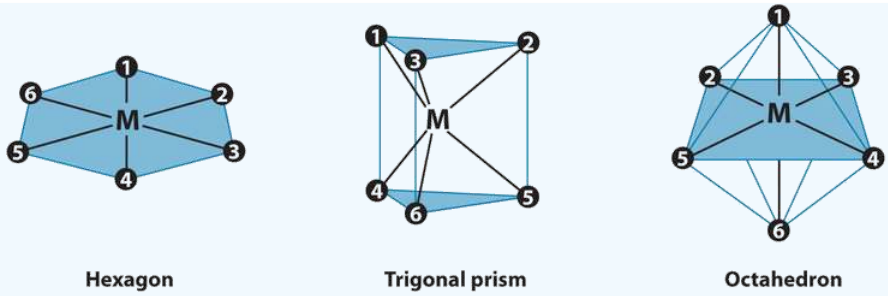
Solution

In this problem you are given

- the stochiometry of the complexes, MA_4B_2
- three possible coordination geometries - hexagonal, trigonal prismatic, and octahedral.

In order to calculate the number of isomers that could be present for each geometry it is best to follow a systematic approach. Since there are fewer B type ligands than A type ligands, the easiest way to do this for each geometry is to start by placing a B ligand at one vertex and then to determine how many different positions are available for the second B ligand.

The three regular six-coordinate structures are shown here, with each coordination position numbered so that we can keep track of the different arrangements of ligands. For each structure, all vertices are equivalent. We begin with a symmetrical MA_6 complex and simply replace two of the A ligands in each structure to give an MA_4B_2 complex:



For the hexagon, we place the first B ligand at position 1. There are now **three** possible places for the second B ligand:

- position 2 (or 6)
- position 3 (or 5)
- position 4

The (1, 2) and (1, 6) arrangements are chemically identical because the two B ligands are adjacent to each other. The (1, 3) and (1, 5) arrangements are also identical because in both cases the two B ligands are separated by an A ligand. Those of you who remember your ogranic chemistry might recognize that this situation is formally analogous to the *ortho-*, *meta-*, and *para-* isomerism in disubstituted benzenes.

Turning to the trigonal prism, we place the first B ligand at position 1. Again, there are three possible choices for the second B ligand:

- at position 2 or 3 on the same triangular face
- position 4 (on the other triangular face but adjacent to 1)
- position 5 or 6 (on the other triangular face but not adjacent to 1).

The (1, 2) and (1, 3) arrangements are chemically identical, as are the (1, 5) and (1, 6) arrangements.

In the octahedron, however, if we place the first B ligand at position 1, then we have only two choices for the second B ligand:

- position 2 (or 3 or 4 or 5)
- position 6.

In the latter, the two B ligands are at opposite vertices of the octahedron, with the metal lying directly between them. Although there are four possible arrangements for the former, they are chemically identical because in all cases the two B ligands are adjacent to each other.

The number of possible MA_4B_2 arrangements for the three geometries is thus: hexagon, 3; trigonal prism, 3; and octahedron, 2. The fact that only two different forms were known for all MA_4B_2 complexes that had been prepared suggested that the correct structure was the octahedron but did not prove it. For some reason one of the three arrangements possible for the other two structures could have been less stable or harder to prepare and had simply not yet been synthesized. When combined with analogous results for other types of complexes (e.g., MA_3B_3), however, the data were best explained by an octahedral structure for six-coordinate metal complexes.

? Exercise 3.6.1.1

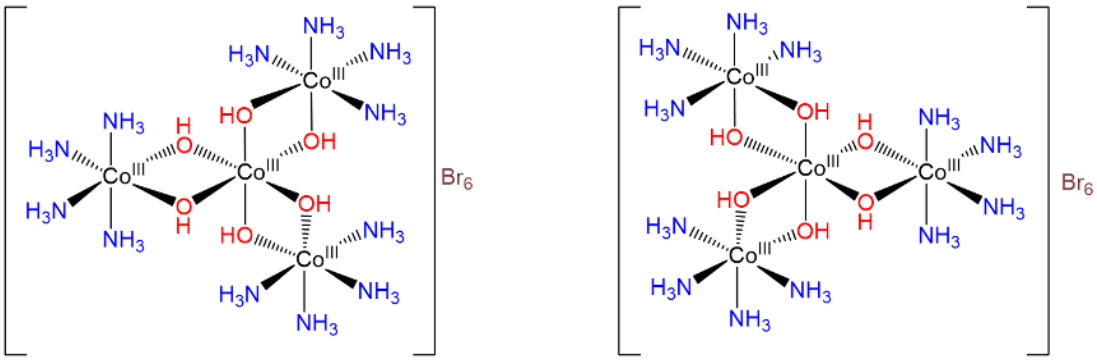
Determine the maximum number of structures that are possible for a four-coordinate MA_2B_2 complex with either a square planar or a tetrahedral symmetrical structure.

Answer

square planar, 2; tetrahedral, 1

Even Werner's explanation of isomerism in coordination complexes in terms of octahedral and other recognized coordination geometries did not convince all chemists until he was able to resolve a racemic mixture of *d*- and *l*-$[Co\{Co(NH3)_4(OH)_2\}_3]$ into its

enantiomers, which are shown in Scheme **3.6.1.II**. By doing so Werner demonstrated to chemists of his time (virtually none of whom knew group theory) that tetrahedral carbon atoms were not required for chirality; D_3 octahedral complexes were also chiral.



Scheme **3.6.1.II**: d- and l-enantiomers of $[Co\{Co(NH3)_4(OH)_2\}_3]$, colloquially referred to as hexol. This work by Stephen Contakes is licensed under a Creative Commons Attribution 4.0 International License.

3.6.1: History is shared under a CC BY-NC-SA 4.0 license and was authored, remixed, and/or curated by LibreTexts.

- **24.1: Werner's Theory of Coordination Compounds** by Anonymous is licensed CC BY-NC-SA 4.0.

3.6.2: Nomenclature and Ligands

Introduction

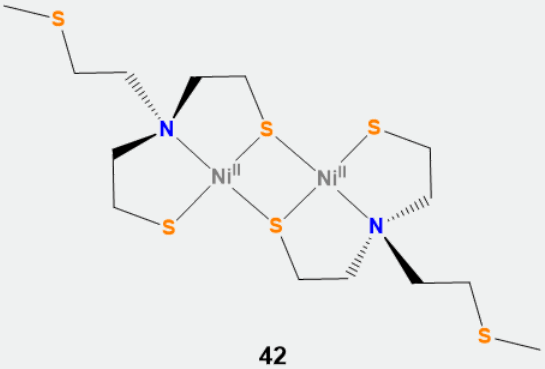
There are well-established rules for both naming and writing the formulae of coordination compounds. The purpose of these rules is to facilitate clear and precise communication among chemists. As with all such rules some are more burdensome than others to employ and some serve more crucial roles in the communication process while others are more peripheral - and all are poorly used in the service of pedantic tyranny, especially when against those who are otherwise doing good work. For this reason, you are urged to approach the rules in a spirit of generosity towards others in

- naming and writing formulas as reasonably accurately as you can so that ligands and metals are where readers expect them and thus can understand what you mean more easily.
- being gracious towards the many professional inorganic chemists who adhere loosely to some of the rules you are about to learn.
- recognizing that in cases when a structure is particularly complex and a picture may make be particularly useful you should supply one (See the note below).

Note 3.6.2.1: Sometimes the most helpful name to give a compound is 42.

Even though the IUPAC nomenclature rules permit specification of even the most complex structures, it is often much easier and more effective to supply a numbered structure that can be referred to instead of the IUPAC name. Consider bis{[(μ-2-mercaptoethyl)(2-mercaptoethyl)-methylthioethylaminato (2-)]Nickel(II)}. Which is easier, to expect readers and hearers to work out the structure from that name or to just refer them to compound **42** in Scheme 3.6.2.I?

Scheme 3.6.2.I. Structure of bis{[(μ-2-mercaptoethyl)(2-mercaptoethyl)-methylthioethylaminato (2-)]Nickel(II)}. The authors of the synthesis of this compound in *Inorganic syntheses*[1] may have had to figure out an IUPAC name for this compound but if you have this scheme in your paper and your instructor is OK with it you can just call it **42**.



42

Coordination Complex Nomenclature

A variety of systems have been used for naming coordination compounds since the development of the discipline in the time of Alfred Werner. In this section the most common approaches as they are currently used by practicing chemists will be described. Those who need a more thorough and accurate acquaintance with the full IUPAC nomenclature rules are encouraged to consult the IUPAC brief guide to inorganic nomenclature followed by complete guidelines, commonly known as the IUPAC red book. If those are still not enough a careful read of note **3.6.2.1** is suggested.

The systems for naming coordination compounds used at present are additive, meaning that they consider coordination compounds as comprised of a central metal to which are added ligands. To specify the structure and bonding in this metal-ligand complex then involves

1. When there are several different ways of attaching the metal and ligands, specifying the structural or stereoisomer

2. systematically listing the ligands in a way that, as necessary, conveys information about how they are linked to the metal and their stereochemistry

3. providing the identity of the metal and its oxidation state, or if the oxidation state is unclear, at least the overall charge on the complex

4. specifying any counterions present

Since the stereochemistry of coordination compounds forms the subject of the next section, in this section it will be addressed in this section by simply giving the prefixes that designate stereochemistry as if they were self-evident. Do not worry about these for now. They will make sense after you have learned more about stereochemistry in the next section. At that time, you can go back over the examples in that section to solidify your understanding of how to name coordination compounds.

However, in order to name coordination compounds accurately you will need to learn about how to think about and name ligands first.

Ligands

Ligands are classified based on whether they bind to the metal center through a single site on the ligand or whether they bind at multiple sites. Ligands which bind through only a single site are called **monodentate** at the Latin word for tooth; in contrast those those which bind through multiple sites are called **chelating** after the Greek $\chi\alpha\lambda\epsilon$ for "claw". These relationships are summarized in Figure 3.6.2.1.

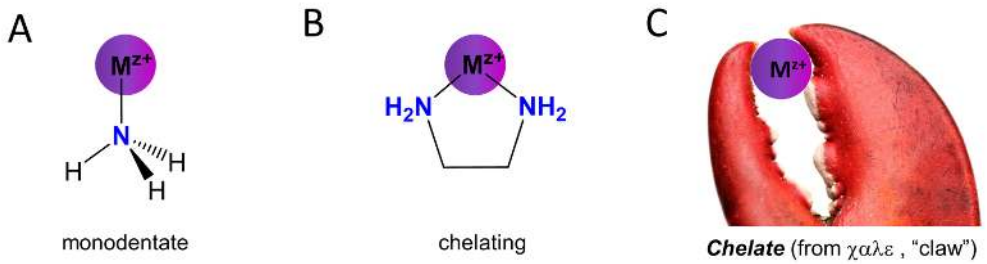
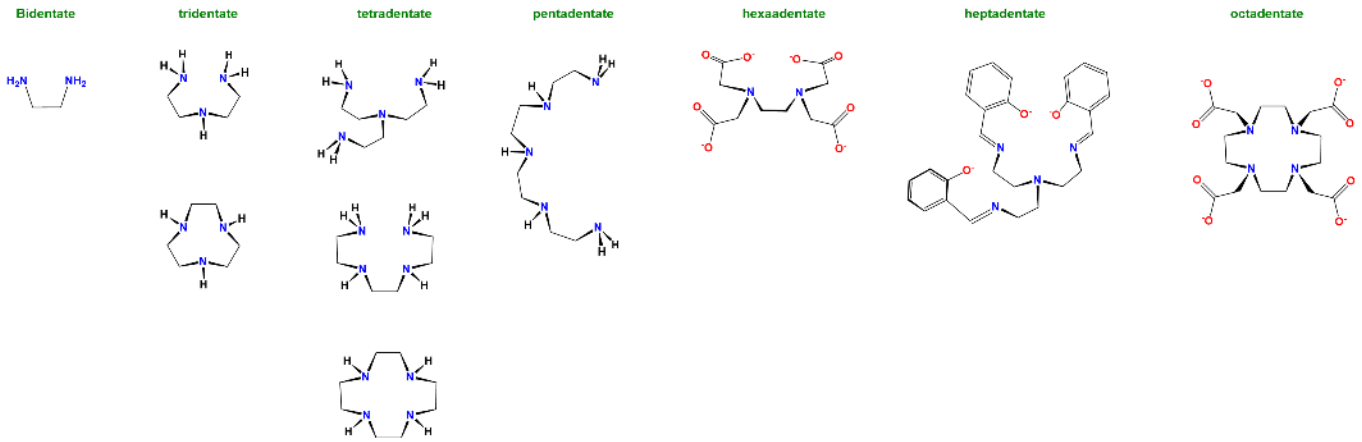


Figure 3.6.2.1. (A) Ammonia is monodentate ligand while (B) ethylene diamine is a chelating ligand owing to its capacity to bind metals via its two amine functional groups. (C) Chelating ligands act like a Lobster claw in attaching to the metal via multiple sites. The lobster claw image is adapted from https://www.clipart.email/download/1127636.html. Otherwise this work by Stephen Contakes is licensed under a Creative Commons Attribution 4.0 International License.

Following naturally from the classification of non-chelating ligands as monodentate, chelating ligands are further classified according to the number of sites which they can use to bind a metal center. This number of binding sites is called the denticity and ligands are referred to as monodentate (non chelating), bidentate, tridentate, etc. based on the number of sites available. Ligands with two binding sites have a denticity of two and are said to be bidentate; those with three are tridentate, four tetradentate, and so on. To illustrate this classification system examples of chelating ligands classified according to denticity are given in Scheme 3.6.2.I.

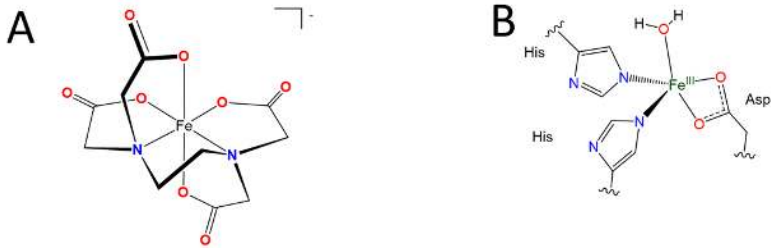
Scheme 3.6.2.I. A selection of chelating ligands classified according to denticity. this work by Stephen Contakes is licensed under a Creative Commons Attribution 4.0 International License.



The classification of several of the ligands in Scheme **3.6.2.I** requires a bit of explanation, specifically as to why the dentificity of the carboxylate-containing ligands is less than the total number of lone-pair bearing oxygen and nitrogens present. This is because only one of the carboxylate oxygens is counted. Only one is counted because in most cases only one oxygen binds to a metal at any given time. When that oxygen is bound the other oxygen faces away from the metal, as depicted for the iron complex shown in Scheme **3.6.2.IIA**. Because only one oxygen per carboxylate *typically* binds only one is counted when assigning a ligand's denticity.

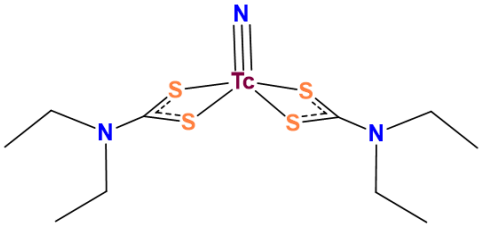
Although only one carboxylate oxygen usually binds to a metal it is still possible to bind a metal using both oxygens. As shown in Scheme **3.6.2.IIB** complexes in which both carboxylates bind to a metal are known, and in fact are common in the active sites of some enzymes. It is just that the binding of both oxygens gives a strained four-membered ring that is usually unstable.

Scheme 3.6.2.II. (A) Only one oxygen per carboxylate counts towards the denticity of EDTA since on binding the other oxygen generally points away from the metal center, as in the structure of $Fe(EDTA)^-$. This does not mean that both oxygens of a carboxylate can *never* both bind to metal centers in a complex. (B) Structures in which both oxygens of a carboxylate side chain bind to a metal are sometimes found in the active sites of some of the nonheme iron enzymes your body uses to break down amino acids. this work by Stephen Contakes is licensed under a Creative Commons Attribution 4.0 International License.



As was the case for carboxylate groups above, sometimes the classification of a group's denticity is based on experimental knowledge of their common binding modes. Carboxylates might commonly act as monodentate ligands but dithiocarbamates more commonly bind metals through both sulfur atoms (Scheme **3.6.2.III**) and are classified as bidentate.

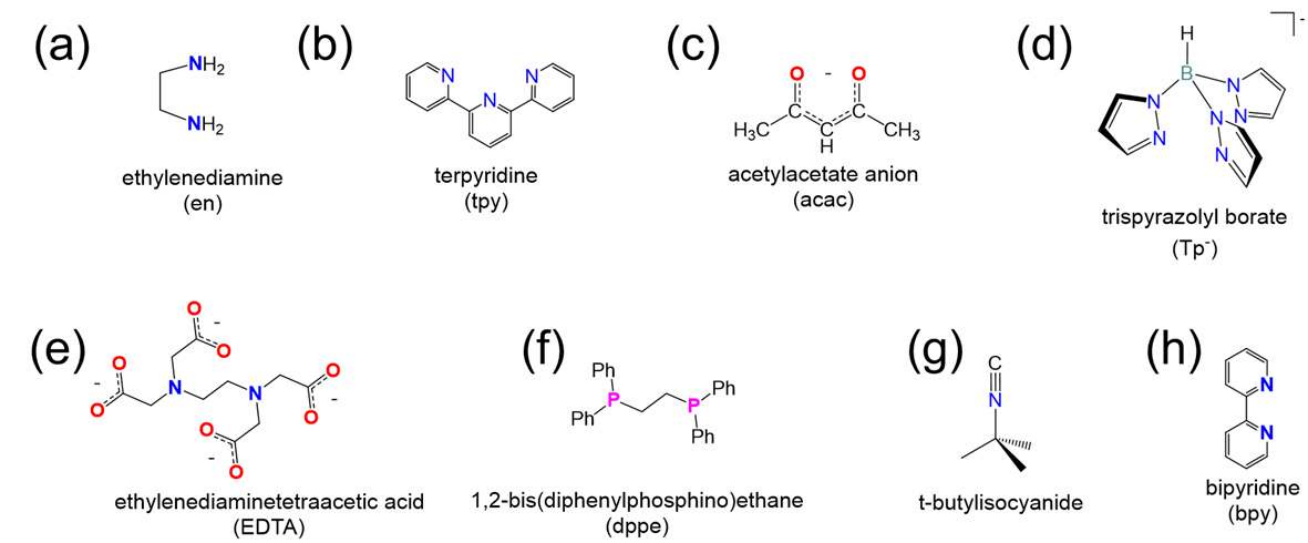
Scheme 3.6.2.III. As in this complex, dithiocarbamates commonly bind metals through both sulfur atoms. Consequently, dithiocarbamates are classified as bidentate. this work by Stephen Contakes is licensed under a Creative Commons Attribution 4.0 International License.



Because of these factors it is technically more correct to say that carboxylates *usually act as* monodentate ligands and dithiocarbamates bidentate ones than it is to say that carboxylates *are* monodentate ligands and dithiocarbamates bidentate ones. So in other words the ligand classifications presented here are just represent common binding modes.

Exercise 3.6.2.1

Determine the denticity of each ligand in the list below and classify them as monodentate, tridentate, etc.



Answer

(a) bidentate

(b) tridentate

(c) bidentate

(d) tridentate (only the lower N on each ring has a lone pair that can be used to bind the metal)

(e) hexadentate (remember that each carboxylate only counts as one point of attachment)

(f) bidentate

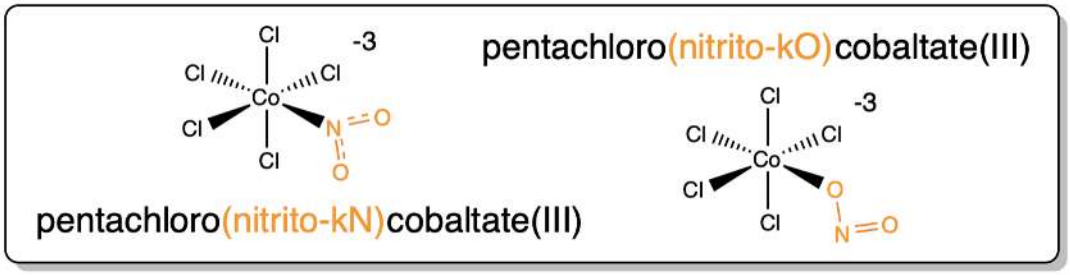
(g) monodentate (through the lone pair on the isocyanide C)

(h) bidentate

This experimentally-based classification of dithiocarbamates as bidentate and carboxylates as monodentate can be confusing to a beginner. Fortunately, such experimentally based classifications are embedded in the lists of common monodentate ligands are given in Table **3.6.2.1** and common chelating ligands in Table **3.6.2.2**.

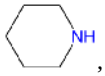
A perusal of the ligands in Table **3.6.2.1** reveals that several can bind to a metal in multiple ways. For example, thiocyanate, SCN^- can bind metal's through its S or N atoms. Such ligands are called **ambidentate ligands**. When naming an ambidentate ligand the atom through which it attaches to the metal is commonly specified after the ligand name using the italicized element symbol or, more formally a κ followed by the italicized element symbol. An example is given in Scheme **3.6.2.I.**[2]

Scheme 3.6.2.I. Two possible binding modes of nitrite acting as a ligand.[3]



https://chem.libretexts.org/@go/page/484727

Table 3.6.2.1. Common monodentate ligands. Most chemists still prefer common names over the IUPAC ones.

Ligand	Common name	IUPAC name
H^- (H ligands are always considered anions for naming purposes)	hydrido	hydrido
F^-	fluoro	fluorido
Cl^-	chloro	chlorido
Br^-	bromo	bromido
I^-	iodo	iodido
CN^-, M-CN	cyano	cyanido or cyanido-κC or cyanido-*C*
CN^-, as M-NC	isocyano	isocyanido or cyanido-κN or cyanido-*N*
CH_3NC	methylisocanide	methylisocyanide
N_3^-	azido	azido
SCN^-, *e.g.* thiocyanate as M-SCN	thiocyanato	thiocyanato-κS or thiocyanato-*S*
NCS^-, *e.g.* thiocyanate as M-NCS	isothiocyanato	thiocyanato-κN or thiocyanato-*N*
$CH_3CO_2^-$	acetato	ethanoato
N^{3-}	nitrido	nitrido
NH^{2-}	imido	azanediido
NH_2^-	amido	azanido
NH_3	ammine	ammine
RNH_2, R_2NH, R_3N	alkylamine, dialkylamine, trialkalyamine (*e.g.* methylamine for CH_3NH_2)	alkylamine, dialkylamine, trialkalyamine (*e.g.* methylamine for CH_3NH_2)
 , piperidine, abbreviated pip	piperidine	piperidine
 , pyridine, abbreviated py	pyridine	pyridine
CH_3CN, acetonitrile, abbreviated MeCN	acetonitrile	acetonitrile
P^{3-}	phosphido	phosphido
PH_3	phosphine	phosphane
PR_3	trialkylphosphine (*e.g.* trimethylphosphine for Me_3P)	trialkylphosphane (*e.g.* trimethylphosphane for Me_3P)
PAr_3	triarylphosphine (*e.g.* triphenylphosphine for Ph_3P)	triarylphosphine (*e.g.* triphenylphosphane for Ph_3P)
 , dimethylsulfoxide or DMSO or dmso	dimethylsulfoxide (sometimes called dimethylsulfoxo but this usage is rare and violates the nomenclature rules for neutral ligands)	(methanesulfinyl)methane or dimethyl(oxido)sulfur

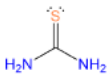
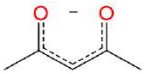
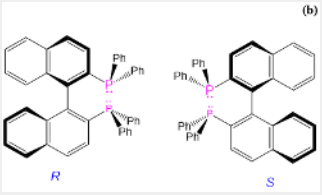
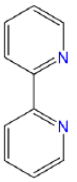
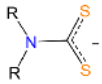
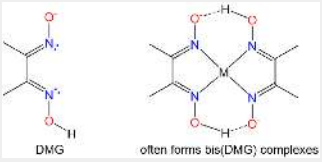
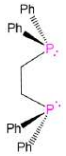
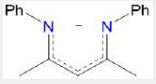
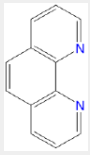
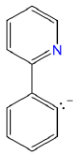
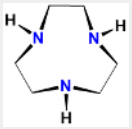
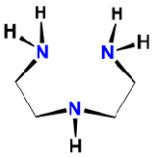
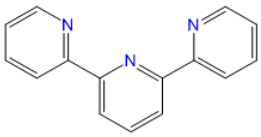
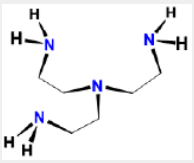
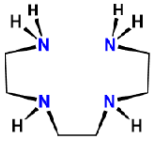
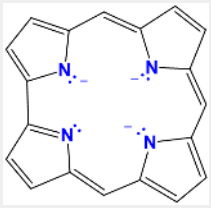
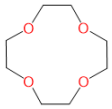
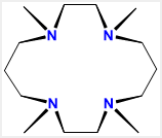
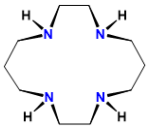
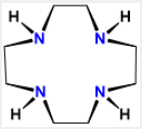
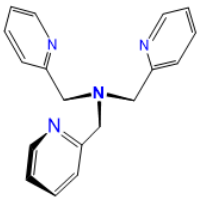
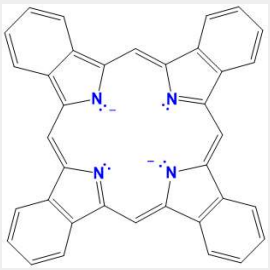
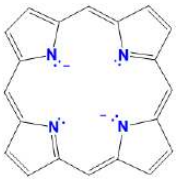
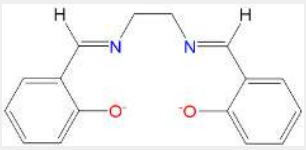
, thiourea or tu	thiourea	thiourea
O^{2-}	oxo	oxido
OH^-	hydroxo	hydroxido
H_2O	aqua	aqua
S^{2-}	sulfo	sulfo
HS^-	hydrosulfido	hydrosulfido
RS^-	alkanethiolate (*e.g.* ethanthiolate for EtS^-)	thioalkanoate
H_2S	hydrogen sulfide	hydrogen sulfide
R_2S	alkylsulfanylalkane (*e.g.* ethylsulfanylethane for Et_2S)	dialkyl sulfide
O_2	dioxygen	dioxygen
O_2^-, superoxide	superoxido	dioxido(1-) or superoxido
O_2^{2-}, peroxide	peroxido	dioxido(2-) or peroxido
N_2	dinitrogen	dinitrogen
NO (are always considered neutral for naming purposes)	nitrosyl	nitrosyl
CO	carbonyl	carbonyl
CS	thiocarbonyl	thiocarbonyl
SO, as M-SO	sulfino	sulfur monoxide-κ*S* or sulfur monoxide-*S*
NO_2, as M-NO_2	nitryl	nitrogen dioxide-κN or nitrogen dioxide-*N*
CO_3^{2-}	carbonato	carbonato
NO_2^-, as M-NO_2	nitro or nitrito-*N*	nitrito-κ*N* or nitrito-*N*
NO_2^-, as M-ONO	nitrito or nitrito-*O*	nitrito-κ*O* or nitrito-*O*
NO_3^-	nitrato	nitrato
SO_3^{2-}	sulfito	sulfito
SO_4^{2-}	sulfato	sulfato
$S_2O_3^{2-}$, as M-S-SO_2-O^-	thiosulfato-*S*	thiosulfato-κ*S* or thiosulfato-*S*
$S_2O_3^{2-}$, as M-O-SO_2-S^-	thiosulfato-*O*	thiosulfato-κ*O* or thiosulfato-*O*

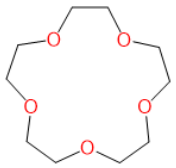
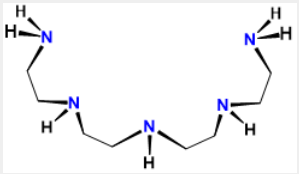
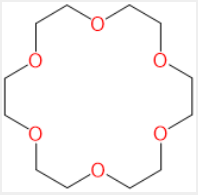
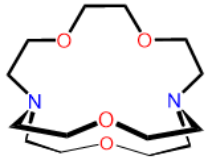
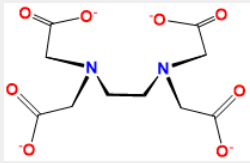
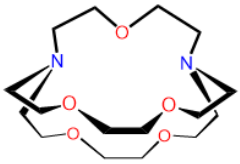
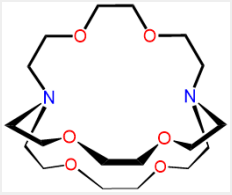
Table 3.6.2.2. Common chelating ligands organized by denticity. Most chemists use the common names and abbreviations to

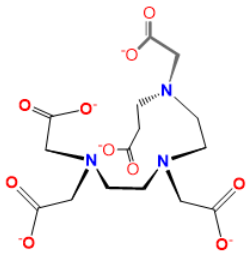
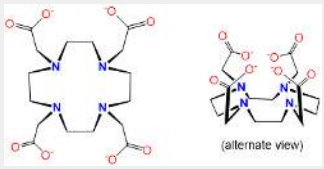
describe these ligands.

Common Ligand name	IUPAC ligand name	abbreviation (if applicable)	structure or representative/parent structure (shown in the ionization state in which they bind to a metal)
bidentate ligands			
acetylacetonato	2,4-pentanediono	acac	
R-BINAP and *S*-BINAP	*R*- or *S*-2,2'-bis(diphenylphosphino)-1,1'-binapthyl	BINAP	
2,2'-bipyridine	2,2'-bipyridine	bpy or bipy	
cyclooctadiene	1,5-cyclooctadiene	COD	 (binding to the metal occurs through the alkene π cloud)
dialkyldithiocarbamato	dialkylcarbamodithiolato	$R_2NCS_2^-$ or dtc	
dimethylgloximato	butanedienedioxime	Hdmg or DMG	
diphenylphosphinoethane or 1,2-(diphenylphosphino)ethane	Ethane-1,2-diylbis(diphenylphosphane)	dppe	
ethylenediamine	Ethane-1,2-diamine	en	
ethylenedithiolato	Ethane-1,2-dithiolato	$C_2H_2S_2^{2-}$	
nacnac	*N*,*N*'-diphenyl-2,4-pentanediiminato	nacnac	

oxalato	oxalato	ox	
1,10-phenanthroline or *o*-phenanthroline	1,10-phenanthroline	phen or *o*-phen	
phenylpyridinato	2-phenylpyridinato-C^2,*N* or 2-phenylpyridinato-κC^2,*N*	ppy	
tridentate ligands			
triazacyclononane	1,3,7-triazacyclononane	tacn	
diethylenetriamine	1,4,7-triazaheptane	dien	
pyrazoylborato (scorpionate)	hydrotris(pyrazo-1-yl)borato	Tp	
terpyridine or 2,2';6',2''-terpyridine	1^2,2^2:2^6,3^2-terpyridine or 2,6-bis(2-pyridyl)pyridine, tripyridyl, 2,2′:6′,2″-terpyridine	tpy or terpy	
tetradentate ligands			
β, *β*', *β*''-triaminotriethylamine	*β*, *β*', *β*''-tris(2-aminoethyl)amine	tren	
triethylenetetramine	1,4,7,10-tetraazadecane	trien	

corroles	variable and generally not used	cor or Cor	
12-crown-4	1,4,7,10-tetraoxacyclododecane	12-crown-4	
tetramethylcyclam	1,4,8,11-tetramethyl-1,4,8,11-tetraazacyclotetradecane	TMC or cyclam	
cyclam	1,4,8,11-tetraazacyclotetradecane	cyclam	
cyclen	1,4,7,10-tetraazacyclododecane	cyclen	
tris(2-pyridylmethyl)amine	1-pyridin-2-yl-*N*,*N*-bis(pyridin-2-ylmethyl)methanamine	tpa or TPA	
phthalocyanines	variable and generally not used	variable, usually a modified Pc	
porphyrins	variable and generally not used	variable, usually a modified por, Por, or P (e.g. TPP = tetraphenylporphyrin)	
salen	2,2'-ethylenebis(nitrilomethylidene) diphenoxido	salen	
pentadentate ligands			

15-crown-5	1,4,7,10,13-Pentaoxacyclopentadecane	15-crown-5	
tetraethylenepentamine	1,4,7,10,13-pentaazatridecane	tepa or TEPA	
hexadentate ligands			
18-crown-6	1,4,7,10,13,16-hexaoxacyclooctadecane	18-crown-6	
2,1,1-cryptand	4,7,13,18-Tetraoxa-1,10-diazabicyclo[8.5.5]icosane	2,1,1-crypt or [2.1.1]-cryptand kryptofix 211 and variations thereof	
ethylenediaminetetraaceto	2,2′,2″,2‴-(Ethane-1,2-diyldinitrilo)tetraaceto	EDTA, edta, Y^{4-}	
heptadentate ligands			
2,2,1-cryptand	4,7,13,16,21-pentaoxa-1,10-diazabicyclo[8.8.5]icosane	2,2,1-crypt or [2.2.1]-cryptand kryptofix 221 and variations thereof	
octadentate ligands			
2,2,2-cryptand	4,7,13,16,21,24-Hexaoxa-1,10-diazabicyclo[8.8.8]hexacosan	2,2,2-crypt or [2.2.2]-cryptand kryptofix 222 and variations thereof	

pentetato acid or diethylenetriaminepentaacetato or DTPA	2-[bis[2-[bis(carboxylatomethyl)amino]ethyl]amino]acetato	DTPA	
DOTA or tetraxetan	1,4,7,10-Tetraazacyclododecane-1,4,7,10-tetraacetic acid	Dota, DOTA	

Rules for Naming Coordination Compounds

As explained above, the name of a coordination compound communicates

- As appropriate, information about isomerism
- systematically listing the ligands in a way that as necessary conveys information about their oxidation state and how they are linked to the metal
- the identity of the metal and its oxidation state
- any counterions present

Before going into these rules it is worth pointing out a few things.

1. It is easiest to learn these rules by starting with one or two of the rules, learning how to apply them, and then adding additional rules one at a time. To that end, instructors who wish to use a more programmed approach may find it convenient to first direct their students to this page which focuses on getting the names of the ligands and metal right, without working about isomerism or stereochemistry.

2. The rules also assume some familiarity with common coordination geometries and patterns of isomerism in metal complexes. Thus it might be easiest to learn about common coordination geometries first, followed by common patterns of isomerism in metal complexes before beginning this section. If you decide to dive right in to this section you might find it helpful to know that when applying nomenclature and formula rules most textbooks *assume*

- complexes in which the metal has a coordination number of six are octahedral
- complexes in which the metal has a coordination number of five are trigonal bipyramidal
- complexes in which Pt^{II} , Pd^{II} , or Rh^{I}, or Ir^{I} have a coordination number of four are square planar
- other complexes in which the metal has a coordination number of four are tetrahedral

Like all assumptions these don't always work in real life but they should be good enough to get you through your first inorganic chemistry course.

For the pedants among you, note that the complexes given as examples and in exercises on this page have been selected for pedagogical utility. Although many are well-known compounds, others are hypothetical.

Now on to the rules.

Name the cation first, followed by the anion.

Examples:

$K_2[Pt^{II}Cl_4]$ potassium tetrachloroplatinate(2-)

$[Co^{III}(NH_3)_6](NO_3)_3$ hexaamminecobalt(3+) nitrate

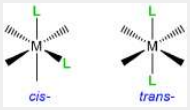
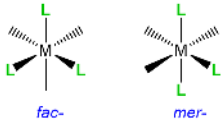
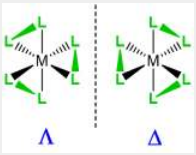
$[Co^{III}(NH_3)_6][Cr^{III}(C_2O_4)_3]$ hexaamminecobalt(3+) tris(oxalato)chromium(3-)

Designate the isomer in italics in front of the name

If you have not yet learned about isomerism in coordination compounds skip this rule for now and return to it after you have.

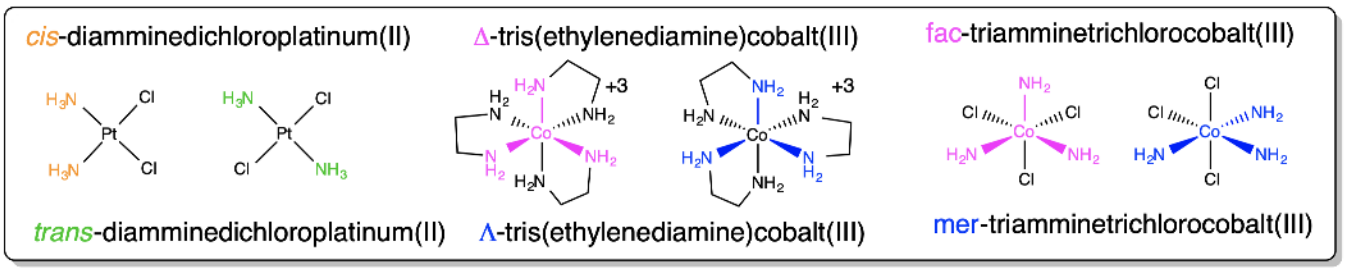
When a complex might exist as one of two stereosisomers prefixes are commonly used to designate which isomer is present. The most common cases are listed in Table **3.6.2.3**.

Table3.6.2.3. Prefixes used to specify isomerism about a metal center when naming and writing coordination compounds' formulae.

Type of isomerism	Graphical reminder	Prefixes
Geometric, *cis-* , *trans-*		*cis-* or *trans-*
Geometric, *fac- /mer-*		*fac-* or *mer-*
Enantiomers, **Λ-**, **Δ-**		**Λ-** or **Δ-**

Examples of how isomerism about a metal center is designated are given in Scheme **3.6.2.II**.

Scheme 3.6.2.II. Application of nomenclature rules for stereosimerism about a metal.[3]



There are a number of other cases where it might be advisable to specify the stereochemistry of a complex. These cases involve specifying

- the coordination geometry about a metal center (octahedral, trigonal prismatic, tetrahedral, square planar, etc.)
- the geometry cannot be unambigouously described by a single *cis/trans* or *fac/mer* relaionship of ligands

These cases may also be handled by using a designator to specify the coordination geometry and, as necessary, giving the position of ligated atoms in terms of designated numbered positions for that geometry. See the IUPAC red book for details as such cases fall outside the scope of what is normally advisable for an undergraduate course.

Specify the identity and number of the ligands in alphabetical order by ligand name.

Before specifying the metal, the ligands are written as prefixes of the metal.

In specifying the ligands several rules are followed.

1. The ligands are written in alphabetical order by the ligand name only; symbols are not considered and prefixes do not count in determining alphabetical order.

   Example: In the name of the complex ion $[Co(NH)_3Cl]^{2+}$, pentamminechlorocobalt(II), the ammine ligand is named before the chloro ligand because the order is alphabetical by the ligand name by virtue of which ammine comes before chloro.

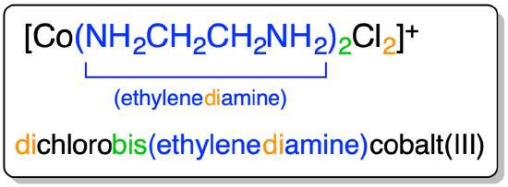
2. Prefixes are used to indicate the number of each ligand present. Specifically, *di-*, *tri-*, *tetra-* , *penta-*, *hexa-*, *etc.* prefixes are used to indicate multiple ligands of the same type EXCEPT when the ligand is polydentate or its name already has a *di-*, *tri-*, *tetra-* etc. In that case *bis-*,*tris-*, *tetrakis-*, etc. are used instead. These prefix rules are summarized in Table **3.6.2.3**.

Table 3.6.2.3. Prefixes used to specify the number of a given ligand present.

Number of identical ligands	prefix used when the ligand name is simple	prefix used when the ligand is polydentate or its name already has a *di-*, *tri-*, *tetra-* etc.
2	di-	bis-
3	tri-	tris-
4	tetra-	tetrakis-
5	penta-	pentakis-
6	hexa-	hexakis-
7	hepta-	heptakis-
8	octa-	octakis-
9	nona-	nonakis-
10	deca-	decakis-

An example of the application of the prefix rule is given in Scheme **3.6.2.III**.

Scheme 3.6.2.III. Example of the use of prefixes to specify the number of ligands of each type in a complex.[3]



3. Ligand names are based on their charge

- Neutral and cationic ligand names are the same as the names of their neutral compounds with two caveats

  i. names that involve spaces should either be put in parentheses or the spaces should be eliminated (preferred)

  Example: cis-dichlorobis(**dimethyl sulfoxide**)platinum(II) or *cis*-dichlorobis(**dimethylsulfoxide**)platinum(II)

  ii. A few ligands are given common names.

  - H_2O = aqua
  - NH_3 = ammine (notice that there are two m's)
  - CO = carbonyl
  - CS = thiocarbonyl
  - NO = nitrosyl

- For anionic ligands, the vowel at the end of their anion names is changed to an -"o"

  Examples: Cl^- = chlorido, NH_2^- = amido, N_3^- = azido

  Caveat: some anionic ligands have common names that may also be used

  Examples:

  I^- = iodo or iodino

  CN^- = cyano or cyanido

O^{2-} = oxo or oxido

The IUPAC and common names of many ligands are given in Tables **3.6.2.1**. and **3.6.2.2**.

4. When an ambidentate ligand is present the atom through which it is bound to the metal is indicated by giving either its element symbol or a κ and its element symbol in italics after the ligand name

   Example:

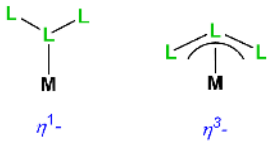
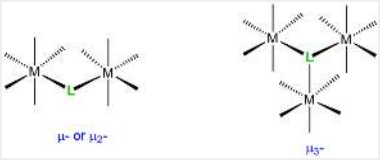
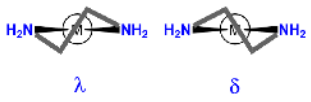
   M-SCN is thiocyanato-*S* or thiocyanato-κ*S*

   M-NCS = thiocyanato-*N or* thiocyanato-κ*N*

   The use of κ and an element symbol to indicate how a ligand and metal are linked is called a **k-term**. More complex k-terms might also involve specifying the atoms by number, though their use is outside the scope of this text.

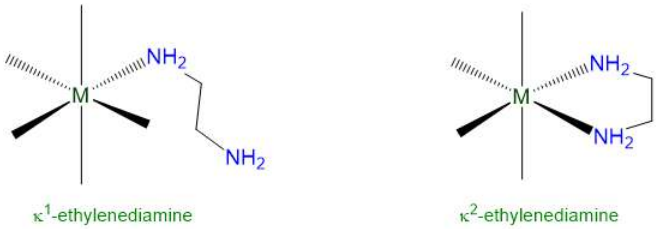
5. As appropriate, additional information about the way a ligand is bound to the metal center and/or its stereochemistry is specified using a prefix. The prefixes to provide linkage and stereochemistry for ligands are given in Table**3.6.2.4**.

Table3.6.2.4. Prefixes used to specify ligands' isomerism when naming and writing coordination compounds' formulae. Some of these types of isomerism will be discussed in later pages.

Type of isomerism	Graphical reminder	Prefixes
when a multidentate ligand binds through less than the full number of atoms		κ^n where n is the number of attached atoms; used when the attached atoms are not directly connected by a chemical bond. The metal-ligand bonding usually involves σ-type coordination.
hapticity		η^n where n is the number of attached atoms; used when the coordinated atoms are all connected by bonds. Usually the metal-ligand bonding involves for π-type coordination. In speech, η^1=monohapto; η^2=dihapto; η^3 =trihapto, etc.
bridging ligands		μ_n where n is the number of atoms bridged. The number n is usually omitted when n =2.
chelating ligand ring twist		λ- or δ-

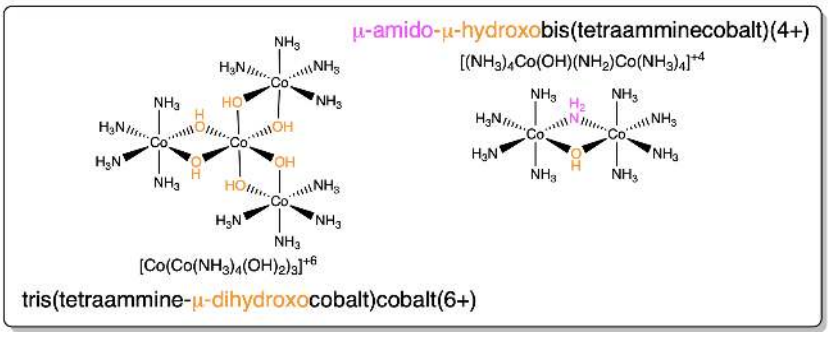
A example showing how the nomenclature rule is applied to a ligand that can have two coordination modes is given in Scheme **3.6.2.IV**.

Scheme 3.6.2.IV. Use of the κ notation to specify the number of attached groups in a multidentate ligand.



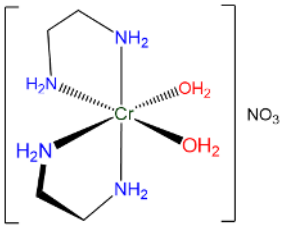
Two examples showing how the nomenclature rule is applied to bridging ligands are given in Scheme **3.6.2.V**. The names of the complexes follow the rules described in 9.2.6: multinuclear coordination complexes.

Scheme 3.6.2.V. Use of the μ notation to specify bridging ligands in metal complexes.[3]



6. If desired, parentheses *may* be used to delineate a ligand name to make it easier to identify in the name. This can be particularly helpful when the name contains a lot of information to keep track of. An example is given in Scheme **3.6.2.VI**.

   Scheme 3.6.2.VI. When naming the complex shown *cis*-diaquabis(ethylenediamine)chromium(III) nitrate is easier to read than *cis*-diaquabisethylenediaminechromium(III) nitrate.



Specify the metal

- In neutral and cationic complexes the metal's name is used directly

  - *e.g.* as in hexammineruthenium(III) for $[Ru(NH_3)_6]^{3+}$

- In anionic complexes, *-ate* replaces *-ium*, *-en*, or *–ese* or adds to the metal name.

  e.g. as in hexachloromanganate(IV) for $MnCl_6^{2-}$

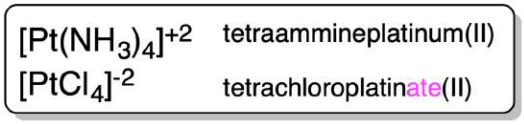
- In anionic complexes of some metals a Latin-derived name is used instead of the element's English name. These names are given in Table **3.6.2.5**.

  Table 3.6.2.5. Latin terms for Select Metal Ions. Redrawn from this page describing the nomenclature of coordination complexes.

Transition Metal	Latin
Copper	Cuprate
Gold	Aurate
Iron	Ferrate
Lead	Plumbate
Silver	Argentate
Tin	Stannate

An example of the application of the metal naming rules is given in Scheme \sf{\PageIndex{VII}}\).

Scheme 3.6.2.VII. Example of the application of the metal specification rules to a cationic and anionic platinum complexes.[3]



Specify the oxidation state of the metal.

Two different systems are used to specify the oxidation state of the metal.

1. In the **Stock system** the metal's oxidation state is indicated in Roman numerals after the metal name.

   Examples:

   $[CoCl(NH_3)_5]Cl_2$ = pentamminechlorocobalt(III) chloride

   $[PtBr_2(bpy)]$ = bipyridinedibromoplatinium(II)

   $K[Ag(SCN)_2]$ = potassium di-*S*-thiocyanatoargentate(I)

2. In the **Ewing-Bassett system** the charge on the complex is specified in Arabic numerals after the complex name. This provides a way of specifying a complex even when the oxidation state of the metal isn't known and, in cases where it is known, the value of the metal's oxidation state may be inferred from the complex ion's charge.

   $[CoCl(NH_3)_5]Cl_2$ = pentamminechlorocobalt(2+) chloride

   $[PtBr_2(bpy)]$ = bipyridinedibromoplatinium(0)

   $K[Ag(SCN)_2]$ = potassium di-*S*-thiocyanatoargentate(1-)

Summary

A graphical summary of the **rules for naming complexes** along with a few examples that you can use to review the nomenclature rules is given in Figure 3.6.2.1. This work by Stephen Contakes is licensed under a Creative Commons Attribution 4.0 International License.

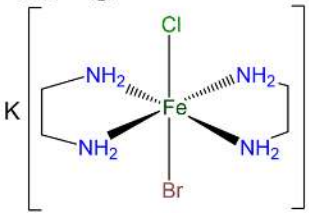
stereochemical prefix-	**Specify Ligands**	**Indicate Metal**	**Charge on the complex or metal oxidation state**
As appropriate use *cis-*, *trans-*, *fac-*, *mer-*, Λ-, Δ-, to indicate stereochemistry.	What ligands and how many? – List alphabetically by ligand name • Neutral – ligand name • Carionic – ligand name • Anionic – change last vowel to "o" – Indicate # by di-, tri-, tetra-, etc. (or bis-, tris-, tetrakis-, etc. if there is a di-, tri-, tetra, etc. in the ligand name) As appropriate, how are the ligands arranged? – Ambidentate – indicate linkage point by κ & italicized element symbol - other structure – use κ^n, η^n, μ_n, λ-, δ- For clarity, parentheses may be used to delineate ligands	Neutral, cationic: English name Anionic – change ending to "ate" - Latin names for Ag, Au, Cu, Fe, Pb, Sn; English for others	Stock system: Metal Oxidation state in capital Roman numerals Ewing-Bassett system: Complex's charge in Arabic numerals

Examples:

$[Ru(NH_3)_6](NO_3)_3$ hexammineruthenium(3+) nitrate or hexammineruthenium(III) nitrate

$K_2[PtCl_4]$ potassium tetrachloroplatinate(2-) or potassium tetrachloroplatinate(II)

$K[Ag(CN)_2]$ potassium dicyanoargentate(1-) or potassium dicyanoargentate(I)



potassium *trans*- bromochlorobis(ethylenediamine)iron(1+) (Ewing-Bassett)

-or-

potassium *trans*-bromochlorobis(ethylenediamine)iron(III) (Stock)

Figure **3.6.2.1**. Summary of nomenclature rules for coordination complexes along with a few examples of their application.

When learning chemical nomenclature practice makes perfect. The following examples and exercises are provided to give you this practice. Additional examples and exercises on the https://chem.libretexts.org/ site include a set of simple examples with explained solutions, a set of simple exercises with solutions, and a set of more challenging exercises without solutions.

Exercise **3.6.2.2**. Assigning metal oxidation states in a complex

In order to name a complex in the Stock system it is necessary to assign a formal oxidation state to the metal.

For this reason it is important to be able to assign the oxidation state of a metal in a complex. Fortunately, this is easy to do if you remember

1. The sum of all atom's oxidation states will equal the overall charge on the complex
2. When determining the metal's oxidation state the ligands can be treated as having an oxidation state equal to their charge - *i.e.* the charge they possess in the form they coordinate the metal so if they need to lose a proton to bind don't forget to account for that.

Given the above, assign the oxidation state of the metal in the following real and hypothetical complexes.

a. $K_3[Fe(CN)_6]$
b. $[CoCl(NH_3)_5](NO_3)_2$
c. $K_2[PtCl_4]$
d. [MnCl(por)]
e. $[Ru(bpy)_3]Cl_2$
f. $[PdCl_2(dppe)]$
g. $[Mn(en)_2(SCN)_2]$

Answer for $K_3[Fe(CN)_6]^{3-}$.

This contains $[Fe(CN)_6]^{3-}$; so O.S.$_{Fe}$ + 6 x (-1) (for CN^-) = -3 (the complexes' charge) so O.S.$_{Fe}$ = +3 or Fe^{3+}.

Answer for $[CoCl(NH_3)_5](NO_3)_2$.

This contains $[CoCl(NH_3)_5]^{2+}$; so O.S.$_{Co}$ + 1 x (-1) (for Cl^-) + 0 x 5 (for NH_3) = +2 (the complexes' charge) so O.S.$_{Co}$ = +3 or Co^{3+}.

Answer for $K_2[PtCl_4]$.

This contains $2K^+$ and $[PtCl_4]^{2-}$; so O.S.$_{Pt}$ + 4 x (-1) (for Cl^-) = -2 (the complexes' charge) so O.S.$_{Pt}$ = +2 or Pt^{2+}.

Answer for [MnCl(por)].

O.S.$_{Pt}$ + 1 x (-2) (for por; see table 9.2.2) + 1 x (-1) (for Cl^-) = +0 (the complexes' charge) so O.S.$_{Mn}$ = +3 or Mn^{3+}.

Answer $[Ru(bpy)_3]Cl_2$.

The complex is $[Ru(bpy)3]^{2+}$ so O.S.$_{Ru}$ + 0 x 3 (for bpy) = +2 (the complexes' charge) so O.S.$_{Ru}$ = +2 or Ru^{2+}.

Answer $[PdCl_2(dppe)]$.

O.S.$_{Pd}$ + 2 x (-1) (for Cl^-) + 0 x 3 (for dppe) = +0 (the complexes' charge) so O.S.$_{Pd}$ = +2 or Pd^{2+}.

Answer $[Mn(en)_2(SCN)_2]$.

O.S.$_{Mn}$ + (2 x 0) (for en) + 2 x (-1) (for SCN^-) = +0 (the complexes' charge) so O.S.$_{Mn}$ = +2 or Mn^{2+}.

Exercise 3.6.2.3: Simple Nomenclature Problems.

Name the following compounds in both the Stock and Ewing-Bassett systems:

a. $[Ru(NH_3)_6](NO_3)_3$
b. $K_2[PtCl_4]$
c. $K[Ag(CN)_2]$
d. $Cs[CuBrCl_2F]$
e. $[Cu(acac)_2]$

Answer

	Complex	Stock system name	Ewing-Bassett System name
a	$[Ru(NH_3)_6](NO_3)_3$	hexammineruthenium(III) nitrate	hexammineruthenium(3+) nitrate
b	$K_2[PtCl_4]$	potassium tetrachloroplatinate(II)	potassium tetrachloroplatinate(2-)
c	$K[Ag(CN)_2]$	potassium dicyanoargentate(I)	potassium dicyanoargentate(1-)
d	$Cs_2[CuBrCl_2F]$	cesium bromodichloroflourocuprate(II)	cesium bromodichloroflourocuprate(2-)
e	$[Cu(acac)_2]$	bis(acetylacetonato)copper(II)	bis(acetylacetonato)copper(0)

Exercise 3.6.2.4: More simple nomenclature problems.

Name the following compounds and ions in both the Stock and Ewing-Bassett systems.

a. $Cu(OH)_4^-$
b. $[AuXe_4]^{2+}$
c. $AuCl_4^-$
d. $Fe(CN)_6^{3-}$
e. $K_4[Fe(CN)_6]$
f. *trans*-$[Cu(en)_2(NO_2)_2]$ (the N is bound to Cu)
g. cis-$IrCl_2(CO)(PPh_3)$ (ignore stereochemistry)
h. $IrCl(PPh_3)$

Answer

	Compound	Stock System Name	Ewing-Bassett System Name
a	$Cu(OH)_4^-$	tetrahydroxocuprate(III) or tetrahydroxidocuprate(III)	tetrahydroxidocuprate(1-) or tetrahydroxidocuprate(1-)
b	$[AuXe_4]^{2+}$	tetraxenongold(II)	tetraxenongold(2+)
c	$AuCl_4^-$	tetrachloroaurate(III)	tetrachloroaurate(1-)
d	$Fe(CN)_6^{3-}$	hexacyanoferrate(III) or hexacyanidoferrrate(III)	hexacyanoferrate(3-) or hexacyanidoferrate(3-)
e	$K_4[Fe(CN)_6]$	potassium hexacyanoferrate(II) or potassium hexacyanidoferrrate(II)	potassium hexacyanoferrate(4-) or potassium hexacyanidoferrrate(4-)
f	*trans*-$[Cu(en)_2(NO_2)_2]$ (the N is bound to Cu)	bis(ethylenediamine)bisnitrocopper(II) or bis(ethylenediamine)bis(nitrito-*κN*)copper(II)	bis(ethylenediamine)bisnitrocopper(0) or bis(ethylenediamine)bis(nitrito-*κN*)copper(0)
g	*cis*-$IrCl_2(CO)(PPh_3)$	*cis*-dichlorocarbonyltriphenylphosphineiridium(I) or *cis*-dichloro(carbonyl)(triphenylphosphine)iridium(I)	*cis*-dichlorocarbonyltriphenylphosphineiridium(0) or *cis*-dichloro(carbonyl)(triphenylphosphine)iridium(0)
h	$IrCl(PPh_3)$	chlorotris(triphenylphosphine)iridium(I)	chlorotris(triphenylphosphine)iridium(0)

Exercise 3.6.2.5: Even more simple nomenclature problems.

Name the following compounds and ions in both the Stock and Ewing-Bassett systems. Ignore prefixes for designating isomers if you haven't learned about those.

a. $Fe(acac)_3$
b. $K_2[CuBr_4]$
c. ReH_9
d. $[Ag(NH_3)_2]BF_4$
e. $[Ag(NH_3)_2][Ag(CN)_2]$

f. $[Ni(CN)_4]^{2-}$
g. $[Co(N_3)(NH_3)_5]SO_4$
h. $[CoBrCl(H_2O)(NH_3)]I$ (ignore stereochemistry)

Sample Answers

	Complex	Stock system name	Ewing-Bassett System name
a	$Fe(acac)_3$	tris(acetoacetato)iron(III)	tris(acetoacetato)iron(0)
b	$Na_2[CuBr_4]$	sodium tetrabromocuprate(II)	sodium tetrabromocuprate(2-)
c	$[Co(NH_3)_6][Co(ox)_3]$	hexamminecobalt(III) tris(oxalato)cobalt(III)	hexamminecobalt(3+) tris(oxalato)cobalt(3-)
d	$[Ag(NH_3)_2]BF_4$	diamminesilver(I) tetrafluoroborate	diamminesilver(1+) tetrafluoroborate
e	$[Ag(NH_3)_2][Ag(CN)_2]$	diamminesilver(I) dicyanoargentate(I) or diamminesilver(I) dicyanidoargentate(I)	diamminesilver(1+) dicyanoargentate(1-) or diamminesilver(1+) dicyanidoargentate(1-)
f	$[Ni(CN)_4]^{2-}$	tetracyanonickelate(II) or tetracyanonickelate(II) ion	tetracyanonickelate(2-) or tetracyanonickelate(2-) ion
g	$[Co(N_3)(NH_3)_5]SO_4$	pentammineazidocobalt(III) sulfate	pentammineazidocobalt(2+) sulfate
h	$[CoBrCl(H_2O)(NH_3)]I$ (ignore stereochemistry)	ammineaquabromochlorocobalt(III) iodide	ammineaquabromochlorocobalt(1+) iodide

Exercise 3.6.2.6: Nomenclature problems, some of which involve consideration of isomerism.

Name the following compounds and ions in both the Stock and Ewing-Bassett systems. Ignore prefixes for designating isomers if you haven't learned about those.

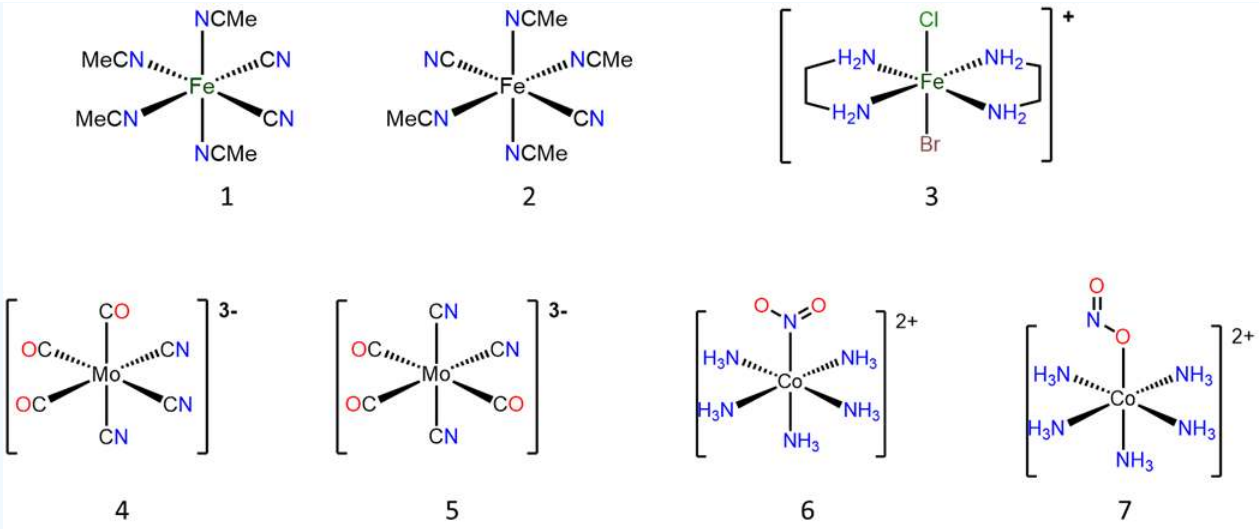
a. *trans*-$[Cu(dppe)_2(NO_2)_2]$ (the N is bound to Cu)
b. $[Pd(en)_2(SCN)_2]$, with the thiocyanates bound Pd-SCN
c. $[Mn(CO)_6]BPh_4$ (BPh_4 = tetraphenylborate)
d. $Rb[AgF_4]$
e. K_2ReH_9
f. K_3CrCl_6
g. $[Ru(H_2O)_6]Cl_2$
h. [*cis*-$Fe(CO)_4I_2$]
i. K_2[*trans*-$Fe(CN)_4(CO)_2$]
j. [*cis*-$MnCl(H_2O)_4(NH_3)$](NO_3)
k. K_3[*fac*-$RuCl_3(PMe_3)_3$]

Answer

	Complex	Stock system name	Ewing-Bassett System name
a	*trans*-$[Cu(dppe)_2(NO_2)_2]$	*trans*-bis(diphenylphosphinoethane)bisnitrocopper(II) or *trans*-bis(diphenylphosphinoethane)bis(nitrito-κN)copper(II)	*trans*-bis(diphenylphosphinoethane)bisnitrocopper(0) or *trans*-bis(diphenylphosphino)ethane bis(nitrito-κN)copper(0)
b	$[Pd(en)_2(SCN)_2]$, with the thiocyanates bound Pd-SCN	bis(ethylenediamine)bisthiocyanatopalladium(II) or bis(ethylenediamine)bis(thiocyanato-*S*)palladium(II) or bis(ethylenediamine)bis(thiocyanato-κS)palladium(II)	bis(ethylenediamine)bisthiocyanatopalladium(0) or bis(ethylenediamine)bis(thiocyanato-*S*)palladium(0) or bis(ethylenediamine)bis(thiocyanato-κS)palladium(0)
c	$[Mn(CO)_6]BPh_4$	hexacarbonylmanganese(I) tetraphenylborate	hexacarbonylmanganese(I) tetraphenylborate
d	$Rb[AgF_4]$	rubidium tetraflouroargentate(III)	rubidium tetraflouroargentate(1-)
e	K_2ReH_9	potassium nonahydridorhenium(VII)	potassium nonahydridorhenium(2-)
f	K_3CrCl_6 or $K_3[CrCl_6]$	potassium hexachlorochromium(III) or potassium hexachloridochromium(III)	potassium hexachlorochromium(3-) or potassium hexachloridochromium(3-)
g	$[Ru(H_2O)_6]Cl_2$	hexaaquaruthenium(II) chloride	hexaaquaruthenium(2+) chloride
h	[*cis*-$Fe(CO)_4I_2$]	*cis*-tetracarbonyldiiodoiron(II)	*cis*-tetracarbonyldiiodoiron(0)
i	K_2[*trans*-$Fe(CN)_4(CO)_2$]	potassium *trans*-dicarbonyltetracyanoferrate(II)	potassium *trans*-dicarbonyltetracyanoferrate(2-)
j	[*cis*-$MnCl(H_2O)_4(NH_3)$] (NO_3)	*cis*-amminetetraaquachloromanganese(0) nitrate	*cis*-amminetetraaquachloromanganese(1+) nitrate
k	K[*fac*-$RuCl_3(PMe_3)_3$]	potassium *fac*-trichlorotris(triphenylphosphine)ruthenium(II)	potassium *fac*-trichlorotris(triphenylphosphine)ruthenium(1-)

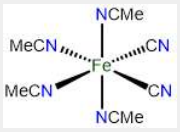
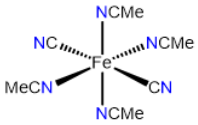
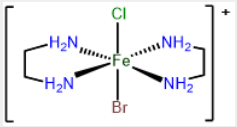
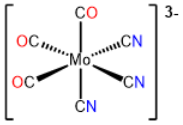
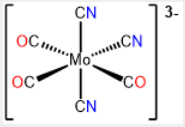
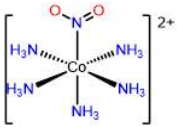
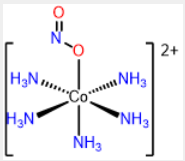
Exercise 3.6.2.7

Name the compounds and ions belowusing both the Stock and Ewing-Bassett systems. Ignore prefixes for designating isomers if you haven't learned about those.



https://chem.libretexts.org/@go/page/484727

Answer

#	Structure	Stock system name	Ewing-Bassett system name
1		*cis*-tetraacetonitriledicyanoiron(II) or *cis*-tetraacetonitriledicyanidoiron(II)	*cis*-tetraacetonitriledicyanoiron(0) or *cis*-tetraacetonitriledicyanoiron(0)
2		*trans*-tetraacetonitriledicyanoiron(II) or *trans*-tetraacetonitriledicyanidoiron(II)	*trans*-tetraacetonitriledicyanoiron(0) or *trans*-tetraacetonitriledicyanidoiron(0)
3		*trans*-bromochlorobis(ethylenediamine)iron(III) or *trans*-bromidochloridobis(ethylenediamine)iron(III)	*trans*-bromochlorobis(ethylenediamine)iron(1+) or *trans*-bromidochloridobis(ethylenediamine)iron(1+)
4		*fac*-tricarbonyltricyanomolybdate(0) or *fac*-tricarbonyltricyanidomolybdate(0)	*fac*-tricarbonyltricyanomolybdate(3-) or *fac*-tricarbonyltricyanidomolybdate(3-)
5		*mer*-tricarbonyltricyanomolybdate(0) or *mer*-tricarbonyltricyanidomolybdate(0)	*mer*-tricarbonyltricyanomolybdate(3-) or *mer*-tricarbonyltricyanidomolybdate(3-)
6		pentammineitrito-*N*-cobalt(III), pentammineitrito-κ*N*-cobalt(III), or pentammineitrocobalt(III)	pentammineitrito-*N*-cobalt(2+), pentammineitrito-κ*N*-cobalt(2+), or pentammineitrocobalt(2+)
7		pentammineitrito-*O*-cobalt(2+), pentammineitrito-κ*O*-cobalt(2+), or pentammineitritocobalt(2+)	pentammineitrito-*O*-cobalt(2+), pentammineitrito-κ*O*-cobalt(2+), or pentammineitritocobalt(2+)

Exercise 3.6.2.8

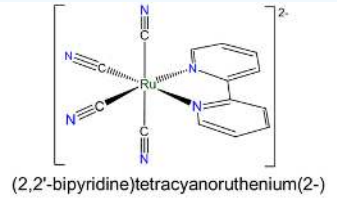
Draw structural formulae for the following compounds and ions. You may assume that

- complexes in which the metal has a coordination number of six are octahedral
- complexes in which the metal has a coordination number of five are trigonal bipyramidal
- complexes in which Pt^{II} , Pd^{II} , or Rh^{I}, or Ir^{I} have a coordination number of four are square planar
- other complexes in which the metal has a coordination number of four will be tetrahedral

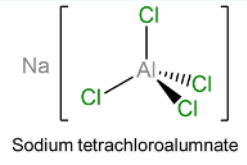
a. (2,2'-bipyridine)tetracyanoruthenium(2-)
b. sodium tetrachloroalumnate (note that since Al is a main group metal with a generally fixed oxidation state no oxidation state is given)
c. pentaamminechlorocobalt(2+) sulfate
d. carbonylhydridotris(triphenylphosphine)rhodium(I) (the ligands in this complex occupy sterically preferred positions)
e. bromotrichlorocobaltate(III)
f. hexaaquacopper(2+) sulfate
g. sodium tris(oxalato)cobalt(III)
h. *fac*-(1,10-phenanthroline)tricarbonylchlororhenium(I)
i. *mer*-triaquatrichlorochromium(III)
j. *trans*-dichlorobis(ethylenediamine)platinum(IV)

Answers

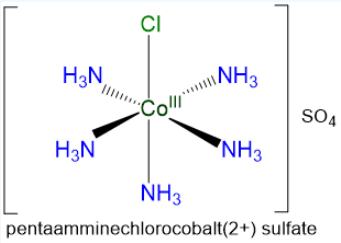
a



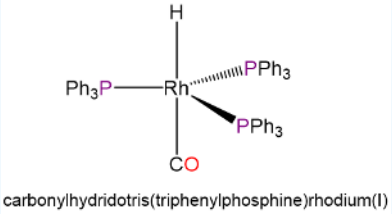
b



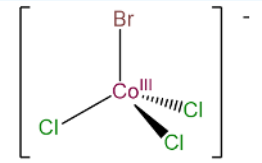
c



d

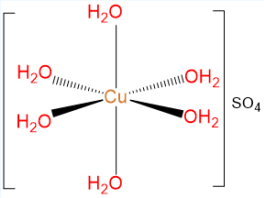


e



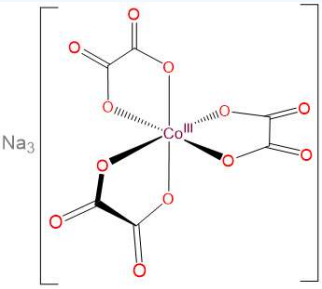
bromotrichlorocobaltate(III)

f



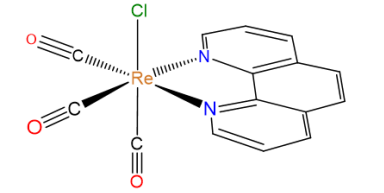
hexaaquacopper(2+) sulfate

g



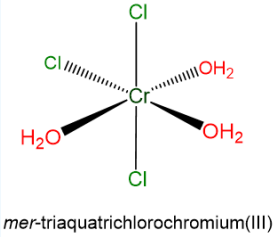
sodium tris(oxalato)cobalt(III)
Λ-enantiomer shown

h



fac-(1,10-phenanthroline)tricarbonylchlororhenium(I)

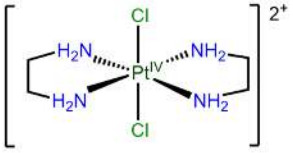
i



mer-triaquatrichlorochromium(III)

j

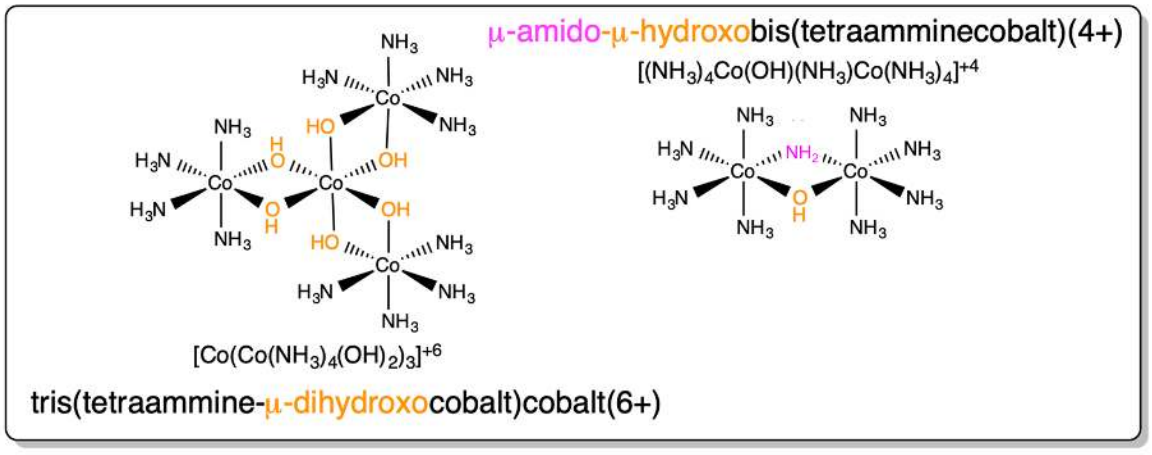
https://chem.libretexts.org/@go/page/484727



trans-dichlorobis(ethylenediamine)platinum(IV)

Exercise 3.6.2.9.

The name of the structure named tris(tetraammine-μ-dihydroxocobalt)cobalt(6+) in Scheme **3.6.2.III** (reproduced below) is incomplete. Give the complete name of the structure in both the Stock and Ewing-Basset systems.



Answer

Δ-tris(tetraammine-μ-dihydroxocobalt)cobalt(6+) or **Δ**-tris(tetraammine-μ-dihydroxocobalt(III)cobalt(III)

Rules for Writing Chemical Formulas

The rules for writing the formulas of coordination compounds follow the same general convention used to specify their names, but are not always adhered to in the chemical literature. Organized predictable formulae can be easier to read and understand than haphazardly written ones the rules for writing the formulae of coordination compounds have value. The rules as given here are adapted from a summary by Robert Lancashire.

1.If there are multiple ions present list the cations before anions.

2.Enclose all the constituents of each complex ion in square brackets.

3.For each complex ion,

- Give the **central metal** atom first.
- Then **ligands** next, listed in alphabetical order, ignoring prefixes according to the first letters in the ligand's symbol as written. This is true regardless of whether the symbol is an element symbol (like C, N, O, etc.) or a symbol for the ligand name (bpy, en, MeCN, etc.). Contrary to widely-circulated myths, the ligand's charge does not matter.[4]
- The formulae or abbreviations (*e.g.* en) for all polyatomic ligands should be enclosed in ordinary parentheses.
- As appropriate, use italicized atom symbols to indicate linkage isomerism and prefixes such as *cis*-, *trans*-, *fac*-, *mer*-, **Λ**-, **Δ**-, κ^n, η^n , μ_n, **λ**-, \or (\delta\)- to indicate stereochemistry.
- When a ligand is bound to a metal through a particular atom, preferably place that atom closest the metal - *e.g.* $[Fe(CN)_6]^{3-}$ not $[Fe(NC)_6]^{3-}$ (Note: this rule primarily is used for ambidentate ligands; although IUPAC reccomends that aqua ligands be written as OH_2 when the O would be closest to its coordinated metal they are still usually written as H_2O).

These rules are graphically summarized in Figure **3.6.2.2**.

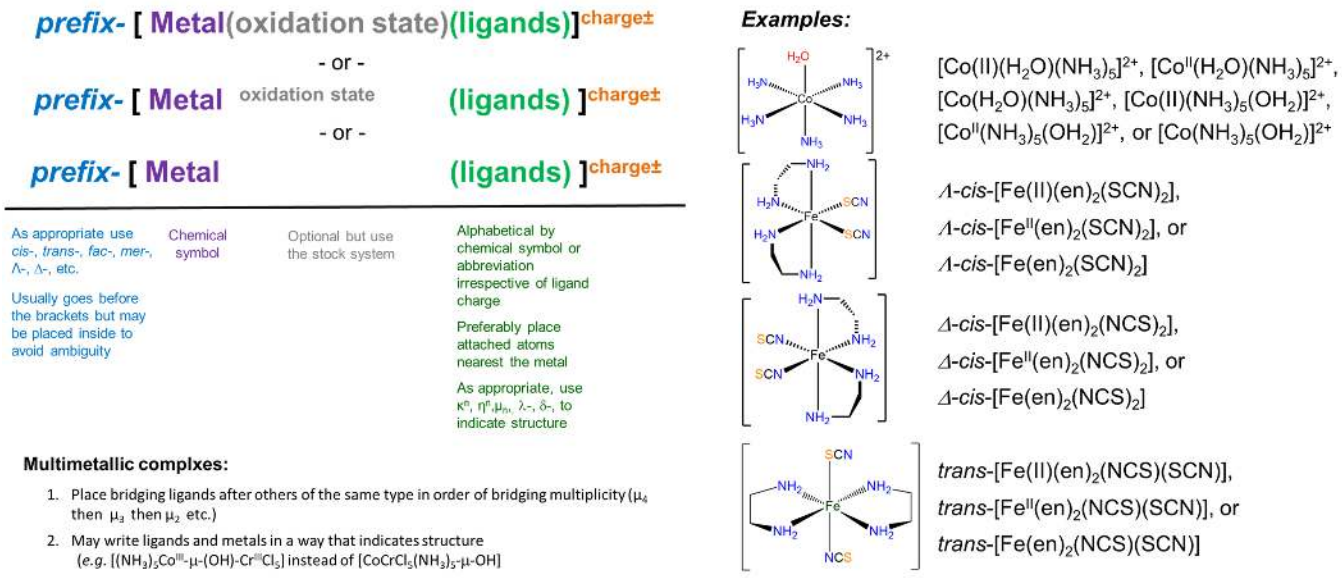
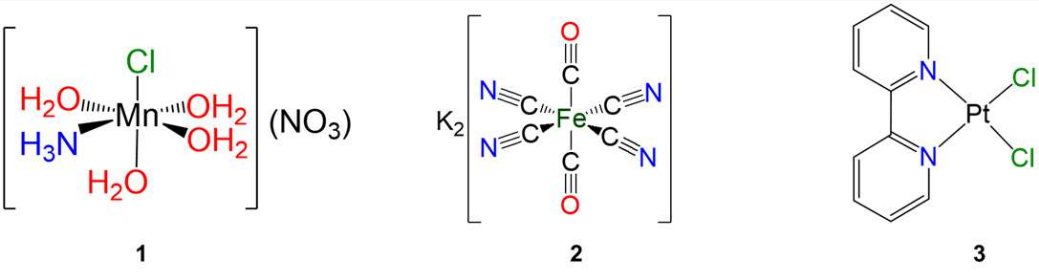


Figure **3.6.2.2.** Summary of the rules for writing the formula of a coordination complexes along with a few examples of their application. This work by Stephen Contakes is licensed under a Creative Commons Attribution 4.0 International License.

Exercise 3.6.2.10

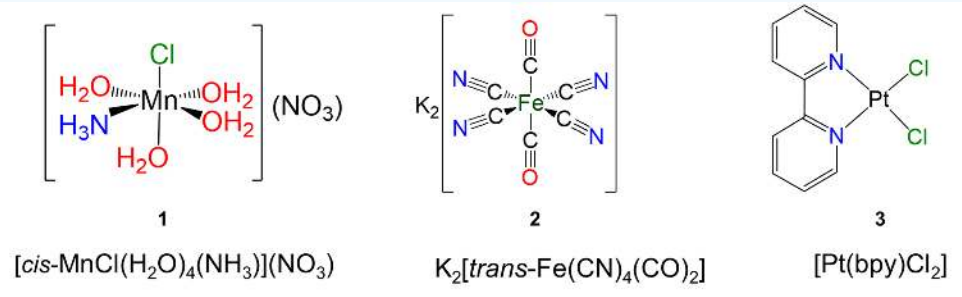
Give the formulae of the following complexes.



1 2 3

.

Answer



1 2 3

[*cis*-MnCl(H2O)4(NH3)](NO3) K2[*trans*-Fe(CN)4(CO)2] [Pt(bpy)Cl2]

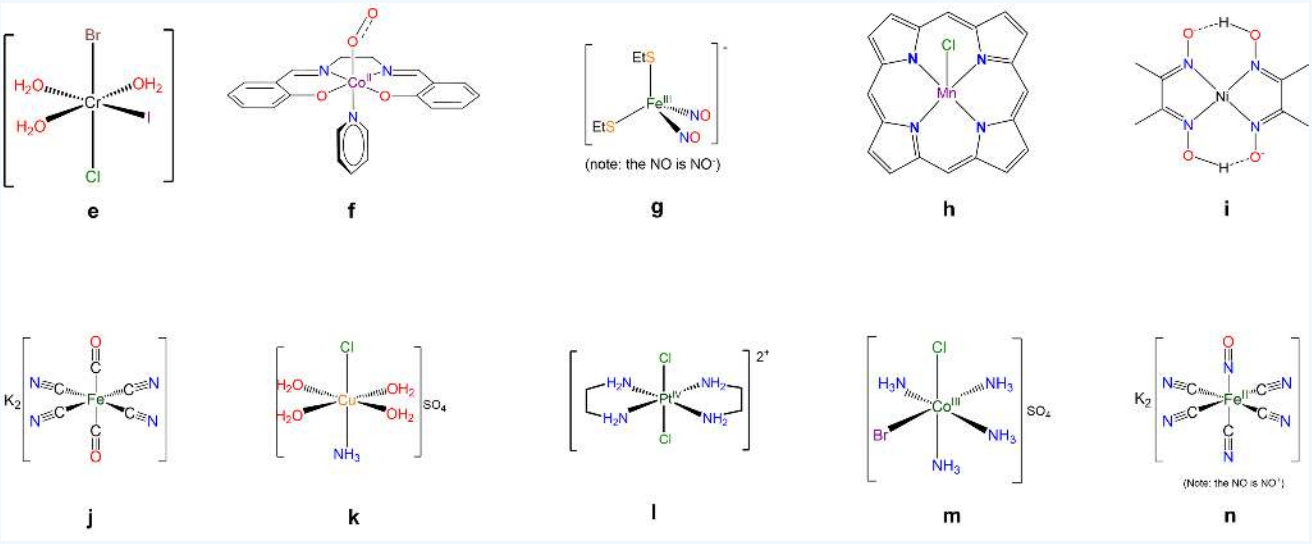
Exercise 3.6.2.11

Write formulae for each of the following compounds and ions. When multidentate ligands are present use suitable abbreviations.

a. pentaamminechlorocobalt(2+) sulfate
b. Δ-diamminebis(oxalato)manganate(III)

c. *trans*-tetraacetonitriledicyanoiron(II)

d. tricarbonyldichlorobis(triphenylphosphine)molybdenum



Answers

a.

$[CoCl(NH_3)_5](SO_4)$

b.

Δ-$[Mn(NH_3)_2(ox)_2]^-$

c.

trans-$[Fe(CN)_2(NCMe)_4]$

d.

$[MoCl_2(CO)_3(PPh_3)]$ or $MoCl_2(CO)_3(PPh_3)$

e.

mer-$[CrBrCl(H_2O)_3I]$

f.

$[Co(O_2)py(salen)]$

g.

$[Fe(NO)_2(SEt)_2]^-$

h.

[NiCl(por)] or $[MnCl(porphyrin)]^-$

i.

$[Ni(DMG)_2]$ or $[Ni(Hdmg)_2]$

j.

potassium *trans*-$[Fe(CN)_2(CO)_4]$

k.

trans-$[CuCl(H_2O)_4(NH_3)]SO_4$

l.

trans-$[PtCl_2(en)_2]^{2+}$

m.

cis-$[CoBrCl(NH_3)_4]SO_4$

n.

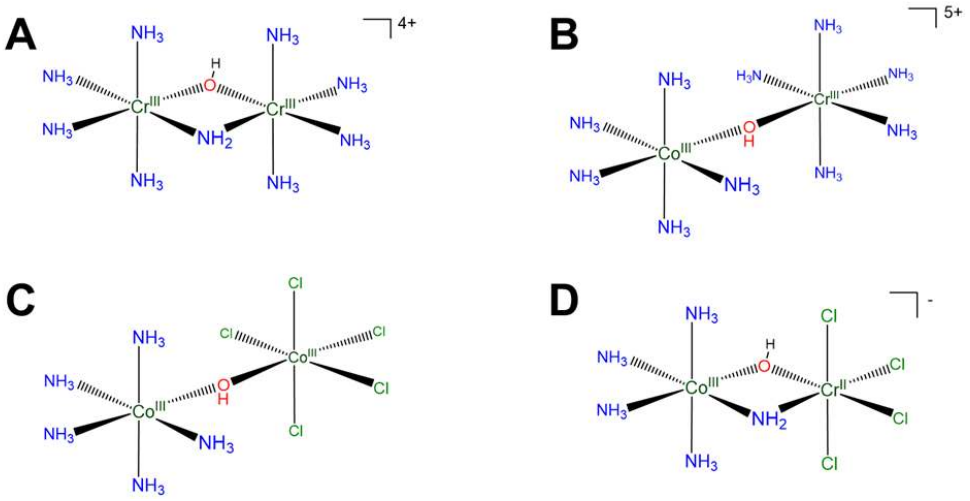
$K_2[Fe(CN)_5NO]$

Multinuclear Coordination Complexes

Multinuclear coordination complexes contain multiple metals connected by one or more bridging ligands. The structures of bridging complexes can usually be inferred from their μ-tagged ligands in their names and formulae. For the benefit of instructors who wish to have their students name multinuclear complexes.

Multinuclear complexes are named differently depending on whether the groups on either side of the bridging ligands are identical or different, as shown in Scheme **3.6.2.VIII**.

Scheme 3.6.2.VIII. Multinuclear coordination complexes may be named differently depending on whether the groups on either side of the bridging ligands are the same or different. The groups are the same if the metal, ligands, and ligand arrangement are identical. This is true in A but in B the metals differ, in C the ligands differ, and in D both the metal and ligands differ.



Naming multinuclear complexes

Let's look at the rules for naming symmetric and asymmetric multinuclear complexes.

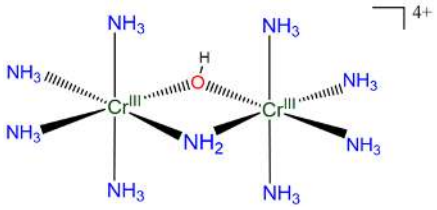
Symmetric complexes

The IUPAC naming system helpfully avoids the sort of ambiguities and *ad hoc* choices involved in most textbook-level nomenclature systems for multimetallic complexes. Unfortunately, it is correspondingly difficult for beginners to employ. Thus it will only be applied in depth to the case of symmetric complexes. Symmetric complexes are particularly easy to name in the IUPAC system and several of its variants that find common use. In these

1. The ligands are given in alphabetical order. When there are bridging and non-bridging ligands of the same type the bridging ligands are given first. When there are multiple bridging ligands of the same type but which use different bridging modes (*e.g.* μ_4-, μ_3-, μ_2-) the bridging ligands are specified in decreasing order of bridging multiplicity, *e.g.* μ_3 -sulfido-di-μ-sulfido.
2. The groups bridged are given afterwards using names that follow the ordinary rules. Generally this either involves
   a. naming all the ligands followed by all the metals, in both cases using prefixes to indicate the number of each
   b. naming each group of atoms individually as in the less formal naming system, using prefixes to indicate the number of ligands (this is an unofficial variant of the IUPAC system that some textbook authors seem to prefer).

These two rules are sufficient to describe simple symmetric bridging complexes.

Example: The compound in Scheme **3.6.2.VIIIA**



may be named

[μ-amido-μ-hydroxo-octaamminedichromium(4+)] ion

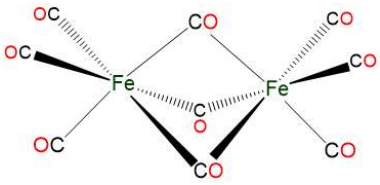
or

[μ-amido-μ-hydroxo-bis(tetraamminechromium(III))] ion

or

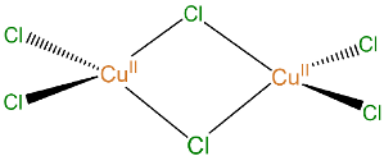
[μ-amido-μ-hydroxo-bis(tetraamminechromium)(4+)] ion

Example: The complex[5]



may be named [tri-μ-carbonyl-bis(tricarbonyliron)(0)], [tri-μ-carbonyl-bis(tricarbonyliron(0))], or [tri-μ-carbonyl-hexacarbonyldiiron)(0)]

Example: The complex



may be named di-μ-chlorido-tetrachloridodicopper(II), di-μ-chlorido-bis(dichlorocopper(II)), or di-μ-chlorido-bis(dichlorocopper)(0)

Asymmetric complexes

For a symmetrical complex like the $[Cu_2Cl_4(\mu\text{-}Cl)_2]$ considered above it is enough to specify the existence of the two bridging and four terminal chloro ligands; there is no need to number the chloro ligands or to specify exactly which ones are involved in bridging or to clarify that the bridging involves κ^2 coordination of the chloro ligands. In cases where the two metal centers or the chloro ligands differ it is necessary to specify the exact ligands and metals involved and how they are connected.

For example, a more extensive IUPAC name for $[Cu_2Cl_4(\mu\text{-}Cl)_2]$ in which the chloro ligands are individually and more completely specified would read di-μ_2-chlorido-tetrachlorido-1κ^2Cl,2κ^2Cl-dicopper(II).

Even more extensive systems would involve numbering the metals and specifying how they are connected together too. The details of how this is done are typically beyond the level of most undergraduate and graduate courses in inorganic chemistry. Those who want to know the details should consult the red book. In many cases it is sufficient to reserve the use of formal IUPAC names for use in publications and to employ a comvenient shorthand naming system for everyday use. An example of one type of system that is sometimes employed is given next.

Unofficial methods

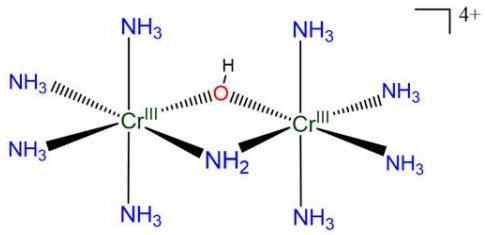
It can be quite complicated to use the IUPAC system to name asymmetric multinuclear coordination complexes. Fortunately it is rarely necessary and there are a variety of simpler somewhat *ad hoc* methods that work well for such cases. Since these methods

are commonly used by textbooks and inorganic instructors it is likely worth your while to learn about their general features. In these methods

1. A multinuclear complex is named as a derivative of one of the metal centers and the other metal centers and their ligands are treated as ligands to the prioritized metal center.
2. Unfortunately, most of the time the choice of which metals are part of the ligands and which one is central is made haphazardly. In other words, there is no agreed upon system for assigning which metal center is the central metal and which should be regarded as part of the ligands around it. One way to be more systematic about the selection of the central and ligand-embedded metals is to assign the central metal as the metal of highest priority in the IUPAC priority rules. In the IUPAC priority rules he central metal is the highest priority metal alphabetically by name; then if there is a tie the ligands on each tied metal center are ranked alphabetically and the tied metal center with the highest priority (or most highest priority) ligands wins.
3. The metal centers not chosen as the primary metal center and all ligands around them, including those bridging to the winning metal center, are then treated as a single ligand that coordinates the winning metal center.
4. When naming the ligands and the overall complex, again there is much that is haphazard. However, in the best systems each coordination sphere is named using the same rules as for mononuclear complexes - *i.e.* the ligands are given in alphabetical order, etc.
    - This is true of any metal center-containing ligands.
    - When there is a bridging and non-bridging ligand of the same type the bridging ligands are given first. When there are multiple bridging ligands of the same type but which use different bridging modes (*e.g.* μ_4-, μ_3-, μ_2-) the ligands are specified in decreasing order of bridging multiplicity, *e.g.* μ_3 -sulfido-di-μ-sulfido.

Let's apply these rules to the examples in Scheme **3.6.2.VIII**.

Compound A:



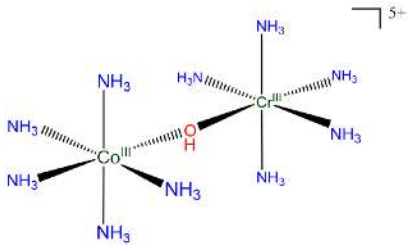
Using hydroxo for the OH^- it may be named

[(μ-amido-tetraammine-μ-hydroxochromium(III))tetraamminechromium(III)] ion

or

[(μ-amido-tetraammine-μ-hydroxochromium)chromium(4+)] ion

Compound B:



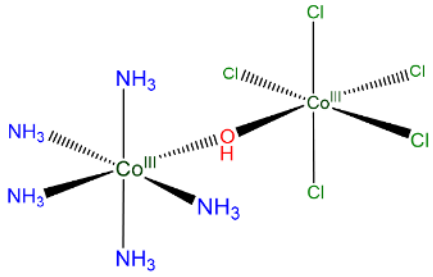
Using hydroxo for OH^- it may be named

[(pentaammine-μ-hydroxocobalt(III))tetraamminechromium(III)] ion

or

[(pentaammine-μ-hydroxocobalt)tetraamminechromium(5+)] ion

Compound C:



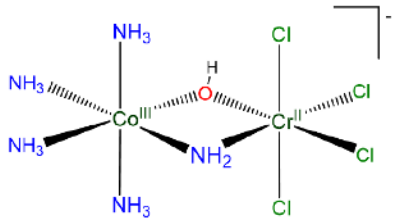
Using hydroxo for OH^- it may be named

[pentaammine(pentachloro-μ-hydroxocobalt(III))cobalt(III)]

or

[pentaammine(pentachloro-μ-hydroxocobalt)cobalt](0)]

Compound D:



Using hydroxo for OH^- and chloro for Cl^- it may be named

[pentaammine(pentachloro-μ-hydroxocobalt(III))chromate(III)] ion

or

[(tetrammine-μ-ammine-μ-hydroxocobalt)tetrachlorochromate](1-)] ion

As can be seen from the examples above this system gives serviceable names for multimetallic complexes but those names are not the IUPAC names and so should not be used to describe complexes outside of pedagogical and informal settings.

Writing and interpreting formulas for multinuclear complexes

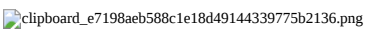
The rules for writing formulae for multinuclear complexes are the same as form mononuclear ones with two added details

1. Write bridging ligands after nonbridging ligands of the same type. For example, Cu_2Cl_6 should be written as $[Cu_2Cl_4$-μ-$Cl)_2]$
2. Although you may ignore that and other rules if you find it helpful to keep groups of metals and ligands together in a way that better convey how the atoms are connected. Just as the structure of ethane may be more clearly conveyed as H_3CCH_3 instead of CH_3CH_3 the complex $[Cu_2Cl_4\mu$-$Cl)_2]$ may be written as $[(Cl_2Cu)(\mu$-$Cl)_2(CuCl_2)]$

Other Examples:

For dichromate write, $[Cr_2O_6(\mu$-$O)]^{2-}$ or $[O_5Cr$-μ-O-$CrO_5]^{2-}$

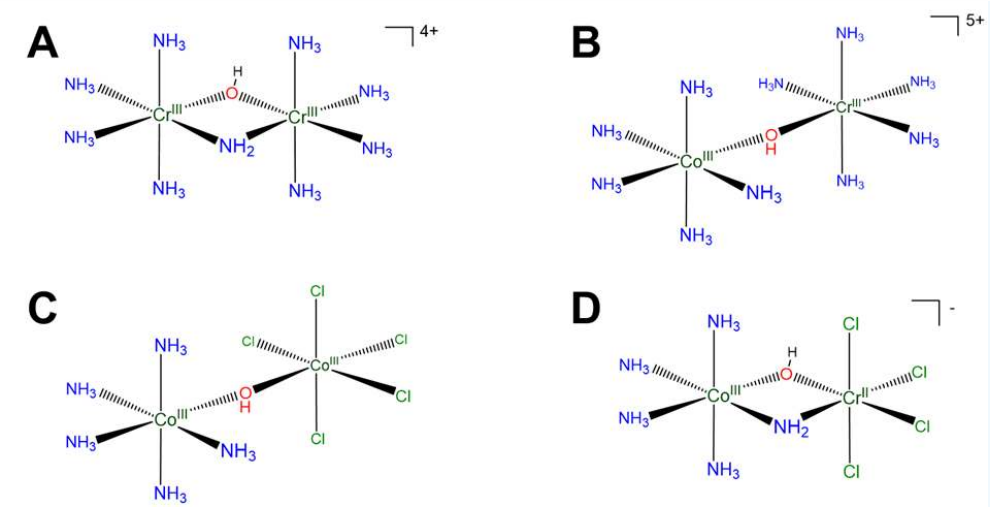
For compound C of Scheme **3.6.2.VIII**.



write $[Co_2Cl_5(NH_3)_5(\mu$-$OH)]$ or, even better, $[(H_3N)_5Co(\mu$-$OH)CoCl_5]$.

Exercise 3.6.2.10

Write reasonable formulae for complexes A, B, and D in Scheme **3.6.2.VIII**, which for convenience is reproduced below.



Sample answers for A

$[Cr_2(NH_3)_8\text{-}\mu(NH_2)\text{-}\mu(OH)]^{4+}$ or $[(H_3N)_4Cr^{III}\text{-}\mu(NH_2)\text{-}\mu(OH)\text{-}Cr^{II}(NH_3)_4]$ and variants thereof involving writing the H_3N as NH_3, μ as μ_2, etc.

Sample answers for B

$[CoCr(NH_3)_{10}\text{-}\mu(OH)]^{5+}$ or, better, $[(H_3N)_5Co^{III}\text{-}\mu(OH)\text{-}Cr^{III}(NH_3)_5]^{5+}$

Sample answers for C

This was already done as an example above, $[Co_2Cl_5(NH_3)_5\text{-}\mu(OH)]$ or, better, $[(NH_3)_5Co^{III}\text{-}\mu(OH)\text{-}Co^{III}Cl_5]$ and variants thereof

Sample answers for D

$[CoCrCl_4(NH_3)_4\text{-}\mu(NH_2)\text{-}\mu(OH)]$ or, better, $[(H_3N)_4Co^{III}\text{-}\mu(NH_2)\text{-}\mu(OH)\text{-}Cr^{II}Cl_4]$

References

1. International Union of Pure and Applied Chemistry *Nomenclature of Inorganic Chemistry* Cambridge, UK, 2005.

2. The structure and name is taken from Choudhury, S. B.; Allan, C. B.; Maroney, M.; Wodward, A. D.; Lucas, C. R. *Inorg. Synth.* **1998**, *32*, 98-107.

3. Haas, K. Naming Transition Metal Complexes. https://chem.libretexts.org/Courses/Saint_Mary's_College%2C_Notre_Dame%2C_IN/CHEM_342%3A_Bio-inorganic_Chemistry/Readings/Week_2%3A_Introduction_to_Metal-Ligand_Interactions_and_Biomolecules/2.1_Transition_metal_complexes/2.1.6%3A_Naming_Transition_Metal_Complexes

4. There is a widely-circulated myth that anionic ligands should be names before neutral ones. This myth is false. According to the IUPAC red book (bolding mine):

IR-2.15.3.4: Ordering ligands in formulae and names In formulae of coordination compounds,

The formulae or abbreviations representing the ligands **are cited in alphabetical order as the general rule**. Bridging ligands are cited immediately after terminal ligands of the same kind, if any, and in increasing order of bridging multiplicity. (See also Sections IR-9.2.3 and IR-9.2.5.)

IR-9.2.3.1 Sequence of symbols within the coordination formula

(i) The central atom symbol(s) is (are) listed first.

(ii) The **ligand symbols (line formulae, abbreviations or acronyms) are then listed in alphabetical order** (see Section IR-4.4.2.2).5 Thus, CH_3CN, MeCN and NCMe would be ordered under C, M and N respectively, and CO precedes Cl

because single letter symbols precede two letter symbols. **The placement of the ligand in the list does not depend on the charge of the ligand.**

(iii) More information is conveyed by formulae that show ligands with the donor atom nearest the central atom; this procedure is recommended wherever possible, even for coordinated water.

5. Technically organometallic complexes are named according to slightly different rules but the coordination compound naming system works here. Note that this complex was once thought to possess an Fe-Fe bond, in accordance with the predictions of the 18 electron rule. Consequently, older sources often give an [*Fe-Fe*] after the name to reflect the presence of that bond. However, as the complex is no longer though to possess an Fe-Fe bond it is omitted here.

Contributors and Attributions

Stephen Contakes, Westmont College, to whom comments, corrections, and criticisms should be addressed.

with some examples taken from Naming Transition Metal Complexes by Kathryn Haas.

Consistent with the policy for original artwork made as part of this project, all unlabeled drawings of chemical structures are by Stephen Contakes and licensed under a Creative Commons Attribution 4.0 International License.

3.6.2: Nomenclature and Ligands is shared under a CC BY-NC-SA 4.0 license and was authored, remixed, and/or curated by LibreTexts.

- **9.3: Nomenclature and Ligands** by Stephen M. Contakes has no license indicated.
- **8.2: Nomenclature and Ligands** is licensed CC BY-NC-SA 4.0.

SECTION OVERVIEW

3.6.3: Acid-Base and Donor-Acceptor Chemistry

3.6.3.1: Acid-Base Models as Organizing Concepts

3.6.3.2: Lewis Concept and Frontier Orbitals

3.6.3.2.1: The frontier orbital approach considers Lewis acid-base reactions in terms of the donation of electrons from the base's highest occupied orbital into the acid's lowest unoccupied orbital.

3.6.3.2.2: All other things being equal, electron withdrawing groups tend to make Lewis acids stronger and bases weaker while electron donating groups tend to make Lewis bases stronger and acids weaker

3.6.3.2.3: The electronic spectra of charge transfer complexes illustrate the impact of frontier orbital interactions on the electronic structure of Lewis acid-base adducts

3.6.3.2.4: Substances' solution phase Lewis basicity towards a given acid may be estimated using the enthalphy change for dissociation of its adduct with a reference acid of similar hardness.

3.6.3.2.5: In the boron trifluoride affinity scale, the enthalphy change on formation of an adduct between the base and boron trifluoride is taken as a measure of Lewis basicity.

3.6.3.2.6: Lewis base strength may also be estimated by measuring structural or energy changes upon formation of a Lewis acid-base complex, as illustrated by efforts to spectroscopically assess the strengths of halogen bonds

3.6.3.2.7: Bulky groups weaken the strength of Lewis acids and bases because they introduce steric strain into the resulting acid-base adduct.

3.6.3.2.8: Frustrated Lewis pair chemistry uses Lewis acid and base sites within a molecule that are sterically restricted from forming an adduct with each other.

3.6.3.3: Hard and Soft Acids and Bases

3.6.3.3.1: Hard-Hard and Soft-Soft preferences may be explained and quantified in terms of electrostatic and covalent and electronic stabilization on the stability of Lewis acid-base adducts

3.6.3.3.2: Quantitative Measures of Hardness, Softness, and Acid-Base Interactions from a Hard Soft Acid-Base Principle Perspective Involve Orbital Energies and/or Apportioning Acid-Base Bonding in Terms of Electrostatic and Covalent Factors

3.6.3.4: Problems

3.6.3: Acid-Base and Donor-Acceptor Chemistry is shared under a CC BY-NC-SA 4.0 license and was authored, remixed, and/or curated by LibreTexts.

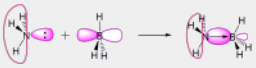
3.6.3.1: Acid-Base Models as Organizing Concepts

> *In a very real sense, we can make an acid anything we wish. The differences between the various acid-base concepts are not concerned with which is 'right', but which is most convenient to use in a particular situation.*
>
> *James E. Huheey, Ellen A. Keiter, and Richard L. Keiter*

The concept of acids and bases is often associated with the movement of hydrogen ions from one molecule or ion to another. However, a host of acid-base concepts have been developed to help chemists organize and make sense of a wide range of reactions (Table 6.1).

Table 6.1. Summary of major acid-base models.

Definition	Theoretical paradigm and notable features.	Acid	Base	Illustrative sample reactions
Arrhenius (1894)	Interested in what the substance does to the state of an aqueous solution. In particular it assesses proton donation to & removal from water using [H_3O^+] as a proxy. Readily accommodates the pH concept as a measure of the state of a solution.	Increases [H_3O^+]	Decreases [H_3O^+]	$\underset{acid}{HCl} + H_2O \rightarrow H_3O^+ + Cl^-$ $\underset{base}{NH_3} + H_2O \rightarrow NH_4^+ + OH^-$
Brønsted-Lowry (1923)	Envisions acid-base reactivity in terms of the transfer of an H^+ from one substance to another. Allows for conjugate acids and bases and solvent autoionization.	Donates H^+	Accepts H^+	$\underset{acid}{HCl} + \underset{base}{NH_3} \rightarrow \underset{conj.\ acid}{NH_4^+} + \underset{conj.\ base}{Cl^-}$ $\underset{acid}{HOAc} + \underset{base}{NH_3} \rightarrow \underset{conj.\ acid}{NH_4^+} + \underset{conj.\ base}{OAc^-}$ $\underset{amphoteric}{2\ H_2O} \rightarrow \underset{conj.\ acid}{H_3O^+} + \underset{conj.\ base}{OH^-}$
Lux-Flood (1939-~47)	Describes reactions involving oxides and oxyanions in terms of the transfer of oxide ion (O^{2-}). Mainly used in geochemistry, although it also can be used to describe some redox reactions.	Oxide acceptor	Oxide donor	$\underset{acid}{SiO_2} + \underset{base}{CaO} \rightarrow CaSiO_3$ $\underset{base}{H_2O} + \underset{acid}{CO} \rightarrow H_2 + CO_2$
Solvent System	Applies aspects of the Arrhenius , Brønsted-Lowry, and Lux-Flood acid base concepts to solvent cation & anion formation in a generalized reaction. Can be used to describe solution chemistry in nonaqueous solvent systems like BrF_3.	Is a solvent cation or increases the solvent cation concentration, often by receiving a lone pair- bearing group	Is a solvent anion or increases the solvent anion concentration, often by donating a lone pair- bearing group	$\underset{acid}{SbF_5} + \underset{base}{BrF_3} \rightarrow \underset{conj.\ base}{SbF_6^-} + \underset{conj.\ acid}{BrF_2^+}$ $\underset{amphoteric}{2\ BrF_3} \rightarrow \underset{conj.\ acid}{BrF_2^+} + \underset{conj.\ base}{BrF_4^-}$
Lewis (1923)	Envisions acid-base reactivity in terms of electron pair donation. Encompasses the Arrhenius , Brønsted-Lowry, Lux-Flood, and Solvent System definitions and readily	Accepts an electron pair	Donates an electron pair	$\underset{base}{:NH_3} + \underset{acid}{BF_3} \rightarrow H_3N + BF_3$

Definition	Theoretical paradigm and notable features.	Acid	Base	Illustrative sample reactions
	integrates with molecular orbital descriptions of chemical reactivity in Frontier orbital theory.			
Nucleophile-Electrophile	Applies the Lewis concept to organic reactivity. Nucleophiles are Lewis bases which tend to react to form a bond with Lewis acid sites called electrophilic centers.	(The electrophile) Tends to react by receiving an electron pair from a nucleophile, forming a bond in the process	(The nucleophile) Donates an electron pair to form a bond to an electrophile	$\underset{base}{Br^-} + \underset{acid}{CH_3-Cl} \rightarrow Br-CH_3 + Cl^-$
Usanovich (1939)	Extends Lewis theory to include the donation and acceptance of any number of electrons, whether through the formation of an adduct or electron transfer.	Accepts electrons	Donates electrons	$\underset{base}{:NH_3} + \underset{acid}{BH_3} \rightarrow \underset{adduct}{H_3N-BH_3}$ $\underset{acid}{Fe^{2+}} + \underset{base}{Zn^0} \rightarrow Fe^0 + Zn^{2+}$
Frontier Orbital (1960s)	Envisions Lewis Acid-base/Electrophile-nucleophile reactions in terms of the donation and acceptance of electrons between the reactant's frontier orbitals. Specifically, the reaction is envisioned in terms of donation of the base's HOMO electrons into the acid's LUMO level.	Possesses a LUMO capable of forming an occupied bonding MO on mixing with a base's HOMO.	Possesses an electron-bearing HOMO capable of forming a filled bonding MO on mixing with an acid's LUMO.	 base acid adduct

Some concepts involve defining acids and bases in particular ways that allow for the understanding of particular types of chemical systems. For example, the familiar Arrhenius and Brønsted acid and base concepts used in general chemistry help chemists make sense of the behavior of compounds which can transfer H^+ ions among themselves, often in aqueous solution. However, the solvent system acid-base concept defines acids and bases in terms of the transfer of a lone-pair bearing group and is particularly useful for conceptualizing the reactivity of main group halides, oxides, and related compounds. Some acid-base definitions seek to encompass an extremely wide range of chemical reactions. For instance, the Lewis acid-base definition encompasses the Arrhenius , Brønsted, and solvent system definitions and has also found wide use in inorganic chemistry owing to the ease with which Lewis acid-base interactions may be described by the Frontier Orbital approach in terms of interacting molecular orbitals on the acid and base.

References

Huheey, J. E.; Keiter, E. A.; Keiter, R. L., *Inorganic Chemistry: Principles of Structure and Reactivity. 4th ed.*; HarperCollins: New York, NY, 1993, pg. 318.

3.6.3.1: Acid-Base Models as Organizing Concepts is shared under a CC BY-NC-SA 4.0 license and was authored, remixed, and/or curated by Stephen M. Contakes.

- **6.1: Acid-Base Models as Organizing Concepts** by Stephen M. Contakes is licensed CC BY 4.0.

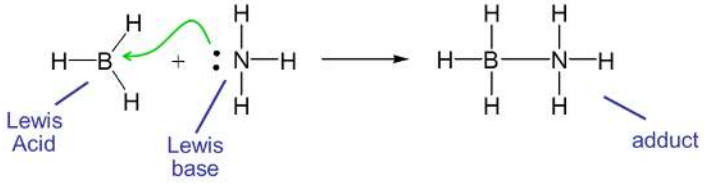
3.6.3.2: Lewis Concept and Frontier Orbitals

The Lewis acid-base concept generalizes the Brønsted and solvent system acid base concepts by describing acid-base reactions in terms of the donation and acceptance of an electron pair.

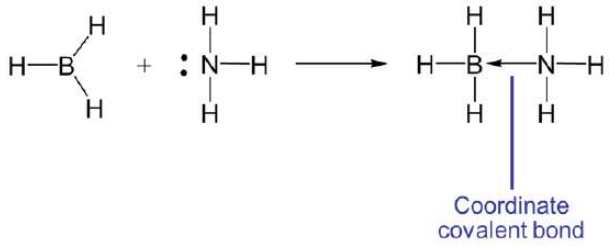
Under the Lewis definition

- **Lewis acids** are electron pair acceptors
- **Lewis bases** are electron pair donors

and in Lewis acid-base reactions, a Lewis base donates an electron pair to the Lewis acid, which accepts it. The reaction between borane, BH_3, and NH_3 is the classic example:

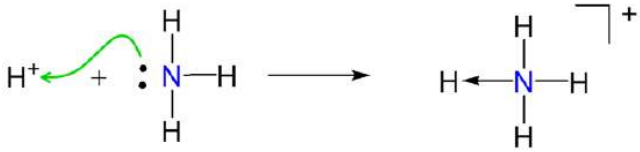


In this case the Lewis acid-base reaction results in the formation of a bond between BH_3, and NH_3. When the acid and base combine to form a larger unit, that unit is said to be an adduct, and the resulting bond is said to be a coordinate covalent or dative bond. Such coordinate covalent bonds are often represented by an arrow that indicates the direction of electron donation from the base to the acid. For instance, the reaction between BH_3 and NH_3 could also have been written as

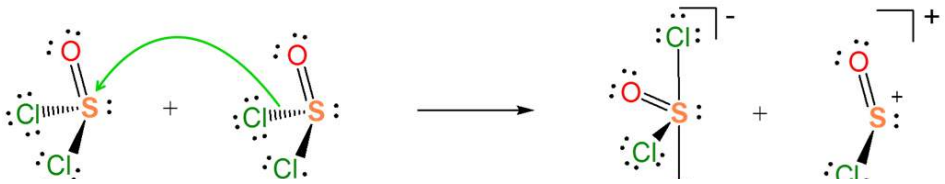


The arrow notation for the coordinate covalent bond is really just a convenient formalism - a bookkeeping tool to help keep track of where the electrons came from and where they might return if the reverse reaction occurs. In actuality a coordinate covalent bond is just an ordinary covalent bond like any other.

For example, in Brønsted acid-base reactions, the hydrogen ion is an acid because it accepts an electron pair from the Brønsted base. Consequently, under the Lewis acid-base concept, Brønsted acid-base reactions involve the formation of an adduct between H^+ and a base.



The Lewis acid-base concept nicely explains ionization reactions involving nonaqueous solvents. For instance, the autoionization of $SOCl_2$ is an acid-base reaction between two $SOCl_2$ molecules.



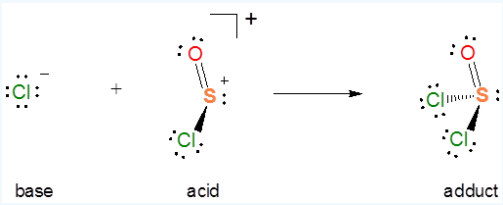
:Cl:

Example 3.6.3.2.1

Explain how the autoionization of $SOCl_2$ is a Lewis acid-base displacement reaction.

Solution

In the autoionization of $SOCl_2$ the pair of electrons donated comes from the S-Cl bond, and the S-Cl bond is broken to give a lone pair bearing a Cl^- base and an $SOCl^+$ Lewis acid fragment. If you are having trouble seeing how this works, it can be instructive to consider the reverse of this process. It is a Lewis acid-base reaction to give a Lewis acid-base adduct:

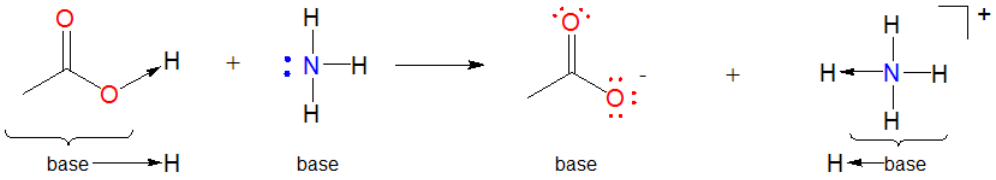


From the autoionization reaction it is also apparent that $SOCl_2$ itself acts as a Lewis acid towards the liberated Cl^-. So the autoionization reaction involves a transfer of the Cl^- base between the two Lewis acids - a Lewis acid-base displacement reaction.



It can be helpful to keep several distinctions in mind when using the Lewis acid-base concept to describe chemical reactions.

1. Many Lewis-Acid base reactions are displacement reactions. This is because the hydrogen ion is usually bound to something at the start of the reaction. In such cases the Lewis acid H^+ unit is transferred from one Lewis base to another :



Such acid-base reactions are sometimes called displacement reactions since the base group in the initial Lewis acid-base complex is displaced by the incoming Lewis base to generate another complex.

2. Substances are sometimes considered amphoteric because they exhibit Lewis acidity and basicity at different types of atomic centers. The classic example is aluminum hydroxide, $Al(OH)_3$. In water $Al(OH)_3$ can act as a Lewis acid towards OH^- ion. The reaction occurs by formation of an adduct at $Al(OH)_3$'s Al^{3+} center:

$$Al(OH)_3 + OH^- \rightarrow Al(OH)_4^-$$

Notice that in addition to acting as a Lewis acid, in this reaction $Al(OH)_3$

- does not act as a Brønsted acid or base since no H^+ ion transfer occurs
- but does act as an Arrhenius acid since OH^- ion is consumed from solution, decreasing $[OH^-]$ and increasing $[H^+]$

In water $Al(OH)_3$ also acts as a Lewis base towards H^+ through the lone pairs on its hydroxide ligands.

$$Al(OH)_3 + 3H^+ + 3H_2O \rightarrow Al(H_2O)_6^{3+}$$

Notice that in addition to acting as a Lewis base, in this reaction $Al(OH)_3$ also acts as a

- Brønsted base, since a H^+ ion is transferred onto the OH^- ligand
- Arrhenius base, since H^+ ion is consumed from solution, decreasing $[H^+]$
- Lewis acid at its Al^{3+} center, since Al-O metal-ligand bonds are formed

Substances that rapidly undergo Lewis acid-base reactions are called nucleophiles and electrophiles.

Two factors govern the course of chemical reactions - thermodynamics and kinetics. Thermodyamics determines what possible fates of the reaction can take place while kinetics determines which among those possible fates will take place quickly under a particular set of reaction conditions. Because of this, it can be helpful to distinguish Lewis acids and bases that tend to undergo reaction quickly with one another from those which do so more slowly. For this reason, synthetic chemists use the terms electrophile and nucleophile to refer to Lewis acids and bases that react quickly:

- electrophile - Lewis acids that rapidly react with a given Lewis base or class of Lewis bases are said to be good electrophiles
- nucleophile - Lewis bases that rapidly react with a given Lewis acid or class of Lewis acids are said to be good nucleophiles

The electrophile-nucleophile concept is sometimes referred to as the Ingold-Robinson acid-base concept after two organic chemists who did much to illustrate the utility of thinking about Lewis acid-base reactions in kinetic terms.

Several distinctions that should be kept in mind when using the electrophile-nucleophile/Ingold-Robinson concept to think about chemical reactivity:

1. Whether a given Lewis acid or base is able to react rapidly depends on the reaction conditions and the substrate (substance it is reacting with). This means that in principle, the terms nucleophile and electrophile should not be used without appropriately qualifying what the substances act as a nucleophile or electrophile towards and under what conditions. Unfortunately this is rarely done. In such cases, the conditions and substrate must be inferred from the context. For instance, when you learned that the chloride ion is a good nucleophile when studying organic chemistry, what was meant is that chloride is a good nucleophile towards electrophilic carbon atoms in organic molecules.

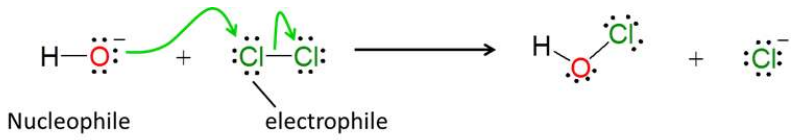
2. Acid and base strength and electrophilicity-nucleophilicity are not exactly the same thing. In many contexts where Lewis acids and bases are classified as electrophilic and nucleophilic substances, it is common to also refer to substances as being good acids or bases on the basis of their Brønsted acidity and basicity. In these contexts, the terms acid and base typically refer to the thermodynamic propensity of a substance to give and accept hydrogen ions while the terms nucleophile and electrophile refer to a substance's kinetic propensity to react with carbon-based Lewis acids and bases, respectively.

A substance may be both a good nucleophile and a strong Brønsted base. For instance, alkyllithium carbanion reagents and alkali metal hydrides are strong bases and good nucleophiles towards electrophilic carbon atoms in organic solvents at moderate temperatures. However, this is not always the case. Under such conditions iodide ion, I^-, is a good nucleophile towards electrophilic carbon atoms but is a poor Brønsted base (it is the conjugate of the strong acid HI). In fact, for the halide ions the order of Brønsted basicity is the opposite of the order of nucleophilicity towards electrophilic carbon:

stronger Brønsted base: F^-, Cl^-, Br^-, I^-: weaker Brønsted base

better nucleophlie: I^-, Br^-, Cl^-, F^-: poorer nucleophile

3. Although the nucleophile-electrophile concept is most often used to describe organic reactions, it is also useful for describing inorganic reactions as well. For instance, the formation of hypochlorite ion in chlorine water possibly involves nucleophilic attack of hydroxide on an electrophilic chlorine atom in an S_N2 type process:



The Usanovich Acid-base Concept

The Usanovich Acid-base concept encompasses a wider range of reactions than the Lewis acid-base concept but is perhaps too general to serve as a convenient framework for understanding reaction chemistry. The Usanovich acid-base concept was developed by the Russian chemist Mikhail Usanovich and extends the Lewis acid-base concept's definition of acids and bases as electron pair donors and acceptors even further. Within the Usanovich definition:

- Acids are anything that accepts electrons, increases cation concentrations, decreases anion concentrations, or reacts with bases
- Bases are anything that donates electrons, increases anion concentrations, decreases cation concentrations, or reacts with acids

These definitions essentially expand the Lewis definition by removing the requirement that the electrons donated or accepted be a pair and practically mean that Usanovich acid-base reactions include Lewis acid-base reactions plus oxidation-reduction reactions. In other words:

- Usanovich acids are Lewis acids plus oxidants
- Usanovich bases are Lewis bases plus reductants

Under this definition BF_3, Fe^{3+}, and $[Fe(CN)_6]^{3-}$ all act as acids, and : NH_3, CN^-, and Zn are all bases:

$$\underset{acid}{BF_3} + \underset{base}{NH_3} \rightarrow F_3B-NH_3$$

$$\underset{acid}{Fe^{3+}} + 6\underset{base}{CN:^-} \rightarrow [Fe(CN)_6]^{3-}$$

$$2\underset{acid}{[Fe(CN)_6]^{3-}} + \underset{base}{Zn} \rightarrow 2[Fe(CN)_6]^{3-} + Zn^{2+}$$

However, notice that while it is easy to think about how any acids might interchangeably react with a given base (and vice versa), under the other acid-base concepts chemists have found it more difficult to think about reactions between oxidants/reductants and Lewis acids and bases. For example, it is difficult to think about how a reaction between BF_3 and Zn metal might occur. Would two Zn donate a pair of electrons to the BF_3? For this reason, most chemists find it more convenient to think about Lewis acid-base and redox reactions under separate categories rather than unite them under the Usanovich definition.

$$2\underset{oxidant}{[Fe(CN)_6]^{3-}} + \underset{reductant}{Zn} \rightarrow 2[Fe(CN)_6]^{3-} + Zn^{2+}$$

Again, it can be helpful to remember Huheey's dictum that deciding between acid-base concepts is not a matter of which concept is the most correct but rather of which is more convenient for a given application.

3.6.3.2: Lewis Concept and Frontier Orbitals is shared under a CC BY-NC-SA 4.0 license and was authored, remixed, and/or curated by Stephen M. Contakes.

- **6.4: Lewis Concept and Frontier Orbitals** by Stephen M. Contakes is licensed CC BY 4.0.

3.6.3.2.1: The frontier orbital approach considers Lewis acid-base reactions in terms of the donation of electrons from the base's highest occupied orbital into the acid's lowest unoccupied orbital.

Another way the Lewis-Acid base concept is widely employed for understanding chemical reactivity is through the frontier orbital approach to chemical reactions. The frontier orbital concept conceptualizes chemical bonding and reactivity in terms of the interactions between frontier orbitals on the chemical species undergoing an interaction (*e.g.* molecules, atoms, ions, or groups as they interact to form a bond or undergo a reaction). Frontier orbitals are those at the frontier between occupied and unoccupied. They are often taken to be the highest energy occupied and lowest energy unoccupied molecular orbitals, called the HOMO and LUMO levels. However, it can sometimes be more convenient to think about them as atomic orbitals or Valence Bond approach-derived orbitals. When developing rough qualitative frontier orbital descriptions of the orbital interactions involved in a given system, the choice of what types of orbitals to use is often a matter of what is the most informative and convenient.

In particular, the frontier orbital concept envisions a Lewis acid-base interaction as involving an interaction between some of the frontier orbitals of the Lewis acid and base, specifically the donation of electrons from the base's HOMO level into the acid's LUMO level. For example, in the frontier orbital approach, adduct formation between $\boldsymbol{NH_3}$ and $\boldsymbol{BH_3}$ involves the donation of electrons from ammonia's a_1 HOMO into BH_3's a_2'' LUMO level.

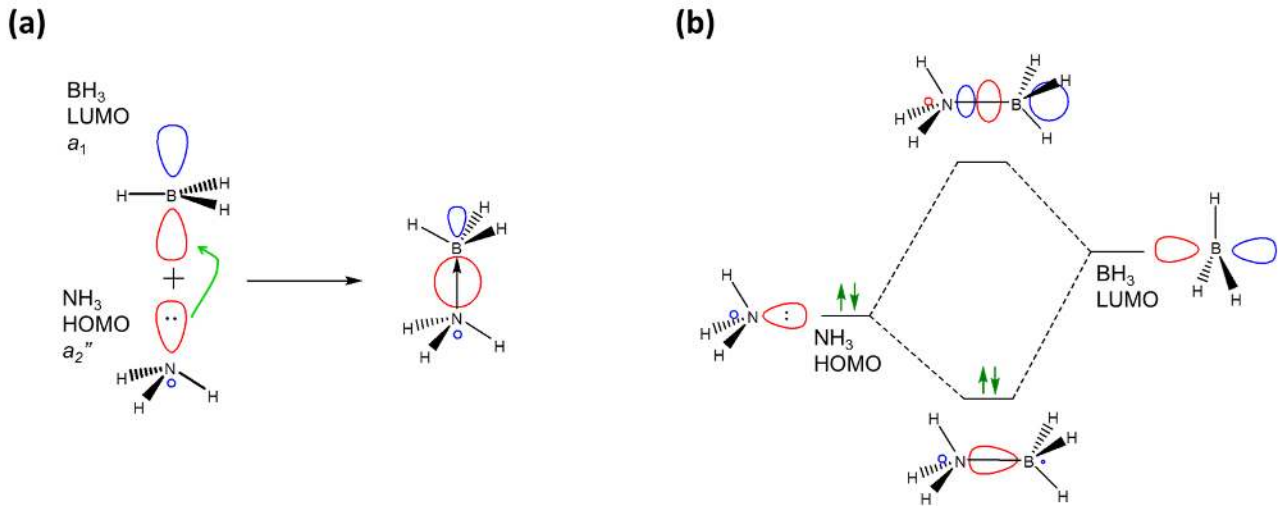


Figure **3.6.3.2.1.1**. Frontier orbital picture of adduct formation between ammonia and borane. (a) As $\boldsymbol{NH_3}$ and $\boldsymbol{BH_3}$ approach one another, interaction between the $\boldsymbol{NH_3}$ HOMO and $\boldsymbol{BH_3}$ LUMO gives a bonding MO. (b) Partial molecular orbital diagram for $\boldsymbol{NH_3} \rightarrow \boldsymbol{BH_3}$ showing the stabilization of the base ($\boldsymbol{NH_3}$) lone pair in a sigma bonding MO upon adduct formation.

As expected when two orbitals of the appropriate symmetry combine, the result of the interaction is the formation of a lower energy bonding orbital between the acid and base (Figure **3.6.3.2.1.1**). Since it is occupied by an electron, the net result of the interaction is the lowering of the base's lone pair energy as it interacts with the Lewis acid. In this case the interaction just follows the general pattern for Lewis-Acid base adduct formation, which is:

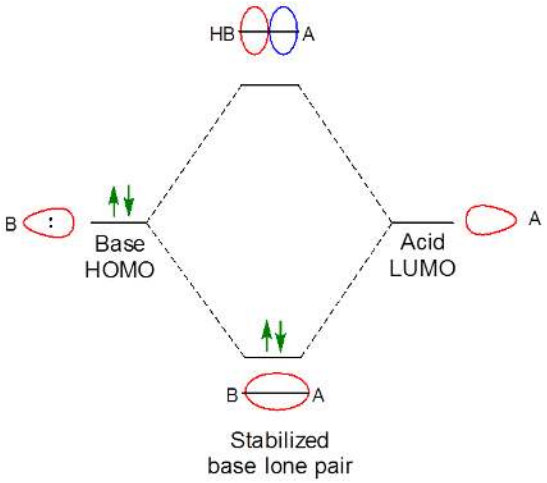
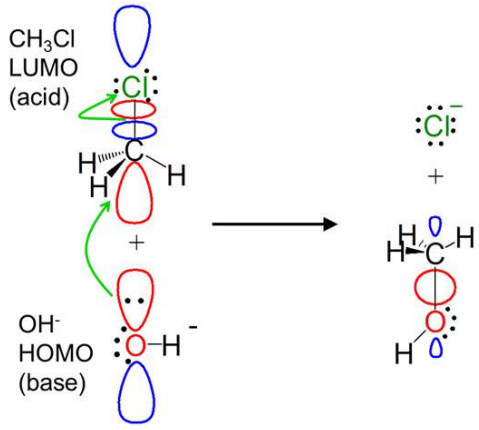


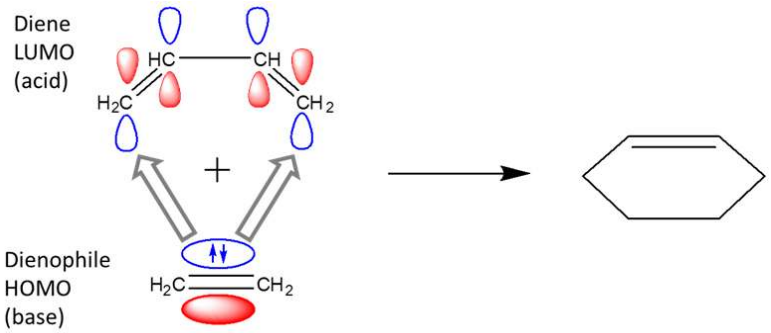
Figure **3.6.3.2.1.2**. Generalized frontier orbital picture for adduct formation between a Lewis base (B) and a Lewis acid (A) involving stabilization of the lone pair of the base HOMO by formation of a bonding orbital with the acid LUMO. The relative energies of the acid LUMO and base HOMO affect the character of the bonding and antibonding MOs but are otherwise unimportant in determining the general features of the interaction. In some cases the base HOMO is higher in energy; in others the acid LUMO is higher in energy; in still others they are equal in energy. In any case the net result is the stabilization of the base lone pair.

The frontier orbital concept illuminates the orbital interactions involved in reactions. For instance, from a frontier orbital perspective the alkyl halide substitution reaction between hydroxide and CH_3Cl via the S_N2 mechanism involves a Lewis acid-base interaction:

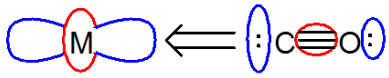


Notice how the frontier orbital approach even explains the displacement of the chloride leaving group. The donation of electrons from the hydroxide HOMO populates the antibonding CH_3Cl LUMO, breaking the C-Cl bond.

With the frontier orbital approach, it becomes apparent that pericyclic reactions are Lewis acid-base reactions. For example, in the Diels-Alder reaction, the dienophile acts as a Lewis base and the diene as a Lewis acid.



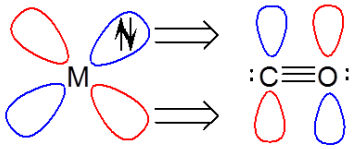
The orbital interactions involved in a given reaction can include both reactants acting as both an acid and base. In these cases the HOMO of each reactant interacts with the LUMO of the other. A good example of this involves **Π**-type interactions between a metal ion with occupied *d* orbitals and a pi-acceptor ligand. The ligand acts as a base and the metal as an acid to give a M-CO single bond:



Metal LUMO (d_{z^2}) acts as an acid

Carbon monoxide HOMO acts as a base

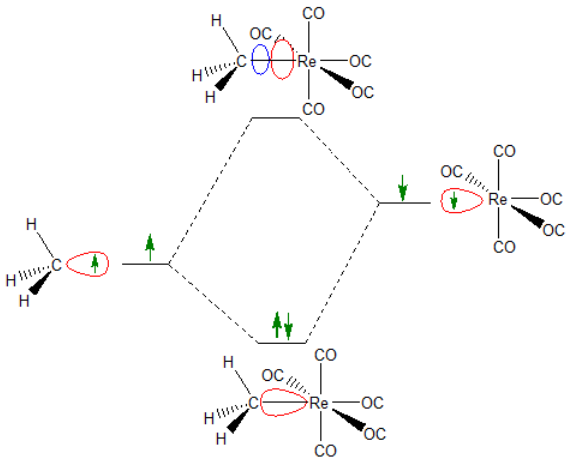
However, the metal can also act as a base towards the ligand LUMO (π^*) orbitals.



Metal HOMO (d_{xz}, d_{xz}) acts as a base

Carbon monoxide LUMO (π^*) acts as an acid

The frontier orbital concept can also be used to describe interactions between one or more singly occupied frontier orbitals. In fact, when approximate molecular orbital diagrams are being constructed, it can often be helpful to focus on one or two particularly instructive interactions. In these cases, it is sometimes convenient to think about a chemical bond as involving the formation of bonding and antibonding interactions between singly occupied frontier orbitals on different molecular fragments. For instance, when thinking about the chemistry of $CH_3Re(CO)_5$ it can sometimes be helpful to think about the C-Re bond as arising from the interaction between a singly-occupied sp^3 type orbital on a CH_3 group and a singly occupied d^2sp^3 orbital on the Re.



In introducing singly occupied orbitals, the frontier orbital concept formally handles interactions that the Lewis acid-base concept does not, since Lewis acid-base behavior is formally confined to the acceptance and donation of electron *pairs*.

3.6.3.2.1: The frontier orbital approach considers Lewis acid-base reactions in terms of the donation of electrons from the base's highest occupied orbital into the acid's lowest unoccupied orbital. is shared under a CC BY-NC-SA 4.0 license and was authored, remixed, and/or curated by Stephen M. Contakes.

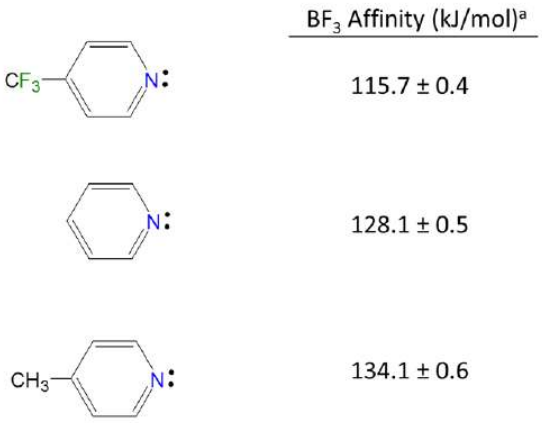
- **6.4.1: The frontier orbital approach considers Lewis acid-base reactions in terms of the donation of electrons from the base's highest occupied orbital into the acid's lowest unoccupied orbital.** by Stephen M. Contakes is licensed CC BY 4.0.

3.6.3.2.2: All other things being equal, electron withdrawing groups tend to make Lewis acids stronger and bases weaker while electron donating groups tend to make Lewis bases stronger and acids weaker

The electrons donated from a Lewis base to a Lewis acid in a Lewis acid-base reaction are donated and accepted at particular atomic centers. For instance, the formation of an adduct between ammonia and BF_3 involves the donation of the lone pair on the ammonia nitrogen atom to the Lewis acid site on BF_3.



Because Lewis acid-base reactions involve electron donation and acceptance at particular sites, substituent groups which alter the electron density at a site through inductively donating or withdrawing electron density will affect the Lewis acid-base properties of that site. For instance, the BF_3 affinities of 4-substituted pyridines increase slightly as the substituent on the aromatic ring is changed from electron donating Me to electron withdrawing CF_3.



a) Data from Laurence, C.; Gal, J.-F. o., *Lewis basicity and Affinity Scales: Data and Measurement. John Wiley: Chichester, West Sussex, U.K., 2010; pp. 91-101.*

Substituent inductive effects are much as one might predict. Since Lewis bases donate electron pairs and Lewis acids accept them:

- electron withdrawing substituents tend to decrease the Lewis basicity of basic sites while electron donating substituents increase site Lewis basicity by making them more electron rich.
- electron withdrawing substituents increase the Lewis acidity of acidic sites by making those sites more electron deficient while electron donating substituents tend to decrease Lewis acidity by making sites less electron deficient.

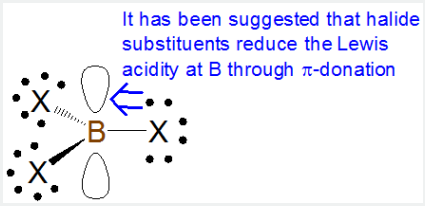
Nevertheless it can be difficult to predict substituent-based trends in Lewis acidity and basicity by inductive effects alone. This is because inductive effects are modest and often exists in competition with other substituent effects, such as

- Steric effects, discussed in section 6.4.7
- Hardness effects, discussed in section 6.6
- π-donation and acceptance effects, which can increase or decrease electron density at a given site as well as create an energy barrier for any structural distortions that might occur upon adduct formation.

Avoid misconceptions about the impact of π donation and acceptance on Lewis acid-base affinity

As with σ-based induction effects, π-donation tends to increase Lewis basicity and decrease Lewis acidity while π-withdrawal tends to decrease Lewis basicity and increase Lewis acidity. However, care needs to be taken in assessing the effect of π-

donation effects on Lewis acidity and basicity. For example, some textbooks claim that the Lewis acidity of boron trihalides is dominated by the reduction of boron acidity through π-donation from the halide substituents:

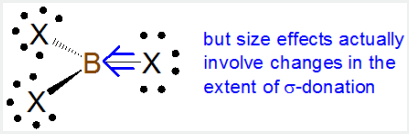


According to this explanation, the extent of this π-donation decreases down the halogen group as the boron-halogen bond distance decreases. This is consistent with the observed trend in Lewis acidity of the boron trihalides towards most bases, which runs counter to that suggested by inductive effects alone:

$$BI_3 > BBr_3 > BCl_3 >> BF_3$$

However, computational work suggests that this explanation is incorrect, since

- atomic size effects are important mainly for substituents in which the connected atom is in row 3+ or higher;
- atomic size effects mainly involve changes in the extent of σ-overlap. In other words, the larger halogens are less able to reduce the electron deficiency at the boron center through σ interactions while π-interactions play little or no role.



References:

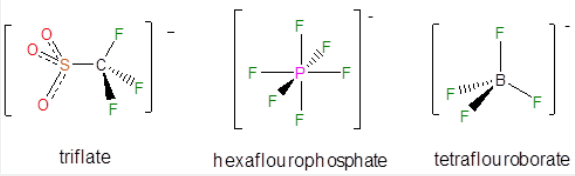
1. Plumley, J. A.; Evanseck, J. D., Periodic Trends and Index of Boron Lewis Acidity. *The Journal of Physical Chemistry A* 2009, 113 (20), 5985-5992.

2. Jupp, A. R.; Johnstone, T. C.; Stephan, D. W., Improving the Global Electrophilicity Index (GEI) as a Measure of Lewis Acidity. *Inorganic Chemistry* 2018, 57 (23), 14764-14771.

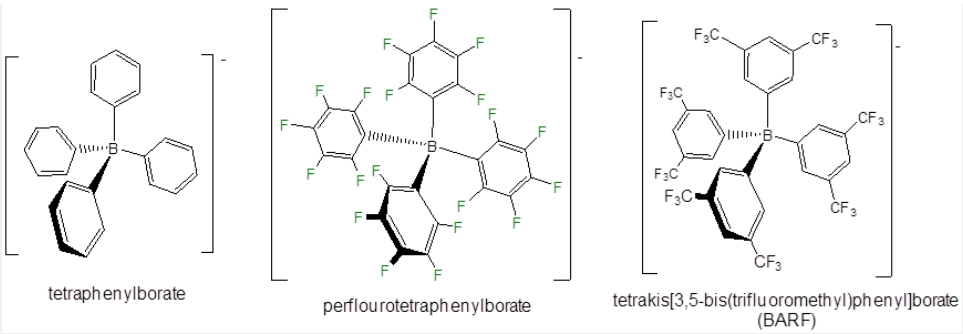
The conjugate bases of many Brønsted superacids have electron-withdrawing substituents that make them such poor Lewis bases that they are useful as noncoordinating anions.

The nonreactivity of Brønsted superacids' conjugate bases towards hydrogen ions is often mirrored in nonreactivity towards other Lewis Acids/electrophiles, most notably metals. This makes these substances useful as inert or noncoordinating ions, although since all are reactive towards suitably electrophilic centers, they are perhaps better understood as weakly coordinating.

A number of noncoordinating anions are commonly used in synthetic and other applications. The conjugate base of perchloric acid, perchlorate, was a common noncoordinating inert anion in classical coordination chemistry and continues to be used widely in electrochemistry. In contrast, the conjugate bases of triflic acid, hexafluoroboric acid, and tetrafluoroboric acid are now more commonly used as counterions for isolating reactive cations.



Even less reactive noncoordination anions include derivatives of tetraphenylborate, particularly those with electron withdrawing substituents.



Other classes of noncoordinating ions include fluoroantimonate clusters, derivatives of the carborane anion ($CB_{11}H_{11}^-$), and fluorinated aluminum tetraalkoxides.

References

Engesser, T. A.; Lichtenthaler, M. R.; Schleep, M.; Krossing, I., Reactive p-block cations stabilized by weakly coordinating anions. *Chemical Society reviews* **2016**, *45 (4)*, 789-899.

3.6.3.2.2: All other things being equal, electron withdrawing groups tend to make Lewis acids stronger and bases weaker while electron donating groups tend to make Lewis bases stronger and acids weaker is shared under a CC BY-NC-SA 4.0 license and was authored, remixed, and/or curated by Stephen M. Contakes.

- **6.4.2: All other things being equal, electron withdrawing groups tend to make Lewis acids stronger and bases weaker while electron donating groups tend to make Lewis bases stronger and acids weaker** by Stephen M. Contakes is licensed CC BY 4.0.

3.6.3.2.3: The electronic spectra of charge transfer complexes illustrate the impact of frontier orbital interactions on the electronic structure of Lewis acid-base adducts

When a Lewis acid-base adduct is formed, electron density and negative charge are transferred from the Lewis base to the acid.

The formation of a Lewis-acid base complex involves the transfer of electron density from the base to the acid.



Figure 6.4.2.**3.6.3.2.3.1**.

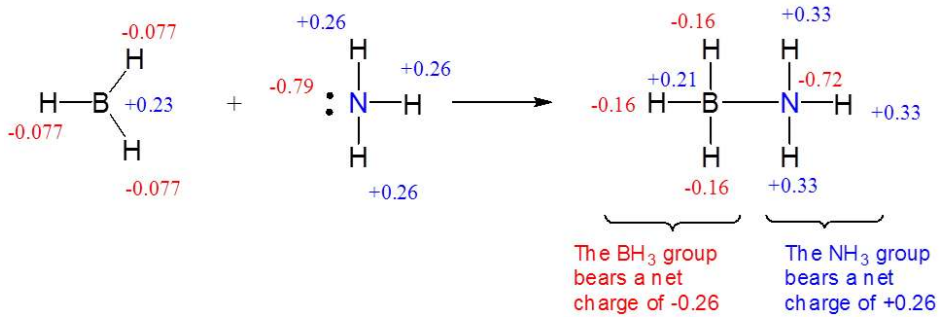


Figure 6.4.2.**3.6.3.2.3.1**. Calculated change in atomic charge distribution upon formation of an adduct between BH_3 and NH_3 in the gas phase. All partial charges were calculated for geometry-optimized molecules at the 6-31G** level.

Weakly bound Lewis acid-base adducts in which charge is incompletely transferred are called charge transfer complexes.

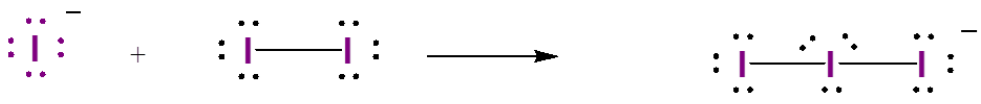
In many weakly bound Lewis acid-base complexes, the transfer of electron density and, consequently, charge from the base group to the acid group is only partial:

$$A + B \rightleftharpoons A^{\delta-}B^{\delta+}$$

Such Lewis acid-base adducts are commonly called **charge transfer complexes (CT complexes)** or **donor-acceptor complexes (DA complexes)**. In these

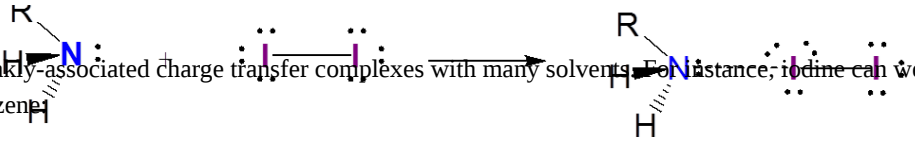
- the base is called the **donor (D)** since it is a net donor of electrons and, consequently, their negative charge
- the acid is called the **acceptor (A)** since it is a net acceptor of electrons and, consequently, their negative charge

A particularly well-known class of charge transfer complexes is the iodine charge transfer complexes. In iodine charge transfer complexes the I_2 acts as a Lewis acid. This is possible since iodine is a Row 3+ element and so is capable of forming hypervalent complexes on reaction with a Lewis base. For example, I_2 reacts with I^- to give the triiodide ion.

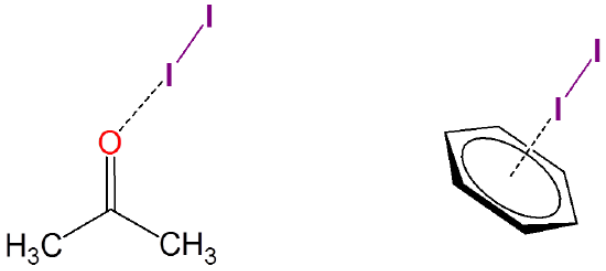


Triiodide is well-known from introductory chemistry from the bright blue color that appears when the triiodide complexes with starch to give the dark blue starch-iodide complex.

In contrast to the stable triiodide anion, iodine charge transfer complexes are only weakly associated. Complexes between iodine and amines are a well known example:

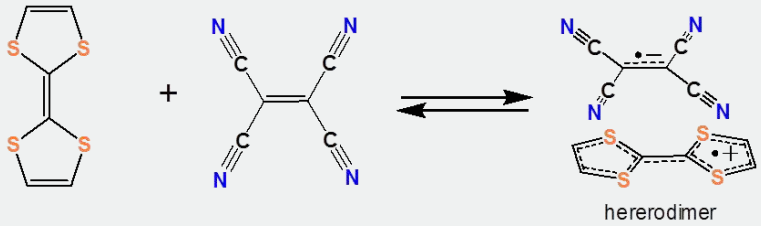


Iodine also forms weakly-associated charge transfer complexes with many solvents. For instance, iodine can weakly associate with both acetone and benzene:

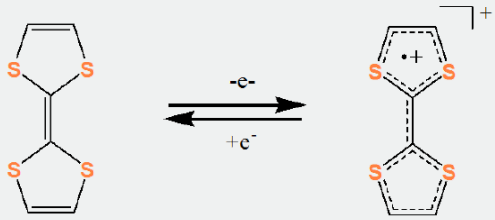


Organic Charge Transfer Complexes

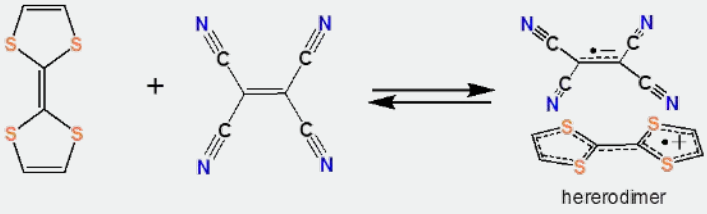
It is worth noting in passing that several organic charge transfer complex systems have been developed in which organic electron donors and acceptors weakly associate with each other. These are of considerable interest for use in molecular electronics applications, and as a result, a large variety of organic electron donors and acceptors have been developed. An example of an organic electron acceptor is tetracyanoethylene (TCNE):



and an example of an organic electron acceptor is tetrathiofulvalene (TTF).



Together they form a charge transfer complex:



Similar organic charge transfer systems have been investigated for use in organic photovoltaic cells. There is considerable interest in developing such organic photovoltaic devices owing to the ease with which organic materials may be fabricated from organic solutions and suspensions.

Charge transfer complexes exhibit charge transfer transitions in which absorption triggers the transfer of an electron from the donor to the acceptor.

When iodine is dissolved in solutions of donor solvents, the striking purple color of molecular iodine is replaced by a yellow-brown color. This is because charge transfer complexes like those formed by I_2 can absorb light in ways that neither the donor nor the

acceptor can on their own. Specifically, charge transfer complexes exhibit **charge transfer bands (CT bands)** in their absorption spectra. In the charge transfer transition the initial partial transfer of charge from the donor Lewis base to the acceptor Lewis acid in the charge transfer complex is pushed further by photoexcitation.

$$D^{\delta+} - A^{\delta-} \xrightarrow{h\nu_{CT}} D^{+} - A^{-}$$

The nature of these charge transfer transitions is seen from the orbital description of binding for iodine charge transfer complexes. When a donor-I_2 complex forms, the formation of donor-I_2 bonding and antibonding orbitals results in a shift in the $I2\sigma \rightarrow \sigma*$ transition to higher energy, as a new charge transfer band is formed, associated with the excitation of an electron from the largely amine-centered amine-I_2 σ orbital to the largely I_2-centered amine-I_2 $\sigma*$ orbital.

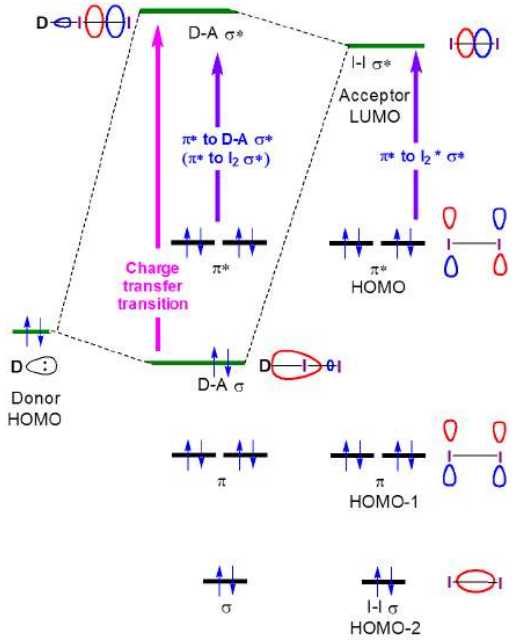


Figure 6.4.2.**3.6.3.2.3.2**. Frontier orbital interactions that give rise to changes in the absorption spectra of iodine when it forms a charge transfer complex with a Lewis base donor.

Solutions of I_2 as mixtures with Lewis bases such as amines and in donor solvents clearly have charge transfer bands in their absorption spectra. Several such spectra are given in Figure 6.4.2.3.

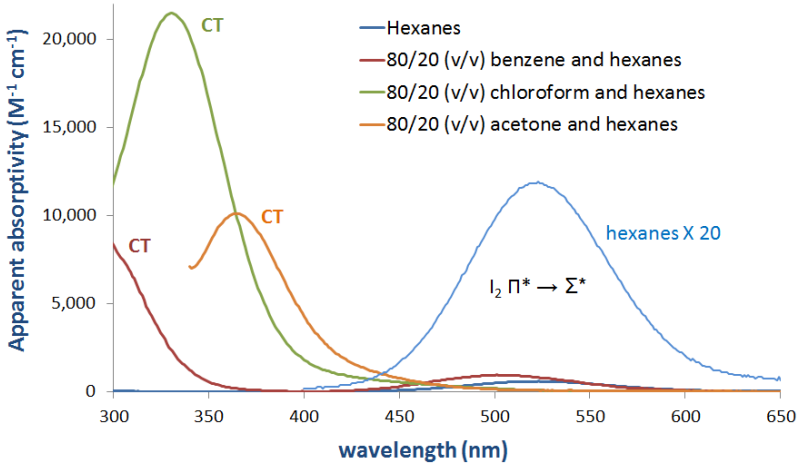


Figure **3.6.3.2.3.3**. Absorption spectrum of molecular iodine (I_2) in various solvents showing the appearance of a CT band in donor solvents.*

In principle, the energies of both the charge transfer and $I_2\ \pi* \rightarrow D-A\ \sigma*$ transitions both increase with donor strength, as shown in Figure 6.4.2.4.

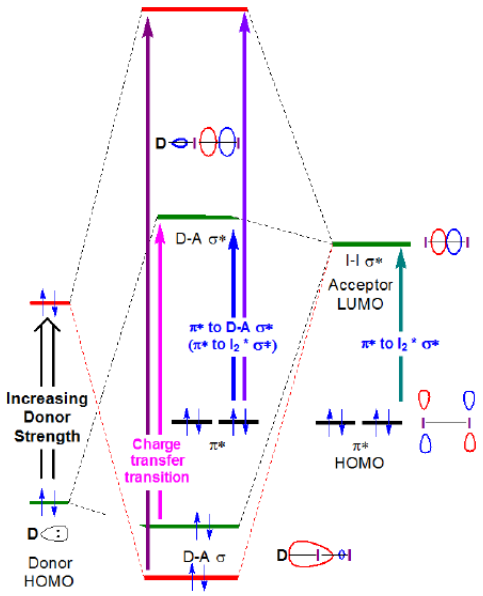


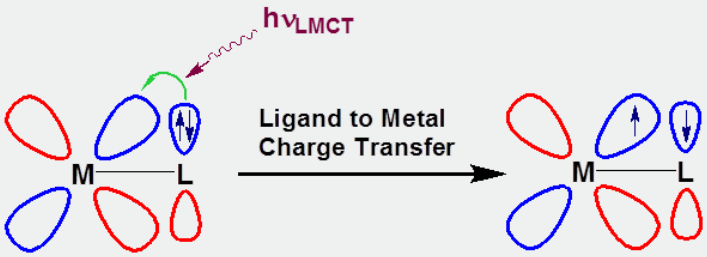
Figure **3.6.3.2.3.4**. Expected change in the frontier orbital energies associated with I_2 donor acceptor complex formation when the HOMO energy of the donor is increased.

As can be seen in Figure 6.4.2, the charge transfer band energy might be expected to increase as the donor HOMO increases in energy to become closer in energy to the acceptor LUMO. Although care should be taken when interpreting the solution phase spectra of I_2, this expectation is borne out by a cursory and qualitative analysis of the spectra in Figure 6.4.2.3. The CT transition energy shifts towards lower wavelengths (and thus higher energy) as the highest occupied atomic orbital energy for the donor atom increases on going from acetone (oxygen, -15.85 eV) to chloroform (chlorine, -13.67eV) and finally benzene (carbon, -10.66 eV).**

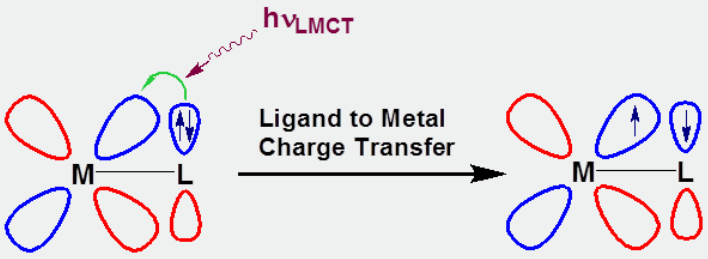
Charge Transfer Bands in Transition Metal Chemistry

Charge transfer transitions are responsible for the intense color of many transition metal complexes. In these cases, however, the weak Lewis acid-base interaction involves incomplete electron donation and acceptance in a $p\pi - d\pi$ (or $p\pi - d\pi*$)-bond between a metal and ligand. The charge transfer bands in the absorption spectra of these complexes involve the transfer of electrons between the metal and ligand. In particular,

- Metal to ligand charge transfer (MLCT or CTTL) bands involve the transfer of an electron from a filled or partly filled metal *d* orbital to a ligand $\pi*$-type orbital.



- Ligand to metal charge transfer (LMCT or CTTM) bands involve the transfer of an electron from a filled or partly filled ligand orbital to a metal *d*-orbital.



- Metal to metal charge transfer bands can be observed in some bimetallic complexes. However, these are usually thought of only as an electron transfer rather than as a shift in the status of a Lewis acid-base interaction.

Because metal-ligand charge transfer bands involve intermolecular electron transfer between the metal and ligand to generate a high energy redox state, the CT excited state is both a better oxidant and reductant than the ground state. Consequently there has been intense research into the development of metal complexes whose charge transfer excited states are powerful oxidants and reductants in the expectation that they will be able to drive the photocatalytic oxidation and reduction of substrates.

* The apparent absorptivity of I_2 in hexanes was calculated from the absorption spectrum of 215 μM I_2 in hexanes. All other apparent absorptivities were calculated from absorption spectra of solutions that were 44 μM in I_2.

** The band positions are not the CT band energies, and the HOMO energies given are atomic energy levels and do not necessarily correspond to the HOMO of the donor in solution. Because of this and other simplifications this analysis is not intended to replace a rigorous computational analysis of the factors that give rise to CT band positions.

References

1. Meyerstein, D.; Treinin, A., Charge-transfer complexes of iodine and inorganic anions in solution. Transactions of the Faraday Society 1963, 59 (0), 1114-1120.
2. Baskar, A. J. A.; Rajpurohit, A. S.; Panneerselvam, M.; Jaccobb, M.; RoopSingh, D.; Kannappan, V., Experimental and theoretical analysis of substituent effect on charge transfer complexes of iodine and some alkylbenzenes in n-hexane solution at 303K. Chemical Data Collections 2017, 7-8, 80-92.

3.6.3.2.3: The electronic spectra of charge transfer complexes illustrate the impact of frontier orbital interactions on the electronic structure of Lewis acid-base adducts is shared under a CC BY-NC-SA 4.0 license and was authored, remixed, and/or curated by Stephen M. Contakes.

- **6.4.3: The electronic spectra of charge transfer complexes illustrate the impact of frontier orbital interactions on the electronic structure of Lewis acid-base adducts** by Stephen M. Contakes is licensed CC BY 4.0.

3.6.3.2.4: Substances' solution phase Lewis basicity towards a given acid may be estimated using the enthalphy change for dissociation of its adduct with a reference acid of similar hardness.

A number of spectroscopic and thermodynamic scales have been developed to quantify the strength of Lewis acids and bases.[1,2] For the sake of simplicity only thermodynamic scales will be described. Thermodynamic scales are based on the energetics of Lewis acid-base reactions. When substances act as a Lewis base (**B**) they form adducts with a Lewis acid (**A**):

$$B: \ + \ A \rightleftharpoons B-A$$

Various thermodynamic parameters for this process may be taken as a measure of the strength of the Lewis base towards that acid. For instance, in the case of iodine charge transfer complexes, the equilibrium constant for adduct formation is sometimes used as an informal measure of Lewis base strength.

The thermodynamic parameters used to define Lewis acid and base strength are similar to those used to define Brønsted acidity and basicity. Just as Brønsted acidity and basicity were defined in terms of the free energy change for the dissociation and association of a hydrogen ion, Lewis acidities and basicities are defined in terms of the free energy change for adduct formation:

$$B: \ + \ A_{reference} \rightleftharpoons B-A \qquad -\Delta G \ = \ Lewis \ basicity \ of \ B \ towards \ A$$

$$B:_{reference} \ + \ A \rightleftharpoons B-A \qquad -\Delta G \ = \ Lewis \ acidity \ of \ A \ towards \ B$$

The physical meaning of Lewis acidities and basicities may be easier to grasp by considering that Lewis acidities and basicities correspond to the free energy for dissociation of acid-base adducts:

$$B-A \rightleftharpoons B: \ + \ A_{reference} \qquad \Delta G \ = \ Lewis \ basicity \ of \ B \ towards \ A$$

$$B-A \rightleftharpoons B:_{reference} \ + \ A \qquad \Delta G \ = \ Lewis \ acidity \ of \ A \ towards \ B$$

Since in practice it is much easier to measure the reaction enthalpies for these processes, many scales use the enthalpy change instead of the free energies. To distinguish these enthalpy changes from Lewis *acidities* and *basicities*, the enthalpy changes are called Lewis acid and base *affinities*. Of these, however, Lewis acid affinities are poorly characterized at present (perhaps one of you readers will help redress this). Thus the remainder of this section will focus on Lewis base affinities.

Before discussing Lewis base affinities it is worth noting that there is no universal reference scale of Lewis base strength. That is because the thermodynamics of a given Lewis acid-base interaction is contingent on a number of factors, including:

- The relative hardness of the acid and base according to Pearson's hard-soft acid base principle. Roughly, Lewis acids tend to associate more strongly with Lewis bases with similar charge densities and polarizabilities. This means that the affinity of a given base for Lewis acids is not a static parameter. Rather it differs markedly with the acid's hardness.
- Steric effects. Sterically hindered Lewis acid-base interactions will be weaker than sterically accessible ones.
- Solvent effects. In solutions, the adduct and the free acid and base pair will in general be differentially stabilized. To avoid solvent effects, some scales quantify Lewis acid and base strength in terms of gas phase adduct formation. However, it is not always possible or desirable to quantify a Lewis acid or base's strength in the gas phase, since gas phase affinities do not always allow for adequate prediction of the strength of a Lewis acid-base interaction in solution.

Because Lewis base affinity depends on hardness, steric effects, and solvent effects care should be taken when acid-base parameters are used to predict the strength of a given interaction. In particular, steric effects should be considered separately, and if predictions are made using scales that employ reference acids or bases that differ markedly in hardness from the interaction to be predicted or which correspond to unrealistic solvent conditions, they should always be taken as tentative.

References

1. Laurence, C.; Graton, J.; Gal, J.-F., An Overview of Lewis Basicity and Affinity Scales. Journal of Chemical Education 2011, 88 (12), 1651-1657.
2. Laurence, C.; Gal, J.-F. o., Lewis basicity and affinity scales: data and measurement. John Wiley: Chichester, West Sussex, U.K., 2010.

3.6.3.2.4: Substances' solution phase Lewis basicity towards a given acid may be estimated using the enthalphy change for dissociation of its adduct with a reference acid of similar hardness. is shared under a CC BY-NC-SA 4.0 license and was authored, remixed, and/or curated by Stephen M. Contakes.

- **6.4.4: Substances' solution phase Lewis basicity towards a given acid may be estimated using the enthalphy change for dissociation of its adduct with a reference acid of similar hardness.** by Stephen M. Contakes is licensed CC BY 4.0.

3.6.3.2.5: In the boron trifluoride affinity scale, the enthalpy change on formation of an adduct between the base and boron trifluoride is taken as a measure of Lewis basicity.

The physical meaning of Lewis acid and base affinities are defined as the negative of the enthalpy for formation of an adduct with a reference base and acid, respectively:

$$B + A_{reference} \rightleftharpoons B-A \qquad -\Delta H = \text{Lewis basicity of B towards A}$$

$$B_{reference} + A \rightleftharpoons B-A \qquad -\Delta H = \text{Lewis acidity of A towards B}$$

Two common scales of Lewis base affinity involve the use of $SbCl_5$ and BF_3 as the reference base. Specifically,

- In the **Guttman donor-acceptor scale,** Lewis bases' **donor numbers** are equal to the negative enthalpy change for formation of the base's $SBCl_5$ adduct in dilute 1,2-dichloroethane (EDC*):

$$Base(EDC\ solution) + SbCl_5(EDC\ solution) \rightarrow Base-SbCl_5(EDC\ solution) \qquad -\Delta H = \text{Guttman Donor Number}$$

- The **BF_3 affinity scale** has largely supplanted the Guttman scale owing to the ease with which its results may be correlated with computational data (it is easier to calculate energies for adducts of BF_3 than of SbF_5). In the BF_3 affinity scale, Lewis bases' **BF_3 affinities** are equal to the negative enthalpy change for formation of a solution phase adduct between the base and gaseous BF_3. The reaction is:

$$Base(solution) + BF_3(g) \rightarrow Base-BF_3(solution) \qquad -\Delta H = \text{BF}_3\text{ Affinity}$$

BF_3 affinity values for a wide range of organic bases were compiled by Laurence, Graton, and Gal in reference 2 and salient trends in this data will be discussed in subsequent sections.

References

1. Laurence, C.; Graton, J.; Gal, J.-F., An Overview of Lewis Basicity and Affinity Scales. Journal of Chemical Education 2011, 88 (12), 1651-1657.
2. Laurence, C.; Gal, J.-F. o., Lewis basicity and affinity scales: data and measurement. John Wiley: Chichester, West Sussex, U.K., 2010.

Notes

* EDC stands for ethylene dichloride, the common name of 1,2-dichloroethane.

3.6.3.2.5: In the boron trifluoride affinity scale, the enthalpy change on formation of an adduct between the base and boron trifluoride is taken as a measure of Lewis basicity. is shared under a CC BY-NC-SA 4.0 license and was authored, remixed, and/or curated by Stephen M. Contakes.

- **6.4.5: In the boron trifluoride affinity scale, the enthalpy change on formation of an adduct between the base and boron trifluoride is taken as a measure of Lewis basicity.** by Stephen M. Contakes is licensed CC BY 4.0.

3.6.3.2.6: Lewis base strength may also be estimated by measuring structural or energy changes upon formation of a Lewis acid-base complex, as illustrated by efforts to spectroscopically assess the strengths of halogen bonds

When a Lewis acid and base form an adduct, it shifts the bond lengths, and strengths in the acid and base also shift.

According to the frontier orbital description of Lewis acid-base interactions, adduct formation results in a net transfer of electron density from the base HOMO to the acid LUMO. This transfer

- increases the electron density between the acid (A) and base (D)
- alters the strength of the bonding within the base as the base LUMO becomes partially populated.

These changes result in structural and spectroscopic shifts on adduct formation that can be taken as a measure of the strength of the Lewis acid-base interaction. Since these shifts depend on the nature of the bonding in the acid and base, in practice structural and spectroscopic measurements of Lewis basicity are applied to a few classes of Lewis acid-base interactions, most notably hydrogen bonding and halogen bonding. Since hydrogen bonds will be discussed in section 6.5.1. the remainder of this subsection will focus on halogen bonds.

Halogen bonds are coordinate covalent bonds formed between a Lewis base and an organohalogen.

The halogens in compounds containing a singly-bonded halogen can engage in a special type of intermolecular interaction called halogen bonding, since the bonded halogens are electrophilic on the opposite side of the bond. This electrophilicity is apparent from the charge distribution in CF_5I shown in Figure 4.5.1, in which the charge is distributed on the I such that the I is Lewis basic perpendicular to the C-I bond and Lewis acidic opposite to it. This region of diminished electron density on the halogen opposite the existing sigma bond is called a σ-hole.*

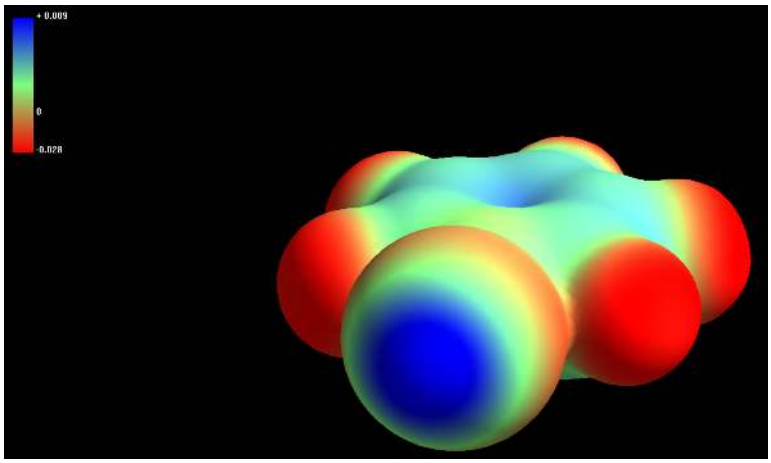
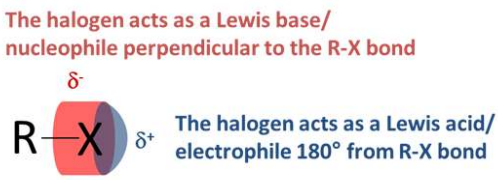
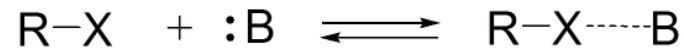


Figure **3.6.3.2.6.1**. Electrostatic surface calculated for CF_5I at the STO-3-21G level oriented so that the C-I bond is facing toward the viewer. The sigma hole shown is the region of positive electron density on the I atom at the front of the image. This work by Stephen Contakes is licensed under a Creative Commons Attribution 4.0 International License.

Schematically,



Since the halogen can act as a Lewis acid in the direction opposite the R-X bond it can form adducts with Lewis bases in that direction.



The bonds holding these adducts together are called **halogen bonds**, often abbreviated XB.

The halogen is said to act as a halogen bond donor when it forms a halogen bond with a base along that direction, with the base acting as the halogen bond acceptor. Consequently, the two previous schemes may also be given as:



The ability of singly-bonded halogen atoms to form halogen bonds forms the basis of many efforts to engineer structures in which halogen-containing compounds are held together into chains, sheets, or 3D structures using halogen bonds. One easy-to-see example involves 1D chains formed between *p*-diiodotetrafluorobenzene and *p*-bis(dimethylamino)benzene.[3]

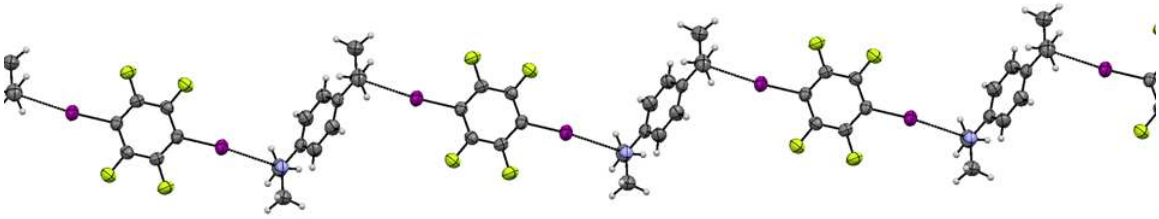
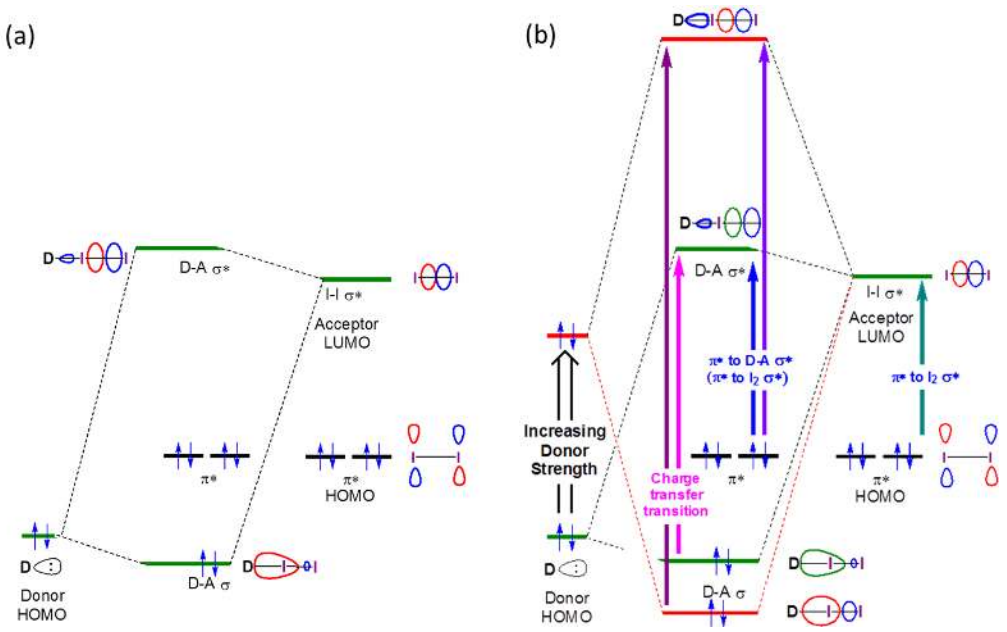


Figure **3.6.3.2.6.2**. 1D chains of *p*-tetrafluorodiiodobenzene and *p*-bis(dimethylamino)benzene molecules in which I is shown in purple, N in blue, F in yellow, and C in grey. The chains are held together by C-I---N halogen bonds with a contact angle of 174 degrees. The figure was produced using Mercury 3.5.1 based on Cambridge crystallographic database entry 172272. This work by Stephen Contakes is licensed under a Creative Commons Attribution 4.0 International License.

Trends in halogen bond strength in a closely-related series of compounds may be assessed by examining how the vibrational stretching frequency of I_2 and the I_2 π^* to σ^* transition energy change upon formation of the adduct.

From the description of halogen bonding above it should be apparent that the iodine charge transfer complexes described in section 6.4.2 are held together by halogen bonds. This means that the description of the bonding in I_2 charge transfer complexes given in that section illustrate how vibrational and electronic transitions shift when a halogen-bonded adduct is formed between a halogen bond donor and acceptor.

The orbital interactions involved in halogen bond formation are shown in Figure 6.4.5.3. As can be seen from that figure, the formation of an adduct between I_2 and a Lewis base is expected to result in weakening of the I-I bond and a shift in the I_2 $\pi^* \rightarrow \sigma^*$ transition energy to higher energy/shorter wavelengths (*i.e.*, a blueshift). Further, both the weakening of the I-I bond and the I_2 $\pi^* \rightarrow \sigma^*$ blueshift are expected to increase with the HOMO energy of the Lewis base.



Figures 6.4.2.2 and 6.4.2.4. This work by Stephen Contakes is licensed under a Creative Commons Attribution 4.0 International License.

Because the I-I bond strength and $I_2\ \pi^* \rightarrow \sigma^*$ blueshift increase with the Lewis basicity of the donor, the blueshift and the I-I vibrational stretching frequency are sometimes used as measures of donor's halogen bond affinity. However, the data obtained from such spectroscopic measurements should be interpreted with a degree of caution. As seen in Table 6.4.5.1, the extent to which the I-I bond is weakened (indicated by $\Delta\nu_{I-I}$) and the $I_2's\ \pi^* \rightarrow \sigma^*$ band is blue shifted are imperfectly correlated overall. However, a careful comparison of the data in 6.4.5.1. reveals that the I-I bond weakening and $I_2's\ \pi^* \rightarrow \sigma^*$ blue shift correlate well for Lewis bases of a given type. Consequently, shifts in the I-I stretching frequency and $I_2\ \pi^* \rightarrow \sigma^*$ absorption band are not useful as an absolute measure of Lewis basicity but can be used to rank the halogen bond affinity of a closely-related set of donors.**

Table **3.6.3.2.6.1**. Spectroscopic measures of Lewis basicity for I_2 adducts of selected bases arranged in order of extent of blue shift. The data are excerpted from the extensive compilation given in reference 4.

Base (type)	$\Delta\nu_{I-I}\ cm^{-1}$	Blue shift of $I_2's\ \pi* \rightarrow \sigma*$
4-methylpyridine (pyridines)	29.1	4730
pyridine (pyridines)	27.4	4560
tetrahydrothiophene (thioethers)	44.5	3640
tetrahydrofuran, THF (ethers)	6.4	2280
diethyl ether (ethers)	5.5	1950
acetone (ketone)	5.0	1850
acetophenone (ketone)	4.6	1650
acetonitrile (nitrile)	4.1	1610
hexamethylbenzene (aromatic)	10.4	1070
benzene (aromatic)	4.3	450

References and Further Reading

1. Cavallo, G.; Metrangolo, P.; Milani, R.; Pilati, T.; Priimagi, A.; Resnati, G.; Terraneo, G., The Halogen Bond. *Chemical Reviews* 2016, *116 (4)*, 2478-2601.
2. Politzer, P.; Murray, J.S. σ-Hole Interactions: Perspectives and Misconceptions. *Crystals* **2017**, *7*, 212.

3. R.Liantonio, S.Luzzati, P.Metrangolo, T.Pilati, G.Resnati, *Tetrahedron*, 2002, 58, 4023, DOI: 10.1016/S0040-4020(02)00264-8
4. Laurence, C.; Gal, J.-F. o., *Lewis Basicity and Affinity scales: Data and Measurement*. John Wiley: Chichester, West Sussex, U.K., 2010.

Notes

* Other compounds also exhibit σ-holes (and π-holes) that can be used in crystal engineering. For details see reference 2.

** for more details consult reference 4, pp. 286-309.

Contributors and Attributions

Consistent with the policy for original artwork made as part of this project, all unlabeled drawings of chemical structures are by Stephen Contakes and licensed under a Creative Commons Attribution 4.0 International License.

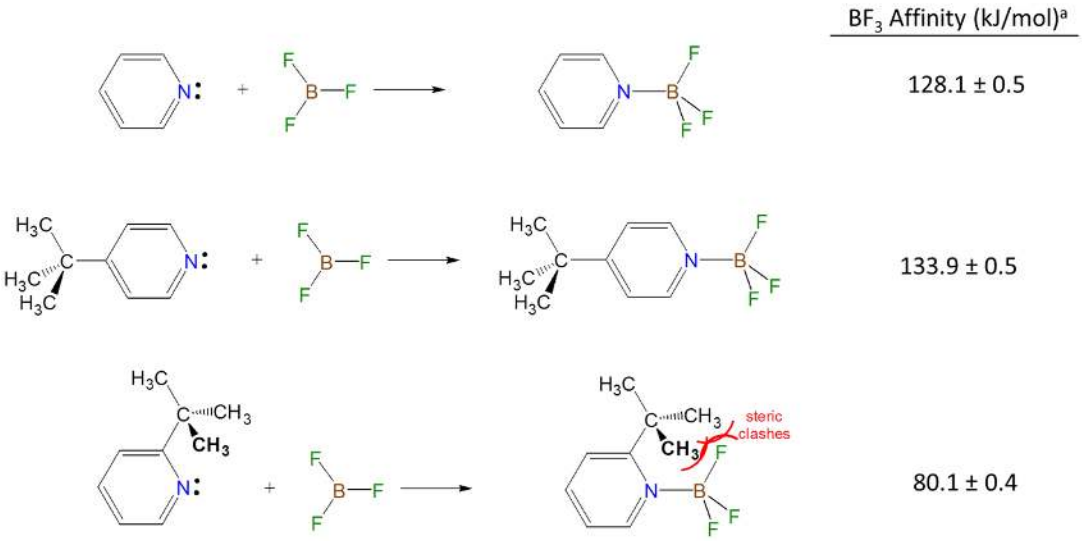
3.6.3.2.6: Lewis base strength may also be estimated by measuring structural or energy changes upon formation of a Lewis acid-base complex, as illustrated by efforts to spectroscopically assess the strengths of halogen bonds is shared under a CC BY-NC-SA 4.0 license and was authored, remixed, and/or curated by Stephen M. Contakes.

- **6.4.6: Lewis base strength may also be estimated by measuring structural or energy changes upon formation of a Lewis acid-base complex, as illustrated by efforts to spectroscopically assess the strengths of halogen bonds** by Stephen M. Contakes is licensed CC BY 4.0.

3.6.3.2.7: Bulky groups weaken the strength of Lewis acids and bases because they introduce steric strain into the resulting acid-base adduct.

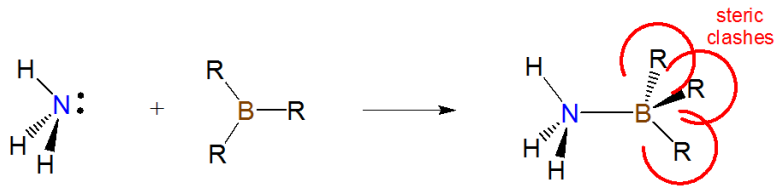
Steric effects can influence the ability of a Lewis acid or base to form adducts by introducing:

- **front strain (F-strain)** whereby bulky groups make it difficult for the Lewis acid and Lewis base centers to approach and interact.



a) Data from Laurence, C.; Gal, J.-F. o., *Lewis basicity and Affinity Scales: Data and Measurement. John Wiley: Chichester, West Sussex, U.K., 2010; pp. 91-101.*

- **back strain (B-strain)** associated with steric interactions that do not directly impede the Lewis acid and base centers from interacting but instead occur as the acid and base rearrange upon adduct formation. For instance, when trivalent boron compounds form adducts with amines, the boron center changes from a more open trigonal geometry to a more hindered tetrahedral one:



- **internal strain (I-strain)** is also associated with the geometry changes incident on adduct formation. However, while B-strain involves direct steric clashes that occur on adduct formation, I-strain is the strain involved in deforming bond and torsional angles away from more stable local geometries. Thus it is more important for Lewis base centers embedded in rings or clusters.

References

1. Alder, R. W., Strain effects on amine basicities. *Chemical Reviews* 1989, 89 (5), 1215-1223.

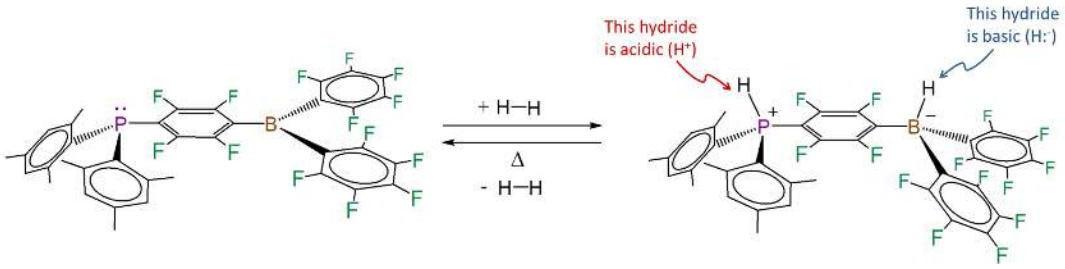
3.6.3.2.7: Bulky groups weaken the strength of Lewis acids and bases because they introduce steric strain into the resulting acid-base adduct. is shared under a CC BY-NC-SA 4.0 license and was authored, remixed, and/or curated by Stephen M. Contakes.

- **6.4.7: Bulky groups weaken the strength of Lewis acids and bases because they introduce steric strain into the resulting acid-base adduct.** by Stephen M. Contakes is licensed CC BY 4.0.

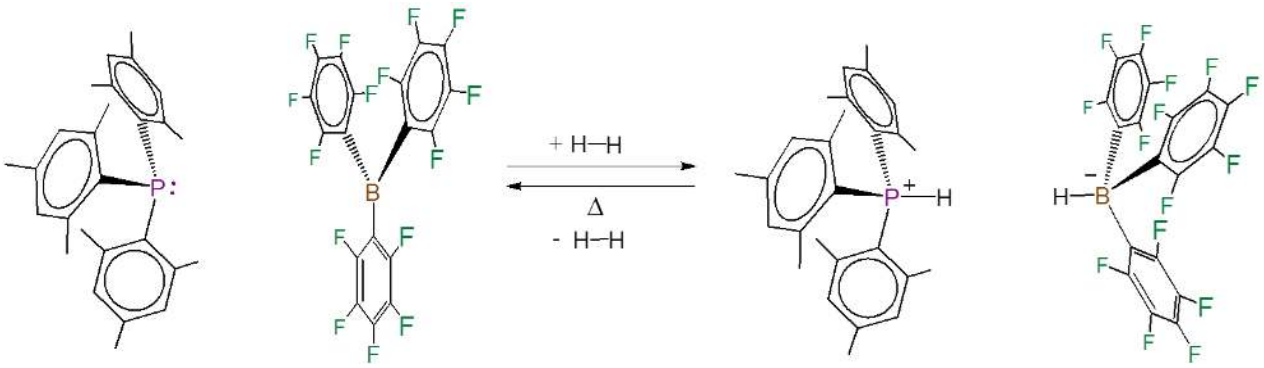
3.6.3.2.8: Frustrated Lewis pair chemistry uses Lewis acid and base sites within a molecule that are sterically restricted from forming an adduct with each other.

In certain cases when a Lewis acid-base adduct is sterically hindered from quantitatively forming an adduct (and perhaps even when they are so able), the Lewis acid and Lewis base can act together to heterolytically cleave chemical bonds. In such cases the pair of electrons that would otherwise be donated by the base is said to be a **frustrated Lewis pair (FLP)** and in performing the heterolytic cleavage the Lewis acid and base are said to exhibit **frustrated Lewis pair chemistry**.

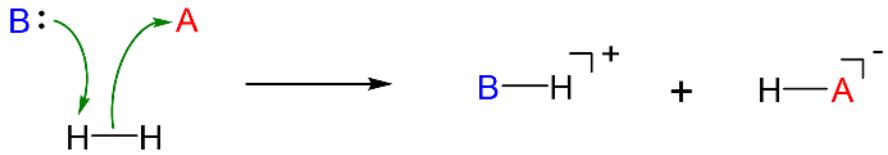
The **Stephan's phosphinoborane** illustrates how FLP chemistry works. It reversibly cleaves dihydrogen to give a zwitterionic species containing both acidic and basic element hydride bonds.



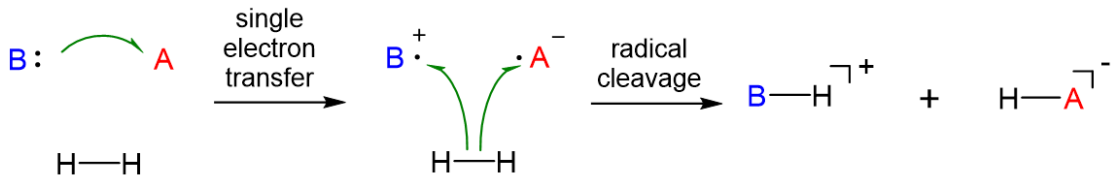
Note that the Lewis acid and base do not need to be part of the same molecule. Hydrogen is also heterolytically cleaved by mixtures of sterically encumbered triarylphosphines and triarylboranes. This time the reaction gives phosphonium and hydroborate ions:



Given the description of FLP systems as frustrated Lewis acid-base adducts, it is natural to think about the cleavage of substrates like H_2 as involving nucleophilic attack by the Lewis base while the Lewis acid acts like an electrophile in a heterolytic cleavage mechanism.



However, only some FLP systems cleave substrates through this mechanism. In others the mechanism involves homolytic cleavage by a diradical intermediate.



In either case, when substrates like H_2 are cleaved by FLPs, they are generally separated into more reactive fragments (e.g., in the case of H_2, H^+ and H^-). Because of this the substrates are said to be activated to undergo further reactions. Because FLP systems can cleave and activate substrates, there is considerable interest in the development of FLP systems that can facilitate reactions of economic or environmental interest. So far FLP systems have been developed that can catalyze various hydrogenations and activate numerous substrates, including CO, SO_2, and N_2.

References

1. Stephan, D. W., Frustrated Lewis Pairs: From Concept to Catalysis. *Accounts of Chemical Research* 2015, 48 (2), 306-316.
2. Fontaine, F.-G.; Stephan D. W., On the concept of frustrated Lewis pairs. *Philosophical Transactions of the Royal Society A: Mathematical, Physical and Engineering Sciences* 2017, 375 (2101), 20170004.
3. Jupp, A. R.; Stephan, D. W., New Directions for Frustrated Lewis Pair Chemistry. *Trends in Chemistry* 2019, 1 (1), 35-48.

3.6.3.2.8: Frustrated Lewis pair chemistry uses Lewis acid and base sites within a molecule that are sterically restricted from forming an adduct with each other. is shared under a CC BY-NC-SA 4.0 license and was authored, remixed, and/or curated by Stephen M. Contakes.

- **6.4.8: Frustrated Lewis pair chemistry uses Lewis acid and base sites within a molecule that are sterically restricted from forming an adduct with each other.** by Stephen M. Contakes is licensed CC BY 4.0.

3.6.3.3: Hard and Soft Acids and Bases

Origin of the Hard-Soft Acid-Base Principle

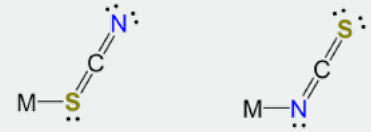
One of the strengths of the Lewis acid-base concept is the readiness with which it illuminates the role that covalent and electrostatic interactions in acid base behavior, specifically through its ability to explain chemical interactions in terms of frontier orbitals and the interactions between charged groups as electrons are donated from a base to an acid. However, simply acknowledging the presence of such interactions does little to illuminate the degree to which each mode of explanation best explains the bonding in a given system? To what extent is a given adduct better described as held together by covalent bonds as opposed to ionic ones - *e.g.* better described as a molecule rather than an ion pair? Moreover, does it even matter, given that the orbitals of quantum mechanics result from the combination of electrons' wavelike behavior with their electrostatic attraction to nuclei in either case?[1] These questions and more are addressed by one of the most important conceptual tools in contemporary inorganic chemistry, the Hard-Soft acid-base principle.

The **Hard-Soft acid-base principle (HSAB principle)** stems from the recognition that some Lewis acids and bases seem to have a natural affinity for one another.* Consider the following:

- Some metals are commonly found in nature as salts of chloride or as oxide ores while others are found in combination with sulfur. Geochemists even use the Goldschmidtt classification scheme to classify the halide and oxide formers as lithophiles and the sulfide formers as chalcophiles.
- In living systems small highly charged metals ions like Fe^{3+} are usually found bound to N and O atoms while larger metals with lower charges such as Zn^{2+} are often found attached to at least one S atom. Similarly, metals prefer to bind to one coordination site over the other when forming complexes with ambidentate ligands. The most well-known instances involve complexes of cyanate and thiocyanate, which can coordinate metals through either the N or chalcogen atom. For instance, Cu^{2+} and Zn^{2+} form *N*-thiocyanato complexes in species like $[Cu(NCS)_2(py)_2]$ and $[Zn(NCS)_4]^{2-}$ while their larger cogeners Au^{3+} and Hg^{2+} preferentially forms *S*-thiocyanato complexes, giving species like $[Hg(SCN)_4]^{2-}$.

Ambidentate ligands

Ambidentate ligands possess multiple coordination sites through which a metal may bind. For instance, thiocyanate may coordinate metals (M) at either the S or N to give *S*-thiocyanato or *N*-thiocyanato complexes.



S-thiocyanato *N*-thiocyanato

- The solubility trends for the alklai metal halides and silver halides are opposite, even though both involve salts of formula M^+X^- (salts can be thought of as involving Lewis acid-base adduct formation between the anions and cations). Specifically, although the silver halides are all relatively insoluble in water, the very modest solubility they possess follows the order:

$$X = F >> Cl > Br > I \text{ (for the solubility of AgX)}$$

In contrast, the much more ample solubility of the alkali metal halides** follows the opposite order. For example, the order for the lithium halides is

$$X = F << Cl < Br << I \text{ (for the solubility of LiX)}$$

Notes

1. Albeit suitably fudged through such niceties as the Aufbau principle and other approximations.

* Despite the fruitfulness of this observation, in general it is important to reduce the potential for observer bias by checking observations like these against compounds reported in the chemical literature and databases like the Inorganic Crystal Structure and Cambridge Crystallographic Databases.

** These are very soluble in water, to the point where some solutions are perhaps better described as solutions of water in the halide.

† This can be predicted based on the relative hardness of BF_3, BR_3, and BH_3 in the list of hard and soft acids. However, for those of you who may be confused as to why H is considered a better electron donor for the purposes of softening a Lewis acid center while alkyl groups are better electron donors for the purposes of stabilizing carbocations in organic chemistry, the dominant effect is the lower electronegativity of H relative to carbon (in CH_3). The effect of electron donation due to hyperconjugation isn't as great for thermodynamically stable bases like BX_3/BR_3.

3.6.3.3: Hard and Soft Acids and Bases is shared under a CC BY-NC-SA 4.0 license and was authored, remixed, and/or curated by Stephen M. Contakes.

- **6.6: Hard and Soft Acids and Bases** by Stephen M. Contakes is licensed CC BY 4.0.

3.6.3.3.1: Hard-Hard and Soft-Soft preferences may be explained and quantified in terms of electrostatic and covalent and electronic stabilization on the stability of Lewis acid-base adducts

The Hard Soft Acid Base Principle is a Conceptual Tool for Thinking About Patterns of Lewis Acid-Base Reactivity

The explanation of the trends in metal distribution, halide salt solubility, and preferred metal coordination patterns is rooted in Arland, Chatt, and Davies' observation that *Lewis acids and bases could be classified into two groups based on their propensity to form stable compounds with one another* (*e.g.* acids in a class tend to form more stable adducts with bases in the same class than they did with bases in the other).[1] Arland, Chatt, and Davies somewhat boringly termed these groups class a and class b but today they are known by Ralph Pearson's name for them. Pearson called the class a acids and bases hard and class b acids and bases soft. These terms reflect how "soft" these substance's electron clouds are towards distortion or, in other words, their polarizability (Figure **3.6.3.3.1.1**). Pearson terms acids and bases which are relatively polarizable **soft** and those which are difficult to polarize **hard.**

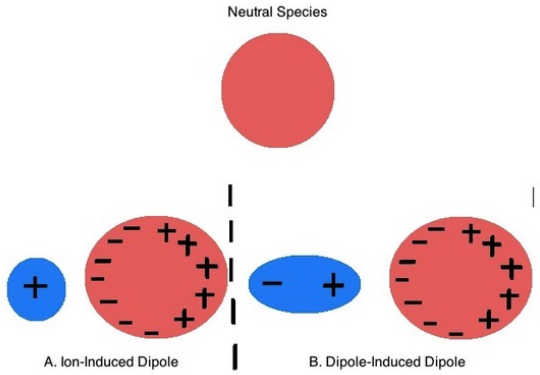


Figure **3.6.3.3.1.1**: Polarizability refers to the ease with which a substance's electron cloud may be distorted under the action of an electric field. A fragment's polarizability determines the degree to which its electron cloud is distorted by A.) an Ion and B.) a polar molecule to induce a dipole moment. The figure is taken from (and the caption expanded from) Cox, Kelly and Dana Reusser "Polarizability"

Recognizing Hard and Soft Acids and Bases

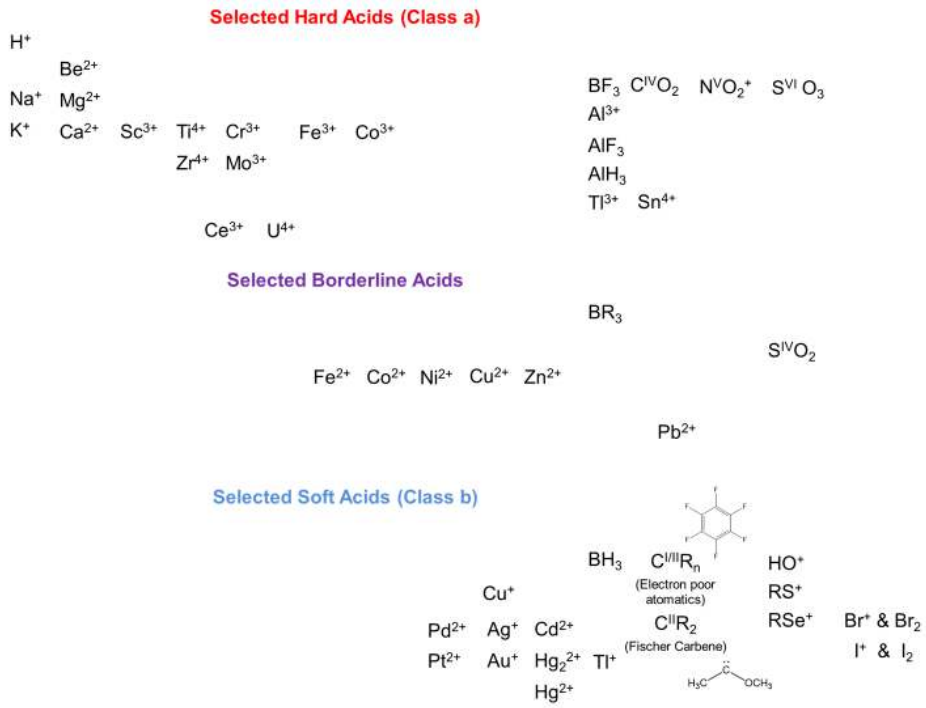
Hard acids and bases come in two varieties:

1. hard acid and base sites that possess few valence electrons and for which polarization therefore involves distorting core electrons, which are difficult to distort because they are close to the nucleus and experience a high nuclear charge. The most common examples of such substances are Lewis acid hard acids towards the left of the periodic table.
2. hard acid and base sites with a high charge density (highly charged relative to size) and/or which are electron deficient. In these cases polarization involves distorting electrons that already experience strong unshielded electrostatic interactions.

Soft acids and bases also come in two varieties

1. soft acids and bases which posses many valence electrons and so are more readily polarized. In consequence, all other things being equal, soft acids and bases are more likely to be found towards the middle or right of the periodic table.
2. soft acids and bases with little charge density and/or which are relatively electron rich.

Note that the hard-soft classification should not be thought of as if all hard acids and bases are equally hard and all soft acids and bases equally soft. There is a graduation in hardness and softness and a number of intermediate acids and bases which do not fit neatly in either category. With this caveat in mind, representative **hard, soft, and borderline acids** are given below. Notice how they illustrate the trends just outlined.



As expected, hard acids tend to be found towards the left side of the periodic table and involve higher oxidation states and/or electron donating substituents while soft acids are more common to the right of the periodic table and involve lower oxidation states and/or electron donating substituents.

Illustrative hard, soft, and borderline bases are given below. Again, notice how these substances illustrate the general trends.

Selected Hard Bases (Class a)

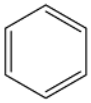
Nitrogen bases	Oxygen bases		small halides
NH_2^-	OH^-	CO_3^{2-}	F^-
NH_3	H_2O	RCO_2^-	Cl^-
RNH_2	ROH	NO_3^-	
NH_2NH_2	ROR	PO_4^{3-}	
		SO_4^{2-}	

Selected Borderline Bases

electron-poor Nitrogen bases		low oxidation state element oxyanions	intermediate halides
N_3^-		NO_2^-	
NO_2^-			
SCN^-		SO_3^{2-}	Br^-
N_2			

Selected Soft Bases (Class b)

Carbon bases	P and As bases	Sulfur bases	large halides & pseudohalides
R^-	PR_3	RS^-	H^-
CO	$P(OR)_3$	RSH	I^-
CN^-	AsR_3	RSR	
RNC		SCN^-	
$R_2C{=}CR_2$ (alkenes)			



(electron-rich aromatics)

Qualitative Estimation of the Relative Hardness and Softness of Lewis Acids and Bases

As can be seen from the examples above, **hard acids are relatively electron-poor and hard bases electron-rich** since they have comparatively

- small frontier orbitals, reflective of their relatively small atom/ion/fragment sizes
- high (for acids) or low (for bases) oxidation states on the base atom, reflected in a large positive formal charge (for acids) or negative formal charge (for bases)
- low polarizability, due to loss or gain of substantial numbers of electrons, or the localization of
  - positive charge on an electropositive element or an atom bearing electron-withdrawing substituents
  - negative charge on an electronegative element or an atom bearing electron-donating substituents

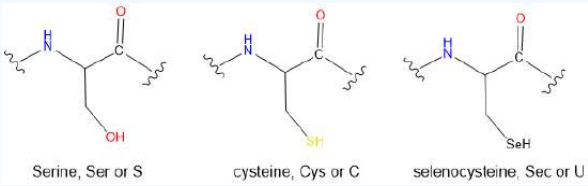
In contrast to hard acids and bases, **soft acids are relatively electron-rich and soft bases larger and more electron poor** since they have comparatively

- large frontier orbitals, reflective of their relatively large atom/ion/fragment sizes
- low oxidation states, often resulting in small or nonexistent atomic charges
- high polarizability, as might be expected of species in which electron-electron repulsions are lower and electrons are spread over a large volume. Sometimes this is indicated by
  - positive charge on an electronegative element or an atom bearing electron-donating substituents
  - negative charge on an electropositive element or an atom bearing electron-withdrawing substituents

Exercise 3.6.3.3.1.1

Rank the acids or bases in each set in increasing order of expected hardness.

a. Cr^{2+} and Cr^{3+}
b. H^+, Cs^+, and Tl^+
c. SCN^- (acting as a base at N) and SCN^- (acting as a base at S)
d. AlF_3, AlH_3, $AlMe_3$
e. The side chains of the following proteinogenic amino acids

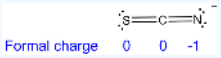


Answer

(a) $Cr^{2+} < Cr^{3+}$ All other things being equal, hardness increases with oxidation state.

(b) $Tl^+ < Cs^+ < H^+$ The order reflects Cs^+ and Tl^+'s larger size relative to H^+ (which doesn't possess any electrons that can be polarized anyway) and that Tl^+ still possesses two valence electrons while Cs^+ possesses none.

(c) SCN^- (acting as a base at S) < SCN^- (acting as a base at N). The order reflects the greater electronegativity of N than S and N's possession of a more negative formal charge of -1.



(d) $AlH_3 < AlMe_3 < AlF_3$. The hardness increases as the substituents on the Lewis acid Al center become less electron donating and more electron withdrawing (and, incidentally, harder bases) as their electronegativity increases in the order $H^- < CH_3^- < F^-$. Note that the order of electron donating ability for H^- and CH_3^- is the opposite observed for carbocations, for which hyperconjugation plays a larger role.

(e) Sec < Cys < Ser. The hardness increases as the electronegativity of the Lewis base chalcogen increases on going from a selenol to a thiol to an alcohol.

The Hard-Soft Acid-Base Principle (HSAB Principle)

The **Hard-Soft acid-base principle (HSAB Principle) explains patterns in Lewis acid-base reactivity in terms of a *like reacts with like preference***. Both thermodynamically and kinetically, hard acids prefer hard bases and soft acids soft bases. Specifically,

- Thermodynamically, hard acids form stronger acid-base complexes with hard bases while soft acids form stronger complexes with soft bases.
- Kinetically, hard acids/electrophiles react more quickly with hard bases/nucleophiles while soft acids/electrophiles react more quickly with soft bases/neucleophiles.

Applications of the HSAB principle include

1. Predicting the equilibrium or speed of *Lewis acid-base metathesis and displacement reactions.* In a Lewis acid-base **metathesis reaction** the acids and bases swap partners

$$\mathbf{A_1 : B_1 + A_2 : B_2 \overset{k_1,\, K_{eq_1}}{\rightleftharpoons} A_1 : B_2 + A_2 : B_1}$$

For example, the equilibrium position of the metathesis reaction between $\mathbf{TlF}$ and $\mathbf{K_2S}$ favors the products:

$$\mathbf{2\,TlF + H_2S \rightleftharpoons Tl_2S + 2\,KF}$$

consistent with the HSAB's hard-hard and soft-soft preference.



The HSAB principle also allows for prediction of the position of displacement reactions, in which a Lewis acid or base forms an adduct using a base or acid from an existing Lewis acid-base complex. In these reactions, the displacement of acid or base from the reactant complex may be thought of as a sort of metathesis reaction, one in which in the unbound acid or base switches places with one in the complex. For example, the reaction between **HI** and methylmercury cation

$$\mathbf{HI + HgSCH_3^+ \rightleftharpoons CH_3SHgI + H^+}$$

involves displacement of an iodide from **HI** to give $\mathbf{CH_3HgI}$. The position of the equilibrium favors $\mathbf{CH_3HgI}$ since both $\mathbf{CH_3Hg^+}$ and $\mathbf{I^-}$ are soft, while $\mathbf{H^+}$ is a hard acid.



? Exercise 3.6.3.3.1.2

Predict the position of equilibrium for the following reaction.

$$\mathbf{Fe_2O_3 + 3\,Ag_2S \rightleftharpoons Fe_2S_3 + 3\,Ag_2O}$$

Answer

The equilibrium will favor the reactants (K<1) since the hard-hard and soft-soft interactions in the reactants are more stable than the hard-soft interactions in the products.



? Exercise 3.6.3.3.1.3

Predict whether K for the following equilibria will be <<1, ~1, or >>1.

a. $\mathbf{2\,HF + (CH_3Hg)_2S \rightleftharpoons 2\,CH_3HgF + H_2S}$
b. $\mathbf{Ag(NH_3)_2^+ + 2\,PH_3 \rightleftharpoons Ag(PH_3)_2^+ + 2\,NH_3}$
c. $\mathbf{Ag(PH_3)_2^+ + 2\,H_3B{-}SH_2 \rightleftharpoons 2\,H_3B{-}PH_3 + Ag(SH_2)_2^+}$
d. $\mathbf{H_3B{-}NH_3 + F_3B{-}SH_2 \rightleftharpoons H_3B{-}SH_2 + F_3B{-}NH_3}$

Answer

a. K< < 1 since the reactant adducts are hard-hard and soft-soft while the products involve hard-soft interactions.

b. K>>1 since the reactant complex, diamine silver(I), is a complex of a hard base, NH_3, with the soft acid, Ag^+, while the product is a complex of the same soft acid with the soft base phosphine.

c. K~1 since all the adducts amongst the reactants and products involve soft acids and bases.

d. K>>1 since BH_3 is a softer acid than BF_3, so it will form a stronger complex with the softer base H_2S while the harder BF_3 forms a stronger complex with the harder base NH_3.

2. Predicting the relative strengths of a given set of *Lewis acids or bases towards a particular substrate*. Consider, for example, the relative strengths of a BH_3, BMe_3, and BF_3 towards group 15 hydrides like NH_3, PH_3, and AsH_3. Of the

boranes listed, the hardest acid BF_3 is the strongest acid towards the hard base NH_3 while BH_3 is the strongest towards AsH_3.[†]

? Exercise 3.6.3.3.1.4

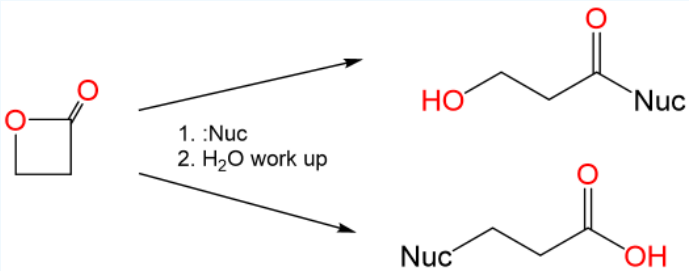
Which acid will form the most stable complex with **CO**: $\mathbf{BH_3}$, $\mathbf{BF_3}$, or $\mathbf{BMe_3}$?

Answer

$\mathbf{BH_3}$. Since **CO** forms complexes primarily through its carbon lone pair, it is a soft base and so will form the strongest complex with the softest Lewis acid.

? Exercise 3.6.3.3.1.5

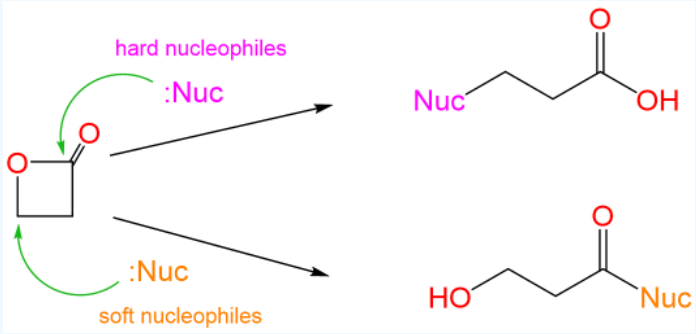
When lactones react with nucleophiles, they can undergo ring opening reactions to give either an alcohol or a carboxylic acid, as shown for propiolactone below:



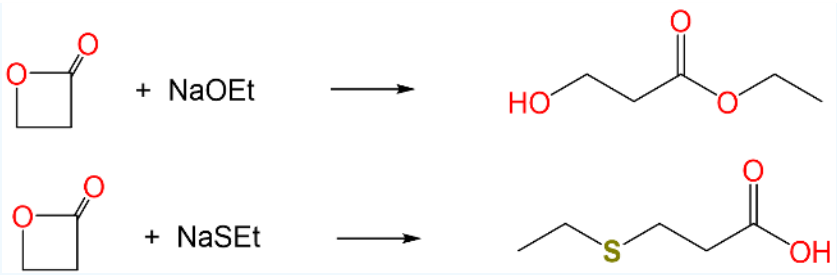
In the reaction above, sterically unhindered alkoxides give one product and sterically unhindered thioalkoxides the other. Explain why this is the case and predict the products of the reaction between propiolactone and the sodium salts of ethoxide and thioethoxide.

Answer

The two reaction products correspond to nucleophilic attack at the lactones' two electrophilic carbon centers. Specifically, the acid is produced by attack at the softer C^{I} center of the CH_2 directly attached to the ester oxygen and the alcohol by nucleophilic attack at the harder C^{III} center of the ester carbonyl.



Consequently, it is reasonable to expect that the harder base ethoxide will nucleophilically attack the harder carbonyl carbon while the softer thioethoxide will attack the softer methylene carbon.



The theoretical interpretation of the hard-soft acid-base principle is that hard-hard preferences reflect superior electrostatic stabilization while soft-soft preferences reflect superior covalent stabilization.

The hard-hard and soft-soft preferences in Lewis acid-base interactions reflect that

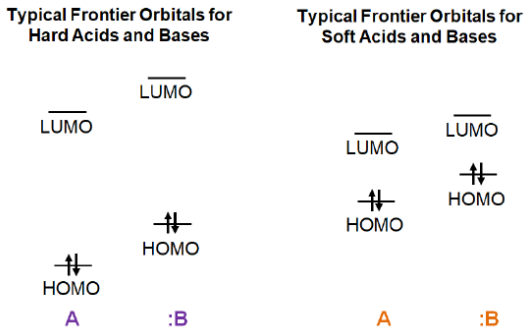
- The lone pair of a hard base is strongly stabilized electrostatically by a hard acid.
- The lone pair of a soft base is strongly stabilized by forming a covalent bond with a soft acid.
- The lone pair of a hard or soft base is comparatively weakly stabilized by an acid opposite to it in hardness or softness since the overall electrostatic and covalent stabilization of the adduct is comparatively weak.

To see why this is the case it is helpful to divide the contributions to the interaction energy between an acid and a base as follows:

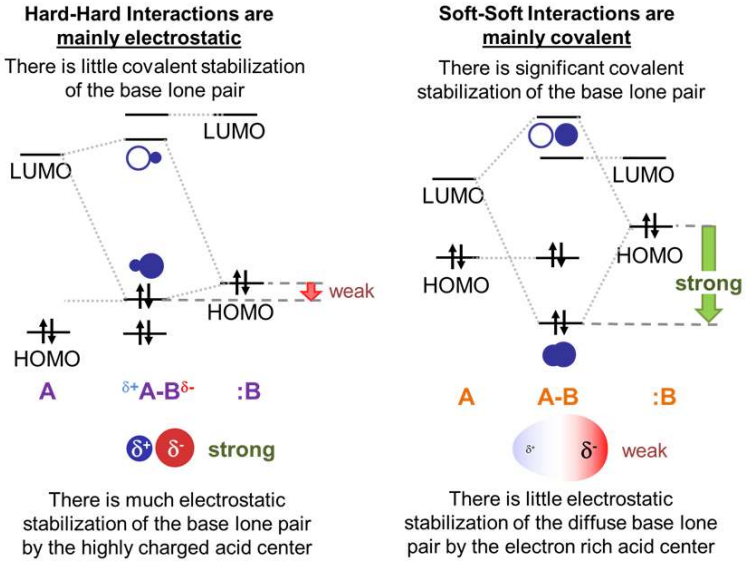
$$\text{Interaction Energy} = \underbrace{\text{Electrostatic attractions and repulsions of partial atomic charges}}_{\text{Ionic term}} + \underbrace{\text{Interactions between filled orbitals on one fragment and unfilled orbitals on the other}}_{\text{Covalent term}} + \underbrace{\text{Electrostatic repulsions between filled orbitals on the two fragments}}_{\text{Steric term}}$$

Of the three contributions to the interaction energy, only the ionic and covalent terms directly relate to the hardness of the interacting acid and base. One approach to thinking about how hardness influences the ionic and covalent contributions is to consider the frontier orbitals involved in the acid-base interaction. This is sometimes done through the use of the Salem-Klopman equation,[1,*] although in the treatment which follows a more qualitative approach will be employed.

Both hard acids and bases will have comparatively low energy HOMO levels and high energy LUMO levels, with a correspondingly high HOMO-LUMO gap. In contrast, soft acids and bases will have comparatively high-energy HOMO levels and low-energy LUMO levels, giving a comparatively smaller HOMO-LUMO gap.



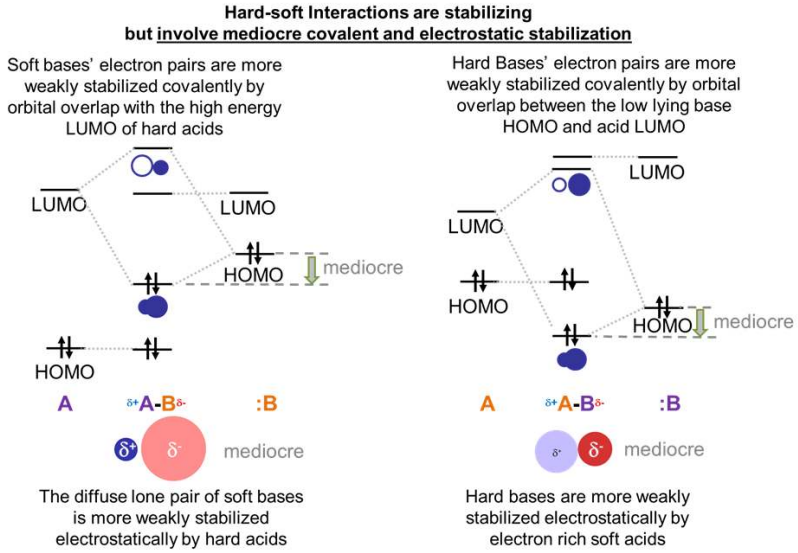
Given this, consider the frontier orbital interactions involved in the formation of an acid-base complex for the possible cases, as illustrated schematically below.



The large gap in energy between hard bases' highly stabilized HOMO lone pairs and the high energy LUMO of hard acids ensures that in **hard acid-hard base adducts the dominant stabilizing interaction will involve electrostatic attraction between the base lone pair and the electropositive Lewis acid center**. Fortunately, since the electron clouds in hard bases are relatively dense and electron rich while hard Lewis acids are highly charged and small, these electrostatic interactions are strong.

In contrast, in **soft acid-soft base adducts, the dominant stabilizing interaction will be covalent.** This is because the small gap in energy between a soft base HOMO and soft acid LUMO enables the formation of a well-stabilized bonding orbital with significant electron density between the acid and base.

The orbitals' interactions between hard acids and soft bases and soft acids and hard bases are intermediate between the hard acid-hard base and soft acid-soft base cases.



This means that the adducts are stable relative to free acid and base – just not as well stabilized as in the hard acid and hard base case. In the case of hard acids and soft bases the hard acids are less able to stabilize the soft bases' relatively diffuse electron pair electrostatically and there isn't as much covalent stabilization as in adducts of soft acids and bases due to the hard acid's high energy.

References

1. Ahrland, S.; Chatt, J.; Davies, N. R., The relative affinities of ligand atoms for acceptor molecules and ions. Quarterly Reviews, Chemical Society 1958, 12 (3), 265-276.

2. Pearson, R. G., Hard and Soft Acids and Bases. Journal of the American Chemical Society 1963, 85 (22), 3533-3539.

3. Fleming, I., Molecular orbitals and organic chemical reactions. Reference ed.; Wiley: Hoboken, N.J., 2010.

Notes

* Despite the fruitfulness of this observation, in general it is important to reduce the potential for observer bias by checking observations like these against compounds reported in the chemical literature and databases like the Inorganic Crystal Structure and Cambridge Crystallographic Databases.

** These are very soluble in water, to the point where some solutions are perhaps better described as solutions of water in the halide.

† This can be predicted based on the relative hardness of BF_3, BR_3, and BH_3 in the list of hard and soft acids. However, for those of you who may be confused as to why H is considered a better electron donor for the purposes of softening a Lewis acid center while alkyl groups are better electron donors for the purposes of stabilizing carbocations in organic chemistry, the dominant effect is the lower electronegativity of H relative to carbon (in CH_3). The effect of electron donation due to hyperconjugation isn't as great for thermodynamically stable bases like BX_3/BR_3.

†† For more on the Salem-Klopman equation see Fleming, I., Molecular orbitals and organic chemical reactions. Reference ed.; Wiley: Hoboken, N.J., 2010; pp. 138-143.

3.6.3.3.1: Hard-Hard and Soft-Soft preferences may be explained and quantified in terms of electrostatic and covalent and electronic stabilization on the stability of Lewis acid-base adducts is shared under a CC BY-NC-SA 4.0 license and was authored, remixed, and/or curated by Stephen M. Contakes.

- **6.6.2: Hard-Hard and Soft-Soft preferences may be explained and quantified in terms of electrostatic and covalent and electronic stabilization on the stability of Lewis acid-base adducts** by Stephen M. Contakes is licensed CC BY 4.0.

3.6.3.3.2: Quantitative Measures of Hardness, Softness, and Acid-Base Interactions from a Hard Soft Acid-Base Principle Perspective Involve Orbital Energies and/or Apportioning Acid-Base Bonding in Terms of Electrostatic and Covalent Factors

Pearson Absolute Hardness is a useful metric of hardness based on orbital energies

The recognition that hard acids and bases possess a large HOMO-LUMO gap suggests that the gap size itself might serve as a useful index of hardness. The basis for this idea may be found by considering Pearson's definition of absolute hardness, η.[1] **Pearson's absolute hardness, η**, is half the second derivative of a species' energy with respect to changes in total number of electrons, N_{e^-}.

$$\text{Pearson's absolute hardness} = \eta = \frac{1}{2}\frac{d^2E}{dN_{e^-}^2}$$

$$(in \;\; eV)$$

and, since acids' and bases' hardness and softness are inversely related, Pearson's absolute softness, σ, is just the inverse of hardness.

$$\text{Pearson's softness} = \frac{1}{\eta}$$

Of these, Pearson's absolute hardness is related to the **Mulliken definition of electronegativity** as the first derivative of a species' energy with respect to changes in total number of electrons.

$$\text{Mulliken electronegativity} = \chi = \frac{dE}{dN_{e^-}}$$

$$(in \;\; eV)$$

Operationally, both the Pearson hardness and Mulliken electronegativity are approximated in terms of the energies associated with unit changes in the number of electrons – *i.e.*, in terms of ionization energies and electronegativities. Specifically,

$$\text{Pearson's absolute hardness} = \eta \approx \frac{IE–EA}{2}$$

$$\text{Mulliken electronegativity} = \chi \approx \frac{IE + EA}{2}$$

where IE and EA are in eV.

The connection between Pearson's absolute hardness/softness and the HOMO-LUMO gap then follows from Koopman's theorem, in which the ionization energy (IE) is just the opposite of the HOMO energy.

$$IE = -E_{HOMO}$$

Similarly, the electron affinity (EA), defined as the opposite of the energy released on absorption of an electron, may be taken as an approximation of the LUMO energy.

$$E_{LUMO} \approx -EA$$

So Pearson's absolute hardness is just half the HOMO-LUMO gap (band gap) size in electron volts:

$$\text{Pearson's absolute hardness} = \eta \approx \frac{E_{LUMO}–E_{HOMO}}{2}$$

where all values are given in eV,

and the Mulliken electronegativity is just the average of the HOMO and LUMO energies (~Fermi energy):

$$Mulliken\ electronegativity, \chi \approx -\frac{E_{LUMO} + E_{HOMO}}{2}$$

$$where\ all\ values\ are\ given\ in\ eV$$

The relationships between the Pearson absolute hardness, Mulliken electronegativity, and HOMO and LUMO energies are depicted schematically for the group 1A monocations in Figure **3.6.3.3.2.1**.

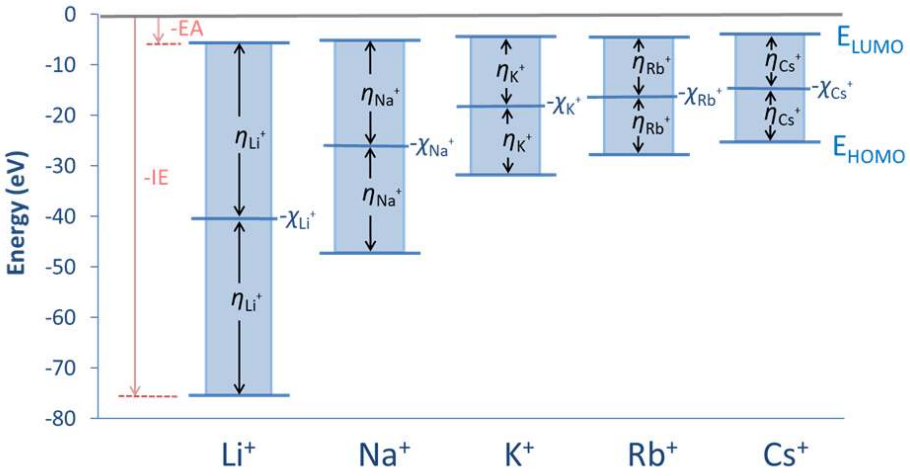


Figure **3.6.3.3.2.1**. Relationships between Pearson absolute hardness, Mulliken electronegativity, and HOMO and LUMO energies for the group 1A monocations.

Values of the Pearson hardness and Mulliken electronegativity for several acids and bases are given in Table **3.6.3.3.2.1**. The values in the table confirm the expected trends, showing an increase in hardness with size (down a group), with increasing charge, and as substituent electronegativity increases for a series of isolobal ions.

Table **3.6.3.3.2.1**: Pearson Absolute Hardness and Related Parameters for Selected Acids and Bases.[2] Taken from Pearson, R. G., Absolute electronegativity and hardness: application to inorganic chemistry. Inorganic Chemistry 1988, 27 (4), 734-740.

Species	Ionization Energy, IE or I (eV)	Electron Affinity, EA or A (eV)	Mulliken Electronegativity, χ (eV)	Pearson Absolute Hardness, η (eV)
Selected Acids				
Group 1A monocations				
Li^+	75.64	5.39	40.52	35.12
Na^+	47.29	5.14	26.21	21.08
K^+	31.63	4.34	17.99	13.64
Rb^+	27.28	4.18	15.77	11.55
Cs^+	25.1	3.89	14.5	10.6
Group 11 monocations				
Cu^+	20.29	7.73	14.01	6.28
Ag^+	21.49	7.58	14.53	6.96
Au^+	20.5	9.23	14.9	5.6
Isoelectronic Row 3 Metal Cations				
Na^+	47.29	5.14	26.21	21.08
Mg^{2+}	80.14	15.04	47.59	32.55
Al^{3+}	119.99	28.45	74.22	45.77
Changes with Transition Metal Ion Charge				
Fe^{2+}	30.65	16.18	23.42	7.24
Fe^{3+}	54.8	30.65	42.73	12.08
Co^{2+}	33.50	17.06	25.28	8.22
Co^{3+}	51.3	22.5	42.4	8.9
Boron trihalides				
BF_3	15.81	-3.5	6.2	9.7
BCl_3	11.60	0.33	5.97	5.64
BBr_3	10.51	0.82	5.67	4.85
CO_2	13.8	-3.8	5.0	8.8
CS_2	10.08	0.62	5.35	5.56
Selected Bases				
Group 17 monoanions (taken to be identical to the free atom values; for arguments as to why this is reasonable see Pearson, R. G., Inorg. Chem. 1988, 27 (4), 734-740.)				
F^-	17.42	3.40	10.41	7.01
Cl^-	13.01	3.62	8.31	4.70
Br^-	11.84	3.36	7.60	4.24
I^-	10.45	3.06	6.76	3.70

Species	Ionization Energy, IE or I (eV)	Electron Affinity, EA or A (eV)	Mulliken Electronegativity, χ (eV)	Pearson Absolute Hardness, η (eV)
Group 15 hydrides				
NH_3	10.7	-5.6	2.6	8.2
PH_3	10.0	-1.9	4.1	6.0
Trimethylpnictides				
NMe_3	7.8	-4.8	1.5	6.3
PMe_3	8.6	-3.1	2.8	5.9
$AsMe_3$	8.7	-2.7	3.0	5.7
Group 16 hydrides				
H_2O	12.6	-6.4	3.1	9.5
H_2S	10.5	-2.1	4.2	6.2
Phosphorous trihalides				
PF_3	12.3	-1.0	5.7	6.7
$PC1_3$	10.2	0.8	5.5	4.7
PBr_3	9.9	1.6	5.6	4.2

Drago-Wayland Acid-Base Parameters allow for estimation of the electrostatic and covalent contributions to the enthalpy of formation of a Lewis acid-base adduct.

Although Pearson hardness values are a useful metric of acids' and bases' hardness, they cannot easily be used to estimate the Lewis acid-base interaction energy. This is not the case for the EC model developed by Drago and Wayland.[3] In the **Drago and Wayland's EC Model,** the enthalpy of formation of an acid-base adduct, AB,

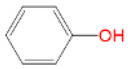
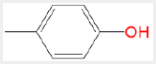
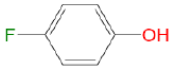
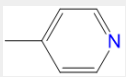
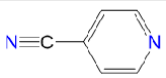
$$A + B \rightleftharpoons AB \qquad \Delta H_{AB\ adduct}$$

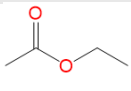
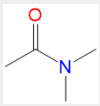
from the acid (A) and base (B) can be calculated as the sum of products of electrostatic (E) and covalent (C) factors that reflect the propensity of the acid and base to engage in strong electrostatic and covalent interactions with one another:

$$-\Delta H_{AB\ adduct} = E_A E_B + C_A C_B$$

where E_A and C_A are the electrostatic and covalent parameters for the acid and E_B and C_B the electrostatic and covalent parameters for the base given in units of $kcal^{½}\ mol^{-½}$. E and C parameters for selected acids and bases are given in Table **3.6.3.3.2.2** .

Table **3.6.3.3.2.2**: E and C Parameters for selected Lewis acids and bases according to the ECW model.[4,5] Taken from Vogel, G. C.; Drago, R. S., The ECW Model. *Journal of Chemical Education* 1996, 73 (8), 701 and Drago, R. S. A modern approach to acid-base chemistry. *Journal of Chemical Education* 1974, 51 (5), 300 (for BF_3).

Species	E (kcal^{½} mol$^{-½}$)	C (kcal^{½} mol$^{-½}$)	W (kcal mol^{-1})	C/E
Acids				
I_2	0.5†	2†	0	4
ICl	2.92	1.66	0	0.57
H_2O	1.31	0.78	0	0.59
SO_2	0.51	1.56	0	3.1
$HCCl_3$ (chloroform)	1.56	0.44	0	0.28
$(CH_3)_3COH$	1.07	0.69	0	0.65
$(CF_3)_3COH$	3.06	1.88	-0.87	0.61
	2.27	1.07	0	0.47
	2.23	1.03	0	0.46
	2.30	1.11	0	0.48
	1.38	0.68	0	0.49
BF_3	1.62	9.88		6.10
$B(CH_3)_3$	2.90	3.60	0	1.2
$Al(CH_3)_3$	8.66	3.68	0	0.43
$Ga(C_2H_5)_3$	6.95	1.48	0	0.21
$In(CH_3)_3$	6.60	2.15	0	0.33
$Zn[N(Si(CH_3)_3)]_2$	2.75	2.32	0	0.84
$Cd[N(Si(CH_3)_3)]_2$	2.50	1.83	0	0.73
Bases				
NH_3	2.31	2.04		0.88
CH_3NH_2	2.16	3.13		1.4
$(CH_3)_2NH$	1.80	4.21		2.3
$(CH_3)_3N$	1.21	5.61		4.6
	1.78	3.54		2.0
	1.81	3.73		2.0
	1.53	2.94		1.9

Species	E ($kcal^{½}$ $mol^{-½}$)	C ($kcal^{½}$ $mol^{-½}$)	W ($kcal$ mol^{-1})	C/E
CH_3CN	1.64	0.71		0.43
$ClCH_2CN$	1.67	0.33		0.20
$CH_3C(O)CH_3$	1.74	1.26		0.72
$(C_2H_5)_2O$	1.80	1.63		0.91
	1.64	2.18		1.3
 (EtOAc)	1.63	0.95		0.58
	2.35†	1.31		0.56
$(CH_3)_2S$	0.25	3.75		15
$(CH_3CH_2)_2S$	0.24	3.92†		15
	0.26	4.07		16
$(CH_3)_2Se$	0.05	4.24		83
$(CH_3)_2SO$	2.4	1.47		0.61
$(CH_3)_3P$	0.25	5.81		24
$(CH_3O)_3P$	0.13	4.83		37
$(C_6H_5)_3PO$	2.59	1.67		0.64
$(C_6H_5)_3PS$	0.35	3.65		10
C_6H_6	0.70	0.45		0.64

† These values were fixed to parameterize the rest of the E and C parameters.

Trends in the relative values of C and E for the acids and bases in Table **3.6.3.3.2.2** are very roughly consistent with the trends in hardness and softness outlined earlier. However, the parameters suggest that some trends in hardness reflect changes in species' ability to engage in ionic interactions while others reflect changes in species' ability to engage in strong covalent interactions. For example, C_B for the dimethylchalcogenides increases steadily from 1.5 to 4.25 $kcal^{½}$ $mol^{-½}$ on going from Me_2O to Me_2Se while E_B decreases from 1.68 to 0.05 $kcal^{½}$ $mol^{-½}$, suggesting that electrostatic and covalent factors are both involved in a decrease in base hardness down group 16. However, in the case of phosphines and amines it appears that electrostatic factors are primarily responsible for the decrease in hardness down group 15. On going from Me_3N to Me_3P, C_B only increases slightly from 5.61 to 5.81 $kcal^{½}$ $mol^{-½}$ while E_B decreases from 1.21 to 0.25 $kcal^{½}$ $mol^{-½}$ - *i.e.*, to 20% of the Me_3N value.

However, some species tend to have very high values for both E and C, reflecting their ability to engage in strong electrostatic and covalent interactions, while others have small values for both, reflecting their relative stability as free species in solution.

As can be seen by comparing the acids and bases listed in the absolute hardness table (Table **3.6.3.3.2.1**) and the EC parameters table (Table **3.6.3.3.2.2**). The EC model has primarily been applied to organic and main group organometallic acids and bases. However, a variety of extensions have been proposed that enable its wider applicability.

The simple EC model only includes electrostatic and covalent considerations and thus ignores steric, lattice energy, and other contributions to the interaction energy. Thus it is only useful for analyzing the interaction energies of sterically unhindered adducts in which solvation energy and other contributions to the overall interaction energy are insignificant. However, additional refinements of the model attempt to extend its usefulness by accomodating various factors, such as

- *Steric strain.* Specifically, Hancock and Martell[6] introduced a D parameter to account for any additional steric strain introduced upon adduct formation,* giving

$$-\Delta H_{AB\ adduct} = E_A E_B + C_A C_B - D_A D_B$$

- *Charge transfer upon adduct formation.* As discussed in section 6.4.2, the formation of a Lewis acid-base complex results in a net transfer of electron density from the electron donor (base) to the acceptor (acid). Drago and Wong[7] extended the EC model to include that charge transfer by adding what they called receptance factors that account for the acid's ability to receive electron density (R_A) and transference factors that account for the base's ability to donate electron density (T_B), giving

$$-\Delta H_{AB\ adduct} = E_A E_B + C_A C_B + R_A T_B$$

  This extension of the EC model is called the **electrostatic-covalent-transfer or ECT model**. Notably, it has been applied successfully to adducts involving ions, for which the $R_A T_B$ term can account for as much as 31% of the interaction energy.

- *Any constant energy term, such as the energy needed to cleave a dimer in order to make the Lewis acid (e.g., $Al_2Cl_6 \rightarrow 2AlCl_3$).* Drago and Vogel[4] extended the EC model to accommodate these constant energy terms, which they designated W. The resulting model is called the **ECW model,** for which

$$-\Delta H_{AB\ adduct} = E_A E_B + C_A C_B + W$$

where

$$W = W_A + W_B$$

A simple application of EC and extended EC models is that they allow the enthalpy of adduct formation to be calculated. These enthalpy calculations based on the EC model are consistent with the superior interaction energy of hard-hard and soft-soft interactions compared to hard-soft ones. Consider, for example, the transfer of I_2 between BF_3 and $InMe_3$, H_3N-BF_3, and H_3N-$InMe_3$.

$$H_3N - BF_3 + InMe_3 \rightleftharpoons BF_3 + H_3N - InMe_3$$

Since H_3N is a hard base and BF_3 and $InMe_3$ are harder and softer acids, respectively, the equilibrium is expected to favor the reactant, H_3N-BF_3. Assuming the equilbrium is enthalpically driven, this qualitative analysis is consistent with the expected endothermic enthalpy of the reaction, as may be seen from the calculated enthalpies of adduct formation for both H_3N-BF_3 and H_3N-$InMe_3$.

For H_3N-BF_3:

$$-\Delta H_{H_3N-BF_3} = E_{BF_3} E_{NH_3} + C_{BF_3} C_{NH_3}$$

$$-\Delta H_{H_3N-BF_3} = (1.62)(2.31) + (9.88)(2.04)$$

$$-\Delta H_{H_3N-BF_3} = 3.74\ kcal/mol + 20.1\ kcal/mol = 23.8\ kcal/mol$$

$$\Delta H_{H_3N-BF_3} = -23.8\ kcal/mol$$

For H_3N-$InMe_3$:

$$-\Delta H_{H_3N-InMe_3} = E_{InMe_3} E_{NH_3} + C_{InMe_3} C_{NH_3}$$

$$-\Delta H_{H_3N-InMe_3} = (6.6)(2.31) + (2.15)(2.04)$$

$$-\Delta H_{H_3N-InMe_3} = 15.25\ kcal/mol + 4.39\ kcal/mol = 19.63\ kcal/mol$$

$$\Delta H_{H_3N-InMe_3} = -19.63\ kcal/mol$$

So H_3N-BF_3 is enthalpically favored by -4.2 kcal/mol [=-23.8 kcal/mol - (-19.63 kcal/mol) according to Hess' Law].

In addition to their utility for estimating enthalpies of Lewis acid-base complex formation, EC and related models serve as a useful tool for estimating the relative importance of ionic, covalent, and steric factors in complex formation. Specifically,

- The relative contributions of ionic and covalent factors can be calculated directly, as from the E and C terms. This can provide insight into why some complexes are more stable than others. Such calculations reveal that the hard-hard adduct H_3N-BF_3 is favored over the hard-soft adduct H_3N-$InMe_3$ because of the strong covalent interaction holding together H_3N-BF_3. The covalent term accounts for 84% of the energy of the H_3N-BF_3 interaction and is largely lost upon formation of H_3N-$InMe_3$, for which it contributes only 22% of the interaction energy. When the electrostatic term is accounted for, it can be seen that the formation of H_3N-$InMe_3$ from H_3N-BF_3 is disfavored, since it would result in a loss of 15.7 kcal/mol of covalent stabilization that would be incompletely compensated for by a gain of 11.5 kcal/mol of electrostatic stabilization.
- The role of other contributions to the bonding in a Lewis acid-base complex may be estimated from the discrepancy between the experimental and EC model calculated stabilization energies. This is because the EC parameters assume sigma bonding and so any deviation between the calculated and experimental enthalpies of complex formation can be attributed to non-sigma contributions.
    - This is done explicitly in extensions of the EC model. For instance, in the case of the Hancock and Martell, ECT, and ECW extensions of the EC model, the contributions of the steric, charge transfer, and constant energy factors (like dimer dissociation) are directly computed in the model.
    - Comparisons of the difference between the energies calculated using ordinary EC parameters and the observed enthalpies has also been used as an estimate of the
        - steric strain energy in strained adducts, which exhibit a less exothermic heat of adduct formation than expected
        - π-backbonding energy in adducts which are capable of such interactions and exhibit a more exothermic heat of formation than expected.[8-10]
    - For examples see (a) Drago, R. S., The interpretation of reactivity in chemical and biological systems with the E and C model. Coordination Chemistry Reviews 1980, 33 (3), 251-277; (b) Drago, R. S.; Bilgrien, C. J., Inductive transfer and coordination of ligands in metal—metal bonded systems. Polyhedron 1988, 7 (16), 1453-1468; (c) Drago, R. S., The question of a synergistic metal-metal interaction leading to .pi.-back-bond stabilization in dirhodium tetrabutyrate adducts. Inorganic Chemistry 1982, 21 (4), 1697-1698.
- The role of electrostatic, covalent, and other contributions to the spectroscopic behavior of Lewis acid-base complexes can be assessed similarly using specialized versions of the ECW or ECT model that allow for calculation of changes in spectroscopic parameters upon adduct formation - *e.g.*, OH stretching frequencies. Details are beyond the scope of this text but may be found in the original literature,[11] for example, Drago, R. S.; Vogel, G. C. *JACS* 1992, 114 (24), 9527-9532; Vogel, G. C.; Drago, R. S., *J. Chem. Educ.* 1996, 73 (8), 701; Drago, R. S.; Wong, N. M., *J. Chem. Educ.* 1996, 73 (2), 123.).

Pearson Softness Parameters have been proposed as a means of calculating the equilibrium constant for formation of a Lewis acid-base adduct, although they are more commonly used to estimate metal toxicity

Pearson also proposed a softness parameter that can be used to estimate the thermodynamics of Lewis acid-base complex formation, this time in the form of the equilibrium constant for

$$A + B \overset{K}{\rightleftharpoons} AB$$

for which Pearson proposed

$$logK = S_A S_B + \sigma_A \sigma_B$$

where S_A and S_B are acid and base parameters related to the strength of the acid-base interaction and σ_A and σ_B are acid and base parameters related to softness. This approach hasn't found as wide an acceptance in studies of chemical reactivity as the Drago-Wayland and absolute hardness parameters. However, because the toxicity of metal ions sometimes depends on their propensity to bind soft Lewis bases in living systems, the softness parameters which Pearson and Mawby subsequently proposed based on the relative energies of metal fluorine and metal iodine bonds[12] have been widely used as a tool for predicting metal ion toxicity.[13]

References

1. Pearson, R. G., Absolute electronegativity and absolute hardness of Lewis acids and bases. *Journal of the American Chemical Society* 1985, 107 (24), 6801-6806.

2. Pearson, R. G., Absolute electronegativity and hardness: application to inorganic chemistry. *Inorganic Chemistry* 1988, 27 (4), 734-740.

3. Drago, R. S.; Wayland, B. B., A Double-Scale Equation for Correlating Enthalpies of Lewis Acid-Base Interactions. *Journal of the American Chemical Society* 1965, 87 (16), 3571-3577.

4. Vogel, G. C.; Drago, R. S., The ECW Model. *Journal of Chemical Education* 1996, 73 (8), 701.

5. Drago, R. S. A modern approach to acid-base chemistry. *Journal of Chemical Education* 1974, 51 (5), 300

6. Hancock, R. D.; Martell, A. E., Hard and Soft Acid-Base Behavior in Aqueous Solution: Steric Effects Make Some Metal Ions Hard: A Quantitative Scale of Hardness-Softness for Acids and Bases. *Journal of Chemical Education* 1996, 73 (7), 654.

7. Drago, R. S.; Wong, N. M., The Role of Electron-Density Transfer and Electronegativity in Understanding Chemical Reactivity and Bonding. *Journal of Chemical Education* 1996, 73 (2), 123.

8. Drago, R. S., The interpretation of reactivity in chemical and biological systems with the E and C model. Coordination Chemistry Reviews 1980, 33 (3), 251-277.

9. Drago, R. S.; Bilgrien, C. J., Inductive transfer and coordination of ligands in metal—metal bonded systems. Polyhedron 1988, 7 (16), 1453-1468.

10. Drago, R. S., The question of a synergistic metal-metal interaction leading to .pi.-back-bond stabilization in dirhodium tetrabutyrate adducts. Inorganic Chemistry 1982, 21 (4), 1697-1698.

11. Drago, R. S.; Vogel, G. C., Interpretation of spectroscopic changes upon adduct formation and their use to determine electrostatic and covalent (E and C) parameters. *Journal of the American Chemical Society* 1992, 114 (24), 9527-9532.

12. Pearson, R. G.; Mawby, R. J. The Nature of Metal-Halogen Bonds in Gutmann, V. *Halogen Chemistry, vol. 3.* Academic Press: London, 1967, pp. 55-84.

13. Kinraide, T. B. Improved Scales for Metal Ion Softness and Toxicity *Environmental Toxicology and Chemistry* 2009, 28 (3), 525-533.

Notes

* More precisely, the D parameters account for the difference in steric strain in the adduct relative to a water adduct of the Lewis acid.

3.6.3.3.2: Quantitative Measures of Hardness, Softness, and Acid-Base Interactions from a Hard Soft Acid-Base Principle Perspective Involve Orbital Energies and/or Apportioning Acid-Base Bonding in Terms of Electrostatic and Covalent Factors is shared under a CC BY-NC-SA 4.0 license and was authored, remixed, and/or curated by Stephen M. Contakes.

- **6.6.1: Quantitative Measures of Hardness, Softness, and Acid-Base Interactions from a Hard Soft Acid-Base Principle Perspective Involve Orbital Energies and/or Apportioning Acid-Base Bonding in Terms of Electrostatic and Covalent Factors** by Stephen M. Contakes is licensed CC BY 4.0.

3.6.3.4: Problems

6.07: Problems

3.6.3.4: Problems is shared under a CC BY-NC-SA 4.0 license and was authored, remixed, and/or curated by LibreTexts.

3.6.4: Coordination Numbers and Structures

Why Do Coordination Complexes Form the Structures They Do?

As with all chemical structure, coordination complexes form the structures they do so as to best stabilize the metal center and ligands through the formation of metal-ligand bonds. while avoiding destabilizing interactions like steric repulsions. The issue then is how many metal-ligand bonds should be formed and how those bonds should be arranged spatially to give the largest net stabilization possible. This question will eventually be considered in detail in connection with the nature of bonding in coordination compounds. For now, it will be helpful to think about it in terms of seven factors:

The stabilizing effect of metal-ligand bond formation

The driving force for complex formation is the stabilization of electrons in covalent chemical bonds. In the vast majority of cases this largely involves stabilization of the ligand lone pair is as it experiences the effective nuclear charge of the metal, although in a few involves stabilization of metal electrons by ligand nuclei (inverse ligand fields). Regardless, metal-ligand bond formation is stabilizing and classified in the way its effect is to preference the addition of ligands to the complex.

Steric effects

One reason coordination numbers do not increase indefinitely is that only so many ligands can fit around a metal. Exactly how many can fit depends on:

- **Size of metal center:** This is one of the more important factors and many metals tend to exhibit preferred coordination numbers, which depend on their oxidation state and size as shown in Figure **3.6.4.1**. Larger inner transition metals like the lanthanides and actinides can accommodate 9-12 sterically undemanding ligands while the smaller transition metals tend to accommodate up to six, although larger coordination numbers are more common for larger low valent metals. Thus molybdenum forms seven and eight coordinate $[Mo^{III}(CN)_7]^{4-}$ and $[Mo^{IV}(CN)_8]^{4-}$ with the sterically undemanding cyano ligand.
- **Size and shape of ligands:** As long as ligands are not excessively rigid and bulky their size is less important than the size of the metal in determining the number of ligands that coordinate. Ligands' ability to donate electrons to the metal center also tends to influence coordination number more than ligand size. However, all other things being equal for a given metal and ligand donor ability, small ligands allow higher coordination numbers while fewer bulky ligands will fit around the metal center. Ligands that are more sterically demanding in the vicinity of the metal center tend to limit the ability of other ligands to bind than those which bind through a small extended group. For example, a bulky isocyanide like tBuCN will sterically crowd the metal less than a bulky phosphine like $^{t}BuH_2P$ would. For this reason the effective size of a ligand is sometimes rated in terms of either a cone angle of space they are estimated to occupy around the metal (called the Tolman cone angle, it is commonly used to evaluate phosphines' steric bulk) or the in terms of the percentage of the metal's coordination sphere the ligand occupies (called the percent buried volume, it is used to estimate the steric impact of *N*-heterocyclic carbenes).

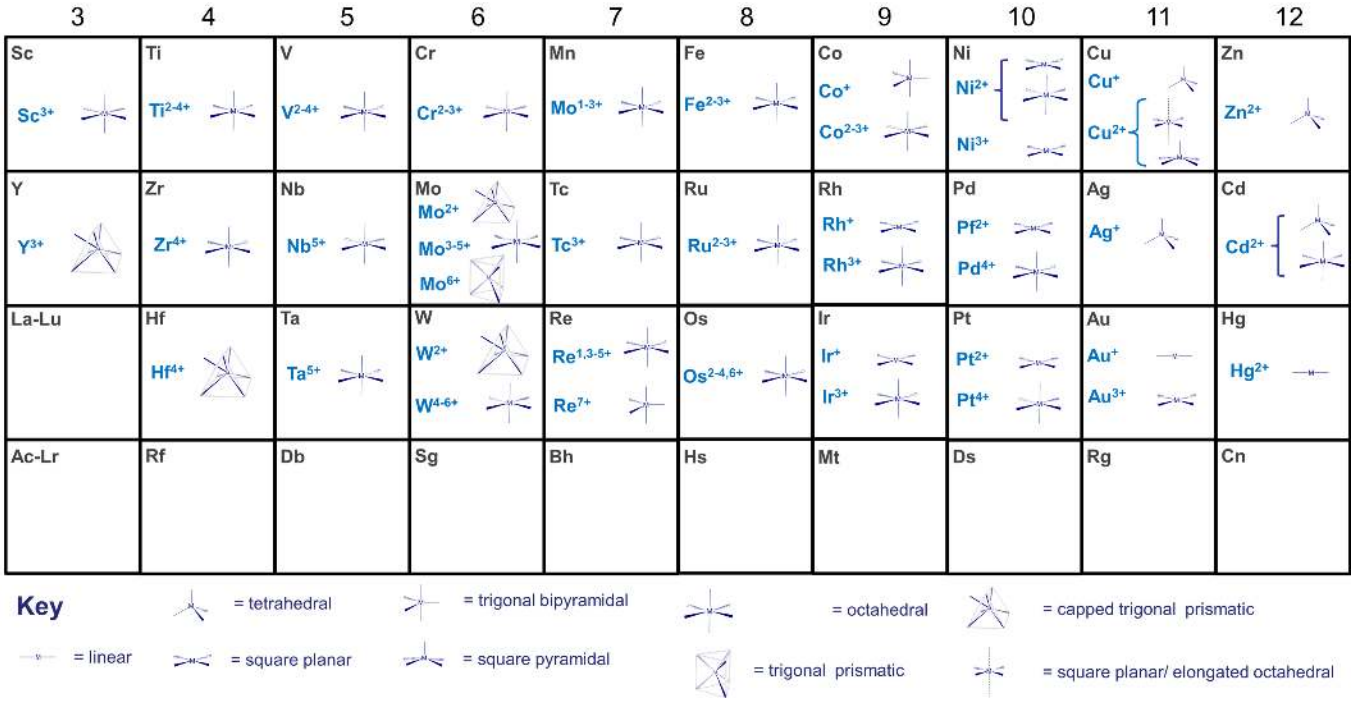


Figure **3.6.4.1**. Preferred coordination geometries of the transition elements. Assignments are as reported in reference 1 except for Cu^{2+}, which is assigned above as square planar/elongated octahedral instead of the square planar assignment given in that work. This work by Stephen Contakes is licensed under a Creative Commons Attribution 4.0 International License.

Repulsion between M-L bonding electrons

For many complexes steric effects are neither the only effects nor the most important. Among the additional factors that should be considered are the repulsions that occur between the electrons that different ligands donate to the metal-ligand bonding. These electron-electron repulsions affect the

- **Coordination number:** When a ligand donates its electrons to a metal center to form a new metal-ligand bond, the electron density around the metal increases, raising the overall energy of the other M-L bonding electrons. This increased repulsion often limits the number of coordinated ligands. As more ligands are added the electron-electron repulsions keep increasing until the lowering of energy of the ligand electrons in the new bond is insufficient to compensate for the raising of energy of the existing M-L bonding electrons. Based on this effect alone:
  - larger metals tend to achieve higher coordination numbers than smaller ones because the electron-electron repulsions are spread across a larger coordiantion sphere.
  - With a given metal, more electron donating ligands have a greater tendency to form complexes with lower coordination numbers than similar neutral ones do. This is why anionic ligands (which tend to be better electron donors) tend to give lower coordination numbers than comparable neutral ligands (which tend to be weaker donors). Thus Co^{2+} forms $CoCl_4^{2-}$ with chloro ligands but $[Co(H_2O)_6]^{2+}$ with aqua ligands.
- **Coordination geometry:** In the Kepert model for the shapes of coordination complexes, this intraligand repulsion determines the most stable coordination geometry by causing the ligands to move as far apart form one another on the metal's coordination sphere as possible.

Formally, according to the Kepert model:

- any of the metal's valence electrons not involved in metal-ligand bonds occupy (n-1)*d* orbitals and function as core electrons. As core electrons they do not influence the molecular shape
- electrons involved in bonding to a given ligand constitute an electron group that repels all other electron groups around the metal.
- all other things being equal the complex will form the geometry that minimizes the repulsions between electron groups.

Notice the similarities of these postulates to those of VSEPR theory. In predicting coordination geometries in terms of electron-electron repulsions, the Kepert model is just an extension of VSEPR theory to coordination compounds. The difference between VSEPR theory and the Kepert model is that in the Kepert model only electrons involved in metal-ligand bonds count.

Coordination geometries predicted by the Kepert model for coordination numbers two through nine are given in Figure **3.6.4.2**. As may be seen from the geoemtries listed in Figure **3.6.4.2**, these are just equivalent to VSEPR geometries for cases in which the number of electron groups is equal to the coordination number.

The difference between optimal and suboptimal coordination geometries is greater with few ligands and becomes smaller and ligands become increasingly dispersed across the metal's coordination sphere. In complexes containing five, seven, eight, or higher coordinate metals a number of geometries that are similar in energy to the preferred geometry. These geometries, which should be regarded as accessible, are also listed in Figure **3.6.4.2**.

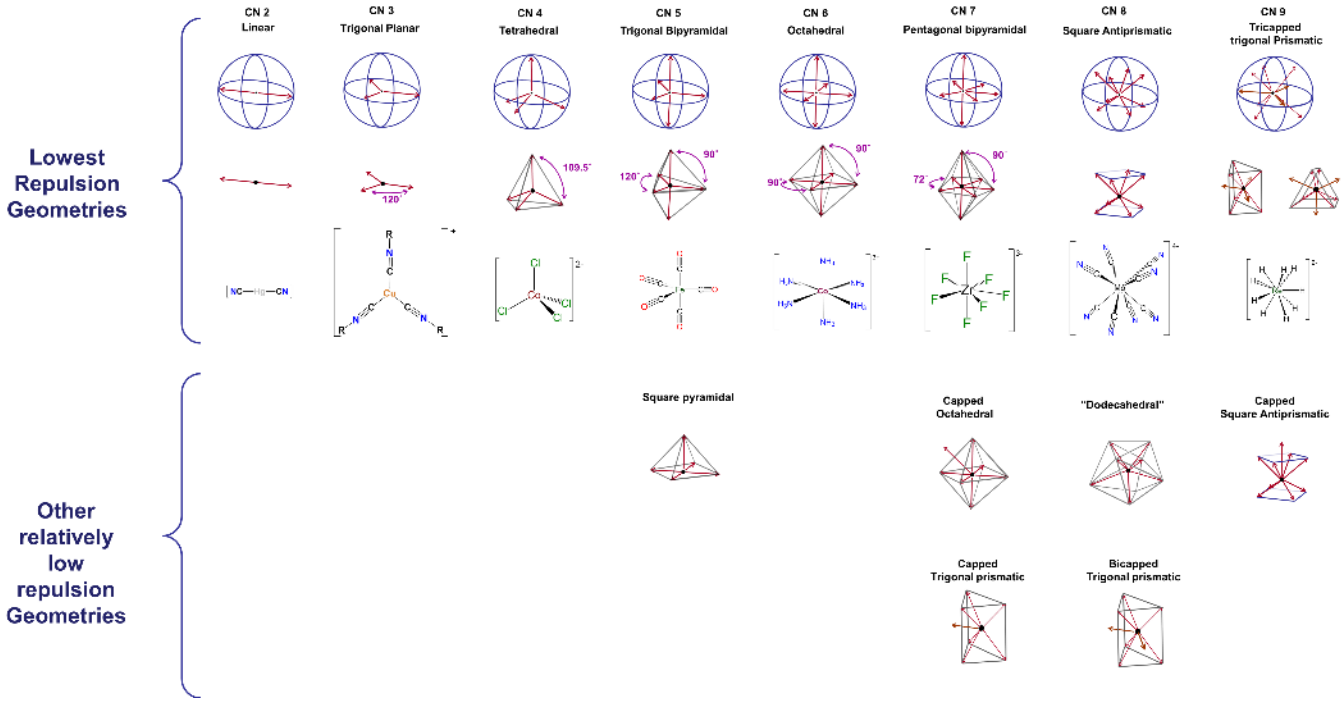


Figure **3.6.4.2**. Coordination geometries predicted by the Kepert model for coordination numbers two through nine along with other coordination geometries similar in energy to the lowest repulsion geometry. This work by Stephen Contakes is licensed under a Creative Commons Attribution 4.0 International License.

Ligand field effects

A few coordination geometries are noticeably absent from the Kepert-preferred and Kepert-accessible geometries in Figure **3.6.4.2**. These include the trigonal prismatic geometries formed by compounds like $W(CH_3)_6$ and the very common square planar geometry illustrated by complexes like $[PtCl_4]^{2-}$ and $[IrClH(PPh_3)_2]$. One of the reasons the Kepert model fails to predict the existence of such structures is its neglect of directional interactions involving *d* electrons on the metal center. Metal *d* electrons exert on profound influence on almost all properties of transition metal complexes, including their structures. The way in which this occurs will be explored at length in the next chapter. For now, it is enough to note that both the ligand-donated electrons surrounding a metal center and the electrons occupying particular *d* orbitals on that metal are oriented in specific directions relative to one another. Because of this the strength of the interactions between the ligand and metal *d* electrons depend on both the number of *d* electrons present, how strongly metal-ligand binding affects their energy, and how the ligands are arranged about the metal center. The impact of these effects, here termed ligand field effects, differ from case to case and can include

- distortions of the complex's geometry. For instance, an ideal octahedral coordination geometry might be tetragonally distorted by flattening or elongating it.
- imparting a strong preference for a non-Kepert coordination geometries. This is why, for example, 2nd and 3rd row complexes in which the metal has a d^8 electron configuration are almost always square planar.

- stabilizing non-Kepert geometries enough to permit complexes to adopt them in the presence of a rigid or semirigid ligand that prefers to coordinate the metal in that geometry.[3]

Because of these effects square planar and trigonal prismatic geometries are also observed and the list of coordination geometries given in Figure **3.6.4.2** may be extended to that shown in Figure **3.6.4.3**.

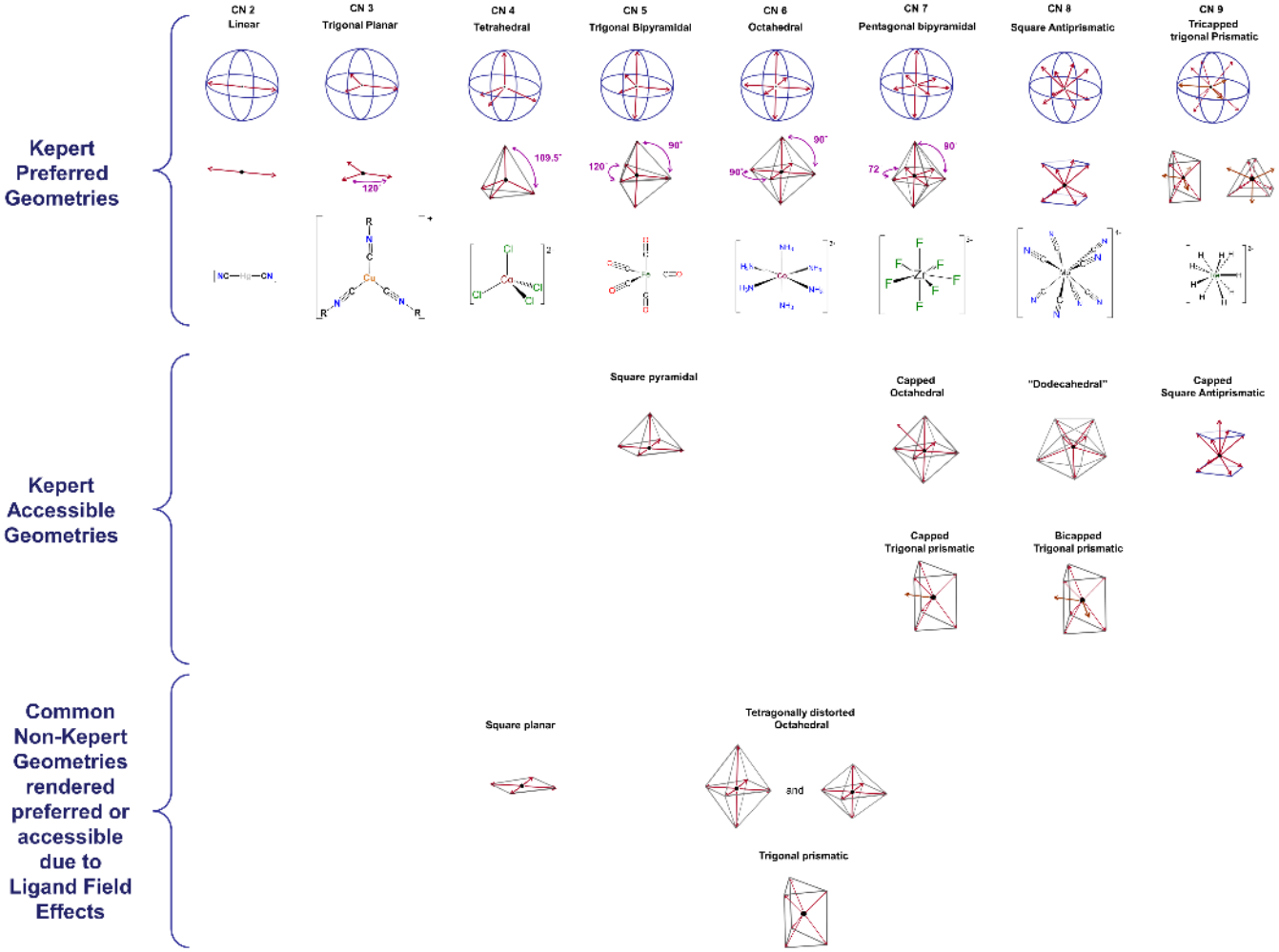


Figure **3.6.4.3**. Coordination geometries accessible in for 2-9 coordinate complexes even without constraint by rigid or semirigid ligands. This work by Stephen Contakes is licensed under a Creative Commons Attribution 4.0 International License.

Ligand geometry constraints

Rigid or semirigid ligands influence the coordination geometry of metal complexes in two main ways:

- Bulky rigid ligands that crowd the metal center prevent other ligands from binding. Such ligands are useful for preparing low-coordinate complexes.
- Rigid and semirigid ligands can impose their preferred coordination geometry on a metal center. This is because these ligands energetically prefer to adopt a particular conformation when they bind a metal center. In doing so they shift the coordination geometry energy landscape toward that preferred geometry. If the shift is large enough relative to the native preference due to ligand repulsion and ligand field effects the complex will either adopt the ligand-preferred geometry or be distorted in the direction of the ligand-preferred geometry. Examples are given in Figure **3.6.4.4**.

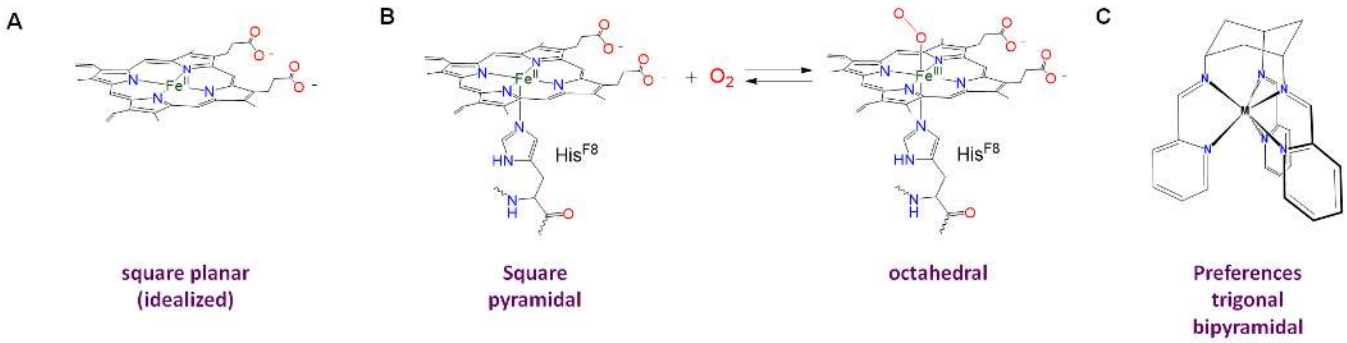


Figure **3.6.4.4**. Examples of rigid or semirigid ligands that can impose their preferred coordination geometry on a metal center. Porphyrins, phyhalocyanines and related macrocycles tend to impose a slightly bent square planar coordination geometry, although (B) many such complexes, including the iron of myoglobin's heme cofactor coordinate additional ligands to give square pyramidal or octahedral complexes. (C) Synthetic multidentate ligands have been developed to preference trigonal prismatic coordination geometries, including the one shown here. It forms roughly trigonal prismatic complexes with Co^{II} and $Zn^{II,}$ albeit imperfect ones.[3]
This work by Stephen Contakes is licensed under a Creative Commons Attribution 4.0 International License.

The influence of ligands on coordination geometry is important in living systems in which proteins and nucleic acids can act as rigid or semirigid ligands. The ability of these ligands to distort the coordination geometries of metal atoms in ways that enable them to perform specific functions is so common that the resulting distorted geometries are termed entactic states. A particulary spectacular case of an entactic state involves the blue copper proteins azurin and plastocyanin, the structure of which is given in Figure **3.6.4.5**.

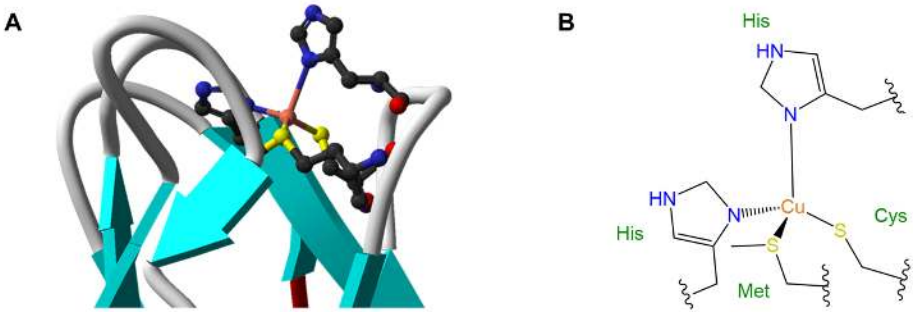


Figure **3.6.4.5**. (A) Structure and (B) schematic of the plastocyanin active site showing the distorted tetrahedral coordination environment that the protein imposes on the copper center (tan), which is most evident from the long vertically oriented Cu-Histidine bond. The image in part A is cropped from an original image by Ben Mills - Own work, Public Domain, https://commons.wikimedia.org/w/inde...?curid=6202620. The image in part B is by Stephen Contakes and licensed under a Creative Commons Attribution 4.0 International License.

As may be seen from the structure in Figure **3.6.4.5**, the copper in plastocyanin exibits a distorted tetrahedral coordination geometry. The protein is said to act like a medieval torture device called a rack in stretching the metal into its distorted geometry. This distortion makes its easier for the copper center to undergo facile redox reactions, enabling it to better function as an electron carrier.

Crystal packing effects

This effect is similar to that of ligand constraints except that in this case arise not from the structure internal to a ligand but out of the forces involves in maximizing the stabilization energy of a crystal. With lower coordination number complexes packing effects can shift the conformations of flexible ligands but only give rise to very small distortions of the overall coordination geometry. Packing effects can drive a shift in the overall coordination geometry of higher coordination number complexes, for which packing effects are significant relative to the small difference in energy between geometries. Thus while $[Mo(CN)_8]^{4-}$ has a square antiprismatic coordination geometry in solution it exhibits a docecahedral coordination geometry in the crystals of many of its salts.

Relatavistic effects on orbital energies

The proximity of fast moving electrons to massive nuclei in the heavier transition elements results in relatavistic expansion and contraction of orbitals. The net results are that

- heavier elements tend to be smaller than expected. This effect preferences lower coordination numbers.
- the relative energies of orbitals shift. Orbitals which become contracted are lowered in energy while those which are expanded increase in energy, as shown for the case of gold in Figure **3.6.4.6*A***.

The combination of smaller sizes and altered orbital energies affect coordination preferences. Relatavistic effects contribute to the greater tendency of Au(I) relative to other group 11 metals to form linear two coordinate complexes. As shown in Figure **3.6.4.6*B***, the relative closeness in energy of the 6*s* and 5*d* orbitals of gold makes mixing of these orbitals more favorable, facilitating the ability of gold to form two coordinate complexes with strong sigma bonds oriented 180° from one another.

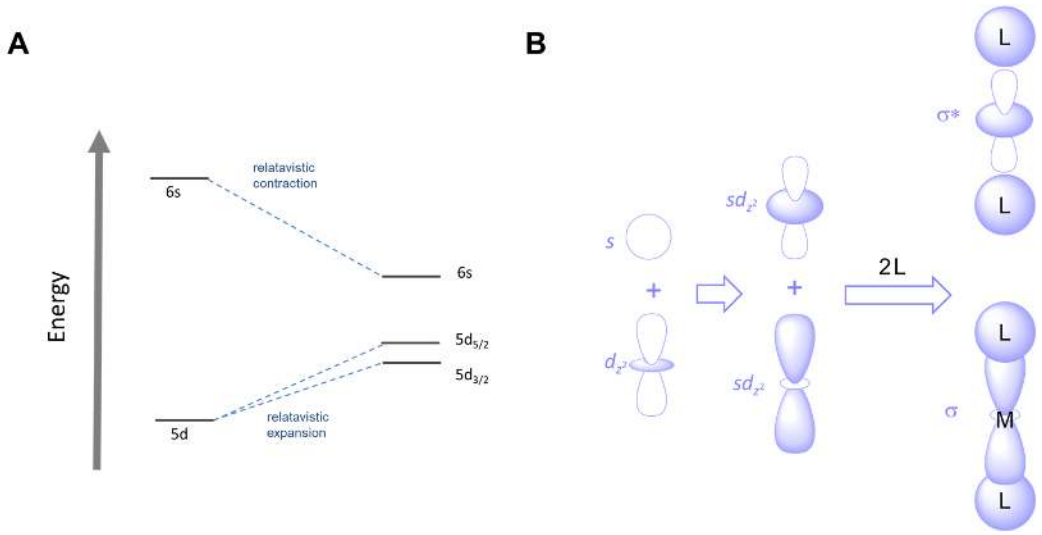


Figure **3.6.4.6**. (A) Gold experiences relatavistic expansion and contraction of its 5*d* and 6*s* orbitals, resulting in shifts to their relative energies. (B) This makes mixing of these orbitals more favorable, facilitating the ability of gold to form two coordinate complexes with strong sigma bonds that involve considerable sd_{z^2} character. This work by Stephen Contakes is licensed under a Creative Commons Attribution 4.0 International License.

What Structures do Coordination Complexes Form?

Metal complexes with coordination numbers ranging from one to 16 are known, although values greater than seven are rare for the transition metals. In this section examples of common coordination geometries will be presented in order of coordination number.

Coordination Number 1

Condensed phase monocoordinate complexes are unknown for the transition metals, although the post transition metals Tl and In form monocoordinate complexes with the bulky ligands triazapentadienyl and 2,6-tris(2,4,6-triisoprophylphenyl)benzene as shown in Figure **3.6.4.7**.

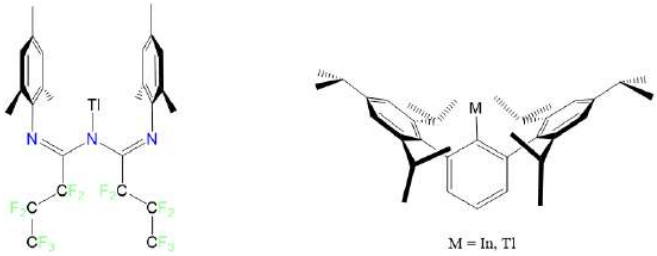
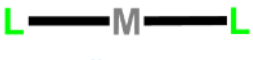


Figure **3.6.4.7**. No monocoordiante transition metal complexes are known but Tl^+ and In^+ form monocoordinate complexes with extremely bulky ligands. This work by Stephen Contakes is licensed under a Creative Commons Attribution 4.0 International License.

Coordination Number 2

This coordination number is rare outside of d^{10} complexes of the group 11 metals and mercury, specifically, Cu^+, Ag^+, Au^+, and Hg^{2+}. In accordance with the predictions of the Kepert model these give linear complexes.



linear

Among these:

- Cu^+ more commonly gives tetrahedral complexes but can be coaxed to give linear ones. The most prominent example is $[CuCl_2]^-$, which forms when CuCl is treated with concentrated HCl under anerobic conditions.
- Ag^+ also commonly forms tetrahedral or trigonal planar complexes but can give linear ones. The most prominent example is $[Ag(NH_3)_2]^+$, which can be formed by treating silver salts with concentrated aqueous or liquid ammonia.
- Au^+ almost always forms linear complexes but many of these formally two coordinate complexes associate as depicted in Figure **3.6.4.8**. The ability of Au^+ to form linear complexes with cyanide is even used to selectively extract metallic gold from low grade ores. The stability of $[Au(CN)_2]^-$ means that the dissolution of metallic gold in aqueous cyanide is thermodynamically favorable under aerobic conditions.

$$4\ Au + 8\ CN^- + O_2 + 2\ H_2O \longrightarrow 4\ [Au(CN)_2]^- + 4\ OH^- \qquad (3.6.4.1)$$

- Hg^{2+}, like Au^+, benefits from relativistic effects and more commonly forms two-coordinate complexes with a linear geometry. Among these is $[Hg(CN)_2]$. However, its preference for linearity is not as rigid as for Au^+ and so complexes with a variety of coordination geometries are known.

An by means of honorary mention the mercury(I),Hg_2^{2+}, forms linear complexes of the type L-Hg-Hg-L, although since Hg_2^{2+} is often considered as a single unit these aren't always considered to be two coordinate complexes.

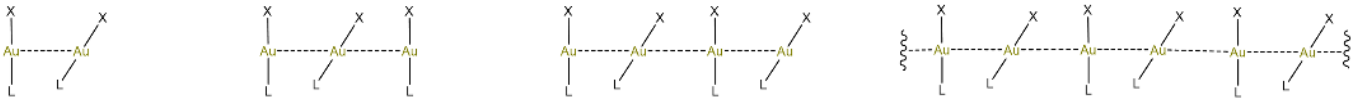
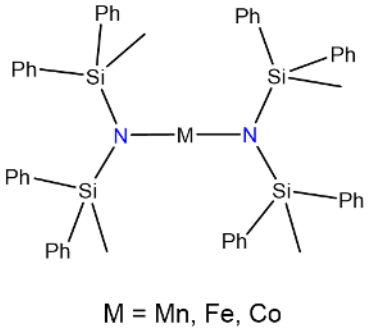


Figure **3.6.4.8**. Many "linear" gold complexes associate side-on to form dimers, trimers, tetramers, and chains. Although in this chapter L is usually taken to represent a generic ligand, in this scheme L represents a neutral ligand that donates two electrons to the metal (py, PR_3, CO etc.) and X an anionic one (*e.g.* Cl^-, CN^-, etc.). Exactly which structure forms depends on the identity of L and X. Redrawn from reference 5. This work by Stephen Contakes is licensed under a Creative Commons Attribution 4.0 International License.

Two coordinate complexes may also be formed through the use of bulky ligands that only allow for the binding of two to the metal center. Classic examples are given in Figure **3.6.4.9**.

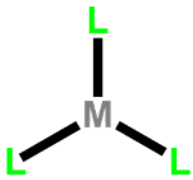


M = Mn, Fe, Co

Figure **3.6.4.9**. Two coordinate complexes form between Mn^{2+}, Fe^{2+}, and Co^{2+} and $N(SiMePh_2)_2$.[6] This work by Stephen Contakes is licensed under a Creative Commons Attribution 4.0 International License.

Coordination Number 3

Three coordinate complexes are similar to two coordinate ones in that they are rare and, aside from the constraining influence of ligands, usually limited to d^{10} metal ions such as Cu^+, Ag^+, Au^+, Hg^{2+}, and Pt^0. As expected from the Kepert model, in the absence of constraining ligands three coordinate complexes are trigonal planar.



Trigonal planar

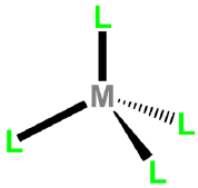
Many of the examples involve soft ligands. They include $[Cu(SPMe_3)_3]^+$, $[Ag(PPh_3)_3]^+$, $[Au(PPhCy_2)_3]^+$, HgI_3^-, and $[Pt(PPh_3)_3]$. Non-d^{10} metal centers have successfully been constrained to adopt a three coordinate trigonal planar geometry using bulky and semirigid ligands. Examples of such three-coordinate complexes are given in Figure **3.6.4.10**.



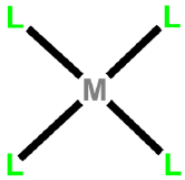
Figure **3.6.4.10**: Three coordinate complexes prepared using bulky and semirigid ligands. This work by Stephen Contakes is licensed under a Creative Commons Attribution 4.0 International License.

Coordination Number 4

Four is one of the most common coordination numbers found in transition metal complexes. The two common four coordinate geometries are tetrahedral and square planar.



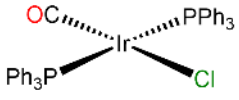
tetrahedral



Square planar

Tetrahedral complexes are commonly formed by metals possessing either a d^0 or d^{10} electron configuration. Monometallic examples of the former include $TiCl_4$, VO_4^{3-}, WS_4^{2-}, MnO_4^-, CrO_4^{2-}, and OsO_4 while d^{10} examples are $[Ni(CO)_4]$, $[HgBr_4]^{2-}$, $[ZnCl_4]^{2-}$, $[CdI_4]^{2-}$. Otherwise tetrahedral complexes are known but much less common. Examples usually involve good donor ligands and include $[FeCl_4]^-$ (d^5), $[CoCl_4^{2-}]$ (d^6), and $[NiCl_4]^{2-}$ (d^7).

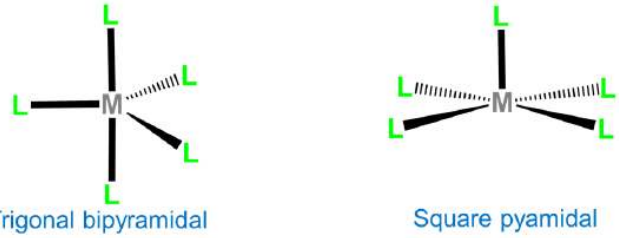
Second and third row transition metal centers with d^8 electron configurations like Rh^+, Ir^+, Pd^{2+}, and Pt^{2+}, Au^{3+} almost exclusively exhibit square planar geometries. Beyond this, square planar geometries are often formed by Ni^{2+} (d^8), Ni^{3+} (d^7), and Cu^{2+} (d^9). Examples of square planar complexes include $[Cu(acac)_2]$; $[PtCl_4]^{2-}$;Wilkinson's catalyst, $[RhCl(PPh_3)_3]$; and Vaska's complex, *trans*-$[Ir(CO)Cl(PPh_3)_2]$. Porphyrins, phthalocyanines, and other rigid macrocycles can also impose a square planar geometry on coordinated metals.



Vaska's Complex

Coordination Number 5

The two common coordination geometries for five coordinate complexes are trigonal bipyramidal and square pyramidal.



Five coordinate complexes are rare. Complexes that exhibit trigonal bipyramidal geometry include $[Fe(CO)_5]$ and $[CuCl_5]^{3-}$ and complexes containing tripodal ligands that preference formation of a trigonal pyramidal structure with an open coordination site, as shown in Figure **3.6.4.11**.

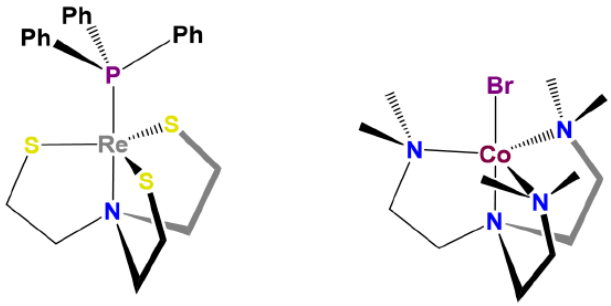


Figure **3.6.4.11**: Some tripodal ligands preference the formation of trigonal bipyramidal complexes. This work by Stephen Contakes is licensed under a Creative Commons Attribution 4.0 International License.

Homoleptic $[Ni(CN)_5]^{3-}$ possesses a square pyramidal structure, although the geometry is more common for macrocyclic complexes like the iron protoporphyrin of deoxymyoglobin shown in Figure **3.6.4.4** and for complexes containing oxo and nitrido ligands, examples of which are shown in Figure **3.6.4.12**.

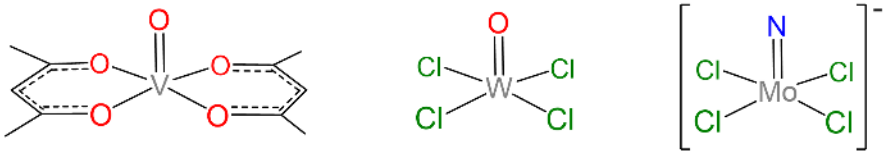


Figure **3.6.4.12**: Some square pyramidal oxo and nitrido complexes. This work by Stephen Contakes is licensed under a Creative Commons Attribution 4.0 International License.

In the absence of rigid constraining ligands the relatively low energy difference between the trigonal bipyramidal and square pyramidal coordination geometries provides a mechanism for interconversion of the axial and equatorial ligands in a trigonal planar complex. For example, pentacarbonyliron(0) exhibits fluxionality involving a square pyramidal intermediate via a Berry pseudorotation mechanism, as shown in Figure **3.6.4.13**

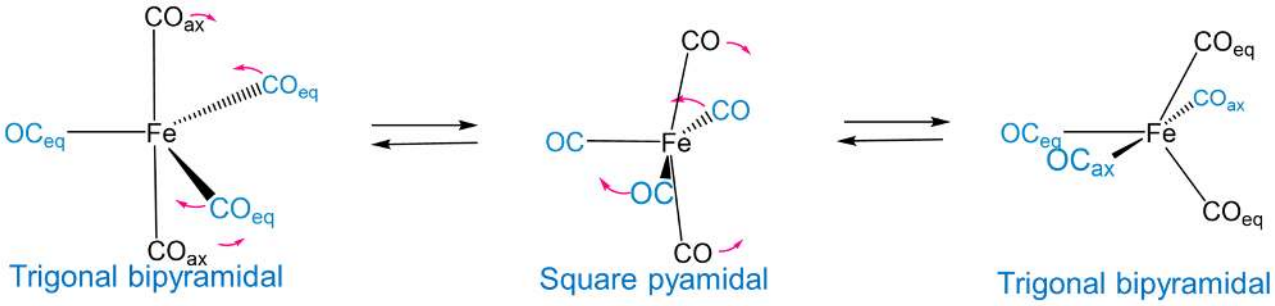
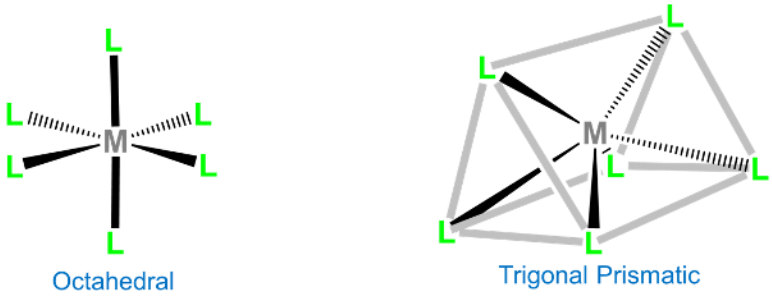


Figure **3.6.4.13**: Fluxionality in pentacarbonyliron(0) involves exchange of axial and equatorial carbonyl ligands via Berry pseudorotation. Interconversion of the axial and equatorial carbonyl groups occurs faster than the NMR timescale at room temperature. As a result the ^{13}C NMR spectrum of $Fe(CO)_5$ exhibits a single signal rather than two separate signals for the axial and equatorial carbonyl carbons. This work by Stephen Contakes is licensed under a Creative Commons Attribution 4.0 International License.

Coordination Number 6

The two common octahedral coordination geometries are octahedral and trigonal prismatic.



Octahedral

Of these octahedral is by far the most common mode of coordination exhibited by transition metals. Most metals can be induced to form octahedral complexes and examples exist for every d electron configuration ranging from d^0 to d^{10}. Among these are the 28 metal oxidation states listed in Figure **3.6.4.1** for which octahedral is the most common coordination geometry. Because of this it is worth pointing out that octahedral complexes possessing d^4, d^7 , or d^9 electron configurations commonly exhibit tetragonal distortions depicted in Figure **3.6.4.14**.

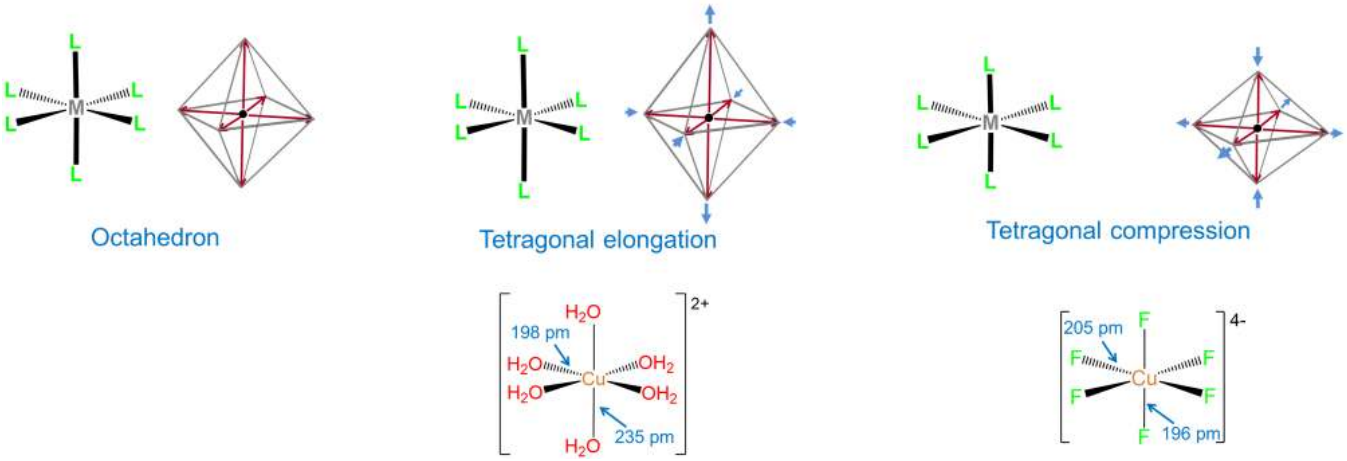


Figure **3.6.4.14**: Tetragonal distortions commonly occur for d^4, d^7 , and d^9 octahedral complexes. The most common type involves axial elongation in which the octahedron is stretched along a single *trans*-L-M-L axis but axial compressions in which the octahedron is compressed along such an axis instead are sometimes observed. An example of an axial elongated complex is $[Cu(H_2O)_6]^{2+}$ in solution while $[CuF_6]^{4-}$ is axially compressed when doped into a Ba_2ZrF_6 lattice (it is elongated when doped into a Bond distances are taken from references 7 and 8. This work by Stephen Contakes is licensed under a Creative Commons Attribution 4.0 International License.

Trigonal prismatic

Trigonal prismatic coordination is related to octahedral coordination as shown in Figure **3.6.4.15**. As may be seen in Figure **3.6.4.15**, an octahedral coordination sphere is just a trigonal antiprism in which all edge lengths are identical. Rotation of one triangular face relative to its opposite until the two are eclipsed gives a triganal prismatic geometry. In fact, since continuation of this rotation gives another octahedral complex the trigonal prismatic geometry is an intermediate in isomerization reactions involving octahedral complexes.

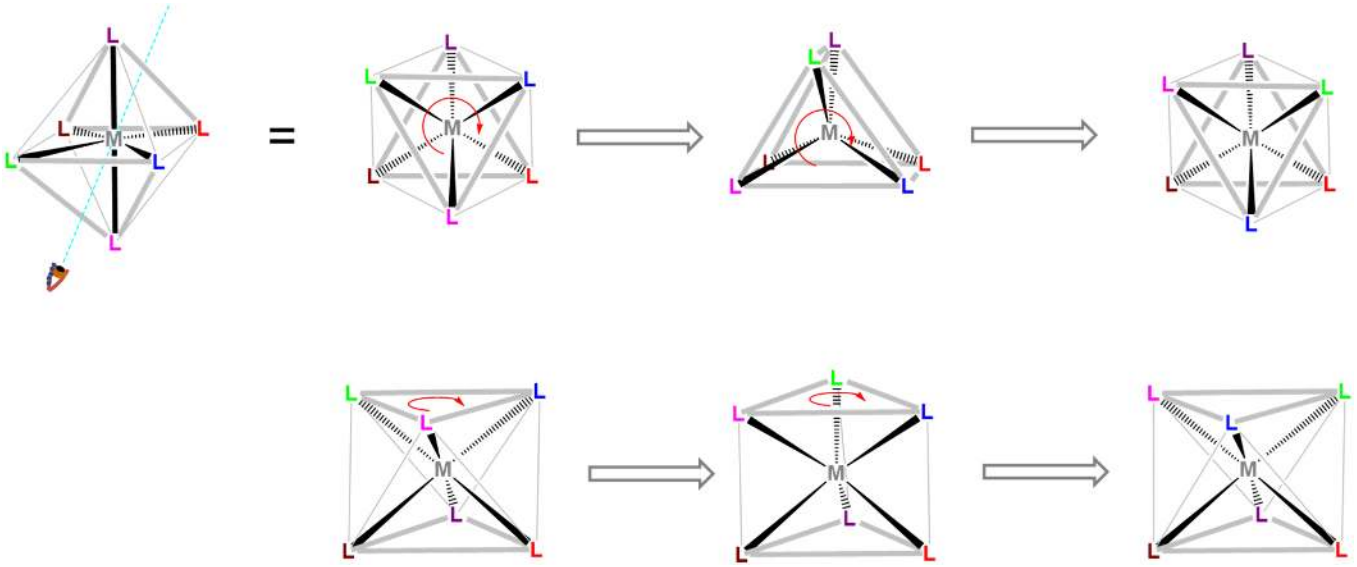


Figure 3.6.4.15: Since an octahedron is a trigonal antiprism a trigonal prism may be produced by rotating or "twisting" one face of the octahedron relative to its opposite. Since continuation of the rotation gives an isomer of the original octahedron, when the energy landscape for twists like these is thermally or photochemically accessible twists like these provide one pathway for isomerisation reactions involving octahedral complexes. In tris- and bis-chelates such isomerizations are said to occur by Bailar and Ray-Dutt twists, which differ only in the relationship between the chelate rings and the faces twisted. Top: View down looking down an axis bisecting a pair of opposing faces. Bottom: View perpendicular to that shown at top. This work by Stephen Contakes is licensed under a Creative Commons Attribution 4.0 International License.

In contrast to octahedral coordination geometries, trigonal prismatic coordination (and distorted versions thereof) are rare and occur mostly for d^0, d^1, and d^2 configurations. Examples of trigonal prismatic metal centers include the d^2 Mo^{4+} centers in MoS_2, d^1 $[Re(S_2C_2Ph_2)_3]^-$, and d^0 $[Ta(CH_3)_6]^-$, of which the latter two structures are given in Figure 3.6.4.16. Semirigid ligands like that shown in Figure 3.6.4.4*C* may be used to encourage the adoption of a trigonal prismatic geometry, although once the number of *d* electrons present the preference for octahedral coordination is too great for a trigonal prismatic geometry to occur.

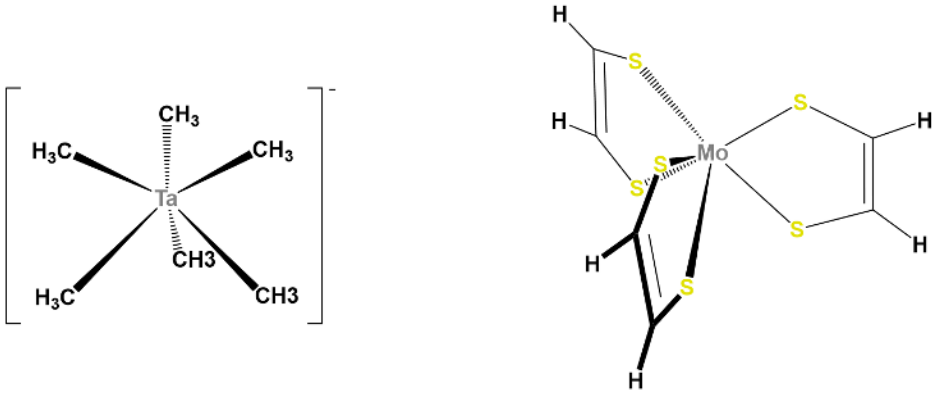
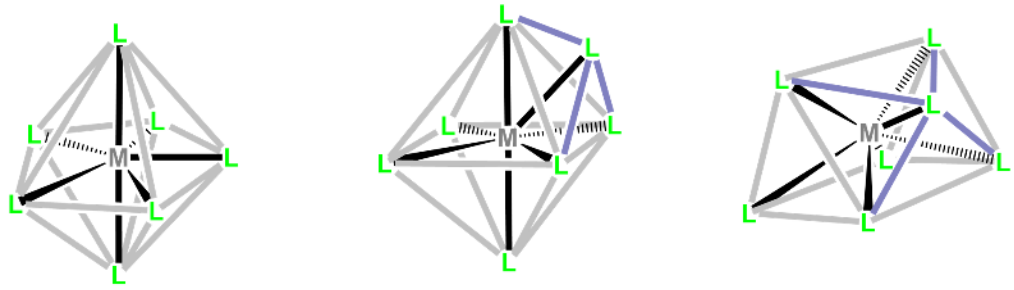


Figure 3.6.4.16: The complexes $[Ta(CH_3)_6]^-$ and $[Mo(S_2C_2H_2)_3]$ adopt a trignal prismatic geometry. Trigonal primatic coordination is common for d^0 and d^1 complexes with alkyl and dithiolene ligands. It is also typical for the dithiolene ligands to coordinate along the rectangular edges of the trigonal prism instead of the triangular ones. This work by Stephen Contakes is licensed under a Creative Commons Attribution 4.0 International License.

Coordination Number 7

Seven coordinate complexes are rare outside of the relatively large early transition metals, lanthanides, and actinides. The three common seven coordinate geometries are pentagonal bipyramidal, monocapped octahedral, and monocapped trigonal prismatic. The latter two are often called capped octahedral, and capped trigonal prismatic, with the mono- prefix being understood.



Although intraligand repulsions are smaller in the pentagonal bipyramidal coordination geometry than the capped octahedral and capped trigonal prismatic geometries the difference is small and the three structures are often close in energy. As a result the structure observed is often dependent on ligand-based constraints, crystal packing, and solvent effects that preference one geometry over the others.

Heptacyano complexes are often pentagonal bipyramidal. Examples include $[Mo(CN)_7]^{3-}$, $[W(CN)_7]^{3-}$, and $[Os(CN)_7]^{3-}$. Seven coordinate complexes containing oxo ligands commonly are pentagonal bipyramidal with the oxo ligand(s) in the less sterically hindered axial position. Examples include $[NbOF_6]^{3-}$ and, for the inner transition metals, $[UO_2F_5]^{3-}$. Ligands that have been used to promote formation of seven-coordinate species include 15-crown-5 and 2,2':6',2":6",2"'-quaterpyridine and 15-crown-5. Representative complexes are given in (Figure **3.6.4.17**.

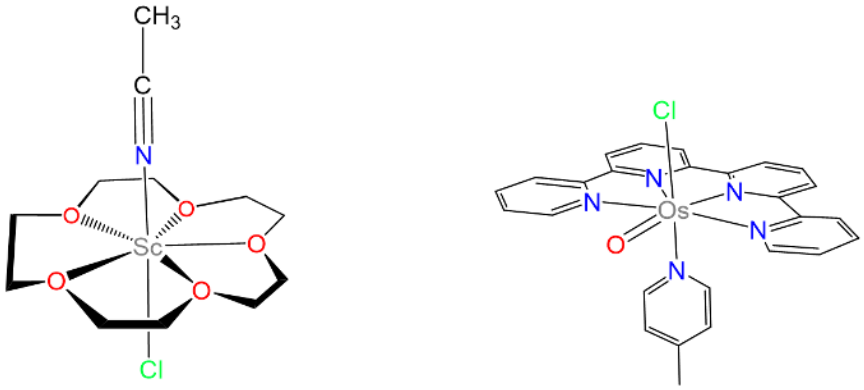


Figure **3.6.4.17**: Seven coordinate complexes containing ligands that encourage the formation of seven-coordinate geometries. Note that while in $[NbOF_6]^{3-}$ and $[UO_2F_5]^{3-}$ the oxo ligands occupy axial positions the Osmium complex shown possesses an oxo ligand in an equatorial position. This is likely because the parent octahedral complex, in which the oxo ligand is not present, possesses an expanded outer N-Os-N angle of 121.655° that opens to 154.161° to accommodate the oxo group. Drawn based on the structures reported in references 9 and 10. This work by Stephen Contakes is licensed under a Creative Commons Attribution 4.0 International License.

Capped trigonal prismatic geometries are common for complexes of the early transition metals. Examples include $[NbF_7]^{2-}$, $[TaF_7]^{2-}$, and $[ZrF_7]^{3-}$ in $(NH_4)_3[ZrF_7]$.

Capped octahedral geometries are found in $[MoMe_7]^-$, $[WMe_7]^-$, and $[WBr_3(CO)_4]$, which contains three pairs of *trans*-Br and CO with the final CO capping the octahedron's $(CO)_3$ face, as shown in Figure **3.6.4.18**.

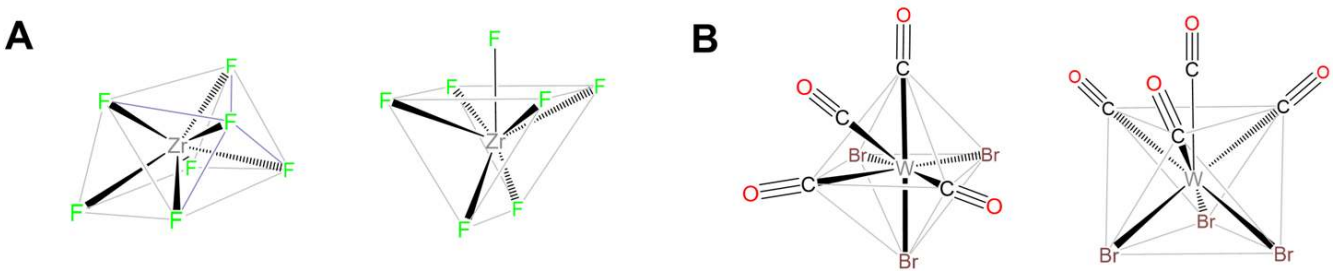


Figure **3.6.4.18**: Examples of complexes that adopt monocapped triconal prismatic and monocapped octahedral geometries.(A) Two views of the structure of (A) capped trigonalprismatic $[ZrF_7]^{3-}$ and (B) capped octahedral $[WBr_3(CO)_4]$. This work by Stephen Contakes is licensed under a Creative Commons Attribution 4.0 International License.

In seven and higher coordinate complexes ligand and crystal packing effects frequently give distorted coordination geometries. These geometries are intermediate between two or more of the idealized seven coordinate geometries, making it difficult to tell exactly which structure they are a distortion of (Figure **3.6.4.19**.

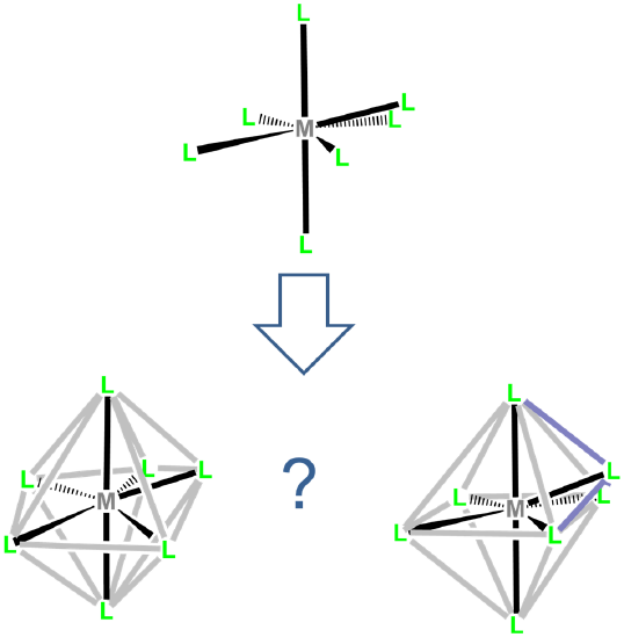
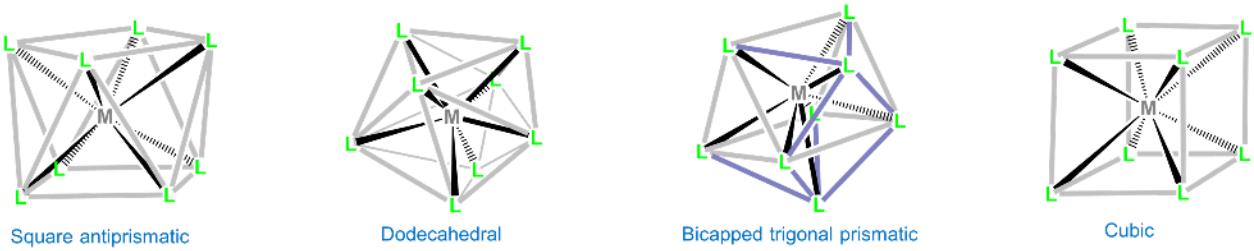


Figure **3.6.4.19**: Many seven-coordinate structures are distorted and can be difficult to classify. For example, how should the geometry of this complex be described - as distorted trigonal bipyramidal or distorted monocapped octahedral? This work by Stephen Contakes is licensed under a Creative Commons Attribution 4.0 International License.

Coordination Number 8

Eight coordinate complexes are rare and occurs in discrete molecules and ions only for the relatively large early transition metals, lanthanides, actinides. The three common eight coordinate geometries are square antiprismatic, dodecahedral, and bicapped trigonal prismatic. In contrast, the cubic coordination geometry is only found in ionic lattices like that of CsCl and in complexes of the inner transition metals such as $Na_3[UF_8]$.



The simplest structure is the cube, which is rare because it does not minimize interligand repulsive interactions. Square antiprismatic, dodecahedral, and bicapped trogonal prismatic coordination are more common. Of these the square antirpismatic and dodecahedral geometries can both be considered as distorted cubic structures. As shown in Figure **3.6.4.20**, the square antiprism may be made by twisting one face of a cube relative to one another and the dodecahedron by folding opposing faces towards one another.

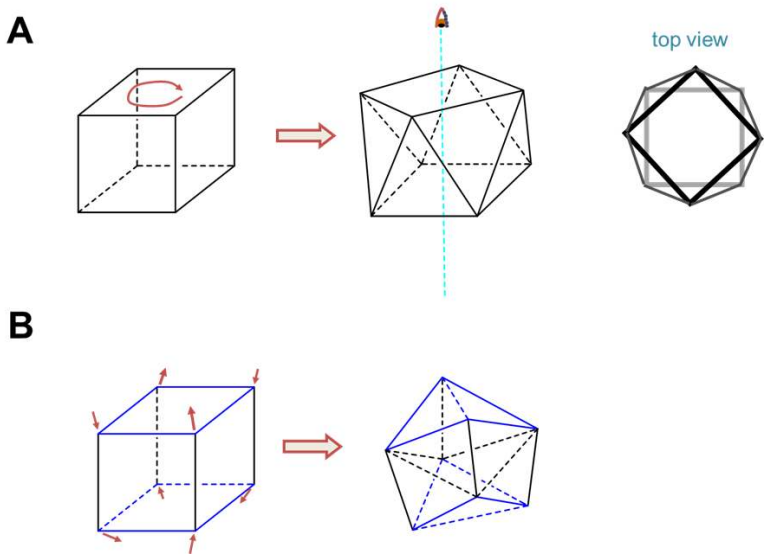


Figure **3.6.4.20**: The (A) square antiprismatic and (B) dodecahedral coordination geometries are distorted cubic geometries. (A) The square antiprismaric coordination geometry is just a cubic coordination geometry in which one face has been rotated 45° relative to its opposite (and for which the distance between those faces need not be equal to the distance between adjacent atoms within a face) (B) The dodecahedral geometry may be thought of as a cube in which opposing faces are folded up and down relative to one another as shown. This work by Stephen Contakes is licensed under a Creative Commons Attribution 4.0 International License.

As with other high-coordinate structures the energy difference between these eightfold coordination geometries is small enough that packing effects can significantly influnece the observed structure. For example, octacyanomolybdates commonly adopt a square antiprismatic coordination geometry but depending on the counterions present can give dodecahedral or bicapped trigonal prismatic complexes. Examples are given in Figure **3.6.4.21**.

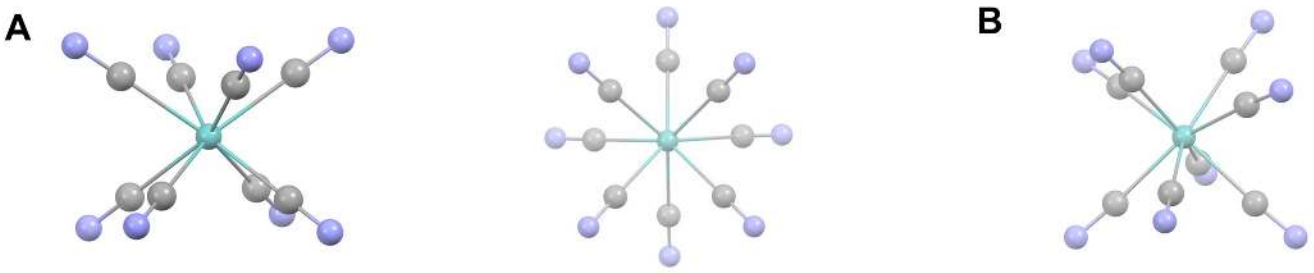
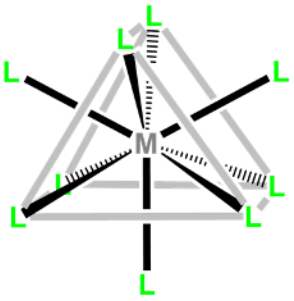


Figure **3.6.4.21**: Structures reported for (A) square antiprismatic $[Mo(CN)_8]^{3-}$ as a solid 4,4'-Diazenediyldipyridinium salt and (B) dodecahedral $[Mo(CN)_8]^{4-}$ as a solid tetra-n-butylammonium salt.

Coordination Number 9

Again, nine coordinate complexes typically require larger transition metals, lanthanides, and actinides. Coordination geometries are typically either tricapped trigonal prismatic or idosynchraitcally determined by the ligands. Simpleexamples include the aqua complexes $[Sc(H_2O)_9]^{3+}$, $[Y(H_2O)_9]^{3+}$, and $[La(H_2O)_9]^{3+}$ as well as $[TcH_9]^{2-}$ and $[ReH_9]^{2-}$.



The classic example of a nine-coordinate complex, $[ReH_9]^{2-}$, is shown in Figure **3.6.4.22**.

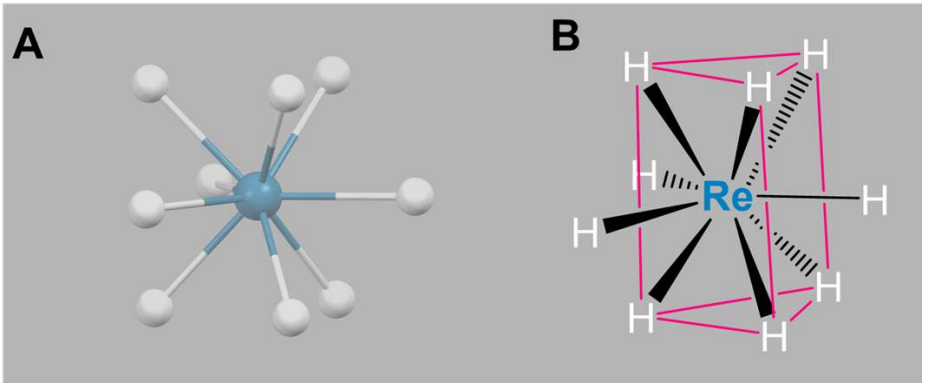


Figure **3.6.4.22**: (A) Structure of $[ReH_9]^{2-}$ in $K_2[ReH_9]$ and (B) schematic showing how the structure maps onto a tricapped trigonal pyramidal coordination geometry. This work by Stephen Contakes is licensed under a Creative Commons Attribution 4.0 International License.

Coordination Numbers 10-16

Coordination numbers higher than nine are extremely rare for compounds that bind in κ fashion (form conventional metal-ligand bonds)[14] and usually involve some combination of large metals, sterically undemanding ligands, and special ligand structures that promote higher coordination. Noteworthy examples include

1. Twelve-coordinate $[Hf(BH_4)_4]$, which illustrates how small multidentate ligands promote higher coordination numbers. As shown in Figure **3.6.4.23**, $[Hf(BH_4)_4]$ has a cubooctahedral structure in which BH_4^- acts as a tridentate ligand, with BH_3 units occupying triangular faces of the cubooctahedron to give a tetrahedron of BH_4^- ligands around the Hf.

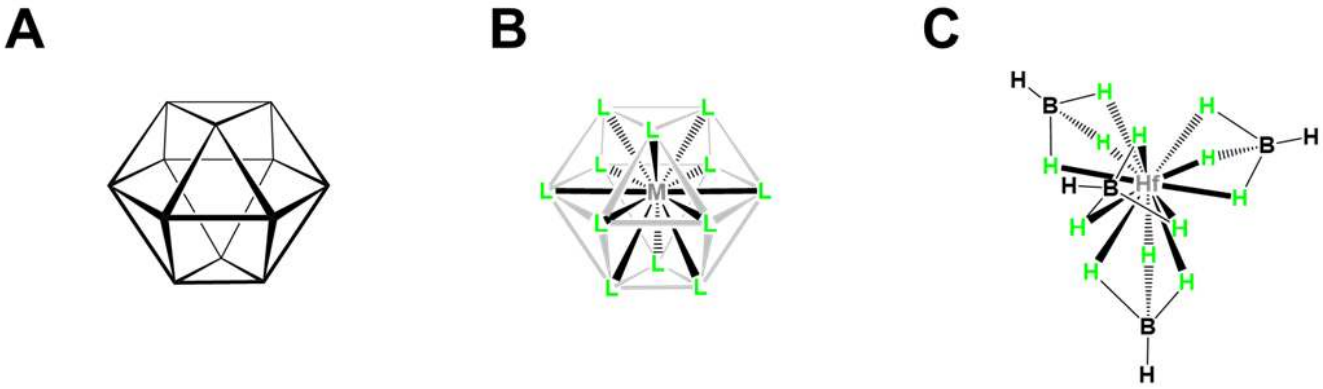


Figure **3.6.4.23**: The anticubooctahedral coordination geometry is observed for $[Hf(BH_4)_4]$. (A) An anticubooctahedron consists of a hexagonal ring capped with antiparallel triangles above and below the ring. (B) Idealized anticubooctahedral complex. (C) Structure of $[Hf(BH_4)_4]$. This work by Stephen Contakes is licensed under a Creative Commons Attribution 4.0 International License.

2. Twelve coordinate $[Ce(NO_3)_6]^{2-}$, in which the nitrate oxygens define an icosahedral coordination geometry as shown in Figure **3.6.4.24**. The nitrates in the structure bind the Ce center in bidentate fashion in an octahedral array.

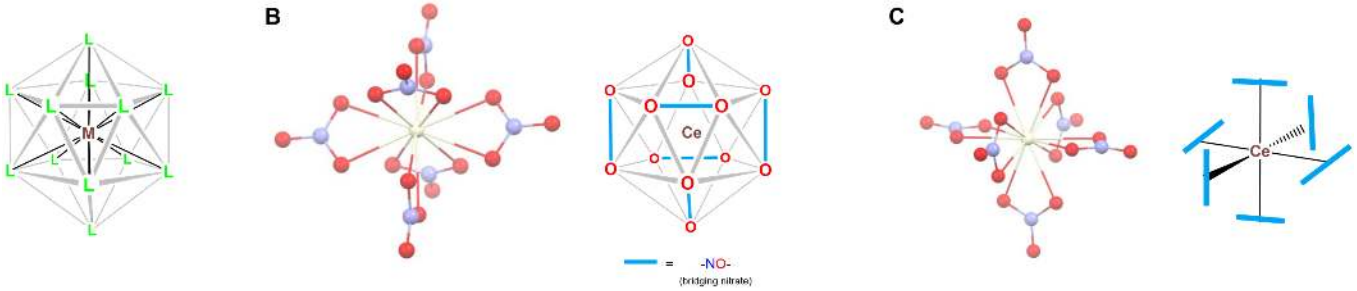


Figure **3.6.4.24**: Coordination geometry of $[Ce(NO_3)_6]^{2-}$ in $[Mg(H_2O)_6][Ce(NO_3)_6]\cdot H_2O$. (A) Idealized icosahedral coordination. (B) View of the structure of $[Ce(NO_3)_6]^{2-}$ showing how it maps onto the icosahedral coordination geometry. (C) The structure may also be thought of as comprising an octahedral geometry in which each vertex of the octahedron is occupied by a κ^2-NO_3^-. The structure of $[Ce(NO_3)_6]^{2-}$ is rendered in Mercury from the cif data in reference 15. This work by Stephen Contakes is licensed under a Creative Commons Attribution 4.0 International License.

3. Fifteen-coordinate, $[Th(H_3BNMe_2BH_3)_4]$, which also uses bridging H-B-H units that occupy little of the coordination sphere. In $[Th(H_3BNMe_2BH_3)_4]$ three of the four $H_3BNMe_2BH_3$ bind in κ^4 fashion and one binds κ^3, giving the fifteen fold coordination.[16]

4. Sixteen-coordinate $[CoB_{16}]^-$, which possesses the highest coordination number yet observed. Its structure is given in Figure **3.6.4.25** The coordination geometry is an octahedral antiprism and the complex should be considered as involving a Co center in the midst of a B_{16}^- "molecular drum" held together by cluster bonds.

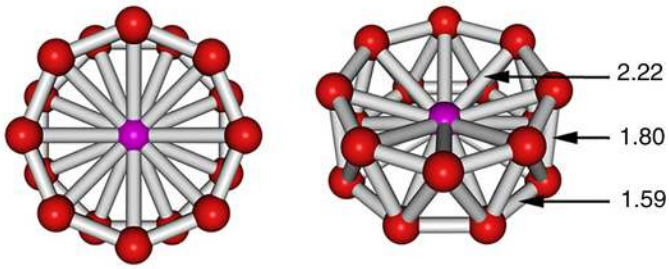


Figure **3.6.4.25**: Structure of the D_{8d} isomer of the 16 coordinate complex $[CoB_{16}]^-$, with distances shown in Ångstroms. The image is Figure 2A from from Popov, I., Jian, T., Lopez, G. *et al*. Cobalt-centred boron molecular drums with the highest coordination number in the CoB_{16}^- cluster. *Nat Commun* **6,** 8654 (2015). https://doi.org/10.1038/ncomms9654, which is is licensed in that publication under a Creative Commons Attribution 4.0 International License.

References

1. Dudev, M.; Wang, J.; Dudev, T.; Lim, C., Factors Governing the Metal Coordination Number in Metal Complexes from Cambridge Structural Database Analyses. *The Journal of Physical Chemistry B* **2006**, *110(4)*, 1889-1895.

2. Kuppuraj, G.; Dudev, M.; Lim, C., Factors Governing Metal−Ligand Distances and Coordination Geometries of Metal Complexes. *The Journal of Physical Chemistry B* 2009, 113 (9), 2952-2960.

3. Cremades, E.; Echeverría, J.; Alvarez, S., The Trigonal Prism in Coordination Chemistry. *Chemistry – A European Journal* 2010, 16 (34), 10380-10396.

4. Xiong, X.-G.; Wang, Y.-L.; Xu, C.-Q.; Qiu, Y.-H.; Wang, L.-S.; Li, J., On the gold–ligand covalency in linear $[AuX_2]^-$ complexes. *Dalton Transactions* 2015, 44 (12), 5535-5546.

5. Concepción Gimeno, M. The Chemistry of Gold in Laguna, Antonio (ed.) *Modern Supramolecular Gold Chemistry: Gold-Metal Interactions and Applications*. Wiley, 2008.

6. Andersen, R. A.; Faegri, K.; Green, J. C.; Haaland, A.; Lappert, M. F.; Leung, W. P.; Rypdal, K., Synthesis of bis[bis(trimethylsilyl)amido]iron(II). Structure and bonding in M[N(SiMe3)2]2 (M = manganese, iron, cobalt): two-coordinate transition-metal amides. *Inorganic Chemistry* 1988, 27 (10), 1782-1786.

7. Persson, I., Hydrated metal ions in aqueous solution: How regular are their structures? Pure and Applied Chemistry 2010, 8*2(10)*, 1901.

8. Aramburu, J. A.; García-Fernández, P.; García-Lastra, J. M.; Moreno, M., Jahn–Teller and Non-Jahn–Teller Systems Involving CuF_6^{4-} Units: Role of the Internal Electric Field in Ba2ZnF6:Cu2+ and Other Insulating Systems. *The Journal of Physical Chemistry C* 2017, *121(9)*, 5215-5224.

9. Brown, M. D.; Levason, W.; Murray, D. C.; Popham, M. C.; Reid, G.; Webster, M., Primary and secondary coordination of crown ethers to scandium(iii). Synthesis, properties and structures of the reaction products of ScCl3(thf)3, ScCl3·6H2O and Sc(NO3)3·5H2O with crown ethers. Dalton Transactions 2003, (5), 857-865.

10. Liu, Y.; Ng, S.-M.; Lam, W. W. Y.; Yiu, S.-M.; Lau, T.-C., A Highly Reactive Seven-Coordinate Osmium(V) Oxo Complex: [OsV(O)(qpy)(pic)Cl]2+. Angewandte Chemie International Edition 2016, 55 (1), 288-291.

11. Popov, I., Jian, T., Lopez, G. *et al.* Cobalt-centred boron molecular drums with the highest coordination number in the CoB_{16}^- cluster. *Nat Commun* **6,** 8654 (2015). https://doi.org/10.1038/ncomms9654

12. The structures are rendered from cif data reported in the following publications (A) square antiprismatic $[Mo(CN)_8]^{3-}$: Wen-Yan Liu, Hu Zhou, Ai-Hua Yuan, *Acta Crystallographica Section E: Structure Reports Online*, 2008, 64, m1151, (B) dodecahedral $[Mo(CN)_8]^{4-}$: B.J.Corden, J.A.Cunningham, R.Eisenberg, *Inorganic Chemistry*, 1970, 9, 356.

13. The structure of ReH_9^{2-} is rendered from the structure reported in Abrahams, S.C.; Ginsberg, A.P.; Knox, K. Transition metal-hydrogen compounds. II. The crystal and molecular structure of potassium rhenium hydride, K_2ReH_9 *Inorganic Chemistry*, **1964**, *3*, 558-567.

14. There are other complexes in which a metal may be said to interact with more than sixteen "ligand atoms" but these are not usually considered to possess a higher coordination number. For example in some π complexes like η^5-Cp_4U technically there are 20 C atoms fastened to the U but these complexes are better considered as 12 coordinate than twenty (since each cyclopentadienl ring is isolobal with a *fac* coordinated set of 3 L ligands) while the metal centers in endohedral fullerene species like $La@C_{60}$ do not interact with all sixty carbon atoms at once are so are better thought of as a metal trapped in a spacious sixty-carbon cage.

15. Zalkin, A.; Forrester, J.D.; Templeton, D.H. Crystal structure of cerium magnesium nitrate hydrate *Journal of Chemical Physics*, **1963**, *39*, 2881-2891.

16. Daly, S. R.; Piccoli, P. M. B.; Schultz, A. J.; Todorova, T. K.; Gagliardi, L.; Girolami, G. S., Synthesis and Properties of a Fifteen-Coordinate Complex: The Thorium Aminodiboranate [Th(H3BNMe2BH3)4]. Angewandte Chemie International Edition 2010, 49 (19), 3379-3381.

17. Popov, I., Jian, T., Lopez, G., Boldyrev, A. I.; Wang, L-S. Cobalt-centred boron molecular drums with the highest coordination number in the CoB_{16}^- cluster. *Nat Commun* **6,** 8654 (2015).

Contributors

Stephen Contakes, Westmont College, to whom comments, corrections, and criticisms should be addressed.

Consistent with the policy for original artwork made as part of this project, all unlabeled drawings of chemical structures are by Stephen Contakes and licensed under a Creative Commons Attribution 4.0 International License.

3.6.4: Coordination Numbers and Structures is shared under a CC BY-NC-SA 4.0 license and was authored, remixed, and/or curated by LibreTexts.

- **9.5: Coordination Numbers and Structures** by Stephen M. Contakes is licensed CC BY 4.0.
- **8.3: Coordination Numbers and Structures** is licensed CC BY-NC-SA 4.0.

3.6.5: Isomerism

Metal complexes present a rich, interesting, and diverse structural chemistry. Major points of variation in the structural chemistry of metal complexes include

1. **coordination number** and **coordination geometry**, which involve differences in how many ligands surround a central metal and their overall geometric arrangement. Examples of the latter include the tetrahedral and square planar geometries commonly observed for four-coordinate metal centers. Tetrahedral, square planar, and octahedral coordination serve as a backdrop to the discussion of isomerism on this page. Readers who are unfamiliar with these structures might consider reading the section on coordination geometries before this one.
2. **structural iosmerism** involves differences in how potential ligand atoms are bound to metals in a complex. Possibilities for structural isomerism include
   - linkage or ambidentate isomerism
   - hydrate/solvate isomerism
   - ionization isomerism
   - coordination isomerism.

   Of these, linkage isomerism should always be considered when working with ambidentate ligands. As classifications, the last three forms of structural isomerism are mainly of academic interest since they represent permutations of ordinary structure patterns for solvates, salts, and coordination complexes, respectively.
3. **stereochemistry**, which includes
   - which coordination geometry is adopted for a metal with a given set of ligands in a particular oxidation state. For instance, $[Ni^{II}Cl_4]^{2-}$ is tetrahedral while $[Pt^{II}Cl_4]^{2-}$ is square planar. Since this geometry is usually fixed by the metal and ligands it is typically not a source of stereoisomeric varierty.
   - metal-centric stereoisomerism involving possible variations in where ligands are located relative to one another around the metal. The possibilities depend on the coordination number, geometry, and number of different types of ligands. For instance, square planar complexes can exhibit *cis-/trans-* isomerism while tetrahedral ones cannot. Tetrahedral complexes with four different ligands exhibit *R* and *S* chirality but complexes of that type are relatively rare. The more common cases include *cis* and *trans* isomerism in square planar complexes and *cis* & *trans-*, *mer* & *fac-*, and Λ & Δ isomerism in octahedral ones, although some multidentate ligands present additional possibilities for stereochemical variation
   - Stereoisomerism centered on the ligands bound to a metal center. Possibilities include
     - stereoisomerism inherent to a ligand. This would include cases where the ligand itself is chiral or, as in the case of amines, exists as a rapidly interconverting mixture of isomers. Thus this sort of stereoisomerism is an extension of the isomerism encountered in ordinary organic and other main group compounds. The main new issues introduced by binding of such ligands to a metal center involve the creation of new possibilities for diastereoisomerism based on the stereochemistry of the metal center and the freezing out of stereocenter inversion on binding to a metal. The latter is particularly important for amines, which as free amines racemize rapidly by nitrogen inversion.
     - or conformational isomerism involving five-membered **chelate rings** created when a multidentate ligand binds to a metal. This isomerism is often called chelate ring twist since individual rings can exhibit one of two conformations depending on how they twist on binding.

A summary of these forms of isomerism is given in Figure **3.6.5.1**.

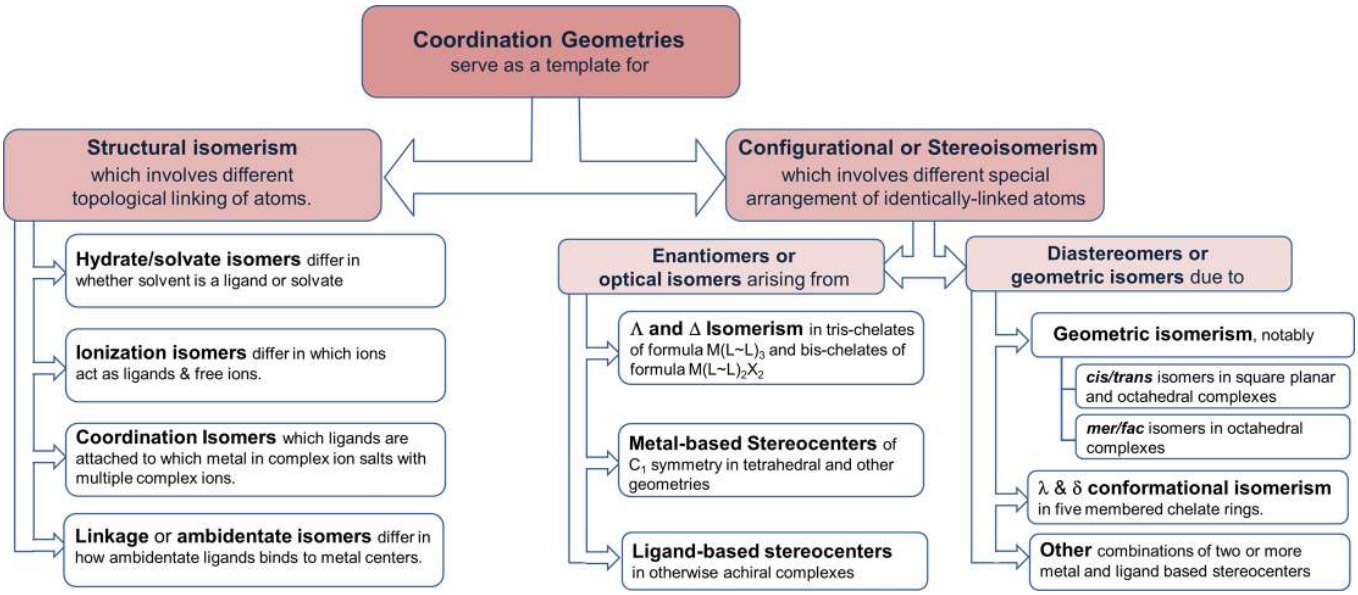


Figure **3.6.5.1**. Relationship among the common types of isomerism in metal complexes. This work by Stephen Contakes is licensed under a Creative Commons Attribution 4.0 International License.

Structural isomers

Structural isomerism involves different topological linkages of atoms. Differences in atomic linkages distinctive to coordination chemistry involve the linkages between metals and ligands. The main variations are:

1. Hydrate/solvate isomerism

Solvate isomers differ in terms of whether a molecule acts as a ligand or whether it acts as a solvate by occupying a lattice site in the crystal. Among solvate isomers, the case in which water is the ligand or solvate is the best known. The resulting isomers are called **hydrate isomers** after the term for water acting as a solvate, hydrate. A well-known example that illustrates how solvate isomerism works is the series $[CrCl_x(H_2O)_{6-x}]Cl_{3-x}{\cdot}xH_2O$, for which x = 0-2. The structures of the complex ions involved in this series are shown in Figure **3.6.5.2**.[1]

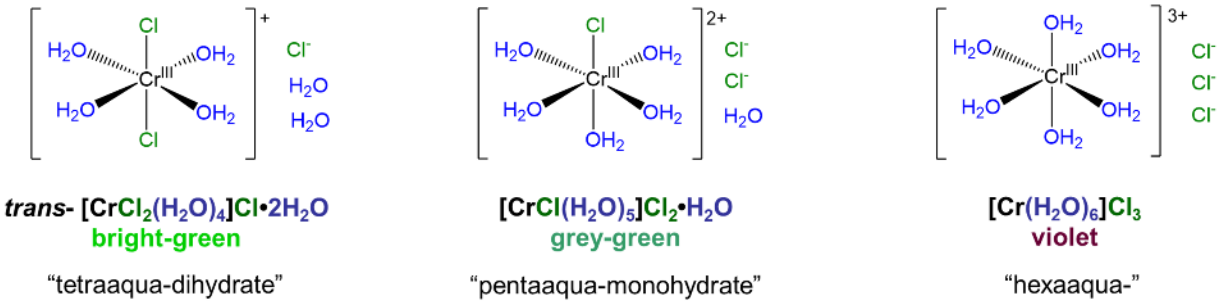


Figure **3.6.5.2**. Complexes of the hydrate isomer series $[CrCl_x(H_2O)_{6-x}]Cl_{3-x}{\cdot}xH_2O$ (x = 0-2). This work by Stephen Contakes is licensed under a Creative Commons Attribution 4.0 International License.

As can be seen from the compounds in Figure **3.6.5.2**, hydrate isomers differ both in terms of whether water acts as a ligand or hydrate *and* in terms of whether a potential counterion acts as a counterion or ligand. Thus, in *trans*-$[CrCl_2(H_2O)_4]Cl{\cdot}2H_2O$ two chlorides act as chloro ligands and four waters as aqua ligands while in $[CrCl(H_2O)_5]Cl_2{\cdot}H_2O$ five water molecules act as aqua ligands while only one chloride acts as a chloro ligand. In this way, solvate isomers simply represent cases in which two or more of the possible permutations for metal ligand binding among a set of solvent and counterion molecules are stable.

2. Ionization isomerism

In **ionization isomerism** there are two or more potential ions that can act as ligands. The ionization isomers differ in terms of which of these ions act as counterions and which act as ligands. Consider, for instance, the complexes shown in Figure **3.6.5.3**. These complexes differ in terms of whether the chloride or sulfate acts as a ligand, with the other acting as a counterion.

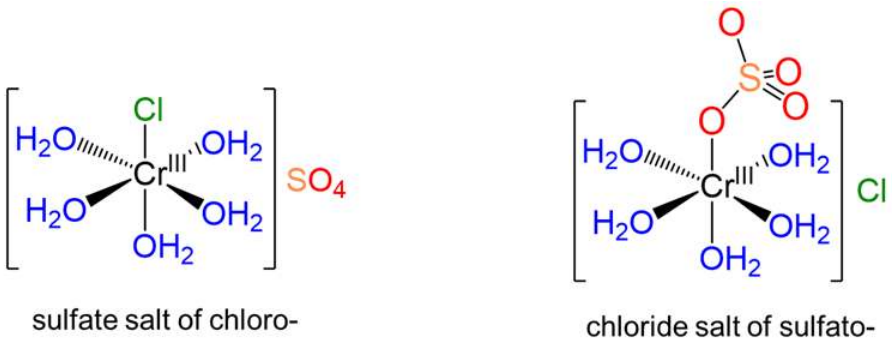


Figure **3.6.5.3**. Ionization isomers comprising a pentaaquachromium(III) fragment and the anions chloride and sulfate. As with all ionization isomers, the isomers differ in terms of which anion acts as a ligand and which a counterion. This work by Stephen Contakes is licensed under a Creative Commons Attribution 4.0 International License.

3. Coordination isomerism

Coordination isomers exist in compounds containing two or more complexes, each of which possesses a different set of ligands that can in principle be swapped with a ligand of the other complex. An example involves $[Co^{III}(NH_3)_6][Cr^{III}(ox)_3]$, depicted in Figure **3.6.5.4A**.[1] Coordination isomers of this complex involve swapping the ammine ligands around the Co^{3+} center for oxalato ligands surrounding the Cr^{3+} center. For instance, swapping all the ammine and oxalato ligands between the metal centers gives the coordination isomer $[Cr^{III}(NH_3)_6][Co^{III}(ox)_3]$ shown in Figure **3.6.5.4B**.

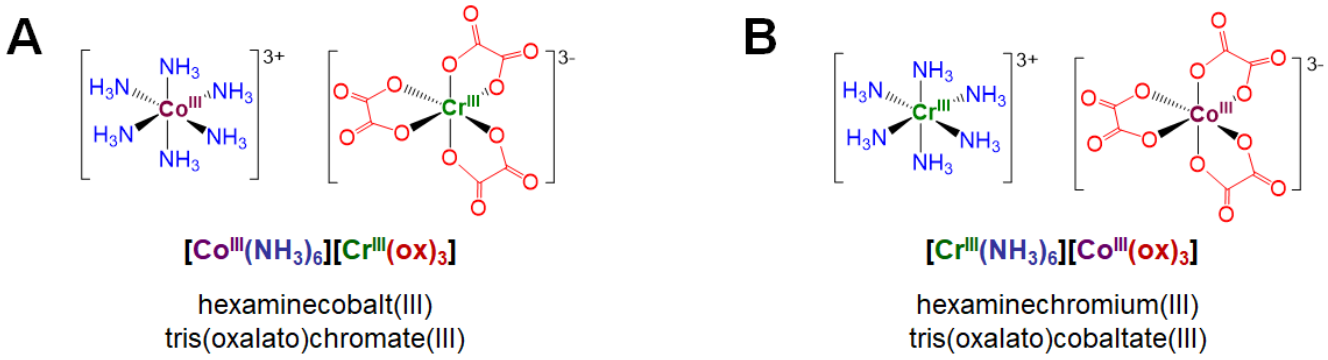
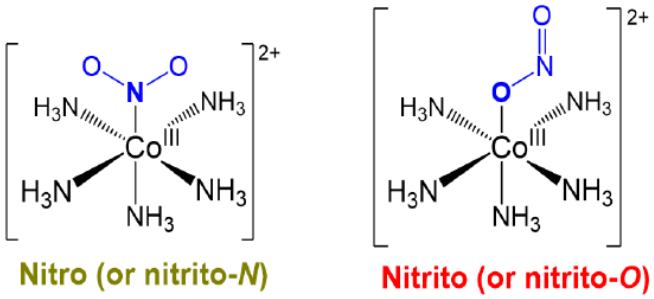


Figure **3.6.5.4**. Two coordination isomers comprising a Co^{3+} ,Cr^{3+}, six NH_3. and three oxalato ligands. The isomers differ in terms of which ligand type is bound to which metal. This work by Stephen Contakes is licensed under a Creative Commons Attribution 4.0 International License.

As classifications, hydrate/solvate, ionization, and coordination isomerism represent permutations of ordinary structure patterns for solvates, salts, and coordination complexes, respectively. As a result these forms of isomerism are rarely used as independent conceptual frameworks when thinking and talking about the structure of coordination compounds. Not so the final type of structural isomerism, linkage isomerism. That is because linkage isomerism has to do with the special *capacity* of ambidentate ligands to bind metals in multiple ways.

4. Linkage or ambidentate isomerism

Linkage or ambidentate isomers differ in how one or more ambidentate ligands bind to metal centers in a complex. The classic example dating from the work of Jørgensen and Werner is given in Scheme **3.6.5.I**.



Scheme **3.6.5.I**. Linkage isomers of penaamminenitritocobalt(III) ion. This work by Stephen Contakes is licensed under a Creative Commons Attribution 4.0 International License.

Just as alkenes exist as *E* and *Z* isomers, compounds possessing ambidentate ligands exist as one among the possible linkage isomers. As such, when working with ambidentate ligands the particular linkage isomer formed should be determined experimentally and considered when interpreting the complex's chemical and physical behavior.

The main ambidentate ligands which give rise to linkage isomerism are

- cyanide, CN^-
- thiocyanate, SCN^-, and the O and Se analogues, OCN^- and $SeCN^-$
- nitrite, NO_2^-
- sulfite, SO_3^-
- nitrosyl, NO

Although ambidentate ligands can bind metals in multiple ways, most exhibit a preferred binding mode (*i.e.*, prefer to bind metal centers in one of the possible ways). For instance, cyanide almost always binds through its carbon atom and thiocyanate almost always binds through its nitrogen (*μ-N*). However, the other binding mode can sometimes be formed kinetically or by using conditions that particularly favor its formation. Thus thiocyanate forms M-SCN^- linkages in the presence of exceptionally soft metal centers or in hard polar solvents (in which Lewis acid groups can stablize the terminal nitrogen of a bound thiocyanate ligand).

Ambidentate ligands are of significant research interest because many don't just bind to metal centers in two ways; the linkage isomers sometimes have significantly different physical properties. In addition, the possibility of two binding modes introduces the possibility of exploiting linkage isomerism to take advantage of some of these ligands:

a. different structural chemistry in different coordination modes. In mononuclear complexes the coordination mode influences which side of the ligand faces away from the complex and might be susceptible to stabilization by interaction with solvent. Additionally, the orientation of the ligand relative to the metal center might differ between one coordination mode and another. For instance, as predicted from the minor contributor to its resonance structure, thiocyanate binds nonlinearly via its S atom and linearly via its N (Figure **3.6.5.5**). Because of this the apparent steric bulk of the ligand around the metal center might differ between forms.

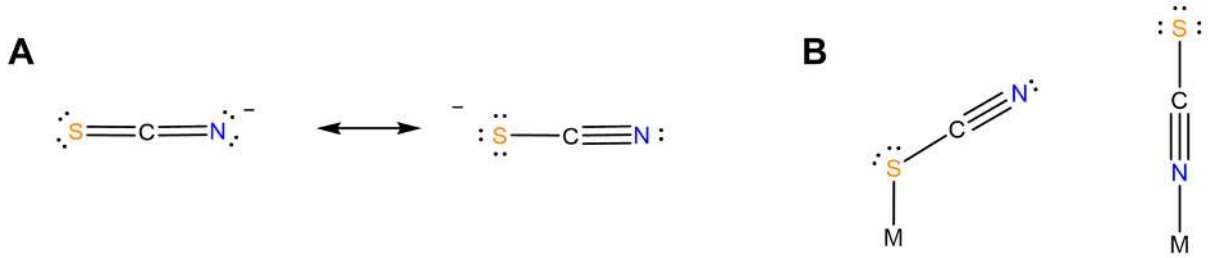


Figure **3.6.5.5**. Thiocyanate generally prefers to bind metals nonlinearly but in some cases forms linear M-SCN bonds. This work by Stephen Contakes is licensed under a Creative Commons Attribution 4.0 International License.

b. bind two different metal centers at the same time, linking them together. Perhaps the best-known examples involve thiocyanate and cyanide. The latter forms linkages of the type M-C≡N-M'. In the dye Prussian blue these take the form Fe^{II}-C≡N-Fe^{III}. An example from the author's graduate research involved tetrahedral clusters containing four metal atoms linked by six cyano ligands, as shown in Figure **3.6.5.6**.

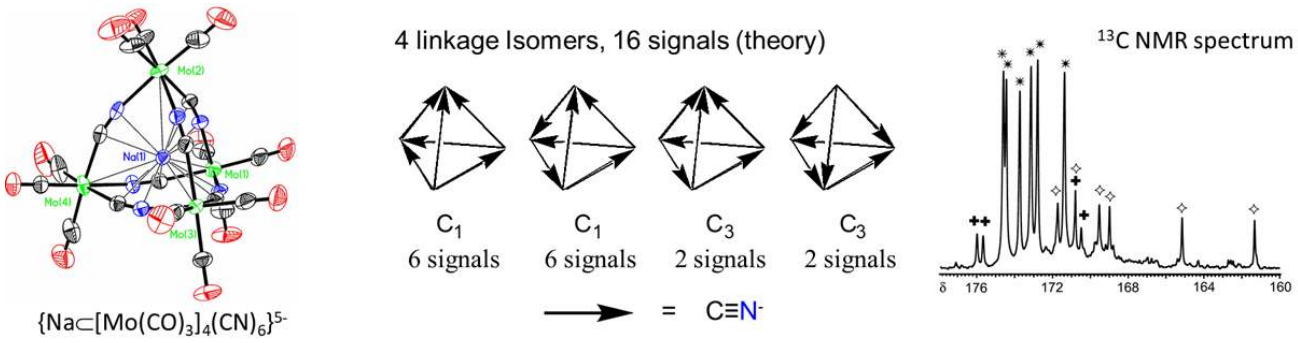


Figure **3.6.5.6**. (A) Structure of $\{Na@[Mo(CO)_3]_4(CN)_6\}$ showing the linking of four Mo centers by six CN ligands. Thermal ellipsoids for the C atoms are shown in black; those of the N atoms in blue. (B) The complex exists as a mixture of four linkage isomers in which the bridging CN^- ligands are oriented in different ways, as may be seen from the presence of the expected sixteen signals in its ^{13}C NMR spectrum. Based on work reported in reference 2.

c. can be induced to change from one binding mode to another in response to a stimulus. The classic example involves the light-driven transformation of the thermodynamically more stable yellow nitro complex of pentamminecobalt(III), $[Co(NH_3)_5NO_2]^{2+}$ to the less stable red *O*-nitrito complex, $[Co(NH_3)_5ONO]^{2+}$. Less stable cyanometallate coordination networks like those in the red $K\{Fe^{II}[Cr^{III}(CN)_6]\}$ transform into the more stable green $K\{Fe^{II}[Cr^{III}(NC)_6]\}$ form on heating, as shown in Figure **3.6.5.7**.[3]

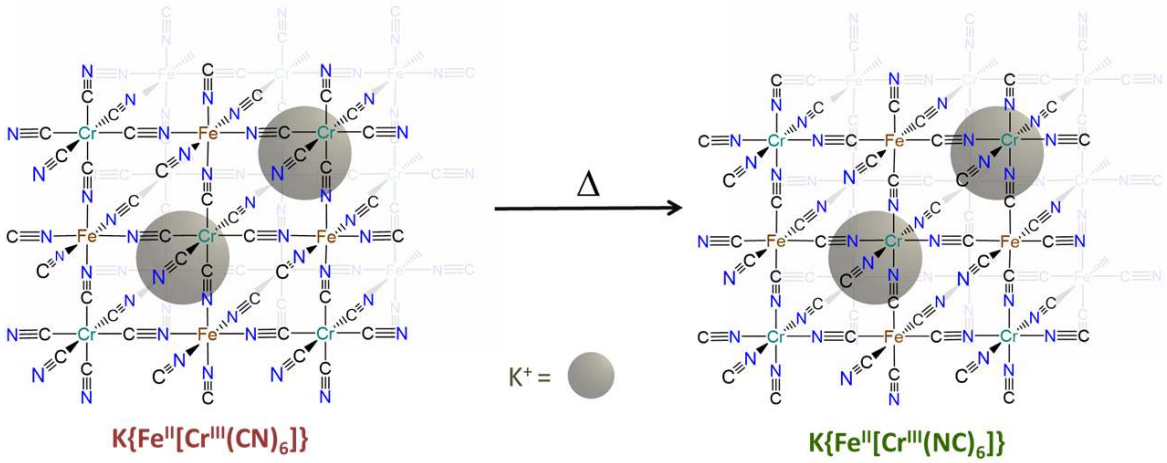


Figure **3.6.5.7**. Thermally-induced transformation of one $K\{Fe^{II}[Cr^{III}(CN)_6]\}$ into its more stable green linkage isomer $K\{Fe^{II}[Cr^{III}(NC)_6]\}$ involves "flipping" the cyano ligands. This work by Stephen Contakes is licensed under a Creative Commons Attribution 4.0 International License.

? Exercise 3.6.5.1: Bridging ambidentate ligands and the Hard-Soft Acid- Base Principle.

The hard-soft acid-base principle helps explain the preference of bridging ambidentate ligands for particular binding modes. How might the greater stability of the green $K\{Fe^{II}[Cr^{III}(NC)_6]\}$ over red $K\{Fe^{II}[Cr^{III}(CN)_6]\}$ be explained in terms of the hard and soft acid-base concept?

Answer

The greater stability of $K\{Fe^{II}[Cr^{III}(NC)_6]\}$ over $K\{Fe^{II}[Cr^{III}(CN)_6]\}$ reflects the greater stability of the Fe^{II}-CN-Cr^{III} linkages in the former over the Fe^{II}-NC-Cr^{III} linkages in the latter. This is consistent with the preference for hard-hard and soft-soft Lewis acid-base interactions of the Hard-Soft Acid-Base Principle.

The Fe^{II}-CN-Cr^{III} linkages are more stable because they possess bonds between

- the softer Lewis acid (Fe^{II}) and Lewis base (the C end of CN^-)
- the harder Lewis acid (Cr^{III}) and Lewis base (the N end of CN^-)

In contrast, the Fe^{II}-NC-Cr^{III} linkages in the less stable linkage isomer involve bonds between

- the softer base (the C end of CN^-) and harder acid (Cr^{III})
- the harder base (the N end of CN^-) and softer acid (Fe^{II})

Stereoisomerism

Optical Isomerism/Chirality

Molecules of D_n, C_n, or C_1 symmetry with only proper rotation axes (including $E = C_1$) are chiral and exhibit optical isomerism. As described in Figure **3.6.5.1**, the main sources of such optical isomerism in coordination chemistry are:

1. Chirality inherent to an organic or main group ligand.

   This type of isomerism is just an extension of the sort described in undergraduate organic texts and consequently does not merit separate discussion here, other than to note that some forms of optical isomerism which are of little importance in organic chemistry lead to optical activity in coordination compounds. In particular, the nitrogen inversion process which serves to rapidly racemize chiral amines is frozen out on formation of a metal-ligand bond. Because of this chiral amine, ligands bound to a metal form non-interconvertible *R* and *S* enantiomers, as shown in Figure **3.6.5.8**.

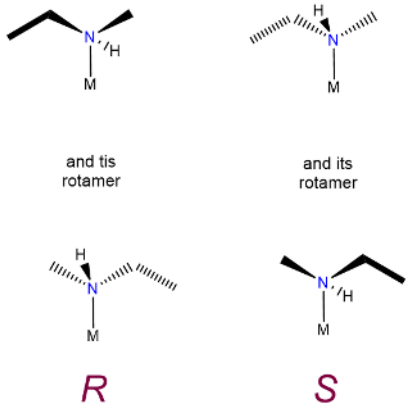


Figure **3.6.5.8**. Two views of *R* and *S* enantiomers formed when the chiral amine ethylmethylamine binds a metal that are commonly used to represent chiral amines in complexes. This work by Stephen Contakes is licensed under a Creative Commons Attribution 4.0 International License.

2. Chirality arising from the symmetry of ligands about a metal center.

   The two common situations through which such chirality arises involve:

   i. Chirality at a tetrahedral metal center surrounded by four different ligand attachment points.

   Such cases are often referred to as MABCD or Mabcd where M stands for the metal and a, b, c, and d the four different ligand attachment points. An example of such a complex is given in Figure **3.6.5.9A**. The chirality of such complexes is analogous to the chirality arising from a tetrahedral carbon stereocenter. There are two caveats, though. First, it is not enough to have a four-coordinate complex; the metal must possess tetrahedral symmetry since, as shown in Figure **3.6.5.9B**, square planar M complexes with four different ligands are identical to their mirror images. Second, such chirality is most easily realized using macrocyclic ligands like proteins. Metal ligand bonds involving sterically unhindered monodentate complexes like that in the example of Figure **3.6.5.9A** are in general weaker and more flexible than analogous carbon-carbon bonds. Consequently, in such cases it is likely that the enantiomers would interconvert through a fluxional process, making their resolution difficult if not impossible.

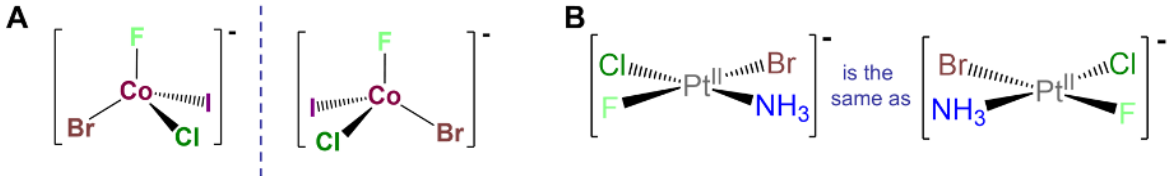


Figure **3.6.5.9**. (A) In principle tetrahedral metal centers surrounded by four different ligands (Mabcd) exhibit chirality analogous to the chirality of tetrahedral carbon stereocenters; (B) in contrast, square planar Macbd complexes like $[PtBrClF(NH_3)]^-$ are not chiral since they are the same as their mirror images. (It is easiest to see this by either working out its point group (C_s) or by rotating the left $[PtBrClF(NH_3)]^-$ structure clockwise 180 degrees to give its mirror image. This work by Stephen Contakes is licensed under a Creative Commons Attribution 4.0 International License.

ii. **Λ** and **Δ** isomerism at octahedral metal centers surrounded by two or three chelating ligands.

Specifically,

a. Octahedral tris-chelates of formula $M(L\sim L)_3$ exhibit D_3 symmetry.
b. cis-octahedral bis-chelates of formula $M(L\sim L)_2XY$ exhibit C_2 or C_1 symmetry: C_2 if X = Y and C_1 if $X \neq Y$.

As shown in Figure **3.6.5.10A**, octahedral tris-chelates like $[V(ox)_3]^{3-}$ are chiral and can exist as nonsuperimposable **Λ** and **Δ** enantiomers. The chirality of these tris-chelates is analogous to that of pinwheels. As shown in Figure **3.6.5.10B**, when looking directly at the head of any individual pinwheel from above, the blades will be angled from back to front going around the pinwheel in either the clockwise or counterclockwise direction. As shown in Figure **3.6.5.10C**, the case for which the blades are angled in the clockwise direction is analogous to the **Λ** enantiomer and the case when they are angled in the counterclockwise direction the **Δ**.

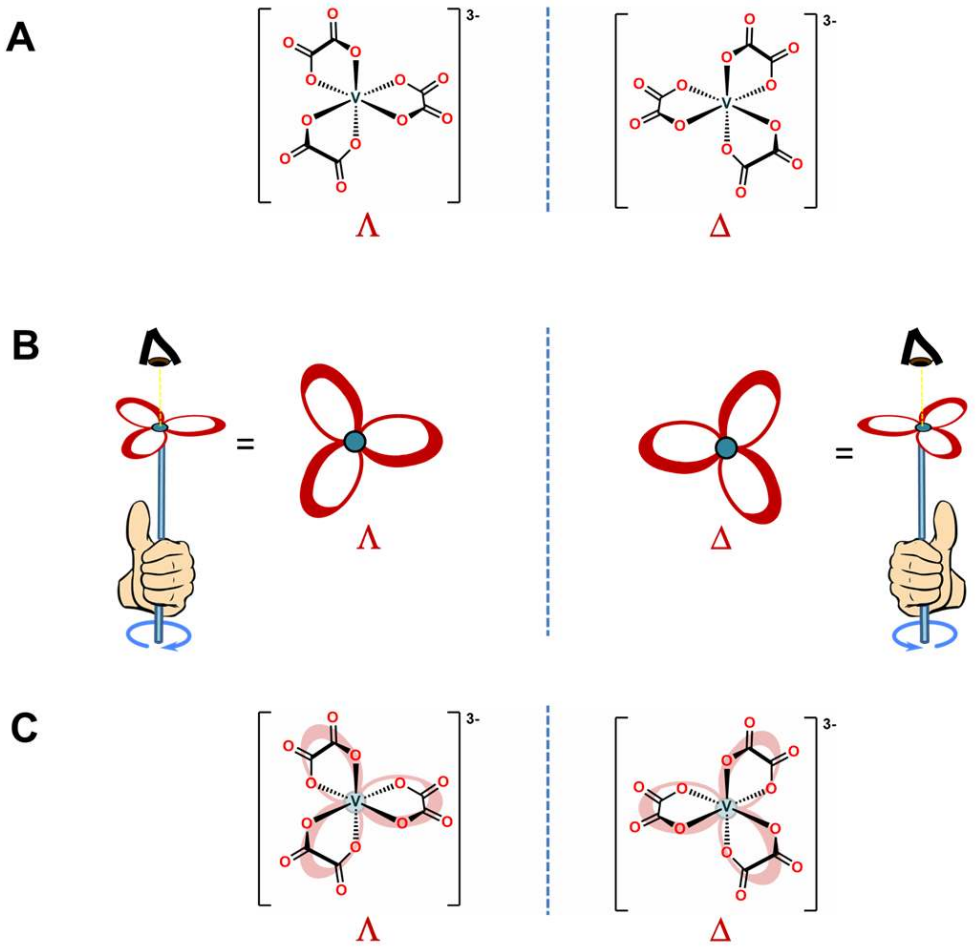


Figure **3.6.5.10**. (A) Octahedral tris-chelates like $[V(ox)_3]^{3-}$ are chiral and can exist as **Λ** and **Δ** enantiomers. (B) The chirality in these systems is analogous to that of a pinwheel, with the **Λ** enantiomer exhibiting the symmetry of a left-handed pinwheel and the **Δ** enantiomer that of a right handed one. (C) The pinwheel-like nature of **Λ** and **Δ** enantiomers is easiest to see by overlaying the structures of $[V(ox)_3]^{3-}$ from A with the pinwheel structures of B. One way to recognize **Λ** and **Δ** enantiomers is to draw them in these projections. If a left hand is curled around the **Λ** enantiomer with the thumb facing up the curl of the fingers will flow from the back of each ligand towards the front. The same will be true if the right hand is curled around the **Δ** enantiomer. Credits: Although the image is largely an original drawing, the hand images used in part B are adapted from an image by SVGguru / CC BY-SA (https://creativecommons.org/licenses/by-sa/4.0). Otherwise this work by Stephen Contakes is licensed under a Creative Commons Attribution 4.0 International License.

The **Λ** and **Δ** chirality in octahedral bis-chelates is analogous to that in the tris-chelates except this time the third chelating ligand is replaced by an arbitrary pair of ligands. This lowers the symmetry of the complex to either C_2 or C_1, as shown for the C_2 complex $[CoCl_2(en)_2]^+$ in Figure **3.6.5.11A**. In either case the result is that such complexes exist as **Λ** and **Δ** enantiomers analogous to those in the metal tris-chelates, as shown in Figure **3.6.5.11B**.

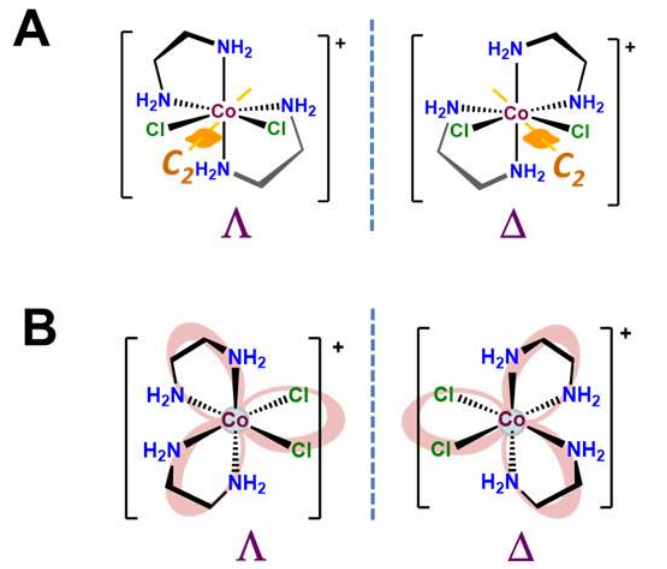


Figure **3.6.5.9C**. This work by Stephen Contakes is licensed under a Creative Commons Attribution 4.0 International License.

Octahedral complexes containing ligands with denticities of four or more also exhibit **Λ** and **Δ** chirality; it is just that in such cases the bound ligand defines multiple rings within the complex that can be defined as existing in either **Λ** or **Δ** orientations relative to each other. The procedure for making these assignments is beyond the scope of most introductory inorganic courses but the result is that such complexes are designated as **ΛΛ**, **ΔΔ**, **ΔΛ**, **ΔΔΔ**, etc., depending on the number of relationships involving the rings defined by the bound ligand. Interested readers should consult reference 4 for more details.

Circular dichroism may be used to characterize optically active metal complexes.

At the present the most definitive way to determine the absolute configuration of an optically active coordination compound is to determine its 3D molecular structure using single crystal X-ray crystallography.[5] However, as that is not always possible or convenient, the optical activity of coordination complexes is also commonly studied using circular dichroism (CD) spectroscopy. CD spectroscopy is used because, unlike most chiral organics, optically active coordination complexes possess low-energy electronic transitions that occur in the far UV and visible range. This means that it is often convenient to use the ability of a complex to refract and absorb different circular polarizations of light to derive information about both the configuration of an optically active complex and its electronic structure. The focus of this section will be to explain how the determination of absolute configuration by circular dichroism and optical rotatory dispersion work, as well as the relationship of these techniques to the more ordinary sort of polarimetry used to measure optical rotation in organic systems. Only brief notes will be made about the instrumental and electronic structure applications of these techniques since the electronic spectra of metal complexes will be discussed in Chapter 11: Coordination Chemistry III - Electronic Spectra and the instrumental aspects of CD are well-treated elsewhere.

Both polarimetry and circular dichroism spectroscopy are grounded in the recognition that plane polarized light is equivalent to a superposition of left and right circularly polarized light, as shown in Figure **3.6.5.12**.

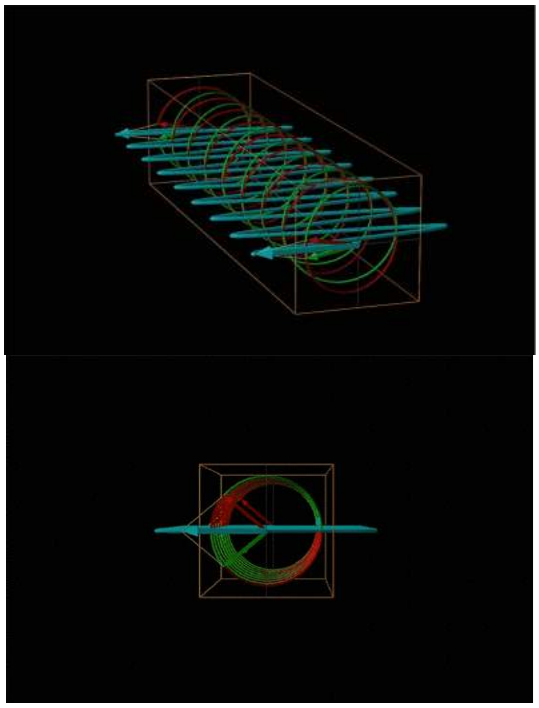


Figure **3.6.5.12**. Angled and front view of plane polarized light (light blue) as the vector sum of left circularly polarized light (red) and right circularly polarized light (green). Created using EMANIM Version 1.2 (2011 July) by Andras Szilagyi (www.enzim.hu/~szia/emanim). This work by Stephen Contakes is licensed under a Creative Commons Attribution 4.0 International License.

When plane polarized light passes through a chiral medium, its left and right circularly polarized components move at different rates (*i.e.*, have different indices of refraction). This causes the plane of polarization to rotate in the direction of the faster component according to the relationship

$$\alpha = \frac{n_l - n_r}{\lambda}$$

where α is the angle of rotation, λ the light's wavelength, and n_l and n_r the refractive indices experienced by left and right circularly polarized light.

An example of such a rotation is shown in Figure **3.6.5.13**.

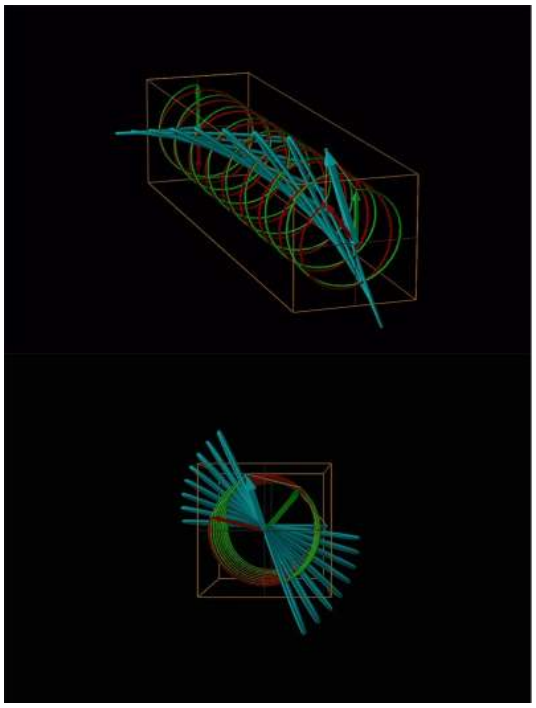


Figure **3.6.5.13**. Angled and front view of plane polarized light (light blue) as it passes through a medium (represented by the orange box) in which left circularly polarized light (red) experiences a higher refractive index (and so moves slower) than right circularly polarized light (green). Created using EMANIM Version 1.2 (2011 July) by Andras Szilagyi (www.enzim.hu/~szia/emanim) with a refractive index of 1.05 for left circularly polarized light and 1.00 for right circularly polarized light. This work by Stephen Contakes is licensed under a Creative Commons Attribution 4.0 International License.

Chemists typically call this rotation of light by a chiral medium optical rotation. In organic chemistry it is common to measure the optical rotation at the sodium D wavelength of 589.29 nm, a much longer wavelength than most organics are able to absorb. Because of this the optical rotations commonly measured by organic chemists are largely independent of absorption and mainly serve as a characteristic physical property similar to melting points or are used to establish the purity of a mixture of enantiomers. The sort of spectroscopic data used to characterize chiral coordination compounds more commonly makes use of the relationship between absorption and optical rotation.

In coordination chemistry the wavelength-dependence of optical rotation is used to discern information about compounds' electronic spectra. This measurement of the wavelength dependence of optical rotation is called **optical rotatory dispersion (ORD)** and the resulting plots are called optical rotatory dispersion or ORD spectra or curves. Such ORD curves are useful for characterizing the chiral environment in a coordination complex because the ORD curves exhibit a characteristic shape. This characteristic shape is because according to the **Cotton Effect,** the optical rotation changes sign at the absorption maximum of a chromophore in the compound. For one configuration the rotation will go from negative to positive with increasing wavelength and is called a **positive cotton effect**; for the other configuration the rotation will go from positive to negative or exhibit a **negative cotton effect**. This behavior is summarized in the top two curves of Figure **3.6.5.14**.

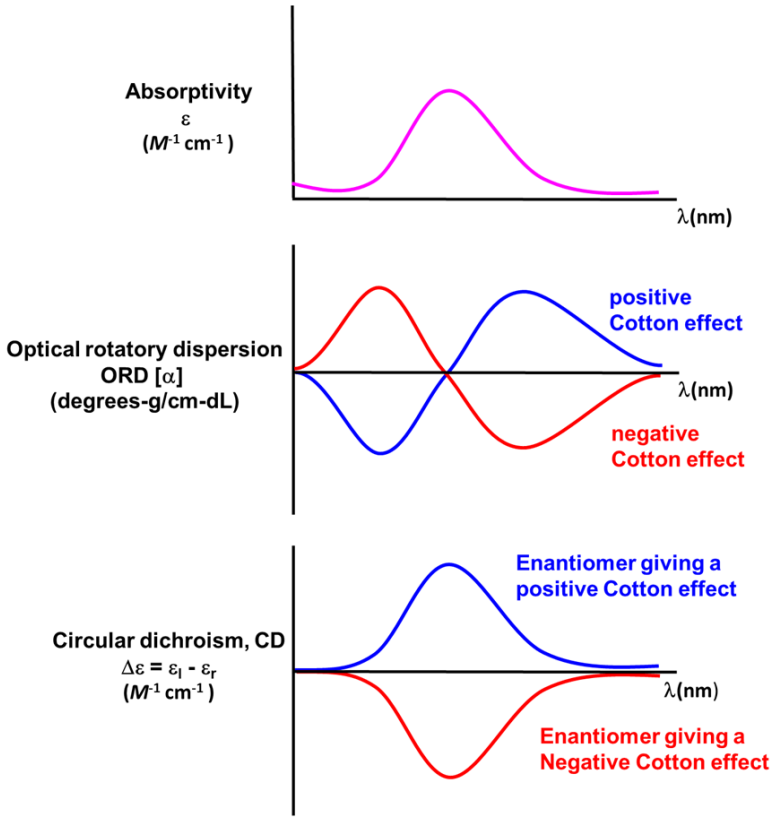


Figure 3.6.5.14. Idealized relationship between absorbance, ORD, and CD spectra for enantiomers exhibiting a positive and negative Cotton effect. This work by Stephen Contakes is licensed under a Creative Commons Attribution 4.0 International License.

A technique used even more often than ORD is **circular dichroism (CD)**, represented by the lowest spectrum in Figure 3.6.5.14. Circular dichroism arises from the differential absorption of left and right circularly polarized light by a chiral compound. This gives elliptically polarized light as shown in Figure 3.6.5.15.

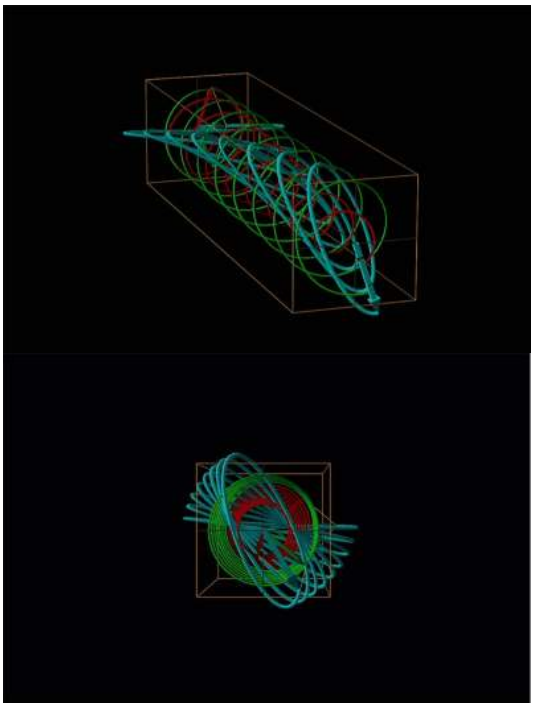


Figure **3.6.5.15**. Angled and front view of plane polarized light (light blue) as it passes through a medium (represented by the orange box) in which left circularly polarized light (red) both experiences a higher refractive index and greater absorption than right circularly polarized light (green). Created using EMANIM Version 1.2 (2011 July) by Andras Szilagyi (www.enzim.hu/~szia/emanim) with a refractive index of 1.05 and an extinction coefficient of 0.05 for left circularly polarized light and a refractive index of 1.00 and extinction coefficient of 0 for right circularly polarized light. This work by Stephen Contakes is licensed under a Creative Commons Attribution 4.0 International License.

In circular dichroism (CD) spectroscopy a sample is irradiated with polarized light resulting in the transmission of elliptically polarized light due to differential refraction and absorption of the polarized light's left and right circularly polarized components. For achiral molecules the handedness doesn't affect absorbance, but for chiral molecules, which chiral ground and excited states the handedness of an EM wave affects can determine how readily that wave can distort the chiral ground state into the chiral excited one. For this reason chiral molecules absorb left and right circularly polarized light differently.

In CD spectroscopy the magnitudes of the left and right circularly polarized components of light that is transmitted by the sample are measured and used to determine how much light of each was absorbed (just as in regular absorbance spectroscopy). The difference in absorption between left and right circularly polarized light constitutes the primary signal in CD spectroscopy. More specifically, circular dichroism spectra (CD spectra) show the difference in extinction coefficients for left and right circularly polarized light, $\Delta\epsilon$, as a function of wavelength, where

$$\Delta\epsilon = \epsilon_l - \epsilon_r$$

where Missing open brace for subscript and Missing open brace for subscript are the extinction coefficients observed with left and right circularly polarized light, respectively.

As with ORD spectra, the signs of the features in CD spectra like that of Δ–$[Co(en)_3]Cl_3$ given in Figure **3.6.5.16** are enantiomer-dependent. As illustrated in the lower spectrum in Figure **3.6.5.14** , the CD spectra of enantiomers mirror one another. Because of this difference in behavior it is possible in principle to determine the absolute configuration of a complex from its CD spectrum.

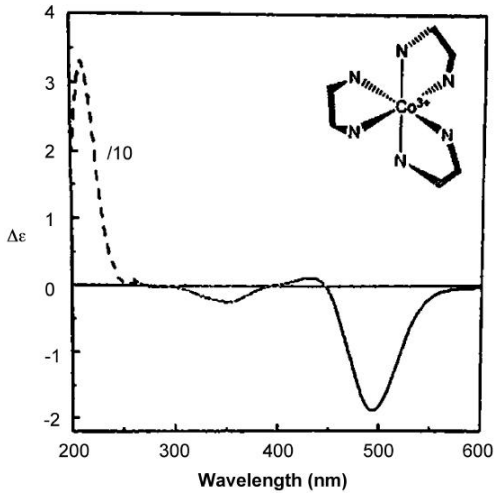


Figure **3.6.5.16**. CD spectrum of Δ–$[Co(en)_3]Cl_3$. Taken from reference 6.

There are several ways that ORD and CD spectra can be useful for determining the absolute configuration of a chiral complex.

1. First, the sign of the Cotton effect and peaks in CD spectra exhibited by a given absolute configuration is often consistent across a series of compounds. Thus if a new member of the series is isolated, its configuration can be determined based on which enantiomer has the same Cotton effect. For instance, if both the **Λ** isomer of a metal diimine complex like $[Ru(bpy)_3]^{2+}$ exhibit a positive Cotton effect and a newly resolved metal diimine exhibits a negative Cotton effect it might reasonably be inferred that the newly-resolved complex is in the opposite or **Δ** configuration.
2. Second, for some systems the expected sign of the Cotton effect and CD peaks for each enantiomer may be predicted semi-empirically based on the spatial locations of substituents relative to the chromophore (the part of the molecule that changes electronic structure during the transition), although the details are beyond the scope of the present discussion.
3. Consideration of interactions between multiple chromophores in a compound can be used to infer absolute configuration. Again, the details are beyond the scope of the present discussion. Interested readers are referred to reference 7 for details.

Common patterns of Diastereomerism

Geometric isomerism

Geometric isomerism involves differences in the geometric placement of atoms in a compound. In coordination chemistry, geometric isomerism involves differences in the relative placement of a set of ligands about a metal center. There are two main types:

cis and *trans* isomerism

This type of isomerism has to do with how two ligands are oriented relative to one another in a square planar or octahedral complex. As shown in Figure **3.6.5.17**, ligands that are next to one another with a L-M-L bond angle of 90° are said to be *cis*; those on opposite sides of the metal with a L-M-L bond angle of 180° are in the *trans* arrangement.



Figure **3.6.5.17**. *cis* and *trans* arrangement of ligands around (A) square planar and (B) octahedral metal centers. Since both types of complexes feature 90° L-M-L bond angles, the arrangements are fundamentally the same in both cases. This work by Stephen Contakes is licensed under a Creative Commons Attribution 4.0 International License.

Simple *cis* and *trans* geometric isomers can be identified when there are two identical ligands (A) or chelating ligands with distinguishable attachment points (A~B) oriented about either a square planar or octahedral center. Examples are given in Figure

3.6.5.18. Notice from the example given in Figure **3.6.5.18C** that multidentate ligands have the potential to constrain complexes to adopt a particular geometry.

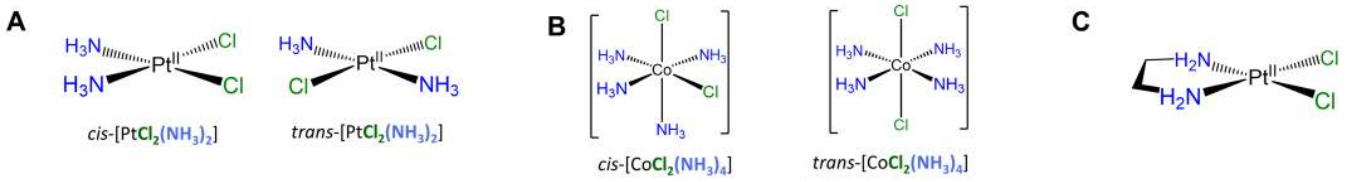


Figure **3.6.5.18**. Examples of square planar and octahedral *cis* and *trans* isomers. (A) *cis* and *trans* isomers of $[PtCl_2(NH_3)_2]$; the former is medicinally important. Sold under the name cisplatin, the *cis* isomer is used as a chemotheraphy against various forms of cancer. (B) *cis* and *trans* isomers of $[CoCl_2(NH_3)_4]$, a compound of more academic interest. (C) $PtCl_2$(en) only exists as the *cis* isomer because the chelating en ligand can only bind in a *cis* arrangement. This work by Stephen Contakes is licensed under a Creative Commons Attribution 4.0 International License.

Slightly more involved examples involve perturbations of the simple cases above in which there are multiple distinguishable *cis* and/or *trans* relationships. Two square planar examples are given in Figure **3.6.5.19**.

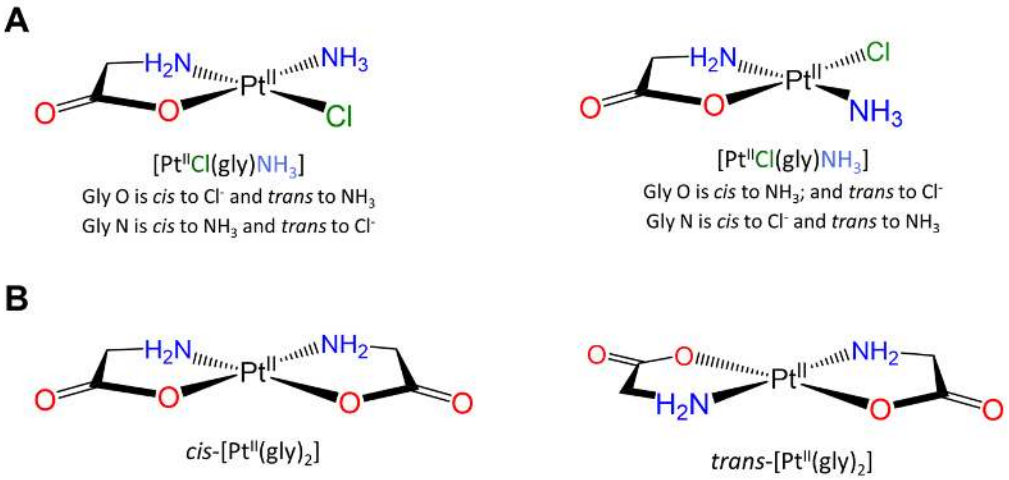


Figure **3.6.5.19**. Examples of more complex square planar systems. (A) Geometric isomers of $[PtCl(gly)NH_3]$, a MA_2BC system for which A = gly^-, B = Cl^-, and C = NH_3. Swapping of the ammine and chloro ligands changes both the *cis* and *trans* relationships involving the Gly ligand. (B) Geometric isomers of $[Pt(gly)_2]$, an $M(A\sim B)_2$ system for which A = the κO glycine carboxy group and B its κN amine. The only possible geometric isomerism involves swapping the orientation of one glycine relative to the other. For this reason the two complexes shown can be designated as *cis* and *trans* isomers based on whether the κO and κN ends of the glycine are *cis* or *trans* to one another. This work by Stephen Contakes is licensed under a Creative Commons Attribution 4.0 International License.

More complex examples of *cis* and *trans* relationships between ligands in octahedral complexes are given in the exercises that conclude this page, which also demonstrates how a systematic approach may be used to identify isomers.

mer and *fac* isomerism

This type of isomerism has to do with how three ligands are oriented relative to one another in an octahedral complex. The arrangements are represented in Figure **3.6.5.20**.

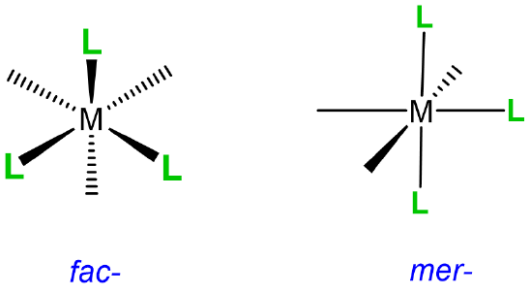


Figure 3.6.5.20. Simple representation of the *fac* and *mer* arrangements of ligands around an octahedral metal center. This work by Stephen Contakes is licensed under a Creative Commons Attribution 4.0 International License.

Since it can help to visualize the *mer* and *fac* geometry from multiple points of view, several representations are given in Figure 3.6.5.21. As shown in Figure 3.6.5.21, in ***fac*** or **facial arrangements**, the ligands occupy the same "face" of the octahedral coordination sphere, while in the ***mer*** or **meridional geometry** the ligands form a T shape in the same plane or its "meridian."[8]

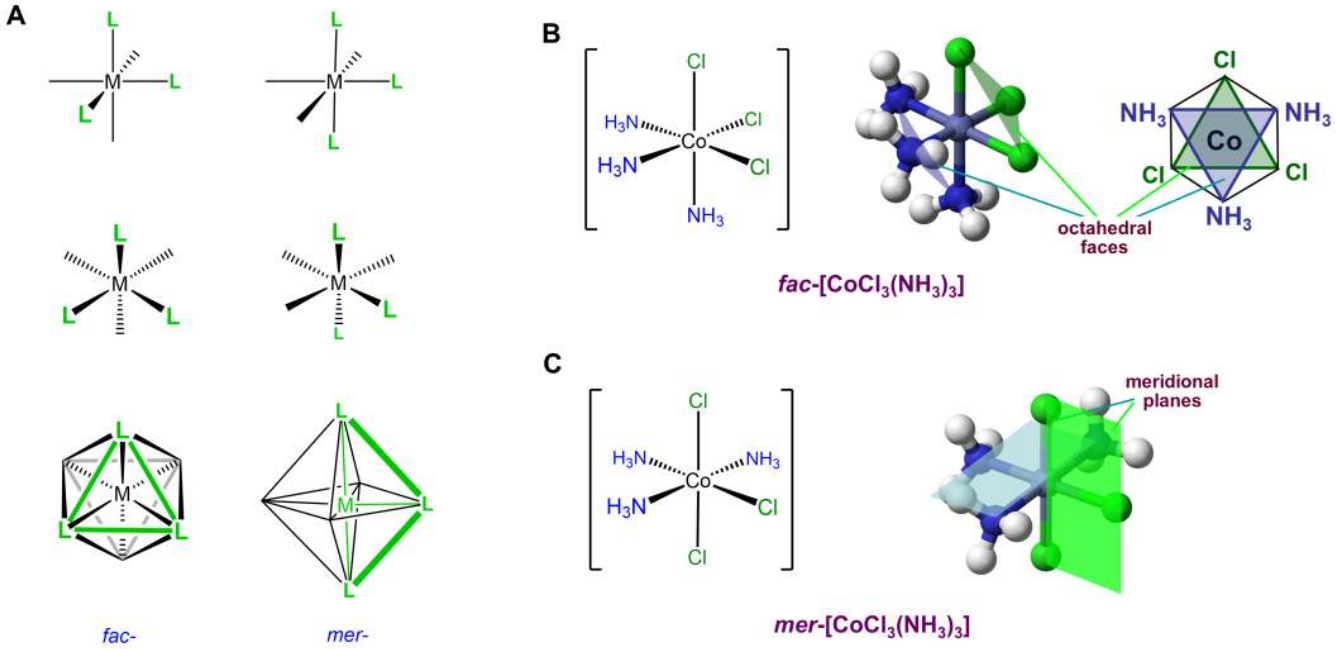
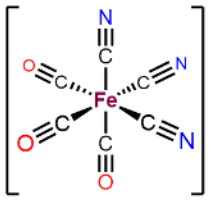
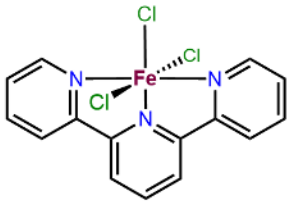
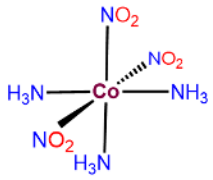


Figure 3.6.5.21. (A) Three projections of *fac* and *mer* arrangements of ligands around an octahedral metal center emphasizing that in the *fac* arrangement the ligands are oriented along a face of the octahedron while in the *mer* arrangement they are oriented in a plane. (B) Structure of *fac*-$[CoCl_3(NH_3)_3]$ showing the octahedral faces occupied by the chloro and amine ligands. (C) Structure of *mer*-$[CoCl_3(NH_3)_3]$ showing the planar arrangement of the chloro and ammine ligands. The ball and stick models are modified from images by Benjah-bmm27 - Own work, Public Domain, https://commons.wikimedia.org/w/inde...?curid=1874872 and curid=1874873. Otherwise this work by Stephen Contakes is licensed under a Creative Commons Attribution 4.0 International License.

Octahedral complexes with three identical ligands oriented about an octahedral center can only exist in *mer* and *fac* arrangements. Consequently, such complexes can be designated as *mer* and *fac* isomers. Examples are given in Figure 3.6.5.22.







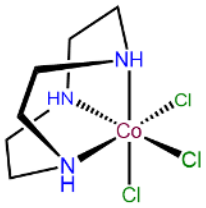


Figure 3.6.5.22. Examples of *fac* and *mer* octahedral complexes. Note how some chelating ligands preferentially bind to the metal in a *fac* or *mer* arrangement and, in so doing, force the other ligands to also form a *mer* or *fac* arrangement. This work by Stephen Contakes is licensed under a Creative Commons Attribution 4.0 International License.

Diastereomerism arising from multiple ligand-associated chiral centers

Diastereomerism can also arise when two or more chiral ligands bind to a metal center. Such cases typically give rise to a complex mixture of isomers, as shown by the example in Figure 3.6.5.23. As may be seen from Figure 3.6.5.23, the differences between these isomers can arise from both changes in the stereochemical configuration of the ligand and the relationship of particular ligand centers relative to one another. For instance, the leftmost two structures in Figure 3.6.5.23 possess one *R* and *S* nitrogen center each but differ in whether the centers are oriented so that the *R* and *S* centers on the two ligands are *trans* or *cis* to one another.

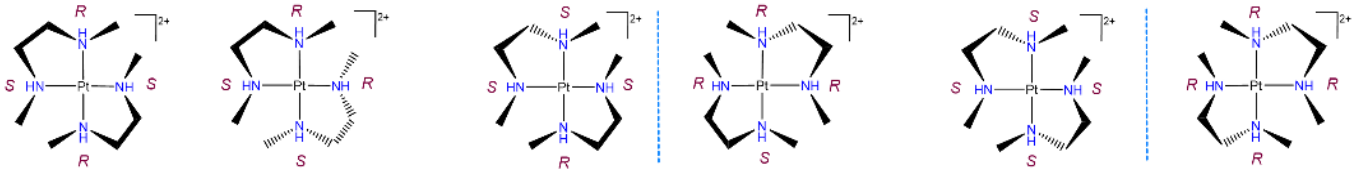


Figure 3.6.5.23. Diastereomers that can in principle be formed when two *N*,*N*′-dimethylethylenediamine ligands coordinate a Pt^{2+} center. This work by Stephen Contakes is licensed under a Creative Commons Attribution 4.0 International License.

Diastereomerism arising from λ and δ ring conformation isomerism.

Chelate rings are formed when a chelating ligand binds a metal

As may also be seen from the structures in Figure 3.6.5.23, when a multidentate ligand coordinates a metal, the ligand and metal center comprise one or more **chelate rings**. Examples of such chelate rings are shown in Figure 3.6.5.24.

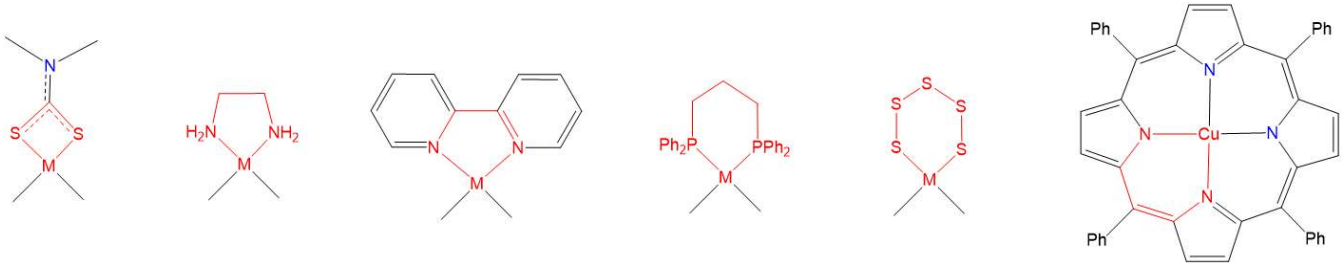


Figure 3.6.5.24. Four, five, and six-membered chelate rings (shown in red) formed by coordination of selected bidentate ligands to a metal center. This work by Stephen Contakes is licensed under a Creative Commons Attribution 4.0 International License.

As may be inferred from the examples in Figure 3.6.5.24, chelate rings may be of different sizes, although four, six, and especially five-membered rings are particularly common. Exactly which ring sizes will be more stable for a given system depends on the

coordination geometry and, due to differences in M-L bond lengths, to a lesser degree on the metal. As a result, for octahedral and square planar complexes with 90° L-M-L bond angles between *cis* ligands, *five-membered rings tend to be especially stable* (Figure **3.6.5.25**).

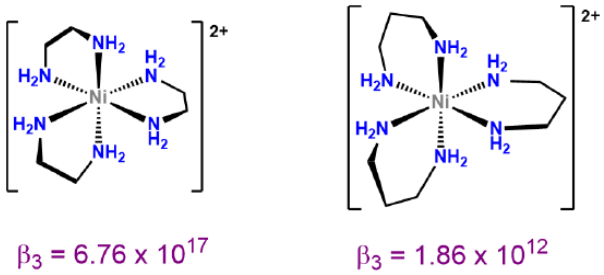


Figure **3.6.5.25**. The greater stability of five-membered chelate rings involving Ni^{2+} and organic ligands is reflected in the higher overall formation constant (β_3) for the five-membered chelate rings contained in $[Ni(en)_3]^{2+}$ compared to that of $[Ni(et)_3]^{2+}$, which has six-membered rings. The data in this figure is taken from Stability of Metal Complexes and Chelation by Robert Lancashire. This work by Stephen Contakes is licensed under a Creative Commons Attribution 4.0 International License.

Not all metal chelates prefer to form five-membered rings. The steric requirements of chelate rings depend on both the preferred coordination geometry of the metal center and the stereochemistry of the ligand. Both of these effects are typically considered in terms of preferred L-M-L bond angles. From the perspective of the metal center, the preferred bond angle is determined by the coordination geometry. Octahedral and square planar metals prefer 90° L-M-L bond amgles, trigonal bipyramidal systems 90 and 120° L-M-L bond angles, and tetrahedral complexes 109.5° L-M-L angles. The larger preferred bond angles in tetrahedral and trigonal bipyramidal systems often require the formation of larger six or seven-membered chelate rings for maximum stability. The size of the chelate ring actually formed between a metal and ligand is determined by the ligand's structure. As the contributor of all the atoms in the chelate ring but one, the ligand directly determines the chelate ring size. More subtly, ligands naturally prefer to coordinate metals at a particular L-M-L angle, called the **bite angle**, as shown in Figure **3.6.5.26A**. Ligands with bite angles corresponding to the ideal L-M-L angle for a metal's preferred geometry tend to form more stable complexes, although in turn ligand bite angles can cause metals with a weak coordination geometry preference to adopt the ligand's preferred geometry instead.[10] As may be seen from the values in Figure **3.6.5.26B**, bite angles roughly increase with the size of the chelate ring formed but are also influenced by the types of structures used to connect the ligand's Lewis base sites. This facilitates the use of diphosphine ligands to tailor the structure and reactivity of phosphine-containing organometallic catalysts.



Figure **3.6.5.26**. (A) Definition of the bite angle as the angle at which the ligand's preferred L-M-L angle when coordinating a metal center. (B) Bite angles of selected diphosphines.[9] The bite angles of many such diphosphines have been determined to facilitate the design of phosphine-containing organometallic catalysts. This work by Stephen Contakes is licensed under a Creative Commons Attribution 4.0 International License.

λ and δ isomerism involves differences in the conformation of nonplanar five-membered chelate rings

As shown in Figure **3.6.5.27**, some chelate ring systems are planar while others are not.

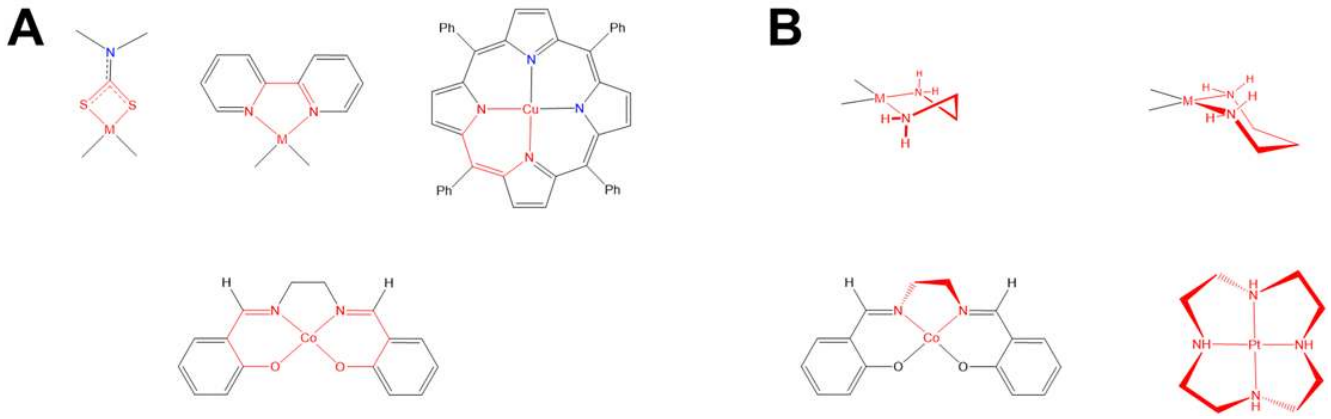


Figure 3.6.5.27. (A) Planar and (B) Nonplanar chelate rings shown highlighted in red. Notice how [Co(salen)] possesses a nonplanar chelate ring and two planar ones. This work by Stephen Contakes is licensed under a Creative Commons Attribution 4.0 International License.

Among the nonplanar chelate ring systems are ligands like en and dppe, which contain tetrahedral C, N, O, P, and S atoms. Because these atoms create kinks in the chelate ring they introduce additional opportunities for diastereomerism due to differences in the chelate ring conformation, called **ring twist**. Ring twist in nonplanar systems has been most extensively explored for five-membered chelates like those formed by dppe and by en and other chelating amines. Unlike the more rigid four-membered chelate rings, five-membered chelates tend to be conformationally flexible, but not so conformationally flexible that their conformers are rapidly interconverting at room temperature (at least not when the rings are substituted to introduce additional steric strain). This balance between flexibility and rigidity enables some five-membered chelate rings to exist as mixtures of distinguishable conformational isomers at room temperature.

To understand the two most stable conformers that five-membered chelates rings tend to form, it is helpful to think of five-membered chelate rings as involving two components (Figure 3.6.5.28):

- a planar L-M-L group, where L are the atoms directly attached to the metal, M, and
- the remaining two ring atoms, E, which form a rigid E-E bar across the back of the chelate ring.

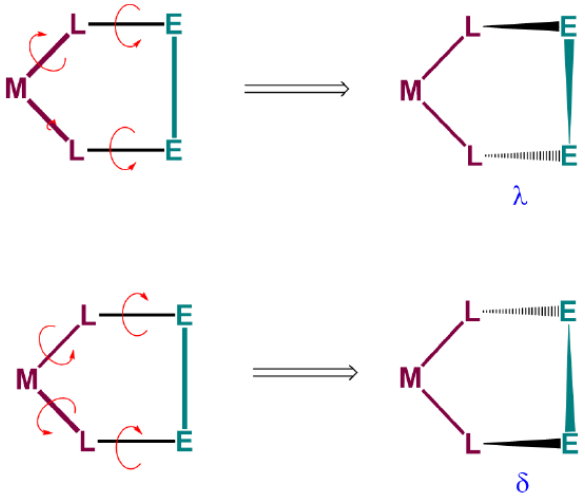


Figure 3.6.5.28. Five-membered chelate rings consist of a planar L-M-L group connected to a rigid E-E bar. Conformers arise as rotation about the M-L and L-E bonds causes twisting of the E-E bar relative to the L-M-L plane. This work by Stephen Contakes is licensed under a Creative Commons Attribution 4.0 International License.

As can be seen from Figure 3.6.5.28 , rotation about the M-L and L-E bonds causes twisting of the E-E bar relative to the L-M-L plane. The two most stable conformers produced by these motions are the λ or δ conformations as shown in Figures 3.6.5.29 and 3.6.5.29.

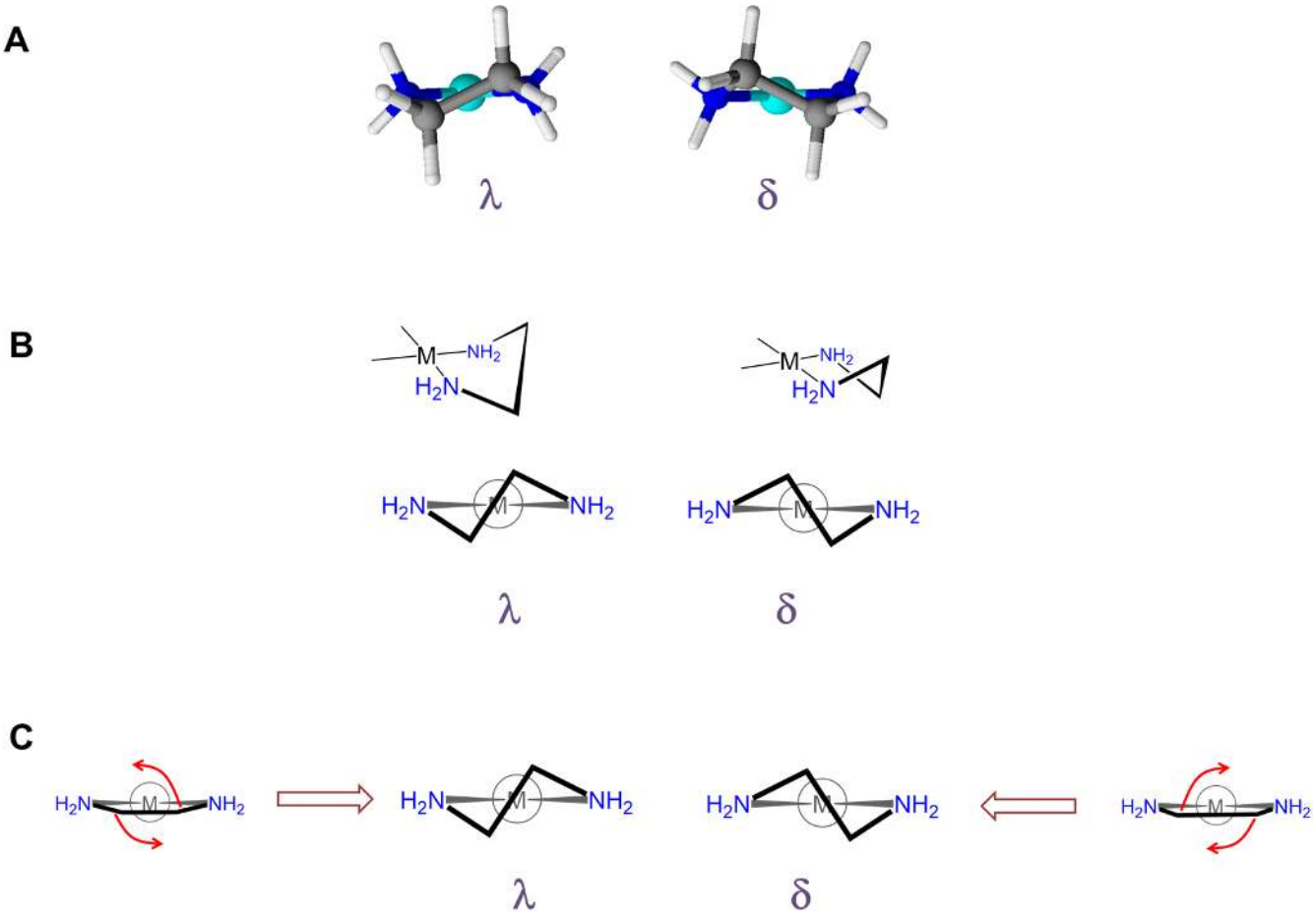


Figure **3.6.5.29**. (A) **λ** and ***δ*** ring twist in a square planar metal ethylenediamine complex (B) along with several ways to represent it in line drawing form. (C) Of these, the projection looking down an axis bisecting the chelate ring makes it easiest to see that, starting with a planar chelate ring the **λ** conformer corresponds to a counterclockwise twist of the CH_2CH_2 bond relative to the N-M-N plane and the ***δ*** conformer a clockwise twist relative to the N-M-N plane. This work by Stephen Contakes is licensed under a Creative Commons Attribution 4.0 International License.

The relative stability of the **λ** and ***δ*** conformers will depend on the configuration of any stereocenters present and steric factors. As with organic ring systems, steric effects tend to favor conformers in which bulky groups are placed in the less sterically strained equatorial positions while the configuration of the stereocenters present can serve to restrict the allowable ring twist conformations, as illustrated in Figure **3.6.5.30**. A detailed treatment of such systems is beyond the scope of this page. Interested readers are referred to reference 12 for more details.

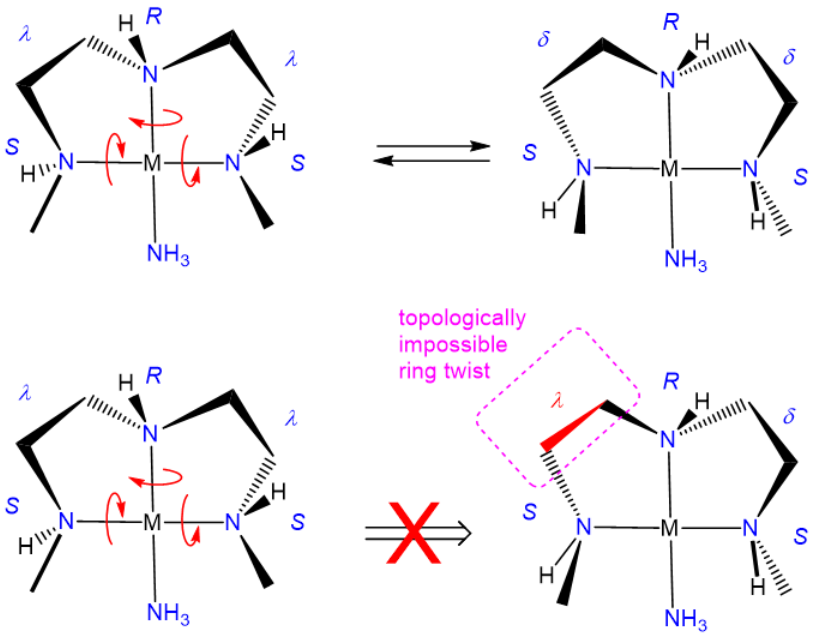


Figure 3.6.5.30. The configurations at nitrogen in the complex shown restrict the chelate ring conformations to either a λλ or δδ conformation because the rotations needed to enable a λδ configuration are topologically impossible. This work by Stephen Contakes is licensed under a Creative Commons Attribution 4.0 International License.

In closing, it should be noted that it might seem to be making much of small effects in pointing out that one source of diastereomerism in metal complexes involves the freezing out of chelate ring conformations. However, that would be to mistake the impacts that ring conformations can have on the steric accessibility of a coordination site and shaping the course of processes that might occur there. As illustrated in Figure 3.6.5.31, a simple shift in the conformation of one ring in a square planar, pyramidal, or octahedral complex containing coplanar ethylene diamine ligands can exert a significant effect on the steric profile of the complex perpendicular to the MN_4 square plane. Because of effects like these, ring conformation isomerism plays a role in the design of stereoselective transition metal catalysts.

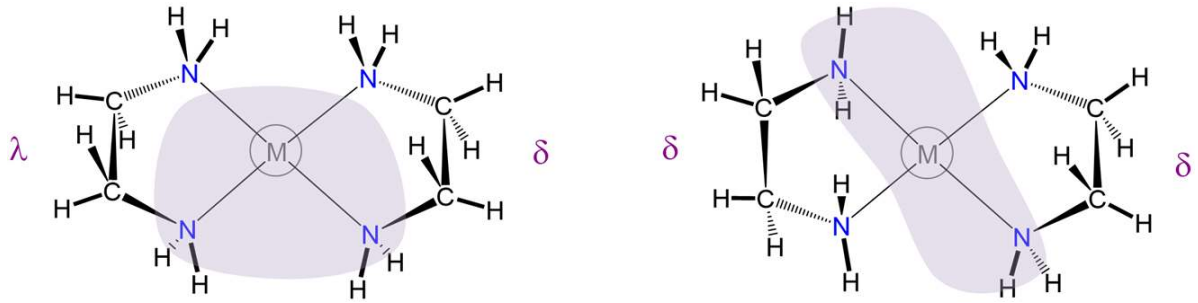


Figure 3.6.5.31. Schematic illustrating how the conformation of ethlyenediamine ligands bound to a metal center affects the steric accessibility of the metal (shown shaded in violet) to potential ligands attempting to bind from above the MN_4 plane. This work by Stephen Contakes is licensed under a Creative Commons Attribution 4.0 International License.

Exercises

? Exercise 3.6.5.1. Identify the type of isomerism

What type of isomers are

a. $[CoCl(NH_3)_5](NO_3)$ and $[Co(NH_3)_5(N\text{-}NO_2)]Cl$?
b. $[Co(NH_3)_5\text{-}CN\text{-}Ru(NH_3)_5]^{4+}$ and $[Co(NH_3)_5\text{-}NC\text{-}Ru(NH_3)_5]^{4+}$
c. $[Cr(CN)_5\text{-}CN\text{-}Co(NH_3)_5]$ and $[Co(CN)_5\text{-}CN\text{-}Cr(NH_3)_5]$
d. *cis*-$[Mn(en)_2(CN)_2]$ and *trans*-$[Mn(en)_2(CN)_2]$

Answer a.

Ionization isomers.

Answer b.

Linkage isomers.

Answer c.

Coordination isomers.

Answer d.

Geometric isomers, specifically *cis*/*trans* isomers.

Exercise 3.6.5.2. Assigning metal oxidation states in a complex

Many properties of transition metal complexes depend on the metal's oxidation state. For instance,

- octahedral complexes of Co^{II} lose and gain ligands rapidly
- octahedral complexes of Co^{III} lose and gain ligands very slowly
- four-coordinate complexes are generally tetrahedral
- EXCEPT four-coordinate complexes of metals like Pt^{II} , Pd^{II} , Rh^{I}, and Ir^{I}, among others, are square planar

For this reason it is important to be able to estimate the formal oxidation state of a metal in a complex. Fortunately, this is easy to do if you remember

1. The sum of all atoms' oxidation states will equal the overall charge on the complex
2. When determining the metal's oxidation state, the ligands can be treated as having an oxidation state equal to their charge - *i.e.*, the charge they possess in the form in which they coordinate the metal - so if they need to lose a proton to bind, don't forget to account for that.

Given the above, estimate the oxidation state of the metal in the following real and hypothetical complexes.

a. $Na_4[Fe(CN)_6]$
b. $[Cu(phen)_2]BF_4$
c. $[PtF_4(NH_3)_2]$
d. $[Ni(en)_2]SO_4$
e. $Co(acac)_3$
f. [MnCl(O)(salen)]

Answer for $Na_4[Fe(CN)_6]$.

This contains $[Fe(CN)_6]^{4-}$; so $O.S._{Fe}$ + 6 x (-1) (for CN^-) = -4 (the complex's charge) so $O.S._{Fe}$ = +2 or Fe^{2+}.

Answer for $[Cu(phen)_2]BF_4$.

Since tetrafluoroborate is a monoanion, the complex is $[Cu(phen)_2]^+$ so $O.S._{Cu}$ + 0 x 2 (for phen) = +1 (the complex's charge) so $O.S._{Cu}$ = +1 or Cu^+.

Answer for $[PtF_4(NH_3)_2]$.

$O.S._{Pt}$ + 4 x (-1) (for F^-) + 0 x 2 (for NH_3) = +0 (the complex's charge) so $O.S._{Pt}$ = +4 or Pt^{4+}.

Answer $[Ni(en)_2]SO_4$.

The complex is $[Ni(en)_2]^+$ so $O.S._{Ni}$ + 0 x 2 (for en) = +2 (the complex's charge) so $O.S._{Ni}$ = +2 or Ni^{2+}.

Answer $Co(acac)_3$.

$O.S._{Co}$ + 3 x (-1) (for acac; see table 9.2.2) = +0 (the complex's charge) so $O.S._{Co}$ = +3 or Co^{3+}.

Answer [MnCl(O)(salen)].

$O.S._{Mn}$ + 1 x (-1) (for Cl^-) + 1 x (-2)(for oxo) + 1 x (-2) (for salen; see table 9.2.2) = +0 (the complex's charge) so $O.S._{Mn}$ = +5 or Mn^{5+}.

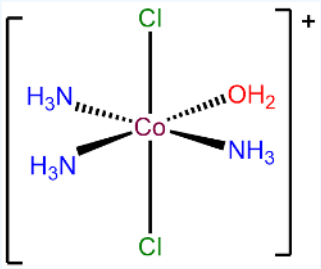
Exercise 3.6.5.3. Drawing isomers from descriptions

Draw structures that match the descriptions given, assuming that

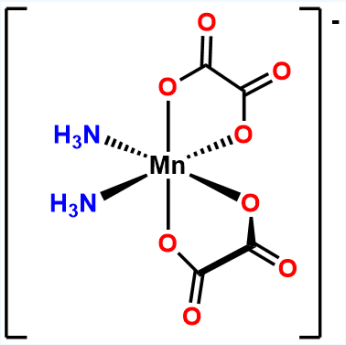
- complexes in which the metal has a coordination number of six are octahedral
- complexes in which the metal has a coordination number of five are trigonal bipyramidal
- complexes in which Pt^{II} , Pd^{II} , or Rh^{I}, or Ir^{I} have a coordination number of four are square planar
- other complexes in which the metal has a coordination number of four will be tetrahedral

a. *mer*-triammineaqua-*trans*-dichlorocobalt(III) ion
b. **Δ**-diaminebis(oxalato)manganate(III)
c. $[CoCl_4]^{2-}$
d. *trans*-diamminebis(ethylenediamine)Nickel(2+) tetracyanopalladate(2-)
e. **Λ**-bis(ethylenediamine)cobalt(III)- μ-amido μ-hydroxo-**Δ**-bis(ethylenediamine)cobalt(III)

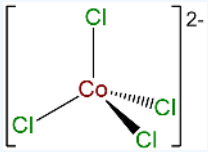
Answer a. *mer*-triammineaqua-*trans*-dichlorocobalt(III) ion.



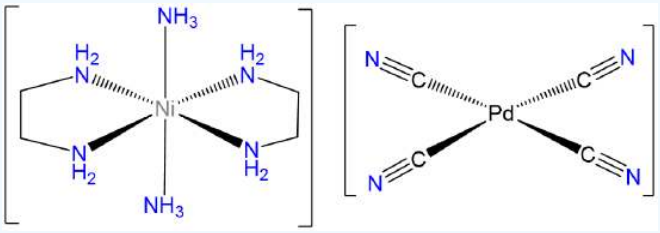
Answer b. Δ-diaminebis(oxalato)manganate(III).



Answer c. $[CoCl_4]^{2-}$.

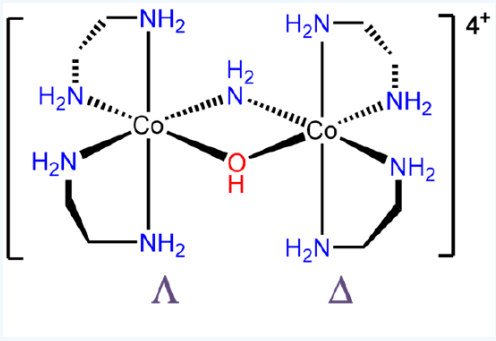


Answer d. *trans*-diamminebis(ethylenediamine)Nickel(2+) tetracyanopalladate(2-).



Note that since the Pd in $[Pd(CN)_4]^{2-}$ is Pd^{2+} it will be square planar.

Answer e. Λ-bis(ethylenediamine)cobalt(III)- μ-amido μ-hydroxo-Δ-bis(ethylenediamine)cobalt(III).



? Exercise 3.6.5.4. Stereoisomers of complexes containing only monodentate ligands.

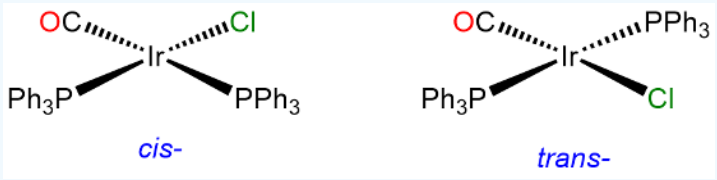
Draw all the stereoisomers of the following real and hypothetical complexes. You may assume that

- complexes in which the metal has a coordination number of six are octahedral
- complexes in which the metal has a coordination number of five are trigonal bipyramidal
- complexes in which Pt^{II} , Pd^{II} , or Rh^{I}, or Ir^{I} have a coordination number of four are square planar
- other complexes in which the metal has a coordination number of four will be tetrahedral

a. $[IrCl(CO)(PPh_3)_2]$
b. $[CoCl_3(NH_3)_3]$
c. $[CoCl_2(H_2O)_2(NH_3)_2]^+$
d. $[CoBrCl(H_2O)_2(NH_3)_2]^+$
e. $[CoBrClI(NH_3)_3]$

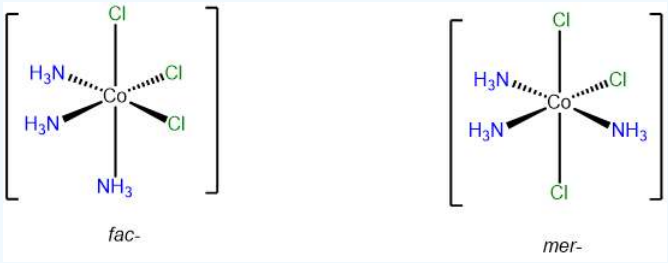
Answer a. $[IrCl(CO)(PPh_3)_2]$

This is a 4-coordinate Ir^{I} complex and, as such will be square planar. Since two of the ligands are identical, it will have *cis* and *trans* isomers. The *trans* isomer is famous for its ability to form adducts and is called Vaska's complex.



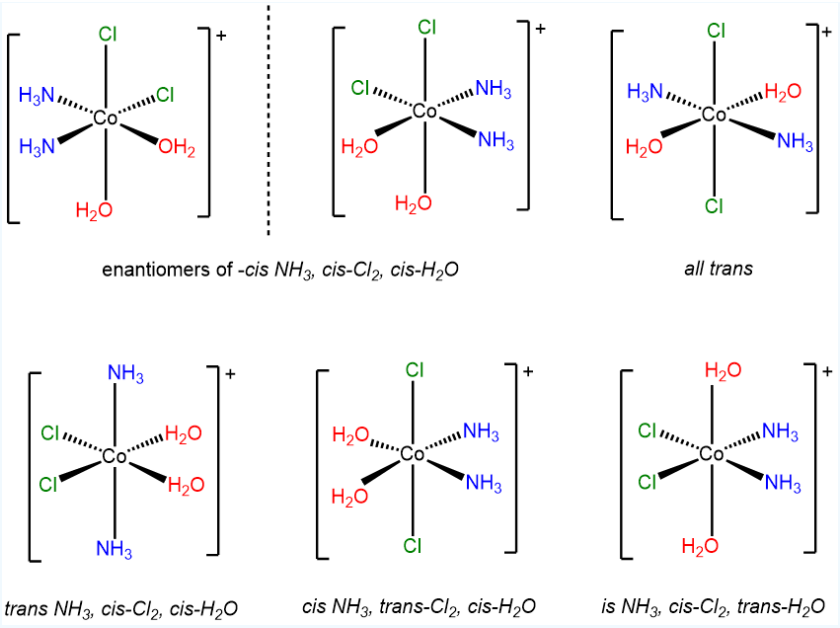
Answer b. $[CoCl_3(NH_3)_3]$

This complex contains three ammine and three chloro ligands and so will have *fac* and *mer* isomers.



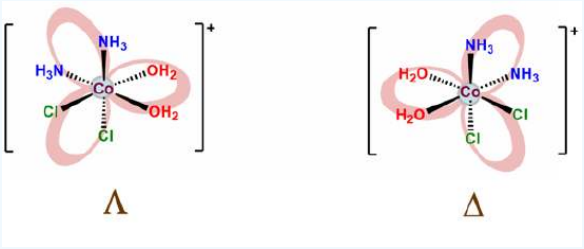
Answer c. $[CoCl_2(H_2O)_2(NH_3)_2]^+$

This is a case of an $MA_2B_2C_2$ system (A = Cl^-, B = H_2O, C = NH_3) involving multiple *cis* and *trans* relationships. The six stereoisomers are shown below.



Since it may not be obvious how to arrive at a set of isomers like the ones above, it is worth considering how one might work through the possibilities for a system of ligands like this one. Several systems may be used to systematically identify isomers. Once approach is the Macbdef system described in Note **3.6.5.1** at the end of these exercises. The solutions presented here and in subsequent problems employ a variant of that approach.

- Start by fixing one set of ligands. In this case the chloro ligands were first fixed as *cis* to one another. Then the remaining ligands might be *cis* or *trans* to one another, although since the *chloro* ligands are already *cis*, the ammine and aqua ligands cannot both be *trans* at the same time. Thus for *cis* chloro ligands the possibilities for the others are:
  - *cis*-H_2O ,*cis*-NH_3,
  - *cis*--H_2O, *trans*-NH_3
  - *trans*-H_2O, *cis*-NH_3
- Swap the configuration of the ligand set you started with. In this case it means placing the chloro ligands *trans* to one another. From that configuration, the possibilities for the ammine and aqua ligands are
  - *cis*-H_2O ,*cis*-NH_3,
  - *trans*-H_2O, *trans*-NH_3
- Check for enantiomers and create mirror images of any chiral complexes you drew. The easiest way to do this is to assign point groups. However, it turns out that the octahedral all-*cis* case is D_3 and formally equivalent to the symmetry of a tris chelate, as shown below.

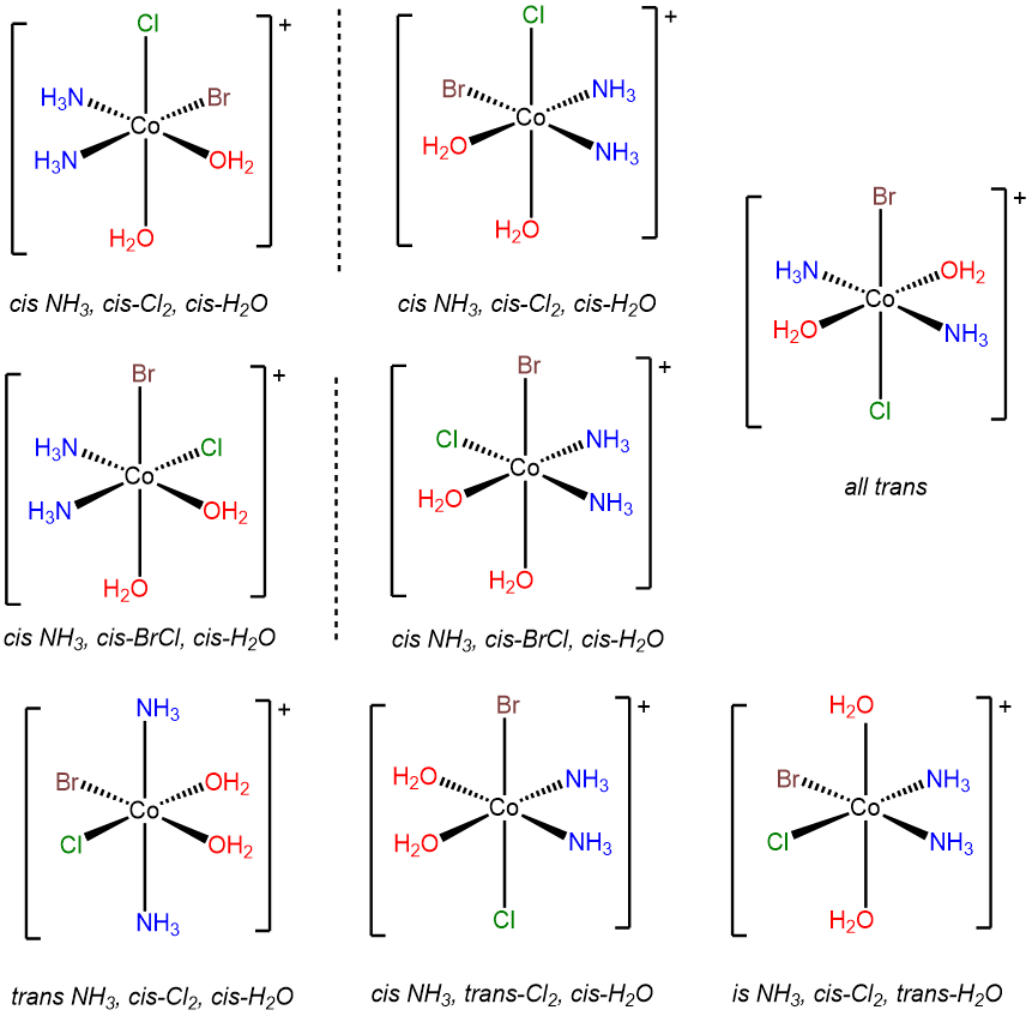


- finally, check to make sure you didn't include the same complex twice. Humans do make mistakes after all.

Answer d. $[CoBrCl(H_2O)_2(NH_3)_2]^+$

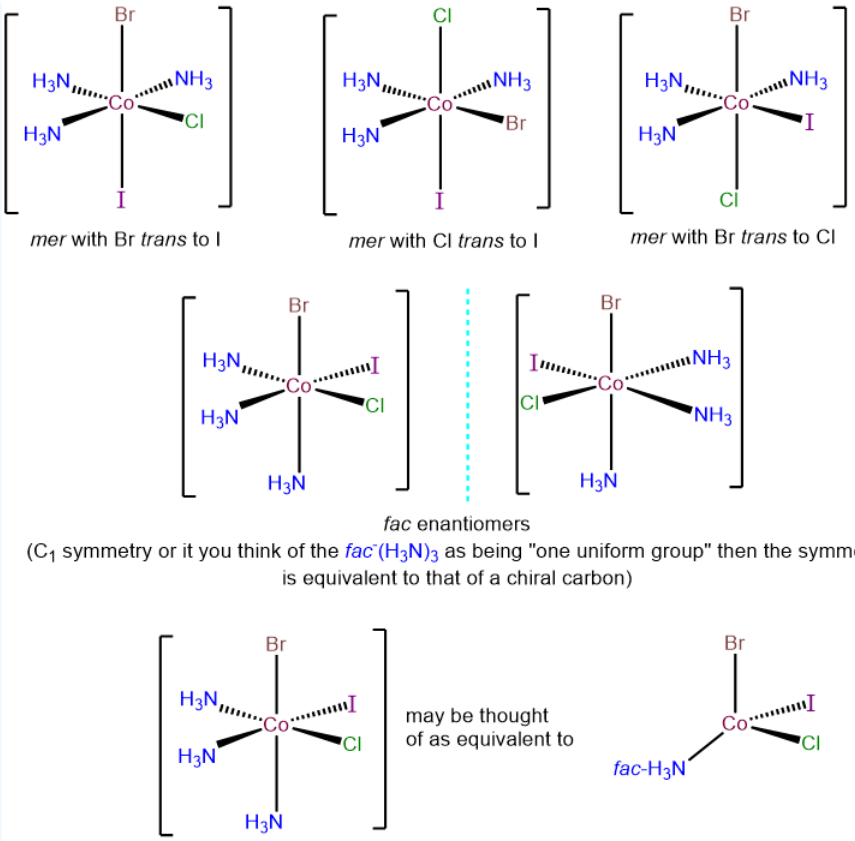
This problem is analogous to the one above except that this complex contains a bromo and chloro ligand in place of the two chloro ligands in $[CoCl_2(H_2O)_2(NH_3)_2]^+$. Consequently, when the bromo and chloro ligands are *cis* to one

another, additional possibilities for isomers arise based on whether ammine or aqua ligands are *trans* to the chloro and bromo. The result is eight isomers.



Answer e. [$CoBrClI(NH_3)_3$]

There are two possibilities for this complex - a *fac*-$(NH_3)_3$ and a *mer*-$(NH_3)_3$ arrangement. These may be taken as starting points for examining the possible permutations for the Cl^-, Br^-, and I^- ligands. The top row presents the three possibilities within the *mer*-$(NH_3)_3$ arrangement; each corresponds to a different ligand *trans* to an ammine ligand. The bottom row presents the two possible isomers with a *fac*-$(NH_3)_3$ arrangement. In each, the Cl^-, Br^-, and I^- ligands are *trans* to ammine ligands. However, the complexes possess C_1 symmetry and so are chiral and exist as enantiomers.



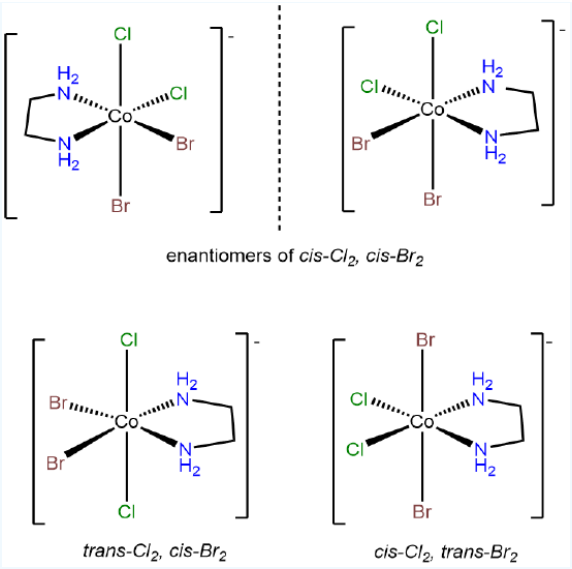
? Exercise 3.6.5.5. Stereoisomers of complexes with bidentate ligands (ignoring ring twist).

Ignoring ring twist, draw all the stereoisomers of the following real and hypothetical octahedral complexes.

a. $[CoBr_2Cl_2(en)]^-$
b. $[CoBrCl(en)_2]^+$
c. $[CoBrCl(gly)_2]^-$
d. $[Co(en)_3]^{3+}$
e. $[Co(gly)_3]$

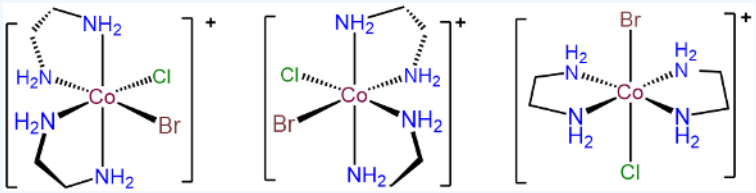
Answer a. $[CoBr_2Cl_2(en)]^-$

This complex is analogous to $[CoCl_2(H_2O)_2(NH_3)_2]^+$ in possessing pairs of identical ligating groups. The main difference is that in $[CoBr_2Cl_2(en)]^-$ the two amine ligating group of the en ligand are restricted to a *cis* arrangement. Under the MABCDEF system explained in Note **3.6.5.1**, $[CoCl_2(H_2O)_2(NH_3)_2]^+$ may be $MA_2B_2C_2$, but this complex, $[CoBr_2Cl_2(en)]^-$, is $M(AA)B_2C_2$. The isomers are:



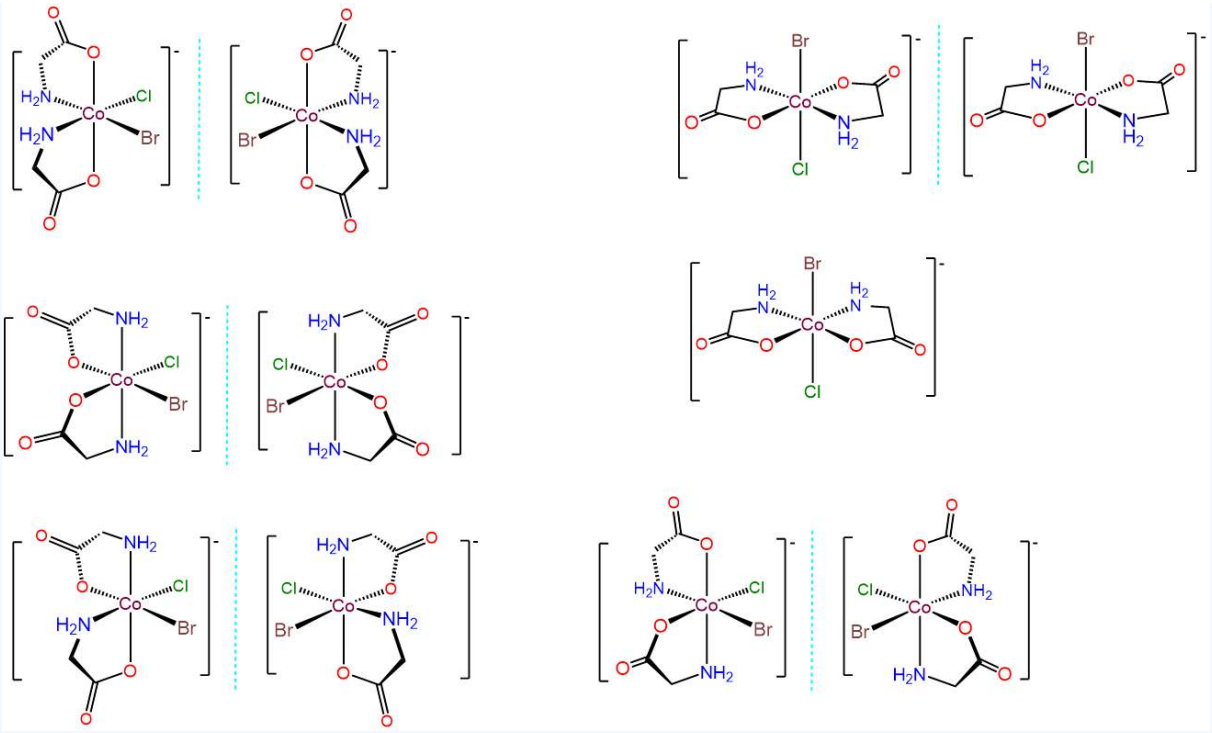
Answer b. $[CoBrCl(en)_2]^+$

The key to problems like this is to focus on the unique ligands, in this case Br^- and Cl^-. These can exist in either a *cis* or *trans* arrangement. The *trans* form is achiral, but in the case where Br^- and Cl^- are *cis*, **Λ** and **Δ** enantiomers are possible. The result is three isomers.



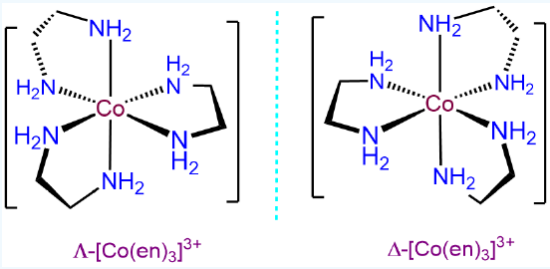
Answer c. $[CoBrCl(gly)_2]^-$

This case is analogous to the one above, but this time the bidentate ligand, gly, possesses distinguishable binding sites. Thus there are additional permutations involving how the gly ligands are bound relative to one another and/or whether the O or N end of the gly is bound *trans* to Br or Cl. The result is 11 different isomers, which are given below.



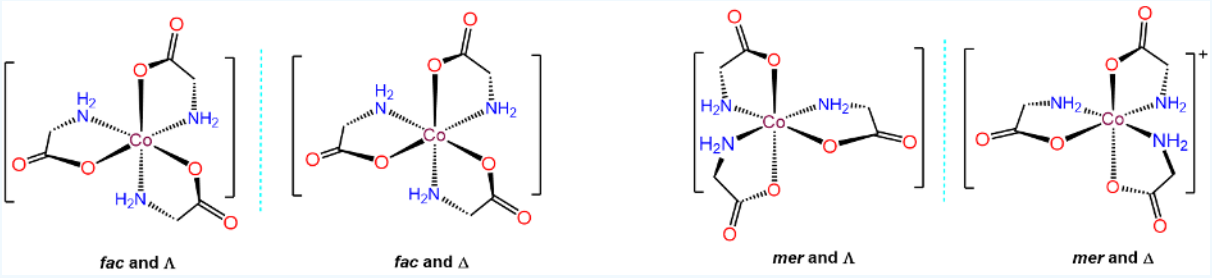
Answer d. $[Co(en)_3]^{3+}$

As a tris-chelate of symmetric bidentate ligands, ignoring ring twist, $[Co(en)_3]^{3+}$ will only exhibit **Λ** and **Δ** isomerism.



Answer e. $[Co(gly)_3]$

Since there are three gly ligands, each of which have carboxy and amine ends, the allowable arrangements involve whether the resulting three carboxy and three amine ends are oriented in a *mer* or *fac* arrangement. This gives two possibilities, each of which can exist as either the **Λ** or **Δ** enantiomer, for a total of four isomers, which are given below.



Exercise 3.6.5.6. More stereoisomers: Now featuring linkage isomerism

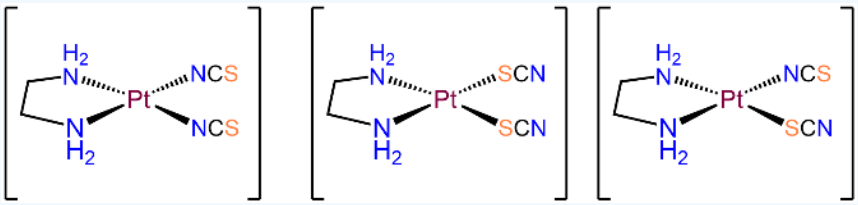
Ignoring ring twist, draw all chemically reasonable stereoisomers for the following real and hypothetical complexes. You may assume that

- complexes in which the metal has a coordination number of six are octahedral
- complexes in which the metal has a coordination number of five are trigonal bipyramidal
- complexes in which Pt^{II} , Pd^{II} , or Rh^{I}, or Ir^{I} have a coordination number of four are square planar
- other complexes in which the metal has a coordination number of four will be tetrahedral

a. $[Pt(en)(SCN)_2]$
b. $[Pt(NH_3)_2(SCN)_2]$
c. $[Co(en)_2(SCN)_2]^+$

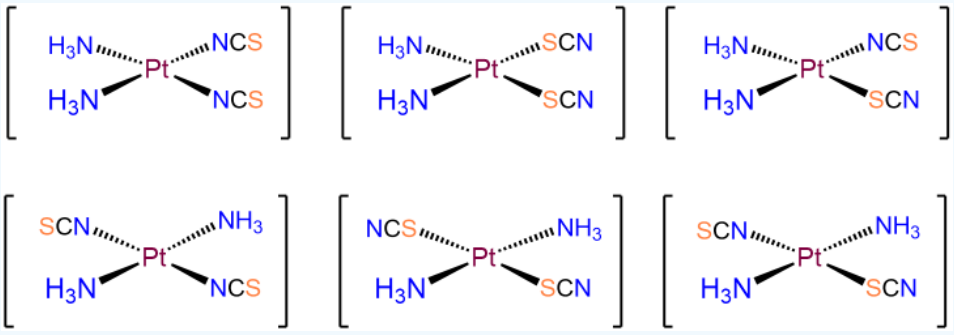
Answer a. $[Pt(en)(SCN)_2]$

The Pt in this neutral complex must be Pt^{2+} to balance the negative charges of the two SCN^- ligands. Complexes of Pt^{2+} are square planar and four coordinate, consistent with the bidentate en and two thiocyanato ligands. Of the ligands, the en ligand must bind in a *cis* arrangement. Consequently, the two SCN^- ligands will be in a *cis* arrangement as well. The isomers will therefore only differ in whether the two SCN^- bind κN or κS. The possibilities are:

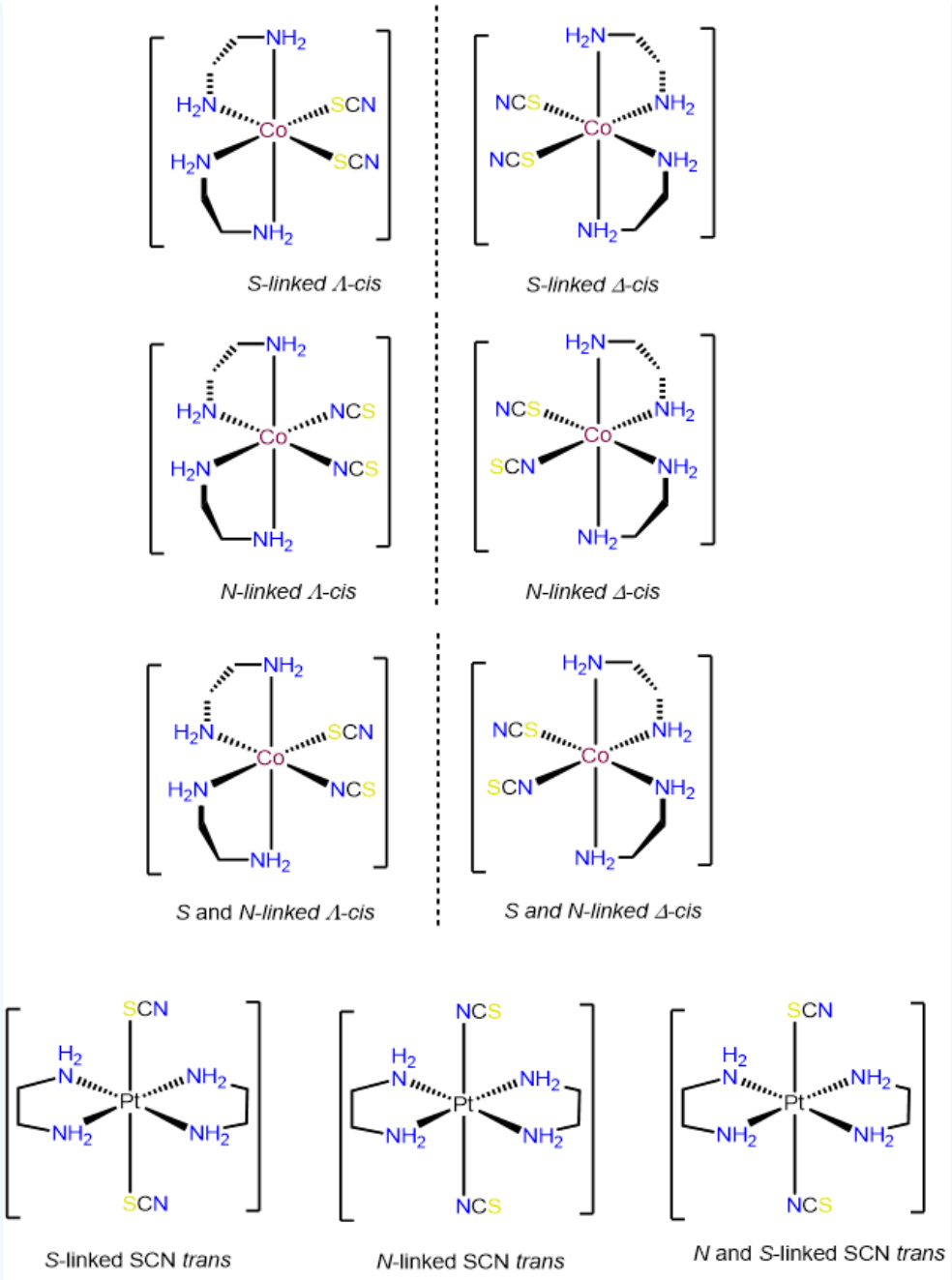


Answer b. $[Pt(NH_3)_2(SCN)_2]$

As with the preceding example, this will be a square planar Pt^{2+} complex. The main difference is that this time the coordinated nitrogens are not constrained to adopt a *cis* arrangement so there will be both *cis* and *trans* isomers.



Answer c. $[Co(en)_2(SCN)_2]^+$



? Exercise 3.6.5.7. Stereoisomer free for all.

Ignoring ring twist, draw all chemically reasonable stereoisomers for the following real and hypothetical complexes. You may assume that

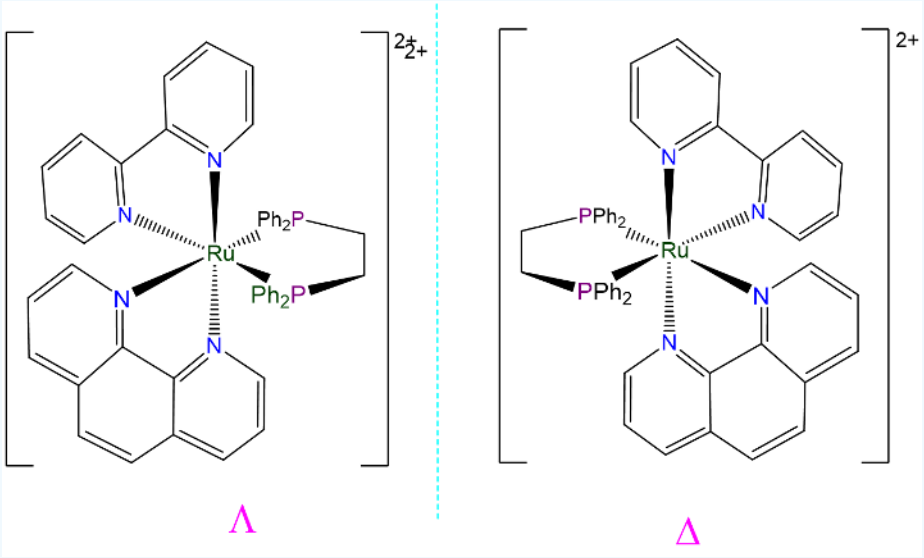
- complexes in which the metal has a coordination number of six are octahedral
- complexes in which the metal has a coordination number of five are trigonal bipyramidal
- complexes in which Pt^{II} , Pd^{II} , or Rh^{I}, or Ir^{I} have a coordination number of four are square planar
- other complexes in which the metal has a coordination number of four will be tetrahedral

a. $[Ru(bpy)(phen)(dppe)]^{2+}$
b. $[CoClF(PPh_3)(py)]^{-}$
c. $[Ni(en)_2(NO_2)_2]$

d. $[Fe(H_2O)_3(SCN)_3]$
e. $[PtClF(PPh_3)(py)]$
f. $[CoBr_2Cl(NH_3)_3]$

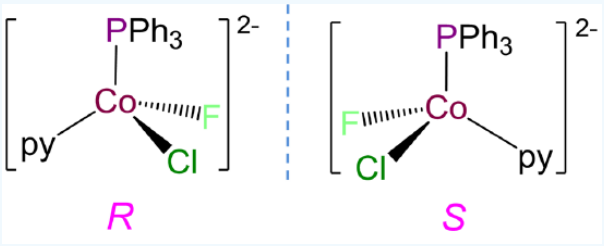
Answer a. $[Ru(bpy)(phen)(dppe)]^{2+}$

This complex is an octahedral tris-chelate containing symmetric ligands. As such it will exhibit **Λ** and **Δ** isomers:



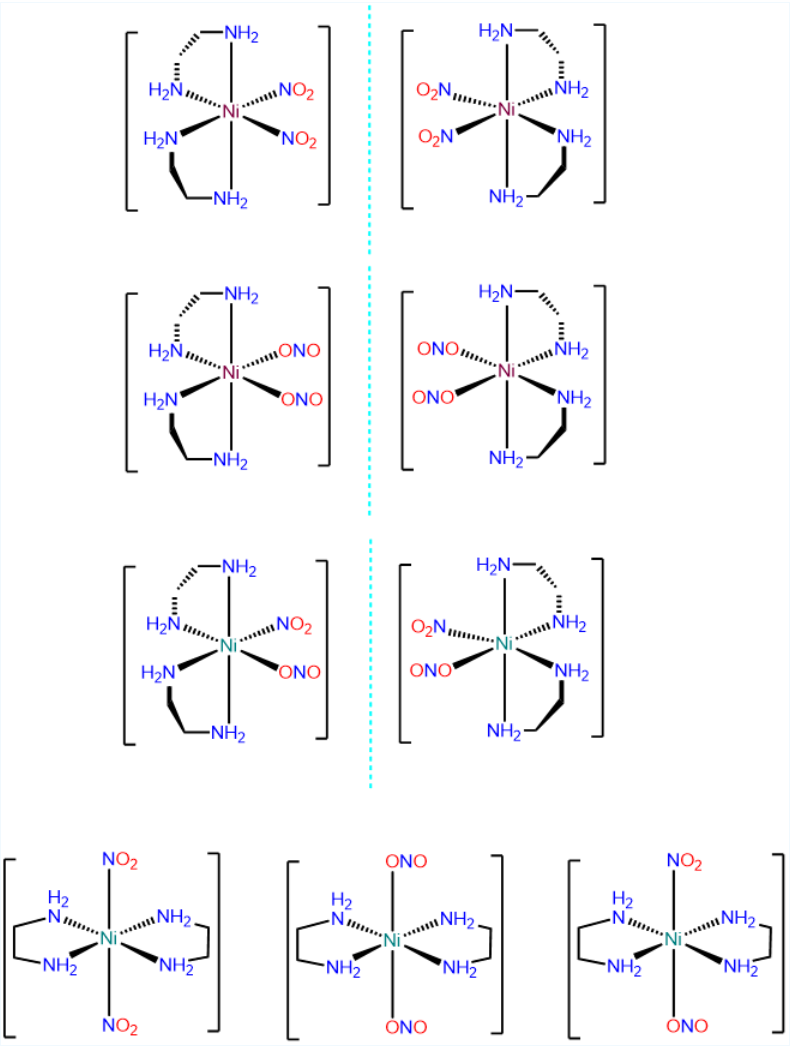
Answer b. $[CoClF(PPh_3)(py)]^-$

This complex has a coordination number of 4 and contains a Co^{2+} ion with a d^7 electron configuration, so a tetrahedral geometry is expected. Tetrahedral complexes like this one with four different ligands are chiral and can form *R* and *S* enantiomers.



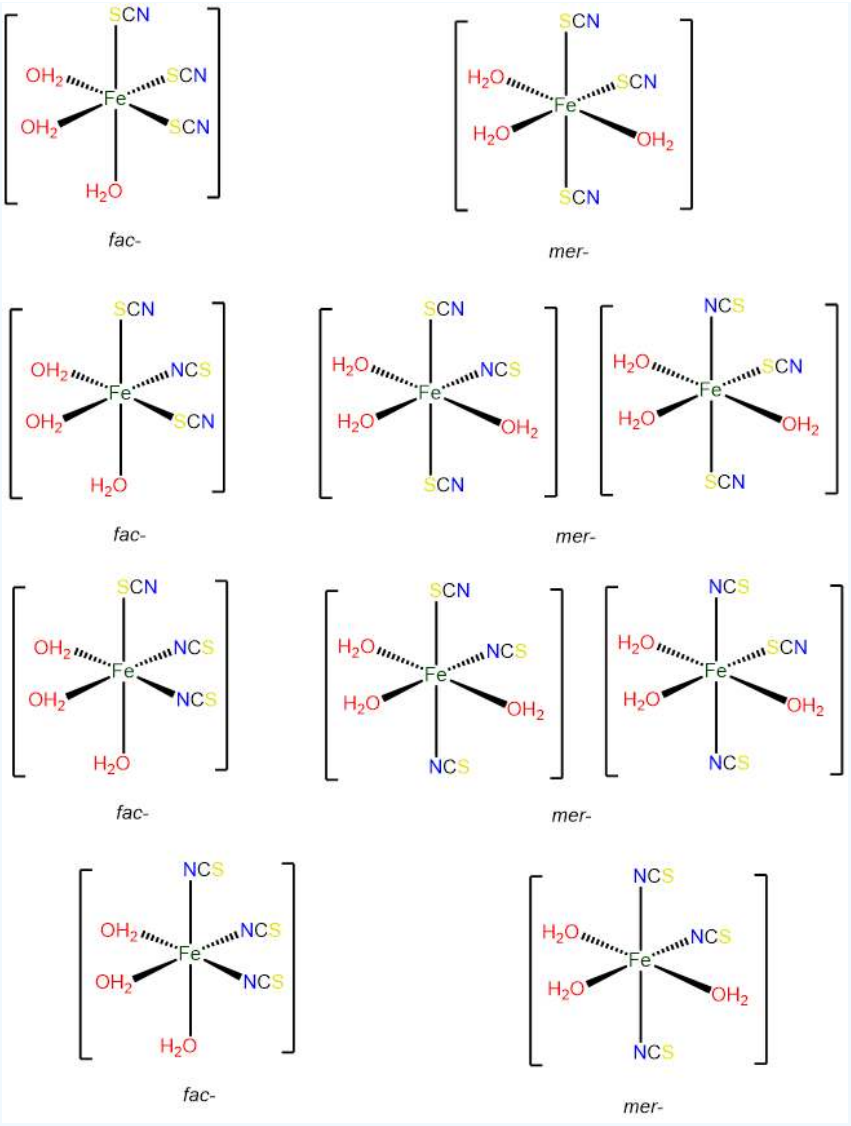
Answer c. $[Ni(en)_2(NO_2)_2]$

This is an octahedral bis-chelate and will exist in **Λ** and **Δ** configurations. Within each configuration the NO_2^- ligands can exist as ***κN*** and ***κO***, leading to the following possibilities:



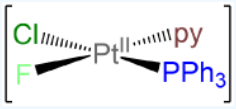
Answer d. $[Fe(H_2O)_3(SCN)_3]$

As an octahedral complex with three identical ligands it can exist in *mer* and *fac* configurations, with the ambidentate SCN ligand providing additional possibilities for isomerism.



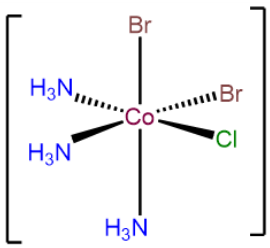
Answer e. [PtClF(PPh$_3$)(py)]

As a square planar complex with four nonidentical ligands, this complex exists as a single isomer.

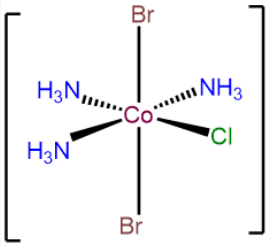


Answer f. [CoBr$_2$Cl(NH$_3$)$_3$]

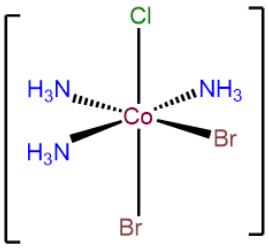
As an octahedral complex with three identical ligands it will exhibit *mer* and *fac* isomerism. In addition, it will have two *mer* configurations that differ in terms of the cis and trans relationships between the bromo and chloro ligands.



fac



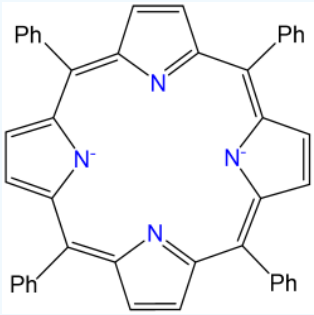
mer with Br *trans* to Br



mer with Cl *trans* to Br

Exercise 3.6.5.8

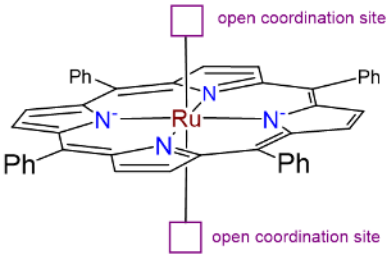
Complexes of formula $Ru(TPP)py_2$ have been prepared, in which TPP is tetraphenylporphyrin, which binds metals in the form given below. Draw all isomers of $Ru(TPP)py_2$.

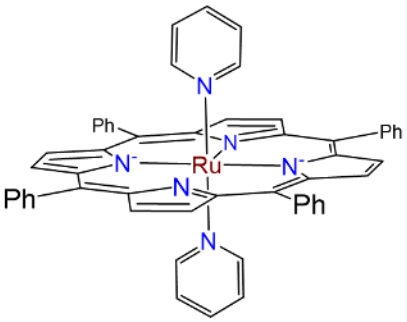


Answer

There is only one isomer. While normally complexes containing two identical ligands (in this case py) can exhibit *cis* and *trans* isomerism, in this case the planar tetraphenylporphyrin ring ligates the Ru^{2+} ion in a square planar arrangement, as shown at left in the image below. This leaves only a pair of *trans* coordination sites for the chloro ligands to occupy, giving the isomer shown at right below.

When TPP ligates Ru^{2+} it leaves only *trans* open coordination sites so only the *trans* isomer can form.

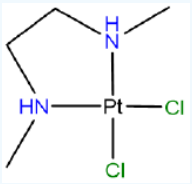




trans-[$Ru(py)_2(TPP)$]

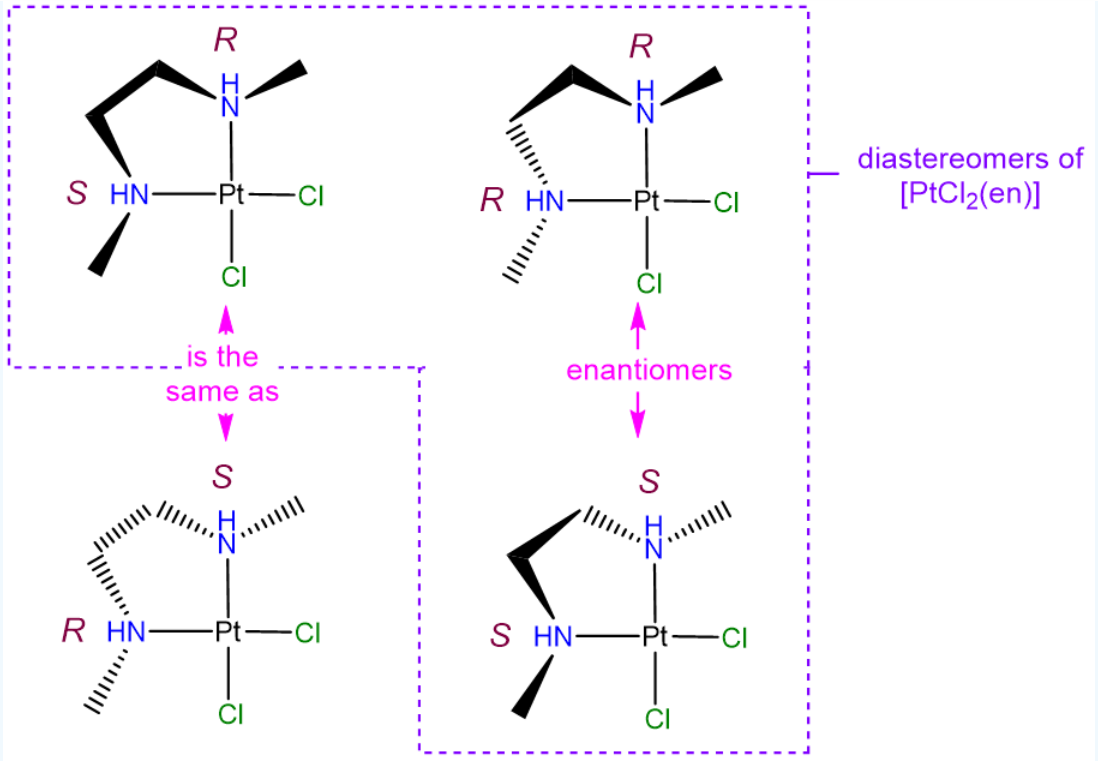
Exercise 3.6.5.9

Draw the diastereomers formed due to the chirality of the amine nitrogen atoms in [$PtCl_2$(*N*,*N*'-dimethylethane-1,2-diamine)] which has the atomic connectivity represented below



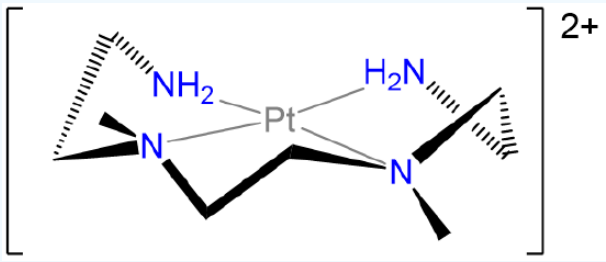
Answer

The diastereomers will differ in whether the N atoms adopt an *R* or *S* configuration at the nitrogen atoms. The possible permutations are (*R*,*R*), (S,*S*), (*R*,*S*), and (S,*R*). However, as may be seen from the image below, the (*R*,*S*) and (S,*R*) configurations are identical (the two projections shown can be interconverted through a C_2 rotation along an axis bisecting the Cl-Pt-Cl unit). As a result there are only three unique isomers. Of these, the (*R*,*R*) and (S,*S*) configurations are enantiomers (they are mirror images by reflection in the $PtCl_2N_2$ plane). Note that in solving problems like this one it can be helpful to keep track of possible isomers by assigning the stereochemistry at each chiral center as *R* or *S* using the Cahn-Ingold-Prelog-convention, though it is not strictly necessary to do so.

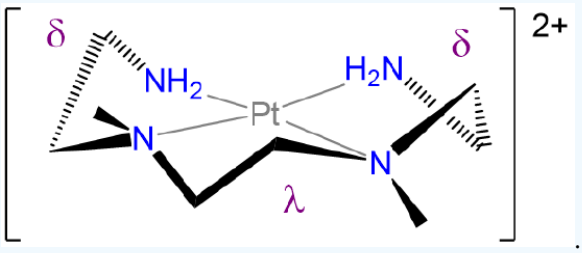


? Exercise 3.6.5.10

Label the conformations of all chelate rings in the structure below.



Answer



Appendix: The MABCDEF bookkeeping system for identifying isomers

The Mabcdef or MABCDEF system is one method for identifying the number of isomers in an octahedral complex, although since it is really just a bookkeeping and organizational system it can easily be extended to other geometries as well. The M in Mabcdef stands for metal and the other letters are used to stand in for ligands. The basic approach involves

- classifying the ligands as A, B, C, D, E, or F in order of multiplicity. Thus for

$[Cr(NH_3)_6]^{3+}$ A = NH_3; there are no B, C, D,E, or F ligands; and the complex is classified as MA_6

$[CoCl(NH_3)_5]^{2+}$ A = NH_3, B = Cl^-, and the complex is MA_5B

$[CrCl_2(H_2O)_2(NH_3)_2]^+$ A = Cl^-, B = H_2O, C = NH_3, and the complex is $MA_2B_2C_2$

- in the classification above, multidentate ligands are typically classified before monodentate ones and are designated AA, AB, ABC, ABA, etc. based on the symmetry of the attachment points. Thus

  en has identical attachment amine points and is AA

  gly has a carboxy and amine attachment points and is AB

  trien is ABA

  $CoCl_2(en)_2^+$ is $M(AA)_2B_2$

  $CoCl_2(gly)_2^-$ is $M(AB)_2C_2$

  $CoCl_2(en)(gly)$ is $M(AA)(AB)C_2$

- Systematically list out the possible *trans* arrangements of ligands by
  1. assigning one pair of ligands to be *trans* to one another.
  2. Then systematically list out the other possible *trans* pairs by permuting the remaining trans arrangements. It can help to organize the permutations in a table, such as that shown below for an MABCDEF complex where A and B are assigned *trans*. In looking at the table notice how the second set of trans permutations is systematically varied. This helps ensure that no possibility is skipped.
  3. Go through the list of isomers and remove any duplicates you generated so far. For instance, notice in the table below that the last three stereoisomers are identical with the first three (*e.g.*, stereoisomer 4 is identical to stereoisomer 3, 5 with 2, and 6 with 1).

Stereoisomer 1	Stereoisomer 2	Stereoisomer 3	Stereoisomer 4 (same as isomer 3)	Stereoisomer 5 (same as isomer 2)	Stereoisomer 6 (same as isomer 1)
trans AB (fixed)	*trans* AB (fixed)	*trans* AB (fixed)	*trans* AB (fixed)	*trans* AB (fixed)	*trans* AB (fixed)
trans CD	*trans* CE	*trans* CF	*trans* DE	*trans* DF	*trans* EF
trans EF	*trans* DF	*trans* DE	*trans* CF	*trans* CE	*trans* CD

  4. If the complex possesses multidentate ligands that demand that certain groups exist and *cis* pairs, then also remove any configurations which do not agree with the known binding capability of the ligand (*e.g.*, the two amine groups of ethylenediamine cannot be *trans* to one another, so if you have an en ligand, remove configurations like that from the list).

5. Next, swap or permute the original *trans* pair and repeat the process you just followed. In the case of Mabcdef this gives the following results:

Isomer	"fixed" trans pair	Additional trans pairs	
1	AB	CD	EF
2	AB	CE	DF
3	AB	CF	DE
4	AC	BD	EF
5	AC	BE	BF
6	AC	BF	DE
7	AD	BC	EF
8	AD	BE	CF
9	AD	BF	CE
10	AE	BC	DF
11	AE	BD	CF
12	AE	BF	CD
13	AF	BC	DE
14	AF	BD	CE
15	AF	BE	CD

- Since the procedure explained above only identifies isomers based on unique *trans* pairings, **it does not identify when a configuration is chiral and corresponds to a pair of enantiomers.** Any enantiomers can be identified by drawing out the complexes and either classifying their point groups or by drawing their mirror images and checking if they are superimposable. In the MABCDEF case - *i.e.*, where all the ligands are different - all of the isomers identified have C_1 symmetry so are chiral. This means there will be a pair of enantiomers for each, giving 15 x 2 = 30 different stereoisomers.

References

1. These examples are taken from http://wwwchem.uwimona.edu.jm/courses/inorgnom.html

2. Contakes S. M.; Rauchfuss, T.B. *Chem. Commun.* 2001, 553-554.

3. Shriver, D. F.; Shriver, S. A.; Anderson, S. E., *Inorg. Chem.* 1965, *4(5)*, 725-730.

4. Zelewsky, A. v., *Stereochemistry of Coordination Compounds* Wiley, 1996.

5. In the past it was difficult to determine absolute configurations from X-ray data alone, but recent advances have made it easier to do so.

6. Pavan M. V. Raja & Andrew R. Barron "Circular Dichroism Spectroscopy and its Application for Determination of Secondary Structure of Optically Active Species" in *Physical Methods in Chemistry and Nano Science* https://chem.libretexts.org/Bookshelves/Analytical_Chemistry/Book%3A_Physical_Methods_in_Chemistry_and_Nano_Science_(Barron)/07%3A_Molecular_and_Solid_State_Structure/7.07%3A_Circular_Dichroism_Spectroscopy_and_its_Application_for_Determination_of_Secondary_Structure_of_Optically_Active_Species

7. Berova, N.; Bari, L. D.; Pescitelli, G., *Chemical Society Reviews* 2007, 36 (6), 914-931.

8. Of course, if one set of ligands occupies a meridional plane, then the other three ligands will be oriented in an equatorial one. The reason they may both be considered meridional is because if the complex were rotated, the equatorial plane would be meridional and vice versa. From that point of view both might be considered meridional planes - albeit not at the same time.

9. Bite angles are taken from Mansell, S. M., Catalytic applications of small bite-angle diphosphorus ligands with single-atom linkers. Dalton Transactions 2017, 46 (44), 15157-15174.

10. Hancock, R. D., The pyridyl group in ligand design for selective metal ion complexation and sensing. Chemical Society Reviews 2013, 42 (4), 1500-1524.

11. Sasi, D.; Ramkumar, V.; Murthy, N. N., Bite-Angle-Regulated Coordination Geometries: Tetrahedral and Trigonal Bipyramidal in Ni(II) with Biphenyl-Appended (2-Pyridyl)alkylamine N,N'-Bidentate Ligands. ACS Omega 2017, 2 (6), 2474-2481.

12. Ehnbom, A.; Ghosh, S. K.; Lewis, K. G.; Gladysz, J. A., Octahedral Werner complexes with substituted ethylenediamine ligands: a stereochemical primer for a historic series of compounds now emerging as a modern family of catalysts. Chemical Society Reviews 2016, 45 (24), 6799-6811.

3.6.5: Isomerism is shared under a CC BY-NC-SA 4.0 license and was authored, remixed, and/or curated by LibreTexts.

- **9.4: Isomerism** by Stephen M. Contakes is licensed CC BY 4.0.

SECTION OVERVIEW

3.7: Coordination Chemistry- Bonding

With the exception of molecular orbital theory, the bonding models discussed in previous courses for main group complexes are not easily applied to transition metal complexes. This chapter describes bonding models that are used to explain the bonding and electronic structures of coordination complexes. As with many theories, the crystal field and ligand field theories discussed in this chapter were developed because existing bonding theories couldn't explain the observed properties of some transition metal complexes.

As an example let us consider the following two transition metal complexes, $[Fe(NH_3)_6]^{2+}$ and $[Co(NH_3)_6]^{3+}$. The Fe^{2+} and the Co^{3+} centers both have a valence electron configuration of $3d^6$ and have the same ligands coordinated. Lewis, VSEPR, and valence bond theories predict that two isoelectronic molecules should have very similar properties, but in the case of $[Fe(NH_3)_6]^{2+}$ and $[Co(NH_3)_6]^{3+}$ that is not true. The light absorption properties (and colors) of the two are quite different. The iron complex absorbs very little visible light and therefore appears a very pale yellow color and the cobalt complex strongly absorbs visible light and has a dark red-orange color. Also, the iron complex is paramagnetic (having unpaired electrons) and the cobalt complex is diamagnetic (having no unpaired electrons). Crystal field theory, and later ligand field theory were developed in part to explain the spectroscopic and magnetic properties of transition metal complexes.

Complex	**$[Fe(NH_3)_6]^{2+}$**	**$[Co(NH_3)_6]^{3+}$**
Valence electron configuration	[Ar] $3d^6$	[Ar] $3d^6$
Color	pale yellow	Red-orange
Magnetic properties	paramagnetic	diamagnetic

Learning Objectives

- Draw a crystal field diagram for a given metal complex and use to identify the number of unpaired electrons
- Identify whether a given metal complex will be high or low spin
- Calculate the crystal field stabilization energy for a given metal complex
- Use ligand field theory to explain the spectrochemical series

3.7.1: Crystal Field Theory

3.7.2: Crystal Field Stabilization Energy

3.7.3: Factors That Affect Crystal Field Splitting

3.7.4: Ligand Field Theory

3.7.5: Metal-Metal Bonds

3.7.5.1: Metal-Metal Multiple Bonds

3.7.6: Jahn-Teller Distortions

3.7: Coordination Chemistry- Bonding is shared under a CC BY-NC-SA 4.0 license and was authored, remixed, and/or curated by LibreTexts.

3.7.1: Crystal Field Theory

Crystal Field Theory

Crystal field theory (CFT) describes the breaking of orbital degeneracy in transition metal complexes due to the presence of ligands. CFT qualitatively describes the strength of the metal-ligand bonds. Based on the strength of the metal-ligand bonds, the energy of the system is altered. This may lead to a change in magnetic properties as well as color. This theory was developed by Hans Bethe and John Hasbrouck van Vleck in the late 1920's. Crystal field theory is a purely electrostatic theory and uses classical potential energy equations that take into account the attractive and repulsive interactions between charged particles (that is, Coulomb's Law interactions).

$$E \propto \frac{q_1 q_2}{r} \tag{3.7.1.1}$$

with

- E the bond energy between the charges and
- q_1 and q_2 are the charges of the interacting ions and
- r is the distance separating them.

For this simple approach to work, CFT makes some assumptions and simplifications. All ligands are modeled as negative point charges with no orbitals and the metal orbitals are modeled as clouds of negative charge. This approach leads to the correct prediction that large cations of low charge, such as K^+ and Na^+, should form few coordination compounds. For transition metal cations that contain varying numbers of d electrons in orbitals that are NOT spherically symmetric, however, the situation is quite different. The shape and occupation of these d-orbitals then becomes important in an accurate description of the bond energy and properties of the transition metal compound.

Orientation of *d*-Orbitals

To understand CFT, one must first understand the shape and orientation of the d orbitals:

- d_{xy}: lobes lie in-between the x and the y axes.
- d_{xz}: lobes lie in-between the x and the z axes.
- d_{yz}: lobes lie in-between the y and the z axes.
- $d_{x^2-y^2}$: lobes lie on the x and y axes.
- d_{z^2}: there are two lobes on the z axes and there is a donut shape ring that lies on the xy plane around the other two lobes.

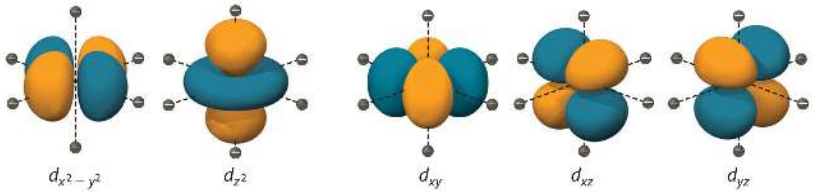


Figure **3.7.1.1**: Spatial arrangement of ligands in the an octahedral ligand field with respect to the five d-orbitals.

Octahedral Crystal Field

When examining a single transition metal ion in free space, the five d-orbitals have the same energy (Figure **3.7.1.2**). When ligands approach the metal ion, the ligand negative point charges destabilize the metal d-orbital based on the geometric structure of the molecule. Since ligands approach from different directions, not all d-orbitals interact equally. These interactions, however, create a splitting due to the electrostatic environment, orbitals with more interaction are higher in energy and orbitals with less interaction are lower in energy.

Definition: Barycenter

In crystal field theory the barycenter is the energy of the d orbitals in a spherical crystal field, where the negative lignad charges are evenly distributed around the metal ion in a sphere. The splitting of the d orbitals in other crystal fields will be symmetric around the barycenter (i.e. the total amount of stabalization will always be equal to the total amount of destabalization)

For example, consider a molecule with octahedral geometry. Ligands approach the metal ion along the x, y, and z axes. Therefore, the electrons in the d_{z^2} and $d_{x^2-y^2}$ orbitals (which lie along these axes) experience greater repulsion and are therefore at higher energy. Compared to a spherical field, where ligands are evenly distributed around the metal center, the d orbitals that lie between the axes (d_{xy}, d_{xz}, and d_{yz} experience less repulsion when the ligands are in an octahedral arrangement and are stabilized. This causes a splitting in the energy levels of the d-orbitals, known as crystal field splitting. For octahedral complexes, crystal field splitting is denoted by Δ_o (or Δ_{oct}) (in older texts and papers it may also be labeled as 10Dq). Any orbital that has a lobe on the axes moves to a higher energy level. The energies of the e_g symmetry orbitals (d_{z^2} and $d_{x^2-y^2}$) increase due to greater interactions with the ligands. The t_{2g} symmetry orbitals (d_{xy}, d_{xz}, and d_{yz}) decrease in energy with respect to the spherical energy level and become

more stable. This splitting is symmetric around the barycenter (the theoretical energy of the d orbitals with spherical charge distribution) which means that the energy levels of e_g are higher (by $0.6\Delta_o$) while t_{2g} are lower (by $0.4\Delta_o$). It should be noted that the labels t_{2g} and e_g come from group theory and the octahedral point group. The energy difference between the t_{2g} and e_g orbitals dictates the energy that the complex will absorb causing electrons to move from one level to the next. For transition metal complexes, the absorbed energy is typically in the visible part of the spectrum and thus this will determine the color of the complex. Whether the complex is paramagnetic or diamagnetic will be determined by the spin state. If there are unpaired electrons, the complex is paramagnetic; if all electrons are paired, the complex is diamagnetic.

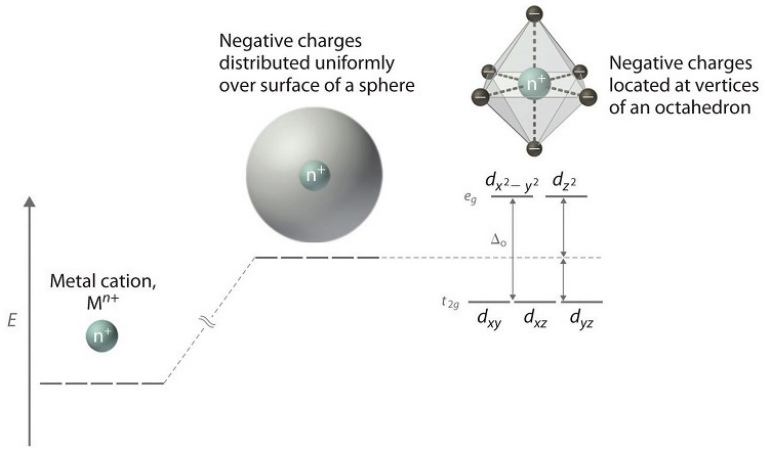


Figure **3.7.1.2**: (a) Distributing a charge of −6 uniformly over a spherical surface surrounding a metal ion causes the energy of all five d orbitals to increase due to electrostatic repulsions, but the five d orbitals remain degenerate. Placing a charge of −1 at each vertex of an octahedron causes the d orbitals to split into two groups with different energies: the $d_{x^2-y^2}$ and d_{z^2} orbitals increase in energy, while the, d_{xy}, d_{xz}, and d_{yz} orbitals decrease in energy. The average energy of the five d orbitals is the same as for a spherical distribution of a −6 charge, however. Attractive electrostatic interactions between the negatively charged ligands and the positively charged metal ion (far right) cause all five d orbitals to decrease in energy but does not affect the splittings of the orbitals. (b) The two e_g orbitals (left) point directly at the six negatively charged ligands, which increases their energy compared with a spherical distribution of negative charge. In contrast, the three t_{2g} orbitals (right) point between the negatively charged ligands, which decreases their energy compared with a spherical distribution of charge.

Filling Electrons in Orbitals

d^1 - d^3

For one, two, or three d electrons the filling is straightforward. According to the Aufbau principle, electrons are filled from lower to higher energy orbitals. In an octahedral crystal field, this corresponds to the d_{xy}, d_{xz}, and d_{yz}) orbitals. Following Hund's rule, electrons are filled in order to have the highest number of unpaired electrons. Therefore, each electron occupies one of the t_{2g} symmetry orbitals d_{xy}, d_{xz}, or d_{yz}) and all the electrons are orientated in the same direction to maximize spin multiplicity as shown in Figure **3.7.1.3**.

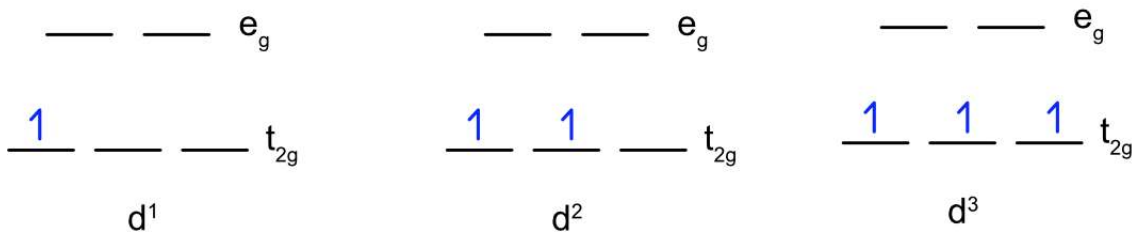


Figure **3.7.1.3**: Arrangement of the d electrons in a octahedral crystal field for 1, 2, and 3 d electrons. (CC-BY-NC-SA; Catherine McCusker)

d^4 - d^7

When a complex has between 4 and 7 d electrons there are two ways the electrons can be arranged into the d orbitals. As an example, in d^4 the first three electrons are placed one in each of the t_{2g} symmetry orbitals. The fourth electron can either be placed in one of the empty e_g symmetry orbitals or it can be paired in one or the t_{2g} symmetry orbitals, as shown in Figure **3.7.1.4**. The first configuration is called high spin because it maximizes the number of unpaired electrons and the second is called low spin. Whether a complex will have the high spin or low configuration depends on the relative magnitude of the spin pairing energy (the energy required to place two negatively charged electrons in the same orbital) and the crystal field splitting (Δ_o). In cases where the spin pairing energy is larger than Δ_o the complex will adopt the high spin configuration because it requires less energy to place an electron in a higher energy e_g orbital than is does to pair two electrons in the same t_{2g} orbital. In cases where Δ_o is larger than the spin pairing energy the complex will adopt a low spin configuration because it requires less energy to place a second electron in a t_{2g} orbital than it does to place one in the higher energy e_g orbitals.

Definition: Spin Pairing Energy

The spin pairing energy is the energy required to pair two electrons in an orbital. It is based on the Coulombic repulsion between the two negative charges. Larger, more diffuse orbitals will have lower spin pairing energy because the two electrons can be further apart

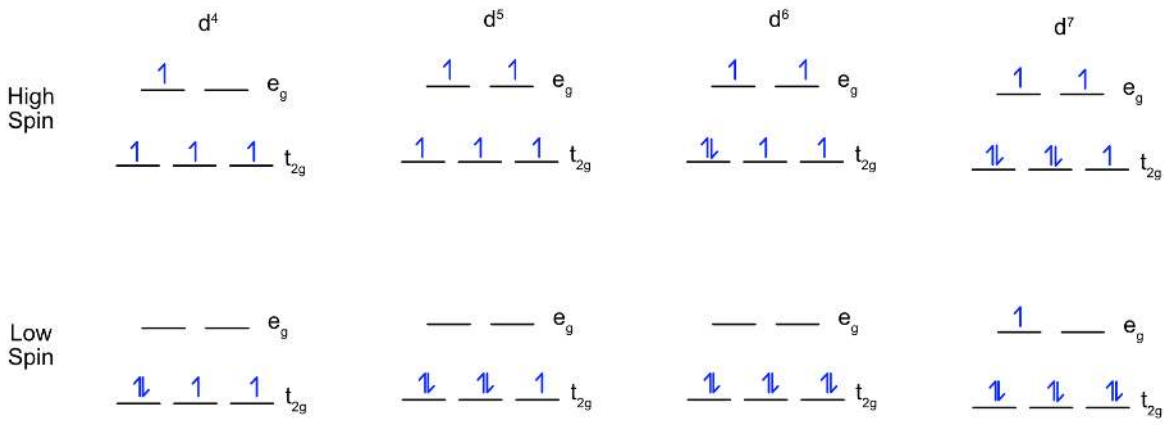


Figure 3.7.1.4: High spin and low spin arrangements of electrons for d^4 - d^7. (CC-BY-NC-SA; Catherine McCusker)

d^8 - d^{10}

For complexes with 8 - 10 d electrons there is again only one way to arrange the electrons. Whether or not the e_g orbitals are filled before electrons are paired in the t_{2g} orbitals the final electron configurations are as shown in Figure 3.7.1.5.

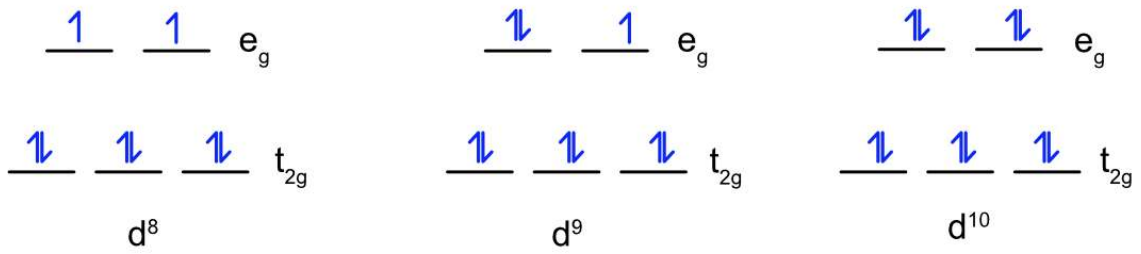


Figure 3.7.1.5: Arrangement of the d electrons in a octahedral crystal field for 8, 9, and 10 d electrons. (CC-BY-NC-SA; Catherine McCusker)

Tetrahedral Crystal Field

In a tetrahedral complex, the four ligands are orientated at opposite corners of a cube as shown in Figure 3.7.1.6*a* rather than along the axes. With the ligands between the axes, the three d orbitals which lie between the axes, d_{xy}, d_{xz}, and d_{yz} (t_2 symmetry in tetrahedral), now interact more with the ligands and are destabilized relative to the spherical crystal field. Conversely, the two d orbitals that lie along the axes, $d_{x^2-y^2}$ and d_{z^2} (e symmetry in tetrahedral), now interact less with the d orbitals and are stabilized relative to the spherical crystal field. As shown in Figure 3.7.1.6*b* the splitting of the d orbitals in a tetrahedral crystal field is essentially the inverse of the octahedral crystal field. The crystal field splitting energy in a tetrahedral crystal field is Δ_t. Because a tetrahedral complex has fewer ligands than an octahedral complex, and those ligands are not ideally orientated to overlap with the d orbitals Δ_t is less than Δ_o for the same metal and ligands:

$$\Delta_t \approx \frac{4}{9}\Delta_o \tag{3.7.1.2}$$

Consequentially, Δ_t is typically smaller than the spin pairing energy, so tetrahedral complexes are usually high spin. As seen with octahedral compounds, the labels for the groups of orbitals, t_2 and e in this case, come from group theory and the tetrahedral point group.

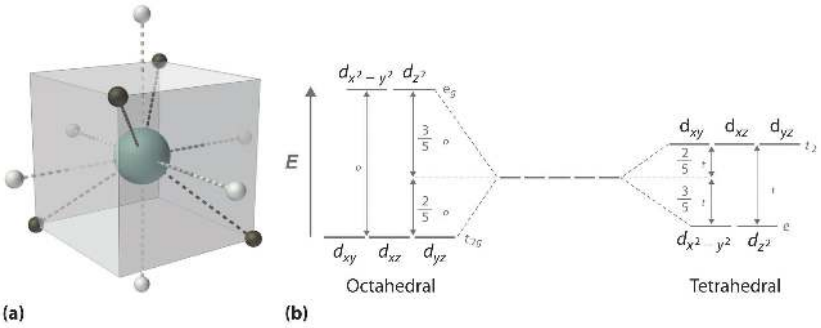


Figure **3.7.1.6**: (a) Tetrahedral ligand field surrounding a central transition metal (teal sphere). (b) Splitting of the degenerate d-orbitals (without a ligand field) due to an octahedral ligand field (left diagram) and the tetrahedral field (right diagram).

Square Planar Crystal Field

In a complex with four ligands, the other possible arrangement of ligands is square planar. The easiest way to visualize the square planar geometry is to start with an octahedral complex and remove the two ligands that are along the z axis. The four remaining ligands are in the xy plane, along the x and y axes. From a crystal field splitting perspective, when the z ligands are removed the d orbitals split further. In an octahedral crystal field both $d_{x^2-y^2}$ and d_{z^2} are destabilized. When the z ligands are removed the d_{z^2} orbital is stabilized because it no longer interacts with ligands on the z axis. Conversely the $d_{x^2-y^2}$ orbital is further destabilized because all of the ligand negative charges are concentrated in the xy plane. Removing the z ligand has a similar effect on the d_{xy}, d_{xz}, and d_{yz} orbitals, although the magnitude of the stabilization and destabilization is less because those orbitals do not directly interact with the ligands. The d_{xy} orbital is destabilized because it also lies in the xy plane and the d_{xz} and d_{yz} orbitals are stabilized because they have lost the (indirect) interaction with the ligands on the z axis. Overall the $d_{x^2-y^2}$ orbital is significantly more destabilized than the other d orbitals, meaning the square planar geometry is most favored in complexes with 8 electrons where the $d_{x^2-y^2}$ is empty and the other more stabilized d orbitals are filled.

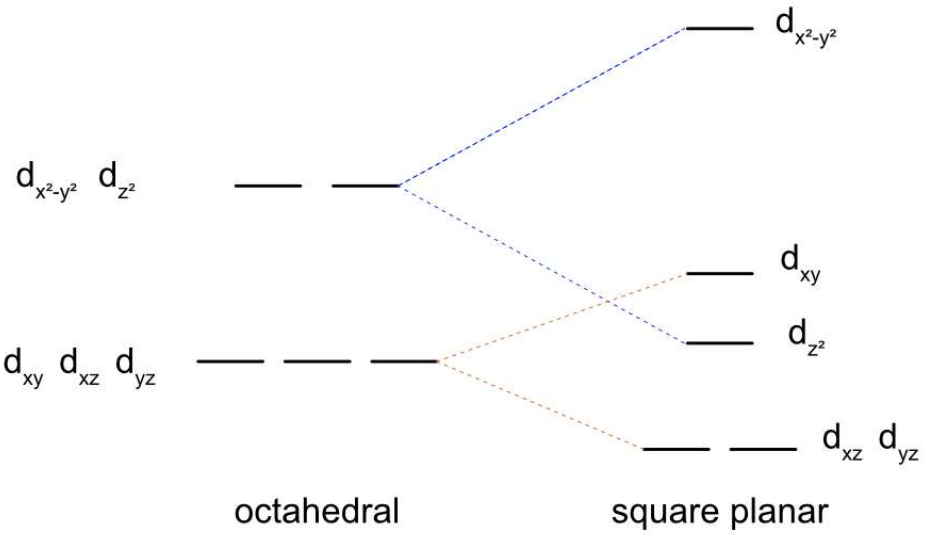
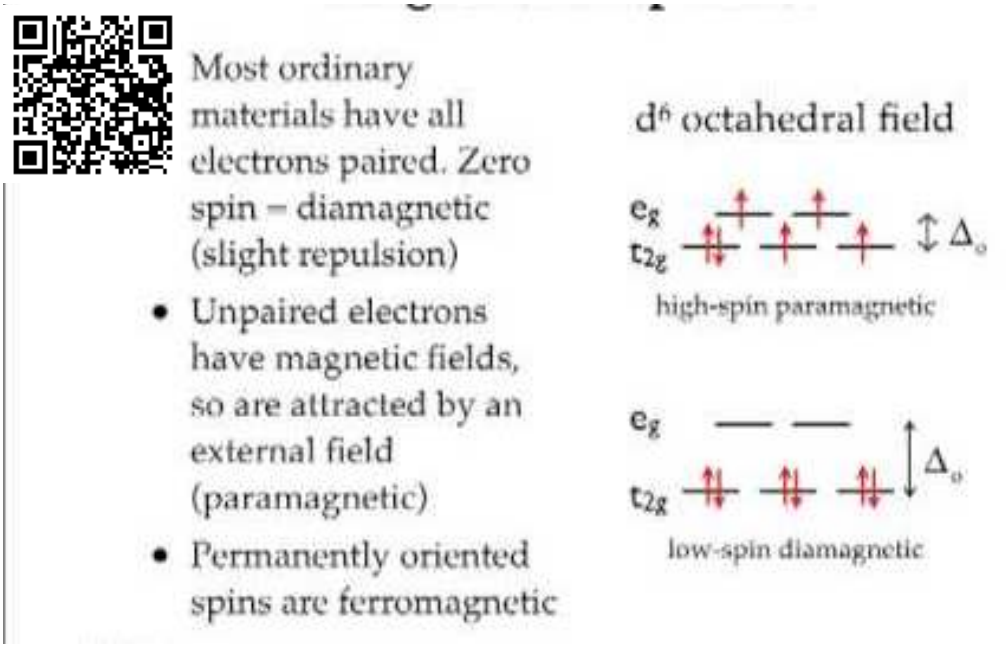


Figure **3.7.1.7**: Comparison between octahedral and square planar crystal field splittings, showing how the energies of the d orbitals change when the two z ligands are removed from an octahedral complex to form a square planar complex. (CC-BY-NC-SA; Catherine McCusker)

Video:



Tetrahedral vs Square Planar

From VSEPR theory we know that sterically the most favorable way to arrange four ligands around a metal ion is in the tetrahedral arrangement. That puts the most possible space between the four ligands. Because of this, a four coordinate metal complex will prefer a tetrahedral geometry UNLESS there is a larger crystal field stabilization energy (CFSE) for the square planar arrangement. As discussed above, this means square planar is the preferred geometry for most metal complexes with 8 d electrons, especially when the crystal field splitting (Δ) is large. While not every d^8 complex is square planar, almost all square planar complexes are d^8 (there are examples of d^7 and d^9 square planar complexes but they are less common)

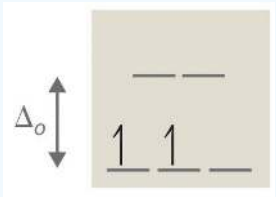
Exercise 3.7.1.3

For each of the following, sketch the d-orbital splitting diagram, fill the diagram with the correct number of d-electrons, list the number of unpaired electrons, and label whether they are paramagnetic or diamagnetic:

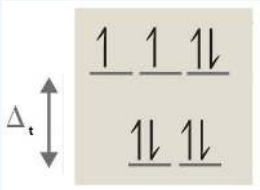
1. $[Ti(H_2O)_6]^{2+}$
2. $[NiCl_4]^{2-}$ (tetrahedral)
3. $[CoF_6]^{3-}$ (high spin)
4. $[Co(NH_3)_6]^{3+}$ (low spin)

Answer

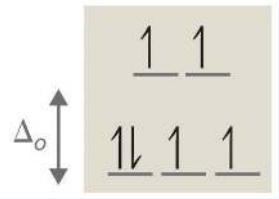
1. 2 unpaired electrons, paramagnetic



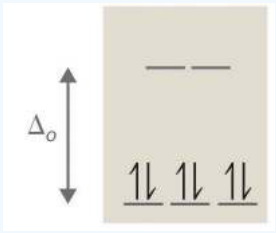
2. 2 unpaired electrons, paramagnetic



3. 4 unpaired electrons, paramagnetic



4. 0 unpaired electrons, diamagnetic



Contributors and Attributions

- Asadullah Awan (UCD), Hong Truong (UCD)
- Prof. Robert J. Lancashire (The Department of Chemistry, University of the West Indies)
- Modified by Catherine McCusker (East Tennessee State University)

3.7.1: Crystal Field Theory is shared under a CC BY-NC-SA 4.0 license and was authored, remixed, and/or curated by LibreTexts.

- **9.1: Crystal Field Theory** is licensed CC BY-NC-SA 4.0.

3.7.2: Crystal Field Stabilization Energy

Crystal Field Stabilization Energy

A consequence of crystal field theory is that the distribution of electrons in the d orbitals may lead to net stabilization (decrease in energy) of some complexes depending on the specific ligand geometry and metal d-electron configurations. It is a simple matter to calculate this stabilization since all that is needed is the electron configuration and knowledge of the splitting patterns.

Definition: Crystal Field Stabilization Energy (CFSE)

The crystal field stabilization energy is defined as the energy of the electron configuration in the crystal field minus the energy of the electronic configuration in the spherical field.

$$CFSE = \Delta E = E_{\text{crystal field}} - E_{\text{spherical field}} \tag{3.7.2.1}$$

The CSFE will depend on multiple factors including:

- Geometry (crystal field splitting pattern)
- Number of d-electrons
- Spin Pairing Energy (the contribution of spin pairing energy is often negligible in comparison to other contributions and is omitted at times)

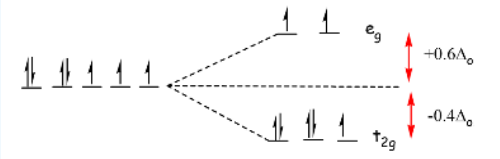
For an octahedral complex, each of the more stable t_{2g} orbitals are stabilized by $-0.4\Delta_o$ relative to spherical field whereas the higher energy e_g orbitals are destabilized by $+0.6\Delta_o$. For a complex the stabilization or destabilization of each electron is summed. Any electrons that are paired within a single orbital, also contribute spin pairing energy (+P). The overall CFSE for a complex is expressed as a multiple of the crystal field splitting parameter Δ_o.

Example 3.7.2.1: CFSE for a high Spin d^7 complex

What is the CFSE for a high spin d^7 octahedral complex?

Solution

The splitting pattern and electron configuration for both spherical and octahedral ligand fields are compared below.



The energy of the spherical field ($E_{\text{spherical field}}$) is

$$E_{\text{spherical field}} = 7 \times 0 + 2P = 2P$$

The energy of the octahedral crystal field $E_{\text{oct field}}$ is

$$E_{\text{oct field}} = (5 \times -0.4\Delta_o) + (2 \times 0.6\Delta_o) + 2P = -0.8\Delta_o + 2P$$

So via Equation 3.7.2.1, the CFSE is

$$\begin{aligned} CFSE &= E_{\text{oct field}} - E_{\text{spherical field}} \\ &= (-0.8\Delta_o + 2P) - 2P \\ &= -0.8\Delta_o \end{aligned}$$

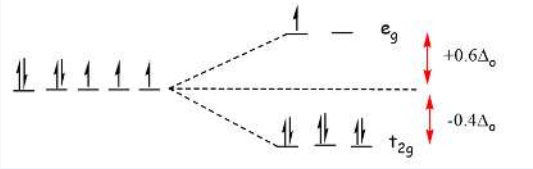
Notice that the spin pairing energy cancels out in this case (and will when calculating the CFSE of high spin complexes) since the number of paired electrons in the octahedral field is the same as that in spherical field of the free metal ion.

Exercise 3.7.2.1

What is the CFSE for a low spin d^7 octahedral complex?

Answer

The splitting pattern and electron configuration for both spherical and octahedral ligand fields are compared below.



The energy of the spherical field is the same as calculated for the high spin configuration in Example 1:

$$E_{\text{spherical}} = 7 \times 0 + 2P = 2P$$

The energy of the octahedral ligand\) field $E_{\text{oct field}}$ is

$$\begin{aligned} E_{\text{oct field}} &= (6 \times -0.4\Delta_o) + (1 \times 0.6\Delta_o) + 3P \\ &= -1.8\Delta_o + 3P \end{aligned}$$

So via Equation 3.7.2.1, the CFSE is

$$\begin{aligned} CFSE &= E_{\text{oct field}} - E_{\text{spherical field}} \\ &= (-9/5\Delta_o + 3P) - 2P \\ &= -9/5\Delta_o + P \end{aligned}$$

This appears more a more stable configuration than the high spin d^7 configuration in Example **3.7.2.1**, but we have then to take into consideration the pairing energy P to know definitely, which varies between $200 - 400\ kJ\ mol^{-1}$ depending on the metal.

Table 3.7.2.1: Crystal field stabilization energies (CFSE) for high and low spin octahedral complexes

Total d-electrons	Spherical Field	Octahedral Field				Crystal Field Stabilization Energy	
		High Spin		Low Spin			
	$E_{\text{spherical field}}$	Configuration	$E_{\text{crystal field}}$	Configuration	$E_{\text{crystal field}}$	High Spin	Low Spin
d^0	0	$t_{2g}^0\ e_g^0$	0	$t_{2g}^0 e_g^0$	0	0	0
d^1	0	$t_{2g}^1\ e_g^0$	-2/5 Δ_o	$t_{2g}^1 e_g^0$	-2/5 Δ_o	-2/5 Δ_o	-2/5 Δ_o
d^2	0	$t_{2g}^2\ e_g^0$	-4/5 Δ_o	$t_{2g}^2 e_g^0$	-4/5 Δ_o	-4/5 Δ_o	-4/5 Δ_o
d^3	0	$t_{2g}^3\ e_g^0$	-6/5 Δ_o	$t_{2g}^3 e_g^0$	-6/5 Δ_o	-6/5 Δ_o	-6/5 Δ_o
d^4	0	$t_{2g}^3\ e_g^1$	-3/5 Δ_o	$t_{2g}^4 e_g^0$	-8/5 Δ_o + P	-3/5 Δ_o	-8/5 Δ_o + P
d^5	0	$t_{2g}^3\ e_g^2$	0 Δ_o	$t_{2g}^5 e_g^0$	-10/5 Δ_o + 2P	0 Δ_o	-10/5 Δ_o + 2P
d^6	P	$t_{2g}^4\ e_g^2$	-2/5 Δ_o + P	$t_{2g}^6 e_g^0$	-12/5 Δ_o + 3P	-2/5 Δ_o	-12/5 Δ_o + P
d^7	2P	$t_{2g}^5\ e_g^2$	-4/5 Δ_o + 2P	$t_{2g}^6 e_g^1$	-9/5 Δ_o + 3P	-4/5 Δ_o	-9/5 Δ_o + P
d^8	3P	$t_{2g}^6\ e_g^2$	-6/5 Δ_o + 3P	$t_{2g}^6 e_g^2$	-6/5 Δ_o + 3P	-6/5 Δ_o	-6/5 Δ_o
d^9	4P	$t_{2g}^6\ e_g^3$	-3/5 Δ_o + 4P	$t_{2g}^6 e_g^3$	-3/5 Δ_o + 4P	-3/5 Δ_o	-3/5 Δ_o
d^{10}	5P	$t_{2g}^6\ e_g^4$	0 Δ_o + 5P	$t_{2g}^6 e_g^4$	0 Δ_o + 5P	0	0

P is the spin pairing energy and represents the energy required to pair up electrons within the same orbital. For a given metal ion P (pairing energy) is constant, but it does not vary with ligand and oxidation state of the metal ion).

Octahedral Preference

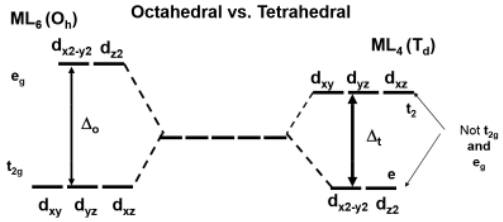
Similar CFSE values can be constructed for non-octahedral ligand field geometries once the knowledge of the d-orbital splitting is known and the electron configuration within those orbitals known, e.g., the tetrahedral complexes in Table **3.7.2.2**. These energies geoemtries can then be contrasted to the octahedral CFSE to calculate a thermodynamic preference for a metal-ligand combination to favor the octahedral geometry. This is quantified via an octahedral site preference energy defined below.

Definition: Octahedral Site Preference Energies (OSPE)

The octahedral site preference energy (OSPE) is defined as the difference of CFSE energies for a non-octahedral complex and the octahedral complex. For comparing the preference of forming an octahedral ligand field vs. a tetrahedral ligand field, the OSPE is thus:

$$OSPE = CFSE_{(oct)} - CFSE_{(tet)} \tag{3.7.2.2}$$

The OSPE quantifies the preference of a complex to exhibit an octahedral geometry vs. another geometry. The OSPE for octahedral vs tetrahedral geometries is illustrated below.



Note: the conversion between Δ_o and Δ_t used for these calculations is:

$$\Delta_t \approx \frac{4}{9}\Delta_o \tag{3.7.2.3}$$

which is applicable for comparing octahedral and tetrahedral complexes that involve same ligands only.

Table **3.7.2.2**: Octahedral Site Preference Energies (OSPE)

Total d-electrons	CFSE(Octahedral)	CFSE(Tetrahedral)	OSPE (for high spin complexes)**

Total d-electrons	CFSE(Octahedral)		CFSE(Tetrahedral)		OSPE (for high spin complexes)**
	High Spin	Low Spin	Configuration	**Always High Spin***	
d^0	0 Δ_o	0 Δ_o	e^0	0 Δ_t	0 Δ_o
d^1	-2/5 Δ_o	-2/5 Δ_o	e^1	-3/5 Δ_t	-6/45 Δ_o
d^2	-4/5 Δ_o	-4/5 Δ_o	e^2	-6/5 Δ_t	-12/45 Δ_o
d^3	-6/5 Δ_o	-6/5 Δ_o	$e^2t_2^1$	-4/5 Δ_t	-38/45 Δ_o
d^4	-3/5 Δ_o	-8/5 Δ_o + P	$e^2t_2^2$	-2/5 Δ_t	-19/45 Δ_o
d^5	0 Δ_o	-10/5 Δ_o + 2P	$e^2t_2^3$	0 Δ_t	0 Δ_o
d^6	-2/5 Δ_o	-12/5 Δ_o + P	$e^3t_2^3$	-3/5 Δ_t	-6/45 Δ_o
d^7	-4/5 Δ_o	-9/5 Δ_o + P	$e^4t_2^3$	-6/5 Δ_t	-12/45 Δ_o
d^8	-6/5 Δ_o	-6/5 Δ_o	$e^4t_2^4$	-4/5 Δ_t	-38/45 Δ_o
d^9	-3/5 Δ_o	-3/5 Δ_o	$e^4t_2^5$	-2/5 Δ_t	-19/45 Δ_o
d^{10}	0	0	$e^4t_2^6$	0 Δ_t	0 Δ_o

P is the spin pairing energy and represents the energy required to pair up electrons within the same orbital.

Note

Tetrahedral complexes are always high spin since the splitting is appreciably smaller than ***P*** (Equation 3.7.2.3).

After conversion with Equation 3.7.2.3. The data in Tables **3.7.2.1** and **3.7.2.2** are represented graphically by the curves in Figure **3.7.2.1** below for the high spin complexes only. The low spin complexes require knowledge of ***P*** to graph, which will vary depending on the identiy of the metal ion.

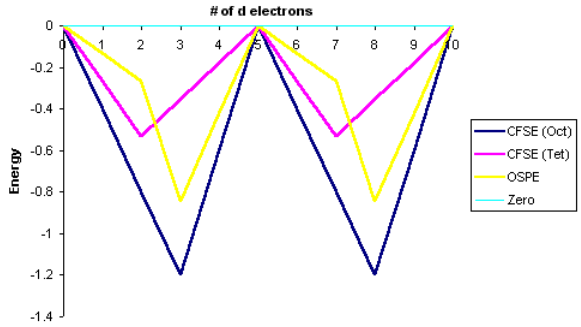


Figure **3.7.2.1**: Crystal Field Stabilization Energies for both high spin octahedral fields ($CFSE_{oct}$) and tetrahedral fields ($CFSE_{tet}$). Octahedral Site Preference Energies (OSPE) are in yellow. This is for high spin complexes only.

From a simple inspection of Figure **3.7.2.1**, the following observations can be made:

- The OSPE is *small* in d^1, d^2, d^5, d^6, d^7 high spin complexes and other factors influence the stability of the complexes including steric factors
- The OSPE is *large* in d^3 and d^8 high spin complexes which strongly favor octahedral geometries

Applications

The "double-humped" curve in Figure **3.7.2.1** is found for various properties of the first-row transition metals, including hydration and lattice energies of the M(II) ions, ionic radii as well as the stability of M(II) complexes. This suggests that these properties are somehow related to crystal field effects.

In the case of hydration energies describing the complexation of water ligands to a bare metal ion:

$$M^{2+}(g) + H_2O \rightarrow [M(OH_2)_6]^{2+}(aq) \qquad (3.7.2.4)$$

Table **3.7.2.3** and Figure **3.7.2.2** shows this type of curve. Note that in any series of this type not all the data are available since a number of ions are not very stable in the M(II) state in water.

Table **3.7.2.3**: Hydration energies of M^{2+} ions

M	ΔH°/kJmol^{-1}	M	ΔH°/kJmol^{-1}
Ca	-2469	Fe	-2840
Sc	no stable 2+ ion	Co	-2910
Ti	-2729	Ni	-2993
V	-2777	Cu	-2996
Cr	-2792	Zn	-2928
Mn	-2733		

Graphically the data in Table 2 can be represented by:

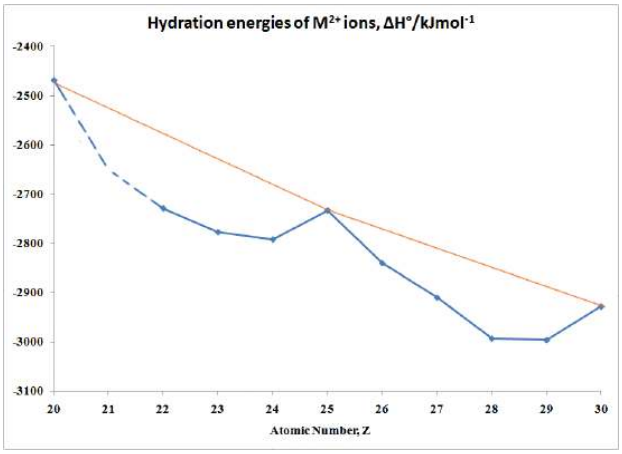


Figure **3.7.2.2**: Hydration energies of M^{2+} ions

Contributors and Attributions

- Prof. Robert J. Lancashire (The Department of Chemistry, University of the West Indies)

3.7.2: Crystal Field Stabilization Energy is shared under a CC BY-NC-SA 4.0 license and was authored, remixed, and/or curated by LibreTexts.

- **9.2: Crystal Field Stabilization Energy** is licensed CC BY-NC-SA 4.0.

3.7.3: Factors That Affect Crystal Field Splitting

Magnitude of Crystal Field Splitting

The magnitude of the crystal field splitting (Δ) dictates whether a complex with four, five, six, or seven d electrons (in an octahedral complex) is high spin or low spin, which affects its magnetic properties, structure, and reactivity. Large values of Δ (i.e., Δ > P) yield a low-spin complex, whereas small values of Δ (i.e., Δ < P) produce a high-spin complex. The magnitude of Δ depends on four factors: the valence of the metal, the principal quantum number of the metal (and thus its location in the periodic table), the geometry, and the nature of the ligand(s). Values of Δ for some representative transition metal complexes are given in Table **3.7.3.1**.

Table **3.7.3.1**: Crystal Field Splitting Energies for Some Octahedral (Δ_o)* and Tetrahedral (Δ_t) Transition-Metal Complexes

Octahedral Complexes	Δ_o (cm^{-1})	Octahedral Complexes	Δ_o (cm^{-1})	Tetrahedral Complexes	Δ_t (cm^{-1})
$[Ti(H_2O)_6]^{3+}$	20,300	$[Fe(CN)_6]^{4-}$	32,800	VCl_4	9010
$[V(H_2O)_6]^{2+}$	12,600	$[Fe(CN)_6]^{3-}$	35,000	$[CoCl_4]^{2-}$	3300
$[V(H_2O)_6]^{3+}$	18,900	$[CoF_6]^{3-}$	13,000	$[CoBr_4]^{2-}$	2900
$[CrCl_6]^{3-}$	13,000	$[Co(H_2O)_6]^{2+}$	9300	$[CoI_4]^{2-}$	2700
$[Cr(H_2O)_6]^{2+}$	13,900	$[Co(H_2O)_6]^{3+}$	27,000		
$[Cr(H_2O)_6]^{3+}$	17,400	$[Co(NH_3)_6]^{3+}$	22,900		
$[Cr(NH_3)_6]^{3+}$	21,500	$[Co(CN)_6]^{3-}$	34,800		
$[Cr(CN)_6]^{3-}$	26,600	$[Ni(H_2O)_6]^{2+}$	8500		
$Cr(CO)_6$	34,150	$[Ni(NH_3)_6]^{2+}$	10,800		
$[MnCl_6]^{4-}$	7500	$[RhCl_6]^{3-}$	20,400		
$[Mn(H_2O)_6]^{2+}$	8500	$[Rh(H_2O)_6]^{3+}$	27,000		
$[MnCl_6]^{3-}$	20,000	$[Rh(NH_3)_6]^{3+}$	34,000		
$[Mn(H_2O)_6]^{3+}$	21,000	$[Rh(CN)_6]^{3-}$	45,500		
$[Fe(H_2O)_6]^{2+}$	10,400	$[IrCl_6]^{3-}$	25,000		
$[Fe(H_2O)_6]^{3+}$	14,300	$[Ir(NH_3)_6]^{3+}$	41,000		

*Energies obtained by spectroscopic measurements are often given in units of wave numbers (cm^{-1}); the wave number is the reciprocal of the wavelength of the corresponding electromagnetic radiation expressed in centimeters: 1 cm^{-1} = 11.96 J/mol.

Source of data: Duward F. Shriver, Peter W. Atkins, and Cooper H. Langford, Inorganic Chemistry, 2nd ed. (New York: W. H. Freeman and Company, 1994).

Valence of the metal

Increasing the valence of a metal ion has two effects: the radius of the metal decreases and ligands are more strongly attracted to it due to Coulombic attraction. Both factors decrease the metal–ligand distance, which in turn causes the ligands to interact more strongly with the d-orbitals. Consequently, the magnitude of Δ_o increases as the valence of the metal increases. Typically, Δ_o for a M(III) is about 50% greater than for the M(II) of the same metal; for example, for $[V(H_2O)_6]^{2+}$, Δ_o = 11,800 cm^{-1}; for $[V(H_2O)_6]^{3+}$, Δ_o = 17,850 cm^{-1}.

Principal quantum number of the metal

For a series of complexes of metals from the same group in the periodic table with the same charge and the same ligands, the magnitude of Δ_o increases with increasing principal quantum number: Δ (3d) < Δ (4d) < Δ (5d). The data for hexaammine complexes of the trivalent Group 9 metals illustrate this point:

$$[Co(NH_3)_6]^{3+}: \Delta_o = 22{,}900\ cm^{-1}$$

$$[Rh(NH_3)_6]^{3+}: \Delta_o = 34{,}100\ cm^{-1}$$

$$[Ir(NH_3)_6]^{3+}: \Delta_o = 40{,}000\ cm^{-1}$$

The increase in Δ with increasing principal quantum number is due to the larger radial extension of the d orbitals as n increases. In addition, repulsive ligand–ligand interactions are most important for smaller metal ions. Relatively speaking, this results in shorter M–L distances and stronger d orbital–ligand interactions. The increase in Δ going from 3d to 4d and 5d is so large that all 4d and 5d metals will form low spin complexes.

Geometry of the complex

The number of ligands in a complex as well as how well the ligand geometry overlaps with the d orbitals is also a factor in the magnitude of the crystal field splitting. For example, comparing octahedral and tetrahedral geometries the octahedral geometry has 6 ligands, and those 6 ligands overlap directly with the two d orbitals that lie along the axes, $d_{x^2-y^2}$ and d_{z^2}. The tetrahedral geometry has fewer ligands than octahedral, and those ligands overlap less ideally with the ligands that lie between the axes, d_{xy}, d_{xz}, and d_{yz}. Because of this the crystal field splitting of a tetrahedral complex is generally less than half ($\frac{4}{9}$ than an octahedral complex with the same metal and ligands. For example $[FeCl_4]^-$ has a $\Delta_t = 5{,}200\ cm^{-1}$ and $[FeCl_6]^{3-}$ has a $\Delta_o = 11{,}600\ cm^{-1}$.

Nature of the ligands

In crystal field theory ligands are all modeled as negative point charges, which means that all ligands should behave identically. Experimentally, it is found that the Δ_o observed for a series of complexes of the same metal ion depends strongly on the nature of the ligands. For a series of chemically similar ligands, the magnitude of Δ_o decreases as the size of the donor atom increases. For example, Δ_o values for halide complexes generally decrease in the order F > Cl > Br > I because smaller, more localized charges, such as we see for F, interact more strongly with the d-orbitals of the metal. In addition, a small neutral ligand with a highly localized lone pair, such as NH_3, results in significantly larger Δ_o values than might be expected. Because the lone pair points directly at the metal ion, the electron density along the M–L axis is greater than for a spherical anion such as F. The experimentally observed order of the crystal field splitting energies produced by different ligands is called the spectrochemical series.

Ligands are classified as strong field or weak field based on the spectrochemical series:

weak field $I^- < Br^- < Cl^- < \underline{S}CN^- < F^- < OH^- < ox^{-2} < \underline{O}NO < H_2O < SC\underline{N}^- < NH_3 <$ en $< \underline{N}O_2 < CN^-$, CO strong field

Note that SCN and NO_2 ligands are represented twice in the above spectrochemical series since there are two different Lewis base sites (e.g., free electron pairs to share) on each ligand (e.g., for the SCN ligand, the electron pair on the sulfur or the nitrogen can form the bond to a metal). The specific atom that binds in such ligands is underlined. Ligands on the weak field end of the series (halogens, OH, H_2O) will tend to form high spin complexes and ligands on the strong field end of the series (CN, CO, NO_2) will tend to form low spin complexes. Intermediate ligands in the midle of the series could form high or low spin complexes depending on other factors.

How to determine if a complex is high or low spin

1. How many d electrons does the complex have?
   - Only complexes with 4-7 d electrons have high spin and low spin configurations
2. What period is the metal?
   - 3d metals could either be high or low spin
   - 4d and 5d metals will ALWAYS be low spin
3. What is the geometry of the complex?
   - Tetrahedral complexes with 3d metals will almost always be high spin because Δt is generally less than spin pairing energy

- Square planar complexes will almost always be low spin because they are favored over tetrahedral when crystal field splitting is large
- Octahedral complexes could be either high or low spin

4. What are the ligands?
   - Strong field ligands will form low spin complexes
   - Weak field ligands will form high spin complexes
   - Intermediate field ligands could form high or low spin complexes. Additional information (like number of unpaired electrons) is needed

- Adapted by Catherine McCusker (East Tennessee State University)

3.7.3: Factors That Affect Crystal Field Splitting is shared under a CC BY-NC-SA 4.0 license and was authored, remixed, and/or curated by LibreTexts.

- **9.4: Factors That Affect Crystal Field Splitting** is licensed CC BY-NC-SA 4.0.

3.7.4: Ligand Field Theory

Extension of Crystal Field Theory

Experimentally it is known that the nature of the ligand plays an important role in the magnitude of the crystal field splitting in metal complexes and can determine whether a complex is high or low spin. Empirically ligands can be ordered in the spectrochemical series, but using crystal field theory we cannot rationalize where ligands fall in the series. For example, why is the neutral CO one of the strongest field ligands in the series while the anionic halogens are weak field ligands? To understand why ligands behave differently we have to consider how ligand orbitals interact with the metal d orbitals. Ligand field theory is essentially a combination between crystal field theory and molecular orbital theory where we focus only on the orbital overlap between the metal d orbitals and select ligand orbitals (rather than considering all of the valence orbitals on both the metal and ligand)

Metal-Ligand σ Bonding

The bond between a metal and a ligand is primarily a Lewis acid-base interaction where the ligand is a Lewis base and donates a pair of electron to the metal, the Lewis acid. This interaction forms a coordinate covalent bond. As with molecular orbital theory we have to decide how (or if) the ligand lone pairs will overlap with each of the d orbitals, and what type of bonding will be formed In an octahedral complex the ligands and their lone pairs lie along the x, y, and z axes. As shown in Figure **3.7.4.1**, the two on axis d orbitals ($d_{x^2-y^2}$ and d_{z^2}) have to correct orientation to form sigma bonds with the ligands. With the three off axis d orbitals (d_{xy}, d_{xz}, and d_{yz}) the ligand lone pair overlaps with a node in these orbitals (Figure **3.7.4.1***c*). This means there is no net overlap and no bonding (or antibonding) molecular orbital can be formed.

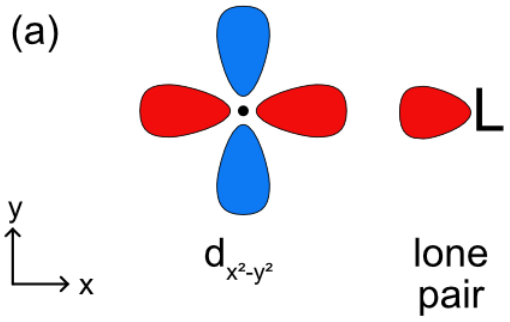


Figure **3.7.4.1***a*: Overlap between a ligand lone pair orbital and the metal $d_{x^2-y^2}$ orbital to form a sigma bond (CC BY-NC-SA, Catherine McCusker)

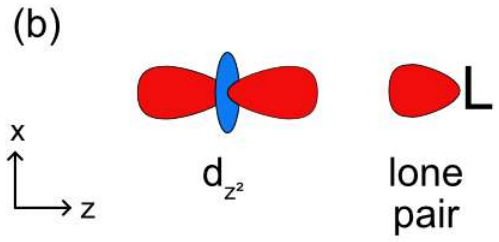


Figure **3.7.4.1***b*: Overlap between a ligand lone pair orbital and the metal d_{z^2} orbital to form a sigma bond (CC BY-NC-SA, Catherine McCusker)

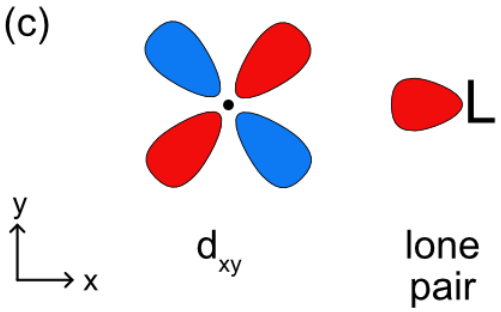


Figure **3.7.4.1***c*: There is no net overlap between the ligand lone pair orbital and the d_{xy} metal orbital, so this is a non bonding interaction (CC BY-NC-SA, Catherine McCusker)

Knowing this, we can construct a ligand field splitting diagram (a simplified molecular orbital diagram) (Figure **3.7.4.2**). In the free metal ion all 5 of the d orbitals are degenerate and before they interact with the metal all 6 of the ligand lone pair orbitals are at the same energy as well. Generally, based on electronegativity the ligand lone pair orbitals will be lower in energy than the metal d orbitals. When the ligand lone pairs interact with metal d orbitals the on axis set of d orbitals ($d_{x^2-y^2}$ and d_{z^2}) will form sigma bonding (e_g) and sigma antibonding (e_g*) molecular orbitals. The off axis set of d orbitals are nonbonding and are not stabilized or destabilized by the ligand lone pairs. Unlike a complete molecular orbital diagrams, a ligand field diagram won't necessarily have the same number of molecular orbitals as atomic orbitals becuse not every possible bonding interaction is included (for example, any overlap between the ligand orbitals and the metal s and p orbitals are not included). As in crystal field theory we can define an octahedral ligand field splitting energy (Δ_o), which will be the difference between the two molecular orbitals with the most metal d orbital character. In Figure **3.7.4.2** the t_{2g} set of d orbitals are nonbonding and therefore 100% metal character. The e_g bonding orbital is closer in energy to the ligand lone pairs and will have a higher % contribution from the ligands, and the e_g* antibonding orbital is closer in energy to the metal d orbitals and will have a higher % contribution from the metal. The relevant energy difference is between the t_{2g} and e_g* orbitals, as highlighted in green in Figure **3.7.4.2**. The splitting energy will increase as there is a stronger interaction between the metal and ligand orbitals (based on the criteria discussed previously) and the e_g* is more destabilized.

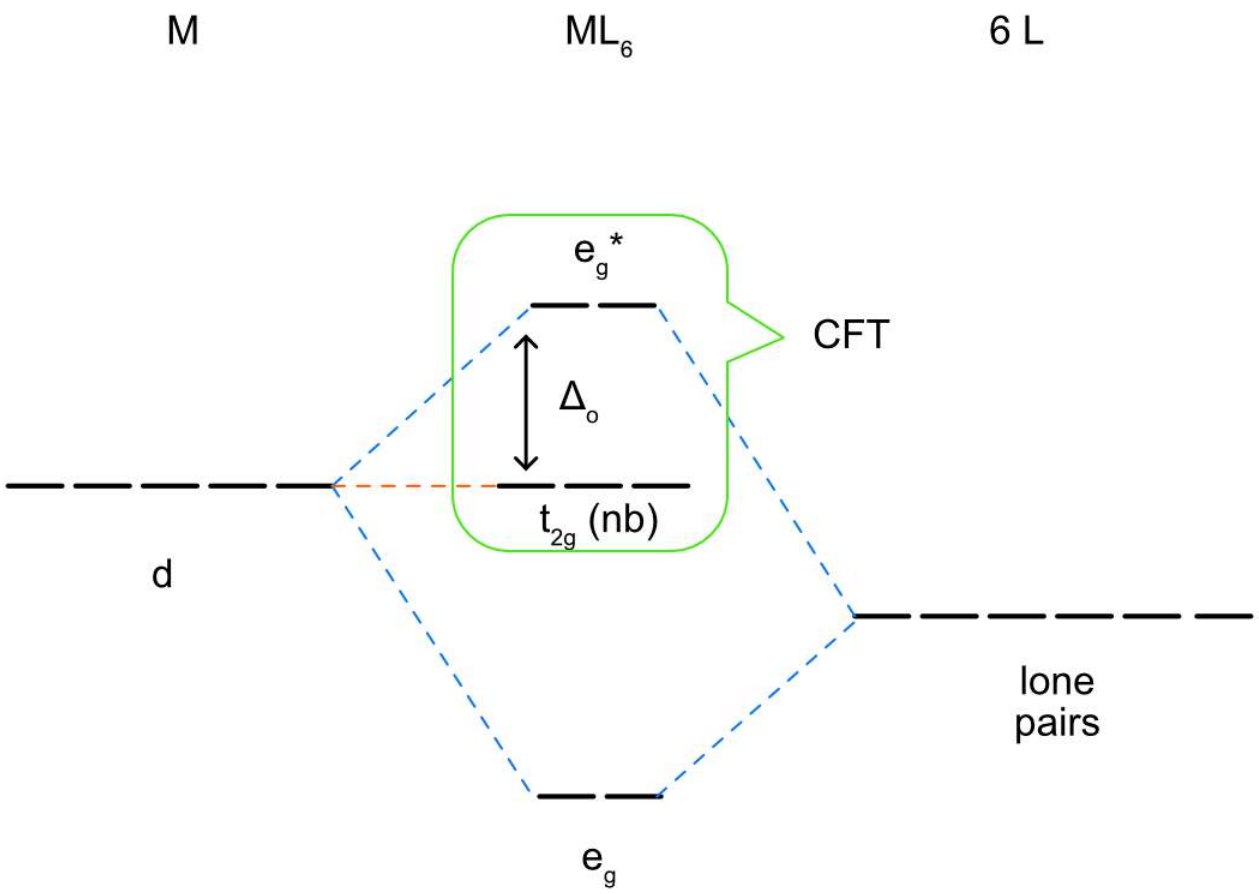


Figure **3.7.4.2**: Octahedral ligand field splitting diagram for only sigma bonding. The $d_{x^2-y^2}$ and d_{z^2} metal orbitals form sigma bonding (e_g) and antibonding molecular orbitals (e_g*). The d_{xy}, d_{xz}, and d_{yz} orbital are nonbonding (t_{2g} (nb)). The green outline highlights the portion of the diagram that is equivalent to the crystal field splitting diagram. (CC BY-NC-SA; Catherine McCusker)

Metal-Ligand π Bonding

In addition to sigma bonding, some ligands have orbitals available which can form π bonds with metals as well. These could include p orbitals on a single donor atom such as a halogen ion or π bonding or antibonding molecular orbitals on a molecular ligand. To determine how π bonding will change the ligand field splitting picture in Figure **3.7.4.2**, we will visualize how a ligand p orbital will interact with the metal d orbitals. The $d_{x^2-y^2}$ and d_{z^2} orbitals do not have the correct symmetry to form any type of bond with a ligand p orbital as shown in Figures **3.7.4.3***a* – *b* The d_{xy}, d_{xz}, and d_{yz} orbitals all have the correct symmetry to form π bonds with a ligand p orbital (Figure **3.7.4.3***c*).

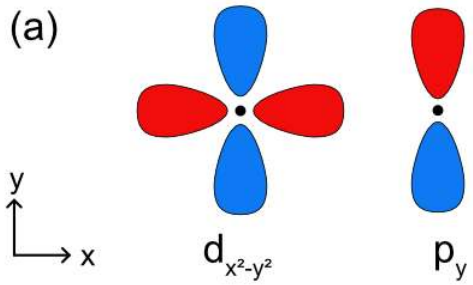


Figure **3.7.4.3a**: There is no net overlap between the ligand p orbital and the $d_{x^2-y^2}$ metal orbital, so this is a non bonding interaction (CC BY-NC-SA, Catherine McCusker)

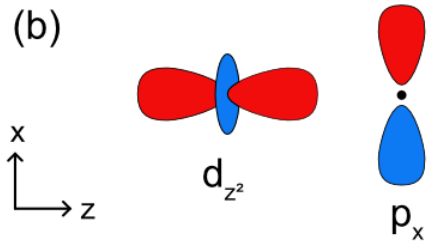


Figure **3.7.4.3b**: There is no net overlap between the ligand p orbital and the d_{z^2} metal orbital, so this is a non bonding interaction (CC BY-NC-SA, Catherine McCusker)

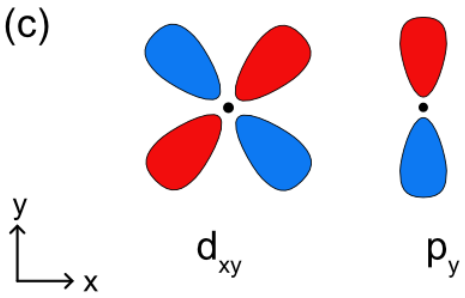


Figure **3.7.4.3c**: Overlap between a ligand p orbital and the metal d_{xy} orbital to form a π bond (CC BY-NC-SA, Catherine McCusker)

Unlike metal-ligand σ bonding, where electrons are always donated from the ligand to the metal, electrons in metal-ligand π bonding can be donated from either the metal or the ligand depending on the nature of the orbitals involved. In cases where ligands have empty p or π symmetry orbitals that are close in energy to the metal d orbitals, they can accept electrons from a filled metal orbital. This is also known as π backbonding because the direction of electron donation is opposite of that found in sigma metal ligand bonding. These ligands are called π acceptor ligands. In cases where ligands have filled p or π symmetry orbitals that are close in energy to the metal d orbitals, they can donate electrons to an empty metal orbital. These ligands are called π donor ligands.

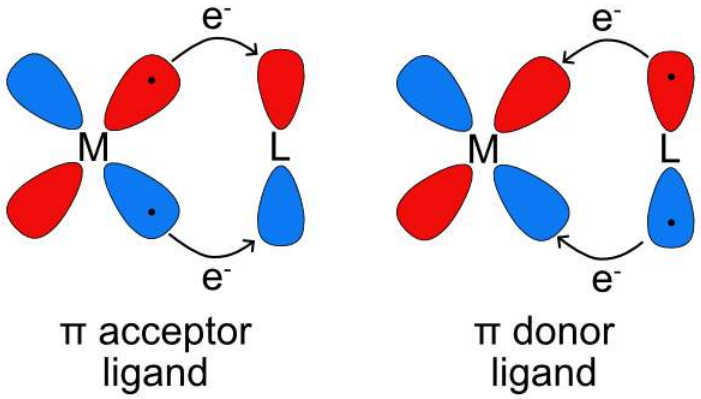


Figure **3.7.4.4**: Illustration of metal-ligand π bonding with π acceptor and donor ligands. Filled orbitals are represented with black dots. (CC BY-NC-SA, Catherine McCusker)

π Acceptors

Ligands that are π acceptors have empty, low energy π symmetry orbitals available to accept electrons from the metal center. Most often this is a π^* antibonding molecular orbital but it could also be an empty p orbital. Due to the aufbau principle, these empty orbitals will be higher in energy than any filled lone pairs on the ligands and will also generally be higher energy than the metal d orbitals. Similar to multiple bonding in main group compounds π bonding always occurs in combination with sigma bonding so in the ligand field splitting diagram of metal-ligand bonding with a π acceptor ligand the lone pairs for sigma bonding must be included as well as the empty orbitals for π bonding. As seen in Figure **3.7.4.3**, the $d_{x^2-y^2}$ and d_{z^2} orbitals do not overlap with the ligand p orbitals. The on axis d orbitals will form sigma bonding (e_g) and sigma antibonding (e_g*) molecular orbitals. Unlike the sigma bonding only diagram, the off axis d orbitals (d_{xy}, d_{xz}, and d_{yz}) overlap with the ligand p orbitals to form π bonding (t_{2g}) and π antibonding (t_{2g}*) molecular orbitals as seen in Figure **3.7.4.5**. Rather than being nonbonding, like in the sigma bonding only picture, the metal based t_{2g} molecular orbital is bonding. This increases the energy difference between the t_{2g} and e_g* and therefore increases Δ_o.

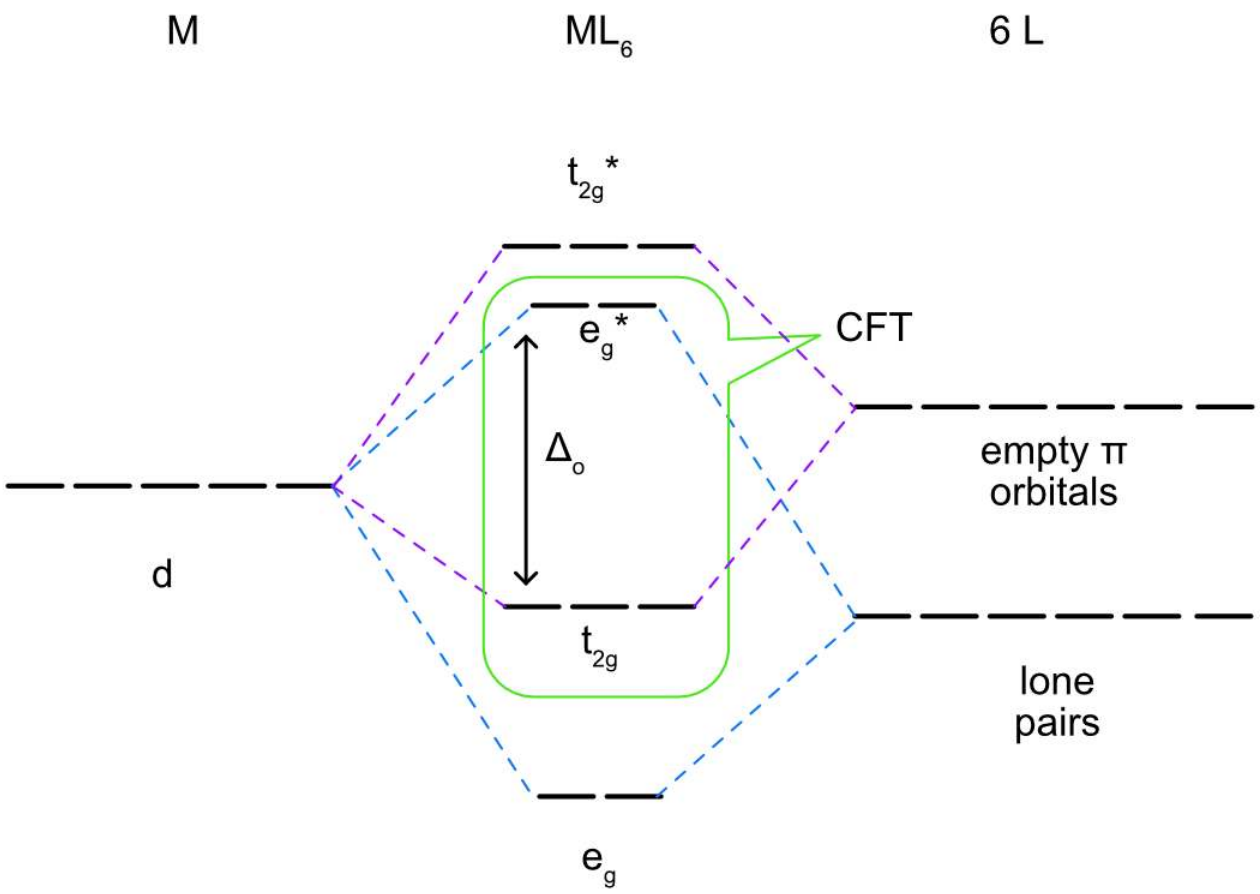


Figure 3.7.4.5: Octahedral ligand field splitting diagram with a π acceptor ligand. The $d_{x^2-y^2}$ and d_{z^2} metal orbitals form sigma bonding (e_g) and antibonding molecular orbitals (e_g*) with the ligand lone pairs. The d_{xy}, d_{xz}, and d_{yz} orbital form pi bonding (t_{2g}) and pi antibonding molecular orbitals (t_{2g}*) with the empty π symmetry orbitals. The green outline highlights the portion of the diagram that is equivalent to the crystal field splitting diagram. (CC BY-NC-SA; Catherine McCusker)

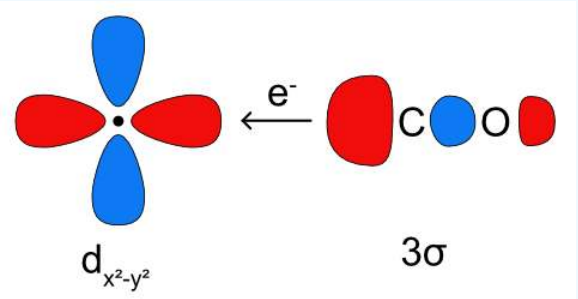
Exercise 3.7.4.1

Carbon monoxide is one of the most common, and strongest π acceptor ligands in inorganic chemistry. Refer to the molecular orbital diagram of CO and sketch likely metal-ligand orbital interactions for both sigma and pi bonding in a metal-CO complex. Indicate the direction of electron donation in both cases.

Answer

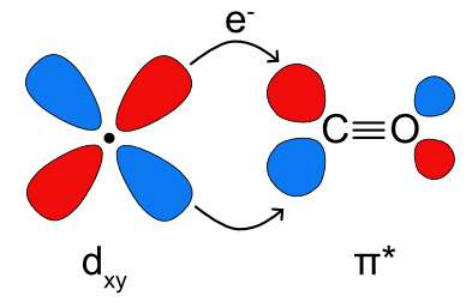
Sigma bonding:

Sigma bonding between a metal ion and a CO ligand involves overlap between the HOMO of CO (3σ) and the metal $d_{x^2-y^2}$ or d_{z^2} orbitals. Electrons are donated from the ligand to the metal.



Pi bonding:

Pi bonding between a metal ion and CO ligand involves overlap between the LUMO of CO (π^*) and the metal d_{xy}, d_{xz}, or d_{yz} orbitals. Electrons are donated from the metal to the ligand.



π Donor Ligands

Ligands that are π donors have filled π symmetry orbitals that are high enough in energy to donate electrons to the metal center. Most often this is a filled p orbital, but it could also be a π bonding molecular orbital. As lone pairs are generally the highest occupied orbitals is a molecule, the filled π orbitals will be lower in energy as seen in Figure **3.7.4.6**. The sigma interaction between the ligand lone pairs and the metal $d_{x^2-y^2}$ and d_{z^2} remain the same as previously described, forming the e_g bonding and e_g* antibonding molecular orbitals. The d_{xy}, d_{xz}, and d_{yz} overlap with the filled π orbitals to form π bonding (t_{2g}) and π antibonding (t_{2g}*) molecular orbitals. The difference between the *pi* acceptor and donor ligands is the energy and character of the t_{2g} and t_{2g}* molecular orbitals. In the π acceptor case above, the t_{2g} orbital is above the e_g and has a higher contribution from the metal and the t_{2g}* is above the e_g* and has a higher contribution from the ligand. In the π donor case the opposite is true. The t_{2g} orbital is below the e_g and has a higher contribution from the ligand and the t_{2g}* is below the e_g* and has a higher contribution from the metal. In this case Δ_o is smaller than in the sigma only picture because the t_{2g} symmetry molecular orbital has gone from nonbonding to antibonding and the energy difference between t_{2g}* and e_g* is smaller.

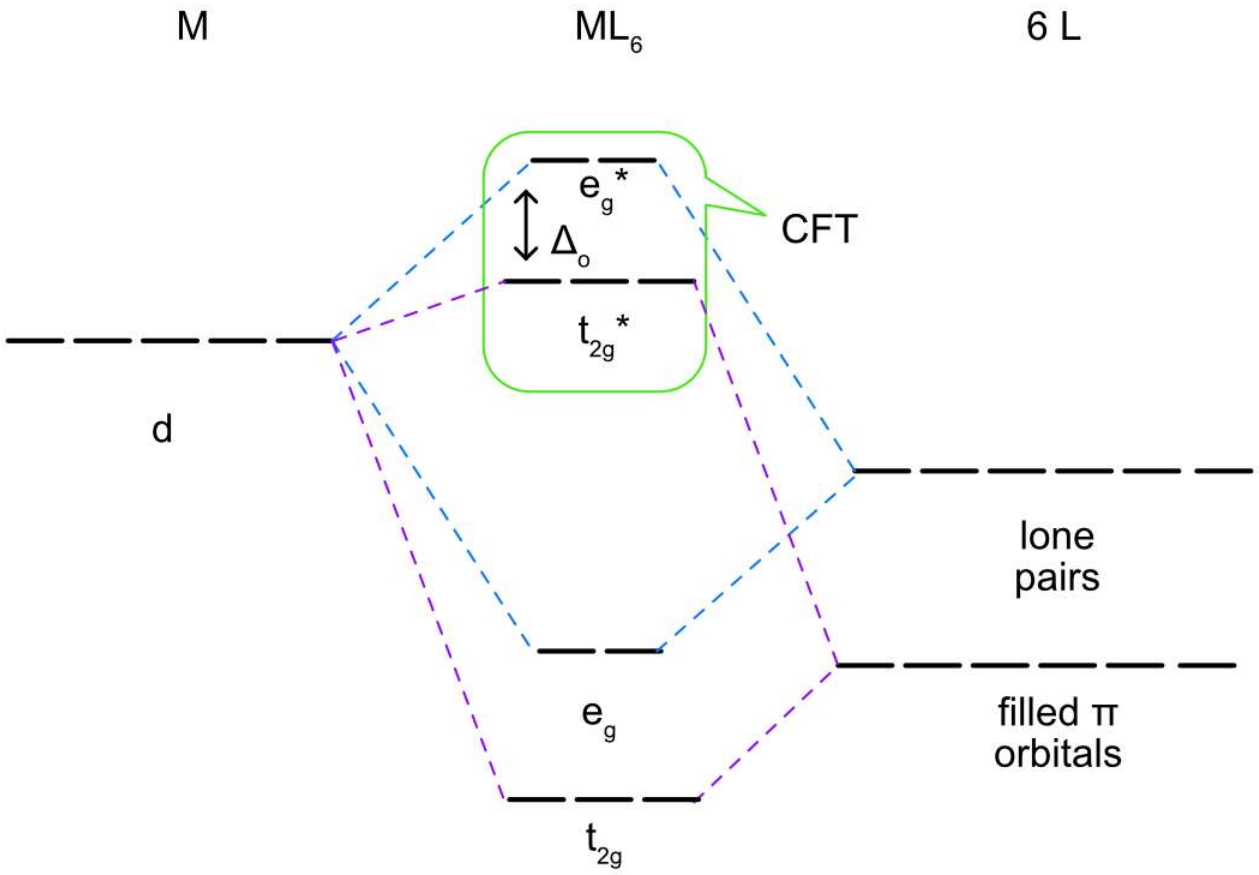


Figure **3.7.4.6**: Octahedral ligand field splitting diagram with a π donor ligand. The $d_{x^2-y^2}$ and d_{z^2} metal orbitals form sigma bonding (e_g) and antibonding molecular orbitals (e_g*) with the ligand lone pairs. The d_{xy}, d_{xz}, and d_{yz} orbital form pi bonding (t_{2g}) and pi antibonding molecular orbitals (t_{2g}*) with the filled π symmetry orbitals. The green outline highlights the portion of the diagram that is equivalent to the crystal field splitting diagram. (CC BY-NC-SA; Catherine McCusker)

The Spectrochemical Series

As discussed above, crystal field theory alone can't distinguish the behaviors of different ligands or explain why some ligands inherently produce larger splittings than others. Armed with ligand field theory we can now revisit the spectrochemical series and explain why ligands fall where they do within the series.

Strong field ligands

Strong field ligands are ones that produce large splittings between the d orbitals and form low spin complexes. Examples of strong field ligands include CO, CN^-, and NO_2. From a ligand field theory perspective all three of these ligands have strong π bonds (either double or triple bonds) and have empty π* molecular orbitals available for backbonding. Strong field ligands are both sigma donors (all ligands are sigma donors) and π acceptors. π backbonding between a metal and a ligand stabilizes the metal based t_{2g} molecular orbital and increases Δ_o.

Weak field ligands

Weak field ligands are ones that produce small splittings between the d orbitals and form high spin complexes. Examples of weak field ligands include the halogens, OH^- and H_2O. From a ligand field perspective these ions or molecules all have filled orbitals

which can π bond with the metal d orbitals. In the case of the halogens these are filled p orbitals and in the case of OH^- and H_2O these are lone pairs which are perpendicular to the metal-ligand bond. Weak field ligands are both sigma donors and π donors. The π donation from the ligand to the metal destabilizes the metal based t_{2g} molecular orbital and decreases Δ_o.

Intermediate field ligands

Intermediate field ligands produce intermediate splittings between the d orbitals and could form high or low spin complexes. Examples of intermediate field ligands include NH_3 or ethylenediamine (en). From a ligand field perspective these ligands only have a single lone pair available for sigma bonding. All of the other orbitals on nitrogen are used for sigma bonding to the H or C atoms within the molecule. Intermediate ligands are those which are only sigma donors, and are not π donors or π acceptors. In this case the t_{2g} symmetry d orbitals are nonbonding and the Δ_o is determined by the strength of the metal ligand sigma interaction (and amount of destabilization of the e_g* molecular orbital)

This page titled 3.7.4: Ligand Field Theory is shared under a CC BY-NC-SA 4.0 license and was authored, remixed, and/or curated by Catherine McCusker.

- **9.5: Ligand Field Theory** by Catherine McCusker is licensed CC BY-NC-SA 4.0.

3.7.5: Metal-Metal Bonds

Molecular orbital considerations in Dinuclear Metal Complexes with Multiple M-M Bonds

Let us begin a new chapter and think about dinuclear transition metal complexes with multiple metal-metal bonds. What is the maximum bond order that we could expect? The transition metals have five d-orbitals available, and in order to determine the maximum possible bond order we need to see how they overlap to form molecular orbitals (Fig. 11.1.1).

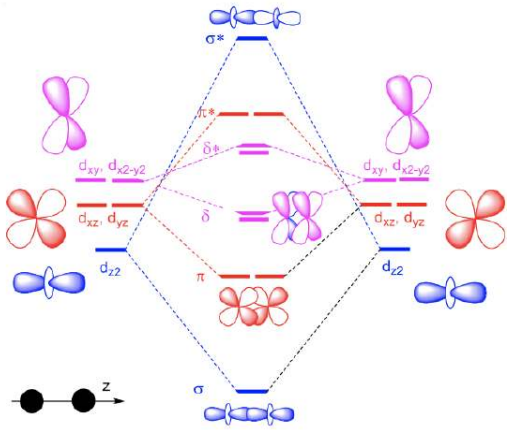


Figure 11.1.1 Molecular orbital overlap of metal d-orbitals forming M-M bonds

If we define the M-M bond axis as the z-axis, then two d_{z^2}-orbitals can overlap in σ-fashion to form a bonding and an anti-bonding σ-molecular orbital. A d_{xz}, and a d_{yz} can overlap with another d_{xz} and another d_{yz} in π-fashion to form two degenerated bonding π and two degenerated anti-bonding π*-orbitals. π-overlap is smaller than σ-overlap, therefore the split in energy between the bonding and the anti-bonding π-orbitals is smaller than the split between the bonding and the anti-bonding σ-orbitals. The d_{xy} orbital can overlap with another d_{xy} orbital in ***δ***-fashion, and so can the $d_{x^2-y^2}$ with another $d_{x^2-y^2}$. This gives two bonding ***δ***-orbitals and two anti-bonding ***δ***-orbitals. The ***δ***-overlap is even smaller than the π-overlap, therefore the energy split between the bonding and the anti-bonding ***δ***-orbitals is even smaller than those for the π and π*-orbitals. So what would be the maximum bond order that could be achieved? The maximum bond order would be achieved when all bonding MOs were full, and all anti-bonding MOs were empty. We have overall five bonding MOs that we could fill with ten electrons from two metal atoms with d^5-electron configuration. The maximum bond order BO would therefore be BO=5. However, in practice only bond orders up to 4 are well known. This is because the $d_{x^2-y^2}$ orbital is usually too involved in the bonding with the ligands thereby becoming unavailable for metal-metal interactions. The $d_{x^2-y^2}$ orbital makes the strongest interactions with the ligands because most ligands approach on or near the x and the y-axes.

Electron Configurations and Multiple M-M Bonds

We can easily predict now which electron configuration leads to which metal-metal bond order. The bond order increases from 1 to 4 with the electron configuration changing from d^1 to d^4. At d^4 all bonding MOs are full with eight electrons.

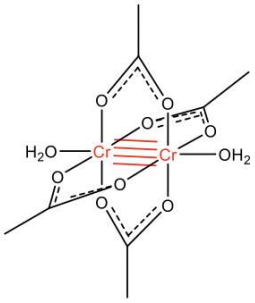


Figure 11.1.2 Tetraacetatodiaquadichromium complex

An example of a complex with a bond order of 4 is the tetraacetatodiaquadichromium complex shown (Fig. 11.1.2). Cr is in the oxidation state +2, which makes the chromium a d^4 species. We can quickly show this by counting the valence electrons. A neutral

Cr atom has 6 VE, and an electron configuration $3d^5 4s^1$. There are four acetate ligands having a 1- charge each which gives four negative charges overall. The complex is overall neutral which means that each Cr must have formally a 2+ charge, and the electron configuration is $3d^4$.

d^1	d^2	d^3	d^4	d^5	d^6	d^7	d^8
1	2	3	4	3	2	1	0

Figure 11.1.3 Relationship between metal-metal bond order and electron configuration

With even more electrons in the metal d-orbitals the bond order begins to decrease again as anti-bonding MOs need to be filled (Fig. 11.1.3). The combination of two metals with d^5 electron configuration leads to a triple bond, two d^6-metals give a double bond, and two d^7 metals give a single bond. A metal-metal bond should not exist for two d^8-metals because then the bond order is zero.

Evidence for M-M Multiple Bonds

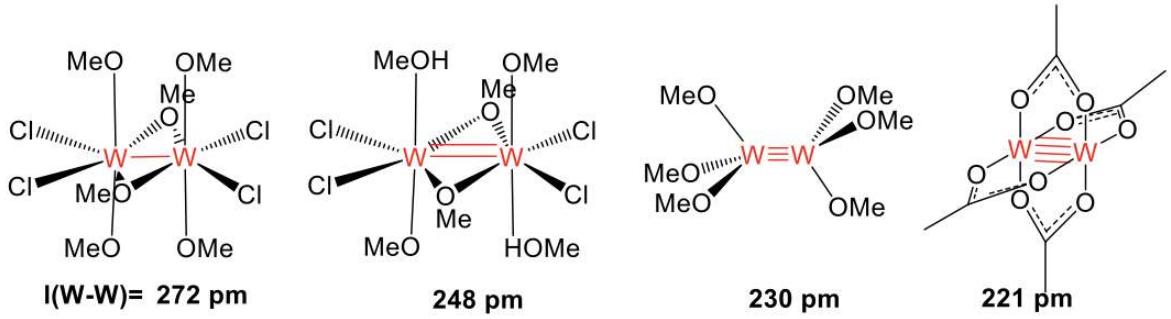


Figure 11.1.4 M-M bond length in four tungsten complexes

What experimental evidence can support the existence of a particular bond order (Fig. 11.1.4)? One argument is the bond length which can be obtained through the crystal structure determination of the complex. The shorter the bond, the higher the bond order. For instance, in the four tungsten complexes shown the bond lengths decrease from 272 pm, to 248 pm, to 230 pm to 221 pm corresponding to a single, double, triple, and quadruple bond, respectively.

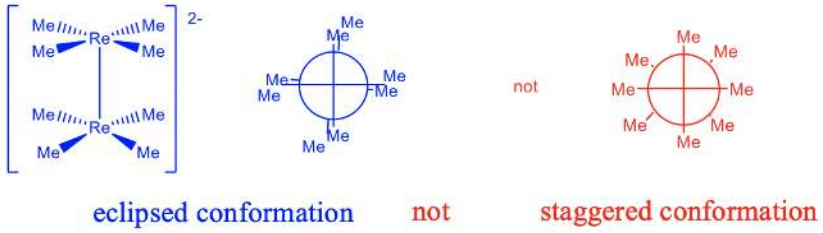


Figure 11.1.5 $ReMe_4$ confirmations

Another hint can be the conformation of a molecule (Fig. 11.1.5). For instance, the two square-planar units of the $Re_2Me_8^{2-}$ complex anion show eclipsed conformation. Steric repulsion arguments would favor the staggered conformation, so there must be a reason why the two $ReMe_4$ units are eclipsed. The rhenium is in the oxidation state +3, thus it is a d^4 species, and we would argue that there may be a Re-Re quadruple bond. This quadruple bond can only form when the d_{xy} orbitals are in eclipsed conformation, and this is only possible when the two $ReMe_4$ fragments are in eclipsed conformation. The very short bond length of 218 pm further supports the existence of the quadruple bond.

Dr. Kai Landskron (Lehigh University). If you like this textbook, please consider to make a donation to support the author's research at Lehigh University: Click Here to Donate.

3.7.5: Metal-Metal Bonds is shared under a CC BY-NC-SA 4.0 license and was authored, remixed, and/or curated by LibreTexts.

- **11.1: Complexes with Multiple Metal-Metal Bonds** by Kai Landskron is licensed CC BY 4.0.

3.7.5.1: Metal-Metal Multiple Bonds

Molecular orbital considerations in Dinuclear Metal Complexes with Multiple M-M Bonds

Let us begin a new chapter and think about dinuclear transition metal complexes with multiple metal-metal bonds. What is the maximum bond order that we could expect? The transition metals have five d-orbitals available, and in order to determine the maximum possible bond order we need to see how they overlap to form molecular orbitals (Fig. 11.1.1).

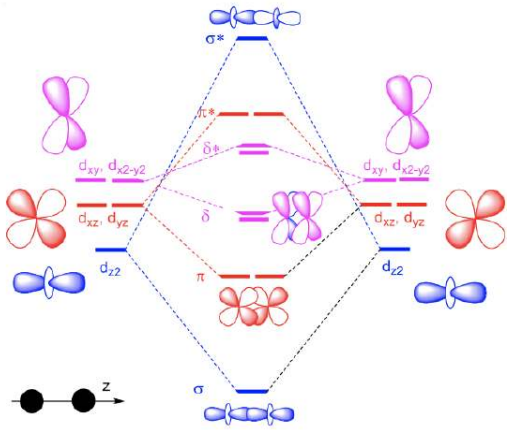


Figure 11.1.1 Molecular orbital overlap of metal d-orbitals forming M-M bonds

If we define the M-M bond axis as the z-axis, then two d_{z^2}-orbitals can overlap in σ-fashion to form a bonding and an anti-bonding σ-molecular orbital. A d_{xz}, and a d_{yz} can overlap with another d_{xz} and another d_{yz} in π-fashion to form two degenerated bonding π and two degenerated anti-bonding π*-orbitals. π-overlap is smaller than σ-overlap, therefore the split in energy between the bonding and the anti-bonding π-orbitals is smaller than the split between the bonding and the anti-bonding σ-orbitals. The d_{xy} orbital can overlap with another d_{xy} orbital in ***δ***-fashion, and so can the $d_{x^2-y^2}$ with another $d_{x^2-y^2}$. This gives two bonding ***δ***-orbitals and two anti-bonding ***δ***-orbitals. The ***δ***-overlap is even smaller than the π-overlap, therefore the energy split between the bonding and the anti-bonding ***δ***-orbitals is even smaller than those for the π and π*-orbitals. So what would be the maximum bond order that could be achieved? The maximum bond order would be achieved when all bonding MOs were full, and all anti-bonding MOs were empty. We have overall five bonding MOs that we could fill with ten electrons from two metal atoms with d^5-electron configuration. The maximum bond order BO would therefore be BO=5. However, in practice only bond orders up to 4 are well known. This is because the $d_{x^2-y^2}$ orbital is usually too involved in the bonding with the ligands thereby becoming unavailable for metal-metal interactions. The $d_{x^2-y^2}$ orbital makes the strongest interactions with the ligands because most ligands approach on or near the x and the y-axes.

Electron Configurations and Multiple M-M Bonds

We can easily predict now which electron configuration leads to which metal-metal bond order. The bond order increases from 1 to 4 with the electron configuration changing from d^1 to d^4. At d^4 all bonding MOs are full with eight electrons.

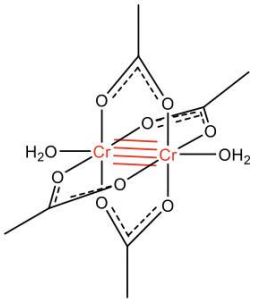


Figure 11.1.2 Tetraacetatodiaquadichromium complex

An example of a complex with a bond order of 4 is the tetraacetatodiaquadichromium complex shown (Fig. 11.1.2). Cr is in the oxidation state +2, which makes the chromium a d^4 species. We can quickly show this by counting the valence electrons. A neutral

Cr atom has 6 VE, and an electron configuration $3d^5 4s^1$. There are four acetate ligands having a 1- charge each which gives four negative charges overall. The complex is overall neutral which means that each Cr must have formally a 2+ charge, and the electron configuration is $3d^4$.

d^1	d^2	d^3	d^4	d^5	d^6	d^7	d^8
1	2	3	4	3	2	1	0

Figure 11.1.3 Relationship between metal-metal bond order and electron configuration

With even more electrons in the metal d-orbitals the bond order begins to decrease again as anti-bonding MOs need to be filled (Fig. 11.1.3). The combination of two metals with d^5 electron configuration leads to a triple bond, two d^6-metals give a double bond, and two d^7 metals give a single bond. A metal-metal bond should not exist for two d^8-metals because then the bond order is zero.

Evidence for M-M Multiple Bonds

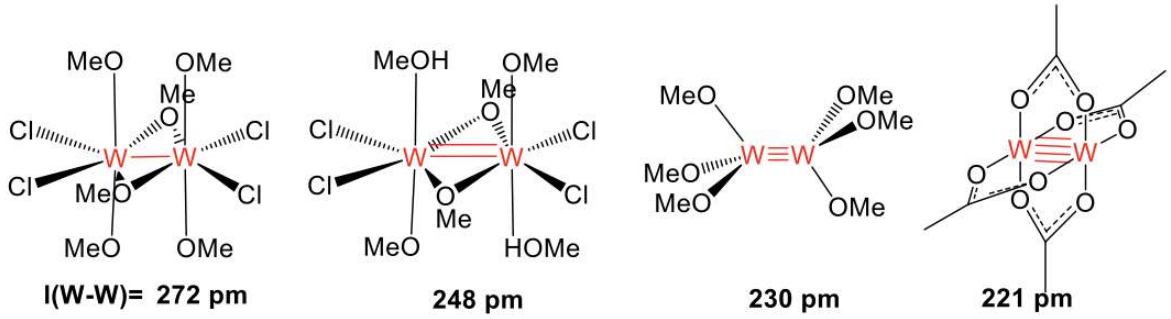


Figure 11.1.4 M-M bond length in four tungsten complexes

What experimental evidence can support the existence of a particular bond order (Fig. 11.1.4)? One argument is the bond length which can be obtained through the crystal structure determination of the complex. The shorter the bond, the higher the bond order. For instance, in the four tungsten complexes shown the bond lengths decrease from 272 pm, to 248 pm, to 230 pm to 221 pm corresponding to a single, double, triple, and quadruple bond, respectively.

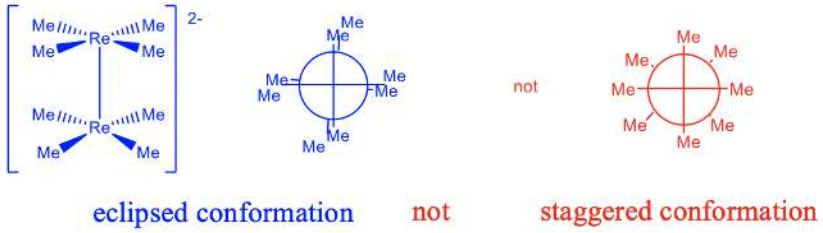


Figure 11.1.5 $ReMe_4$ confirmations

Another hint can be the conformation of a molecule (Fig. 11.1.5). For instance, the two square-planar units of the $Re_2Me_8^{2-}$ complex anion show eclipsed conformation. Steric repulsion arguments would favor the staggered conformation, so there must be a reason why the two $ReMe_4$ units are eclipsed. The rhenium is in the oxidation state +3, thus it is a d^4 species, and we would argue that there may be a Re-Re quadruple bond. This quadruple bond can only form when the d_{xy} orbitals are in eclipsed conformation, and this is only possible when the two $ReMe_4$ fragments are in eclipsed conformation. The very short bond length of 218 pm further supports the existence of the quadruple bond.

Dr. Kai Landskron (Lehigh University). If you like this textbook, please consider to make a donation to support the author's research at Lehigh University: Click Here to Donate.

3.7.5.1: Metal-Metal Multiple Bonds is shared under a CC BY-NC-SA 4.0 license and was authored, remixed, and/or curated by LibreTexts.

- **11.1: Complexes with Multiple Metal-Metal Bonds** by Kai Landskron is licensed CC BY 4.0.

3.7.6: Jahn-Teller Distortions

The Jahn-Teller effect is a geometric distortion of a non-linear molecular system that reduces its symmetry and energy. This distortion is typically observed among octahedral complexes where the two axial bonds can be shorter or longer than those of the equatorial bonds. This effect can also be observed in tetrahedral compounds. This effect is dependent on the electronic state of the system.

Introduction

In 1937, Hermann Jahn and Edward Teller postulated a theorem stating that "stability and degeneracy are not possible simultaneously unless the molecule is a linear one," in regards to its electronic state.[1] This leads to a break in degeneracy which stabilizes the molecule and by consequence, reduces its symmetry. Since 1937, the theorem has been revised which Housecroft and Sharpe have eloquently phrased as "any non-linear molecular system in a degenerate electronic state will be unstable and will undergo distortion to form a system of lower symmetry and lower energy, thereby removing the degeneracy."[2] This is most commonly observed with transition metal octahedral complexes, however, it can be observed in tetrahedral compounds as well.

For a given octahedral complex, the five d atomic orbitals are split into two degenerate sets when constructing a molecular orbital diagram. These are represented by the sets' symmetry labels: t_{2g} (d_{xz}, d_{yz}, d_{xy}) and e_g (d_{z^2} and $d_{x^2-y^2}$). When a molecule possesses a degenerate electronic ground state, it will distort to remove the degeneracy and form a lower energy (and by consequence, lower symmetry) system. The octahedral complex will either elongate or compress the z ligand bonds as shown in Figure **3.7.6.1** below:

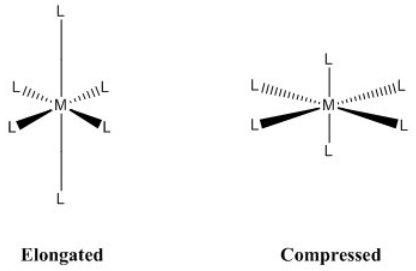


Figure **3.7.6.1**: Jahn-Teller distortions for an octahedral complex.

When an octahedral complex exhibits elongation, the axial bonds are longer than the equatorial bonds. For a compression, it is the reverse; the equatorial bonds are longer than the axial bonds. Elongation and compression effects are dictated by the amount of overlap between the metal and ligand orbitals. Thus, this distortion varies greatly depending on the type of metal and ligands. In general, the stronger the metal-ligand orbital interactions are, the greater the chance for a Jahn-Teller effect to be observed.

Elongation

Elongation Jahn-Teller distortions occur when the degeneracy is broken by the stabilization (lowering in energy) of the d orbitals with a *z* component, while the orbitals without a *z* component are destabilized (higher in energy) as shown in Figure **3.7.6.2** below:

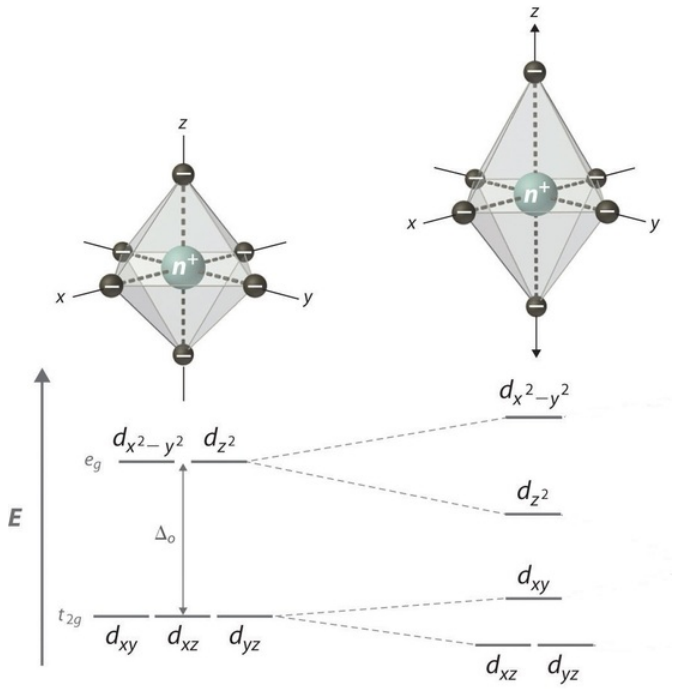


Figure **3.7.6.2**: Illustration of tetragonal distortion (elongation) for an octahedral complex.

This is due to the d_{xy} and $d_{x^2-y^2}$ orbitals having greater overlap with the ligand orbitals, resulting in the orbitals being higher in energy. Since the $d_{x^2-y^2}$ orbital is antibonding, it is expected to increase in energy due to elongation. The d_{xy} orbital is still nonbonding, but is destabilized due to the interactions. Jahn-Teller elongations are well-documented for copper(II) octahedral compounds. A classic example is that of copper(II) fluoride as shown in Figure **3.7.6.3**.

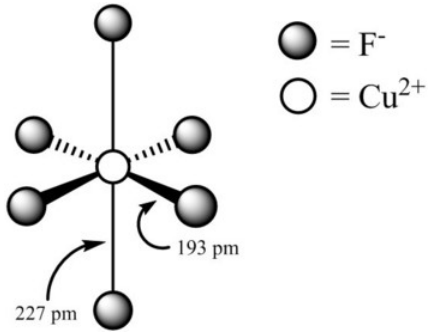


Figure **3.7.6.3**: Structure of octahedral copper(II) fluoride.[3]

Notice that the two axial bonds are both elongated and the four shorter equatorial bonds are the same length as each other. According the theorem, the orbital degeneracy is eliminated by distortion, making the molecule more stable based on the model presented in Figure **3.7.6.2**.

Compression

Compression Jahn-Teller distortions occur when the degeneracy is broken by the stabilization (lowering in energy) of the d orbitals *without* a *z* component, while the orbitals with a *z* component are destabilized (higher in energy) as shown in Figure **3.7.6.4** below:

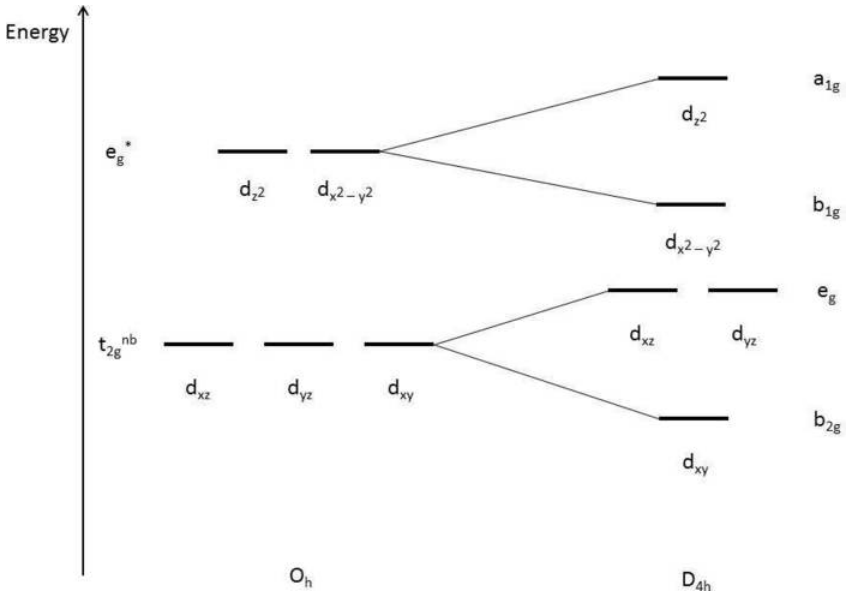


Figure **3.7.6.4**: Illustration of tetragonal distortion (compression) for an octahedral complex.

This is due to the *z*-component d orbitals having greater overlap with the ligand orbitals, resulting in the orbitals being higher in energy. Since the d_{z^2} orbital is antibonding, it is expected to increase in energy due to compression. The d_{xz} and d_{yz} orbitals are still nonbonding, but are destabilized due to the interactions.

Electronic Configurations

For Jahn-Teller effects to occur in transition metals there must be degeneracy in either the t_{2g} or e_g orbitals. The electronic states of octahedral complexes depend on the number of d-electrons and the splitting energy, **Δ**. When **Δ** is large and is greater than the energy required to pair electrons, electrons pair in t_{2g} before occupying e_g. On the other hand, when **Δ** small and is less than the pairing energy, electrons will occupy e_g before pairing in t_{2g}. The **Δ** of an octahedral complex is dictated by the chemical environment (ligand identity), and the identity and charge of the metal ion. If there electron configurations for any d-electron count is different depending on **Δ**, the configuration with more paired electrons is called low spin while the one with more unpaired electrons is called high spin.

The electron configurations diagrams for d1 through d10 with large and small **Δ** are illustrated in the figures below. Notice that the electron configurations for d^1, d^2, d^3, d^8, d^9, and d^{10} are the same no matter what the magnitude of **Δ**. Low spin and high spin configurations exist only for the electron counts d^4, d^5, d^6, and d^7.

Large Δ

Figure **3.7.6.5** (below) shows the various electronic configurations for octahedral complexes with large **Δ**, including the low-spin configurations of d^4, d^5, d^6, and d^7:

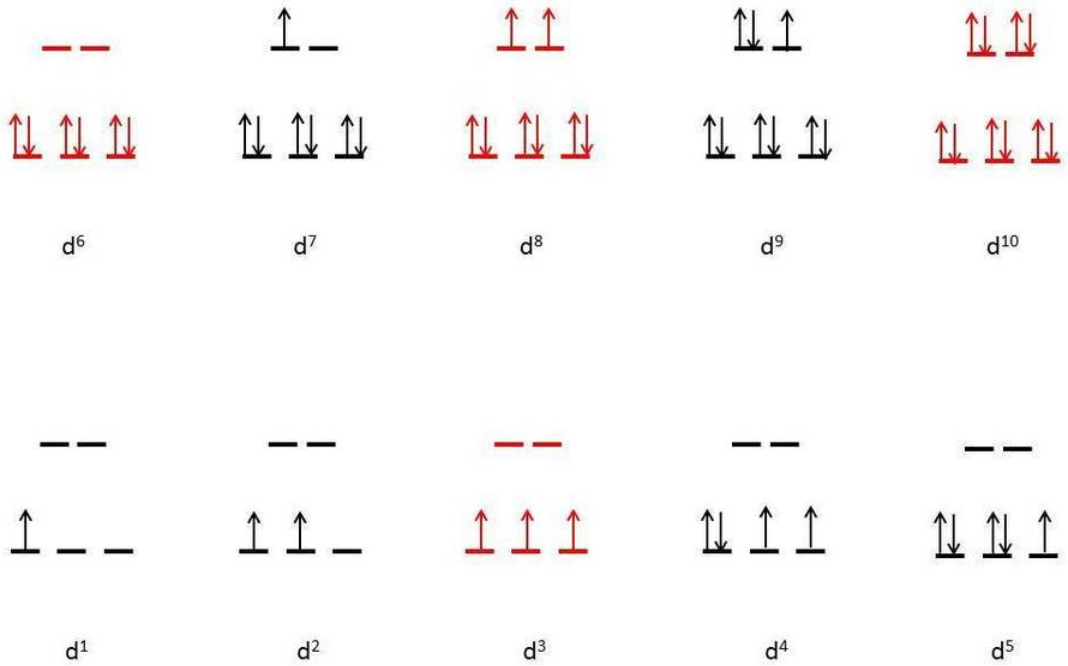


Figure **3.7.6.5**: Electron configuration diagram of octahedral complexes (red indicates no degeneracies possible, thus no Jahn-Teller effects).

The figure illustrates the electron configurations in the case of large **Δ**. The electron configurations highlighted in red (d^3, low spin d^6, d^8, and d^{10}) **do not** exhibit Jahn-Teller distortions. On the other hand d^1, d^2, low spin d^4, low spin d^5, low spin d^7, and d^9, would be expected to exhibit Jhan-Teller distortion. These electronic configurations correspond to a variety of transition metals. Some common examples include Cr^{3+}, Co^{3+}, and Ni^{2+}.

Small Δ

Figure **3.7.6.6** (below) shows the various electronic configurations for octahedral complexes with small **Δ**, including the high-spin configurations of d^4, d^5, d^6, and d^7::

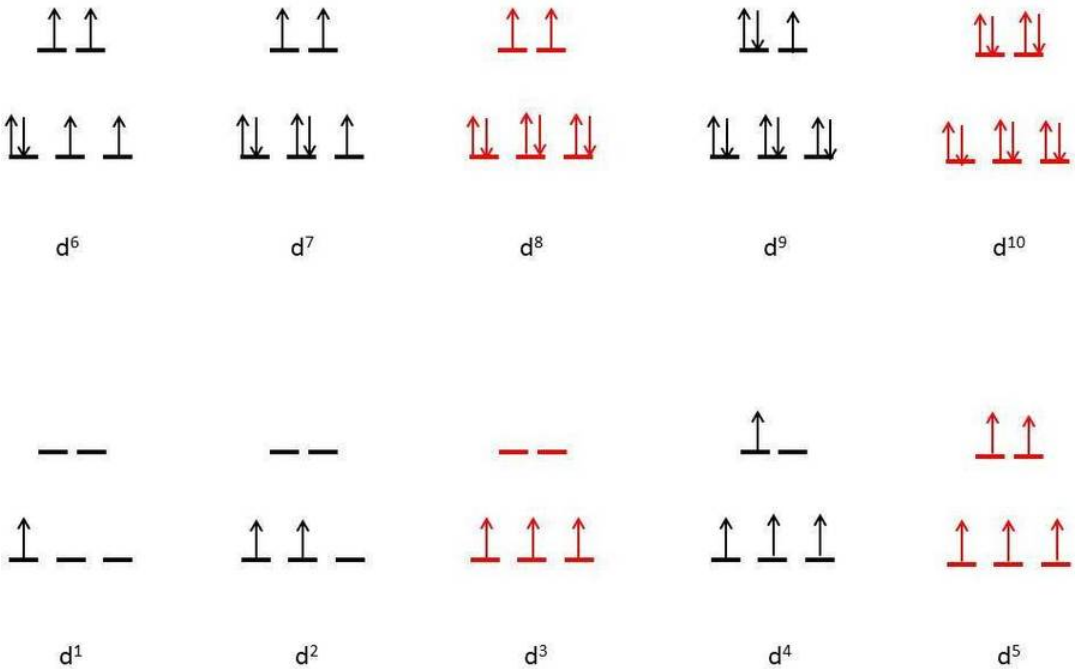


Figure **3.7.6.6**: High spin octahedral coordination diagram (red indicates no degeneracies possible, thus no Jahn-Teller effects).

The figure illustrates the electron configurations in the case of small Δ. The electron configurations highlighted in red (d^3, high spin d^5, d^8, and d^{10}) **do not** exhibit Jahn-Teller distortions. In general, degenerate electronic states occupying the e_g orbital set tend to show stronger Jahn-Teller effects. This is primarily caused by the occupation of these high energy orbitals. Since the system is more stable with a lower energy configuration, the degeneracy of the e_g set is broken, the symmetry is reduced, and occupations at lower energy orbitals occur.

Spectroscopic Observation

Jahn-Teller distortions can be observed using a variety of spectroscopic techniques. In UV-VIS absorption spectroscopy, distortion causes splitting of bands in the spectrum due to a reduction in symmetry (O_h to D_{4h}). Consider a hypothetical molecule with octahedral symmetry showing a single absorption band. If the molecule were to undergo Jahn-Teller distortion, the number of bands would increase as shown in Figure **3.7.6.7** below:

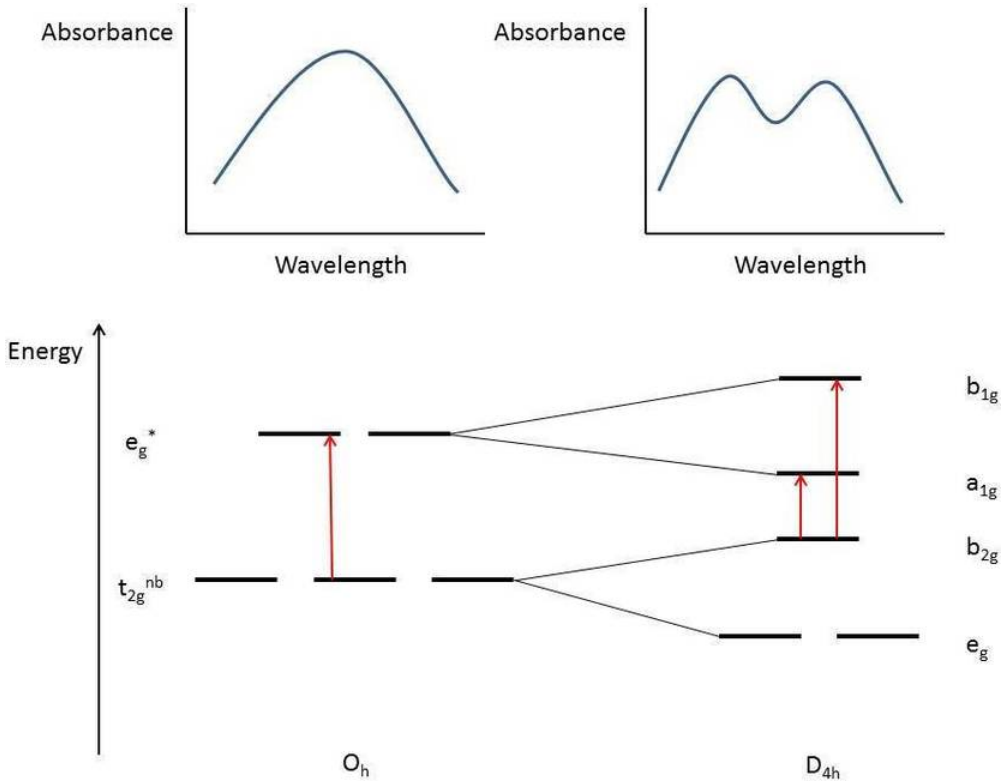


Figure **3.7.6.7**: Hypothetical absorption spectra of an octahedral molecule (left) and the same molecule with Jahn-Teller elongation (right). The red arrows indicate electronic transitions.

A similar phenomenon can be seen with IR and Raman vibrational spectroscopy. The number of vibrational modes for a molecule can be calculated using the 3n - 6 rule (or 3n - 5 for linear geometry) rule. If a molecule exhibits an O_h symmetry point group, it will have fewer bands than that of a Jahn-Teller distorted molecule with D_{4h} symmetry. Thus, one could observe Jahn-Teller effects through either IR or Raman techniques. This effect can also be observed in EPR experiments as long as there is at least one unpaired electron.

Table **3.7.6.1**: Examples of Jahn-Teller distorted complexes

$CuBr_2$	4 Br at 240 pm 2 Br at 318 pm
$CuCl_2$	4 Cl at 230 pm 2 Cl at 295 pm
$CuCl_2.2H_2O$	2 O at 193 pm 2 Cl at 228 pm 2 Cl at 295 pm
$CsCuCl_3$	4 Cl at 230 pm 2 Cl at 265 pm
CuF_2	4 F at 193 pm 2 F at 227 pm
$CuSO_4.4NH_3.H_2O$	4 N at 205 pm 1 O at 259 pm 1 O at 337 pm
K_2CuF_4	4 F at 191 pm 2 F at 237 pm
$KCuAlF_6$	2 F at 188 pm 4 F at 220 pm
CrF_2	4 F at 200 pm 2 F at 243 pm
$KCrF_3$	4 F at 214 pm 2 F at 200 pm
MnF_3	2 F at 209 pm 2 F at 191 pm 2 F at 179 pm

The Jahn-Teller Theorem predicts that distortions should occur for *any degenerate state*, including degeneracy of the t_{2g} level, however distortions in bond lengths are much more distinctive when the degenerate electrons are in the e_g level.

References

1. Jahn, H. A.; Teller, E. *Proc. R. Soc. London A*, **1937**, *161*, 220-235. DOI: 10.1098/rspa.1937.0142
2. Housecroft, C.; Sharpe, A. G. *Inorganic Chemistry*. Prentice Hall, 3rd Ed., 2008, p. 644. ISBN: 978-0-13-175553-6
3. Billy, C.; Haendler, H. A. *J. Am. Chem. Soc.*, **1957**, *79*, 1049–1051. DOI: 10.1021/ja01562a011

References

- Janes, R.; Moore, E. A. *Metal-ligand bonding*. The Open University, 2004, p. 23. ISBN 0-85404-979-7
- P.T.Miller, P.G.Lenhert and M.D.Joesten, *Inorg. Chem.*, 11, 2221, 1972.
- J.S.Wood, C.P.Keijzers and R.O.Day, *Acta Crystallogr., Sect.C (Cr. Str. Comm.)*, 40, 404, 1984.
- M.D.Joesten, M.S.Hussain and P.G.Lenhert, *Inorg. Chem.*, 9, 151, 1970.

Practice Questions

1. Why do d^3 complexes not show Jahn-Teller distortions?
2. Does the spin system (high spin v. low spin) of a molecule play a role in Jahn-Teller effects?
3. What spectroscopic method would one utilize in order to observe Jahn-Teller distortions in a diamagnetic molecule?
4. What spectroscopic method(s) would one utilize in order to observe Jahn-Teller distortions in a paramagnetic molecule?
5. Why are Jahn-Teller effects most prevalent in inorganic (transition metal) compounds?

Answers

1. Complexes with d^3 electron configurations do not show Jahn-Teller distortions because there is no ground state degeneracy.
2. Yes. Examining the d^5 electron configuration, one finds that the high spin scenario contains all singly occupied d orbitals (no degeneracy). However, the low spin d^5 electron configuration shows degeneracy, which then leads to possible Jahn-Teller effects.
3. UV-VIS absorption spectroscopy is one of the most common techniques for observing these effects. In general, it is independent of magnetism (diamagnetic v. paramagnetic). Thus, one would see the effect in the spectrum of UV-VIS absorption analysis. Note that EPR requires at least one unpaired electron, and therefore not EPR active.
4. Inorganic, specifically transition metal, complexes are most prevalent in showing Jahn-Teller distortions due to the availability of d orbitals. The most common geometry that the Jahn-Teller effect is observed is in octahedral complexes (see **Figures 2, 4, 5** and **6** above) due to the splitting of d orbitals into two degenerate sets. Due to stabilization, the degeneracies are removed, making a lower symmetry and lower energy molecule.

5. In addition to UV-VIS absorption, one can also employ EPR spectroscopy if a molecule possesses and unpaired electron.

3.7.6: Jahn-Teller Distortions is shared under a CC BY-NC-SA 4.0 license and was authored, remixed, and/or curated by LibreTexts.

- **9.3: Jahn-Teller Distortions** by Kamran Ghiassi, Robert Lancashire is licensed CC BY-NC-SA 4.0.

CHAPTER OVERVIEW

4: Electronic Structure and Spectra of d-Metal Complexes

4.1: Absorption of Light

4.1.1: Beer-Lambert Absorption Law

4.2: Quantum Numbers of Multielectron Atoms

4.2.1: Finding Microstates and Term Symbols

4.2.2: Spin-Orbit Coupling

4.3: Electronic Spectra of Coordination Compounds

4.3.1: Symmetry labels for split terms

4.3.2: Correlation Diagrams

4.3.3: Tanabe-Sugano Diagrams

4.3.4: Applications of Tanabe-Sugano Diagrams

4.3.5: Tetrahedral Complexes

4.3.6: Selection Rules

4.3.7: Charge-Transfer Spectra

4.3.8: Applications of Charge-Transfer

4: Electronic Structure and Spectra of d-Metal Complexes is shared under a CC BY-NC-SA 4.0 license and was authored, remixed, and/or curated by LibreTexts.

4.1: Absorption of Light

Introduction

The d-orbital splitting in coordination complexes results in a gap (Δ) that happens to be just the right magnitude to absorb visible light. Because metal complexes can absorb visible light, they display an array of colors. Not only is the color attractive to the eye, it is an indication of the chemical and physical properties of the metal complex. The color (like the magnitude of Δ) depends on the identity of the metal ion, the coordination geometry, and the ligand identity. Chemists don't just "look" at color, though - we measure it using electronic absorption spectroscopy. This is usually done in a lab using a UV-visible spectrophotometer.

An example of such a measurement is shown below in Figure **4.1.1** for a Cu(II) complex. The sample appears a pink color to the eye, and when it is measured using a UV-visible spectrometer, it is shown to absorb visible light at approximately 530 nm. The absorption spectrum can indicate the oxidation state of Cu, the ligands bound to the Cu(II) ion, and the coordination geometry. The color of the solution in Figure **4.1.1** is a shade of pink.

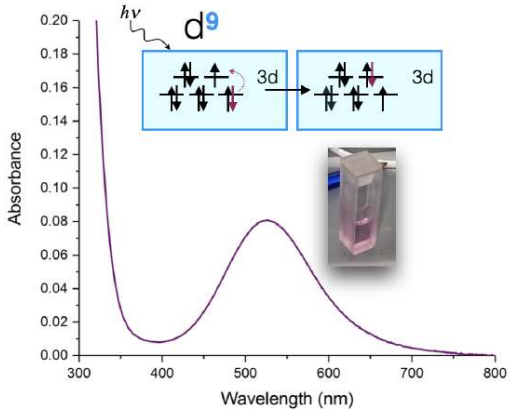


Figure **4.1.1**: A UV-visible spectrum of a Cu(II)-peptide complex. A photo of the sample shows its pink color. The splitting diagram for its approximation as an octahdral complex is shown, where an electronic transition from t_{2g} to e_g is shown. (CC-BY-NC-SA; Kathryn Haas)

We observe the complementary color of light absorbed

The absorption spectrum shown above in Figure **4.1.1** is a simple case in which only one absorption band is observed in the visible region of the spectrum. In a simple case like this, the color of a complex can be predicted as the complementary color of the light absorbed by the solution. When a solution or object absorbs a certain wavelength, we see the complementary color; or the color opposite to the absorbed wavelength on the color wheel in Figure **4.1.2**. In the case of the Cu(II) complex spectrum shown in Figure **4.1.1**, the color of the light absorbed at 530 nm is green, and the predicted color observed is pink.

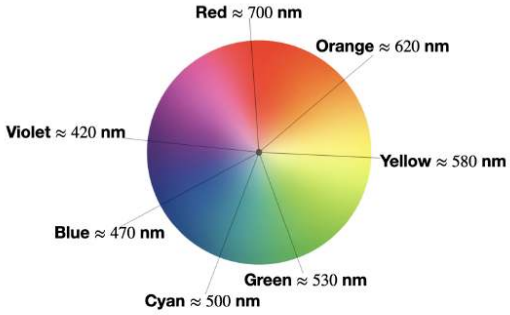


Figure **4.1.2**: Color wheel with approximate wavelengths of colors. (CC-BY-NC-SA; Kathryn Haas)

The table below lists the approximate colors of absorption corresponding to wavelengths of light absorbed, and gives similar information to that deduced from Figure **4.1.2**.

Table **4.1.1**: Approximate wavelengths of absorption and their complementary colors observed. * This prediction is limited to simple cases where there is only one absorption band in the visible spectrum.

λ absorbed	E (cm^{-1})	E (eV)	Approximate color absorbed	Predicted color observed (by eye)
> 700 nm	$< 14,000 \frac{1}{cm}$	< 1.77 eV	Infrared	not observable
$\approx 700 - 635$ nm	$\approx 14,300 - 16,000 \frac{1}{cm}$	$\approx 1.77 - 1.95$ eV	Red	Green
$\approx 635 - 590$ nm	$\approx 15,700 - 16,900 \frac{1}{cm}$	$\approx 1.95 - 2.10$ eV	Orange	Blue
$\approx 590 - 560$ nm	$\approx 16,900 - 17,900 \frac{1}{cm}$	$\approx 2.10 - 2.21$ eV	Yellow	Violet
$\approx 560 - 520$ nm	$\approx 17,900 - 19,200 \frac{1}{cm}$	$\approx 2.21 - 2.38$ eV	Green	Red
$\approx 520 - 490$ nm	$\approx 19,200 - 20,400 \frac{1}{cm}$	$\approx 2.38 - 2.53$ eV	Cyan	Red-Orange
$\approx 490 - 450$ nm	$\approx 20,400 - 22,200 \frac{1}{cm}$	$\approx 2.53 - 2.76$ eV	Blue	Orange
$400 - 450$ nm	$\approx 22,200 - 25,000 \frac{1}{cm}$	$\approx 2.76 - 3.10$ eV	Violet	Yellow
<400 nm	$> 25,000 \frac{1}{cm}$	> 3.10 eV	Ultraviolet (UV)	not observable

Energy of electronic absorption

The absorption spectrum of a metal complex can be used to calculate the splitting energy, Δ, when the absorption corresponds to a $d \rightarrow d$ transition. Let's use the d^9 Cu(II) complex (discussed above) as an example. A d^9 metal ion has only one visible-light $d \rightarrow d$ transition. Let's assume that the coordination geometry is *approximately* octahedral (although it is actually a Jahn-Teller distorted octahedron, and more like a square plane). If we assume it's octahedral, then the d-orbital splitting diagram (see Figure **4.1.1**) leads us to expect one electronic transition: an electron is excited from the t_{2g} to e_g. The energy absorbed is equal to the energy of the Δ.

Many cases are not as simple as a d^9 octahedral case because there are multiple possible electronic transitions, and also multiple absorption bands in the UV-vis spectrum. In these more complex cases, the actual energy of the transition are affected by differences in electron-electron repulsion energies in the ground state and the excited states. We will learn how to account for multiple possible excited states and electron-electron repulsions using Tanabe-Sugano diagrams later in this chapter.

This page titled 4.1: Absorption of Light is shared under a CC BY-NC-SA 4.0 license and was authored, remixed, and/or curated by Kathryn Haas.

- **11.1: Absorption of Light** by Kathryn Haas has no license indicated.

4.1.1: Beer-Lambert Absorption Law

When light passes through a solution that absorbs light, it enters the solution with an initial intensity (I_o) at a given wavelength, and it emerges with an intensity, I.

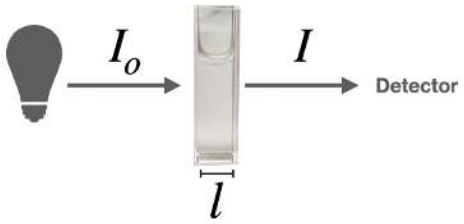


Figure **4.1.1.1**: Initial intensity (I_o) of light passes through a solution and emerges as intensity, I. The path length is l. (CC-BY; Kathryn Haas)

The Beer-Lambert Law defines the relationship between absorbance at a given wavelength and the concentration of the solution.

$$\log\left(\frac{I_o}{I}\right) = A = \varepsilon lc \tag{4.1.1.1}$$

The absorbance (A) is a unitless number because $\frac{I_o}{I}$ is unitless. The absorbance depends on the concentration (c) and the path length (l). The concentration of the sample solution is measured in molarity (M) and the length of the light path in centimeters (cm). The Greek letter epsilon (ε) in these equations is called the **molar absorptivity** (also called the **molar absorption coefficient**). The units of ε are $\frac{L}{mol \times cm}$ or $L \times mol^{-1} \times cm^{-1}$.

Chemists most often measure and report absorbed light in terms of wavelength (λ) in units of nanometers (nm). But the wavelength scale is inconvenient for measuring energy because it is inversely proportional to both frequency and energy. In other disciplines, like physics for example, absorption spectra are more often reported in terms of frequency (ν) using units of inverse centimeters (cm^{-1}). The relationships between energy (E), ν, and λ are given by the equation below:

$$E = h\nu = \frac{hc}{\lambda} = hc\left(\frac{1}{\lambda}\right) = hc\bar{\nu} \tag{4.1.1.2}$$

This page titled 4.1.1: Beer-Lambert Absorption Law is shared under a CC BY-NC-SA 4.0 license and was authored, remixed, and/or curated by Kathryn Haas.

- **11.1.1: Beer-Lambert Absorption Law** by Kathryn Haas has no license indicated.

4.2: Quantum Numbers of Multielectron Atoms

Note

The quantum numbers of atoms (and ions) correspond to quantized energy states, called microstates, that depend on the electron configuration. Electrons within a subshell or orbital can adopt different configurations of their electrons, with different individual quantum numbers. These different electron configurations are **microstates**, and they can be grouped into **terms** and ordered according to their relative energies. Since electronic transitions occur between terms of different energies, knowledge of the terms for a given atom or ion can aid in the interpretation of electronic spectra.

Introduction

Transition metal ions can give rise to a spectrum of beautifully colored colored complexes. The colors are often caused by absorption of visible light due to electronic transitions involving metal d-orbitals. These electronic transitions are not only attractive to the eye, they are useful spectroscopic signals because the transitions occur between quantized electronic energy states, called microstates. Spectroscopy, coupled with knowledge of the possible microstates and their energies can yield clues about molecular structure.

To learn what a microstate is, let's use the simple example of a carbon atom with a $1s^2 2s^2 2p^2$ electron configuration. The s subshell is full, and there is only one way to put two electrons into an s subshell. Both electrons must occupy the orbital having $m_l = 0$, and each must have opposite spins, ($m_s = +\frac{1}{2}$), and ($m_s = -\frac{1}{2}$). On the other hand, the p subshell of carbon has two electrons that can occupy any of three orbitals (Figure 4.2.1). This leaves room for different orientations of the electrons within the p subshell. Each different electron configuration is a **microstate**, and each has an energy that can be distinguished using electronic spectroscopy (UV-vis for example). In the case of a carbon atom with a two p electrons, there are 15 different possible microstates, as illustrated in Figure 4.2.1.

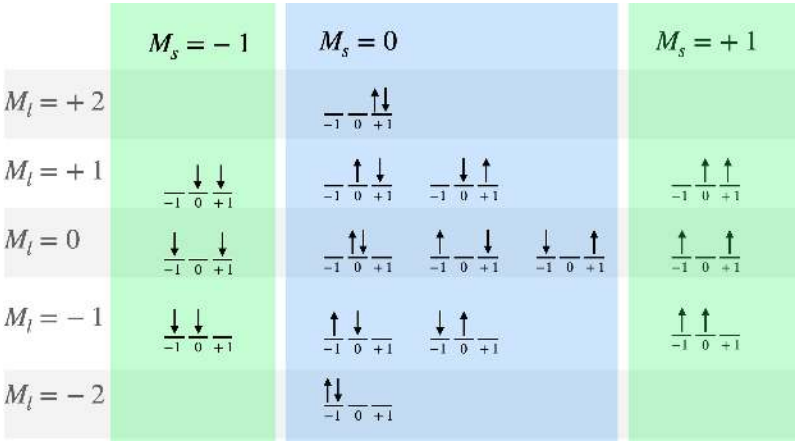


Figure 4.2.1: Fifteen possible microstates for two electrons in a p subshell. These microstates are organized according to their total spin (M_s) and total magnetic (M_l) quantum numbers. Arrows pointing upward represent electrons with $m_s = +\frac{1}{2}$, and those pointing downward represnt $m_s = -\frac{1}{2}$. Each horizontal line represents a p orbital, and m_l values are indicated under each orbital. (CC-BY-NC; Kathryn Haas)

Just as individual electrons have quantum numbers (n, l, m_l, m_s), the electronic states of atoms have quantum numbers (L, M_l, M_s, S, J). Each individual microstate in Figure 4.2.1 can be described by quantum numbers M_l and M_s. The values of total angular momentum (L), and total intrinsic spin (S) arise from sets of microstates, and are related to quantum numbers M_l and M_s for individual microstates. The relative energies of the terms for 3d metals and other light atoms can be predicted (roughly) by Hund's Rules, according to values of S and L. These atomic quantum numbers and Hund's rules are described below.

A closer look at electronic spectra

Let us take a closer look at optical absorption spectra, also called electronic spectra, of coordination compounds. We have previously argued that ligand field theory can predict and explain the electronic spectra. However, ligand field theory (LFT) is sufficient to explain the spectra in only a few cases. For example the $[Ni(H_2O)_6]^{2+}$ ion is an octahedral d^8-complex ion. According

to LFT, the metal d-orbitals in an octahedral field are the t_{2g} and the e_g–orbitals (Figure 4.2.2). Six electrons are in the t_{2g} orbitals, and two electrons are in the e_g orbitals (Figure 4.2.2). Ligand field theory (LFT) would predict that there is one electron transition possible, namely the promotion of an electron from a t_{2g} into an e_g orbital. This process would be triggered by the absorption of light whereby the wavelength of the light would depend on the Δ_o between the t_{2g} and the e_g orbitals. Overall, this should lead to a single absorption band in the absorption spectrum of the complex. We can check this prediction by experimentally recording the absorption spectrum of the complex (Figure 4.2.2).

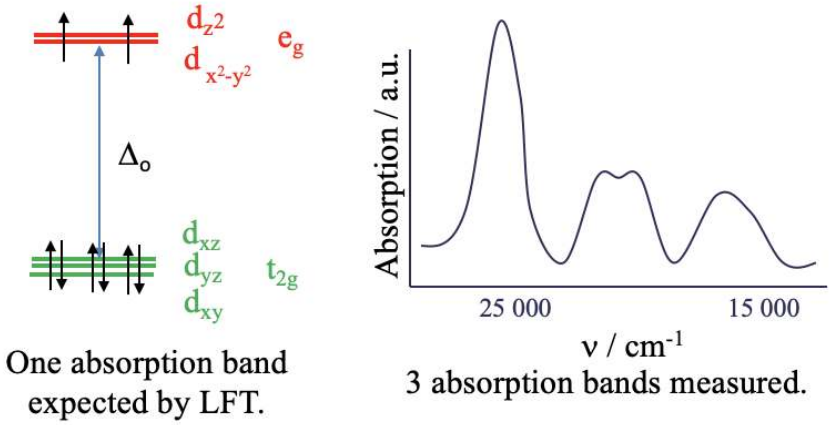


Figure 4.2.2. Electron transition according to LFT and actual absorption spectrum of the $[Ni(H_2O)_6]^{2+}$ complex ion. Attribution: E.R. Schofield.

What we find is that the absorption spectrum is far more complex than expected. Instead of just a single absorption band there are multiple ones. Obviously, LFT is unable to explain this spectrum. The question is: why? The answer is: LFT assumes that there are no electron-electron interactions. However, in reality there is repulsion between electron in d-orbitals and this has an effect on their energy. And, electrons within the d-subshell, for example, repel each other to different extents depending on the relative orientations of their orbitals in space.

To illustrate how electrons in different orbitals might have different interactions, let's consider the case of a d^2 excited state in an octahedral ligand field (Figure 4.2.3).

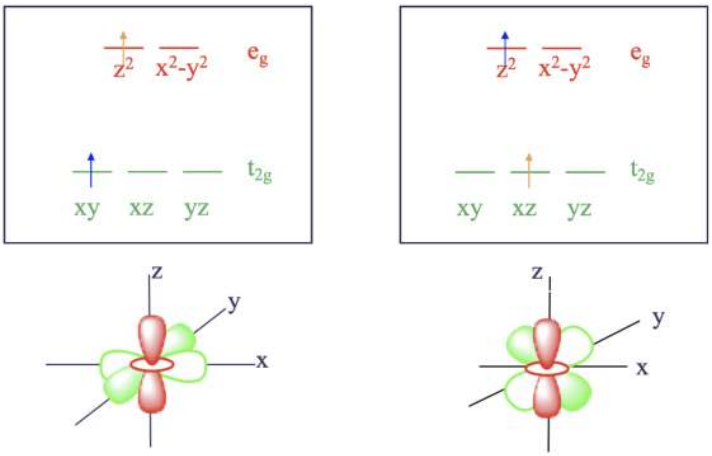


Figure 4.2.3: Two microstates with different energies for a d^2 ion in an octahedral ligand field. Electron configurations of two different microstates are shown on the top, and the orbitals associated with each shown underneath each configuration. Left: An excited microstate with one electron in the d_{xy} orbital (shown in green) and one electron in the d_{z^2} (shown in red). Right: An excited microstate with one electron in the d_{xz} orbital (shown in green) and one electron in the d_{z^2} (shown in red).

According to LFT, both electrons would be in the t_{2g} orbitals in the ground state. For instance, they could be in the microstate where one electron is in d_{xy}, and the other is in the d_{xz} orbital (not pictured). This configuration is called a microstate of a state because there are other combinations of orbitals possible. For example, the ground state would also be realized by a microstate in which the electrons were in the d_{xz} and the d_{yz} orbitals. Upon absorption of light, the electron in the d_{xy} orbital could be excited into one of the higher-energy e_g orbitals. That excited electron could occupy either the d_{z^2} or the $d_{x^2-y^2}$ orbitals. Those two possibilities

reflect two different microstates associated with the excited state. For a moment, let's assume that the excited electron goes into the d_{z^2} orbital. In this microstate one electron would be in the d_{xz} orbital and the other one in the d_{z^2} orbital (Figure **4.2.3**, right). There is another possibility for how to excite an electron from the ground state. We could assume that instead of the d_{xy} electron being promoted, the d_{xz} electron gets promoted. In this case, we would realize a microstate in which one electron in the d_{xy} orbital and the other one in the d_{z^2} orbital (Figure **4.2.3**, left).

Now let us compare the two cases shown in Figure **4.2.3**. Ligand field theory would argue that both excited microstates have the same energy. However, in fact they do not. Why? It is because the electrons in the first excited microstate interact differently than those of the second excited microstate. This difference becomes plausible when considering the orbital shapes and orientations (Figure **4.2.3**, bottom). The d_{xz} orbital has electron density on the z-axis, while the d_{xy} orbital is perpendicular to d_{z^2}. The different relative orientations of d_{xy} and d_{xz} with respect to d_{z^2} cause electrons in the d_{z^2} orbital to interact differently with an electron in a d_{xy} than in a d_{xz}. As a result, the two excited microstates do not have the same energy. In other words, to achieve either of these different excited microstates from the ground state, we need different amounts of energy. Thus, the complex would absorb light with different energies (or wavelengths). This is in contrast to what LFT predicts.

If LFT cannot predict the number of electronic transitions, then how can we correctly predict how many absorption bands we get? The answer is, we must find all possible microstates for the d^2 electron configuration and group together those with the same energy. A group of microstates with the same energy is called a **term**. *The number of electron transitions can then be predicted from the number of terms.*

Quantum Numbers

The table below summarizes the quantum numbers of atoms (individual microstates and sets of microstates). You may wish to review the quantum numbers for individual electrons and then refer to this table as you read this and the next sections. Recall the meanings of the quantum numbers for individual electrons (n, l, m_l, m_s that were described in a previous section (Section 2.2.2).

Symbol	Name	Allowed Range	Comment
L	Total Orbital Angular Momentum	$\lvert l_1 + l_2\rvert, \lvert l_1 + l_2\text{-}1\rvert, \ldots, \lvert l_1\text{-}l_2\rvert$	Total *orbital* angular momentum of a *collection of microstates*, designated as S, P, D, F..etc
S	Total Intrinsic Spin	$\lvert m_{s1} + m_{s2}\rvert, \lvert m_{s1} + m_{s2}\text{-}1\rvert, \ldots, \lvert m_{s1}\text{-}m_{s2}\rvert$	Total spin of a *collection of microstates*
M_l	Magnetic Quantum Number	$L, L-1, L-2, \ldots, -L$	Direction of total angular momentum for an individual microstate
M_s	Spin Magnetic Quantum Number	$S, S-1, S-2, \ldots -S$	Total spin of electrons for an individual microstate
J	Total Angular Momentum	$L+S, \ldots, \lvert L-S\rvert$	Total angular momentum

Quantum Numbers S and L for sets of microstates

The quantum numbers S and L represent sets of microstates. Once these values are found, they can be ordered in terms of relative energies, first according to the value of S, then L.

Total Orbital Angular Momentum Quantum Number: L

L gives the total sum of orbital angular momentum vectors in a multielectron atom. The possible values of L can be found from the values of l for individual electrons in the system. For example, in a system with two electrons with values of m_{l_1} and m_{l_2}, the possible values of L are:

$$L = \sum_i^n m_{l_i} = \lvert m_{l_1} + m_{l_2}\rvert, \lvert m_{l_1} + m_{l_2}\text{-}1\rvert, \ldots, \lvert m_{l_1}\text{-}m_{l_2}\rvert \tag{4.2.1}$$

The absolute value symbols indicate that L cannot be a negative value. The values of L correspond to different energy levels for groups of microstates. Microstates with values of $L = 0, 1, 2, 3...$ correspond to symbols $S, P, D, F...$ respectively. This is analogous to the relationship between the electron quantum number, l, and the $s, p, d, f..$ orbital subshells. However, the capital letters used for microstates do not indicate orbital or subshell assignments for the electrons.

The Total Intrinsic Spin Quantum Number: S

The sum total of the spin vectors of all of the electrons is called S. The values of S are computed from m_s in a manner very similar to how L is computed from m_l. Because S measures the magnitude of a vector, it cannot be negative. For a system with two electrons, each with spin m_{s1}, and m_{s2}, the possible values of S are given below.

$$S = \sum_{i}^{n} m_{si} = |m_{s1} + m_{s2}|, |m_{s1} + m_{s2}\text{-}1|, ..., |m_{s1}\text{-}m_{s2}| \tag{4.2.2}$$

The possible values of S fall into a series that depend on whether there are an odd or even number of electrons.

- Odd number of electrons: $S = \frac{1}{2}, \frac{3}{2}, \frac{5}{2}, ...$
- Even number of electrons: $S = 0, 1, 2, 3, ...$

Example 11.2.1 : Total Orbital Angular Momentum of Carbon

What are the possible L values for the electrons in the $1s^2 2s^2 2p^2$ configuration of carbon?

Solution

Both electrons (i.e., the 2p electrons) are $l = 1$. The possible combinations are 0, 1, and 2 corresponding to symbols S, P, and D, respectively.

Example 11.2.2 : Total Orbital Angular Momentum of Unknown Species

What are the possible L values for the electrons in the $[Xe]6s^2 4f^1 5d^1$?

Solution

We can ignore the electrons in the $[Xe]$ core and the electrons in the $6s$ block. So all we have to consider is the lone f electron ($l = 3$) and the lone d electron ($l = 2$).

The two extremes for possible L values are $3 + 2 = 5$ and $3\text{-}2 = 1$.

Thus, possible values of L for this Xe atom are 5(H), 4(G), 3(F), 2(D), and 1(P).

Example 11.2.5 : The Hydrogen Ground State

Find S for $1s^1$.

Solution

S must be $\frac{1}{2}$, since that's the spin of a single electron and there's only one electron.

Example 11.2.6 : The Beryllium Excited State

Find S for $1s^2 2s^1 2p^1$.

Solution

$S = 1, 0$

Example 11.2.7 : The Carbon Ground State

Find S for carbon atoms with the $1s^2 2s^2 2p^2$ electron configuration.

Solution

$S = 1, 0$ This is the same as the previous problem. Notice that S is not affected by which orbitals are occupied by electrons. S depends only on the number of unpaired electrons. These are usually the electrons in partially-filled subshells (i.e., unpaired electrons in open shells).

Example 11.2.8 : The Nitrogen Ground State

Find S for nitrogen atoms with the $1s^2 2s^2 2p^3$ electron configuration.

Solution

S can be $S = \frac{3}{2}, \frac{1}{2}$.

Quantum numbers M_l and M_s for individual microstates

Once S and L are found, the allowed values of M_l and M_s can be calculated.

The Total Magnetic Quantum Number: M_l

The Total Magnetic Quantum Number M_l is the total z-component of all of the relevant electrons' orbital momentum. While L describes the total angular momentum in the system, M_l tells you which direction it is pointing. L can be assigned to a collection of microstates, but M_l is unique to a specific microstate in that group. Unlike L, M_l is allowed to have negative values. The possible values of M_l are integer values ranging from the largest positive sum to the most negative sum of possible m_l values:

$$M_l = L, L-1, L-2, ..., -L \tag{4.2.3}$$

For the p^2 case, the m_l values of p orbitals are $-1, 0, +1$. The largest value of M_l would come from a state where both electrons occupy $m_l = +1$, thus the maximum is $M_l = L = 2$. Likewise, the minimum value of M_l comes from both electrons occupying $m_l = -1$ to give $M_l = -L = -2$. The possible M_l values for p^2 are the series of integer values $+2, +1, 0, -1, -2$.

It is worth noting that there are values of M_l that are forbidden due to the Pauli exclusion principle. For example, the value of $M_l = +3$ could only come from three electrons occupying the $m_l = +1$ orbital. That is impossible because more than one electron would possess the same set of electron quantum numbers.

The Total Spin Magnetic Quantum Number: M_s

M_s is the sum total of the z-components of the electrons' inherent spin in an individual microstate. The difference between S and M_s is subtle, but important. M_s indicates the total z-component of the electrons' spins, while S indicates the entire resultant vector. It is also distinct from M_l, which is the sum total of the z-component of the *orbital angular momentum*. M_s can be computed from S, as shown below. Note that while S must be positive, M_s can have negative values.

$$M_s = S, S-1, S-2, ... -S \tag{4.2.4}$$

For the p^2 case, the possible values of M_s are $M_s = +1, 0, -1$. The value $M_s = +1$ comes from the sum of two electrons with spin "up", $m_s = +\frac{1}{2}$. The value $M_s = -1$ comes from the sum of two electrons with spin "down", $m_s = -\frac{1}{2}$. And the value $M_s = 0$ comes from the sum of one electron with $m_s = +\frac{1}{2}$ and the other with $m_s = -\frac{1}{2}$.

There are some values of M_s that will be forbidden, but not in the case of p^2. However in the case of a p^4, for example, the value M_s =2 is forbidden because there is no way to put four "up" electrons in three orbitals without violating the Pauli exclusion principle.

Example 11.2.3 : Total Magnetic Quantum Number of the Zirconium Ground State

What are the possible values M_l of a zirconium atom with the $[Kr]5s^2 4d^2$ electron configuration?

Solution

Both open-shell electrons (i.e., the 4d electrons) are $l = 2$, so the values are 4, 3, 2, 1, 0, -1, -2, -3, -4.

Example 11.2.4 : Total Spin Magnetic Quantum Number of the Carbon Ground State

What are the M_s values for $1s^2 2s^2 2p^2$?

Solution

This system is paramagnetic, with two unpaired electrons in the $2p$ orbital. The three p orbitals have values of $m_s = -1, 0, 1$. The maximum value of $M_s = +1$ would come from the two electrons occupying $m_{s_1} = +1$ and $m_{s_2} = 0$. The minimum value, $M_s = -1$ would come from the two electrons occupying $m_{s_1} = -1$ and $m_{s_2} = 0$. Thus, the possible values for the total spin magnetic quantum number are $M_s = 1, 0, -1$, where the value of $M_s = 0$ comes from a configuration where, for example, $m_{s_1} = +1$ and $m_{s_2} = -1$.

Example 11.2.4 : Total Spin Magnetic Quantum Number of the Nitrogen Ground State

What are the M_s values for $1s^2 2s^2 2p^3$?

Solution

$M_s = +\frac{3}{2}, +\frac{1}{2}, -\frac{1}{2}, -\frac{3}{2}$

This page titled 4.2: Quantum Numbers of Multielectron Atoms is shared under a CC BY-NC-SA 4.0 license and was authored, remixed, and/or curated by Kathryn Haas.

- **8.8: Term Symbols Gives a Detailed Description of an Electron Configuration** by Mattanjah de Vries is licensed CC BY 4.0.
- **8.1: Microstates and Terms** by Kai Landskron is licensed CC BY 4.0.

4.2.1: Finding Microstates and Term Symbols

Constructing "Free Ion" Term Symbols and their Relative Energies

The different electronic states of an atom or ion are described by L and S in the form of a **term symbol** (Figure 4.2.1.1). Keep in mind that M_l is related to L, and M_s is related to S, and in some cases their values are equal.

One term symbol can describe one or more microstates with the same energy. The free ion terms are useful in the interpretation of electronic spectra. These term symbols are also commonly called *free ion terms (*or *Russell-Saunders terms*) because they describe the atomic or ionic state, free of any ligands. The term symbol indicates the total orbital angular momentum of the atom, (L), and the multiplicity, ($2S+1$), of the state. The multiplicity can be found with the formula, ($2S+1$), but it is also equal to the number of unpaired electrons plus one.

Misplaced '#'

The generic form of a free ion term symbol is shown in Figure 4.2.1.1. Recall that $L = 0, 1, 2, 3...$ is denoted by a capital letter $S, P, D, F...$, respectively. The latter designation for L is used in the term symbol.

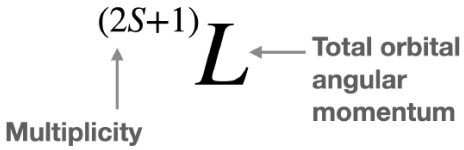


Figure 4.2.1.1: A term symbol of the free ion takes the form ${}^{(2S+1)}L$, where L is the total orbital angular momentum quantum number, and S is the total intrinsic spin quantum number. The value $2S+1$ is called the multiplicity. (CC-BY-NC; Kathryn Haas)

Example 11.2.1.1 : Hydrogen Ground State

What is the free ion term symbol of an H atom in the ground state ($1s^1$)? How many microstates are there for the ground state hydrogen atom? Comment on the degeneracy and multiplicity of the state.

Solution

There is only one electron in a s orbital. That electron must have $l = 0$, and s could be either $+\frac{1}{2}$ or $-\frac{1}{2}$. This is two possible microstates, one with spin "up" and one with spin "down". In either case there is only one value of the total intrinsic spin quantum number, $S = +\frac{1}{2}$. Therefore, the only possible value of spin multiplicity is Multiplicity $= 2 \times (+\frac{1}{2}) + 1 = 2$. The s orbital corresponds to $l = 0$, so $L = 0$, or S. Thus the term symbol is ${}^2S$.

There are two possible microstates of the ground state (both represented by the ground state term). One microstate has $m_s = +\frac{1}{2}$ and the other has $m_s = -\frac{1}{2}$.

The question about degeneracy specifically asks about degeneracy of *the state*. Let's give the most complete answer possible. In terms of energy levels (the ground state in this case), there are two microstates with approximately equal (degenerate) energy, thus the degeneracy of the state is two (2) and is the same as the multiplicity ($2S+1 = 2$). However, sometimes we also refer to the "degeneracy" of electron configurations. It is important to recognize that ground state electron configuration with $M_s = m_s = +\frac{1}{2}$ is singly degenerate, and the same is true for $M_s = m_s = -\frac{1}{2}$. Recognising degeneracy of electron configurations will be useful later in this chapter because the degeneracy of an electron configuration can be helpful for interpreting term symbols in an octahedral field.

Exercise 4.2.1.1

Find the term symbols for the following cases:

a. $L = 0,\ S = 0$
b. $L = 0,\ S = \frac{1}{2}$
c. $L = 1,\ S = 1$
d. $L = 2,\ S = \frac{3}{2}$

e. $L = 3,\ S = 2$

Answer

(a) ^1S
(b) ^2S
(c) ^3P
(d) ^4D
(e) ^5F

Finding all possible microstates for an atom or ion

What are the possible microstates and the overall number of microstates for a free ion with d^2-electron configuration? We can express this in a so-called microstate table (**4.2.1.2**).

M_s \ M_L	-4	-3	-2	-1	0	+1	+2	+3	+4
-1	Not possible (Pauli principle)	$-2^-\ -1^-$	$-2^-\ 0^-$	$-2^-\ 1^-$ $-1^-\ 0^-$	$-2^-\ 2^-$ $-1^-\ 1^-$	$-1^-\ 2^-$ $0^-\ 1^-$	$0^-\ 2^-$	1^-2^-	Not possible (Pauli principle)
0	$-2^-\ -2^+$	$-2^-\ -1^+$ $-2^+\ -1^-$	$-2^-\ 0^+$ $-2^+\ 0^-$ $-1^-\ -1^+$	$-2^-\ 1^+$ $-2^+\ 1^-$ $-1^-\ 0^+$ $-1^+\ 0^-$	$-2^-\ 2^+$ $-2^+\ 2^-$ $-1^-\ 1^+$ $-1^+\ 1^-$ $0^-\ 0^+$	$-1^-\ 2^+$ $-1^+\ 2^-$ $0^-\ 1^+$ $0^+\ 1^-$	$0^-\ 2^+$ $0^+\ 2^-$ $1^-\ 1^+$	1^-2^+ 1^+2^-	$2^-\ 2^+$
+1	Not possible (Pauli principle)	$-2^+\ -1^+$	$-2^+\ 0^+$	$-2^+\ 1^+$ $-1^+\ 0^+$	$-2^+\ 2^+$ $-1^+\ 1^+$	$-1^+\ 2^+$ $0^+\ 1^+$	$0^+\ 2^+$	1^+2^+	Not possible (Pauli principle)

Figure **4.2.1.2**. d^2 electron configuration microstate table. This table is organized with M_l values increasing horizontally and M_s values decreasing vertically. You may see different ways to organize a microstate table, and there is no wrong orientation to use, as long as you can use it to correctly find and organize microstates. Each microstate is indicating using notion $(m_l)^{m_s}$, where only the sign of m_s is indicated for simplicity. For example, an electron in $m_l = -2$ with $m_s = +\frac{1}{2}$ is notated -2^+.

You can see the microstate table for the d^2 electron configuration depicted above. Each column represents a possible value M_l. For the d^2 configuration, M_l can adopt values from -4 to +4, hence there there are 9 columns. Each row represents possible M_s value. For the d^2 electron configuration, M_s can vary between +1 and -1. $M_s = +1$ means both electrons have the spin $+\frac{1}{2}$, $M_s = 0$ means one electron has the spin $+\frac{1}{2}$ and the other one has the spin $-\frac{1}{2}$. The $M_s = -1$ value is adopted when both electrons have the spin $-\frac{1}{2}$. Now we can combine each M_s value with each M_l value, which defines a particular field in the table. You can see that some fields are empty due to the Pauli principle. For example, the field for $M_l = -4$ and $M_s = -1$ is not filled because in this case both electrons would have the same quantum numbers, namely $m_l = 2$, and $m_s = -\frac{1}{2}$. We can further see that for some fields only one combination of electrons is possible, while for others there are multiple possible microstates. For example, for the field with $M_l = 4$ and $M_s = 0$ there is only one combination of electrons possible. You can see the notation "2^-2^+" in this field. This means that the first electron has an m_l value of 2 and a spin of $-\frac{1}{2}$ and the second electron also has an m_l value of 2 and an m_s value of $+\frac{1}{2}$. The most populated field is the field for $M_l = 0$ and $M_s = 0$; there are overall five microstates with that combination of M_l and M_s values. If we count the overall number of microstates in the table then we arrive at the number 45. This is consistent with what we would expect according to the following formula.

Misplaced '#'

In our example L=4 and S = 1, and thus the number of microstates is: $((2x4) + 1)((2x1) + 1) = 45$. **In general for a d^n electron configuration with n d-electrons, the number of microstates is** $(10!)/((10 - n)!n!)$**.**

One useful property of a microstate table is that we can derive all possible terms and term symbols for a particular electron configuration from it. For simplification's sake, we indicate a possible microstate in the table in Figure **4.2.1.5** just by an "x". Then we draw the largest possible rectangular box into the microstate table that contains only fields with at least one possible electron combination (Figure **4.2.1.5**).

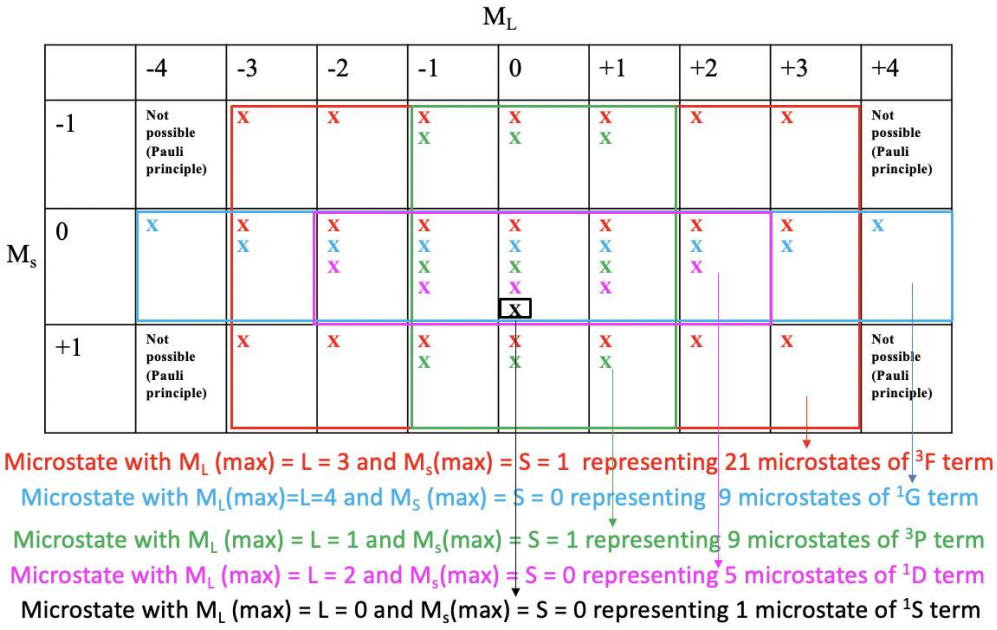


Figure **4.2.1.5**. Deriving the terms and term symbols for the d^2 electron configuration from the microstate table

You can see that the largest possible box is the red box drawn (Figure **4.2.1.5**). This box contains the microstates that belong to the first term of the electron configuration d^2. The number of microstates is equal to the number of fields within the red box. That makes $7 \times 3 = 21$ microstates. What is the term symbol for this term? In order to answer this question we need to find the microstate in the red box that has the highest M_l and the highest M_s value. You can see that it is the one with $M_l = 3$ and $M_s = 2$. Thus, L=3 and S=1. This defines the term as a ^{3}F term because 2S+1 = 3, and L=3 corresponds to the term symbol F. This term is a triplet term. Note that a triplet term also includes microstates with opposite spins. Overall seven of the 21 microstates have $M_s = 0$.

Next, we look what is the next-largest rectangular box we can draw, and which contains microstates we did not consider yet. We can see that the blue box contains nine fields equaling nine microstates. The microstate within this box that has the highest M_l and M_s values is the one with $M_l = 4$ and $M_s = 0$. This defines a ^{1}G term. This is a singlet term. Note that a singlet term ONLY has microstates with paired spins (M_s=0).

There is another rectangular box which also contains nine microstates. It is the green one. The microstate with the highest M_l and M_s values is the one with $M_l = 1$ and $M_s = 1$. Thus, $L = 1$, and $2S + 1 = 3$, which defines a ^3P term. Note that despite this being a triplet term, which indicates two unpaired electrons (\S=1\), the term also contains three microstates that have opposite spins with a total $M_s = 0$.

The next-largest box is the purple one containing five fields and five microstates. What is the term with the highest M_l and M_s values? It is the one with $M_l = 2$ and $M_s = 0$. This means that L=2 and S=0, which defines a ^{1}D term, a singlet term with only microstates with paired spins. There is one microstate left that we did not consider thus far, the one with $M_l = 0$ and $M_s = 0$. These are the highest M_l and M_s values because there is no other microstate. Thus, this term contains only one microstate and the term symbol is ^1S. Now we have found all the terms and term symbols.

✔ Example 11.2.1.2 : Boron

What are the possible term symbols for $1s^2 2s^2 2p^1$ electronic configuration of boron? Which is the ground state?

Solution

We only need to consider the one electron in the $2p$ orbital, since that is the only open shell electron. For one electron, there is only one value of $S = ½$, so multiplicity must be $2S + 1 = 2$. The possible values of L for one electron in a p orbital are $L = 0, 1$ (or S, and P terms). This gives the free ion term symbols ^2P and ^2S. Both of these terms have multiplicity of 2, so the ground state would be the one with the highest value for L. The ground state term is ^2P.

Example 11.2.1.3 : Beryllium Excited State

What are the term symbols for the $1s^2 2s^1 2p^1$ excited-state electronic configuration of Beryllium?

Solution

The term symbols will be of the form ^1P and ^3P. For the ^1P state, $L = 1$ and $S = 0$, so the total angular momentum $J = 1$. For the second state, $L = 1$ and $S = 1$, so the possible values of $J = 2, 1, 0$. There are four microstates for this configuration with term symbols of $^1P_1$ and $^3P_2$, $^3P_1$, and $^3P_0$.

Finding The Ground State Term

...from a list of microstates

Each term symbol represents an atomic state with an associated energy level. If you have found all the possible microstates using a microstate table, and have identified their terms, then the term with the lowest energy (ie the ground state) can be found using Hund's first two rules. In abbreviated form, Hund's rules state...

1. The lowest energy electron configuration has the maximum multiplicity (the maximum number of unpaired electrons).
2. For a given multiplicity, the configuration with the largest total orbital angular momentum (L) value has the lowest energy.

In the case of the p^2 carbon atom (see Figure 4.2.1.1), the lowest energy state would have a multiplicity of 3 (two unpaired electrons). Of the states with a multiplicity of 3, the largest value of L is 1 (and thus, P). Thus, the ground state term for carbon is ^3P. These rules are reliable for identifying the ground state term for any atom, but have limited use for ordering relative energies outside of the ground state for 3d metal ions and other light atoms. For heavier atoms (e.g., 4d metals) another type of interaction, called jj coupling must be considered, but this is outside the scope of this discussion. **Tip:** There is a deep symmetry that connects different electronic configurations. It turns out that a p^1 configuration has the same term symbols as a p^5. Similarly, $p^2 = p^4$. A similar relationship can be used to figure out high electron number term symbols for the d and f orbitals.

...if you just want the find Ground State term

To assign transitions in an electronic spectrum, we should know the ground state term, as well as all other terms and their relative energies for a given atom or ion. However, the identification of all possible terms becomes tedious with more than one or two electrons in the d orbitals. Fortunately, there are tools (like correlation diagrams) that can help us find all terms for an atom or ion, as long as the ground state term can be identified. Here is a quick shortcut for finding the ground state term for transition metal complex with partially-filled d shell.

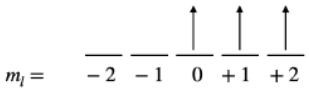
Quickly find the ground state free ion tern

In this case, we'll focus on transition metal d-orbitals. To begin, you'll need to know the metal ion identity and its oxidation state. These instructions assume that the d orbital is the only shell that is partially filled.

1. Determine the number of d-electrons.
2. Then fill these electrons into an electron orbital diagram of five degenerate orbitals, putting electrons into the highest value of m_l first, and filling orbitals with single electrons before pairing them (just as you may have done in an introductory chemistry course).
3. Calcuate the total intrinsic spin (\S\) and spin multiplicity using the diagram drawn in #2.
4. Calculate L using the diagram drawn from #2.
5. Write the term symbol for the ground state.

Let's use the example of the $[Cr(NH_3)_6]^{3+}$ complex ion, and determine its ground state term following the shortcut described above.

1. Determine the number of d-electrons.
   $[Cr(NH_3)_6]^{3+}$ contains Cr^{3+}, which is a d^3 metal ion. There are three d electrons.
2. Draw a diagram of five degenerate d orbitals, with m_l values labeled. Fill in the electrons to maximize m_s and m_l.



3. Calculate spin multiplicity (should be the maximum possible value!).
   $S = m_{s_1} + m_{s_2} + m_{s_3} = +\frac{1}{2} + +\frac{1}{2} + +\frac{1}{2} = \frac{3}{2}$
   Spin multiplicity = $2S + 1 = 2\frac{3}{2} + 1 = 4$
4. Calculate L (should be the maximum possible value after spin is maximized.
   $L = m_{l_1} + m_{l_2} + m_{l_3} = 2 + 1 + 0 = 3$
5. Write the ground state free ion term:
   ${}^{(2S+1)}L = {}^4F$

? Exercise 4.2.1.2

Earlier on this page, you found all the terms for a d^2 metal ion. Use both of the methods (Hund's rule, and the shortcut method) described here to identify the ground state term for d^2.

Answer

Using Hund's rule: The terms identified for d^2 are ${}^3F$, ${}^1G$, ${}^3P$, ${}^1D$, and ${}^1S$. Hund's first rule tells us that either ${}^3F$ or ${}^3P$ could be the ground state because these two terms have the highest multiplicity. Hund's second rule tells us that ${}^3F$ must be the ground state because it has the largest value of L.

Using the shortcut: The drawing is shown below, with one electron in $m_l = +2$ and the second electron in $m_l = +1$. Both electrons are unpaired with $m_s = +\frac{1}{2}$. This gives $L = 3$ or an F term. And, $S = 1$ with a multiplicity of 3. The ground state term is ${}^3F$.

? Exercise 4.2.1.3

Find the ground state free ion terms for the metal ions in the following cases:

(a) $[Ti(H_2O)_6]Cl_2$

(b) $[Ti(NH_3)_6]Cl_3$

(c) $[Cu(H_2O)_6]Cl_2$

Answer

(a) Ti^{2+} is a d^2 metal ion, ${}^3F$

(b) Ti^{3+} is a d^1 metal ion, ${}^2D$

(c) Cu^{1+} is a d^9 metal ion, ${}^2D$. Note that d^9 and d^1 are related by the symmetry of their electronic states.

This page titled 4.2.1: Finding Microstates and Term Symbols is shared under a CC BY-NC-SA 4.0 license and was authored, remixed, and/or curated by Kathryn Haas.

- **8.8: Term Symbols Gives a Detailed Description of an Electron Configuration** by Mattanjah de Vries is licensed CC BY 4.0.
- **8.1: Microstates and Terms** by Kai Landskron is licensed CC BY 4.0.

4.2.2: Spin-Orbit Coupling

The magnetic fields created by S and L are not isolated from one another; they interact through **spin-orbit coupling** *(aka Russell-Saunders coupling)*. We will consider only this simple form of coupling in this text. Its application is limited to the elements with $z < 40$, including the first row of the transition elements. In the case of heavier elements, we must also consider jj coupling; however, we will not discuss the latter here.

In the Russell-Saunders spin-orbit coupling scheme, the interaction between S and L is expressed by an additional quantum number, the total angular momentum quantum number (J). The possible values of J are values between $L+S$ and $|L-S|$.

$$J = L+S,\ L+S-1,\ L+S-2,\ ...,\ |L-S| \tag{4.2.2.1}$$

A value of J must be positive or zero for a multielectron system. J values can fall into series $\frac{1}{2}, \frac{3}{2}, \frac{5}{2}, ...$ or $0, 1, 2, ...$ The quantum number J is added to the term symbol as a subscript to the right of the letter describing the term. A full term symbol is as follows:

$$^{(2S+1)}L_J \tag{4.2.2.2}$$

The result of spin-orbit coupling is that a term for the free ion is split into states of different energies. For example, a ^3P state of a carbon atom with a p^2 electron configuration would be split into three different energy states (according to the three possible J values 0, 1, and 2): $^3P_0, ^3P_1, ^3P_2$.

The relative energies of the states can be predicted from Hund's Third Rule.

Hund's third Rule:

- For subshells that are less than half-filled, the lowest energy state has the lowest J value.
- For subshells that are exactly half-filled, there is only one J value, thus it is the lowest energy.
- For subshells that are more than half-filled, the lowest energy state has the largest J value.

Thus, in this case where the p subshell is less than half full, the lowest energy state from the ^3P free ion term would be that with $J = 0$, $^3P_0$, followed by $J = 1$ and $J = 2$. The splitting and relative energies are depicted in Figure 4.2.2.1. Spin-orbit coupling and the splitting of the free ion terms have important implications for electronic spectra because they affect the energies of electronic transitions.

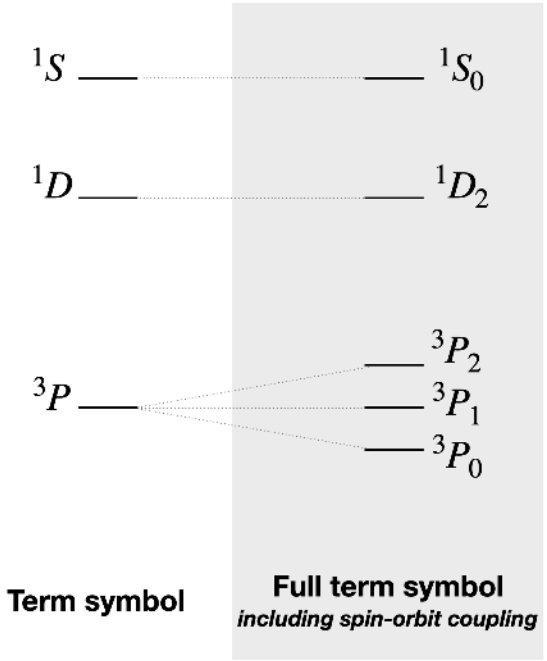


Figure 4.2.2.1: The effects of spin-orbit (Russell-Sauders) coupling on the "free ion" term symbols for. Energy splitting not shown to scale. (CC-BY-NC; Kathryn Haas)

4.2.2: Spin-Orbit Coupling is shared under a CC BY-NC-SA 4.0 license and was authored, remixed, and/or curated by LibreTexts.

- **8.1: Microstates and Terms** by Kai Landskron is licensed CC BY 4.0.
- **11.2.2: Spin-Orbit Coupling** has no license indicated.

SECTION OVERVIEW

4.3: Electronic Spectra of Coordination Compounds

Types of transitions related to the metal ion:

1. **d-d transitions**: d-d transitions are electronic transitions that occur between the molecular orbitals (MOs) that are mostly metal in character: specifically, the orbitals that we think of as the d-orbitals of a transition metal complex. These transitions are useful in determining the energy of splitting and can be used to indicate coordination chemistry (geometry and ligand sets). In octahedral complexes, d-d transitions occur between the t_{2g} and e_g orbitals (across Δ). These transitions cannot occur in metal complexes where the d-orbital is completely empty (d^0) or completely full (d^{10}). In other words, a d-d transition is only possible in $d^1 - d^9$ metal ions. In a UV-visible absorption spectrum, d-d transitions appear as relatively weak absorptions with extinction coefficients (ε) less than 1,000.
2. **Charge transfer (CT) transitions**: Charge transfer transitions occur between MOs that are mostly metal in character and those that are mostly ligand in character. These transitions depend on the type of ligand: they occur only when the metal is bound to ligands that are π-donors or π-acceptors. And there are two types of CT transitions. If the metal is bound to a π-donor ligand, electrons from lower-energy MO's that are mostly ligand in character can become excited to MO's that are mostly metal in character. These are **ligand to metal charge transfers (LMCT) transitions** (Figure **4.3.1**, left diagram). If the the metal is bound to ligands that are π-acceptors, electrons from the MO's that are mostly metal in character can become excited to higher-energy orbitals that are mostly ligand in character. These are **metal to ligand charge transfer (MLCT)** transitions (Figure **4.3.1**, right diagram). In a UV-visible absorption spectrum, CT transitions appear as relatively intense absorptions with extinction coefficients (ε) much greater than 1,000.

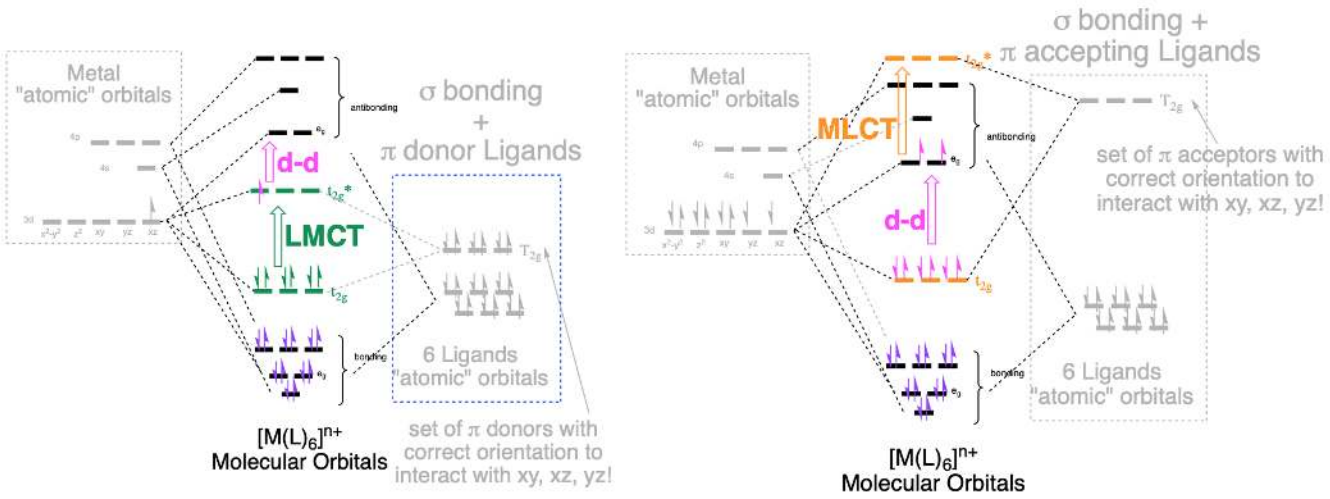


Figure **4.3.1**: Abbreviated and annotated MO diagrams for example cases of metal ions in octahdral geometry with sets of π-donor and π-acceptor lignads. In both example MO diagrams, d-d transitions are shown (pink, open arrow from t_{2g} to e_g). **Left:** LMCT transitions are possible with π-donor ligands when electrons are excited from MOs that are mostly ligand in character to MOs that are mostly metal in character. An example of LMCT is shown (green, open arrow from t_{2g} to $t*_{2g}$). **Right:** MLCT transitions are possible with π-acceptor ligands when electrons from MOs that are mostly metal in character are excited to orbitals that are mostly ligand in character (the π^* orbitals from ligands). An example MLCT is shown ((orange, open arrow from e_g to $t*_{2g}$).

4.3.1: Symmetry labels for split terms

4.3.2: Correlation Diagrams

4.3.3: Tanabe-Sugano Diagrams

4.3.4: Applications of Tanabe-Sugano Diagrams

4.3.5: Tetrahedral Complexes

4.3.6: Selection Rules

4.3.7: Charge-Transfer Spectra

4.3.8: Applications of Charge-Transfer

This page titled 4.3: Electronic Spectra of Coordination Compounds is shared under a CC BY-NC-SA 4.0 license and was authored, remixed, and/or curated by Kathryn Haas.

4.3.1: Symmetry labels for split terms

While the free ion terms symbols are derived using Russell-Saunders terms, we only briefly discussed how the term symbols may be found from a character table upon ligand-field splitting. The symmetry labels (called Mulliken Labels) that are used in character tables to describe the symmetry of wavefunctions were described in a previous section (Section 4.3.3). Just as orbitals are wavefunctions that are described by the irreducible representations that are part of a character table, so are the terms. When we are discussing the terms of an octahedral complex, we can apply what we already know about octahedral symmetry and symmetry labels to understand how the terms labels are assigned.

Upon close inspection of any of the Tanabe-Sugano diagrams shown previously, or in the Resources Section, you may notice that each free ion term (listed at the right of the diagram) splits into a term or set of terms that retain the same multiplicity (the left superscript). Under an octahedral field, all terms have symbols A, B, E or T because they are singly, doubly, or triply degenerate. While some of these terms have subscripts "1" or "2", all the terms also have "g" subscripts due to the symmetry of the d orbitals. Some of the symbols might also look familiar, as they are similar to the labels you know for splitting of d orbitals, like E_g and T_{2g}.

It is useful to know that under an octahedral field, the D, F, G, H, I terms split, but the terms S, P do not split. From inspection of the O_h character table, we find that free ion terms will split as follows:

Free Ion Term	Terms under O_h
S	A_{1g}
P	T_{1g}
D	$T_{2g} + E_g$
F	$A_{2g} + T_{2g} + T_{1g}$
G	$A_{1g} + E_g + T_{2g} + T_{1g}$
H	$E_g + T_{1g} + T_{1g} + T_{2g}$
I	$A_{1g} + A_{2g} + E_g + T_{1g} + T_{2g} + T_{2g}$

The term symbols under an octahedral field have symmetry that matches symmetry of other elements within the molecule, including the d-orbitals. A reminder of their symmetry meanings is below (see also Section 4.3.3).

Review of Mulliken Labels

Each wavefunction (including terms) can be described by a Mulliken label (symmetry label). The labels used for terms in an octahedral ligand field are listed in the table below.

Mulliken Labels	meaning
A or B	singly degenerate
E	doubly degenerate
T	triply degenerate
Subscripts	**meaning**
1	symmetric to σ_v or perpendicular C_2
2	anti-symmetric to σ_v or perpendicular C_2
g	symmetric to inversion center
u	anti-symmetric to inversion center

We can use our knowledge of symmetry to derive the term labels for a given electron configuration under an octahedral field. Let's focus only on the capital letter that is assigned as the term symbol. Assignment of the octahedral term subscripts will not be described here, but are similar to assignment of these same subscripts to orbitals with matching symmetry.

For example, the d^1 electron configuration has a free ion ground state term of ^2D. According to the table shown above, these terms will split into E_g and T_{2g} terms. Which would be its ground state term under an octahedral field? And which is the excited state term? To answer these questions we need to look at the electron configurations of the ground and excited states in an octahedral field. It is convenient to know that the term symbol under an octahedral field indicates the *degeneracies of the related electron configurations*.

Let's take a look at the electron configurations of the split d-orbitals to determine which term is the ground state. In the ground state of a d^1 under an octahedral ligand field, there would be one electron in the t_{2g} orbitals, thus the electron configuration is $t_{2g}^1 e_g^0$. For simplicity we can consider only the cases where m_s values are $+\frac{1}{2}$. There are three ways to put the electron in t_{2g} therefore, the ground state is triply degenerate, with a symbol "T". This is illustrated in the left panel of Figure 4.3.1.1.

In the excited state of a d^1 under an octahedral ligand field, there would be one electron in the e_g orbitals, or a configuration of $t_{2g}{}^0 e_g^1$. There are two ways to arrange the electron with $m_s = +\frac{1}{2}$ in the e_g orbitals (Figure 4.3.1.1, left). Therefore, the excited state is doubly degenerate, with a symbol "E".

In summary, the ^2D free ion term for d^1 splits into a lower-energy $^2T_{2g}$ and a higher-energy ^2E_g term under an octahedral field (Figure 4.3.1.1, left).

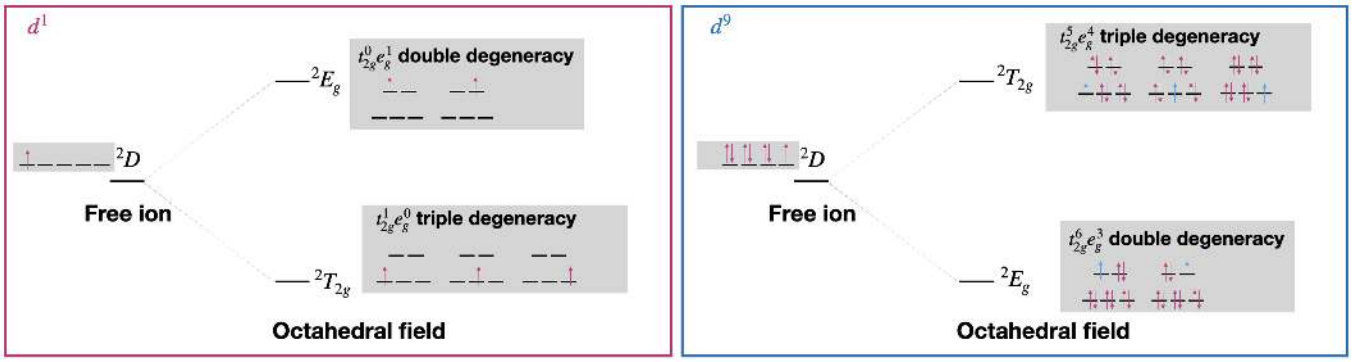


Figure 4.3.1.1: Term splitting of d^1 and d^9 free ion terms in an octahedral field. The symbols of the octahedral terms match the degeneracies of the electron configurations. (CC-BY-SA; Kathryn Haas)

We could use a similar treatment to derive the relative energies and terms of a d^9 ion in an octahedral field. The ground state term of d^9 is the same as for d^1: it is ^2D. If we look at the ground state and excited state electron configurations of a d^9 ion, we find that the ground state configuration is $t_{2g}^6 e_g^3$, which is doubly degenerate. On the other hand, the excited state has an electron configuration of $t_{2g}^5 e_g^4$, and has triple degeneracy. In summary, in the case of d^9, the ^2D free ion term splits into a lower energy ^2E_g term and a higher-energy $^2T_{2g}$ term. *This is exactly the opposite of d^1!*

The d^1 and d^9 cases are opposite because they are related by what is said to be a "positive hole" concept. The d^9 configuration could be derived from a d^{10} configuration with one positive "hole" (an electron removed). The positive hole is similar to the lone electron in d^1 except that in the ground state, the hole is in e_g, while the electron in d^1 is in t_{2g}; thus the two situations are exact opposites.

Just as d^1 and d^9 are related by the hole concept, so are d^4 and d^6. If you consider that d^1 is the addition of one electron to the totally symmetric d^0 case, then perhaps you can see how d^6 is similar in that it is the addition of one electron to the totally symmetric d^5 case. Thus, d^1 and d^6 have similar splittings under the octahedral field. Similarly, d^9 is created by removing one electron from the totally symmetric case of d^{10} and d^4 is created by removing one electron from d^5. Thus d^4 and d^9 have identical splittings for their ground state free ion terms, which in these cases are a D term.

Due to the relationships between d^1, d^4, d^6, and d^9, the same Orgel Diagram is used to show term splitting for these cases (Figure 4.3.1.2). Orgel diagrams are yet another form of correlation diagrams.

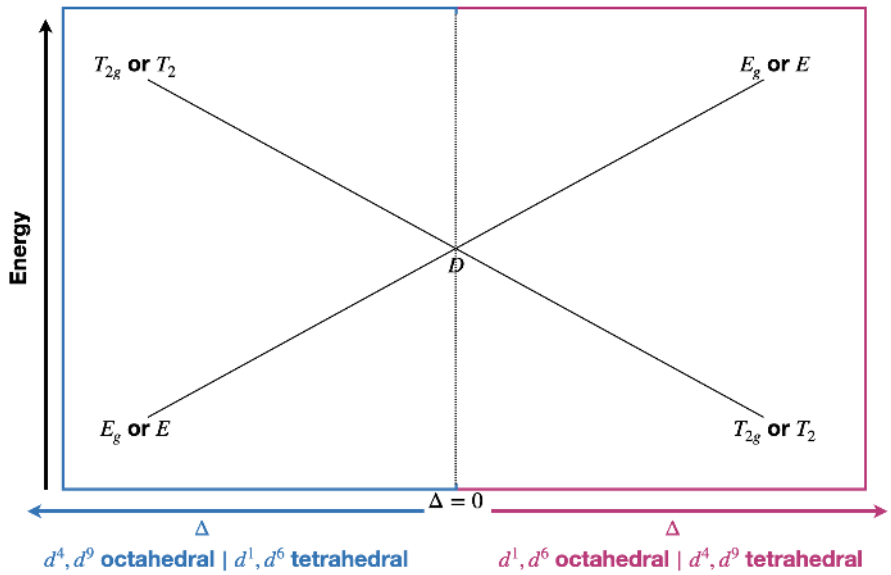


Figure **4.3.1.2**: Orgel diagram for splitting of the ground state ***D*** term of d^1, d^4, d^6, and d^9 ions in an tetrahedral or octahedral field. (CC-BY-SA; Kathryn Haas)

Just as there are relationships between d^1, d^4, d^6, and d^9, there are similar relationships between d^2, d^3, d^7, and d^8, and there is an Orgel diagram that can represent the splitting of their relevant free-ion terms.

Tetrahedral splitting

Because tetrahedral field splitting has the opposite pattern to octahedral field splitting of the d-orbitals, there are relationships between tetrahedral and octahedral terms. In general, for a tetrahedral field with d^n electrons, the Tanabe-Sugano diagram of an octahedral diagram for d^{10-n} can be used to interpret the tetrahedral case. The Orgel diagrams are labeled in general terms for this reason. They can be applied to both tetrahedral and octahedral cases.

Jahn-Teller distortions

We can also see what would happen to the terms in the case of Jahn-Teller distortion. In the case of a Jahn-Teller distortion (most common for d^9 and high-spin d^4 where the e_g orbitals are asymmetrically occupied), we can use the degeneracy of orbital electron configurations to identify term labels. Let's walk through an example using the most simple case: a d^1 metal ion (Figure **4.3.1.3**).

Jahn-teller usually causes a tetragonal distortion of an octahedron. This would be a change from O_h to D_{4h} symmetry.

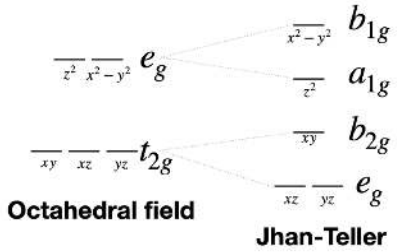


Figure **4.3.1.3**: Splitting of d-orbitals from O_h to D_{4h} symmetry by Jahn-Teller distortion. (CC-BY-SA; Kathryn Haas)

The t_{2g} orbitals (the set d_{xy}, d_{xz}, d_{yz} are split into e_g (d_{xz}, d_{yz}) and b_{2g} (d_{xy}) by this symmetry change. Thus, we can expect any T_{2g} terms to be split similarly into E_g and B_{2g} terms by Jahn-Teller distortion. The e_g orbitals under O_h are split into a_1g (d^{z^2}) and b_1g ($d_{x^2-y^2}$) under D_{4h}. Thus, we can expect E_g terms to be split into B_{1g} and A_{1g} terms by Jahn-Teller distortion (Figure **4.3.1.4**).

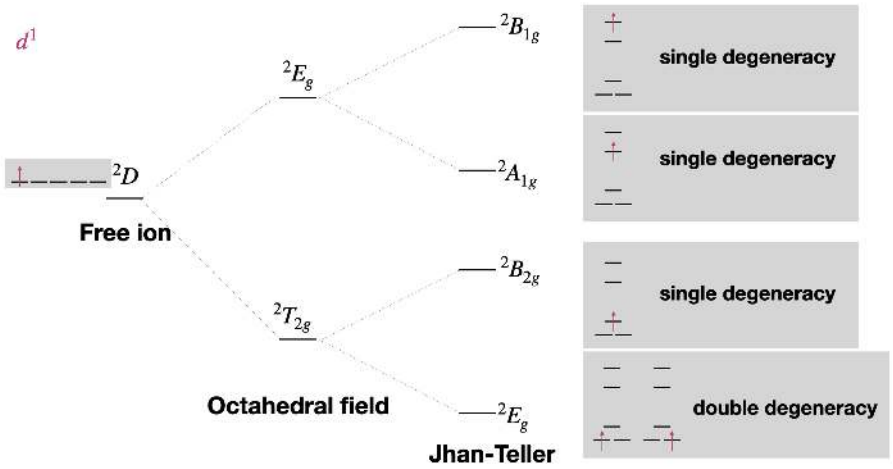


Figure **4.3.1.4**: Splitting of d^1 from an octahedral field to D_{4h} by Jhan-Teller tetragonal distortion. (CC-BY-SA; Kathryn Haas)

Just as d^1 and d^9 gave opposite order of their terms under an octahedral field, they also give opposite order of terms in the Jahn-Teller distortion.

This page titled 4.3.1: Symmetry labels for split terms is shared under a CC BY-NC-SA 4.0 license and was authored, remixed, and/or curated by Kathryn Haas.

- **4.3.3: Character Tables** by Kathryn Haas is licensed CC BY-NC-SA 4.0.

4.3.2: Correlation Diagrams

Splitting of Terms in an Octahedral Field

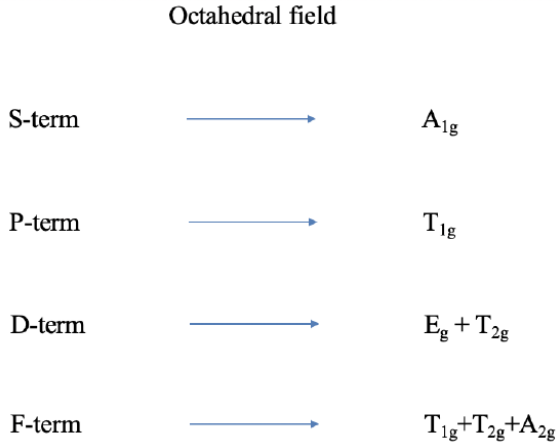


Figure 4.3.2.1: Octahedral field term splitting

Thus far we have only considered free ion terms, which means terms without the presence of a ligand field. Let us think next about the influence of an octahedral field on a term. Terms are wavefunctions, just like orbitals, and therefore they behave like orbitals in a ligand field. For example, the d-orbitals split into $t_{2g}$and e_g orbitals in an octahedral ligand field. A D-term behaves similarly. It splits into T_{2g} and E_g terms (note the capital letters that describe term, and the lower-case letters that describe orbitals!). \The p-orbitals are triple-degenerate, having T_{1g} symmetry in the O_h (octahedral) point group, and do not split in energy: they give the t_{1g} orbitals under an octahedral field. Similarly, the P-terms have the same symmetry and also do not split. The P-term becomes a T_{1g} term in an octahedral field.

Following analogous arguments, S terms become A_{1g} terms. F terms do split in energy like f-orbitals and become T_{1g}, T_{2g}, and A_{2g} terms. Overall, the presence of the octahedral field increases the number of terms from four to seven (Figure 4.3.2.1). It is easy to see that the ligand field leads to many states, and many potential electron transitions. Thus, we would expect quite complicated spectra. For other ligand fields, the terms also behave analogously to orbitals. For, instance in a tetrahedral field D-terms split into E and T_2 terms, and so forth.

Term Splitting for octahedral d^2 metal complexes

Now let us think about how the term energies of our free d^2-ion changes when placed in an octahedral ligand field, depending on the ligand field strength. We can express this by a correlation diagram (Figure 4.3.2.2). In a correlation diagram, we plot the energies of the terms relative to the field strength.

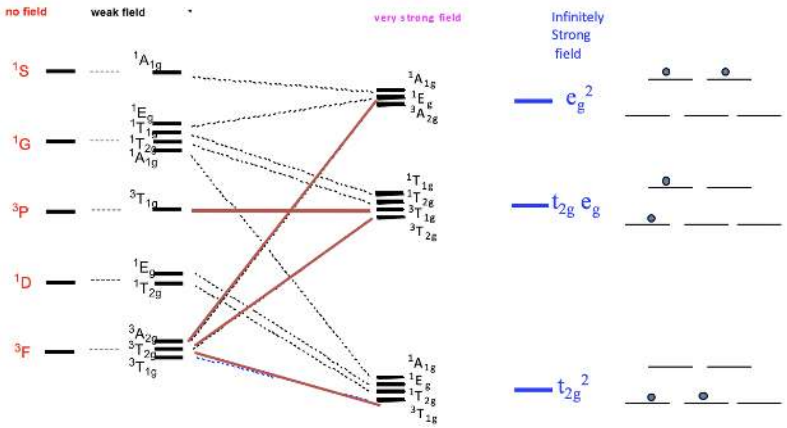


Figure 4.3.2.2: Correlation diagram

On the left side we plot the terms without any field according to their energies. In the case of a d^2 ion, the energies are

$$^3F < ^1D < ^3P < ^1G < ^1S.$$

Next, we plot the relative energies in a weak octahedral ligand field, and label the terms according to their symmetry. We can see that the D, F, and G terms split in energy, while the S and P terms do not. Because of the weak field, energy differences are very small. Now let us increase the ligand field strength continuously, until we have reached a very strong ligand field. We see that some of the terms move up in energy, while other terms move down as the ligand field increases. For example, two of the three terms resulting from the F-terms increase in energy while one decreases. It is also possible that a term does not change its energy. For example, the $^3T_{1g}$ term from the ^3P term does not change its energy. In very strong ligand field there are three groups of terms that have similar energy. In the hypothetical case of an infinitely strong ligand field, the terms that belong to a particular group become identical in energy. In this case, there are only three states for the electrons possible. The field is considered so strong that the energy associated with electron-electron interactions become negligible compared to the energy of the field. The electrons behave as though there were no electron-electron interactions. Therefore, we can call the lowest energy state the t_{2g}^2 state. It is equivalent to the state of the two electrons being in the t_{2g} orbitals. The second state is called the $t_{2g}e_g$ state. It is equivalent to the state of one electron being in the t_{2g} and one electron being in the e_g orbitals. The third state is called the e_g^2 state, which is equivalent to the state with both electrons in the e_g^2-orbitals.

This page titled 4.3.2: Correlation Diagrams is shared under a CC BY-NC-SA 4.0 license and was authored, remixed, and/or curated by Kai Landskron.

- **8.2: Term splitting in ligand fields, selection rules, Tanabe-Sugano diagrams. Metal to ligand, and ligand to metal transitions** by Kai Landskron is licensed CC BY 4.0.

4.3.3: Tanabe-Sugano Diagrams

Tanabe-Sugano diagrams are modified forms of correlation diagrams. The modification is simply that the energies of terms are plotted in terms of transition energy and Δ divided by a constant, B, called the Racha parameter. Terms are plotted relative to the lowest-energy term; in other words, the ground state term is plotted as the horizontal axis (x-axis). The Tanabe-Sugano diagram of a d^2 transition metal complex is shown below in Figure **4.3.3.1**. Tanabe-Sugano diagrams for other d-electron counts are available in the Reference Section of LibreTexts.

Tanabe-Sugano diagram of a d^2 octahedral complex

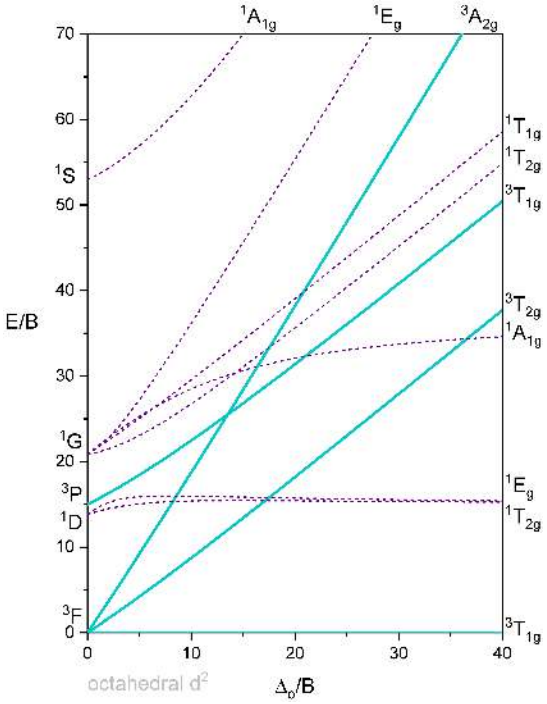


Figure **4.3.3.2**: d^3: Tanabe-Sugano Diagram for octahedral metal complex with two d electrons. For convenience, terms that can accommodate spin-allowed transitions from the ground state are indicated by solid lines. Terms that have different multiplicity than the ground state are shown in dashed lines. (CC-BY-SA; Kathryn Haas)

The difference between the diagram shown in Figure **4.3.3.1** and the previously-discussed correlation diagram for a d^2 metal ion is that the energy of the ground state is plotted horizontally, and the energy of all other terms are plotted relative to that. In the case of the d^2 electron configuration, the $^3T_{1g}$ term is the ground term and is plotted as a horizontal line. We can see that the ligand field strength on the x-axis is given in units of B (specifically as $\frac{\Delta}{B}$), and the energy of the terms is also given in units of B (specifically $\frac{E}{B}$. B is a so-called Racah parameter, which is a quantum-mechanical energy unit for the electromagnetic interactions between the electrons. It is chosen because it provides “handy” numbers.

You can see that some lines in Figure **4.3.3.1** are bent (eg the two $^1A_{1g}$ terms), and some are straight. Bending of lines occurs when two terms interact with each other because they are close in energy and have the same symmetry. This is again an analogy to orbitals. Just as orbitals interact when they have the same symmetry type and similar energy, terms also interact when they have the same symmetry and similar energy. Without taking their interactions into account, their energies can cross when the energy of term A declines and the energy of term B increases with increasing field strength (Figure **4.3.3.2**). The closer the terms come to the point where they cross, the stronger their interactions, because their energies become more and more similar. These interactions lead to the "bending away" of the terms from each other, leading to bent curves. This means that curves for two terms of the same symmetry type will bend away in a Tanabe-Sugano diagram and never cross. For example the terms for the two $^1A_{1g}$ terms bend away from each other and do not cross.

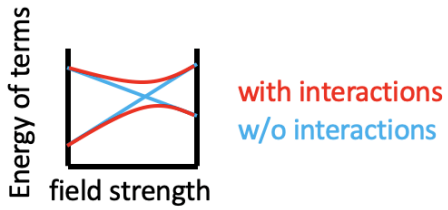


Figure **4.3.3.2**: Origin of line-bending in Tanabe-Sugano diagrams.

Next, let us think about which electron transitions would be allowed by considering spin selection and the Laporte rule. First, notice that all the terms in Figure **4.3.3.1** have "gerade" symmetry and are labeled with a "g" subscript. In fact, this is the case for the terms of any octahedral complex. What does this mean for the allowance of electron transitions? It means that no electron transition would be allowed by the Laporte Rule, and that would imply that the complex could not absorb light. The Laporte selection rule, however, does not hold strictly. It only says that the probability of the electron-transition is reduced - but not forbidden. This means that an absorption band that disobeys the Laporte rule will have lower intensity compared to one that follows the Laporte rule, but it can still be observed. The spin-selection rule, however, holds strictly, and transitions between terms of different spin multiplicity are strictly forbidden, meaning that they have near zero probability to occur. Overall, we can therefore excite an electron from the $^3T_1$ ground state to other triplet terms, namely the $^3T_2$ term, and the $^3A_2$ term (Figure **4.3.3.1**).

Tanabe-Sugano diagram of d^3 octahedral complexes

Now, let us have a look at the Tanabe-Sugano diagram of a d^3 ion in an octahedral ligand field (Figure **4.3.3.3**). What is the ground term? We can see that the term designation on the horizontal line reads "$^4A_{2g}$", therefore this term is the ground term. How many electron transitions from the ground state should we expect? To answer this question we need to count the number of other quartet terms. There is the $^4T_{2g}$, the $^4T_{1g}$, and another $^4T_{1g}$. Thus, there are overall three electron transitions possible.

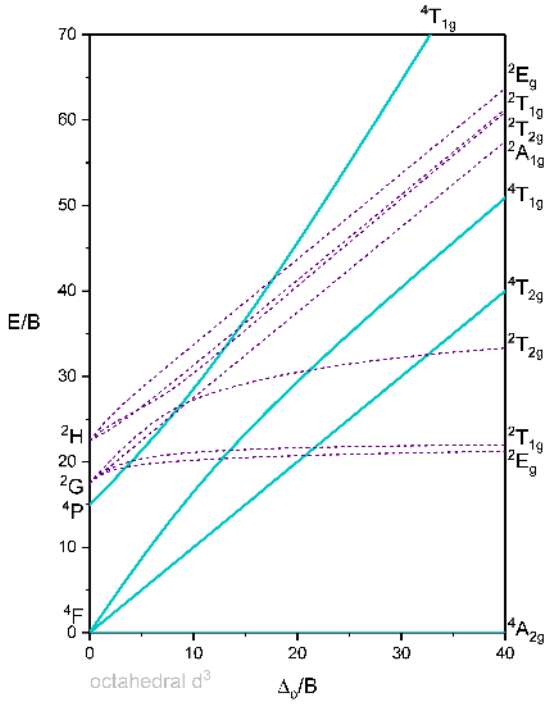


Figure **4.3.3.3**: d^3: Tanabe-Sugano Diagram for octahedral metal complex with three d electrons. For convenience, terms that can accommodate spin-allowed transitions from the ground state are indicated by solid lines. Terms that have different multiplicity than the ground state are shown in dashed lines. (CC-BY-SA; Kathryn Haas)

Can we understand why the ground state is a quartet term? It helps to consider how we would fill the electrons into the d-orbitals for the electron configuration d^3. All three electrons would be filled spin-up in the t_{2g} orbital following Hund's rule (Figure **4.3.3.4**). Because each electron has the spin +1/2 the total spin of all three electrons is 3x1/2=3/2. Thus, the spin multiplicity is ((2x3/2)+1)=4. Note that the microstate we have drawn is actually only one of the (2L+1)(2S+1) microstates. S=3x1/2=3/2, but

what is L? You can see on the left side of the diagram that the $^4A_2$ term originated from a ^4F term. This means L=3, and (2L+1)((2S+1)=7x4=28. This means that there are actually 27 other microstates that have the same energy as the microstate that we drew. Why did we draw this microstate in favor of the others? This is because this microstate is the state with the maximum M_L (=L) and M_s (=S) values determining the term symbol.

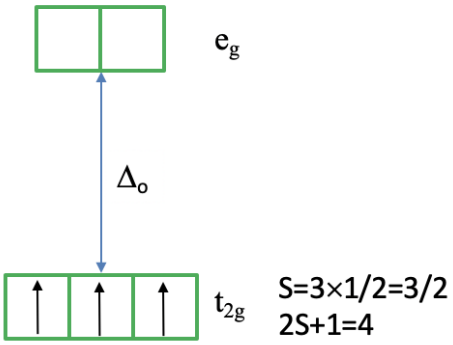


Figure **4.3.3.4**: d-orbitals in an octahedral ligand field for the electron configuration d^3

Tanabe-Sugano diagram of d^4 octahedral complexes

Now let us look at the Tanabe-Sugano diagram of a d^4 octahedral complex (Figure **4.3.3.5**). You can see that this diagram is separated into two parts separated by a vertical line. The line indicates the ligand field strength at which the complex changes from a high spin complex to a low spin complex. At lower ligand field strengths, the ground term is a ^5E_g term (solid turquoise line). At higher field strength the ground term is a $^3T_{1g}$ term (dashed purple line).

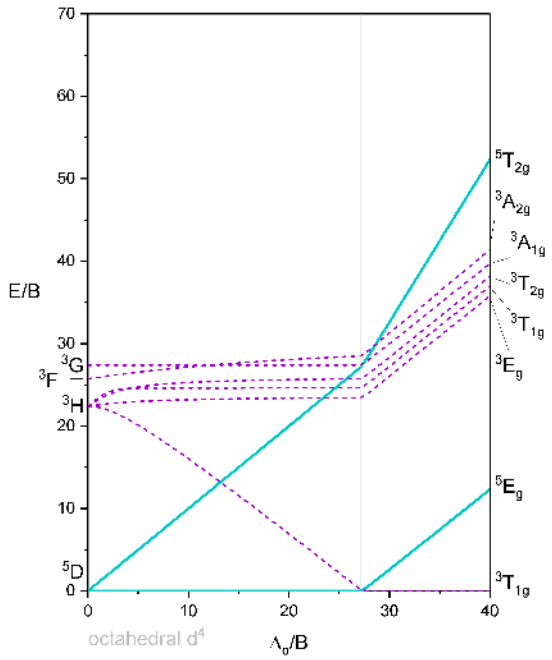
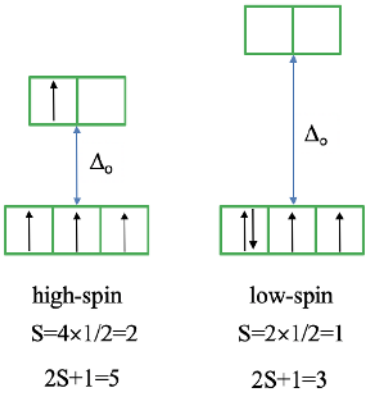


Figure **4.3.3.5**: d^4, simplified: Tanabe-Sugano Diagram for octahedral metal complex with four d electrons. A grey vertical line at 27.2 $\frac{\Delta_o}{B}$ divides high spin from low spin cases. For convenience, terms that can accommodate spin-allowed transitions from the pentet ground state in high spin (left of grey line) are indicated by heavy solid lines. Terms that can accommodate spin-allowed transitions from the low spin triplet ground state are shown in heavy dashed lines. This version of the d^4 Tanabe Sugano Diagram is abbreviated in that it shows only the spin-allowed terms that are most relevant for interpreting UV-visible spectra. For the full version of a d^4 diagram, see the Resources section. (CC-BY-SA; Kathryn Haas)

We can rationalize this again by drawing the orbital box representation of the d-orbitals in the octahedral ligand field. In the high spin state, there are four unpaired electrons, thus S=4x1/2=2, and 2S+1=5. In the low spin state, there are two unpaired electrons, and thus S=2x1/2=1, and 2S+1=3. This explains the quintet and the triplet nature of the high and low spin ground terms. Note

again, that the two microstates represented by the orbital box diagrams (**4.3.3.6**) are not the only microstates that have the respective energy. They are only the "representative" microstates because they have the maximum M_L and M_S values.



4.3.3.6: d-orbitals in the octahedral ligand field for the electron configuration d^4.

How many electron transitions are possible from the ground term? For a high spin complex there is only one because the is only one other quintet term, namely the $^5T_{2g}$ term. For the low spin complex, there are five transitions because there are five other triplet terms.

Tananbe-Sugano diagram of d^5 octahedral complexes

The Tanabe-Sugano diagram of a d^5 octahedral complex is also divided into two parts separated by a vertical line (Figure **4.3.3.7**). The left part reflects the high spin and the right part the low spin complex.

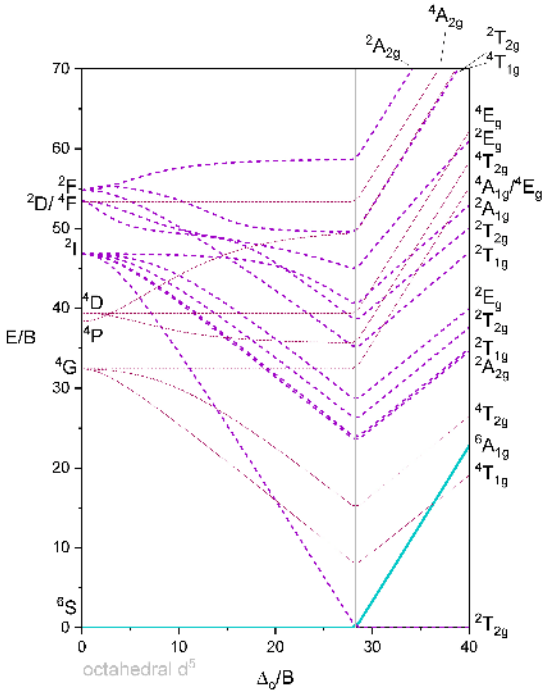


Figure **4.3.3.7**: d^5, simple: Tanabe-Sugano Diagram for octahedral metal complex with five d electrons. A grey vertical line at 27.3 $\frac{\Delta_o}{B}$ divides high spin from low spin cases. For convenience, terms that can accommodate spin-allowed transitions from the sextet ground state in low spin (right of grey line) are indicated by heavy solid lines. Terms that can accommodate spin-allowed transitions from the low spin doublet ground state are shown in heavy dashed lines. Terms that have different multiplicity than ground states are shown in lighter dotted lines. This version of the d^5 Tanabe Sugano Diagram is abbreviated for simplicity and for the purpose of interpreting UV-visible spectra. For the full version of a d^5 diagram, see the Resources section. (CC-BY-SA; Kathryn Haas)

The high spin ground state is a sextet term, and the low spin ground state is a doublet term. We can understand the sextet and doublet nature of the terms when considering that the associated electron box diagrams have five and one unpaired electrons

respectively. S=5x1/2=5/2 and 2S+1=6 for the high spin term, and S=1x1/2=1/2 and 2S+1=2 for the low spin term. What are the possible electron transitions from the ground state? For the high-spin complex there is no other sextet term, meaning that there is no electron transition possible. Hence, high-spin octahedral d^5-complexes are colorless. An example is the hexaaqua manganese (2+) complex. A solution of this complex is near colorless, only very slightly pinkish. The slight color is because also spin-forbidden transitions can occur, albeit at a very low probability. For a d^5-low spin complex there are three additional doublet states, and thus there are three electron transitions possible.

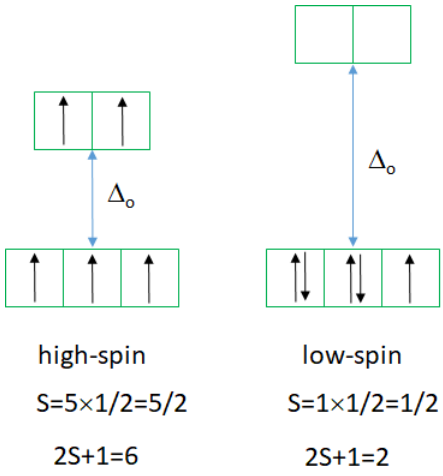


Figure 4.3.3.8: d-orbitals in the octahedral ligand field for the electron configuration d^5

Tanabe-Sugano diagram of d^6 octahedral complexes

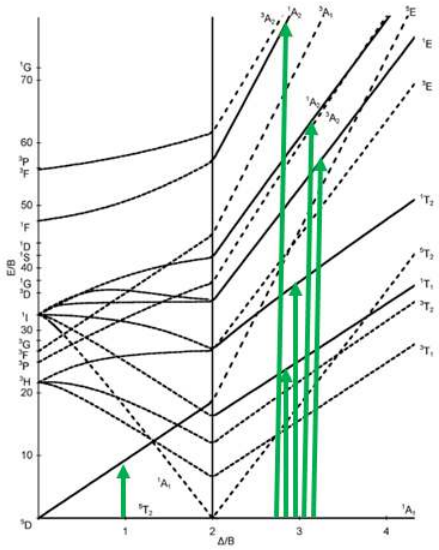


Figure 8.2.13 Tanabe-Sugano diagram of the d^6 octahedral complex (Chem507f091 / Public domain https://commons.wikimedia.org/wiki/F...no_diagram.png)

The next diagram is the one for the d^6 electron configuration (Fig. 8.2.13). Again, the diagram is separated into parts for high and low spin complexes. The dashed lines in the diagram indicate the terms that have a different spin multiplicity than the ground term. This way we can more easily see how many electron transitions are allowed.

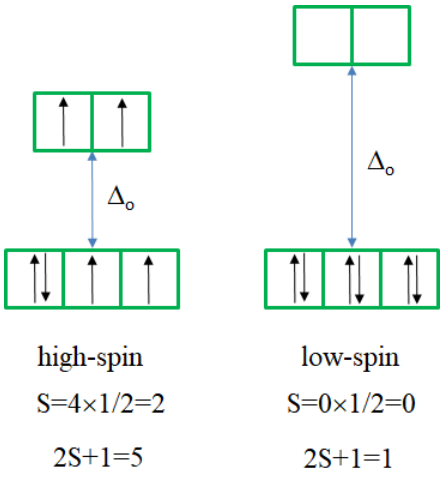


Figure 8.2.14 d-orbitals in the octahedral ligand field for the electron configuration d^6

The ground term for the high-spin complex is the quintet $^5T_2$ term. It is a quintet term because four electrons in the d-orbitals are unpaired, and two are paired. The value for S is thus 4x1/2=2, and the spin multiplicity is 2S+1=5. The ground term for the low spin complex is a $^1A_1$ term. It is a singlet term because all electrons are paired, and thus S=0, and 2S+1=1. How many electron transitions are there for the high-spin complex? There is only one because the ^5E term is the only other quintet term. There are five transitions possible for the low-spin case because there are five additional singlet terms.

Tanabe-Sugano diagram of d^7 octahedral complexes

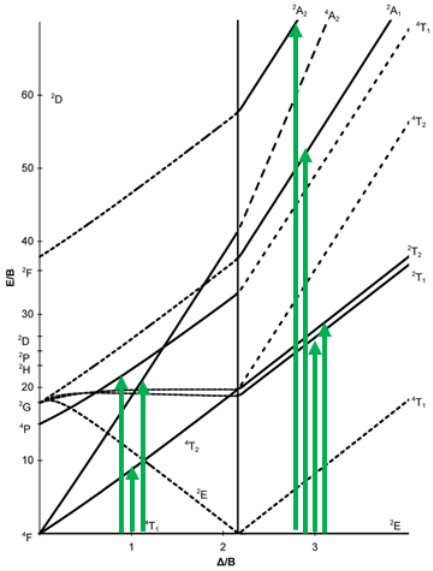


Figure 8.2.15 Tanabe-Sugano diagram of the d^7 octahedral complex (Attribution: Chem507f091 / Public domain https://commons.wikimedia.org/wiki/F...no_diagram.png)

Next, let us look at the Tanabe-Sugano diagram of a d^7 octahedral complex (Fig. 8.2.15). In this case, the high spin complex has a $^4T_1$ ground term, and the low spin complex has a ^2E ground term.

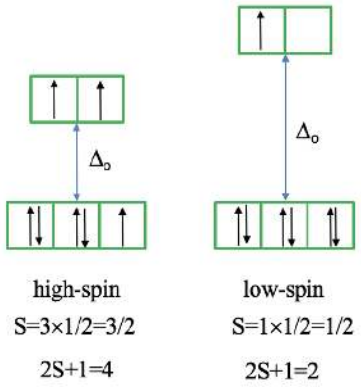


Figure 8.2.16 d-orbitals in the octahedral ligand field for the electron configuration d^7

The microstate that "represents" the high spin ground term has three unpaired electrons, hence the spin quantum number S=3/2 and the spin multiplicity is 2S+1=4. The microstate that represents the low spin ground term has one unpaired electron, an S value of ½, and a spin multiplicity of 2. There are three other quartet terms, and four other doublet terms, hence there are three electron transitions for the high-spin complex, and four for the low spin complex.

Tanabe-Sugano diagram of d^8 octahedral complexes

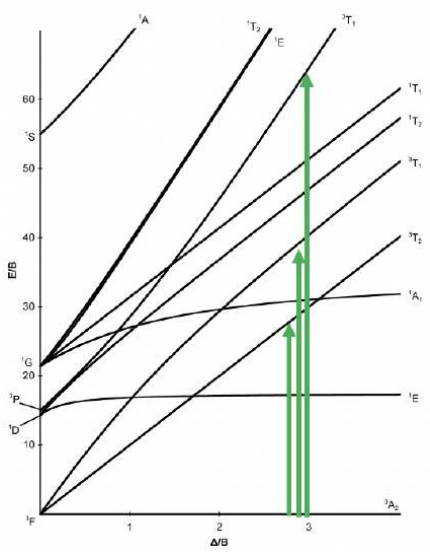


Figure 8.2.17 Tanabe-Sugano diagram of the d^8 octahedral complex (Attribution: Chem507f091 / Public domain https://commons.wikimedia.org/wiki/F...no_diagram.png)

Now let us look at an octahedral complex with d^8 electron configuration. For this electron configuration, there are no high and low spin complexes possible, therefore, the Tanabe-Sugano diagram is no longer divided into two parts (Fig. 8.2.17).

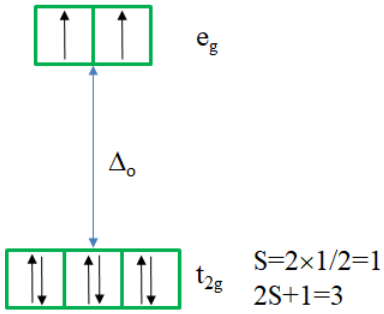


Figure 8.2.18 d-orbitals in the octahedral ligand field for the electron configuration d^8

There is a single ground term of the type $^3A_2$. It is a triplet state because the microstate representing the term has two unpaired electrons in the e_g orbitals (Fig. 8.2.18). Thus, S=2x1/2=1, and the spin multiplicity is 2S+1=2. How many electron transitions would you expect? There are three other triplet states, namely the $^3T_2$ and two $^3T_1$ terms. Therefore, there are three electron transitions possible.

Unnecessary diagrams for d^1, d^9, d^10

We could also ask: Are there Tanabe-Sugano diagrams for d^1, d^9, and d^{10}? For, d^1 there are no electron-electron interactions, thus the simple orbital picture is sufficient. The ^2D term splits into T_{2g} and E_g terms, and there is only one electron transition possible. The d^9 electron configuration is the "hole-analog" of the d^1 electron configuration. It has also just one ^2D term which splits into a T_{2g} and an E_g term in the octahedral ligand field. Therefore, also in this case there is only one electron transition from the T_{2g} into the E_g term possible. In the case of d^{10} all microstates are filled with orbitals, and there is only the ^1S term which does not split in an octahedral ligand field. Therefore, there are no electron transitions in this case.

Jahn-Teller distortions and other geometries

Some of the electron configurations discussed above are ones that are particularly susceptible to Jahn-Teller distortion. The Jahn-Teller theorem predicts that electron configurations with asymmetrically populated orbitals (i.e., those that have spin multiplicity of a doublet or greater), will distort. Distortions affect the electronic spectra of coordination complexes, and in practice Jahn-Teller distortions are significant only in the cases where the e_g orbitals are asymmetrically populated (e.g., octahedral d^9 and high spin d^4).

Finally, it should be mentioned that it is also possible to construct Tanabe-Sugano diagrams for other shapes such as the tetrahedral shape, but we will not discuss these further here.

Dr. Kai Landskron (Lehigh University). If you like this textbook, please consider to make a donation to support the author's research at Lehigh University: Click Here to Donate.

This page titled 4.3.3: Tanabe-Sugano Diagrams is shared under a CC BY-NC-SA 4.0 license and was authored, remixed, and/or curated by Kai Landskron.

- **8.2: Term splitting in ligand fields, selection rules, Tanabe-Sugano diagrams. Metal to ligand, and ligand to metal transitions** by Kai Landskron is licensed CC BY 4.0.

4.3.4: Applications of Tanabe-Sugano Diagrams

The Tanabe-Sugano diagrams can be used to interpret absorption spectra and gain insight into the properties of a coordination complex. For example, you could use the appropriate diagram to predict the number of transitions, assign the identity of a specific transition, or calculate the value of Δ for a specific metal complex.

How to use the Tanabe-Sugano Diagrams

1. Determine the d-electron count of the metal ion of interest.
2. Choose the appropriate Tanabe-Sugano diagram: this is the one matching the d-electron count of the metal ion. There is a full list of Tanabe-Sugano diagrams in the Resources Section.
3. Acquire an electronic spectrum of the metal complex and identify λ_{max} for spin-allowed (strong intensity) and spin forbidden (weak intensity) transitions.
4. Convert wavelength (λ_{max}) to energy (E) in wavenumbers (cm^{-1}) and generate energy ratios relative to the lowest-energy allowed transition. (i.e. $\frac{E_2}{E_1}$ and $\frac{E_3}{E_1}$).
5. Using a ruler, slide it across the printed Tanabe-Sugano diagram until the E/B ratios between lines is equivalent to the ratios found in step 4.
6. Solve for B using the E/B values (y-axis, step 4) and Δ_{oct}/B (x-axis, step 5) to yield the ligand field splitting energy, $Delta$ (Sometimes this is labeled as $10D_q$, and it is useful to know that $\Delta = 10D_q$).

Example 4.3.4.1: Chromium Splitting

A Cr^{3+} metal complex has strong transitions and λ_{max} at

- 431.03 nm,
- 781.25 nm, and
- 1,250 nm.

Determine the Δ_{oct} for this complex.

Solution

1. Cr has 6 electrons. Cr^{3+} has three electrons, so it has a d-configuration of d^3
2. Locate the d^3 Tanabe-Sugano diagram
3. Convert to wavenumbers:

$$\frac{10^7(nm/cm)}{1250\ nm} = 8,000\ cm^{-1} \quad (4.3.4.1)$$

$$\frac{10^7(nm/cm)}{781.25\ nm} = 13,600\ cm^{-1} \quad (4.3.4.2)$$

$$\frac{10^7(nm/cm)}{431.03\ nm} = 23,200\ cm^{-1} \quad (4.3.4.3)$$

4. Allowed transitions are $^4T_{1g} \leftarrow {}^4A_{2g}$, $^4T_{1g} \leftarrow {}^4A_{2g}$ and $^4T_{2g} \leftarrow {}^4A_{2g}$.

Transition	Energy cm^{-1}	Ratios to lowest
$^4T_{1g} \leftarrow {}^4A_{2g}$	23,200	2.9
$^4T_{1g} \leftarrow {}^4A_{2g}$	13,600	1.7
$^4T_{2g} \leftarrow {}^4A_{2g}$	8,000	1

5. Sliding the ruler perpendicular to the x-axis of the d^3 diagram yields the following values:

Δ_{oct}/B	10	20	30	40
Height E(ν_3)/B	29	45	64	84
Height E(ν_2)/B	17	30	40	51
Height E(ν_1)/B	10	20	30	40
Ratio E(ν_3)/E(ν_1)	2.9	2.25	2.13	2.1
Ratio E(ν_2)/E(ν_1)	1.7	1.5	1.33	1.275

6. Based on the two tables above it should be assessed that the Δ_{oct}/B value is 10. B is found by dividing E by the height.

Energy cm^{-1}	Height	B
23,200	29	800
13,600	17	800
8,000	10	800

7. Next multiply Δ_{oct}/B by B to yield the Δ_{oct} energy.

$$10 \times 800 = 8000\ cm^{-1} = \Delta_{oct} \tag{4.3.4.4}$$

Each problem is of varying complexity as several steps may be needed to find the correct Δ_{oct}/B values that yield the proper energy ratios.

This page titled 4.3.4: Applications of Tanabe-Sugano Diagrams is shared under a CC BY-NC-SA 4.0 license and was authored, remixed, and/or curated by Kathryn Haas.

4.3.5: Tetrahedral Complexes

Transitions in tetrahedral complexes are Laporte-allowed

Tetrahedral metal complexes often have more intense electronic transitions than their octahedral counterparts. This is due to the fact that the $d-d$ transitions in a tetrahedron are allowed by the Laporte selection rule, while $d-d$ transitions in an octahedral complex are Laporte-forbidden. Recall that the Laporte selection rule applies to centrosymmetric complexes only. The Laporte rule applies to octahedral complexes but not to tetrahedral complexes because a tetrahedron does not have a center of inversion. Notice that the terms (and orbital labels) in a tetrahedron do not include the g subscripts that are present under octahedral symmetry (Figure **4.3.5.1**). The splitting pattern of a tetrahedral complex is exactly opposite to the octahedral case. In the case of a tetrahedron, however, the "g" subscripts are inappropriate because of the tetrahedron's lack of a center of inversion, and transitions between the terms in a tetrahedron do not violate the Laporte Rule.

Another way to explain this in terms of electron transitions between orbitals is through the orbital mixing required to form a tetrahedral complex. Orbital types (i.e., s, p, d) must mix to form the moleculare orbitals of a tetrahedral transition metal complex. The mixing of s and p orbitals with the d orbitals allows transitions that are forbidden in the case of pure d-orbitals.

It is also worth noting that $\Delta_t = \frac{4}{9}\Delta_o$. The smaller Δ for transition metals means that the tetrahedral complexes can absorb at a lower energy and longer wavelength relative to an analogous octahedron.

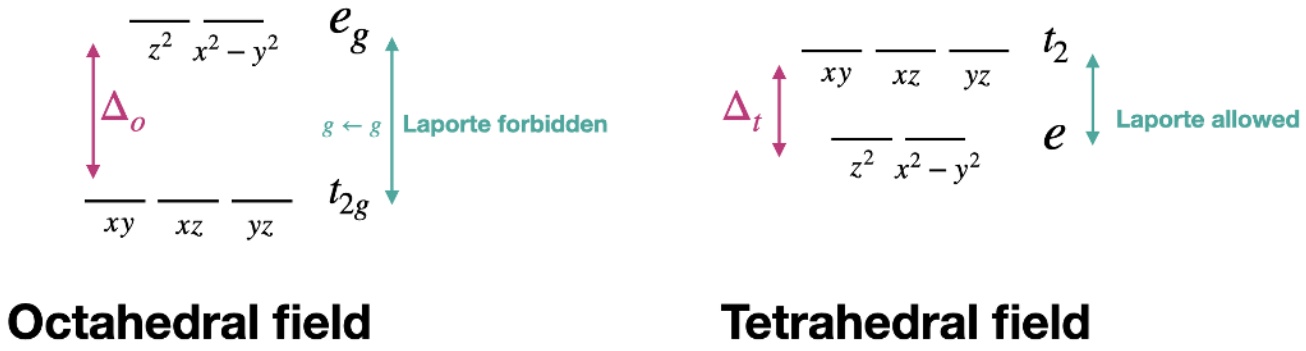


Figure **4.3.5.1**: $d-d$ transitions in octahedral complexes are Laporte-forbidden, while those in tetrahedral complexes are Laporte-allowed. (CC_BY_SA; Kathryn Haas)

Tanabe-Sugano diagrams for tetrahedral complexes

Due to the opposite splitting pattern, the transitions for a d^n tetrahedral complex are sufficiently represented by the d^{10-n} Tanabe-Sugano diagram (just drop the g subscripts from the diagrams). For example, the electronic spectrum of a d^8 tetrahedral complex (e.g., $[Ni(H_2O)_6]^{2+}$) can be interpreted using the d^2 Tanabe-Sugano diagram.

This page titled 4.3.5: Tetrahedral Complexes is shared under a CC BY-NC-SA 4.0 license and was authored, remixed, and/or curated by Kathryn Haas.

4.3.6: Selection Rules

Electronic transitions between states of different energies give rise to electronic spectra. However, some transitions are more probable, and thus more intense, than others. In UV-vis spectroscopy, for example, the transitions that are "allowed" can give rise to absorption bands that are much more intense than transitions that are "forbidden". To be clear, "forbidden" transitions are still possible, and are sometimes observable, but are less intense because they happen less frequently than "allowed" transition when the molecules are exposed to electromagnetic radiation.

Selection Rules that govern Electronic Transitions

The Selection Rules governing transitions between electronic energy levels (including microstates and terms) are:

1. **The Spin Selection Rule**, $\Delta S = 0$.
2. **The Laporte (or orbital) Selection Rule**, for centrosymmetric molecules $g \rightarrow u$ or $u \rightarrow g$, or $\Delta l = \pm 1$.

Selection rules that govern electronic transitions

Spin selection rule

The Spin Selection Rule forbids transitions between states with different total spin, and thus different spin multiplicity. This rule allows transitions only between states with the same total intrinsic spin ($\Delta S = 0$), and thus the same spin multiplicity value in the term symbol. In other words, the direction of the promoted electron's spin should not change. Just in case it is not obvious yet, the spin multiplicity is the left superscript in the term symbol, so this rule allows transitions between terms with the same superscript. For example, this rule would allow a transition from a ^3T term to a ^3A term, but not from ^3T to ^2D.

Laporte (orbital) Selection Rule

The Laporte Selection Rule applies to molecules that have a center of symmetry (aka center of inversion, centrosymmetric). This rule forbids transitions between states with the same parity (symmetry) with respect to an inversion center (i). Parity is indicated on molecular orbitals and on term symbols with subscripts g (gerade, or even) and u (ungerade, or uneven). Transitions between u and g terms are allowed (eg $T_{2g} \rightarrow T_{1u}$ is allowed), but those between two g or two u terms are forbidden (eg $T_{2g} \rightarrow T_{1g}$ is forbidden). Because different types of orbitals have different symmetries with respect to i, this rule is sometimes referred to as the "orbital selection rule". It forbids transitions within one type of orbital subshell. For example, p orbitals are antisymmetric with respect to i, while both s and d orbitals are symmetric with respect to i. This rule forbids $s \rightarrow s$, $p \rightarrow p$, $d \rightarrow d$, and $d \rightarrow s$ transitions, but allows transition between $d \rightarrow p$ and $d \rightarrow s$ orbitals. This rule is important in transition metal complexes because it fobids $d - d$ transitions in centrosymmetric geometries, including octahedral and linear coordination geometries.

Despite these selection rules, $d \rightarrow d$ transitions are a hallmark feature of octahedral transition metal complexes, and are often responsible for their brilliant colors. These $d \rightarrow d$ transtions, and other forbidden transitions may still occur, primarily through relaxation of these rules in specific cases.

Breaking the rules!

Relaxation of the Laporte and Spin Selection Rules rules can occur through:

- **Vibronic coupling:** the bonds of metal complexes vibrate and may cause temporary distortions in molecular symmetry. These distortions can cause temporary loss in symmetry (as well as some orbital mixing), and thus allow $d \rightarrow d$ transitions in those moments of distortion. Despite being forbidden by the Laporte Selection rule, the $d \rightarrow d$ transitions in octahedral complexes appear, but are weak (of low intensity) with molar absorptivities $\leq 100\ M^{-1}cm^{-1}$.
- **Orbital Mixing**: In the case of octahedral complexes, π-acceptor and π-donor ligands can mix with the d-orbitals so that transitions are no longer purely $d \rightarrow d$ (but these are usually considered "charge transfer" transitions, not $d \rightarrow d$). In the case of tetrahedral complexes, the molecule has no center of symmetry (thus no u or g subscripts on the terms). In the valence orbital model, a tetrahedral molecule is said to have sp^3 and sd^3 hybridized orbitals, while MO theory predicts MO's with mixtures of some s, p, and d character - this mixing of orbital types can allow transitions between "mixed" orbitals that

would otherwise be forbidden in "pure" orbitals. A similar phenomenon would occur in octahedrons with significant distortion, or in other coordination geometries that provide potential for orbital mixing.

- **Spin-Orbit coupling**: This gives rise to spin-forbidden bands of low intensity, usually with very weak molar absorptivities approximately $\leq 1 M^{-1} cm^{-1}$. This phenomenon is usually more important for transition metals of the second row $4d$ and beyond.

? Exercise 4.3.6.1

Consider the d^2 case presented in a previous section. The free ion terms for d^2 were found to be ^3F, ^1G, ^3P, ^1D, ^1S. First, identify the ground state term. Then identify the Spin-Allowed excitations starting from the ground state.

Answer

The ground state is ^3F. There is only one spin-allowed transition: $^3F \rightarrow ^3 P$.

The spin-forbidden transitions from ^3F include $^3F \rightarrow ^1 D$, $^3F \rightarrow ^1 G$, and $^3F \rightarrow ^1 S$.

This page titled 4.3.6: Selection Rules is shared under a CC BY-NC-SA 4.0 license and was authored, remixed, and/or curated by Kathryn Haas.

- **Selection Rules for Electronic Spectra of Transition Metal Complexes** by Robert J. Lancashire is licensed CC BY 4.0.

4.3.7: Charge-Transfer Spectra

Charge Transfer Transitions

Zn^{2+}		d^{10} ion	white
$[Cu(MeCN)_4]^+$	Cu(I)	d^{10} ion	colourless
$[Cu(phen)_2]^+$	Cu(I)	d^{10} ion	dark orange
TiF_4		d^0 ion	white
$TiCl_4$		d^0 ion	white
$TiBr_4$		d^0 ion	orange
TiI_4		d^0 ion	dark brown
$[MnO_4]^-$	Mn(VII)	d^0 ion	extremely purple
$[Cr_2O_7]^-$	Cr(VI)	d^0 ion	bright orange

Figure **4.3.7.1**: Some examples of complexes with d^0 and d^{10} electron configurations, and their colors. Attribution: E.R. Schofield.

We are still not done with our electronic spectra. Thus far, we have only considered transitions of d-electrons between d-orbitals, and their terms. These are called d-d transitions. However, there are also so-called charge transfer transitions possible, which are not d-d transitions. We can easily see that there must be transitions other than d-d transitions when we look at the colors of d^{10} and d^0 ions. For those, there are no d-d transitions possible. Therefore, they all should be colorless. However, that is not always true. Some of these ions are indeed colorless, but some are not (Figure **4.3.7.2**). For example, Zn^{2+}, a d^{10} ion, is colorless in complexes, but not Cu(I), which is also d^{10}. While tetrakis(acetonitrile)copper(+) is colorless, bis(phenanthrene) copper(+) is dark orange. d^0 ions have similar properties: While TiF_4 and $TiCl_4$ are colorless, $TiBr_4$ is orange, and TiI_4 is brown. Some d^0 species are even extremely colorful, for example, permanganate with Mn^{7+}, which is extremely purple, and dichromate with Cr(VI), which is bright orange.

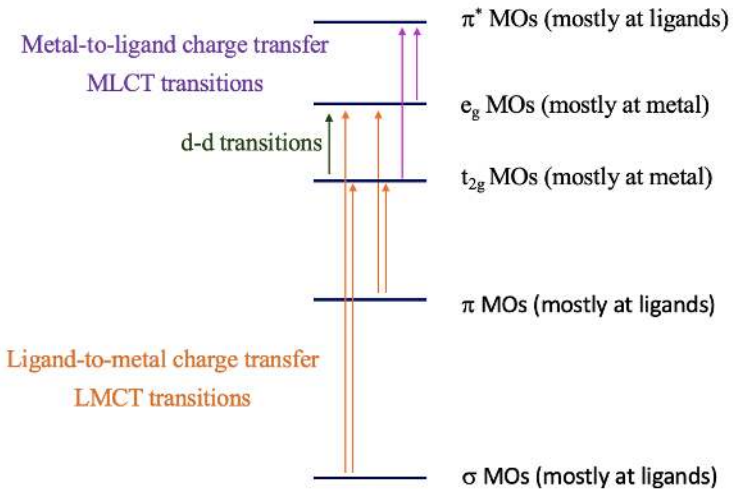


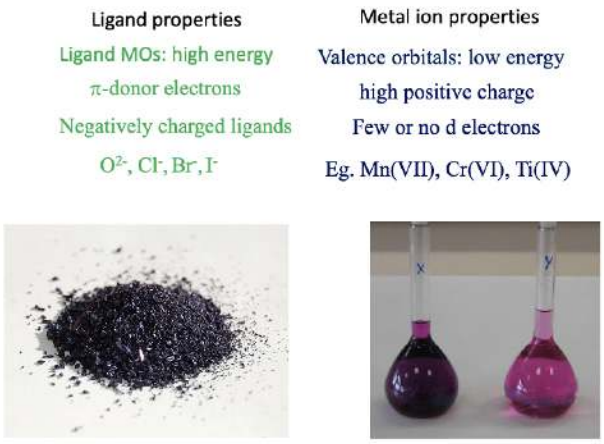
Figure **4.3.7.2**: Charge-transfer transitions. Attribution: E.R. Schofield.

The explanation for these phenomena is charge-transfer transitions (**4.3.7.2**). There are two types of charge-transfer transitions: ligand-to-metal (LMCT) and metal-to-ligand (MLCT) charge transfer transitions. For the ligand-to-metal transitions, electrons from bonding σ and π-orbitals get excited into metal d-orbitals in the ligand field, for example the t_{2g} and the e_g orbitals in an octahedral complex. If the energy difference between the σ/π-orbitals and the d-orbitals is small enough, then this electron transition is associated with the absorption of visible light. The transition is called a ligand-to-metal transition because the ligand σ/π-orbitals are mostly located at the ligands, while the metal-d-orbitals in a ligand field are mostly located at the metal. Vice versa,

the metal-to-ligand transition involves the transition of an electron from metal d-orbitals in a ligand field to ligand π*-orbitals. This essentially moves electron density from the metal to the ligand, hence the name ligand-to-metal-charge transfer transition. If the energy-difference between the ligand π* and the metal orbitals is small enough, then the absorption occurs in the visible range. Charge-transfer transitions are usually both spin- and Laporte allowed; hence, if they occur, the color is often very intense. How can we distinguish between d-d and charge transfer transitions? Charge transfer transitions often change in energy as the solvent polarity is varied (solvatochromic), as there is a change in polarity of the complex associated with the charge transfer transition. This can be used to distinguish between d-d transitions and charge-transfer bands.

LMCT Transitions

Can we predict when the energy windows between the bonding molecular orbitals and the metal d-orbitals are small enough for LMCT transitions in the visible to take place? Generally, it would be desirable if the energy of the metal orbitals were as low as possible and the energy of the bonding ligand orbitals were as high as possible. The energy of metal d-orbitals decreases with increasing positive charge at the metal because the effective nuclear charge on the metal increases. This means that very high metal oxidation states favor LMCT transitions. The d-orbitals should have few or no electrons, so that electrons can be promoted into the orbitals, and orbital energy decreases because electron-electron repulsion is minimized. Examples are Mn(VII), Cr(VI), and Ti(IV). The energy of MOs from bonding ligand orbitals increases when the ligand orbitals have high energy; this is typically the case for π-donor ligands with a negative charge (Fig. 8.2.21).



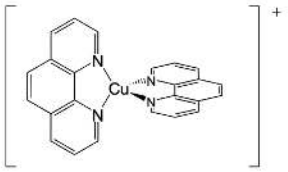
4.3.7.1: The properties of the metal ions and ligands suitable for LMCT transitions. MnO_4^- is deep purple due to LMCT transitions (Attribution: Benjah-bmm27 / Public domain https://commons.wikimedia.org/wiki/F...ate-sample.jpg) and (Attribution: Pradana Aumars / CC0 https://commons.wikimedia.org/wiki/F...entrations.jpg), respectively.

Examples of ligands are oxo- and halo ligands. This explains, for example, the LMCT transitions in permanganate. The Mn is in the very high oxidation state +7, and the ligands are oxo-ligands, which are π-donors with a 2- negative charge. The transitions are both Laporte and spin-allowed, leading to a very high intensity of light absorption, and thus color (Fig. 8.2.21).

MLCT Transitions

What are favorable metal ion and ligand properties for a metal-to-ligand transition, then? In this case we would like to keep the energy of the metal orbitals as high as possible so that the energy difference between a metal d-orbital and a π*-orbital is minimized. This is accomplished when the positive charge at the metal ion is small, and there are many d-electrons that can repel each other, thereby increasing orbital energies, for example Cu(I), Fig. 8.2.22.

Metal ion properties	Ligand properties
low metal ion charge	π-acceptor ligand with low-lying π* orbitals
many electrons	
Cu(I), d^{10} ion	1,10-phenanthroline, CN^-, CO, SCN^-



$[Cu(phen)_2]^+$, dark orange

4.3.7.3: bis(phenanthroline) copper(+). Attribution: E.R. Schofield.

The ligand should be a π-acceptor with low-lying π*-orbitals - for example, phenanthroline, CN^-, SCN^-, and CO. The bis(phenanthroline) copper(+) ion, for instance, is dark orange and has an MLCT absorption band at 458 nm. This MLCT transfer is both spin and Laporte-allowed.

It should be mentioned that some complexes allow for both metal-to-ligand and ligand-to-metal transitions. For example, in the $Cr(CO)_6$ complex, the σ-orbitals are high enough and the π*-orbitals are low enough in energy to allow for light absorption in the visible range. Finally, intraligand bands are also possible when the ligand is a chromophore.

Dr. Kai Landskron (Lehigh University). If you like this textbook, please consider to make a donation to support the author's research at Lehigh University: Click Here to Donate.

This page titled 4.3.7: Charge-Transfer Spectra is shared under a CC BY-NC-SA 4.0 license and was authored, remixed, and/or curated by Kathryn Haas.

- **8.2: Term splitting in ligand fields, selection rules, Tanabe-Sugano diagrams. Metal to ligand, and ligand to metal transitions** by Kai Landskron is licensed CC BY 4.0.

4.3.8: Applications of Charge-Transfer

Transition metal complexes with strong π-accepting ligands have proven quite useful across many applications in industry, materials science, and medicine due to their intense absorption of light, photostability, and unique geometric, redox, and photodynamic properties. These complexes usually have low-valent metal ions (low oxidation state) with π-accepting ligands constructed of conjugated poly-aromatic rings. Intense light absorption occurs through metal-to-ligand charge transfer (MLCT), causing a formal oxidation of the metal ion and reduction of the ligand. These compounds are used as sensors, and their excited states can be used as indispensable reactants. Some examples of their applications are discussed briefly below.

Ruthenium bypyridine derivatives

Let's use the example of a simple and interesting metal complex: tris(bypyridine)ruthenium(II), or $[Ru(bpy)_3]^{2+}$. This molecule is the most generic form of a family of derivatives that have this core structure in common. $[Ru(bpy)_3]^{2+}$ absorbs ultraviolet light at 452 nm due to an intense MLCT. It also absorbs light at shorter wavelenghts due to ligand-centered $\pi* \leftarrow \pi$, metal-centered $d \leftarrow d$, and LMCT transitions. The ground state is a singlet state (all paired electrons), and the spin-selection rule allows formation of a singlet excited state. However, in the case of high-atomic-number d^6 metal ions, like Ru, there is intense spin-orbit coupling that favors intersystem crossing. **Intersystem crossing** is the phenomenon by which a system's spin multiplicity can change by the transition of an electron's spin without energy cost. In the case of $[Ru(bpy)_3]^{2+}$, the excited singlet state transitions to an isoenergetic (or degenerate) triplet excited state. $[Ru(bpy)_3]^{2+}$ has a long-lived excited state due to the fact that the transition between the triplet excited state and the singlet ground state is spin-forbidden. The excited state can relax to the singlet ground state radiatively (releasing a photon) or non-radiatively (as phonons/heat).

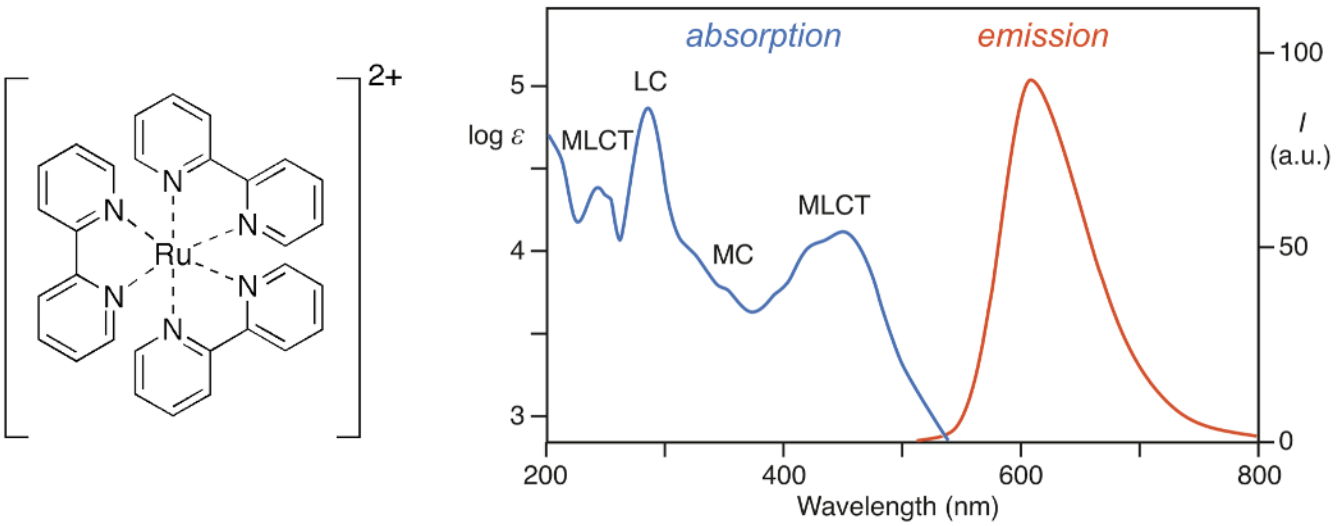


Figure **4.3.8.1**: Structure of $[Ru(bpy)_3]^{2+}$ (left) and its absorption and emission spectrum (right). (CC-BY-SA: Albris, Ru(bpy)32+ absorption&emission, Added structure of Ru(bpy)3 by Kathryn Haas)

Bioimaging

The $[Ru(bpy)_3]^{2+}$ complex is fluorescent, with a quantum yeld of approximately 2%. Derivatives of this core structure offer a variety of interesting properties, including a tunable color of emission. Other modifications have been made to make Ru bipyridine derivatives more functional for cellular imaging. For example, these metal complexes have been modified to bind to carbohydrates, specific organelles, or specific organs for targeted biological imaging applications.

Energy and catalysis

Due to the long lifetime of the $[Ru(bpy)_3]^{2+}*$ excited triplet state, this molecule has potential as a photosensitizer for the oxidation and reduction of water (water splitting) for energy production. The MLCT excitation is essentially a removal of an electron from Ru (an oxidation of Ru) and a placement of an electron onto a bpy ligand (a reduction of the ligand). The resultant $[Ru^{3+}]$ center is a powerful oxidant, capable of oxidizing water, while the unpaired electron on reduced bpy is a powerful reductant. The power of

this complex for catalyzing the splitting of water has been demonstrated using an electron mediator, methyl viologin, a Pt catalyst, and a sacrificial reductant. Once the excited $[Ru(bpy)_3]^{2+*}$ has formed, the excited electron can be captured by methyl viologen and passed to a Pt catalyst which reduces hydrogen ion (H^+) to H_2. The oxidized $[Ru(bpy)_3]^{3+}$ complex is then reduced by reaction with a sacrificial reductant like EDTA or triethanolamine to re-form $[Ru(bpy)_3]^{2+}$.

$[Ru(bpy)_3]^{2+}$ is also used as a photosensitizer for organic synthesis. Many analogues of $[Ru(bpy)_3]^{2+}$ are employed as well. These transformations exploit the redox properties of excited $[Ru(bpy)_3]^{2+*}$ and its reductively quenched derivative $[Ru(bpy)_3]^{+}$. (from Wikipedia)

Other applications

Derivatives of $[Ru(bpy)_3]^{2+}$ are numerous. Such complexes are widely discussed for applications in biodiagnostics, photovoltaics, and organic light-emitting diodes, but no derivative has been commercialized. Application of $[Ru(bpy)_3]^{2+}$ and its derivatives to fabrication of optical chemical sensors is arguably one of the most successful areas so far. (from Wikipedia)

This page titled 4.3.8: Applications of Charge-Transfer is shared under a CC BY-NC-SA 4.0 license and was authored, remixed, and/or curated by Kathryn Haas.

CHAPTER OVERVIEW

5: Reactions of d-Metal Complexes

Learning Objectives

- Determine whether an metal ion will be labile or inert.
- Use kinetic data to determine if a ligand substitution occurs by an associative or dissociative mechanism
- Predict the product of a square planar ligand substitution reaction based on the trans effect and trans influence
- Explain the difference between and inner sphere and outer sphere electron transfer reaction

5.1: Thermodynamic Stability of Metal Complexes
5.2: Trends in Kinetic Lability
5.3: Ligand Substitution Mechanisms
5.4: Substitutions in Square Planar Complexes
5.4.1: Kinetics and Stereochemistry of Square Planar Reactions
5.4.2: Evidence for Associative Reactions
5.5: The Trans Effect Observation
5.6: The Trans Effect Explanation
5.7: Redox Mechanisms
5.7.1: Outer Sphere Electron Transfer
5.7.2: Inner Sphere Electron Transfer

5: Reactions of d-Metal Complexes is shared under a CC BY-NC-SA 4.0 license and was authored, remixed, and/or curated by LibreTexts.

5.1: Thermodynamic Stability of Metal Complexes

Chelate Complexes

As seen in Chapter 8, ligands like chloride, water, and ammonia are monodentate More complex ligands can, however, be bidentate, tridentate, or, in general, polydentate Ethylenediamine ($H_2NCH_2CH_2NH_2$, often abbreviated as en) and diethylenetriamine ($H_2NCH_2CH_2NHCH_2CH_2NH_2$, often abbreviated as dien) are examples of a bidentate and a tridentate ligand, respectively, because each nitrogen atom has a lone pair that can be shared with a metal ion. When a bidentate ligand such as ethylenediamine binds to a metal such as Ni^{2+}, a five-membered ring is formed. A metal-containing ring like that shown is called a chelate ring. Correspondingly, a polydentate ligand is a chelating agent, and complexes that contain polydentate ligands are called chelate complexes.



A chelate complex

Experimentally, it is observed that metal complexes of polydentate ligands are significantly more stable than the corresponding complexes of chemically similar monodentate ligands; this increase in stability is called the chelate effect. For example, the complex of Ni^{2+} with three ethylenediamine ligands, $[Ni(en)_3]^{2+}$, should be chemically similar to the Ni^{2+} complex with six ammonia ligands, $[Ni(NH_3)_6]^{2+}$. In fact, the equilibrium constant for the formation of $[Ni(en)_3]^{2+}$ is almost 10 orders of magnitude larger than the equilibrium constant for the formation of $[Ni(NH_3)_6]^{2+}$ (Table E4):

$$[Ni(H_2O)_6]^{2+} + 6NH_3 \rightleftharpoons [Ni(NH_3)_6]^{2+} + 6H_2O(l) \quad K_f = 4 \times 10^8 \tag{5.1.1}$$

$$[Ni(H_2O)_6]^{2+} + 3en \rightleftharpoons [Ni(en)_3]^{2+} + 6H_2O(l) \quad K_f = 2 \times 10^{18} \tag{5.1.2}$$

The formation constants are formulated as ligand exchange reactions with aqua ligands being displaced by new ligands (NH_3 or en) in the examples above.

> *Chelate complexes are more stable than the analogous complexes with monodentate ligands.*

The stability of a chelate complex depends on the size of the chelate rings. For ligands with a flexible organic backbone like ethylenediamine, complexes that contain five-membered chelate rings, which have almost no strain, are significantly more stable than complexes with six-membered chelate rings, which are in turn much more stable than complexes with four- or seven-membered rings. For example, the complex of nickel (II) with three ethylenediamine ligands is about 363,000 times more stable than the corresponding nickel (II) complex with trimethylenediamine ($H_2NCH_2CH_2CH_2NH_2$, abbreviated as tn):

$$[Ni(H_2O)_6]^{2+} + 3en \rightleftharpoons [Ni(en)_3]^{2+} + 6H_2O(l) \quad K_f = 6.76 \times 10^{17} \tag{5.1.3}$$

$$[Ni(H_2O)_6]^{2+} + 3tn \rightleftharpoons [Ni(tn)_3]^{2+} + 6H_2O(l) \quad K_f = 1.86 \times 10^{12} \tag{5.1.4}$$

*The above measurements were done in a solution of ionic strength 0.15 at 25° C.

Example 5.1.1

Arrange $[Cr(en)_3]^{3+}$, $[CrCl_6]^{3-}$, $[CrF_6]^{3-}$, and $[Cr(NH_3)_6]^{3+}$ in order of increasing stability.

Given: four Cr(III) complexes

Asked for: relative stabilities

Strategy:

A Determine the relative basicity of the ligands to identify the most stable complexes.

B Decide whether any complexes are further stabilized by a chelate effect and arrange the complexes in order of increasing stability.

Solution

A The metal ion is the same in each case: Cr^{3+}. Consequently, we must focus on the properties of the ligands to determine the stabilities of the complexes. Because the stability of a metal complex increases as the basicity of the ligands increases, we need to determine the relative basicity of the four ligands. Our earlier discussion of acid–base properties suggests that ammonia and ethylenediamine, with nitrogen donor atoms, are the most basic ligands. The fluoride ion is a stronger base (it has a higher charge-to-radius ratio) than chloride, so the order of stability expected due to ligand basicity is

$$[CrCl_6]^{3-} < [CrF_6]^{3-} < [Cr(NH_3)_6]^{3+} \approx [Cr(en)_3]^{3+}.$$

B Because of the chelate effect, we expect ethylenediamine to form a stronger complex with Cr^{3+} than ammonia. Consequently, the likely order of increasing stability is

$$[CrCl_6]^{3-} < [CrF_6]^{3-} < [Cr(NH_3)_6]^{3+} < [Cr(en)_3]^{3+}.$$

Exercise 5.1.1

Arrange $[Co(NH_3)_6]^{3+}$, $[CoF_6]^{3-}$, and $[Co(en)_3]^{3+}$ in order of decreasing stability.

Answer: $[Co(en)_3]^{3+} > [Co(NH_3)_6]^{3+} > [CoF_6]^{3-}$

The Chelate Effect

The chelate effect can be seen by comparing the reaction of a chelating ligand and a metal ion with the corresponding reaction involving comparable monodentate ligands. For example, comparison of the binding of 2,2'-bipyridine with pyridine or 1,2-diaminoethane (ethylenediamine=en) with ammonia. It has been known for many years that a comparison of this type always shows that the complex resulting from coordination with the chelating ligand is **much more thermodynamically stable**. This can be seen by looking at the values for adding two monodentates compared with adding one bidentate, or adding four monodentates compared to two bidentates, or adding six monodentates compared to three bidentates.

> *The Chelate Effect is that complexes resulting from coordination with the chelating ligand is much more thermodynamically stable than complexes with non-chelating ligands.*

A number of points should be highlighted from the formation constants in Table E4. In Table **5.1.1**, it can be seen that the ΔH° values for the formation steps are almost identical, that is, heat is evolved to about the same extent whether forming a complex involving monodentate ligands or bidentate ligands. What is seen to vary significantly is the ΔS° term which changes from negative (unfavorable) to positive (favorable). Note as well that there is a dramatic increase in the size of the ΔS° term for adding two compared to adding four monodentate ligands. (-5 to -35 $JK^{-1}mol^{-1}$). What does this imply, if we consider ΔS° to give a measure of disorder?

In the case of complex formation of Ni^{2+} with ammonia or 1,2-diaminoethane, by rewriting the equilibria, the following equations are produced.

$$\begin{array}{lcl} [Ni(H_2O)_6]^{2+} + 6\,NH_3 \overset{\beta_6}{\Leftrightarrow} [Ni(NH_3)_6]^{2+} & & \textbf{1f} \\ [Ni(NH_3)_6]^{2+} \Leftrightarrow [Ni(H_2O)_6]^{2+} + 6\,NH_3 & & \textbf{1d} \\ [Ni(H_2O)_6]^{2+} + 3\,en \overset{\beta_3}{\Leftrightarrow} [Ni(en)_3]^{2+} & & \textbf{2f} \\ \hline [Ni(NH_3)_6]^{2+} + 3\,en \Leftrightarrow [Ni(en)_3]^{2+} + 6NH_3 & & \textbf{3} \end{array}$$

Using the equilibrium constant for the reaction (3 above) where the *three* bidentate ligands replace the *six* monodentateligands, we find that at a temperature of 25° C:

$$\Delta G° = -2.303\,RT\,\log_{10} K \tag{5.1.5}$$

$$= -2.303\,RT\,(18.28 - 8.61) \tag{5.1.6}$$

$$= -54\ \text{kJ mol}^{-1} \tag{5.1.7}$$

Based on measurements made over a range of temperatures, it is possible to break down the $\Delta G°$ term into the enthalpy and entropy components.

$$\Delta G^\circ = \Delta H^\circ - T\Delta S^\circ \tag{5.1.8}$$

The result is that: $\Delta H^\circ = -29 kJ mol^{-1}$

$$- T\Delta S^\circ = -25 \text{ kJ mol}^{-1}$$
and at 25C (298K)
$$\Delta S^\circ = +88 \text{ J K}^{-1} \text{ mol}^{-1}$$

Caution

For many years, these numbers have been **incorrectly recorded** in textbooks. For example, the third edition of "Basic Inorganic Chemistry" by F.A. Cotton, G. Wilkinson and P.L. Gaus, John Wiley & Sons, Inc, 1995, on page 186 gives the values as:

$$\Delta G^\circ = -67 \text{ kJ mol}^{-1}$$
$$\Delta H^\circ = -12 \text{ kJ mol}^{-1}$$
$$-T\Delta S^\circ = -55 \text{ kJ mol}^{-1}$$

The conclusion they drew from these incorrect numbers was that the chelate effect was essentially an entropy effect, since the $T\Delta S^\circ$ contribution was nearly 5 times bigger than ΔH°.

In fact, the breakdown of the ΔG° into ΔH° and $T\Delta S^\circ$ shows that the two terms are nearly equal (-29 and -25 kJ mol^{-1}, respectively) with the ΔH° term a little bigger! The entropy term found is still much larger than for reactions involving a non-chelating ligand substitution at a metal ion. How can we explain this enhanced contribution from entropy? One explanation is to count the number of species on the left and right hand side of the equation above.

It will be seen that on the left-hand-side there are 4 species, whereas on the right-hand-side there are 7 species, that is a net gain of 3 species occurs as the reaction proceeds. This can account for the increase in entropy since it represents an increase in the disorder of the system. An alternative view comes from trying to understand how the reactions might proceed. To form a complex with 6 monodentates requires 6 separate favorable collisions between the metal ion and the ligand molecules. To form the tris-bidentate metal complex requires an initial collision for the first ligand to attach by one arm but remember that the other arm is always going to be nearby and only requires a rotation of the other end to enable the ligand to form the chelate ring.

If you consider dissociation steps, then when a monodentate group is displaced, it is lost into the bulk of the solution. On the other hand, if one end of a bidentate group is displaced the other arm is still attached and it is only a matter of the arm rotating around and it can be reattached again. **Both** conditions favor the formation of the complex with bidentate groups rather than monodentate groups.

This page titled 5.1: Thermodynamic Stability of Metal Complexes is shared under a CC BY-NC-SA 4.0 license and was authored, remixed, and/or curated by Robert J. Lancashire.

- **10.1: Thermodynamic Stability of Metal Complexes** by Robert J. Lancashire is licensed CC BY-NC-SA 4.0.

5.2: Trends in Kinetic Lability

Introduction

Kinetics is a branch of chemistry that is concerned with the rates of chemical reactions. In this section, we will discuss the rates of metal-ligand (M-L) substitution reactions.

Let's start with some examples. In the table below are three examples of ligand substitution reactions of hexaaquo metal complexes to form hexaammine complexes. These reactions are nearly identical with the exception of the metal ion. The products are thermodynamically favored in all cases.

Reaction	Rate constant (k)	Labile or Inert
$[Ni(OH_2)]^{2+} + 6NH_3 \rightleftharpoons [Ni(NH_3)_6]^{2+}$	$k = 10^4 s^{-1}$	Labile (happens in < 1 min)
$[Cr(OH_2)]^{3+} + 6NH_3 \rightleftharpoons [Cr(NH_3)_6]^{3+}$	$k = 10^{-3} s^{-1}$	Inert (slow, takes hours)
$[Cu(OH_2)]^{2+} + 6NH_3 \rightleftharpoons [Cu(NH_3)_6]^{2+}$	$k = 10^8 s^{-1}$	Very Labile (happens in seconds)

Definitions

- **Labile** - Metal complexes that undergo "kinetically fast" substitution reactions are **labile**. These reactions usually happen in less than one minute.
- **Inert** - Metal complexes that undergo "kinetically slow" substitution reactions are **inert** or **non-labile**. These reactions usually take hours.
- **Intermediate** - Metal complexes that undergo "kinetically intermediate" substitution reactions are **intermediate**.

A common pitfall is to confuse the meaning of kinetic terms, like *labile* and *inert*, with thermodynamic terms, like *stable* and *unstable*. It is important to distinguish between kinetics and thermodynamics. For example, the complex $[Fe(H_2O)Cl]^{2+}$ has a large formation constant and is thermodynamically stable; yet it is also labile. On the other hand, the complex $[Co(NH_3)_6]^{3+}$ is unstable in acidic aqueous solution and decomposes spontaneously to $[Co(H_2O)_6]^{3+}$; yet it decomposes slowly because it is inert. It is good practice to distinguish between meanings by using terms such as "kinetically labile" or "kinetically inert" and "thermodynamically stable" and "thermodynamically unstable".

Reaction Coordinate Diagrams

One way to visualize chemical reactions is through reaction coordinate diagrams (Figure **5.2.1**). These diagrams illustrate the relative free energy of the reactants and products, when the free energy of the products is lower than the reactants ΔG_{rxn} is negative and the reaction is spontaneous. This is what determines thermodynamic stability. These diagrams also illustrate the changes in free energy as the reaction progresses from reactants to products. In the case of a single step, concerted reaction the reactants go through a higher energy transition state before (potentially) forming products. The free energy difference between the reactants and the transition state is the free energy of activation ($\Delta G^{\ddagger}$), which determines the rate of the reaction. A larger $\Delta G^{\ddagger}$ yields a slower reaction rate because fewer reactants have sufficient energy to form products. In cases where the reaction occurs in 2 steps an intermediate is formed. The step with the largest $\Delta G^{\ddagger}$ will be the slowest, rate determining step. The magnitude of $\Delta G^{\ddagger}$ is what determines kinetic lability.

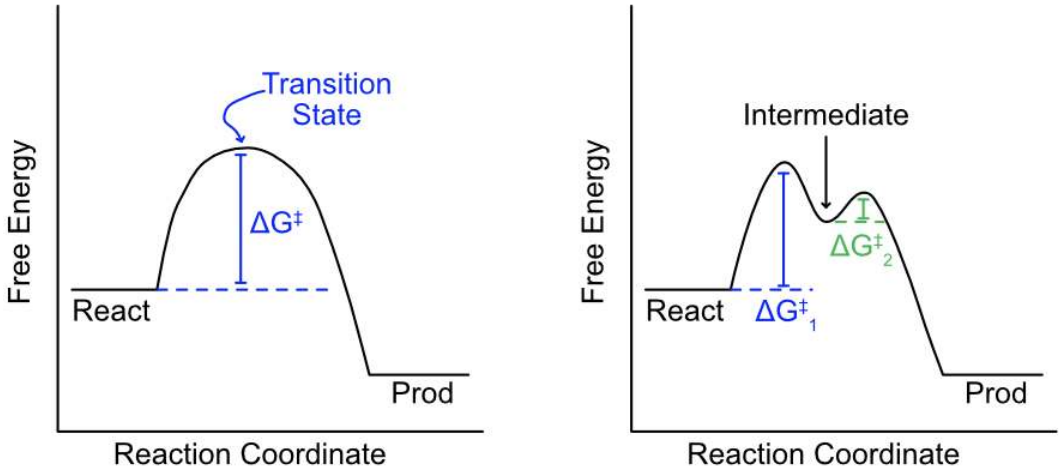


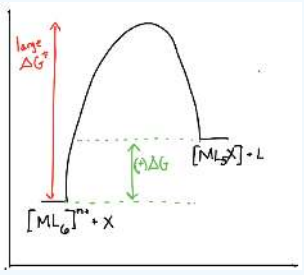
Figure **5.2.1**: Example reaction coordinate diagrams for a single step reaction (left) and a reaction with an intermediate (right). $\Delta G^{\ddagger}$ is the free energy of activation. (CC BY-NC-SA; Catherine McCusker)

Exercise 5.2.1

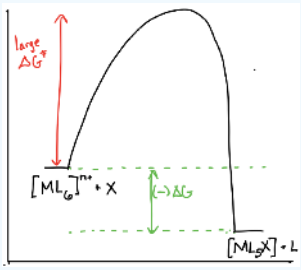
Draw the reaction coordinate diagrams for a reaction of the form $[ML_6]^{n+} + X \rightleftharpoons [ML_5X]^{n+} + L$ in the following scenarios:

a. $[ML_6]^{n+}$ is thermodynamically stable and kinetically inert.
b. $[ML_6]^{n+}$ is thermodynamically unstable and kinetically inert.
c. $[ML_6]^{n+}$ is thermodynamically stable and kinetically labile.
d. $[ML_6]^{n+}$ is thermodynamically unstable and kinetically labile.

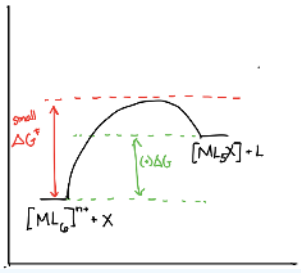
Answer a)



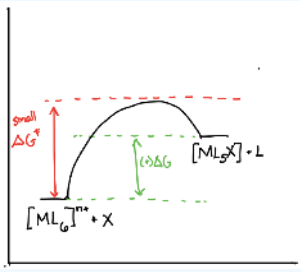
Answer b)



Answer c)



Answer d)



Self Exchange Reactions

$$[ML_5L]^{n+} + L \rightleftharpoons [ML_5L]^{n+} + L \tag{5.2.1}$$

The rate of a chemical reaction depends on both thermodynamic and kinetic factors. One way to isolate the kinetic factors is to study self exchange reactions. In a self exchange reaction the incoming and outgoing ligand are the same and the ΔG_{rxn} of the reaction is 0. In practice this is often done by dissolving hexaaqua metal complexes in isotopically labeled water and monitoring the ligand exchange reaction by NMR. These experiments have found reaction rates for different metals that span more than 12 orders of magnitude as shown in Figure 5.2.2.

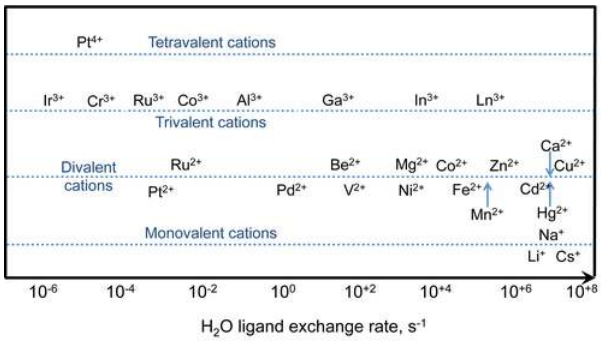


Figure 5.2.2: Water exchange rates measured by NMR for a series of metal ions. (CC BY-SA; Tem5psu via Wikimedia)

Factors that Affect Rates of Substitution Reactions

Some of the factors that affect rates of ligand substitution reactions are those that also affect thermodynamic stability. It is important to remember that kinetic and thermodynamic factors are related, yet separate. The same factors that make a complex stable can also make it more inert. However, it is incorrect to assume that stability is always correlated with reaction rates.

Why are kinetic factors related to thermodynamic stability? For a complex to react or exchange one ligand for another, it must change its geometry to form an intermediate or transition state. For example, inert octahedral complexes often have stable electron configurations. When the reactant electron configuration is particularly stable, it can result in a higher activation energy associated with moving away from the stable configuration.

Factors to consider

1. Electron configuration and LFSE: Electron configurations that place electrons in higher-energy orbitals (particularly antibonding orbitals) result in more labile complexes. As long as there are not electrons in higher-energy orbitals, the lability correlates roughly with LFSE. The more negative the LFSE, the more inert.
2. Size and charge of the metal ion: In general, higher charge density on the metal ion leads to stronger electrostatic attraction between metal and ligand; higher charge density generally correlates with slower rates of ligand substitution.

Taube's Observations of Substitution Rates

Henry Taube (Nobel Prize, 1983) tried to understand lability by comparing the factors that govern bond strengths in ionic complexes to observations about the rates of reaction of coordination complexes. He saw some things that were unsurprising. He also drew some new conclusions based on ligand field theory. Taube observed that many M^{+1} ions are more labile than many M^{+3} ions, in general. That isn't too surprising, since metal ions function as electrophiles or Lewis acids and ligands function as nucleophiles or Lewis bases in forming coordination complexes. In other words, metals with higher charges ought to be stronger Lewis acids, and so they should bind ligands more tightly. However, there were exceptions to that general rule. For example, Taube also observed that Mo^{+5} compounds are more labile than Mo^{+3} compounds. So, there must be more going on here than just the effects of electrostatic attraction.

Another factor that governs ionic bond strengths is the size of the ion. Typically, ions with smaller atomic radii form stronger bonds than ions with larger radii. Taube observed that Al^{3+}, V^{3+}, Fe^{3+} and Ga^{3+} ions are all about the same size. All these ions exchange ligands at about the same rate. That isn't surprising, because they have the same charge and the same radius. However, Cr^{3+} is also about the same size as those ions and it also has the same charge, but it is much less labile. Once again, there are exceptions to our regular expectations based on simple electrostatic considerations. Furthermore, 4d and 5d transition metals (Y→Cd, and Ac→Hg) are much more inert than 3d transition metals (Sc→Zn). This is unexpected when we consider size; the 4d and 5d metals are much larger than the 3d metals. This unexpected behavior tells us that electrostatics alone cannot predict lability.

Exercise 5.2.2

In which compound from each pair would you expect the strongest ionic bonds? Why?

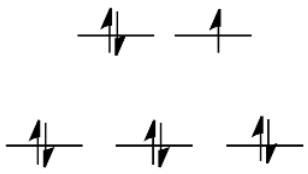
a) LiF vs KBr
b) $CaCl_2$ vs. KCl

Answer a

The ions in LiF are both smaller than in KBr, so the force of attraction between the ions in LiF is greater because of the smaller separation between the charges.

Answer b

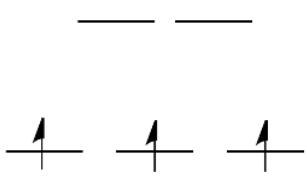
Calcium has a 2+ charge in $CaCl_2$, whereas potassium has only a + charge, so the chloride ions are more strongly attracted to the calcium than to the potassium.



Cu^{2+}

Taube came up with a hypothesis that could explain the seeming contradictory observations described above: *kinetic lability must be affected by d-electron configuration*. This idea forms the basis of Taube's rules about lability. For example, metals like Ni^{2+} and Cu^{2+} are very labile. The d orbital splitting diagrams for those compounds would have d electrons in the e_g set. Remember, the e_g

set arises from interaction with the ligand donor orbitals; this set corresponds to a σ antibonding level. By comparison, V^{2+} is rather inert. The d orbital splitting diagram in this case has electrons in the t_{2g} set, but none in the e_g set. So, having electrons in the higher energy, antibonding e_g level weakens the bond to the ligand, so the ligand can be replaced more easily. In the absence of those higher energy electrons, the bond to the ligand is stronger, and the ligand isn't replaced as easily.



V^{2+}

On the other hand, metals like Ca^{2+}, Sc^{3+} and Ti^{4+} are pretty labile. The d orbital splitting diagrams in those cases are pretty simple: there are no d-electrons at all in these ions. That means having no electrons in these mostly non-bonding levels leaves the complex susceptible to ligand replacement. But it's hard to see why population of an orbital that is mostly non-bonding would have an effect on ligand bond strength. Instead, this factor probably has something to do with the part of ligand substitution that we have ignored so far. Not only does one ligand need to leave, but a second one needs to bond in its place. So, having an empty orbital for the ligand to donate electrons into (or, put another way, not having electrons in the way that may complicate donation from the ligand) makes that part of the reaction easier.

Electron configurations can be generally classified as inert or labile based on crystal field stabilization energy. Configurations with high CFSE will be inert and configurations with low CFSE will be labile. Configurations that are most susceptible to Jahn-Teller distortions will be exceptionally labile, as the elongated bonds will be weaker and those ligands more easily exchanged.

Labile and inert electron configurations

Inert	Labile	Very labile
d^3, ls d^4, ls d^5, ls d^6,	d^1, d^2, hs d^5, hs d^6, hs d^7, d^{10}	hs d^4, d^9

Exercise 5.2.3

Put the metal ions in order of decreasing reaction rate (from labile to inert):

a) Al^{3+}, Na^{+}, Mg^{2+}

b) $Ca^{2+}, Mg^{2+}, Sr^{2+}$

Answer (a)

Most labile to most inert: $Na^{+} > Mg^{2+} > Al^{3+}$

These are metal ions with similar size and varying charge. They are in order of increasing charge and increasing density from left to right.

Answer (b)

Most labile to most inert: $Sr^{2+} > Ca^{2+} > Mg^{2+}$

These metal ions have the same charge, and vary in size. They are in order of decreasing charge and increasing charge density from left to right.

Exercise 5.2.4

Predict whether octahedral complexes of the following metals are labile or inert

a) Co^{3+} (high spin)

b) Co^{3+} (low spin)

c) Fe^{2+} (low spin)

d) Fe^{2+} (high spin)

e) Zn^{2+}

Answer a

hs d^6 labile (electrons in higher energy d orbital set)

Answer b

ls d^6 inert (all electrons in lower energy d orbitals)

Answer c

ls d^6 inert (all electrons in lower energy d orbitals)

Answer d

hs d^5 labile (electrons in higher energy d orbital set, CFSE = 0)

Answer e

d^{10} labile (electrons in higher energy d orbital set, CFSE = 0)

Overall Generalizations for Kinetics

1. s-block metals are very labile, except for those with very high charge density (eg. Mg^{2+} *is inert*)
2. d^{10} metals are labile (eg: Zn^{2+}, Cu^{+}, Hg^{2+})
3. Other ions with a full shell are labile (eg: La^{3+} of f-block)
4. 3d M^{2+}, *when high spin*, are generally labile (eg. Cu^{2+}*is very labile*)
5. 4d and 5d are usually inert due to higher CFSE (low spin, high CFSE)
6. M^{2+} is more labile than the same metal as M^{3+}
7. d^3 and low spin d^6 are inert (eg. Cr^{3+}, Co^{3+}, low spin Fe^{2+})

Attribution

Chris P Schaller, Ph.D., (College of Saint Benedict / Saint John's University)

Curated or created by Kathryn Haas

- Modified by Catherine McCusker (East Tennessee State University)

5.2: Trends in Kinetic Lability is shared under a CC BY-NC-SA 4.0 license and was authored, remixed, and/or curated by LibreTexts.

- **10.2: Trends in Kinetic Lability** has no license indicated.

5.3: Ligand Substitution Mechanisms

Ligand Substitution Reactions

Ligand substitution is one of the simplest reactions a metal complex may undergo. In general, ligand substitution involves the exchange of one ligand for another, with no change in oxidation state at the metal center. The incoming and outgoing ligands may be neutral or ionic but the charge of the complex changes if the ligand charge changes. Keep charge conservation in mind when writing out ligand substitutions.

How do we know when a ligand substitution reaction is favorable? The thermodynamics of the reaction depend on the relative strength of the two metal-ligand bonds, and the stability of the departing and incoming ligands (or salts of the ligand, if they're ionic). It's often useful to think of X-for-X substitutions like acid-base reactions, with the metal and spectator ligands serving as a "glorified proton." Like acid-base equilibria in organic chemistry, we look to the relative stability of the two charged species (the free ligands) to draw conclusions. Of course, we don't necessarily need to rely just on thermodynamics to drive ligand substitution reactions. Photochemistry, neighboring-group participation, relative concentrations, and other tools can facilitate otherwise difficult substitutions.

Ligand substitution is characterized by a continuum of mechanisms bound by associative (A) and dissociative (D) extremes. At the associative extreme, the incoming ligand first forms a bond to the metal, then the departing ligand takes its lone pair and leaves. At the dissociative extreme, the order of events is opposite—the departing ligand leaves, then the incoming ligand comes in. Associative substitution is common for square planar (like d8 complexes of Ni, Pd, and Pt), while dissociative substitution is more common for octahedral complexes. Then again, reality is often more complicated than these extremes. In some cases, evidence is available for simultaneous dissociation and association, and this mechanism has been given the name interchange (IA or ID).

Associative Substitution

The associative substitution reaction is the inorganic analog of an S_{N2} reaction. In associative ligand substitution, the incoming ligand (Y) forms a new bond with the metal (M) before the bond to the leaving ligand (X) breaks. The first step, formation of the new M-Y bond is generally rate-determining. A typical mechanism for associative ligand substitution in both octahedral and square planar complexes is shown in Figure 5.3.1.

$$ML_nX \xrightarrow{Y} ML_nXY \rightarrow ML_nY + X \tag{5.3.1}$$

In an octahedral complex the intermediate is 7 coordinate, so associative ligand exchange in octahedral complexes is rare and only favored with larger metal ions and ligands that are not sterically demanding. In contrast, ligand substitution in square planar complexes almost always occurs via an associative mechanism, involving approach of the incoming ligand to the open coordination sites above or below the plane. Let's begin with the kinetics of the reaction. How can we spot an associative mechanism in experimental data, and what are some of the consequences of this mechanism?

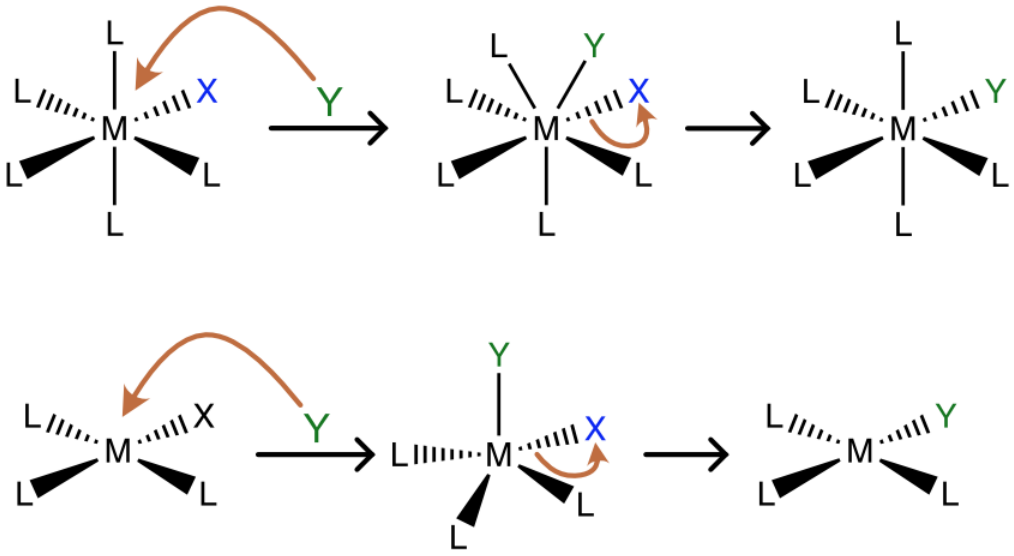


Figure 5.3.1: Scheme of associative ligand substitution in an octahedral (top) and square planar (bottom) metal complex. (CC BY-NC-SA; Catherine McCusker)

Reaction Kinetics

$$L_nM\text{–}X + Y \xrightarrow{k_1} L_nM\text{–}Y + X \tag{5.3.2}$$

$$\frac{d[L_nM\text{–}Y]}{dt} = rate = k_1[L_nM\text{–}X][Y] \tag{5.3.3}$$

Reaction kinetics are commonly used to elucidate reaction mechanisms, and ligand substitution is no exception. Different mechanisms of substitution may follow different rate laws, so plotting the dependence of reaction rate on concentration often allows us to distinguish mechanisms. In the associative mechanism, the rate law is second order overall, first order in both L_nMX and Y. (Figure 5.3.2). If a large excess of Y is used in the reaction is will become pseudo first order, where the reaction appears first order because the [Y] doesn't change significantly over the course of the reaction.

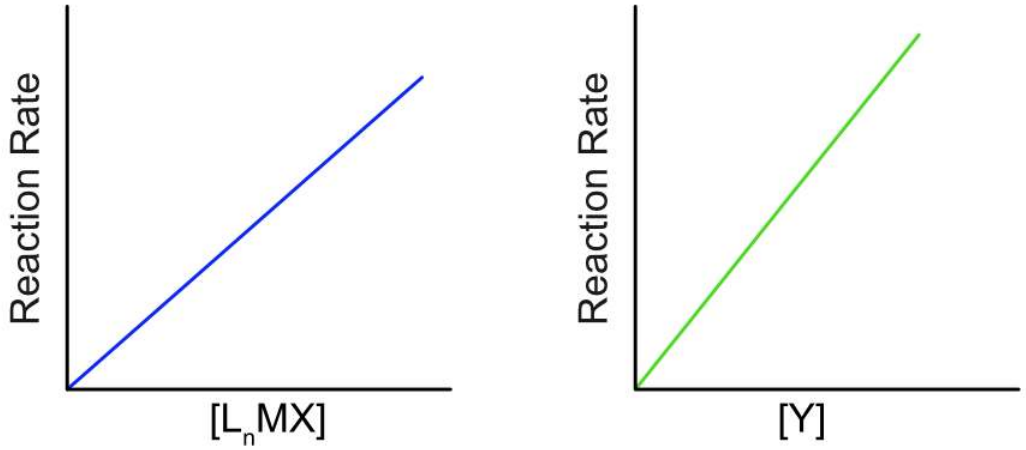


Figure 5.3.2: Dependence of associative reaction rate on concentration of the starting metal complex [ML_nX] and the incoming ligand [Y]. (CC BY-NC-SA; Catherine McCusker)

Dissociative Substitution

The associative substitution mechanism is unlikely for 6 coordinate complexes. For octahedral complexes dissociative substitution mechanisms involving 5 coordinate intermediates are more likely. In

a slow step, the departing ligand leaves, generating a coordinatively unsaturated 5 coordinate intermediate. The incoming ligand then enters the coordination sphere of the metal to generate the product. We'll focus on the kinetics of the reaction and the nature of the unsaturated intermediate (which influences the stereochemistry of the reaction). The reverse of the first step, re-coordination of the departing ligand (rate constant k_{-1}), is often competitive with dissociation.

$$ML_nX \rightarrow ML_n + X + Y \rightarrow ML_nY + X \tag{5.3.4}$$

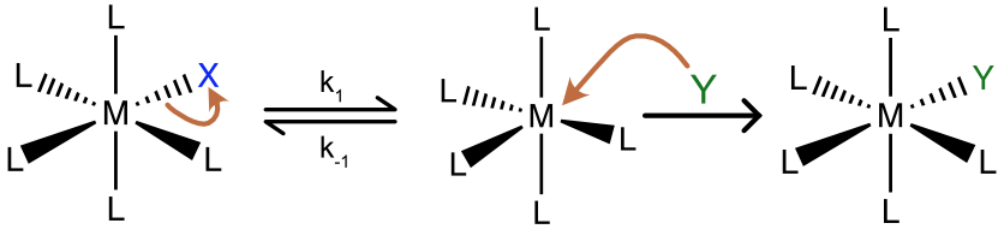


Figure 5.3.3: A general scheme for dissociative ligand substitution in an octahedral complex. (CC BY-NC-SA; Catherine McCusker)

Reaction Kinetics

Let's begin with the general situation in which k_1 and k_{-1} are similar in magnitude. Since k_1 is rate limiting, k_2, the rate of the second step is assumed to be much larger than k_1 and k_{-1}. Most importantly, we need to assume that variation in the concentration of the unsaturated intermediate is essentially zero. This is called the steady state approximation, and it allows us to set up an equation that relates reaction rate to observable concentrations.

$$\text{rate} = k_2[L_nM][Y] \tag{5.3.5}$$

Of course, the unsaturated complex is present in very small concentration and is unmeasurable, so this equation doesn't help us much. We need to remove the concentration of the unmeasurable intermediate from (1), and the steady state approximation helps us do this. We can express variation in the concentration of the unsaturated intermediate as (processes that make it) minus (processes that destroy it), multiplying by an arbitrary time length to make the units work out. All of that equals zero, according to the steady state approximation.

$$\Delta[L_nM] = 0 = (k_1[L_nM\text{–}X] – k_{-}1[L_nM][X] – k_2[L_nM][Y])\Delta t \tag{5.3.6}$$

$$0 = k_1[L_nM\text{–}X] – k_{-1}[L_nM][X] – k_2[L_nM][Y] \tag{5.3.7}$$

Rearranging to solve for [L_nM], we arrive at the following.

$$[L_nM] = k_1\frac{[L_nM\text{–}X]}{(k_{-1}[X] + k_2[Y]} \tag{5.3.8}$$

Finally, substituting into Equation 5.3.5 we reach a verifiable rate equation.

$$\text{rate} = k_2k_1\frac{[L_nM\text{–}X][Y]}{(k_{-1}[X] + k_2[Y])} \tag{5.3.9}$$

When k_{-1} is negligibly small, Equation 5.3.9 reduces to the familiar Equation 5.3.10, typical of dissociative reactions like S_N1.

$$\text{rate} = k_1[L_nM\text{–}X] \tag{5.3.10}$$

This rate does not depend on the concentration of incoming ligand. For reactions that are better described by Equation 5.3.9, we can use a large excess of Y to make $k_2[Y]$ far greater than $k_{-1}[X]$, essentially forcing the reaction to fit Equation 5.3.10.

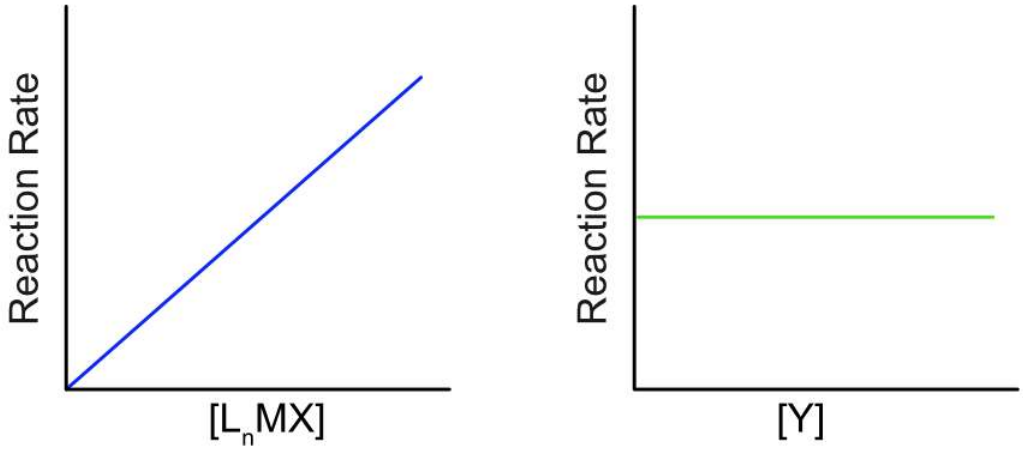


Figure **5.3.4**: Dependence of dissociative reaction rate on concentration of the starting metal complex [ML_nX] and the incoming ligand [Y]. (CC BY-NC-SA; Catherine McCusker)

Stereochemistry

Dissociation of a ligand from an octahedral complex generates an unsaturated ML_5 intermediate. The five coordinate intermediate could adopt either a trigonal bipyramidal (TBP) geometry or a square pyramidal geometry (SP). Both steric and electronic factors combine to determine which geometry is most favorable. For example, with 6 d electrons an issue arises with the TBP geometry. With 6 d electrons, the TBP geometry has two unpaired electrons in degenerate orbitals. Unpaired electrons in degenerate orbitals lead to Jahn-Teller distortion. For a TBP geometry, distortion to a SP or a distorted TBP geometry removes the degeneracy, and so five-coordinate d6 complexes typically have square pyramidal or distorted TBP geometries.

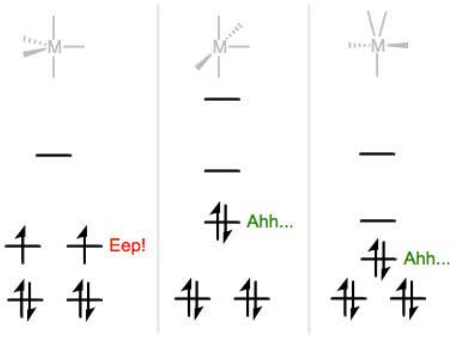


Figure **5.3.5**: TBP geometry (left) is electronically disfavored for d6 metals. Distorted TBP (right) and SP (center) geometries are favored.

When the intermediate adopts square pyramidal geometry, the incoming ligand can simply approach where the departing ligand left, resulting in retention of stereochemistry. Inversion is more likely when the intermediate is a distorted trigonal bipyramid.

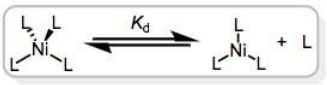
Factors That Favor Dissociative Substitution

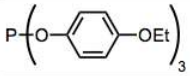
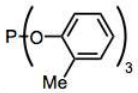
In general, introducing structural features that either stabilize the unsaturated intermediate or destabilize the starting complex can encourage dissociative substitution. Both of these strategies lower the activation barrier for the reaction.

Let's begin with features that stabilize the unsaturated intermediate. Electronically, the intermediate loves it when its d electron count is nicely matched to its crystal field orbitals. As you study inorganic chemistry, you'll learn that there are certain "natural" d electron counts for particular geometries that fit well with the metal-centered orbitals predicted by crystal field theory. Octahedral geometry is great for six d electrons, for example, and square planar geometry loves eight d electrons. Complexes with "natural" d electron counts—but bearing one extra ligand—are ripe for dissociative substitution. The classic examples are d^8 TBP complexes, which become d^8 square planar complexes (think Pt(II) and Pd(II)) upon dissociation. Similar factors actually can also stabilize the

starting complexes, making them less reactive in dissociative substitution reactions. Fro example, low spin d^6 octahedral complexes are particularly happy, and react most slowly in dissociative substitutions.

Destabilization of the starting complex is commonly accomplished by adding steric bulk to its ligands. Naturally, dissociation relieves steric congestion in the starting complex. Chelation has the opposite effect, and tends to steel the starting complex against dissociation.



L	Cone Angle	K_d
$P(OEt)_3$	109	$< 10^{-10}$
	128	$6 * 10^{-10}$
$P(Oi\text{-}Pr)_3$	130	$2.7 * 10^{-5}$
	141	$4 * 10^{-2}$
PPh_3	145	huge

As steric bulk on the ligand increases, dissociation becomes more favorable.

Interchange Substitution

Real life chemical reactions don't always fall neatly into one of the categories above. In some cases the M-X bond can break and the M-Y bond can form simultaneously. An interchange reaction is a concerted reaction without an intermediate. The transition state is a species where the bond to Y is partially formed and the bond to X is partially broken as seen in Figure **5.3.6**. If the new M-Y bond forms faster than the M-X bond breaks tat is an associative interchange (IA) reaction and if the M-X bond breaks faster than the new M-Y bond forms that is a dissociative interchange reaction (ID)

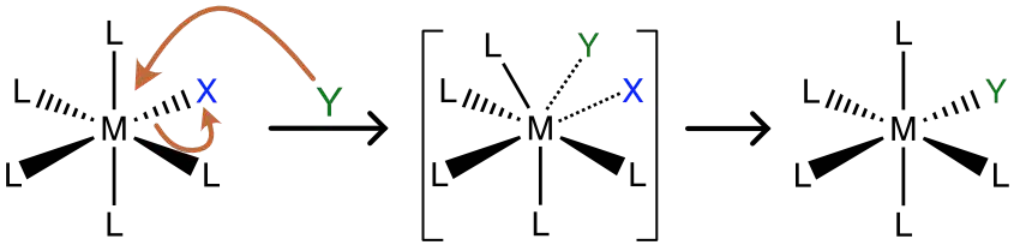


Figure **5.3.6**: A general scheme for an interchange ligand substitution reaction. Species in brackets is the transition state, not an intermediate. (CC BY-NC-SA; Catherine McCusker)

Contributors and Attributions

- Dr. Michael Evans (Georgia Tech)
- Modified by Catherine McCusker (East Tennessee State University)

This page titled 5.3: Ligand Substitution Mechanisms is shared under a CC BY-NC-SA 4.0 license and was authored, remixed, and/or curated by Michael Evans.

- **10.3: Ligand Substitution Mechanisms** by Michael Evans is licensed CC BY-NC-SA 4.0.
- **4.2: Associative Ligand Substitution** by Michael Evans is licensed CC BY-NC-SA 4.0.
- **4.3: Dissociative Ligand Substitution Reactions** by Michael Evans is licensed CC BY-NC-SA 4.0.
- **4.4: Ligand substitution** by Michael Evans is licensed CC BY-NC-SA 4.0.

5.4: Substitutions in Square Planar Complexes

Substitutions in square planar complexes tend to occur through mechanisms with associative character, although the degree of associative character may vary (eg A, I_a, I_d. The outcome of square planar substitutions depend on the identities of the leaving group, the ligand trans to the leaving group, and the entering group. The reactions of Pt(II) are well studied and will serve as the primary examples in this section. Pt(II) complexes are of particular interest because of their role as effective chemotherapeutics in the treatment of several types of solid tumor cancers.

The generic chemical equation for substitution in a square planar complex is shown below, where X is the leaving group, Y is the entering group, and $[ML_3X]$ is the reactant complex:

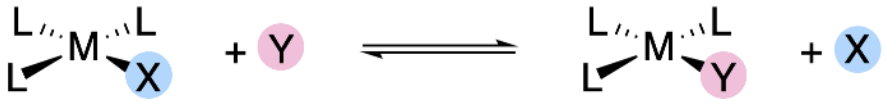


Figure 5.4.1: Generic form of square planar metal complex undergoing a substitution reaction. (CC-BY-SA; Kathryn Haas)

This page titled 5.4: Substitutions in Square Planar Complexes is shared under a CC BY-NC-SA 4.0 license and was authored, remixed, and/or curated by Kathryn Haas.

5.4.1: Kinetics and Stereochemistry of Square Planar Reactions

Kinetics

In general, the reaction kinetics of square-planar associative substitution takes the form of the following rate law, which has two terms:

$$\frac{d[ML_3Y]}{dT} = k_1[ML_3X] + k_2[ML_3X][Y]$$

Each of the terms corresponds to one of the two possible reaction pathways. The term, $k_2[ML_3X][Y]$, is second-order, and corresponds to a simple associative pathway. The $k_1[ML_3X]$ term is first-order, although it also corresponds to an associative pathway. The reason it appears to be first order is because square planar complexes can react through a solvent-assisted pathway where bulk solvent replaces the leaving group, and then is replaced by the entering group (Figure **5.4.1.2**). Because solvent concentration does not appreciably change as the reaction proceeds, it is not part of the rate law term even though it is involved in the rate-determining association. The step in which solvent is substituted by the entering group must happen faster than the solvent-assisted replacement of X.

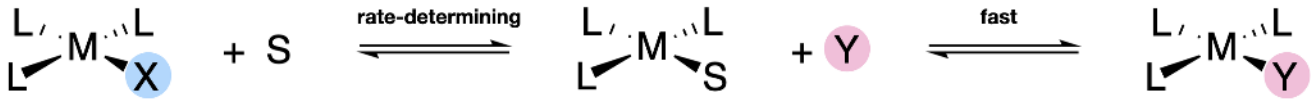


Figure **5.4.1.2**: Solvent-assisted substitution pathway where X is the leaving group, Y is the entering group, and S is solvent. (CC-BY-SA; Kathryn Haas)

The kinetic rate constats in square planar substitution can depend on the identities of the leaving group, the ligand trans to the leaving group, and the entering group. The ligands that are in the ***cis*** positions with respect to the leaving group do not have a significant affect on the rate, and these are referred to as spectator ligands.

Stereochemistry

Square planar complexes react to give products in which the stereochemistry of the reactant is retained. In other words, a *trans*-reactant will give a *trans*-product, and a *cis*-reactant will give a *cis*-product (Figure **5.4.1.3**). The identity of the trans ligand has particular importance in the outcome of square planar substitutions (discussed further in the next sections). We will designate the trans ligand generally with the symbol T to indicate its position (Figure **5.4.1.3**), the leaving group as X, and the entering group as Y. The spectator ligands (ligands that are ***cis*** to X) will be desginated L and L'. For the discussion that follows, the plane of the metal complex will be designated as the xy plane, while the z axis is perpendicular to the plane (Figure **5.4.1.3**). The x and y axes will run colinear to the bond axes, with the x axis running colinear to the T-M-X bonds (Figure **5.4.1.3**).

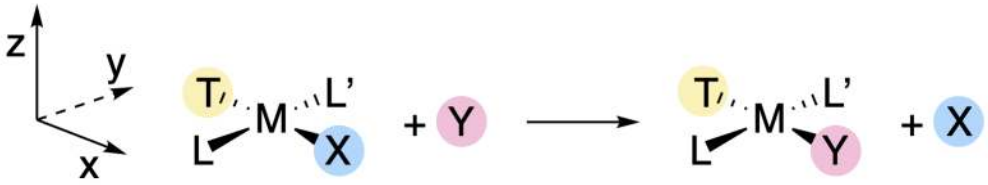


Figure **5.4.1.3**: Stereochemistry is strictly retained in the reactions of square planar complexes. By convention, the plane of the metal complex is the xy plane, with the x axis colinear with the T-M-X bonds. M = metal ion | X = leaving group ligand | Y = entering group ligand | T = ligand trans to the leaving/entering group. (CC-BY-SA; Kathryn Haas)

The retention of stereochemistry, and the fact that X, Y, and T can influence the rate of reaction provide hints at the nature of intermediates and/or transition states involved in these reactions. The existence of five-coordinate square pyramidal structures, like those of $[Ni(CN)_5]^{3-}$ and $[Pt(SnCl_3)_5]^{3-}$, suggests that five-coordinate intermediates are possible. However the substitutions of square planar complexes are generally classified as associative interchange mechanisms (I_a) because isolation of a true intermediate is rarely accomplished. In any case, the retention of stereochemistry is explained by a five-coordinate trigonal bipyramidal transition state in which X, Y, and T are each in the trigonal plane (along with the metal center). As the M-X bond is breaking, the M-Y bond is forming and Y replaces X in the position trans to T. Because T, Y and X are in the trigonal plane in the

transition state, all three ligands are able to interact with the same ***d*** orbitals of the central metal ion. Thus the identities of X, Y, and T should influence the ability of the M-X bond to break and the M-Y bond to form. On the other hand, L and L' are in a perpendicular plane, and would interact with different orbitals than X and Y. This explains why spectator ligands L and L' have little effect on the reaction rate, as they are interacting with different orbitals than those involved in bond breaking and bond making.

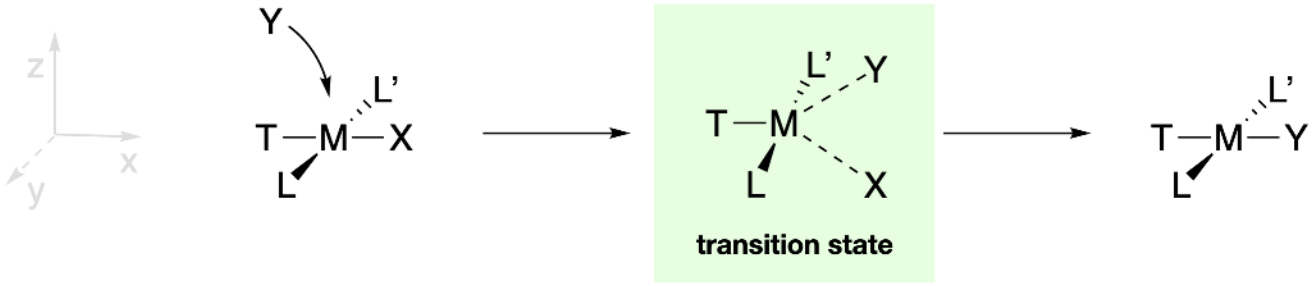


Figure **5.4.1.4**: Mechanism for simple I_a substitution. The structure of the transition state is trigonal bipyramidal, with T, X, and Y in the trigonal plane with M. The spectator ligands, L and L', are in a perpendicular plane and are coplanar with T and M. (CC-BY-SA; Kathryn Haas)

The solvent-assisted pathway can occur through similar transition states and mechanistic steps, except that there are additional steps involving solvent association and displacement.

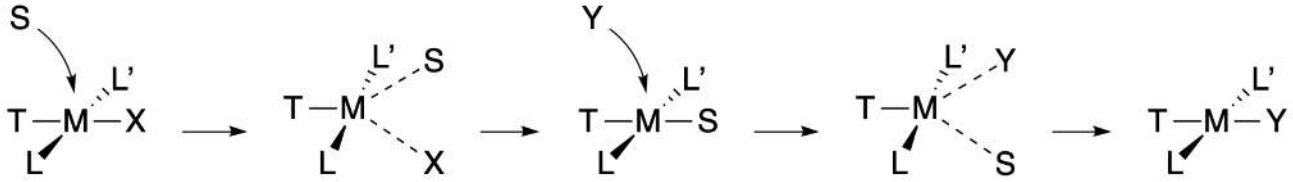


Figure **5.4.1.5**: Solvent-assisted I_a substitution. Compare to Figure **5.4.1.4**. S is solvent. (CC-BY-SA; Kathryn Haas)

Although there is general consensus that square planar complexes react through associative pathways, the characterization of intermediates and/or transition states has remained elusive, and there is still debate as to the intricate details of the reaction mechanisms involving square planar complexes. For example, there are arguments that a six-coordinate transition state may exist in the solvent-assistant pathway.

This page titled 5.4.1: Kinetics and Stereochemistry of Square Planar Reactions is shared under a CC BY-NC-SA 4.0 license and was authored, remixed, and/or curated by Kathryn Haas.

5.4.2: Evidence for Associative Reactions

The reactions of Pt(II) complexes have been thoroughly investigated, and there are several lines of experimental evidence that have lead to the general conclusion that square planar complexes react through associative mechanisms. The experimental evidence is presented here.

The entering group

In the reaction of $\mathbf{trans-[PtL_2Cl_2]}$, the rate of reaction depends on the identity of the incoming ligand Y.

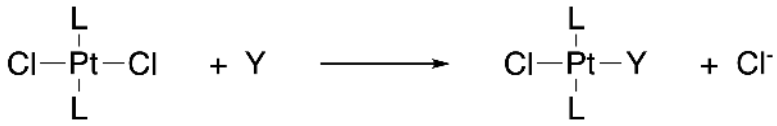


Figure **5.4.2.1**: Substitution reaction of $\mathbf{trans-[PtL_2Cl_2]}$. (CC-BY-SA; KAthryn Haas)

For example, the rate of the reaction shown above depends heavily on the ligand, Y, as follows:

$$\mathbf{most\ kinetically\ labile\ PR_3 > CN^- > SCN^- > I^- > Br^- > N_3^- > NO_2^- > py > NH_3 \quad Cl^- > CH_3OH\ most\ kinetically\ inert}$$

In general, ligands that would form the strongest bonds with Pt(II) due to their soft character or π-binding ability react fastest. The rate constants in the above series range by nearly ten orders of magnitude. This huge range of rate constants as a factor of Y demonstrates suggests that M-Y bond formation is part of the rate limiting step. This is evidence for rate-determining association $\boldsymbol{A}$ or $\boldsymbol{I_a}$.

The leaving group

Since the leaving group occupies a similar position in the transition state as the entering group, we should expect the leaving group to have a similar effect on the rate constants as was found for Y. In fact, this is true. For the reaction of $\mathbf{[Pt(diene)X]^+}$ with pyridine, the follow trend was observed by varying the leaving group, X:

$$\mathbf{most\ kinetically\ labile\ NO_3^- > Cl^- > Br^- > I^- > N_3^- > SCN^- > NO_2^- > CN^-\ most\ kinetically\ inert}$$

The rate of reaction follows an order that is nearly opposite as that observed for Y: The softer the ligand, the slower the dissociation. The rate constants in this series span a range of approximately five orders of magnitude, illustrating that breaking of the M-X bond is part of the rate-determining step. This is evidence for a mechanism involving associative interchange character ($\boldsymbol{I_a}$ or $\boldsymbol{I_d}$. The importance of the leaving group somewhat depends on the identity of the entering group, and vice-versus.

The trans ligand

The trans ligand also occupies a similar position to X and Y in the transition state. So, as you might expect, it too has influence on the rate of reaction. In general, the rate of substitution of X in Pt(II) complexes general follows the order given below when T is varied as:

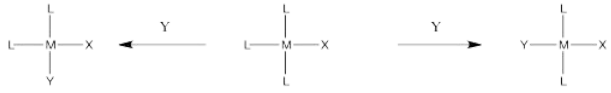
$$\mathbf{M\text{-}X\ most\ kinetically\ labile\ CN^- \quad CO \quad C_2H_4 > PH_3 \quad SH_2 > NO_2^- > I^- > Br^- > py \quad NH_3 > OH^- > H_2O\ M\text{-}X\ most\ kinetically\ inert}$$

The effect of the trans ligand deserves a more through discussion, and will be addressed in the next section. It is mentioned here because it is evidence for the trigonal bipyramidal intermediate that was described earlier for associative substitution in square planar metal complexes.

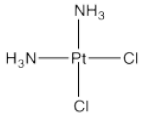
This page titled 5.4.2: Evidence for Associative Reactions is shared under a CC BY-NC-SA 4.0 license and was authored, remixed, and/or curated by Kathryn Haas.

5.5: The Trans Effect Observation

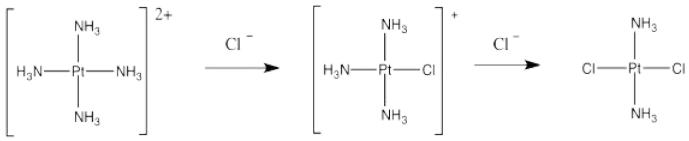
Occasionally in ligand substitution there is a situation in which there are two identical ligands that could be replaced, but two different products would result depending on which ligand left. This situation often happens in square planar complexes, for example. Replacement of one ligand would lead to a *cis* product. Replacement of the other one would lead to a *trans* product.



An important example of this issue is in the synthesis of cis-platin, an antitumour medication frequently used to treat ovarian and testicular cancer.

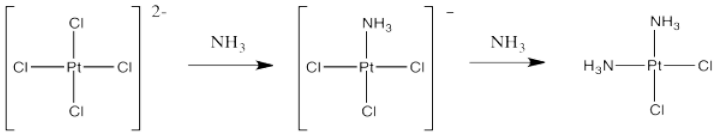


Cis-platin could be made from treatment of tetraammineplatinum(II) with chloride salts. The chloride ion could replace two of the ammonia ligands.



But that doesn't work. That synthesis results in the formation of *trans*-platin, a compound that has all of the nasty side effects of the *cis* isomer but with none of the therapeautic benefit.

If instead you were to start with tetrachloroplatinate salts and treat them with ammonia, you could replace two of the chloride ligands. That works really well, and it provides *cis*-platin, not *trans*-platin.



? Exercise 5.5.1

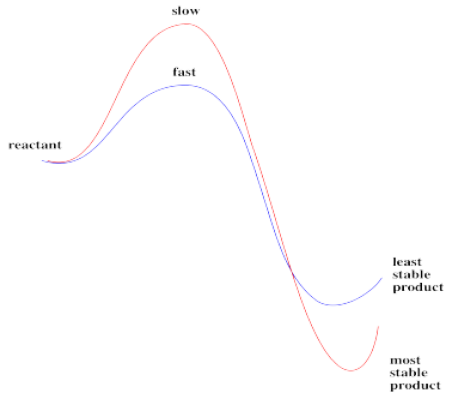
What do you think is the mechanism of substitution of the two reactions above? Why?

Answer

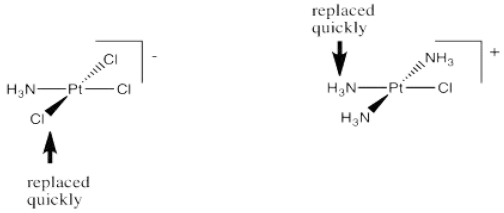
This is probably an associative mechanism because of the square planar geometry.

This reaction, if run under these conditions, is clearly not always under thermodynamic control. Two different products result, depending on how the reaction is done. One of those isomers is probably more stable than the other; if thermodynamics were in charge, it would form the same thing both times.

Instead, there may be an element of kinetic control for at least one of the pathways. A given product might be made, not because it is more stable, but simply because it forms more quickly than the other one.



Take another look at those two reactions. One of the things that they have in common is that the ligand that gets replaced is *trans* to a chloride. It is not *trans* to an ammonia. Maybe the other ligands in the complex can influence how quickly one ligand can leave.



Specifically, the "*trans* effect" is the role of *trans*-ligands in influencing substitution rates in square planar complexes.

The following kinetic data were obtained for substitutions on square planar platinum complexes, in the reaction:

$$trans-(PEt_3)_2PtLCl + py \rightarrow trans-(PEt_3)_2PtLpy^+ + Cl^-$$

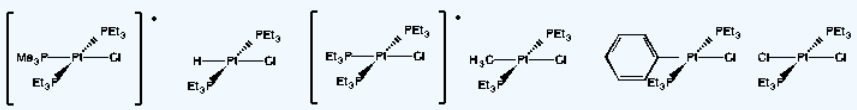
L	k_{obs} (s^{-1})	T, °C
PMe_3	0.20	0
H^-	0.047	0
PEt_3	0.041	0
CH_3^-	6.0×10^{-4}	25
$C_6H_5^-$	1.2×10^{-4}	25
Cl^-	3.5×10^{-6}	25

Ref: Cooper Langford & Harry Gray, *Ligand Substitution Processes*, W.A. Benjamin, NY, 1965, p. 25.

? Exercise 5.5.2

Draw structures for each of the complexes listed in the table.

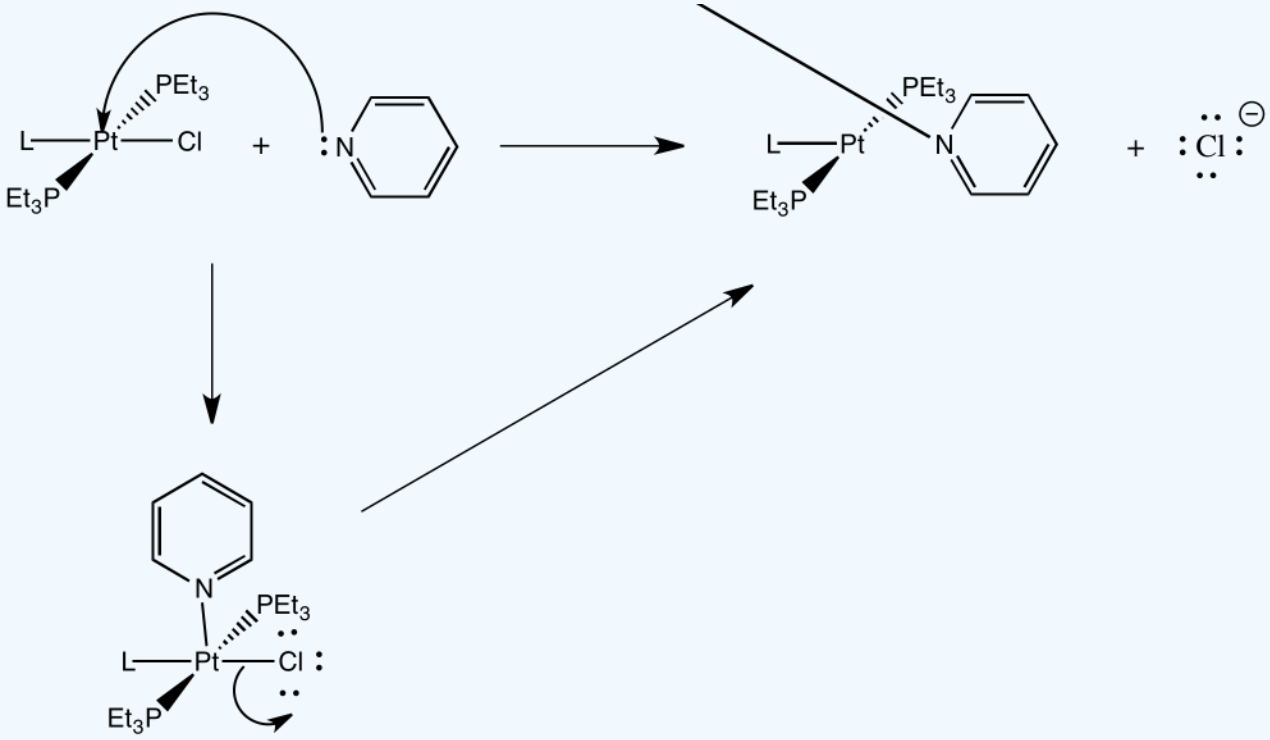
Answer



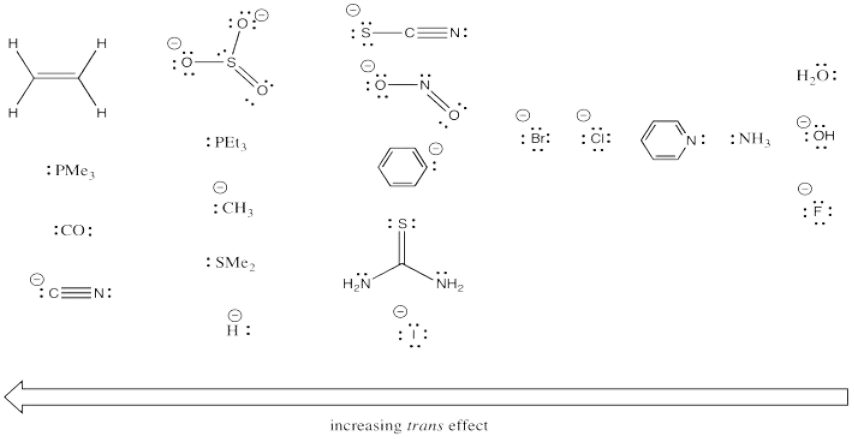
Exercise 5.5.3

Provide a mechanism with arrows for the reaction studied in the table.

Answer



Clearly that *trans* ligand has a dramatic effect on how quickly the chloride can be substituted in the above study. Additional studies like this one have led to some general trends. Below, the ligands on the left have strong *trans*-effects. Ligands *trans* to them are substituted very quickly. The ligands on the right have very modest *trans* effects. Ligands *trans* to them are substituted only slowly.



Exercise 5.5.4

Look for empirical trends in the series of ligands above. Without trying to explain exactly why, find chemically relevant factors that may be responsible for these reactivity trends.

Answer

There is an electronegativity trend: the less electronegative, the greater the *trans* effect (see the halogens, as well as the series O,N,C and also the orders within several pairings: S,P; O,S and N,P).

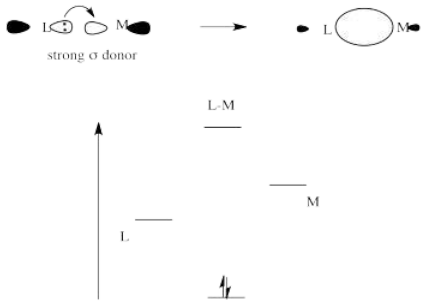
Alternatively, some of the above could be described by a polarizability trend: more polarizable atom, greater *trans* effect (for example, the halogens).

Most of the ligands containing π-bonds have strong *trans* influence (but not all).

Most of the π-donors have a weaker *trans* influence. However, these ligand cover a very broad range in this series.

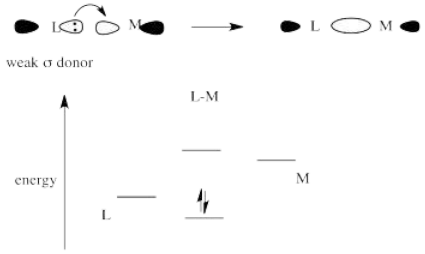
In general, explanations of the trans effect have focused on two separate types of ligands. These are strong sigma donors and strong pi acceptors.

Strong sigma donors donate electrons very effectively to the metal via a sigma bond. Because the ligand trans to this donor would be bonding via donation to the same metal p orbital, there is a competition. The metal p orbital bonds more favorably with the strong sigma donor, and the ligand trans to it is left with a weaker bond.



The strong sigma donor gets good overlap with the metal orbital and the resulting interaction goes down low in energy.

The weak sigma donor gets poorer overlap with the metal orbital and only weak stabilization of the donor electrons.



Place these two choices together, and the metal orbital will engage in a strong bonding interaction with the strong σ-donor. Doing so lowers the electronic energy significantly. It won't interact very much with the weak σ-donor, because doing that won't result in as much lowering of electronic energy. The result is a strong bond on one side of the metal and a weak bond on the other. That weak bond will break easily and that ligand will be replaced easily.



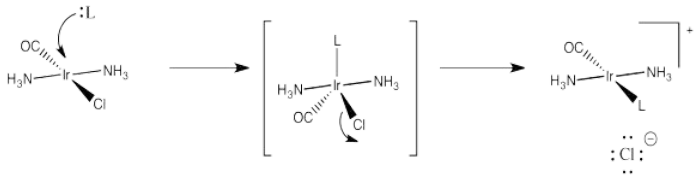
? Exercise 5.5.5

Which of the ligands in the *trans* effect series are probably strong σ-donors? Why?

Answer

The strongest σ-donors are typically those with more polarizable donor atoms (such as S, P, I) as well as those with less electronegative donor ions such as C^- and H^-.

Strong pi acceptors exert their trans effect in a different way. They are thought to stabilize a particular geometry of the five-coordinate intermediate in substitution of square planar complexes. We haven't worried too much about the geometry of that intermediate, but it is probably trigonal bipyramidal. It would have three ligands in an equatorial plane and two more directly opposite each other, in the axial positions.



Essentially, the incoming ligand pushes two of the ligands down from the square plane to form this trigonal bipyramid. When it comes time for a ligand to leave, it is probably going to be one of these ligands that is already on the move. They are already on a trajectory out of the square plane, anyway.

A strong pi acceptor like CO exerts its *trans* effect by making sure it, along with the ligand opposite it, gets into that equatorial plane. It does that by a stabilizing delocalization that happens when the π-acceptor is in the electron-rich equatorial plane. In that position, it can draw electron density via π-donation from two different donors. If it were in an axial position, it could still delocalize electrons this way, but it would draw most effectively from just one donor rather than two.



favoured

So which of those two ligands is going to keep moving and leave the complex? It certainly won't be the one that is exerting a stabilizing, delocalizing effect on the complex via its strong bonding interactions. It will be the unlucky *trans* ligand that got dragged along with it.

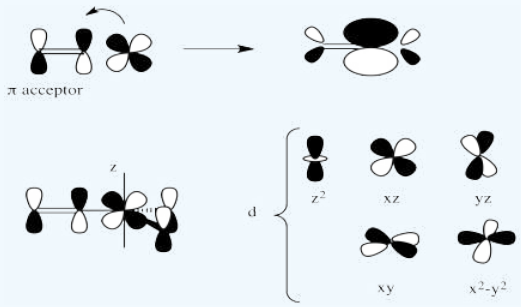
? Exercise 5.5.6

Which of the ligands in the *trans*-effect series are probably strong π-acceptors? Show why.

? Exercise 5.5.7

Draw an orbital picture showing the -delocalization described in the trigonal bipyramidal intermediate. Label the orbitals, assuming the z axis is along the axis of the trigonal bipyramid (i.e. the equatorial plane is the xy plane).

Answer



? Exercise 5.5.8

Substitution of trans ligands in μ-oxo-bis(μ-acetato)diruthenium complexes: Synthesis and kinetic studies. Hussain, Bhatt, Kumar, Thorat, Padhiyar and Shukla, *Inorganica Chemica Acta*, **2009**, *362*, 1101-1108.

Given the structure $[Ru_2O(L)_6(acetate)_2](PF_6)_2$, in which L is a neutral donor,

a) Draw the structure of the counterion, PF_6^-.

b) Provide an account of the valence electron count in the ruthenium coordination complex.

Valence electrons on metal	
Total charge on ligands	
Charge on the metal	
Revised count on metal	
Electrons donated by ligands	
Total electrons on metal in complex	

Data shows that the ligands L are *trans* to the bridging oxo ligand are labile.

c) Use orbital cartoons and words to provide an explanation for this effect.

When water is added to an acetone solution of $[Ru_2O(pyridine)_4(L)_2(acetate)_2](PF_6)_2$, then $[Ru_2O(pyridine)_4(H_2O)_2(acetate)_2](PF_6)_2$ is formed.

d) Draw the product of this reaction.

When pyridine is added to $[Ru_2O(pyridine)_4(H_2O)_2(acetate)_2](PF_6)_2$, then $[Ru_2O(pyridine)_6(acetate)_2](PF_6)_2$ is formed. The following rate constants were observed for this reaction.

[pyridine] mol L^{-1}	k_{obs} s^{-1} (x 10^{-3})
0.005	1.75
0.012	2.53
0.025	9.7
0.049	16.7
0.100	35.2

e) Use the data from this table to determine the order in pyridine. Provide an explanation for your conclusion.

f) Draw a mechanism for the reaction, consistent with the data.

g) Write a rate law for the reaction.

h) The authors studies the same reaction with different ligands instead of pyridine. They observed an increase in rate constants with increasing basicity of the incoming ligands. Provide an explanation for this observation.

Answer a



5 valence electrons - 6 bonds - 0 nonbonding = -1

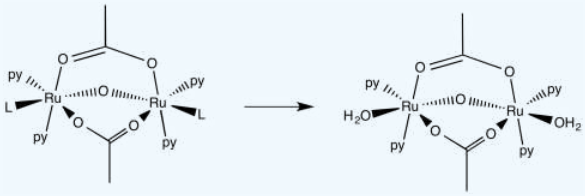
Answer b

Valence electrons on metal	8
Total charge on ligands	-4 (-2 per Ru)
Charge on the metal	+2
Revised count on metal	6
Electrons donated by ligands	12
Total electrons on metal in complex	18

Answer c

The oxo is a strong sigma donor and hogs the orbital with the metal thus leaving very little room for orbital bonding trans to the sigma donor.

Answer d



Answer e

First order. Although there is some amount of error in the data, doubling the pyridine concentration generally results in a doubling of the rate.

Answer f

The mechanism you draw would have to involve a first associative step; because the complex is already 18 electrons, associative interchange is likely.

Answer g

$$Rate = k[ML_n][py]$$

Answer h

Basic ligands have stronger attraction to the metal thus accelerating the reaction.

This page titled 5.5: The Trans Effect Observation is shared under a CC BY-NC-SA 4.0 license and was authored, remixed, and/or curated by Kathryn Haas.

- **3.7: The Trans Effect** by Chris Schaller is licensed CC BY-NC 3.0. Original source: https://employees.csbsju.edu/cschaller/ROBI2.htm.

5.6: The Trans Effect Explanation

The trans effect is an ancient but venerable observation. First noted by Chernyaev in 1926, the trans effect and its conceptual siblings (the trans influence, cis influence, and cis effect) are easy enough to comprehend. That is, it's simple enough to know what they are. To understand why they are, on the other hand, is much more difficult.

Definitions & Examples

Let's begin with definitions: what is the trans effect? There's some confusion on this point, so we need to be careful. The trans effect proper, which is often called the kinetic trans effect, refers to the observation that certain ligands increase the rate of ligand substitution when positioned trans to the departing ligand. The key word in that last sentence is "rate"—the trans effect proper is a kinetic effect. The trans influence refers to the impact of a ligand on the length of the bond trans to it in the ground state of a complex. The key phrase there is "ground state"—this is a thermodynamic effect, so it's sometimes called the thermodynamic trans effect. Adding to the insanity, cis effects and cis influences have also been observed. Evidently, ligands may also influence the kinetics or thermodynamics of their cis neighbors. All of these phenomena are independent of the metal center, but do depend profoundly on the geometry of the metal (more on that shortly).

Kinetic trans and cis effects are shown in the figure below. In both cases, we see that X1 exhibits a stronger effect than X2. The geometries shown are those for which each effect is most commonly observed. The metals and oxidation states shown are prototypical.

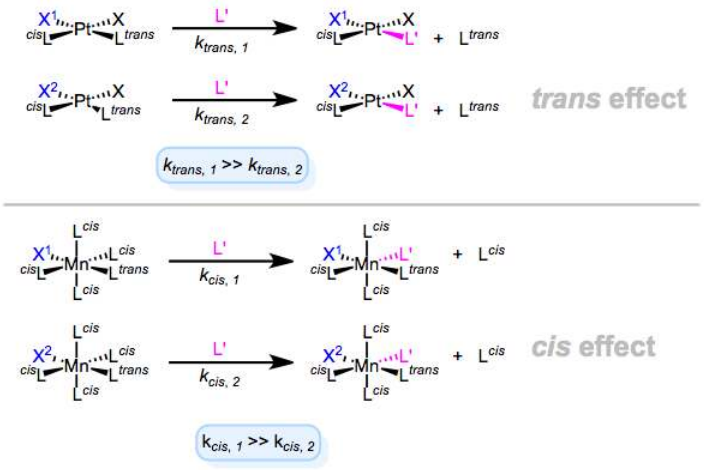


Figure 1: *The kinetic trans and cis effects in action. X^1 is the stronger (trans/cis)-effect ligand in these examples.*

On to the influences, which are simpler to illustrate since they're concerned with ground states, not reactions. The lengthened bonds below are exaggerated.

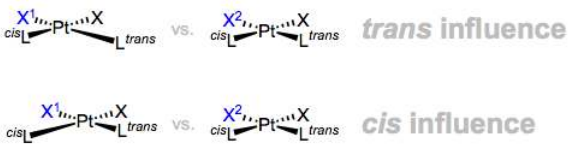


Figure 2: *The trans and cis influences in action. Note the elongated bond lengths.*

And there we have it folks, the thermodynamic and kinetic cis/trans effects. It's worth keeping in mind that the kinetic trans effect is most common for d8 square planar complexes, and the kinetic cis effect is most common for d6 octahedral complexes (particularly when the departing L is CO). But a lingering question remains: what makes for a strong trans effect ligand?

Origins of Effects & Influences

The trans effect and its cousins are all electronic, not steric effects. So, the electronic properties of the ligand dictate the strength of its trans effect. Let's finally dig into the trans effect series:

(weak) F^-, HO^-, H_2O <NH_3 < py < Cl^- < Br– < I–, SCN^-, NO_2^-, $SC(NH_2)_2$, Ph^- < SO_3^{2-} < PR_3 < AsR_3, SR_2, H_3C^- < H^-, NO, CO, NC^-, C_2H_4 (strong)

What's the electronic progression here? It's clear that electronegativity decreases across the series: F^- < Cl^- < Br^- < I^- < H_3C^-. From a bonding perspective, we can say that ligands with strong trans effects are strong σ-donors (or σ-bases). Yet σ-donation doesn't tell the whole story. What about ethylene and carbon monoxide, which both appear at the top of the heap? Neither of these ligands are strong σ-donors, but their π systems do interact with the metal center through backbonding. Consider the following sub-series: S=C=N– < PR_3 < CO. Backbonding increases across this series, along with the strength of the trans effect. Strong backbonders—better known as π-acceptors or π-acids—exhibit strong trans effects.

Strong trans effect = strong σ-donor + strong π-acceptor

Wonderful! Using these ideas we can identify ligands with strong trans effects. But we can dive deeper down the rabbit hole: why does this particular combination of electronic factors lead to a strong trans effect? To understand this, we need to know the mechanism of the ligand substitution reaction that's sped up by strong trans effect ligands. For 16-electron Pt(II) complexes, associative substitution is par for the course. The incoming ligand binds to the metal first, forming an 18-electron complex (yay!), which jettisons a ligand to yield a new 16-electron product. The mechanism in all its glory is shown in the figure below.

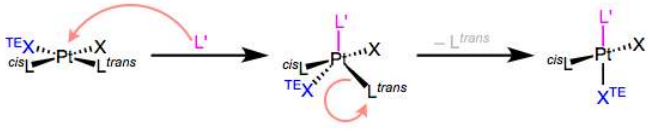


Figure 3: *The mechanism of associative ligand substitution of Pt(II) complexes.*

Some very important points about this mechanism:

- The incoming ligand always sits at an equatorial site in the trigonal bipyramidal intermediate. More on this another day, but I think of this result as governed by the principle of least motion. Consider the molecular gymnastics that would have to happen to place the incoming ligand in an axial position.
- Two ligands in the square plane are "pushed down" and become the other two equatorial ligands.
- Owing to microscopic reversibility, the leaving group must be one of the equatorial ligands.

The third point reveals that once L' has "pushed down" XTE and Ltrans, Ltrans has no choice but to leave (assuming XTE stays put). Thus, the trans effect has nothing to do with the second step of the mechanism, which is not rate determining anyway. The key is the first step—in particular, the "pushing down" event. Apparently, ligands with strong trans effects like to be pushed down. They like to occupy the equatorial plane of the TBP intermediate. Now here's the kicker: the equatorial sites of the TBP geometry are more π basic than the axial sites. The equatorial plane is just the xy-plane of the metal center, and the d orbitals in that plane (when occupied) are great electron sources for π-acidic ligands. Thus, π-acidic ligands want to occupy those equatorial sites, to receive the benefits of strong backbonding! Boom; strong π-acids encourage loss of the ligand trans to themselves.



Figure 4: *The equatorial sites of TBP metals are rich in electrons that can π bond.*

What about those pesky σ donors? Well, we can imagine that in a square planar complex, a ligand and its trans partner are competing for donation into the same d orbital. Strong σ donation from a ligand should thus weaken the bond trans to it. Although this is the thermodynamic trans effect (trans influence) in action, the resulting destabilization of the ground state relative to the transition state is a kinetic effect. On the whole, the barrier to substitution of the trans ligand goes down as σ-donating strength goes up.

This idea of "competition for the metal center" is a nice heuristic to use when thinking about the trans and cis influences. The type of metallic orbital involved in M–L bonding determines the strength of L's trans and cis influences on neighboring ligands that also need that metallic orbital for bonding. For example: both influences are large if the metal's s orbital is a significant contributor to

M–L bonding, since it's non-directional; the trans influence is much greater than the cis influence when metallic p orbitals are primarily involved in M–L. For a deeper explanation of these ideas, see this paper.

Summing up

Perhaps the most valuable lesson from a study of the trans effect is that many concepts from organometallic chemistry involve more than meets the eye. Geometric effects and influences are real icebergs, in the sense that the observations and trends are easy to grasp, but difficult to explain. We had to dig all the way into the mechanism of associative ligand substitution before a satisfactory explanation emerged!

Contributors

Dr. Michael Evans (Georgia Tech)

5.6: The Trans Effect Explanation is shared under a CC BY-NC-SA 4.0 license and was authored, remixed, and/or curated by LibreTexts.

5.7: Redox Mechanisms

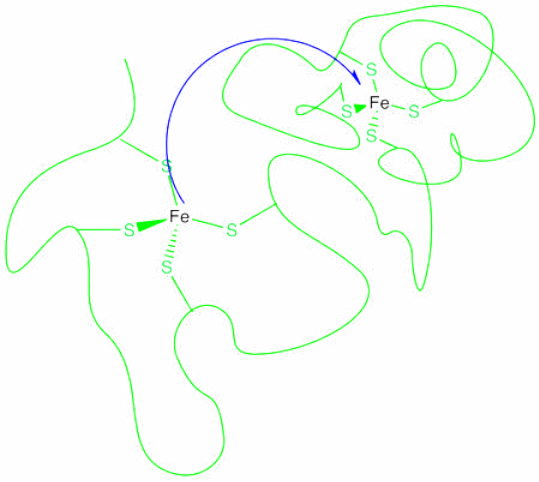
The oxidation state of a metal ion can be changed by **red**uction/**ox**idation (redox) reactions in which electrons are transferred between a metal center and another species. The other species could be another metal ion or some other redox partner. In the case of metal complexes, the electron transfer often occurs at the metal center, changing the oxidation state of the metal ion(s) involved. This section will focus on the redox reactions involving change in metal ion oxidation state.

There are two general mechanisms by which electrons can be transferred to or from a metal center. The definition of these two mechanisms depends on whether the redox partner is bound within the metal ion's inner sphere (bound directly to the metal ion), or whether it is just nearby the metal complex (in the metal ion's outer sphere). If the redox partner is bound to the metal ion itself, it is called an **inner-sphere electron transfer**. Electrons can also be transferred between two species that are close in proximity, but not bound to one another. When electrons are transferred to or from a metal through close proximity, but not through direct bonds to the metal center, it is an **outer-sphere electron transfer**.

This page titled 5.7: Redox Mechanisms is shared under a CC BY-NC-SA 4.0 license and was authored, remixed, and/or curated by Kathryn Haas.

5.7.1: Outer Sphere Electron Transfer

How does an electron get from one metal to another? This might be a more difficult task than it seems. In biochemistry, an electron may need to be transfered a considerable distance. Often, when the transfer occurs between two metals, the metal ions may be constrained in particular binding sites within a protein, or even in two different proteins.



That means the electron must travel through space to reach its destination. Its ability to do so is generally limited to just a few Angstroms (remember, an Angstrom is roughly the distance of a bond). Still, it can react with something a few bond lengths away. Most things need to actually bump into a partner before they can react with it.

This long distance hop is called an outer sphere electron transfer. The two metals react without ever contacting each other, without getting into each others' coordination spheres. Of course, there are limitations to the distance involved, and the further away the metals, the less likely the reaction. But an outer sphere electron transfer seems a little magical.

Barrier to Reaction: A Qualitative Picture of Marcus Theory

So, what holds the electron back? What is the barrier to the reaction? Rudy Marcus at Caltech has developed a mathematical approach to understanding the kinetics of electron transfer, in work he did beginning in the late 1950's. We will take a very qualitative look at some of the ideas in what is referred to as "Marcus Theory". An electron is small and very fast. All those big, heavy atoms involved in the picture are lumbering and slow. The barrier to the reaction has little to do with the electron's ability to whiz around, although even that is limited by distance. Instead, it has everything to do with all of those things that are barely moving compared to the electron.

Imagine an iron(II) ion is passing an electron to an iron(III) ion. After the electron transfer, they have switched identities; the first has become an iron(III) and the second has become an iron(II) ion.

Nothing could be simpler. The trouble is, there are big differences between an iron(II) ion and an iron(III) ion. For example, in a coordination complex, they have very different bond distances. Why is that a problem? Because when the electron hops, the two iron atoms find themselves in sub-optimal coordination environments.

? Exercise 5.7.1.1

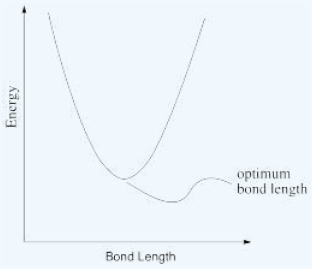
Suppose an electron is transferred from an Fe(II) to a Cu(II) ion. Describe how the bond lengths might change in each case, and why. Don't worry about what the specific ligands are.

Answer

The bonds to iron would contract because the increased charge on the iron would attract the ligand donor electrons more strongly. The bonds to copper would lengthen because of the lower charge on the copper.

Exercise 5.7.1.2

In reality, a bond length is not static. If there is a little energy around, the bond can lengthen and shorten a little bit, or vibrate. A typical graph of molecular energy vs. bond length is shown below.



a. Why do you think energy increases when the bond gets shorter than optimal?
b. Why do you think energy increases when the bond gets longer than optimal?
c. In the following drawings, energy is being added as we go from left to right. Describe what is happening to the bond length as available energy increases.

Answer a

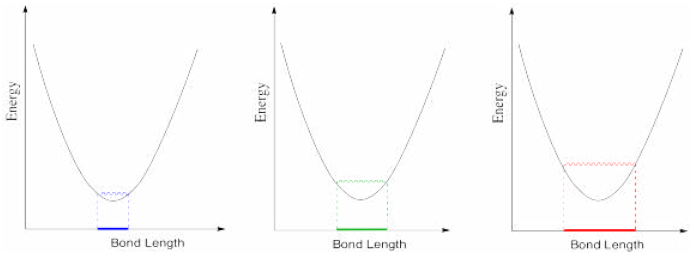
a) Most likely there are repulsive forces between ligands if the bonds get too short.

Answer b

b) Insufficient overlap between metal and ligand orbitals would weaken the bond and raise the energy.

Answer c

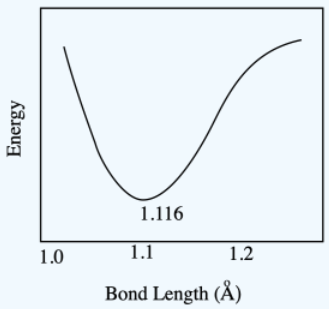
c) The range of possible bond lengths gets broader as energy is increased. The bond has more latitude, with both longer and shorter bonds allowed at higher energy.



Exercise 5.7.1.3

The optimum C-O bond length in a carbon dioxide molecule is 1.116 Å. Draw a graph of what happens to internal energy when this bond length varies between 1.10 Å and 1.20 Å. Don't worry about quantitative labels on the energy axis.

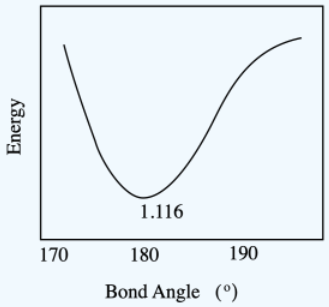
Answer



Exercise 5.7.1.4

The optimum O-C-O bond angle in a carbon dioxide molecule is 180 °. Draw a graph of what happens to internal energy when this bond angle varies between 170 ° and 190 °. Don't worry about quantitative labels on the energy axis.

Answer



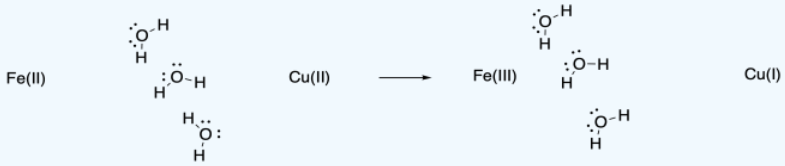
The barrier to electron transfer has to do with reorganizations of all those big atoms before the electron makes the jump. In terms of the coordination sphere, those reorganizations involve bond vibrations, and bond vibrations cost energy. Outside the coordination sphere, solvent molecules have to reorganize, too. Remember, ion stability is highly influenced by the surrounding medium.

Exercise 5.7.1.5

Draw a Fe(II) ion and a Cu(II) ion with three water molecules located somewhere in between them. Don't worry about the ligands on the iron or copper. Show how the water molecules might change position or orientation if an electron is transferred from iron to copper.

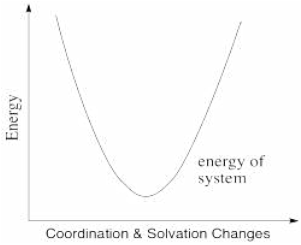
Answer

The water molecules may pivot toward the more highly charged Fe(III), or they may shift closer to it because of the attraction between the ion and the dipole of the water molecule.



Keep in mind that such adjustments would happen in non-polar solvents, too, although they would involve weaker IMFs such as ion - induced dipole interactions.

Thus, the energetic changes needed before electron transfer can occur involve a variety of changes, including bond lengths of several ligands, bond angles, solvent molecules, and so on. The whole system, involving both metals, has some optimum set of positions of minimum energy. Any deviations from those positions requires added energy. In the following energy diagram, the x axis no longer defines one particular parameter. Now it lumps all changes in the system onto one axis. This picture is a little more abstract than when we are just looking at one bond length or one bond angle, but the concept is similar: there is an optimum set of positions for the atoms in this system, and it would require an input of energy in order to move any of them move away from their optimum position.

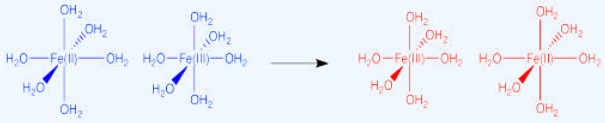


It is thought that these kinds of reorganizations -- involving solvent molecules, bond lengths, coordination geometry and so on -- actually occur prior to electron transfer. They happen via random motions of the molecules involved. However, once they have happened, there is nothing to hold the electron back. Its motion is so rapid that it can immediately find itself on the other atom before anything has a chance to move again.

Consequently, the barrier to electron transfer is just the amount of energy needed for all of those heavy atoms to get to some set of coordinates that would be accessible in the first state, before the electron is transferred, but that would also be accessible in the second state, after the electron is transfered.

? Exercise 5.7.1.6

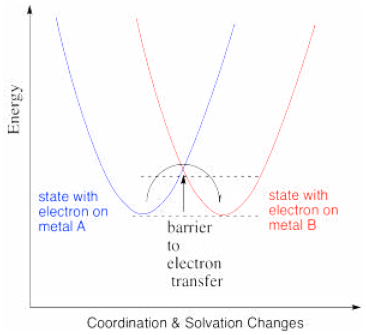
Describe some of the changes that contribute to the barrier to electron transfer in the following case.



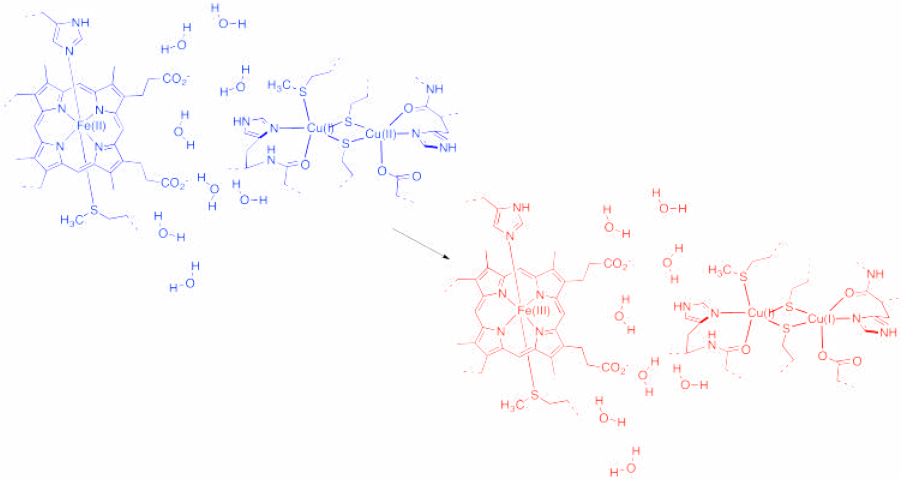
Answer

The reactants and products are very similar in this case. However, the Fe(III) complex has shorter bonds than the Fe(II) complex because of greater electrostatic interaction between the metal ion and the ligands. These changes in bond length needed in order to get ready to change from Fe(III) to Fe(II) (or the reverse) pose a major barrier to the reaction.

In the drawing below, an electron is transferred from one metal to another metal of the same kind, so the two are just switching oxidation states. For example, it could be an iron(II) and an iron(III), as pictured in the problem above. In the blue state, one iron has the extra electron, and in the red state it is the other iron that has the extra electron. The energy of the two states are the same, and the reduction potential involved in this transfer is zero. However, there would be some atomic reorganizations needed to get the coordination and solvation environments adjusted to the electron transfer. The ligand atoms and solvent molecules have shifted in the change from one state to another, and so our energy surfaces have shifted along the x axis to reflect that reorganization.



That example isn't very interesting, because we don't form anything new on the product side. Instead, let's picture an electron transfer from one metal to a very different one. For example, maybe the electron is transferred from cytochrome c to the "copper A" center in cytochrome c oxidase, an important protein involved in respiratory electron transfer.



? Exercise 5.7.1.7

In the drawing above, some water molecules are included between the two metal centres.

a. Explain what happens to the water molecules in order to allow electron transfer to occur, and why.
b. Suppose there were a different solvent, other than water, between the complexes. How might that affect the barrier to the reaction?

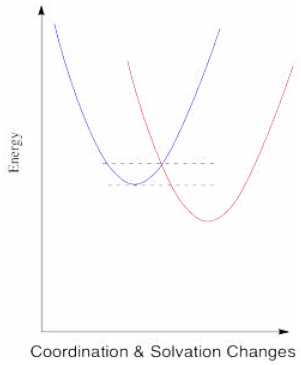
Answer a

a) The drawing is an oversimplification, but in general the water molecules are shown reorienting after the electron transfer because of ion-dipole interactions. In this case, the waters are shown orienting to present their negative ends to the more positive iron atom after the electron transfer. In reality, in a protein there are lots of other charges (including charges on the ligand) that may take part in additional ion-dipole interactions.

Answer b

b) Because electron transfer is so fast, atomic and molecular reorganisations are actually thought to happen before the electron transfer. The water molecules would happen to shift into a position that would provide the greatest possible stabilisation for the ions and then the electron would be transferred. A less polar solvent than water would be less able to stabilize ions and the electron would be slower to transfer as a result. In addition, a less polar solvent than water would be a poor medium to transmit an electron, which is charged and therefore stabilized by interactions with polar solvents.

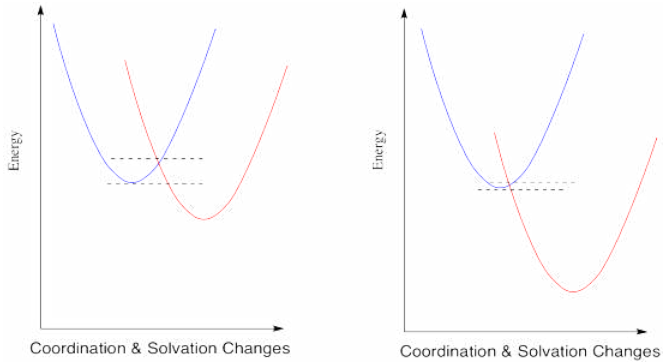
The energy diagram for the case involving two different metals is very similar, except that now there is a difference in energy between the two states. The reduction potential is no longer zero. We'll assume the reduction potential is positive, and so the free energy change is negative. Energy goes down upon electron transfer.



Compare this picture to the one for the degenerate case, when the electron is just transferred to a new metal of the same type. A positive reduction potential (or a negative free energy change) has the effect of sliding the energy surface for the red state

downwards. As a result, the intersection point between the two surfaces also slides downwards. Since that is the point at which the electron can slide from one state to the other, the barrier to the reaction decreases.

What would happen if the reduction potential were even more positive? Let's see in the picture below.



The trend continues. According to this interpretation of the kinetics of electron transfer, the more exothermic the reaction, the lower its barrier will be. It isn't always the case that kinetics tracks along with thermodynamics, but this might be one of them.

But is all of this really true? We should take a look at some experimental data and see whether it truly works this way.

Oxidant	E°	k ($M^{-1}s^{-1}$) (margin of error shown in parentheses)
$Co(diene)(NH_3)_2^{3+}$	0.12	3.0(4)
$Co(diene)H_2O)NCS^{2+}$	0.38	11(1)
$Co(diene)(H_2O)_2^{3+}$	0.53	800(100)
Co(EDTA)	0.60	6000(1000)

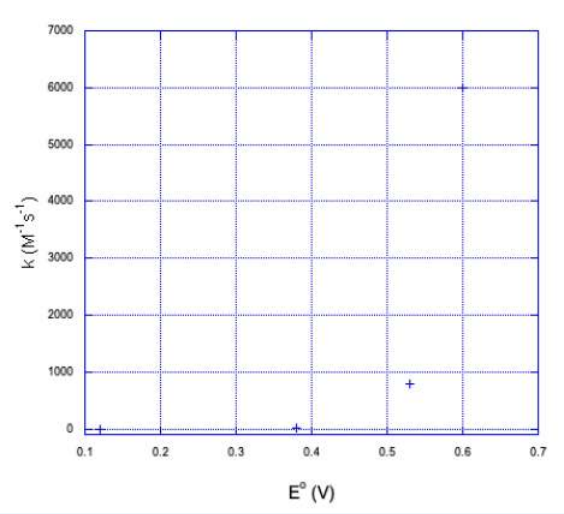
As the reduction potential becomes more positive, free energy gets more negative, and the rate of the reaction dramatically increases. So far, Marcus theory seems to get things right.

? Exercise 5.7.1.8

a. Plot the data in the above table.
b. How would you describe the relationship? Is it linear? Is it exponential? Is it direct? Is it inverse?
c. Plot rate constant versus free energy change. How does this graph compare to the first one?

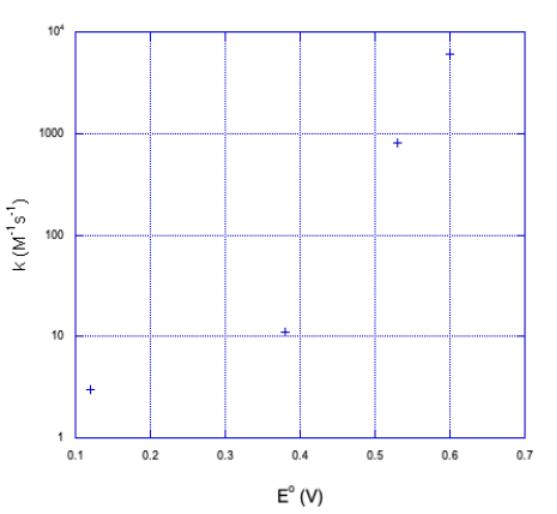
Answer a

a) Here is a plot of the data.



Answer b

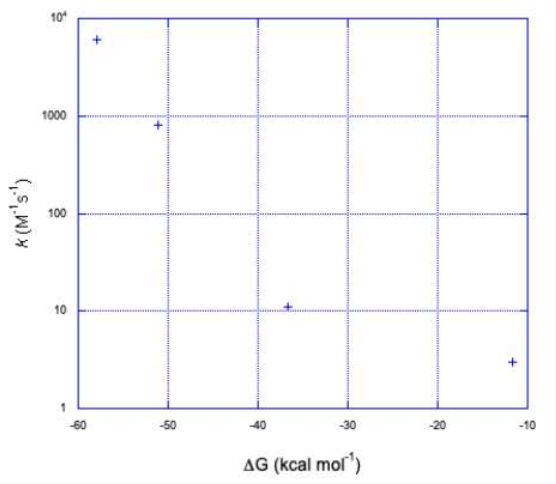
b) It doesn't look linear. If we plot the y axis on a log scale, things become a little more linear.



It looks closer to a logarithmic relationship than a linear one.

Answer c

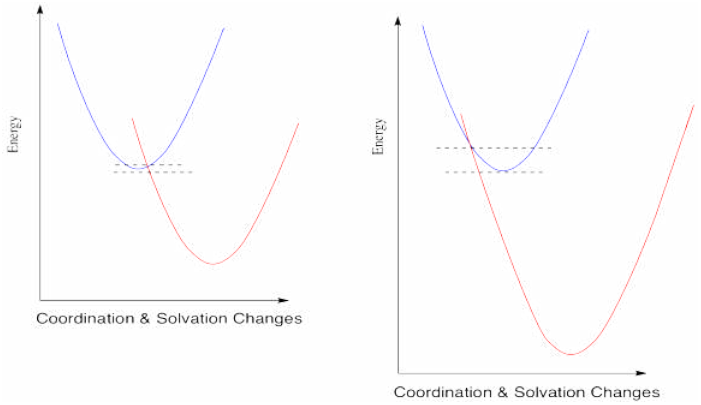
c) Assuming one electron transfer:



The graph takes the same form but in the opposite direction along the x axis.

Marcus Inverted Region

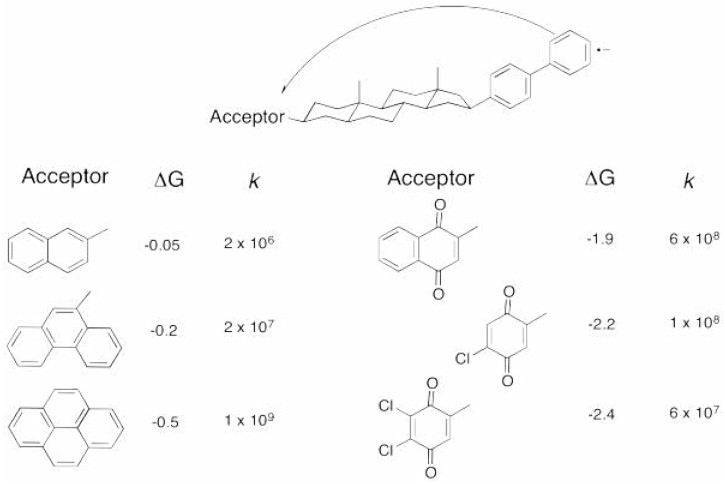
When you look a little closer at Marcus theory, though, things get a little strange. Suppose we make one more change and see what happens when the reduction potential becomes *even more* positive.



So, if Marcus is correct, at some point as the reduction potential continues to get more positive, reactions start to slow down again. They don't just reach a maximum rate and hold steady at that plateau; the barrier gets higher and higher and the reactions get slower and slower. If you feel a little skeptical about that, you're in good company.

Marcus always maintained that this phenomenon was a valid aspect of the theory, and not just some aberration that should be ignored. The fact that nobody had ever actually observed such a trend didn't bother him. The reason we didn't see this kind of thing, he said, was that we just hadn't developed technology that was good enough to measure these kind of rates accurately.

But technology did catch up. Just take a look at the following data (from Miller, *J. Am.Chem. Soc.* **1984**, *3047*).



Don't worry that there are no metals involved anymore. An electron transfer is an electron transfer. Here, an electron is sent from the aromatic substructure on the right to the substructure on the left. By varying the part on the left, we can adjust the reduction potential (or the free energy change, as reported here.

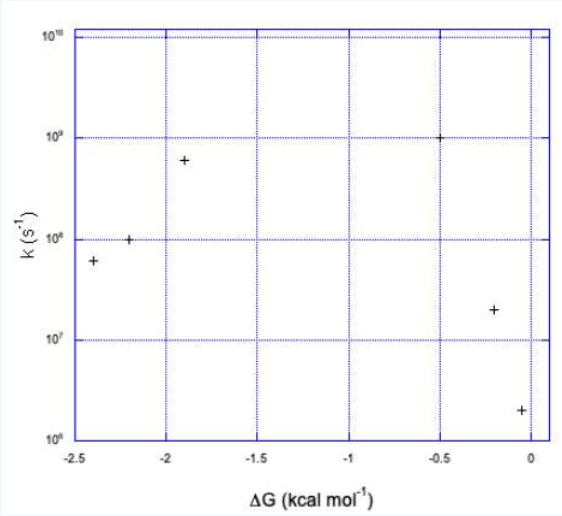
? Exercise 5.7.1.9

a. Plot the data in the above table.

b. How would you describe the relationship?

Answer a

a)



Answer b

b) We can see two sides of an inverted curve. The reaction gets much faster as the free energy becomes more negative, but at some point the rate begins to decrease again.

As the reaction becomes more exergonic, the rate increases, but then it hits a maximum and decreases again. Data like this means that the "Marcus Inverted Region" is a real phenomenon. Are you convinced? So were other people. In 1992, Marcus was awarded the Nobel Prize in Chemistry for this work.

Exercise 5.7.1.10

Take a look at the donor/acceptor molecule used in Williams' study, above. a) Why do you suppose the free energy change is pretty small for the first three compounds in the table? b) Why does the free energy change continue to get bigger over the last three compounds in the table?

Answer

The acceptor compound becomes an anion when it accepts an electron. The first three compounds do not appear to be strongly electrophilic; they can accept electrons simply because of resonance stability of the resulting anion. The last three have electron withdrawing groups (chlorines and oxygens) that would stabilize the anion even further.

Exercise 5.7.1.11

The rates of electron transfer between cobalt complexes of the bidentate bipyridyl ligand, $Co(bipy)_3^{n+}$, are strongly dependent upon oxidation state in the redox pair. Electron transfer between Co(I)/Co(II) occurs with a rate constant of about 10^9 $M^{-1}s^{-1}$, whereas the reaction between Co(II)/Co(III) species proceeds with k = 18 $M^{-1}s^{-1}$.

a. What geometry is adopted by these complexes?
b. Are these species high spin or low spin?
c. Draw d orbital splitting diagrams for each complex.
d. Explain why electron transfer is so much more facile for the Co(I)/Co(II) pair than for the Co(II)/Co(III) pair.

Answer a

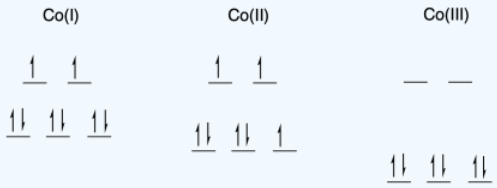
a) octahedral; bpy is a bidentate ligand.

Answer b

b) Co is first row; Co(I) and Co(II) have relatively low charge. Usually we would expect them to be high spin. Co(III) is at a cut-off point in the first row; it is just electronegative enough that it is usually low spin.

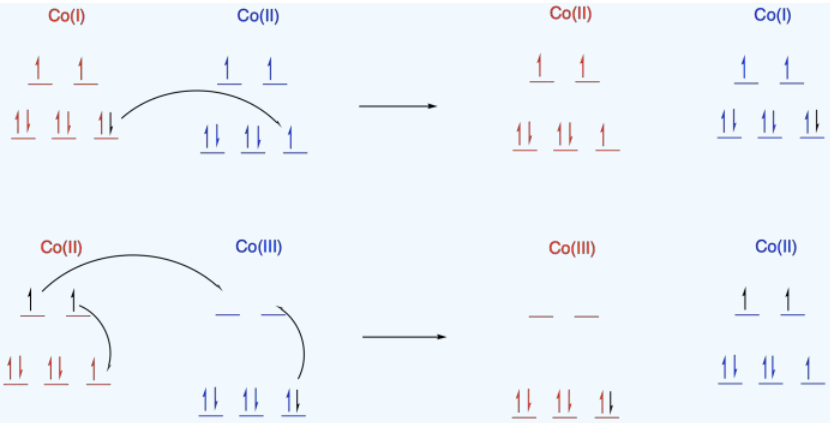
Answer c

c)



Answer d

d) In a transfer from Co(II) to Co(III), there is additional reorganization needed because the metal changes between high and low spin. Not only does one electron have to move from one metal to another metal, but additional electrons have to shuffle from one orbital to another on the same metal to accommodate the change. These reorganizations have a barrier, slowing the reaction.



This page titled 5.7.1: Outer Sphere Electron Transfer is shared under a CC BY-NC-SA 4.0 license and was authored, remixed, and/or curated by Kathryn Haas.

- **1.9: Outer Sphere Electron Transfer** by Chris Schaller is licensed CC BY-NC 3.0. Original source: https://employees.csbsju.edu/cschaller/ROBI3.htm.

5.7.2: Inner Sphere Electron Transfer

In some cases, electron transfers occur much more quickly in the presence of certain ligands. For example, compare the rate constants for the following two electron transfer reactions, involving almost exactly the same complexes:

$$Co(NH_3)_6^{3+} + Cr^{2+} \longrightarrow Co^{2+} + Cr^{3+} + 6\,NH_3 \;\; k = 10^{-4} M^{-1} s^{-1}$$

$$Co(NH_3)_5Cl^{2+} + Cr^{2+} \longrightarrow Co^{2+} + CrCl^{2+} + 6\,NH_3 \;\; k = 6 \times 10^{5} M^{-1} s^{-1}$$

(Note: aqua ligands are omitted for simplicity. Ions, unless noted otherwise, are aqua complexes.)

Notice two things: first, when there is a chloride ligand involved, the reaction is much faster. Second, after the reaction, the chloride ligand has been transferred to the chromium ion. Possibly, those two events are part of the same phenomenon.

Similar rate enhancements have been reported for reactions in which other halide ligands are involved in the coordination sphere of one of the metals.

In the 1960's, Henry Taube of Stanford University proposed that halides (and other ligands) may promote electron transfer via bridging effects. What he meant was that the chloride ion could use one of its additional lone pairs to bind to the chromium ion. It would then be bound to both metals at the same time, forming a bridge between them. Perhaps the chloride could act as a conduit for electron transfer. The chloride might then remain attached to the chromium, to which it had already formed a bond, leaving the cobalt behind.

Electron transfers that occur via ligands shared by the two metals undergoing oxidation and reduction are termed "inner sphere" electron transfers. Taube was awarded the Nobel Prize in chemistry in 1983; the award was based on his work on the mechanism of electron transfer reactions.

? Exercise 5.7.2.1

Take another look at the two electron transfer reactions involving the cobalt and chromium ion, above.

a. What geometry is adopted by these complexes?
b. Are these species high spin or low spin?
c. Draw d orbital splitting diagrams for each complex.
d. Explain why electron transfer is accompanied by loss of the ammonia ligands from the cobalt complex.
e. The chloride is lost from the cobalt complex after electron transfer. Why does it remain on the chromium?

Answer a

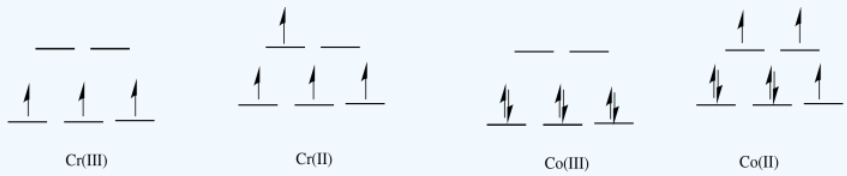
a) octahedral

Answer b

b) In the first row, 2^+ complexes are almost always high spin. However, 3^+ complexes are sometimes low spin.

Answer c

c)



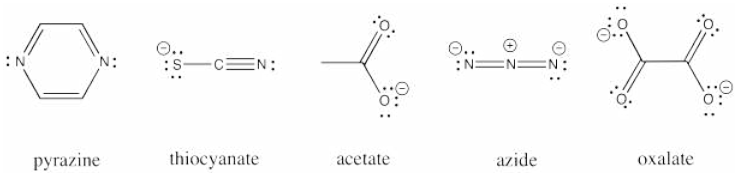
Answer d

d) The Co(II) complex is high spin and labile. The ligands are easily replaced by water.

Answer e

e) The Cr(III) complex is only d^3; it is inert.

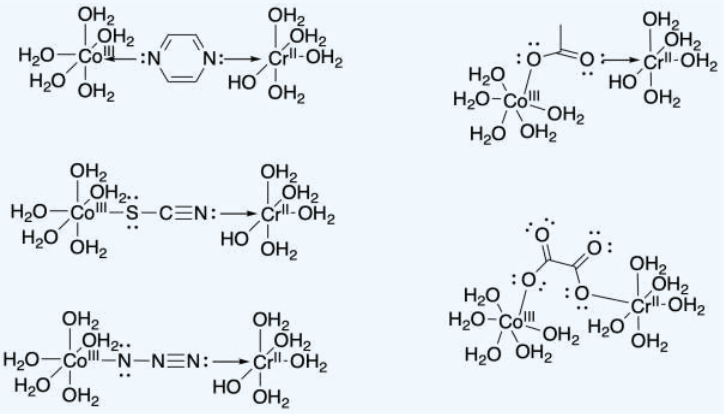
Other ligands can be involved in inner sphere electron transfers. These ligands include carboxylates, oxalate, azide, thiocyanate, and pyrazine ligands. All of these ligands have additional lone pairs with which to bind a second metal ion.



Exercise 5.7.2.2

Draw an example of each of the ligands listed above bridging between a cobalt(III) and chromium(II) aqua complex.

Answer

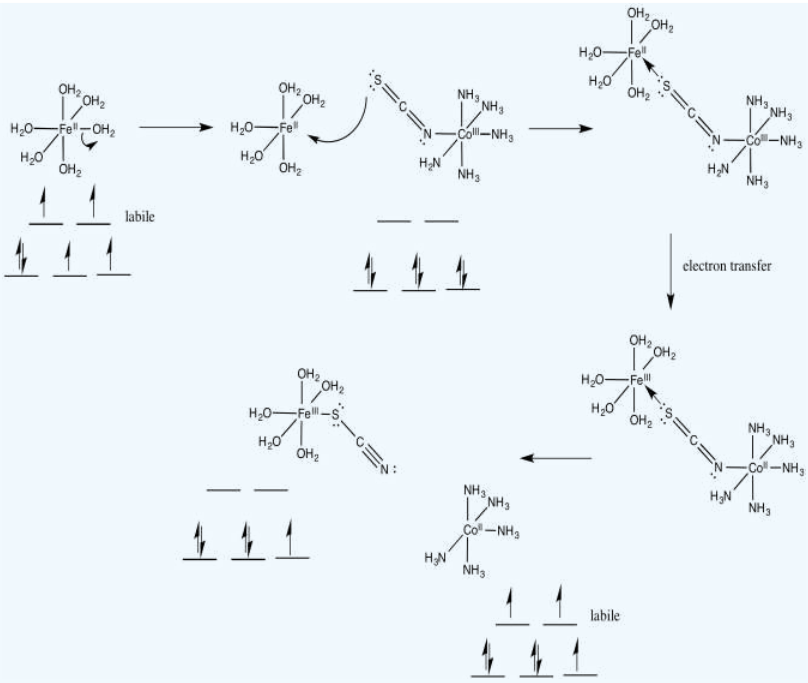


Exercise 5.7.2.3

Explain, with structures and d orbital splitting diagrams, how the products are formed in the following reaction, in aqueous solution.

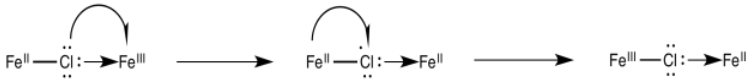
$$Fe(OH_2)_6^{2+} + (SCN)Co(NH_3)_5^{2+} \longrightarrow (NCS)Fe(OH_2)_5^{2+} + Co(OH_2)_6^{2+} + 5\,NH_3$$

Answer



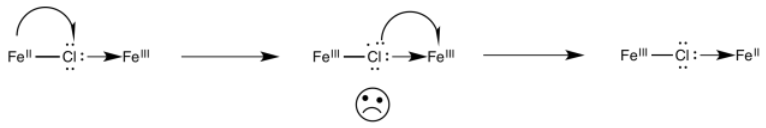
How does the electron travel over the bridge?

Once the bridge is in place, the electron transfer may take place via either of two mechanisms. Suppose the bridging ligand is a chloride. The first step might actually involve an electron transfer from chlorine to the metal; that is, the chloride could donate one electron from one of its idle lone pairs. This electron could subsequently be replaced by an electron transfer from metal to chlorine.



Sometimes, we talk about the place where an electron *used to be*, describing it as a "hole". In this mechanism, the electron donated from the bridging chloride ligand leaves behind a hole. The hole is then filled with an electron donated from the other metal.

Alternatively, an electron might first be transferred from metal to chlorine, which subsequently passes an electron along to the other metal. In the case of chlorine, this idea may be unsatisfactory, because chlorine already has a full octet. Nevertheless, some of the other bridging ligands may have low-lying unoccupied molecular orbitals that could be populated by this extra electron, temporarily.

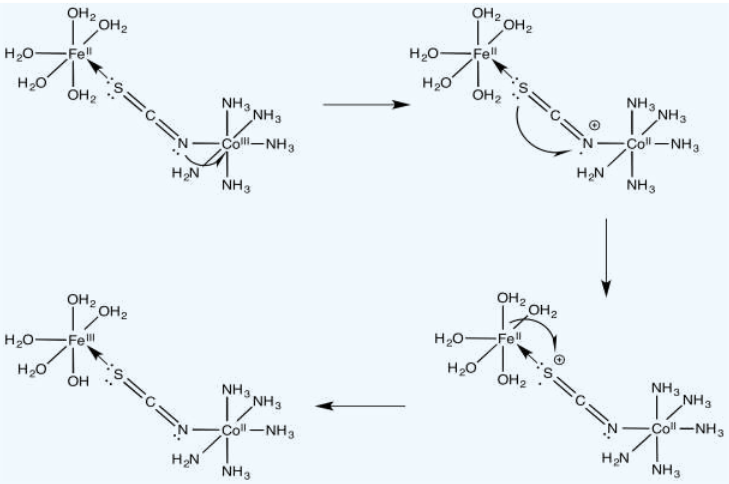


? Exercise 5.7.2.4

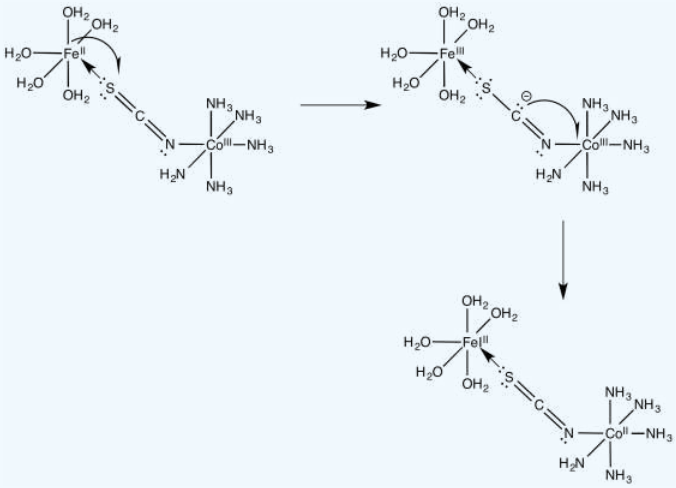
For the iron / cobalt electron transfer in problem Exercise **5.7.2.3** (RO9.3.), show

a. an electron transfer mechanism via a hole migration along the bridge
b. an electron transfer mechanism via an electron migration along the bridge

Answer a



Answer b



Exercise 5.7.2.5

One of the many contributions to the barrier for electron transfer between metal ions is internal electronic reorganization.

a) Draw d orbital splitting diagrams for each of the following metal ions in an octahedral environment.

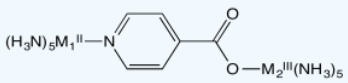
Ru(II) or Os(II)

Ru(III) or Os(III)

Co(II)

Co(III)

Flash photolysis is a method in which an electron can be moved instantly "uphill" from one metal to another (e.g. from M_2^{II} to M_1^{III}, below); the electron transfer rate can then be measured as the electron "drops" back from M_1^{II} to M_2^{III}.



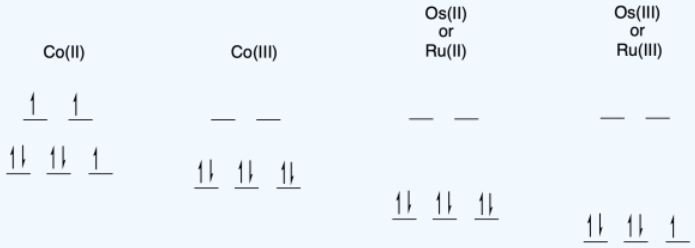
b) Explain the relative rates of electron transfer reaction in this system, as measured by flash photolysis in the table below.

M_1^{II}	M_2^{III}	k_{obs} s^{-1}
Os	Ru	> 5 x 10^9
Os	Co	1.9 x 10^5

c) Does the reaction above probably occur via an inner sphere or by an outer sphere pathway? Why?

Answer a

a)



Answer b

b) The electron transfer between Os(II) and Ru(III) will not involve any electron reorganization because both are low spin to begin with. However, the electron transfer between Os(II) and Co(III) will result in cobalt changing from low spin to high spin. The need to move electrons between different d orbitals on the cobalt will add to the barrier, slowing down the reaction.

Answer c

c) The pathway is probably inner sphere because of the bridging ligand. Furthermore, the conjugation in the bridging ligand would help in conducting an electron from one end of the ligand to the other, either through an electron mechanism or a hole mechanism.

? Exercise 5.7.2.6

Outer sphere electron transfer rates depend on the free energy change of the reaction (ΔG°) and the distance between oxidant and reductant (d) according to the relation

Rate constant = $k = Ae^{(-\Delta G)}e^{-d}$

a) What happens to the rate of the reaction as distance increases between reactants?

One potential problem in measuring rates of intramolecular electron transfer (i.e. *within* a molecule) is competition from intermolecular electron transfer (*between* molecules).

b) What would you do in the flash photolysis experiment above to discourage intermolecular electron transfer?

c) How could you confirm whether you were successful in discouraging intermolecular reaction?

Answer a

a) The rate decreases exponentially as distance increases.

Answer b

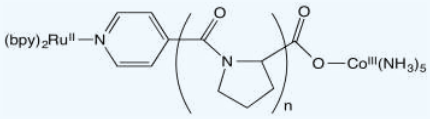
b) You might keep the concentration low in order to increase the distance between molecules, reducing the likely hood of an outer-sphere electron transfer.

Answer c

c) If you ran the experiment at a series of dilutions, intramolecular electron transfer would be unaffected but outer sphere electron transfer would not. If the rates were the same across a number of different concentrations, the reaction would probably be intramolecular.

Exercise 5.7.2.7

Stephan Isied and coworkers at Rutgers measured the following electron transfer rates between metal centers separated by a peptide. (*Chem Rev* **1992**, *92*, 381-394)



a. The proline repeating unit is crucial in ensuring a steady increase in distance between metal centers with increased repeat units, n. Why?
b. An inner sphere pathway in this case is expected to be somewhat slow because of the lack of conjugation in the polyproline bridge. Explain why.
c. Plot the data below, with log*k* on the y axis (range from 4-9) and d on the x axis (12-24 Angstroms).

n	d (Å)	k_{obs} (s^{-1})
1	12.2	5×10^{8}
2	14.8	1.6×10^{7}
3	18.1	2.3×10^{5}
4	21.3	5.1×10^{4}
5	24.1	1.8×10^{4}

d) A linear relationship is in agreement with Marcus theory; log*k* = - c x d. Is your plot linear?

Isied offers a number of possible explanations for the data, all of which involve two competing reaction pathways.

e) Suggest one explanation for the data.

Answer a

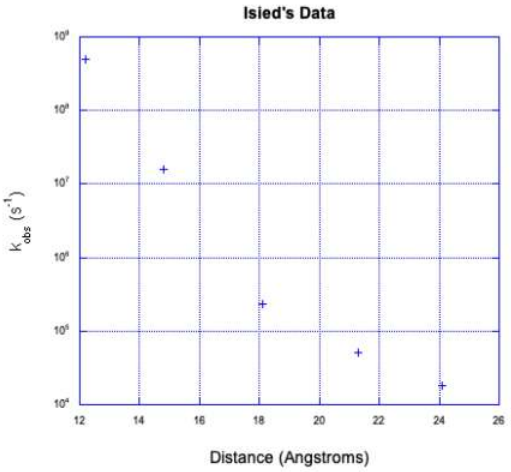
a) Rings are frequently used to introduce conformational rigidity (or decrease conformational flexibility), limiting the range of potential shapes a molecule could adopt. If the molecule can't wiggle around as much, then the distance between the ends of the molecule should be more constant.

Answer b

b) Although the ligand is bridging, it would be difficult to picture either an electron or hole mechanism of inner sphere electron transfer. There are few pi bonds or lone pairs to use as places to put electrons or temporarily remove electrons from, shuttling the electrons from place to place along the ligand. A conjugated system would be much more likely to carry out inner sphere electron transfer.

Answer c

c)



Answer d

d) The data is not linear.

Answer e

e) The data appear to show two lines that cross. That's a classic symptom of two competing mechanisms. The faster mechanism, to the left, is probably an intramolecular electron transfer. The slower mechanism, to the right, may be an intermolecular electron transfer.

This page titled 5.7.2: Inner Sphere Electron Transfer is shared under a CC BY-NC-SA 4.0 license and was authored, remixed, and/or curated by Kathryn Haas.

- **1.10: Inner Sphere Electron Transfer** by Chris Schaller is licensed CC BY-NC 3.0. Original source: https://employees.csbsju.edu/cschaller/ROBI3.htm.

CHAPTER OVERVIEW

6: Organometallic Chemistry

6.1: Introduction to Organometallic Chemistry
6.2: Nomenclature, Ligands, and Classification
6.3: Electron Counting in Organometallic Complexes
6.3.1: The 18 Electron Rule
6.3.2: Simplifying the Organometallic Complex by Deconstruction
6.4: Survey of Organometallic Ligands
6.4.1: Carbon Monoxide (Carbonyl Complexes)
6.4.2: Ligands similar to CO
6.4.3: Hydrides and Dihydrogen Complexes
6.5: Bonding between Metal Atoms and Organic Pi Systems
6.5.1: Linear π Systems
6.5.2: Cyclic π systems
6.5.3: Odd-numbered π Systems
6.5.4: Fullerene Complexes
6.6: Metal-Carbon Bonds
6.6.1: Metal Alkyls
6.6.2: Carbenes
6.6.3: Carbyne (Alkylidyne) Complexes
6.6.4: Carbido and Cumulene Complexes
6.6.5: Carbon Wires- Polyyne and Polyene Bridges
6.7: Characterization of Organometallic Complexes

This page titled 6: Organometallic Chemistry is shared under a CC BY-NC-SA 4.0 license and was authored, remixed, and/or curated by Kathryn Haas.

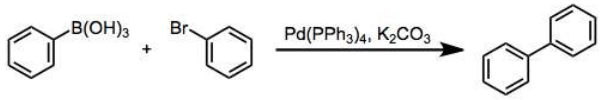
6.1: Introduction to Organometallic Chemistry

What is Organometallic Chemistry?

This chapter will introduce a subfield of inorganic coordination chemistry; organometallic chemistry. Let's begin with a few simple questions: what is organometallic chemistry? What, after studying organometallic chemistry, will we know about the world that we didn't know before? Why is the subject worth studying? And what kinds of problems is the subject meant to address? The purpose of this introduction is twofold: (1) to help motivate us as we move forward (that is, to remind us that there is a point to all this!); and (2) to illustrate the kinds of problems we'll be able to address using concepts from the field. You might be surprised by the spine-chilling power you feel after learning about the behavior of organometallic compounds and reactions!

Put most bluntly, **organometallic chemistry is the study of compounds containing, and reactions involving, metal-carbon bonds**. The metal-carbon bond may be transient or temporary, but if one exists during a reaction or in a compound of interest, we're squarely in the domain of organometallic chemistry. Despite the denotational importance of the M-C bond, bonds between metals and the other common elements of organic chemistry also appear in organometallic chemistry: metal-nitrogen, metal-oxygen, metal-halogen, and even metal-hydrogen bonds all play a role. Metals cover a vast swath of the periodic table and include the alkali metals (group 1), alkali earth metals (group 2), transition metals (groups 3-12), the main group metals (groups 13-15, "under the stairs"), and the lanthanides and actinides. We will focus most prominently on the behavior of the transition metals, so called because they cover the transition between the electropositive group 2 elements and the more electron-rich main group elements.

Why is organometallic chemistry worth studying? Well, for me, it mostly comes down to synthetic flexibility. There's a reason the "organo" comes first in "organometallic chemistry"—our goal is usually the creation of new bonds in *organic* compounds. The metals tend to just be along for the ride (although their influence, obviously, is essential). And the fact is that you can do things with organometallic chemistry that you cannot do using straight-up organic chemistry. Case in point:



The venerable Suzuki reaction...unthinkable without palladium!

The establishment of the bond between the phenyl rings through a means other than dumb luck seems unthinkable to the organic chemist, but it's natural for the palladium-equipped metal-organicker. Bromobenzene looks like a potential electrophile at the bromine-bearing carbon, and if you're familiar with hydroboration you might see phenylboronic acid as a potential nucleophile at the boron-bearing carbon. Catalytic palladium makes it all happen! Organometallic chemistry is full of these mind-bending transformations, and can expand the synthetic toolbox of the organic chemist considerably.

To throw another motive into the mix for the non-specialist (or the synthesis-spurning chemist), organometallic chemistry is full of intriguing stories of scientific inquiry and discovery. Exploring how researchers take a new organometallic reaction from "ooh pretty" to strong predictive power is instructive for anyone interested in "how science works," in a practical sense. We'll examine a number of classical experiments in organometallic chemistry, both for their value to the field and their contributions to the general nature of scientific inquiry.

What kinds of problems should we be able to address as we move forward? Here's a bulleted list of the most commonly encountered types of problems in an organometallic chemistry course:

- Describe the structure of an organometallic complex…
- Predict the product of the given reaction conditions…
- Draw a reasonable mechanism based on evidence…
- Devise a synthetic route to synthesize a target organometallic compound…
- Explain the observation(s)…
- Predict the results of a series of experiments…

The first four are pretty standard organic-esque problems, but it's the last two, more general classes that really make organometallic chemistry compelling. Just imagine putting yourself in the shoes of the pioneers and making the same predictions they did!

There you have it, a short introduction to organometallic chemistry and why it's worth studying. The rest of this chapter will describe what organometallic chemistry really is…it will be helpful to keep these motives in mind as you study. Keep a thirst for predictive power, and it's hard to go wrong with organometallic chemistry!

Resources for learning organometallic chemistry

For the penny-pinching student or layman, there are several good resources for organometallic chemistry on the Web. Nothing as exhaustive as Reusch's Virtual Textbook of Organic Chemistry exists for organometallic chemistry, but the base of resources available on the Web is growing. Rob Toreki's Organometallic HyperTextBook could use a CSS refresh, but contains some nice introductions to different organometallic concepts and reactions. Try the electron-counting quiz!

VIPER is a collection of electronic resources for teaching and learning inorganic chemistry, and includes a nice section on organometallic chemistry featuring laboratory assignments, lecture notes, and classroom activities. Awesome public lecture notes are available from Budzelaar at the University of Manitoba and Shaughnessy at Alabama (Roll Tide?). For practice problems, check out Fu's OpenCourseWare material from MIT and Shaughnessy's problem sets.

Historical Background and Introduction to Metallocenes

Definition: Organometallic Complex

Organometallic Complex: A complex with bonding interactions between a metal atom and one or more carbon atoms of an organic group or molecule.

An **organometallic complex** is defined as a complex with bonding interactions between one or more carbon atoms of an organic group or molecule and at least one metal atom. It is important to understand that *just the presence of an organic ligand is not sufficient to define an organometallic compound*. If there are organic ligands present, but no metal-carbon bonds, the complex is said to be "**metal-organic**". There must be interactions between a carbon and a metal for the complex to be considered organometallic.

Example 6.1.1

Which of the molecules below is an organometallic complex?

$$[Sn(Me)_4] \qquad Sn(OMe)_4 \qquad cis\text{–}[PtCl_2(NH_3)_2] \tag{6.1.1}$$

Solution

The tetramethyl tin ($Sn(Me)_4$) has metal-carbon bonds, and thus it is an organometallic complex.

Tetramethoxy tin ($Sn(OMe)_4$) has metal-oxygen bonds. It lacks metal-carbon bonds, but it does contain organic ligands; thus it is a "metal-organic" complex rather than organometallic.

Cisplatinum ($cis\text{–}[PtCl_2(NH_3)_2]$) contains no carbon and thus it is neither organometallic or metal-organic; it is just a coordination compound.

Industrial Importance of Organometallic Compounds

Organometallic compounds are a very important class of compounds in industry. For example, tens of thousand of tons of aluminum and tin alkyl compounds are produced each year for industrial purposes. The use of organometallic compounds as catalysts to produce other compounds is even more important. Organometallic catalysts are used for a range of industrial syntheses from manufacture of commodity polymers like polypropylene and polyethylene to production of simple organic molecules like acetaldehyde and acetic acid. These compounds are produced at a scale in the order of millions of tons per year.

Let us take a historical approach to organometallic chemistry and see how the field has evolved. Arguably, the first organometallic compound was kakodyl oxide, an organo-arsenic compound (Figure **6.1.2**). It was accidentally produced by the French chemist Louis Cadet in 1760 when he was working on inks. He heated arsenic oxide and potassium acetate and obtained a red-brown oily liquid, known as Cadet's fuming liquid. It consists mostly of cacodyl and cacodyl oxide (Figure **6.1.2**). In cacodyl, there is an As-As bond and two methyl groups attached to each As atom. In the other product, cacodyl oxide, there is an O atom bridging the two As atoms, and each As is bound to two methyl groups. The names of these two compounds come from the greek word "kakodes", meaning "bad smell". Indeed, they have a very intense, garlic-like smell. The reaction can be used to identify arsenic in samples. For instance, if you suspected your food was poisoned with arsenic, you could heat a sample together with potassium acetate. If a bad, garlic-like smell evolved, this would indicate that there is arsenic in your sample.

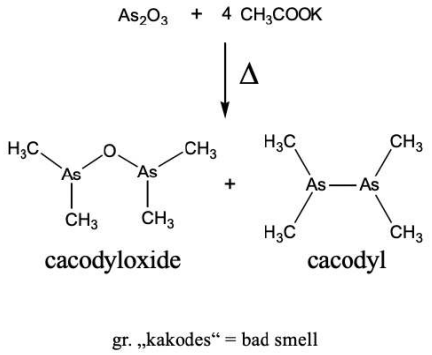


Figure **6.1.2**: Cacodyl and cacodyl oxide

Another important milestone in coordination chemistry was the discovery of Zeise's salt by the Danish chemist William Zeise in 1827 (Figure **6.1.3**). Zeise's salt was the first olefin complex in which an olefin was bound side-on to a metal using its π-electrons for σ-bonding. Zeise observed that when sodium hexachloroplatinate (2-) was heated in ethanol, a compound with the composition $Na[PtCl_3(C_2H_4)]$ could be isolated. The chemical composition of the compound suggested that there was a C_2H_4 organic fragment bonded to the platinum, but it was not clear how.

This question was only answered more than 100 years later in 1969 with the crystal structure analysis of Zeise's salt. The crystal structure revealed that an ethylene molecule was bound side-on to the platinum (Figure **6.1.3**). The two carbon atoms had about the same distance to the Pt arguing that they were equally strongly involved in the bonding with Pt. The first C had a distance of 216 pm while the second carbon had a distance of 215 pm. The ethylene molecule was oriented perpendicular to the plane made of the three chloro ligands and the platinum atom. The Cl-Pt-Cl bond angles were near 90°. Overall, the structure could be described as a structure derived from a square planar structure with the ethylene as the fourth ligand that would stand perpendicular to the plane in order to minimize steric repulsion with the chloro ligands.

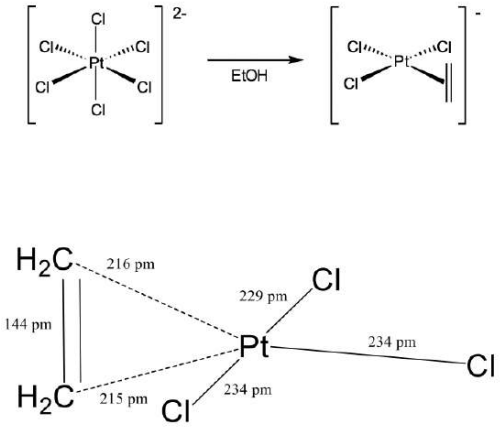


Figure **6.1.3**: Zeise's salt: Synthesis and crystal structure.

An important question was how to describe the bonding in the compound. It was noteworthy that the C-C bond length in Zeise's salt was significantly longer (144 pm) than that in a free ethylene molecule (134 pm). Based on the bond-strength bond-length concept this argued that the bond was weaker than a regular C=C double bond, and that the bond order was smaller than 2. What could explain this lower bond order and the side-on coordination of the ethylene in Zeise's salt?

The answer is that the ethylene molecule uses its π-electrons for σ-bonding with a metal d-orbital (Figure **6.1.4**). You can see above that the lobe of a $d_{x^2-y^2}$ orbital has the correct orientation to overlap with the bonding π-orbitals of the ethylene ligand in a σ-fashion. Through this interaction electron density gets donated from the bonding ligand π-orbital into the metal-d-orbital. This results in a lower electron density for π-bonding within the ligand, and thus the bond order is decreased. In addition, there is another effect that lowers the bond order. A metal d-orbital can interact with the π*-orbitals in π-fashion. In this process, electron density can be donated from the metal d-orbital into the empty π-orbitals of the ligand. The increased electron density in the π-orbitals further decreases the bond order.

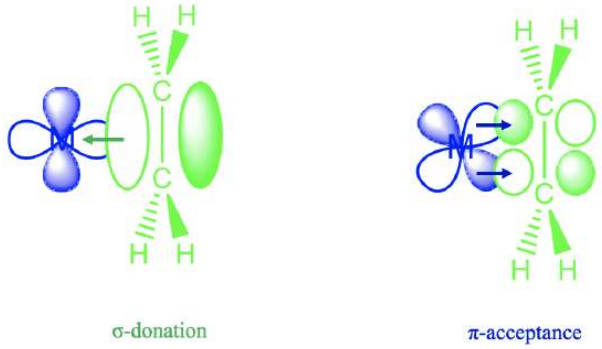


Figure **6.1.4**: An orbital view of bonding in Zeise's salt

In 1890, a further milestone in organometallic chemistry was reached with the synthesis of the first carbonyl complex, the nickel tetracarbonyl. Nickel tetracarbonyl is a colorless liquid that boils at 43°C. The compound was prepared by the German chemist Ludwig Mond. Nickel tetracarbonyl forms spontaneously from nickel metal and carbon monoxide at room temperature. The reaction is the basis of the Mond-process that is used up to date in order to purify nickel (Figure **6.1.5**). Carbon monoxide gas can be streamed over impure Ni metal at temperatures of 50-60°C to form $Ni(CO)_4$ in gaseous form. Impurities are left behind in solid form. Then, the nickel tetracarbonyl is thermally decomposed at ca. 220° to form nickel and carbon monoxide. The process can be varied to produce nickel in powder form, as spheres (Figure **6.1.5**), and as coatings. The Mond process is still used despite the very high toxicity of nickel tetracarbonyl.

$$\mathrm{Ni_{(s,\ impure)} + 4\,CO_{(g)} \longrightarrow Ni(CO)_{4\,(g)}} \qquad \mathbf{50-60^{\circ}C\ (also\ spontaneous\ at\ room\ temp)}$$

$$\mathrm{Ni(CO)_{4\,(g)} \longrightarrow Ni_{(s,\ purified)} + 4\,CO} \qquad \mathbf{220-250^{\circ}C\ (Ni\ is\ purified)}$$



Figure **6.1.5**: Purified Ni spheres prepared through the Mond process (René Rausch, Nickel kugeln, CC BY-SA 3.0 DE)

In 1900 the first Grignard reagents were discovered. Victor Grignard (Figure **6.1.9**) was an enthusiastic young French chemist who discovered how to make organomagnesium halides (RMgX) while working for his Ph.D.. His supervisor, Sabatier, had been trying this chemistry for some time, but Victor was the genius who solved the problem. Organomagnesium halides form from magnesium and organic halides in ethers. This discovery in 1900 changed the course of organic chemistry and won Grignard and Sabatier the Nobel Prize in 1912.

Extra close brace or missing open brace

In 1917, the first lithium alkyls were prepared by Wilhelm Schlenk. Like Grignard reagents, lithium alkyls are very valuable reactants in synthetic organic chemistry. Lithium alkyls are very air-sensitive compounds, and some even self-ignite in air (for example tert-butyl lithium is explosive when exposed to air). Therefore, they need to be handled carefully under inert gas. So that the reactions could be carried out under air0free conditions, Wilhelm Schlenk made an important invention: The Schlenk-lines (Figure **6.1.6**). The Schlenk lines allows a chemist to remove all gas (air) from a reaction flasks and back-fill the flask with an inert gas. A Schlenk line has a dual manifold with several ports. One manifold is connected to a source of purified inert gas, while the other is connected to a vacuum pump. The inert-gas line is vented through an oil bubbler, while solvent vapors and gaseous reaction products are prevented from contaminating the vacuum pump by a liquid nitrogen or dry ice/acetone cold trap. Special stopcocks or Teflon taps allow vacuum or inert gas to be selected without the need for placing the sample on a separate line.



Figure **6.1.6**: A Schlenk-line (Polimerek, Double vac line front view, CC BY-SA 3.0)

Discovery of Metallocenes

The discoveries discussed above were important milestones in the development of organometallic chemistry. But the field expanded more rapidly with the discovery of the first metallocene: ferrocene. Like often in science, ferrocene was discovered through an accident. In 1951 Peter Pauson and Thomas Kealy attempted to synthesize the organic compound fulvalene through oxidative coupling of cyclopentadienyl magnesium chloride with iron (III) chloride. However, instead of obtaining fulvalene they observed the formation hydrofulvalene together with an orange powder with “remarkable stability”. Analysis of the powder showed that the chemical compound contained two cyclopentadienyl rings and one iron atom. According to the knowledge on bonding in organometallic compounds that was known at the time Kealy and Pauson suggested a structure for the molecule in which two cyclopentadienyl group were bound to a single Fe atom via two Fe-C bonds (Figure **6.1.7**).

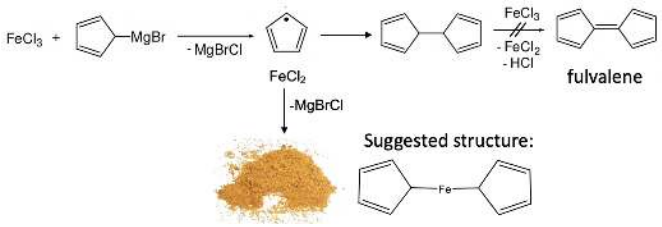
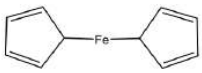


Figure **6.1.7**: Synthesis of ferrocene (Attribution: T.J. Kealy, P.L. Pauson, Nature 1951, 168, 1039.)

However, the remarkable stability of the compound was in contradiction to the proposed structure. The structure would be a 10 electron complex which would be highly coordinatively unsaturated. This would be inconsistent with the observed stability. We can briefly practice our electron counting skills again in order to prove that there are only 10 electrons (Figure **6.1.8**). (Electron counting will be discussed in more depth later in this chapter)

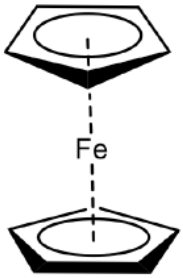


Structure is coordinatively unsaturated and has 10 valence electrons.

Fe:	8e
Ox-State (+2):	-2e
Ligands:	2x2e = 4e
Sum:	10e

Figure **6.1.8**: Electron counting in the wrong structure for $Fe(Cp)_2$

The compound was stable in air, and could be sublimed without decomposition. Further, the double-bonds in the cyclopentadienyl rings resisted hydrogenation. In addition, the structure was inconsistent with spectroscopic observations. Only one C-H stretch vibration was observed in the IR and only one signal was observed in the ^1H NMR. Kealy and Pauson's structure would have been consistent with three C-H stretch vibrations and three NMR resonances. For these reasons, Kealy's and Pausons structure was soon questioned. Ernst Otto Fischer at University of Munich and Sir Geoffrey Wilkinson at Harvard University (Figure **6.1.9**) suggested an alternative structure that was very different from all known organometallic structures. The bonding in this structure was completely different from all bonding concepts considered thus far for organometallics. What structure did they propose? They proposed a sandwich structure in which the two aromatic cyclopentadienyl anions would sandwich an Fe^{2+} ion. What would be the bonding in this structure? The cylopentadienyl anion would donate its six π-electrons into the valence orbitals of the metal. Thus, all five carbon atoms would be equally involved in the bonding, the ligand would act as a η^5-ligand. Because of the donation of π-electrons in the cycopentadiene unit, the structure was called "ferrocene". The ferrocene structure would explain the stability and low reactivity of the compound.



Ferrocene

Figure **6.1.9**: The sandwich structure of ferrocene

Electron-counting gives an 18 electron complex (Figure **6.1.10**). Let us verify this using the oxidation state method. Fe would contribute eight electrons in the neutral state. The ligands would be considered as cyclopendienyl anions with a 1- charge. This would give an oxidation state of +2 for Fe reducing the number of electrons from eight to six. The two ligands would contribute six electrons each giving twelve electrons. 12+6=18. Hence, the structure fulfills the 18 electron rule. The structure is also consistent with the spectroscopic observation of one NMR resonance and one C-H stretch vibration. All these were excellent arguments to support the ferrocene sandwich structure, however they were not an absolute proof. The proof finally came with the X-ray crystal structure determination which unambiguously confirmed the sandwich structure.

Fe:	8e
Ox-State (+2):	-2e
Ligands:	2x6e = 12e
Sum:	18e

Figure **6.1.10**: Electron counting in ferrocene using the oxidation state method

---

Dr. Kai Landskron (Lehigh University). If you like this textbook, please consider to make a donation to support the author's research at Lehigh University: Click Here to Donate.

This page titled 6.1: Introduction to Organometallic Chemistry is shared under a CC BY-NC-SA 4.0 license and was authored, remixed, and/or curated by Kathryn Haas.

- **1.2: What is Organometallic Chemistry?** by Michael Evans is licensed CC BY-NC-SA 4.0.
- **1.1: Resources for Organometallic Chemistry** by Michael Evans is licensed CC BY-NC-SA 4.0.
- **10.1: Historical Background and Introduction into Metallocenes** by Kai Landskron is licensed CC BY 4.0.

6.2: Nomenclature, Ligands, and Classification

The nomenclature of coordination compounds was described in an earlier section (Section 9.2). Organometallic compounds are named using this same system, so it may be helpful to review before proceeding. Here, we will point out some of the symbols and terminology that are used heavily in naming organometallic complexes.

Hapticity

The eta (η) symbol is used to indicate the variable **hapticity** of ligands with conjugated π systems. For example, the cyclopentadiene anion (Cp, $\mathbf{C_5H_5}$) ligand has the capability to coordinate a metal ion in several ways due to its cyclic conjugated π system. The hapticity (the number of atoms involved in the metal bonding interaction) must be indicated in the formula with the η^n notation, and in the name with the appropriate prefix. Figure **6.2.1** illustrates three different hapticities, and the relevant formula symbols and names.

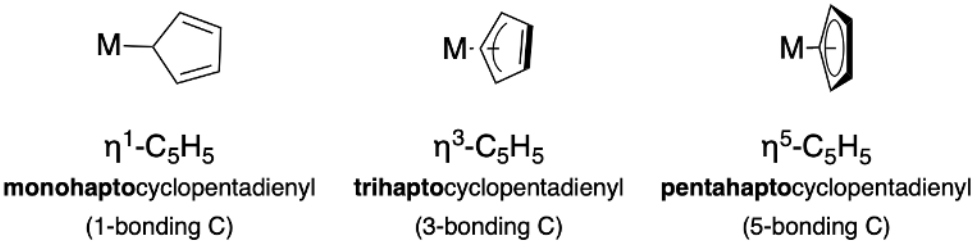


Figure **6.2.1**: The cyclopentadiene anion is shown coordinating to a metal ion (M) using three different coordination modes: On the left, Cp as a monohapto ligand. In the center, Cp is shown bonding to a metal in a trihapto fashion where the metal interacts with three carbons. On the right, Cp is shown bonding in a pentahapto fashion, where the five ligand carbons interact equally through the π system . (CC-BY-SA 4.0; Kathryn Haas)

Another common ligand is the π-allyl anion ($\mathbf{C_3H_3}$), which can coordinate in either an η^1 or η^3 fashion, as illustrated below (Figure **6.2.2**).

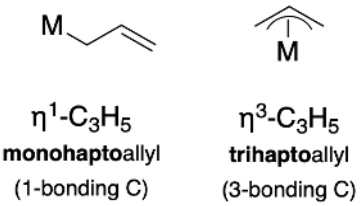


Figure **6.2.2**: The allyl anion is shown coordinating in a η^1 and eta^3 modes. (CC-BY-SA 4.0; Kathryn Haas)

Bridging ligands

Ligands that bridge two or more metal ions are indicated using the symbol, mu (μ). For a ligand that bridges n metal ions, the symbol is written as μ_n. However the subscript is often ommitted when $n = 2$. Some examples of the carbonyl ligand are given below. More specific rules for naming are found in Section 9.2.

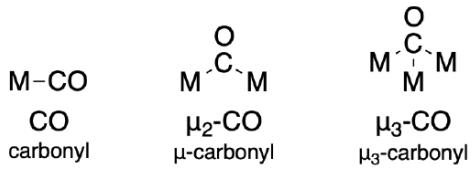
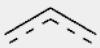
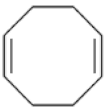


Figure **6.2.3**: The carbonyl ligand is shown as a terminal ligand (with no μ necessary), bridging two metals (μ_2), and bridging three metals μ_3). (CC-BY-SA 4.0; Kathryn Haas)

Common Ligands and Classifications

Some common organic ligands found in organometallic compounds are listed below with their names and structures.

Name	Structure	CBC description
Alkyl		X
Carbonyl		L
Carbene (alkylidene)		X_2
Carbyne (alkylidyne)		X_3
Ethylene		L
Acteylene		L
Acyl		X
π-allyl ($C_3H_5^-$)		X for η^1 LX for η^3
Cyclopropenyl (cyclo-C_3H_3)		X for η^1 LX for η^3
Cyclobutadiene (cyclo-C_4H_4)		L_2 for η^4
Cyclopentadienyl (cyclo-C_5H_5, Cp)		X for η^1 LX for η^3 L_2X for η^5
Benzene		L_3 for η^6
1,5-cyclooctadiene (1,5-COD)		L_2 for η^4

Covalent Bond Classification Method (CBC)

Later in this chapter, you will learn to count electrons. The way in which you count depends on what counting scheme you choose to use. But in any case, the way in which we "count" the electrons from ligands depends on the ligand type. The covalent bond classification method (CBC) has been in use since the late 1990's to classify ligands in organometallic complexes. This method classifies ligands into three main types as follows. (see Application of the Covalent Bond Classification Method for the Teaching of Inorganic Chemistry. Malcolm L. H. Green and Gerard Parkin, Journal of Chemical Education 2014 91 (6), 807-816, DOI: 10.1021/ed400504f.)

CBC Ligand Class/Type	Examples	Use in neutral Ligand Method of Electron Counting	Use in Donor Pair Method of Electron Counting
X-type	H^-, Cl^-, H_3C^-	Considered neutral Donates 1 electron to the metal	Considered anionic Donates 2 electrons to the metal
L-type	CO, NH_3, H_2O	Considered neutral Donates 2 electrons to the metal	Considered neutral Donates 2 electrons to the metal
Z-type (rarely used)	BR_3, Lewis acids	Considered neutral Accepts 2 electrons	Considered cationic Donates 0 electrons

This page titled 6.2: Nomenclature, Ligands, and Classification is shared under a CC BY-NC-SA 4.0 license and was authored, remixed, and/or curated by Kathryn Haas.

6.3: Electron Counting in Organometallic Complexes

In this section we will learn how to **count valence electrons in coordination compounds**. Electron counting is important because the number of electrons in a complex can be used to predict the compound's stability and reactivity. There are two different methods that are commonly used, and each is described below. Each of the two methods will lead to the same result if done correctly. Which method you prefer is “personal taste”, but each method is about equally common in the literature, so it is good to be familiar with both of them.

This page titled 6.3: Electron Counting in Organometallic Complexes is shared under a CC BY-NC-SA 4.0 license and was authored, remixed, and/or curated by Kathryn Haas.

- **Chapter 6.1: The 18 Electron Rule** by Kai Landskron is licensed CC BY 4.0.

6.3.1: The 18 Electron Rule

Method A for counting electrons: The Donor Pair Method

The donor pair method consider ligands to donate pairs of electrons to the metal. Each ligand-metal bond is considered a pair of electrons donated to the metal by the ligand. The method consists of the steps described in the box below.

How to count with the DONOR PAIR METHOD

1. **Determine the oxidation state of the metal center.** This step can be done by first deconstructing the complex so that each ligand "keeps" its bonded electrons (See Figure **6.3.1.2**). by considering the overall charge of the complex and the charge of each ligand, the oxidation state of the metal center can be determined. An alternative to deconstruction is to consider each ligand's class according to the Covalent Bond Classification (CBC) method discussed earlier.
2. **Determine the number of metal ion valence electrons**. The number of valence electrons can be determined from the metal's group on the periodic table and its oxidation state. If the oxidation state is positive we subtract electrons from the group number, if it is negative, which is rare, then we add electrons.
3. **Determine the number of bonded electrons derived from ligands**. Each ligand single bond provides two electrons, double bonds provide four electrons, etc.
4. **Add** the number of electrons from the metal ion valence (step 2) to the number of bonded electrons from the ligands to get the total valence electron count for the complex.

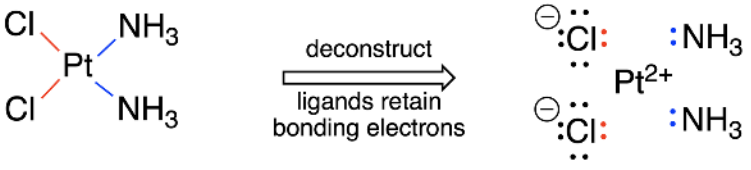
Below is an example of using the donor pair method to count electrons in the chemotherapy drug **cis**–$[PtCl_2(NH_3)_2]$, also called *cis*-platinum (Figure **6.3.1.1**). This compound is neutral in charge.

Step 1: Deconstruction of the complex using the donor pair method would convert each metal-ligand bond to a pair of electrons on the ligand. Without consulting the Covalent Bond Classification (CBC) method, we can determine the charge on each ligand using the simple Lewis dot diagrams that result. The ligands consist of two neutral ammines and two negatively charged chlorides. The ligands account for a total negative charge of -2. Since the metal complex is neutral, there must be a +2 change on the metal. Thus, the metal oxidation state is +2.

Step 2: With the knowledge that the Pt has an oxidation state of +2, and is in group 10 of the periodic table, we can determine the number of valence electrons on Pt(II). Subtract the oxidation state from the group number to get 8 valence electrons on the Pt(II) ion.

Step 3: Each of the ligands had one bond to Pt, thus each is a 2-electron donor. The ligands combined contribute a total of 8 electrons.

Step 4: Adding the 8 electrons from Pt(II) and the 8 electrons from the ligands gives a total electron count of 16.



Fragment	Electron Count
Pt(II)	8
2x Cl^-	4
2x NH_3	4
Total	**16**

Figure **6.3.1.1**: Example of the oxidation state method

Method B for counting electrons: The Neutral Atom Method (aka Neutral Ligand Method)

The “neutral atom method”, is sometimes called "the neutral ligand method". In this method, each ligand is considered to donate the number of electrons that it would *if the ligand were neutral*. The neutral atom method is carried out according to the steps described below.

How to count using the NEUTRAL LIGAND/ATOM METHOD

1. Determine the number of valence electrons on the metal center, as if it were a neutral atom. Add those electrons to the total count.
   Hint: The number valence electrons is the same as the group number of the transition metal in the periodic table (groups 3-12 for the transition metals).
2. Account for the ionic charge on the entire coordination complex. If the charge is neutral, you can ignore this step. If the complex has a positive charge, you subtract that many electrons from the total count. If the complex is an anion, you add the anionic charge to the total electron count.
3. Determine how many electrons are contributed by each ligand. (This is the most complicated step)
   - Deconstruct the metal ion (break its M-L bonds) so that each resulting ligand fragment and the central metal are neutral.
   - Then count the number of electrons from each ligand that contributed to the bond. Add the sum of those electrons from all the ligands to the total count.
     (Remeber you've already accounted for the electrons from the neutral atom in step #1)
4. Add the metal ion valence electrons (step 1), the total ligand electrons (step 3), and accounting for the charge of the complex (step 2). The total sum is the total valence electron count for the metal complex.

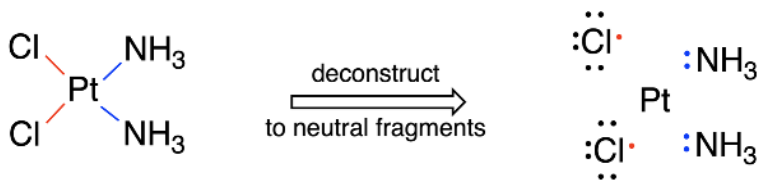
Below is an example of applying the neutral atom method to count electrons in the *cis*-platinum complex ($[Pt(Cl)_2(NH_3)_2]$ (Figure \(\PageIndex{2}\))).

Step 1: The metal is platinum which is located in group 10 of the periodic table. Therefore, a neutral platinum atom has ten valence electrons.

Step 2: The complex is neutral, this we can ignore this step.

Step 3: Each Cl is considered to donate 1 electron and each ammine ligand is considered to donate two electrons. The Cl's donate a total of two electrons, and the ammines donate a total of four electrons to give a total of 6 from all ligands.

Step 4: Ten electrons from Pt and six electrons from the ligands combine to give a total electron count of 16.



Neutral fragment	Electron Count
Pt	10
2x Cl	2
2x NH_3	4
Total	**16**

Figure 6.3.1.2: Example of applying the neutral fragment method to count the total valence electrons in $[Pt(Cl)_2(NH_3)_2]$.

There are pros and cons to each of the methods presented above. The neutral atom method has the advantage that we do not have to calculate charges of ligands or the metal oxidation states to reach the final answer. However, the disadvantage is that we must think about how to cleave bonds to create neutral fragments. We may need to cleave bonds in an way that is contrary to the real donor-acceptor nature of a coordination compound. The donor-pair method does account for the donor-acceptor nature of a coordination compound because the bonds are considered dative bonds, and the electrons are assigned to the ligands and metals accordingly. And advantage to the donor-pari method is that we do not need to think how to cleave bonds in artificial ways because we cleave the bonds always heteroleptically. However, the disadvantage is that it requires us to calcuate charges at the ligands to determine metal oxidation states, which is an additional, non-trivial step.

The 18 Electron Rule

Electron counting is a critical step in the context of an important rule in coordination chemistry: The 18 electron rule. **The 18 electron rule states that transition metal complexes are *normally* most stable when they have a total count of 18 electrons in the valence shell**. In other words, for *d*-block metal complexes, a valence configuration that fills all valence orbitals (ns^2 $(n-1)d^{10}$ np^6) is most stable; it is equivalent to a nobel-gas configuration for the metal atom, and is analogous to the "octet rule" for the

main-group elements. Complexes that have 18 electrons in their count are considered to be **coordinatively saturated**. In general, coordinatively saturated compounds are considered to be relatively stable, and when they react they usually undergo dissociation or oxidation reactions that decrease the electron count. If the there are less than 18 electrons, the species is **coordinatively unsaturated**, and considered less stable than a species with 18 electrons. In general, coordinatively unsaturated complexes tend to react in ways that can increase the electron count. They tend to undergo reactions involving associations to add more electrons to the system and/or tend to gain electrons through redox reactions (the metal becomes reduced). If a species has more than 18 electrons it is **coordinatively oversaturated** and tends to lose ligands. It is usually easily oxidized. Both loss of ligands and oxidation reduces to the number of electrons to or at least closer to 18.

Definitions:

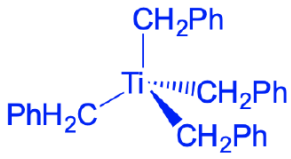
Coordinatively saturated: when the complex has an electron count =18 electrons. These complexes are considered most stable.

Coordinatively unsaturated: when the complex has an electron count <18 electrons. These complexes tend to add more ligands, and to become reduced.

Coordinatively oversaturated: when the complex has an electron count >18 electrons. These complexes tend to lose ligands and become oxidized.

Exceptions to the 18-electron rule:

The 18 electron rule has many exceptions, and therefore needs to be applied with caution. In particular, group 3, 4, and 10 complexes deviate often from the 18 electron rule.



Contribution metal:	4e
Oxidation state: +4	-4e
Electrons contributed by ligands:	4x2e=8e
Sum:	**8e**

Figure **6.3.1.3**: Example of counting electrons in the tetrahedral tetrabenzyltitanium(0) complex using the oxidation state method

For illustration purposes, let us count the number of electrons of the tetrahedral tetrabenzyltitanium(0) complex by the oxidation state method. We could also use the neutral atom method, which would give the same results. This complex is a group 4 complex because titanium is in group 4. How many electrons will the titanium contribute? Because the number of electrons is always the same as the group number, it will contribute four electrons. Next, what is oxidation state of Ti? To determine it we must determine the charge at the ligands. To do that we cleave the bonds heteroleptically. This will give benzylate anions with -1 charge. There are four of these ions, and therefore there will be four negative charges overall. The complex is charge-neutral, and thus the oxidation state is +4 because -4+4=0. Therefore, we need to subtract four electrons. Because we cleaved the bond heteroleptically, each ligand contributes two electrons, giving overall eight electrons coming from the four ligands. This means that we have overall eight electrons, or an 8-electron complex. This is far, far away from 18 electrons. Nonetheless, the complex is stable. How can we explain this? The answer is that in order to achieve 18 electrons it would need to add five additional ligands if each ligand is considered a 2-electron donor. This would increase the coordination number to 9 which is too high to produce a stable complex. In order to reduce the complex to an 18 electron complex, 10 electrons would need to be added. This would produce a complex with a -10 charge which is way to high to be stable. The arguments are generalizable for group 3 and group 4 complexes. Because these elements only have a few d electrons, the ligands would need to contribute a lot of electrons to produce an 18 electron complex. This would require just too many ligands to add. The coordination numbers would get too high. If electrons are added instead of ligands, the negative charge at the complex would be to high to be stable based on electron-electron repulsion arguments.



Contribution metal:	10e
Charge:	0e
Electrons contributed by Cl ligands:	2x1e=2e
Electrons contributed by NH_3 ligands:	2x2e=4e
Sum:	**16e**

Figure **6.3.1.4**: Counting electrons in the diamminedichloro palladium complex using the neutral atom method.

These arguments cannot be applied for group 10 elements, because these elements have many d electrons. The explanation in this case is that these elements like to make square planar complexes when in the oxidation number is +2. Square planar complexes prefer 16 instead of 18 electrons. We will learn later, when we discuss bonding in coordination compounds, why this is. You can see that the square planar diamminedichloro palladium complex shown is square planar and has sixteen electrons. There are 10 electrons coming from Pd. If we use the neutral atom method, no electrons need to be added or subtracted due to the charge at the complex. The complex is charge-neutral. To assess how many electrons come from the ligands we need to cleave the bonds so that neutral ligands are produced. The Pd-Cl bonds need to be cleave homoleptically, the Pd-N bonds need to be cleave heteroleptically. Therefore, the two chloro ligands are 1e donors, and the two ammine ligands are 2e donors. This gives 10+4+2=16 electrons.

Dr. Kai Landskron (Lehigh University). If you like this textbook, please consider to make a donation to support the author's research at Lehigh University: Click Here to Donate.

This page titled 6.3.1: The 18 Electron Rule is shared under a CC BY-NC-SA 4.0 license and was authored, remixed, and/or curated by Kathryn Haas.

- **Chapter 6.1: The 18 Electron Rule** by Kai Landskron is licensed CC BY 4.0.

6.3.2: Simplifying the Organometallic Complex by Deconstruction

Organometallic complexes, which consist of centrally located metals and peripheral organic compounds called ligands, are the workhorses of organometallic chemistry. Just like organic intermediates, understanding something about the structure of these molecules tells us a great deal about their expected reactivity. Some we would expect to be stable, and others definitely not! A big part of our early explorations will involve describing, systematically, the principles that govern the stability of organometallic complexes. From the outset, I will say that these principles are not set in stone and are best applied to well controlled comparisons. Nonetheless the principles are definitely worth talking about, because they form the foundation of everything else we'll discuss. Let's begin by exploring the general characteristics of organometallic complexes and identifying three key classes of organic ligands.

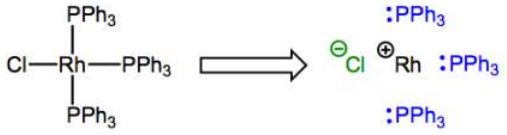
When we think of metals we usually think of electropositive atoms or even positively charged ions, and many of the metals of OM chemistry fit this mold. In general, it is useful to imagine organic ligands as electron donors and metals as electron acceptors. When looking at a pair of electrons shared between a transition metal and main-group atom (or hydrogen), I imagine the cationic metal center and anionic main-group atom racing toward one another from oblivion like star-crossed lovers. In the opposite direction (with an important caveat that we'll address soon), we can imagine ripping apart metal–R covalent bonds and giving both electrons of the bond to the organic atom. This heterolytic bond cleavage method reproduces the starting charges on the metal and ligand. Unsurprisingly, the metal is positive and the ligand negative.

FYI, you might see the blue bipyridine referred to as an L2 ligand elsewhere; this just means that a single bipyridine molecule possesses two L-type binding points. Ligands with multiple binding points are also known as chelating or polydentate ligands. Chelating ligands may feature mixed binding modes; for instance, the allyl ligand is of the LX-type. Chelating ligands can also bind to two different metal centers; when they act in this way, they're called bridging ligands. But don't let all this jargon throw you! Deconstruct complexes one binding point at a time, and you cannot go wrong.

Next, we'll take a closer look at the metal center and expand on the purpose of the deconstruction process described here.

"Bookkeeping" through deconstruction of organometallic complexes

Now it's time to turn our attention to the metal center, and focus on what the deconstruction process can tell us about the nature of the metal in organometallic complexes. Let's turn our attention now to a new complex. I've gone ahead and deconstructed it for us.



Say hello to rhodium (Rh)! Don't fret; it's just a group 9 element.

The complex possesses one X-type and three L-type ligands, so the rhodium atom ends up with a formal charge of +1. The formal charge on the metal center after deconstruction has a very special name that you will definitely want to commit to memory: it's called the oxidation state. It's usually indicated with a roman numeral next to the atomic symbol of the metal (the "+" is implied). In the complex shown above, rhodium is in the Rh(I) or +1 oxidation state. Oxidation state is most useful because changes in oxidation state indicate changes in electron density at the metal center, and this can be a favorable or unfavorable occurrence depending on the other ligands around. We will see this principle in action many, many times! Get used to changes in oxidation state as everyday events in organometallic reaction mechanisms. Unlike carbon (with the exception of carbene…what's its oxidation state?!) and other second-row elements, the transition metals commonly exhibit multiple different oxidation states. More on that later, though. For now, training yourself to rapidly identify the oxidation state of a complexed metal is most important. Please note that when a complex possesses an overall charge, the oxidation state is affected by this charge!

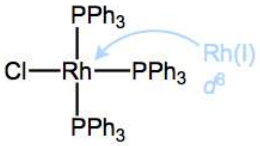
oxidation state = number of X-type ligands bound to metal + overall charge of complex

What of this number of d electrons concept? A very useful way to think about "number of d electrons" is as the "number of non-bonding electrons on the metal center," and you're probably familiar with identifying non-bonding electrons from organic chemistry. The numbers of valence electrons of each organic element are set in stone: carbon has four, nitrogen has five, et cetera.

Furthermore, using this knowledge, it's straightforward to determine the number of lone pair electrons associated with an atom by subtracting its number of covalent bonds from its total number of valence electrons. E.g., for a neutral nitrogen atom in an amine NR3, 5 – 3 = 2 lone pair electrons, typically. The extension to organometallic chemistry is natural! We can analyze complexed metal centers in the same way, but they tend to have a lot more non-bonding electrons than organic atoms, and the number depends on the metal's oxidation state. For instance, the deconstructed rhodium atom in the figure above has 8 d electrons: 9 valence electrons minus 1 used for bonding to Cl. Dative bonds don't affect d electron count since both electrons in the bond come from the ligand.

number of non-bonding electrons = number of d electrons = metal's group number – oxidation state

Drawing all the non-bonding d electrons out as lone pairs would clutter things up, so they are never drawn…but we must remember that they're around! Why? Because the number of d electrons profoundly affects a complex's geometry. We will return to this soon, but the key idea is that the ligands muck up the energies of the d orbitals as they approach the metal (recall the "star-crossed lovers" idea), and the most favorable way to do so depends on the number of non-bonding electrons on the metal center.



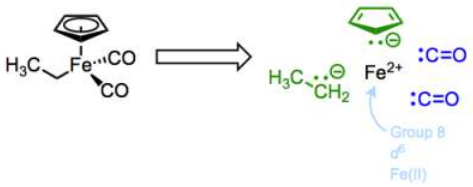
Oxidation state and d electron count: two tools the OM chemist can't live without!

This post introduced us to two important bookkeeping tools, oxidation state and number of d electrons. In the final installment of the "Simplifying the Organometallic Complex" series, we'll bring everything together and discuss total electron count. We'll see that total electron count may be used to draw a variety of insightful conclusions about organometallic complexes.

Apply deconstruction to gain insight

So far, we've seen how deconstruction can reveal useful "bookkeeping" properties of organometallic complexes: number of electrons donated by ligands, coordination number, oxidation state, and d electron count (to name a few). Now, let's bring everything together and discuss total electron count, the sum of non-bonding and bonding electrons associated with the metal center. Like oxidation state, total electron count can reveal the likely reactivity of OM complexes—in fact, it is often more powerful than oxidation state for making predictions. We'll see that there is a definite norm for total electron count, and when a complex deviates from that norm, reactions are likely to happen.

Let's begin with yet another new complex. This molecule features the common and important cyclopentadienyl and carbon monoxide ligands, along with an X-type ethyl ligand.



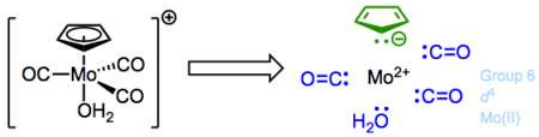
What is the total electron count of this Fe(II) complex?

The Cp or cyclopentadienyl ligand is a polydentate, six-electron L2X ligand. The two pi bonds of the free anion are dative, L-type ligands, which we'll see again in a future post on ligands bound through pi bonds. Think of the electrons of the pi bond as the source of a dative bond to the metal. Since both electrons come from the ligand, the pi bonds are L-type binders. The anionic carbon in Cp is a fairly standard, anionic X-type binder. The carbon monoxide ligands are interesting examples of two-electron L-type ligands—notice that the free ligands are neutral, so these are considered L-type! Carbon monoxide is an intriguing ligand that can teach us a great deal about metal-ligand bonding in OM complexes…but more on that later.

After deconstruction, we see that the Fe(II) center possesses 6 non-bonding d electrons. The total electron count is just the d electron count plus the number of electrons donated by the ligands. Since the d electron count already takes overall charge into account, we need not worry about it as long as we've followed the deconstruction procedure correctly.

total electron count = number of d electrons + electrons donated by ligands

For the Fe(II) complex above, the total electron count is thus 6 + (6 + 2 + 2 + 2) = 18. Let's work through another example: the complex below features an overall charge of +1. Water is a dative ligand—that "2" is very important!

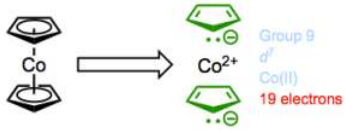


Note that the overall charge is lumped into the oxidation state and d electron count of Mo.

The oxidation state of molybdenum is +2 here…remember that the overall charge factors in to that. When everything is said and done, the total electron count is 4 + (6 + 2 + 2 + 2 + 2) = 18.

What's up with 18?! As it turns out, 18 electrons is a very common number for stable organometallic complexes. So common that the number got its own rule—the 18-electron rule—which states that stable transition-metal complexes possess 18 or fewer electrons. The rule is analogous to organic chemistry's octet rule. The typical explanation for the 18-electron rule points out that there are 9 valence orbitals (1 s, 3 p, 5 d) available to metals, and using all of these for bonding seems to produce the most stable complexes. Of course, as soon as the rule left the lips of some order-craving chemist, researchers set out to find counterexamples to it, and a number of counterexamples are known. Hartwig describes the rule as an "empirical guideline" with little theoretical support. In fact, theoretical studies have shown that the participation of p orbitals in complex MOs is unlikely. I know that's not what you want to hear—but hang with me! The 18-electron rule is still a very useful guideline. It's most interesting, in fact, when it is not satisfied.

One last example…how would you expect the complex below to react?



Cobaltocene: jonesing for chemical change.

If we assume that the 18-electron rule is true, then cobaltocene has a real problem. It possesses 7 + (6 + 6) = 19 total valence electrons! Yet, we can also reason that this complex will probably react to relieve the strain of not having 18 electrons by giving up an electron. Guess what? In practice, cobaltocene is a great one-electron reducing agent, and can be used to prepare anionic complexes through electron transfer.

$$CoCp_2 + ML_n \rightarrow [CoCp_2] + [ML_n]^- \tag{6.3.2.1}$$

This post described how to calculate total electron count and introduced the power of the 18-electron rule for predicting whether a complex will donate or accept electrons. We will definitely see these ideas again! But what happens when the electron counts of two complexes we're interested in comparing are the same? We'll need more information. In the next post, we'll explore the periodic trends of the transition series. Our goal will be to make meaningful comparisons between complexes of different metals.

Contributors and Attributions

- Dr. Michael Evans (Georgia Tech)

This page titled 6.3.2: Simplifying the Organometallic Complex by Deconstruction is shared under a CC BY-NC-SA 4.0 license and was authored, remixed, and/or curated by Kathryn Haas.

- **3.5: Simplifying the Organometallic Complex (Part 1)** by Michael Evans is licensed CC BY-NC-SA 4.0.
- **3.6: Simplifying the Organometallic Complex (Part 2)** by Michael Evans is licensed CC BY-NC-SA 4.0.
- **3.7: Simplifying the Organometallic Complex (Part 3)** by Michael Evans is licensed CC BY-NC-SA 4.0.

6.4: Survey of Organometallic Ligands

Organometallic chemistry may be taught in many ways. Some textbooks spend a significant chunk of time discussing ligands, while others forego ligand surveys to dive right in to reactions and mechanisms. I like the ligand survey approach because it allows you to get a grip on expected behaviour for each type of ligand before you see them pop up as intermediates in reaction cycles. With the general principles in hand, it becomes easier to generate explanations for observed each ligan's effect on a reactions. Instead of generalizing from complex, specific examples in the context of reaction mechanisms, we'll look at general trends first and apply these to reaction intermediates and mechanisms later. This section will kick off with carbon monoxide, a simple but fascinating ligand.

This section begins a survey of some of the most common or most interesting ligands in organometallic complexes. We will begin with a survey of ligands that participate in "dative" bonding to metal ions in this section (Runaway argument for \eatSpaces?), followed by ligands that interact with metal ions through their π electrons, and those that have multiple metal-carbon bonds in the following sections.

This page titled 6.4: Survey of Organometallic Ligands is shared under a CC BY-NC-SA 4.0 license and was authored, remixed, and/or curated by Michael Evans.

- **2.2: Carbon Monoxide** by Michael Evans has no license indicated.

6.4.1: Carbon Monoxide (Carbonyl Complexes)

Introduction into Carbonyl Complexes

In this chapter we will look closer at carbonyl complexes, often just called carbonyls. Why? They are interesting for a number of reasons. Firstly, they are a quite extensive class of compounds with a diverse coordination chemistry. We will learn that the CO ligand can bind to a metal in various, sometimes non-obvious ways. Further, carbonyls are frequently used as starting materials for other coordination compounds. This is because the carbonyl ligand has no charge and carbon monoxide is a gas. Because of that a ligand substitution reaction can be easily driven to the right side by purging CO out of the reaction vessel. CO is a C_1 unit, and this is frequently used in catalysis with carbonyls. Carbonyls are often intermediates in reactions that add a single carbon atom to a hydrocarbon chain. A fascinating fundamental property of carbonyls is that its π-accepting properties stabilize metals in low, sometimes even negative oxidation numbers.

Bonding in CO

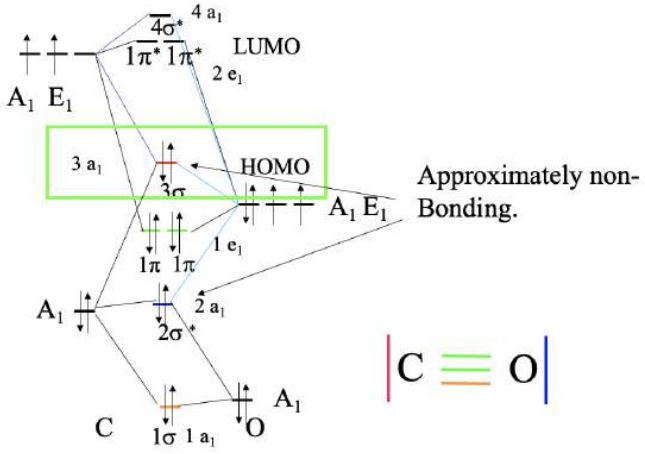


Figure **6.4.1.1**: Bonding in the CO molecule. MO diagram (left), and corresponding valence bond structure (right). For more explaination click here.

The carbon in the CO molecule is the more reactive end, and thus CO prefers to bind with the carbon to a metal, and not with oxygen. This is not obvious because the carbon is less electronegative than oxygen. The reason is that the HOMO of the CO molecule is an approximately non-bonding orbital which is primarily localized at the carbon (Figure **6.4.1.1**). In the valence bond picture it is resembled by the electron-lone pair at the carbon atom. The electron lone pair at the oxygen is resembled by the $2a_1$ molecular orbital which has a significantly lower energy, therefore it is rarely used in bonding. Both the π and π*-orbitals are relatively close in energy to the HOMO, and thus these orbitals can also be used for bonding in carbonyls. This explains the diverse coordination chemistry of carbonyls.

σ-binding Modes of The Carbonyl Ligand

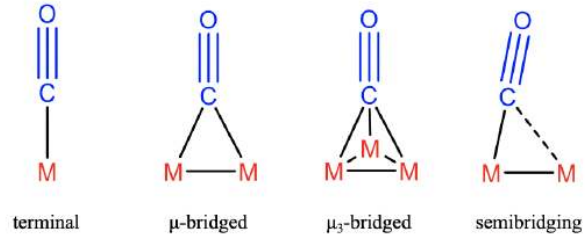


Figure **6.4.1.2**: σ-binding modes of the carbonyl ligand. Attribution: W. Petz

In the most simple case the CO uses its electron lone pair at the carbon to bind to single metal atom M (Figure **6.4.1.2**). In this case we call CO a terminal carbonyl ligand. In addition, it is possible that the electron lone pair is shared between two or even three metals that are interconnected via metal-metal bonds. In these cases, we say that the CO acts as a μ-bridged, and μ_3-brigded ligand,

respectively. If two metals held together by a metal-metal bond are different, then the interaction of CO with one metal may be stronger than with the other. In this case the CO ligand acts as a semibridging ligand. In all these cases CO acts as a 2-electron donor because it donates its two electrons in the electron lone pair in the carbon atom.

In addition to the electron lone pair at the carbon the CO ligand can also use its binding π-orbitals for electron-donation into metal orbitals (Figure **6.4.1.3**). However, these electrons can only be used in conjunction with the electron lone pair at C because the electron pair has a higher energy than the π-electrons, and electrons of higher energy are always used first. For steric reasons the electron lone pair and the π-electrons are always donated to different metals that are held together by metal-metal bonds.

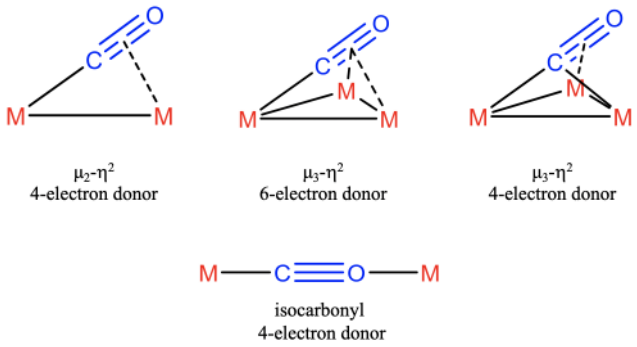


Figure **6.4.1.3**: Binding in π-orbitals for electron-donation into metal orbitals. Attribution: W. Petz

In the most simple case the CO ligand binds in μ_2-η_2-mode which implies that the electron lone pair binds to one metal and two π-electrons bind to another. In this this case the CO ligand acts as a 4-electron donor. In addition, it is possible that all four π-electrons are involved involved in the bonding in addition to the electron lone pair. In this case three metal atoms are involved. The first one interacts with the electron-lone pair, the second one with the two π-electrons, and the third one with the other two π-electrons. Because three metals are bridged and both atoms of the ligand are involved in the bonding with the metal we can say that CO binds in μ_3-η_2-fashion and acts as a 6-electron donor. It is also possible that the electron-lone pair is being shared between two metals, and two π-electrons are donated to the third metal. Also in this case the ligand binds in μ_3-η_2-fashion, but acts as a 4-electron donor. Another way the CO ligand can act as 4-electron donor is when it acts as an isocarbonyl ligand. In this case it uses its electron pairs at both the C and the O-atoms. This is only possible when steric circumstances favor the utilization of the O-electron lone pair over the energetically higher π-electrons. This is rare.

π-binding Modes of The Carbonyl Ligand

The carbonyl ligand can use its π*-orbitals for bonding with metal d-orbitals in π-fashion. The ligand acts as a π-acceptor. There are two possibilities for the binding (Figure **6.4.1.4**).

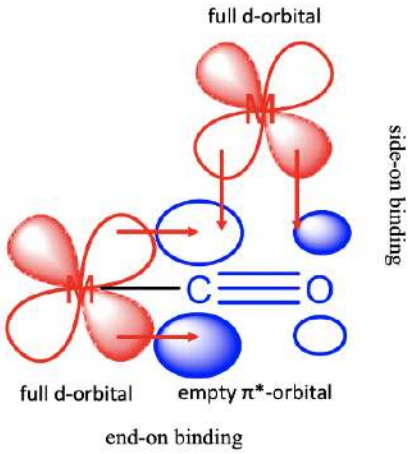


Figure **6.4.1.4**: π-binding modes of the carbonyl ligand

The first one occurs when the CO-ligand acts as a terminal ligand binding end-on. In this case the two lobes of the π*-orbitals at the carbon interact with the the lobes of a metal d-orbital. Also the bonding π-orbitals have the right symmetry to overlap with the

metal d-orbital in this mode, but their energies are much further away from those of the d-orbitals, so that these interactions can be neglected. The second possibility is that the CO binds side-on to the a metal-d-orbital. In this case one lobe at C and one lobe at O interacts with the metal d-orbital. These interactions are less strong compared to the end-on interactions because the orbital overlap is less efficient due to the unequal size of the lobes of the π^*-orbital. The π^*-orbital is mostly localized at the carbon-atom because the carbon atom is the more electropositive atom. Note that the bonding π-orbitals do not have the right symmetry to overlap with a metal-d orbital in π-fashion, they can only overlap in σ-fashion when the binding is side-on.

The Dewar-Chatt-Duncanson model

The σ-donor and the π-acceptor interactions in carbonyl complexes synergistically reinforce each other. This synergistic effect is called the Dewar-Chatt-Duncanson model for carbonyls. How can we understand the synergistic interactions. Let us consider a carbonyl ligand that binds end-on to a metal.

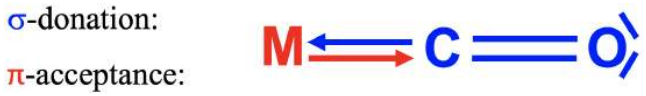


Figure **6.4.1.5**: σ-donor and the π-acceptor interactions in carbonyl complexes.

Let us first look at the σ-donor interactions. The electron lone pair at the carbon donates electron density into empty metal d-orbitals and a dative bond is formed between the metal and the carbon. The donated electron density enhances the energy of the metal d-electrons due to increased electron-electron repulsion. Because of their increased energy the d-electrons get more easily accepted by the carbonyl ligand through the π-acceptor interactions. The π-acceptor interactions increase the bond order between the metal and the carbon bond. At the same time the bond order between carbon and oxygen gets decreases because electron density has been transferred from the metal into the π^*-orbitals (Figure **6.4.1.5**).

The strength of the π-acceptor interactions can differ significantly in carbonyls. One can draw three different structures for weak, intermediate, and strong π-acceptor interactions (Figure **6.4.1.6** to **6.4.1.8**).



Figure **6.4.1.6**: Weak π-acceptor interactions

When only weak interactions are present we can represent the M-C bond as a single bond, and the C-O bond as a triple bond.



Figure **6.4.1.7**: Intermediate π-acceptor interactions

When the interactions have intermediate strength we can represent both the M-C bond and the C-O bond as a double-bonds.



Figure **6.4.1.8**: Strong π-acceptor interactions

When the π-acceptor interactions are strong then the M-C bond becomes a triple bond and the C-O bond becomes a single bond.

On what does the strength of the π-acceptor interactions depend? It depends mostly on the charge on the carbonyl. Carbonyl cations with a charge of +2 or higher tend to have weak π-acceptor interactions. Neutral carbonyls or carbonyls with a +1 or -1 charge have intermediate π-acceptor interactions. and those with a negative charge of 2- or higher have strong π-acceptor interactions. One can see from this that the smaller the positive charge and the higher the negative charge, the higher the metal-carbon bond-order, and the stronger the metal-carbon bond. As a consequence negative charges tend to stabilize carbonyls, while positive charges destabilize them. Therefore, carbonylate anions tend to be more stable compared to carbonyl cations. The stability of neutral carbonyls is intermediate.

Homoleptic Carbonyls of The Transition Metals

After having understood the principles of the bonding in carbonyls let us next think about what structures transition metal carbonyls make. The structures follow mostly the 18 electron rule. For the most simple homoleptic carbonyls, in which the carbonyl ligand binds end-on to the transition metal acting as a two-electron donor, we would just assemble as many ligands as

needed until we have 18 electrons. This would give us the coordination number in the carbonyl from which we could deduct the structure. This works well for transition metals with an even number of valence electrons.

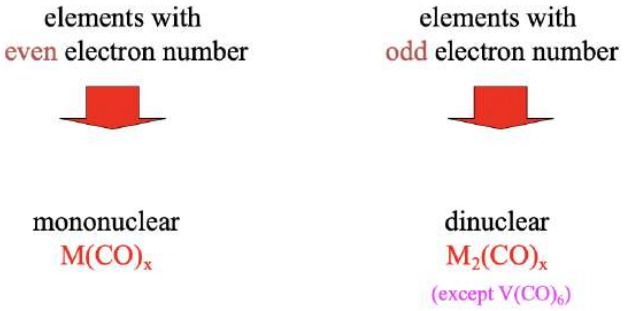


Figure **6.4.1.9**: Mononuclear carbonyls vs dinuclear carbonyls. Attribution: W. Petz

In this case the number of ligands x is just 18 minus the number of metal electrons divided by 2. We would therefore expect a mononuclear carbonyl of the type $M(CO)_x$ (Figure **6.4.1.9**). For metals with an odd number of electrons, the situation is more complicated because an odd number times two multiplied with an integer number never gives 18. In this case, as many ligands x as needed to make a 17 valence electron complex are added to the metal, and then the 17 valence electron complex dimerizes to form a dinuclear carbonyl of the composition $M_2(CO)_x$. An exception is the vanadium. It makes a 17 valence electron vanadium hexacarbonyl that does not dimerize because a coordination number of 7 is not favorable.

Homoleptic carbonyls of the 6th group (M = Cr, Mo, W)

Now let us look closer at the carbonyls with metals with an even number of electrons. We can start out with group 6 which contains the elements chromium, molybdenum, and tungsten. Our task is to determine the composition and structure of the carbonyls.

sum:	18e
metal electrons:	6e
charge:	0 e
# ligand electrons needed:	18-6=12e
# of ligands needed:	12/2=6

$M(CO)_6$
(octahedral)

Figure **6.4.1.10**: Determining the composition and structure of carbonyls via electron counting

According to the 18 electron rule we need 18 electrons overall. How many are contributed by the metal? Because the metals are in group 6, they all have six electrons. The carbonyls carry no charge, so there are no electrons to be subtracted or added. How many ligand electrons do we need to get to 18? Well, that is 18-6=12 electrons. How many carbonyl ligands are needed then? Because each ligand is considered a two electron donor, we need 12/2=6 ligands. The composition of the carbonyl will therefore be $M(CO)_6$. The carbonyl adopts octahedral shape in order to maximize the distance of the ligands from each other. The group 6 carbonyls are colorless, crystalline, and sublimable solids.

	ν(CO)/cm^{-1}		ν(CO)/cm^{-1}		ν(CO)/cm^{-1}
$[Co(CO)_6]^{3+}$		$[Rh(CO)_6]^{3+}$		$[Ir(CO)_6]^{3+}$	2254
$[Fe(CO)_6]^{2+}$	2204	$[Ru(CO)_6]^{2+}$	2199	$[Os(CO)_6]^{2+}$	2190
$[Mn(CO)_6]^{+}$	2100	$[Tc(CO)_6]^{+}$	not reported	$[Re(CO)_6]^{+}$	2085
$Cr(CO)_6$	1986	$Mo(CO)_6$	1986	$W(CO)_6$	1977
$[V(CO)_6]^{-}$	1847	$[Nb(CO)_6]^{-}$	1850	$[Ta(CO)_6]^{-}$	1850
$[Ti(CO)_6]^{2-}$	1750	$[Zr(CO)_6]^{2-}$	1757	$[Hf(CO)_6]^{2-}$	1757

Figure **6.4.1.11** Charged octahedral 18 electron carbonyls and the wave number of their C-O stretch vibrations. Green: Known charged carbonyls, Red: Unknown charged carbonyls.

Are there also other 18 e carbonyls of the type $M(CO)_6$ with other metals but group 6 metals? Yes, but the charge at the carbonyl needs to be adjusted so that the complex has 18 electrons. For instance, we can replace Cr by V, but then the we need a 1- charge which results in a carbonylate of the formula $V(CO)_6^-$. Why? The vanadium is in group 5 and has one electron less than chromium. For that reason, we must add an electron which gives the complex a 1- charge. Also the higher homologues $Nb(CO)_6^-$ and $Ta(CO)_6^-$ are known. What if we go further to the left in the periodic table? Titanium is left to the vanadium, and has four valence electrons. Therefore, the 18 valence electron hexacarbonyl of titanium has a 2- charge, and the formula is $Ti(CO)_6^{2-}$. Again, the higher homologues of $Ti(CO)_6^{2-}$, the $Zr(CO)_6^{2-}$ and the $Hf(CO)_6^{2-}$ are also known. Can we also go to the right in the periodic table? Manganese sits to the right of the chromium. The manganese has one electron more than the chromium, therefore the 18 electron hexacarbonyl of manganese must be a carbonyl cation with a 1+ charge, and the formula is $Mn(CO)_6^{2+}$. Of the higher homologues, both the $Tc(CO)_6^+$ and the $Re(CO)_6^+$ are known, too. To the right of the Mn, there is the Fe which has 8 valence electrons. Therefore the 18 electron iron hexacarbonyl must have a 2+ charge, and the formula is $Fe(CO)_6^{2+}$. The higher homologues $Ru(CO)_6^{2+}$ and $Os(CO)_6^{2+}$ are also known. Can we go even further to the left, to the Co? The expected formula for Co carbonyl would be $Co(CO)_6^{3+}$, but it is not known, and neither is the higher homologue, the $Rh(CO)_6^{3+}$. Only the $Ir(CO)_6^{3+}$ has been isolated. This reflects a general trend in carbonyl chemistry. Positive charges destabilize the carbonyl, and carbonyls with high positive charges are frequently not stable. On the other hand, negative charges stabilize a carbonyl and even carbonylates with high negative charges are stable. We can easily explain this by the fact that the bond order between the metal and the carbon decreases with increasing positive charge, and increases with increasing negative charge. Increasing bond order strengthens the stability of the carbonyl. We see from this that the π-acceptor properties are quite important for the stability of carbonyls. We also see that in carbonylates the oxidation numbers of the metals are negative. Negative oxidation numbers are quite unusual for metals. We conclude that the carbonyl ligand has the unusual property to stabilize the metal in negative oxidation states.

Is there a way to easily measure the bond order of an M-C bond? We can do this indirectly by measuring the IR-spectrum of the carbonyl. Because the bond order of the C-O bond decreases with increasing bond order for the M-C bond, the wavenumber for the

C-O stretch vibration can be used as a measure for the M-C bond order. The lower the wavenumber, the lower the C-O bond order, and the higher the M-C bond order. When we look at the numbers for the different carbonyls within a period we see that as expected the wavenumbers increase with increasing group number indicating a decreasing bond order. We can also look down the groups. We see that in this case, the numbers hardly change, meaning that the bond order is hardly affected by the period of the metal.

Homoleptic Carbonyls of the 8th Group (Fe, Ru, Os)

What charge-neutral carbonyls would we expect for the group 8 elements Fe, Ru, and Os?

sum:	18e
metal electrons:	8e
charge:	0 e
# ligand electrons needed:	18-8=10e
# of ligands needed:	10/2=5

$M(CO)_5$
(trigonal-bibyramidal)

Figure **6.4.1.12**: Carbonyls for the group 8 elements

Overall, these carbonyl need to have 18 electrons. In this case the metals have 8 electrons. The charge is 0. This means that we would have 18-8=10 electrons that would need to come from the ligand. The number of ligands needed would therefore be 10/2=5. Thus, we would expect pentacarbonyls of the composition $M(CO)_5$ (Figure **6.4.1.12**). These carbonyls adopt the trigonal-bipyramidal shape. The group 8 carbonyls are all liquids. The iron pentacarbonyl has a light-orange color while the ruthenium and the osmium carbonyls are colorless.

Charged Trigonal-Bipyramidal Carbonyls with 18 electrons

$[Ni(CO)_5]^{2+}$	$[Pd(CO)_5]^{2+}$	$[Pt(CO)_5]^{2+}$
$[Co(CO)_5]^{+}$	$[Rh(CO)_5]^{+}$	$[Ir(CO)_5]^{+}$
$Fe(CO)_5$	$Ru(CO)_5$	$Os(CO)_5$
$[Mn(CO)_5]^{-}$	$[Tc(CO)_5]^{-}$	$[Re(CO)_5]^{-}$
$[Cr(CO)_5]^{2-}$	$[Mo(CO)_5]^{2-}$	$[W(CO)_5]^{2-}$
$[V(CO)_5]^{3-}$	$[Nb(CO)_5]^{3-}$	$[Ta(CO)_5]^{3-}$

Figure **6.4.1.13**: 18 Charged trigonal-bipyramidal carbonyls with 18 electrons. Green: Known charged carbonyls, Red: unknown charged carbonyls.

We can again ask if there are charged isosteric pentacarbonyls with 18 e of metals other than group 8 metals. The answer is yes. The manganese is left to the iron in the periodic table and has one electron less. Therefore its pentacarbonyl needs to have a 1- charge and the composition is $Mn(CO)_5^-$. Also the higher homologues, the $Tc(CO)_5^-$ and the $Re(CO)_5^-$ exist. The Cr has one electron less than than the Mn, therefore its pentacarbonyl has a 2- charge and the formula is $Cr(CO)_5^{2-}$. $Mo(CO)_5^{2-}$ and $W(CO)_5^{2-}$ are also known. The vanadium has another electron less because it is in the 5th group, therefore its pentacarbonyl has a 3- charge, and the formula is $V(CO)_5^{3-}$. Again, the higher homologues, the $Nb(CO)_5^{3-}$ and the $Ta(CO)_5^{3-}$ are also stable. Also for the pentacarbonylates high negative charges are no problem for the stability of the complexes due to the stabilizing effect of the π-acceptor interactions. What about carbonyl cations with trigonal bipyramidal shape? As we go from Fe to Co, we need a 1+ charge

at the carbonyl to achieve 18 electrons. The respective $Co(CO)_5^+$ cation is stable, and so are their higher homologues, the $Rh(CO)_5^+$ and the $Ir(CO)_5^+$. However, the group 10 pentacarbonyl cations $Ni(CO)_5^{2+}$, $Pd(CO)_5^{2+}$, and $Pt(CO)_5^{2+}$ are not stable. The 2+ positive charge weakens the metal-carbon bond too much. This behavior is consistent with the weakening of the M-C bond with increasing positive charge due to weaker π-acceptor effects.

Homoleptic carbonyls of group 10 (Ni, Pd, Pt)

What about the group 10 carbonyls?

sum:	18e
metal electrons:	10e
charge:	0 e
# ligand electrons needed:	18-10=8e
# of ligands needed:	8/2=4

$M(CO)_4$
(tetrahedral)

Figure 6.4.1.14: Carbonyls for the group 10 elements

In this case the metals have 10 electrons. There is no charge. The number of ligand electrons needed is 18-10 = 8 electrons. Thus, the number of ligands is 8/2=4. Therefore, the composition is $M(CO)_4$ (Figure 6.4.1.14). The shape is tetrahedral because we have an 18 and not a 16 valence electron complex. Nickel tetracarbonyl is a volatile, colorless liquid. The higher homologues, the $Pd(CO)_4$ and the $Pt(CO)_4$ are not stable. We can explain this when remembering that the π-orbital overlap in tetrahedral complexes is generally weak. Therefore, the M-C carbon bond is less effectively stabilized by the π-acceptor interactions compared to octahedral and trigonal-bipyramidal carbonyls. This effect is even more pronounced for the Pd and Pt carbonyls because they have larger orbitals that can overlap even less effectively with the relatively small π^*-orbitals of the CO ligand. In this case the π-acceptor interactions are so weak so that the entire molecule is no longer stable.

Charged Tetrahedral Carbonyls with 18 electrons

$[Cu(CO)_4]^+$	$[Ag(CO)_4]^+$	$[Au(CO)_4]^+$
$Ni(CO)_4$	$Pd(CO)_4$	$Pt(CO)_4$
$[Co(CO)_4]^-$	$[Rh(CO)_4]^-$	$[Ir(CO)_4]^-$
$[Fe(CO)_4]^{2-}$	$[Ru(CO)_4]^{2-}$	$[Os(CO)_4]^{2-}$
$[Mn(CO)_4]^{3-}$	$[Tc(CO)_4]^{3-}$	$[Re(CO)_4]^{3-}$
$[Cr(CO)_4]^{4-}$	$[Mo(CO)_4]^{4-}$	$[W(CO)_4]^{4-}$

Figure 6.4.1.15: Charged tetrahedral carbonyls with 18 electrons. Green: Known carbonyls. Red: Unknown carbonyls.

What about charged 18 electron tetrahedral carbonyls with other metals? Again, negatively charged carbonylates are stable, even with high negative charges. $Co(CO)_4^-$, $Fe(CO)_4^{2-}$, $Mn(CO)_4^{3-}$, and $Cr(CO)_4^{4-}$ are all stable and so are their higher homologues. The $Cu(CO))_4^+$ which has a 1+ positive charge is also known, but its higher homologues, the $Ag(CO)_4^+$ and the $Au(CO)_4^+$ are not.

Overall Stability Trends

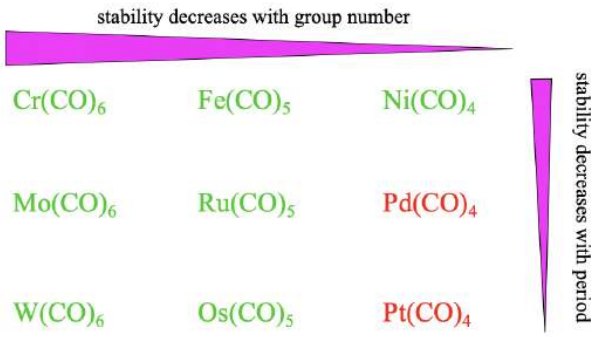


Figure **6.4.1.16**: Stability trends. Attribution: W. Petz

Overall the stability of carbonyls tends to decrease from group 6 to group 8 to group 10 (Figure **6.4.1.16**). This trend is because the octahedral shape allows for the best orbital overlap for π-acceptor interactions, followed by the trigonal bipyramidal, followed by the tetrahedral shape. The stability also tends to decline from the 4th to the 6th period. This trend can be explained by less efficient orbital overlap due to increasingly different orbital size between the ligand and the metal orbitals. These effects are sufficiently large for $Pd(CO)_4$ and $Pt(CO)_4$ to make them instable.

Group 4 and Group 12 Carbonyls (non-existing)

We have discussed group 6, 8, and 10 carbonyls, but not group 4 and group 12. Why? Because no carbonyls of these groups are stable. What is the reason? For group 4 carbonyls, we would need seven carbonyl ligands. This would lead to a coordination number of seven which is unacceptably high for carbonyls. For group 12 carbonyls, we would only need three carbonyl ligands. This would lead to an unacceptably low coordination number of 3.

Homoleptic carbonyls of the 7th group (M = Mn, Tc, Re)

Now let us think about what structures the homoleptic carbonyls with metals having an odd number of electrons form. Let us start with the 7th group which consists of the metals Mn, Tc, and Re. Our approach is to see how many ligands we need to produce a 17 valence electron fragment, and then dimerize that fragment.

sum:	17e
metal electrons:	7e
charge:	0 e
# ligand electrons needed:	17-7=10e
# of ligands needed:	10/2=5

$(CO)_5M\text{-}M(CO)_5 = M_2(CO)_{10}$

(derived from octahedral $M(CO)_5L$ (L=$M(CO)_5$))

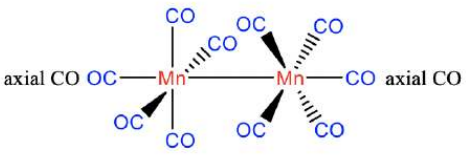


Figure **6.4.1.17**: Homoleptic carbonyls with group 7 metals. Attribution: W. Petz.

The group 7 metals have seven valence electrons. Again, we will assume that there is no charge on the carbonyl. The number of ligand electrons to produce the 17 valence electrons fragment will therefore be 17-7 = 10. The number of ligands needed is therefore 10/2=5 assuming that the carbonyl ligand is a 2-electron donor binding end-on to the metal. This gives an $M(CO)_5$ fragment that dimerizes to form an $M_2(CO)_{10}$ carbonyl with a metal-metal bond. The structure can be thought to be derived from an octahedral structure in which each metal is surrounded octahedrally by five CO ligands and an $M(CO)_5$ fragment acting as the sixth ligand. Each $M(CO)_5$ unit has one axial ligand and four equatorial ligands, whereby the axial ligand is co-directional with the metal-metal bond. The four equatorial ligands of the first metal are in staggered conformation relative to the four equatorial ligands of the second metal due to steric repulsion arguments.

Charged Isoelectronic Carbonyls of the Type $M_2(CO)_{10}$

Can we make charged isoelectronic carbonyls of the type $M_2(CO)_{10}$ with other metals? The answer is yes, but only carbonylate anions with low negative charge, and no carbonyl cations. The formation of carbonyl cations is prohibited because of the weakening of the π-acceptor interactions that result from the positive charge. High negative charges are not possible because too many negative charges on the metal atoms lead to electrostatic repulsion and the destabilization of the metal-metal bonds.

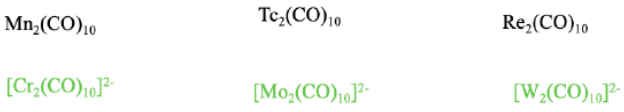


Figure **6.4.1.18**: Charged isoelectronic carbonyls of the type $M_2(CO)_{10}$

There are therefore only $Cr_2(CO)_{10}^{2-}$, and the higher homologues $Mo_2(CO)_{10}^{2-}$ and $W_2(CO)_{10}^{2-}$, but no other M_2CO_{10} type carbonyl ions.

Homoleptic carbonyls of the 9th group (M = Co, Rh, Ir)

What are the expected structures for the homoleptic carbonyls of group 9?

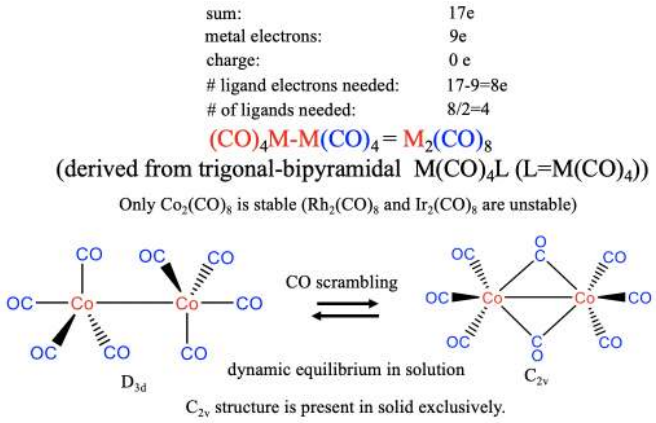


Figure **6.4.1.19**: Homoleptic carbonyls of the group 9 metals. Attribution: W. Petz.

In this case, the metal contributes 9 electrons, and this means that 17-9=8 electrons need to come from the carbonyl ligand. We therefore need 8/2=4 CO molecules to produce an $M(CO)_4$ 17 valence electron fragment. Two of the fragments then dimerize to form a dinuclear carbonyl of the composition M_2CO_8. In nature, however, only the Co-carbonyl is realized, the Rh and the Ir analogs are unstable. The structure of the $Co_2(CO)_8$ carbonyl can be derived from an $M(CO)_4L$ trigonal-pyramid, whereby L is the second $M(CO)_4$ unit (Fig. 10.2.19). According to that, the coordination number is 5. There are two axial and six equatorial ligands whereby the equatorial ligands are oriented in a staggered conformation. In solution this structure is in dynamic equilibrium with a second structure with C_{2v} symmetry in which two CO ligands are bridging. Due to this equilibrium there is constant ligand scrambling, meaning that the CO ligands constantly move from axial to equatorial positions, and migrate from one metal atom to the other. In solid state the C_{2v}-type structure is present exclusively indicating that it is slightly more stable.

Charged Isoelectronic Carbonyls of the Type $M_2(CO)_8$

The charged, isoelectronic carbonyls of the type $M_2(CO)_8$ behave similarly to that of the type $M_2(CO)_{10}$. There are no highly charged binuclear carbonylate anions, and no carbonyl cations.

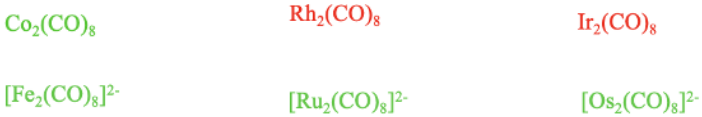


Figure **6.4.1.20**: Charged isoelectronic carbonyls of the type $M_2(CO)_8$ (green: stable carbonyl. red: unstable carbonyl)

There are only the weakly negatively charged $[Fe_2(CO)_8]^{2-}$, $[Ru_2(CO)_8]^{2-}$, and $[Os_2(CO)_8]^{2-}$. The weakly negative charge stabilizes the metal-carbon bond without destabilizing the metal-metal bond too much. We can further see from this that a weakly negative

charge is better for the stability of the species than no charge at all.

Homoleptic Carbonyls of the 11th Group (M = Cu, Ag, Au)

The group 11 metals Cu, Ag, and Au have eleven valence electrons.

sum:	17e
metal electrons:	11e
charge:	0 e
# ligand electrons needed:	17-11=6e
# of ligands needed:	6/2=3

$(CO)_3M\text{-}M(CO)_3 = M_2(CO)_6$
(derived from tetrahedral $M(CO)_3L$ ($L=M(CO)_3$))

$Cu_2(CO)_6$, $Ag_2(CO)_3$, and $Au_2(CO)_3$ are not known. but....

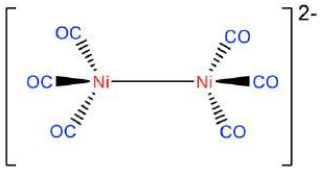


Figure **6.4.1.21**: Homoleptic carbonyls of the 11th group metals (Attribution: W. Petz)

Therefore, six ligand electrons are needed to achieve 17 electrons (Figure **6.4.1.21**). This means that 6/2=3 CO ligands are required to produce the 17 valence electron fragment. The dimer of it has the composition $M_2(CO)_6$ and its structure can be derived from a tetrahedral $M(CO)_3L$ structure in which L is the second $M(CO)_3$ fragment. Neither the Cu, nor the Ag, nor the Au carbonyl are known due to the weak π-overlap in tetrahedral coordination. However, the weakly negatively $[Ni_2(CO)_6]^{2-}$ ion is known which may be explained by the stabilizing effect of one negative charge on the M-C bond.

Overall Stability Trends

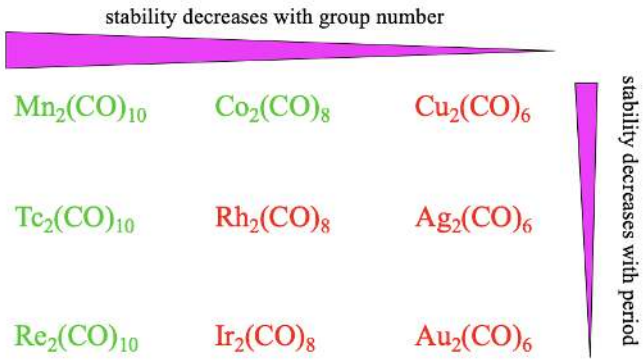


Figure **6.4.1.22**: Overall stability trends for dinuclear carbonyls. Green: stable. Red: Unstable.

Overall, we see the same stability trends for the dinuclear carbonyls as compared to the mononuclear ones. The stability decreases with the group number because π-overlap becomes smaller with smaller coordination numbers. Also, we see that the stability decreases with the period because of decreasing match of orbital sizes.

Homoleptic carbonyls of the 5th group (M = V, Nb, Ta)

The 17 valence electron fragment of the carbonyl of vanadium has the composition $V(CO)_6$. It does not dimerize because the coordination number of 6 is much more favorable compared to the coordination number 7. $V(CO)_6$ is a dark violet radical of octahedral shape. The radical electron is sterically inactive. $V(CO)_6$ can be used as an oxidant because it can be reduced easily to the 18 valence electron species $V(CO)_6^-$. The higher homologues $Nb(CO)_6$ and $Ta(CO)_6$ are not known. This may be explained by the weaker orbital overlap between the relatively small π^*-orbitals of the carbonyl ligand and the large metal d-orbitals of Nb and Ta.

Dr. Kai Landskron (Lehigh University). If you like this textbook, please consider to make a donation to support the author's research at Lehigh University: Click Here to Donate.

Synthesis

Metal carbonyl complexes containing only CO ligands abound, but most cannot be synthesized by the method we all wish worked, bathing the elemental metal in an atmosphere of carbon monoxide (entropy is a problem, as we already discussed for $W(CO)_6$). This method does work for nickel(0) and iron(0) carbonyls, however.

$M + n\ CO \rightarrow M(CO)_n$ [M = Fe, n = 5; M = Ni, n = 4]

Other metal carbonyl complexes can be prepared by **reductive carbonylation**, the treatment of a high-oxidation-state complex with CO. These methods usually require significant heat and pressure. One example:

$WCl_6 + CO + \text{heat, pressure} \rightarrow W(CO)_6$

Still other methods employ **deinsertion** from organic carbonyl compounds like dimethylformamide. These methods are particularly useful for preparing mixed carbonyl complexes in the presence of reducing ligands like phosphines.

$IrCl_3(H_2O)_3 + 3\ PPh_3 + HCONMe_2 + PhNH_2 \rightarrow IrCl(CO)(PPh_3)_2 + (Me_2NH_2)Cl + OPPh_3 + (PhNH_3)Cl + 2\ H_2O$

The key thing to notice about the reaction above is that the CO ligand is derived from dimethylformamide (DMF).

This page titled 6.4.1: Carbon Monoxide (Carbonyl Complexes) is shared under a CC BY-NC-SA 4.0 license and was authored, remixed, and/or curated by Kai Landskron.

- **10.2: Principles of carbonyl complexes** by Kai Landskron is licensed CC BY 4.0.
- **2.2: Carbon Monoxide** by Michael Evans has no license indicated.

6.4.2: Ligands similar to CO

Now let us leave the CO ligand, consider a number of related ligands, and discuss similarities and differences compared to the CO ligand.

The cyano ligand (CN^-)

Let us start with the cyano ligand CN^-. This ligand is isoelectronic to the CO ligand. The N atom has one electron less than O, but the negative charge at the cyanide ligand compensates for that. One question we can ask is: What is the reactive end? The answer is: In analogy to the carbonyl ligand the reactive end is the carbon atom. We can explain this by the fact that the MO diagram is similar to that of CO, only the differences in atomic orbital energies are smaller due to the smaller electronegativity difference between C and N compared to C and O. Therefore, like in CO, the HOMO is represented by the electron lone pair at the C, which makes C the more reactive end. Due to the smaller electronegativity difference, the difference in energy between the lone pair at C and the lone pair at N is smaller, therefore, in contrast to CO, the cyano ligand acts far more often as a bridging ligand between two metals using both of its electron lone pairs.

Would we expect the cyano ligand to be a stronger or weaker σ-donor compared to the CO ligand? Think about it for a moment. The answer is: It is a stronger σ-donor because of its negative charge. The negative charge at the ligand increases electrostatic repulsion between the electrons, and this increases the orbital energies. Therefore, there is a stronger tendency to donate the electrons. Our next question is: Is the CN^- ligand a stronger or weaker π-acceptor than CO? The energy of the π^*-orbitals is higher compared to CO because of the negative charge at the ligand. Because of that, electrons from the metal cannot be as easily accepted by the ligand. Therefore, the cyano ligand is a weaker π-acceptor than the carbonyl ligand. Our last question is: Are cyano complexes more stable with metals in high or low oxidation states. Because of electrostatic arguments a cyanide anion interacts more strongly with a metal cation rather than a metal in a zero or negative oxidation state. Therefore, unlike CO, CN^- does not stabilize metals in low oxidation states. It prefers to make complexes with metal in high, positive oxidation numbers.

The Nitrosyl Ligand NO

The nitrosyl ligand NO is another ligand similar to CO. It has one more electron that CO because N has one more electron than C. The additional electron makes NO an "odd" molecule with a radical electron. Like in CO and CN^-, the more electropositive element is the reactive end. In the case of NO it is the N atom. The radical electron is the most reactive electron that can be most easily donated, however the electron lone pair at N may be donated in addition. In the former case, the NO is a 1-electron donor, in the latter it is a 3-electron donor. How can we tell if one or three electrons have been donated? When only one electron is donated, the electron lone pair at the nitrogen is sterically active and leads to a bent structure (Fig. 6.4.2.1).

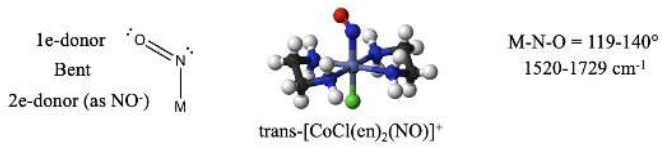


Figure 6.4.2.1: The Trans-bis-(ethylenediamine)chloronitrosyl cobalt (1+) cation as an example of an NO complex with NO as 1e donor.

An example is the trans-bis-(ethylenediamine)chloronitrosyl cobalt (1+) cation. Generally, the O–N–M bond angle in nitrosyl complexes with NO as a 1e-donor can vary between 119 and 140°. We can also identify a bent nitrosyl ligand in the IR spectrum. Typical wave numbers are 1520-1729 cm^{-1}.

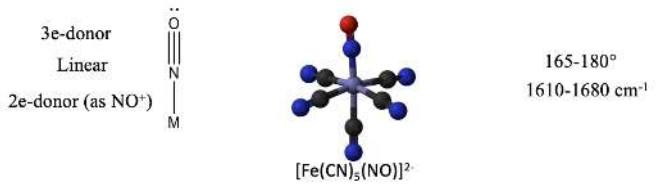


Figure 6.4.2.2: THe Nitroprusside anion as an example of a complex with NO as a 3e donor. (Attribution: Benjah-bmm27 / Public domain https://commons.wikimedia.org/wiki/F...l-3D-balls.png)

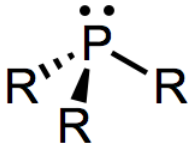
When the nitrosyl ligand donates all three electrons, then it binds to the metal in a linear fashion (Fig. **6.4.2.2**). The electron lone pair is no longer sterically active because it is involved in the bonding. An example is the nitroprusside anion $[Fe(CN)_5(NO)]^{2-}$. It is used as a medication for the treatment of high blood pressure. The bond angles in complexes with **NO** as the 3-electron donor are often not exactly 180°, but vary between 165 and 180°. It can also be identified in the IR because it has a characteristic band between 1610-1680 cm^{-1}.

There is a also a different view on nitrosyl complexes with linear and bent structures. In bent structures we can also consider the ligand as an NO^- anion that donates two electrons. The NO^- anion has two electron lone pairs at N. When it donates two electrons then one sterically active electron lone pair remains at the nitrogen atom. In linear structures we can regard the ligand also as an NO^+ cation that donates two electrons. An NO^+ cation has one electron lone pair at N, and when it donates that lone pair then there is no sterically active electron at the nitrogen left, and thus the ligand binds in a linear fashion.

We could also ask: What can neutral **NO** not be a 2-electron donor with the radical electron left at N? The answer is: The radical electron is the highest energy electron, and is always used first in interactions with a metal.

Phosphine Ligands

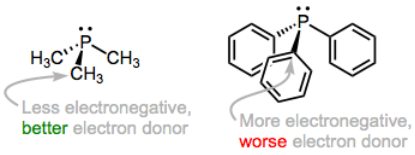
Phosphines are most notable for their remarkable electronic and steric tunability and their "innocence"—they tend to avoid participating directly in organometallic reactions, but have the ability to profoundly modulate the electronic properties of the metal center to which they're bound. Furthermore, because the energy barrier to umbrella flipping of phosphines is quite high, "chiral-at-phosphorus" ligands can be isolated in enantioenriched form and introduced to metal centers, bringing asymmetry just about as close to the metal as it can get in chiral complexes. Phosphorus NMR is a technique that Just Works (thanks, nature). Soft phosphines match up very well with the soft low-valent transition metals. Electron-poor phosphines are even good π-acids!



Like CO, phosphines are dative, L-type ligands that formally contribute two electrons to the metal center. Unlike CO, most phosphines are not small enough to form more than four bonds to a single metal center (and for large R, the number is even smaller). Steric hindrance becomes a problem when five or more PR_3 ligands try to make their way into the space around the metal. An interesting consequence of this fact is that many phosphine-containing complexes do not possess 18 valence electrons. Examples include $Pt(PCy_3)_2$, $Pd[P(t\text{-}Bu)_3]_2$, and $[Rh(PPh_3)_3]^+$. Doesn't that just drive you crazy? It drives the complexes crazy as well—and most of these coordinatively unsaturated compounds are wonderful catalysts.

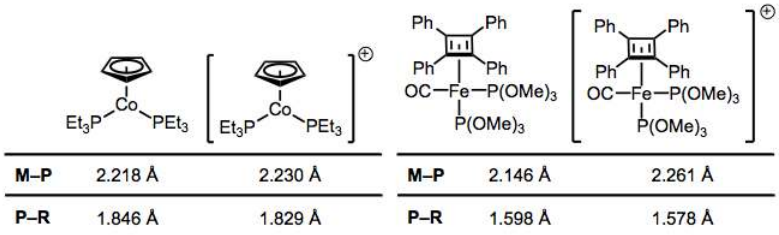
Bridging by phosphines is extremely rare, but ligands containing multiple phosphine donors that bind in an L_n ($n > 1$) fashion to a single metal center are all over the place. These ligands are called chelating or polydentate to indicate that they latch on to metal centers through multiple binding sites. For entropic reasons, chelating ligands bind to a single metal center at multiple points if possible, instead of attaching to two different metal centers (the aptly named chelate effect). An important characteristic of chelating phosphines is bite angle, defined as the predominant P–M–P angle in known complexes of the ligand. We'll get into the interesting effects of bite angle later, but for now, we might imagine how "unhappy" a ligand with a preferred bite angle of 120° would be in the square planar geometry. It would much rather prefer to be part of a trigonal bipyramidal complex, for instance.

The predominant orbital interaction contributing to phosphine binding is the one we expect, a lone pair on phosphorus interacting with an empty metallic d orbital. The electronic nature of the R groups influences the electron-donating ability of the phosphorus atom. For instance, alkylphosphines, which possess P–Csp^3 bonds, tend to be better electron donors than arylphosphines, which possess P–Csp^2 bonds. The rationale here is the greater electronegativity of the sp^2 hybrid orbital versus the sp3 hybrid, which causes the phosphorus atom to hold more tightly to its lone pair when bound to an sp^2 carbon. The same idea applies when electron-withdrawing and -donating groups are incorporated into R: the electron density on P is low when R contains electron-withdrawing groups and high when R contains electron-donating groups. Ligands (and associated metals) in the former class are called electron poor, while those in the latter class are electron rich.



As we add electronegative R groups, the phosphorus atom (and the metal to which it's bound) become more electron poor.

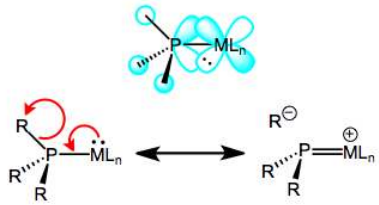
Like CO, phosphines participate in backbonding to a certain degree; however, the phenomenon here is of a fundamentally different nature than CO backbonding. For one thing, phosphines lack a π* orbital. In the days of yore, chemists attributed backbonding in phosphine complexes to an interaction between a metallic dπ orbital and an empty 3d orbital on phosphorus. However, this idea has elegantly been proven bogus, and a much more organicker-friendly explanation has taken its place (no d orbitals on P required!). In an illuminating series of experiments, M–P and P–R bond lengths were measured via crystallography for several redox pairs of complexes. I've chosen two illustrative examples, although the linked reference is chock full of other pairs. The question is: how do we explain the changes in bond length upon oxidation?



M–P	2.218 Å	2.230 Å	**M–P**	2.146 Å	2.261 Å
P–R	1.846 Å	1.829 Å	**P–R**	1.598 Å	1.578 Å

Upon oxidation, M–P bond lengths increase and and P–R bond lengths decrease. Why?

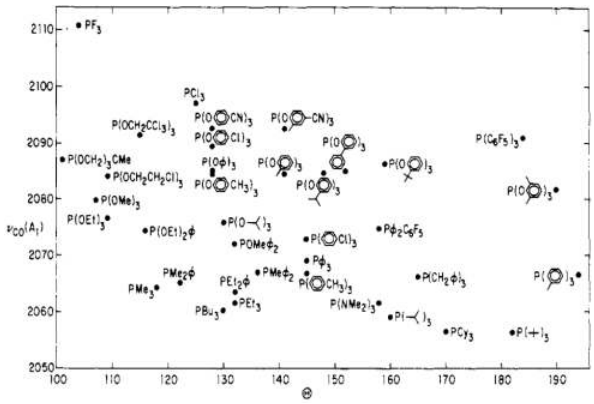
Oxidation decreases the ability of the metal to backbond, because it removes electron density from the metal. This explains the increases in M–P bond length—just imagine a decrease the M–P bond order due to worse backbonding. And the decrease in P–R bond length? It's important to see that invoking only the phosphorus 3d orbitals would not explain changes in the P–R bond lengths, as the 3d atomic orbitals are most definitely localized on phosphorus. Instead, we must invoke the participation of σ*P–R orbitals in phosphine backbonding to account for the P–R length decreases. When all is said and done, the LUMO of the free phosphine has mostly P–R antibonding character, with some 3d thrown into the mix. The figure below depicts one of the interactions involved in M–P backbonding, a dπ → σ* interaction (an orthogonal dπ → σ* interaction also plays a role). As with CO, a resonance structure depicting an M=P double bond is a useful heuristic! Naturally, R groups that are better able to stabilize negative charge—that is, electron-withdrawing groups—facilitate backbonding in phosphines. Electron-rich metals help too.



Backbonding in phosphines, a sigma-bond-breaking affair.

The steric and electronic properties of phosphines vary enormously. Tolman devised some intriguing parameters that characterize the steric and electronic properties of this class of ligands. To address sterics, he developed the idea of cone angle—the apex angle of a cone formed by a point 2.28 Å from the phosphorus atom (an idealized M–P bond length), and the outermost edges of atoms in the R groups, when the R groups are folded back as much as possible. Wider cone angles, Tolman reasoned, indicate greater steric congestion around the phosphorus atom. To address electronics, Tolman used a not-so-old friend of ours—the CO stretching frequency (νCO) of mixed phosphine-carbonyl complexes. Specifically, he used Ni(CO)3L complexes, where L is a tertiary phosphine, as his standard. Can you anticipate Tolman's logic? How should νCO change as the electron-donating ability of the phosphine ligands increases?

Tolman's logic went as follows: more strongly electron-donating phosphines are associated with more electron-rich metals, which are better at CO backbonding (due fundamentally to higher orbital energies). Better CO backbonding corresponds to a lower νCO due to decreased C–O bond order. Thus, better donor ligands should be associated with lower νCO values (and vice versa for electron-withdrawing ligands). Was he correct? Exhibit A…



Tolman's map of the steric and electronic properties of phosphine ligands.

Notice the poor ligand trifluorophosphine stuck in the "very small, very withdrawing" corner, and its utter opposite, the gargantuan tri(tert-butyl)phosphine in the "extremely bulky, very donating" corner. Intriguing! One can learn a great deal just by studying this chart.

Dr. Michael Evans (Georgia Tech)

Bonding in Phosphine Complexes

Let us have a look at the MO diagram of the $\mathbf{PH_3}$ molecule and compare it with the $\mathbf{NH_3}$ molecule. As one would expect, the MOs are overall similar, but there is one important difference. While the LUMO in $\mathbf{NH_3}$ is the anti-bonding $3a_1$ orbital, the LUMOs in the $\mathbf{PH_3}$ molecule are the anti-bonding 2e orbitals. The relative energies of the $3a_1$ and 2e orbitals in the $\mathbf{PH_3}$ and $\mathbf{NH_3}$ molecules are swapped up. This can be attributed to the fact that the the P atom uses the 3s and the 3p orbitals as valence orbitals, while N uses the 2s and 2p orbitals. The 3s and the 3p orbitals are larger and overlap less effectively with the small 1s orbitals of the hydrogen. They also have a higher energy making the P-H bonds less polar than the N-H bonds. The energy of the $\mathbf{PH_3}$ HOMO is higher than that of the $\mathbf{NH_3}$ HOMO. Both the HOMO and the LUMO of $\mathbf{PH_3}$ are more diffuse and polarizable than the respective orbitals in $\mathbf{NH_3}$.

The higher energy of the HOMO in $\mathbf{PH_3}$ makes it a better donor than $\mathbf{NH_3}$. In addition, the $\mathbf{PH_3}$ has π-acceptor properties because the 2e LUMO are relatively low-lying anti-bonding 2e orbitals and have suitable shape for π-overlap with metal d-orbitals. $\mathbf{NH_3}$ does not have these π-acceptor properties because its LUMO is the $3a_1$ orbital, and not the 2e orbitals. The 2e orbitals in $\mathbf{NH_3}$ are energetically too high in order to allow for significant π-acceptor interactions.

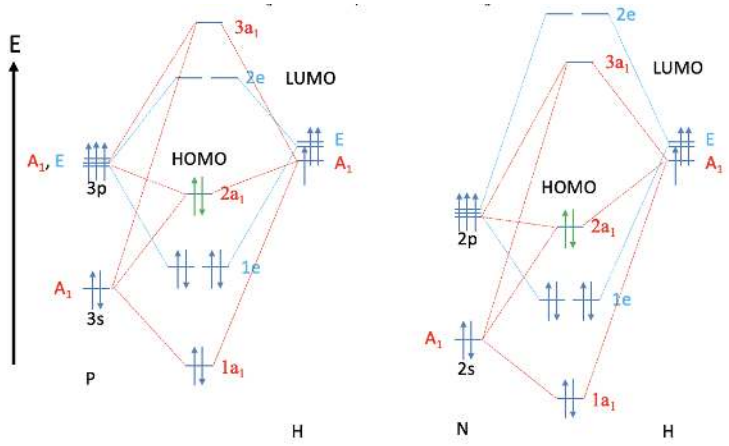


Figure 6.4.2.3: MO diagrams of $\mathbf{PH_3}$ and $\mathbf{NH_3}$

The σ-donor and π-acceptor properties of the phosphine ligand can be modified by substituting H by other groups. Generally, more electron donating groups increase the energy of the HOMO and the LUMO. This strengthens the σ-donor and reduces the π-acceptor properties. Vice versa, more electron withdrawing groups decrease the energy of the HOMO and the LUMO. As a consequence, the ligand becomes a weaker σ-donor and a stronger π-acceptor (Fig. **6.4.2.4**).

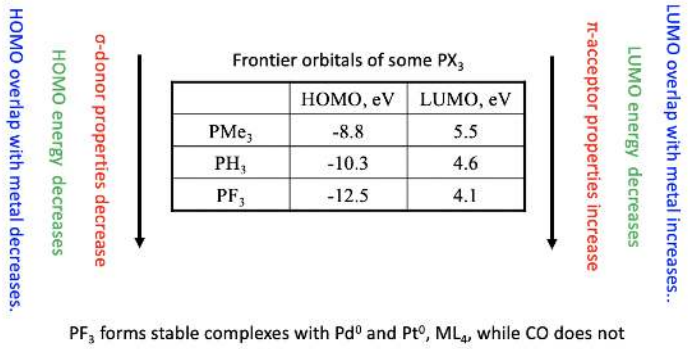


Figure **6.4.2.4**: HOMO and LUMO energies of three phosphines

The table above shows the HOMO and LUMO energies of three phosphines. As expected the HOMO and LUMO energies decrease from **PMe_3** to **PH_3** to **PF_3** due to the increasingly electron-withdrawing nature of the substituent. As a consequence, the σ-donor properties weaken and the π-acceptor properties strengthen from to **PMe_3** to **PH_3** to **PF_3**.

Not only the energies, but also the orbital overlap is important for the strength of the π-acceptor properties of the phosphine ligands. The more strongly electron-withdrawing the group is the more the anti-bonding e-type LUMO orbitals are located at the P atom. The more these orbitals are localized at P, the better they can overlap with the ligand. Vice versa the localization of the HOMO shifts toward the group as the group becomes more electron-withdrawing, thereby weakening the σ-donor properties.

Phosphine ligands with strongly electron withdrawing groups such as **PF_3** have π-acceptor properties strong enough to stabilize metals in low oxidation numbers, similar to **CO**. For example, the **PF_3** ligand forms stable complexes with Pd and Pt atoms in the oxidation number 0, while the respective Pd and Pt carbonyls are not known.

Dr. Kai Landskron (Lehigh University). If you like this textbook, please consider to make a donation to support the author's research at Lehigh University: Click Here to Donate.

6.4.2: Ligands similar to CO is shared under a CC BY-NC-SA 4.0 license and was authored, remixed, and/or curated by LibreTexts.

- **10.3: The Concept of Isolobality, Carbonyl Clusters, and Ligands Related to CO** by Kai Landskron is licensed CC BY 4.0.
- **2.9: Phosphines** by Michael Evans is licensed CC BY-NC-SA 4.0.

6.4.3: Hydrides and Dihydrogen Complexes

Ligands can, shockingly enough, bind through the electrons in their own σ bonds in an L-type fashion. This binding mode depends as much on the metal center as it does on the ligand itself—to see why, we need only recognize that σ complexes look like intermediates in concerted oxidative additions. With a slight reorganization of electrons and geometry, an L-type σ ligand can become two X-type ligands. Why, then, are σ complexes stable? How can we control the ratio of σ complex to X_2 complex in a given situation? How does complexation of a σ bond change the ligand's properties? We'll address these questions and more in this post.

General Properties

The first thing to realize about σ complexes is that they are highly sensitive to steric bulk. Any old σ bond won't do; hydrogen at one end of the binding bond or the other (or both) is necessary. The best studied σ complexes involve dihydrogen ($\mathbf{H_2}$), so let's start there.

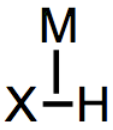


Figure **6.4.3.1**: A bonding interaction between a metal ion and the σ bond of a generic $\mathbf{X–H}$ ligand.

Mildly backbonding metals may bind dihydrogen "side on." Like side-on binding in π complexes, there are two important orbital interactions at play here: The first is a sigma bonding interaction ($\sigma\mathbf{H–H} \rightarrow \mathrm{d}\sigma$), as pictured on the left in Figure **6.4.3.2**; the second is a π bonding interaction ($\mathrm{d}\,\pi \rightarrow \sigma^*\mathbf{H–H}$), as pictured on the right in Figure **6.4.3.2**. Dihydrogen complexes can "tautomerize" to hydride $(\mathbf{H})_2$ isomers through cleavage of the $\mathbf{H–H}$ bond to the metal (this is an oxidative addition reaction, as discussed in the chapter on organometallic reactions).

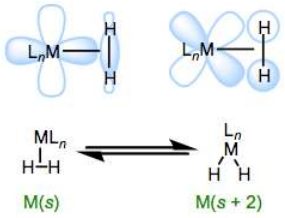


Figure **6.4.3.2**: Orbital interactions and $\mathbf{L–X_2}$ equilibrium in σ complexes.

$\mathbf{H_2}$ binding in an L-type fashion massively acidifies the ligand. Changes in of over thirty pKa units have been observed upon metal binding! Analogous acidifications of X–H bonds, rarely exhibit ΔpKa > 5. What's causing the different behavior of X–H and H–H ligands? The key is to consider the conjugate base of the ligand—in particular, how much it's stabilized by a metal center relative to the corresponding free anion. The principle here is analogous to the famous dictum of organic chemistry: consider charged species when making acid/base comparisons. Stabilization of the unhindered anion $\mathbf{H^-}$ by a metal is much greater than stabilization of larger, more electronegative anions like $\mathbf{HO^-}$ and $\mathbf{NH_2^-}$ by a metal. As a result, it's more favorable to remove a proton from metal-complexed $\mathbf{H_2}$ than from larger, more electronegative X–H ligands.

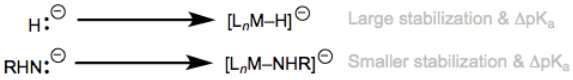


Figure **6.4.3.3**: When the conjugate base is stabilized, the pKa of the acid is decreased. The metal ion has a more important stabilizing effect on $\mathbf{H^-}$ compared to any other conjugate base ($\mathbf{X^-}$).

Remarkably large stabilization by an acidic metal fragment, without any counterbalancing from steric factors, explains the extreme acidification of dihydrogen upon metal binding.

The electronic nature of the metal center has two important effects on σ complexes. The first concerns the acidity of $\mathbf{H_2}$ upon metal binding. The principle here is consistent with what we've hammered into the ground so far. In the same way cationic organic acids are stronger than their neutral counterparts, σ complexes of electron-poor metals—including (and especially) cations—are stronger

acids than related complexes of electron-rich metals. The second concerns the ratio of L-type to X_2-type binding. We should expect more electron-rich metal centers to favor the X2 isomer, since these should donate more strongly into the σ*H–H orbital. This idea was masterfully demonstrated in a study by Morris, in which he showed that H_2 complexes of π-basic metal centers show all the signs of X2 complexes, rather than L complexes. More generally, metal centers in σ complexes need a good balance of π basicity and σ acidity (I like to call this the "Goldilocks effect"). Because of the need for balance, σ complexes are most common for centrally located metals (groups 6-9).

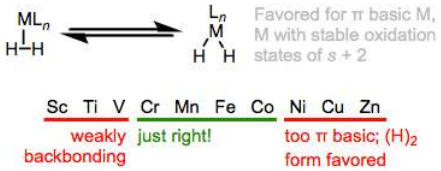


Figure **6.4.3.4**: Oxidative addition of H_2 is important for electron-rich, π-basic metal centers. Groups 6-9 hit the "Goldilocks" spot.

The M–H bond in hydride complexes is a good base—anyone who's ever quenched lithium aluminum hydride can attest to this! Intriguingly, because it's a good base, the M–H bond can participate in hydrogen bonding with an acidic X–H bond, where X is a heteroatom. This kind of bonding, called dihydrogen bonding (since two hydrogen atoms are involved), is best described as a sort of σM–H→σ*X–H orbital interaction. Think of it as analogous to a traditional hydrogen bond, but using a σ bond instead of a lone pair. Crazy, right?!

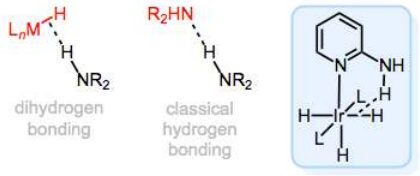


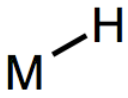
Figure **6.4.3.1**:

Dihydrogen bonding in metal hydrides: a sort of "interrupted protonation" of M–H.

Other kinds of σ complexes are known, but these are rarer than H–H complexes. One class that we've seen before involve agostic interactions of C–H bonds in alkyl ligands. σ Complexes of inorganic ligands like silanes and stannanes may involve complex bonding patterns, but we won't concern ourselves with those here.

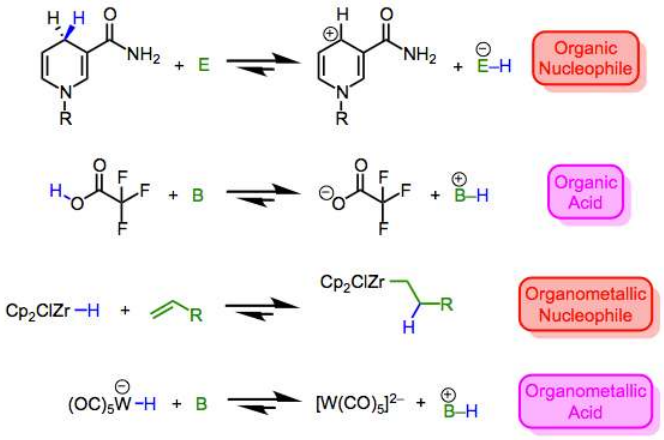
Hydride Complexes

Metal-hydrogen bonds, also known (misleadingly) as **metal hydrides**, are ubiquitous X-type ligands in organometallic chemistry. There is much more than meets the eye to most M-H bonds: although they're simple to draw, they vary enormously in polarization and pKa. They may be acidic or hydridic or both, depending on the nature of the metal center and the reaction conditions. In this post, we'll develop some heuristics for predicting the behavior of M-H bonds so that later, we can discuss their major modes of reactivity (acidity, radical reactions, migratory insertion, etc.).



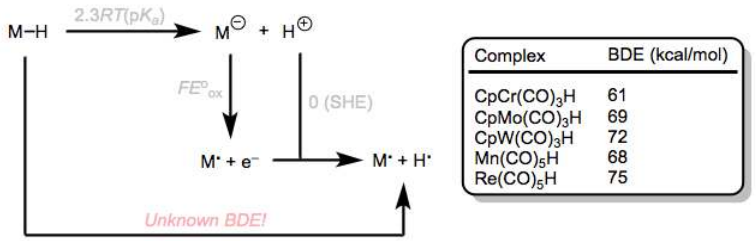
General Properties

Metal hydrides run the gamut from nucleophilic/basic to electrophilic/acidic. Then again, the same can be said of X–H bonds in organic chemistry, which may vary from mildly nucleophilic (consider Hantzsch esters and NADH) to extremely electrophilic (consider triflic acid). As hydrogen is what it is in both cases, it's clear that the nature of the X fragment—more specifically, the stability of the charged fragments X+ and X−—dictate the character of the X–H bond. Compare the four equilibria outlined below—the stabilities of the ions dictate the position of each equilibrium. By now we shouldn't find it surprising that the highly π-acidic W(CO)5 fragment is good at stabilizing negative charge; for a similar reason, the ZrCp2Cl fragment can stabilize positive charge.*



Metal-hydrogen bonds may be either hydridic (nucleophilic) or acidic (electrophilic). The nature of other ligands and the reaction conditions are keys to making predictions.

Let's turn our attention now to *homolytic* M–H bond strength. A convenient thermodynamic cycle allows us to use the acidity of M–H and the oxidation potential of its conjugate base in order to determine bond strength. This clever method, employed by Tilset and inspired by the inimitable Bordwell, uses the cycle in the figure below. BDE values for some complexes are provided as well. From the examples provided, we can see that bond strength increases down a group in the periodic table. This trend, and the idea that bridging hydrides have larger BDEs than terminal M–H bonds, are just about the only observable trends in M–H BDE.

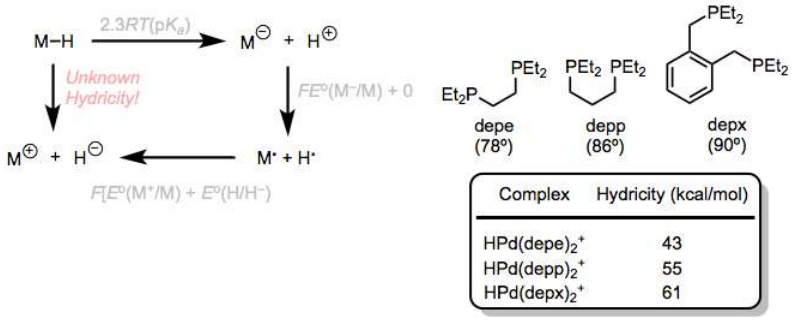


Complex	BDE (kcal/mol)
$CpCr(CO)_3H$	61
$CpMo(CO)_3H$	69
$CpW(CO)_3H$	72
$Mn(CO)_5H$	68
$Re(CO)_5H$	75

A clever cycle for determining BDEs from other known quantities, with select BDE values. I've left out solvation terms from the thermodynamic cycle. For more details, see the Tilset link above.

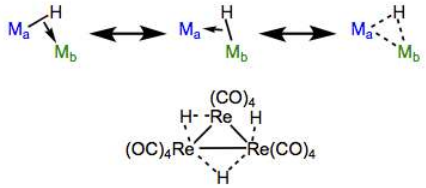
Why is knowing M-H BDEs useful? For one thing, the relative BDEs of M-C and M-H bonds determine the thermodynamics of β-hydride elimination, which results in the replacement of a covalent M-C bond with an M-H bond. Secondly, complexes containing weak M-H bonds are often good hydrogen transfer agents and may react with organic radicals and double bonds, channeling stannane and silane reductants from organic chemistry.

Hydricity refers to the tendency of a hydride ligand to depart as H–. A similar thermodynamic cycle relates the energetics of losing H– to the oxidation potentials of the conjugate base and the oxidized conjugate base; however, this method is complicated by the fact that hydride loss establishes an open coordination site. I've provided an abridged version of the cycle below. Hydricities are somewhat predictable from the electronic and steric properties of the metal center: inclusion of electron-donating ligands tends to increase hydricity, while electron-withdrawing or acidic ligands tend to decrease it. For five-coordinate hydrides that form 16-electron, square planar complexes upon loss of hydride, the bite angle of chelating phosphines plays an interesting role. As bite angle increases, hydricity does as well.



A thermodynamic cycle for hydricity, with some examples. Hydricity and bite angle are well correlated in five-coordinate palladium hydrides.

Bridging hydrides are an intriguing class of ligands. A question to ponder: how can a ligand associated with only two electrons possibly bridge two metal centers? How can two electrons hold three atoms together? Enter the magic of three-center, two-electron bonding. We can envision the M–H sigma bond as an electron donor itself! With this in mind, we can imagine that hydrides are able to bind end-on to one metal (like a standard X-type ligand) and side-on to another (like an L-type π system ligand, but using sigma electrons instead). Slick, no? We'll see more side-on bonding of sigma electrons in a future post on sigma complexes.



Resonance forms of bridging hydrides, with an example. Sigma complexes like these show up in other contexts, too!

Consistent with the idea that bridging is the result of "end-on + side-on" bonding, bond angles of bridging hydrides are never 180°.

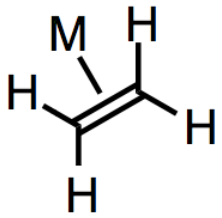
Dr. Michael Evans (Georgia Tech)

This page titled 6.4.3: Hydrides and Dihydrogen Complexes is shared under a CC BY-NC-SA 4.0 license and was authored, remixed, and/or curated by Michael Evans.

- **2.3: σ Complexes** by Michael Evans is licensed CC BY-NC-SA 4.0.
- **2.6: Metal Hydrides** by Michael Evans is licensed CC BY-NC-SA 4.0.

6.5: Bonding between Metal Atoms and Organic Pi Systems

With this section, we finally reach our first class of dative **actor** ligands, **π systems**. In contrast to the **spectator** L-type ligands we've seen so far, π systems most often play an important role in the reactivity of the OM complexes of which they are a part (since they act in reactions, they're called "actors"). π Systems do useful chemistry, not just with the metal center, but also with other ligands and external reagents. Thus, in addition to thinking about how π systems affect the steric and electronic properties of the metal center, we need to start considering the metal's effect on the ligand and how we might expect the ligand to behave as an active participant in reactions. To the extent that structure determines reactivity—a commonly repeated, and extremely powerful maxim in organic chemistry—we can think about possibilities for chemical change without knowing the elementary steps of organometallic chemistry in detail yet.



This page titled 6.5: Bonding between Metal Atoms and Organic Pi Systems is shared under a CC BY-NC-SA 4.0 license and was authored, remixed, and/or curated by Kathryn Haas.

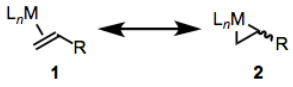
- **2.10: π Systems** by Michael Evans is licensed CC BY-NC-SA 4.0.

6.5.1: Linear π Systems

General Properties

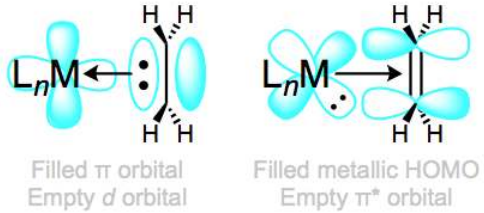
The π bonding orbitals of alkenes, alkynes, carbonyls, and other unsaturated compounds may overlap with dσ orbitals on metal centers. This is the classic ligand HOMO → metal LUMO interaction that we've beaten into the ground over the last few posts. Because of this electron donation from the π system to the metal center, coordinated π systems often act electrophilic, even if the starting alkene was nucleophilic (the **Wacker oxidation** is a classic example; water attacks a palladium-coordinated alkene). The π → dσ orbital interaction is central to the structure and reactivity of π-system complexes.

Then again, a theme of the last three posts has been the importance of orbital interactions with the opposite sense: metal HOMO → ligand LUMO. Like CO, phosphines, and NHCs, π systems are often subject to important backbonding interactions. We'll focus on alkenes here, but these same ideas apply to carbonyls, alkynes, and other unsaturated ligands bound through their π clouds. For alkene ligands, the relative importance of "normal" bonding and backbonding is nicely captured by the relative importance of the two resonance structures in the figure below.



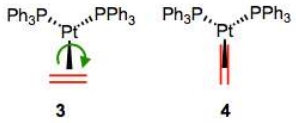
Resonance forms of alkene ligands.

Complexes of weakly backbonding metals, such as the electronegative late metals, are best represented by the traditional dative resonance structure **1**. But complexes of strong backbonders, such as electropositive Ti(II), are often best drawn in the **metallacyclopropane** form **2**. Organic hardliners may have a tough time believing that **1** and **2** are truly resonance forms, but several studies—e.g. of the Kulinkovich cyclopropanation—have shown that independent synthetic routes to metallacyclopropanes and alkene complexes containing the same atoms result in the same compound. Furthermore, bond lengths and angles in the alkene change substantially upon coordination to a strongly backbonding metal. We see an elongation of the C=C bond (consistent with decreased bond order) and some pyramidalization of the alkene carbons (consistent with a change in hybridization from sp2 to sp3). A complete orbital picture of "normal" bonding and backbonding in alkenes is shown in the figure below.



Normal bonding and backbonding in alkene complexes.

Here's an interesting question with stereochemical implications: what is the orientation of the alkene relative to the other ligands? From what we've discussed so far, we can surmise that one face of the alkene must point toward the metal center. Put differently, the bonding axis must be normal to the plane of the alkene. However, this restriction says nothing about rotation about the bonding axis, which spins the alkene ligand like a pinwheel. Is a particular orientation preferred, or can we think about the alkene as a circular smudge over time? The figure below depicts two possible orientations of the alkene ligand in a trigonal planar complex. Other orientations make less sense because they would involve inefficient orbital overlap with the metal's orthogonal d orbitals. Which one is favored?



Two limiting cases for alkene orientation in a trigonal planar complex.

First of all, we need to notice that these two complexes are **diastereomeric**. They have different energies as a result, so one must be favored over the other. Naive steric considerations suggest that complex **4** ought to be more stable (in most complexes, steric factors dictate alkene orientation). To dig a little deeper, let's consider any electronic factors that may influence the preferred geometry. We've already seen that electronic factors can overcome steric considerations when it comes to complex geometry! To begin, we need to consider the crystal field orbitals of the complex as a whole. Verify on your own that in this d10, Pt(0) complex, the crystal-field HOMOs are the dxy and dx2–y2 orbitals. Where are these orbitals located in space? In the xy-plane! Only the alkene in **3** can engage in efficient backbonding with the metal center. In cases when the metal is electron rich and/or the alkene is electron poor, complexes like **3** can sometimes be favored in spite of sterics. The thought process here is very similar to the one developed in an earlier post on geometry. However, please note that this situation is fairly rare—steric considerations often either match or dominate electronics where alkenes are concerned.

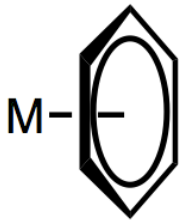
Dr. Michael Evans (Georgia Tech)

This page titled 6.5.1: Linear π Systems is shared under a CC BY-NC-SA 4.0 license and was authored, remixed, and/or curated by Kathryn Haas.

- **2.10: π Systems** by Michael Evans is licensed CC BY-NC-SA 4.0.

6.5.2: Cyclic π systems

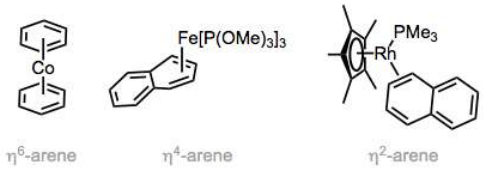
Arene or **aromatic ligands** are the subject of this post, the second in our series on π-system ligands. Arenes are dative, L-type ligands that may serve either as actors or spectators. Arenes commonly bind to metals through more than two atoms, although η2-arene ligands are known. Structurally, most η6-arenes tend to remain planar after binding to metals. Both "normal" bonding and backbonding are possible for arene ligands; however, arenes are stronger electron donors than CO and backbonding is less important for these ligands. The reactivity of arenes changes dramatically upon metal binding, along lines that we would expect for strongly electron-donating ligands. After coordinating to a transition metal, the arene usually becomes a better electrophile (particularly when the metal is electron poor). Thus, metal coordination can enable otherwise difficult **nucleophilic aromatic substitution** reactions.



General Properties

The coordination of an aromatic compound to a metal center through its aromatic π MOs removes electron density from the ring. I'm going to forego an in-depth orbital analysis in this post, because it's honestly not very useful (and overly complex) for arene ligands. π → dσ (normal bonding) and dπ → π* (backbonding) orbital interactions are possible for arene ligands, with the former being much more important, typically. To simplify drawings, you often see chemists draw "toilet-bowl" arenes involving a circle and single central line to represent the π → dσ orbital interaction. Despite the single line, it is often useful to think about arenes as L3-type ligands. For instance, we think of η6-arenes as six-electron donors.

Multiple coordination modes are possible for arene ligands. When all six atoms of a benzene ring are bound to the metal (η6-mode), the ring is flat and C–C bond lengths are slightly longer than those in the free arene. The ring is bent and non-aromatic in η4-mode, so that the four atoms bound to the metal are coplanar while the other π bond is out of the plane. η4-Arene ligands show up in both stable complexes (see the figure below) and reactive intermediates that possess an open coordination site. To generate the latter, the corresponding η6-arene ligand undergoes **ring slippage**—one of the π bonds "slips" off of the metal to create an open coordination site. We'll see ring slippage again in discussions of the aromatic cyclopentadienyl and indenyl ligands.



Arene ligands exhibit multiple coordination modes.

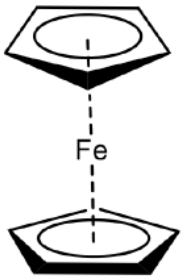
Even η2-arene ligands bound through one double bond are known. Coordination of one π bond results in **dearomatization** and makes η2-benzene behave more like butadiene, and furan act more like a vinyl ether. With naphthalene as ligand, there are multiple η2 isomers that could form; the isomer observed is the one that retains aromaticity in the free portion of the ligand. In fact, this result is general for polycyclic aromatic hydrocarbons: binding maximizes aromaticity in the free portion of the ligand. In the linked reference, the authors even observed the coordination of two different rhodium centers to naphthalene—a bridging arene ligand! Other bridging modes include σ, π-binding (the arene is an LX-type ligand, and one C–M bond is covalent, not dative) and L2-type bridging through two distinct π systems (as in biphenyl).

Arene ligands are usually hydrocarbons, not heterocycles. Why? Aromatic heterocycles, such as pyridine, more commonly bind using their basic lone pairs. That said, a few heterocycles form important π complexes. Thiophene is perhaps the most heavily studied, as the desulfurization of thiophene from fossil fuels is an industrially useful process.

Dr. Michael Evans (Georgia Tech)

Bonding in Ferrocene

Ferrocene was the first metallocene to be discovered and characterized. The structure of ferrocene is shown below.



Ferrocene

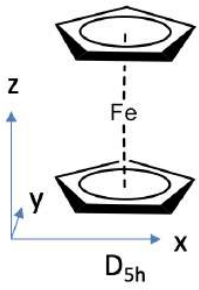
Figure **6.5.2.9**: The sandwich structure of ferrocene

Can the stability of the ferrocene structure also be explained by molecular orbital theory? Let us check! First, we need to decide on the point group. We will make the simplification that the two C_p cyclopentadienyl rings are in eclipsed formation, and then the point group is D_{5h}. Actually, the rings are in staggered confirmation and the point group is D_{5d}, but the energy difference is minimal, and there is a very small activation barrier between the two conformers.

$\mathbf{D_{5h}}$	E	$2C_5$	$2C_5^2$	$5C_2$	σ_h	$2S_5$	$2S_5^2$	$5\sigma_h$	$h = 20$	
A_1'	1	1	1	1	1	1	1	1		x^2+y^2, z^2
A_2'	1	1	1	−1	1	1	1	−1	R_z	
E_1'	2	$2cos(72°)$	$2cos(144°)$	0	2	$2cos(72°)$	$2cos(144°)$	0	$(x,\ y)$	
E_2'	2	$2cos(144°)$	$2cos(72°)$	0	2	$2cos(144°)$	$2cos(72°)$	0		$(x^2-y^2,\ xy)$
A_1''	1	1	1	1	−1	−1	−1	−1		
A_2''	1	1	1	−1	−1	−1	−1	1	z	
E_1''	2	$2cos(72°)$	$2cos(144°)$	0	−2	$-2cos(72°)$	$-2cos(144°)$	0	$(R_x,\ R_y)$	$(xz,\ yz)$
E_2''	2	$2cos(144°)$	$2cos(72°)$	0	−2	$-2cos(144°)$	$-2cos(72°)$	0		

(6.5.2.1)

We can define the z-axis standing perpendicular to the Cp rings, and the xy plane to be coplanar with the Cp rings.



$3d_{yz}$, $3d_{xz}$	E_1''
$3d_{x2-y2}$, $3d_{xy}$	E_2'
$3d_{z2}$	A_1'
4s	A_1'
$4p_x$, $4p_y$	E_1'
$4p_z$	A_2''

Figure **6.5.2.18**: The coordinate system for ferrocene, Fe valence orbitals, and their symmetry types.

The Fe 3d, 4s and 4p orbitals will be our frontier orbitals and we can read their symmetry types from the character table of D_{5h}. The $3d_{xz}$ and $3d_{yz}$ have E_1'' symmetry, the $3d_{x^2-y^2}$ and the $3d_{xy}$ have E_2' symmetry, the $3d_{z^2}$ has A_1' symmetry, the 4s has A_1' symmetry, and the $4p_x$ and the $4p_y$ orbitals have E_1' symmetry, and the $4p_z$ has A_2'' symmetry.

Next, we need to determine the ligand group orbitals. We know that the π-ligand molecular orbitals are the ones that donate the electrons into the metal-orbitals, thus we have to have a closer look at these orbitals. The π-MOs of the ligand are made from the

five $2p_z$ orbitals of the carbon atoms that stand perpendicular to the ring. This means that there are 5 MOs to consider.

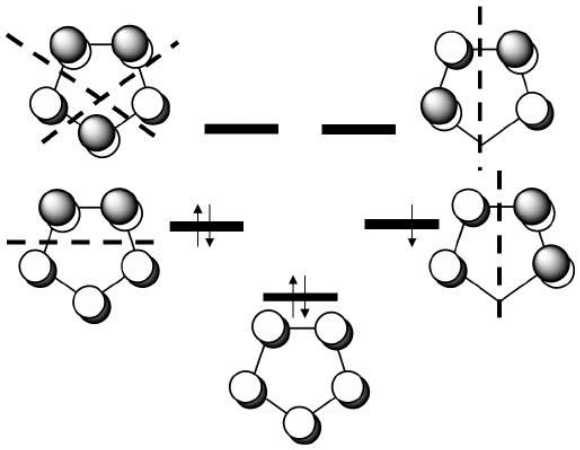


Figure **6.5.2.19**: MOs of the cyclopentadienyl ligand and their relative energy

You can see the five MOs and their relative energy above. One is strongly bonding and has no node. Then, there are two double-generate weakly bonding ones that have one node, and finally there are two anti-bonding ones that have two nodes. Because the cyclopentadienyl anion has six π electrons, the bonding MO and the two weakly bonding MOs are full, the anti-bonding MOs are empty.

Because we have two Cp^- anions to consider we have overall 10 MOs to combine. We would therefore expect ten ligand group orbitals (LGOs). We can determine their symmetry type by determining the reducible and irreducible representations. The results are shown below.

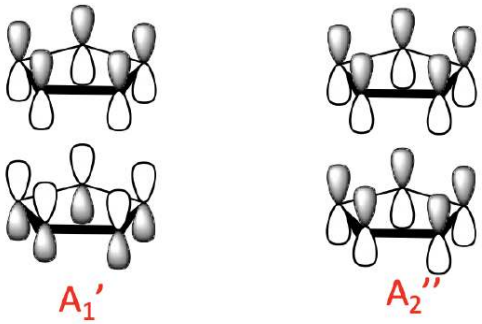


Figure **6.5.2.20**: 0-node LGOs

We can generally divide the LGOs into three groups with a different number of nodes. There are two 0-node LGOs with A_1' and A_2'' symmetry. They are made from the 0-node MOs of the ligand. There is a bonding an anti-bonding combination possible. In the bonding combination the 0–node ligand MOs have the lobes with the same algebraic sign pointing toward each other. The anti-bonding combination has the lobes with opposite algebraic sign pointing toward each other.

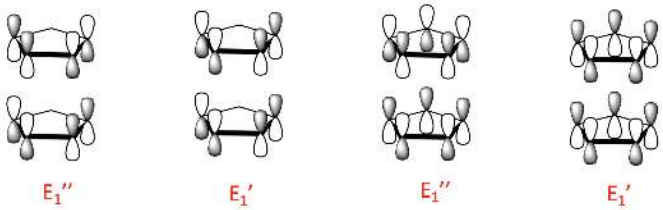


Figure **6.5.2.21**: 1-node LGOs

There are four 1-node LGOs with E_1' and E_1'' symmetry. They are constructed from the two 1-node ligand MOs. Like for the 0-node orbitals, there is a bonding and an anti-bonding combination possible.

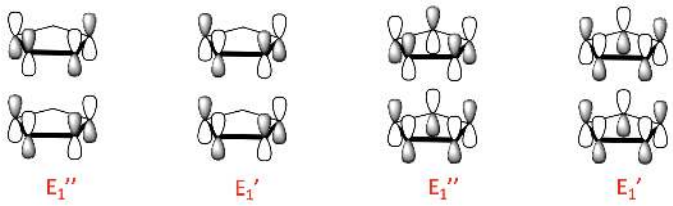


Figure **6.5.2.22**: 2-node LGOs

Finally, there are four 2-node LGOs with E_2' and E_2'' symmetry. They are made from the 2-node ligand MOs and there is also a bonding and an anti-bonding combination possible.

The Molecular Orbital Diagram of Ferrocene

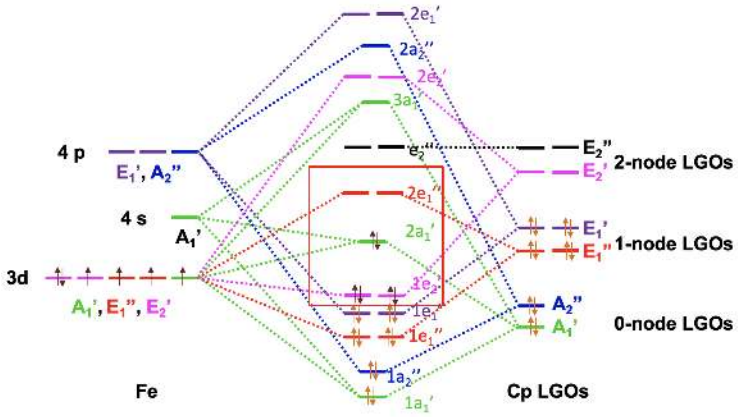


Figure **6.5.2.23**: MO diagram of ferrocene

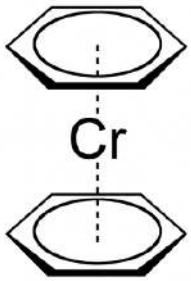
Now we have all the information to draw the molecular orbital diagram of ferrocene. As usual we plot the metal frontier orbitals on the left and label their symmetry. We plot the Cp LGOs on the right and also label the symmetry. We can order the LGOs according to energy with the 0-node LGOs having the lowest energy and the 2-node LGOs having the highest energy. Then, we can start to combine orbitals of the same symmetry type to form MOs. There are two metal AOs of the A_1' type and one A_1' LGO giving three MOs of this symmetry type, one bonding, one approximately non-bonding, and third one anti-bonding. We can connect AOs, LGOs, and MOs with dotted lines. Next, we can combine the A_2'' AO and the A_2'' LGO to form a bonding and an anti-bonding MO. We again connect the AOs, LGOs, and MOs with dotted lines. Then, we can produce two bonding e_1'' and two anti-bonding e_1'' MOs from the E_1'' metal AOs and the E_1'' LGOs and connect the orbitals with dotted lines. There are two E_1' LGOs and two E_1' AOs that can be combined to two bonding $1e_1$' and two anti-bonding $2e_1$' MOs and we again connect the orbitals with dotted lines. The two E_2' LGOs can be combined with the two E_2' d-orbitals to form a pair of bonding $1e_2$' and anti-bonding $2e_2$' molecular orbitals. Lastly, we notice that the E_2'' LGOs do not find a partner, and we have to write them as non-bonding with the same energy into the MO diagram.

Now we need to fill the electrons into the orbitals. The ligands have twelve electrons overall. They can be filled into the six orbitals of the lowest energy. This fills the $1a_1$', the $1a_2$'', the $1e_1$'', the and $1e_1$' orbitals. We notice that all MOs are bonding which supports the stability of the molecule. We still need to consider the metal d-orbitals. We have an Fe^{2+} ion and thus six metal d-electrons. They would go into the $1e_2$' orbital which is bonding and the $2a_1$' orbital which is weakly bonding. The $2a_1$ is the HOMO, and the next higher $2e_1$'' is the LUMO. We can see that we can fill all metal electrons into bonding MOs. The LUMO is an anti-bonding orbital, and thus overall all bonding MOs are filled, and no non-bonding and anti-bonding orbitals need to be filled. This is the ideal situation for a stable molecule. We can also see that the MO diagram explains the 18 electron rule. All 18 electrons are in bonding MOs.

We can consider the $1e_2$', the $2a_1$', and the $2e_1$'' metal d-orbitals in the ligand field produced by the Cp-ligands as these 5 orbitals can hold the maximum possible number of 10 d-electrons, have similar energy then the d-orbitals, and have contributions from them.

Metallocenes with other cyclic π-ligands

Is it possible to make metallocenes with other π-conjugated rings but the cylopentadienyl anion?



Bis-(benzene) chromium (0)

Figure **6.5.2.24**: Bis-(benzene) chromium

The answer is yes, for instance benzene is known to act as a ligand bis-(benzene) chromium (0). In this case the ligand acts as a η^6-ligand because all six carbon atoms are involved in the bonding. Why does chromium give stable metallocene complex with benzene? We can explain this again with the 18 electron rule. In bis-(benzene) chromium (0), chromium is in the oxidation state 0 because the benzene ligand has no charge. Thus, chromium contributes six electrons. Adding the 12 π-electrons from the two benzene ligands gives 18 electrons.

Other cyclic π-ligands

Also cyclobutadiene can act as a cylic π-ligand in complexes. The cyclobutadiene is is different from the cyclopentadienyl anion and the benzene ligand in two ways. Firstly, it has much more ring strain then the previous two, and secondly it is not an aromatic, but an anti-aromatic ligand. Remember, we have an aromatic ring when there are 4n+2 π-electrons, whereby n is an inter number. This means that rings with two (n=0), six (n=1), and ten (n=2) π-electrons are aromatic. Anti-aromatic rings are those that have 4n electrons, such as four (n=1), eight (n=2) and so forth. Cyclobutadiene has four electrons, and thus it is anti-aromatic. Anti-aromatic rings are less stable than aromatic ones because not all π-electrons are in bonding molecular orbitals. Let us illustrate this by constructing the MO diagram for the π-system of the cyclobutadiene molecule (Figure **6.5.2.25**)

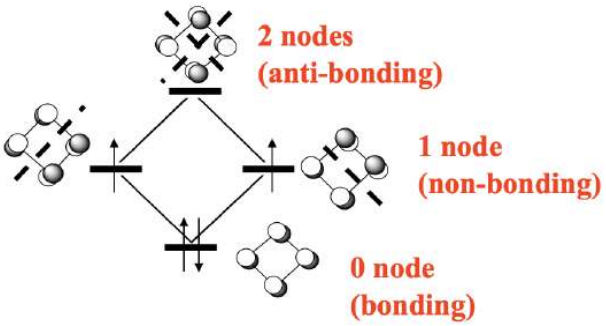


Figure **6.5.2.25**: MO diagram for the π-system of the cyclobutadiene molecule

The π-system is made of four carbon atoms contributing a half-filled $2p_z$ orbital each (if we define the plane of the molecule as the xy plane). That makes four p-orbitals with four electrons that give four molecular orbitals. There is a bonding MO with no node, two doubly-degenerate non-bonding ones with one node, and one anti-bonding one with two nodes (Figure **6.5.2.25**). There are four electrons. We can fill two electrons into the bonding MO, but the other two must go into the two non-bonding ones under obedience of Hund's rule.

Jahn-Teller distortion in cyclobutadiene

One may think that the cyclobutadiene is a square planar molecule because of complete delocalization of the π-electrons, but that is actually not the case. There are two shorter double-bonds and two longer single-bonds, and the shape of the molecules is a rectangle. This means that the two double bond are localized. We can view this effect as a Jahn-Teller distortion.

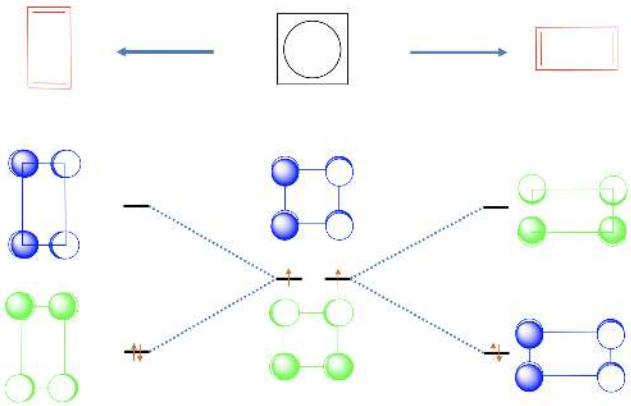


Figure 6.5.2.26: Jahn-Teller distortion in cyclobutadiene

The distortion of the square to form a rectangle is energetically favorable because it lowers the energy of the two non-bonding electrons. Why? Let us look at the non-bonding orbital 1 first and elongate in x-direction, and squeeze in y-direction (Figure 6.5.2.26). We can see that we bring the p-orbitals with bonding interactions further apart, and bring those with anti-bonding interactions closer together. This means that the energy of this orbital goes up and the orbital becomes anti-bonding. Let us do the same with non-bonding orbital 2. We see that the opposite happens. The bonding interactions are enhanced and the anti-bonding interactions are weakened. Therefore, this orbital becomes bonding and the energy goes down. We can now fill the two electrons into the bonding MO. We see that we have lowered the energy of the electrons through the distortion.

We could also have squeezed in x-direction and elongated in y-direction. In this case orbital 1 would have become bonding and orbital 2 anti-bonding. However, this distortion is symmetry-equivalent to the previous one, and does not produce a new molecule. Both molecules can be superposed by a simple 90° rotation.

Cyclobutadiene as η^4-ligand

Cyclobutadiene (Cb) in its free form is not stable because of the high ring strain and the anti-aromaticity, but complexes with cyclobutadiene as a ligand are stable. We would expect that 18 electron complexes are most stable.

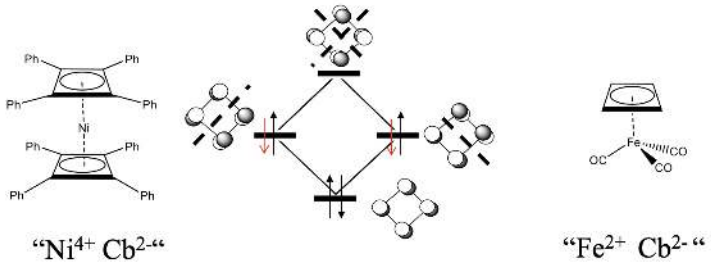
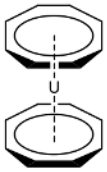


Figure 6.5.2.27: Complexes with cyclobutadiene

What would be an 18 electron sandwich complex with two cyclobutadiene ligands? Because each cyclobutadiene contributes four electrons, ten electrons would need to come from the metal, and we would expect a nickel cyclobutadienyl complex $Ni(Cb)_2$. This complex is not known, but derivatives are. For example a Ni complex with two tetraphenyl butadiene ligands are known (Figure 6.5.2.27). Another example is the butadienyl tricarbonyl iron (0) complex. Interestingly, when cyclobutadiene acts as a η^4-ligand, then it is not distorted, but square planar. An explanation is that we can formally treat the cyclobutadiene ligand as an Cb^{2-} ligand binding to a metal cation. For instance in $FeCb(CO)_3$ the Fe would be an Fe^{2+}, in the nickel complex, the nickel would be a Ni^{4+}. The Cb^{2-} anion would formally aromatic because it has 4n+2=6 electrons. The additional two electrons would be in the non-bonding orbitals. Because the two non-bonding orbitals are completely filled now, there would be no longer a driving force for the distortion. Note though that is is a formal view only, and there are arguments that speak against this view. One is that the addition of the two electrons to the ligand should further destabilize the ring because the added electrons are non-bonding. Aromaticity would rather be achieved by removing two electrons to form a Cb^{2+} cation that would have only two electrons in the bonding orbital.

Cyclooctetraene (cot) as a ligand

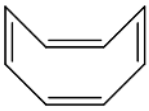
Also metallocenes with cyclooctatetraene (cot) acting as η^8-ligand is known. However, because of the large ring size only metals with large atomic radii, can make metallocenes with this ligand. For example uranium makes a uranocenes with two cyclooctatetraene ligands (Figure **6.5.2.28**).



planar, formally aromatic (cot^{2-})

Figure **6.5.2.28**: Aromatic Cot^{2-} ligand

Like cyclobutadiene, cyclooctatetraene is an anti-aromatic ligand with 4n=8 π-electrons (n=2). In the free cyclooctatetraene molecule is non-planar and the π-electrons are localized (Figure **6.5.2.29**).



non-planar, antiaromatic

Figure **6.5.2.29**: Free cyclooctatraene is non-planar, thus π electrons are localized.

In metallocenes however, the ring becomes planar (Figure **6.5.2.28**). One can again formally explain that by assuming an aromatic cot^{2-} ligand that binds to a metal 2+ cation, however one should keep in mind again that this is a formal view and not necessarily reflects the bonding situation in the compound.

Metals having smaller atomic radius can bind to *cot* in η^2, η^4, and less commonly in η^6-mode. The 18 electron rule holds in most cases. For instance, *cot* can make a η^4-complex in tricarbonyl cyclooctatetraene ruthenium (0) (Figure **6.5.2.30**).

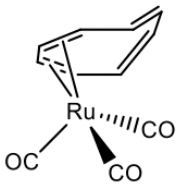


Figure **6.5.2.30**: tricarbonyl cyclooctatetraene ruthenium (0)

Also two metals can bind to a single *cot*-ligand. This is for instance realize in μ-cyclooctetraene bis(tricarbonyl ruthenium (0) (Figure **6.5.2.31**).

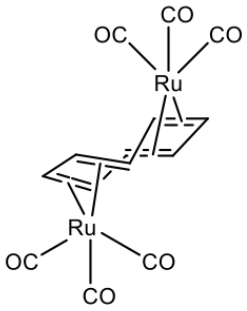


Figure **6.5.2.31**: bis(tricarbonyl) cyclooctetraene ruthenium (0)

Dr. Kai Landskron (Lehigh University). If you like this textbook, please consider to make a donation to support the author's research at Lehigh University: Click Here to Donate.

6.5.2: Cyclic π systems is shared under a CC BY-NC-SA 4.0 license and was authored, remixed, and/or curated by LibreTexts.

- **2.10: π Systems** by Michael Evans is licensed CC BY-NC-SA 4.0.
- **10.1: Historical Background and Introduction into Metallocenes** by Kai Landskron is licensed CC BY 4.0.

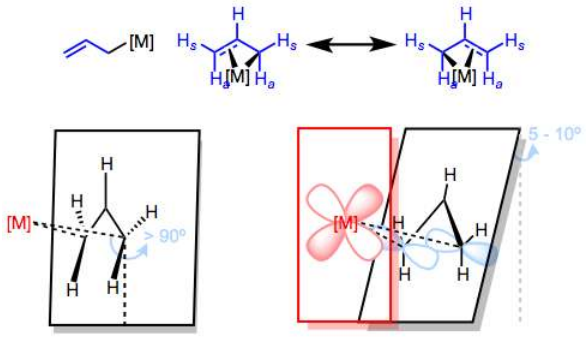
6.5.3: Odd-numbered π Systems

Odd-numbered π systems—most notably, the allyl and cyclopentadienyl ligands—are formally LnX-type ligands bound covalently through one atom (the “odd man out”) and datively through the others. This formal description is incomplete, however, as resonance structures reveal that multiple atoms within three- and five-atom π systems can be considered as covalently bound to the metal. To illustrate the plurality of equally important resonance structures for this class of ligands, we often just draw a curved line from one end of the π system to the other. Yet, even this form is not perfect, as it obscures the possibility that the datively bound atoms may dissociate from the metal center, forming σ-allyl or ring-slipped ligands. What do the odd-numbered π systems really look like, and how do they really behave?



General Properties

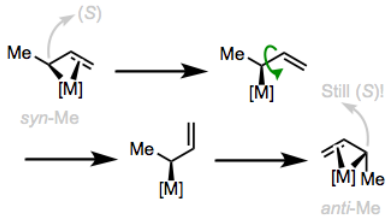
Allyls are often actor ligands, most famously in allylic substitution reactions. The allyl ligand is an interesting beast because it may bind to metals in two ways. When its double bond does not become involved in binding to the metal, allyl is a simple X-type ligand bound covalently through one carbon—basically, a monodentate alkyl! Alternatively, allyl can act as a bidentate LX-type ligand, bound to the metal through all three conjugated atoms. The LX or “trihapto” form can be represented using one of two resonance forms, or (more common) the “toilet-bowl” form seen in the general figure above. I don’t like the toilet-bowl form despite its ubiquity, as it tends to obscure the important dynamic possibilities of the allyl ligand.



Can we use FMO theory to explain the wonky geometry of the allyl ligand?

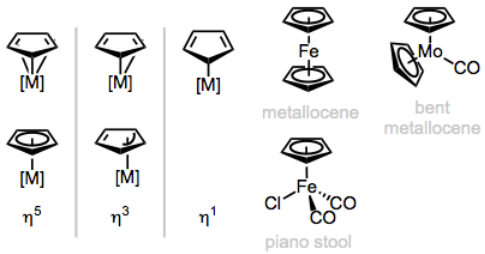
The lower half of the figure above illustrates the slightly weird character of the geometry of allyl ligands. In a previous post on even-numbered π systems, we investigated the orientation of the ligand with respect to the metal and came to some logical conclusions by invoking FMO theory and backbonding. A similar treatment of the allyl ligand leads us to similar conclusions: the plane of the allyl ligand should be parallel to the xy-plane of the metal center and normal to the z-axis. In reality, the allyl plane is slightly canted to optimize orbital overlap—but we can see at the right of the figure above that π2–dxy orbital overlap is key. Also note the rotation of the anti hydrogens (anti to the central C–H, that is) toward the metal center to improve orbital overlap.

Exchange of the syn and anti substituents can occur through σ,π-isomerization followed by bond rotation and formation of the isomerized trihapto form. Notice that the configuration of the stereocenter bearing the methyl group is unaffected by the isomerization! It should be noted that 1,3-disubstituted allyl complexes almost exclusively adopt a syn,syn configuration without danger of isomerization.



The methylene and central C–H simply change places!

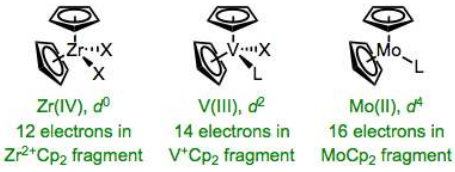
Upon deconstruction, the cyclopentadienyl (Cp) ligand yields the aromatic cyclopentadienyl anion, an L2X-type ligand. Cp is normally an η5-ligand, but η3 (LX) and η1 (X) forms are known in cases where the other ligands on the metal center are tightly bound. η1-Cyclopentadienyl ligands can sometimes be fluxional—the metal has the ability to "jump" from atom to atom. Variations on the Cp theme include Cp* (C5Me5) and the monomethyl version (C5H4Me). Cp may be found as a loner alongside other ligands (in "half-sandwich" or "piano-stool" complexes), or paired up with a second Cp ligand in metallocenes. The piano-stool and bent metallocene complexes are most interesting for us, since these have potential for open coordination sites—plain vanilla metallocenes tend to be relatively stable and boring.



Binding modes of Cp and general classes of Cp complexes.

Research for this post has made me appreciate the remarkable electron-donating ability of the cyclopentadienyl (Cp) ligand, which renders its associated metal center electron rich. The LUMO of Cp is high in energy, so the ligand is a weak π-acid and is, first and foremost, a σ-donor. This effect is apparent in the strong backbonding displayed by Cp carbonyl complexes. Despite its strong donating ability, Cp is rarely an actor ligand unless another ligand shakes things up—check out the nucleophilic reactivity of doubly jazzed-up ferrocene for a nice example.

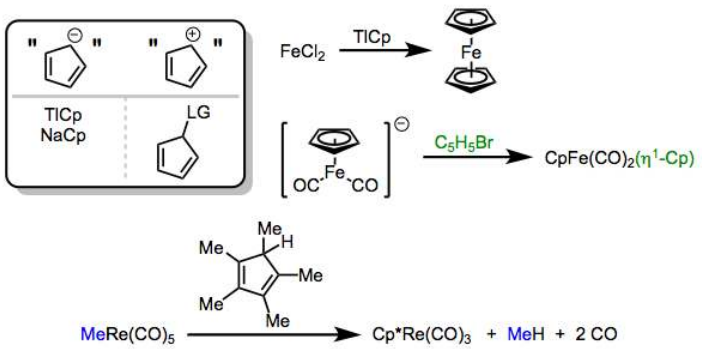
It's critical to recognize that η5-Cp is a six-electron ligand (!). Because Cp piles on electrons, the numbers of ligands bound to the metal in Cp complexes tend to be lower than we might be used to, especially in bent metallocenes containing two Cp's. Still, the number of ligands we'd expect on the metal center in these complexes is perfectly predictable. We just need to keep in mind that the resulting complexes are likely to contain 16 or 18 total electrons.



By considering the MCp2 fragment, we can predict the nature of ancillary ligands in bent metallocenes.

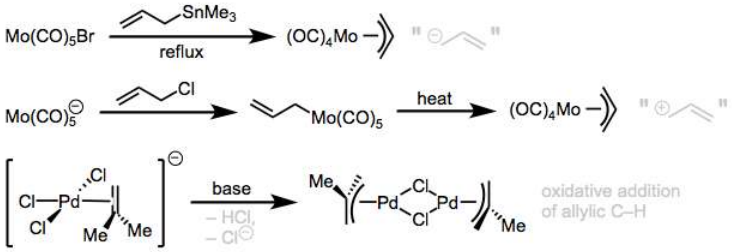
Synthesis

Crabtree cleanly divides methods for the synthesis of Cp complexes into those employing Cp+ equivalents, Cp– equivalents, and the neutral diene. Naturally, the first class of reagents are appropriate for electron-rich, nucleophilic complexes, while the second class are best used in conjunction with electron-poor, electrophilic complexes. The figure below provides a few examples.



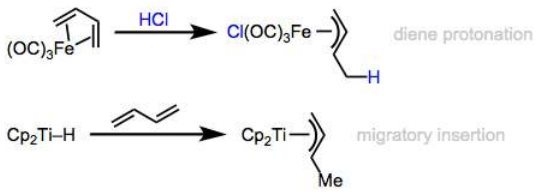
Methods for the synthesis of Cp complexes. The possibilities are exhausted by anionic, cationic, and neutral Cp equivalents!

Methods for synthesizing allyl complexes can also be classified according to whether the allyl donor is a cationic, anionic, or neutral allyl equivalent. In metal-catalyzed allylic substitution reactions, the allyl donor is usually a good electrophile bearing a leaving group displaced by the metal (an allyl cation equivalent). However, similar complexes may be obtained through oxidative addition of an allylic C–H bond to the metal, as in the synthesis of methallyl palladium chloride dimer below. Transmetalation of nucleophilic allyls from one metal to another, which we can imagine as nucleophilic attacks of an anionic allyl group, are useful when the metal is electron-poor.



Nucleophilic, electrophilic, and neutral allyl donors.

Complexes containing conjugated dienes are also viable precursors to allyl complexes. Migratory insertion of a diene into the M–H bond is a nice route to methyl-substituted allyl complexes, for example. Interestingly, analogous insertions of fulvenes do not appear to lead to Cp complexes, but some funky reductive couplings that yield ansa-metallocenes are known. External electrophilic attack (e.g., protonation) and nucleophilic attack on coordinated dienes also result in allyl complexes. In essence, one double bond of the diene becomes a part of the allyl ligand in the product; the other is used as a "handle" to establish the key covalent bond to the allyl ligand.

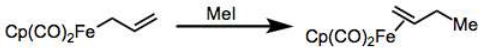


Dienes: brave crusaders in the quest for allyl complexes.

Reactions

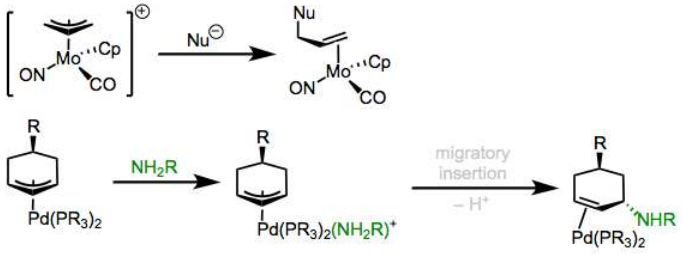
Since the Cp ligand is typically a spectator, we'll focus in this section on the reactivity of allyl ligands. As usual, the behavior of the allyl ligand depends profoundly on the nature of its coordinated metal center, which depends in turn on the metal's ancillary ligands. Avoid "tunnel vision" as you study the examples below—depending on the issue at hand, the ancillary ligands may be as important as (or more important than) the actor ligand.

Nucleophilic allyl complexes react with electrophiles like H+, MeI, X+, and acylium ions to yield cationic alkene complexes.



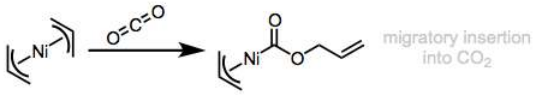
Attack of electrophiles on nucleophilic allyl complexes. Notice the donating Cp ligand!

In a conceptually related process, nucleophiles can attack allyl ligands bound to electrophilic metals. This process is key in allylic substitution reactions. In some cases, the nucleophile is known to bind to the metal first, then transfer to the allyl ligand through reductive elimination. Alternatively, direct attack on the allyl ligand may occur on the face opposite the metal. The figure below illustrates both possibilities.



External and internal attack of nucleophiles on coordinated allyl ligands.

Migratory insertion of allyl ligands is known, and is analogous to insertions involving alkyl ligands (see the figure below). Movement of the allyl ligand toward the coordination site of the dative ligand is assumed. Of course if oxidative addition to form allyl complexes is possible, reductive elimination of allyl ligands with other X-type ligands is also possible. We'll hit on these process in more detail in their dedicated posts.



Like alkyl ligands, allyls can migrate onto dative ligands like CO and π bonds.

One final post on σ-complexes will bring this series to a temporary close. In the next post, we'll look at ligands that, rather surprisingly, bind through their σ-electrons. These "non-classical" ligands behave like other dative ligands we've seen before, but are important for many reactions that involve main-group single bonds, such as oxidative addition. Before their discovery, the relevance of σ-ligands for reaction mechanisms went unappreciated by organometallic chemists.

This page titled 6.5.3: Odd-numbered π Systems is shared under a CC BY-NC-SA 4.0 license and was authored, remixed, and/or curated by Kathryn Haas.

- **2.8: Odd-numbered π Systems** by Michael Evans is licensed CC BY-NC-SA 4.0.

6.5.4: Fullerene Complexes

The π systems of fullerenes (eg buckmisterfullerene, C_{60}) also act as ligands for metal complexes. Most transition metal-fullerene complexes are derived from C_{60}. The structure of $C_{60}[IrCl(CO)(PMe_3)_2]_2$ is shown in Figure **6.5.4.1**.

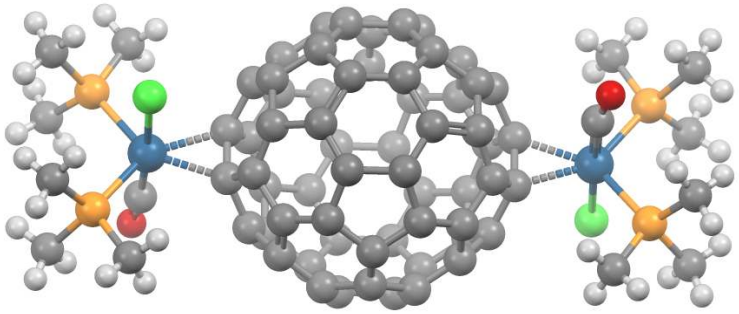


Figure **6.5.4.1**: Structure of $C_{60}[IrCl(CO)(PMe_3)_2]_2$. doi=10.1021/ic00101a015. (Smokefoot, YEMVOB, CC BY-SA 4.0)

As ligands, fullerenes behave similarly to electron-deficient alkenes, and they prefer coordination to electron-rich metal centers (metal ions with softer character like those of the 4d and 5d transition metals). They almost always coordinate in a dihapto (η^2) fashion. The η^2 metal binding most often occurs on the junction of two 6-membered rings, as shown for $[[Ph_3P]_2Pt]_6(\eta^2\text{-}C_{60})$ on the left of Figure **6.5.4.2**. In (\ce{Ru3(CO)9(C60)}\), the fullerene binds to the triangular face of the cluster as shown on the right in Figure **6.5.4.2**.

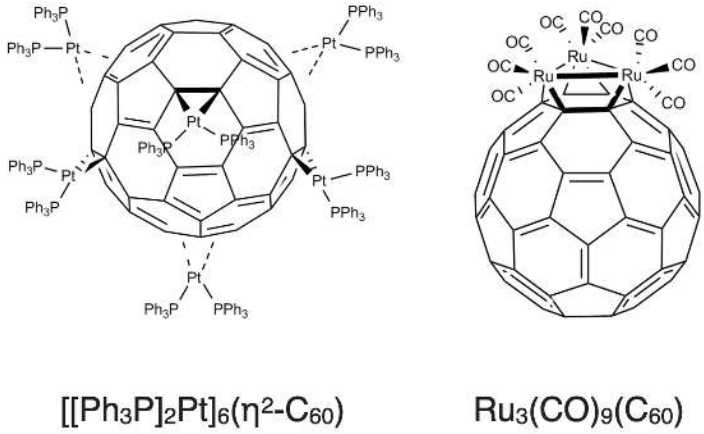
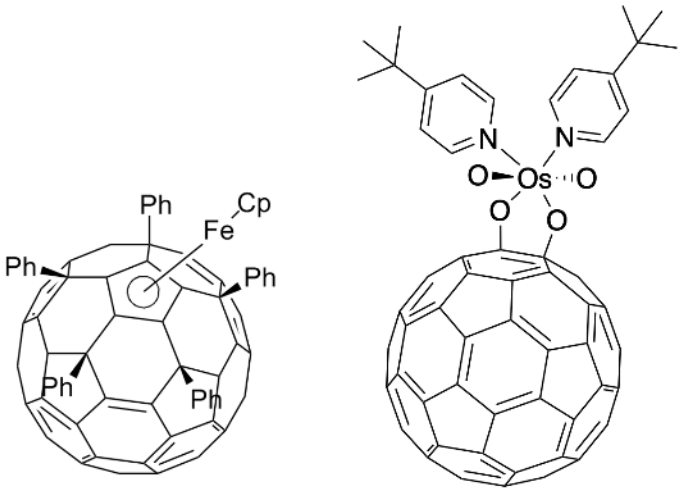


Figure **6.5.4.2**: Structures of two η^2 fullerene complexes. Left, $[[Ph_3P]_2Pt]_6(\eta^2\text{-}C_{60})$. Right, $Ru_3(CO)_9(C_{60})$. (CMSherwood, Fullerene 4 and Fullerene 2, CC BY-SA 3.0)

Hexahapto and pentahato binding is possible, but is less common that dihapto coordination. Modification of the fullerene with phynyl substituents makes the fullerene a more electron rich ligand so that penta- and hexahapto coordination is more favorable. For example, the pentaphenyl anion, $C_{60}Ph_5^-$, binds to Fe in a pentahpto (η^5) fashion, similar to the interactions in ferrocene (Left, Figure **6.5.4.3**).



Complexes of modified C_{60}

Figure **6.5.4.3**: Structures of two modified fullerenes. Left, a ferrocene-like complex of the pentaphynyl bucknisterfullerene anion (CMSherwood, Fullerene 3, CC BY-SA 3.0). Right, the structure of \(\ce{C60(OsO4)(4-*t*-butylpyridine)2}\), which was important for the original determination of the structure for C_{60}
(CC-BY-SA; Kathryn Haas).

The first X-ray structure that gave insight into the spherical structure of fullerenes was derived from an oxygen adduct of osmium tetroxide (Right, Figure **6.5.4.3**).

6.5.4: Fullerene Complexes is shared under a CC BY-NC-SA 4.0 license and was authored, remixed, and/or curated by LibreTexts.

SECTION OVERVIEW

6.6: Metal-Carbon Bonds

6.6.1: Metal Alkyls

6.6.2: Carbenes

6.6.3: Carbyne (Alkylidyne) Complexes

6.6.4: Carbido and Cumulene Complexes

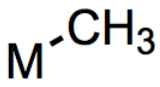
6.6.5: Carbon Wires- Polyyne and Polyene Bridges

This page titled 6.6: Metal-Carbon Bonds is shared under a CC BY-NC-SA 4.0 license and was authored, remixed, and/or curated by Kathryn Haas.

6.6.1: Metal Alkyls

Part 1:

With this post we finally reach the defining ligands of organometallic chemistry, alkyls. Metal alkyls feature a metal-carbon σ bond and are usually actor ligands, although some alkyl ligands behave as spectators. Our aim will be to understand the general dependence of the behavior of alkyl ligands on the metal center and the ligand's substituents. Using this knowledge, we can make meaningful comparisons between related metal alkyl complexes and educated predictions about their likely behavior. Because alkyl ligands are central to organometallic chemistry, I've decided to spread this discussion across multiple posts. We'll deal first with the general properties of metal alkyls.



In the Simplifying the Organometallic Complex series, we decomposed the M–C bond into a positively charged metal and negatively charged carbon. This deconstruction procedure is consistent with the relative electronegativities of carbon and the transition metals. It can be very useful for us to imagine metal alkyls essentially as stabilized carbanions—but it's also important to understand that M–C bonds run the gamut from extremely ionic and salt-like ($NaCH_3$) to essentially covalent ($[HgCH_3]^+$). The reactivity of the alkyl ligand is inversely related to the electronegativity of the metal center.

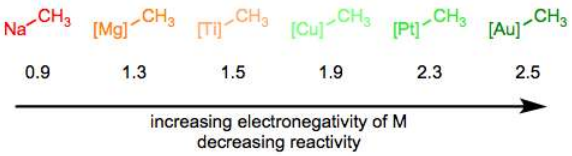


Figure **6.6.1.1**: Reactivity decreases as the metal's electronegativity increases. Values given are Pauling electronegativities. (Michael Evans)

The hybridization of the carbon atom is also important, and the trend here follows the trend in nucleophilicity as a function of hybridization in organic chemistry. *sp*-Hybridized ligands are the least nucleophilic, followed by sp^2 and sp^3 ligands respectively.

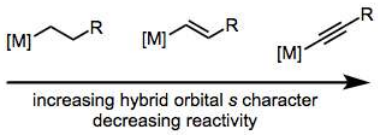


Figure **6.6.1.1**: Note that this trend is similar to the nucleophilicity of carbanions as a function of hybridization. (Michael Evans)

The history of transition metal alkyls is an intriguing example of an incorrect scientific paradigm. After several unsuccessful attempts to isolate stable metal alkyls, organometallic chemists in the 1920s got the idea that metal-carbon bonds were weak in general. However, later studies showed that it was *kinetic instability*, not thermodynamic, that was to blame for our inability to isolate metal alkyls. In other words, most metal alkyls are susceptible to decomposition pathways with low activation barriers—the instability of the M–C bond *per se* is not to blame. Crabtree cites typical values of 30-65 kcal/mol for M–C bond strengths.

What are the major decomposition pathways of metal alkyl complexes? **β-hydride elimination** is the most common. Thermodynamically, the ubiquity of β-hydride elimination makes sense—M–C bonds run 30-65 kcal/mol, while M–H bonds tend to be stronger. The figure below summarizes the accepted mechanism and requirements of β-hydride elimination. We'll revisit this fundamental reaction of organometallic complexes in a future post.

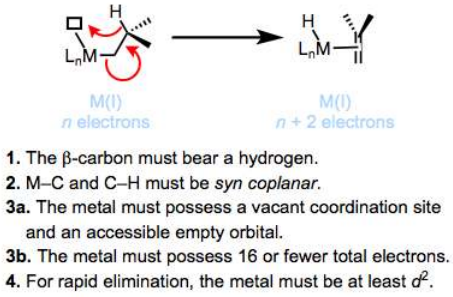


Figure **6.6.1.1**: What kinds of metal alkyl complexes violate the requirements for beta-hydride elimination? (Copyright; author via source)

Kinetically stable metal alkyl complexes violate one of the requirements for β-hydride elimination. Methyl and neopentyl complexes lack β-hydrogens, violating requirement 1. Tightly binding, chelating ligands may be used to prevent the formation of an empty coordination site, violating requirements 3a and 3b. Titanium complexes are known that violate requirement 4 and eliminate only very slowly—back-donation from the metal to the σ^*_{C-H} is required for rapid elimination (see below).

Reductive elimination is a second common decomposition pathway. The alkyl ligand hooks up with a second X-type ligand on the metal, and the metal is reduced by two units with a decrease in the total electron count by two units. I've omitted curved arrows here because different mechanisms of reductive elimination are known. We'll discuss the requirements of reductive elimination in detail in a future post; for now, it's important to note that the thermodynamic stability of C–X versus that of (M–X + M–C) is a critical driving force for the reaction.

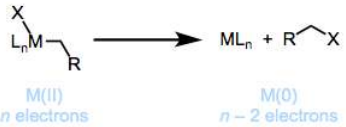


Figure **6.6.1.1**: The thermodynamics of reductive elimination can present problems for some alkyl complexes. (Copyright; author via source)

When X = H, reductive elimination is nearly always thermodynamically favorable; thus, isolable alkyl hydride complexes are rare. This behavior is a feature, not a bug, when we consider that hydrogenation chemistry depends on it! On the other hand, when X = halogen reductive elimination is usually disfavored. Reductive elimination of C–C (X = C) can be favored thermodynamically, but is usually slower than the corresponding C–H elimination.

Complexes that cannot undergo β-hydride elimination are sometimes susceptible to **α-elimination**, a mechanistically similar process that forms a metal carbene. This process is particularly facile when the α-position is activated by an adjacent electron donor (Fischer carbenes are the result).

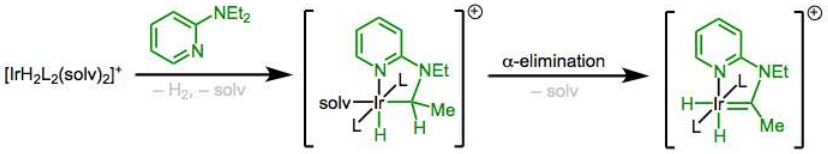


Figure **6.6.1.1**: Oxidative addition followed by alpha-elimination, forming a Fischer carbene from an alkyl complex. (Copyright; author via source)

In some metal alkyl complexes, C–H bonds at the α, β, or even farther positions can serve as electron donors to the metal center. This idea is supported by crystallographic evidence and NMR chemical shifts (the donating hydrogens shift to high field). Such interactions are called **agostic interactions**, and they resemble an "interrupted" transition state for hydride elimination. Alkyl complexes that cannot undergo β-hydride elimination for electronic reasons (high oxidation state, d^0 metals) and vinyl complexes commonly exhibit this phenomenon. The fact that β-hydride elimination is slow for d^0 metals—agostic interactions are seen instead—suggests that back-donation from a filled metal orbital to the σ^*_{C-H} is important for β-hydride elimination. Here's an interesting, recent-ish review of agostic interactions.

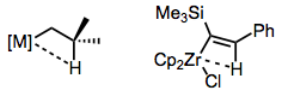


Figure **6.6.1.1**: Copy and Paste Caption here. (Copyright; author via source)

In the next post in this series, we'll explore the synthesis of metal alkyl complexes in more detail, particularly clarifying the question: how can we conquer β-hydride elimination?

Part 2:

In this post, we'll explore the most common synthetic methods for the synthesis of alkyl complexes. In addition to enumerating the reactions that produce alkyl complexes, this post will also describe strategies for getting around β-hydride elimination when isolable alkyl complexes are the goal. Here we go!

Properties of Stable Alkyl Complexes

Stable alkyl complexes must be resistant to β-hydride elimination. In the last post we identified four key conditions necessary for elimination to occur:

1. The β-carbon must bear a hydrogen.
2. The M–C and C–H bonds must be able to achieve a *syn* coplanar orientation (pointing in the same direction in parallel planes).
3. The metal must bear 16 total electrons or fewer and possess an open coordination site.
4. The metal must be at least d^2.

Stable alkyl complexes must violate at least one of these conditions. For example, titanium(IV) complexes lacking *d* electrons β-eliminate very slowly. The complex below likely also benefits from chelation (see below).

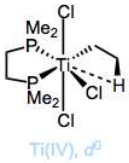


Figure **6.6.1.1**: No d electrons here! (Michael Evans)

Complexes have been devised that are unable to achieve the *syn* coplanar orientation required for elimination, or that lack β-hydrogens outright. A few examples are provided below—one has to admire the cleverness of the researchers who devised these complexes. The metallacyclobutane is particularly striking!

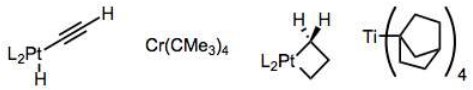


Figure **6.6.1.1**: Complexes whose beta-C–H bonds cannot align in a syn coplanar manner with the M–C bond. (Copyright; author via source)

Using tightly binding, chelating ligands or a directing group on the substrate, the formation of 16-electron complexes susceptible to β-hydride elimination can be discouraged. Notice how the hyrdrogen-bonding L_2 ligands in the central complex below hold the metal center in a death grip.

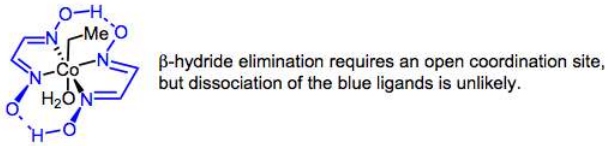


Figure **6.6.1.1**: Tightly chelating ligands prevent the opening of a coordination site. (Copyright; author via source)

Finally, it's worth noting that complexes with an open coordination site—such as 16-electron, square-planar complexes of Ni, Pd, and Pt important for cross-coupling—are susceptible to reactions with solvent or other species at the open site. Bulky alkyl ligands help prevent these side reactions. In the example below, the methyl groups of the *o*-tolyl ligands extend into the space above and below the square plane, discouraging the approach of solvent molecules perpendicular to the plane.

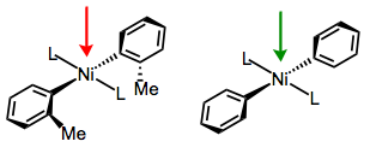


Figure **6.6.1.1**: The approach of solvent perpendicular to the square plane is slowed by methyl groups on the aryl ligand. (Copyright; author via source)

Many transition metal complexes catalyze (*E*)/(*Z*) isomerization and the isomerization of terminal alkenes (α-olefins) to internal isomers via β-hydride elimination. This is a testament to the importance of this process for alkyl complexes. Of course, transient alkyl complexes may *appear* to be susceptible to β-hydride elimination, but if other processes are faster, elimination will not occur. Thus, the optimization of many reactions involving alkyl complexes as intermediates has involved speeding up other processes at the expense of β-hydride elimination—hydrocyanation is a good example.

Synthesis of Alkyl Complexes

The dominant synthetic methods for alkyl complexes are based on nucleophilic attack, electrophilic attack, oxidative addition, and migratory insertion. The first two methods should be intuitive to the organic chemist; the second two are based on more esoteric (but no less important) reactions of organometallic complexes.

Metals bearing good leaving groups are analogous to organic electrophiles, and are susceptible to **nucleophilic attack** by organolithiums, Grignard reagents, and other polarized organometallics. These reactions can be viewed as a kind of **transmetalation**, as the alkyl ligand moves from one metal to another. Electron-withdrawing X-type ligands like –Cl and –Br should jump out as good leaving groups. On the other hand, clean substitution of L-type ligands by anionic nucleophiles is much more rare (anionic complexes would result).



Figure **6.6.1.1**: Simple and straightforward: nucleophile attacks electrophilic metal. (Copyright; author via source)

Many anionic metal complexes are nucleophilic enough to attack electrophilic sources of carbon such as alkyl and acyl halides in an **electrophilic attack** mode. An available lone pair on the metal and open coordination site are prerequisites for this chemistry. The charge on the complex increases by one unit (in effect, negative charge is transferred to the electrophile's leaving group). We can classify these as oxidative ligation reactions—notice that the oxidation state of the metal increases by two units.

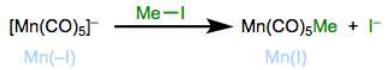


Figure **6.6.1.1**: Oxidative ligation for the synthesis of alkyl complexes. Total electron count does not change. (Copyright; author via source)

Oxidative addition results in the cleavage of a W–Z bond and placement of two new X-type ligands (–W and –Z) on the metal center, with an increase in the oxidation state of the metal and the total electron count by two units. Organic halides are extremely common substrates for this reaction, the first step in the mechanism of cross-coupling reactions. The oxidized metal complex containing new alkyl and halide ligands is the final product. Notice that *two* open coordination sites are required (not necessarily simultaneously), the metal center must be amenable to two-electron oxidation, and the number of total electrons of the complex increases by two. In essence, the electrons of the W–Z bond join the complex's party. Take note that there are many known mechanisms for oxidative addition! We'll explore these different mechanisms in detail in a future post.

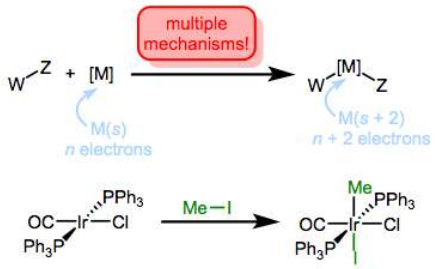


Figure **6.6.1.1**: Oxidative addition, with a representative example, for the synthesis of metal alkyl complexes. (Copyright; author via source)

Finally, **migratory insertion** of unsaturated organic compounds is an important method for the synthesis of certain alkyl complexes, and an important step of organometallic reactions that result in addition across π bonds. Migratory insertion is the microscopic reverse of β-hydride elimination. The clever among you may notice that the use of migratory insertion to synthesize alkyl complexes seems inconsistent with our observation that its reverse is ubiquitous for metal alkyls—shouldn't equilibrium favor the olefin hydride complex? In many cases this is the case; however, there are some notable exceptions. For example, perfluoroalkyl complexes are exceptionally stable (why?), so the insertion of fluoroalkenes is often favored over elimination.

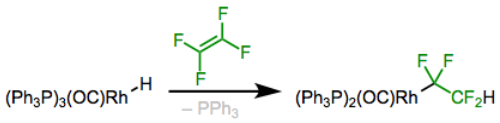


Figure **6.6.1.1**: Why does this work? Thank fluorine! (Copyright; author via source)

As we noted above, we can still invoke kinetically stable alkyl complexes as *intermediates* in reactions provided subsequent steps are faster. In the next post, we'll examine the general classes of reactions in which alkyl complexes find themselves the major players, focusing on the specific mechanistic steps that involve the alkyl complex (reductive elimination, transmetalation, migratory insertion, and [naturally] β-hydride elimination).

Part 3:

In this last post on alkyl ligands, we'll explore the major modes of reactivity of metal alkyls. We've discussed β-hydride elimination in detail, but other fates of metal alkyls include reductive elimination, transmetallation, and migratory insertion into the M–C bond. In a similar manner to our studies of other ligands, we'd like to relate the steric and electronic properties of the metal alkyl complex to its propensity to undergo these reactions. This kind of thinking is particularly important when we're interested in controlling the relative rates and/or extents of two different, competing reaction pathways.

Reactions of Metal Alkyl Complexes

Recall that **β-hydride elimination** is an extremely common—and sometimes problematic—transformation of metal alkyls. Then again, there are reactions for which β-hydride elimination is desirable, such as the Heck reaction. Structural modifications that strengthen the M–H bond relative to the M–C bond encourage β-hydride elimination; the step can also be driven by trapping of the metal hydride product with a base (the Heck reaction uses this idea).

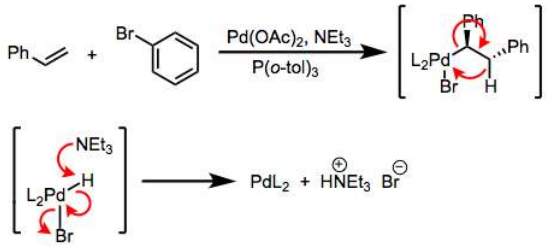


Figure **6.6.1.1**: During the Heck reaction, beta-hydride elimination is driven by a base. (Copyright; author via source)

On the flip side, stabilization of the M–C bond discourages elimination and encourages its reverse: migratory insertion of olefins into M–H. Previously we saw the example of perfluoroalkyl ligands, which possess exceptionally stable M–C bonds. The fundamental idea here—that electron-withdrawing groups on the alkyl ligand stabilize the M–C bond—is quite general. Hartwig

describes an increase in the "ionic character" of the M–C bond upon the addition of electron-withdrawing groups to the alkyl ligand (thereby strengthening the M–C bond, since ionic bonds are stronger than covalent bonds). Bond energies from organic chemistry bear out this idea to an extent; for instance, see the relative BDEs of Me–Me, Me–Ph, and Me–CCH in this reference. I still find this explanation a little "hand-wavy," but it serves our purpose, I suppose.

Metal alkyls are subject to **reductive elimination**, the microscopic reverse of oxidative addition. The metal loses two covalent ligands, its formal oxidation state decreases by two units, total electron count decreases by two units, and an R–X bond forms. Reductive elimination is favorable when the R–X bond in the organic product is more stable than the M–R and M–X bonds in the starting complex (a thermodynamic issue). It should be noted, however, that the kinetics of reductive elimination depend substantially on the steric bulk of the eliminating ligands. Concerted reductive elimination of R–H usually possesses a lower activation energy than R–R elimination.

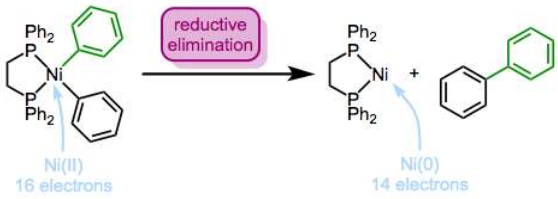


Figure **6.6.1.1**: An example of reductive elimination. Intuitively, the electron density at the metal center increases as this step proceeds. (Copyright; author via source)

Transmetalation involves the transfer of an alkyl ligand from one metal to the other. An interesting problem concerns the relative reactivity of metal alkyls toward transmetalation. Assuming similar, uncomplicated ligand sets, which of two metal centers is more likely to hold on to an alkyl ligand? Consider the two situations below.

$$\mathbf{MR + M' \rightleftharpoons M + M'R}$$

$$\mathbf{MR + M'R' \rightleftharpoons MR' + M'R}$$

The first is a *bona fide* transmetalation; the second is really a double replacement reaction. The distinction is rarely drawn in practice, but it's important! The difference is that in the first case, a single-electron transfer of sorts must take place, while in the second case, no redox chemistry is necessary. Favorability in the first case is governed by the relative reduction potentials of M and M' (the reaction goes forward when M' is more easily oxidized than M); in the second case, the relative electropositivities of the metals is key, and other factors like lattice energies may be important. The distinction between transmetalation *per se* and double replacement explains the paradoxical synthetic sequence in the figure below. In practice, both are called "transmetalation." See these slides (page 6) for a summarizing reference.

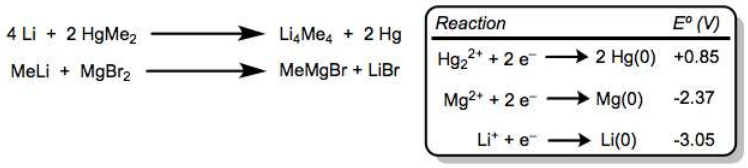


Figure **6.6.1.1**: How are both of these reactions favorable? The first is a true transmetalation; the second is a double replacement. (Copyright; author via source)

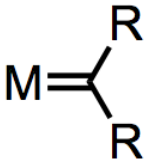
This brings our extended look at metal alkyl complexes to a temporary close. Of course, metal alkyls are *everywhere* in organometallic chemistry…so seeing them again is pretty much inevitable! The next installment in the Epic Ligand Survey series concerns allyl, cyclopentadienyl, and other odd-membered pi systems. These L_nX-type ligands can, like arenes, pile as many as six electrons on the metal center at once.

This page titled 6.6.1: Metal Alkyls is shared under a CC BY-NC-SA 4.0 license and was authored, remixed, and/or curated by Kathryn Haas.

- **2.5: Metal Alkyls** by Michael Evans is licensed CC BY-NC-SA 4.0.

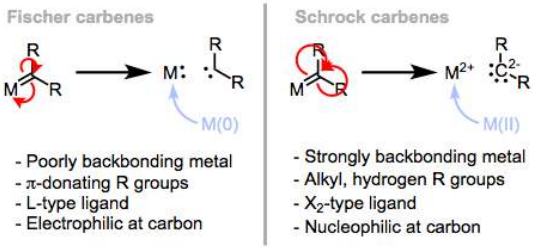
6.6.2: Carbenes

In a previous post, we were introduced to the N-heterocyclic carbenes, a special class of carbene best envisioned as an L-type ligand. In this post, we'll investigate other classes of carbenes, which are all characterized by a metal-carbon double bond. Fischer carbenes, Shrock carbenes, and vinylidenes are usually actor ligands, but they may be either nucleophilic or electrophilic, depending on the nature of the R groups and metal. In addition, these ligands present some interesting synthetic problems: because free carbenes are quite unstable, ligand substitution does not cut the mustard for metal carbene synthesis.



General Properties

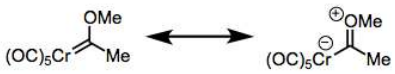
Metal carbenes all possess a metal-carbon double bond. That's kind of a given. What's interesting for us about this double bond is that there are multiple ways to deconstruct it to determine the metal's oxidation state and number of d electrons. We could give one pair of electrons to the metal center and one to the ligand, as we did for the NHCs. This procedure nicely illustrates why compounds containing M=C bonds are called "metal carbenoids"—the deconstructed ligand is an L-type carbenoid. Alternatively, we could give both pairs of electrons to the ligand and think of it as an X2-type ligand. The appropriate procedure depends on the ligand's substituents and the electronic nature of the metal. The figure below summarizes the two deconstruction procedures.



The proper method of deconstruction depends on the electronic nature of the ligand and metal.

When the metal possesses π-acidic ligands and the R groups are π-basic, the complex is best described as an L-type Fischer carbene and the oxidation state of the metal is unaffected by the carbene ligand. When the ligands are "neutral" (R = H, alkyl) and the metal is a good backbonder—that is, in the absence of π-acidic ligands and electronegative late metals—the complex is best described as an X2-type Schrock carbene. Notice that the oxidation state of the metal depends on our deconstruction method! Thus, we see that even the oxidation state formalism isn't perfect.

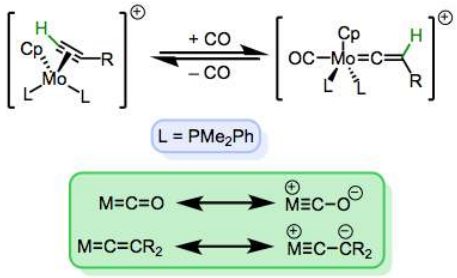
Deconstruction reveals the typical behavior of the methylene carbon in each class of complex. The methylene carbon of Schrock carbenes, on which electron density is piled through backbonding, is nucleophilic (the 2– charge screams nucleophilic!). On the other hand, the methylene carbon of Fischer carbons is electrophilic, because backbonding is weak and does not compensate for σ-donation from the ligand to the metal. To spot a Fischer carbene, be on the lookout for reasonable zwitterionic resonance structures like the one at right below.



Thanks to the pi-accepting CO ligands, the metal handles the negative charge well. This is a Fischer carbene.

The clever reader may notice that we haven't mentioned π-acidic R groups, such as carbonyls. Complexes of this type are best described as Fischer carbenes as well, as the ligand is still electrophilic. However, complexes of this type are difficult to handle and crazy reactive (see below) without a π-basic substituent to hold them in check.

Vinylidenes are the organometallic analogues of allenes, and are best described as intermediate in behavior between Fischer and Schrock carbenes. They are electrophilic at the α carbon and nucleophilic at the β carbon—in fact, a nice analogy can be made between vinylidenes and carbon monoxide. Tautomerization to form alkyne π-complexes is common, as the vinylidene and alkyne complexes are often comparable in stability.



Vinylidene tautomerization, and an analogy between vinylidenes and CO.

Take care when diagnosing the behavior of metal carbenes. In these complexes, there is often a subtle interplay between the R groups on the carbene and other ligands on the metal. In practice, many carbenes are intermediate between the Fischer and Schrock ideals.

Synthesis

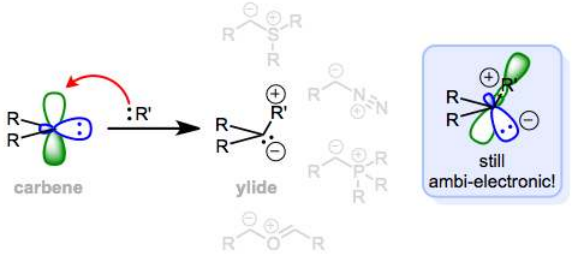
Metal carbenes present a fascinating synthetic problem. A cursory look at the deconstruction procedures above reveals that these complexes cannot be made using ligand substitution reactions, because the free ligands are far too unstable. Although the synthetic methods introduced here will be new for us, the attuned organic chemist will find them familiar. The conceptual foundations of metal carbene synthesis are similar to methods for the synthesis of alkenes in organic chemistry.

In the post on NHCs, we saw that the free carbene is both nucleophilic (via the lone pair in its σ system) and electrophilic (via its empty 2pz orbital). Organic precursors to metal carbenes and alkenes also possess this property—they can act both as nucleophiles and electrophiles. Fundamentally, this “ambi-electronic” behavior is useful for the creation of double bonds. One bond comes from “forward flow,” and the other from “reverse flow.” Naturally, the other reacting partner also needs to be ambi-electronic for this method to work.



A fundamental paradigm for double bond synthesis: ambi-electronic compounds doing what they do.

What sets carbene precursors apart from free carbenes? What other kinds of molecules may act as both nucleophiles and electrophiles at the same atom? Watch what happens when we tack a third group onto the free carbene…the figure below shows the result in general and a few specific examples in gray.

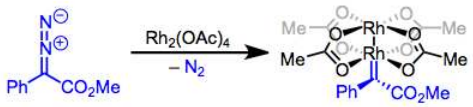


A "dative ligand" R' is the difference between a carbene and an ylide. Both are ambi-electronic.

An ylide, which contains adjacent positive and negative charges, results from this purely hypothetical process. Ylides (diazo compounds, specifically) are the most common precursors to metal carbene complexes. Like free carbenes, ylides are ambi-electronic. The electrophilic frontier orbital of an ylide is just the σ* orbital of the bond connecting the charged atoms, which

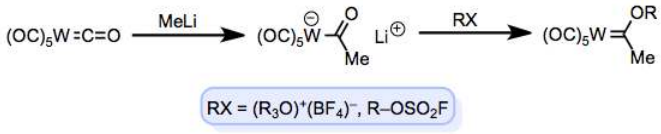
makes sense if we consider the positively charged fragment as a good leaving group (it always is). The lone pair is still nucleophilic. The figure above depicts some of the most famous ylides of organic chemistry, including those used for alkene synthesis (Corey-Chaykovsky and Wittig) and cycloaddition reactions (the carbonyl ylide).

Although diazo compounds are most commonly drawn with charges on the two nitrogen atoms, the diazo carbon is a good nucleophile and can attack electrophilic metal centers to initiate metal carbene formation. A slick 15N kinetic isotope effect study showed that C–N bond cleavage is the rate-limiting step of the reaction below. Visualize the carbanionic resonance structure to kick off the mechanism! Don't think too hard about the structure of rhodium(II) acetate here. Rhodium, copper, ruthenium, and iridium all form carbene complexes with diazo compounds in a similar way.



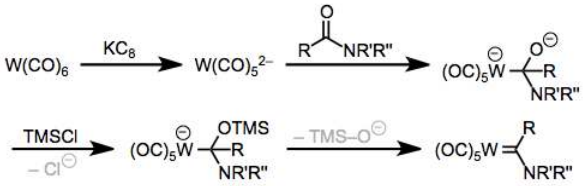
After association of the nucleophilic carbon to Rh, elimination with loss of nitrogen gas is the slow step of this reaction.

Diazo compounds work well for metal carbene formation when they possess an electron-withdrawing group, which stabilizes the ylide through conjugation. What about Fischer carbenes, which possess electron-donating groups on the carbene carbon? An interesting method that still involves a "push-and-pull" of electron flow (but not ylides) employs metal-CO complexes. Upon addition of a strong nucleophile ("forward flow") to the carbonyl carbon, a metalloenolate of sorts is produced. Treatment with an electrophile RX that prefers oxygen over the metal ("reverse flow") results in an OR-substituted Fischer carbene. Reactions reminiscent of transesterification trade out the OR group for an –SR group (using a thiol) or an –NR2 group (using a secondary amine).



Fischer's classical route to L-type carbenes.

As counterintuitive as it may seem, it's possible to use metal dianions for the synthesis of Fischer carbenes via a method pioneered by Hegedus and Semmelhack. Potassium intercalated in graphite—the mysterious "KC8"—reduces group 6 metal carbonyl complexes to the corresponding dianions, which subsequently unleash a deluge of electrons on a poor, unsuspecting amide to afford NR2-substituted Fischer carbenes after treatment with trimethylsilyl chloride.

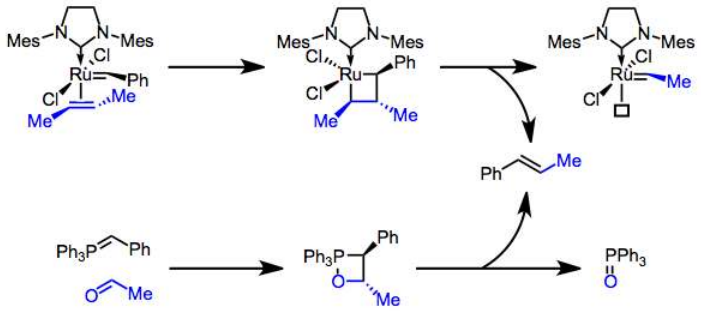


One-directional electron flow for Fischer carbene synthesis: the Hegedus-Semmelhack approach.

For other methods for the synthesis of Fischer carbenes, check out this nice review from the Baran group.

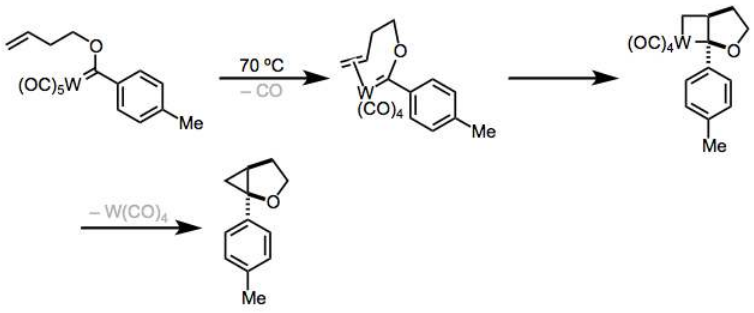
Reactions

In many ways, the reactivity of metal carbenes parallels that of ylides. Olefin metathesis catapulted metal carbenes to international stardom, but in many ways, metathesis is conceptually similar to the Wittig reaction, which employs phosphorus ylides. During both mechanisms, an ylide/carbene hooks up with another doubly bound molecule to form a four-membered ring. This step is followed by what we might call "orthogonal breakdown" to yield two new double bonds.



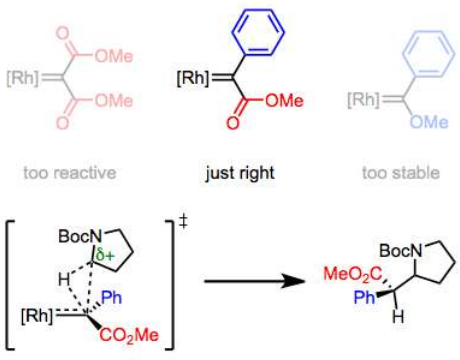
Wittig, Grubbs, and Schrock: Lords of the Chemical Dance. Ambi-electronic molecules are the dancers!

In my opinion, bond insertion reactions are the most interesting processes in which carbenes regularly engage. Bond insertions may be subdivided into cyclopropanation (π-bond insertion) and σ-bond insertion. Evidence suggests that most cyclopropanations take place by a mechanism that overlaps with metathesis—instead of orthogonal breakdown, reductive elimination occurs to release the three carbon atoms as a cyclopropane.



The metallacyclobutane mechanism of cyclopropanation.

σ-Bond insertion involves electron-rich C–H bonds most prominently, suggesting that electrophilic Fischer carbenes should be best for this chemistry. Fischer carbenes incorporating electron-withdrawing groups love to dimerize to form olefins and/or cyclopropanate olefins—how might we put the brakes on this behavior? If we simply tack a π-basic substituent onto the carbene carbon, the reactivity of these complexes is “just right” for C–H insertion. Notably, no covalent organometallic intermediates are involved; the electrophilic carbene carbon snuggles in between C and H in a single step. The transition state of this step resembles the transfer of a hydride from the organic substrate to the carbene, with “rebound” of electron density toward the partial positive charge.



Donor-acceptor carbenoids are the "Goldilocks complexes" of C–H insertion.

Let’s end with a nod to the similarity between Fischer carbenes and carboxylic acid derivatives (esters and amides). Transesterification-type reactions allow the chemist to swap out heteroatomic substituents on the carbene carbon at will (see above). Alkyl substitutents can even be deprotonated at the α carbon, just like esters! When we see the electronic similarities between the M=C bond of a Fischer carbene and the O=C bond of carboxylic acid derivatives, the similar behavior is only natural.

This page titled 6.6.2: Carbenes is shared under a CC BY-NC-SA 4.0 license and was authored, remixed, and/or curated by Kathryn Haas.

- **2.1: Carbenes** by Michael Evans is licensed CC BY-NC-SA 4.0.

6.6.3: Carbyne (Alkylidyne) Complexes

Learning Objectives

In this lecture you will learn the following

- The metal−ligand multiple bonding and their relevance in.
- The Fischer type carbyne complexes.
- The Schrock type carbyne complexes.

The metal−ligand multiply bonded systems even extended beyond the doubly bonded Fischer and the Schrock carbenes to the triply bonded $L_nM{\equiv}CR$ type Fischer carbyne and the Schrock carbyne complexes. Similar to carbene that exists in a singlet and a triplet spin state, the carbyne also exists in two other spin states *i.e* in a doublet and a quartet form.

Upon binding to the metal in its doublet spin state as in the Fischer carbene system, the carbyne moiety donates two electrons *via* its *sp* hybridized lone pair containing orbital to an empty metal *d* orbital to yield a $L_nM \leftarrow CR$ type ligand to metal dative bond. It also makes a covalent π−bond through one of its singly occupied p_z orbital with one of the metal *d* orbitals. The carbyne−metal interaction consist of two ligand to metal interactions namely a dative one and a covalent one that together makes the carbyne moiety a LX type of a ligand. In addition to these two types of ligand to metal bonding interactions, there remains an empty p_y orbital on the carbyne−C atom that can accommodate electron donation from a filled metal *d* orbital to give a metal to ligand π−back bonding interaction (Figure **6.6.3.1**).

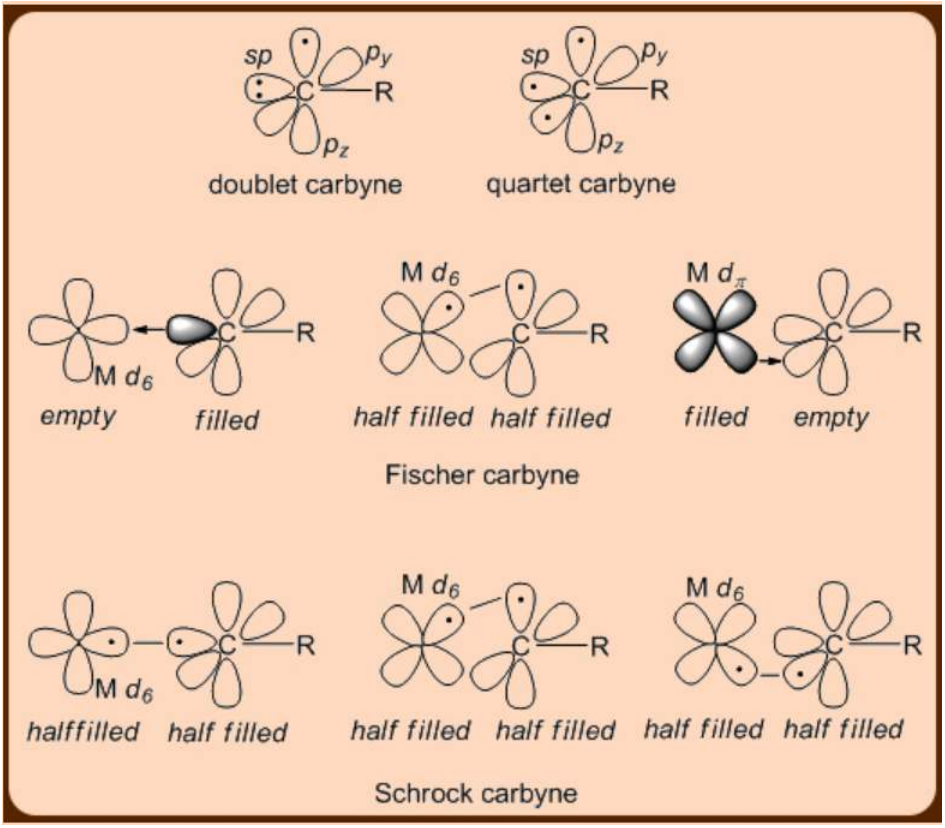


Figure **6.6.3.1**: Metal−ligand multiple bonding in the Fischer and Schrock carbyne system

Analogously, in the quartet carbyne spin state in the Schrock carbyne systems three covalent bonds occur between the singly occupied *sp*, $p_y$and p_z orbitals of carbyne−C moiety with the respective singly occupied metal *d* orbitals (Figure **6.6.3.1**).

Similar to what has been observed earlier in the case of the Fischer carbenes and Schrock carbenes, the Fischer carbyne complexes are formed with metal centers in lower oxidation states for *e.g.* as in $Br(CO)_4W{\equiv}CMe$, while the Schrock carbyne complexes are formed with metals in higher oxidation state, *e.g.* as in $(t{-}BuO)_3W{\equiv}Ct{-}Bu$.

Carbyne complexes can be prepared by the following methods.

i. The Fischer carbyne complexes can be prepared by the electrophilic abstraction of a methoxy group from a methoxy methyl substituted Fischer carbene complex.

$$L(CO)_4M{=}C(OMe)Me + 2\,BX_3 \longrightarrow [L(CO)_4M{\equiv}CMe]^+BX_4^- + BX_2(OMe) \longrightarrow X(CO)_4M{\equiv}CMe$$

ii. Schrock carbynes can be prepared by the deprotonation of a α−CH bond of a metal−carbene complex.

$$CPCl_2Ta{=}CHR \xrightarrow[(ii)Ph_3P{=}CH_2]{(i)PMe_3} Cp(PMe_3)ClTa{\equiv}CR$$

iii. by an α−elimination reaction on a metal−carbene complex

$$Cp \cdot Br_2Ta{=}CHt{-}Bu \xrightarrow[(ii)Na/Hg]{(i)dmpe} Cp \cdot (dmpe)HTa{\equiv}Ct{-}Bu$$

iv. by metathesis reaction

$$(t\text{-}BuO)_3W{\equiv}W(Ot{-}Bu)_3 + t\text{-}BuC{\equiv}Ct{-}Bu \longrightarrow 2\,(t\text{-}BuO)_3W{\equiv}Ct{-}Bu$$

The reactivities of Fischer and the Schrock carbynes mirror that of the Fischer and Schrock carbenes. For example, the Fischer carbyne undergo nucleophilic attack at the carbyne−C atom while the Schrock carbyne undergo electrophilic attack at the carbyne−C atom.

Summary

The theme of metal−ligand multiple bonding extends beyond the doubly bonded Fischer and the Schrock carbene systems to even triply bonded Fischer and the Schrock carbyne systems. The carbyne moieties in these Fischer and the Schrock carbyne systems respectively exist in a doublet and a quartet spin state. The carbyne complexes are generally prepared from the respective carbene analogues by the abstraction of alkoxy (OR), proton (H^+), hydride (H^-) moieties, the α−elimination reactions and the metathesis reactions. The reactivity of the Fischer and the Schrock carbyne complexes parallel the corresponding Fischer and the Schrock carbene counterparts with regard to their reactivities toward electrophiles and nucleophiles.

This page titled 6.6.3: Carbyne (Alkylidyne) Complexes is shared under a CC BY-NC-SA 4.0 license and was authored, remixed, and/or curated by Kathryn Haas.

- **13.2: Metal-Carbynes** by M. S. Balakrishna & Prasenjit Ghosh is licensed CC BY-NC-SA 4.0. Original source: https://nptel.ac.in/courses/104101006.

6.6.4: Carbido and Cumulene Complexes

Carbido ligand: One single carbon

A metal carbido (aka carbide, or simply carbon) complex is a metal complex that contains the ligand, carbon (C). Most molecular carbido complexes are clusters, usually featuring carbide as a six-fold bridging ligand. Examples include $[Rh_6C(CO)_{15}]^{2-}$, and $[Ru_6C(CO)_{16}]^{2-}$. The iron carbonyl carbides exist not only in the encapsulated carbon ($[Fe_6C(CO)_{16}]^{2-}$) but also with exposed carbon centres as in $Fe_5C(CO)_{15}$ and $Fe_4C(CO)_{13}$.

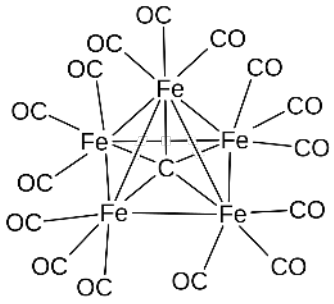


Figure 6.6.4.1: Structure of $Fe_5C(CO)_{15}$ containing a carbido bridging five iron centers. (Public domain)

In rare cases, carbido ligands are terminal ligands (Figure 6.6.4.2, left). Although it is tempting to extend the model of metal-carbon bonds from the alkyl (M—C), carbene (M=C, and carbyne (M ≡ C) ligands and evoke the idea of a quadruple bond between metal and carbon in the case of a carbido, experimental data is more consistent with a triple bonded to a metal ion ((M ≡ C_1)). For example, the metal-carbon bond in the $RuC(PCy_3)_2Cl_2$ complex is similar to the bond length of other complexes with C ≡ M (Figure 6.6.4.2).

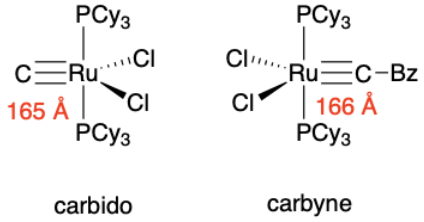


Figure 6.6.4.2: Carbido-metal bonds are similar in length to the C ≡ M of metal carbynes. Cy = cyclohexane, Bz = benzyl. (CC-BY-SA; Kathryn Haas)

Source: https://en.Wikipedia.org/wiki/Metal_carbido_complex

Cumulene ligands: Chains of carbon atoms with consecutive double bonds

Chains of carbon atoms that have consecutive (cumulated) double bonds are intriguing ligands for metal complexes due to their potential utility as molecular wires in nano or optical devices. The first reported complex containing a vinylidene ligand was $Ph_2C_2Fe_2(CO)_8$. The first monometallic vinylidene complex was $(C_5H_5)Mo(P(C_6H_5)_3)(CO)_2[C{=}C(CN)_2]Cl$. Just as in the case of conjugated pi systems, the longer the length of a cumulated diene, the closer the HOMO/LUMO gap, and thus the more conductive. To date, the longest cumulenylidene ligand reported is heptahexaenylidene (Figure 6.6.4.3).

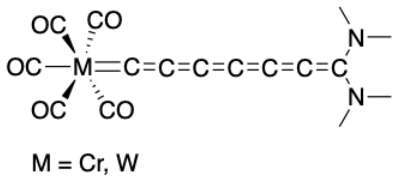


Figure 6.6.4.3: Structure of a metal complex with a heptahexaenylidene ligand. (CC-BY-SA; Kathryn Haas)

Source: https://en.Wikipedia.org/wiki/Cumule...ply%20cumulene.

This page titled 6.6.4: Carbido and Cumulene Complexes is shared under a CC BY-NC-SA 4.0 license and was authored, remixed, and/or curated by Kathryn Haas.

https://chem.libretexts.org/@go/page/488744

6.6.5: Carbon Wires- Polyyne and Polyene Bridges

Organic molecules with conjugated π systems are known to have interesting optical and electronic properties. When ligands with conjugated π systems are used to bridge two metal centers, the two metals can behave in a cooperative way because the electronic state of one metal ion is conjugated to the other. The most intensely investigated complexes are bimetallic metal complexes (two metal ions) that are bridged by long carbon chains with alternating single and double bonds. Some examples are given below. (This topic is reviewed in Aguirre-Etcheverry D. O'Hare, *Chem. Rev.*, **2010**, *110*, 4839, doi: 10.1021/cr9003852)

Polyene

Polyenes are organic molecules with alternating double and single bonds. In other words, they contain a series of consecutive \(\ce{(-C= C-)_{n}}\) with $n > 1$. Aromatic and cyclic polyenes were discussed in a previous section. One of the longest ligands reported as of 2010 was a $\mathbf{Ru{-}(CH)_{14}{-}Ru}$ complex (shown in Figure **6.6.5.1**).

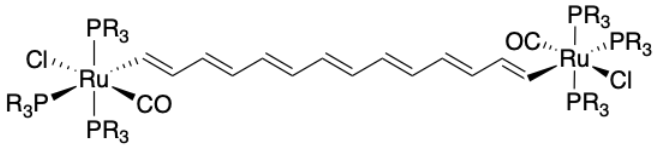


Figure **6.6.5.1**: Structure of linear polyene complex of Ru with and 14-carbon polyene. (CC-BY-SA; Kathryn Haas)

Source: Aguirre-Etcheverry D. O'Hare, *Chem. Rev.*, **2010**, *110*, 4839, doi: 10.1021/cr9003852

Polyyne ligands

Polyynes are organic molecules with alternating single and double bonds. In other words, they contain a series of consecutive $\mathbf{(-C \equiv C-)_n}$ with $n > 1$.

Organometallic polyynes capped with metal complexes are well characterized. As of the mid-2010s, the most intense research had concerned rhenium (ReC_nRe, n=6-20), ruthenium ($RuRuC_nRuRu$, n = 8–20), iron ($FeC_{12}CFe$), platinum (PtC_nPt, n = 16–28), palladium (ArC_nPd, n = 6–10), and cobalt ($Co_3C_nCo_3$, n = 14–26) complexes (Figure **6.6.5.1**).

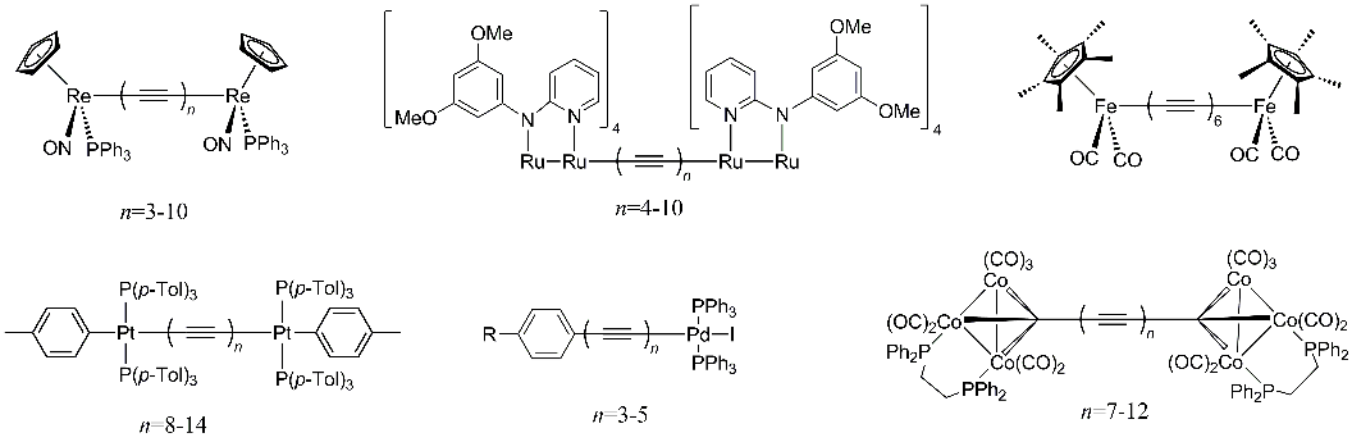


Figure **6.6.5.1**: Examples of known polyyne organometallic complexes. (Pigulski, Organometallic polyynes, CC BY-SA 4.0)

Source: https://en.Wikipedia.org/wiki/Polyyne

This page titled 6.6.5: Carbon Wires- Polyyne and Polyene Bridges is shared under a CC BY-NC-SA 4.0 license and was authored, remixed, and/or curated by Kathryn Haas.

6.7: Characterization of Organometallic Complexes

Learning Objectives

In this lecture you will learn the following

- The characterization techniques of organometallic compounds.
- The NMR analysis of these compounds.
- The IR analysis of these compounds.
- The X-ray single crystal diffraction studies of these compounds.

The characterization of an organometallic complex involves obtaining a complete understanding of the same right from its identification to the assessment of its purity content, to even elucidation of its stereochemical features. Detailed structural understanding of the organometallic compounds is critical for obtaining an insight on its properties and which is achieved based on the structure-property paradigm.

Synthesis and isolation

Synthesis and isolation are two very important experimental protocols in the overall scheme of things of organometallic chemistry and thus these needs to be performed carefully. The isolation of the organometallic compounds is essential for their characterization and reactivity studies. Fortunately, many of the methods of organic chemistry can be used in organometallic chemistry as the organometallic compounds are mostly nonvolatile crystalline solids at room temperature and atmospheric pressure though a few examples of these compounds are known to exist in the liquid [$(CH_3C_5H_4Mn(CO)_3$] and even in the vapor [$Ni(CO)_4$] states. The organometallic compounds are comparatively more sensitive to aerial oxygen and moisture, and because of which the manipulation of these compounds requires stringent experimental skills to constantly provide them with anaerobic environment for their protection. All of these necessities led to the development of the so-called special Schlenk techniques, requiring special glasswares and which in conjunction with a high vacuum line and a dry box allow the lab bench-top manipulation of these compounds. Successful isolation of organometallic compounds naturally points to the need for various spectroscopic techniques for their characterizations and some of the important ones are discussed below.

1H NMR spectroscopy

The ^1H NMR spectroscopy is among the extensively used techniques for the characterization of organometallic compounds. Of particular interest is the application of ^1H NMR spectroscopy in the characterization of the metal hydride complexes, for which the metal hydride moiety appear at a distinct chemical shift range between 0 ppm to −40 ppm to the high field of tetramethyl silane (TMS). This upfield shift of the metal hydride moiety is attributed to a shielding by metal *d*−electrons and the extent of the upfield shift increases with higher the d^n configuration. Chemical shifts, peak intensities as well as coupling constants from the through-bond couplings between adjacent nuclei like that of the observation of $J_{P\text{-}H}$, if a phosphorous nucleus is present within the coupling range of a proton nucleus, are often used for the analysis of these compounds. The ^1H NMR spectroscopy is often successfully employed in studying more complex issues like fluxionality and diastereotopy in organometallic molecules (Figure **6.7.1**).

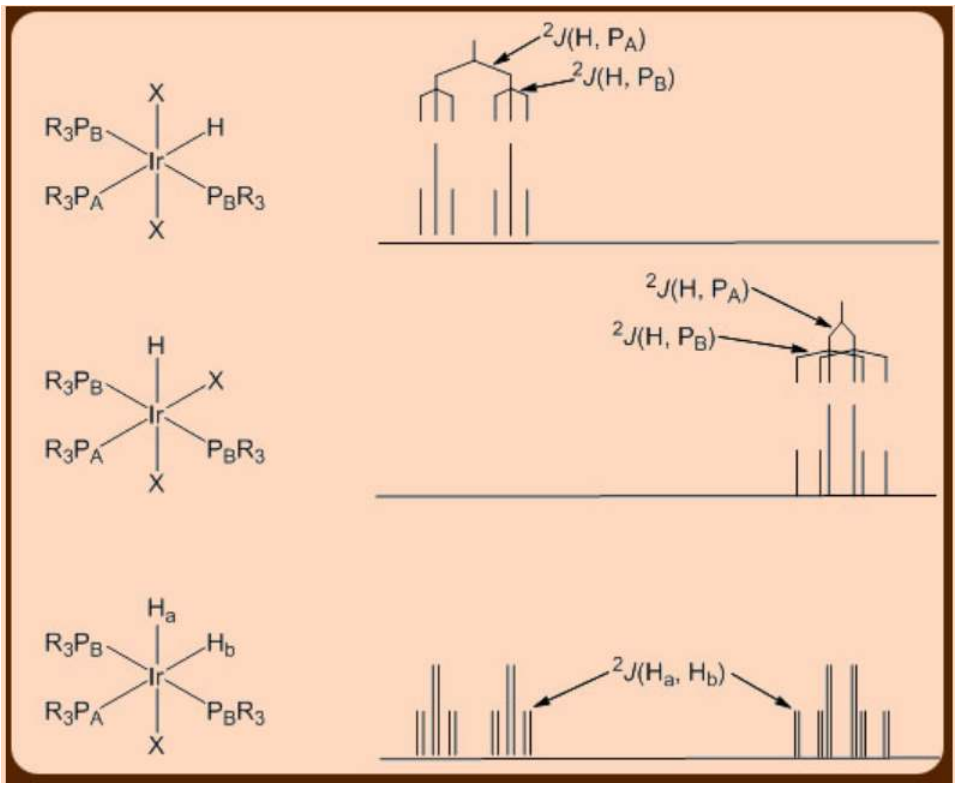


Figure **6.7.1**: Different phosphorous-proton coupling patterns in various iridium hydride complexes.

The paramagnetic organometallic complexes show a large range of chemical shifts, for example, $(\eta^6{-}C_6H_6)_2V$ exhibits proton resonances that extend even up to 290 ppm.

13C NMR spectroscopy

Although the natural abundance of NMR active ^{13}C (I = ½) nuclei is only 1 %, it is possible to obtain a proton decoupled $^{13}C\{^1H\}$ NMR spectra for most of the organometallic complexes. In addition, the off−resonance ^1H decoupled ^{13}C experiments yield $^1J_{C\text{-}H}$ coupling constants, which contain vital structural information, and hence are very critical to the ^{13}C NMR spectral analysis. For example, the $^1J_{C\text{-}H}$ coupling constants directly correlate with the hybridization of the C−H bonds with *sp* center exhibiting a $^1J_{C\text{-}H}$ coupling constant of ~250 Hz, a sp^2 center of 160 Hz and a sp^3 center of 125 Hz. Similar to what is seen in ^1H NMR, a phosphorous−carbon coupling is also observed in a ^{13}C NMR spectrum with the *trans* coupling (~100 Hz) being larger than the *cis* coupling (~10 Hz).

^{31}P NMR spectroscopy

The ^{31}P NMR spectroscopy, which in conjunction with ^1H and ^{13}C NMR spectroscopies, is a useful technique in studying the phosphine containing organometallic complexes. The ^{31}P NMR experiments are routinely run under ^1H decoupled conditions for simplification of the spectral features that allow convenience in spectral analysis. Thus, for this very reason, many mechanistic studies on catalytic cycle are conveniently undertaken by ^{31}P NMR spectroscopy whenever applicable.

IR spectroscopy

Qualitative to semi-quantitative analysis of organometallic compounds using IR spectroscopy are performed whenever possible. In general the signature stretching vibrations for chemical bonds are more conveniently looked at in these studies. The frequency (ν) of a stretching vibration of a covalent bond is directly proportional to the strength of the bond, usually given by the force constant (k) and inversely proportional to the reduced mass of the system, which relates to the masses of the individual atoms.

$$\nu = \frac{1}{2\pi C}\sqrt{\frac{k}{m_r}}$$

$$m_r = \frac{m_1 m_2}{m_1 + m_2}$$

The organometallic compounds containing carbonyl groups are regularly studied using IR spectroscopy, and in which the **CO** peaks appear in the range between 2100−1700 cm^{-1} as distinctly intense peaks.

Crystallography

The solid state structure elucidation using single crystal diffraction studies are extremely useful techniques for the characterization of the organometallic compounds and for which the X-ray diffraction and neutron diffraction studies are often undertaken. As these methods give a three dimensional structural rendition at a molecular level, they are of significant importance among the various available characterization methods. The X-ray diffraction technique is founded on Bragg's law that explains the diffraction pattern arising out of a repetitive arrangement of the atoms located at the crystal lattices.

$$2d \sin\theta = n\lambda$$

A major limitation of the X-ray diffraction is that the technique is not sensitive enough to detect the hydrogen atoms, which appear as weak peaks as opposed to intense peaks arising out of the more electron rich metal atoms, and hence are not very useful for metal hydride compounds. Neutron diffraction studies can detect hydrogens more accurately and thus are good for the analysis of the metal hydride complexes.

Summary

Along with the synthesis, the isolation and the characterization protocols are also integral part of the experimental organometallic chemistry. Because of their air and moisture sensitivities, specialized experimental techniques that succeed in performing the synthesis, isolation and storage of these compounds in an air and moisture-free environment are often used. The organometallic compounds are characterized by various spectroscopic techniques including the ^{1}H NMR, ^{13}C NMR and IR spectroscopies and the X-ray and the neutron diffraction studies.

This page titled 6.7: Characterization of Organometallic Complexes is shared under a CC BY-NC-SA 4.0 license and was authored, remixed, and/or curated by M. S. Balakrishna & Prasenjit Ghosh via source content that was edited to the style and standards of the LibreTexts platform.

- **12.1: Characterization of Organometallic Complexes** by M. S. Balakrishna & Prasenjit Ghosh is licensed CC BY-NC-SA 4.0. Original source: https://nptel.ac.in/courses/104101006.

CHAPTER OVERVIEW

7: Organometallic Reactions and Catalysis

Introduction

This chapter is a survey of common organometallic reactions and catalytic cycles. The reactions of organometallic complexes are divided into two main categories: (1) Reactions that involve gain or loss of ligands, and (2) Reactions involving modification of ligands.

7.1: Reactions Involving Gain or Loss of Ligands

7.1.1: Ligand Dissociation and Substitution

7.1.2: Oxidative Addition

7.1.3: Reductive Elimination

7.1.4: Sigma Bond Metathasis

7.1.5: Application of Pincer Ligands

7.2: Reactions Invloving Modification of Unsaturated Ligands

7.2.1: Introduction to Insertion

7.2.2: CO Insertions (Alkyl Migration)

7.2.3: Migratory Insertion-1,2-Insertions

7.2.4: β-Elimination Reactions

7.2.5: Abstraction and Addition

7.3: Organometallic Catalysts

7.3.1: Catalytic Deuteration

7.3.2: Hydroformylation

7.3.3: Monsanto Acetic Acid Process

7.3.4: Wacker (Smidt) Process

7.3.5: Hydrogenation by Wilkinson's Catalyst

7.3.6: Olefin Metathesis

7.4: Heterogeneous Catalysts

7.4.1: Ziegler-Natta Polymerizations

7.4.2: Water-Gas Shift Reaction

7.5: Problems

7.5.1: Concept Review Questions Chapter 12

7.5.2: Homework Problems Chapter 12

This page titled 7: Organometallic Reactions and Catalysis is shared under a CC BY-NC-SA 4.0 license and was authored, remixed, and/or curated by Kathryn Haas.

SECTION OVERVIEW

7.1: Reactions Involving Gain or Loss of Ligands

Many reactions of organometallic complexes involve change in coordination number. In a dissociation reaction, one or more ligands are eliminated from the complex and the coordination number decreases. In an association, one or more ligands are added to the complex and the coordination number increases. If the coordination number changes while the metal oxidation state remains constant, the reactions are considered **association/addition** reactions or **dissociation** reactions. Reactions can also occur where the coordination number changes while the metal oxidation state also changes. These reactions are considered **reductive eliminations** or **oxidative additions** (or a combination of these).

Types of reactions involving gain or loss of ligands

- **Association or Addition Reaction**: a reaction in which the coordination number increases; metal oxidation state is unchanged.
- **Dissociation Reaction**: a reaction in which the coordination number decreases; metal oxidation state is unchanged.
- **Oxidative Addition**: a reaction in which coordination number increases while metal oxidation state increases.
- **Reductive Elimination**: a reaction in which coordination number decreases while metal oxidation state decreases.

7.1.1: Ligand Dissociation and Substitution

7.1.2: Oxidative Addition

7.1.3: Reductive Elimination

7.1.4: Sigma Bond Metathasis

7.1.5: Application of Pincer Ligands

This page titled 7.1: Reactions Involving Gain or Loss of Ligands is shared under a CC BY-NC-SA 4.0 license and was authored, remixed, and/or curated by Kathryn Haas.

7.1.1: Ligand Dissociation and Substitution

As discussed in Chapter 13, ligand substitution is characterized by a continuum of mechanisms bound by associative (A) and dissociative (D) extremes. At the associative extreme, the first step is an Associative reaction; the incoming ligand forms a bond to the metal and creates an intermediate of higher coordination number. Then the departing ligand takes its lone pair and leaves. At the dissociative extreme, the fist step is a Dissociative reaction and the order of events is opposite; a ligand departs and a new complex with lower coordination number forms. Then, a new ligand associates with the complex in the second step. Sometimes, instead of reacting, the "intermediate" is simply a stable complex with a different coordination number than the reactant.

The most common reactions that are used to create new complexes are Dissociations and Substitutions (involving both Dissociation and Association steps). Associative substitution is common for 16-electron complexes (like d^8 complexes of Ni, Pd, and Pt), while both Dissociation and Dissociative Substitution are the norm for 18-electron complexes. Then again, reality is often more complicated than these extremes. In some cases, evidence is available for interchange (I_a or I_d).

In this subsection, we'll explore ligand substitution reactions and mechanisms in the context of organometallic chemistry. We'd like to be able to (a) predict whether a mechanism is likely to be associative or dissociative; (b) propose a reasonable mechanism from given experimental data; and (c) describe the results we'd expect given a particular mechanism. Keep these goals in mind as you learn the theoretical and experimental nuts and bolts of substitution reactions.

Dissociation

Carbonyl compounds are known to undergo dissociation reactions upon heating or irradiation with light. For example, upon heating, the the cyclopentadienylmolybdenum tricarbonyl dimer ($Cp_2Mo_2(CO)_6$), where Cp is the cyclopentadienyl ligand) loses a CO ligand from each Mo ion, and a triple bond between the Mo ions is formed (Top, Figure 7.1.1.1). An example of a photoactivated dissociation of CO is the case of neutral iron pentacarbonyl, $Fe(CO)_5$. Irradiation of $Fe(CO)_5$ with UV produces $Fe(CO)_4$ (Bottom, Figure 7.1.1.1).

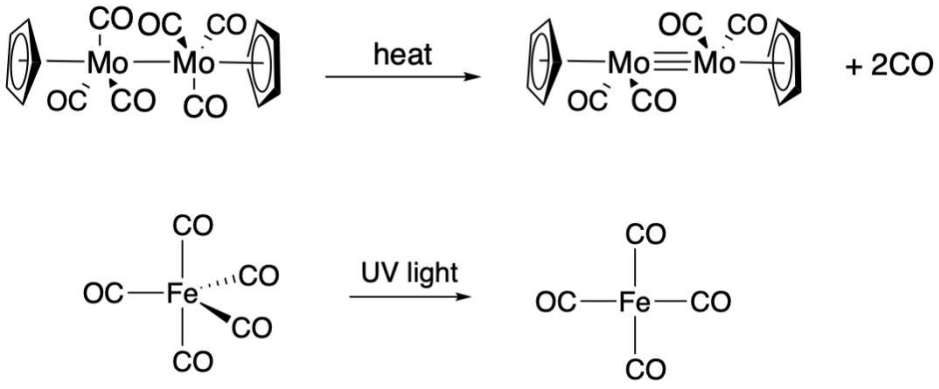


Figure 7.1.1.1: Dissociation reactions: Top, the thermally-activated dissociation of CO from cyclopentadienylmolybdenum tricarbonyl dimer. Bottom, the photochemically-activated dissociation of CO from ironpentacarbonyl. (CC-BY-SA; Kathryn Haas)

However, in each of the cases shown above, the product complex is reactive toward ligand association, usually resulting in an overall substitution. The cyclopentadienylmolybdenum dicarbonyl dimer shown on the top of Figure 7.1.1.1 binds a variety of substrates across the metal-metal triple bond. And the iron tetracarbonyl complex shown on the bottom in Figure 7.1.1.1 readily captures a variety of ligands to result in an overall substitution (example given below); when a ligand doe not associate with it, $Fe_2(CO)_9$ is produced.

Sources: Iron Pentacarbonyl and Cyclopentadienylmolybdenum tricarbonyl dimer articles from Wikipedia.

Dissociative Substitution

Associative substitution is unlikely for saturated, 18-electron complexes—coordination of another ligand would produce a 20-electron intermediate. For 18-electron complexes, dissociative substitution mechanisms involving 16-electron intermediates are more likely. In a slow step with positive entropy of activation, the departing ligand leaves, generating a coordinatively unsaturated intermediate. The incoming ligand then enters the coordination sphere of the metal to generate the product. For the remainder of this post, we'll focus on the kinetics of the reaction and the nature of the unsaturated intermediate (which influences the stereochemistry of the reaction). The reverse of the first step, re-coordination of the departing ligand (rate constant k–1), is often competitive with dissociation.

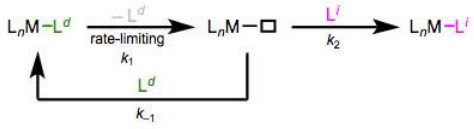


Figure 7.1.1.7: A general scheme for dissociative ligand substitution. There's more to the intermediate than meets the eye! (Michael Evans)

Reaction Kinetics

Let's begin with the general situation in which k_1 and k_{-1} are similar in magnitude. Since k_1 is rate limiting, k_2 is assumed to be much larger than k_1 and k_{-1}. Most importantly, we need to assume that variation in the concentration of the unsaturated intermediate is essentially zero. This is called the steady state approximation, and it allows us to set up an equation that relates reaction rate to observable concentrations Hold onto that for a second; first, we can use step 2 to establish a preliminary rate expression.

$$\text{rate} = k_2[L_nM\text{–}\Diamond][Li] \tag{1}$$

Of course, the unsaturated complex is present in very small concentration and is unmeasurable, so this equation doesn't help us much. We need to remove the concentration of the unmeasurable intermediate from (1), and the steady state approximation helps us do this. We can express variation in the concentration of the unsaturated intermediate as (processes that make it) minus (processes that destroy it), multiplying by an arbitrary time length to make the units work out. All of that equals zero, according to the SS approximation. The painful math is almost over! Since Δt must not be zero, the other factor, the collection of terms, must equal zero.

$$\Delta[L_nM\text{–}\Diamond] = 0 = (k1[L_nM\text{–}L^d]\text{–}k\text{–}1[L_nM\text{–}\Diamond][L^d]\text{–}k_2[L_nM\text{–}\Diamond][Li])\Delta t \tag{2}$$

$$0 = k_1[L_nM\text{–}Ld]\text{–}k_{-1}[L_nM\text{–}\Diamond][Ld]\text{–}k_2[L_nM\text{–}\Diamond][Li] \tag{3}$$

Rearranging to solve for $[L_nM\text{–}\Diamond]$, we arrive at the following.

$$[L_nM\text{–}\Diamond] = k_1\frac{[L_nM\text{–}L_d]}{(k_{-1}[L_d] + k_2[Li]} \tag{4}$$

Finally, substituting into equation (1) we reach a verifiable rate equation.

$$\text{rate} = k_2k_1\frac{[L_nM\text{–}Ld][Li]}{(k_{-1}[L_d] + k_2[Li]} \tag{5}$$

When k_{-1} is negligibly small, (5) reduces to the familiar equation (6), typical of dissociative reactions like S_N1.

$$\text{rate} = k_1[L_nM\text{–}L_d] \tag{6}$$

Unlike the associative rate law, this rate does not depend on the concentration of incoming ligand. For reactions that are better described by (5), we can drown the reaction in incoming ligand to make $k_2[Li]$ far greater than $k_{-1}[Ld]$, essentially forcing the reaction to fit equation (6).

The Unsaturated Intermediate & Stereochemistry

Dissociation of a ligand from an octahedral complex generates an usaturated ML5 intermediate. When all five of the remaining ligands are L-type, as in Cr(CO)5, the metal has 6 d electrons for a total electron count of 16. The trigonal bipyramidal geometry

presents electronic problems (unpaired electrons) for 6 d electrons, as the figure below shows. The orbital energy levels come from crystal field theory. Distortion to a square pyramid or a distorted TBP geometry removes the electronic issue, and so five-coordinate d6 complexes typically have square pyramidal or distorted TBP geometries. This is just the geometry prediction process in action!

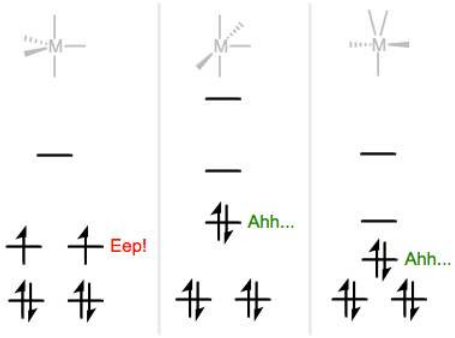


Figure **7.1.1.8**: TBP geometry is electronically disfavored for d6 metals. Distorted TBP and SP geometries are favored. (Michael Evans)

When the intermediate adopts square pyramidal geometry (favored for good π-acceptors and σ-donors…why?), the incoming ligand can simply approach where the departing ligand left, resulting in retention of stereochemistry. Inversion is more likely when the intermediate is a distorted trigonal bipyramid (favored for good π-donors). As we've already seen for associative substitution, fluxionality in the five-coordinate intermediate can complicate the stereochemistry of the reaction.

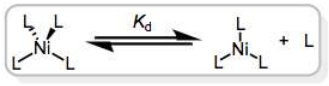
Encouraging Dissocative Substitution

In general, introducing structural features that either stabilize the unsaturated intermediate or destabilize the starting complex can encourage dissociative substitution. Both of these strategies lower the activation barrier for the reaction. Other, quirky ways to encourage dissociation include photochemical methods, oxidation/reduction, and ligand abstraction.

Let's begin with features that stabilize the unsaturated intermediate. Electronically, the intermediate loves it when its d electron count is nicely matched to its crystal field orbitals. As you study organometallic chemistry, you'll learn that there are certain "natural" d electron counts for particular geometries that fit well with the metal-centered orbitals predicted by crystal field theory. Octahedral geometry is great for six d electrons, for example, and square planar geometry loves eight d electrons. Complexes with "natural" d electron counts—but bearing one extra ligand—are ripe for dissociative substitution. The classic examples are d8 TBP complexes, which become d8 square planar complexes (think Pt(II) and Pd(II)) upon dissociation. Similar factors actually stabilize starting 18-electron complexes, making them less reactive in dissociative substitution reactions. d6 octahedral complexes are particularly happy, and react most slowly in dissociative substitutions. The three most common types of 18-electron complexes, from fastest to slowest at dissociative substitution, are:

$$d^8 \text{ TBP} > d^{10} \text{ tetrahedral} > d^6 \text{ octahedral}$$

Destabilization of the starting complex is commonly accomplished by adding steric bulk to its ligands. Naturally, dissociation relieves steric congestion in the starting complex. Chelation has the opposite effect, and tends to steel the starting complex against dissociation.



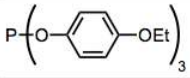
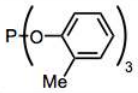
L	Cone Angle	K_d
$P(OEt)_3$	109	$< 10^{-10}$
	128	$6 * 10^{-10}$
$P(Oi\text{-}Pr)_3$	130	$2.7 * 10^{-5}$
	141	$4 * 10^{-2}$
PPh_3	145	huge

Figure **7.1.1.9**: As steric bulk on the ligand increases, dissociation becomes more favorable. (Michael Evans)

I plan to cover the "quirky" methods in a post of their own, but these include strategies like N-oxides for CO removal, photochemical cleavage of the metal–departing ligand bond, and the use of silver cation to abstract halide ligands. Oxidation and reduction can also be used to encourage substitution: 17- and 19-electron complexes are much more reactive toward substitution than their 18-electron analogues.

Associative Substitutions

Despite the sanctity of the 18-electron rule in organometallic chemistry, a wide variety of stable complexes possess fewer than 18 total electrons at the metal center. Perhaps the most famous examples of these complexes are 14- and 16-electron complexes of group 10 metals (Ni, Pt, Pd). Ligand substitution in complexes of this class typically occurs via an associative mechanism, involving approach of the incoming ligand to the complex before departure of the leaving group. If we keep this principle in mind, it seems easy enough to predict when ligand substitution is likely to be associative. But how can we spot an associative mechanism in experimental data, and what are some of the consequences of this mechanism?

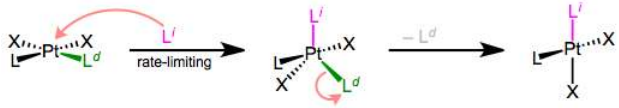


Figure **7.1.1.2**: Associative substitution. (Michael Evans)

The prototypical mechanism of associative ligand substitution. The first step is rate-determining. A typical mechanism for associative ligand substitution is shown above. It should be noted that square pyramidal geometry is also possible for the intermediate, but is less common. Let's begin with the kinetics of the reaction.

Reaction Kinetics for Associative Reactions

Reaction kinetics are commonly used to elucidate organometallic reaction mechanisms, and ligand substitution is no exception. Different mechanisms of substitution may follow different rate laws, so plotting the dependence of reaction rate on concentration often allows us to distinguish mechanisms. Associative substitution's rate law is analogous to that of the S_N2 reaction—rate depends on the concentrations of both starting materials.

$$L_nM\text{–}L^d + L_i \rightarrow L_nM\text{–}L_i + L^d \tag{7.1.1.1}$$

$$\frac{d[L_nM\text{–}L^i]}{dt} = rate = k_1[L_nM\text{–}L^d][L^i] \tag{7.1.1.2}$$

The easiest way to determine this rate law is to use pseudo-first-order conditions. Although the rate law is second order overall, if we could somehow render the concentration of the incoming ligand unchanging, the reaction would appear first order. The observed rate constant under these conditions reflects the constancy of the incoming ligand's concentration ($k_{obs} = k_1[L^i]$, where both k_1 and $[Li]$ are constants). How can we make the concentration of the incoming ligand invariant, you ask? We can drown the reaction in ligand to achieve this. The teensy weensy bit actually used up in the reaction has a negligible effect on the concentration of the "sea" of starting ligand we began with. The observed rate is equal to $k_{obs}[L_nM\text{–}L^d]$, as shown by the purple trace below. By

determining k_{obs} at a variety of $[L^i]$ values, we can finally isolate k_1, the rate constant for the slow step. The red trace below at right shows the idea.

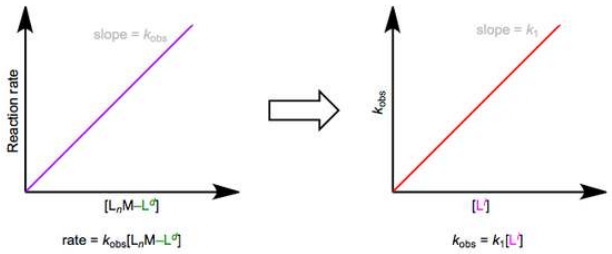


Figure 7.1.1.3: Associative substitution under pseudo-first-order conditions. The reaction is "swamped out" with incoming ligand. (Michael Evans)

In many cases, the red trace ends up with a non-zero y-intercept…curious, if we limit ourselves to the simple mechanism shown in the first figure of this post. A non-zero intercept suggests a more complex mechanism. We need to add a new term (called k_s for reasons to become clear shortly) to our first set of equations:

$$rate = (k_1[L_i] + k_s)[L_nM–L^d] \tag{7.1.1.3}$$

$$k_{obs} = k_1[L_i] + k_s \tag{7.1.1.4}$$

The full rate law suggests that some other step (with rate ks[LnM–Ld]) independent of incoming ligand is involved in the mechanism. To explain this observation, we can invoke the solvent as a reactant. Solvent can associate with the complex first in a slow step, then incoming ligand can displace the solvent in a fast step. Solvent concentration doesn't enter the rate law because, well, it's drowning the reactants and its concentration undergoes negligible change! An example of this mechanism in the context of Pt(II) chemistry is shown below.

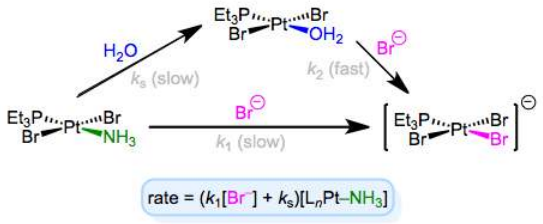


Figure 7.1.1.4: Associative substitution with solvent participation—a head-scratching mechanism for many an organometallic grad student! (Michael Evans)

As an aside, it's worth mentioning that the entropy of activation of associative substitution is typically negative. Entropy decreases as the incoming ligand and complex come together in the rate-determining step. Dissociative substitution shows the opposite behavior: loss of the departing ligand in the RDS increases entropy, resulting in positive entropy of activation.

Stereochemistry of Associative Substitution

As we saw in discussions of the trans effect, the entering and departing ligands both occupy equatorial positions in the trigonal bipyramidal intermediate. Microscopic reversibility is to blame: the mechanism of the forward substitution (displacement of the leaving by the incoming ligand) must be the same as the mechanism of the reverse reaction (displacement of the incoming by the leaving ligand). This can be a confusing point, so let's examine an alternative mechanism that violates microscopic reversibility.

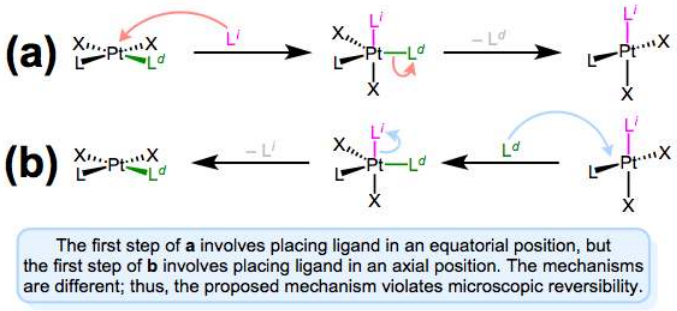


Figure 7.1.1.5: A mechanism involving approach to an axial position and departure from an equatorial position violates microscopic reversibility. Forward and reverse reactions a and b differ! (Michael Evans)

The figure above shows why a mechanism involving axial approach and equatorial departure (or vice versa) is not possible. The forward and reverse reactions differ, in fact, in both steps. In forward mechanism a, the incoming ligand enters an axial site. But in the reverse reaction, the incoming ligand (viz., the departing ligand in mechanism a) sits on an equatorial site. The second steps of each mechanism differ too—a involves loss of an equatorial ligand, while b involves loss of an axial ligand. Long story short, this mechanism violates microscopic reversibility. And what about a mechanism involving axial approach and axial departure? Such a mechanism is unlikely on electronic grounds. The equatorial sites are more electron rich than the axial sites, and σ bonding to the axial d_{z^2} orbital is expected to be strong. Intuitively, then, loss of ligand from an axial site is less favorable than loss from an equatorial site.

I know what you're thinking: what the heck does all of this have to do with stereochemistry? Notice that, in the equatorial-equatorial mechanism (first figure of this post), the axial ligands don't move at all. The configuration of the starting complex is thus retained in the product. Although retention is "normal," complications often arise because five-coordinate TBP complexes—like other odd-coordinate organometallic complexes—are often fluxional. Axial and equatorial ligands can rapidly exchange through a process called Berry pseudorotation, which resembles the axial ligands "cutting through" a pair of equatorial ligands like scissors (animation!). Fluxionality means that all stereochemical bets are off, since any ligand can feasibly occupy an equatorial site. In the example below, the departing ligand starts out cis to L, but the incoming ligand ends up trans to L.

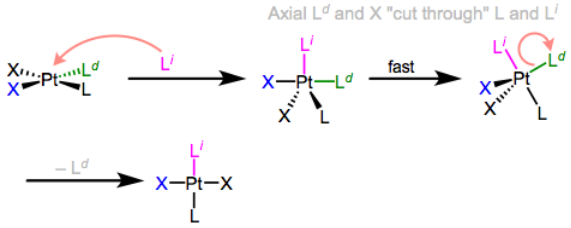


Figure 7.1.1.6: Berry pseudorotation in the midst of associative ligand substitution. (Michael Evans)

Associative Substitution in 18-electron Complexes?

Associative substitution can occur in 18-electron complexes if it's preceded by the dissociation of a ligand. For example, changes in the hapticity of cyclopentadienyl or indenyl ligands may open up a coordination site, which can be occupied by a new ligand to kick off associative substitution. An allyl ligand may convert from its π to σ form, leaving an open coordination site where the π bond left. A particularly interesting case is the **nitrosyl ligand**—conversion from its linear to bent form opens up a site for coordination of an external ligand.

Summary of Associative Substitution

Associative ligand substitution is common for complexes with 16 total electrons or fewer. The reaction is characterized by a second-order rate law, the possibility of solvent participation, and a trigonal bipyramidal intermediate that is often fluxional. An open coordination site is essential for associative substitution, but such sites are often hidden in the dynamism of 18-electron complexes with labile ligands.

Dr. Michael Evans (Georgia Tech)

Quirky Substitutions

Over the years, a variety of "quirky" substitution methods have been developed. All of these have the common goal of facilitating substitution in complexes that would otherwise be inert. It's an age-old challenge: how can we turn a stable complex into something unstable enough to react? Photochemical excitation, oxidation/reduction, and radical chains all do the job, and have all been well studied. We'll look at a few examples in this post—remember these methods when simple associative or dissociative substitution won't get the job done.

Photochemical Substitution

Substitution reactions of dative ligands—most famously, CO—may be facilitated by photochemical excitation. We just discussed the photochemically-activated dissociation of CO from ironpentacarbonyl above; that reaction is often used to accomplish substitution of a CO ligand. Other CO complexes also undergo photochemically-activated CO substitution reactions. Two examples are shown below. The first reaction yields only monosubstituted product without ultraviolet light, even in the presence of a strongly donating phosphine.

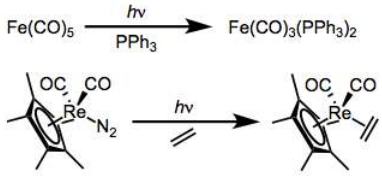


Figure 7.1.1.10:Dissociative photochemical substitutions of CO and dinitrogen. (Michael Evans)

All signs point to dissociative mechanisms for these reactions (the starting complexes have 18 total electrons each). Excitation, then, must increase the M–L antibonding character of the complex's electrons; exactly how this increase in antibonding character happens has been a matter of some debate. Originally, the prevailing explanation was that the LUMO bears M–L antibonding character, and excitation kicks an electron up from the HOMO to the LUMO, encouraging cleavage of the M–L bond. A more recent, more subtle explanation backed by calculations supports the involvement of a metal-to-ligand charge-transfer state along with the "classical" ligand-field excited state.

Oxidation/Reduction

Imagine a screaming baby without her pacifier—that's a nice analogy for an odd-electron organometallic complex. Complexes bearing 17 and 19 total electrons are much more reactive toward substitution than their even-electron counterparts. Single-electron oxidation and reduction ("popping out the pacifier," if you will) can thus be used to efficiently turn on substitution. As you might expect, oxidation and reduction work best on electron-rich and electron-poor complexes, respectively. The Mn complex in the oxidative example below, for instance, includes a strongly donating MeCp group (not shown).

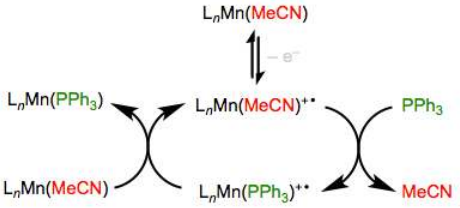


Figure 7.1.1.11: Oxidation accelerates substitution in electron-rich complexes through a chain process. (Michael Evans)

Reduction works well for electron-poor metal carbonyl complexes, which are happy to accept an additional electron.

There is a two-electron oxidation method that's also worth knowing: the oxidation of CO with amine oxides. This nifty little method releases carbon dioxide, amine, and an unsaturated complex that may be quenched by a ligand hanging around. The trick is addition to the CO ligand followed by elimination of the unsaturated complex. As the oxidized CO2 and reduced amine float away, the metal complex finds another ligand.

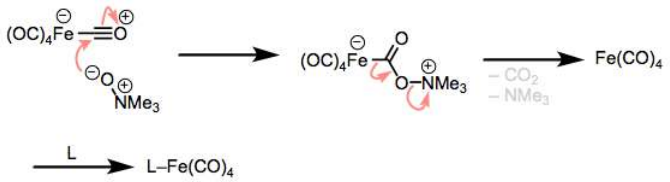


Figure 7.1.1.12: Oxidation of CO with amine oxides. A fun method for dissociative substitution of metal carbonyls! (Michael Evans)

Radical Chain Processes

Atom abstraction from 18-electron complexes produces neutral 17-electron intermediates, which are susceptible to ligand substitution via radical chain mechanisms. The fact that the intermediates are neutral distinguishes these methods from oxidation-based methods. First-row metal hydrides are great for these reactions, owing to their relatively weak M–H bonds. One example is shown below.

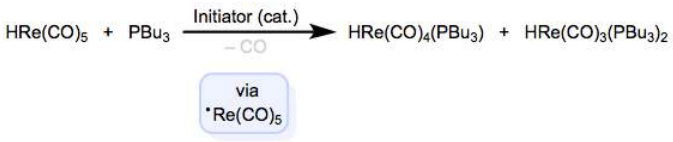


Figure 7.1.1.13: Radical-chain substitution involving atom abstraction. (Michael Evans)

After abstraction of the hydrogen atom by initiator, substitution is rapid and may occur multiple times. Propagation begins anew when the substituted radical abstracts hydrogen from the starting material to regenerate the propagating radical and form the product. These quirky methods are nice to have in your back pocket when you're backed into a synthetic corner—sometimes, conventional associative and dissociative substitution just won't do the job. In the next post, we'll press on to oxidative addition.

Template:Evans

This page titled 7.1.1: Ligand Dissociation and Substitution is shared under a CC BY-NC-SA 4.0 license and was authored, remixed, and/or curated by Kathryn Haas.

- **4.4: Ligand substitution** by Michael Evans is licensed CC BY-NC-SA 4.0.
- **4.3: Dissociative Ligand Substitution Reactions** by Michael Evans is licensed CC BY-NC-SA 4.0.
- **4.2: Associative Ligand Substitution** by Michael Evans is licensed CC BY-NC-SA 4.0.
- **4.10: Quirky Ligand Substitutions** by Michael Evans is licensed CC BY-NC-SA 4.0.

7.1.2: Oxidative Addition

An **oxidative addition** is a reaction in which the coordination number and the oxidation state of the metal ion both increase by 2. In other words, the metal becomes oxidized by two electrons as the coordination number increases by 2 ligands. The microscopic reverse of oxidative addition is reductive elimination (discussed in the next section).

Oxidative addition can occur in a cis- or trans-fashion. A cis-addition means that two ligands are added so that they have cis-orientation to each other after the reaction is complete. A trans-addition implies that two new ligands are in opposite, trans-position after they have been added. We can further distinguish between mononuclear and dinuclear additions. Mononuclear addition involves a complex with a single metal. Dinuclear additions are additions to a metal-metal bond. The addition cleaves the metal-metal bond and adds one ligand to each fragment.

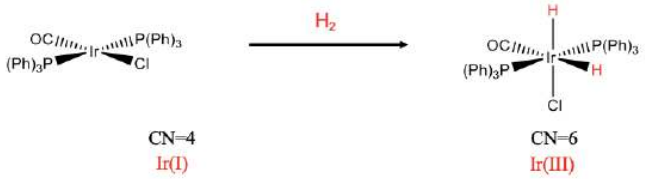


Figure **7.1.2.1**: Mononuclear oxidative cis-addition (Attribution: A. Vedernikov, U Maryland (modified))

Let's explore a few examples. The first example is a mononuclear cis-addition (Fig. **7.1.2.1**). In the reaction we add dihydrogen to a square planar iridium complex. After the reaction there are two additional hydrido ligands, and the coordination number has increased from 4 to 6. We can see that the two hydrido ligands are oriented in cis-fashion relative to each other. We can verify that the addition of the hydrido ligands oxidized the metal by determining the oxidation number of the metal before and after the reaction. There are three neutral ligands and one negatively charged chloro ligand. There is no overall charge at the complex. This means that the oxidation number of Ir is +1. After the reaction, there are the two hydrido ligands that have both a -1 charge. Remember, we get the charge at a ligand by cleaving the metal-ligand bond so that all electrons in the bond get assigned to the ligand. This means the oxidation number must be increased by +2, and is +3 after the reaction.

We can rationalize why the addition occurs in cis-fashion and not in trans-fashion. The two hydrido ligands are the smallest ligands, therefore, steric repulsion is minimized in the complex is minimized when the two hydrido ligands are in cis-position.

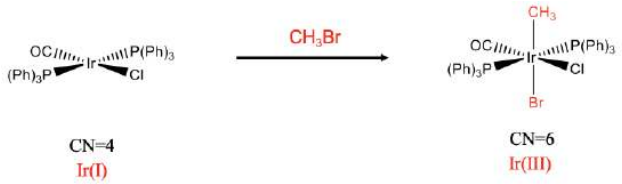


Figure **7.1.2.2**: Mononuclear oxidative trans-addition (Attribution: A. Vedernikov, U Maryland (modified))

The second example is a mononuclear trans-addition (Fig. **7.1.2.2**). In this reaction CH_3Br is added to the iridium complex. In this case the two new ligands, a CH_3 and the Br group are in opposite position. Again, the coordination number increases from four to six. We can again verify that an oxidation has occurred by analyzing the oxidation number of Ir. As previously determined, the oxidation number of iridium in the reactant complex is +1. Let us analyze the product complex. The chloro ligand and the bromo ligand have a 1- charge. In addition to that also the CH_3 ligand has a 1- charge assuming that we treat the Ir-C bond as a dative bond. Thus, the oxidation number of Ir must be +3 to give a neutral complex.

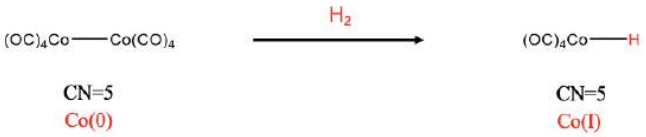


Figure **7.1.2.3**: Dinuclear addition (Attribution: A. Vedernikov, U Maryland (modified))

The third example is a dinuclear addition (Fig. **7.1.2.3**). This addition is neither cis nor trans because it cleaves a metal-metal bond, and the one new ligand is added to each fragment. In the example the Co-Co bond of the dicobalt octacarbonyl gets cleaved upon

the reaction with dihydrogen, and two $HCo(CO)_4$ complexes with Co-H bonds form. In this case the coordination number does not increase. Both the reactant and the products have the coordination number 5. We can see that an oxidation of Co has occurred by comparing the oxidation numbers. In the reactant the oxidation number of Co is zero because all CO ligands are neutral and the complex is overall neutral. In the carbonyl hydride product, Co has the oxidation number +1, because the hydrido ligand has a 1- charge.

Oxidative Additions with Intact Ligands

In the previous examples, the ligands that reacted with the complexes lost their integrity. The H-H bond in the H_2 molecule cleaved to form the hydrido ligands, and the C-Br bond in CH_3Br was cleaved to form separate Br and methyl ligands. Not all ligands lose their integrity upon their addition, in particular when they contain multiple bonds. These ligands are called intact ligands. In these cases the bond order *between two atoms in the ligand* is decreased, but the bond order is still at least 1. For example, the alkyne ligand shown belo decreases from a carbon-carbon bond order of three to a bond order of two after it binds to Pt.

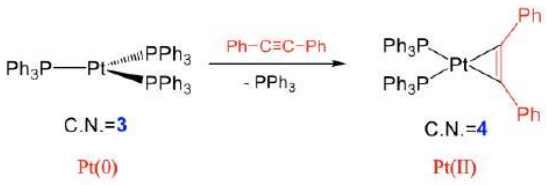


Figure **7.1.2.4**: Oxidative addition with intact ligands (Attribution: A. Vedernikov, U Maryland (modified))

Examples for intact ligands are are alkenes, alkynes, O_2, etc. In an oxidative addition with an alkyne for example, the alkyne binds side-on to the transition metal under the formation of two metal-C single bonds, and the reduction of the bond order within the alkyne from 3 to 2 (Fig. **7.1.2.4**). In the shown reaction, a diphenyl ethine molecule adds to tris(triphenyl phosphine) platinum under the formation of two Pt-C single bonds. The C-C triple bond in the ligand becomes a double bond. This reaction occurs under loss of one of the three triphenyl phosphine ligands. The coordination number at the metal increases from 3 to 4. We can again show that the reaction is oxidative by comparing the oxidation numbers of the metal. In the reactant, Pt has the oxidation number 0 because the three triphenyl phosphine ligands have no charge and the complex has overall no charge. After the reaction, the oxidation number of Pt is +2. This is because when we assign the four electrons of the two Pt-C single bonds to the ligand, the ligand becomes a $(Ph\text{-}C{=}C\text{-}Ph)^{2-}$ ligand with each C atom carrying a 1- charge. Because the product complex is overall neutral, the oxidation number of Pt is +2.

Nucleophilic Displacement Reactions

Another important reaction is the nucleophilic displacement reaction. This type of reaction can be classified as an oxidative addition although it does not strictly meet the definnition. In these reactions a metal complex (typically an anion) acts as a nucleophile. A ligand is added, but no electrons are added to the complex. The reactions can be extremely useful for the synthesis of organic compounds. The utility results mostly from the fact that an organic electrophile is turned into a nucleophile.

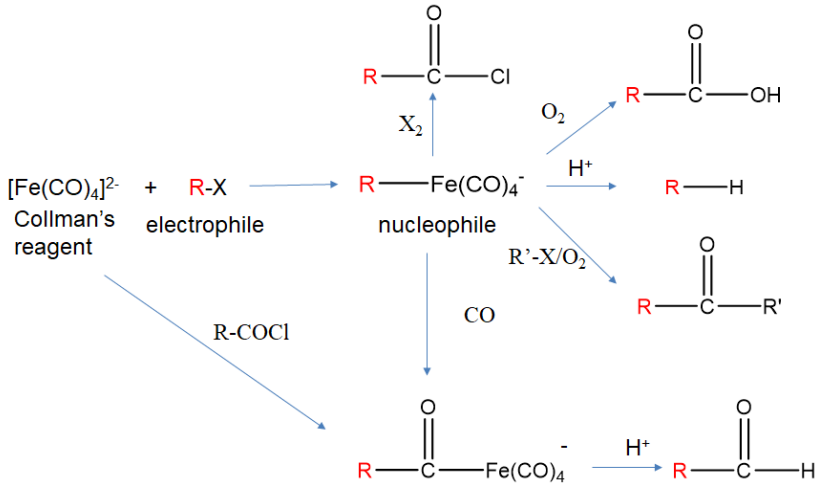


Figure 7.1.2.5: Mononuclear oxidative trans-addition (Attribution: A. Vedernikov, U Maryland (modified)): Examples of nucleophilic displacement reactions

For example, tetracarbonyl ferrate (2-), also known as Collman's reagent reacts with alkyl halides to form alkyl tetracarbonyl ferrate (-) (Fig. 7.1.2.5). We can check that the addition of the alkyl group did not add any electrons by counting the electrons before and after the reaction. The $Fe(CO)_4^{2-}$ anion is an 18e complex. Applying the neutral atom method to the electron counting in $[R\text{-}Fe(CO)_4]^-$ means that Fe contributes 8e, the 1- charge adds 1e, the CO ligands 4x2=8 electrons and the alkyl ligand 1e. This gives 8+1+8+1=18 electrons. Also the oxidation number of Fe has not changed upon the addition of the ligand. It is -2 before and after the reaction.

In the alkyltetracarbonyl ferrate (1-) anion, the group R which was formerly an electrophile in R-X, can now act as a nucleophile due to the fact that the Fe-C bond is polarized toward the C-atom. As a nucleophile it can for instance react with protons to form an alkane. It can also react with oxygen to form a carboxylic acid. In the presence of another alkyl halide R'-X it can form a ketone R-C(O)-R'. It can also insert CO into the Fe-C bonding in a so-called migratory insertion reaction, and the reaction product can react with acid to form an aldehyde. With dihalogens X_2 it can form acyl chloride. Collman's reagent cannot only add alkyl halides by also acyl halides to form acyl tetracarbonyl ferrates (-).

This page titled 7.1.2: Oxidative Addition is shared under a CC BY-NC-SA 4.0 license and was authored, remixed, and/or curated by Kathryn Haas.

- **12.1: Organometallic reactions** by Kai Landskron is licensed CC BY 4.0.

7.1.3: Reductive Elimination

Reductive Elimination Reactions

Reductive elimination is the microscopic reverse of oxidative addition. The reductive elimination can only occur when the two ligands to be eliminated are in cis-position.

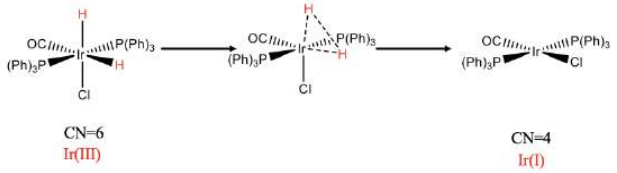


Figure **7.1.3.1**: Reductive elimination (Attribution: A. Vedernikov, U Maryland.)

For instance the previously discussed oxidative cis-addition of H_2 to the iridium complex is reversible, and the reverse is called the reductive elimination (Fig. **7.1.3.1**). The cis-orientation of the two hydrido ligands is necessary to form an H-H bond. The reaction can be thought of going along a reaction path in which the Ir-H bonds become gradually larger and and the H-H distance gradually smaller until the H_2 molecule is eliminated from the complex.

During reductive elimination, the electrons in the M–X bond head toward ligand Y, and the electrons in M–Y head to the metal. The eliminating ligands are always X-type! On the whole, the oxidation state of the metal decreases by two units, two new open coordination sites become available, and an X–Y bond forms. What does the change in oxidation state suggest about changes in electron density at the metal? As suggested by the name “reductive,” the metal gains electrons. The ligands lose electrons as the new X–Y bond cannot possibly be polarized to both X and Y, as the original M–X and M–Y bonds were. Using these ideas, you may already be thinking about reactivity trends in reductive elimination…hold that thought.

It’s been observed in a number of cases that a ligand dissociates from octahedral complexes before concerted reductive elimination occurs. Presumably, dissociation to form a distorted TBP geometry brings the eliminating groups closer to one another to facilitate elimination.

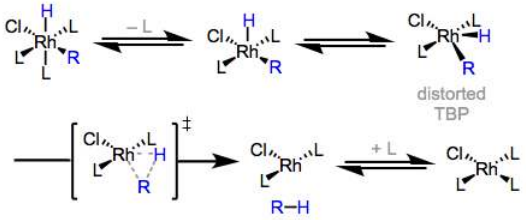


Figure **7.1.3.2**: Reductive elimination is faster from five-coordinate than six-coordinate complexes. (Michael Evans)

Square planar complexes may either take on an additional fifth ligand or lose a ligand to form an odd-coordinate complex before reductive elimination. Direct reductive elimination without dissociation or association is possible, too.

Reactivity trends in reductive elimination are opposite those of oxidative addition. More electron-rich ligands bearing electron-donating groups react more rapidly, since the ligands lose electron density as the reaction proceeds. More electron-poor metal centers—bearing π-acidic ligands and/or ligands with electron-withdrawing groups—react more rapidly, since the metal center gains electrons. Sterically bulky ancillary ligands promote reductive elimination since the release of X and Y can “ease” steric strain in the starting complex. Steric hindrance helps explain, for example, why coordination of a fifth ligand to a square planar complex promotes reductive elimination even though coordination increases electron density at the metal center. A second example: trends in rates of reductive eliminations of alkanes parallel the steric demands of the eliminating ligands: C–C > C–H > H–H.

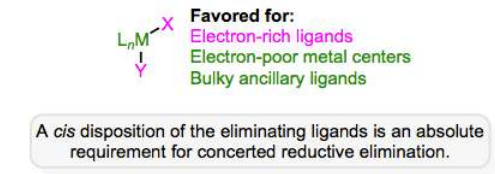


Figure **7.1.3.3**: Reactivity trends for reductive eliminations. (Michael Evans)

Mechanistic trends for reductive elimination actually parallel trends in mechanisms of oxidative addition, since these two reactions are the microscopic reverse of one another. Non-polar and moderately polar ligands react by concerted or radical mechanisms; highly polarized ligands and/or very electrophilic metal complexes react by ionic (S_N2) mechanisms. The thermodynamics of reductive elimination must be favorable in order for it to occur! Most carbon–halogen reductive eliminations, for example, are thermodynamically unfavorable (this has turned out to be a good thing, especially for cross-coupling reactions).

Reductive elimination is an important step in many catalytic cycles—it usually comes near the "end" of catalytic mechanisms, just before product formation. For some catalytic cycles it's the turnover-limiting step, making it very important to consider! Hydrocyanation is a classic example; in the mechanism of this reaction, reductive elimination of C–CN is the slow step. Electron-poor alkyl ligands, derived from electron-poor olefins like unsaturated ketones, are bad enough at reductive elimination to prevent turnover altogether! Of course, the electronegative CN ligand is not helping things either…how would you design the ancillary ligands L to speed up this step?

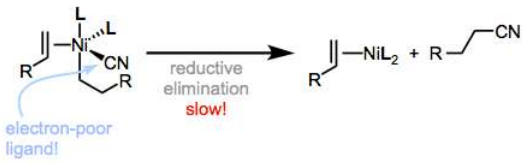


Figure **7.1.3.4**: Reductive elimination is the turnover-limiting step of hydrocyanation. How would you design L to speed it up? (Michael Evans)

Dr. Michael Evans (Georgia Tech)

Dr. Kai Landskron (Lehigh University). If you like this textbook, please consider to make a donation to support the author's research at Lehigh University: Click Here to Donate.

This page titled 7.1.3: Reductive Elimination is shared under a CC BY-NC-SA 4.0 license and was authored, remixed, and/or curated by Kathryn Haas.

- **12.1: Organometallic reactions** by Kai Landskron is licensed CC BY 4.0.
- **4.11: Reductive Elimination- General Ideas** by Michael Evans is licensed CC BY-NC-SA 4.0.

7.1.4: Sigma Bond Metathasis

Metal compounds with d^0 electron count are able to activate C-H bonds through σ bond metathesis reactions. **σ-bond metathesis** is a chemical reaction wherein a metal-ligand σ bond undergoes metathesis (exchange of parts) with the sigma bond in some other reagent. The reaction is illustrated by the exchange of lutetium(III) methyl complex with a hydrocarbon (R-H) (Figure **7.1.4.1**). The oxidation state of the metal ion does not change during the reaction. This reactivity was first observed by Patricia L. Watson, a researcher at duPont.

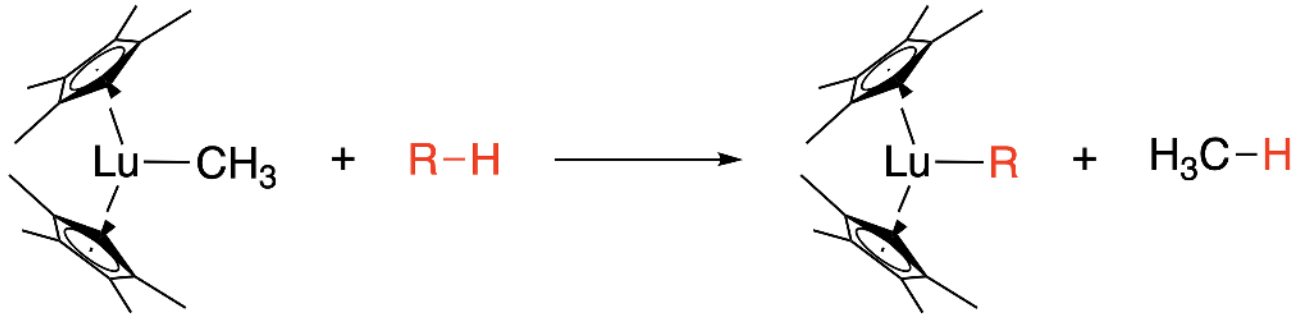


Figure **7.1.4.1**: Example of σ bond metathesis; exchange of lutetium(III) methyl complex with a hydrocarbon. The R-H bond is activated and a new C-H bond is created. (CC-BY-SA; Kathryn Haas)

The reaction is mainly observed for complexes of metals with d^0 electron configuration, e.g. complexes of Sc(III), Zr(IV), Nb(IV), Ta(V), etc. Complexes of the f-block elements also participate, regardless of the number of f-electrons. For metals unsuited for redox, sigma bond metathesis provides a pathway for introducing substituents.

The details of the reaction mechanism are somewhat a matter of debate, however a currently accepted model is that it precedes through a cycloaddition and via a "kite-shaped" transition state (Figure **7.1.4.2**). Indeed, the rate of the reaction is characterized by a highly negative entropy of activation, indicating an ordered transition state.

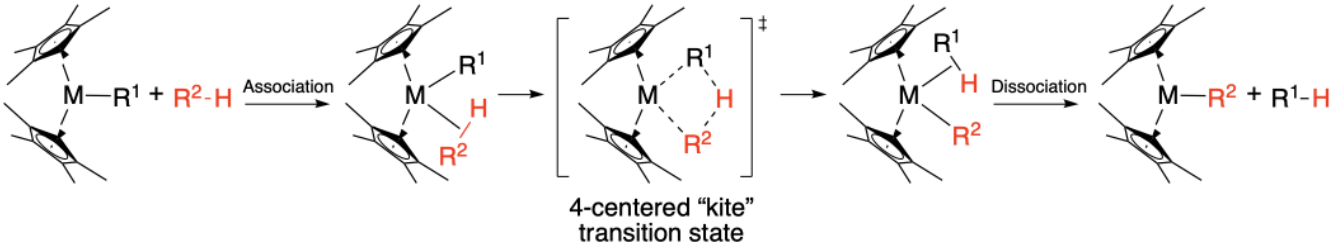


Figure **7.1.4.2**: The currently accepted mode for the mechanism of σ bond metathesis involving a kite-like transition state. (CC-BY-SA; Kathryn Haas)

The reaction attracted much attention because hydrocarbons are normally unreactive substrates, whereas some sigma-bond metatheses are facile. Unfortunately the reaction does not readily allow the introduction of functional groups. It has been suggested that dehydrocoupling reactions proceed via sigma-bond metathesis.

Sources:

- https://en.Wikipedia.org/wiki/Sigma-bond_metathesis
- *Waterman, Rory (2013). "σ-Bond Metathesis: A 30-Year Retrospective". Organometallics. **32**: 7249–7263. doi:10.1021/om400760k.*

This page titled 7.1.4: Sigma Bond Metathasis is shared under a CC BY-NC-SA 4.0 license and was authored, remixed, and/or curated by Kathryn Haas.

7.1.5: Application of Pincer Ligands

Pincer ligands are chelating agents that bind tightly to three adjacent coplanar sites of a metal complex. Stoichiometric and catalytic applications of pincer complexes have been studied at an accelerating pace since the mid-1970s.

Pincers often include one anionic, two-electron donor flanked by two neutral, two-electron donor groups. It consists of a rigid, planar backbone, usually consisting of aryl frameworks. The inflexibility of the pincer-metal interaction confers high thermal stability to the resulting complexes. This stability is in part ascribed to the constrained geometry of the pincer, which inhibits ligand exchange and cyclometallation of the pincer. In contrast, cyclometallation is often a significant deactivation process in the case of other types of chelates, in particular limiting their ability to effect C-H bond activation. The pincer ligand also creates a hydrophobic pocket around the reactive coordination site.

There are various types of pincer ligands that are used in transition metal catalysis. Often, they have the same two-electron donor flanking the metal centre, but this is not a requirement. Early examples of pincer ligands were anionic with a carbanion as the central donor site and flanking phosphine donors; these compounds are referred to as **PCP pincers**. Although the most common class of pincer ligands features PCP donor sets, variations have been developed where the phosphines are replaced by thioethers and tertiary amines. Many pincer ligands also feature nitrogenous donors at the central coordinating group position (see figure), such as pyridines. By altering the properties of the pincer ligands, it is possible to significantly alter the chemistry at the metal centre. Changing the hardness/softness of the donor, using electron-withdrawing groups (EWGs) in the backbone, and the altering the steric constraints of the ligands are all methods used to tune the reactivity at the metal centre.

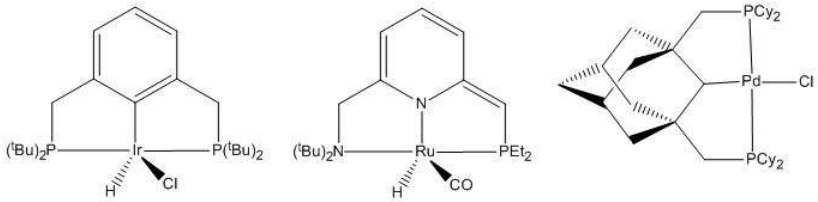


Figure **7.1.5.1**: Examples of transition metal pincer complexes. (Scott0, Examples pincer complexes, CC BY-SA 3.0)

The Role of Pincer Complexes in Catalysis

Suzuki-Miyaura coupling

Pincer complexes have been shown to catalyse Suzuki-Miyaura coupling reactions, a versatile carbon-carbon bond forming reaction. Suzuki-Miyaura coupling (or Suzuki coupling) is a metal catalyzed reaction, typically with Pd, between an alkenyl (vinyl), aryl, or alkynyl organoborane (boronic acid or boronic ester, or special cases with aryl trifluoroborane) and halide or triflate under basic conditions. This reaction is used to create carbon-carbon bonds to produce conjugated systems of alkenes, styrenes, or biaryl compounds (Scheme 1).



R^1= aryl, alkene (vinyl), alkyne **R**^{2}= H (boronic acid), alkyl (boronic ester) **R**^{3}= aryl, alkene (vinyl), alkyne

X = halide (I, Br, Cl*) triflate (-OTf) *Cl requires special conditions for activation

Scheme **7.1.5.2**: General reaction scheme of Suzuki cross coupling reaction. (Suzuki-Miyaura Coupling)

Modified conditions have demonstrated reactivity with less reactive substrates such as alkyl boranes (BR_3) or aryl or alkenyl chlorides by amending the base and ligands employed.

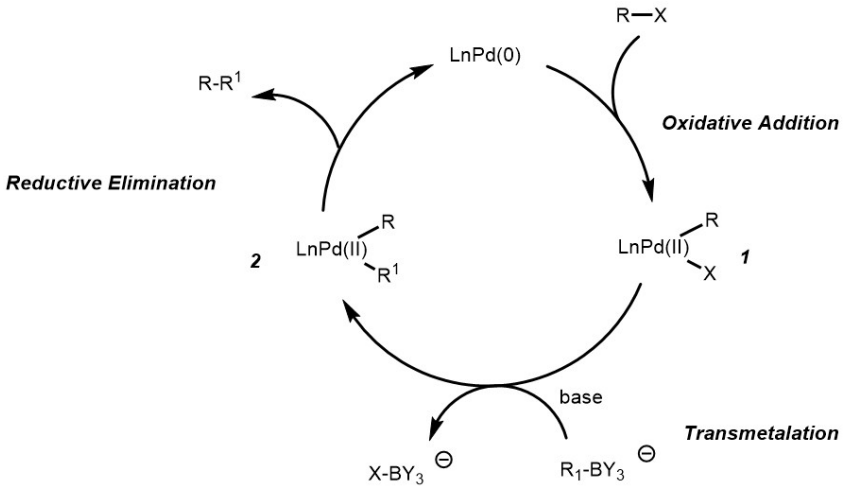
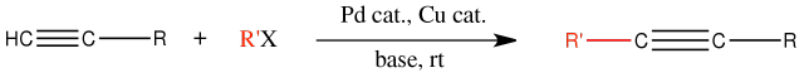


Figure 7.1.5.3: Suzuki coupling proceeds via three basic steps: oxidative addition, transmetallation, and reductive elimination. (Suzuki-Miyaura Coupling)

Sonogashira Coupling

The Sonogashira reaction (also called the Sonogashira-Hagihara reaction) is the cross coupling of aryl or vinyl halides with terminal alkynes to generate conjugated enynes and arylalkynes (Scheme 1). The reaction typically proceeds in the presence of a palladium(0) catalyst, a copper(I) cocatalyst, and an imine base. Alternative procedures describe Sonogashira coupling reactions performed without the Cu(I) cocatalyst.



R' = Aryl, Vinyl

X = I, Br, Cl, OTf

Scheme 7.1.5.4: *General reaction for Sonogashira Coupling*. (Jcap17, Sonogashira Cross-Coupling Reaction, CC BY-SA 3.0)

Dehydrogenation of alkanes

Alkanes undergo dehydrogenation at high temperatures. Typically this conversion is promoted heterogeneously because typically homogeneous catalysts do not survive the required temperatures (~200 °C) The corresponding conversion can be catalyzed homogeneously by pincer catalysts, which are sufficiently thermally robust. Proof of concept was established in 1996 by Jensen and co-workers. They reported that an iridium and rhodium pincer complex catalyze the dehydrogenation of cyclooctane with a turnover frequency of 12 min^{-1} at 200 °C. They found that the dehydrogenation was performed at a rate two orders of magnitude greater than those previously reported. The iridium pincer complex was also found to exhibit higher activity than the rhodium complex. This rate difference may be due to the availability of the Ir(V) oxidation state which allows stronger Ir-C and Ir-H bonds.

The homogeneously catalyzed process can be coupled to other reactions such as alkene metathesis. Such tandem reactions have not been demonstrated with heterogeneous catalysts.

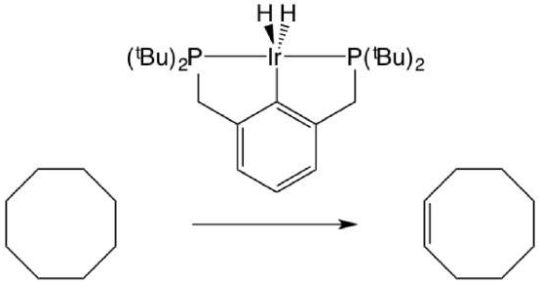


Figure 7.1.5.5: Iridium pincer complex catalyzing the dehydrogenation of cyclooctane to cyclooctene. (Paul Gray, Iridium Pincer Catalysis, CC BY-SA 3.0)

Sources:

- https://en.Wikipedia.org/wiki/Transi...pincer_complex
- Sonogashira Coupling
- Suzuki-Miyaura Coupling

This page titled 7.1.5: Application of Pincer Ligands is shared under a CC BY-NC-SA 4.0 license and was authored, remixed, and/or curated by Kathryn Haas.

SECTION OVERVIEW

7.2: Reactions Invloving Modification of Unsaturated Ligands

This section will describe organometallic reactions that involve modification of unsaturated ligands.

7.2.1: Introduction to Insertion

7.2.2: CO Insertions (Alkyl Migration)

7.2.3: Migratory Insertion-1,2-Insertions

7.2.4: β-Elimination Reactions

7.2.5: Abstraction and Addition

This page titled 7.2: Reactions Invloving Modification of Unsaturated Ligands is shared under a CC BY-NC-SA 4.0 license and was authored, remixed, and/or curated by Kathryn Haas.

7.2.1: Introduction to Insertion

We've seen that the metal-ligand bond is generally polarized toward the ligand, making the ligand nucleophilic. The ligand is especially nucleophilic in the case of X-type (anionic) ligands. When a nucleophilic, X-type ligand is positioned *cis* to a neutral, unsaturated ligand (L) in an organometallic complex, a migratory insertion reaction can occur. In a **migratory insertion reaction**, an anionic ligand (X^-) and a neutral unsaturated ligand (L) couple to form a new anionic ligand (^-LX)*thatisattachedtothesamemetal*(*Figure*\(7.2.1.1). The overall result is that an M-X bond is broken and M and X are added across a π bond of L. There is no change in oxidation state at the metal (unless the ligand is an alkylidene/alkylidyne), but the total electron count of the complex decreases by two during the actual insertion event.

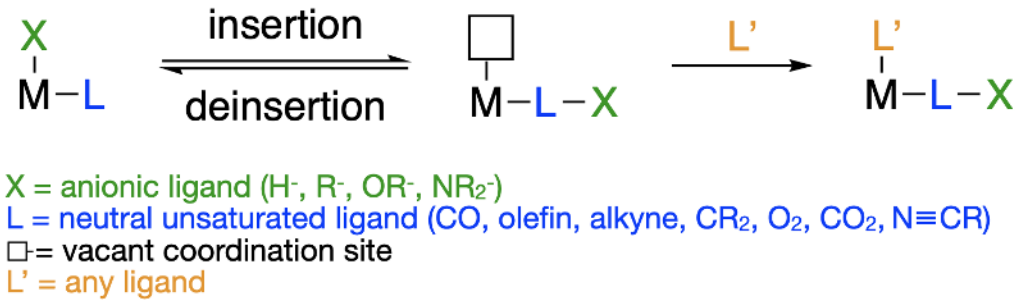


Figure 7.2.1.1: Migratory insertion (CC-BY-SA; Kathryn Haas)

The migratory insertion results in a decrease in coordination number and the creation of an open coordination site on the complex. The open coordination site can be filled by an added ligand (L') (Figure 7.2.1.1). The reverse of the insertion reaction is called a **deinsertion**. To drive the chemical equilibrium in the forward (insertion) direction, the reactant neutral ligand (or another neutral ligand) can be added in excess so that the neutral ligand fills the vacancy in the product complex and prevents the reverse (deinsertion) reaction. Typical neutral, unsaturated ligands are CO, olefins, alkynes, carbenes, dioxygen, carbon dioxide, and nitriles. Typical anionic ligands are hydrido, alkyl, aryl, alkoxy, and amido-ligands Figure 7.2.1.1.

The open site may appear where the unsaturated ligand was *or* where the X-type ligand was, depending on which group actually moved (see below). It is more common that the anionic X ligand moves (Figure 7.2.1.2).

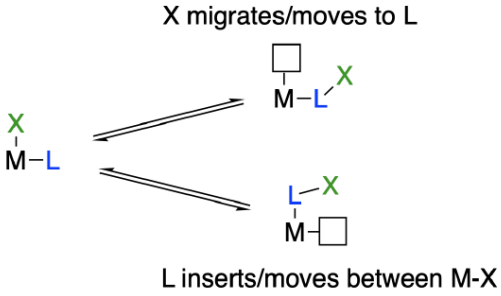


Figure 7.2.1.2: X can migrate onto unsaturated ligand L, or L can move to the original position of X. The former is more common for CO insertions. (CC-BY-SA; Kathryn Haas)

We can distinguish between two types of insertions, which differ in the number of atoms in the unsaturated ligand involved in the step. Insertions of CO, carbenes, and other η^1 unsaturated ligands are called **1,1-insertions** because the X-type ligand moves from its current location on the metal to one spot over, on the atom bound to the metal. η^2 ligands like alkenes and alkynes can also participate in migratory insertion; these reactions are called **1,2-insertions** because the X-type ligand slides two atoms over, from the metal to the distal atom of the unsaturated ligand (Figure 7.2.1.4).

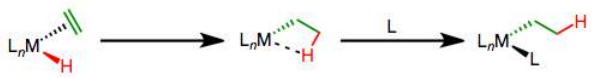


Figure 7.2.1.4: 1,2-insertion of an alkene and hydride. In some cases, an agostic interaction has been observed in the unsaturated intermediate. (Michael Evans)

This is really starting to look like the addition of M and X across a π bond! However, we should take care to distinguish this completely intramolecular process from the attack of a nucleophile or electrophile on a coordinated π system, which is a different beast altogether. Confusingly, chemists often jumble up all of these processes using words like “hydrometalation,” “carbometalation,” “aminometalation,” etc. Another case of big words being used to obscure ignorance! We’ll look at nucleophilic and electrophilic attack on coordinated ligands in separate posts.

This page titled 7.2.1: Introduction to Insertion is shared under a CC BY-NC-SA 4.0 license and was authored, remixed, and/or curated by Kathryn Haas.

- **12.1: Organometallic reactions** by Kai Landskron is licensed CC BY 4.0.

7.2.2: CO Insertions (Alkyl Migration)

One of the most common types of migratory insertions is carbonyl insertion (Figure **7.2.2.3**). The carbonyl insertion produces an acyl group. Notice in the example below that the complex goes from 18 to 16 total electrons after insertion. A dative ligand comes in to fill the empty coordination site. L can be a neutral or anionic ligand, and it can even be the carbonyl oxygen itself. To drive the reaction, the reaction can be carried out in the presence of a neutral ligand like free CO, which occupies the vacant site.

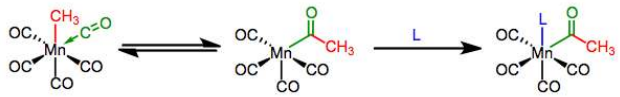


Figure **7.2.2.1**: Migratory insertion into a metal-carbon bond. (Michael Evans)

Reactivity Trends in CO Insertions

Certain conditions *must* be met for migratory insertion to occur: the two ligands undergoing the process must be *cis*, and the complex must be stable with two fewer total electrons. Thermodynamically, the formed Y–X and covalent M–Y bonds must be more stable than the broken M–X and dative M–Y bonds for insertion to be favored. When the opposite is true, the microscopic reverse (**elimination** or **deinsertion**) will occur spontaneously.

Migratory aptitudes for insertion into CO have been studied extensively, and the general conclusion here is “it’s complicated.” A few ligands characterized by remarkably stable metal-ligand bonds don’t undergo insertion for thermodynamic reasons—the M–X bond is just too darn strong. Perfluoroalkyl complexes and metal hydrides are two notable examples. Electron-withdrawing groups on the X-type ligand, which strengthen the M–X bond, slow down insertion (likely for thermodynamic reasons though… Hammond’s postulate in action).

What factors affect the relative speed (kinetics) of favorable insertions? Sterics is one important variable. Both 1,1- and 1,2-insertions can relieve steric strain at the metal center by spreading out the ligands involved in the step. In 1,2-insertions, the X-type ligand removes itself completely from the metal! Unsurprisingly, then, bulky ligands undergo insertions more rapidly than smaller ligands. Complexes of the first-row metals tend to react more rapidly than analogous second-row metal complexes, and second-row metal complexes react faster than third-row metal complexes. This trend fits in nicely with the typical trend in M–C bond strengths: first row < second row < third row. Lewis acids help accelerate insertions into CO by coordinating to CO and making the carbonyl carbon more electrophilic. For a similar reason, CO ligands bound to electron-poor metal centers undergo insertion more rapidly than CO’s bound to electron-rich metals. Finally, for reasons that are still unclear, one-electron oxidation often increases the rate of CO insertion substantially.

Although the thermodynamics of alkene 1,2-insertion are more favorable for metal-carbon than metal-hydrogen bonds, M–H bonds react *much* more rapidly than M–C bonds in 1,2-insertions. This fact has been exploited for olefin hydrogenation, which would be much less useful if it had to complete with olefin polymerization (the result of repeated insertion of C=C into M–C) in the same reaction flask! More on that in the next post.

Stereochemistry in CO Insertions

Migratory insertion steps are full of stereochemistry! Configuration at the migrating alkyl group is retainedduring insertion—a nice piece of evidence supporting a concerted, intramolecular mechanism of migration.

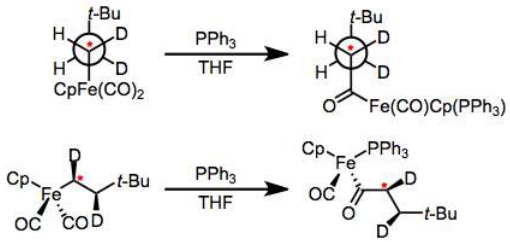


Figure **7.2.2.2**: Migratory insertion occurs with retention of configuration at the migrating alkyl group. Two different views of the same reaction are shown here. (Michael Evans)

What about stereochemistry at the metal center? Migratory insertion may create a stereogenic center at the metal—see the iron example above. Whether the X-type ligand moves onto the unsaturated ligand or *vice versa* will impact the configuration of the product complex. Calderazzo's study of this issue is one of my favorite experiments in all of organometallic chemistry! He took the simple labeled substrate in the figure below and treated it with dative ligand, encouraging insertion. Four products of insertion are possible, corresponding to reaction of the four CO ligands *cis* to the methyl ligand. Try drawing a few curved arrows to wrap your mind around the four possibilities, and consider both CO migration and Me migration as possible at this point.

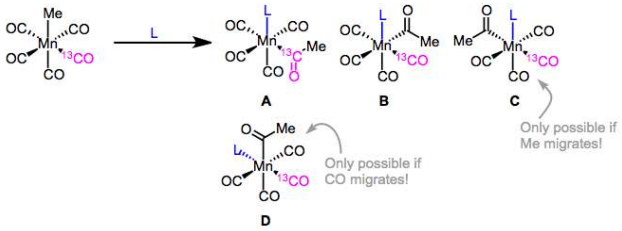


Figure **7.2.2.3**: Insertion of the labeled complex shown could produce four products. Calderazzo did not observe product **D**, supporting a mechanism involving Me migration to CO. (Michael Evans)

Note that product **D** is impossible if we only allow the Me group to migrate—the spot *trans* to the labeled CO is another CO ligand, so that spot can only pick up L if CO migrates (not if Me migrates). On the other hand, product **C** must have come from the migration of Me, since the Me group has moved from a *cis* to a *trans*position relative to the labeled CO in product **C**. Calderazzo observed products **A**, **B**, and **C**, but not **D**, supporting a mechanism involving Me migration. Other experiments since support the idea that most of the time, the alkyl group migrates onto CO. Slick, huh?

I won't address insertions into alkylidenes, alkylidynes, and other one-atom unsaturated ligands in this post, as insertions into CO are by far the most popular 1,1 insertions in organometallic chemistry. In the next post, we'll dig more deeply into 1,2-insertions of alkenes and alkynes. Thanks for reading!

This page titled 7.2.2: CO Insertions (Alkyl Migration) is shared under a CC BY-NC-SA 4.0 license and was authored, remixed, and/or curated by Kathryn Haas.

7.2.3: Migratory Insertion-1,2-Insertions

Insertions of π systems into M-X bonds are appealing in the sense that they establish two new σ bonds in one step, in a stereocontrolled manner. As we saw in the last post, however, we should take care to distinguish these fully intramolecular migratory insertions from intermolecular attack of a nucleophile or electrophile on a coordinated π-system ligand. The reverse reaction of migratory insertion, β-elimination, is not the same as the reverse of nucleophilic or electrophilic attack on a coordinated π system.

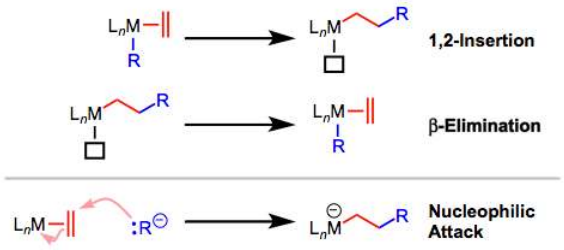


Figure 7.2.3.1: 1,2-Insertion is dinstinct from nucleophilic/electrophilic attack on coordinated ligands. (Michael Evans)

Like 1,1-insertions, 1,2-insertions generate a vacant site on the metal, which is usually filled by external ligand. For unsymmetrical alkenes, it's important to think about site selectivity: which atom of the alkene will end up bound to metal, and which to the other ligand? To make predictions about site selectivity we can appeal to the classic picture of the M–X bond as M + X^-. Asymmetric, polarized π ligands contain one atom with excess partial charge; this atom hooks up with the complementary atom in the M–R bond during insertion. Resonance is our best friend here!

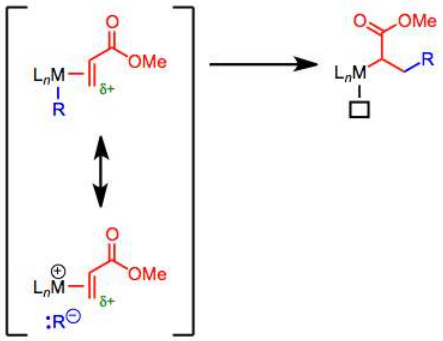


Figure 7.2.3.2: The site selectivity of 1,2-insertion can be predicted using resonance forms and partial charges. (Michael Evans)

A nice study by Yu and Spencer illustrates these effects in homogeneous palladium- and rhodium-catalyzed hydrogenation reactions. Unactivated alkenes generally exhibit lower site selectivity than activated ones, although steric differences between the two ends of the double bond can promote selectivity.

Reactivity Trends in 1,2-Insertions

The thermodynamics of 1,2-insertions of alkenes depend strongly on the alkene, but we can gain great insight by examining the structure of the product alkyl. Coordinated alkenes that give strong metal-alkyl bonds after migratory insertion tend to undergo the process. Hence, electron-withdrawing groups, such as carbonyls and fluorine atoms, tend to encourage migratory insertion—remember that alkyl complexes bearing these groups tend to have stable M–C bonds.

Insertions of alkenes into both M–H and M–R (R = alkyl) are favored thermodynamically, but the kinetics of M–R insertion are much slower. This observation reflects a pervasive trend in organometallic chemistry: M–H bonds react more rapidly than M–R bonds. The same is true of the reverse, β-elimination. Even in cases when both hydride and alkyl elimination are thermodynamically favored, β-hydride elimination is much faster. Although insertion into M–R is relatively slow, this elementary step is critical for olefin polymerizations that form polyalkenes (Ziegler-Natta polymerization). This reaction deserves a post all its own!

As the strength of the M–X bond increases, the likelihood that an L-type π ligand will insert into the bond goes down. Hence, while insertions into M–H and M–C are relatively common, insertions into M–N and M–O bonds are more rare. Lanthanides and palladium are known to promote insertion into M–N in some cases, but products with identical connectivity can come from external attack of nitrogen on a coordinated π ligand. The diastereoselectivity of these reactions provides mechanistic insight—since migratory insertion is syn (see below), a syn relationship between Pd and N is to be expected in the products of migratory insertion. An anti relationship indicates external attack by nitrogen or oxygen.

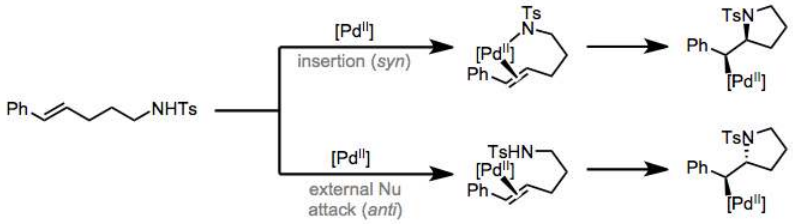


Figure **7.2.3.3**: The diastereoselectivity of formal insertions provides insight about their mechanisms. (Michael Evans)

Stereochemistry of 1,2-Insertions

1,2-Insertion may establish two stereocenters at once, so the stereochemistry of the process is critical! Furthermore, 1,2-insertions and β-eliminations are bound by important stereoelectronic requirements. An analogy can be made to the E2 elimination of organic chemistry, which also has strict stereoelectronic demands. For migratory insertion to proceed, the alkene and X-type ligand must be syncoplanar during insertion; as a consequence of this alignment, X and MLn end up on the same face of the alkene after insertion. In other words, insertions into alkenes take place in a syn fashion. Complexes that have difficulty achieving a coplanar arrangement of C=C and M–X undergo insertion very slowly, if at all.

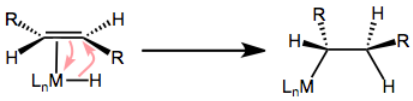


Figure **7.2.3.4**: 1,2-Insertions take place in a syn fashion. The metal and X end up bound to the same face of the alkene. (Michael Evans)

This observation has important implications for β-elimination, too—the eliminating X and the metal must have the ability to align syn.

Insertions of Other π Systems

To close this post, let's examine insertions into π ligands other than alkenes briefly. Insertions of alkynes into metal-hydride bonds are known, and are sometimes involved in reactions that I refer to collectively as "hydrostuffylation": hydrosilylation, hydroesterification, hydrogenation, and other net H–X additions across the π bond. Strangely, some insertions of alkynes yield trans products, even though cis products are to be expected from syn addition of M–X. The mechanisms of these processes involve initial syn addition followed by isomerization to the trans complex via an interesting resonance form. The cis complex is the kinetic product, but it isomerizes over time to the more thermodynamically stable trans complex.

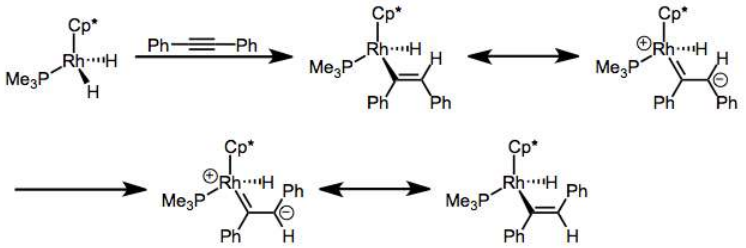


Figure **7.2.3.5**: Migratory insertions of alkynes into M–H produce alkenyl complexes, which have been known to isomerize. (Michael Evans)

The strongly donating Cp* ligand supports the legitimacy of the zwitterionic resonance form—and suggests that the C=C bond may be weaker than it first appears!

Polyenes can participate in migratory insertion, and insertions of polyenes are usually quite favored because stabilized π-allyl complexes result. In one mind-bending case, a coordinated arene inserts into an M–Me bond in a syn fashion!

Have you ever stopped to consider that the addition of methyllithium to an aldehyde is a formal insertion of the carbonyl group into the Li–Me bond? It's true! We can think of these as (very) early-metal "insertion" reactions. Despite this precedent, migratory insertion reactions of carbonyls and imines into late-metal hydride and alkyl bonds are surprisingly hard to come by. Rhodium is the most famous metal that can make this happen—rhodium has been used in complexes for arylation and vinylation, for example. Insertion of X=C into the M–R bond is usually followed by β-hydride elimination, which has the nifty effect of replacing H in aldehydes and aldimines with an aryl or vinyl group.

Contributors and Attributions

Dr. Michael Evans (Georgia Tech)

This page titled 7.2.3: Migratory Insertion-1,2-Insertions is shared under a CC BY-NC-SA 4.0 license and was authored, remixed, and/or curated by Kathryn Haas.

- **4.5: Migratory Insertion- 1,2-Insertions** by Michael Evans is licensed CC BY-NC-SA 4.0.

7.2.4: β-Elimination Reactions

In organic chemistry class, one learns that elimination reactions involve the cleavage of a σ bond and formation of a π bond. A nucleophilic pair of electrons (either from another bond or a lone pair) heads into a new π bond as a leaving group departs. This process is called β-elimination because the bond β to the nucleophilic pair of electrons breaks. Transition metal complexes can participate in their own version of β-elimination, and metal alkyl complexes famously do so. Almost by definition, metal alkyls contain a nucleophilic bond—the M–C bond! This bond can be so polarized toward carbon, in fact, that it can promote the elimination of some of the world's worst leaving groups, like –H and –CH3. Unlike the organic case, however, the leaving group is not lost completely in organometallic β-eliminations. As the metal donates electrons, it receives electrons from the departing leaving group. When the reaction is complete, the metal has picked up a new π-bound ligand and exchanged one X-type ligand for another.

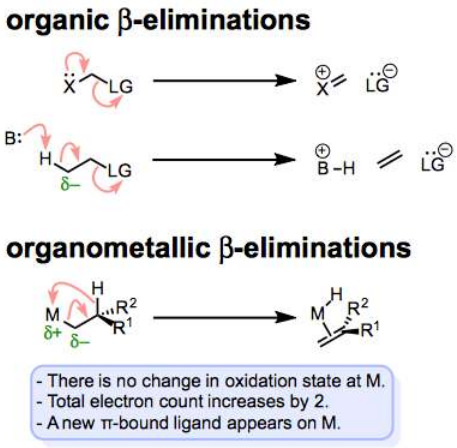


Figure **7.2.4.1**: Comparing organic and organometallic β-eliminations. A nucleophilic bond or lone pair promotes loss or migration of a leaving group. (Michael Evans)

In this post, we'll flesh out the mechanism of β-elimination reactions by looking at the conditions required for their occurrence and their reactivity trends. Many of the trends associated with β-eliminations are the opposite of analogous trends in 1,2-insertion reactions. A future post will address other types of elimination reactions.

β-Hydride Elimination

The most famous and ubiquitous type of β-elimination is **β-hydride elimination**, which involves the formation of a π bond and an M–H bond. Metal alkyls that contain β-hydrogens experience rapid elimination of these hydrogens, provided a few other conditions are met.

The complex must have an open coordination site and an accessible, empty orbital on the metal center. The leaving group (–H) needs a place to land. Notice that after β-elimination, the metal has picked up one more ligand—it needs an empty spot for that ligand for elimination to occur. We can envision hydride "attacking" the empty orbital on the metal center as an important orbital interaction in this process.

The M–C_α and C_β–H bonds must have the ability to align in a syn coplanar arrangement. By "syn coplanar" we mean that all four atoms are in a plane and that the M–C_α and C_β–H bonds are on the same side of the C_α–C_β bond (a dihedral angle of 0°). You can see that conformation in the figure above. In the syn coplanar arrangement, the C–H bond departing from the ligand is optimally lined up with the empty orbital on the metal center. Hindered or cyclic complexes that cannot achieve this conformation do not undergo β-hydride elimination. The need for a syn coplanar conformation has important implications for eliminations that may establish diastereomeric olefins: β-elimination is stereospecific. One diastereomer leads to the (E)-olefin, and the other leads to the (Z)-olefin.

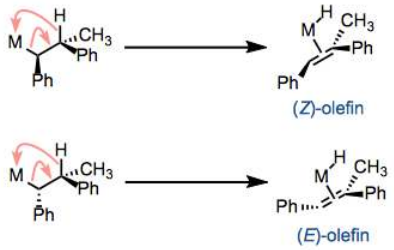


Figure 7.2.4.2: β-elimination is stereospecific. One diastereomer of reactant leads to the (Z)-olefin and the other to the (E)-olefin. (Michael Evans)

The complex must possess 16 or fewer total electrons. Examine the first figure one more time—notice that the total electron count of the complex increases by 2 during β-hydride elimination. Complexes with 18 total electrons don't undergo β-elimination because the product would end up with 20 total electrons. Of course, dissociation of a loose ligand can produce a 16-electron complex pretty easily, so watch out for ligand dissociation when considering the possibility of β-elimination in a complex. Ligand dissociation may be reversible, but β-Hydride elimination is almost always irreversible.

The metal must bear at least 2 d electrons. Now this seems a bit strange, as the metal has served as nothing but an empty bin for electrons in our discussion so far. Why would the metal center need electrons for β-hydride elimination to occur? The answer lies in an old friend: backbonding. The $\sigma_{C-H} \rightarrow M$ orbital interaction mentioned above is not enough to promote elimination on its own; an $M \rightarrow \sigma^*_{C-H}$ interaction is also required! I've said it before, and I'll say it again: backbonding is everywhere in organometallic chemistry. If you can understand and articulate it, you'll blow your instructor's mind.

Other β-Elimination Reactions

The leaving group does not need to be hydrogen, of course, and a number of more electronegative groups come to mind as better candidates for leaving groups. β-Alkoxy and β-amino eliminations are usually thermodynamically favored thanks to the formation of strong M–O and M–N bonds, respectively. These reactions are so favored in β-alkoxyalkyl "complexes" of alkali and alkaline earth metals (R–Li, R–MgBr, etc.) that using these as σ-nucleophiles at carbon is untenable. Such compounds eliminate immediately upon their formation. I had an organic synthesis professor in undergrad who was obsessed with this—using a β-alkoxyalkyl lithium or β-alkoxyalkyl Grignard reagent in a synthesis was a recipe for red ink. β-Haloalkyls were naturally off limits too.

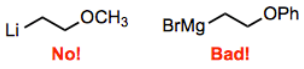


Figure 7.2.4.3: Watch out…these are not stable compounds! (Michael Evans)

The atom bound to the metal doesn't have to be carbon. β-Elimination of alkoxy ligands affords ketones or aldehydes bound at oxygen or through the C=O π bond (this step is important in many transfer hydrogenations, and an analogous process occurs in the Oppenauer oxidation). Amido ligands can undergo β-elimination to afford complexes of imines; however, this process tends to be slower than β-alkoxy elimination.

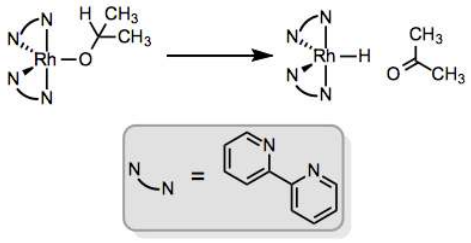


Figure 7.2.4.4: β-Elimination helps transfer the elements of dihydrogen from one organic compound to another.. (Michael Evans)

Incidentally, I haven't seen any examples in which the β atom is not carbon, but would be interested if anyone knows of an example!

Applications of β-Eliminations

As with many concepts in organometallic chemistry, there are two ways to think about applications of β-elimination. One can take either the “inorganic” perspective, which focuses on the metal center, or the “organic” perspective, which focuses on the ligands.

With the metal center in focus, we can recognize that β-hydride elimination has the wonderful side effect of establishing an M–H bond—a feat generally difficult to achieve in a selective manner via oxidative addition of X–H. If the ligand from which the hydrogen came displaced something more electronegative, the whole process represents reduction at the metal center. For example, imagine rhodium(III) chloride is mixed with sodium isopropoxide, $NaOCH(CH_3)_2$. The isopropoxide easily displaces chloride, and subsequent β-hydride elimination affords a rhodium hydride, formally reduced with respect to the chloride starting material. See p. 236 of this review for more.

With the ligand in focus, we see that the organic ligand is oxidized in the course of β-hydride elimination. Notice that the metal is reduced and the ligand oxidized! A π bond replaces a σ bond in the ligand, and if the conditions are right, this represents a bona fide oxidation (as opposed to a mere elimination). For example, oxidative addition into a C–H bond followed by β-hydride elimination at a C–H bond next door sets up an alkene where two adjacent C–H bonds existed before, an oxidation process. These dehydrogenation reactions are incredibly appealing in a theoretical sense, but still at an early stage when it comes to scope and practicality.

Summary

We already encountered β-hydride elimination in an earlier series of posts on metal alkyl complexes, where we noted that it’s a very common decomposition pathway for metal alkyls. β-Hydride elimination isn’t all bad, however, as it can be an important step in catalytic reactions that result in the oxidation of organic substrates (dehydrogenations and transfer hydrogenations) and in reactions that reduce metal halides to metal hydrides. The general idea of β-elimination involves the transfer of a leaving group from a ligand to the metal center with simultaneous formation of a π bond in the ligand. β-Elimination requires an open coordination site and at least two d electrons on the metal center, and eliminations of chiral complexes are stereospecific. The leaving group is commonly hydrogen, but need not be—the more electronegative the leaving group, the more favorable the elimination. Stronger π bonds in the product also encourage β-elimination, so eliminations that form carbonyl compounds or imines are common.

In the next post, we’ll explore other types of organometallic elimination reactions, which establish π bonds at different positions in metal alkyl or other complexes. α-Eliminations, for example, establish metal-carbon, -oxygen, or -nitrogen multiple bonds, which are generally difficult to forge through other means

Contributors and Attributions

- Dr. Michael Evans (Georgia Tech)

This page titled 7.2.4: β-Elimination Reactions is shared under a CC BY-NC-SA 4.0 license and was authored, remixed, and/or curated by Kathryn Haas.

- **4.1: β-Elimination Reactions** by Michael Evans is licensed CC BY-NC-SA 4.0.

7.2.5: Abstraction and Addition

The nucleophilic and electrophilic addition and abstraction reactions can be viewed as ways of activating a ligand toward reaction with an external reagent. The external reagent reacts directly with the ligand, not with the metal center. The external reagent may be a nucleophile (Lewis Base) or an electrophile (Lewis acid).

Nucleophilic Addition and Abstraction

The reaction of an activated ligand with a nucleophilic reagent is favored if the activated ligand is electron poor. When the metal complex is either cationic and/or has spectator ligands that are are electron withdrawing, the reactive ligand becomes activated by being depleted of electron density. The attack of the nucleophile may result in the formation of a new bond between the nucleophile and the activated unsaturated substrate, in which case it is called nucleophilic addition. Alternatively, the reaction may result in an abstraction of a part or the whole of the activated ligand, in which case it is called the nucleophilic abstraction. Some examples of nucleophilic addition and the abstraction reactions are discussed below.

Nucleophilic Addition

An example of a nucleophilic addition reaction is shown in Figure **7.2.5.1**. The olefin is activated by its interaction with platinum. Pyridine is the nucleophile, and the result is a new **C–N** bond.

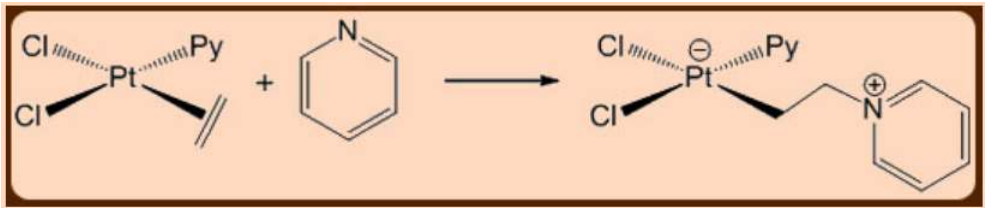


Figure **7.2.5.1**: An example of addition of a nucleophile to an activated ligand.

Nucleophilic Abstraction

An example of a nucleophilic abstraction reaction is shown in Figure **7.2.5.2**.

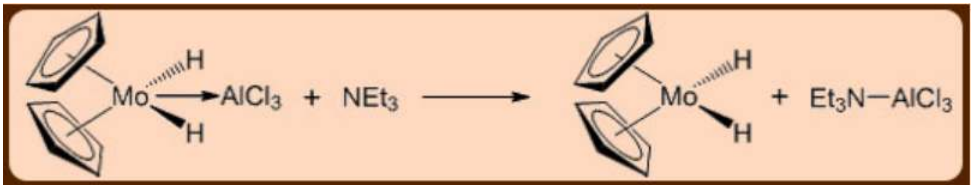


Figure **7.2.5.2**: An example of abstraction by a nucleophile.

Electrophilic Addition and Abstraction

Similar to the nucleophilic addition and abstraction reactions, the electrophilic counterparts of these reactions also exist. An electrophilic attack is favored if the ligand-metal fragment is more electron rich. When the complex is anionic, the metal center is at low oxidation state, and/or when the spectator ligands are electron donating, the ligand becomes activated toward reaction with an electrophile. The reaction of activated ligands with electrophilic substrates may result in the formation of a new bond between the electrophile and the activated unsaturated substrate, in which case it is called electrophilic addition, or may result in an abstraction of a part or the whole of the activated ligand, in which case it is called the electrophilic abstraction.

Electrophilic Addition

An example of an electrophile being added to an activated ligand is shown in Figure **7.2.5.3**. The allylic anion ligand uses its π electrons to react with hydrogen ion. This adds a hydrogen to the ligand, converting it from an anionic X-type ligand to a neutral L-type ligand .

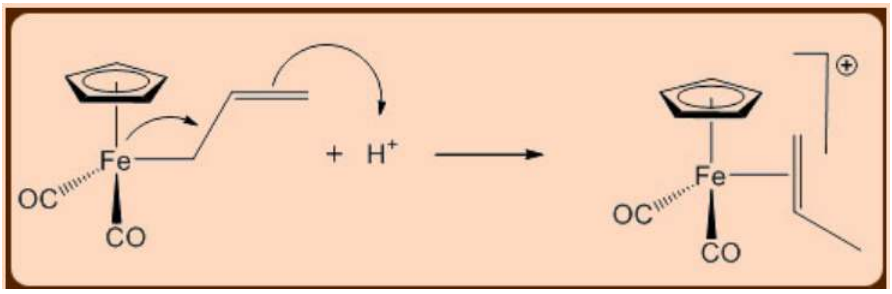


Figure **7.2.5.3**: An example of electrophilic addition to an activated ligand.

Electrophilic Abstraction

Depending on whether the abstraction occurs at the α or β position with respect to the metal ion, the reaction is either classified as an α-abstraction or a β-abstraction.

An example of an α electrophilic abstraction reaction is shown in Figure **7.2.5.4**.

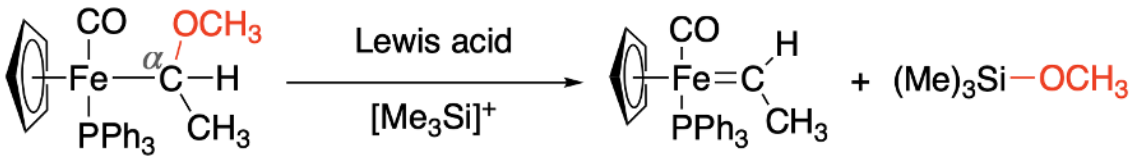


Figure **7.2.5.4**: An example of an electrophilic α-abstraction. (CC-BY-SA; Kathryn Haas)

Two examples of a β electrophilic abstraction are shown in Figure **7.2.5.5**.

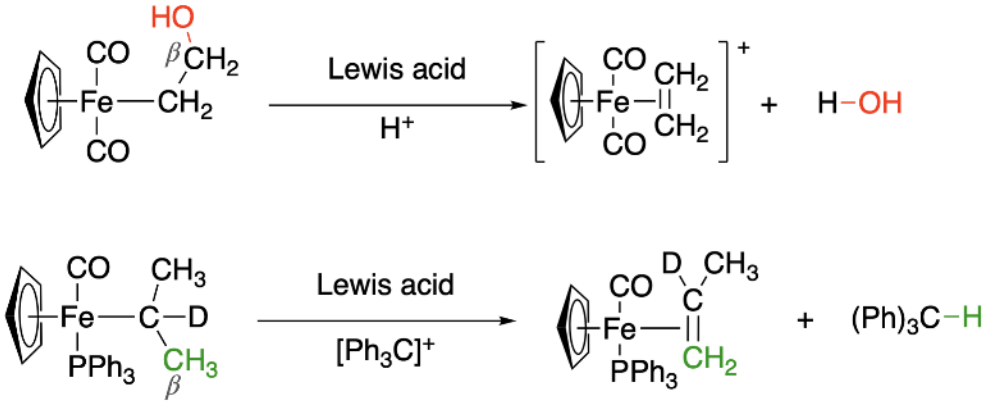


Figure **7.2.5.5**: Two examples of electrophilic β-abstraction. (CC-BY-SA; Kathryn Haas)

This page titled 7.2.5: Abstraction and Addition is shared under a CC BY-NC-SA 4.0 license and was authored, remixed, and/or curated by Kathryn Haas.

- **10.3: Nucleophilic and Electrophilic Addition and Abstraction** by M. S. Balakrishna & Prasenjit Ghosh is licensed CC BY-NC-SA 4.0. Original source: https://nptel.ac.in/courses/104101006.

SECTION OVERVIEW

7.3: Organometallic Catalysts

One of the most important uses of organometalic complexes is in the catalysis of chemical reactions. In this section, we will apply knowledge of reaction types and the skill of electron counting to understand organometalic catalytic cycles.

7.3.1: Catalytic Deuteration

7.3.2: Hydroformylation

7.3.3: Monsanto Acetic Acid Process

7.3.4: Wacker (Smidt) Process

7.3.5: Hydrogenation by Wilkinson's Catalyst

7.3.6: Olefin Metathesis

This page titled 7.3: Organometallic Catalysts is shared under a CC BY-NC-SA 4.0 license and was authored, remixed, and/or curated by Kathryn Haas.

7.3.1: Catalytic Deuteration

Catalytic Deuteration of Benzene

Combinations of oxidative additions and reductive eliminations have many applications in the synthesis of organic molecules using an organometallic reactant.

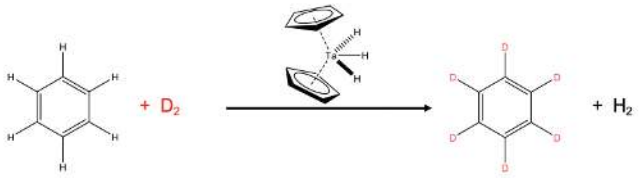


Figure **7.3.1.1** Deuteration of benzene

An example is the deuteration of benzene (Fig. **7.3.1.1**). Deuterated benzene is an important solvent in NMR spectroscopy. Industrially, the deuteration is done using a dicyclopentadienyltrihydridotantalum(V) catalyst starting out from benzene and D_2. The D_2 is provided in excess to drive the chemical equilibrium to the right side.

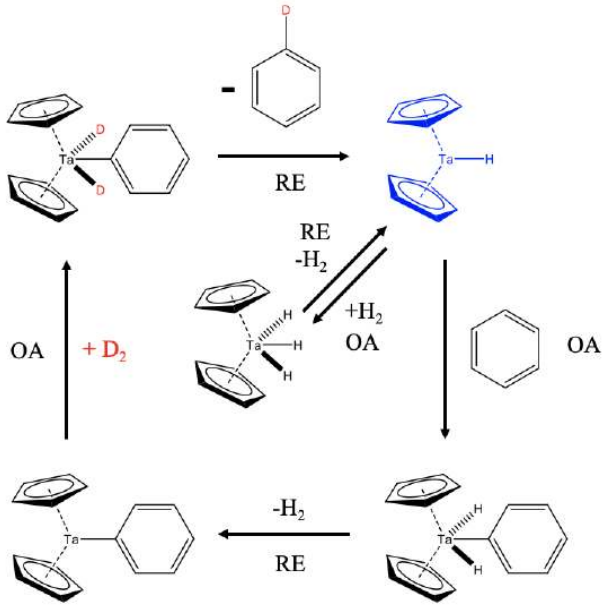


Figure **7.3.1.2** Mechanism of the catalytic deuteration of benzene

How does this reaction work mechanistically? This 18e Cp_2TaH_3 is actually a precatalyst that is in chemical equilibrium with H_2 and the 16e dicyclopentadienylhydrido tantalum(III) which is the actual catalyst (Fig. **7.3.1.2**). Elimination of H_2 from the Ta(V) catalyst is a reductive elimination (RE) and the re-addition of H_2 to the Ta(III) species an oxidative addition (OA). In the presence of benzene, the Ta(III) species can oxidatively add benzene to form an 18e Ta(V) complex. This complex can reductively eliminate H_2 to form a 16e Cp_2Ta(III)-Ph complex. In the presence of deuterium this complex can add D_2 oxidatively to form an 18e Cp_2D_2Ta(V)-Ph complex. This species can then reductively eliminate a monodeuterated benzene molecule under formation of Cp_2Ta(III)-D. In the presence of enough D_2 this monodeuterated benzene can be further deuterated in subsequent catalytic cycles.

This page titled 7.3.1: Catalytic Deuteration is shared under a CC BY-NC-SA 4.0 license and was authored, remixed, and/or curated by Kathryn Haas.

- **12.1: Organometallic reactions** by Kai Landskron is licensed CC BY 4.0.

7.3.2: Hydroformylation

Catalytic Olefin Hydroformylation

An important industrial reaction is the catalytic hydroformylation reaction, also known as oxo-process (Figure **7.3.2.1**). It was discovered in 1938 by Otto Roelen at BASF. In the hydroformylation reaction an H atom and a formyl group are added to an alkene to form aldehydes. The reaction can produce both branched an linear aldehydes from terminal alkenes, CO, and H_2 using a carbonyl hydrides such as $HCo(CO)_4$ as a catalyst. The reaction is performed at about 100°C at a pressure of up to 100 atm.

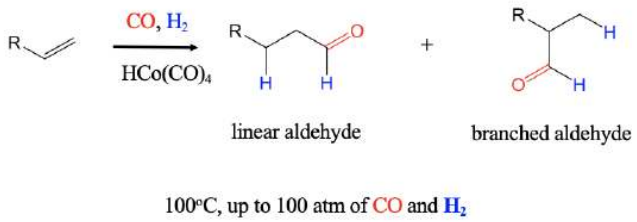


Figure **7.3.2.1**: Catalytic olefin hydroformylation

Mechanism of the Catalytic Olefin Hydroformylation by $HCo(CO)_4$

How does the hydroformylation work mechanistically?

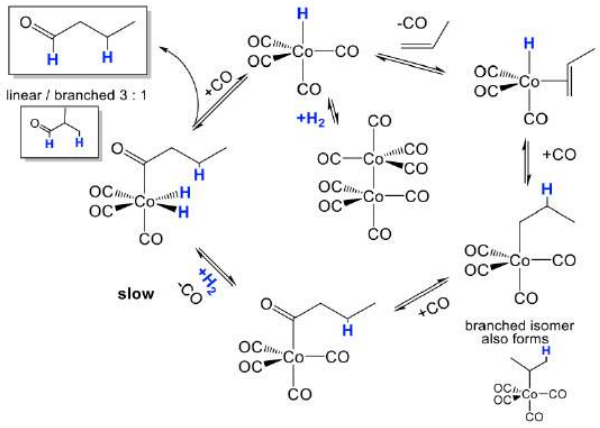


Figure **7.3.2.2**: Mechanism of the catalytic olefin hydroformylation by $HCo(CO)_4$ (Attribution: A. Vedernikov, U Maryland (modified).)

The mechanism is illustrated for the hydroformylation of propene (Fig. **7.3.2.2**:). The actual catalyst $HCo(CO)_4$ is first formed from its precatalyst $Co_2(CO)_8$ in the presence of H_2 in a dinuclear oxidative addition reaction. The catalyst can undergo a substitution reaction in which a CO ligand is replaced by the olefin that binds side-on to the cobalt. This species can then undergo a migratory olefin insertion reaction. This leads to a mixture of linear and branched alkyl groups attached to the Co. A new CO ligand can add to the vacant site. The alkyl group can then insert into a carbonyl group in another migratory insert step, and the vacant site can be reoccupied by a new CO molecule. Then, H_2 is added in an oxidative addition. This is the slowest and rate-limiting step in the catalytic cycle. From the addition product the aldehyde can then be eliminated in a reductive elimination reaction. Addition of CO regenerates the catalyst, and the catalytic cycle can begin again.

Hydrocarbonylations

After the hydroformylation, a number of other hydrocarbonylations were developed, and industrially deployed.

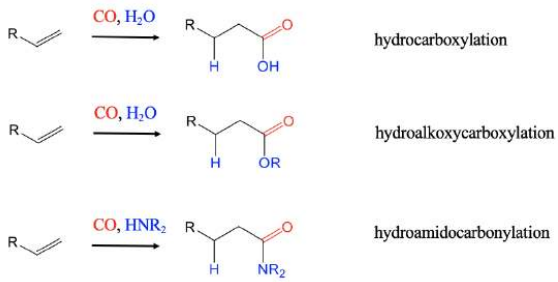


Figure **7.3.2.3**: Hydrocarbonylation reactions

When hydrogen is replaced by H_2O hydrocarboxylations of alkenes lead to carboxylic acids (Fig. **7.3.2.3**:). With an alcohol instead of H_2 hydroalkoxycarbonylcations lead to esters. The employment of amines instead of H_2 leads to amides in hydroamidocarbonylation reactions.

This page titled 7.3.2: Hydroformylation is shared under a CC BY-NC-SA 4.0 license and was authored, remixed, and/or curated by Kathryn Haas.

- **12.2: Organometallic Catalysts** by Kai Landskron is licensed CC BY 4.0.

7.3.3: Monsanto Acetic Acid Process

The Monsanto Acetic Acid Process

Another carbonylation reaction involving an organometallic catalyst is the Monsanto acetic acid process (Figure **7.3.3.1**). It has been introduced by Monsanto in the 1970s for the industrial production of acetic acid from methanol. The reaction involves dual catalysis with HI and $[RhI_2(CO)_2]^-$ as a co-catalysts. How does this reaction work?

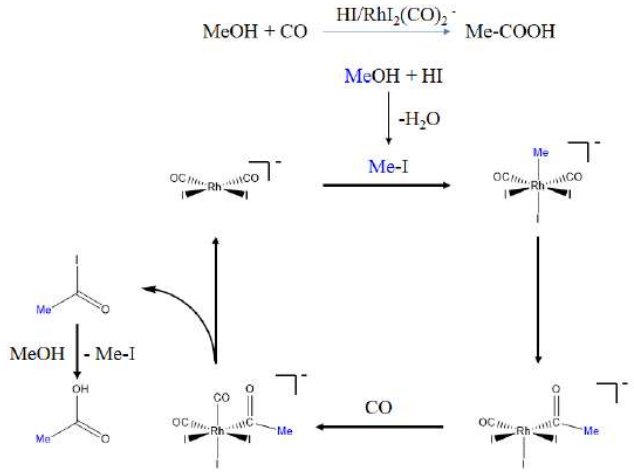


Figure **7.3.3.1**: The catalytic cycle in the Monsanto acetic acid process

In the first step methanol reacts with HI to form methyl iodide. The methyl iodide then reacts with the Rh-catalyst in an oxidative addition reaction in which a methyl and an iodo group are added in trans-fashion to the square-planar Rh-complex to give an octahedral complex. The octahedral complex then undergoes a migratory insertion reaction with CO producing an acyl group and a vacant site. A CO molecule can then add to the vacant site. The acetyl iodide can then be eliminated in a reductive elimination to reform the Rh-catalyst thereby closing the catalytic cycle. The acetyl iodide can then react with methanol to form new methyl iodide and acetic acid. The methyl iodide can start a new catalytic cycle with the Rh-catalyst.

This page titled 7.3.3: Monsanto Acetic Acid Process is shared under a CC BY-NC-SA 4.0 license and was authored, remixed, and/or curated by Kathryn Haas.

- **12.2: Organometallic Catalysts** by Kai Landskron is licensed CC BY 4.0.

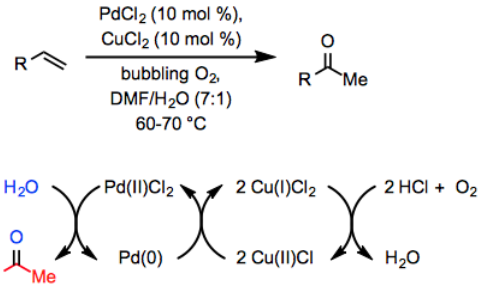
7.3.4: Wacker (Smidt) Process

See also Wacker Oxidation (Wikipedia)

The **Wacker oxidation** refers generally to the transformation of a terminal or 1,2-disubstituted alkene to a ketone through the action of catalytic palladium(II), water, and a co-oxidant. Variants of the reaction yield aldehydes, allylic/vinylic ethers, and allylic/vinylic amines. Because of the ease with which terminal alkenes may be prepared and the versatility of the methyl ketone group installed by the reaction, the Wacker oxidation has been employed extensively in organic synthesis.[1]

Introduction

The stoichiometric conversion of ethylene to acetaldehyde by an acidic, aqueous solution of $PdCl_2$ was discovered over a century ago,[2] but fifty years passed between the discovery of this reaction and the development of a catalytic method. In 1959, researchers at Wacker Chemie reported that a similar transformation takes place in an aqueous, acidic solution of catalytic $PdCl_2$ and a stoichiometric amount of $CuCl_2$ through which oxygen is bubbled (Equ. **7.3.4.1**).[3]



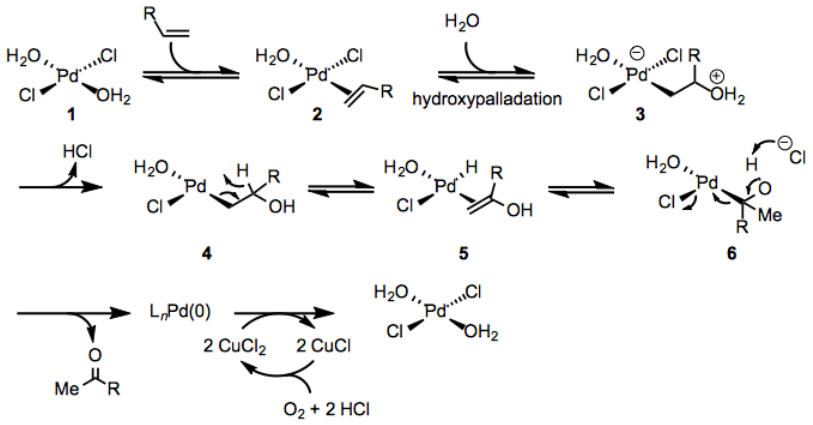
Equation **7.3.4.1**

Since this initial report, the Wacker process has been widely applied in organic synthesis and has been extended to other classes of substrates and products. To encourage mixing of the organic reactants with the aqueous phase, a co-solvent is generally employed along with water. Dimethylformamide (DMF) is a common choice; when DMF is used as a co-solvent with a stoichiometric amount of CuCl under balloon pressure of oxygen, the reaction is called the "Tsuji-Wacker oxidation."[4] Applications of the Wacker oxidation to organic synthesis typically involve the installation of a methyl ketone moiety, which may subsequently undergo nucleophilic addition or deprotonation to form an enolate.

Mechanism and Stereochemistry

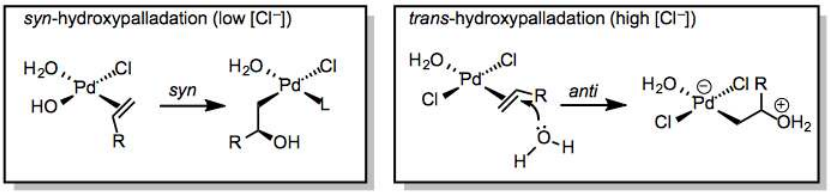
Prevailing Mechanism: Water Nucleophile

The mechanism of the Wacker oxidation has been studied both experimentally and theoretically (Eq. 2). The first step of the Wacker oxidation involves coordination of the the alkene to the palladium center to form π-complex **2**. Evidence for this step is provided by the relative sluggishness of electron-poor alkenes, which generally require higher catalyst loadings than unactivated alkenes. Hydroxypalladation then occurs to yield either zwitterionic complex **3** or neutral complex **4** depending on the mode of hydroxypalladation (see below). Studies employing deuterated substrates suggest that β-hydride elimination then occurs to afford enol complex **5**, which re-inserts into the Pd-H bond to afford complex **6**.[5] Computational studies support the involvement of chloride-assisted deprotonation in the subsequent step,[6] which affords the product and palladium(0). Oxidation of palladium(0) by copper(II) then occurs, regenerating palladium(II) species **1**. The role of copper(II) in the mechanism is poorly understood at present.



Equation **7.3.4.2**

The mode of hydroxypalladation is an important issue for the Wacker oxidation. Hydroxypalladation may occur either in a *syn* fashion through an inner-sphere mechanism or in an *anti* fashion via nucleophilic attack on the coordinated alkene (Eq. 3). Although the stereocenter in **4** is ultimately destroyed upon elimination, the mode of hydroxypalladation can influence the site selectivity of the reaction. Markovnikov-type addition of water to the more substituted carbon of the alkene forms a methyl ketone, while attack of water at the less substituted position ultimately yields an aldehyde. The mode of hydroxypalladation has been shown to affect the distribution of ketone and aldehyde products, and is also important in stereoselective Wacker cyclization reactions. ***(2)***

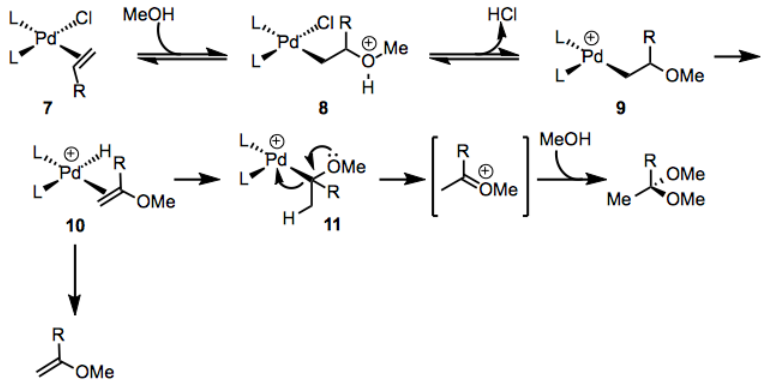


Equation **7.3.4.3**

At low concentrations of chloride ion, *syn*-hydroxypalladation appears to be the norm.[7] Water coordinates to the metal and migratory insertion into the Pd-OH bond occurs to generate **4** directly. At high concentrations of chloride ion, chloride competes with hydroxide for binding at palladium, and thus *anti*-hydroxypalladation may occur.[8] ***(3)***

Prevailing Mechanism: Alcohol Nucleophiles

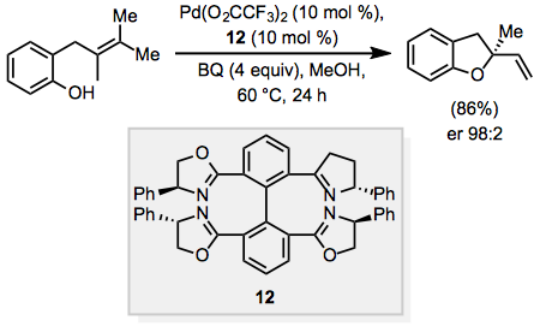
Alcohols may also be employed as nucleophiles in the Wacker process. The initial steps of the mechanism are similar to those for the Wacker oxidation with water, but the mechanisms diverge at alkoxy complex **11** (Eq. 4). Elimination of palladium occurs to generate an oxocarbenium ion, which may be captured by solvent to generate an acetal. Small amounts of vinyl ether products support the intermediacy of complex **10**.[9]



Equation **7.3.4.4**

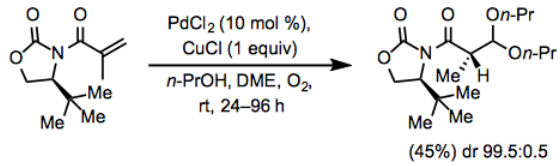
Enantioselective Variants

When the substrate contains a tethered nucleophile, such as a hydroxyl group or protected amine, the nucleophile may react to form a cyclic, allylic or vinylic ether or amine after β-hydride elimination. This process is known as the "Wacker cyclization," and when the product is allylic, a stereocenter may be established. Chiral ligands have been used to render the Wacker cyclization enantioselective. For example, use of tetra(dihydrooxazoline) ligand **12** and benzoquinone (BQ) as a co-oxidant resulted in formation of allylic ether product in an enantiomeric ratio of 98:2 (Eq. 5). [10]



Equation **7.3.4.5**

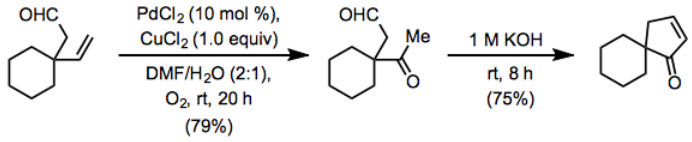
The Wacker process may also establish a stereocenter in 1,1-disubstituted alkenes via acetal formation. A chiral auxiliary in the alkene has been used successfully to generate chiral acetals with high diastereomeric ratio. The acetal forms at the more electron-deficient site of the alkene (Eq. 6).[11]



Equation **7.3.4.6**

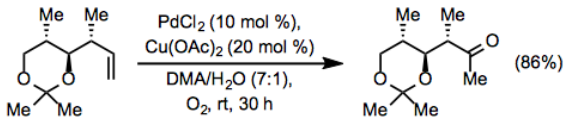
Scope and Limitations

Terminal alkenes are the most commonly employed substrates for the Wacker oxidation. Oxygen-containing functionality far from the reactive alkene is well tolerated by the reaction because palladium reacts selectively with the alkene in preference to lone pairs on oxygen. Wacker oxidation followed by intramolecular aldol condensation is a convenient method for the rapid synthesis of carbocycles (Eq. 7).[12]



Equation **7.3.4.7**

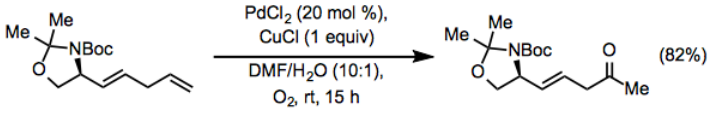
The original Wacker process and Tsuji-Wacker conditions can present problems for substrates containing acid-sensitive functionality, such as acetals and silyl ethers. Use of copper(II) chloride leads to the generation of strongly acidic hydrochloric acid. To mitigate this issue, a method employing copper(II) acetate has been developed. Some acid-sensitive groups are able to withstand the milder acetic acid generated by this method (Eq. 8).[13] Under similar conditions involving copper(I) chloride, a yield of only 56% was obtained.



Equation **7.3.4.8**

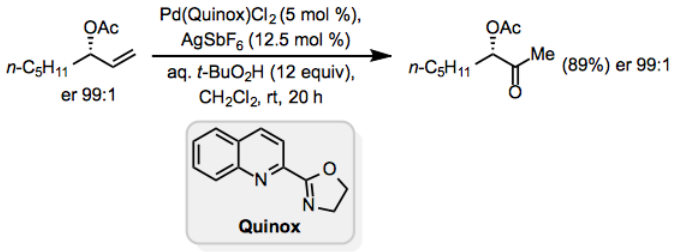
Unprotected amines coordinate strongly to palladium and thus cause problems for Wacker oxidations. Amines protected with electron-withdrawing substituents often do not interfere in Wacker oxidations,[14] although they may participate in aza-Wacker cyclizations if appropriately positioned in the substrate (see below).

Tri-substituted alkenes are completely inert to the conditions of the Wacker oxidation; only terminal and 1,1-disubstituted alkenes react. Terminal alkenes are usually oxidized selectively over internal alkenes, except under rather specialized circumstances.[15] Eq. 9 represents a typical case of selectivity for terminal alkenes.[14]



Equation **7.3.4.9**

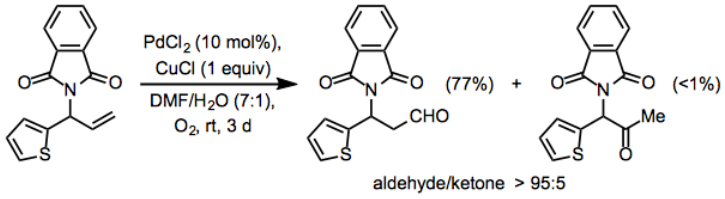
Lewis-basic functionality in the allylic or homoallylic position relative to the reactive alkene may cause unpredictable site selectivity in Wacker oxidations. Under standard Tsuji-Wacker conditions, unprotected allylic alcohols form mixtures of methyl ketone and aldehyde products.[16] The catalyst Pd(Quinox)Cl_2 was developed to address this problem; allylic alcohols react selectively in the presence of this catalyst to afford methyl ketones (Eq. 10).[17] *tert*-Butyl hydroperoxide (TBHP) is used as the oxygen source in this reaction.



Equation **7.3.4.10**

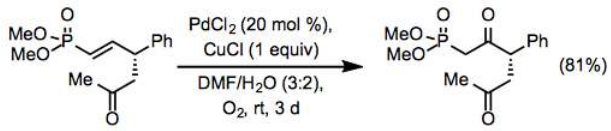
Protected, homoallylic alcohols generally form the methyl ketone selectively, but results are more unpredictable for unprotected homoallylic alcohols.[18]

Protected allylic amines generally give higher yields of aldehyde than comparable protected allylic alcohols; these results suggest that coordination of palladium to the Lewis base is responsible for the formation of aldehydes. Using a phthalimide group in the allylic position, the Wacker oxidation may be rendered completely selective for aldehydes (Eq. 11).[19]



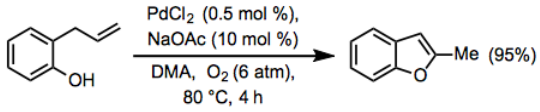
Equation **7.3.4.11**

Site selectivity in reactions of internal alkenes is low unless an allylic or homoallylic Lewis base is present in the substrate. Electron-withdrawing groups can direct oxidation to the β position of the alkene (Eq. 12), but relatively high catalyst loadings are required.[20]



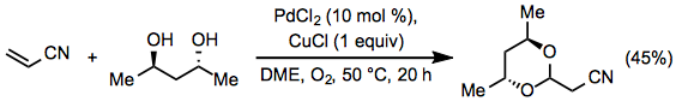
Equation **7.3.4.12**

When an appropriately situated nucleophile is present in the substrate, Wacker cyclization may occur to yield an allylic or vinylic ether (Eq. 13).[21] The aza-Wacker cyclization involves protected amino nucleophiles such as sulfonamides.[22]



Equation
7.3.4.13

When an alcohol is used in stoichiometric or solvent quantities or a diol is present in the substrate, acetal formation may occur. Acetal formation, like ketone formation, generally occurs with Markovnikov selectivity. For example, a Michael acceptor forms an acetal at the β position in the presence of (*R*,*R*)-2,4-pentanediol (Eq. 14).[23]

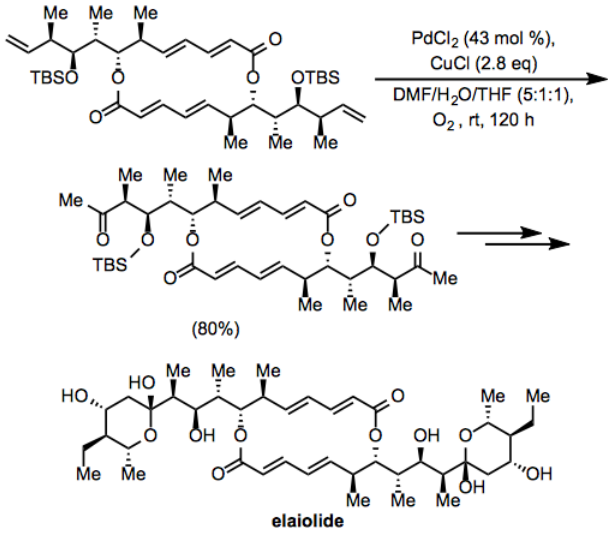


Equation
7.3.4.14

Synthetic Applications

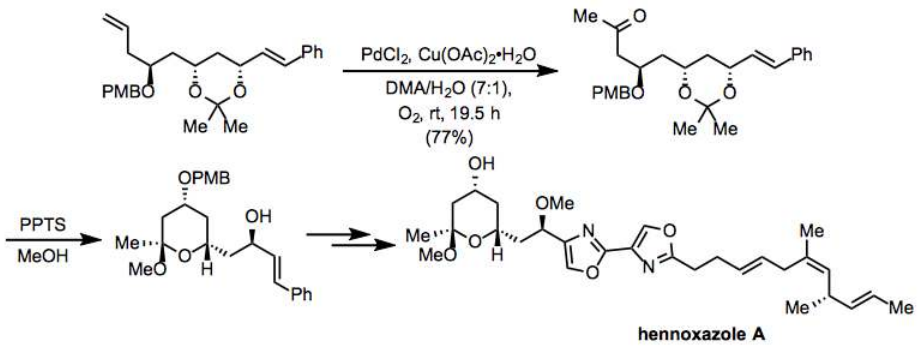
The Wacker oxidation has been used extensively in organic synthesis. A number of methods exist for the installation of terminal alkenes and the methyl ketone products of the reaction can be elaborated easily to more complex compounds. In addition, the reaction is aerobic and operationally simple.

The Wacker oxidation was employed in the course of synthesis of the macrolide elaiolide. Oxidation at two terminal alkenes in a C_2-symmetric intermediate afforded a diketone, which was subsequently elaborated to the symmetric natural product (Eq. 15).[24] Notably, the internal alkenes and esters in the intermediate appeared not to affect the oxidation.



Equation
7.3.4.15

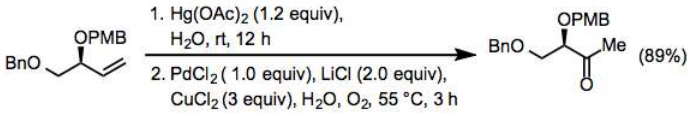
A modification of Tsuji-Wacker conditions employing copper(II) acetate was used in the course of a synthesis of hennoxazole A (Eq. 16).[25] After the oxidation, deprotection under acidic conditions led to the intramolecular formation of an acetal present in the target compound.



Equation
7.3.4.16

Comparison to Other Methods

Few true alternatives to the Wacker oxidation (that is, other hydration-oxidation reactions) are known. One rather harsh method involves oxymercuration followed by transmetalation to palladium (Eq. 17).[26]



Equation
7.3.4.17

Experimental Conditions and Procedure

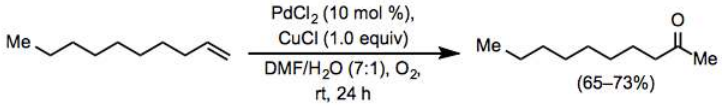
Typical Conditions

Tsuji-Wacker conditions represent a good starting point for experimental conditions for this reaction. Water is mixed with an organic co-solvent (often DMF) and 10 mol% $PdCl_2$, stoichiometric CuCl, and 1 atmosphere of oxygen gas. Copper(I) salts are generally superior to copper(II) salts because the former minimize the concentration of chloride in solution, encouraging *syn*-hydroxypalladation. Copper(I) is rapidly oxidized to copper(II) by dissolved oxygen; a period of 30 minutes prior to the introduction of the substrate is used to ensure that this oxidation is complete. For situations in which Tsuji-Wacker conditions fail, a wide variety of modifications of the reaction conditions may be employed.

Using high oxygen pressure and a judicious choice of solvent, Wacker oxidations can be carried out without the need for a co-oxidant. Certain ligands also promote direct O_2-coupled oxidations.[27]

Peroxides may also be used as the oxygen source in Wacker oxidations; these reactions do not require a co-oxidant. In the Pd(Quinox)/TBHP system, silver hexafluoroantimonate serves as a scavenger of chloride ions.

Experimental Procedure[4]



Equation
7.3.4.18

A 100-mL, 3-necked, round-bottomed flask was fitted with a magnetic stirring bar and a pressure-equalizing dropping funnel containing 1-decene (4.2 g, 30 mmol, 1.0 equiv). The flask was charged with a mixture of $PdCl_2$ (0.53 g, 3 mmol, 0.1 equiv), CuCl (2.97 g, 30 mmol, 1.0 equiv) and aqueous DMF (DMF/H_2O = 7:1, 24 mL). With the other outlets securely stoppered and wired down, an oxygen-filled balloon was placed over one neck, and the mixture was stirred at rt to allow oxygen uptake. After 1 h, the 1-decene (4.2 g, 30 mmol) was added over 10 min, and the solution was stirred vigorously at rt under an oxygen balloon. The color of the solution turned from green to black within 15 min and returned gradually to green. After 24 h, the mixture was poured into cold 3 N HCl (100 mL) and extracted with five, 50 mL portions of ether. The extracts were combined and washed successively with 50 mL of saturated aqueous $NaHCO_3$ solution, 50 mL of brine, and then dried over anhydrous magnesium sulfate. The solvent was

removed by evaporation and the residue was distilled using a 15 cm Vigreux column to give 2-decanone as a colorless oil (3.0–3.4 g, 65–73%): bp 43.5 °C (1 mm Hg); IR (neat) 1722 cm^{-1}; ^1H NMR (CCl_4) δ 2.37 (t, J = 7 Hz, 2H), 2.02 (s, 3H), 0.7–1.8 (m, 15H).

References

1. Michel, B. W.; Steffens, L. D.; Sigman, M. S. *Org. React.* **2014**, *84*, 2. (doi: 10.1002/0471264180.or084.02)
2. Phillips, F. C. *Am. Chem. J.* **1894**, *16*, 255.
3. Smidt, J.; Hafner, W.; Jira, R.; Sedlmeier, J.; Sieber, R.; Ruttinger, R.; Kojer, H. *Angew. Chem.* **1959**, *71*, 176.
4. [a] [b] Tsuji, J.; Nagashima, H.; Nemoto, H. *Org. Synth.* **1984**, *62*, 9.
5. Smidt, J.; Hafner, W.; Jira, R.; Sieber, R.; Sedlmeier, J.; Sabel, A. *Angew. Chem.* **1962**, *74*, 93.
6. Eshtiagh-Hosseini, H.; Beyramabadi, S. A.; Morsali, A.; Housaindokht, M. R. *J. Mol. Struct.: THEOCHEM* **2010**, *941*, 138.
7. Henry, P. M. *J. Am. Chem. Soc.* **1964**, *86*, 3246.
8. Bäckvall, J. E.; Akermark, B.; Ljunggren, S. O. *J. Chem. Soc., Chem. Commun.* **1977**, 264.
9. Balija, A. M.; Stowers, K. J.; Schultz, M. J.; Sigman, M. S. *Org. Lett.* **2006**, *8*, 1121.
10. Zhang, Y. J.; Wang, F.; Zhang, W. *J. Org. Chem.* **2007**, *72*, 9208.
11. Hosokawa, T.; Yamanaka, T.; Itotani, M.; Murahashi, S.-I. *J. Org. Chem.* **1995**, *60*, 6159.
12. Srikrishna, A.; Kumar, P. P. *J. Indian Chem. Soc.* **1999**, *76*, 521.
13. Smith, A. B., III; Cho, Y. S.; Friestad, G. K. *Tetrahedron Lett.* **1998**, *39*, 8765.
14. [a] [b] Reginato, G.; Mordini, A.; Verrucci, M.; Degl'Innocenti, A.; Capperucci, A. *Tetrahedron: Asymmetry* **2000**, *11*, 3759.
15. Ho, T.-L.; Chang, M. H.; Chen, C. *Tetrahedron Lett.* **2003**, *44*, 6955.
16. Muzart, J. *Tetrahedron* **2007**, *63*, 7505.
17. Michel, B. W.; Camelio, A. M.; Cornell, C. N.; Sigman, M. S. *J. Am. Chem. Soc.* **2009**, *131*, 6076.
18. Kang, S.-K.; Jung, K.-Y.; Chung, J.-U.; Namkoong, E.-Y.; Kim, T.-H. *J. Org. Chem.* **1995**, *60*, 4678.
19. Weiner, B.; Baeza, A.; Jerphagnon, T.; Feringa, B. L. *J. Am. Chem. Soc.* **2009**, *131*, 9473.
20. Yan, B.; Spilling, C. D. *J. Org. Chem.* **2008**, *73*, 5385.
21. Mitsudome, T.; Umetani, T.; Nosaka, N.; Mori, K.; Mizugaki, T.; Ebitani, K.; Kaneda, K. *Angew. Chem., Int. Ed.* **2006**, *45*, 481.
22. Hegedus, L. S.; McKearin, J. M. *J. Am. Chem. Soc.* **1982**, *104*, 2444.
23. Hosokawa, T.; Ataka, Y.; Murahashi, S. *Bull. Chem. Soc. Jpn.* **1990**, *63*, 166.
24. Barth, R.; Mulzer, J. *Tetrahedron* **2008**, *64*, 4718.
25. Yokokawa, F.; Asano, T.; Shioiri, T. *Tetrahedron* **2001**, *57*, 6311.
26. Ellis, J. M.; Crimmins, M. T. *Chem. Rev.* **2008**, *108*, 5278.
27. Cornell, C. N.; Sigman, M. S. *Org. Lett.* **2006**, *8*, 4117.

Contributors

- This page is based on *Organic Reactions*. The primary collection of full *Organic Reactions* chapters is maintained by John Wiley & Sons.

This page titled 7.3.4: Wacker (Smidt) Process is shared under a CC BY-NC-SA 4.0 license and was authored, remixed, and/or curated by Kathryn Haas.

7.3.5: Hydrogenation by Wilkinson's Catalyst

Organometallic Compounds as Hydrogenation Catalysts

Migratory insertions play an important role in catalysis.

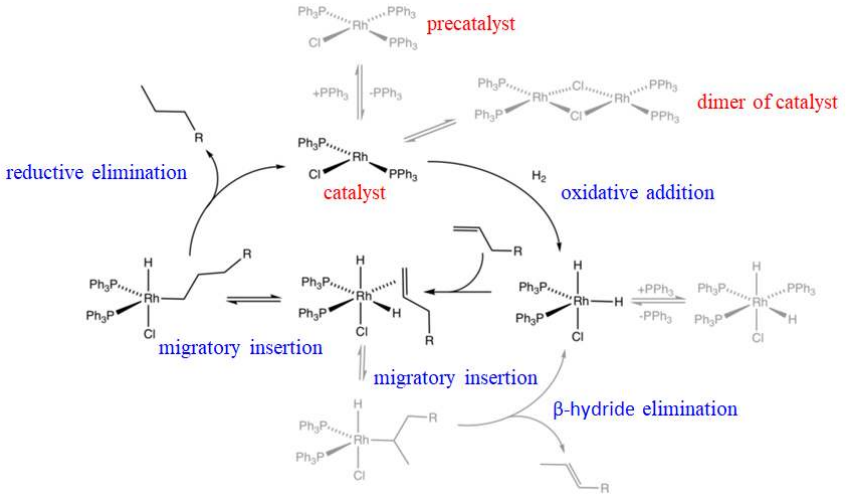


Figure **7.3.5.1**: Mechanism of the Wilkinson hydrogenation catalyst (Attribution: Smokefoot / CC BY-SA (https://creativecommons.org/licenses/by-sa/4.0) https://commons.wikimedia.org/wiki/F...cleJMBrown.png)

For example a Rh-catalyst called the Wilkinson catalyst is an effective hydrogenation catalyst for olefins. The mechanism of the hydrogenation involves a combination of oxidative additions, olefin migratory insertions, and reductive eliminations (Fig. **7.3.5.1**). Wilkinson's catalyst is the square planar chloro tris(triphenylphosphine) rhodium(I) complex. This molecule is actually a precatalyst that becomes the actual catalyst when it statistically loses a triphenylphosphine ligand producing chloro bis(triphenylphosphine) rhodium(I). The loss of this ligand is a reversible reaction, and thus the catalyst is in chemical equilibrium with the precatalyst. The actually catalyst is in a second chemical equilibrium with its dimer. The chloro bis(triphenylphosphine) rhodium(I) catalyst can undergo an oxidative addition in the presence of hydrogen to form a trigonal bipyramidal chlorodihydrido bis(triphenylphosphine) (III) rhodium complex. This species is in chemical equilibrium with an octahedral chlorodihydrido tris(triphenyl phosphine) rhodium(III) species that can form due to the presence of free triphenylphosphine ligands in the system. The trigonal bipyramidal species can then add an olefin that binds side-on to the Rh. Because the olefin is in cis-position to the hydride ligand it can undergo an olefin insertion. The Rh-C bond can either form with the first or the second carbon in the carbon chain of the olefin, giving a linear and a branched alkyl complex, respectively. The branched complex can undergo a β-hydride elimination thereby reforming the trigonal bipyramidal Rh-complex, and an olefin. This reaction is a side-reaction because the branched alkyl complex is sterically more crowded than the linear complex. The linear alkyl Rh complex can undergo a reductive elimination to form the linear alkane and the $RhCl(PPh_3)_2$ catalyst. This completes the catalytic cycle, and a new cycle can start.

This page titled 7.3.5: Hydrogenation by Wilkinson's Catalyst is shared under a CC BY-NC-SA 4.0 license and was authored, remixed, and/or curated by Kathryn Haas.

- **12.2: Organometallic Catalysts** by Kai Landskron is licensed CC BY 4.0.

7.3.6: Olefin Metathesis

Olefin Metathesis

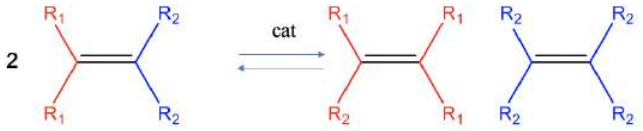


Figure **7.3.6.1**: Olefin metathesis

Olefin metathesis is a reaction which allows to cut and rearrange C=C double bonds in olefins to make new olefins (Fig. **7.3.6.1**). Formally, the carbon-carbon bond of the reactant is cleaved homoleptically and the two carbene fragments are combined in a different way. This reaction is typically an equilibrium reaction, and neither the reactants nor the products are clearly favored. This reaction is catalyzed by molybdenum arylamido carbene complexes or ruthenium carbene complexes.

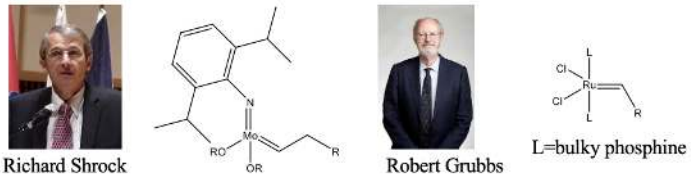


Figure **7.3.6.2**: Shrock catalyst (Attribution: R._Schrock_-_IChO_2012_Opening_Ceremony.JPG: A.mela93derivative work: Materialscientist / CC BY-SA (https://creativecommons.org/licenses/by-sa/3.0) https://commons.wikimedia.org/wiki/F...hrock_2012.jpg) and (Attribution: The Royal Society / CC BY-SA (https://creativecommons.org/licenses/by-sa/3.0) https://commons.wikimedia.org/wiki/F...al_Society.jpg)

The former are called Shrock catalysts, and the latter Grubbs catalysts named after their discoverers Richard Shrock and Robert Grubbs who received the Nobel prize for Chemistry in 2005 (Fig. **7.3.6.2**). The Schrock catalysts are more active, but also very sensitive to air and water. The Grubbs catalysts, while less active, are less sensitive to air and water.

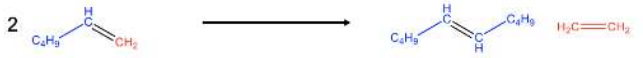


Figure **7.3.6.3**: Regular metathesis

Olefin metathesis often allows for simpler preparation of olefins compared to other methods. Olefin metathesis is particularly powerful when one olefin product is gaseous because then it can be quite easily removed from the chemical equilibrium by purging. This drives the chemical equilibrium to the right side. An example is the preparation of 5-decene from 1-hexene. Cleavage of the C=C double bond in the hexene leads to C_5 and C_1 carbene fragments (Fig. **7.3.6.3**). The two C_1 fragments can combine to form ethylene and the two C_5 fragments combine to 5-decene. The ethylene is volatile and can be purged from the reaction system thereby driving the chemical reaction to the right side.

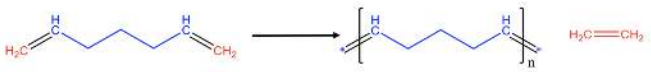


Figure **7.3.6.4**: Acylic diene metathesis (ADMET)

The same principles can also be applied to produce polymers from dienes with two terminal C=C double bonds at the chain ends. This is called acylic diene metathesis (ADMET), Fig. **7.3.6.4**. For instance the cleavage of the two terminal double bonds in a diene with seven C atoms leads to C_1 and C_5 fragments. The C_1 fragments can combine to form ethylene, and the C_5 fragments can combine to make an unsaturated polymer of the type $[CH(CH_2)_3CH]_n$. Again, the reaction can be driven to the right side by removing the gaseous ethylene from the reaction mixture through purging.

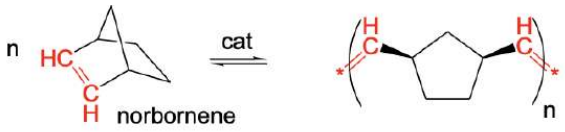


Figure **7.3.6.5**: Ring-opening metathesis polymerization (ROMP)

Another variation of olefin metathesis is ring-opening metathesis polymerization (ROMP). It allows to make polymers from strained cycloolefins, for example norbornene. The reaction driving force is the relief of the strain. Because the strain is removed in the polymer, the chemical equilibrium lies far on the right side. The reaction product in norbornene is a polymer with 5-membered rings that are interconnected by ethylene -CH=CH- units (Fig. **7.3.6.5**).

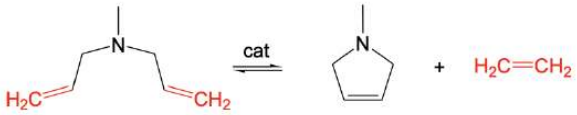


Figure **7.3.6.6**: Ring-closing metathesis (RCM)

The opposite of ROMP is ring-closure metathesis (RCM). RCM allows for the preparation of unstrained rings with C=C double bonds from dienes with C=C double bonds that are five or six carbon atoms apart. This distance is suitable to produce unstrained rings. In the shown example a five-membered ring with a C=C double bond is formed from a diene with terminal C=C double bonds that are five atoms apart.

The Mechanism of Olefin Metathesis

What is the mechanism of olefin metathesis?

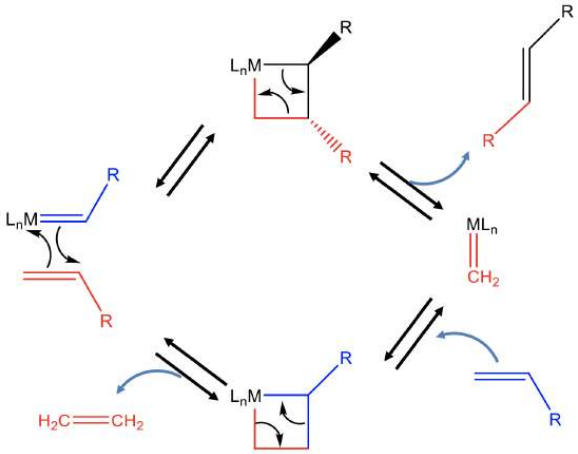


Figure **7.3.6.7**: The mechanism of olefin metathesis

In the first step, the alkene adds to the the carbene fragment of the catalyst in a 2+2 cycloaddition reaction to produce an unstable intermediate with a highly strained four-membered ring (Fig. **7.3.6.7**). This four membered ring can open to produce the first new alkene product R-CH=CH-R and a metal carbene species. This metal carbene can react with another reactant olefin to form another highly stained 4-ring intermediate via a 2+2 cycloaddition reaction. This ring can then reopen again to produce the second alkene metathesis product, in this case ethylene, and the original catalyst. The regenerated catalyst can then start a new catalytic cycle.

Dr. Kai Landskron (Lehigh University). If you like this textbook, please consider to make a donation to support the author's research at Lehigh University: Click Here to Donate.

This page titled 7.3.6: Olefin Metathesis is shared under a CC BY-NC-SA 4.0 license and was authored, remixed, and/or curated by Kathryn Haas.

- **12.2: Organometallic Catalysts** by Kai Landskron is licensed CC BY 4.0.

7.4: Heterogeneous Catalysts

Heterogeneous Catalysis

In **heterogeneous catalysis**, the catalyst is in a different phase from the reactants. At least one of the reactants interacts with the solid surface in a physical process called adsorption in such a way that a chemical bond in the reactant becomes weak and then breaks. Poisons are substances that bind irreversibly to catalysts, preventing reactants from adsorbing and thus reducing or destroying the catalyst's efficiency.

An example of heterogeneous catalysis is the interaction of hydrogen gas with the surface of a metal, such as Ni, Pd, or Pt. As shown in part (a) in Figure **7.4.2**, the hydrogen–hydrogen bonds break and produce individual adsorbed hydrogen atoms on the surface of the metal. Because the adsorbed atoms can move around on the surface, two hydrogen atoms can collide and form a molecule of hydrogen gas that can then leave the surface in the reverse process, called desorption. Adsorbed H atoms on a metal surface are substantially more reactive than a hydrogen molecule. Because the relatively strong H–H bond (dissociation energy = 432 kJ/mol) has already been broken, the energy barrier for most reactions of H_2 is substantially lower on the catalyst surface.

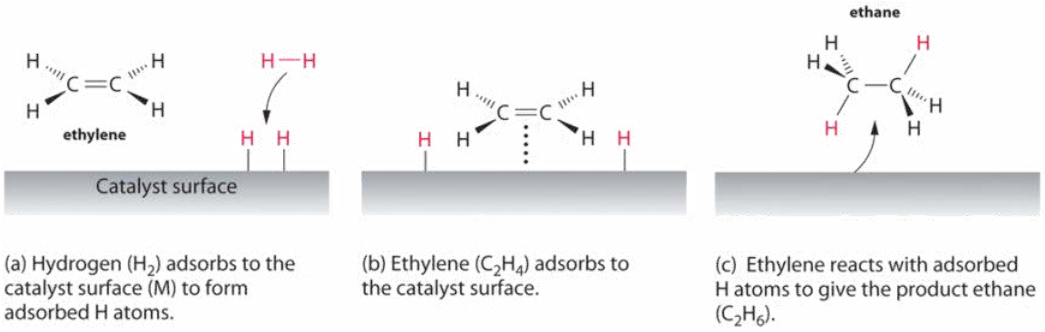


Figure **7.4.1**: Hydrogenation of Ethylene on a Heterogeneous Catalyst. When a molecule of hydrogen adsorbs to the catalyst surface, the H–H bond breaks, and new M–H bonds are formed. The individual H atoms are more reactive than gaseous H_2. When a molecule of ethylene interacts with the catalyst surface, it reacts with the H atoms in a stepwise process to eventually produce ethane, which is released. (CC BY-NC-SA; anonymous)

Figure **7.4.1** shows a process called *hydrogenation*, in which hydrogen atoms are added to the double bond of an alkene, such as ethylene, to give a product that contains C–C single bonds, in this case ethane. Hydrogenation is used in the food industry to convert vegetable oils, which consist of long chains of alkenes, to more commercially valuable solid derivatives that contain alkyl chains. Hydrogenation of some of the double bonds in polyunsaturated vegetable oils, for example, produces margarine, a product with a melting point, texture, and other physical properties similar to those of butter.

Several important examples of industrial heterogeneous catalytic reactions are in Table **7.4.1**. Although the mechanisms of these reactions are considerably more complex than the simple hydrogenation reaction described here, they all involve adsorption of the reactants onto a solid catalytic surface, chemical reaction of the adsorbed species (sometimes via a number of intermediate species), and finally desorption of the products from the surface.

Table **7.4.1**: Some Commercially Important Reactions that Employ Heterogeneous Catalysts

Commercial Process	Catalyst	Initial Reaction	Final Commercial Product
contact process	V_2O_5 or Pt	$2SO_2 + O_2 \rightarrow 2SO_3$	H_2SO_4
Haber process	Fe, K_2O, Al_2O_3	$N_2 + 3H_2 \rightarrow 2NH_3$	NH_3
Ostwald process	Pt and Rh	$4NH_3 + 5O_2 \rightarrow 4NO + 6H_2O$	HNO_3
water–gas shift reaction	Fe, Cr_2O_3, or Cu	$CO + H_2O \rightarrow CO_2 + H_2$	H_2 for NH_3, CH_3OH, and other fuels
steam reforming	Ni	$CH_4 + H_2O \rightarrow CO + 3H_2$	H_2
methanol synthesis	ZnO and Cr_2O_3	$CO + 2H_2 \rightarrow CH_3OH$	CH_3OH
Sohio process	bismuth phosphomolybdate	$\mathbf{CH_2{=}CHCH_3 + NH_3 + \frac{3}{2}O_2 \rightarrow CH_2{=}CHCN + 3H_2O}$	$\mathbf{CH_2{=}CHCN}$ acrylonitrile
catalytic hydrogenation	Ni, Pd, or Pt	RCH=CHR′ + H2 → RCH_2—CH_2R'	partially hydrogenated oils for margarine, and so forth

This page titled 7.4: Heterogeneous Catalysts is shared under a CC BY-NC-SA 4.0 license and was authored, remixed, and/or curated by Kathryn Haas.

- **14.7: Catalysis** is licensed CC BY-NC-SA 3.0.

7.4.1: Ziegler-Natta Polymerizations

Another example of an organometallic catalytic reaction is the Ziegler-Natta olefin polymerization. This reaction is of high industrial importance for the production of olefins like polyethylene. There are both heterogeneous and homogeneous Ziegler-Natta catalysts. The mechanism for the homogeneous catalysts is generally well understood. Homogeneous catalysts are typically metallocene catalysts.

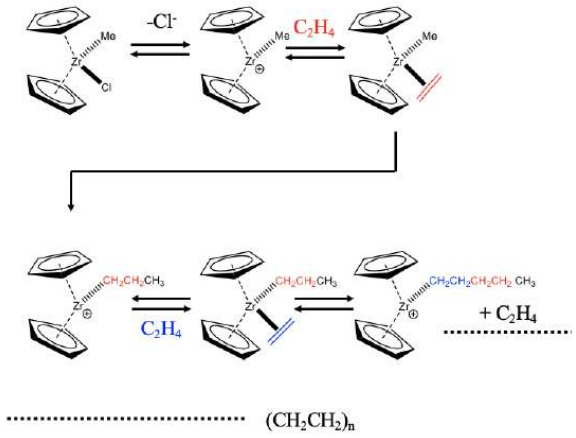


Figure **7.4.1.1**: Zirconium-based Ziegler-Natta catalyst (Attribution: A. Vedernikov, U Maryland (modified).)

An example of a zirconium-based catalyst is shown (Fig. **7.4.1.1**). The catalyst is a coordinatively unsaturated complex cation with two cyclopentadienyl rings and a methyl group. The catalyst is formed from its precatalyst, a neutral molecule with an additional chloro ligand. The catalyst oxidatively adds an olefin like an ethylene molecule to the coordinatively unsaturated site. This step is followed an olefin insertion step that produces a propyl group. The migratory insertion leads to the formation of a vacant site, that can be re-oocupied by another ethylene molecule. This molecule can insert into the propyl chain thereby prolonging the propyl chain to a pentyl chain. The olefin insertion step generates another vacant site that can be reoccupied by a new ethylene molecule. Repeating the catalytic cycle many times eventually leads to polyethylene.

The Ziegler-Natta (ZN) catalyst, named after two chemists: Karl Ziegler and Giulio Natta, is a powerful tool to polymerize α-olefins with high linearity and stereoselectivity (Figure 1). A typical ZN catalyst system usually contains two parts: a transition metal (Group IV metals, like Ti, Zr, Hf) compound and an organoaluminum compound (co-catalyst). The common examples of ZN catalyst systems include $TiCl_4$ + Et_3Al and $TiCl_3$ + $AlEt_2Cl$.

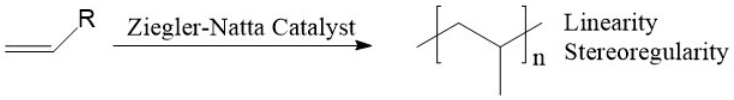


Figure **7.4.1.2**: The generic reaction equation for polymerization of -olefins.

In 1953, German chemist Karl Ziegler discovered a catalytic system able to polymerize ethylene into linear, high molecular weight polyethylene which conventional polymerization techniques could not make.[1] The system contained a transition metal halide with a main group element alkyl compound (Figure **7.4.1.3**).

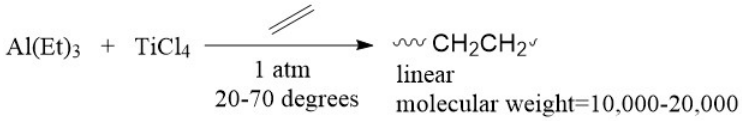


Figure **7.4.1.3**: Linear polyethylene obtained by Ziegler's catalytic system (20-70).

Following the catalytic design, Italian chemist Giulio Natta found that polymerization of α-olefins resulted in stereoregular structures,[2] either syndiotactic or isotactic, depending on the catalyst used (Figure **7.4.1.4**). Because of these important discoveries, Karl Ziegler and Giulio Natta shared the Nobel Prize in Chemistry in 1963.

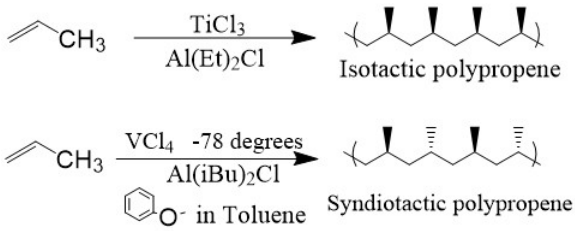


Figure **7.4.1.4**: The ZN catalytic polymerization of linear polypropene with two different stereoregular structures.

Advantages over traditional polymerization method

Traditionally, polymerization of α-olefins was done by radical polymerization (Figure **7.4.1.5**). Problem with this technique was that the formation of undesired allylic radicals leaded to branched polymers.[3] For example, radical polymerization of propene gived branched polymers with large molecular weight distribution. Also, radical polymerization had no control over stereochemistry. Linear unbranched polyethylene and stereoregulated polypropylene could not be fabricated by free radical polymerization. This technique largely limited the potential applications of these polymeric materials.

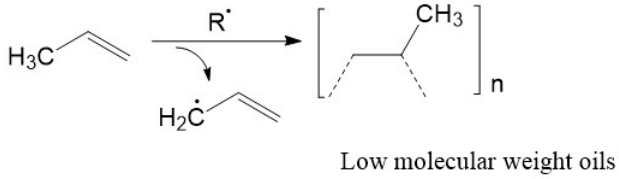


Figure **7.4.1.5**: The radical polymerization of propylene using traditional method.

The invention of ZN catalyst successfully addressed these two problems. The catalyst can give linear α-olefin polymers with high and controllable molecular weights. Moreover, it makes the fabrication of polymers with specific tacticity possible. By controlling the stereochemistry of products, either syndiotactic or isotactic polymers can be achieved.

Mechanism of Ziegler-Natta catalytic polymerization

Activation of Ziegler-Natta catalyst

It is necessary to understand the catalyst's structure before understanding how this catalyst system works. Herein, $TiCl_4$+$AlEt_3$ catalyst system is taken as an example. The titanium chloride compound has a crystal structure in which each Ti atom is coordinated to 6 chlorine atoms. On the crystal surface, a Ti atom is surrounded by 5 chlorine atoms with one empty orbital to be filled. When Et_3Al comes in, it donates an ethyl group to Ti atom and the Al atom is coordinated to one of the chlorine atoms. Meanwhile, one chlorine atom from titanium is kicked out during this process. Thus, the catalyst system still has an empty orbital (Figure **7.4.1.6**). The catalyst is activated by the coordination of $AlEt_3$ to Ti atom.

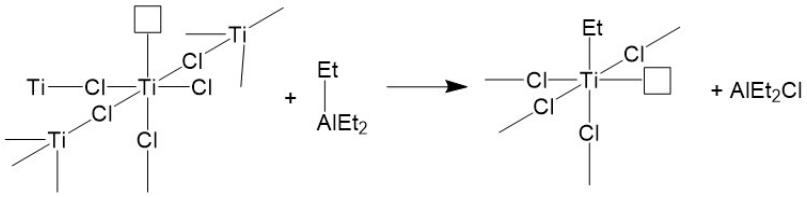


Figure **7.4.1.6**: The activation of ZN catalyst system by coordination of $AlEt_3$ to Ti atom.

Initiation step

The polymerization reaction is initiated by forming alkene-metal complex. When a vinyl monomer like propylene comes to the active metal center, it can be coordinated to Ti atom by overlapping their orbitals. As shown in Figure **7.4.1.7**, there is an empty dxy orbital and a filled dx^2-y^2 orbital in Ti's outermost shell (the other four orbitals are not shown here). The carbon-carbon double bond of alkene has a pi bond, which consists of a filled pi-bonding orbital and an empty pi-antibonding orbital. So, the alkene's pi-bonding orbital and the Ti's dxy orbital come together and share a pair of electrons. Once they're together, that Ti's dx^2-y^2 orbital comes mighty close to the pi-antibonding orbital, sharing another pair of electrons.

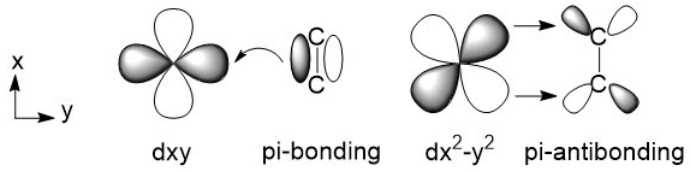


Figure **7.4.1.7**: Molecular orbitals representation of monomer coordinating to metal center.

The formed alkene-metal complex (1) then goes through electron shuffling, with several pairs of electrons shifting their positions: The pair of electrons from the carbon-carbon pi-bond shifts to form Ti-carbon bond, while the pair of electrons from the bond between Ti and AlEt3' ethyl group shifts to form a bond between the ethyl group and the methyl-substituted carbon of propylene (Figure **7.4.1.8**). After electron shuffling, Ti is back with an empty orbital again, needing electrons to fill it (2).

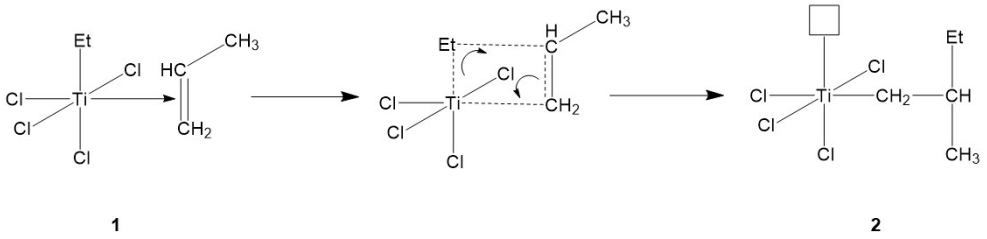


Figure **7.4.1.8**: The formation process of alkene-metal complex.

Propagation step

When other propylene molecules come in, this process starts over and over, giving linear polypropylene (Figure **7.4.1.9**).

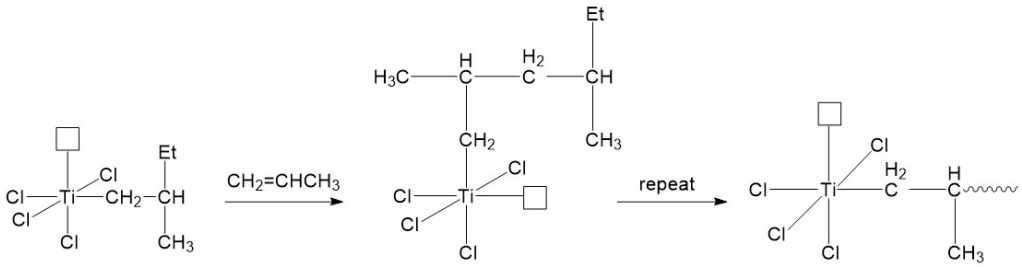


Figure **7.4.1.9**: Propagation towards polymeric chains.

Termination step

Termination is the final step of a chain-growth polymerization, forming "dead" polymers (desired products). Figure **7.4.1.10** illustrates several termination approaches developed with the aid of co-catalyst $AlEt_3$.[4]

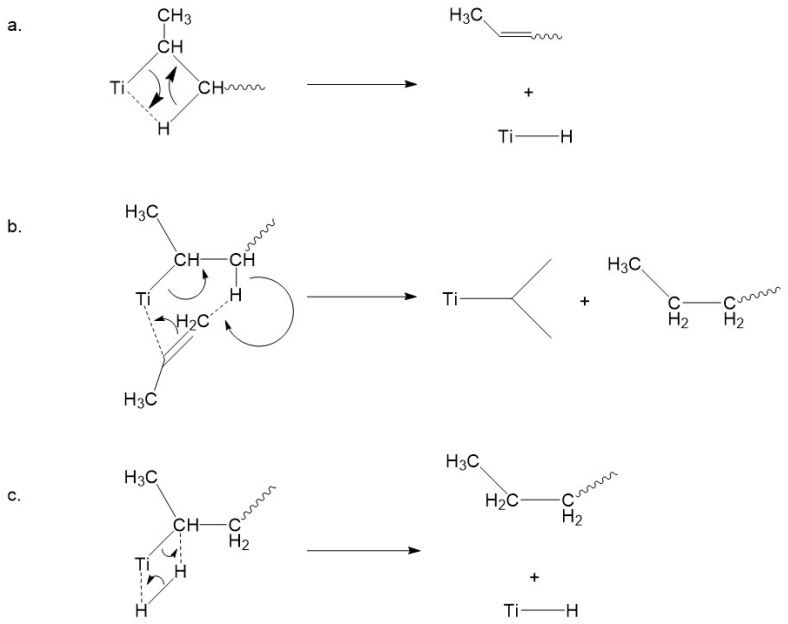


Figure 7.4.1.10: Three termination approaches: (a) β-elimination from the polymer chain, forming metal hydride; (b) β-elimination with hydrogen transfer to monomer; (c)hydrogenation.

Mechanistic study: kinetic isotope effect experiments

Unlike the mechanism discussed above, there is also a competing mechanism proposed by Ivin and coworkers.[5] They proposed that a 1,2-hydrogen shift occurs prior to monomer association, giving a carbene intermediate (Figure 7.4.1.11).

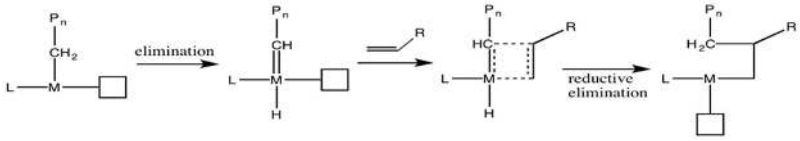


Figure 7.4.1.11: Alternative propagation mechanism: hydride shift prior to monomer association.

To determine the actual mechanism, Grubbs[6] conducted kinetic isotope effect (KIE) experiments. Due to their different weights, carbon-deuterium bond reacts slower than carbon-hydrogen bond (Figure 7.4.1.12). If such bonds are involved in the rate-determining step, the isotopic species should proceed in lower rate.

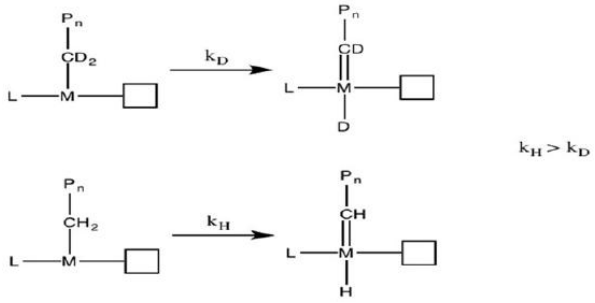


Figure 7.4.1.12: Carbon-deuterium bonds react slower than carbon-hydrogen bonds.

In Grubbs's experiment, deuterated ethylene and normal ethylene were catalyzed by Ziegler-Natta catalyst with 1:1 ratio (Figure 7.4.1.13). The result showed that H/D ratio in the resulting polymers was still 1:1.6 This indicated that no carbon-hydrogen bond cleavage or formation is involved in the rate determining step. Therefore, the mechanism proposed by Ivin was excluded.

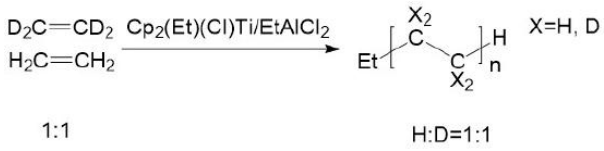


Figure **7.4.1.13**: KIE experiment excludes Ivin's mechanism.

Regio- and stero-selectivity

Regio-selectivity

For propene polymerization, most ZN catalysts are highly regioselective, favoring 1,2-primary insertion [M-R + CH2=CH(Me)=M-CH2-CH(Me)(R)] (Figure **7.4.1.14**), due to electronic and steric effects.[7]

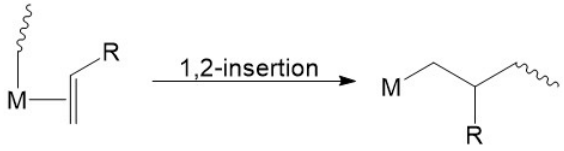


Figure **7.4.1.14**: Primary insertion occurs in ZN-catalytic system to give regioselective products.

Stereo-selectivity

Stereochemistry of polymers made from ZN-catalyst can be well regulated by rational design of ligands. By using different ligand system, either syndiotactic or isotactic polymers can be obtained (Figure **7.4.1.15**).

The relative stereochemistry of adjacent chiral centers within a macromolecule is defined as tacticity. Three kinds of stereochemistry are possible: isotactic, syndiotactic and atactic. In isotactic polymers, substituents are located on the same side of the polymer backbone, while substituents on syodiotactic polymers have alternative positions. In atactic polymers, substituents are placed randomly along the chain.

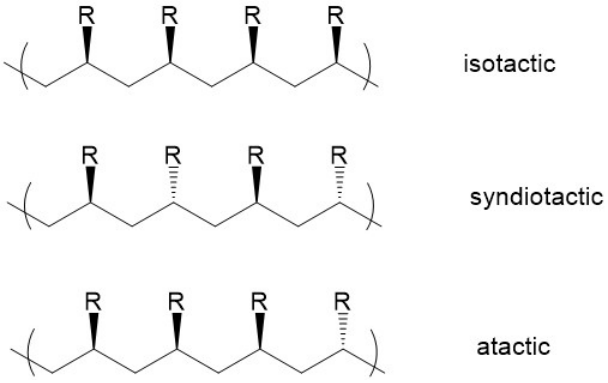


Figure **7.4.1.15**: Tacticity of macromolecules

Choice of ZN catalyst regulates the stereochemistry. We use propylene polymerization as an example here. Recall the mechanism section, a monomer approaches the metal center and forms a four-membered ring intermediate. The binding of a monomer to the reactive metal-carbon bond should occur in from the least hindered site.[8] As shown in Figure **7.4.1.16**, the trans-complex in which methyl on the growing chain is trans to the methyl group on the incoming monomer, should be energetically favored than the cis-complex, as the trans-complex experience less steric effect.

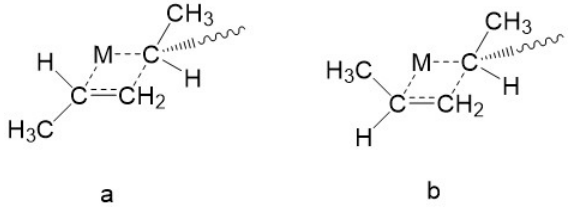


Figure **7.4.1.16**: The active state a (trans) is more stable than b (cis) due to less steric effects of methyl groups.

Following the trans- complex, the methyl group on the newly added monomer is trans to that on the previous monomer. The step repeats so that a syndiotactic polypropylene is obtained (Figure **7.4.1.17**a). However, if the metal center is coordinated with bulky ligands (e.g. –iBu, -Et2 groups), as denoted by Y in Figure **7.4.1.17**b, the incoming monomer will adopt a cis-conformation to avoid serious steric effect with the bulky ligand. Thus, at the presence of bulky ligand, the propylene monomer is cis to the growing chain. This results in a isotactic product.

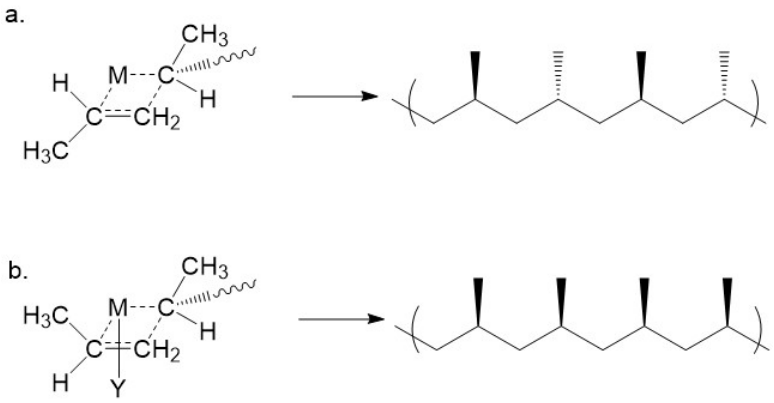


Figure **7.4.1.17**: a. Trans-intermediate avoids 1,3-strain of methyl groups, producing syndiotactic polypropylene; b. at the presence of bulky ligand Y, a cis-intermediate is adopted, generating isotactic polypropylene.

Applications

ZN catalysts have provided a worldwide profitable industry with production of more than 160 billion pounds and creation of numerous positions.[9] These products have been extensively applied in different areas, largely improving the quality of people's life. They can catalyze α-olefins to produce various commercial polymers, like polyethylene, polypropylene and Polybutene-1. Polyethylene and polypropylene is reported to be the top two widely used synthetic plastic in the word.[10]

Among the polyethylene fabricated by ZN catalysts, there are three major classes: high density polyethylene (HDPE), linear low density polyethylene (LLDPE), and ultra-high molecular weight polyethylene (UHMWPE). HDPE, a linear homopolymer, is widely applied in garbage containers, detergent bottles and water pipes because of its high tensile strength. Compared with HDPE whose branching degree is quite low, LLDPE has many short branches. Its better toughness, flexibility and stress-cracking resistance makes it suitable for materials like cable coverings, bubble wrap and so on. UHMWPE is polyethylene with a molecular weight between 3.5 and 7.5 million. This material is extremely tough and chemically resistant. Therefore, it is often used to make gears and artificial joints.

Compared to polyethylene, polypropylene has enhanced mechanical properties and thermal resistance because of the additional methyl group. Moreover, isotactic polypropylene is stiffer and more resistant to creep than atactic polypropylene. Polypropylene has a wide range of applications in clothing, medical plastics, food packing, and building construction.

Substrate scope and limitations

ZN catalysts are effective for polymerization of α-Olefins (ethylene, propylene) and some dienes (butadiene, isoprene). However, they don't work for some other monomers, such as 1.2 disubstituted double bonds. Vinyl chloride cannot be polymerized by ZN catalyst either, because free radical vinyl polymerization is initiated during the reaction. Another situation that ZN catalysts don't work is when the substrate is acrylate. The reason is that ZN catalysts often initiate anionic vinyl polymerization in those monomers.[11]

References

1. Ziegler, K.; Holzkamp, E.; Breil, H.; Martin, H., Polymerisation Von Athylen Und Anderen Olefinen. Angew Chem Int Edit 1955, 67 (16), 426-426.
2. Natta, G., Une Nouvelle Classe De Polymeres D Alpha-Olefines Ayant Une Regularite De Structure Exceptionnelle. J Polym Sci 1955, 16 (82), 143-154.
3. Mulhaupt, R., Catalytic polymerization and post polymerization catalysis fifty years after the discovery of Ziegler's catalysts. Macromol Chem Phys 2003, 204 (2), 289-327.

4. Sinn, H.; Kaminsky, W., Ziegler-Natta Catalysis. In Advances in Organometallic Chemistry, Stone, F. G. A.; Robert, W., Eds. Academic Press: 1980; Vol. Volume 18, pp 99-149.
5. Ivin, K. J.; Rooney, J. J.; Stewart, C. D.; Green, M. L.; Mahtab, R., Mechanism for the stereospecific polymerization of olefins by Ziegler–Natta catalysts. Journal of the Chemical Society, Chemical Communications 1978, (14), 604-606.
6. Soto, J.; Steigerwald, M. L.; Grubbs, R. H., Concerning the Mechanism of Ziegler-Natta Polymerization - Isotope Effects on Propagation Rates. J Am Chem Soc 1982, 104 (16), 4479-4480.
7. Busico, V.; Cipullo, R.; Pellecchia, R.; Ronca, S.; Roviello, G.; Talarico, G., Design of stereoselective Ziegler-Natta propene polymerization catalysts. P Natl Acad Sci USA 2006, 103 (42), 15321-15326.
8. Zambelli, A., Stereoregulation of Propylene Polymerization. Abstr Pap Am Chem S 1974, 34-34.
9. Ittel, S. D.; Johnson, L. K.; Brookhart, M., Late-metal catalysts for ethylene homo- and copolymerization. Chem Rev 2000, 100 (4), 1169-1203.
10. Macbride, R. R., High Molecular-Weight Polyethylene Drums Show Signs of Becoming Big Business. Mod Plast 1975, 52 (12), 10-&.
11. Ivan, B., Comparison of Living Polymerization Systems. Macromol Symp 1994, 88, 201-215.

Contributors and Attributions

- Fangyuan Dong and Ru Deng

This page titled 7.4.1: Ziegler-Natta Polymerizations is shared under a CC BY-NC-SA 4.0 license and was authored, remixed, and/or curated by Kathryn Haas.

- **12.2: Organometallic Catalysts** by Kai Landskron is licensed CC BY 4.0.

7.4.2: Water-Gas Shift Reaction

The **water-gas shift reaction** (WGSR) describes the reaction of carbon monoxide and water vapor (steam) at very high temperatures to form carbon dioxide and hydrogen:

$$\mathrm{CO + H_2O \rightleftharpoons CO_2 + H_2} \tag{7.4.2.1}$$

The WGSR is a highly valuable industrial reaction that is used in the manufacture of ammonia, hydrocarbons, methanol, and hydrogen. Its most important application is in the conversion of carbon monoxide or other hydrocarbons to produce hydrogen gas, an important source of fuel for a modern hydrogen economy. If hydrogen could be produced at low cost and using a renewable resource, it could significantly advance the movement to sustainable energy.

Most of the catalysts that are used for this process are heterogeneous catalysts. Unfortunately, the process using heterogeneous catalysts occurs only at extremely high temperatures and pressures. The high energy cost of performing the reaction limits its industrial utility, and there are efforts to produce homogeneous catalysts that catalyze the reaction at more mild conditions. Another limitation is that the reaction requires sufficient quantities of CO, which are primarily obtained from non-renewable coal or petroleum sources. However, there are processes that can convert methane gas, which is an abundant greenhouse gas, to .

The WGSR has been extensively studied for over a hundred years. The kinetically relevant mechanism depends on the catalyst composition and the temperature. Two mechanisms have been proposed: an associative Langmuir–Hinshelwood mechanism and a redox mechanism. The redox mechanism is generally regarded as kinetically relevant during the high-temperature WGSR (> 350 °C) over the industrial Fe-Cr catalyst. Historically, there has been much more controversy surrounding the mechanism at low temperatures. Recent experimental studies confirm that the associative carboxyl mechanism is the predominant low temperature pathway on metal-oxide-supported transition metal catalysts.

Associative mechanism

In 1920 Armstrong and Hilditch first proposed the associative mechanism. In this mechanism CO and H_2O are adsorbed onto the surface of the catalyst, followed by formation of an intermediate and the desorption of H_2 and CO_2. In general, H_2O dissociates onto the catalyst to yield adsorbed OH and H. The dissociated water reacts with CO to form a carboxyl or formate intermediate. The intermediate subsequently dehydrogenates to yield CO_2 and adsorbed H. Two adsorbed H atoms recombine to form H_2.

There has been significant controversy surrounding the kinetically relevant intermediate during the associative mechanism. Experimental studies indicate that both intermediates contribute to the reaction rate over metal oxide supported transition metal catalysts. However, the carboxyl pathway accounts for about 90% of the total rate owing to the thermodynamic stability of adsorbed formate on the oxide support. The active site for carboxyl formation consists of a metal atom adjacent to an adsorbed hydroxyl. This ensemble is readily formed at the metal-oxide interface and explains the much higher activity of oxide-supported transition metals relative to extended metal surfaces. The turn-over-frequency for the WGSR is proportional to the equilibrium constant of hydroxyl formation, which rationalizes why reducible oxide supports (e.g. CeO_2) are more active than irreducible supports (e.g. SiO_2) and extended metal surfaces (e.g. Pt). In contrast to the active site for carboxyl formation, formate formation occurs on extended metal surfaces. The formate intermediate can be eliminated during the WGSR by using oxide-supported atomically dispersed transition metal catalysts, further confirming the kinetic dominance of the carboxyl pathway.

Redox mechanism

The redox mechanism involves a change in the oxidation state of the catalytic material. In this mechanism, CO is oxidized by an O-atom intrinsically belonging to the catalytic material to form CO_2. A water molecule undergoes dissociative adsorption at the newly formed O-vacancy to yield two hydroxyls. The hydroxyls disproportionate to yield H_2 and return the catalytic surface back to its pre-reaction state.

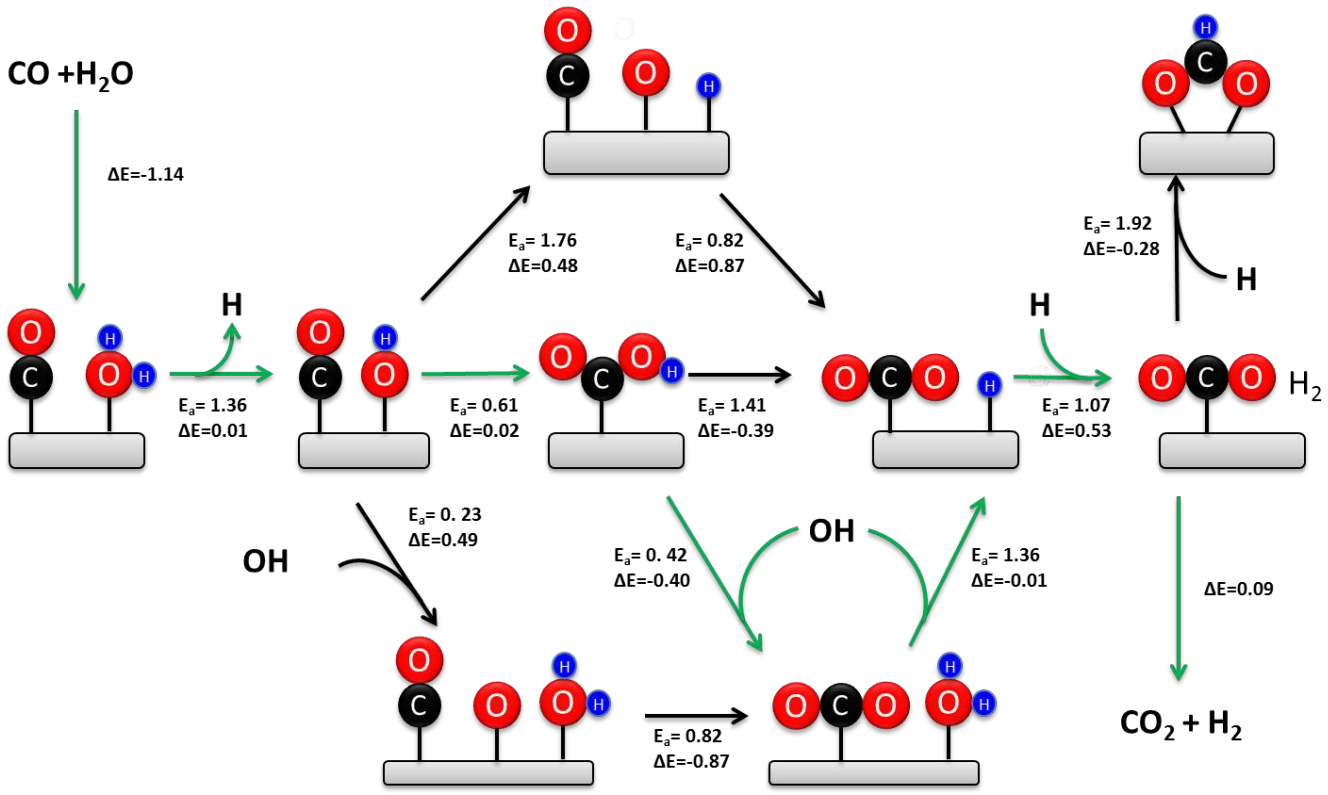


Figure **7.4.2.1**: Proposed associative and redox mechanisms of the water gas shift reaction. (Zwickipedia, WGS mechanism, CC BY-SA 3.0)

Source: https://en.Wikipedia.org/wiki/Water%...shift_reaction

---

This page titled 7.4.2: Water-Gas Shift Reaction is shared under a CC BY-NC-SA 4.0 license and was authored, remixed, and/or curated by Kathryn Haas.

7.5: Problems

This page titled 7.5: Problems is shared under a CC BY-NC-SA 4.0 license and was authored, remixed, and/or curated by Kathryn Haas.

7.5.1: Concept Review Questions Chapter 12

Concept Review Questions

Section 1

1) What is an oxidative addition?

2) What is a reductive elimination?

3) What is a cis and a trans addition, respectively?

4) Does the coordination number in oxidative additions always increase? Explain.

5) What is the reverse reaction of an oxidative addition?

6) What is a migratory insertion?

7) Are migratory insertions reversible reactions?

Section 2

1) Why are transition metal alkyl complexes that have alkyl groups longer than 1 carbon atom often unstable?

2) What is meant by beta-hydride elimination?

3) What is alpha-abstraction?

4) What is a nucleophilic displacement reaction?

5) What is meant by an oxidative addition of an intact ligand?

6) Write the catalytic cyclic for the deuteration of benzene with Cp_2TaH_3 as a catalyst. Name each reaction step.

7) What is Collman's reagent and how is it being used?

8) What is Wilkinson's catalyst, and what reactions can it be used for. Write the catalytic cycle.

9) Write done the reaction mechanism for the Ziegler-Natta olefin polymerization.

10) What is carbene migratory insertion?

11) Write down the catalytic cycle for the hydroformylation of olefins.

12) Name three hydrocarbonylation reactions. What are the reactants?

13) Write down the mechanism for the Monsanto acetic acid process.

14) What is olefin metathesis?

15) What is ring-opening olefin polymerization (ROMP)?

16) What is acyclic diene metathesis?

17) Why are olefins with terminal C=C double bonds particularly useful in olefin metathesis?

18) What is ring-closing metathesis?

19) What are the characteristics of Schrock and Grubbs catalysts, respectively?

20) Write down the catalytic cycle for olefin metathesis.

Dr. Kai Landskron (Lehigh University). If you like this textbook, please consider to make a donation to support the author's research at Lehigh University: Click Here to Donate.

This page titled 7.5.1: Concept Review Questions Chapter 12 is shared under a CC BY-NC-SA 4.0 license and was authored, remixed, and/or curated by Kathryn Haas.

- **Concept Review Questions Chapter 12** by Kai Landskron is licensed CC BY 4.0.

7.5.2: Homework Problems Chapter 12

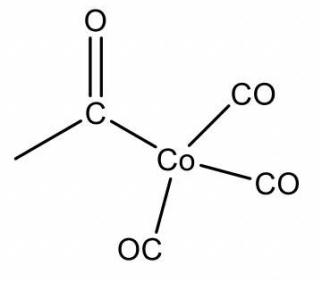
Homework Problems

Section 1

Exercise 1

The coordination compound $CH_3Co(CO)_4$ undegoes a migratory insertion. What is the reaction product?

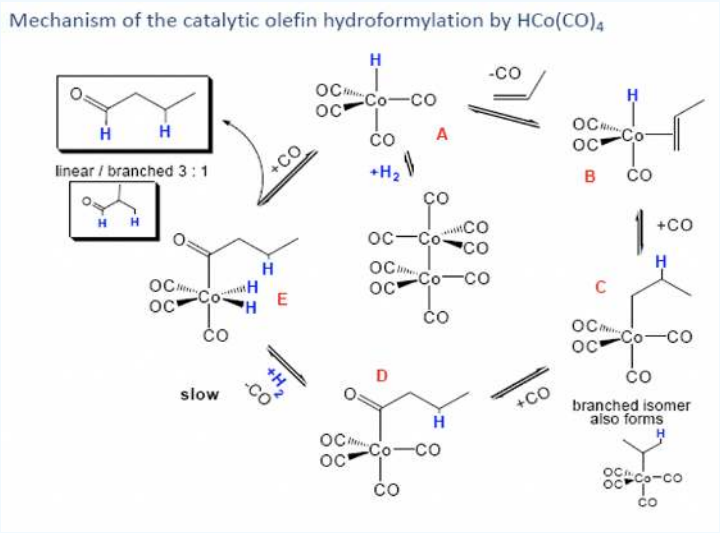
Answer



Section 2

Exercise 1

Identify all oxidative additions in the catalytic cycle of olefin hydroformylation:



Answer

Step D --> E is an oxidative addition

Formation of $HCo(CO)_4$ from $Co_2(CO)_8$ is also an oxidative addition.

Exercise 2

1. What are the reaction products of the following olefin metathesis reactions?

a) 2 CH_2=CH-Ph -->

b) n CH_2=CH-CH=CH_2 -->

Answer

a) $CH_2=CH_2$ and Ph-CH=CH-Ph

b) $CH_2=CH_2$ and $(CH=CH)_n$

Exercise 3

What reaction product would you expect would you expect from the following reaction:

$Fe(CO)_4^{2-} + CH_3CH_2I$ -->

Name the reaction.

Answer

$Fe(CO)_4CH_2CH_3^- + I^-$ Nucleophilic displacement

Exercise 4

Which of the following phosphines would you expect to be most suitable to stabilize metals in low oxidation states:

a) $P(CF_3)_3$

b) $P(CH_3)_3$

c) PH_3

Answer

a) $P(CF_3)_3$

Exercise 5

What reaction product would you expect from the following reaction?

$Pt(PPh_3)_4 + 4\ NPh_3$ -->

Answer

There would be no reaction.

Exercise 6

Which of the following complexes would likely be unstable:

a) $[PtCl_3(C_2H_5)]^{2-}$

b) $[PtCl_3(CH_3)]^{2-}$

c) $PtCl_4^{2-}$

Answer

a) $[PtCl_3(C_2H_5)]^{2-}$

Dr. Kai Landskron (Lehigh University). If you like this textbook, please consider to make a donation to support the author's research at Lehigh University: Click Here to Donate.

This page titled 7.5.2: Homework Problems Chapter 12 is shared under a CC BY-NC-SA 4.0 license and was authored, remixed, and/or curated by Kathryn Haas.

- **Homework Problems Chapter 12** by Kai Landskron is licensed CC BY 4.0.

CHAPTER OVERVIEW

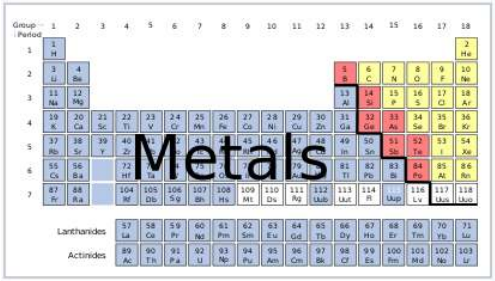
8: Solid State Chemistry

8.1: Prelude to Metals and Alloys
8.2: Unit Cells and Crystal Structures
8.3: Crystal Structures of Metals
8.4: Conduction in Metals
8.5: Atomic Orbitals and Magnetism
8.6: Ferro-, Ferri- and Antiferromagnetism
8.7: Hard and Soft Magnets
8.8: Defects in Metallic Crystals
8.9: X-ray Crystallography
8.10: Miller Indices (hkl)
8.11: Powder X-ray Diffraction
8.12: Prelude to Ionic and Covalent Solids - Structures
8.13: Close-packing and Interstitial Sites
8.14: Structures Related to NaCl and NiAs
8.15: Tetrahedral Structures
8.16: Layered Structures and Intercalation Reactions
8.17: Ionic Radii and Radius Ratios
8.18: Structure Maps
8.19: Energetics of Crystalline Solids- The Ionic Model
8.20: Born-Haber Cycles for NaCl and Silver Halides
8.21: Lattice Energies and Solubility
8.22: Spinel, Perovskite, and Rutile Structures
8.23: Kapustinskii Equation
8.24: New Page

8: Solid State Chemistry is shared under a CC BY-NC-SA 4.0 license and was authored, remixed, and/or curated by LibreTexts.

8.1: Prelude to Metals and Alloys

In the chemistry of molecular compounds, we are accustomed to the idea that properties depend strongly on structure. For example we can rationalize the polarity of the water molecule based on its shape. We also know that two molecules with the same composition (e.g., ethanol and dimethyl ether) have very different properties based on the bonding arrangements of atoms. It should come as no surprise that the properties of extended solids are also connected to their structures, and so to understand what they do we should begin with their crystal structures. Most of the metals in the periodic table have relatively simple structures and so this is a good place to begin.



Over 2/3 of the elements in the periodic table exist in their pure form as metals. All elemental metals (except the three - Cs, Ga, Hg - that are liquid) are crystalline solids at room temperature, and most have one of three simple crystal structures.

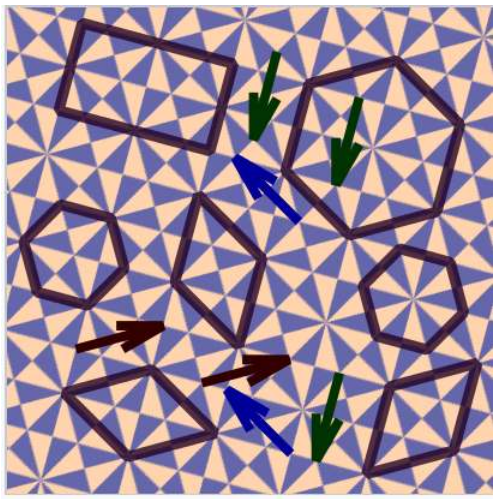
8.1: Prelude to Metals and Alloys is shared under a CC BY-NC-SA 4.0 license and was authored, remixed, and/or curated by LibreTexts.

- **6.1: Prelude to Metals and Alloys** by Chemistry 310 is licensed CC BY-SA 4.0. Original source: https://en.wikibooks.org/wiki/Introduction_to_Inorganic_Chemistry.

8.2: Unit Cells and Crystal Structures

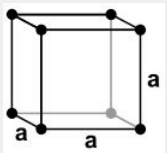
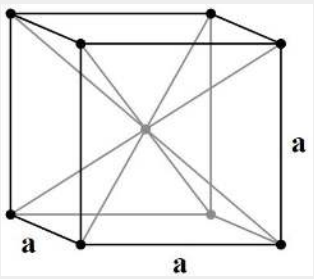
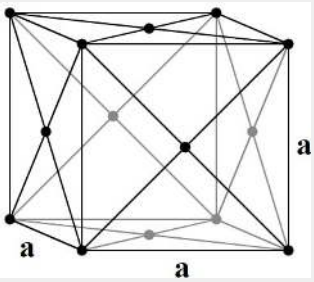
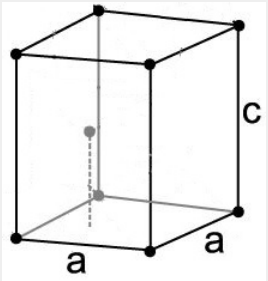
Crystals can be thought of as repeating patterns, much like wallpaper or bathroom tiles, but in three dimensions. The fundamental repeating unit of the crystal is called the **unit cell**. It is a three dimensional shape that can be repeated over and over by unit translations to fill space (and leave minimal gaps) in the structure. Some possible unit cells are shown in the tiling pattern at the right, along with arrows that indicate **unit translation vectors**. In three dimensions, the hexagonal or rhombic unit cells of this pattern would be replaced by three dimensional boxes that would stack together to fill all space. As shown in the figure, the origin of the unit cell is arbitrary. The same set of boxes will fill all space no matter where we define the origin of the lattice. We will see that pure metals typically have very simple crystal structures with cubic or hexagonal unit cells. However the crystal structures of alloys can be quite complicated.

When considering the crystal structures of metals and alloys, it is not sufficient to think of each atom and its neighboring ligands as an isolated system. Instead, think of the entire metallic crystal as a network of atoms connected by a sea of shared valence electrons. The **electrons are delocalized** because there are **not enough of them** to fill each "bond" between atoms with an electron pair. For example, in the crystal structures of s-block and p-block metals, each atom has either 8 or 12 nearest neighbors, but the maximum number of s + p electrons is 8. Thus, there are not enough to put two electrons between each pair of atoms. Transition metals can also use their d-orbitals in bonding, but again there are never enough electrons to completely fill all the "bonds."



Possible unit cells in a periodic tile pattern. The arrows connect translationally equivalent points (lattice points) in the pattern.

The atoms in a metal lattice arrange themselves in a certain pattern which can be represented as a 3D box structure known as the **unit cell** which repeats across the entire metal.

Simple Cubic	Body Centered Cubic	Face Centered Cubic	Hexagonal Close Packed
			
1 atom/cell	2 atoms/cell	4 atoms/cell	2 atoms/cell

Metal atoms can be approximated as spheres, and therefore are not 100 % efficient in packing, the same way a stack of cannonballs has some empty spaces between the balls. Different unit cells have different packing efficiencies. The number of atoms that is

included in the unit cell only includes the fractions of atoms *inside* of the box. Atoms on the corners of the unit cell count as ⅛ of an atom, atoms on a face count as ½, an atom in the center counts as a full atom. Using this, let's calculate the number of atoms in a simple cubic unit cell, a face centered cubic (fcc) unit cell, and a body centered cubic (bcc) unit cell.

Simple Cubic:

8 corner atoms × ⅛ = 1 atom/cell. The packing in this structure is not efficient (52%) and so this structure type is very rare for metals.

Body Centered Cubic, bcc:

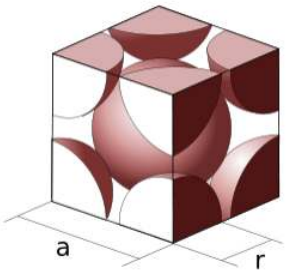
(8 corner atoms × ⅛) + (1 center atom × 1)= 2 atoms/cell. The packing is more efficient (68%) and the structure is a common one for alkali metals and early transition metals. Alloys such as brass (CuZn) also adopt these structures.

Face Centered Cubic, fcc (also called Cubic Close Packed, ccp):

(8 corner atoms × ⅛)+ (6 face atoms × ½)= 4 atoms/cell. This structure, along with its hexagonal relative (hcp), has the most efficient packing (74%). Many metals adopt either the fcc or hcp structure.

Hexagonal Close Packed, hcp:

Like the fcc structure, the packing density of hcp is 74%.

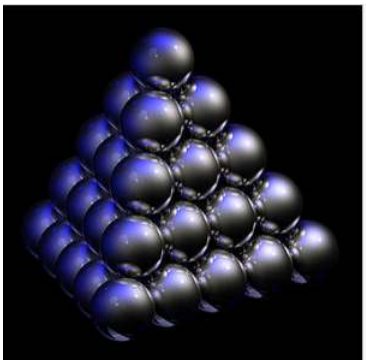


The unit cell of a bcc metal contains two atoms.

Calculating the packing fraction. The packing fractions of the crystal structures shown above can be calculated by dividing the volume of the atoms in the cell by the volume of the cell itself. The volume of the atoms in the cell is equal to the number of atoms/cell times the volume of a sphere, $(4/3)\pi r^3$. The volume of the cubic cells is found by cubing the side length. As an example, let's calculate the packing efficiency of a simple cubic unit cell. As we saw earlier in the section, a simple cubic unit cell contains one atom. The side length of the simple cubic unit cell is 2r, since the centers of each atom occupy the corners of the unit cell.

$$\text{Packing efficiency} = \frac{(1\ atom) \times (\frac{4}{3})\pi r^3}{(2r)^3} = 0.523 \tag{8.2.1}$$

The same method can be applied to bcc and fcc structures.



Face-centered cubic stack of cannonballs.

8.2: Unit Cells and Crystal Structures is shared under a CC BY-NC-SA 4.0 license and was authored, remixed, and/or curated by LibreTexts.

- **6.2: Unit Cells and Crystal Structures** by Chemistry 310 is licensed CC BY-SA 4.0. Original source: https://en.wikibooks.org/wiki/Introduction_to_Inorganic_Chemistry.

8.3: Crystal Structures of Metals

Crystal structures

Most metals and alloys crystallize in one of three very common structures: body-centered cubic (bcc), hexagonal close packed (hcp), or cubic close packed (ccp, also called face centered cubic, fcc). In all three structures the coordination number of the metal atoms (i.e., the number of equidistant nearest neighbors) is rather high: 8 for bcc, and 12 for hcp and ccp. We can contrast this with the low coordination numbers (i.e., low valences - like 2 for O, 3 for N, or 4 for C) found in nonmetals. Atoms in metallic crystals have a tendency to pack in dense arrangments that fill space efficiently.

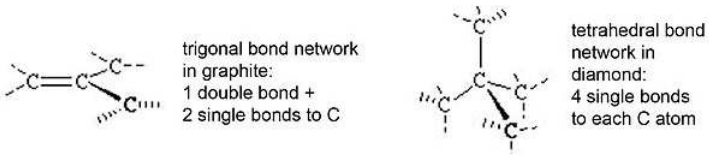
Periodic trends in structure and metallic behavior

Remember where we find the metallic elements in the periodic table - everywhere except the upper right corner. This means that as we go down a group in the p-block (let's say, group IVA, the carbon group, or group VA, the nitrogen group), the properties of the elements gradually change from nonmetals to metalloids to metals. The carbon group nicely illustrates the transition. Starting at the top, the element carbon has two stable allotropes - graphite and diamond. In each one, the valence of carbon atoms is exactly satisfied by making four electron pair bonds to neighboring atoms. In graphite, each carbon has three nearest neighbors, and so there are two single bonds and one double bond. In diamond, there are four nearest neighbors situated at the vertices of a tetrahedron, and so there is a single bond to each one.

The two elements right under carbon (silicon and germanium) in the periodic table also have the diamond structure (recall that these elements cannot make double bonds to themselves easily, so there is no graphite allotrope for Si or Ge). While diamond is a good insulator, both silicon and germanium are semiconductors (i.e., metalloids). Mechanically, they are hard like diamond. Like carbon, each atom of Si and Ge satisfies its valence of four by making single bonds to four nearest neighbors.

The next element under germanium is tin (Sn). Tin has two allotropes, one with the diamond structure, and one with a slightly distorted bcc structure. The latter has metallic properties (metallic luster, malleability), and conductivity about 10^9 times higher than Si. Finally, lead (Pb), the element under Sn, has the ccp structure, and also is metallic. Note the trends in coordination number and conducting properties:

Element	Structure	Coord. no.	Conductivity
C	graphite, diamond	3, 4	semimetal, insulator
Si	diamond	4	semiconductor
Ge	diamond	4	semiconductor
Sn	diamond, distorted bcc	4, 8	semiconductor, metal
Pb	ccp	12	metal



The elements C, Si, and Ge obey the octet rule, and we can easily identify the electron pair bonds in their structures. Sn and Pb, on the other hand, adopt structures with high coordination numbers. They *do not have enough valence electrons* to make electron pair bonds to each neighbor (this is a common feature of metals). What happens in this case is that the valence electrons become "smeared out" or delocalized over all the atoms in the crystal. It is best to think of the bonding in metals as a crystalline arrangement of positively charged cores with a "sea" of shared valence electrons gluing the structure together. Because the electrons are not localized in any particular bond between atoms, they can move in an electric field, which is why metals conduct electricity well. Another way to describe the bonding in metals is nondirectional. That is, an atom's nearest neighbors surround it in every direction, rather than in a few particular directions (like at the corners of a tetrahedron, as we found for diamond). Nonmetals

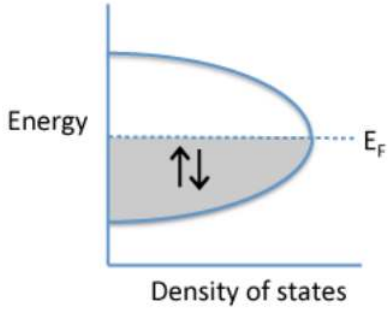
(insulators and semiconductors), on the other hand, have directional bonding. Because the bonding is non-directional and coordination numbers are high, it is relatively easy to deform the coordination sphere (i.e., break or stretch bonds) than it is in the case of a nonmetal. This is why elements like Pb are much more malleable than C, Si, or Ge.

8.3: Crystal Structures of Metals is shared under a CC BY-NC-SA 4.0 license and was authored, remixed, and/or curated by LibreTexts.

- **6.4: Crystal Structures of Metals** by Chemistry 310 is licensed CC BY-SA 4.0. Original source: https://en.wikibooks.org/wiki/Introduction_to_Inorganic_Chemistry.

8.4: Conduction in Metals

In metals, the valence electrons are in molecular orbitals that extend over the entire crystal lattice. Metals are almost always crystalline and the individual crystal grains are typically micron size. This means that the spatial extent of the orbitals is *very large* compared to the size of the atoms or the unit cell. The diagram shows a generic plot of electron energy vs. density of states for a metal such as Na, Cu, or Ag. In these cases, there are N orbitals for N electrons, and each orbital can accommodate two electrons. Therefore the Fermi level, which corresponds to the energy of the highest occupied MO at zero temperature, is somewhere in the middle of the band of orbitals. The energy level spacing between orbitals is very small compared to the thermal energy kT, so we can think of the orbitals as forming a continuous band.



Classically, if the electrons in this band were free to be thermally excited, we would expect them to have a specific heat of 3R per mole of electrons. However, experimentally we observe that C_p is only about 0.02 R per mole. This suggests that *only about 1%* of the electrons in the metal can be thermally excited at room temperature. However, essentially *all* of the valence electrons are free to move in the crystal and contribute to electrical conduction. To understand this apparent paradox, we need to recall that the electrons exist in *quantized energy levels.*

Because of quantization, electrons in metals have a Fermi-Dirac distribution of energies. In this distribution, most of the electrons are spin-paired, although the individual electrons in these pairs can be quite far apart since the orbitals extend over the entire crystal. A relatively small number of electrons at the top of the Fermi sea are unpaired by thermal excitation. This is the origin of the Pauli paramagnetism of metals.

How fast are electrons traveling in a typical metal? Because of the bell shape of the E vs. DOS curve, most of the electrons have $E \approx E_F$. At the midpoint energy (E_F) of the band, the MO's have one node for every two atoms. We can calculate the de Broglie wavelength as twice the distance between nodes and thus:

$\lambda = \mathbf{4a}$ at the midpoint of the band.

where **a** is the interatomic spacing. Since a typical value of **a** is about 2 Å, we obtain the **de Broglie wavelength λ ≈ 8 Å**.

Using the de Broglie relation p = h/λ, we can write:

$$\mathbf{p = \frac{h}{\lambda} = m_e v_F} \tag{8.4.1}$$

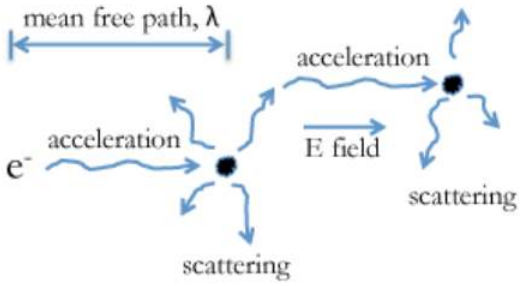
where $\mathbf{m_e}$ is the mass of the electron and $\mathbf{v_F}$ is the velocity of electrons with energy E_F.

Solving for $V_F = \frac{h}{m_e \lambda}$ we obtain $\mathbf{v_F = \frac{(6.62\times10^{-34} Js)}{(9.1\times10^{-31} kg)(8\times10^{-10} m)} = 1.0 \times 10^6 m/s}$

Experimental values of v_F are 1.07 x 10^6 and 1.39 x 10^6 m/s for Na and Ag, respectively, so our approximations are pretty good.

How fast are electrons moving in metals? Really, really fast!! **1,000,000 meters per second!** This is about 1/300 the speed of light, and about 3000 times the speed of sound in air (3 x 10^2 m/s).

However, the **drift velocity** of electrons in metals - the speed at which electrons move in applied electric field - is quite slow, on the order of 0.0001 m/s, or .01 cm/s. You can easily outrun an electron drifting in a metal, even if you have been drinking all night and have been personally reduced to a very slow crawl.



In order to understand the great disparity between the Fermi velocity and the drift velocity of electrons in metals, we need to consider a picture for the scattering of electrons, and their acceleration in an electric field, as shown at the left. If we apply a voltage across a metal (e.g., a metal wire), the electrons are subjected to an electric field **E**, which is the voltage divided by the length of the wire. This electric field exerts a force on the electron, causing it to accelerate. However, the electron is frequently scattered, mostly by phonons (lattice vibrations). Each time the electron is scattered its acceleration starts all over again. The time between scattering events is **τ** and the distance the electrons travel between scattering events is the **mean free path**, **λ**. (Note that this is NOT the same λ as the de Broglie wavelength, they just unfortunately have the same symbol!)

We can write the force on the electron as:

$$\mathbf{F = eE = m_e a = \frac{m_e v_{drift}}{\tau}} \tag{8.4.2}$$

In this equation, **a** is the acceleration in the electric field, $\mathbf{m_e}$ is the mass, and v_{drift} is the **drift velocity** of the electron.

Experimentally, the mean free path is typically obtained by measuring the scattering time. For an electron in Cu metal at 300 K, the scattering time τ is about 2 x 10^{-14} s. From this we can calculate the mean free path as:

$$\mathbf{\lambda = v_{avg}\tau \approx v_F\tau = (1 \times 10^6 m/s)(2 \times 10^{-14}) = 40nm} \tag{8.4.3}$$

The mean free path (40 nm = 400 Å) is quite long compared to the interatomic spacing (2 Å). To put it in perspective, if the interatomic spacing were scaled to the length of a football (0.3 m), the mean free path would be over half the length of the football field (60 m). Thus an electron travels a fairly long way between scattering events and scarcely notices the atomic structure of the metal in which it is traveling.

To summarize, electrons are traveling in metals at the Fermi velocity v_F, which is very, very fast (10^6 m/s), but the flux of electrons is the same in all directions. That is, they are *going nowhere fast*. In an electric field, a very small but directional *drift velocity* is superimposed on this fast random motion of valence electrons.

From F = ma, we obtain the acceleration (a) as:We can calculate the drift velocity of electrons as the acceleration in the electric field times the scattering time:

$$\mathbf{a = \frac{F}{m_e} = \frac{eE}{m_e}} \tag{8.4.4}$$

And thus,

$$\mathbf{v_{drift} = a\tau = \frac{eE\tau}{m_e}} \tag{8.4.5}$$

If we divide both sides of this equation by the magnitude of the electric field (**E**), we obtain the **mobility (μ)**:

$$\mathbf{\mu = \frac{v_{drift}}{E} = \frac{e\tau}{m_e}} \tag{8.4.6}$$

μ has units of velocity/field = cm/s / V/cm = cm^2/Vs

An important consequence of the calculation of v_{drift} is **Ohm's Law**, V = iR. From the equations above, we can see that the drift velocity increases linearly with the applied electric field. The drift velocity (cm/s) is proportional to the current (i, coul/s), and the electric field (E, V/cm) is proportional to the voltage (V):

$$\textbf{Current (i)} = \textbf{nev}_{\textbf{drift}} \times \textbf{area} \tag{8.4.7}$$

$$\textbf{Voltage (V)} = \textbf{E} \times \textbf{length} \tag{8.4.8}$$

Here **n** is the density of valence electrons (#/cm^3) and **e** is the charge of the electron (coul). Combining these equations with our equation for v_{drift} we obtain:

$$V = i(\frac{m_e}{ne^2\tau})\frac{(}{length}area) = iR \tag{8.4.9}$$

Thus, V = iR, where R is the combination of the two terms in parentheses. The first of these is the **resistivity**, ρ, and the second is a geometrical factor.

The **conductivity (σ)** of a metal, which is the inverse of ρ, is proportional to μ, which in turn is proportional to τ (and λ):

$$\sigma = \textbf{ne}\mu = \frac{\textbf{ne}^2\tau}{\textbf{m}_\textbf{e}} \tag{8.4.10}$$

We can use this equation to work out the conductivity of a specific metal (Cu), for which n = 8.5 x 10^{22} cm^{-3} and τ = 2 x 10^{-14} s. Putting in the numbers for m_e and e, we obtain σ = 7 x 10^5 Ω^{-1} cm^{-1} for Cu, in good agreement with the measured value (6 x 10^5 $\Omega^{-1}cm^{-1}$).

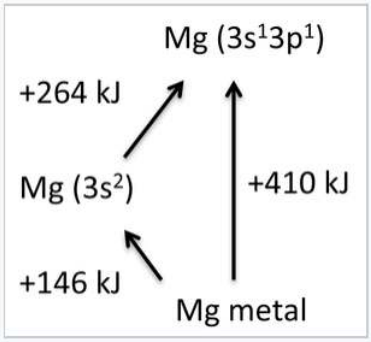
8.4: Conduction in Metals is shared under a CC BY-NC-SA 4.0 license and was authored, remixed, and/or curated by LibreTexts.

- **6.6: Conduction in Metals** by Chemistry 310 is licensed CC BY-SA 4.0. Original source: https://en.wikibooks.org/wiki/Introduction_to_Inorganic_Chemistry.

8.5: Atomic Orbitals and Magnetism

The MO picture we developed in Section 6.4 helps us rationalize the electrical conductivity of Na ($3s^1$), but what about Mg, which (as an atom in the gas phase) has a $3s^2$ electronic configuration? The two valence electrons are spin-paired in atomic Mg, as they are in the helium atom ($1s^2$). When the 3s orbitals of Mg combine to form a band, we would expect the band to be completely filled, since Mg has two electrons per orbital. By this reasoning, solid Mg should be an insulator. But Mg has all the properties of a metal: high electrical and thermal conductivity, metallic luster, malleability, etc. In this case the 3s and 3p bands are sufficiently broad (because of strong orbital overlap between Mg atoms) that they form a continuous band. This band, which contains a total of four orbitals (one 3s and three 3p) per atom, is only partially filled by the two valence electrons.

Another way to think about this is to consider the **hybridization** of the 3s and 3p electrons in Mg. Hybridization requires promotion from the $3s^23p^0$ ground state of an Mg atom to a $3s^13p^1$ excited state. The **promotion energy** (+264 kJ/mol) is more than offset by the **bonding energy** (-410 kJ/mol), the energy released when gaseous atoms in the excited state condense to form the metallic solid. The heat of vaporization, or the cohesive energy of a metal, is the difference between the bonding energy and the promotion energy. Experimentally, we can measure the vaporization energy (+146 kJ/mol) and the promotion energy and use them to calculate the bonding energy. From this we learn that each s or p electron is worth about 200 kJ/mol in bonding energy. The concepts of promotion energy and bonding energy are very useful in rationalizing periodic trends in the bond strengths and magnetic properties of metals, which are described below.

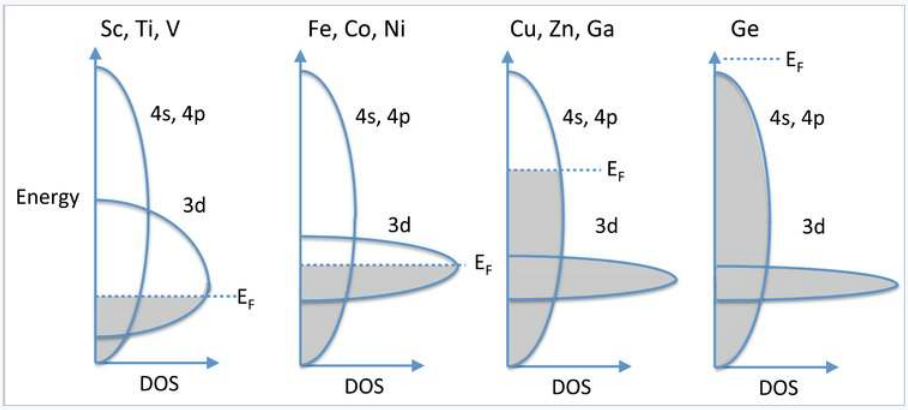


The cohesive energy of Mg metal is the difference between the bonding and promotion energies. The ground state of a gas phase Mg atom is $[Ar]3s^2$, but it can be promoted to the $[Ar]3s^13p^1$ state, which is 264 kJ/mol above the ground state. Mg uses two electrons per atom to make bonds, and the sublimation energy of the metal is 146 kJ/mol.

Filling of the 3d and 4s,4p bands

In the 3d series, we see magnetic behavior for elements and alloys between Cr and Ni. Past Ni, the elements (Cu, Zn, Ga,...) are no longer magnetic and they are very good electrical conductors, implying that their valence electrons are highly delocalized. We can understand this behavior by considering the overlap of 4s, 4p, and 3d orbitals, all of which are close in energy. The 4s and 4p have strong overlap and form a broad, continuous band. On the other hand, the 3d electrons are contracted and form a relatively narrow band. Progressing from the early 3d elements (Sc, Ti, V), we begin to fill the 3d orbitals, which are not yet so contracted that they cannot contribute to bonding. Thus, the valence electrons in Sc, Ti, and V are all spin-paired, except for a small number near the Fermi level that give rise to a weak Pauli paramagnetism. Moving across the 3d series to the magnetic elements (Fe, Co, Ni), the d-orbitals are now so contracted that their electrons unpair and we see cooperative ordering of spins (ferromagnetism and antiferromagnetism). Referring to the band diagram at the right, the 3d band is only partially filled and the Fermi level cuts through it. For Cu, Zn, and Ga, the 3d orbitals are even more contracted and the 3d band is thus more narrow, but now it is completely filled and the Fermi level is in the 4s,4p band. The strong orbital overlap in these bands results in spin pairing and a high degree of

electron delocalization. Consequently, metals in this part of the periodic table (Cu, Ag) are diamagnetic and are among the best electrical conductors at room temperature. Finally, at Ge, the 4s,4p band is completely filled and the solid is a semiconductor.



Progressive filling of the 3d and 4s,4p bands going across the periodic table from Sc to Ge.

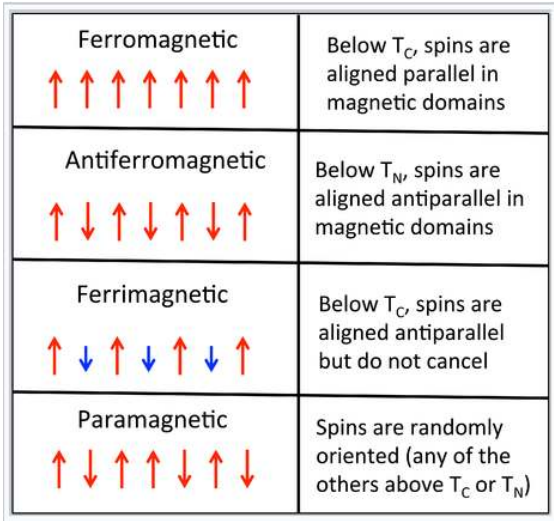
Materials are classified as diamagnetic if they contain no unpaired electrons. Diamagnetic substances are very weakly repelled from an inhomogeneous magnetic field. Molecules or ions that have unpaired spins are paramagnetic and are attracted to a magnet, i.e., they move towards the high field region of an inhomogeneous field. This attractive force results from the alignment of spins with the field, but in the case of paramagnetism each molecule acts independently. In metals, alloys, oxides, and other solid state compounds, the unpaired spins interact strongly with each other and can order spontaneously, resulting in the cooperative magnetic phenomena described below.

8.5: Atomic Orbitals and Magnetism is shared under a CC BY-NC-SA 4.0 license and was authored, remixed, and/or curated by LibreTexts.

- **6.7: Atomic Orbitals and Magnetism** by Chemistry 310 is licensed CC BY-SA 4.0. Original source: https://en.wikibooks.org/wiki/Introduction_to_Inorganic_Chemistry.

8.6: Ferro-, Ferri- and Antiferromagnetism

The magnetism of metals and other materials are determined by the orbital and spin motions of the unpaired electrons and the way in which unpaired electrons align with each other. All magnetic substances are **paramagnetic** at sufficiently high temperature, where the thermal energy (kT) exceeds the interaction energy between spins on neighboring atoms. Below a certain critical temperature, spins can adopt different kinds of ordered arrangements.



A pictorial description of the ordering of spins in ferromagnetism, antiferromagnetism, ferrimagnetism, and paramagnetism

Let's begin by considering an individual atom in the bcc structure of iron metal. Fe is in group VIIIb of the periodic table, so it has eight valence electrons. The atom is promoted to the $4s^1 3d^7$ state in order to make bonds. A localized picture of the d-electrons for an individual iron atom might look like this:



Since each unpaired electron has a spin moment of 1/2, the total spin angular momentum, **S**, for this atom is:

$S = 3\frac{1}{2} = \frac{3}{2}$ (in units of h/2π)

We can think of each Fe atom in the solid as a little bar magnet with a spin-only moment **S** of 3/2. The spin moments of neigboring atoms can align in parallel (↑ ↑), antiparallel (↑ ↓), or random fashion. In bcc Fe, the tendency is to align parallel because of the positive sign of the exchange interaction. This results in **ferromagnetic** ordering, in which all the spins within a magnetic domain (typically hundreds of unit cells in width) have the same orientation, as shown in the figure at the right. Conversely, a negative exchange interaction between neighboring atoms in bcc Cr results in **antiferromagnetic** ordering. A third arrangement, **ferrimagnetic** ordering, results from an antiparallel alignment of spins on neighboring atoms when the magnetic moments of the neighbors are unequal. In this case, the spin moments do not cancel and there is a net magnetization. The ordering mechanism is like that of an antiferromagnetic solid, but the magnetic properties resemble those of a ferromagnet. Ferrimagnetic ordering is most common in metal oxides.

Magnetization and susceptibility

The **magnetic susceptibility**, **χ**, of a solid depends on the ordering of spins. Paramagnetic, ferromagnetic, antiferromagnetic, and ferrimagnetic solids all have $\chi > 0$, but the magnitude of their susceptibility varies with the kind of ordering and with temperature. We will see these kinds of magnetic ordering primarily among the **3d** and **4f** elements and their alloys and compounds. For example, Fe, Co, Ni, $Nd_2Fe_{14}B$, $SmCo_5$, and YCo_5 are all ferromagnets, Cr and MnO are antiferromagnets, and Fe_3O_4 and $CoFe_2O_4$ are ferrimagnets. Diamagnetic compounds have a weak *negative* susceptibility ($\chi < 0$).

Definitions

- H = applied magnetic field (units: Henry (H))
- B = induced magnetic field in a material (units: Tesla (T))
- M = magnetization, which represents the magnetic moments within a material in the presence of an external field H.

Magnetic susceptibility $\chi = M/H$

Usually, χ is given in *molar* units in the *cgs system*:

χ_M = molar susceptibility (units: cm^3/mol)

Typical values of χ_M:

Compound	Type of Magnetism	χ at 300K (cm^3/mol)
SiO_2	Diamagnetic	-3×10^{-4}
Pt metal	Pauli paramagnetic	$+2 \times 10^{-4}$
$Gd_2(SO_4)_3 \cdot 8H_2O$	Paramagnetic	$+5 \times 10^{-2}$
Ni-Fe alloy	Ferromagnetic	$+10^4 - 10^6$

To correlate χ with the number of unpaired electrons in a compound, we first correct for the small diamagnetic contribution of the core electrons:

$$\chi^{corr} = \chi^{obs} - \chi^{diamagnetic\ cores} \tag{8.6.1}$$

Susceptibility of paramagnets

For a paramagnetic substance,

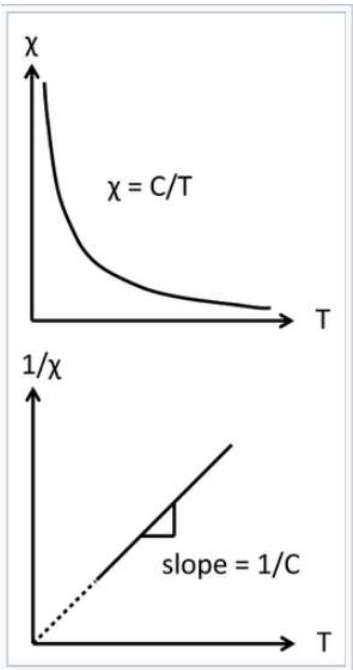
$$\chi_M^{corr} = \frac{C}{T} \tag{8.6.2}$$

The inverse relationship between the magnetic susceptibility and T, the absolute temperature, is called **Curie's Law**, and the proportionality constant C is the **Curie constant**:

$$C = \frac{N_A}{3k_B}\mu_{eff}^2 \tag{8.6.3}$$

Note that C is not a "constant" in the usual sense, because it depends on μ_{eff}, the **effective magnetic moment** of the molecule or ion, which in turn depends on its number of unpaired electrons:

$$\mu_{eff} = \sqrt{n(n+2)}\mu_B \tag{8.6.4}$$



Curie law behavior of a paramagnet. A plot of 1/χ vs. absolute temperature is a straight line, with a slope of 1/C and an intercept of zero.

Here μ_B is the Bohr magneton, a physical constant defined as $\mu_B = eh/4\pi m_e = 9.274 \times 10^{-21}$ erg/gauss (in cgs units).

In cgs units, we can combine physical constants,

$$\frac{N_A}{3k_B}\mu_B^2 = .125 \tag{8.6.5}$$

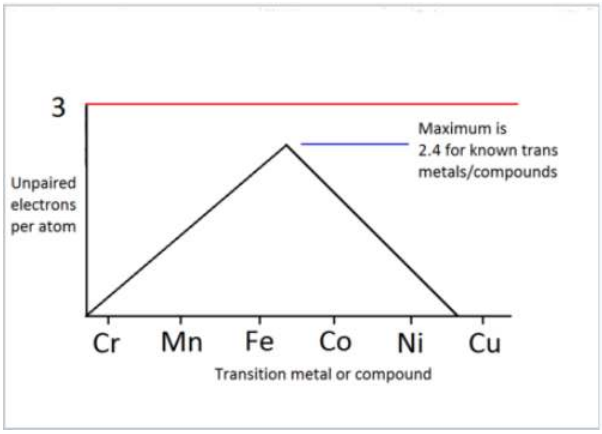
Combining these equations, we obtain

$$\chi_M^{corr} = \frac{.125}{T}\left(\frac{\mu_{eff}}{\mu_B}\right)^2 \tag{8.6.6}$$

These equations relate the molar susceptibility, a bulk quantity that can be measured with a magnetometer, to μ_{eff}, a quantity that can be calculated from the number of unpaired electrons, n. Two important points to note about this formula are:

- The magnetic susceptibility is inversely proportional to the absolute temperature, with a proportionality constant C (Curie's Law)

- So far we are talking only about paramagnetic substances, where there is no interaction between neighboring atoms.



Number of unpaired electrons per atom, determined from Curie constants of transition metals and their 1:1 alloys.

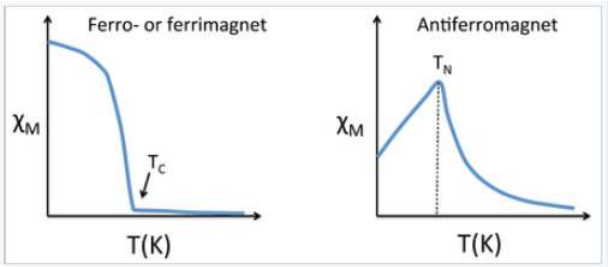
Returning to the isolated Fe atom with its three unpaired electrons, we can measure the Curie constant for iron metal (above the temperature of its transition to a paramagnetic solid) and compare it to the calculation of μ_{eff}. Since n = 3, we calculate:

$$\mu_{eff} = \sqrt{(3)(5)}\mu_B = 3.87\mu_B \tag{8.6.7}$$

The plot at the right shows the number of unpaired electrons per atom, calculated from measured Curie constants, for the magnetic elements and 1:1 alloys in the 3d series. The plot peaks at a value of 2.4 spins per atom, slightly lower than we calculated for an isolated iron atom. This reflects that fact that there is some pairing of d-electrons, i.e., that they do contribute somewhat to bonding in this part of the periodic table.

Susceptibility of ferro-, ferri-, and antiferromagnets

Below a certain critical temperature, the spins of a solid paramagnetic substance order and the susceptibility deviates from simple Curie-law behavior. Because the ordering depends on the short-range exchange interaction, this critical temperature varies widely. Metals and alloys in the 3d series tend to have high critical temperatures because the atoms are directly bonded to each other and the interaction is strong. For example, Fe and Co have critical temperatures (also called the Curie temperature, T_c, for ferromagnetic substances) of 1043 and 1400 K, respectively. The Curie temperature is determined by the strength of the magnetic exchange interaction and by the number of unpaired electrons per atom. The number of unpaired electrons peaks between Fe and Co as the d-band is filled, and the exchange interaction is stronger for Co than for Fe. In contrast to ferromagnetic metals and alloys, paramagnetic salts of transition metal ions typically have critical temperatures below 1K because the magnetic ions are not directly bonded to each other and thus their spins are very weakly coupled in the solid state. For example, in gadolinium sulfate, the paramagnetic Gd^{3+} ions are isolated from each other by SO_4^{2-} ions.

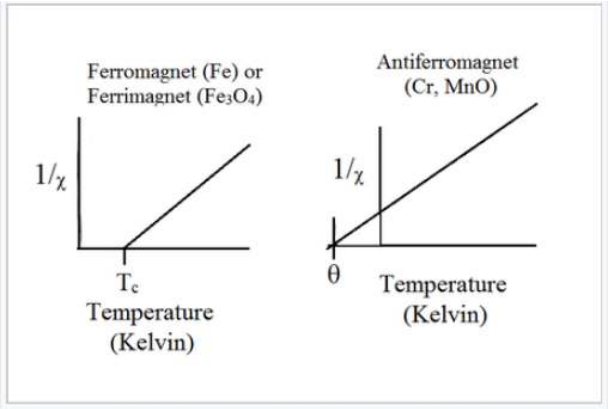


Magnetic susceptibility vs temperature (Kelvin) for ferrimagnetic, ferromagnetic, and antiferromagnetic materials

Above the critical temperature T_C, **ferromagnetic** compounds become paramagnetic and obey the **Curie-Weiss law:**

$$\chi = \frac{C}{T - T_c} \tag{8.6.8}$$

This is similar to the Curie law, except that the plot of $1/\chi$ vs. T is shifted to a positive intercept T_C on the temperature axis. This reflects the fact that ferromagnetic materials (in their paramagnetic state) have a greater tendency for their spins to align in a magnetic field than an ordinary paramagnet in which the spins do not interact with each other. Ferrimagnets follow the same kind of ordering behavior. Typical plots of χ vs. T and $1/\chi$ vs. T for ferro-/ferrimagnets are shown above and below.



Plots of $1/\chi$ vs. T for ferromagnets, ferrimagnets, and antiferromagnets.

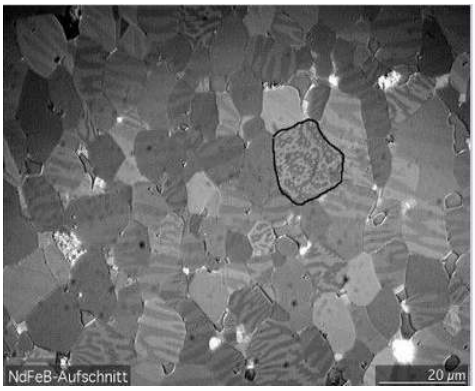
Antiferromagnetic solids are also paramagnetic above a critical temperature, which is called the Néel temperature, T_N. For antiferromagnets, χ reaches a maximum at T_N and is smaller at higher temperature (where the paramagnetic spins are further disordered by thermal energy) and at lower temperature (where the spins pair up). Typically, antiferromagnets retain some positive susceptibility even at very low temperature because of canting of their paired spins. However the maximum value of χ is much lower for an antiferromagnet than it is for a ferro- or ferrimagnet. The Curie-Weiss law is also modified for an antiferromagnet, reflecting the tendency of spins (in the paramagnetic state above T_N) to resist parallel ordering. A plot of $1/\chi$ vs. T intercepts the temperature axis at a negative temperature, $-\theta$, and the Curie-Weiss law becomes:

$$\chi = \frac{C}{T+\theta} \tag{8.6.9}$$

Ordering of spins below T_C

Below T_C, the spins align spontaneously in ferro- and ferrimagnets. Complex magnetization behavior is observed that depends on the history of the sample. For example, if a ferromagnetic material is cooled in the absence of an applied magnetic field, it forms a mosaic structure of magnetic domains that each have internally aligned spins. However, neighboring domains tend to align the opposite way in order to minimize the total energy of the system. This is illustrated in the figure at the left for a Nd-Fe-B magnet. The sample consists of 5-10 μm wide crystal grains that can be easily distinguished by the sharp boundaries in the image. Within

each grain are a series of lighter and darker stripes (imaged by using the optical Kerr effect) that are ferromagnetic domains with opposite orientations. Averaged over the whole sample, these domains have random orientation so the net magnetization is zero.



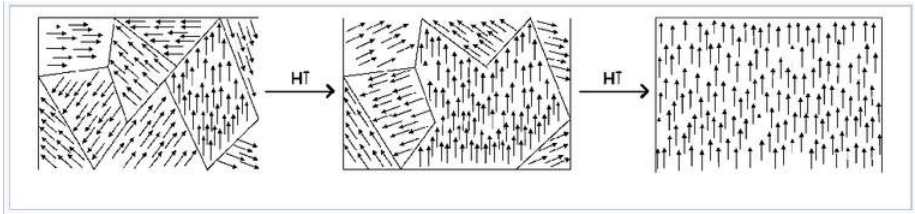
Microcrystalline grains within a piece of $Nd_2Fe_{14}B$ (the alloy used in neodymium magnets) with magnetic domains made visible with a Kerr microscope. The domains are the light and dark stripes visible within each grain.

When a sample like this one is magnetized (i.e., exposed to a strong magnetic field), the domain walls move and the favorably aligned domains grow at the expense of those with the opposite orientation. This transformation can be seen in real time in the Kerr microscope. The domain walls are typically hundreds of atoms wide, so movement of a domain wall involves a cooperative tilting of spin orientation (analogous to "the wave" in a sports stadium) and is a relatively low energy process.



The movement of domain walls in a grain of silicon steel is driven in this movie by increasing the external magnetic field in the "downward" direction, and is imaged using a Kerr microscope. White areas are domains with their magnetization directed up, dark areas - which eventually comprise the entire grain - are domains with their magnetization directed down.

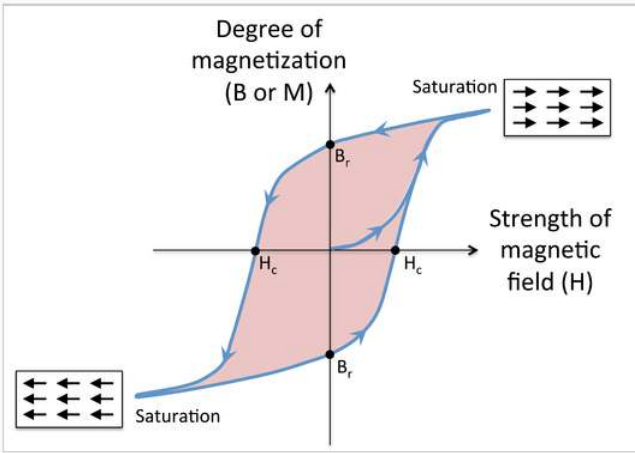
The process of magnetization moves the solid away from its lowest energy state (random domain orientation), so magnetization involves input of energy. When the external magnetic field is removed, the domain walls relax somewhat, but the solid (especially in the case of a "hard" magnet) can retain much of its magnetization. If you have ever magnetized a nail or a paper clip by using a permanent magnet, what you were doing was moving the walls of the magnetic domains inside the ferromagnet. The object thereafter retains the "memory" of its magnetization. However, annealing a permanent magnet destroys the magnetization by returning the system to its lowest energy state in which all the magnetic domains cancel each other.



Rotation of orientation and increase in size of magnetic domains in response to an externally applied magnetic field.

Magnetic hysteresis. Cycling a ferro- or ferrimagnetic material in a magnetic field results in hysteresis in the magnetization of the material, as shown in the figure at the left. At the beginning, the magnetization is zero, but it begins to rise rapidly as the magnetic field is applied. At high field, the magnetic domains are aligned and the magnetization is said to be saturated. When the field is removed, a certain **remanent magnetization** (indicated as the point $\mathbf{B_r}$ on the graph) is retained, i.e., the material is magnetized. Applying a field in the opposite direction begins to orient the magnetic domains in the other direction, and at a field $\mathbf{H_c}$ (the **coercive field**), the magnetization of the sample is reduced to zero. Eventually the material reaches saturation in the opposite direction, and when the field is removed again, it has remanent magnetization Br, but in the opposite direction. As the field continues to reverse, the magnet follows the hysteresis loop as indicated by the arrows. The area of colored region inside the loop is

proportional to the magnetic work done in each cycle. When the field cycles rapidly (for example, in the core of a transformer, or in read-write cycles of a magnetic disk) this work is turned into heat.



Magnetization of a ferro- or ferrimagnet vs. applied magnetic field H. Starting at the origin, the upward curve is the initial magnetization curve. The downward curve after saturation, along with the lower return curve, form the main loop. The intercepts Hc and Br are the coercivity and remanent magnetization.

8.6: Ferro-, Ferri- and Antiferromagnetism is shared under a CC BY-NC-SA 4.0 license and was authored, remixed, and/or curated by LibreTexts.

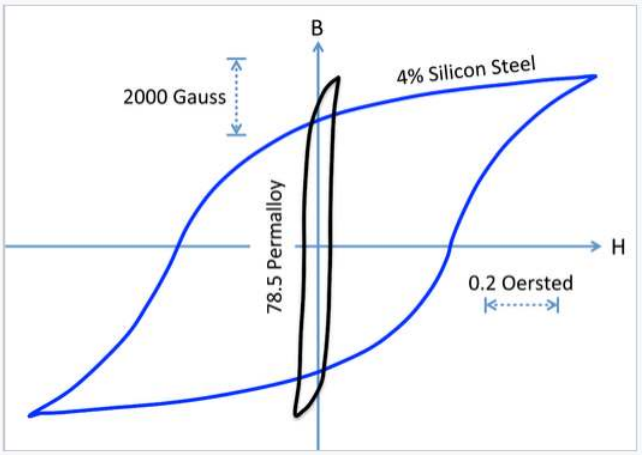
- **6.8: Ferro-, Ferri- and Antiferromagnetism** by Chemistry 310 is licensed CC BY-SA 4.0. Original source: https://en.wikibooks.org/wiki/Introduction_to_Inorganic_Chemistry.

8.7: Hard and Soft Magnets

Whether a ferro- or ferrimagnetic material is a **hard** or a **soft magnet** depends on the strength of the magnetic field needed to align the magnetic domains. This property is characterized by $\mathbf{H_c}$, the coercivity. Hard magnets have a high coercivity (H_c), and thus retain their magnetization in the absence of an applied field, whereas soft magnets have low values.

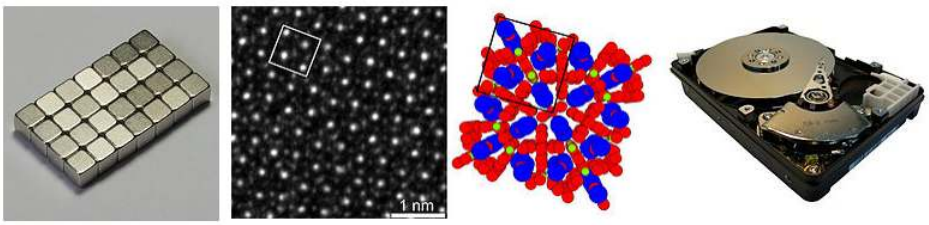
The figure at the right compares hysteresis loops for hard and soft magnets. Recall that the energy dissipated in magnetizing and demagnetizing the material is proportional to the area of the hysteresis loop. We can see that soft magnets, while they can achieve a high value of B_{sat}, dissipate relatively little energy in the loop. This makes **soft magnets** preferable for use in **transformer cores**, where the field is switched rapidly. **Permalloy**, an alloy consisting of about 20% Fe and 80% Ni, is a soft magnet that has very high magnetic permeability μ (i.e., a large maximum slope of the B vs. H curve) and a very narrow hysteresis loop.

Some materials, such as iron metal, can exist as either hard or soft magnets. Whether bcc iron is a hard or soft magnet depends on the crystal grain size. When crystal grains in iron are sub-micron size, and comparable to the size of the magnetic domains, then the magnetic domains are pinned by crystal grain boundaries. When the magnetic domains are pinned a stronger coercive magnetic field needs to be applied to cause them to re-align. When iron is annealed, the crystal grains grow and the magnetic domains become more free to align with applied magnetic fields. This decreases the coercive field and the material becomes a soft magnet.



Hysteresis loops comparing a hard magnet (iron-silicon steel) to a soft magnet (permalloy) on the same scale. H_c for permallloy is 0.05 Oe, about 10 times lower than that of the hard magnet. The remanent magnetizations of the two materials are comparable.

Hard magnets such as CrO_2, γ-Fe_2O_3, and cobalt ferrite ($CoFe_2O_4$) are used in magnetic recording media, where the high coercivity allows them to retain the magnetization state (read as a logical 0 or 1) of a magnetic bit over long periods of time. Hard magnets are also used in disk drives, refrigerator magnets, electric motors and other applications. Drive motors for hybrid and electric vehicles such as the Toyota Prius use the hard magnet $Nd_2Fe_{14}B$ (also used to make strong refrigerator magnets) and require 1 kilogram (2.2 pounds) of neodymium.[6]. A high-resolution transmission electron microscope image of $Nd_2Fe_{14}B$ is shown below and compared to the crystal structure with the unit cell marked.

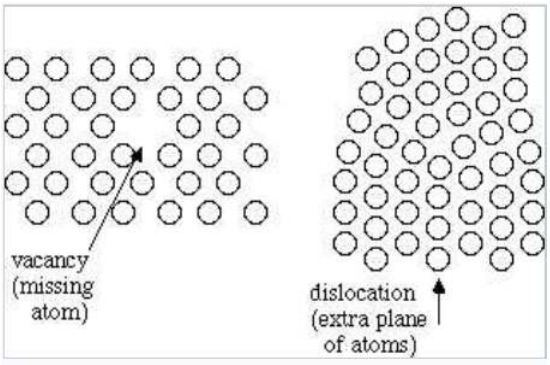


8.7: Hard and Soft Magnets is shared under a CC BY-NC-SA 4.0 license and was authored, remixed, and/or curated by LibreTexts.

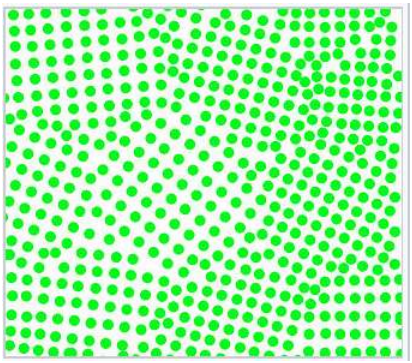
- **6.9: Hard and Soft Magnets** by Chemistry 310 is licensed CC BY-SA 4.0. Original source: https://en.wikibooks.org/wiki/Introduction_to_Inorganic_Chemistry.

8.8: Defects in Metallic Crystals

“Crystals are like people, it is the defects in them which tend to make them interesting!” - *Colin Humphreys.*



Metals, by virtue of their non-directional bonding, are more energetically tolerant of **defects** than are covalent network or ionic solids. Because there is no strong preference for one atomic position over another, the energy of a metallic crystal is not greatly impaired by the vacancy of a single atom or by the dislocation of a group of atoms. These kinds of "mistakes" in the packing of metal atoms within crystals are collectively called defects. The deformability of metals is the direct result of defects in the crystal structure. Defects in metals such as Al and Fe are responsible for the three orders of magnitude difference between the yield stress of annealed polycrystalline samples (i.e., normal articles of commerce) and perfect single crystals.



Grains and grain boundaries in a polycrystalline material

8.8: Defects in Metallic Crystals is shared under a CC BY-NC-SA 4.0 license and was authored, remixed, and/or curated by LibreTexts.

- **7.1: Defects in Metallic Crystals** by Chemistry 310 is licensed CC BY-SA 4.0. Original source: https://en.wikibooks.org/wiki/Introduction_to_Inorganic_Chemistry.

8.9: X-ray Crystallography

X-ray Crystallography is a scientific method used to determine the arrangement of atoms of a crystalline solid in three dimensional space. This technique takes advantage of the interatomic spacing of most crystalline solids by employing them as a diffraction gradient for x-ray light, which has wavelengths on the order of 1 angstrom (10^{-8} cm).

Introduction

In 1895, Wilhelm Rontgen discovered X-rays. The nature of X-rays, whether they were particles or electromagnetic radiation, was a topic of debate until 1912. If the wave idea was correct, researchers knew that the wavelength of this light would need to be on the order of 1 Angstrom (Å) (10^{-8} cm). Diffraction and measurement of such small wavelengths would require a gradient with spacing on the same order of magnitude as the light.

In 1912, Max von Laue, at the University of Munich in Germany, postulated that atoms in a crystal lattice had a regular, periodic structure with interatomic distances on the order of 1 Å. Without having any evidence to support his claim on the periodic arrangements of atoms in a lattice, he further postulated that the crystalline structure can be used to diffract X-rays, much like a gradient in an infrared spectrometer can diffract infrared light. His postulate was based on the following assumptions: the atomic lattice of a crystal is periodic, X-rays are electromagnetic radiation, and the interatomic distance of a crystal are on the same order of magnitude as X-ray light. Laue's predictions were confirmed when two researchers: Friedrich and Knipping, successfully photographed the diffraction pattern associated with the X-ray radiation of crystalline $CuSO_4$ • 5 H_2O. The science of X-ray crystallography was born.

The arrangement of the atoms needs to be in an ordered, periodic structure in order for them to diffract the X-ray beams. A series of mathematical calculations is then used to produce a diffraction pattern that is characteristic to the particular arrangement of atoms in that crystal. X-ray crystallography remains to this day the primary tool used by researchers in characterizing the structure and bonding of organometallic compounds.

Diffraction

Diffraction is a phenomena that occurs when light encounters an obstacle. The waves of light can either bend around the obstacle, or in the case of a slit, can travel through the slits. The resulting diffraction pattern will show areas of constructive interference, where two waves interact in phase, and destructive interference, where two waves interact out of phase. Calculation of the phase difference can be explained by examining Figure 1 below.

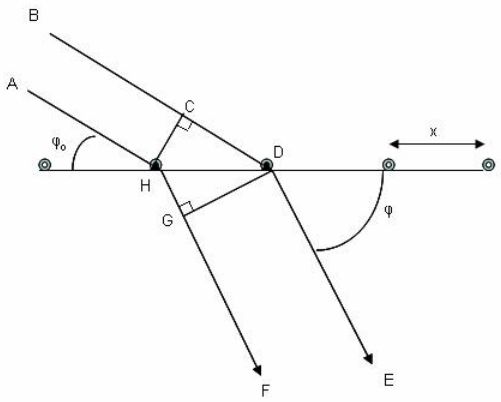


Figure 1: Scattering of light by a diffraction gratting

In the figure below, two parallel waves, BD and AH are striking a gradient at an angle θ_o. The incident wave BD travels farther than AH by a distance of CD before reaching the gradient. The scattered wave (depicted below the gradient) HF, travels father than the scattered wave DE by a distance of HG. So the total path difference between path AHGF and BCDE is CD - HG. To observe a wave of high intensity (one created through constructive interference), the difference CD - HG must equal to an integer number of

wavelengths to be observed at the angle psi, $CD - HG = n\lambda$, where λ is the wavelength of the light. Applying some basic trigonometric properties, the following two equations can be shown about the lines:

$$CD = x\cos(\theta o) \tag{8.9.1}$$

and

$$HG = x\cos(\theta) \tag{8.9.2}$$

where x is the distance between the points where the diffraction repeats. Combining the two equations,

$$x(\cos\theta_o - \cos\theta) = n\lambda \tag{8.9.3}$$

Bragg's Law

Diffraction of an X-ray beam, occurs when the light interacts with the electron cloud surrounding the atoms of the crystalline solid. Due to the periodic crystalline structure of a solid, it is possible to describe it as a series of planes with an equal interplaner distance. As an X-ray's beam hits the surface of the crystal at an angle, θ, some of the light will be diffracted at that same angle away from the solid (Figure 2). The remainder of the light will travel into the crystal and some of that light will interact with the second plane of atoms. Some of the light will be diffracted at an angle θ, and the remainder will travel deeper into the solid. This process will repeat for the many planes in the crystal. The X-ray beams travel different pathlengths before hitting the various planes of the crystal, so after diffraction, the beams will interact constructively only if the path length difference is equal to an integer number of wavelengths (just like in the normal diffraction case above). In the figure below, the difference in path lengths of the beam striking the first plane and the beam striking the second plane is equal to BG + GF. So, the two diffracted beams will constructively interfere (be in phase) only if $BG + GF = n\lambda$. Basic trigonometry will tell us that the two segments are equal to one another with the interplaner distance times the sine of the angle θ. So we get:

$$BG = BC = d\sin\theta \tag{8.9.4}$$

Thus,

$$2d\sin\theta = n\lambda \tag{8.9.5}$$

This equation is known as Bragg's Law, discovered in 1912. {C}{C}Bragg's Law relates the distance between two planes in a crystal and the angle of reflection to the X-ray wavelength. The X-rays that are diffracted off the crystal have to be in-phase in order to signal. Only certain angles that satisfy the following condition will register:

$$\sin\theta = \frac{n\lambda}{2d} \tag{8.9.6}$$

For historical reasons, the resulting diffraction spectrum is represented as intensity vs. 2θ.

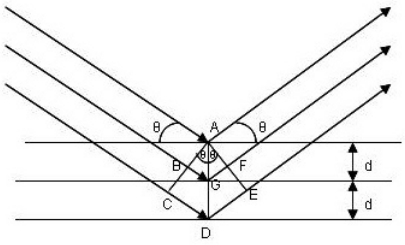


Figure 2: Incident X-ray strikes a set of planes (with an interplaner distance of d) at an angle of θ

Instrument Components

The main components of an X-ray instrument are similar to those of many optical spectroscopic instruments. These include a source, a device to select and restrict the wavelengths used for measurement, a holder for the sample, a detector, and a signal converter and readout. However, for X-ray diffraction; only a source, sample holder, and signal converter/readout are required.

The Source

X-ray tubes provides a means for generating X-ray radiation in most analytical instruments. An evacuated tube houses a tungsten filament which acts as a cathode opposite to a much larger, water cooled anode made of copper with a metal plate on it. The metal plate can be made of any of the following metals: chromium, tungsten, copper, rhodium, silver, cobalt, and iron. A high voltage is passed through the filament and high energy electrons are produced. The machine needs some way of controlling the intensity and wavelength of the resulting light. The intensity of the light can be controlled by adjusting the amount of current passing through the filament; essentially acting as a temperature control. The wavelength of the light is controlled by setting the proper accelerating voltage of the electrons. The voltage placed across the system will determine the energy of the electrons traveling towards the anode. X-rays are produced when the electrons hit the target metal. Because the energy of light is inversely proportional to wavelength ($E = hc = h(1/\lambda)$), controlling the energy, controls the wavelength of the X-ray beam.

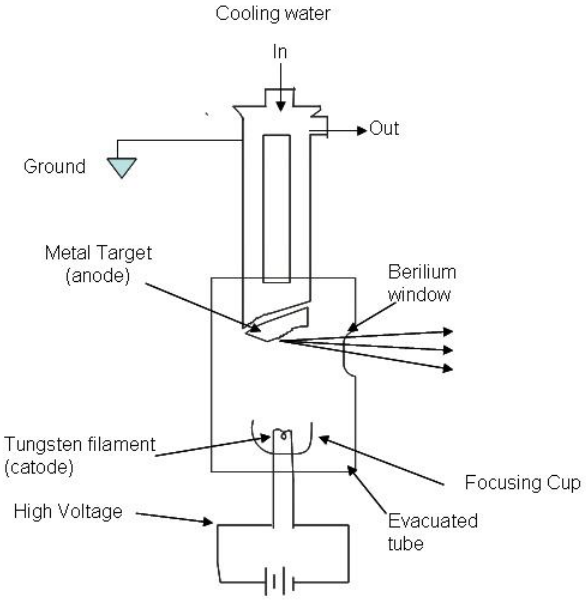


Figure 3: X-ray tube schematic

X-ray Filter

Monochromators and filters are used to produce monochromatic X-ray light. This narrow wavelength range is essential for diffraction calculations. For instance, a zirconium filter can be used to cut out unwanted wavelengths from a molybdenum metal target (see figure 4). The molybdenum target will produce X-rays with two wavelengths. A zirconium filter can be used to absorb the unwanted emission with wavelength $K\beta$, while allowing the desired wavelength, K_α to pass through.

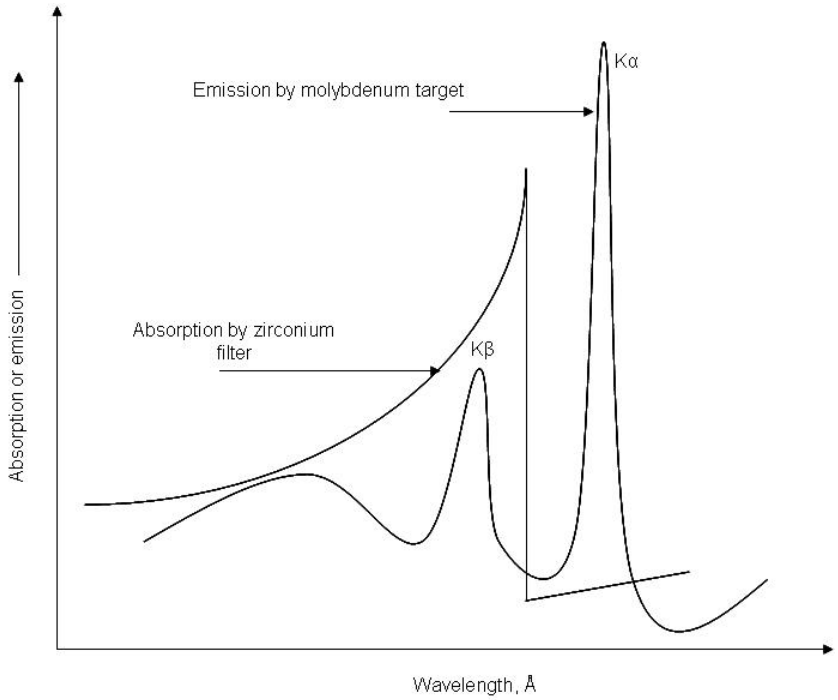


Figure 4: Monochromatic light produce by absorption of unwanted emissions.

Signal Converter

In x-ray diffraction, the detector is a transducer that counts the number of photons that collide into it. This photon counter gives a digital readout in number of photons per unit time.

References

1. Skoog, D . A.; Holler, F. J.; Stanley R. C.; Principles of Instrumental Analysis; Thomson Brooks/Cole: Belmont CA, 2007.
2. Sands, D. E.; Introduction to Crystallography; Dover Publications, Inc.; New York, 1975
3. Drenth, Jan. Principles of Protein x-ray Crystallography, 3rd edition. 2007, Springer Science + Business Media, LLC. pg. 14.
4. Rhodes, Gale. Crystallography Made Crystal Clear, 3rd edition. 2006, Elsevier Inc. pg. 33, 55 - 57.
5. Actual experimentation done of APS Kinase D63N *Penicillium Chrysogenum*.

Contributors and Attributions

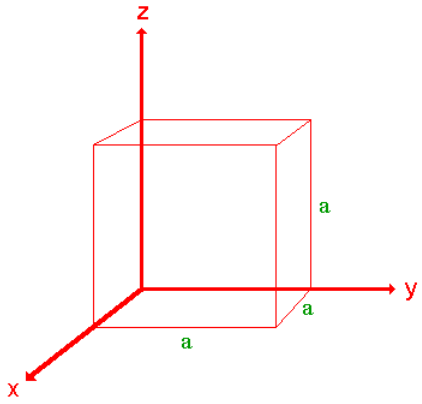
- Roman Kazantsev (UC Davis) and Michelle Towles (UC Davis)

8.9: X-ray Crystallography is shared under a CC BY-NC-SA 4.0 license and was authored, remixed, and/or curated by LibreTexts.

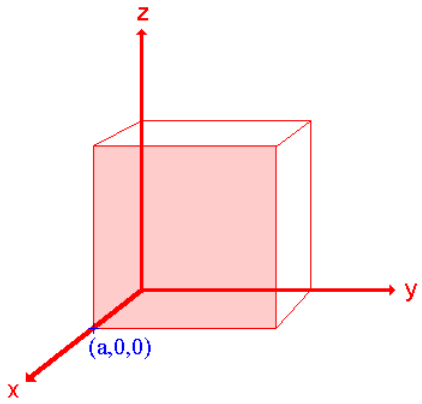
8.10: Miller Indices (hkl)

The orientation of a surface or a crystal plane may be defined by considering how the plane (or indeed any parallel plane) intersects the main crystallographic axes of the solid. The application of a set of rules leads to the assignment of the Miller Indices (*hkl*), which are a set of numbers which quantify the intercepts and thus may be used to uniquely identify the plane or surface.

The following treatment of the procedure used to assign the Miller Indices is a simplified one and only a **cubic** crystal system (one having a cubic unit cell with dimensions a x a x a) will be considered.



The procedure is most easily illustrated using an example so we will first consider the following surface/plane:



Step 1: *Identify the intercepts on the* x- , y- *and* z- *axes.*

In this case the intercept on the x-axis is at x = a (at the point (a,0,0)), but the surface is parallel to the y- and z-axes - strictly therefore there is no intercept on these two axes but we shall consider the intercept to be at infinity (∞) for the special case where the plane is parallel to an axis. The intercepts on the x- , y- and z-axes are thus **a , ∞ , ∞**.

Step 2: Specify the intercepts in fractional co-ordinates

Co-ordinates are converted to fractional co-ordinates by dividing by the respective cell-dimension - for example, a point (x,y,z) in a unit cell of dimensions a x b x c has fractional co-ordinates of (x/a , y/b , z/c). In the case of a cubic unit cell each co-ordinate will simply be divided by the cubic cell constant, a. This gives

Fractional Intercepts = **a/a , ∞/a, ∞/a** i.e. **1 , ∞ , ∞**.

Step 3: Take the reciprocals of the fractional intercepts

This final manipulation generates the Miller Indices which (by convention) should then be specified without being separated by any commas or other symbols. The Miller Indices are also enclosed within standard brackets (….) when one is specifying a unique

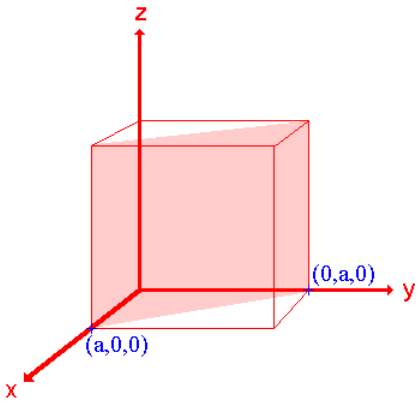
surface such as that being considered here.

The reciprocals of 1 and ∞ are 1 and 0 respectively, thus yielding Miller Indices **(100)**.

So the surface/plane illustrated is the (100) plane of the cubic crystal.

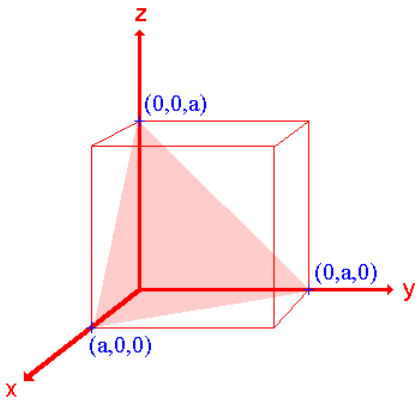
Other Examples

1. The (110) surface



Assignment
Intercepts: a , a , ∞
Fractional intercepts: 1 , 1 , ∞
Miller Indices: **(110)**

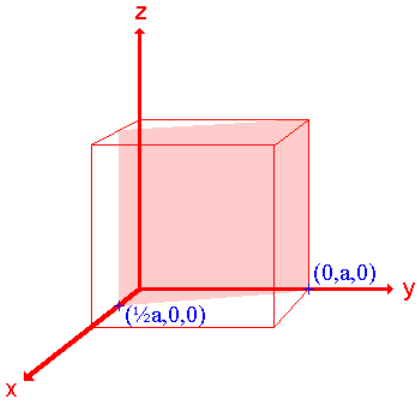
2. The (111) surface



Assignment
Intercepts: a , a , a
Fractional intercepts: 1 , 1 , 1
Miller Indices: **(111)**

The (100), (110) and (111) surfaces considered above are the so-called low index surfaces of a cubic crystal system (the "low" refers to the Miller indices being small numbers - 0 or 1 in this case). These surfaces have a particular importance but there an infinite number of other planes that may be defined using Miller index notation. We shall just look at one more …

3. The (210) surface



Assignment
Intercepts: ½ a , a , ∞
Fractional intercepts: ½ , 1 , ∞
Miller Indices: **(210)**

Further notes:

i. in some instances the Miller indices are best multiplied or divided through by a common number in order to simplify them by, for example, removing a common factor. This operation of multiplication simply generates a parallel plane which is at a different distance from the origin of the particular unit cell being considered. e.g. (200) is transformed to (100) by dividing through by 2 .
ii. if any of the intercepts are at negative values on the axes then the negative sign will carry through into the Miller indices; in such cases the negative sign is actually denoted by overstriking the relevant number. e.g. (00-1) is instead denoted by (00$\bar{1}$)
iii. in the *hcp* crystal system there are four principal axes; this leads to four Miller Indices e.g. you may see articles referring to an *hcp* (0001) surface. It is worth noting, however, that the intercepts on the first three axes are necessarily related and not completely independent; consequently the values of the first three Miller indices are also linked by a simple mathematical relationship.

Contributors and Attributions

- Roger Nix (Queen Mary, University of London)

This page titled 8.10: Miller Indices (hkl) is shared under a CC BY-NC-SA 4.0 license and was authored, remixed, and/or curated by Roger Nix.

8.11: Powder X-ray Diffraction

When an X-ray is shined on a crystal, it diffracts in a pattern characteristic of the structure. In powder X-ray diffraction, the diffraction pattern is obtained from a powder of the material, rather than an individual crystal. Powder diffraction is often easier and more convenient than single crystal diffraction since it does not require individual crystals be made. Powder X-ray diffraction (XRD) also obtains a diffraction pattern for the bulk material of a crystalline solid, rather than of a single crystal, which doesn't necessarily represent the overall material. A diffraction pattern plots intensity against the angle of the detector, 2θ.

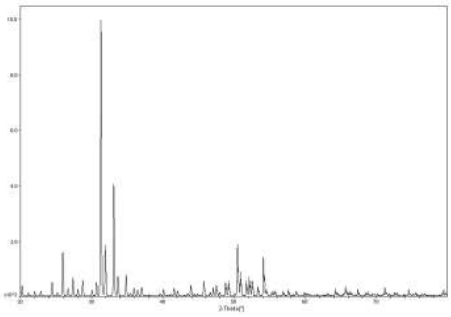
Introduction

Since most materials have unique diffraction patterns, compounds can be identified by using a database of diffraction patterns. The purity of a sample can also be determined from its diffraction pattern, as well as the composition of any impurities present. A diffraction pattern can also be used to determine and refine the lattice parameters of a crystal structure. A theoretical structure can also be refined using a method known as **Rietveld refinement**. The particle size of the powder can also be determined by using the Scherrer formula, which relates the particle size to the peak width. The Scherrer fomula is

$$t = \frac{0.9\lambda}{\sqrt{B_M^2 - B_s^2}\cos\theta} \tag{8.11.1}$$

with

- λ is the x-ray wavelength,
- B_M is the observed peak width,
- B_S is the peak width of a crystalline standard, and
- θ is the angle of diffraction.



To the left is an example XRD pattern for $Ba_{24}Ge_{100}$. The x axis is 2θ and the y axis is the intensity.

References

1. Dann, S.E. *Reactions and Characterization of SOLIDS.* Royal Society of Chemistry, USA (2002).
2. Skoog, D.A.; Holler, F.J.; Crouch, S.R. *Principles of Instrumental Analysis*. Sixth Edition, Thomson Brooks/Cole, USA (2007).

Contributors and Attributions

- Jason Grebenkemper

8.11: Powder X-ray Diffraction is shared under a CC BY-NC-SA 4.0 license and was authored, remixed, and/or curated by LibreTexts.

8.12: Prelude to Ionic and Covalent Solids - Structures

As we noted in our discussion of metal and alloy structures, there is an intimate connection between the structures and the physical properties of materials. As we "graduate" from simple metal structures based on sphere packings to more complex structures, we find that this is still true. In this section we will try to systematize the structures of inorganic solids - metal oxides, halides, sulfides, and related compounds - and develop some rules for which structures to expect based on electronegativity differences, hard-soft acid-base rules, and other periodic trends. We will see that many of these structures are related to the sphere packings that we learned about previously.



The morphology of twinned crystals of iron pyrite (FeS_2) is related to the underlying cubic symmetry of the unit cell. Like NaCl, the pyrite crystal structure can be thought of as a face-centered cubic array of anions (S_2^{2-}) with cations (Fe^{2+}) occupying all the octahedral holes.

Inorganic solids often have simple crystal structures, and some of these structures are adopted by large families of ionic or covalent compounds. Examples of the most common structures include NaCl, CsCl, NiAs, zincblende, wurtzite, fluorite, perovskite, rutile, and spinel. We will develop these structures systematically from the close packed and non-close packed lattices. Some layered structures, such as $CdCl_2$ and CdI_2, can be thought of as relatives of simple ionic lattices with some atoms "missing."

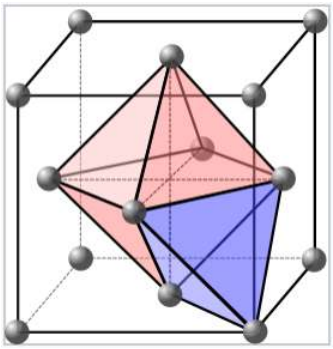
8.12: Prelude to Ionic and Covalent Solids - Structures is shared under a CC BY-NC-SA 4.0 license and was authored, remixed, and/or curated by LibreTexts.

- **8.1: Prelude to Ionic and Covalent Solids - Structures** by Chemistry 310 is licensed CC BY-SA 4.0. Original source: https://en.wikibooks.org/wiki/Introduction_to_Inorganic_Chemistry.

8.13: Close-packing and Interstitial Sites

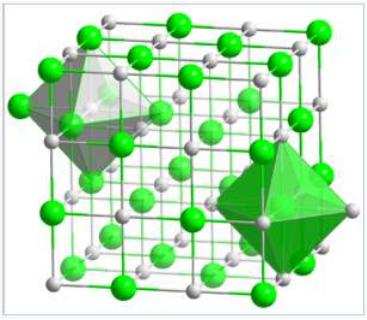
Many common inorganic crystals have structures that are related to cubic close packed (face-centered cubic) or hexagonal close packed sphere packings. These packing lattices contain two types of sites or "holes" that the interstitial atoms fill, and the coordination geometry of these sites is either **tetrahedral** or **octahedral**. An interstitial atom filling a tetrahedral hole is coordinated to four packing atoms, and an atom filling an octahedral hole is coordinated to six packing atoms. In both the hexagonal close packed and cubic close packed lattices, there is one octahedral hole and two tetrahedral holes per packing atom.

Question: Would anions or cations be better as packing atoms?
We might expect that anions, which are often larger than cations, would be better suited to the positions of packing atoms. While this is often true, there are many examples of structures in which cations are the packing atoms, and others in which the distinction is arbitrary. The NaCl structure is a good example of the latter.



One octahedral and one tetrahedral site in a face-centered cubic unit cell. Each cell contains four packing atoms (gray), four octahedral sites (pink), and eight tetrahedral sites (blue).

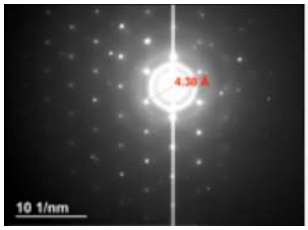
In the NaCl structure, shown on the right, the green spheres are the Cl^- ions and the gray spheres are the Na^+ ions. The octahedral holes in a face-centered cubic lattice can be found at fractional coordinates (1/2 1/2 1/2), (1/2 0 0), (0 1/2 0), and (0 0 1/2). There are four of these holes per cell, and they are filled by the chloride ions. The packing atoms (Na^+) have coordinates (0 0 0), (0 1/2 1/2), (1/2 1/2 0), and (1/2 0 1/2). Note that each of the Na^+ positions is related to a Cl^- position by a translation of (1/2 0 0). Another way of stating this is that the structure consists of **two interpenetrating fcc lattices**, which are related to each other by a translation of half the unit cell along any of the three Cartesian axes. We could have equivalently placed the Cl ions at the fcc lattice points and the Na ions in the octahedral holes by simply translating the origin of the unit cell by (1/2 0 0). Thus the distinction between packing and interstitial atoms in this case is arbitrary.



Crystal structure of NaCl. Both the Na^+ and Cl^- ions are octahedrally coordinated.

NaCl is interesting in that it is a three-dimensional checkerboard, and thus there are no NaCl "molecules" that exist in the structure. When this structure was originally solved (in 1913 by using X-ray diffraction) by W. L. Bragg, his interpretation met resistance by chemists who thought that precise integer stoichiometries were a consequence of the valency of atoms in molecules. The German chemist Pfeiffer noted in 1915 that ‘the ordinary notion of valency didn’t seem to apply’, and fourteen years later, the influential chemist Armstrong still found Bragg’s proposed structure of sodium chloride ‘more than repugnant to the common sense, not

chemical cricket'! Nevertheless, Bragg and his father, W. H. Bragg, persevered and used the then-new technique of X-ray diffraction to determine the structures of a number of other compounds, including diamond, zincblende, calcium fluoride, and other alkali halides. These experiments gave chemists their first real look at the atomic structure of solids, and laid the groundwork for X-ray diffraction experiments that later elucidated the structures of DNA, proteins, and many other compounds. For their work on X-ray diffraction the Braggs received the Nobel prize in Physics in 1915.

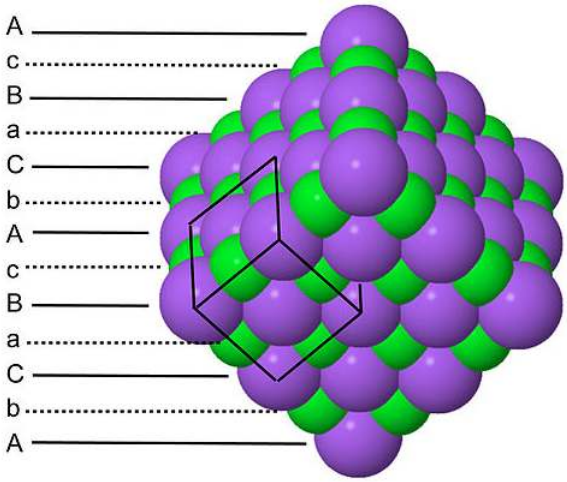


The lattice dimensions and positions of atoms in crystals such as NaCl are inferred from diffraction patterns.

Since each type of atom in the NaCl structure forms a face-centered cubic lattice, there are four Na and four Cl atoms per NaCl unit cell. It is because of this ratio that NaCl has a 1:1 stoichiometry. The shaded green and gray bipyramidal structures in the NaCl lattice show that the Na^+ ions are coordinated to six Cl^- ions, and vice versa. The NaCl structure can be alternatively drawn as a stacking of close-packed layer planes, AcBaCbAcBa... along the body diagonal of the unit cell. Here the uppercase letters represent the packing atoms, and the lower case letters are the interstitial atoms. This layered packing is illustrated below:

NaCl structure

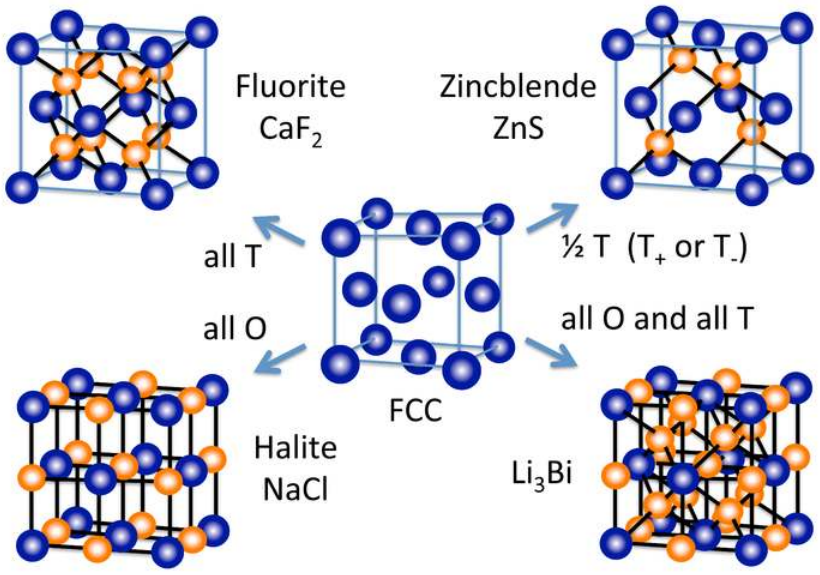
- ---------- A
- - - -c- - - -
- ---------- B
- - - -a- - - -
- ---------- C
- - - -b- - - -
- ---------- A
- - - -c- - - -
- ---------- B
- - - -a- - - -
- ---------- C
- - - -b- - - -
- ---------- A



Note that both the packing atoms and interstitials are stacked in the sequence A-B-C-A-B-C..., in keeping with the fact that each forms a cubic close-packed lattice.

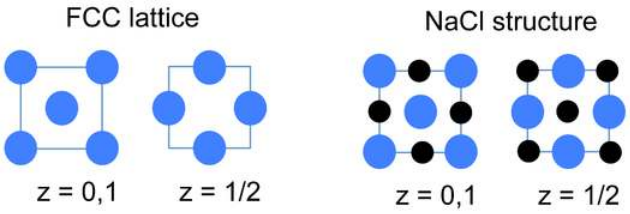
The NaCl structure is fairly common among ionic compounds:

- Alkali Halides (except CsCl, CsBr, and CsI)
- Transition Metal Monoxides (TiO, VO,..., NiO)
- Alkali Earth Oxides and Sulfides (MgO, CaO, BaS... except BeO and MgTe)
- Carbides and Nitrides (TiC, TiN, ZrC, NbC) -these are very stable refractory, interstitial alloys (metallic)



A number of other inorganic crystal structures are formed (at least conceptually) by filling octahedral and/or tetrahedral holes in close-packed lattices. The figure at the right shows some of the most common structures (fluorite, halite, zincblende) as well as a rather rare one (Li_3Bi) that derive from the fcc lattice. From the hcp lattice, we can make the NiAs and wurzite structures, which are the hexagonal relatives of NaCl and zincblende, respectively.

An alternative and very convenient way to represent inorganic crystal structures (especially complex structures such as Li_3Bi) is to draw the unit cell in slices along one of the unit cell axes. This kind of representation is shown at the left for the fcc lattice and the NaCl structure. Since all atoms in these structures have z-coordinates of either 0 or 1/2, only those sections need to be drawn in order to describe the contents of the unit cell. It is a useful exercise to draw some of the fcc compound structures (above) in sections.



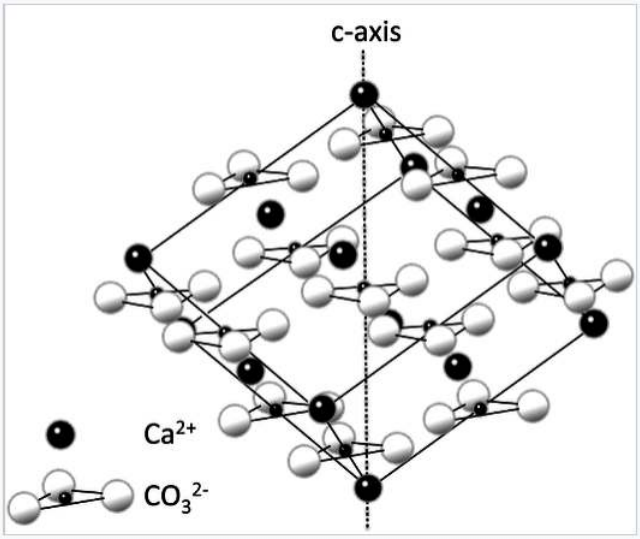
8.13: Close-packing and Interstitial Sites is shared under a CC BY-NC-SA 4.0 license and was authored, remixed, and/or curated by LibreTexts.

- **8.2: Close-packing and Interstitial Sites** by Chemistry 310 is licensed CC BY-SA 4.0. Original source: https://en.wikibooks.org/wiki/Introduction_to_Inorganic_Chemistry.

8.14: Structures Related to NaCl and NiAs

There are a number of compounds that have structures similar to that of NaCl, but have a lower symmetry (usually imposed by the geometry of the anion) than NaCl itself. These compounds include:

- FeS_2 (pyrite, "fools gold"): S_2^{2-} (disulfide) and Fe^{2+}
- CaC_2 (a salt-like carbide): Ca^{2+} and linear C_2^{2-} anions
- $CaCO_3$ (calcite, limestone, marble): Ca^{2+} and triangular CO_3^{2-}.



The rhombohedral unit cell of the calcite crystal structure. The hexagonal c-axis is shown.

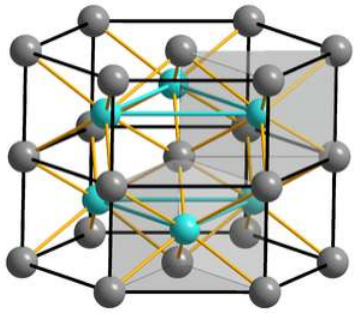
The **calcite** ($CaCO_3$) crystal structure is shown above. Triangular CO_3^{2-} ions fill octahedral holes between the Ca^{2+} ions (black spheres) in a distorted NaCl lattice. As in NaCl, each ion is coordinated by six of the other kind. From this image we can see why the $CaCO_3$ structure has a lower symmetry than that of NaCl. The fourfold rotation symmetry of the NaCl unit cell is lost when the spherical Cl^- ions are replaced by triangular CO_3^{2-} ions. Because of this symmetry lowering, transparent crystals calcite are birefringent, as illustrated below.



Calcite crystals are birefringent, meaning that their refractive indices are different along the two principal crystal directions. This gives rise to the phenomenon of double refraction.

NiAs structure

The NaCl structure can be described a face-centered cubic lattice with all of the octahedral holes filled. What if we start with a hexagonal-close packed lattice rather than a face-centered cubic lattice?



Nickel arsenide crystal structure. The Ni_6As trigonal prisms are shaded gray. One octahedron of six As atoms surrounding a Ni atom is shown in the center of the figure.

This is the structure adopted by **NiAs** and many other transition metal sulfides, phosphides, and arsenides. The cations are shown in gray while the anions are light blue in the figure at the right. The cations are in octahedral coordination, so each cation is coordinated to six anions. The anions are also coordinated to six cations, but they occupy trigonal prismatic sites. In terms of layer stacking, the NiAs structure is AcBcAcBc..., where the A and B sites (the hcp lattice) are occupied by the As atoms, and the c sites, which are eclipsed along the layer stacking axis, are occupied by Ni. Unlike the NaCl structure, where the anion and cation sites are interchangeable, NiAs has unique anion and cation sites. The layer stacking sequence for NiAs is shown below:

- ---------- A
- - - -c- - - -
- ---------- B
- - - -c- - - -
- ---------- A
- - - -c- - - -
- ---------- B
- - - -c- - - -

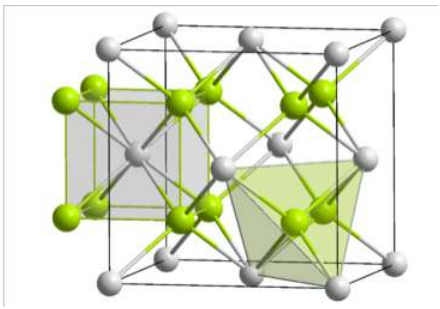
The NiAs structure cannot be adopted by ionic compounds because of the eclipsing cations, because the cation-cation repulsions would be internally destabilizing for an ionic compound. This structure is mainly adopted by covalent and polar covalent MX compounds, typically with "soft" X anions (S, Se, P, As,....) and low-valent transition metal cations. For example, some compounds with the NiAs structure are: MS, MSe, MTe (M=Ti, V, Fe, Co, Ni). Often these are nonstoichiometric or complex stoichiometries with ordered vacancies (Cr_7S_8, Fe_7S_8).

8.14: Structures Related to NaCl and NiAs is shared under a CC BY-NC-SA 4.0 license and was authored, remixed, and/or curated by LibreTexts.

- **8.3: Structures Related to NaCl and NiAs** by Chemistry 310 is licensed CC BY-SA 4.0. Original source: https://en.wikibooks.org/wiki/Introduction_to_Inorganic_Chemistry.

8.15: Tetrahedral Structures

In ccp and hcp lattices, there are two tetrahedral holes per packing atom. A stoichiometry of either M_2X or MX_2 gives a structure that fills all tetrahedral sites, while an MX structure fills only half of the sites. An example of an MX_2 structure is **fluorite**, CaF_2, whose structure is shown in the figure at the left. The packing atom in fluorite is Ca^{2+} and the structure is composed of three interpenetrating fcc lattices. It should be noted that the Ca^{2+} ion (gray spheres) as a packing atom defies our "rule" that anions are larger than cations and therefore must be the packing atoms. The fluorite structure is common for ionic MX_2 (MgF_2, ZrO_2, etc.) and M_2X compounds (Li_2O). In contrast, the hcp relative of the fluorite structure is quite rare because of unfavorable close contacts between like-charged ions.



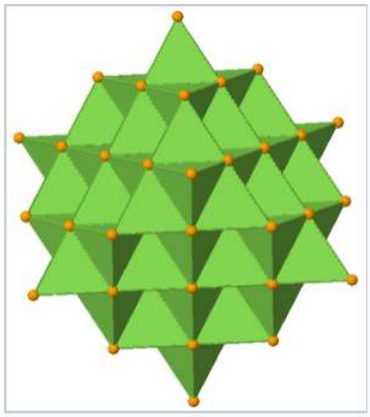
The fluorite (CaF_2) crystal structure showing the coordination environments of the Ca and F atoms

In terms of geometry, Ca^{2+} is in cubic coordination with eight F^- neighbors, and the fluoride ions are tetrahedrally coordinated by four Ca^{2+} ions. The 8:4 coordination geometry is consistent with the 1:2 Ca:F stoichiometry; in all crystal structures the ratio of the coordination numbers is the inverse of the stoichiometric ratio. The three interpenetrating fcc lattices have Ca at 0,0,0 , 1/2,1/2,0 , etc....F at 1/4,1/4,1/4 , 3/4,3/4,1/4 , etc... and F at 3/4,3/4,3/4 , 1/4,1/4/3/4 , etc.

Looking more closely at the tetrahedral sites in fluorite, we see that they fall into two distinct groups: T_+ and T_-. If a tetrahedron is oriented with a vertex pointing upwards along the stacking axis, the site is T_+. Likewise, a tetrahedron with a vertex oriented downward is T_-. The alternation of T_+ and T_- sites allows for efficient packing of ions in the structure. The layer stacking sequence in this structure (including fluoride ions in the T_+ and T_- sites) is:

- ---------- A
- - - -b- - - T_+
- - - -a- - - T_-
- ---------- B
- - - -c- - - T_+
- - - -b- - - T_-
- ---------- C
- - - -a- - - T_+
- - - -c- - - T_-
- ---------- A
- - - -b- - - T_+

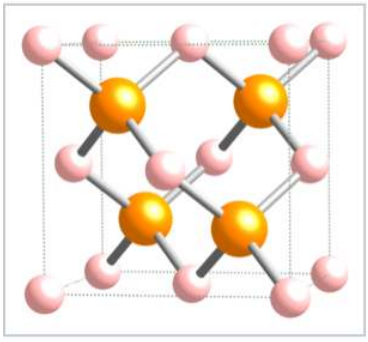
- - - -a- - - T_-



Polyhedral view of the fluorite crystal structure, showing T_+ and T_- Ca_4F tetrahedra. The Ca^{2+} ions are stacked ABCABC... along the body diagonal of the unit cell, which is the vertical direction in this image.

Tetrahedrally bonded compounds with a 1:1 stoichiometry (MX compounds) have only **half** of the tetrahedral sites (either the T_+ or T_- sites) filled. In this case, both the M and the X atoms are tetrahedrally coordinated. The **zincblende** and **wurtzite** structures of ZnS are 1:1 tetrahedral structures based on fcc and hcp lattices, respectively. Both structures are favored by p-block compounds that follow the octet rule, and these compounds are usually semiconductors or insulators. The zincblende structure, shown below, can be thought of as two interpenetrating fcc lattices, one of anions and one of cations, offset from each other by a translation of 1/4 along the body diagonal of the unit cell. Examples of compounds with the zincblende structure include CuCl, CuI, ZnSe, HgS, BeS, CdTe, AlP, GaP, SnSb, CSi, and diamond. Additionally, the compound $CuInSe_2$ is zincblende in an ordered, doubled unit cell (the chalcopyrite structure). The solid solution compounds $CuIn_{1-x}Ga_xSe_2$ with this structure are among the most widely studied materials for use in efficient thin film photovoltaic cells. Using ZnS as a representative of zincblende, the coordination of both Zn and S atoms is tetrahedral. The layer sequence, which is AbBcCaAbBcC..., results in non-planar, six-membered ZnS rings which allows for a relatively long distance between opposite atoms in the ring. The sequence of close-packed layers in zincblende, filling only the T_+ sites and leaving the T_- sites empty, is shown below:

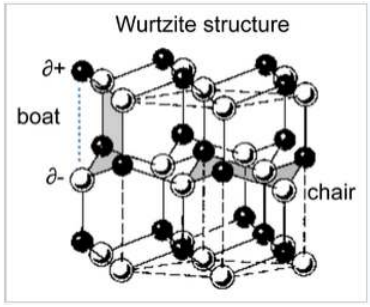
- ---------- A
- - - -b- - - T_+
- - - - - - T_-
- ---------- B
- - - -c- - - T_+
- - - - - - T_-
- ---------- C
- - - -a- - - T_+
- - - - - - T_-



The zincblende unit cell

The wurtzite structure is a close relative of zinc blende, based on filling half the tetrahedral holes in the hcp lattice. Like zincblende, wurtzite contains planes of fused six-membered rings in the chair conformation. Unlike zincblende, however, the rings joining these planes contain non-planar, six-membered rings. The structure aligns the anions so that they are directly above the cations in the structure, a less favorable situation sterically but a more favorable one in terms of electrostatics. As a result, the wurtzite structure tends to favor more polar or ionic compounds (e.g., ZnO, $NH_4^+F^-$) than the zincblende structure. As with zincblende, both ions are in tetrahedral (4:4) coordination and there are typically eight valence electrons in the MX compound. Examples of compounds with this structure include: BeO, ZnO, MnS, CdSe, MgTe, AlN, and NH_4F. The layered structure of wurtzite is AbBaAbB and the layer sequence with T_+ sites filled is illustrated below:

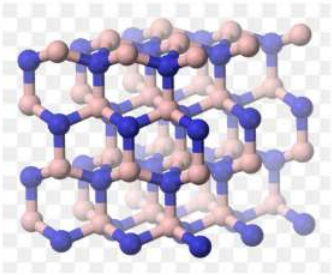
- ---------- A
- - - -b- - - T_+
- - - - - - - T_-
- ---------- B
- - - -a- - - T_+
- - - - - - - T_-
- ---------- A
- - - -b- - - T_+
- - - - - - - T_-
- ---------- B



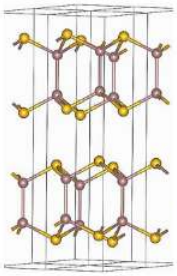
The chair and boat conformations of six-membered ZnS rings in the wurtzite structure.

An interesting consequence of the layer stacking in the wurtzite structure is that the crystals are polar. When cleaved along the c-axis (the stacking axis), crystals of ZnO, ZnS, and GaN have one negatively charged face and an opposite positively charged face. An applied electric field interacts with the crystal dipole, resulting in compression or elongation of the lattice along this direction. For this reason crystals of compounds in the wurtzite structure are typically piezoelectric (increasing the pressure on the material generates a voltage in the material).

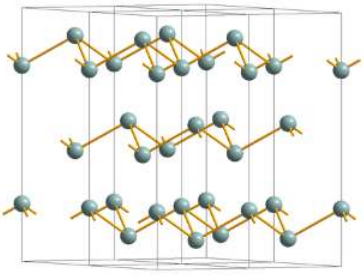
Some compounds are diamorphic and can have either the zincblende or wurtzite structure. Examples of these compounds that have intermediate polarities include CdS and ZnS. SiO_2 exists in polymorphs (crystobalite and tridymite) that resemble zincblende and wurtzite with O atoms midway between each of the Si atoms. The zincblende and wurtzite structures have efficient packing arrangements for tetrahedrally bonded networks and are commonly found in compounds that have tetrahedral bonding. Water, for example, has a tetrahedral hydrogen bonding network and is wurtzite-type. The undistorted wurtzite and zinc blende structures are typically found for AX compounds with eight valence electrons, which follow the octet rule. AX compounds with nine or ten electrons such as GaSe and GaAs crystallize in distorted variants of the wurtzite structure. In GaSe, the extra electrons form lone pairs and this creates layers in the structure, as can be seen in the figure below. To the right of GaSe, the structures of As, Sb, and SbAs show an ever further breakdown of the structure into layers as more valence electrons are added.



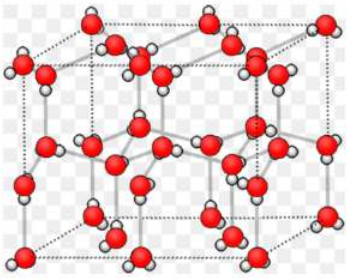
Wurtzite crystal structure



GaSe crystal structure



Crystal structure of Sb, SbAs, and gray As



Crystal structure of hexagonal ice

Hexagonal ice is the most stable polymorph of ice, which is obtained upon freezing at 1 atmosphere pressure. This polymorph (ice-I) has a hcp wurtzite-type structure. Looking at the structure shown at the right, we see that there are irregular arrangements of the O-H---O bonds. In the structure, hydrogen bonding enforces the tetrahedral coordination of each water molecule, resulting in a relatively open structure that is less dense than liquid water. For this reason, ice floats in water.

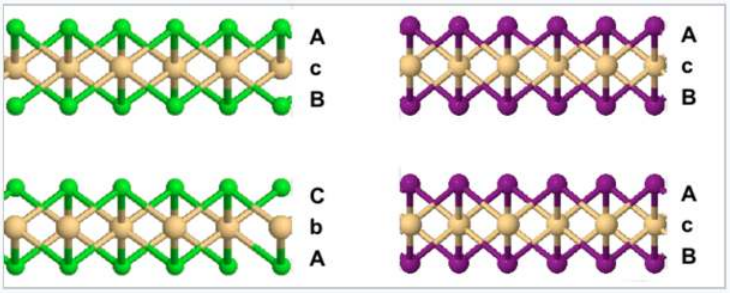
8.15: Tetrahedral Structures is shared under a CC BY-NC-SA 4.0 license and was authored, remixed, and/or curated by LibreTexts.

- **8.4: Tetrahedral Structures** by Chemistry 310 is licensed CC BY-SA 4.0. Original source: https://en.wikibooks.org/wiki/Introduction_to_Inorganic_Chemistry.

8.16: Layered Structures and Intercalation Reactions

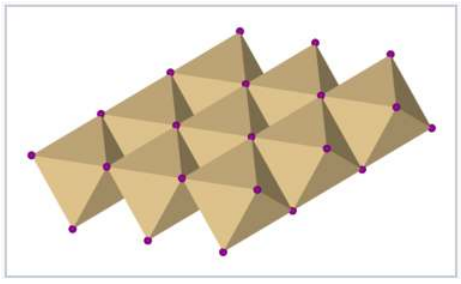
Layered structures are characterized by strong (and typically covalent) bonding between atoms in two dimensions and weaker bonding in the third. A broad range of compounds including metal halides, oxides, sulfides, selenides, borides, nitrides, carbides, and allotropes of some pure elements (B, C, P, As) exist in layered forms. Structurally, the simplest of these structures (for example binary metal halides and sulfides) can be described as having some fraction of the octahedral and/or tetrahedral sites are filled in the fcc and hcp lattices. For example, the $CdCl_2$ structure is formed by filling all the octahedral sites in alternate layers of the fcc lattice, and the CdI_2 structure is the relative of this structure in the hcp lattice.

In the **$CdCl_2$ structure**, the stacking sequence of anion layers is ABCABC...
In the **CdI_2 structure**, the anion stacking sequence is ABAB..., and all the cations are eclipsed along the stacking axis.



Comparison of the $CdCl_2$ (left) and CdI_2 (right) crystal structures

These are examples of **6-3 structures**, because the cations are coordinated by an octahedron of six anions, and the anions are coordinated by three cations to make a trigonal pyramid (like NH_3). Another way to describe these structures is to say that the MX_6 octahedra each share six edges in the MX_2 sheets.



Polyhedral drawing of one layer of the $CdCl_2$ or CdI_2 structure showing edge-sharing MX_6 octahedra

Because these structures place the packing atoms (the anions) in direct van der Waals contact, they are most stable for relatively **covalent** compounds. Otherwise, the electrostatic repulsion between contacting anions would destabilize the structure energetically. More ionic MX_2 compounds tend to adopt the fluorite (CaF_2) or rutile (TiO_2) structures, which are not layered.

Despite the fact that these two structure types are the same at the level of nearest and next-nearest neighbor ions, the CdI_2 structure is much more common than the $CdCl_2$ structure.

$CdCl_2$ structure:

MCl_2 (M = Mg, Mn, Fe, Co, Ni, Zn, Cd)

$NiBr_2$, NiI_2, $ZnBr_2$, ZnI_2

CdI_2 structure:

MCl_2 (M = Ti, V)

MBr_2 (M = Mg, Fe, Co, Cd)

MI_2 (M = Mg, Ca, Ti, V, Mn, Fe, Co, Cd, Ge, Pb, Th)

$M(OH)_2$ (M = Mg, Ca, Mn, Fe, Co, Ni, Cd)

MS_2 (M = Ti, Zr, Sn, Ta, Pt)

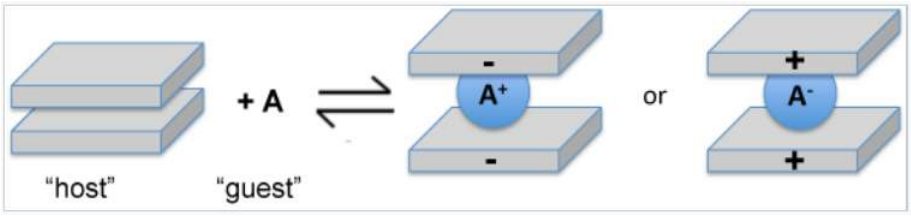
MSe_2 (M = Ti, Zr, Sn, V, Pt)

MTe_2 (M = Ti, Co, Ni, Rh, Pd, Pt)

Physically, layered compounds are **soft** and **slippery**, because the layer planes slide past each other easily. For example, graphite, MoS_2, and talc (a silicate) are layered compounds that are used widely as **lubricants** and lubricant additives.

An important reaction of layered compounds is **intercalation**. In intercalation reactions, guest molecules and ions enter the galleries that separate the sheets, usually with expansion of the lattice along the stacking axis. This reaction is typically reversible if it does not perturb the bonding within the sheets. Often the **driving force for intercalation is a redox reaction**, i.e., electron transfer between the host and guest. For example, lithium metal reacts with TiS_2, MoS_2, and graphite to produce $LiTiS_2$, Li_xMoS_2 ($x < 1$), and LiC_6. In these compounds, lithium is ionized to Li^+ and the sheets are negatively charged. Oxidizing agents such as Br_2, $FeCl_3$, and AsF_5 also react with graphite. In the resulting intercalation compounds, the sheets are positively charged and the intercalated species are anionic.

Intercalation reactions are especially important for electrochemical energy storage in **secondary batteries**, such as **lithium ion** batteries, **nickel-metal hydride** batteries, and **nickel-cadmium** batteries. The reversible nature of the intercalation reaction allows the electrodes to be charged and discharged up to several thousand times without losing their mechanical integrity. In lithium ion batteries, the negative electrode material is typically graphite, which is intercalated by lithium to make LiC_6. Several different oxides and phosphates containing redox active transition metal ions (Mn, Fe, Co, Ni) are used as the positive electrode materials.



Oxidative or reductive intercalation involves the placement of anions or cations between sheets.

Lithium ion batteries based on CoO_2 were first described in 1980[1] by John B. Goodenough's research group at Oxford. In batteries based on CoO_2, which has the CdI_2 structure, the positive electrode half-reaction is:

$$\mathrm{LiCoO_2 \leftrightharpoons Li_{1-x}CoO_2 + x\,Li^+ + xe^-} \tag{8.16.1}$$

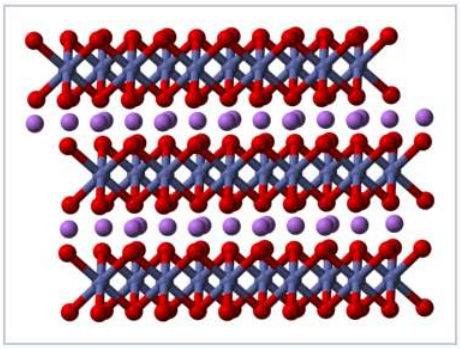
The negative electrode half reaction is:

$$\mathrm{x\,Li^+ + xe^- + x\,C_6 \leftrightharpoons x\,LiC_6} \tag{8.16.2}$$

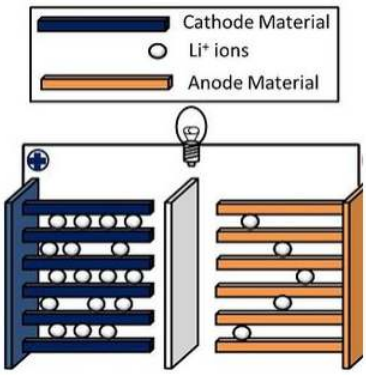
The battery is fully charged when the positive electrode is in the CoO_2 form and the negative electrode is in the LiC_6 form. Discharge involves the motion of Li^+ ions through the electrolyte, forming Li_xCoO_2 and graphite at the two electrodes.



Blue plaque erected by the Royal Society of Chemistry commemorating the development of cathode materials for the lithium-ion battery



Crystal structure of $LiCoO_2$[2]



The lithium ion battery is a "rocking chair" battery, so named because charging and discharging involve moving Li^+ ions from one side to the other. CoO_2 is one example of a positive electrode material that has been used in lithium ion batteries. It has a high energy density, but batteries based on CoO_2 have poor thermal stability. Safer materials include lithium iron phosphate ($LiFePO_4$), and $LiMO_2$ (M = a mixture of Co, Mn, and Ni). These batteries are used widely in laptop computers, portable electronics, cellular telephones, cordless tools, and electric and hybrid vehicles.

A similar intercalation reaction occurs in nickel-cadmium batteries and nickel-metal hydride batteries, except in this case the reaction involves the movement of protons in and out of the $Ni(OH)_2$ lattice, which has the CdI_2 structure:

$$NiO(OH) + H_2O + e^- \longrightarrow Ni(OH)_2 + OH^- \tag{8.16.3}$$

There are many layered compounds that cannot be intercalated by redox reactions, typically because some other stable product is formed. For example, the reaction of layered CdI_2 with Li produces LiI (NaCl structure) and Cd metal.

8.16: Layered Structures and Intercalation Reactions is shared under a CC BY-NC-SA 4.0 license and was authored, remixed, and/or curated by LibreTexts.

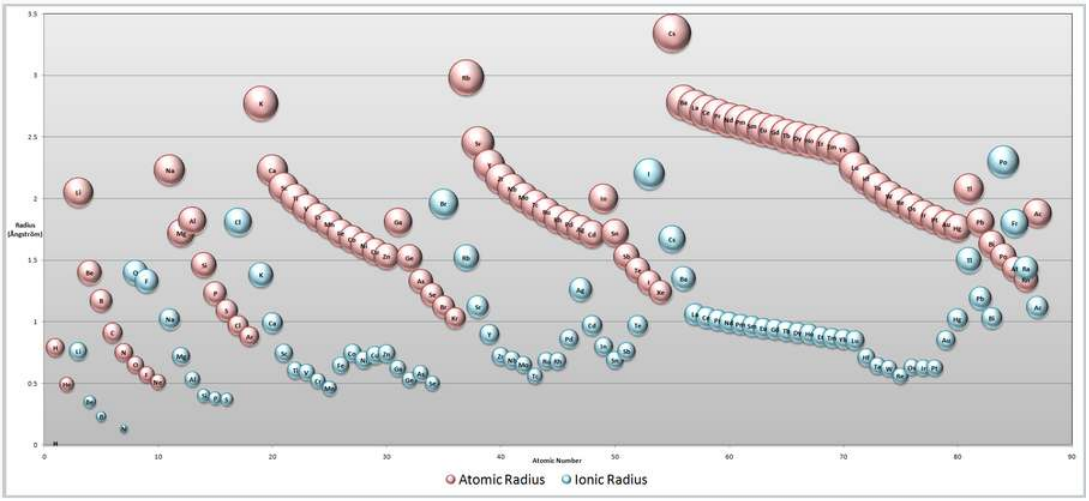
- **8.5: Layered Structures and Intercalation Reactions** by Chemistry 310 is licensed CC BY-SA 4.0. Original source: https://en.wikibooks.org/wiki/Introduction_to_Inorganic_Chemistry.

8.17: Ionic Radii and Radius Ratios

Atoms in crystals are held together by electrostatic forces, van der Waals interactions, and covalent bonding. It follows that arrangements of atoms that can maximize the strength of these attractive interactions should be most favorable and lead to the most commonly observed crystal structures.

Radius ratio rules

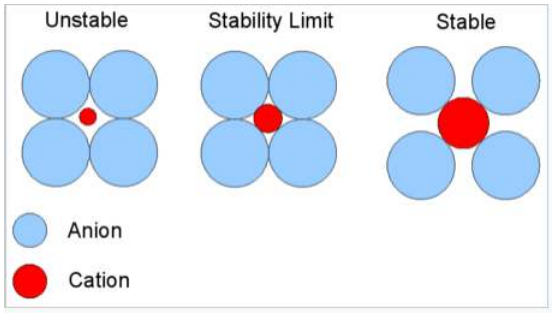
Early crystallographers had trouble solving the structures of inorganic solids using X-ray diffraction because some of the mathematical tools for analyzing the data had not yet been developed. Once a trial structure was proposed, it was relatively easy to calculate the diffraction pattern, but it was difficult to go the other way (from the diffraction pattern to the structure) if nothing was known *a priori* about the arrangement of atoms in the unit cell. It was (and still is!) important to develop some guidelines for guessing the coordination numbers and bonding geometries of atoms in crystals. The first such rules were proposed by Linus Pauling, who considered how one might pack together oppositely charged spheres of different radii. Pauling proposed from geometric considerations that the quality of the "fit" depended on the **radius ratio** of the anion and the cation.



Atomic and Ionic Radii. Note that cations are always smaller than the neutral atom (pink) of the same element, whereas anions are larger. Going from left to right across any row of the periodic table, neutral atoms and cations contract in size because of increasing nuclear charge. (click for larger image)

The basic idea of radius ratio rules is illustrated at the right. We consider that the anion is the packing atom in the crystal and the smaller cation fills interstitial sites ("holes"). Cations will find arrangements in which they can contact the largest number of anions. If the cation can touch all of its nearest neighbor anions, as shown at the right for a small cation in contact with larger anions, then the fit is good. If the cation is too small for a given site, that coordination number will be unstable and it will prefer a

lower coordination structure. The table below gives the ranges of cation/anion radius ratios that give the best fit for a given coordination geometry.



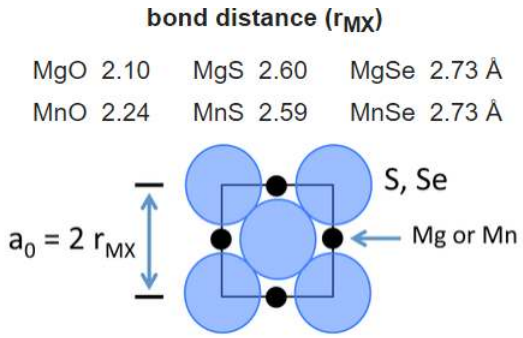
Critical Radius Ratio. This diagram is for coordination number six: 4 anions in the plane are shown, 1 is above the plane and 1 is below. The stability limit is at $r_C/r_A = 0.414$

Coordination number	Geometry	$\rho = r_{cation}/r_{anion}$
2	linear	0 - 0.155
3	triangular	0.155 - 0.225
4	tetrahedral	0.225 - 0.414
4	square planar	0.414 - 0.732
6	octahedral	0.414 - 0.732
8	cubic	0.732 - 1.0
12	cuboctahedral	1.0

There are unfortunately several challenges with using this idea to predict crystal structures:

- We don't know the radii of individual ions
- Atoms in crystals are not really ions - there is a varying degree of covalency depending electronegativity differences
- Bond distances (and therefore ionic radii) depend on bond strength and coordination number (remember Pauling's rule D(n) = D(1) - 0.6 log n)
- Ionic radii depend on oxidation state (higher charge => smaller cation size, larger anion size)

We can build up a table of ionic radii by assuming that the bond length is the sum of the radii ($r_+ + r_-$) if the ions are in contact in the crystal. Consider for example the compounds MgX and MnX, where X = O, S, Se. All of these compounds crystallize in the NaCl structure:



For the two larger anions (S^{2-} and Se^{2-}), the unit cell dimensions are the same for both cations. This suggests that the anions are in contact in these structures. From geometric considerations, the anion radius in this case is given by:

Extra close brace or missing open brace

and thus the radii of the S^{2-} and Se^{2-} ions are 1.84 and 1.93 Å, respectively. Once the sizes of these anions are fixed, we can obtain a self-consistent set of cation and anion radii from the lattice constants of many MX compounds.

How well does this model work? Let's consider the structures of tetravalent metal oxides (MO_2), using Pauling radii and the predictions of the radius ratio model:

Oxide MO_2	Radius ratio	Predicted coord. no.	Observed coord no. (structure)
CO_2	~0.1	2	2 (linear molecule)
SiO_2	0.32	4	4 (various tetrahedral structures)
GeO_2	0.43	4	4 (silica-like structures)
"	0.54	6	6 (rutile)
TiO_2	0.59	6	6 (rutile)
ZrO_2	0.68	6	7 (baddleyite)
"	0.77	8	8 (fluorite)
ThO_2	0.95	8	8 (fluorite)

Note that cations have different radii depending on their coordination numbers, and thus different radius ratios are calculated for Ge^{4+} with coordination numbers 4 and 6, and for Zr^{4+} with coordination numbers 6 and 8.

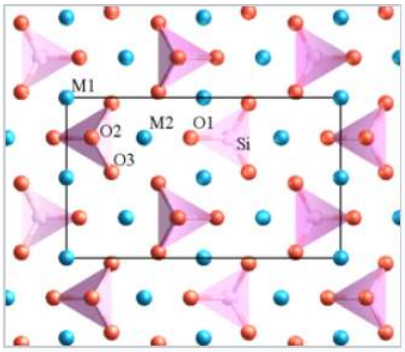
For this series of oxides, the model appears to work quite well. The correct coordination number is predicted in all cases, and borderline cases such as GeO_2 and ZrO_2 are found in structures with different coordination numbers. The model also correctly predicts the structures of BeF_2 (SiO_2 type), MgF_2 (rutile), and CaF_2 (fluorite).

What about the alkali halides NaCl, KBr, LiI, CsF, etc.? All of them have the NaCl structure except for CsCl, CsBr, and CsI, which have the CsCl (8-8) structure. In this case the radius ratio model fails rather badly. The Li^+ salts LiBr and LiI are predicted to have tetrahedral structures, and KF is predicted to have an 8-8 structure like CsCl. We can try adjusting the radii (e.g., making the cations larger and anions smaller), but the best we can do with the alkali halides is predict about half of their structures correctly. Since the alkali halides are clearly ionic compounds, this failure suggests that there is something very wrong with the radius ratio model, and its success with MO_2 compounds was coincidental.

In addition to the radius ratio rule, Linus Pauling developed other useful rules that are helpful in rationalizing and also predicting the structures of inorganic compounds. Pauling's rules[1] state that:

- Stable structures are **locally electroneutral**. For example, in the structure of the double perovskite Sr_2FeMoO_6, MO_6 (M = Fe^{2+}, Mo^{6+}) octahedra share all their vertices, and Sr^{2+} ions fill the cubooctahedral cavities that are flanked by eight MO_6 octahedra.[2] Each O^{2-} ion is coordinated to one Fe^{2+} and one Mo^{6+} ion in order to achieve local electroneutrality, and thus the FeO_6 and MoO_6 octahedra alternate in the structure.
- **Cation-cation repulsion** should be minimized. Anion polyhedra can share vertices (as in the perovskite structure) without any energetic penalty. Shared polyhedral edges, and especially shared faces, cause cation-cation repulsion and should be avoided. For example, in rutile, the most stable polymorph of TiO_2, the TiO_6 octahedra share vertices and two opposite edges, forming ribbons in the structure. In anatase TiO_2, each octahedron shares four edges so the anatase polymorph is less thermodynamically stable.

- **Highly charged cations** in anion polyhedra tend not to share edges or even vertices, especially when the coordination number is low. For example, in orthosilicates such as olivine (M_2SiO_4), there are isolated SiO_4^{4-} tetrahedra.



Structure of olivine. M (Mg or Fe) = blue spheres, Si = pink tetrahedra, O = red spheres.

As we will soon see, all of Pauling's rules are justified on the basis of lattice energy considerations. In ionic compounds, the arrangement of atoms that maximizes anion-cation interactions while minimizing cation-cation and anion-anion contacts is energetically the best.

8.17: Ionic Radii and Radius Ratios is shared under a CC BY-NC-SA 4.0 license and was authored, remixed, and/or curated by LibreTexts.

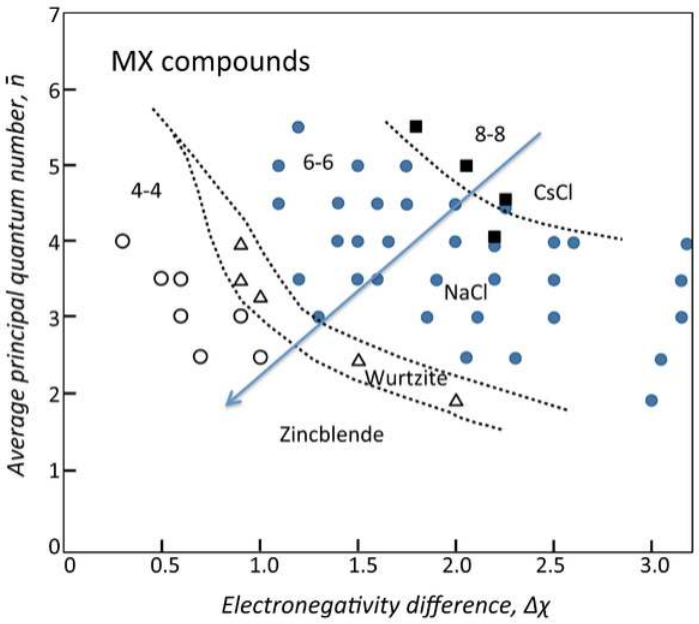
- **9.1: Ionic Radii and Radius Ratios** by Chemistry 310 is licensed CC BY-SA 4.0. Original source: https://en.wikibooks.org/wiki/Introduction_to_Inorganic_Chemistry.

8.18: Structure Maps

Structure maps, which plot structures against properties such electronegativity, are more consistent than radius ratio rules in correctly predicting coordination numbers and crystal structures. One of the early examples of this approach was published by Mooser and Pearson in 1959.[3]

A **Mooser-Pearson diagram** maps crystal structures according to the average principal quantum numbers of the atoms and their electronegativity difference. The basic ideas behind such a plot are:

- The greater the electronegativity difference, the more ionic is the compound. Higher ionicity results in higher coordination numbers because anions like to surround cations (and vice versa).
- Higher principal quantum numbers result in less s-p hybridization, less directional bonding, and therefore higher coordination number. We saw this trend before with the structures of elements in group IV: descending the group the coordination number increases progressively from 3-4 (carbon) to 12 (Pb).



The lines in the Mooser-Pearson diagram separate MX compounds with CsCl, NaCl, and tetrahedral (wurtzite and zincblende) structures. Note that wurtzite has higher ionicity than zincblende in the plot, consistent with our discussion of the "boat" and "chair" ring structures in Chapter 8. Diamorphic compounds tend to fall on the boundaries. On the whole, the Mooser-Pearson diagram makes far fewer errors in predicting structures than the radius ratio rule. There are similar diagrams for MX_2 structures, in which the order of ionicity is CaF_2 (8:4 coordination) > rutile (6:3) > silica structures (4:2).

8.18: Structure Maps is shared under a CC BY-NC-SA 4.0 license and was authored, remixed, and/or curated by LibreTexts.

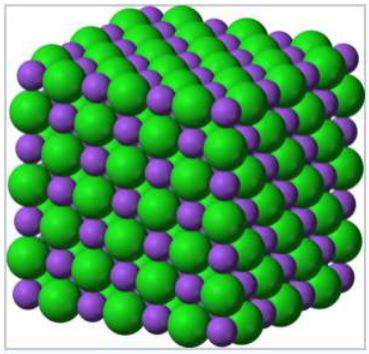
- **9.2: Structure Maps** by Chemistry 310 is licensed CC BY-SA 4.0. Original source: https://en.wikibooks.org/wiki/Introduction_to_Inorganic_Chemistry.

8.19: Energetics of Crystalline Solids- The Ionic Model

Many ionic compounds have simple structures. Because the forces holding the atoms together are primarily electrostatic, we can calculate the cohesive energy of the crystal lattice with good accuracy. Interesting questions to ask about these lattice energy calculations are:

- How accurate are lattice energy calculations?
- What do they teach us about the chemical bonds in ionic crystals?
- Can we use lattice energies to predict properties such as solubility, stability, and reactivity?
- Can we use lattice energies to predict the crystal structures of ionic compounds?

Let's start by looking at the forces that hold ionic lattices together. There are mainly two kinds of force that determine the energy of an ionic bond.



The NaCl crystal structure is the archetype for calculating lattice energies and computing enthalpies of formation from Born-Haber cycles.

1) **Electrostatic Force** of attraction and repulsion (Coulomb's Law): Two ions with charges z_+ and z_-, separated by a distance r, experience a force F:

$$\mathbf{F} = -\frac{e^2}{4\pi\varepsilon_0}\frac{z_+z_-}{r^2} \tag{8.19.1}$$

where

e = 1.6022×10^{-19} C

4 π ε_0 = 1.112×10^{-10} C²/(J m)

This force is attractive for ions of opposite charge.

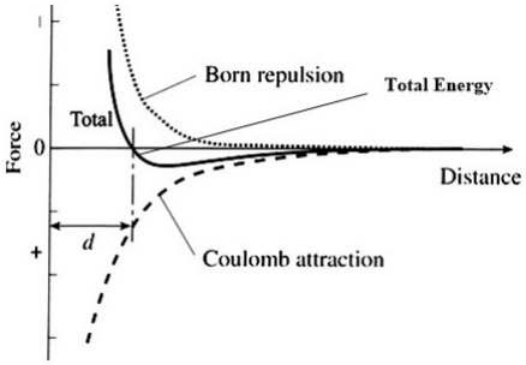
The electrostatic potential energy, E_{elec}, is then given by

$$\mathbf{E}_{elec}\int_{\infty}^{r} F(r)dr = \frac{e^2}{4\pi\varepsilon_0}\frac{z_+z_-}{r} \tag{8.19.2}$$

The sign of E_{elec} is negative for the attractive interaction between a cation and an anion. That is, the closer oppositely charged ions approach each other, the lower the potential energy.

2) **Closed-shell repulsion**. When electrons in the closed shells of one ion overlap with those of another ion, there is a repulsive force comes from the Pauli exclusion principle. A third electron cannot enter an orbital that already contains two electrons. This force is short range, and is typically modeled as falling off exponentially or with a high power of the distance r between atoms. For example, in the Born approximation, B is a constant and ρ is a number with units of length, which is usually empirically determined from compressibility data. A typical value of ρ is 0.345 Å.

$$\mathbf{E}_{repulsion} = Bexp(\frac{-r}{\rho}) \tag{8.19.3}$$



The energy of the ionic bond between two atoms is then calculated as the combination of net electrostatic and the closed-shell repulsion energies, as shown in the figure at the right. Note that for the moment we are ignoring the attractive van der Waals energy between ions, which we will explain below. For a pair of ions, the equilibrium distance between ions is determined by the minimum in the total energy curve. At this distance, the net force on each ion is zero.

Electrostatic energy of a crystal lattice

We can use these equations to calculate the lattice energy of a crystal by summing up the interactions between all pairs of ions. Because the closed-shell repulsion force is short range, this term is typically calculated only for interactions between neighboring ions. However, the Coulomb force is long range, and must be calculated over the entire crystal. This problem was first solved in 1918 by Erwin Madelung, a German physicist.[4]

Consider an ion in the NaCl structure labeled "O" in the diagram at the right. We can see that the nearest neighbor interactions (+ -) with ions labeled "1" are attractive, the next nearest neighbor interactions (- - and + +) are repulsive, and so on. In the NaCl structure, counting from the ion in the center of the unit cell, there are 6 nearest neighbors (on the faces of the cube), 12 next nearest neighbors (on the edges of the cube), 8 in the next shell (at the vertices of the cube), and so on. Their distances from ion "0" increase progressively: r_o, $\sqrt{2}\ r_o$, $\sqrt{3}\ r_o$, and so on, where r_o is the nearest neighbor distance.

We can now write the electrostatic energy at ion "O" as:

$$\mathbf{E}_{elec} = -6\frac{e^2}{4\pi\varepsilon_0}\frac{z_+z_-}{r_o} + 12\frac{e^2}{4\pi\varepsilon_0}\frac{z_+z_-}{\sqrt{2}r_o} - 8\frac{e^2}{4\pi\varepsilon_0}\frac{z_+z_-}{\sqrt{3}r_o} + \ldots \tag{8.19.4}$$

Factoring out constants and the nearest-neighbor bond distance r_o we obtain:

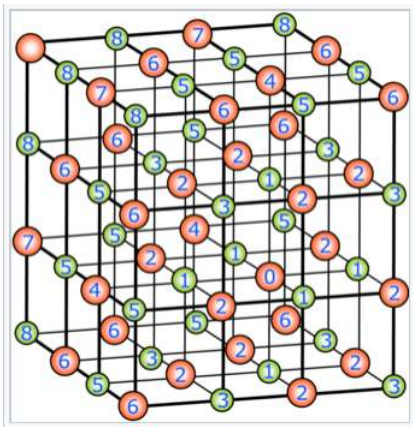
$$\mathbf{E}_{elec} = \frac{e^2}{4\pi\varepsilon_0}\frac{z_+z_-}{r_o}\left(6 - \frac{12}{\sqrt{2}} + \frac{8}{\sqrt{3}} - \frac{6}{\sqrt{4}} + \ldots\right) \tag{8.19.5}$$

Where the sum in parentheses, which is unitless, slowly converges to a value of A = 1.74756. Generalizing this formula for any three-dimensional ionic crystal we get a function:

$$\mathbf{E}_{elec} = \frac{e^2}{4\pi\varepsilon_0}\frac{z_+z_-}{r_o}NA \tag{8.19.6}$$

where N is Avogadro's number (because we are calculating energy per mole of ions) and A is called the *Madelung constant*. The **Madelung constant** depends only on the geometrical arrangement of the ions and so it varies between different types of crystal

structures, but within a given structure type it does not change. Thus MgO and NaCl have the same Madelung constant because they both have the NaCl structure. We will see more about the Madelung constant in an upcoming section.



The Madelung constant is calculated by summing up electrostatic interactions with ion labeled 0 in the expanding spheres method. Each number designates the order in which it is summed. For example, ions labeled 1 represent the six nearest neighbors (attractive interaction), ions labeled 2 are the 12 next nearest neighbors (repulsive interaction) and so on. Note that if the sum is carried out over shells 1-2-3..., it converges very slowly, but there are mathematical methods for summing it which give a rapidly converging series.

Total lattice energy of a crystal

Having in hand a formula for the electrostatic energy, we can now add in the closed-shell repulsion term to obtain an equation that gives us the total lattice energy.

$$E_L = \frac{e^2}{4\pi\varepsilon_0}\frac{z_+z_-}{r_o}NA + NBexp(\frac{-r}{\rho}) \tag{8.19.7}$$

At the equilibrium bond distance, the forces on all the ions are zero, and we can use this fact to eliminate the constant B:

$$[\frac{dE}{dr}]_{r=r_o} = 0 \tag{8.19.8}$$

Expressed this way, E_L is a negative number (because z_+ and z_- have opposite signs). It represents the energy change for forming one mole of solid salt from one mole of the gaseous ions, separated initially at an infinite distance.



Lithium fluoride (shown here as a large single crystal in a beaker of water) is the only alkali halide that is not freely soluble in water. The lattice energy of LiF is the most negative of the alkali fluorides because Li^+ and F^- are both small ions and E_L is proportional to $1/r_0$.

8.19: Energetics of Crystalline Solids- The Ionic Model is shared under a CC BY-NC-SA 4.0 license and was authored, remixed, and/or curated by LibreTexts.

- **9.3: Energetics of Crystalline Solids- The Ionic Model** by Chemistry 310 is licensed CC BY-SA 4.0. Original source: https://en.wikibooks.org/wiki/Introduction_to_Inorganic_Chemistry.

8.20: Born-Haber Cycles for NaCl and Silver Halides

Now that we have an equation for the lattice energy of an ionic crystal, we can ask the question of how accurate it is. Remember, we made several approximations in arriving at this formula. We assumed that the lattice was completely ionic, we ignored the van der Waals attractive energy of the ions, and we assumed that there was no covalent contribution to the bonding.

Let's consider the lattice energy of table salt (NaCl)

$$Na^+_{(g)} + Cl^-_{(g)} \longrightarrow NaCl_{(s)}$$

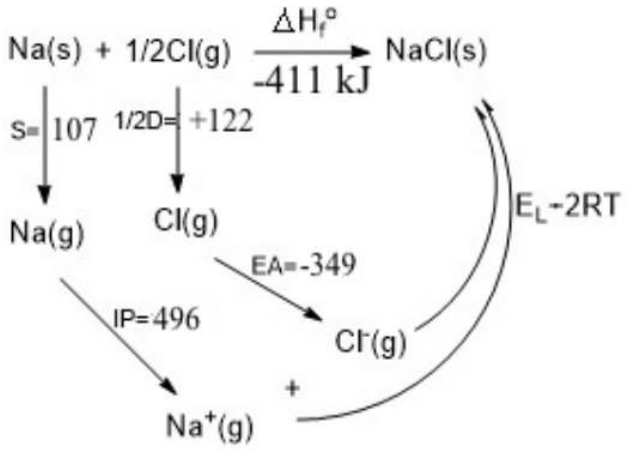
To calculate the lattice energy, we lump together the physical constants:

$$E_L(\frac{kJ}{mol}) = (1389.3)\frac{Aq_1q_2}{r_o}(1 - \frac{.345}{r_o}) \tag{8.20.1}$$

where r_o is expressed in Å. Now we can calculate the lattice energy for NaCl using r_o = 2.814 Å, as:

$$E_L = -(1389.3)\frac{1.7476}{2.814}(1 - \frac{.345}{2.814}) = -766.5\frac{kJ}{mol} \tag{8.20.2}$$

We can alternatively construct a **Born-Haber cycle** for the formation of NaCl from the elements and calculate the lattice energy as the "missing" term in the cycle.



S= Sublimation energy of Na(s)

IP= Ionization potential of Na(g)

D= Bond dissocation energy of Cl_2(g)

EA= Electron affinity of Cl(g)

E_L=Lattice energy of NaCl

R= Gas constant

T= Absolute temperature

From **Hess' Law:** $\Delta H_f = s + \frac{1}{2}D + IP + EA + E_L - 2RT = -396\frac{kJ}{mol}$

Here we have to subtract 2RT to convert our cycle of energies to a cycle of enthalpies, because we are compressing two moles of gas in making NaCl(s) and PΔV = ΔnRT, where Δn = -2.

Experimentally ΔH_f for NaCl is **-411 kJ/mol**

Because all the other numbers in the cycle are known accurately, the error in our calculation is only about 15 kJ (about 2% of E_L). The result is promising because we neglected the van der Waals term.

But....how did we get away with neglecting the van der Waals term?

This is because we used **energy minimization** to obtain the repulsion energy in the Born-Mayer equation. If we underestimate the attractive energy of the crystal lattice, the energy minimization criterion ensures that the repulsion energy is underestimated as well. The two errors partially compensate, so the overall error in the calculation is small.

We can do better by explicitly including the short-range van der Waals attractive energy between ions. The table below shows results of more detailed lattice energy calculations for ionic fluorides in which the van der Waals term is explicitly included. The errors in this case are only about 1% of E_L.

Compound	Calculated Lattice Energy (kJ/mol)	Experimental E_L from Born-Haber Cycle
MgF_2 (rutile structure)	-2,920	-2,908
CaF_2 (fluorite structure)	-2,586	-2,611
BaF_2 (fluorite structure)	-2,326	-2,368

Silver Halides

It is interesting to repeat this exercise for the silver halides, which have either the NaCl structure (AgF, AgCl, AgBr) or zincblende structure (AgI).

Silver Halide	Calculated	Cycle	Difference (kJ/mol)
AgF	-920	-954	34
AgCl	-833	-908	75
AgBr	-816	-900	84
AgI	-778	-883	105

Looking at the table, we see that the error is small for AgF and becomes progressively larger for the heavier silver halides. However we are still obtaining answers within about 12% error even for AgI. Should we interpret the good agreement with values calculated from the ionic model to mean that these compounds are ionic? Clearly, this description is inappropriate for AgI, where the electronegativity difference $\Delta\chi$ is only 0.6 (compare this value to 0.4 for a C-H bond, which we typically view as non-polar).



A drop of siver nitrate solution, when added to a dilute hydrochloric acid solution, results in the immediate formation of a white silver chloride precipitate. This reaction is used as a qualitative test for the presence of halide ions in solutions. The covalent bonding contribution to the lattice energies of AgCl, AgBr, and AgI makes these salts sparingly soluble in water.

Again, we can interpret the fortuitous agreement between the calculated and experimentally obtained energies in terms of compensating errors. Our lattice energy calculation *overestimates* the ionic contribution in the case of the heavier silver halides, but *underestimates* the covalent contribution. Of these compounds, only AgF is soluble in water and should be thought of as an ionic compound. The others are progressively more insoluble in water (K_{sp} is 10^{-10}, 10^{-13}, and 10^{-16} for AgCl, AgBr, and AgI), reflecting increasing covalency as $\Delta\chi$ decreases.

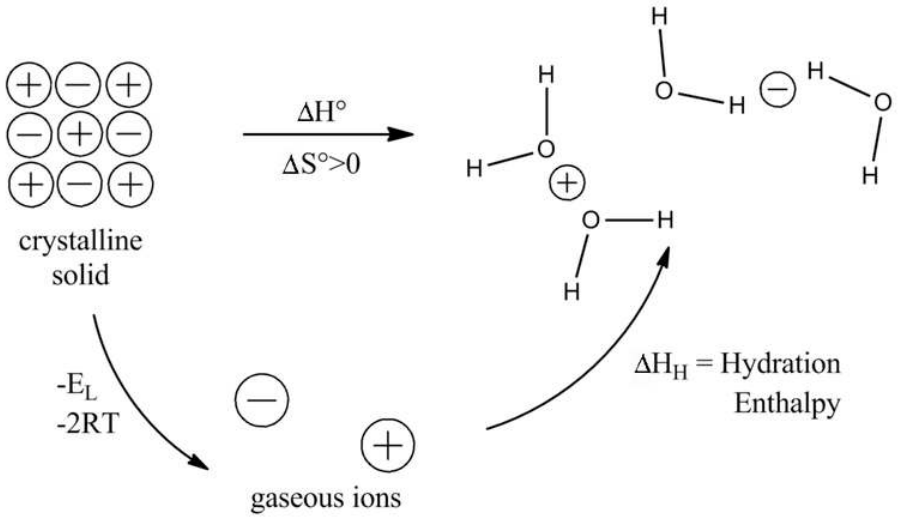
The moral of the story is that simple lattice energy calculations based on the ionic model work well, but *they do not necessarily imply that the compounds are ionic*!

8.20: Born-Haber Cycles for NaCl and Silver Halides is shared under a CC BY-NC-SA 4.0 license and was authored, remixed, and/or curated by LibreTexts.

- **9.4: Born-Haber Cycles for NaCl and Silver Halides** by Chemistry 310 is licensed CC BY-SA 4.0. Original source: https://en.wikibooks.org/wiki/Introduction_to_Inorganic_Chemistry.

8.21: Lattice Energies and Solubility

Lattice energies can also help predict compound solubilities. Let's consider a Born-Haber cycle for dissolving a salt in water. We can imagine this as the sum of two processes: (1) the vaporization of the salt to produce gaseous ions, characterized by the lattice enthalpy, and (2) the hydration of those ions to produce the solution. The enthalpy change for the overall process is the sum of those two steps. We know that the entropy change for dissolution of a solid is positive, so the solubility depends on the enthalpy change for the overall process.



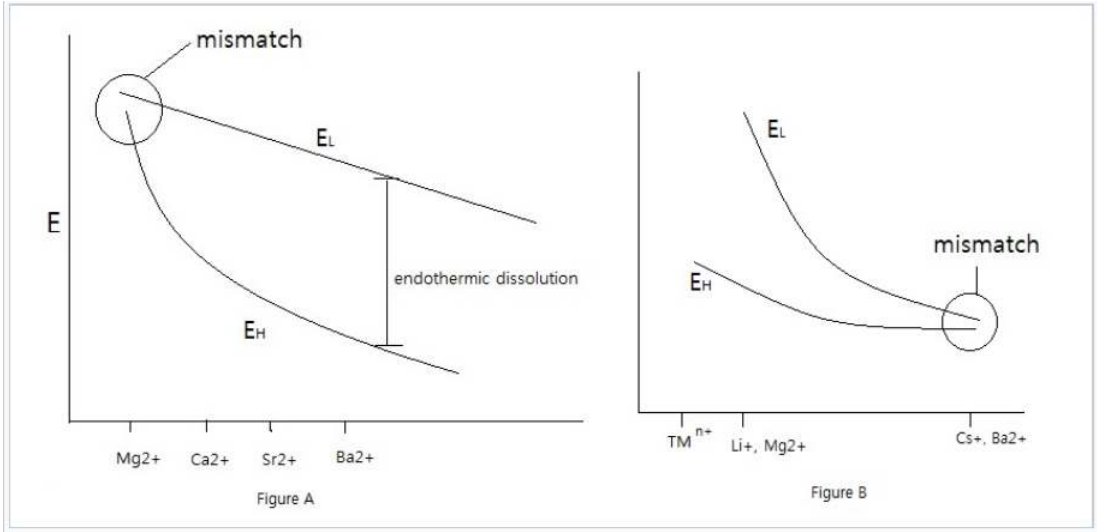
Here we need to consider the trends in both the lattice energy E_L and the hydration energy E_H. The lattice energy depends on the sum of the anion and cation radii ($r_+ + r_-$), whereas the hydration energy has separate anion and cation terms. Generally the solvation of small ions (typically cations) dominates the hydration energy because of the $1/r^2$ dependence.

$$E_L \alpha \frac{1}{r_+ + r_-} \tag{8.21.1}$$

$$E_H \alpha \frac{1}{r_+^2} + \frac{1}{r_-^2} \tag{8.21.2}$$

For salts that contain large anions, E_L doesn't change much as r_+ changes. That is because the anion dominates the $r_+ + r_-$ term in the denominator of the formula for E_L. On the other hand, E_H changes substantially with r_+, especially for small cations.

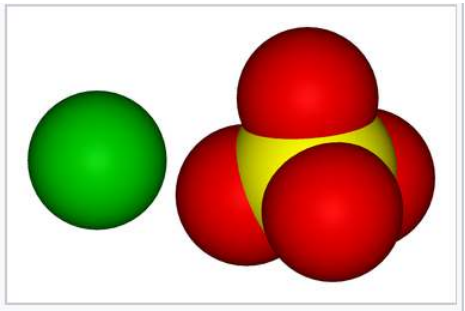
As a result, sulfate salts of small divalent cations, such as $MgSO_4$ (epsom salts), are soluble, whereas the lower hydration energy of Ba^{2+} in $BaSO_4$ makes that salt insoluble ($K_{sp} = 10^{-10}$).



Left: E_L diagram for sulfate salts. The large SO_4^{2-} ion is size-mismatched to small cations such as Mg^{2+}, which have large hydration energies, resulting soluble salts. With larger cations such as Ba^{2+}, which have lower E_H, the lattice energy exceeds the solvation enthalpy and the salts are insoluble.. Right: In the case of small anions such as F^- and OH^-, the lattice energy dominates with small cations such as transition metal ions (TM^{n+}), Mg^{2+}, and Li^+. Anion-cation size mismatch occurs with larger cations, such as Cs^+ and Ba^{2+}, which make soluble fluoride salts.

For small anions, E_L is more sensitive to r_+, whereas E_H does not depend on r_+ as strongly. For fluorides and hydroxides, LiF is slightly soluble whereas CsF is very soluble, and $Mg(OH)_2$ is insoluble whereas $Ba(OH)_2$ is very soluble.

Putting both trends together, we see that **low solubility** is most often encountered when the **anion and cation match well in their sizes**, especially when one or both are **multiply charged**.



Space-filling models showing the van der Waals surfaces of Ba^{2+} and SO_4^{2-}. The similarity in size of the two ions contributes to the low solubility of $BaSO_4$ in water.

Combining all our conclusions about solubility, we note the following trends:

1) Increasing **size mismatch** between the anion and cation leads to greater solubility, so CsF and LiI are the most soluble alkali halides.

2) Increasing **covalency** leads to lower solubility in the salts (due to larger E_L. For example, AgF, AgCl, AgBr, and AgI exhibit progressively lower solubility because of increasing covalency.

AgF > AgCl > AgBr > AgI

3) Increasing the **charge on the anion** lowers the solubility because the increase in E_L is large relative to the increase in E_H.

4) Small, polyvalent cations (having large E_H) make **soluble salts with large, univalent anions** such as I^-, NO_3^-, ClO_4^-, PF_6^-, and acetate.

Examples: Salts of transition metal and lanthanide ions

- Ln^{3+}: Nitrate salts are soluble, but oxides and hydroxides are insoluble.
- Fe^{3+}: Perchlorate is soluble, but sulfate is insoluble.

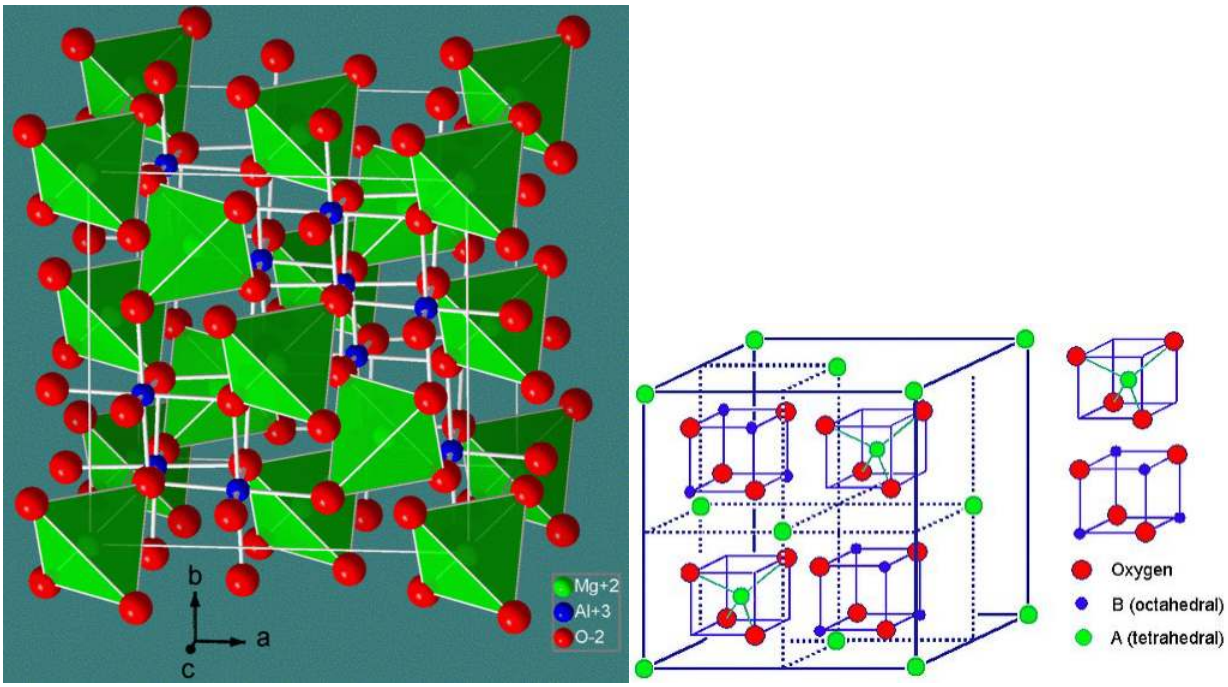
5) Multiple charged anions such as O^{2-}, S^{2-}, PO_4^{3-}, and SO_4^{2-} make insoluble salts with most M^{2+}, M^{3+}, and M^{4+} metals.

8.21: Lattice Energies and Solubility is shared under a CC BY-NC-SA 4.0 license and was authored, remixed, and/or curated by LibreTexts.

- **9.12: Lattice Energies and Solubility** by Chemistry 310 is licensed CC BY-SA 4.0. Original source: https://en.wikibooks.org/wiki/Introduction_to_Inorganic_Chemistry.

8.22: Spinel, Perovskite, and Rutile Structures

There are three more structures, which are derived from close-packed lattices, that are particularly important because of the material properties of their compounds. These are the **spinel** structure, on which ferrites and other magnetic oxides are based, the **perovskite** structure, which is adopted by ferroelectric and superconducting oxides, and the **rutile** structure, which is a common binary 6:3 structure adopted by oxides and fluorides.



The **spinel structure** is formulated MM'_2X_4, where M and M' are tetrahedrally and octahedrally coordinated cations, respectively, and X is an anion (typically O or F). The structure is named after the mineral $MgAl_2O_4$, and oxide spinels have the general formula AB_2O_4.

In the **normal spinel** structure, there is a close-packed array of anions. The A-site cations fill 1/8 of the tetrahedral holes and the B-site cations fill 1/2 of the octahedral holes. A polyhedral view of the normal spinel unit cell is shown at the left, and a simplified view (with the contents of the back half of the cell removed for clarity) is shown above. Each unit cell contains eight formula units and has a composition $A_8B_{16}O_{32}$.

Inverse spinels have a closely related structure (with the same large unit cell) in which the A-site ions and half of the B-site ions switch places. Inverse spinels are thus formulated $B(AB)O_4$, where the AB ions in parentheses occupy octahedral sites, and the other B ions are on tetrahedral sites. There are also mixed spinels, which are intermediate between the **normal** and **inverse** spinel structure.

Some spinel and inverse spinel AB combinations are:

$A^{2+}B^{3+}$, e.g., $MgAl_2O_4$ (normal spinel)

$A^{4+}B^{2+}$, e.g., $Pb_3O_4 = Pb^{II}(Pb^{II}Pb^{IV})O_4$ (inverse spinel)

$A^{6+}B^{+}$, e.g., Na_2WO_4 (normal spinel)

Many magnetic oxides, such as Fe_3O_4 and $CoFe_2O_4$, are spinels.

Normal vs. inverse spinel structure

For transition metal oxide spinels, the choice of the normal vs. inverse spinel structure is driven primarily by the **crystal field stabilization energy** (CFSE) of ions in the tetrahedral and octahedral sites. For spinels that contain 3d elements such as Cr, Mn, Fe,

Co, and Ni, the electron configuration is typically **high spin** because O^{2-} is a **weak field ligand**. We will learn more about these terms in the next section.

Ferrites are compounds of general formula $\mathbf{M^{II}Fe_2O_4}$. We can see that magnetite is one example of a ferrite (with M = Fe). Other divalent metals (M = Mg, Mn, Co, Ni, Zn) also form ferrites. Ferrites can be normal or inverse spinels, or mixed spinels, depending on the CFSE of the M^{II} ion. Based on their CFSE, Fe^{2+}, Co^{2+}, and Ni^{2+} all have a strong preference for the octahedral site, so those compounds are all inverse spinels. $ZnFe_2O_4$ is a normal spinel because the small Zn^{2+} ion (d^{10}) fits more easily into the tetrahedral site than Fe^{3+} (d^5), and both ions have zero CFSE. $MgFe_2O_4$ and $MnFe_2O_4$, in which all ions have zero CFSE and no site preference, are mixed spinels. **Chromite** spinels, $\mathbf{M^{II}Cr_2O_4}$, are always **normal spinels** because the d^3 Cr^{3+} ion has a strong preference for the octahedral site.

Examples of normal and inverse spinel structures:

> $\mathbf{MgAl_2O_4}$ is a **normal spinel** since both Mg^{2+} and Al^{3+} are non-transition metal ions and thus CFSE = 0. The more highly charged Al^{3+} ion prefers the octahedral site, where it is surrounded by six negatively charged oxygen atoms.
>
> $\mathbf{Mn_3O_4}$ is a **normal spinel** since the Mn^{2+} ion is a high spin d^5 system with zero CFSE. The two Mn^{3+} ions are high spin d^4 with higher CFSE on the octahedral sites ($3/5\ \Delta_O$) than on the tetrahedral site ($2/5\ \Delta_t \sim 1/5\ \Delta_O$).
>
> $\mathbf{Fe_3O_4}$ is an **inverse spinel** since the Fe^{3+} ion is a high spin d^5 system with zero CFSE. Fe^{2+} is a high spin d^6 system with more CFSE on an octahedral site than on a tetrahedral one.
>
> $\mathbf{NiFe_2O_4}$ is again an **inverse spinel** since Ni^{2+} (a d^8 ion) prefers the octahedral site and the CFSE of Fe^{3+} (a d^5 ion) is zero.
>
> $\mathbf{FeCr_2O_4}$ is a **normal spinel** since Fe^{2+} is high spin d^6 ion with $CFSE = [4(\frac{2}{5}) - 2(\frac{3}{5})]\Delta_o = \frac{2}{5}\Delta_o$ on an octahedral site, and Cr^{3+} is a d^3 ion with CFSE = $3(2/5)\ \Delta_O = 6/5\ \Delta_O$. Hence it is more energetically favorable for Cr^{3+} to occupy both of the octahedral sites.
>
> $\mathbf{Co_3O_4}$ is a **normal spinel**. Even in the presence of weak field oxo ligands, Co^{3+} is a low spin d^6 ion with very high CFSE on the octahedral sites, because of the high charge and small size of the Co^{3+} ion. Hence the Co^{3+} ions occupy both octahedral sites, and Co^{2+} occupies the tetrahedral site.

Magnetism of ferrite spinels

Ferrite spinels are of technological interest because of their magnetic ordering, which can be ferrimagnetic or antiferromagnetic depending on the structure (normal or inverse) and the nature of the metal ions. Fe_3O_4, $CoFe_2O_4$, and $NiFe_2O_4$ are all inverse spinels and are ferrimagnets. The latter two compounds are used in magnetic recording media and as deflection magnets, respectively.

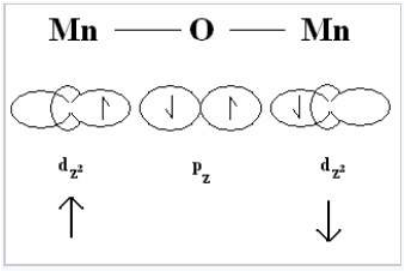
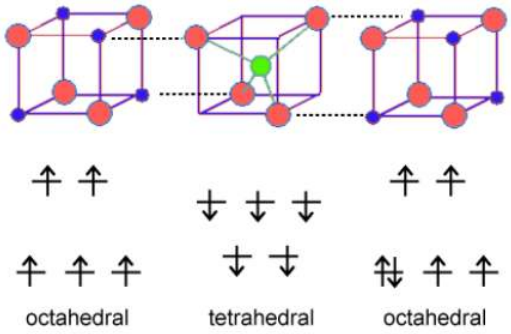


Illustration of antiferromagnetic superexchange between two transition metal cations through a shared oxygen atom.

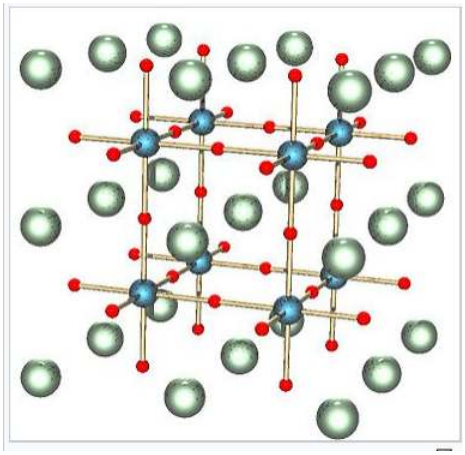
In order to understand the magnetism of ferrites, we need to think about how the unpaired spins of metal ions are coupled in oxides. If an oxide ion is shared by two metal ions, it can mediate the coupling of spins by superexchange as shown at the right. The coupling can be antiferromagnetic, as shown, or ferromagnetic, depending on the orbital filling and the symmetry of the orbitals involved. The **Goodenough-Kanamori rules** predict the local magnetic ordering (ferromagnetic vs. antiferromagnetic) that results from superexchange coupling of the electron spins of transition metal ions. For ferrites, the strongest coupling is between ions on neighboring **tetrahedral and octahedral sites**, and the ordering of spins between these two sites is reliably **antiferromagnetic**.



Because all the tetrahedral and octahedral sites in a spinel or inverse spinel crystal are coupled together identically, it works out that ions on the tetrahedral sites will all have one orientation (e.g., spin down) and ions on all the octahedral sites will have the opposite orientation (e.g., spin up). If the number of spins on the two sites is the same, then the solid will be antiferromagnetic. However, if the **number of spins is unequal** (as in the case of Fe_3O_4, $CoFe_2O_4$, and $NiFe_2O_4$) then the solid will be **ferrimagnetic**. This is illustrated above for Fe_3O_4. The spins on the Fe^{3+} sites cancel, because half of them are up and half are down. However, the four unpaired electrons on the Fe^{2+} ions are all aligned the same way in the crystal, so the compound is ferrimagnetic.

Perovskites are **ternary oxides** of general formula **ABO_3**. More generally, the perovskite formula is ABX_3, where the anion X can be **O, N, or halogen**. The A ions are typically large ions such as Sr^{2+}, Ba^{2+}, Rb^{+}, or a lanthanide 3+ ion, and the B ions are smaller transition metal ions such as Ti^{4+}, Nb^{5+}, Ru^{4+}, etc. The mineral after which the structure is named has the formula $CaTiO_3$.

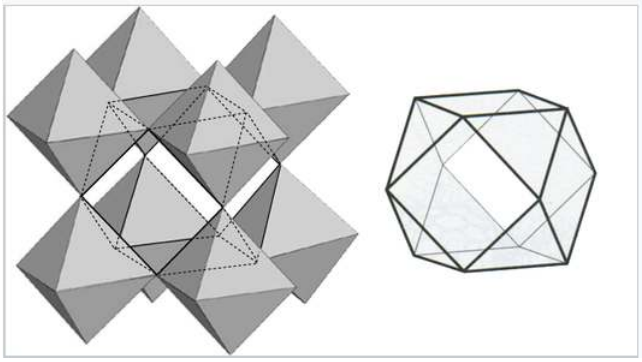
The perovskite structure has simple cubic symmetry, but is related to the fcc lattice in the sense that the A site cations and the three O atoms comprise a fcc lattice. The B-site cations fill 1/4 of the octahedral holes and are surrounded by six oxide anions.



ABX_3 perovskite structure. A, B, and X are white, blue, and red, respectively.

The coordination of the A ions in perovsite and the arrangement of BO_6 octahedra is best understood by looking at the ReO_3 structure, which is the same structure but with the A-site cations removed. In the polyhedral representation of the structure shown at the right, it can be seen that the octahedra share all their vertices but do not share any octahedral edges. This makes the ReO_3 and perovskite structures flexible, like three-dimensional wine racks, in that the octahedra can **rotate and tilt cooperatively**. Eight such

octahedra surround a large **cuboctahedral cavity**, which is the site of the A ions in the perovskite structure. Cations in these sites are coordinated by 12 oxide ions, as expected from the relationship between the perovskite and fcc lattices.



Polyhedral representation of the ReO_3 structure showing the large cuboctahedral cavity that is surrounded by 12 oxygen atoms

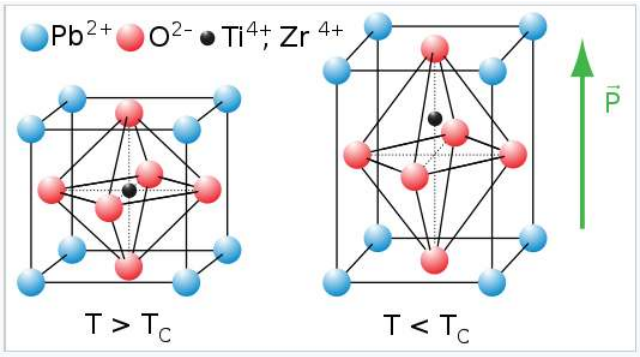
Because the A-site is empty in the ReO_3 structure, compounds with that structure can be reversibly **intercalated** by small ions such as **Li^+ or H^+**, which then occupy sites in the cuboctahedral cavity. For example, smart windows that darken in bright sunlight contain the **electrochromic** material WO_3, which has the ReO_3 structure. In the sunlight, a photovoltaic cell drives the reductive intercalation of WO_3 according to the reaction:

$$x\,H^+ + xe^- + WO_3 \leftrightharpoons H_xWO_3 \tag{8.22.1}$$

WO_3 is a light yellow compound containing d^0 W(VI). In contrast, H_xWO_3, which is mixed-valent W(V)-W(VI) = d^1-d^0, has a deep blue color. Such coloration is typical of mixed-valence transition metal complexes because their d-electrons can be excited to delocalized conduction band levels by red light. Because the electrochemical intercalation-deintercalation process is powered by a solar cell, the tint of the windows can adjust automatically to the level of sunlight.

Ferroelectric perovskites

The flexibility of the network of corner-sharing BO_6 octahedra is also very important in ferroelectric oxides that have the perovskite structure. In some perovsites with small B-site cations, such as Ti^{4+} and Nb^{5+}, the cation is too small to fit symmetrically in the BO_6 octahedron. The octahedron distorts, allowing the cation to move off-center. These distortions can be **tetragonal** (as in the example shown at the right), **rhombohedral**, or **orthorhombic**, depending on whether the cation moves towards a vertex, face, or edge of the BO_6 octahedron. Moving the cation off-center in the octahedron creates an **electric dipole**. In ferroelectrics, these dipoles align in neighboring unit cells through cooperative rotation and tilting of octahedra. The crystal thus acquires a net electrical polarization.



Tetragonal distortion of the perovskite unit cell in the ferroelectric oxide PZT, $PbTi_xZr_{1-x}$

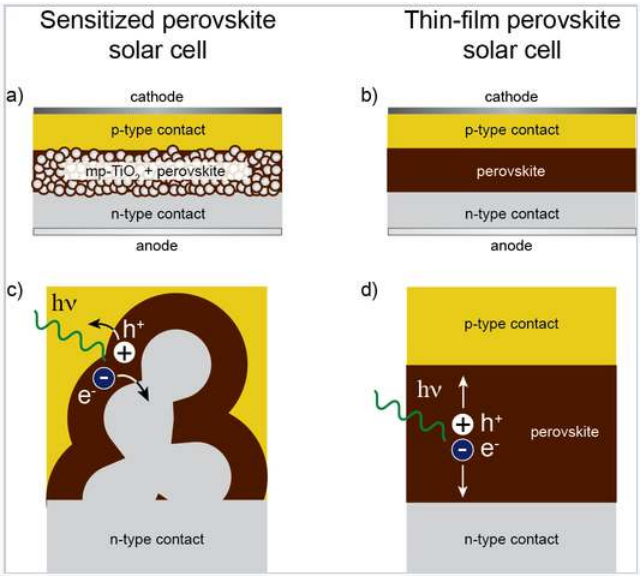
Ferroelectricity behaves analogously to **ferromagnetism**, except that the polarization is electrical rather than magnetic. In both cases, there is a **critical temperature (T_c)** above which the **spontaneous polarization** of the crystal disappears. Below T_c, the

electric polarization of a ferroelectric can be switched with a coercive field, and hysteresis loop of polarization vs. field resembles that of a ferromagnet. Above T_c, the crystal is **paraelectric** and has a high dielectric permittivity.

Ferroelectric and paraelectric oxides (along with piezoelectrics and pyroelectrics) have a wide variety of applications as switches, actuators, transducers, and dielectrics for capacitors. **Ferroelectric capacitors** are important in memory devices (FRAM) and in the tuning circuits of cellular telephones. **Multiferroics**, which are materials that are simultaneously ferroelectric and ferromagnetic, are rare and are being now intensively researched because of their potential applications in electrically adressable magnetic memory.

Halide perovskites (ABX_3, X = Cl, Br, I) can be made by combining salts of monovalent A ions ($A^+ = Cs^+$, NH_4^+, RNH_3^+) and divalent metal salts such as $PbCl_2$ or PbI_2. These compounds have sparked recent interest as light absorbers for **thin film solar cells** that produce electricity from sunlight. Lead and tin halide perovskites can be grown as thin films from solution precursors or by thermal evaporation at relatively low temperatures. In some lead halide perovskites, the mobility of electrons and holes is very high, comparable to that of more expensive III-V semiconductors such as GaAs, which must be grown as very pure single crystals at high temperatures for use in solar cells. Because of their high carrier mobility, some lead halide perovskites are also electroluminescent and are of interest as inexpensive materials for light-emitting diodes (LEDs).

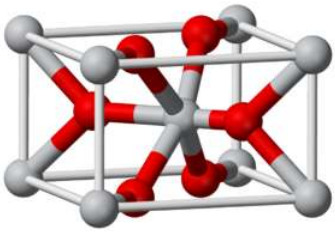
Tin and lead halide perovskites were first studied in the 1990s as materials for thin film electronics,[4] and more recently as light absorbers in dye-sensitized solar cells. Soon after the results on dye-sensitized perovskite cells were reported, it was discovered that halide perovskites could also be used in thin film solid state solar cells. The structures of these solar cells are shown schematically at the right. The highest reported solar power conversion efficiencies of perovskite solar cells have jumped from 3.8% in 2009 [5] to 10.2% in 2012[6] and a certified 20.1% in 2014.[7]. The highest performing cells to date contain divalent lead in the perovskite B cation site and a mixture of methylammonium and formamidinium ions in the perovskite A cation site.



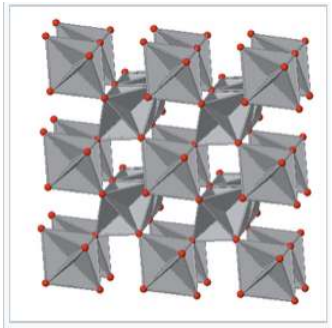
a) Solar cell architecture in which a lead halide perovskite absorber coats a layer of nanocrystalline anatase TiO_2. b) Thin-film solar cell, with a layer of lead halide perovskite sandwiched between two selective contacts. c) Charge generation and extraction in the sensitized architecture and d) in the thin-film architecture.

Despite their very impressive efficiency, perovskite solar cells are stable for relatively short periods of time and are sensitive to air and moisture. Current research is focused on understanding the degradation mechanisms of these solar cells and improving their stability under operating conditions.

The **rutile structure** is an important MX_2 (X = O, F) structure. It is a 6:3 structure, in which the cations are octahedrally coordinated by anions, and as such is intermediate in polarity between the CaF_2 (8:4) and SiO_2 (4:2) structures. The mineral rutile is one of the polymorphs of TiO_2, the others (anatase and brookite) also being 6:3 structures.



The rutile structure can be described as a distorted version of the NiAs structure with half the cations removed. Recall that compounds with the NiAs structure were typically metallic because the metal ions are eclipsed along the stacking axis and thus are in relatively close contact. In rutile, the MO_6 **octahedra share edges** along the tetragonal c-axis, and so some rutile oxides, such as **NbO_2, RuO_2 and IrO_2,** are also **metallic** because of **d-orbital overlap** along that axis. These compounds are important as electrolyzer catalysts and catalyst supports because they combine high catalytic activity with good electronic conductivity.



View down the tetragonal c-axis of the rutile lattice, showing edge-sharing MO_6 octahedra.

Rutile TiO_2, because of its high refractive index, is the base pigment for white paint. It is a wide bandgap semiconductor that has also been extensively researched as an electrode for water splitting solar cells and as a photocatalyst (primarily as the anatase polymorph) for degradation of pollutants in air and water. Self-cleaning glass exploits the photocatalytic properties of a thin film of TiO_2 to remove oily substances from the glass surface and improve the wetting properties of the glass.

8.22: Spinel, Perovskite, and Rutile Structures is shared under a CC BY-NC-SA 4.0 license and was authored, remixed, and/or curated by LibreTexts.

- **8.7: Spinel, Perovskite, and Rutile Structures** by Chemistry 310 is licensed CC BY-SA 4.0. Original source: https://en.wikibooks.org/wiki/Introduction_to_Inorganic_Chemistry.

8.23: Kapustinskii Equation

From the discussion above, it is clear that the lattice energy, E_L, of an ionic crystal can be calculated with reasonable accuracy if the structure is known. But how can we calculate E_L for a new or hypothetical compound of unknown structure? Recall that the reduced Madelung constant is about the same for different crystal structures. Russian chemist A. F. Kapustinskii recognized this fact and devised a formula that allows one to calculate E_L for any compound if we know the univalent radii of the constituent ions. [5]

The Madelung constant, A, is proportional to the number of ions (n) in formula unit, so dividing by the n gives similar values as shown in the table below:

A/n ~ invariant

Structure	A/n
NaCl	0.874
CsCl	0.882
Rutile	0.803
Fluorite	0.800

Kapustinskii noticed that the difference in ionic radii between M^+ and M^{2+} (the monovalent vs. divalent radius) largely compensates for the differences in A/n between monovalent (NaCl, CsCl) and divalent (rutile, CaF_2) structures. He thus arrived at a lattice energy formula using an average Madelung constant, corrected to monovalent radii. In the **Kapustinskii formula**, the lattice energy (kJ/mol) is given by:

$$E_L = \frac{1213.8 z_+ z_- n}{r_+ + r_-}\left(1 - \frac{0.345}{r_+ + r_-}\right) \tag{8.23.1}$$

Here the sum of the monovalent radii is used in place of r_o, the bond distance in the Born-Mayer equation. The beauty of this formula is that it requires no knowledge of the structure of the compound. Therefore it can be used, in combination with Born-Haber cycles, to predict the stability of unknown compounds. As we show below, this is a broadly useful tool in guiding syntheses and predicting the reactivity of inorganic solids.

8.23: Kapustinskii Equation is shared under a CC BY-NC-SA 4.0 license and was authored, remixed, and/or curated by LibreTexts.

- **9.5: Kapustinskii Equation** by Chemistry 310 is licensed CC BY-SA 4.0. Original source: https://en.wikibooks.org/wiki/Introduction_to_Inorganic_Chemistry.

8.24: New Page

8.24: New Page is shared under a CC BY-NC-SA 4.0 license and was authored, remixed, and/or curated by LibreTexts.

CHAPTER OVERVIEW

9: Bioinorganic Chemistry

9.1: Biological Significance of Iron, Zinc, Copper, Molybdenum, Cobalt, Chromium, Vanadium, and Nickel
9.2: Introduction to Amino Acids and Proteins
9.3: Overview of Hemoglobin and Myoglobin
9.3.1: Myoglobin, Hemoglobin, and their Ligands
9.3.2: Oxygen Transport by the Proteins Myoglobin and Hemoglobin
9.4: Ferrodoxins, Hydrogenases, and Nitrogenases - Metal-Sulfide Proteins
9.4.1: Iron-sulfur Proteins and Models
9.4.2: Iron-sulfur Proteins and Models (Part 2)
9.4.3: Iron-sulfur Proteins and Models (Part 3)
9.4.4: Iron-sulfur Proteins and Models (Part 4)
9.5: The Reaction Pathways of Zinc Enzymes and Related Biological Catalysts
9.5.1: About Carbonic Anhydrase
9.5.2: Catalytic Mechanism
9.5.3: Metal Substitution
9.6: Metals in Medicine
9.6.1: Metal Deficiency and Disease
9.6.2: Toxic Effects of Metals
9.6.3: Aspects of Platinum Binding to DNA
9.6.4: Survey of Metals Used for Diagnosis and Chemotherapy
9.6.5: Platinum Anticancer Drugs- A Case Study
9.6.6: Mapping the Major Adducts of cis- and trans-DDP on DNA; Sequence Specificity
9.6.7: Structure of Platinum-DNA Complexes
9.6.8: Site-specifically Platinated DNA \(\;^{154}\)
9.6.9: Bioinorganic Chemistry of Platinum Anticancer Drugs- How Might They Work?
9.6.10: Bioinorganic Chemistry of Platinum Anticancer Drugs; How Might They Work? (Part 2)
9.6.11: Design of New Inorganic Anticancer Drugs
9.7: Electron Transfer

7.5: The Reaction Pathways of Zinc Enzymes and Related Biological Catalysts

7.6: Metals in Medicine

9: Bioinorganic Chemistry is shared under a CC BY-NC-SA 4.0 license and was authored, remixed, and/or curated by LibreTexts.

9.1: Biological Significance of Iron, Zinc, Copper, Molybdenum, Cobalt, Chromium, Vanadium, and Nickel

The transition metals are among the least abundant metal ions in sea water from which contemporary organisms are thought to have evolved (Table 1.1).[1-5] For many of the metals, the concentration in human blood plasma greatly exceeds that in sea water. Such data indicate the importance of mechanisms for accumulation, storage, and transport of transition metals and zinc in living organisms.

Table 1.1: Concentrations of transition metals and zinc in sea water and human plasma.a*Data from References 1 - 5 and 12

Element	Sea Water (M) x 10^8	Human Plasma (M) x 10^8
Fe	0.005 - 2	2230
Zn	8.0	1720
Cu	1.0	1650
Mo	10.0	1000
Co	0.7	0.0025
Cr	0.4	5.5
V	4.0	17.7
Mn	0.7	10.9
Ni	0.5	4.4

The metals are generally found either bound directly to proteins, found in cofactors, or part of clusters that are in turn bound by a protein. The ligands usually contain O, N, S, or C donor atoms. Proteins with transition metals are most commonly associated with the catalysis involving the intramolecular or intermolecular rearrangement of electrons. Although the redox properties of the metals are important in many of the reactions, in others the metal appears to contribute to the structure of the active state, e.g., zinc in the Cu-Zn dismutases and some of the iron in the photosynthetic reaction center. Sometimes equivalent reactions are catalyzed by proteins with different metal centers; the metal binding sites and proteins have evolved separately for each type of metal center.

Iron is the most common transition metal in biology.[6,7] Its use has created a dependence that has survived the appearance of dioxygen in the atmosphere ca. 2.5 billion years ago, and the concomitant conversion of ferrous ion to ferric ion and insoluble rust. All plants, animals, and bacteria use iron, except for a lactobacillus that appears to maintain high concentrations of manganese instead of iron. The processes and reactions in which iron participates are crucial to the survival of terrestrial organisms, and include ribonucleotide reduction (DNA synthesis), energy production (respiration), energy conversion (photosynthesis), nitrogen reduction, oxygen transport (respiration, muscle contraction), and oxygenation (e.g., steroid synthesis, solubilization and detoxification of aromatic compounds). Among the transition metals used in living organisms, iron is the most abundant in the environment. Whether this fact alone explains the biological predominance of iron or whether specific features of iron chemistry contribute is not clear.

Many of the other transition metals participate in reactions equivalent to those involving iron, and can sometimes substitute for iron, albeit less effectively, in natural Fe-proteins. Additional biological reactions are unique to nonferrous transition metals.

Zinc is relatively abundant in biological materials.[8,9] The major location of zinc in the body is metallothionein, which also binds copper, chromium, mercury, and other metals. Among the other well-characterized zinc proteins are the Cu-Zn superoxide dismutases (other forms have Fe or Mn), carbonic anhydrase (an abundant protein in red blood cells responsible for maintaining the pH of the blood), alcohol dehydrogenase, and a variety of hydrolases involved in the metabolism of sugars, proteins, and nucleic acids. Zinc is a common element in nucleic-acid polymerases and transcription factors, where its role is considered to be structural rather than catalytic. Interestingly, zinc enhances the stereoselectivity of the polymerization of nucleotides under reaction conditions designed to simulate the environment for prebiotic reactions. Recently a group of nucleic-acid binding proteins, with a

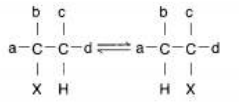
repeated sequence containing the amino acids cysteine and histidine, were shown to bind as many as eleven zinc atoms necessary for protein function (transcribing DNA to RNA).[10] Zinc plays a structural role, forming the peptide into multiple domains or "zinc fingers" by means of coordination to cysteine and histidine. A survey of the sequences of many nucleic-acid binding proteins shows that many of them have the common motif required to form zinc fingers. Other zinc-finger proteins called steroid receptors bind both steroids such as progesterone and the progesterone gene DNA . Much of the zinc in animals and plants has no known function, but it may be maintaining the structures of proteins that activate and deactivate genes.[11]

Copper and iron proteins participate in many of the same biological reactions:

1. reversible binding of dioxygen, e.g., hemocyanin (Cu), hemerythrin (Fe), and hemoglobin (Fe);
2. activation of dioxygen, e.g., dopamine hydroxylase (Cu) (important in the synthesis of the hormone epinephrine), tyrosinases (Cu), and catechol dioxygenases (Fe);
3. electron transfer, e.g., plastocyanins (Cu), ferredoxins, and c-type cytochromes (Fe);
4. dismutation of superoxide by Cu or Fe as the redox-active metal (superoxide dismutases).

The two metal ions also function in concert in proteins such as cytochrome oxidase, which catalyzes the transfer of four electrons to dioxygen to form water during respiration. Whether any types of biological reactions are unique to copper proteins is not clear. However, use of stored iron is reduced by copper deficiency, which suggests that iron metabolism may depend on copper proteins, such as the serum protein ceruloplasmin, which can function as a ferroxidase, and the cellular protein ascorbic acid oxidase, which also is a ferrireductase.

Cobalt is found in vitamin B_{12} , its only apparent biological site.[12] The vitamin is a cyano complex, but a methyl or methylene group replaces CN in native enzymes. Vitamin-B_{12} deficiency causes the severe disease of pernicious anemia in humans, which indicates the critical role of cobalt. The most common type of reaction in which cobalamin enzymes participate results in the reciprocal exchange of hydrogen atoms if they are on adjacent carbon atoms, yet not with hydrogen in solvent water:



(An important exception is the ribonucleotide reductase from some bacteria and lower plants, which converts ribonucleotides to the DNA precursors, deoxyribonucleotides, a reaction in which a sugar -OH is replaced by -H. Note that ribonucleotide reductases catalyzing the same reaction in higher organisms and viruses are proteins with an oxo-bridged dimeric iron center.) The cobalt in vitamin B_{12} is coordinated to five N atoms, four contributed by a tetrapyrrole (corrin); the sixth ligand is C, provided either by C5 of deoxyadenosine in enzymes such as methylmalonyl-CoA mutase (fatty acid metabolism) or by a methyl group in the enzyme that synthesizes the amino acid methionine in bacteria.

Nickel is a component of a hydrolase (urease), of hydrogenase, of CO dehydrogenase, and of S-methyl CoM reductase, which catalyzes the terminal step in methane production by methanogenic bacteria. All the Ni-proteins known to date are from plants or bacteria.[13,14] However, about 50 years elapsed between the crystallization of jack-bean urease in 1925 and the identification of the nickel component in the plant protein. Thus it is premature to exclude the possibility of Ni-proteins in animals. Despite the small number of characterized Ni-proteins, it is clear that many different environments exist, from apparently direct coordination to protein ligands (urease) to the tetrapyrrole F430 in methylreductase and the multiple metal sites of Ni and Fe-S in a hydrogenase from the bacterium *Desulfovibrio gigas*. Specific environments for nickel are also indicated for nucleic acids (or nucleic acid-binding proteins), since nickel activates the gene for hydrogenase.[15]

Manganese plays a critical role in oxygen evolution catalyzed by the proteins of the photosynthetic reaction center. The superoxide dismutase of bacteria and mitochondria, as well as pyruvate carboxylase in mammals, are also manganese proteins.[16,17] How the multiple manganese atoms of the photosynthetic reaction center participate in the removal of four electrons and protons from water is the subject of intense investigation by spectroscopists, synthetic inorganic chemists, and molecular biologists.[17]

Vanadium and chromium have several features in common, from a bioinorganic viewpoint.[18a] First, both metals are present in only small amounts in most organisms. Second, the biological roles of each remain largely unknown.[18] Finally, each has served as a probe to characterize the sites of other metals, such as iron and zinc. Vanadium is required for normal health, and could act *in vivo* either as a metal cation or as a phosphate analogue, depending on the oxidation state, V(lV) or V(V), respectively. Vanadium in a

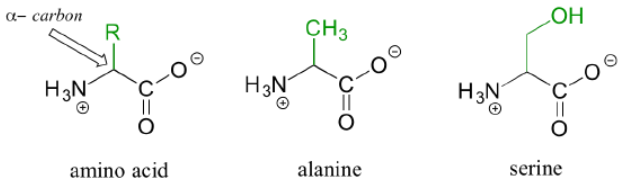
sea squirt (tunicate), a primitive vertebrate, is concentrated in blood cells, apparently as the major cellular transition metal, but whether it participates in the transport of dioxygen (as iron and copper do) is not known. In proteins, vanadium is a cofactor in an algal bromoperoxidase and in certain prokaryotic nitrogenases. Chromium imbalance affects sugar metabolism and has been associated with the glucose tolerance factor in animals. But little is known about the structure of the factor or of any other specific chromium complexes from plants, animals, or bacteria.

Molybdenum proteins catalyze the reduction of nitrogen and nitrate, as well as the oxidation of aldehydes, purines, and sulfite.[19] Few Mo-proteins are known compared to those involving other transition metals. Nitrogenases, which also contain iron, have been the focus of intense investigations by bioinorganic chemists and biologists; the iron is found in a cluster with molybdenum (the iron-molybdenum cofactor, or FeMoCo) and in an iron-sulfur center (Chapter 7). Interestingly, certain bacteria (*Azotobacter*) have alternative nitrogenases, which are produced when molybdenum is deficient and which contain vanadium and iron or only iron. All other known Mo-proteins are also Fe-proteins with iron centers, such as tetrapyrroles (heme and chlorins), Fe-sulfur clusters, and, apparently, non-heme/non-sulfur iron. Some Mo-proteins contain additional cofactors such as the Havins, e.g., in xanthine oxidase and aldehyde oxidase. The number of redox centers in some Mo-proteins exceeds the number of electrons transferred; reasons for this are unknown currently.

9.1: Biological Significance of Iron, Zinc, Copper, Molybdenum, Cobalt, Chromium, Vanadium, and Nickel is shared under a CC BY-NC-SA 4.0 license and was authored, remixed, and/or curated by LibreTexts.

9.2: Introduction to Amino Acids and Proteins

Proteins are polymers of **amino acids**, linked by amide groups known as **peptide bond**s. An amino acid can be thought of as having two components: a 'backbone', or 'main chain', composed of an ammonium group (H_3N^+-C), an 'alpha-carbon' bonded to the nitrogen atom, a carboxylate (COO^-), and a variable 'side chain' (in green below) bonded to the alpha-carbon (Figure **9.2.1**).



(Figure 9.2.1). Structures of amino acids.

There are twenty different side chains in naturally occurring amino acids, and it is the identity of the side chain that determines the identity of the amino acid: for example, if the side chain is a $-CH_3$ group, the amino acid is alanine, and if the side chain is a $-CH_2OH$ group, the amino acid is serine. Many amino acid side chains contain a functional group (the side chain of serine, for example, contains a primary alcohol), while others, like alanine, lack a functional group, and contain only a simple hydrocarbon group.

The two 'hooks' on an amino acid monomer are the ammonium and carboxylate groups. Proteins (polymers of ~50 amino acids or more) and peptides (shorter polymers) are formed when the amino group of one amino acid monomer reacts with the carboxylate carbon of another amino acid to form an amide linkage, which in protein terminology is a **peptide bond**. Which amino acids are linked, and in what order - the protein **sequence** - is what distinguishes one protein from another. This sequence is coded for by an organism's DNA. Protein sequences are written in the ammonium terminal (N-terminal) to carboxylate terminal (C-terminal) direction, with either three-letter or single-letter abbreviations for the amino acids. Below is a four amino acid peptide with the sequence "cysteine - histidine - glutamate - methionine". Using the single-letter code, the sequence is abbreviated CHEM (Figure **9.2.2**).

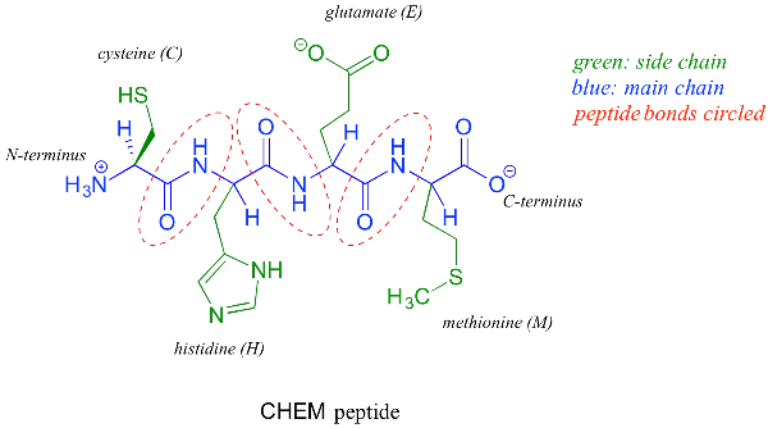


Figure 9.2.2. The CHEM peptide.

When an amino acid is incorporated into a protein it loses a molecule of water and what remains is called a **residue** of the original amino acid. Thus we might refer to the 'glutamate residue' at position 3 of the CHEM peptide above.

Once a protein polymer is constructed, it in many cases folds up very specifically into a three-dimensional structure, which often includes one or more 'binding pockets' in which other molecules can be bound. It is this shape of this folded structure, and the precise arrangement of the functional groups within the structure (especially in the area of the binding pocket) that determines the function of the protein.

Enzymes are proteins which catalyze biochemical reactions. One or more reacting molecules - often called **substrates** - become bound in the **active site** pocket of an enzyme, where the actual reaction takes place. **Receptors** are proteins that bind specifically to

one or more molecules - referred to as **ligands** - to initiate a biochemical process. For example, we saw in the introduction to this chapter that the TrpVI receptor in mammalian tissues binds capsaicin (from hot chili peppers) in its binding pocket and initiates a heat/pain signal which is sent to the brain.

Contributors and Attributions

- Organic Chemistry With a Biological Emphasis by Tim Soderberg (University of Minnesota, Morris)

This page titled 9.2: Introduction to Amino Acids and Proteins is shared under a CC BY-NC-SA 4.0 license and was authored, remixed, and/or curated by Tim Soderberg.

SECTION OVERVIEW

9.3: Overview of Hemoglobin and Myoglobin

9.3.1: Myoglobin, Hemoglobin, and their Ligands

9.3.2: Oxygen Transport by the Proteins Myoglobin and Hemoglobin

---

9.3: Overview of Hemoglobin and Myoglobin is shared under a CC BY-NC-SA 4.0 license and was authored, remixed, and/or curated by LibreTexts.

9.3.1: Myoglobin, Hemoglobin, and their Ligands

Hemoglobin:

- 1st. protein whose molecular weight was determined
- 1st protein to be assigned a specific function - dioxygen transport
- has a prosthetic group (non-amino acid) heme group (protoporphyrin IX with a ferrous ion) covalently attached to the protein. The heme group binds dioxygen.
- 1st protein in which a point mutation (single base pair charge) causes a single amino acid change in the protein, marking the start of molecular medicine
- 1st protein with high resolution x-ray structure
- theory for dioxygen binding explain control of enzyme activity
- the binding of dioxygen is regulated by binding of H^+, CO_2, and bisphosphoglcyerate which bind to sites (allosteric) distant from oxygen binding site.
- crystals of deoxy-Hb shatter on binding dioxygen, indicating significant conformational changes on binding.

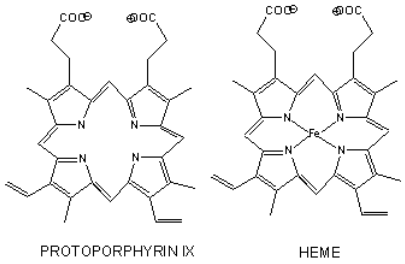


Figure 9.3.1.1. The heme group contains protoporphyrin IX, with four tetrapyrrole rings linked by methene bridges. Attached to the tetrapyrrole structure are four methyl, two vinyl, and two proprionate groups. These can be arranged in 15 ways, only one (IX) occurs in biological systems.

The heme fits into a hydrophobic crevice in the proteins with the proprionate groups exposed to solvent. The Fe^{2+} ion is coordinated to 4 N's on the 4 pyrrole rings, The 5th ligand is a supplied by proximal His (the 8th amino acid on helix F) of the protein. In the absence of dioxygen, the 6 ligand is missing. and the geometry of the complex is square pyramidal with the Fe above the plane of the heme ring. A distal His (E7) is on the opposite side of the heme ring, but too far to coordinate with the Fe. When dioxgen binds, it occupies the 6th coordination site and pulls the Fe into the plane of the ring, leading to octahedral geometry. CO, NO, and H_2S also bind to the 6th site, but with higher affinity than dioxygen, which can lead to CO poisoning. The distal His keeps these ligands (including dioxygen) bound in a bent, non-optimal geometry. This minimizes the chances of CO poisoning.

Myoglobin

- Myoglobin is a relatively small protein that contains 150 amino acids.
- Mb is extremely compact, and consists of 75% alpha helical structure.
- The interior amino acids are almost entirely nonpolar. The only polar amino acids found completely buried are the two His (proximal and distal) found at the active site of dioxygen binding.

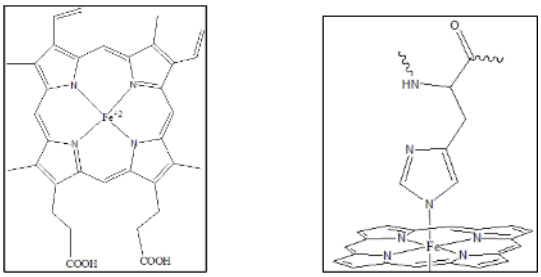


Figure 9.3.1.2. The skeletal structure of the heme prosthetic group found within the structure of myoglobin. The porphyrin ring contains four pyrrole nitrogens bound to a ferrous (Fe(II)) ion center. There are six coordination sites in the Fe(II) ion; four are occupied by the pyrrole nitrogens, one is occupied by a proximal histidine, one site can be occupied by a dioxygen molecule (not shown).

Difference between Hb and Mb

Hb is a tetramer of two α and two β subunits held together by IMF's (an example of quarternary protein structure), and 4 bound hemes, each of which can bind a dioxygen. In a fetus, two other subunits make up Hb (two zeta - ζand two epsilion - ε subunits - analogous to the two αand two β subunits, respectively). This changes in fetuses to two α and two γ subunits. Fetal Hb has higher affinity for dioxygen than adult Hb. Mb is a single polypeptide chains which has higher affinity for dioxygen than Hb.

The α and β chains are similar to Mb, which is unexpected since only 24 of 141 residues in the α and β chains of Hb are identical to amino acids in Mb. This suggests that different sequences can fold to similar structures. The globin fold of Mb and each chain of Hb is common to vertebrates and must be nature's design for dioxygen carriers. A comparison of the sequence of Hb from 60 species show much variability of amino acids, with only 9 identical amino founds. These must be important for structure/function. All internal changes are conservative (e.g. changing a nonpolar for a nonpolar amino acid). Not even Pro's are conserved, suggesting there are different ways to break helices. The two active site His are conserved, as is Gly B6 (required for a reverse turn).

This page titled 9.3.1: Myoglobin, Hemoglobin, and their Ligands is shared under a CC BY-NC-SA 4.0 license and was authored, remixed, and/or curated by Henry Jakubowski.

9.3.2: Oxygen Transport by the Proteins Myoglobin and Hemoglobin

Oxygen Transport

Many microorganisms and most animals obtain energy by respiration, the oxidation of organic or inorganic molecules by O_2. At 25°C, however, the concentration of dissolved oxygen in water in contact with air is only about 0.25 mM. Because of their high surface area-to-volume ratio, aerobic microorganisms can obtain enough oxygen for respiration by passive diffusion of O_2 through the cell membrane. As the size of an organism increases, however, its volume increases much more rapidly than its surface area, and the need for oxygen depends on its volume. Consequently, as a multicellular organism grows larger, its need for O_2 rapidly outstrips the supply available through diffusion. Unless a transport system is available to provide an adequate supply of oxygen for the interior cells, organisms that contain more than a few cells cannot exist. In addition, O_2 is such a powerful oxidant that the oxidation reactions used to obtain metabolic energy must be carefully controlled to avoid releasing so much heat that the water in the cell boils. Consequently, in higher-level organisms, the respiratory apparatus is located in internal compartments called mitochondria, which are the power plants of a cell. Oxygen must therefore be transported not only to a cell but also to the proper compartment within a cell.

Myoglobin and Hemoglobin

Myoglobin is a relatively small protein that contains 150 amino acids. The functional unit of myoglobin is an **iron–porphyrin complex** that is embedded in the protein (Figure 4.2.1). In myoglobin, the heme iron is five-coordinate, with only a single histidine imidazole ligand from the protein (called the proximal histidine because it is near the iron) in addition to the four nitrogen atoms of the porphyrin. A second histidine imidazole (the distal histidine because it is more distant from the iron) is located on the other side of the heme group, too far from the iron to be bonded to it. Consequently, the iron atom has a vacant coordination site, which is where O_2 binds.

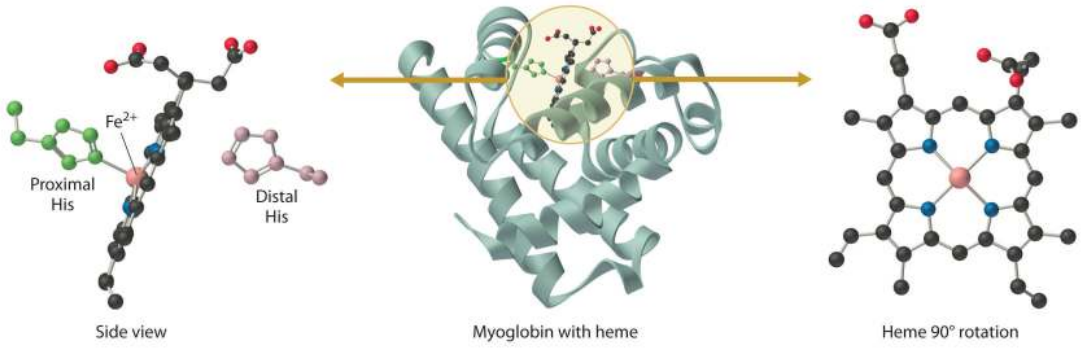


Figure 9.3.2.1. The Structure of Deoxymyoglobin, Showing the Heme Group. The iron in deoxymyoglobin is five-coordinate, with one histidine imidazole ligand from the protein. Oxygen binds at the vacant site on iron.

In the ferrous form (deoxymyoglobin), the iron is five-coordinate and high spin. Because high-spin Fe^{2+} is too large to fit into the "hole" in the center of the porphyrin, it is about 60 pm above the plane of the porphyrin. When O_2 binds to deoxymyoglobin to form oxymyoglobin, the iron is converted from five-coordinate (high spin) to six-coordinate (low spin; Figure 4.2.2). Because low-spin Fe^{2+} and Fe^{3+} are smaller than high-spin Fe^{2+}, the iron atom moves into the plane of the porphyrin ring to form an octahedral complex. The O_2 pressure at which half of the molecules in a solution of myoglobin are bound to O_2 ($P_{1/2}$) is about 1 mm Hg (1.3×10^{-3} atm).

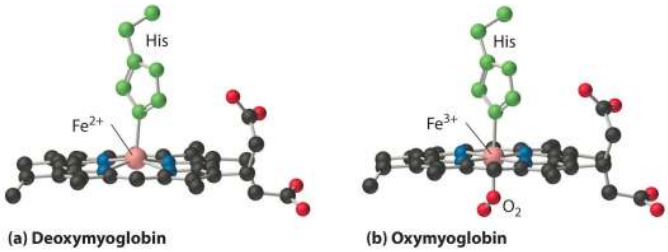


Figure 9.3.2.2. Oxygen Binding to Myoglobin and Hemoglobin. (a) The Fe^{2+} ion in deoxymyoglobin is high spin, which makes it too large to fit into the "hole" in the center of the porphyrin. (b) When O_2 binds to deoxymyoglobin, the iron is converted to low-spin Fe^{3+}, which is smaller, allowing the iron to move into the plane of the four nitrogen atoms of the porphyrin to form an octahedral complex.

Hemoglobin consists of two subunits of 141 amino acids and two subunits of 146 amino acids, both similar to myoglobin; it is called a tetramer because of its four subunits. Because hemoglobin has very different O_2-binding properties, however, it is not simply a "super myoglobin" that can carry four O_2 molecules simultaneously (one per heme group). The shape of the O_2-binding curve of myoglobin can be described mathematically by the following equilibrium:

$$MbO_2 \rightleftharpoons Mb + O_2 \tag{9.3.2.1}$$

$$K_{diss} = \frac{[Mb]\,[O_2]}{[MbO_2]} \tag{9.3.2.2}$$

The O_2-binding curve of hemoglobin is S shaped (Figure 4.2.3). As shown in the curves, at low oxygen pressures, the affinity of deoxyhemoglobin for O_2 is substantially lower than that of myoglobin, whereas at high O_2 pressures the two proteins have comparable O_2 affinities. The physiological consequences of unusual S-shaped O_2-binding curve of hemoglobin are enormous. In the lungs, where O_2 pressure is highest, the high oxygen affinity of deoxyhemoglobin allows it to be completely loaded with O_2, giving four O_2 molecules per hemoglobin. In the tissues, however, where the oxygen pressure is much lower, the decreased oxygen affinity of hemoglobin allows it to release O_2, resulting in a net transfer of oxygen to myoglobin.

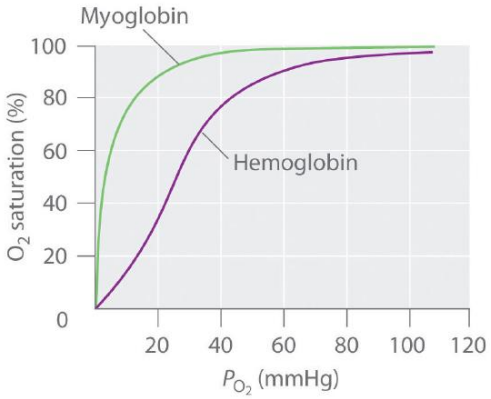


Figure 4.2.3: The O_2-Binding Curves of Myoglobin and Hemoglobin. Plots of Y (fractional saturation) vs L (pO2) are hyperbolic for Mb, but sigmoidal for Hb, suggesting cooperative binding of oxygen to Hb (binding of the first oxygen facilitates binding of second, etc).

The S-shaped O_2-binding curve of hemoglobin is due to a phenomenon called **cooperativity**, in which the affinity of one heme for O_2 depends on whether the other hemes are already bound to O_2. Cooperativity in hemoglobin requires an interaction between the four heme groups in the hemoglobin tetramer, even though they are more than 3000 pm apart, and depends on the change in structure of the heme group that occurs with oxygen binding. The structures of deoxyhemoglobin and oxyhemoglobin are slightly different, and as a result, deoxyhemoglobin has a much lower O_2 affinity than myoglobin, whereas the O_2 affinity of oxyhemoglobin is essentially identical to that of oxymyoglobin. Binding of the first two O_2 molecules to deoxyhemoglobin causes the overall structure of the protein to change to that of oxyhemoglobin; consequently, the last two heme groups have a much higher affinity for O_2 than the first two.

The affinity of Hb, but not of Mb, for dioxygen depends on pH. This is called the **Bohr effect**, after the father of Neils Bohr, who discovered it.

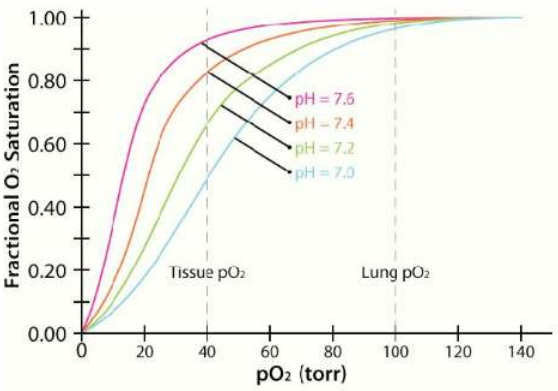


Figure 4.2.4: The Bohr Effect

Decreasing pH shifts the oxygen binding curves to the right (to decreased oxygen affinity). Increased [H^+] will cause protonation of basic side chains. In the pH range for the Bohr effect, the mostly likely side chain to get protonated is His (pKa around 6), which then becomes charged. The mostly likely candidate for protonation is His 146 (on the β chain - CH_3) which can then form a salt bridge with Asp 94 of the β(FG1) chain. This salt bridge stabilizes the positive charge on the His and raises its pKa compared to the oxyHb state. Carbon dioxide binds covalently to the N-terminus to form a negatively charge carbamate which forms a salt bridge with Arg 141 on the alpha chain. BPG, a strongly negatively charged ligand, binds in a pocket lined with Lys 82, His 2, and His 143 (all on the beta chain). It fits into a cavity present between the β subunits of the Hb tetramer in the T state. Notice all these allosteric effectors lead to the formation of more salt bridges which stabilize the T or deoxy state. The central cavity where BPG binds between the β subunits become much smaller on oxygen binding and the shift to the oxy or R state. Hence BPG is extruded from the cavity.

The binding of H^+ and CO_2 helps shift the equilibrium to deoxyHb which faciliates dumping of oxygen to the tissue. It is in respiring tissues that CO_2 and H^+ levels are high. CO_2 is produced from the oxidation of glucose through glycolysis and the Krebs cycle. In addition, high levels of CO_2 increase H^+ levels through the following equilibrium:

$$\mathbf{H_2O + CO_2 \rightleftharpoons H_2CO_3 \rightleftharpoons H^+ + HCO_3^-} \tag{9.3.2.3}$$

In addition, H^+ increases due to production of weak acids such as pyruvic acid in glycolysis .

Hb, by binding CO_2 and H^+, in addition to O_2, serves an additional function: it removes excess CO_2 and H^+ from the tissues where they build up. When deoxyHb with bound H^+ and CO_2 reaches the lungs, they leave as O_2 builds and deoxyHb is converted to oxyHb.

Contributors

Prof. Henry Jakubowski (College of St. Benedict/St. John's University)

Contributed by OpenStax, General Biology at OpenStax CNX

Dr. Kevin Ahern and Dr. Indira Rajagopal (Oregon State University)

9.3.2: Oxygen Transport by the Proteins Myoglobin and Hemoglobin is shared under a CC BY-NC-SA 4.0 license and was authored, remixed, and/or curated by LibreTexts.

SECTION OVERVIEW

9.4: Ferrodoxins, Hydrogenases, and Nitrogenases - Metal-Sulfide Proteins

Transition-metal/sulfide sites, especially those containing iron, are present in all forms of life and are found at the active centers of a wide variety of redox and catalytic proteins. These proteins include simple soluble electron-transfer agents (the ferredoxins), membrane-bound components of electron-transfer chains, and some of the most complex metalloenzymes, such as nitrogenase, hydrogenase, and xanthine oxidase. In this chapter we first review the chemistry of the Fe-S sites that occur in relatively simple rubredoxins and ferredoxins, and make note of the ubiquity of these sites in other metalloenzymes. We use these relatively simple systems to show the usefulness of spectroscopy and model-system studies for deducing bioinorganic structure and reactivity. We then direct our attention to the hydrogenase and nitrogenase enzyme systems, both of which use transition-metalsulfur clusters to activate and evolve molecular hydrogen.

9.4.1: Iron-sulfur Proteins and Models

9.4.2: Iron-sulfur Proteins and Models (Part 2)

9.4.3: Iron-sulfur Proteins and Models (Part 3)

9.4.4: Iron-sulfur Proteins and Models (Part 4)

References

1. F. Armstrong, in A. G. Sykes, ed., *Advances in Inorganic and Bioinorganic Mechanisms*, Vol. **I**, Academic Press, 1982.
2. H. Beinert and S. P. J. Albracht, *Biochim. Biophys. Acta* **683** (1982), 245.
3. A. V. Xavier, J. J. G. Moura, and I. Moura, in J. B. Goodenough *et al.*, eds., *Structure and Bonding*, Springer-Verlag, **43** (1981), 187-213.
4. D. C. Yoch and R. P. Carithers, *Microbiol. Rev*. **43** (1979), 384.
5. H. B. Dunford *et aI.*, eds., *The Biological Chemistry of Iron: A Look at the Metabolism of Iron and Its Subsequent Uses in Living Organisms*, Reidel, 1981.
6. R. K. Thauer and P. Schönheit, in Reference 8, p. 329.
7. A. Bezkorovainy, *Biochemistry of Nonheme Iron*, Plenum, 1980, pp. 343-393.
8. T. G. Spiro, ed., *Iron-Sulfur Proteins*, Wiley-Interscience, 1985.
9. W. Lovenberg, ed., *Iron-Sulfur Proteins*, Vol. I, Academic Press, 1973.
10. Reference 9, Vol. II, Academic Press, 1973.
11. Reference 10, Vol. III, Academic Press, 1977.
12. Nomenclature, *Eur. J. Biochem.* **93** (1979), 427.
13. Nomenclature, *Biochim. Biophys. Acta* 549 (1979), 101.
14. C. F. Yocum, J. N. Sadow, and A. San Pietro, in Reference 9, p. 112.
15. B. B. Buchanan, in Reference 9, p. 129.
16. T. P. Singer and R. R. Ramsay, in A. N. Martonosi, ed., *The Enzymes of Biological Membranes*, Plenum, 1985, pp. 301-332.
17. T. Yagi, H. Inokuchi, and K. Kimura, *Acc. Chem. Res.* **16** (1983), 2; Y. Higuchi *et al.*, *J. Mol. Biol.* **172** (1984), 109.
18. R. Lemberg and J. Barrett, *Cytochromes*, Academic Press, 1973.
19. H. Beinert, in Reference 9, p. 1.
20. K. K. Rao and D. O. Hall, in G. V. Leigh, ed., *Evolution of Metalloenzymes, Metalloproteins, and Related Materials*, 1977, p. 39.
21. D. O. Hall, R. Cammack, and K. K. Rao, *Nature* **233** (1977), 136.
22. T. Ohnishi and J. C. Salerno, in Reference 8, p. 285.
23. F. A. Cotton and G. Wilkinson, *Advanced Inorganic Chemistry*, Wiley, 1980.
24. D. E. McRee *et al.*, *J. Biol. Chem.* **261** (1986), 10277.

25. S. J. N. Burgmayer and E. I. Stiefel, *J. Chem. Educ.* **62** (1985), 943.
26. W. Lovenberg and B. E. Sobel, *Proc. Natl. Acad. Sci. USA* **54** (1965), 193.
27. E. T. Lode and M. J. Coon, in Reference 9, pp. 173-191.
28. I. C. Gunsalus and J. D. Lipscomb, in Reference 11, p. 151.
29. R. W. Estabrook *et al*., in Reference 9.
30. I. Moura *et al*., *Biochem. Biophys. Res. Commun*. **75** (1977), 1037.
31. I. Moura *et al*., *J. Biol. Chem.* **255** (1980), 2493. a) J. LeGall *et al*., *Biochemistry* **27** (1988), 1636.
32. K. D. Watenpaugh, L. C. Sieker, and L. H. Jensen, *J. Mol. Biol*. **138** (1980), 615.
33. E. T. Adman *et al*., *J. Mol. Biol.* **112** (1977), 113. a) C. D. Stout, in Reference 8, p. 97.
34. K. D. Watenpaugh *et al*., *Acta Cryst*. **B29** (1973), 943.
35. R. G. Shulman *et al*., *Proc. Natl. Acad. Sci. USA* **72** (1975), 4003.
36. R. G. Shulman *et al*., *J. Mol. Biol.* **124** (1978), 305.
37. W. D. Phillips *et al*., *Nature* **227** (1970), 574.
38. J. C. Rivoal *et aI*., *Biochim. Biophys. Acta* **493** (1977), 122.
39. D. E. Bennett and M. K. Johnson, *Biochim. Biophys. Acta* **911** (1987), 71. a) M. S. Gebhard *et al*.,*J. Am. Chem. Soc*. **112** (1990), 2217. b) K. D. Butcher, M. S. Gebhard, and E. I. Solomon, *Inorg. Chem*. **29** (1990), 2067.
40. M. C. W. Evans, in Reference 8, p. 249.
41. W. A. Eaton and W. J. Lovenberg, *J. Am. Chem. Soc*. **92** (1970), 7195.
42. M. K. Johnson, A. E. Robinson, and A. J. Thomson, in Reference 8, p. 367.
43. P. J. Stephens *et aI*., *Proc. Natl. Acad. Sci. USA* **75** (1978), 5273.
44. J. Peisach *et al*., *J. Biol. Chem.* 246 (1971), 5877.
45. P. M. Champion and A. J. Siever, *J. Chem. Phys.* **66** (1977), 1819; D. Coucouvanis *et al*., *J. Am. Chem Soc.* **101** (1979), 3392.
46. R. Cammack, D. S. Patil, and V. M. Fernandez, *Biochem. Soc. Trans.* **13** (1985), 572.
47. B. L. Trumpower, *Biochim. Biophys. Acta* **639** (1981), 129.
48. H. Beinert, *Biochem. Soc. Trans.* **13** (1985), 542.
49. G. Palmer, *Biochem. Soc. Trans.* **13** (1985), 548.
50. R. Malkin and A. J. Bearden, *Biochim. Biophys. Acta* **505** (1978), 147.
51. C. E. Johnson, *J. Inorg. Biochem.* **28** (1986), 207.
52. E. Münck and T. A. Kent, *Hyperfine Interactions* **27** (1986), 161.
53. K. K. Rao *et al*., *Biochem. J.* **129** (1972), 1063.
54. I. Bertini and C. Luchinat, eds., *NMR of Paramagnetic Molecules in Biological Systems*, Benjamin/ Cummings, 1986.
55. G. N. La Mar, W. D. Horrocks, Jr., and R. H. Holm, NMR *of Paramagnetic Molecules*, Academic Press, 1973.
56. M. T. Werth *et al*., *J. Am. Chem. Soc.* **109** (1987), 273.
57. T. G. Spiro *et al*., in Reference 8, p. 407. a) T. V. Long and T. M. Loehr, *J. Am. Chem. Soc.* **92** (1970), 6384.
58. G. Christou, B. Ridge, and H. N. Rydon, *J. Chem. Soc. Chem. Commun.* (1979), 20.
59. S. W. May and J.-Y. Kuo, *Biochemistry* **17** (1978), 3333.
60. S. W. May *et al*., *Biochemistry* **23** (1984), 2187.
61. P. Saint-Martin *et al*., *Proc. Natl. Acad. Sci. USA* **85** (1988), 9378.
62. R. W. Lane *et al*., *Proc. Natl. Acad. Sci. USA* **72** (1975), 2868.
63. R. W. Lane *et al*., *J. Am. Chem. Soc.* **99** (1977), 84.
64. D. G. Holah and D. Coucouvanis, *J. Am. Chem. Soc.* **97** (1975), 6917.
65. D. Coucouvanis *et al*., *J. Am. Chem. Soc.* **93** (1976), 5721.
66. M. Millar *et al*., *lnorg. Chem.* **21** (1982), 4105.
67. S. A. Koch and L. E. Madia, *J. Am. Chem. Soc.* **105** (1983), 5944.
68. M. Millar, S. A. Koch, and R. Fikar, *lnorg. Chim. Acta* **88** (1984), L15.
69. J. C. Deaton *et al*., *J. Am. Chem. Soc.* **110** (1988), 6241.
70. D. B. Knaff, *Trends Biochem. Sci.* **13** (1988), 461. a) T. Tsukihara *et al*., *J. Biochem.* **90** (1981), 1763.
71. D. R. Ort and N. E. Good, *Trends Biochem. Sci.* **13** (1988), 467.
72. V. Massey, in Reference 9, p. 301.
73. M. K. Johnson *et al*., *J. Biol. Chem.* **260** (1985), 7368.

74. J. C. Salerno *et al*., *J. Biol. Chem.* **254** (1979), 4828.
75. T. P. Singer, M. Gutman, and V. Massey, in Reference 9, p. 225.
76. H. Twilfer, F.-H. Bernhardt, and K. Gersonde, *Eur. J. Biochem.* **119** (1981), 595.
77. L. Petersson, R. Cammack, and K. Krishna Rao, *Biochim. Biophys. Acta* **622** (1980), 18.
78. B.-K. Teo and R. G. Shulman, in Reference 8, p. 343.
79. T. Tsukihara *et al*., in K. Kimura, ed., *Molecular Evolution, Protein Polymorphism and the Neutral Theory*, Japan Scientific Societies Press and Springer-Verlag, 1982, p. 299.
80. T. Tsukihara *et al*., *BioSystems* **15** (1982), 243.
81. D. Petering and G. Palmer, *Arch. Biochem. Biophys*. **141** (1970), 456.
82. J. F. Gibson *et aI*., *Proc. Natl. Acad. Sci. USA* **56** (1966), 987.
83. W. A. Eaton *et al*., *Proc. Natl. Acad. Soc. USA* **68** (1971), 3015. a) L. B. Dugad *et al*., *Biochemistry* **29** (1990), 2663.
84. J. Rawlings, O. Siiman, and H. B. Gray, *Proc. Natl. Acad. Sci. USA* **71** (1974), 125.
85. I. Salmeen and G. Palmer, *Arch. Biochem. Biophys.* **150** (1972), 767.
86. J. J. Mayerle *et al*., *Proc. Natl. Acad. Sci. USA* **70** (1973), 2429.
87. J. L. Markley *et al*., *Science* **240** (1988), 908. a) L. Banci, I. Bertini, and C. Luchinat, *Structure and Bonding* **72** (1990), 113.
88. V. K. Yachandra *et al*., *J. Am. Chem. Soc.* **105** (1983), 6462.
89. S. Hwa, R. S. Czernuszewicz, and T. G. Spiro, *J. Am. Chem. Soc*. **111** (1989), 3496.
90. S. Hwa *et al*., *J. Am. Chem. Soc.* **111** (1989), 3505.
91. J. R. Rieske, D. H. MacLennan, and R. Coleman, *Biochem. Biophys. Res. Commun*. **15** (1964), 338.
92. W. D. Bonner, Jr., and R. C. Prince, *FEBS Lett.* **177** (1984), 47.
93. J. F. Cline *et al*., *J. Biol. Chem.* **260** (1985), 3251.
94. H.-T. Tsang *et al*., *Biochemistry* **28** (1989), 7233.
95. R. C. Prince, S. J. G. Linkletter, and P. L. Dutton, *Biochem. Biophys. Acta* **635** (1981), 132.
96. J. G. Reynolds and R. H. Holm, *lnorg. Chem*. **19** (1980), 3257; **20** (1981), 1873. a) J. J. Mayerle *et al*., *J. Am. Chem. Soc*. **97** (1977), 1032. b) Y. Do, E. D. Simhon, and R. H. Holm, *lnorg. Chem.* **22** (1983), 3809. c) S. Han, R. Czernuszewicz, and T. G. Spiro, *lnorg. Chem.* **25** (1986), 2276. d) H. Strasdeit, B. Krebs, and G. Henkel, *lnorg. Chim. Acta* **89** (1989), LII.
97. P. K. Mascharak *et al*., *J. Am. Chem. Soc.* **103** (1981), 6110.
98. P. Beardwood *et al*., *J. Chem. Soc.* Dalton Trans. (1982), 2015.
99. D. Coucouvanis *et al*., *J. Am. Chem. Soc*. **106** (1984), 6081.
100. P. Beardwood and J. F. Gibson, *J. Chem. Soc. Chem. Commun.* **102** (1985), 490 and 1345.
101. L. C. Sieker, E. Adman, and L. H. Jensen, *Nature* **235** (1971), 40.
102. J. M. Berg, K. O. Hodgson, and R. H. Holm, *J. Am. Chem. Soc*. **101** (1970), 4586.
103. P. J. Stephens *et al*., *Proc. Natl. Acad. Sci. USA* **82** (1985), 5661.
104. M. W. W. Adams and L. E. Mortenson, in Reference 235a.
105. L. W. Lim *et al*., *J. Biol. Chem.* **261** (1986), 15 and 140.
106. J. C. Salerno *et al*., *Biochem. Biophys. Res. Commun.* **73** (1976), 833.
107. G. Strahs and J. Kraut, *J. Mol. Biol.* **35** (1968), 503.
108. C. W. Carter, Jr., *et al*., *Proc. Natl. Acad. Sci. USA* **69** (1972), 3526.
109. C. W. Carter, Jr., *et al*., *J. Biol. Chem*. **249** (1974), 4212.
110. K. Fukuyama, *J. Mol. Biol.* 199 (1988), 183. a) K. Fukuyama *et al*., *J. Mol. Biol.* **210** (1989), 383.
111. G. H. Stout *et al*., *Proc. Natl. Acad. Sci. USA* **85** (1988), 1020.
112. C. D. Stout, *J. Biol. Chem.* **263** (1988), 9256.
113. A. H. Robbins and C. D. Stout, *Proc. Natl. Acad. Sci. USA* **86** (1989), 3639.
114. E. T. Adman, L. C. Sieker, and L. H. Jensen, *J. Biol. Chem.* **248** (1973), 3987.
115. R. C. Prince and M. W. W. Adams, *J. Biol. Chem.* **262** (1987), 5125.
116. L. E. Mortenson, R. C. Valentine, and J. E. Carnahan, *Biochem. Biophys. Res. Commun.* **7** (1962), 448.
117. W. Lovenberg, B. B. Buchanan, and J. C. Rabinowitz, *J. Biol. Chem*. **254** (1979), 4499.
118. R. Mathews *et al*., *J. Biol. Chem.* **249** (1974), 4326.
119. A. J. Thomson, in P. M. Harrison, ed., *Metalloproteins, Part I: Metal Proteins with Redox Roles*, Verlag Chemie, 1985, pp. 79-120.

120. R. Cammack, *Biochem. Biophys. Res. Commun.* **54** (1973), 548.
121. M. J. Carney *et al.*, *Inorg. Chem.* **27** (1988), 346.
122. M. J. Carney *et al.*, *J. Am. Chem. Soc.* **110** (1988), 6084.
123. L. Noodleman, D. A. Case, and A. Aizman, *J. Am. Chem. Soc.* **110** (1988), 1001.
124. L. Noodleman, *Inorg. Chem.* 27 (1988), 3677.
125. J.-M. Moulis, J. Meyer, and M. Lutz, *Biochemistry* **23** (1984), 6605. a) W. D. Phillips and M. Poe, in Reference 10, p. 255. b) E. L. Packer *et al.*, *J. Biol. Chem.* **252** (1977), 2245. c) J. Bertini *et al.*, *Inorg. Chem.* **29** (1990), 1874. d) B.-K. Teo *et al.*, *J. Am. Chem. Soc.* **101** (1979), 5624.
126. T. Herskovitz *et al.*, *Proc. Natl. Acad. Sci. USA* **69** (1972), 2437.
127. B. A. Averill *et al.*, *J. Am. Chem. Soc.* **95** (1973), 3523.
128. J. M. Berg and R. H. Holm, in Reference 8, p. I.
129. G. B. Wang, M. A. Bobrick, and R. H. Holm, *Inorg. Chem.* **17** (1978), 578.
130. D. Coucouvanis *et al.*, *J. Am. Chem. Soc.* **104** (1982), 1874.
131. A. Müller and N. Schladerbeck, *Chimia* **39** (1985), 23.
132. A. Müller, N. Schladerbeck, and H. Bagge, *Chimia* **39** (1985), 24.
133. S. Rutchik, S. Kim, and M. A. Walters, *Inorg. Chem.* **27** (1988), 1513.
134. W. E. Cleland *et al.*, *J. Am. Chem. Soc.* **105** (1983), 6021.
135. M. G. Kanatzidis *et al.*, *J. Am. Chem. Soc.* **106** (1984), 4500.
136. M. G. Kanatzidis *et al.*, *Inorg. Chem.* **22** (1983), 179.
137. R. E. Johnson *et al.*, *J. Am. Chem. Soc.* **105** (1983), 7280.
138. M. G. Kanatzidis *et al.*, *J. Am. Chem. Soc.* **107** (1985), 4925. a) K. S. Hagen, J. G. Reynolds, and R. H. Holm, *J. Am. Chem. Soc.* **103** (1981), 4054. b) G. Christou and C. D. Gamer, *J. Chem. Soc. Dalton Trans.* (1979), 1093. c) M. J. Carney *et al.*, *Inorg. Chem.* **27** (1988), 346. d) P. Barbaro *et al.*, *J. Am. Chem. Soc.* **112** (1990), 7238.
139. E. J. Laskowski *et al.*, *J. Am. Chem. Soc.* **100** (1978), 5322.
140. E.1. Laskowski *et al.*, *J. Am. Chem. Soc.* **101** (1979), 6562.
141. T. O'Sullivan and M. Millar, *J. Am. Chem. Soc.* **107** (1985), 4096.
142. M. Millar, private communication.
143. T. D. P. Stack and R. H. Holm, *J. Am. Chem. Soc.* **110** (1989), 2484. a) T. D. P. Stack, M. J. Carney, and R. H. Holm, *J. Am. Chem. Soc.* **111** (1989), 1670. b) S. Ciurli *et al.*, *J. Am. Chem. Soc.* **112** (1990), 2654. c) P. R. Challen *et al.*, *J. Am. Chem. Soc.* **112** (1990), 2455.
144. L. Que, Jr., R. H. Holm, and L. E. Mortenson, *J. Am. Chem. Soc.* **97** (1975), 463.
145. N. R. Bastian *et al.*, in Reference 10, p. 227.
146. H. Beinert and A. J. Thomson, *Arch. Biochem. Biophys.* **222** (1983), 333.
147. M. H. Emptage *et al.*, *J. Biol. Chem.* **255** (1980), 1793.
148. W. W. Sweeney, J. C. Rabinowitz, and D. C. Yoch, *J. Biol. Chem.* **250** (1985), 7842.
149. B. A. Averill, J. R. Bal, and W. H. Orme-Johnson, *J. Am. Chem. Soc.* **100** (1978), 3034.
150. C. D. Stout, *Nature* **279** (1979), 83.
151. D. Ghosh *et al.*, *J. Biol. Chem.* **256** (1981), 4185.
152. D. Ghosh *et al.*, *J. Mol. Biol.* **158** (1982), 73.
153. M. K. Johnson *et al.*, *J. Am. Chem. Soc.* **105** (1983), 6671.
154. H. Beinert and A. J. Thomson, *Arch. Biochem. Biophys.* **222** (1983), 333.
155. M. R. Antonio *et al.*, *J. Biol. Chem.* **257** (1982), 6646.
156. E. Miinck, in Reference 8, p. 147.
157. C. E. Johnson, *J. Inorg. Biochem.* **207** (1986), 28.
158. B. H. Huynh *et al.*, *J. Biol. Chem.* **255** (1980), 3242.
159. J. J. G. Moura *et al.*, *J. Biol. Chem.* **257** (1982), 6259. a) H. Beinert and M. C. Kennedy, *Eur. J. Biochem.* **186** (1989), 1865.
160. C. R. Kissinger *et al.*, *J. Am. Chem. Soc.* **110** (1988), 8721. a) S. Ciurli and R. H. Holm, *Inorg. Chem.* **28** (1989), 1685.
161. T. A. Kent *et al.*, *J. Biol. Chem.* **260** (1985), 6871.
162. A. H. Robbins and C. D. Stout, *J. Biol. Chem.* **260** (1985), 2328.
163. M. K. Johnson *et al.*, *J. Biol. Chem.* **258** (1983), 12771.

164. M. C. Kennedy *et al.*, *J. Biol. Chem.* **258** (1983), 11098.
165. J. TeIser *et al.*, *J. Biol. Chem.* **261** (1986), 4840.
166. D. H. Flint, M. H. Emptage, and J. R. Guest, *J. Inorg. Biochem.* **36** (1989), 306. a) R. L. Switzer, *BioFactors* **2** (1989), 77.
167. H. Beinert *et al.*, *Proc. Natl. Acad. Sci. USA* **80** (1983), 393.
168. M. K. Johnson *et al.*, *J. Biol. Chem.* **256** (1981), 9806.
169. T. R. Halbert *et al.*, *J. Am. Chem. Soc.* **106** (1984),1849.
170. G. N. George and S. J. George, *Trends Biochem. Sci.* **13** (1988), 369. a) I. Moura *et al*., *J. Am. Chem. Soc.* **108** (1986), 349. b) K. K. Surerus *et al.*, *J. Am. Chem. Soc.* **109** (1987), 3805. c) R. C. Conover *et al.*, *J. Am. Chem. Soc.* **112** (1990), 4562. d) J. K. Money, J. C. Huffman, and G. Christou, *Inorg. Chem.* **27** (1988), 507.
171. B. H. Huynh *et al*., *Proc. Natl. Acad. Sci. USA* **81** (1984), 3728.
172. T. R. Hawkes and B. E. Smith, *Biochem. J.* 223 (1984), 783.
173. M. A. Whitener *et al.*, *J. Am. Chem. Soc.* **108** (1986), 5607.
174. K. S. Hagen and R. H. Holm, *J. Am. Chem. Soc.* **104** (1982), 5496.
175. K. S. Hagen, A. D. Watson, and R. H. Holm, *J. Am. Chem. Soc.* **105** (1983), 3905. a) J.-J. Girard *et al.*, *J. Am. Chem. Soc.* **106** (1984), 5941.
176. M. C. Kennedy *et al.*, *J. Biol. Chem.* 259 (1984), 14463. a) H. Strasdeit, B. Krebs, and G. Henkel, *Inorg. Chem*. **23** (1983), 1816.
177. M. G. Kanatzidis *et al.*, *J. Chem. Soc. Chem. Commun.* (1984), 356.
178. M. G. Kanatzidis, A. Salifoglou, and D. Coucouvanis, *J. Am. Chem. Soc.* **107** (1985), 3358; *Inorg. Chem*. **25** (1986), 2460.
179. S. Pohl and W. Saak, *Angew. Chem. Int. Ed. Engl.* **23** (1984), 907. a) S. A. AI-Ahmand *et al.*, *Inorg. Chem.* **29** (1990), 927.
180. F. Cecconi, C. A. Ghilardi, and S. Midolini, *J. Chem. Soc. Chem. Commun.* (1981), 640.
181. A. Agresti *et al.*, *Inorg. Chem.* **24** (1985), 689.
182. K. S. Hagen, J. M. Berg, and R. H. Holm, *Inorg. Chim. Acta* **45** (1980), L17. a) B. S. Snyder and R. H. Holm, *Inorg. Chem.* **27** (1988), 1816. b) B. S. Synder *et al.*, *Inorg. Chem.* **27** (1988), 595. c) M. S. Reynolds and R. H. Holm, *Inorg. Chem.* **27** (1988), 4494. d) B. S. Snyder and R. H. Holm, *Inorg. Chem*. **29** (1990), 274.
183. I. Noda, B. S. Snyder, and R. H. Holm, *Inorg. Chem.* **25** (1986), 3851. a) J.-F. You, B. S. Snyder, and R. H. Holm, *J. Am. Chem. Soc.* **110** (1988), 6589. b) J.-F. You *et al.*, *J. Am. Chem. Soc.* **112** (1990), 1067. c) W. R. Hagen, A. J. Pierik, and C. Veeger, *J. Chem. Soc., Faraday Trans. I* **85** (1989), 4083.
184. E. I. Stiefel *et al*., *Adv. Chem. Ser.* **162** (1977), 353. a) I. Moura and J. J. G. Moura, in Reference 5, p. 179. b) J. R. Lancaster, Jr., ed., *The Bioinorganic Chemistry of Nickel*, VCH Publishers, 1988. c) H. J. Grande *et al.*, in Reference 5, p. 193. d M. W. W. Adams, L. E. Mortenson, and J.-S. Chen, *Biochim. Biophys. Acta* **594** (1981), 105. e) J. LeGall and H. D. Peck, Jr., in Reference 5, p. 207. f) J. LeGall *et al.*, in Reference 8, p. 177. g) S. P. Ballantine and D. H. Boxer, *Eur. J. Biochem.* **156** (1986), 276. h) W. H. Onne-Johnson and N. R. Onne-Johnson, in Reference 8, p. 67.
185. B. Bowien and H. G. Schlegel, *Annu. Rev. Microbiol.* **35** (1981), 401.
186. C. R. Bowers and D. P. Weitekamp, *J. Am. Chem. Soc.* **109** (1987), 5541.
187. T. C. Eisenschmid *et al.*, *J. Am. Chem. Soc.* **109** (1987), 8089.
188. M. W. W. Adams *et al.*, *Biochimie* **68** (1986), 35.
189. R. Cammack, V. M. Fernandez, and K. Schneider, in Reference 184b, p. 167. 189a. M. W. W. Adams, *Biochem. Biophys. Acta* **1020** (1990),115.
190. H. J. Grande *et al.*, *Eur. J. Biochem.* **136** (1983), 201.
191. M. W. W. Adams and L. E. Mortenson, *J. Biol. Chem.* **259** (1984), 7045.
192. S. W. Ragsdale and L. G. L. Ljungdahl, *Arch. Microbial*. **139** (1984), 361.
193. C. R. Woese, *Microbial. Rev.* **81** (1987), 221.
194. M. W. W. Adams, E. Eccleston, and J. B. Howard, *Proc. Natl. Acad. Sci. USA* **86** (1989), 4932.
195. D. S. Patil *et al*., *J. Am. Chem. Soc.* **110** (1988), 8533.
196. A. T. Kowal, M. W. W. Adams, and M. K. Johnson, *J. Biol. Chem.* **264** (1989), 4342.
197. W. R. Hagen *et al.*, *FEBS Lett.* **203** (1986), 59.
198. I. C. Zambrano *et al.*, *J. Biol. Chem.* **264** (1989), 20974.
199. M. W. W. Adams, *J. Biol. Chem.* **262** (1987), 15054.
200. T. V. Morgan, R. C. Prince, and L. E. Mortenson, *FEBS Lett*. **206** (1986), 4.

201. W. R. Hagen *et al.*, *FEBS Lett.* **201** (1986), 158.
202. F. M. Rusnak *et al.*, *J. Biol. Chem.* **262** (1987), 38.
203. G. Wang *et al.*, *J. Biol. Chem.* **259** (1984), 14328.
204. J. Telser *et al.*, *J. Biol. Chem.* **262** (1987), 6589.
205. J. Telser *et al.*, *J. Biol. Chem.* **261** (1986), 15536.
206. H. Thomann, M. Bernardo, and M. W. W. Adams, *J. Am. Chem. Soc.* **113** (1991), 7044.
207. A. J. Thomson *et al.*, *Biochem. J.* **227** (1985), 333.
208. K. A. Macor *et al.*, *J. Biol. Chem.* **282** (1987), 9945.
209. G. N. George *et al.*, *Biochem. J.* **259** (1989), 597.
210. R. Cammack, *Adv. Inorg. Chem.* **32** (1988), 297.
211. J. J. G. Moura *et al.*, in Reference 5, p. 191.
212. J. R. Lancaster, *FEBS Lett.* **115** (1980), 285.
213. M. Teixeira *et al.*, *J. Biol. Chem.* **260** (1985), 8942.
214. J. W. Van der Zwaan *et al.*, *FEBS Lett.* **179** (1985), 271.
215. M. K. Eidsness, R. J. Sullivan, and R. A. Scott, in Reference 184b, p. 73.
216. M. K. Eidsness *et al.*, *Proc. Natl. Acad. Sci. USA* **86** (1989), 147.
217. P. A. Lindahl *et al.*, *J. Am. Chem. Soc.* **106** (1984), 3062.
218. R. A. Scott *et al.*, *J. Am. Chem. Soc.* **106** (1984), 6864.
219. S. P. J. Albracht *et al.*, *Biochim. Biophys. Acta* **874** (1986), 116.
220. A. Chapman *et al.*, *FEBS Lett.* **242** (1988), 134.
221. S. L. Tau *et al.*, *J. Am. Chem. Soc.* **106** (1984), 3064.
222. G. J. Kubas *et al.*, *J. Am. Chem. Soc.* **106** (1984), 451.
223. G. J. Kubas and R. R. Ryan, *Polyhedron* **5** (1986), 473.
224. G. J. Kubas *et al.*, *J. Am. Chem. Soc.* **108** (1986), 7000.
225. M. Rakowski DuBois *et al.*, *J. Am. Chem. Soc.* **102** (1980), 7456.
226. C. Bianchini *et al.*, *Inorg. Chem.* **25** (1986), 4617.
227. W. Tremel *et al.*, *Inorg. Chem.* **27** (1988), 3886.
228. W. Tremel and G. Henkel, *Inorg. Chem.* **27** (1988), 3896.
229. I. Dance, *Polyhedron* **5** (1986), 1037; P. J. Blower and J. R. Dilworth, *Coord. Chem. Rev.* **76** (1987), 121.
230. C. L. Coyle and E. I. Stiefel, in Reference 184b, p. 1.
231. M. Kumar *et al.*, *J. Am Chem. Soc.* **111** (1989), 5974.
232. M. Kumar *et al.*, *J. Am. Chem. Soc.* **111** (1989), 8323.
233. T. H. Blackburn, in W. E. Krumbein, ed., *Microbial Geochemistry*, Blackwell Scientific, 1983, p. 63.
234. J. R. Postgate, *Fundamentals of Nitrogen Fixation*, Cambridge University Press, 1982.
235. R. W. F. Hardy, *Treatise on Dinitrogen Fixation*, Wiley, 1979, Section I. a) T. G. Spiro, ed., *Molybdenum Enzymes*, Wiley-Interscience, 1985.
236. W. J. Brill, *NATO Adv. Sci. Inst., Ser. A* **63** (1983), 231.
237. R. Haselkorn, *Annu. Rev. Microbial.* **40** (1986), 525.
238. A. C. Robinson, D. R. Dean, and B. K. Burgess, *J. Biol. Chem.* **262** (1987), 14327.
239. P. J. Stephens, in Reference 235a, p. 117.
240. A. H. Gibson and W. E. Newton, eds., Current *Perspectives in Nitrogen Fixation*, Australian Academy of Science, 1981.
241. E. I. Stiefel, in W. E. Newton and C. Rodriquez-Barrucco, eds., in *Recent Progress in Nitrogen Fixation*, Academic Press, 1977, p. 69.
242. C. Veeger and W. E. Newton, eds., *Advances in Nitrogen Fixation Research*, Nijhoff/Junk, 1984.
243. H. J. Evans, P. J. Bottomley, and W. E. Newton, eds., *Nitrogen Fixation Research Progress*, Martinus Nijhoff, 1985. a) A. Braaksma *et al.*, in Reference 5, p. 223. b) B. H. Huynh, E. Münck, and W. H. Orme-Johnson, in Reference 5, p. 241.
244. E. I. Stiefel, in Reference 240, p. 55.
245. R. V. Hageman and R. H. Burris, *Proc. Natl. Acad. Sci. USA* **75** (1978), 2699.
246. V. Sundaresan and F. M. Ausubel, *J. Biol. Chem.* **256** (1981), 2808. a) R. P. Hausinger and J. B. Howard, *J. Biol. Chem.* **258** (1983), 13486. b) M. M. Georgiadis, P. Chakrabarti, and D. C. Rees, *SSRL Annual Report* (1989), p. 94.

247. L. E. Mortenson, M. N. Walker, and G. A. Walker, in W. E. Newton and C. J. Nyman, eds., *Proceedings of the First International Conference on Nitrogen Fixation*, Washington State University Press (1976), p. 117.
248. W. H. Orme-Johnson et al., in W. E. Newton, J. R. Postgate, and C. Rodriguez Barrucco, eds., *Recent Developments in Nitrogen Fixation*, Academic Press, 1977, p. 131.
249. G. D. Watt and J. W. McDonald, *Biochemistry* **24** (1985), 7226.
250. W. R. Hagen *et al.*, *FEBS Lett.* **189** (1986), 250.
251. L. Noodleman *et al.*, *J. Am. Chem. Soc.* **107** (1985), 3418.
252. G. D. Watt, Z.-C. Wang, and R. R. Knotts, *Biochemistry* **25** (1986),8156; J. Cordewener *et al.*, *Eur. J. Biochem.* **148** (1985), 499.
253. L. E. Mortenson and R. N. F. Thorneley, *Annu. Rev. Biochem.* **48** (1979), 387.
254. A. V. Kulikov *et al.*, *Dokl. Akad. Nauk SSR* **262** (1981), 1177.
255. R. N. F. Thorneley and D. J. Lowe, in Reference 235, p. 221. a) F. A. Schultz, S. F. Gheller, and W. E. Newton, Proc. *Int. Symp. Redox Mech. Interfacial Prop. Mol. Biol. Importance* **3** (1988), 203.
256. B. K. Burgess and W. E. Newton, in A. Müller and W. E. Newton, eds., *Nitrogen Fixation: The Chemical-Biochemical-Genetic Interface*, Plenum, 1983, p. 83.
257. E. I. Stiefel and S. P. Cramer, in Reference 235, p. 88.
258. V. Shah and W. J. Brill, *Proc. Natl. Acad. Sci. USA* **74** (1977), 3249.
259. S. D. Conradson *et al.*, *J. Am. Chem. Soc.* **109** (1987), 7507. a) P. A. McLean *et al.*, *Biochemistry* **28** (1989), 9402. b) D. A. Wink *et al.*, *Biochemistry* **28** (1989), 9407.
260. M. A. Walters, S. K. Chapman, and W. H. Orme-Johnson, *Polyhedron* **5** (1986), 561.
261. P. A. McLean and R. A. Dixon, *Nature* **292** (1981), 655.
262. P. A. McLean and B. E. Smith, *Biochem. J.* **211** (1983), 589.
263. T. R. Hawkes, P. A. McLean, and B. E. Smith, *Biochem. J.* **217** (1984), 317.
264. T. R. Hoover *et al.*, *Biochemistry* **27** (1988), 3647.
265. T. R. Hoover *et al.*, *Biochemistry* **28** (1989), 2768. a) J. Liang *et al.*, *Biochemistry* **29** (1990), 8377. b) M. S. Madden *et al.*, *Proc. Natl. Acad. Sci. USA* **87** (1990), 6517.
266. A. C. Robinson, D. Dean, and B. K. Burgess, *J. Biol. Chem.* **262** (1989), 14327. a) A. C. Robinson *et al.*, *J. Biol. Chem.* **264** (1989), 10088. b) D. J. Scott *et al.*, *Nature* **343** (1990), 188. c) H. M. Kent *et al.*, *Biochem. J.* **264** (1989), 257.
267. W. R. Hagen *et al.*, *Eur. J. Biochem*. **169** (1987), 457.
268. P. A. McLean *et al.*, *J. Biol. Chem.* **262** (1987), 12900.
269. P. A. Lindahl *et al.*, *J. Biol. Chem.* **263** (1988), 19442.
270. G. D. Watt, A. Burns, and D. L. Tennent, *Biochemistry* **20** (1981), 7272; G. D. Watt and Z. C. Wang, *Biochemistry* **25** (1986), 5196.
271. R. Zimmermann *et al.*, *Biochim. Biophys. Acta.* **537** (1978), 185.
272. D. M. Kurtz *et al.*, *Proc. Natl. Acad. Sci. USA* **76** (1979), 4986.
273. R. A. Venters *et al.*, *J. Am. Chem. Soc*. **108** (1986), 3487. a) J. Bolin, in P. M. Gresshoff, L. E. Roth, G. Stacey, and W. E. Newton, eds., *Nitrogen Fixation: Achievements and Objectives*, Chapman and Hall, 1990, p. 111.
274. B. M. Hoffman, J. E. Roberts, and W. H. Orme-Johnson, *J. Am. Chern. Soc.* **104** (1982), 860.
275. A. E. True *et al.*, *J. Am. Chem. Soc.* **110** (1988), 1935. a) A. E. True *et al.*, *J. Am. Chem. Soc.* **112** (1990), 651.
276. G. N. George *et aI.*, *Biochem. J.* **262** (1989), 349.
277. W. B. Mims and J. Peisach, in R. G. Shulman, ed., *Biological Applications of Magnetic Resonance*, Academic Press, 1980, p. 221.
278. W. H. Orme-Johnson *et al.*, in Reference 8, p. 79.
279. H. Thomann *et al.*, *J. Am. Chem. Soc.* **109** (1987), 7913.
280. H. Thomann *et al.*, *Proc. Natl. Acad. Sci. USA*, **88** (1991), 6620.
281. B. H. Huynh, E. Munck, and W. H. Orme-Johnson, *Biochim. Biophys. Acta* **527** (1979), 192.
282. B. H. Huynh *et aI.*, *Biochim. Biophys. Acta* **623** (1980), 124.
283. E. Münck *et al.*, *Biochim. Biophys. Acta* **400** (1975), 32. a) W. E. Newton *et al.*, *Biochem. Biophys. Res. Commun*. **162** (1989), 882.
284. S. D. Conradson, B. K. Burgess, and R. H. Holm, *J. Biol. Chem*. **263** (1988), 13743.

285. W. R. Dunham *et aI*., *Eur. J. Biochem.* **146** (1985), 497.
286. S. P. Cramer *et al*., *J. Am. Chem. Soc*. **100** (1978), 3398.
287. M. K. Eidsness *et al*., *J. Am. Chem. Soc*. **108** (1986), 2746.
288. S. D. Conradson *et aI*., *J. Am. Chem. Soc.* **107** (1985), 7935; Reference 259.
289. B. Hedman *et al*., *J. Am. Chem. Soc*. **110** (1988), 3798.
290. M. R. Antonio *et al*., *J. Am. Chem. Soc.* **104** (1982), 4703.
291. J. M. Arber *et al*., *Biochem. J.* **252** (1988), 421.
292. M. S. Weininger and L. E. Mortenson, *Proc. Natl. Acad. Sci. USA* **79** (1982), 378.
293. N. I. Sosfenov *et al*., *Dokl. Akad. Nauk. SSSR* **291** (1986), 1123.
294. T. Yamane *et al*., *J. Biol. Chem.* **257** (1982), 1221.
295. A. M. Flank *et aI*., *J. Am. Chem. Soc.* **108** (1986), 1049.
296. J. F. Rubinson *et aI*., *Biochemistry* **24** (1985), 273.
297. E. I. Stiefel, *Proc. Natl. Acad. Sci. USA* **70** (1973), 988.
298. K. L. Hadfield and W. A. Bulen, *Biochemistry* **8** (1969), 5103.
299. F. B. Simpson and R. Burris, *Science* **224** (1984), 1095.
300. B. K. Burgess *et al*., *Biochemistry* **20** (1981), 5140.
301. S. Wherland *et aI*., *Biochemistry* **20** (1981), 5132.
302. J. H. Guth and R. H. Burris, *Biochemistry* **22** (1983), 5111.
303. Z.-c. Wang and G. D. Watt, *Proc. Natl. Acad. Sci. USA* **81** (1984), 376.
304. B. E. Smith *et al*., *Phil. Trans. Roy. Soc. London* **B317** (1987), 131.
305. R. N. F. Thorneley, R. R. Eady, and D. J. Lowe, *Nature* **272** (1978), 557.
306. S. Wherland *et al*., *Biochemistry* **20** (1981), 5132.
307. B. K. Burgess *et al*., *Biochemistry* **20** (1981), 5140.
308. H. Bortels, *Arch. Mikrobiol*. **1** (1930), 333.
309. R. C. Bray, *Quart. Rev. Biophys*. **21** (1988), 299.
310. H. Bortels, *Zentbl. Bakt. Parasiten Abt. II* **95** (1935), 193.
311. C. E. McKenna, J. R. Benemann, and T. G. Traylor, *Biochem. Biophys. Res. Commun.* **41** (1970), 1501.
312. R. C. Burns, W. H. Fuchsman, and R. W. F. Hardy, *Biochem. Biophys. Res. Commun.* **42** (1971), 353.
313. J. R. Benemann *et al*., *Biochim. Biophys. Acta* **264** (1972), 25.
314. P. E. Bishop, D. M. L. Jarlenski, and D. R. Hetherington, *Proc. Natl. Acad. Sci. USA* **77** (1980), 7342.
315. P. E. Bishop *et al*., *Science* **232** (1986), 92.
316. B. J. Hales, D. J. Langosch, and E. E. Case, *J. Biol. Chem.* **261** (1986), 15301.
317. B. J. Hales *et al*., *Biochemistry* **26** (1987), 1795.
318. J. Morningstar *et al*., *Biochemistry* **26** (1987), 1795.
319. R. L. Robson *et al*., *Nature* **322** (1986), 388.
320. R. R. Eady *et al*., *Biochem. J.* **244** (1987), 197.
321. M. J. Dilworth *et al*., *Nature* **327** (1987), 167.
322. R. N. Pau, *Trends Biochem. Res.* **14** (1989), 186; P. E. Bishop and R. D. Joerger, *Annu. Rev. Plant Physiol. Plant Mol. Biol*. **41** (1990), 109.
323. J. E. Morningstar and B. J. Hales, *J. Am. Chem. Soc.* **109** (1987), 6854.
324. J. M. Arber *et al*., *Nature* **372** (1987), 325.
325. G. N. George *et al*., *J: Am. Chem. Soc.* **110** (1988), 4057.
326. R. R. Eady *et al*., *Recueil des Travaus Chim. des Pays-Bas* **106** (1987), 175.
327. M. J. Carney *et al*., *J. Am. Chem. Soc.* **108** (1986), 3519.
328. R. H. Holm, *Chem. Soc. Rev.* (1981), 455.
329. G. Christou and C. D. Gamer, *J. Chem. Soc. Dalton Trans.* (1980), 2354.
330. C. D. Gamer *et al*., *Phil. Trans. Roy. Soc. Land.* **A308** (1982), 159. a). R. H. Holm and E. D. Simhon, in Reference 235a, p. 1.
331. W. H. Armstrong, P. K. Mascharak, and R. H. Holm, *Inorg. Chem.* **21** (1982),1699.
332. R. E. Palermo and R. H. Holm, *J. Am. Chem. Soc.* **105** (1983), 4310. a) D. Coucouvanis, E. D. Simhon, and N. C. Baenziger, *J. Am. Chem. Soc.* **102** (1980), 6644. b) G. D. Friesen *et al*., *Inorg. Chem.* **22** (1983), 2203. c) P. Stremple, N. C. Baenziger, and D.

Coucouvanis, *J. Am. Chem. Soc.* **103** (1981), 4601. d) D. Coucouvanis *et al.*, *J. Am. Chem. Soc.* **102** (1980), 1732. e) A. Müller *et al.*, *Inorg. Chim. Acta* **148** (1988), 11. f) A. Müller *et al.*, *Angew. Chem. Int. Ed. Engl.* **21** (1982), 860. g) D. Coucouvanis *et al.*, *Inorg. Chem.* **27** (1988), 4066. h) P. A. Eldridge *et al.*, *J. Am. Chem. Soc.* **110** (1988), 5573. i) K. S. Bose *et al.*, *J. Am. Chem. Soc.* **111** (1989), 8953. j) J. A. Kovacs, J. K. Bashkin, and R. H. Holm, *Polyhedron* **6** (1987), 1445.

333. R. D. Sanner *et al.*, *J. Am. Chem. Soc.* **98** (1972), 8351. a) M. B. O'Regan *et al.*, *J. Am. Chem. Soc.* **112** (1990), 4331.
334. G. Pez, P. Apgar, and R. K. Crissey, *J. Am. Chem. Soc.* **104** (1982), 462.
335. K. Jones *et al.*, *J. Am. Chem. Soc.* **98** (1976), 74.
336. G. J. Leigh, *J. Mol. Catal.* **47** (1988), 363.
337. R. A. Henderson, G. J. Leigh, and C. J. Pickett, *Adv. Inorg. Chem. Radiochem.* **27** (1984), 198. a) M. Hidai and Y. Mizobe, in P. S. Braterman, ed., *Reactions of Coordinated Ligands*, Plenum, **2** (1989),53. b) T. Yoshida *et al.*, *J. Am. Chem. Soc.* **110** (1988), 4872. c) T. Yoshida, T. Adachi, and T. Ueda, *Pure Appl. Chem.* **62** (1990), 1127.
338. D. Sellmann *et al.*, *Angew. Chem. Int. Ed. Engl.* **28** (1989), 1271.
339. A. E. Shilov, in M. Gratzel, ed., *Energy Resources through Chemistry and Catalysis*, Academic Press, 1983, p. 533.
340. W. E. Newton *et al.*, *Inorg. Chem.* **19** (1980), 1997.
341. T. R. Halbert, W.-H. Pan, and E. I. Stiefel, *J. Am. Chem. Soc.* **105** (1983), 5476.
342. M. Rakowski DuBois *et al.*, *J. Am. Chem. Soc.* **101** (1979), 5245.
343. R. H. Crabtree, *Inorg. Chim. Acta* **125** (1986), 27.
344. W. B. Mims and J. Peisach, in J. Berliner and J. Reuben, eds., *Biological Magnetic Resonance*, Plenum, **3** (1981), 213.
345. T. Yamane *et al.*, *J. Biol. Chem.* **257** (1982), 1221.
346. D. C. Rees and J. B. Howard, *J. Biol. Chem.* **2587** (1983), 12733.
347. R. B. Frankel *et al.*, *J. de Physique* **37** (1976), C6.
348. C. E. Johnson, *J. Appl. Phys.* **42** (1971), 1325.
349. P. Middleton *et al.*, *Eur. J. Biochem.* **88** (1978), 135.
350. K. Tagawa and D. I. Amon, *Biochim. Biophys. Acta* **153** (1968), 602.
351. G. Palmer, R. H. Sands, and L. E. Mortenson, *Biochim. Biophys. Acta* **23** (1966), 357.
352. R. H. Sands and W. R. Dunham, *Quart. Rev. Biophys.* **4** (1975), 443.
353. R. Cammack, in M. J. Allen and P. N. R. Usherwood, eds., *Charge and Field Effects in Biosystems*, Abacus Press, 1984, p. 41.
354. J. Cardenas, L. E. Mortenson, and D. C. Yoch, *Biochim. Biophys. Acta* **434** (1976), 244.
355. R. Cammack, M. J. Barber, and R. C. Bray, *Biochem. J.* **157** (1976), 469.
356. R. C. Bray, in *The Enzymes*, 3d ed., **12** (1975), 299.
357. J. A. Fee *et al.*, *J. Biol. Chem.* **259** (1984), 124.
358. R. N. Mullinger *et al.*, *Biochem. J.* **151** (1975), 75.
359. R. Cammack *et al.*, *Biochim. Biophys. Acta* **490** (1977), 311.
360. F. A. Armstrong *et al.*, *FEBS Lett.* **234** (1988), 107.
361. W. R. Hagen *et al.*, *Biochim. Biophys. Acta* **828** (1985), 369.
362. E. deGryse, N. Glandsdorff, and A. Piérard, *Arch. Microbiol.* **117** (1978), 189.
363. V. M. Fernandez, E. C. Hatchikian, and R. Cammack, *Biochim. Biophys. Acta* **832** (1985), 69.
364. V. Niviére, *Biochem. Biophys. Res. Commun.* **139** (1986), 658.
365. M. Teixeira *et al.*, *Biochimie* **68** (1986), 75.
366. D. J. Lowe, B. E. Smith, and R. R. Eady, in N. S. Subba Rao, ed., *Recent Advances in Biological Nitrogen Fixation*, Arnold, 1980, p. 34.
367. R. C. Bums, R. D. Holsten, and R. W. F. Hardy, *Biochem. Biophys. Res. Commun.* **39** (1970), 90.
368. M. G. Yates and K. Planque, *Eur. J. Biochem.* **60** (1975), 467.
369. T. C. Huang, W. G. Zumft, and L. E. Mortenson, *J. Bact.* **113** (1973), 884.
370. P. C. Hallenback, P. J. Kostel, and J. R. Benemann, *Eur. J. Biochem.* **98** (1979), 275.
371. S. Norlund, U. Erikson, and H. Baltscheffsky, *Biochim. Biophys. Acta* **504** (1978), 248.
372. B. K. Burgess *et al.*, in Reference 242.
373. S. D. Conradson *et aI.*, *J. Am. Chem. Soc.* **109** (1987), 7507.
374. S. A. Vaughn and B. K. Burgess, *Biochemistry* **28** (1989), 419.
375. R. W. Miller and R. R. Eady, *Biochim. Biophys. Acta* **952** (1988), 290.

376. B. K. Burgess, in Reference 235a, p. 161.
377. B. J. Hales *et al.*, *Biochemistry* **25** (1986), 7251.
378. M. M. Georgiadis *et al.*, *Science* **257** (1992), 1653.
379. J. T. Bolin *et al.*, in P. M. Greshoff et al., eds., *Nitrogen Fixation: Achievements and Objectives*, Chapman and Hall, 1990, p. 117.
380. J. Kim and D. C. Rees, *Science* **257** (1992), 1677.
381. J. Kim and D. C. Rees, *Nature* **360** (1992), 553.
382. For allowing us to see and quote their work prior to publication, we are grateful to Prof. M. W. W. Adams, Prof. B. K. Burgess, Dr. R. Cammack, Prof. D. Coucouvanis, Prof. S. P. Cramer, Dr. S. J. George, Prof. J. N. Enemark, Prof. J. Lancaster, Dr. Michelle Millar, Prof. M. Maroney, Prof. W. E. Newton, Prof. D. C. Rees, Prof. Dieter Sellman, Prof. A. E. Shilov, Dr. Barry E. Smith, Dr. R. N. F. Thorneley, and Prof. G. D. Watt. We thank Pat Deuel for her superb efforts under difficult circumstances in the preparation of this manuscript.

Contributors and Attributions

- Edward I. Stiefel (Exxon Research and Engineering Company)
- Graham N. George (Exxon Research and Engineering Company)

9.4: Ferrodoxins, Hydrogenases, and Nitrogenases - Metal-Sulfide Proteins is shared under a CC BY-NC-SA 4.0 license and was authored, remixed, and/or curated by LibreTexts.

9.4.1: Iron-sulfur Proteins and Models

Iron sulfide proteins involved in electron transfer are called *ferredoxins* and *rubredoxins*.* The ferredoxins were discovered first, and were originally classified as bacterial (containing Fe_4S_4 clusters) and plant (containing Fe_2S_2 clusters) ferredoxins. This classification is now recognized as being not generally useful, since both Fe_2S_2 and Fe_4S_4 ferredoxins are found in plants,[14,15] animals,[2,6,16] and bacteria.[4] Ferredoxins are distinguished from rubredoxins by their possession of acid-labile sulfide; i.e., an inorganic S^{2-} ion that forms H_2S gas upon denaturation at low pH. Rubredoxins have no acid-labile sulfide, and generally have a single iron in a more or less isolated site. Despite their lack of acid-labile sulfide, rubredoxins are included in this chapter because they have sequences much like those of the ferredoxins, and because their simple mononuclear Fe^{2+} and Fe^{3+} sites provide convenient illustrations of key structural and spectroscopic features.

In most ferredoxins, and in all rubredoxins, the protein ligands are cysteines, which provide four thiolate donors to the 1Fe, 2Fe, or 4Fe center. Additionally, the existence of 3Fe centers and of Fe-S sites that contain a second metal (i.e., heteronuclear clusters) make the Fe-S class a broad and multifunctional one.

Simple cytochromes and simple iron-sulfide proteins are similar, in that both can undergo one-electron transfer processes that are generally uncoupled from proton-, atom-, or group-transfer processes. Some of these proteins, such as cytochrome c_3 from *Desulfovibrio* with four hemes[17] or ferredoxin from *Clostridium pasteurianum* with two Fe_4S_4 centers,[6] can transfer more than one electron, because they have multiple copies of a one-electron transfer group. The cytochromes were discovered in 1886 by McMunn,[18] and their role in metabolism was discovered in the 1920s by Keilin (Chapter 6). The intense optical absorbance of these heme-containing proteins contributed singularly to their discovery and biochemical characterization. In contrast, the iron-sulfur proteins, although red to red-brown, absorb far more weakly in the visible region than do the cytochromes. Their presence is sometimes obscured by the cytochromes, and their frequent air instability made their initial recognition and isolation more difficult. It was not until the early 1960s that discoveries by several research groups[19] led to the isolation, recognition, and characterization of the ferredoxins. The use of EPR spectroscopy and its application to biological systems had a profoundly stimulating effect on the field (see below).

Although cytochromes were discovered first, the ferredoxins are likely to be the older proteins from an evolutionary perspective.[20] Ferredoxins have relatively low-molecular-weight polypeptide chains, require no organic prosthetic group, and often lack the more complex amino acids. In fact, the amino-acid composition in clostridial ferredoxin is close to that found in certain meteorites.[21]

The various Fe-S sites found in electron-transfer proteins (ferredoxins) are also found in many enzymes,[6,11,22.23] where these centers are involved in intraor interprotein electron transfer. For example, sulfite reductase contains a siroheme and an Fe_4S_4 center,[24] which are strongly coupled and involved in the sixelectron reduction of SO_3^{2-} to H_2S. Xanthine oxidase (see Figure 7.1) has two identical subunits, each containing two different Fe_2S_2 sites plus molybdenum and FAD sites. In xanthine oxidase, the Mo(VI) site carries out the two-electron oxidation of xanthine to uric acid, being reduced to Mo(IV) in the process.[25] The Mo(VI) site is regenerated by transferring electrons, one at a time, to the Fe_2S_2 and flavin sites, thereby readying the Mo site for the next equivalent of xanthine. Although the Fe_2S_2 sites do not directly participate in substrate reactions, they are essential to the overall functioning of the enzyme system. The Fe_2S_2 centers in xanthine oxidase play the same simple electron-transfer role as the Fe_2S_2 ferredoxins play in photosynthesis.

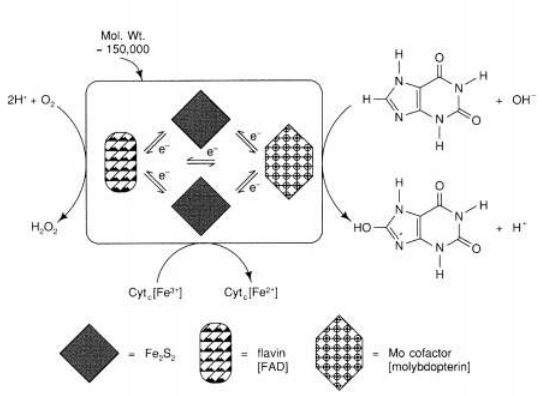


Figure 7.1 - A schematic drawing of xanthine oxidase illustrating the Mo, flavin, and Fe_2S_2 sites and interaction of the enzyme with substrate and oxidant(s).

Structurally, all the iron-sulfur sites characterized to date are built up of (approximately) tetrahedral iron units (see Figure 7.2). In rubredoxins the single iron atom is bound in tetrahedral coordination by four thiolate ligands provided by cysteine side chains. In two-iron ferredoxins the Fe_2S_2 site consists of two tetrahedra doubly bridged through a pair of sulfide ions, i.e., $Fe_2(\mu_2\text{-}S)_2$, with the tetrahedral coordination of each Fe completed by two cysteine thiolates. In four-iron or eight-iron ferredoxins, the 'thiocubane' Fe_4S_4 cluster consists of four tetrahedra sharing edges with triply bridging S^{2-} ions, i.e., $Fe_4(\mu_3\text{-}S)_4$, with each Fe completing its tetrahedron by binding to a single cysteine thiolate. Finally, for Fe_3S_4 clusters, which are now being found in more and more proteins, the well-established structure has one triply bridging and three doubly bridging sulfide ions, $Fe_3(\mu_3\text{-}S)(\mu_2S)_3$. The Fe_3S_4 unit can be thought of as derived from the 'thiocubane' Fe_4S_4 unit by the removal of a single iron atom.

In what follows we will introduce these structures in the order 1Fe, 2Fe, 4Fe, and 3Fe. For each, we will first discuss the physiological role(s) of the particular proteins, then the structural features, followed by the spectroscopic properties and model systems.

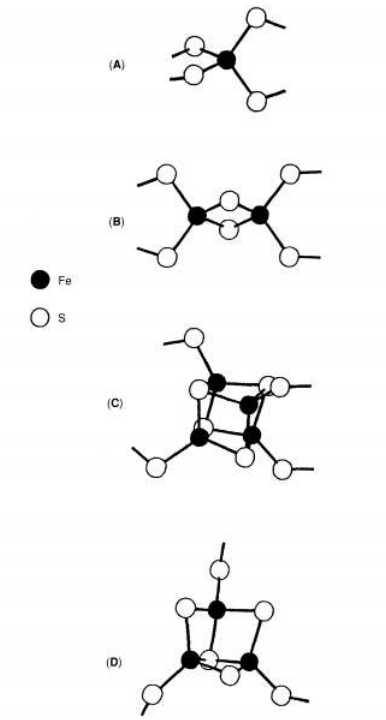


Figure 7.2 - Structural systematics of Fe-S units found in proteins: (A) rubredoxin single Fe center; (B) Fe_2S_2 unit; (C) Fe_4S_4 unit; (d) Fe_3S_4 unit.

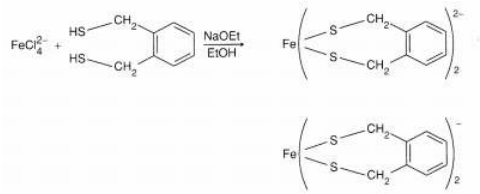
* For review articles, see References 1-11. For a discussion of nomenclature, see References 12 and 13.

9.4.1: Iron-sulfur Proteins and Models is shared under a CC BY-NC-SA 4.0 license and was authored, remixed, and/or curated by LibreTexts.

9.4.2: Iron-sulfur Proteins and Models (Part 2)

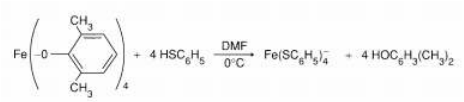
Rubredoxin Model Systems

The simple mononuclear tetrahedral site of Rd has been chemically modeled in both its reduced and its oxidized forms. The bidentate o-xylyl-α,α'-dithiolate ligand forms bis complexes of Fe(II) and Fe(III) that have spectroscopic features quite similar to those of the protein.[62,63] The preparative procedure is relatively straightforward (Equation 7.1).



The UV-visible-NIR spectra, Mössbauer spectra, and magnetic susceptibility differ only slightly from those of oxidized and reduced rubredoxins.

The monodentate benzenethiolate (thiophenolate) ligand, $C_6H_5S^-$, similarly forms the ferrous $Fe(SC_6H_5)_4^{2-}$ complex.[64,65] Although for some time it was felt that the oxidized form, $Fe(SC_6H_5)_4^-$, was inherently unstable, the sterically hindered monothiolate ligand 2,3,5,6-tetramethylbenzenethiolate was found to form[66-68] a stable, quite symmetric Fe(III) tetrathiolate anion. Armed with this information, the preparation of the tetrakis(benzenethiolate) Fe(III) complex was reinvestigated, and the complex successfully synthesized[67] (Equation 7.2).



The Fe(III) and Fe(II) tetrathiolate species now serve as excellent structural models for the Fe sites of both oxidized and reduced Rd.[69]

The structural parameters for the oxidized rubredoxin analogues are very similar to those of the oxidized Rd iron site. The reduced complexes reveal a lengthening of the average Fe-S bond from 2.27 to 2.36 Å, consistent with the change in oxidation state from ferric to ferrous. The addition of an electron has a more profound structural effect in this single-iron center than in some of the multiiron clusters, where electrons are more delocalized.

Clearly, for the single-Fe sites, the dominant structural feature is their near-tetrahedral tetrathiolate coordination. The dominant electronic structural feature is the presence of high-spin Fe^{3+} and Fe^{2+} sites. The important mode of chemical reactivity is a simple one-electron transfer. Each of these features carries over to the 2Fe, 4Fe, and 3Fe sites discussed below.

Fe_2S_2 Ferredoxins

The simple 2Fe-2S proteins are sometimes referred to as "plant" or "plant-type" ferredoxins. The protein from spinach, which serves as an electron acceptor in the photosynthetic apparatus,[14,15,50,70] was among the first to be wellcharacterized and widely studied, and could be considered the prototypical 2Fe-2S ferredoxin, However, 2Fe-2S proteins are also well-known in bacteria.[4] The protein from the cyanobacterium (blue-green alga) *Spirulina platensis* has been structurally elucidated by x-ray crystallography.[47] Putidaredoxin, from *Pseudomonas putida*, which serves as a donor to the P-450 camphor monooxygenase system, has been extensively studied.[28] Fe_2S_2 centers are also well-established in mammalian proteins. Adrenodoxin[29] serves as the electron donor to the P-450 monooxygenase system that carries out the 11-β-hydroxylation of steroids, The so-called "Rieske proteins" are found in the bc_1 complex of mitochondria[47] as well as in the bd complex of the photosynthetic apparatus of plants.[71] In addition, Fe_2S_2 centers are well-known constituents of such redox proteins as xanthine oxidase,[25,72] CO oxidase,[25] succinate dehydrogenase,[73-75] and putidamonooxin.[76] Table 7.1 lists some of the Fe_2S_2 proteins and their properties.

The x-ray crystal structure of only the single 2Fe-2S protein mentioned above has been determined;[70a] the 2Fe-2S ferredoxin from the blue-green alga Spirulina platensis[6,22,47,77,78] shows significant sequence identity with chloroplast ferredoxins typical of higher plants.[79,80] As Figure 7.8 shows, the Fe_2S_2 unit in this 11-kDa protein is bound by Cys-41, Cys-46, Cys-49, and Cys-79, The

binuclear iron cluster is found in a largely hydrophobic region of the protein, but is within 5 Å of the protein surface.[6] The sulfur atoms of the cluster, both inorganic and cysteinyl, are hydrogen-bonded to six peptide NH groups and one serine OH group, which presumably stabilize the cluster/protein complex, The serine involved in the H-bonding, Ser-40, is conserved in all plant and algal 2Fe-2S ferredoxins sequenced, which implies that it plays a crucial structural or functional role.

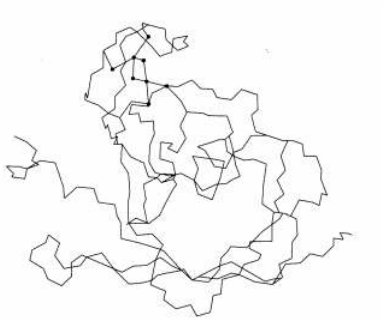


Figure 7.8 - The x-ray crystal structure of the Fe_2S_2 ferredoxin from Spirulina platensis.[70a]

The structure of the 2Fe-2S core in Figure 7.2 reveals a tetrahedron of S ligands surrounding each Fe atom. The two tetrahedra share an edge defined by the two bridging sulfide ions, and the core structure is designated $Fe_2(\mu_2\text{-}S)_2$. Fe-S distances and angles cannot be measured accurately in the structure at the present 2.5-Å resolution;[70a] so we will later discuss these details in terms of model compounds.

The Fe_2S_2 center shows nicely how spectroscopy can be used to deduce the structure of an active site. Indeed, in this case the now well-established active-site structure was deduced by a combination of chemical, spectroscopic, and magnetic methods, and the site was successfully modeled long before the first protein crystallographic study was reported. The presence of acid-labile, inorganic sulfide is a key feature of both the Fe_2S_2 and the Fe_4S_4 centers. The 1:1 stoichiometry between iron and acid-labile sulfide was eventually established analytically for Fe_2S_2 centers.[9-11] Care must be taken to ensure that both the protein and its active-site complement are homogeneous. Although protein homogeneity is usually established by electrophoretic methods, these methods may not distinguish between pure proteins and those with absent or incomplete active centers. Fortunately, absorption at 420 nm is due solely to the Fe_2S_2 cluster, whereas the 275-nm absorption is dominated by the protein. Therefore a good criterion for active-site saturation and homogeneity is the ratio of the absorbances at 420 and 275 nm, $A_{420\ nm}/A_{275\ nm}$, which is ~0.48 for pure spinach ferredoxin.[81] Once homogeneous protein is obtained, the Fe_2S_2 composition of the "plant" ferredoxins can be correctly deduced analytically.

The Fe_2S_2 center displays two redox states that differ by a single electron. The potential range for the couple is -250 to -420 mV, revealing the highly reducing nature of the ferredoxin. The correct structure of the Fe_2S_2 center was first proposed in 1966 based on EPR studies.[82] The reduced state of the cluster shows a rhombic EPR signal with g values of 1.88, 1.94, and 2.04 (Figure 7.6B) characteristic of an $S = \frac{1}{2}$ center. The oxidized state is EPR-silent. The weakness of the sulfur ligand field causes the iron atoms to be high-spin. But how can two sulfur-ligated iron atoms, each with a tendency to be high-spin, produce a state with a single unpaired electron?

The individual Fe atoms in the Fe_2S_2 cluster resemble those in rubredoxin quite closely. The two redox states of the Fe_2S_2 protein correspond to an Fe^{3+}-Fe^{3+} and an Fe^{3+}-Fe^{2+} pair, respectively, as shown in Figure 7.9. In the all-ferric oxidized state, the two Fe^{3+} sites are antiferromagnetically coupled; i.e., the spins of the five d electrons on the two iron atoms are oppositely aligned, such that their pairing produces an effective S = 0, diamagnetic ground state. In the reduced form, a single unpaired electron is present, because the $S = \frac{5}{2}$ Fe^{3+} and S = 2 Fe^{2+} sites are antiferromagnetically coupled, leaving one net unpaired spin and an $S = \frac{1}{2}$ ground state. The profound difference between the electronic properties of rubredoxin and Fe_2S_2 ferredoxin arises because the latter has two Fe atoms in close proximity, which allows for their magnetic coupling.

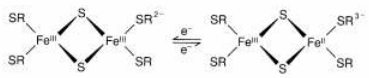


Figure 7.9 - Redox states of Fe_2S_2 proteins: (A) reduced; (B) oxidized.

Strong support for the spin-coupling model in Fe_2S_2 ferredoxins comes from a detailed analysis of their absorption and circular dichroism spectra.[83] As with rubredoxin (see Figure 7.5), we expect no low-energy spin-allowed d-d bands for the ferric site in either the oxidized or the reduced state. Indeed, the oxidized state containing all Fe^{3+} shows no low-energy bands; the reduced state containing a single Fe^{2+} displays low-energy, low-intensity bands in the region 4,000-9,000 cm^{-1}, in close analogy to the situation in reduced rubredoxin. The combined EPR and optical spectra leave little doubt about the structural assignment: two coupled high-spin ferric ions in the oxidized state, and coupled high-spin ferric and ferrous ions in the reduced state. Moreover, the spectra are consistent only with a localized model, i.e., one in which the Fe(II) site is associated with a single iron.[83,83a] The Fe_2S_2 site is inherently asymmetric, and inequivalence of the Fe(llI) sites is spectroscopically detectable in the all-ferric oxidized form.[84] In fact, the localized valence trapping is present in reduced model compounds that contain no ligand asymmetry.

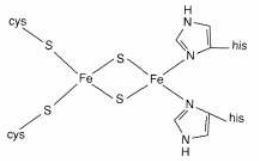
Mössbauer spectra provide additional and striking confirmation of the structural assignment. The spectrum of the oxidized ferredoxin (Figure 7.7) resembles strongly that of oxidized rubredoxin, indicating the presence of high-spin Fe^{3+}, even though the net spin is zero. In the reduced form, the Mössbauer spectrum involves the superposition of signals from a high-spin Fe^{2+} and a high-spin Fe^{3+}, i.e., a reduced and an oxidized rubredoxin, respectively. Clearly, the simplest interpretation of this result consistent with the S = $\frac{1}{2}$ spin state required by the EPR is the localized Fe^{2+}-Fe^{3+} antiferromagnetic coupling model discussed above.

NMR studies of oxidized Fe_2S_2 proteins reveal broad isotropically shifted resonances for the CH_2 protons of the cysteine ligands.[85] Despite the coupling of the irons, the net magnetism at room temperature is sufficient to lead to large contact shifts (-30 to -40 ppm downfield from TMS). The assignment of the resonance was confirmed with the synthesis and spectroscopic analysis of model compounds.[86] Extensive NMR studies of the Fe_2S_2 proteins have been reported.[87,87a]

Resonance Raman spectra of Fe_2S_2 sites[88,89,90] reveal many bands attributable to Fe-S stretching. Detailed assignments have been presented for the four bridging and four terminal Fe-S modes. A strong band at 390 cm^{-1}, which shifts on ^{34}S sulfide labeling, is assigned to the A_{1g} "breathing" mode; another band at 275 cm^{-1} is assigned to B_{3u} symmetry in point group D_{2h}.[57,88] Spectroscopic differences in the terminal, Fe-S(Cys) stretches between plant ferredoxins and adrenodoxin (which also differ somewhat in redox potential) seem to reflect different conformations of the cysteine ligands in the two classes. Evidence for asymmetry of the iron atoms is found in the intensity of the resonance enhancement of certain modes.

Rieske Centers

Within the class of Fe_2S_2 ferredoxins there is a subclass called the Rieske proteins, or the Rieske centers.[47,91,92] The Rieske iron-sulfur centers are found in proteins isolated from mitochondria and related redox chains.[47,92] In addition, the phthalate dioxygenase system from *Pseudomonas cepacia*[93,94] contains one Fe_2S_2 Rieske center as well as one additional nonheme Fe atom. Although the Rieske centers appear to contain an Fe_2S_2 core, there is extensive evidence for nonsulfur ligands coordinated to at least one of the Fe atoms. The proposed model in Scheme (7.3) has two imidazole ligands bound to one Fe atom. The nitrogen atoms are seen in ENDOR (Electron Nuclear Double Resonance) experiments,[93] and are manifest in EXAFS spectra, which are consistent with the presence of a low-Z (atomic number) ligand bound to iron.[94] The potentials for the Rieske proteins range from +350 to -150 mV,[47] in contrast to the plant-type Fe_2S_2 centers, which range from -250 to -450 mV. The strong dependence of redox potential on pH[95] suggests a possible role in coupling protonand electron-transfer processes.



Fe_2S_2 Models

Although spectroscopic studies led to the correct deduction of the structure of the Fe_2S_2 core, the synthesis of model compounds containing this core provided unequivocal confirmation. The model compounds allowed detailed structural analysis unavailable for the proteins. Moreover, by using a uniform set of peripheral ligands, properties inherent to the Fe_2S_2 core could be discerned.

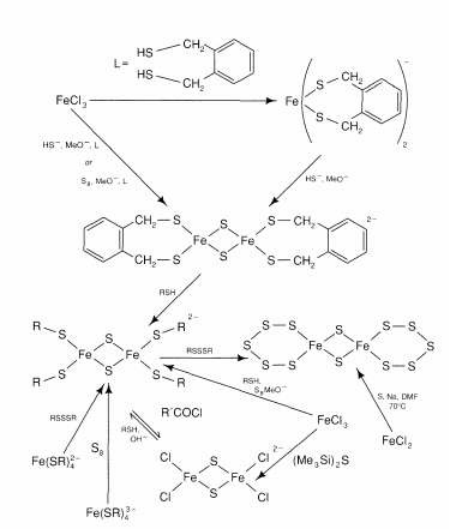


Figure 7.10: Preparative schemes leading to complexes containing the Fe_2S_2 core.[128]

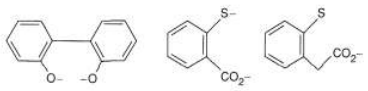
The Fe_2S_2 core has been synthesized by several routes[86,96a,b,c,d] (see Figure 7.10). For example, the reaction of $Fe(SR)_4^{2-}$, the ferrous rubredoxin model, with elemental sulfur produces the complex $Fe_2S_2(SR)_4^{2-}$. In this reaction the sulfur presumably oxidizes the Fe^{2+} to Fe^{3+}, being reduced to sulfide in the process. The Fe_2S_2 core has been prepared with a variety of peripheral S-donor ligands. Metrical details for $Fe_2S_2(SC_6H_4\text{-}p\text{-}CH_3)_4^{2-}$ are given in Table 7.3. Notable distances are the Fe-S (bridging) distance of 2.20 Å, the Fe-S (terminal) distance of 2.31 Å, and the Fe-Fe distance of 2.69 Å.

Table 7.3: Structural parameters for $Fe_2S_2(SC_6H_4-p-CH_3)_4^{2-}$. a) Data from Reference 211.

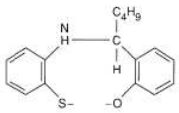
Atoms[a]	Distance Å	Atoms[a]	Angle[a]
Fe-Fe	2.691 (1)	Fe-S-Fe	75.3
Fe-S1 (bridge)	2.200 (1)	S-Fe-S	104.6
Fe-S2 (bridge)	2.202 (1)	S-Fe-S	115.1
Fe-S3	2.312 (1)	S-Fe-S	105.4

To date, all analogue systems structurally characterized contain the Fe^{3+}-Fe^{3+} fully oxidized form. Attempts to isolate the Fe^{3+}-Fe^{2+} form have so far failed. However, the mixed-valence Fe_2S_2 form can be generated and trapped by freezing for spectroscopic examination.[97,98] Mössbauer spectroscopy reveals the presence of distinct Fe^{2+} and Fe^{3+} ions, as found in the proteins, clearly showing that "trapped" valence states are an inherent characteristic of the $Fe_2S_2^{2+}$ core and are *not* enforced by the protein.[97,98]

The existence of noncysteine-bound Fe_2S_2 cores in Rieske-type proteins has led to attempts to synthesize complexes with oxygen and nitrogen ligands.[99-101] Characterized species include $Fe_2S_2(OC_6H_5)_4^{2-}$, $Fe_2S_2(OC_6H_4\text{-}p\text{-}CH_3)_4^{2-}$, $Fe_2S_2(C_4H_4N)_4^{2-}$, and $Fe_2S_2(L)_2^{2-}$, where L is a bidentate ligand.



The potentially tridentate ligand



acts in a bidentate fashion, binding through S and O but not N.

No Fe_2S_2 complexes containing mixed S,N terminal ligands, such as those suggested for the Rieske site, have been prepared. The Se^{2-} bridged analogue has been prepared for some of the complexes.[102,103]

9.4.2: Iron-sulfur Proteins and Models (Part 2) is shared under a CC BY-NC-SA 4.0 license and was authored, remixed, and/or curated by LibreTexts.

9.4.3: Iron-sulfur Proteins and Models (Part 3)

Fe_4S_4 Ferredoxins (including HiPIPs)

We now turn our attention to proteins containing the Fe_4S_4 center. Historically, within this class a strong distinction was made between the "ferredoxins," which are low-potential (as low as -600 mV in chloroplasts) iron-sulfur proteins, and the "HiPIPs" = High Potential Iron Proteins, which have positive redox potentials (as high as +350 mV in photosynthetic bacteria). Although the HiPIP designation is still useful, proteins of both high and low potential are considered ferredoxins, whose key defining feature is the presence of iron and acid-labile sulfide.[13]

The Fe_4S_4 proteins participate in numerous electron-transfer functions in bacteria, and in some organisms (such as *Clostridium*) are the immediate electron donors for the nitrogenase and/or hydrogenase enzymes. The function of the HiPIPs seems obscure at present. In addition, Fe_4S_4 centers have been shown or postulated to occur in numerous microbial, plant, and mammalian redox enzymes, including nitrate reductase,[104] sulfite reductase,[24] trimethylamine dehydrogenase,[105] succinate dehydrogenase,[73,106] hydrogenase, and, possibly, in altered forms, nitrogenase. Table 7.1 lists some of the Fe_4S_4 ferredoxins and their properties.

In the Fe_2S_2 ferredoxins, combined spectroscopic, analytical, and model-system work led to an unequivocal assignment of the structural nature of the active site long before the crystallography was done. In contrast, for Fe_4S_4 systems and in particular the 8Fe-8S = $2Fe_4S_4$ systems from bacteria, the initial chemical suggestions were fallacious, and even the number and stoichiometry of the clusters were in doubt. In these cases, crystallography provided the definitive structural information.

The first indication of the presence of the "thiocubane" structure came in 1968, when a 4-Å resolution study[107] indicated a compact cluster of potentially tetrahedral Fe_4 shape in the HiPIP from *Chromatium vinosum*. This finding did not lead to much excitement, since it was not yet appreciated that HiPIPs and ferredoxins were structurally similar. In 1972, the high-resolution structure solution of both *Chromatium* HiPIP[108] and the 8Fe ferredoxin from *Peptococcus aerogenes* (formerly *Microbacter aerogenes*)[101] confirmed the presence of virtually identical thiocubane clusters in the two proteins.[108] Moreover, the structures for both oxidized and reduced HiPIP were deduced, and these revealed that the Fe_4S_4 cluster remained intact during the redox interconversion.[109] Subsequently, four-iron clusters have been crystallographically confirmed in an Fe_4S_4 ferredoxin from *Bacillus thermoproteolyticus*,[110,110a] in *Azotobacter vinelandii* ferredoxin I (also previously called Shethna Fe-S protein II), which also contains a 3Fe-4S cluster,[111,112] in the active form of aconitase,[113] and in sulfite reductase, where the cluster is probably bridged by cysteine sulfur to a siroheme.

In all the proteins characterized to date, the Fe_4S_4 clusters adopt the thiocubane structure,[108] which is discussed at greater length in the section on models. The clusters are usually bound to their proteins by four cysteine residues. As shown in Figure 7.11, in the *P. aerogenes* protein the two Fe_4S_4 clusters are bound by cysteines numbered 8, 11, 14, 18, 35, 38, 41, and 45.[101,114] The presence of the Cys-x-x-Cys unit is again apparent. However, this sequence seems prominent in all Fe-S proteins, and so is not specific for a particular Fe-S site. At first glance one might expect one cluster to be bound by cysteines 8,11,14, and 18, the other by cysteines 35, 38, 41, and 45. Actually, one cluster is bound by cysteines 8, 11, 14, and 45, the other by cysteines 35, 38, 41, and 18. The binding of a given cluster by cysteine residues from different portions of the polypeptide chain apparently helps stabilize the tertiary structure of the protein and brings the two clusters into relatively close proximity, the center-center distance being 12 Å.[114]

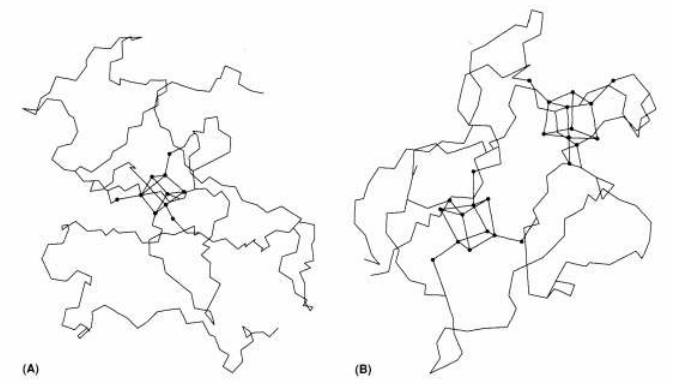


Figure 7.11 - The x-ray crystal structures of (A) *Chromatium vinosum* HiPIP[108] and (B) the 8Fe-8S ferredoxin from *Peptococcus aerogenes*.[101]

The *C. pasteurianum* protein displays weak magnetic coupling, which leads to an unusual EPR spectrum[115] consistent with the 12-Å cluster-cluster separation. However, the redox potentials for the two sites seem virtually identical at -412 mV, thus allowing the 8Fe ferredoxin to deliver two electrons at this low redox potential.[115] Significant sequence identity indicates the likelihood that other 8Fe ferredoxins, such as the well-studied one from *C. pasteurianum*,[116-118] have quite similar structures.

The thiocubane unit of Fe_4S_4 proteins can exist in proteins in at least three stable oxidation states. This so-called three-state model[74,109,119,120] contrasts dramatically with the situation for Rd(1Fe), Fe_2S_2, and Fe_3S_4 systems, in which only two oxidation states are accessible through simple electron transfer for each center. For the thiocubane structure, the three accessible states can be designated $Fe_4S_4^{3+}$, $Fe_4S_4^{2+}$, and $Fe_4S_4^{+}$, corresponding to $[Fe(III)_2Fe(II)]$, $[Fe(III)_2Fe(II)_2]$, and $[Fe(III)Fe(II)_3]$ valence-state combinations, respectively. It is crucial to note that, in sharp contrast to the Fe_2S_2 and Fe_3S_4 sites, the oxidation states are not localized in the Fe_4S_4 clusters. In most cases, each Fe atom behaves as if it had the same average oxidation level as the other Fe atoms in the cluster. The redox interconversion of the Fe4S4 sites is shown in Figure 7.12. The $Fe_4S_4^{3+} \rightleftharpoons Fe_4S_4^{2+}$ couple is the high-potential redox couple characteristic of HiPIPs; the $Fe_4S_4^{2+} \rightleftharpoons Fe_4S_4^{+}$ couple is responsible for the low-potential process characteristic of the classical ferredoxins. In any given protein under physiological conditions, only one of the two redox couples appears to be accessible and functional.

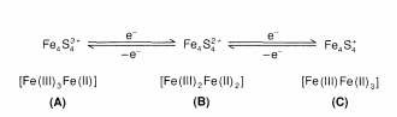


Figure 7.12 - The redox interconversions of Fe_4S_4 sites illustrating the three-state model. The states are found in (A) oxidized HiPIP; (B) reduced HiPIP and oxidized ferredoxin; (C) reduced ferredoxin.

Both the $Fe_4S_4^{+}$ and the $Fe_4S_4^{3+}$ states of the thiocubane cluster are paramagnetic and display characteristic EPR spectra (Figure 7.6C,D). The $Fe_4S_4^{3+}$ site in reduced ferredoxins[46,48,49,119] displays a rhombic EPR signal (Figure 7.6C) with g = 1.88, 1.92, and 2.06. The oxidized form of low-potential ferredoxins is EPR-silent, and attempts to "superoxidize" it to achieve the $Fe_4S_4^{3+}$ state invariably lead to irreversible cluster decomposition, probably through a 3Fe-4S structure. The $Fe_4S_4^{3+}$ signal is usually referred to as the HiPIP signal (Figure 7.6D) and shows distinct g values at 2.04($g_\perp$) and 2.10($g_\parallel$); it is present in oxidized HiPIP but absent in reduced HiPIP.[46,119] Reduction of HiPIP to a "super-reduced" state apparently occurs under partially denaturing conditions in aqueous DMSO.[108] The observed axial EPR signal with g = 1.94 and 2.05 is assigned to the $Fe_4S_4^{+}$ state characteristic of reduced ferredoxins. This result[108] is consistent with structural and spectroscopic identity of the HiPIP and Fd sites, as required by the three-state model of the Fe_4S_4 proteins (Figure 7.12).

In Fe_4S_4 centers at each level of oxidation, electronic transitions give rise to characteristic visible and UV spectra, although the delocalized nature of the electronic states makes detailed assignment difficult. MCD spectra of clusters in the three states of oxidation are clearly distinguishable from each other and from MCD of Fe_2S_2 clusters.[43,119] MCD, magnetic susceptibility, and Mössbauer spectra provide evidence that the S = $\frac{1}{2}$ state, whose EPR signal is so distinct in reduced ferredoxins, may coexist at higher T with S = $\frac{3}{2}$ and perhaps even higher spin states. Indeed, recent studies with model systems[121,122] and theoretical treatments[123,124] clearly support the ability of the Fe_4S_4 cluster to display a number of spin states that are in labile equilibria, which are influenced, perhaps quite subtly, by local structural conditions. The iron protein of nitrogenase also displays this behavior.

The Mössbauer spectra of Fe_4S_4 centers of ferredoxins reveal the equivalence of the Fe sites, and quadrupole splittings and isomer shifts at averaged values for the particular combination of oxidation states present.[3,51,52] Representative spectra are shown in Figure 7.7. Magnetic coupling is seen for the paramagnetic states.

Resonance Raman spectra (and IR spectra) have been extensively investigated in *C. pasteurianum* ferredoxin and in model compounds.[57,125] Selective labeling of either thiolate sulfur or sulfide sulfur with ^{34}S allows modes associated with the Fe_4S_4 core to be distinguished from modes associated with the FeSR ligands. The band at 351 cm^{-1} is assigned to Fe-SR stretching, and Fe_4S_4 modes occur at 248 and 334 cm^{-1} in reduced ferredoxin from *C. pasteurianum.* There is little difference between the oxidized and reduced spectra, although an extra band at 277 cm^{-1} seems present in the oxidized protein. The Fe_4Se_4 substituted protein has also been studied.[125]

As in the 1Fe and 2Fe proteins, ^1H NMR spectra reveal resonances from contact-shifted-CH_2-groups of cysteinyl residues.[125a] However, unlike the other proteins, where all states are at least weakly magnetic, only the reduced ferredoxin and the oxidized HiPIP states show contact shifts.[87a,125a,b,c]

EXAFS studies on proteins and on model compounds clearly identify the Fe-S distance of ~2.35 Å and an Fe-Fe distance of 2.7 Å. These distances, as expected, vary only slightly with state of oxidation.[125d]

Fe_4S_4 Models

Judging from the ease with which models of Fe_4S_4 are prepared under a variety of conditions and their relative stability, the $Fe_4S_4^{2+}$ core structure seems to be a relatively stable entity, a local thermodynamic minimum in the multitude of possible iron-sulfide-thiolate complexes. The initial preparation and structural characterization[126,127] of the models showed that synthetic chemistry can duplicate the biological centers in far-simpler chemical systems, which can be more easily studied in great detail.

The general synthetic scheme for Fe-S clusters is shown in Figure 7.13. Many different synthetic procedures can be used to obtain complexes with the Fe_4S_4 core.[126-138,138a,b] The multitude of preparative procedures is consistent with the notion that the $Fe_4S_4^{2+}$ core is the most stable entity present and "spontaneously self-assembles" when not limited by stoichiometric constraints.

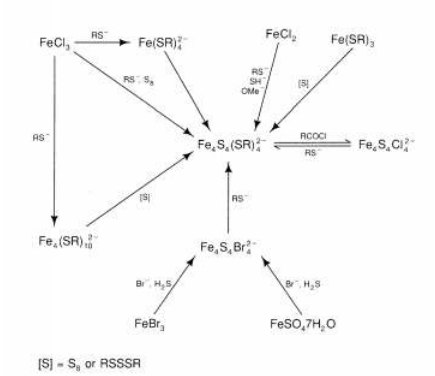


Figure 7.13 - Preparative schemes leading to complexes containing the Fe_4S_4 core.[128]

The thiocubane structure can be viewed as two interpenetrating tetrahedra of 4Fe and 4S atoms. The 4S tetrahedra are the larger, since the S-S distance is ~3.5 Å, compared with the Fe-Fe distance of ~2.7 Å. The S_4 tetrahedron encloses ~2.3 times as much volume as does the Fe_4 tetrahedron.[128] Key distances and angles for $Fe_4S_4(SCH_2C_6H_5)_4^{2-}$ given in Table 7.4 are extremely similar to those found in oxidized ferredoxin and reduced HiPIP centers in proteins.[127]

Table 7.4 - Structural parameters for $Fe_4S_4(SCH_2C_6H_5)_4^{2-}$.

a) Data from References 126 and 127.

Atoms[a]	Average Distances	Number of Bonds	Type
Fe(1)-S(3)	2.310 (3)	8	Sulfide
Fe(1)-S(2)	2.239 (4)	4	Sulfide
Fe(1)-S(5)	2.251 (3)	4	Thiolate
Fe(1)-Fe(2)	2.776 (10)	2	
Fe-Fe(other)	2.732 (5)	4	

Atoms[a]	Average Distances	Number of Bonds	Type
Fe-S-Fe	73.8 (3)	12	
S-Fe-S	104.1 (2)	12	Sulfide-Fe-Sulfide
S-Fe-S	111.7-117.3	12	Sulfide-Fe-Thiolate

The idealized symmetry of $Fe_4S_4^{2+}$ model systems is that of a regular tetrahedron, i.e., T_d. Though the distortion of the cube is quite pronounced, all known examples of the Fe_4S^{2+} core show distortion, which lowers the symmetry at least to D_{2d}. In most Fe_4S^{2+} core structures, this distortion involves a tetragonal compression, which leaves four short and eight long Fe-S bonds.

Complexes with non-S-donor peripheral ligands have been prepared and studied. The halide complexes $Fe_4S_4X_4^{2-}$ (X = Cl^-, Br^-, I^-) have been prepared, and serve as useful starting points for further syntheses.[129-133] The complex $Fe_4S_4(OC_6H_5)_4^{2-}$ can be prepared[134] from the tetrachloride (or tetrathiolate) thiocubane by reaction with $NaOC_6H_5$ (or HOC_6H_5). There are a few examples of synthetic $Fe_4S_4^{2+}$ cores in which the peripheral ligands are not identical. For example, $Fe_4S_4Cl_2(OC_6H_5)_2^{2-}$ and $Fe_4S_4Cl_2(SC_6H_5)_2^{2-}$ have structures characterized by D_{2d} symmetry.[135] The complexes $Fe_4S_4(SC_6H_5)_2[S_2CN(C_2H_5)_2]^{2-}$ and $Fe_4S_4(SC_6H_4OH)_4^{2-}$ are similarly asymmetric, containing both four- and five-coordinate iron.[136-138] The presence of five-coordinate iron in the Fe_4S_4 cluster is notable, since it offers a possible mode of reactivity for the cluster wherever it plays a catalytic role (such as in aconitase). Complexes with Fe_4Se^{2+} and $Fe_4Te_4^{2+}$ cores have also been prepared.[138c,d]

One structural analysis of $Fe_4S_4(SC_6H_5)_4^{3-}$, which contains the reduced $Fe_4S_4^+$ core, revealed a tetragonal elongation[139] in the solid state. In contrast, analysis of $Fe_4S_4(SCH_2C_6H_5)_4^{3-}$ revealed a distorted structure possessing C_{2v} symmetry.[102] It would appear that the $Fe_4S_4^+$ clusters maintain the thiocubane structure, but are nevertheless highly deformable. Interestingly, when the solidstate C_{2v} structure, $Fe_4S_4(SCH_2C_6H_5)_4^{3-}$, is investigated in solution, its spectroscopic and magnetic behavior change to resemble closely those of the $Fe_4S_4(SC_6H_5)_4^{3-}$ cluster,[140] which does not change on dissolution. The simplest interpretation assigns the elongated tetragonal structure as the preferred form for $Fe_4S_4^+$ cores with deformation of sufficiently low energy that crystal packing (or, by inference, protein binding forces) could control the nature of the distortions in specific compounds.[128] The elongated tetragonal structure has four long and eight short bonds in the core structure. The terminal (thiolate) ligands are 0.03-0.05 Å longer in the reduced structure, consistent with the presence of 3Fe(ll) and 1Fe(III) in the reduced form, compared to 2Fe(II) and 2Fe(III) in the oxidized form. There is no evidence for any valence localization.[128]

The oxidized $Fe_4S_4^{3+}$ core defied isolation and crystallization in a molecular complex prior to the use of sterically hindered thiolate ligands. With 2,4,6 tris(isopropyl)phenylthiolate, the $Fe_4S_4L_4^-$ complex could be isolated and characterized.[141] The structure is a tetragonally compressed thiocubane with average Fe-S and Fe-SR distances 0.02 and 0.04 Å shorter than the corresponding distances in the $Fe_4S_4L_4^{2-}$ complex. Again, there is no evidence for Fe inequivalence or more profound structural distortion in this 3Fe(III)-1Fe(II) cluster. Clearly, the Fe_4S_4 clusters have highly delocalized bonding.

Evidence from model systems using sterically hindered thiolate ligands indicates the existence of an $Fe_4S_4^{4+}$, i.e., all-ferric fully oxidized cube.[142] The existence of the complete series $Fe_4S_4[(Cy)_3C_6H_2S]_4^n$ (Cy =cyclohexyl; n = 0, -1, -2, -3) is implied by reversible electrochemical measurements. Clearly, five different states of the Fe_4S_4 core—including the (at least) transient fully oxidized state and the all-ferrous fully reduced state—may have stable existence. Although only the central three states have been shown to exist in biological contexts, one must not rule out the possible existence of the others under certain circumstances.

Recently, specifically designed tridentate ligands have been synthesized that bind tightly to three of the four Fe atoms in the thiocubane structure.[143,143a,b] The remaining Fe atom can then be treated with a range of reagents to produce a series of subsite-differentiated derivatives and variously bridged double-cubane units. These derivatives illustrate the potential to synthesize complexes that mimic the more unusual features of Fe_4S_4 centers that are bound specifically and asymmetrically to protein sites. The recently synthesized complex ion $[(Cl_3Fe_4S_4)_2S]^{4-}$, containing two Fe_4S_4 units bridged by a single S^{2-} ligand, illustrates the potential coupling of known clusters into larger aggregates.[143c]

The model-system work has made an important contribution to our understanding of the Fe_4S_4 centers. The existence of three states, the exchange of ligands, the redox properties, the metrical details of the basic Fe_4S_4 unit, and the subtleties of structural distortion can each be addressed through the study of models in comparison with the native proteins.

9.4.3: Iron-sulfur Proteins and Models (Part 3) is shared under a CC BY-NC-SA 4.0 license and was authored, remixed, and/or curated by LibreTexts.

9.4.4: Iron-sulfur Proteins and Models (Part 4)

Core Extrusion/Cluster Displacement Reactions

Synthetic model-system work led to the realization that the cluster cores can exist outside the protein and undergo relatively facile ligand-exchange reactions.[128] This behavior of the purely inorganic complexes allowed core extrusion reactions[128,144] to be developed. The basic assumption behind these reactions is that the cluster core retains its integrity when it is substituted by low-MW thiolates, especially aryl thiolates, which replace the cysteinyl ligands that bind it to the protein. In order to free the cluster from the protein, one must at least partially denature the protein, usually by using ~80 percent aqueous solution of a polar aprotic solvent, such as DMSO or HMPA. The resulting inorganic clusters can be identified and quantified by measurement of their characteristic electronic absorption or NMR spectra. An alternative approach involves transferal of the unknown cluster in question to an apoprotein that binds a cluster of known type.[145]

Since the 1Fe, 2Fe, and 4Fe sites are each usually bound to the protein by four cysteine residues, it is perhaps not surprising that there have been reports[58] of interconversion of cluster types bound to a given protein. Specifically, in 90 percent aqueous DMSO, the single Fe site in rubredoxin from *C. pasteurianum* is converted to an Fe_4S_4 cluster by the addition of sodium sulfide, ferrous chloride, and ferric chloride in ratio 4:2:1. Presumably the spacing and geometric disposition of the cysteines are suitable to bind a single Fe or the Fe_4S_4 cluster, which is readily formed under the reaction conditions. Another example of cluster rearrangement involves the three-iron center discussed below that does *not* extrude as an Fe_3S_4 center. Rather, at least under *certain* conditions, the Fe_{3Sx} center rearranges to form Fe_2S_2 centers.[146] The facile interconversion of the Fe clusters demonstrated the lability of Fe-S systems, and indicates that caution must be exercised in interpreting the results of cluster-displacement reactions.

Fe_3S_4 Centers

Three-iron centers are a comparatively recent finding,[119,146] and the full scope of their distribution is not yet known. Although they have now been confirmed in dozens of proteins, it often remains uncertain what physiological role these centers play. Indeed, since Fe_3S_4 centers can be produced as an artifact upon oxidation of Fe_4S_4 centers, it has been suggested that 3Fe centers may not be truly physiological, and could be side products of aerobic protein isolation. This caveat notwithstanding, the 3Fe sites are being found in more and more proteins and enzymes. Their physiological *raison d' être* may be more subtle than that of their 1, 2, and 4Fe cousins; we should certainly try to find out more about them. Some proteins containing Fe_3S_4 centers are listed in Table 7.1.

The 3Fe center was first recognized[147] in the protein ferredoxin I from the anaerobic nitrogen-fixing bacterium *Azotobacter vinelandii*. The protein is called *Av* FdI for short. It is instructive to sketch historically the evolution of our understanding of this protein. *Av* ferredoxin I was reported to have 6 to 8 Fe atoms and was first thought to resemble the clostridial 8Fe ferredoxins. However, unlike the clostridial protein, the *Av* FdI clusters appeared to have two quite different redox couples at +320 and -420 mV. Although it might have been thought that this protein contained one HiPIP-type and one Fd- or "ferredoxin"-type Fe_4S_4 cluster, the protein as isolated had an EPR signal with g = 2.01, which differed significantly (Figure 7.6) from that of an oxidized HiPIP or a reduced Fd.[148] Cluster extrusion reactions also seemed to indicate the presence of an unusual cluster type.[149]

Fortunately, the protein was crystallized, and could be studied by x-ray diffraction. Unfortunately, the initial conclusions[150] and subsequent revisions[151,152] of the crystal-structure analysis have proven to be wrong, teaching us in the process that protein x-ray crystallography, taken alone, does not always provide definitive results. Specifically, the first crystallographic report suggested the presence of a conventional Fe_4S_4 cluster and a smaller packet of electron density that was assigned as a 2Fe-2S center.[150] However, upon further refinement, and following the formulation of the 3Fe center by Mössbauer spectroscopy,[147] a 3Fe-3S center was identified and refined.[151,152] The "refined" Fe_3S_3 center was a six-membered alternating iron-sulfide ring with an open, almost flat, twistedboat conformation (Figure 7. 14). The Fe-Fe separation of 4.1 Å and the structural type was unprecedented, and did not agree with the results of resonance Raman spectroscopy,[153] with x-ray absorption spectroscopy on the native protein or on samples from which the Fe_4S_4 center was removed,[103] or even with stoichiometry, which eventually led to the reformulation[154] of the cluster as Fe_3S_4. The x-ray absorption studies (EXAFS) clearly led to the assignment of a 2.7-Å Fe-Fe distance for the 3Fe cluster.[103]

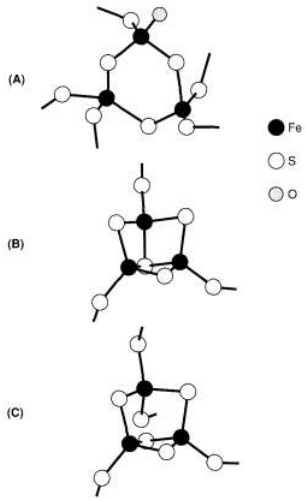


Figure 7.14 - Fe_3S_n structures: (A) open Fe_3S_3 structure proposed from initial x-ray studies (now shown to be in error); (B) the thiocubane fragment structure believed present in most Fe_3S_4 proteins; (C) open Fe_3S_4 structure (not found to date).

In parallel with the studies on *Av* FdI, two additional proteins played key roles in the resolution of the nature of the Fe_3 cluster. These are FdII from *Desulfovibrio gigas* and aconitase from beef heart. Each contains (under certain conditions) only Fe_3S_4 sites, thus enabling more definitive structural, stoichiometric, and spectral information to be acquired. Studies on these proteins using EXAFS,[155] Mössbauer,[52,156,157] EPR,[146] and resonance Raman (to which we will return briefly) clearly favor the closed structure shown in Figure 7.14C. Indeed, x-ray crystallography on aconitase by the same group that did the initial x-ray work on *Av* FdII revealed the compact structure in agreement with the spectroscopy.[20]

In 1988 the structural error in the crystallography of *Av* FdI was found by two groups, and a new refinement in a corrected space group led to a structure in agreement with the spectroscopy.[111,112] The Fe_3S_4 cluster has the apoFe thiocubane structure, with each iron atom bound to the protein by a single cysteinyl thiolate. Clearly, even x-ray crystallography is potentially fallible, and its findings must be critically integrated with the data from other techniques in arriving at full structural definition of metalloenzyme sites.

The studies on the ferredoxins from *D. gigas* present an interesting lesson on the lability of the Fe-S cluster systems. Two distinct proteins from *D. gigas*, FdI and FdII, contain the same polypeptide chain (6 kDa) in different states of aggregation,[158,159] Whereas FdI is a trimer containing three Fe_4S_4 clusters, FdII is a tetramer that contains four Fe_3S_4 clusters. The ferredoxins differ in their redox potentials and appear to have different metabolic functions in *D. gigas*. The oxidation of *D. gigas* FdI with $Fe(CN)_6^{3-}$ leads to FdII, and treatment of FdII with iron salts leads to FdI. The *D. gigas* system reveals the lability and interconvertibility of Fe-S clusters. The recently reported[160] crystal structure of *D. gigas* FdII shown in Figure 7.15 confirms the partial (apoFe) thiocubane Fe_3S_4 center. The iron atoms are ligated by three cysteinyl residues from protein side chains. The cube missing an iron is now firmly established as a viable structural type.

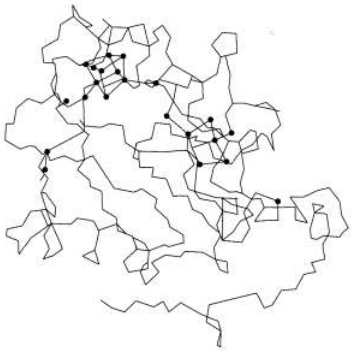
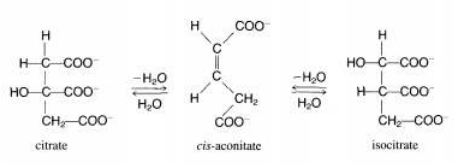


Figure 7.15 - The x-ray crystal structure of D.gigas FdII, illustrating the Fe_4S_4 and Fe_3S_4 centers in this protein.[160]

The aconitase system presents yet another fascinating story.[159a] Aconitase is a key enzyme in the Krebs cycle, catalyzing the conversion of citrate and isocitrate through the intermediacy of cis-aconitate, as shown in Equation (7.6).



This is a hydrolytic nonredox process, and for some time it was thought that aconitase was a simple Fe^{2+} protein wherein the ferrous iron was involved in the Lewis-acid function of facilitating the hydrolytic reaction. Indeed, aconitase is inactive when isolated from mitochondria, and requires the addition of Fe^{2+} to achieve activity.

Surprisingly, the isolated aconitase was found by analysis and Mossbauer spectroscopy to possess an Fe_3S_4 site in its inactive form.[161] Low-resolution crystallographic study supports the presence of an apo-Fe thiocubane, Fe_3S_4 structure in aconitase.[162] Resonance Raman[163] and EXAFS[103,155] studies clearly fingerprint the Fe_3S_4 cluster. The current hypothesis for aconitase activation involves the Fe_3S_4 thiocubane fragment reacting with Fe^{2+} to complete the cube, which is the active form of the enzyme.[164] Recent crystallographic studies[113] confirm the presence of a complete cube in the activated aconitase. The dimensions and positioning of the Fe_3S_4 and Fe_4S_4 centers in the cube are virtually identical. The added Fe^{2+} iron atom is ligated by a water (or hydroxide) ligand, consistent with the absence of any cysteine residues near the exchangeable iron. Since this water (or a hydroxide) is also present in the Fe_3S_4 system, one wonders whether a small ion such as Na^+ might be present in the Fe_3S_4 aconitase system.

Questions of detailed mechanism for aconitase remain open. ENDOR spectroscopy[165] shows that both substrate and water (or OH^-) can bind at the cluster. Does one of its Fe-atom vertices play the Lewis-acid role necessary for aconitase activity? Is the $Fe_3S_4 \rightleftharpoons Fe_4S_4$ conversion a redox- or iron-activated switch, which works as a control system for the activity of aconitase? These and other questions will continue to be asked. If aconitase is indeed an Fe-S enzyme with an iron-triggered control mechanism, it may be representative of a large class of Fe_3/Fe_4 proteins. Other hydrolytic enzymes containing similar Fe-S centers have recently been reported.[166,166a]

Spectroscopically, the Fe_3S_4 center is distinct and clearly distinguishable from 1Fe, 2Fe, and 4Fe centers. The center is EPR-active in its oxidized form, displaying a signal (Figure 7.6) with g = 1.97, 2.00, and 2.06 (*D. gigas* FdII).[158] The Mössbauer spectrum (Figure 7.7) shows a single quadrupole doublet with ΔQ = 0.53 nm/s and isomer shift of 0.27 nm, suggesting the now familiar highspin iron electronic structure.[158,159] In its reduced form, the center becomes EPR-silent, but the Mössbauer spectrum now reveals two quadrupole doublets of intensity ratio 2:1. The suggestion of the presence of a 3Fe center was first made based on this observation.[147] The picture of the reduced Fe_3S_4 state that has emerged involves a coupled, delocalized Fe^{2+}/Fe^{3+} unit responsible for the outer doublet, with a single Fe^{3+} unit responsible for the inner doublet of half the intensity. The oxidized state contains all Fe^{3+} ions, which are coupled in the trinuclear center.

EXAFS studies were consistent and unequivocal in finding an Fe-Fe distance of ~2.7 Å in all putative Fe_3S_4 proteins.[103,155,167] Resonance Raman spectra compared with those of other proteins and of model compounds with known structures[168,169] for other metals also favored the structure of Figure 7.14B. Clearly, what has been termed the spectroscopic imperative[170] has been crucial in the successful elucidation of the 3Fe structure. An interesting excursion has led to isolation of what are presumed to be $ZnFe_3S_4$, $CoFe_3S_4$, and $NiFe_3S_4$ thiocubane structures by adding Zn^{2+}, Co^{2+}, or Ni^{2+}, respectively, to proteins containing reduced Fe_3S_4 cores.[170a,b,c] These modified proteins provide interesting electronic structural insights and, potentially, new catalytic capabilities.

Fe_3 Model Systems

To date, the Fe_3S_4 center is the only structurally characterized biological iron-sulfide center that does not have an analogue in synthetic Fe chemistry. In fact, the closest structural analogue[21,170d] is found in the $Mo_3S_4^{4+}$ or $V_3S_4^{3+}$ core in clusters such as $Mo_3S_4(SCH_2CH_2S)_3^{2-}$, whose structure is shown in Figure 7.16.

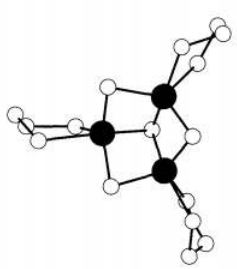


Figure 7.16 - The x-ray crystal structure of $Mo_3S_4(SCH_2CH_2S)_3^{2-}$. (From Reference 10a.)

The resonance Raman spectrum[169] of this complex bears a close resemblance to that of the *D. gigas* ferredoxin II. Since the vibrational bands responsible for the resonance Raman spectrum are not strongly dependent on the electronic properties, it is not surprising that an analogue with a different metal can be identified using this technique.

In synthetic Fe chemistry, although there is no precise structural analogue, it is instructive to consider three types of trinuclear and one hexanuclear center in relation to the three-iron biocenter.

The trinuclear cluster $Fe_3S[(SCH_2)C_6H_4]_3^{2-}$ is prepared[171,172] by the reaction of $FeCI_3$, $C_6H_4(CH_2SH)_2$, $Na^+OCH_3^-$, and p-CH_3-C_6H_4-SH in CH_3OH. As shown in Figure 7.17A, this cluster has, like the biocluster, a single triply bridging sulfide ion but, unlike the biocluster, it uses the sulfur atoms of the ethane 1,2-dithiolate as doubly bridging, as well as terminal, groups. The inorganic ring $Fe_3(SR)_3S_6^{3-}$ (X = CI, Br) has a planar $Fe_3(SR)_3$ core, which resembles the now-discredited structure for *Av* FdI[173] (Figure 7. 14A).

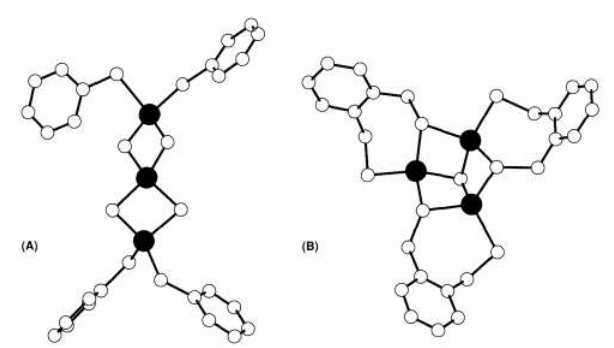


Figure 7.17 - The x-ray crystal structures of trinuclear Fe complexes: (A) $Fe_3S_4(SR)_4^{3-}$; (B) $Fe_3S[(SCH_2)_2C_6H_4]_3^{2-}$. (Data from References 171, 172, 174, 175.)

The complex $Fe_3S_4(SR)_4^{3-}$ is prepared[174,175] by reaction of $Fe(SR)_4^{2-}$ with sulfur. The x-ray-determined structure reveals two tetrahedra sharing a vertex with the linear Fe-Fe-Fe array shown in Figure 7.17B. This complex has distinctive EPR, Mössbauer, and NMR spectra that allow it to be readily identified[174,175,175a] Interestingly, after the complex was reported, a study of (denatured) aconitase at high pH (>9.5) revealed that the thiocubane fragment Fe_3S_4 site in that enzyme rearranged to adopt a structure that was spectroscopically almost identical with that of the linear complex.[176] Although the state may not have any physiological significance, it does show that Fe-S clusters different from the common (conventional) ones already discussed could be important in proteins under certain physiological conditions or in certain organisms; i.e., iron centers first identified synthetically may yet prove to be present in biological systems.

A synthetic cluster that displays features related to the biological Fe_3S_4 cluster is the hexanuclear cluster $Fe_6S_9(SR)_2^{4-}$ shown in Figure 7.18. This cluster contains two Fe_3S_4 units bridged through their diiron edges by a unique quadruply bridging S^{2-} ion (μ_4-S^{2-}) and by two additional μ_2S^{2-} bridges. The inability of synthetic chemists to isolate an Fe_3S_4 analogue may indicate that in proteins this unit requires strong binding. Significant sequestration by the protein may be needed to stabilize the Fe_3S_4 unit against oligomerization through sulfide bridges or, alternatively, rearrangement to the stable Fe_4S_4 center.

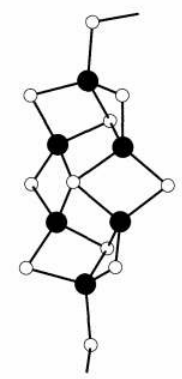


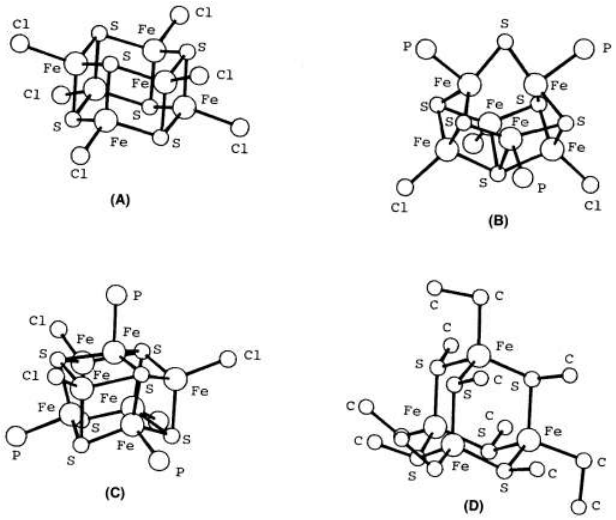
Figure 7.18 - The x-ray crystal structure[176a,b] of $Fe_6S_9(SR)_2^{4-}$.

Fe-S Chemistry: Comments and New Structures

The first successful model system for an iron-sulfur protein was an analogue of the Fe_4S_4 system, i.e., the system with the largest presently established biological Fe cluster. The reactions used to synthesize the cluster shown in Figure 7.13 are said to involve self-assembly, meaning that starting materials are simply mixed together, and thermodynamic control causes the cluster to assemble in its stable form. Interestingly, the Fe_4S_4-containing proteins, such as those of *C. pasteurianum*, are considered to be among the most ancient of proteins. Perhaps on the anaerobic primordial Earth, Fe-S clusters self-assembled in the presence of protein ligands to form the progenitors of the modem ferredoxins.

Much progress has been made in synthetic chemistry, and it is clear that both understanding and control of Fe-S chemistry are continuing to grow. New preparations for known clusters continue to be found, and new clusters continue to be synthesized, Although many of the new clusters appear to be abiological, we should not ignore them or their potential. They add to our understanding of Fe-S chemistry in general, and serve as starting points in the study of heteronuclear clusters, There is also the distinct possibility that one or more of these synthetic clusters represent an existing biological site that has not yet been identified in an isolated system.

Among the "nonbiological" structures that have been synthesized are complexes with $Fe_6S_6^{3+/2+}$ cores[177,178] including the thioprismanes,[108,109,177-179] the octahedron/cube $Fe_6S_8^{3+}$ cores,[180,181] the $Fe_6S_9^{2-}$ cores[176a,b] discussed above, the adamantane-like $Fe_6(SR)_{10}^{4-}$ complexes related to Zn and Cu structures in metallothioneins,[182] basket $Fe_6S_6^{2+}/Fe_6S_6^{+}$ cores,[182a,b,c,d] monocapped prismatic $Fe_7S_6^{3+}$ cores,[183] the cube/octahedron $Fe_8S_6^{5+}$ cores,[179] and the circular Na^+-binding $Fe_{18}S_{30}^{10-}$ unit.[183a,b] Representative ions are shown in Figure 7.19. Some of these cores are stabilized by distinctly nonbiological phosphine ligands. Nevertheless, one should not *a priori* eliminate any of these structures from a possible biological presence. Indeed, recently a novel, apparently six-iron protein from *Desulfovibio gigas* has been suggested[183c] to have the thioprismane core structure first found in model compounds.



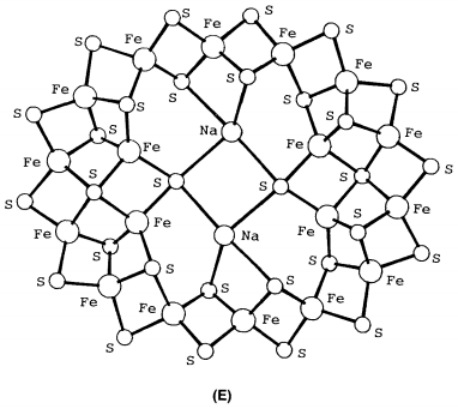


Figure 7.19 - Structures of "to date nonbiological" Fe-S clusters: (A) the thioprismane structure;[177] (B) basket-handle structure;[182a] (C) monocapped prismatic structure;[183] (D) adamantane structure;[182] (E) circular $Fe_{18}S_{30}^{10-}$ core unit.[183a,b]

Detection of Fe-S Sites

Several recent reviews have concentrated on the ways in which the various Fe-S centers can be identified in newly isolated proteins.[5,6,184] It is instructive to summarize the central techniques used in the identification of active sites. Optical spectra are usually quite distinctive, but they are broad and of relatively low intensity, and can be obscured or uninterpretable in complex systems. MCD spectra can give useful electronic information, especially when the temperature dependence is measured. EPR spectra, when they are observed, are distinctive, and are usually sufficiently sharp to be useful even in complex systems. Mössbauer and resonance Raman spectroscopies have each been applied with good effect when they can be deconvoluted, and NMR and magnetic susceptibility have given important information in some simple, lower-MW protein systems. X-ray absorption spectra, especially EXAFS, give accurate Fe-S and Fe-Fe distances when a single type of Fe atom is present. Analytical and extrusion data complement the spectroscopic and magnetic information. Extrusion data must be viewed with considerable caution, because of possible cluster-rearrangement reactions. Even x-ray crystallography has led to incorrect or poorly refined structures. In general, no one technique can unequivocally identify a site except in the very simplest systems, and there is continued need for synergistic and collaborative application of complementary techniques to a given system.

Redox Behavior

Figure 7.20 shows the ranges of redox behavior known for Fe-S centers. Clearly, the Fe-S systems can carry out low-potential processes. The rubredoxins cover the mid-potential range, and the HiPIPs are active in the high-potential region. The lack of extensive Fe-S proteins in the positive potential region may reflect their instability under oxidizing conditions and their preemption by Mn, Cu, or heme-iron sites (such as in cytochrome c), which function in this region.

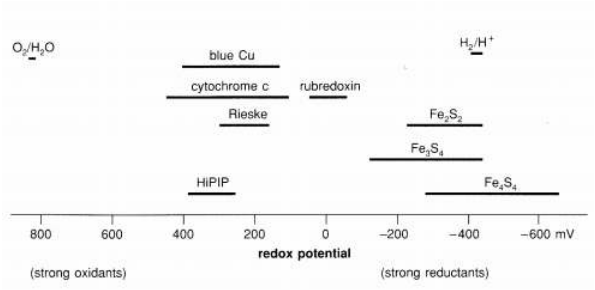


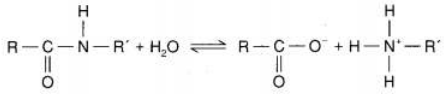
Figure 7.20 - A schematic diagram of the redox potential of the various FeS centers in comparison with other known redox centers.

9.4.4: Iron-sulfur Proteins and Models (Part 4) is shared under a CC BY-NC-SA 4.0 license and was authored, remixed, and/or curated by LibreTexts.

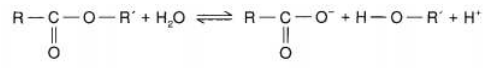
9.5: The Reaction Pathways of Zinc Enzymes and Related Biological Catalysts

I. Introduction

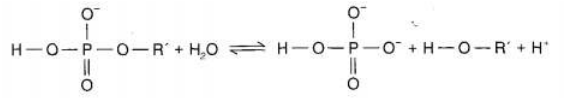
This chapter deals with metalloenzymes wherein the metal acts mainly as a Lewis acid; i.e., the metal does not change its oxidation state nor, generally, its protein ligands. Changes in the coordination sphere may occur on the side exposed to solvent. The substrate interacts with protein residues inside the active cavity and/or with the metal ion in order to be activated, so that the reaction can occur. Under these circumstances the catalyzed reactions involve, as central steps with often complex reaction pathways, the following bond-breaking and/or formation processes:



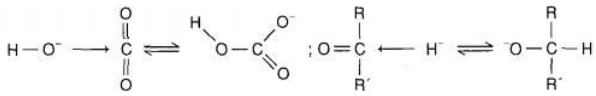
Peptide Hydrolysis



Carboxylic Ester Hydrolysis

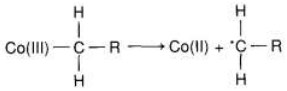


Phosphoric Ester Hydrolysis



Nucleophilic Addition of OH^- and H^-

Scheme (2.3) also pertains to the reactions which need ATP hydrolysis to promote endoenergetic reactions. We will also briefly deal with coenzyme B_{12}; this is a cobalt(III) complex that, by interacting with a number of proteins, produces an R-CH_2 radical by homolytic breaking of the Co-C bond as follows:



After an R-CH_2 radical is formed, it initiates a radical reaction. This is the only system we treat in which the oxidation state changes.

II. The Natural Catalysts

III. Strategies for the Investigation of Zinc Enzymes

A. Why Zinc?

1. The Groups to Which Zinc(II) is Bound
2. The Reactivity of Zinc(II) in Cavities
3. The Investigation of Zinc Enzymes

B. Metal Substitution

IV. Elucidation of Structure-Function Relationships: Carbonic Anhydrase as an Example

A. About the Enzyme

B. Steady-State and Equilibrium Kinetics of Carbonic Anhydrase-Catalyzed CO_2/HCO_3^- Interconversion

C. What Do We Learn from Cobalt Substitution?
   1. Acid-base Equilibria
   2. Coordination Geometries
   3. Coordinated Water and NMR
   4. pH Dependence of Inhibitor Binding

D. What Do We Learn from Copper Substitution?

E. What Do We Learn from Manganese and Cadmium Substitution?

F. Catalytic Mechanism

G. Model Chemistry

V. Other Enzymatic Mechanisms and Model Chemistry

A. Peptide Hydrolysis

B. Ester Hydrolysis and Phosphoryl Transfer

C. Nucleophilic Addition of OH^- and H^-

D. Group Transfer and Vitamin B_{12}
   1. Group Transfer Enzymes
   2. The B_{12}-dependent Enzymes

VI. Perspectives

Although a great deal is known about the biophysical characteristics of the various enzyme derivatives mentioned in this chapter, we are still far from a clear understanding of their mechanisms of action, especially if we take into consideration the role of each amino-acid residue inside the active-site cavity. Although we can successfully discuss why certain metal ions are used in certain biological reactions, we still do not know why nickel(II), for example, is involved in the enzymatic hydrolysis of urea.[199,200] If we are content with the explanations given in Sections III.A or V.D, we would need model compounds that are good catalysts and perform the job in several steps. This latter requirement would make the various models much more interesting, and would represent a new objective in the investigation of the structure-function relationship of catalytically active molecules. Indeed, the synthesis of large polypeptides may in principle provide such models. In this respect we need to know more about protein folding, for which emerging techniques like protein computer graphics and molecular dynamics are very promising.

Chemical modifications of proteins like the alkylation of carboxylate[124,201] or histidine[202] residues have been performed for a long time. A newer approach toward modeling the function of a protein, and understanding the role of the active site, involves cleaving part of a naturally occurring protein through enzymatic or chemical procedures, and then replacing it with a synthetic polypeptide. The use of modem techniques of molecular genetics has allowed site-directed mutagenesis to become in principle a very powerful technique for changing a single residue in a cavity. Site-directed mutagenesis is a very popular approach, and its principal limitation with respect to the synthetic polypeptide route is that only natural amino acids can be used (aside from the technical difficulties in both approaches). Small quantities of site-directed mutants have been obtained for CPA[125-127] and AP,[203] whereas the expression of CA[204,205] is now satisfactory.

Predictions of the changes in structure needed to affect the reaction pathway can nowadays be made with the aid of computers. The occurrence of the predicted change can be checked through x-ray analysis and NMR. The latter spectroscopy is today well-

recognized as being able to provide structural information on small (≲20 kDa) proteins through 2- or 3-dimensional techniques.[206-208] These techniques are increasingly being applied to paramagnetic metalloproteins such as many of those discussed here.[208,209] The advantage of handling a paramagnetic metalloprotein is that we can analyze signals shifted far away from their diamagnetic positions, which correspond to protons close to the metal ion,[69] even for larger proteins. It is possible to monitor the distances between two or more protons under various conditions, such as after the addition of inhibitors or pseudosubstrates, chemical modification, or substitution of a specific amino acid.

VII. References

1. H. Sigel and A. Sigel, eds., *Metal Ions in Biological Systems*, Dekker, **26** (1990).
2. R. K. Andrews, R. L. Blakeley, and B. Zemer, in Reference 1, **23** (1988).
3. K. Doi, B. C. Antanaitis, and P. Aisen, *Struct. Bonding* **70** (1988), I.
4. M. M. Werst, M. C. Kennedy, H. Beinert, and B. M. Hoffman, *Biochemistry* **29** (1990), 10526, and references therein.
5. A. G. Orpen *et al.*, *J. Chem. Soc., Dalton Trans.* **S1** (1989).
6. F. H. Westheimer, *Spec. Publ. Chem. Soc.* **8** (1957), I.
7. F. Basolo and R. G. Pearson, *Mechanisms of Inorganic Reactions*, Wiley, 2d ed., 1967.
8. L. G. Sillen and A. E. Martell, *Stability Constants of Metal-Ion Complexes*, Spec. Publ. Chern. Soc., London, **25**, 1971.
9. E. J. Billo, *Inorg. Nucl. Chem. Lett.* **11** (1975), 491.
10. I. Bertini, G. Canti, C. Luchinat, and F. Mani, *Inorg. Chem.* **20** (1981), 1670.
11. S. Burki, Ph.D. Thesis, Univ. Basel, 1977.
12. P. Wolley, *Nature* **258** (1975), 677.
13. J. T. Groves and R. R. Chambers, *J. Am. Chem. Soc.* **106** (1984), 630.
14. J. T. Groves and J. R. Olson, *Inorg. Chem.* **24** (1985), 2717.
15. L. J. Zompa, *Inorg. Chem.* **17** (1978), 2531.
16. E. Kimura, T. Koike, and K. Toriumi, *Inorg. Chem.* **27** (1988), 3687; E. Kimura *et al.*, *J. Am. Chem. Soc.* **112** (1990), 5805.
17. R. S. Brown *et al.*, *J. Am. Chem. Soc.* **104** (1982), 3188.
18. I. Bertini *et al.*, *Inorg. Chem* **29** (1990), 1460.
19. R. J. P. Williams, *Coord. Chem. Rev.* **100** (1990), 573.
20. D. W. Christianson, *Adv. Prot. Chem.* **42** (1991), 281.
21. I. Bertini, C. Luchinat, and M. S. Viezzoli, in I. Bertini *et al.*, eds., *Zinc Enzymes*, Birkhauser, 1986, p.27.
22. D. S. Auld and B. L. Vallee, in Reference 21, p. 167.
23. G. Formicka-Kozlowska, W. Maret, and M. Zeppezauer, in Reference 21, p. 579.
24. I. Bertini and C. Luchinat, in Reference 30, p. 101.
25. I. Bertini and C. Luchinat, *Adv. Inorg. Biochem.* **6** (1984), 71.
26. H. Sigel, ed., *Metal Ions in Biological Systems*, Dekker, **12** (1981).
27. T. G. Spiro, ed., *Copper Proteins*, Wiley, 1981.
28. J. E. Coleman and P. Gettins, in Reference 21, p. 77.
29. J. E. Coleman and D. P. Giedroc, in Reference 1, **25** (1989).
30. H. Sigel, ed., *Metal Ions in Biological Systems*, Dekker, **15** (1983).
31. N. U. Meldrum and F. J. W. Roughton, *J. Physiol.* **75** (1932), 4.
32. D. Keilin and T. Mann, *Biochem. J.* **34** (1940), 1163.
33. S. Lindskog, in T. G. Spiro, ed., *Zinc Enzymes: Metal Ions in Biology*, Wiley, **5** (1983), 78; D. N. Silverman and S. Lindskog, *Acc. Chem. Res.* **21** (1988), 30.
34. J.-Y. Liang and W. N. Lipscomb, *J. Am. Chem. Soc.* **108** (1986), 5051.
35. K. M. Merz, *J. Am. Chem. Soc.* **112** (1990), 7973.
36. (a) G. Sanyal, *Ann. N. Y. Acad. Sci.* **429** (1984), 165; (b) G. Sanyal and T. H. Maren, *J. Biol. Chem.* **256** (1981), 608.
37. T. Kararli and D. N. Silverman, *J. Biol. Chem.* **260** (1985), 3484.
38. A. Liljas *et al.*, *Nature* **235** (1972), 131.
39. K. K. Kannan *et al.*, *Proc. Natl. Acad. Sci. USA*, **72** (1975), 51.
40. E. A. Eriksson *et al.*, in Reference 21, p. 317.
41. S. Lindskog in Reference 21, p. 307.

42. E. Clementi *et al.*, *FEBS Lett.* **100** (1979), 313.
43. B. P. N. Ko *et al.*, *Biochemistry* **16** (1977), 1720.
44. A. Ikai, S. Tanaka, and H. Noda, *Arch. Biochem. Biophys.* **190** (1978), 39.
45. I. Bertini, C. Luchinat, and A. Scozzafava, *Struct. Bonding* **48** (1982), 45.
46. A useful review by W. W. Cleland on pH-dependent kinetics can be found in *Methods Enzymol.*, 1987, 390.
47. Y. Pocker and S. Sarkanen, *Adv. Enzymol.* **47** (1978), 149.
48. I. Bertini and C. Luchinat, *Acc. Chern. Res.* **16** (1983), 272.
49. S. Lindskog and I. Simonsson, *Eur. J. Biochem.* **123** (1982), 29.
50. B.-H. Jonsson, H. Steiner, and S. Lindskog, *FEBS Lett.* **64** (1976), 310.
51. H. Steiner, B.-H. Jonsson, and S. Lindskog, *Eur. J. Biochem.* **59** (1975), 253.
52. D. N. Silverman *et al.*, *J. Am. Chem. Soc.* **101** (1979), 6734.
53. S. H. Koenig *et al.*, *Pure Appl. Chem.* **40** (1974), 103.
54. I. Simonsson, B.-H. Jonsson, and S. Lindskog, *Eur. J. Biochem.* **93** (1979), 4.
55. T. J. Williams and R. W. Henkens, *Biochemistry* **24** (1985), 2459.
56. I. Bertini, C. Luchinat, and M. Monnanni, in Reference 99, p. 139.
57. I. Bertini *et al.*, in Reference 21, p. 371.
58. I. Bertini *et al.*, *Inorg. Chem.* **24** (1985), 301.
59. I. Bertini *et al.*, *J. Am. Chem. Soc.* **100** (1978), 4873.
60. R. C. Rosenberg, C. A. Root, and H. B. Gray, *J. Am. Chem. Soc.* **97** (1975), 21.
61. B. Holmquist, T. A. Kaden, and B. L. Vallee, *Biochemistry* **14** (1975), 1454, and references therein.
62. M. W. Makinen and G. B. Wells, in H. Sigel, ed., *Metal Ions in Biological Systems*, Dekker, **22** (1987).
63. M. W. Makinen *et al.*, *J. Am. Chem. Soc.* **107** (1985), 5245.
64. A. E. Eriksson, Uppsala Dissertation, Faculty of Science, n. 164, 1988.
65. A. E. Eriksson, A. T. Jones, and A. Liljas, *Proteins* **4** (1989), 274.
66. A. E. Eriksson *et al.*, *Proteins* **4** (1989), 283.
67. I. Bertini *et al.*, *Inorg. Chem.*, **31** (1992), 3975.
68. P. H. Haffner and J. E. Coleman, *J. Biol. Chem.* **248** (1973), 6630.
69. I. Bertini and C. Luchinat, *NMR of Paramagnetic Molecules in Biological Systems*, Benjamin/Cummings, 1986.
70. R. D. Brown III, C. F. Brewer, and S. H. Koenig, *Biochemistry* **16** (1977), 3883.
71. I. Bertini, C. Luchinat, and M. Messori, in Reference 62, vol. 21.
72. I. Solomon, *Phys. Rev.* **99** (1955), 559.
73. I. Bertini *et al.*, *J. Magn. Reson.* **59** (1984), 213.
74. L. Banci, I. Bertini, and C. Luchinat, *Magn. Res. Rev.*, **11** (1986), 1.
75. I. Bertini *et al.*, *J. Am. Chem. Soc.*, **103** (1981), 7784.
76. T. H. Maren, A. L. Parcell, and M. N. Malik, *J. Pharmacol. Exp. Theor.* **130** (1960), 389.
77. J. E. Coleman, *J. Biol. Chem.* **243** (1968), 4574.
78. S. Lindskog, *Adv. Inorg. Biochem.* **4** (1982), 115.
79. G. Alberti *et al.*, *Biochim. Biophys. Acta* **16** (1981), 668.
80. J. I. Rogers, J. Mukherjee, and R. G. Khalifah, *Biochemistry* **26** (1987), 5672.
81. C. Luchinat, R. Monnanni, and M. Sola, *Inorg. Chim. Acta* **177** (1990), 133.
82. L. Morpurgo *et al.*, *Arch. Biochem. Biophys.* **170** (1975),360.
83. I. Bertini and C. Luchinat, in K. D. Karlin and J. Zubieta, eds., *Biological and Inorganic Copper Chemistry,* vol. 1, Adenine Press, 1986.
84. I. Bertini *et al.*, *J. Chem. Soc., Dalton Trans.* (1978), 1269.
85. P. H. Haffner and J. E. Coleman, *J. Biol. Chem.* **250** (1975), 996.
86. I. Bertini *et al.*, *J. Inorg. Biochem.* **18** (1983), 221.
87. I. Bertini, E. Borghi, and C. Luchinat, *J. Am. Chem. Soc.* **102** (1979), 7069.
88. I. Bertini *et al.*, *J. Am. Chem. Soc.* **109** (1987), 7855.
89. P. Yeagle, Y. Lochmtiller, and R. W. Henkens, *Proc. Natl. Acad. Sci. USA* **48** (1975), 1728.
90. P. J. Stein, S. T. Merrill, and R. W. Henkens, *J. Am. Chem. Soc.* **99** (1977), 3194.

91. P. S. Hubbard, *Proc. Roy. Soc. London* **291** (1966), 537.
92. A. Lanir and G. Navon, *Biochemistry* **11** (1972), 3536.
93. J. J. Led and E. Neesgard, *Biochemistry* **26** (1987), 183.
94. N. B.-H. Johnsson *et al.*, *Proc. Natl. Acad. Sci. USA* **77** (1980), 3269.
95. J. L. Evelhoch, D. F. Bocian, and J. L. Sudmeier, *Biochemistry* **20** (1981), 4951.
96. J.-Y. Liang and W. N. Lipscomb, *Proc. Natl. Acad. Sci. USA* **87** (1990), 3675.
97. K. M. Merz, *J. Mol. Biol.* **214** (1990), 799.
98. C. A. Fierke, T. L. Calderone, and J. F. Krebs, *Biochemistry* **30** (1991) 11054.
99. M. Aresta and G. Forti, eds., *Carbon Dioxide as a Source of Carbon*, Reidel, 1987.
100. M. Aresta and J. V. Schloss, eds., *Enzymatic and Model Carboxylation and Reduction Reactions for Carbon Dioxide Utilization*, Kluwer, 1990.
101. C. K. Tu and D. N. Silverman, *J. Am. Chem. Soc.* **108** (1986), 6065.
102. E. Chaffee, T. P. Dasgupta, and J. M. Harris, *J. Am. Chem. Soc.* **95** (1973), 4169.
103. J. B. Hunt, A. C. Rutenberg, and H. Taube, *J. Am. Chem. Soc.* **74** (1983), 268.
104. R. S. Brown, N. J. Curtis, and J. Huguet, *J. Am. Chem. Soc.* **103** (1981), 6953.
105. I. Tabushi and Y. Kuroda, *J. Am. Chem. Soc.* **106** (1984), 4580.
106. I. Bertini *et al.*, *Gazz. Chim. Ital.* **118** (1988), 777.
107. L. Meriwether and F. H. Westheimer, *J. Am. Chem. Soc.* **78** (1956), 5119.
108. D. A. Buckingham, D. M. Foster, and A. M. Sargeson, *J. Am. Chem. Soc.* 92 (1970), 6151.
109. M. L. Bender, R. J. Bergeron, and M. Komiyama, *The Bioorganic Chemistry of Enzymatic Catalysis*, Wiley, 1984.
110. B. Anderson *et al.*, *J. Am. Chem. Soc.* **99** (1977), 2652.
111. M. L. Bender and B. W. Tumquest, *J. Am. Chem. Soc.* **77** (1955), 4271.
112. D. L. Miller and F. H. Westheimer, *J. Am. Chem. Soc.* **88** (1966), 1514.
113. H. Kroll, *J. Am. Chem. Soc.* **74** (1952), 2036.
114. D. A. Buckingham, D. M. Foster, and A. M. Sargeson, *J. Am. Chem. Soc.* **90** (1968), 6032.
115. R. Breslow, in R. F. Gould, ed., *Bioinorganic Chemistry (Advances in Chemistry Series*, vol. **100**), American Chemical Society, 1971; Chapter 2.
116. A. Schepartz and R. Breslow, *J. Am. Chem. Soc.* **109** (1987), 1814.
117. J. T. Groves and R. R. Chambers, Jr., *J. Am. Chem. Soc.* **106** (1984), 630.
118. M. A. Wells and T. C. Bruice, *J. Am. Chem. Soc.* **99** (1977), 5341.
119. H. Sigel, ed., *Metal Ions in Biological Systems*, Dekker, **5** (1976).
120. N. E. Dixon and A. M. Sargeson, in Reference 33.
121. R. W. Hay, G. Wilkinson, R. D. Gillard, and J. A. McCleverty, eds., in *Comprehensive Coordination Chemistry*, Pergamon Press, 1987.
122. D. C. Rees, M. Lewis, and W. N. Lipscomb, *J. Mol. Biol.* **168** (1983), 367.
123. D. C. Rees *et al.*, in Reference 21, p. 155.
124. D. S. Auld, K. Larson, and B. L. Vallee, in Reference 21, p. 133.
125. W. J. Rutter, personal communication.
126. D. Hilvert et al., *J. Am. Chem. Soc.* **108** (1986), 5298.
127. S. J. Gardell *et al.*, *J. Biol. Chem.* **262** (1987), 576.
128. D. S. Auld *et al.*, *Biochemistry*, **31** (1992), 3840; W. L. Mock and J. T. Tsay, *J. Biol. Chem.* **263** (1988), 8635.
129. G. Shoham, D. C. Rees, and W. N. Lipscomb, *Proc. Natl. Acad. Sci. USA* **81** (1984), 7767.
130. K. F. Geoghegan *et al.*, *Biochemistry* **22** (1983), 1847.
131. I. Bertini *et al.*, *J. Inorg. Biochem.* **32** (1988), 13.
132. C. Luchinat *et al.*, *J. Inorg. Biochem.* **32** (1988), 1.
133. R. Bicknell *et al.*, *Biochemistry* **27** (1988), 1050.
134. I. Bertini *et al.*, *Biochemistry* **27** (1988), 8318.
135. M. E. Sander and H. Witzel, in Reference 21, p. 207.
136. M. W. Makinen, in Reference 21, p. 215.
137. D. W. Christianson and W. N. Lipscomb, *Acc. Chem. Res.* **22** (1989), 62.

138. D. W. Christianson *et al.*, *J. Biol. Chem.* **264** (1989), 12849.
139. B. W. Matthews, *Acc. Chem. Res.* **21** (1988), 333, and references therein.
140. B. S. Cooperman, in Reference 119.
141. D. M. Blow, J. J. Birktoft, and B. S. Hartley, *Nature* **221** (1969), 337.
142. R. C. Nordlie, in P. D. Boyer, ed., *T he Enzymes*, Academic Press, 3d ed., **4** (1975), 543.
143. R. Breslow *et al.*, *Proc. Natl. Acad. Sci. USA* **80** (1983), 4585.
144. H. W. Wyckoff *et al.*, *Adv. Enzymol.* **55** (1983), 453.
145. E. E. Kim and H. W. Wyckoff, *J. Mol. Biol.* **218** (1991), 449.
146. L. Banci *et aI.*, *J. Inorg. Biochem.* **30** (1987), 77.
147. P. Gettins and J. E. Coleman, *J. Biol. Chem.* **259** (1984), 11036.
148. I. Bertini *et al.*, *Inorg. Chem.* **28** (1989), 352.
149. A. Chaidaroglou *et al.*, *Biochemistry* **27** (1988), 8338.
150. E. C. Dinovo and P. D. Boyer, *J. Biol. Chem.* **246** (1971), 4586.
151. H. Dutler, A. Ambar, and J. Donatsch, in Reference 21, p. 471.
152. H. Eklund and C.-I. Bränden, in *Biological Macromolecules and Assemblies*, Wiley, 1985.
153. C.-I. Branden *et al.*, *The Enzymes* **11** (1975), 104.
154. E. S. Cedergren-Zeppezauer, in Reference 21, p. 393.
155. H. Theorell, *Feder. Proc.* **20** (1961), 967.
156. M. W. Makinen and W. Maret, in Reference 21, p. 465.
157. J. Kvassman and G. Pettersson, *Eur. J. Biochem.* **103** (1980), 565.
158. P. F. Cook and W. W. Cleland, *Biochemistry* **20** (1981),1805.
159. I. Bertini *et al.*, *J. Am. Chem. Soc.* **106** (1984), 1826.
160. W. Maret *et al.*, *J. Inorg. Biochem.* **12** (1980), 241.
161. H. B. Gray and E. I. Solomon, in Reference 27, p. 1.
162. J. S. Valentine and M. W. Pantoliano, in Reference 27, p. 291.
163. M. F. Dunn, A. K. H. MacGibbon, and K. Pease, in Reference 21, p. 486.
164. I. Bertini *et al.*, *Eur. Biophys. J.* **14** (1987), 431.
165. W. Maret and M. Zeppezauer, *Biochemistry* **25** (1986), 1584.
166. C. Sartorius, M. Zeppezauer, and M. F. Dunn, *Rev. Port. Quim.* **27** (1985), 256; C. Sartorius *et al.*, *Biochemistry* **26** (1987), 871.
167. G. Pettersson, in Reference 21, p. 451.
168. E. Garces and W. W. Cleland, *Biochemistry* **8** (1969), 633.
169. B. Edlund *et al.*, *Eur. J. Biochem.* **9** (1969), 451.
170. R. K. Crane, in M. Horkin and E. H. Stotz, eds., *Comprehensive Biochemistry*, Elsevier, **15** (1964), 200.
171. B. M. Babior and J. S. Krouwer, *CRC Crit. Rev. Biochem.* **6** (1979), 35.
172. C. Brink-Shoemaker *et al.*, *Proc. Roy. Soc. London, Ser. A* **278** (1964), 1.
173. B. T. Golding and P. J. Sellars, *Nature* (1983), p. 204.
174. D. Lexa and J. M. Saveant, *Acc. Chem. Res.* **16** (1983), 235.
175. R. A. Firth *et al.*, *Chem. Commun.* (1967), 1013.
176. G. N. Schrauzer and L. P. Lee, *J. Am. Chem. Soc.* **90** (1968), 6541.
177. R. A. Firth *et al.*, *Biochemistry* **6** (1968), 2178.
178. V. B. Koppenhagen and J. J. Pfiffner, *J. Biol. Chem.* **245** (1970), 5865.
179. H. A. O. Hill, in G. L. Eichhorn, ed., *Inorganic Biochemistry*, Elsevier, **2** (1973), 1067.
180. J. Halpern, *Pure. Appl. Chem.* **55** (1983), 1059.
181. J. Halpern, S. H. Kim, and T. W. Leung, *J. Am. Chem. Soc.* **106** (1984), 8317.
182. R. G. Finke and B. P. Hay, *Inorg. Chem.* **23** (1984), 3041; B. P. Hay and R. G. Finke, *Polyhedron* **4** (1988), 1469; R. G. Finke, in C. Bleasdale and B. T. Golding, eds., *Molecular Mechanisms in Bioorganic Processes*, The Royal Society of Chemistry; Cambridge, England (1990).
183. B. P. Hay and R. G. Finke, *J. Am. Chem. Soc.* **108** (1986), 4820.
184. B. P. Hay and R. G. Finke, *J. Am. Chem. Soc.* **109** (1987), 8012.
185. J. M. Pratt, *Quart. Rev.* (1984), 161.

186. J. Halpern, *Science* **227** (1985), 869.
187. B. M. Babier, *Acc. Chem. Res.* **8** (1975), 376.
188. B. T. Golding, in D. Dolphin, ed., B_{12} , Wiley, **2** (1982), 543.
189. N. Bresciani-Pahor *et al.*, *Coord. Chem. Rev.* **63** (1985), 1.
190. J. M. Pratt, *J. Mol. Cat.* **23** (1984), 187.
191. S. M. Chennaly and J. M. Pratt, *J. Chem. Soc., Dalton Trans.* (1980), 2259.
192. *Ibid*., p. 2267.
193. *Ibid*., p. 2274.
194. L. G. Marzilli *et al.*, *J. Am. Chem. Soc.* **101** (1979), 6754.
195. J. Glusker, in Reference 188, **1** (1982), 23.
196. G. De Alti *et al.*, *Inorg. Chim. Acta* **3** (1969), 533.
197. K. Geno and J. Halpern, *J. Am. Chem. Soc.* **109** (1987), 1238.
198. C. Mealli, M. Sabat, and L. G. Marzilli, *J. Am. Chem. Soc.* **109** (1987), 1593.
199. *Nickel and its Role in Biology*, vol. 23 of Reference 62.
200. C. T. Walsh and W. H. Orme-Johnson, *Biochemistry* **26** (1987), 4901.
201. J. F. Riordan and H. Hayashida, *Biochem. Biophys. Res. Commun.* **41** (1970), 122.
202. R. G. Khalifah, J. I. Rogers, and J. Mukherjee, in Reference 21, p. 357.
203. A. Chaidaroglou *et al.*, *Biochemistry* **27** (1988), 8338.
204. C. Forsman *et al.*, *FEBS Lett.* **229** (1988), 360; S. Lindskog *et al.*, in *Carbonic Anhydrase*, F. Botre, G. Gros, and B. T. Storey, eds., VCH, 1991.
205. C. A. Fierke, J. F. Krebs, and R. A. Venters, in *Carbonic Anhydrase*, F. Botre, G. Gros, and B. T. Storey, eds., VCH, 1991.
206. K. Wüthrich, *NMR in Biological Research*, Elsevier-North Holland, 1976.
207. K. Wüthrich, *NMR of Proteins and Nucleic Acids*, Wiley, 1986.
208. I. Bertini, H. Molinari, and N. Niccolai, eds., *NMR and Biomolecular Structure*, Verlag Chemie, 1991.
209. J. T. J. LeComte, R. D. Johnson, and G. N. La Mar, *Biochim. Biophys. Acta* **829** (1985), 268.
210. Recently, ^{67}Zn has been used as a relaxing probe to monitor the binding of ^{13}C-enriched cyanide to zinc in carbonic anhydrase (see Section IV.C).
211. Recent work on HCA II has improved the resolution to 1.54 Å (K. Hakan *et al.*, *J. Mol. Biol.* **227** (1993), 1192). Mutants at positions 143 (R. S. Alexander, S. K. Nair, and D. W. Christianson, *Biochemistry* **30** (1991), 11064) and 200 (1. F. Krebs et al., Biochemistry 30 (1991),9153; Y. Xue *et al.*, *Proteins* **15** (1993), 80) also have been characterized by x-ray methods.
212. An x-ray study of the cyanate and cyanide derivatives of the native enzyme has shown that the anions sit in the cavity without binding to the metal ion (M. Lindahl, L.A. Svensson, and A. Liljas, *Proteins* **15** (1993), 177). Since NCO^- has been shown to interact with the paramagnetic cobalt(II) center, and ^{13}C-enriched cyanide has been shown to interact with ^{67}Zn-substituted CA (see Reference 67), it appears that the structures in the solid state and solution are strikingly different.
213. Recent x-ray data on the adduct of 1,2,4-triazole with HCA II confirm H-bonding with Thr-200 (S. Mangani and A. Liljas, *J. Mol. Biol.* **232** (1993), 9).
214. An HCO_3^--complex of the His-200 mutant of HCA II has been studied by x-ray methods. The data are consistent with the coordinated oxygen being protonated and H-bonded to Thr-199 (Y. Xue *et al.*, *Proteins* **15** (1993), 80).

Contributors and Attributions

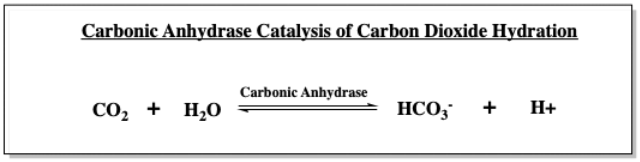
- Ivano Bertini (University of Florence, Department of Chemistry)
- Claudio Luchinat (University of Bologna, Institute of Agricultural Chemistry)

9.5: The Reaction Pathways of Zinc Enzymes and Related Biological Catalysts is shared under a CC BY-NC-SA 4.0 license and was authored, remixed, and/or curated by LibreTexts.

9.5.1: About Carbonic Anhydrase

Introduction

Carbon-dioxide (CO2) hydration and its mechanism in living systems are of fundamental importance for bioinorganic chemistry. In 1932 the existence of an enzyme catalyzing CO2 hydration in red blood cells was established,31 The enzyme was named carbonic anhydrase (abbreviated CA). In 1939 the enzyme was recognized to contain zinc (Zn).32 Because CO2 is either the starting point for photosynthesis or the endpoint of substrate oxidation, carbonic anhydrases are now known to be ubiquitous, occurring in animals, plants, bacteria, and fungi. Different enzymes from different sources, catalyzing the same reaction and usually having homologous structures, are termed isoenzymes. Thus far, a total of 7 distinct classes of CAs have been identified based upon organism: alpha, beta, gamma, delta, zeta, eta, and theta. Each class may contain multiple isoenzymes. Sometimes the same organism has more than one isoenzyme for a particular function, as is true for human carbonic anhydrase. Humans have 15 CAs that belong to the alpha class; these isozymes vary by location in the body and by catalytic activity. CA is a classic example of a hydrolytic enzyme, one that catalyzes addition or removal of water to a substrate molecule. More specifically, CA catalyzes the reversible conversion of carbon dioxide (CO2) to bicarbonate (HCO3-), also referred to as carbonic acid.



Although hydration of CO2 is spontaneous in water at pH 7, the reaction is kinetically slow (k = 10-1 s-1), too slow to convert all CO2 produced in respiration. Only above pH 9 does the uncatalyzed reaction become fast, owing to direct attack of OH-, which is a much better nucleophile than H2O (k = 104 M-1 s-1, where M-1 refers to the OH- concentration). The figure below compares nucleophilic attack of water versus hydroxide (OH-) on CO2.

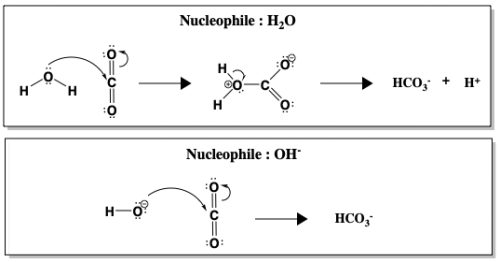


Figure: This figure depicts nucleophilic attack on carbon in carbon dioxide (CO2) in the formation of bicarbonate (HCO3-). In the top panel, H2O is the nucleophile. The bottom panel shows the reaction with hydroxide (OH-) as the nucleophile. Since the OH- is a stronger nucleophile, HCO3- formation is faster when OH- is the nucleophile.

Between H2O and OH-, formation of HCO3- occurs faster when OH- is the nucleophile. A faster reaction at higher pH, when more OH- ions are present, suggests OH- is involved in the rate determining step. However, realistically, the pH of human blood cannot be changed to speed up hydration of CO2. Instead, humans use carbonic anhydrase to catalyse the reaction. When CA is present, the reaction is sped up to a rate of k = 106 s-1.

The ubiquity of CA in different organisms reflects the importance of these enzymes in sustaining life. The speed of CA-catalyzed CO2 hydration is essential to meet the needs of living cells. Some physiological CA functions include pH regulation, electrolyte secretion, ion transport, and CO2 homeostasis. In the digestive tract, CAs plays a role in the secretion of acid and keep saliva neutral by modulating pH.G,H Among these functions, CA most notably plays a role in transport of CO2 and HCO3- related to respiration, the process of atmospheric oxygen and carbon dioxide exchange that occurs when humans inhale oxygen and exhale carbon dioxide. With low solubility, CO2 must be converted to a more soluble form, HCO3-, for transport throughout the body. Bicarbonate ion (HCO3-) eventually reaches the lungs, gets converted back to CO2, and exits the body through exhalation.C

Medical research revolving around CA focuses on the Zn-containing active site as a therapeutic target for various disease treatments; both CA inhibitors and activators are incorporated in drug design. CA inhibitors are used as treatment for epilepsy, ulcers, cancer, obesity, and other neurological disorders. In the eye, CA produces hydrogen ions that maintain optic pressure.

However, too much pressure in the eye can damage the optic nerve and cause glaucoma. CA activity can create a concentration gradient that drives the transport of water to the optical nerve. When too much water is around the optical nerve, pressure around the nerve increases causing damage. Inhibition of CA has become a key treatment of glaucoma.

Beyond pharmaceutical applications, CA has also been investigated for its utility in carbon capture and carbon sensor applications. Carbon capture and storage happens as CAs convert CO2 to bicarbonate. Increased availability of bicarbonate in the presence of calcium ions (Ca2+) causes precipitation of calcite (CaCO3). This process, called bio-mineralization, may be a viable mode of long term storage of CO2 in calcite to mitigate CO2 emissions.

Details about the structure and function of CA's Zn-containing active site have been elucidated over 80 years of research. The current article delves into the metalloenzyme active site using bioinorganic concepts.

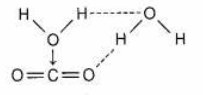
Old Text Below ----------

Carbon-dioxide hydration and its mechanism in living systems are of fundamental importance for bioinorganic chemistry. In 1932 the existence of an enzyme catalyzing CO_2 hydration in red blood cells was established,[31] The enzyme was named carbonic anhydrase (abbreviated CA). In 1939 the enzyme was recognized to contain zinc.[32] Because CO_2 is either the starting point for photosynthesis or the endpoint of substrate oxidation, carbonic anhydrases are now known to be ubiquitous, occurring in animals, plants, and several bacteria. Different enzymes from different sources, catalyzing the same reaction and usually having homologous structures, are termed isoenzymes. Sometimes the same organism has more than one isoenzyme for a particular function, as is true for human carbonic anhydrase.

CO_2 gas is relatively soluble in water (3×10^{-2} M at room temperature under p_{CO2} = 1 atm), equilibrating with hydrogen carbonate at pK_a 6.1:

$$CO_2 + H_2O \rightleftharpoons HCO_3^- + H^- \tag{2.6}$$

The uncatalyzed reaction is kinetically slow around physiological pH ($k \simeq 10^{-1}\ s^{-1}$), whereas, in the presence of the most efficient isoenzyme of CA, the maximal CO_2 turnover number (i.e., the number of substrate molecules transformed per unit time by each molecule of enzyme)[33] is $\simeq 10^6\ s^{-1}$. The uncatalyzed attack by water on CO_2 may be facilitated by two hydrogen-bonded water molecules, one of which activates the carbon by means of a hydrogen bond to a terminal CO_2 oxygen, the other of which binds the carbon atom via oxygen: [34,35]



Only above pH 9 does the uncatalyzed reaction become fast, owing to direct attack of OH^-, which is a much better nucleophile than H_2O ($k \simeq 10^4\ M^{-1}s^{-1}$, where M^{-1} refers to the OH^- concentration):

$$CO_2 + OH^- \rightleftharpoons HCO_3^- \tag{2.8}$$

On the other hand, the rate constant in the presence of the enzyme, called k_{cat}, is pH-independent above pH 8 in every CA isoenzyme (Figure 2.2).[33,36]

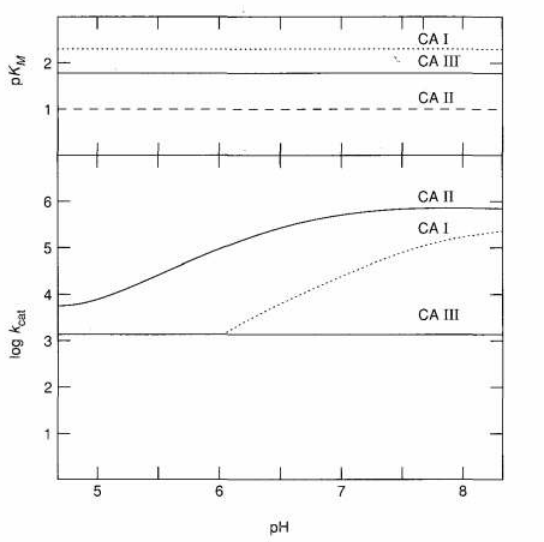


Figure 2.2 - pH dependence of k_{cat} and K_m values for CO_2 hydration catalyzed by carbonic anhydrase I, II, and III isoenzymes.[33,36]

In vitro, carbonic anhydrase is quite versatile, catalyzing several reactions that involve both OH^- and H^+, such as the hydrolysis of esters and the hydration of aldehydes. The various isoenzymes have been characterized to different degrees of sophistication. High-activity forms are labeled II ($k_{cat} \simeq 10^6\ s^{-1}$ at 25 °C); low-activity forms I ($k_{cat} \simeq 10^5\ s^{-1}$), and the very-low-activity forms III ($k_{cat} \simeq 10^3\ s^{-1}$).[37] X-ray structural information at nominal 2 Å resolution is available for HCA I[38] and HCA II,[39] where H indicates human. The structure of HCA II has been refined recently.[40] High-resolution structures of mutants and of their substrate and inhibitor derivatives are being reported.[211] All isoenzymes are single-chain polypeptides, with M.W. about 30 kDa and one zinc ion per molecule. They have the shape of a rugby ball with a crevice 16 Å deep running through the south pole (Figure 2.3 See color plate section, page C-2.). At the bottom of the crevice, the zinc ion is anchored to the protein by three histidine nitrogen atoms and is exposed to solvent. Two histidines (His-94 and His-96, HCA I numbering) are bound to zinc via their Nϵ2 atoms, whereas one (His-119) is bound via its Nδ1 atom (Figure 2.4). It is quite general that histidines bind zinc equally well by either of the two histidine nitrogens, the preference being probably dictated by the steric constraints imposed by the protein folding. The three histidine NH protons are all engaged in H-bonding (Figure 2.4). Histidine-119 is involved in H-bonding with a glutamate residue. As mentioned, this could be a way of controlling the basicity of the metal ligands. A solvent molecule bound to zinc is involved in an H-bond with Thr-199, which in turn is H-bonded to Glu-106. This H-bonding network is important for understanding the subtle structural changes that occur with pH changes; these could, in principle, account for the pH-dependent properties. Although the structure of crystals grown at pH 8 in sulfate-containing buffer gives some indication of a single solvent molecule bound to zinc (Figures 2.3 and 2.5 See color plate section, pages C2, C3.), theoretical studies indicate that two water molecules can be at bonding distances.[42] Such a finding is consistent with spectroscopic studies on other derivatives and with the concept that attachment and detachment of substrates occur through five coordination.

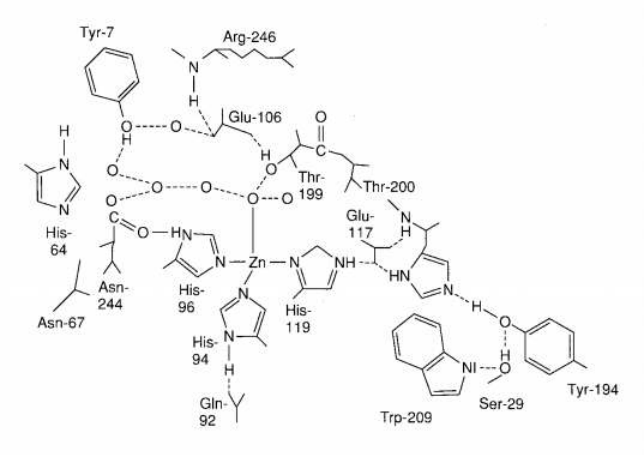


Figure 2.4 - Schematic representation of the active site of human carbonic anhydrase II. Hydrogen bonds (---) and ordered water molecules (o) are indicated.[41]

Just as is true for every zinc enzyme in which zinc is at the catalytic site, activity is lost if the metal is removed, and is restored by zinc uptake. The tertiary structure of carbonic anhydrase is maintained in the absence of zinc; even the denatured apoprotein can refold spontaneously from a random coil to a native-like conformation. Although such a process is accelerated by zinc,[43,44] the presence of the metal does not seem to be an absolute requirement for the correct folding of CA, whereas it is an absolute requirement for several other metalloproteins.[23,29,30]

Anions are attracted in the metal cavity by the positive $Zn(N_3OH_2)^{2+}$ moiety, and are believed to bind to zinc in carbonic anhydrase very effectively; so their use should be avoided as much as possible if the goal is to study the enzyme as it is. When the protein is dialyzed against freshly doubly distilled or carefully deionized water under an inert atmosphere, the pH of the sample approaches the isoelectric point, which is below 6 for HCA I and bovine (BCA II) enzymes. The pH can then be adjusted by appropriate additions of NaOH. All the measurements reported in the literature performed in acetate, phosphate, imidazole, or tris sulfate buffers are affected by the interference of the anion with the metal ion. However, buffer species containing large anions like Hepes (4[(2-hydroxyethyl)-l-piperazinyl]ethanesulfonic acid) can be used,[45] since these anions do not enter the cavity.

There are many indications that zinc in the high-pH form of CA is four-coordinate with an OH group in the fourth coordination site. At low pH the enzyme exists in a form that contains coordinated water; the coordination number can be four (one water molecule) or five (two water molecules). Of course, the occurrence of the low-pH species depends on the pK_a's of the complex acid-base equilibria.

9.5.1: About Carbonic Anhydrase is shared under a CC BY-NC-SA 4.0 license and was authored, remixed, and/or curated by LibreTexts.

9.5.2: Catalytic Mechanism

All the above structural and kinetic information obtained under a variety of conditions with different metal ions can be used to propose a catalytic cycle for carbonic anhydrase (Figure 2.21), As shown by studies on the pH-dependent properties of native and metal-substituted CAs, both type-I and type-II proteins have two acidic groups, the zinc-coordinated water and a free histidine. At physiological pH the enzyme is essentially in the Zn—OH form (step A in Figure 2.21). A Zn—OH moiety is a relatively good nucleophile, poised for nucleophilic attack on carbon dioxide. It is possible that the hydrogen bond with Thr-199, which seems to be consistent with an sp^3 oxygen, orients the OH for attack at the substrate CO_2 . Studies of the copper derivative indicated that the concentration of CO_2 in the cavity is higher than in bulk solution (step B).

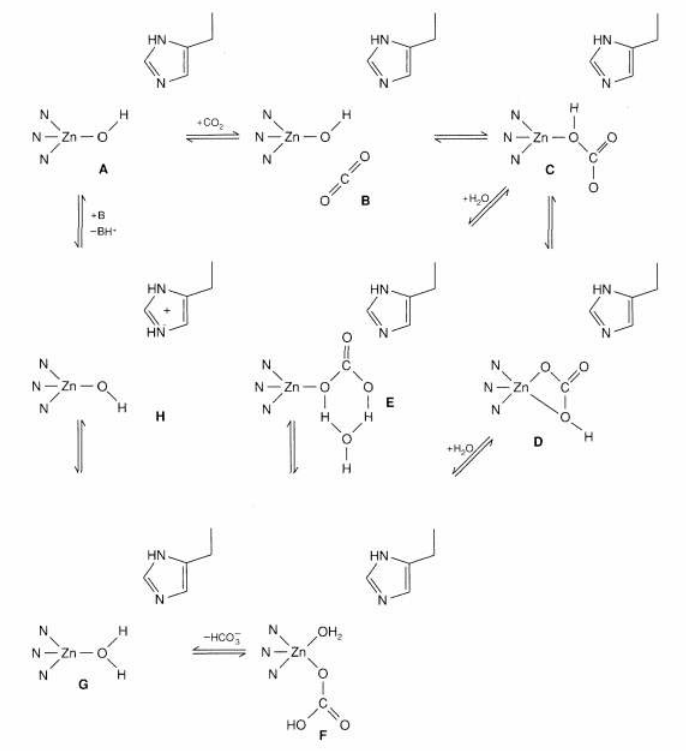


Figure 2.21 - Proposed catalytic cycle of CA.

Molecular dynamics calculations have shown that there are either three[96] or two[97] potential wells for CO_2 in the hydrophobic pocket. It was shown[98] that when Val-143 is replaced by the much larger Phe, the activity decreases by a factor of 10^3. Apparently the large Phe residue does not leave space within the cavity to accomodate CO_2.

It would also be nice if the enzyme were able to activate CO_2. There is no evidence that it does, even though the positive charge around zinc and the NH of Thr-199 would represent two electrostatic attraction points that could activate CO_2. It is well-known that CO_2's interactions with positive charges activate the carbon for nucleophilic attack.[99,100] The positioning of CO_2 between zinc and the peptide NH of Thr-199 would be ideal for the OH attack. Merz[97] locates it as shown in Figure 2.22.

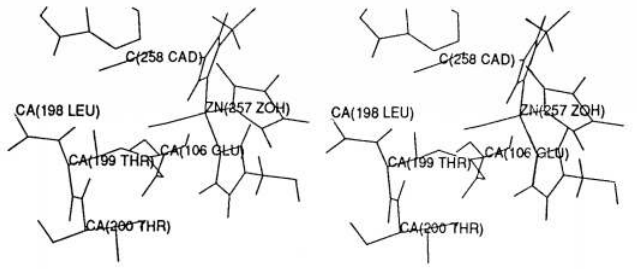


Figure 2.22 - Stereo view of the site of activation of CO_2 in the cavity of CA as proposed by Merz.[97]

It was believed that, once bicarbonate is formed (C), the proton has to transfer to a terminal oxygen atom, either via an intermediate in which bicarbonate is bidentate (D) or via a hydrogen-bond network (E). Indeed, in model compounds one would expect HCO_3^- to bind through a nonprotonated oxygen. However, the possibility of restoring the hydrogen bond with Thr-199 as in sulfonamide adducts could justify the presence of the hydrogen on the coordinating oxygen.[214] The bicarbonate derivative is presumably in equilibrium between four- and five-coordinate species (F), as shown by the electronic spectra of the cobalt derivative.[59] The five-coordinate species provides a low barrier for the substrate detachment step via an associative mechanism involving coordination of a water molecule (G). A possible five-coordinate species would contain bicarbonate in the B site and water in the C site (Figure 2.12). It is reasonable that the measured K_m for the reaction of bicarbonate dehydration is the thermodynamic dissociation constant of the M—HCO_3^- species. Anionic or neutral inhibitors are competitive with bicarbonate because they tend to bind at the same site. At this stage the second substrate, which is H^+, has to be released (H). It is reasonable that the water proton transfers to a group inside the cavity, e.g. , the free histidine mentioned above, and subsequently to the solvent. In the absence of buffers the latter step is rate-limiting for the high-activity isoenzymes, since the diffusion rate cannot exceed the product of the concentration times the diffusion coefficient, i.e., 10^{-7} M x 10^{11} $M^{-1}s^{-1}$. Such a limit is then 10^4 s^{-1}, whereas the turnover rate is 10^6 s^{-1}. The presence of buffer can assist in proton transfer at this stage, in such a way that the rate-limiting step becomes the internal proton transfer. The release of H^+ from the Zn—OH_2 moiety is also the rate-limiting step for the low-activity CA III, as nicely shown by the electronic spectra of CoCA III. These spectra change from the basic form at the beginning of the reaction to the acidic form upon CO_2 addition (Figure 2.23).[101] After the interconversion of CO_2 into bicarbonate, there is an accumulation of the $CoOH_2$ species, the deprotonation of which is slower than the release of HCO_3^-.

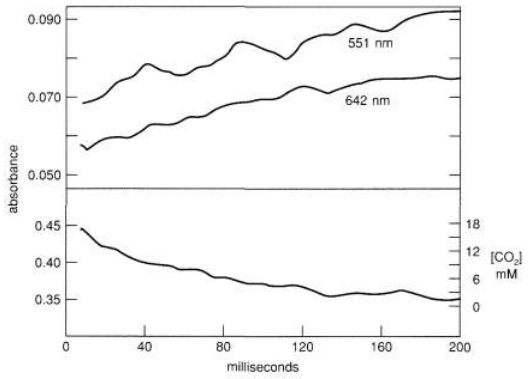


Figure 2.23 - Time dependence of $\epsilon_{15.6}$ and $\epsilon_{18\cdot1}$ of cobalt(II)-substituted CA III after addition of CO_2 to a buffered enzyme solution at pH 8. The initial drop of absorbance reflects the accumulation of a $CoOH_2$ intermediate.[101]

9.5.2: Catalytic Mechanism is shared under a CC BY-NC-SA 4.0 license and was authored, remixed, and/or curated by LibreTexts.

9.5.3: Metal Substitution

With zinc enzymes, metallosubstitution is a convenient tool for monitoring the protein and its function by means of spectroscopic techniques. Furthermore, it is interesting to learn how reactivity depends on the nature of the metal ion and its coordination properties, because much of it depends on the protein structure, which seemingly remains constant. As discussed, zinc enzymes can be studied by replacing zinc with other spectroscopically useful metal ions, whose activities have been checked, and by transferring the information obtained to the native enzyme. The strategy of metal substitution is not limited to zinc enzymes, since it has been used for magnesium-activated enzymes and, occasionally, other metalloenzymes as well.

By dialyzing a protein solution against chelating agents, such as EDTA, 1,10-phenanthroline, or 2,6-dipicolinic acid at moderately acidic pH, or by reversibly unfolding the protein with denaturing agents (as has been done with alkaline phosphatase), one can cause zinc proteins to release their metal ions, giving rise to the corresponding but inactive apoprotein. Sometimes (e.g., by using alcohol dehydrogenase) dialysis against chelating agents can be applied to a suspension of protein microcrystals. In this way the chelating agent is still able to reach and remove the active site metal by slowly diffusing in the crystals through the hydration water, while the apoprotein is maintained in the native conformation by the crystal packing forces and denaturation is avoided. After the chelating agent is dialyzed out, often against a high-salt (e.g., ClO_4^-) buffer to reduce nonspecific binding, a new metalloprotein can obtained by addition of the appropriate metal salt.[23]

Cobalt(II)-substituted zinc proteins often show about as much activity as the native zinc enzymes (Table 2.4). This is a general characteristic of the cobalt-substituted zinc enzymes,[24] since the coordination chemistry of cobalt(II) is very similar to that of zinc(II). The two ions also show virtually identical ionic radii. Cobalt(II) derivatives generally display useful electronic spectra. High-spin cobalt(II) ions are paramagnetic, containing three unpaired electrons ($S = \frac{3}{2}$); thus they can also give rise to EPR spectra. The electronic relaxation times, i.e., the average lifetimes of the unpaired electrons in a given spin state of the S manifold ($-\frac{3}{2}$, $-\frac{1}{2}$, $\frac{1}{2}$, $\frac{3}{2}$), are very short (10^{-11} to 10^{-12} s) at room temperature. In order to detect EPR spectra, the sample temperature is usually decreased, often down to liquid helium temperature, to increase the electronic relaxation times and sharpen the EPR linewidths. On the other hand, as the paramagnetic broadening of the NMR lines in such systems is inversely proportional to the electronic relaxation times (see Section IV.C.3), room-temperature ^1H NMR spectra of cobalt(II) complexes can be easily detected, even in the absence of chemical exchange. Therefore cobalt(II) is an exceptional probe to monitor the structure and reactivity of zinc enzymes. Of course, the transfer of information from the artificial to the native enzyme must be done with caution. However, if we can understand the functioning of the cobalt enzyme, we then have a reference frame by which to understand the kinetic properties of the native enzyme. The spectroscopic properties of cobalt(Il) in cobalt-substituted proteins have been reviewed.[25]

Copper(Il)-substituted zinc proteins are generally inactive with respect to the natural and most artificial substrates (Table 2.4). In model compounds copper(Il) is often principally four-coordinate, with at most two more ligands present at metal-ligand distances that are longer than normal coordination bonds. As a consequence, the ability of zinc to switch between four- and five-coordinate species without any appreciable barrier and with usual metal-donor distances is not mimicked by copper. Furthermore, binding at the four principal coordination positions is generally stronger for copper than for zinc. It follows that substrates may have slow detachment kinetics. These properties are unfavorable for catalysis.

Copper(II) can be easily and meaningfully studied by means of electronic spectroscopy. Moreover, the EPR spectra can be recorded even at room temperature because of the long electronic relaxation times, which are of the order of 10^{-9} s. Because a protein is a macromolecule, it rotates slowly, and the EPR spectra in solution at room temperature look like those of crystalline powders or frozen solutions (powder-like spectra). ENDOR spectra are also easily obtained for copper proteins at low temperatures, because at low temperature the electronic relaxation times are even longer, and saturation of the EPR lines (which is a requirement to obtain ENDOR spectra) is easy to accomplish. The long electronic relaxation times make the broadening effects on the NMR lines of nuclei sensing the metal ion too severe; so these lines, unlike those of cobalt(Il) complexes, generally escape detection. However, if the nucleus under investigation is in fast exchange between a free species in large excess and a bound species, the line may be observed, because the broadening effects are scaled down by a factor equal to the molar fraction of bound species. The nuclear relaxation parameters contain precious structural and/or dynamic information (see Section IV.C.3). The spectroscopic properties of copper(II) in proteins have been extensively reviewed.[26,27]

Cadmium-substituted zinc proteins may also be active (Table 2.4), although usually at higher pH. This observation is readily explained in terms of the pK_a of a coordinated water, which is expected to be higher than that of analogous zinc complexes because

the cadmium ion is larger and polarizes the Cd-OH_2 bond less.

^{113}Cd and ^{111}Cd are nuclei with relatively high sensitivity for NMR spectroscopic study. The ^{113}Cd chemical shift spans from -200 to 800 ppm relative to $CdSO_4$ in H_2O, depending on the number and nature of donor atoms.[24,28] Sulfur donor atoms cause larger downfield shifts than oxygens or nitrogens, and the downfield shift increases with decreasing number of donor atoms. Therefore, ^{113}Cd NMR probes have been used extensively to study zinc enzymes, metal-storage proteins like thioneins, and other proteins with cysteine ligands, and chemical shifts in various cadmium proteins, together with the proposed ligand donor set, have been obtained (Figure 2.1).

Manganese(II)-containing proteins give rise to detectable EPR signals; however, their interpretation in terms of structure and dynamics is not always informative. The electronic relaxation times of Mn^{2+} are the longest among metal ions, of the order of 10^{-8} s at room temperature and at the magnetic fields of interest. This property and the large S = $\frac{5}{2}$ value account for a large NMR linewidth, even larger than in copper(II) systems. Manganese(II)- and nickel(II)- substituted zinc proteins have often been reported to have fractional activity (Table 2.4).[24] Several efforts have been devoted to Mn(II) derivatives, especially by studying the NMR signals of nuclei in molecules that exchange rapidly with the metalloprotein.

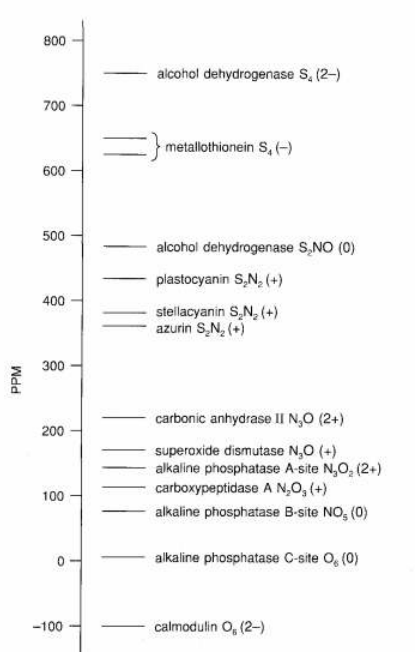


Figure 2.1 - ^{113}Cd chemical shifts in cadmium(II)-substituted metalloproteins. [24,28] Donor sets and overall charges (in parentheses) of the complexes are indicated.

Finally, several other metal-substituted zinc metalloprotein derivatives have been prepared, including those of VO^{2+} , Fe(II), Co(III), Pt(II), and $HgCl_2$. Although these systems add little directly to our understanding of the relationship between structure and function of the enzymes, nonetheless they represent new bioinorganic compounds and are of interest in themselves, or can add information on the coordinating capabilities, and reactivity in general, of the residues present in the active cavity.

Under the heading *zinc enzymes* there are several enzymes in which zinc is essential for the biological function, but is not present in the catalytic site. Among the most-studied enzymes, zinc has a structural role in superoxide dismutase, where the ligands are three histidines and one aspartate. In alcohol dehydrogenase there is a zinc ion that has a structural role, besides the catalytically active one. The former zinc has four cysteine ligands. Cysteine ligands are also present in zinc thioneins, which are zinc-storage proteins. The recently discovered class of genetic factors containing "zinc fingers" are zinc proteins in which the metal has an essentially structural role.[29] Such a role may consist of lowering the folding enthalpy of a protein to induce an active conformation or to stabilize a particular quaternary structure.

Zinc may also have a regulatory role; i.e., it does not participate in the various catalytic steps, but its presence increases the catalytic rate. This is a rather loose but common definition. Typically, zinc in the B site of alkaline phosphatase (Section V.B) has such a role, and the ligands are histidines, aspartates, and water molecules.

The enzymes in which zinc plays a structural or regulatory role will not be further discussed here, because they do not participate in the catalytic mechanisms; see the broader review articles.[23 ,29,30] Rather, we will describe in some detail the enzyme carbonic anhydrase, in order to show how researchers have investigated such complicated systems as enzymes. We will discover as we look at the details of the structures and mechanisms of enzymes that there are large differences between reactivities in solution and in enzymatic cavities. The fundamental properties underlying these differences are still not fully understood.

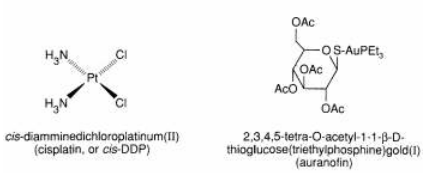
9.5.3: Metal Substitution is shared under a CC BY-NC-SA 4.0 license and was authored, remixed, and/or curated by LibreTexts.

9.6: Metals in Medicine

Metal ions are required for many critical functions in humans. Scarcity of some metal ions can lead to disease. Well-known examples include pernicious anemia resulting from iron deficiency, growth retardation arising from insufficient dietary zinc, and heart disease in infants owing to copper deficiency. The ability to recognize, to understand at the molecular level, and to treat diseases caused by inadequate metal-ion function constitutes an important aspect of medicinal bioinorganic chemistry.

Metal ions can also induce toxicity in humans, classic examples being heavy-metal poisons such as mercury and lead. Even essential metal ions can be toxic when present in excess; iron is a common household poison in the United States as a result of accidental ingestion, usually by children, of the dietary supplement ferrous sulfate. Understanding the biochemistry and molecular biology of natural detoxification mechanisms, and designing and applying ion-specific chelating agents to treat metal overloads, are two components of a second major aspect of the new science that is evolving at the interface of bioinorganic chemistry and medicine.

Less well known than the fact that metal ions are required in biology is their role as pharmaceuticals. Two major drugs based on metals that have no known natural biological function, Pt (cisplatin) and Au (auranofin), are widely used for the treatment of genitourinary and head and neck tumors and of rheumatoid arthritis, respectively. In addition, compounds of radioactive metal ions such as ^{99m}Tc and complexes of paramagnetic metals such as Gd(III) are now in widespread use as imaging agents for the diagnosis of disease. Many patients admitted overnight to a hospital in the U.S. will receive an injection of a ^{99m}Tc compound for radiodiagnostic purposes. Yet, despite the obvious success of metal complexes as diagnostic and chemotherapeutic agents, few pharmaceutical or chemical companies have serious in-house research programs that address these important bioinorganic aspects of medicine.



This chapter introduces three broad aspects of metals in medicine: nutritional requirements and diseases related thereto; the toxic effects of metals; and the use of metals for diagnosis and chemotherapy. Each area is discussed in survey form, with attention drawn to those problems for which substantial chemical information exists. Since there is only a primitive understanding at the molecular level of the underlying biochemical mechanisms for most of the topics, this field is an important frontier area of bioinorganic chemistry. The major focus of this chapter is on the platinum anticancer drug cisplatin, which is presented as a case study exemplifying the scope of the problem, the array of methodologies employed, and the progress that can be made in understanding the molecular basis of a single, if spectacular, metal complex used in medicine today.

II. Metal Deficiency and Disease[1]

A. Essential Metals

B. Anemia and Iron[2]

C. Causes and Consequences of Zinc Deficiency[4-6]

D. Copper Deficiency[7]

E. Summary

III. Toxic Effects of Metals

A. Two Classes of Toxic Metal Compounds

B. Copper Overload and Wilson's Disease[8]

C. Iron Toxicity[9]

D. Toxic Effects of Other Essential Metals[10,11]

E. Plutonium: A Consequence of the Nuclear Age[12]

F. Mercury Toxicity[13] and Bacterial Resistance[14-17]

G. Cadmium and Lead Toxicity[18]

H. Metals as Carcinogens[19,20]

I. Summary

IV. Survey of Metals Used for Diagnosis and Chemotherapy

A. Radiodiagnostic Agents[21,22]

B. Magnetic Resonance Imaging (MRI)[27]

C. Lithium and Mental Health[28-31]

D. Gold and Rheumatoid Arthritis[23,32,33]

E. Anticancer Drugs

1. Platinum Ammine Halides[34,35]
2. Metallocenes and Their Halides: Ti, V, Fe[36,37]
3. Gold and Other Metal Phosphines[39]
4. Other Main Group and Transition-Metal Compounds[36,40,41]

F. Miscellaneous Metals in Medicine

G. Summary and Prospectus

V. Platinum Anticancer Drugs: A Case Study

A. History of Discovery[47]

B. Principles that Underlie Drug Development

1. Strategic Considerations
2. Pre-clinical and Clinical Trials[49]
3. Mechanism of Action Studies

C. Clinical Picture for Cisplatin and Carboplatin[49,52]

1. Responsive Tumors and Combination Chemotherapy
2. Dose-limiting Problems; Toxicology
3. Pharmacology[49,52]

D. Bioinorganic Chemistry of Platinum Anticancer Drugs; How Might They Work?

1. Reactions of *cis*-DDP and Related Compounds in Aqueous, Biological, and Other Media
2. Evidence that DNA is the Target
3. Aspects of Platinum Binding to DNA
4. Mapping the Major Adducts of *cis*- and *trans*-DDP on DNA; Sequence Specificity

5. Structure of Platinum-DNA Complexes
6. Effects of DNA Structure on Platinum Binding
7. Speculations About the Molecular Mechanism
8. Site-Specifically Platinated DNA[154]

E. Design of New Inorganic Anticancer Drugs

1. Objectives
2. Strategies for Drug Development
3. Second- and Third-generation Platinum Anticancer Drugs
4. Nonplatinum Antitumor Metal Complexes

VI. Restrospective

The topics discussed in this chapter are helping to expand bioinorganic chemistry from a subject that arose chiefly from spectroscopic analysis of metal centers in proteins, because they were uniquely convenient functional groups, to a discipline where fundamental knowledge about metal functions and the application of metals as diagnostic and chemotherapeutic agents are making important contributions to medicine. As the case study of cisplatin is intended to demonstrate, progress in understanding how metals function in chemotherapy can be made only by the combined efforts of many disciplines, including synthetic and physical inorganic and organic chemistry, molecular and cell biology, immunology, pharmacology, toxicology, and clinical medicine. Although we have not yet reached the day where chemotherapeutic agents can be rationally designed from knowledge of a molecular mechanism, such a concept does not seem that farfetched. If nothing else, knowledge of fundamental bioinorganic processes related to metal-macromolecule interactions will continue to grow enormously through efforts to achieve this ultimate goal.

VII. References

1. H. Sigel, ed., *Metal Ions in Biological Systems*, Dekker, vol. 14, 1982.
2. D. A. Brown, *Metal Ions Biol. Syst.* **14** (1982), 125.
3. A. D. Young and R. W. Noble, *Methods Enzymol*. **76** (1981), 792.
4. D. A. Phipps, *Metals and Metabolism*, Oxford University Press, 1976, p. 63.
5. G. J. Brewer, *Metal Ions Biol. Syst*. **14** (1982), 57.
6. A. S. Prasad, *Metal Ions Biol. Syst.* **14** (1982), 37.
7. J. R. J. Sorenson, *Metal Ions Biol. Syst*. 14 (1982), 77.
8. D. R. Williams, *An Introduction to Bioinorganic Chemistry*, C. C. Thomas, 1976, p. 327.
9. Reference 8, p. 371.
10. Reference 4, p. 56.
11. Reference 8, p. 372.
12. K. N. Raymond and W. L. Smith, *Struct. Bonding* **43** (1981), 159.
13. Reference 8, p. 366.
14. C. T. Walsh *et al*., *FASEB* **2** (1988), 124.
15. J. G. Wright *et al.*, *Prog. Inorg. Chem*. **38** (1990), 323.
16. J. D. HeImann, L. M. Shewshuck, and C. T. Walsh, *Adv. Inorg. Biochem.* **8** (1990), 331.
17. M. J. Moore *et al*., *Acc. Chem. Res*. **23** (1990), 301.
18. Reference 8, p. 363.
19. Reference I, vol. 10, 1980.
20. K. E. Wetterhahn. *J. Am. Coll. Toxicol*. **8** (1989), 1275.
21. C. J. Mathias *et al.*, *Nucl. Med. Biol.* **15** (1988), 69.
22. A. Yokoyama and H. Saji, *Metal Ions Biol. Syst*. **10** (1980), 313.
23. R. C. Elder and M. K. Eidness, *Chem. Rev*. **87** (1987), 1027.
24. J. C. Dabrowiak, *Adv. lnorg. Chem*. **4** (1982), 70.
25. J. Stubbe and J. W. Kozarich, *Chem. Rev*. **87** (1987), 1107.
26. C. F. Meares and T. G. Wensel, *Acc. Chem. Res*. **17** (1984), 202.

27. R. B. Laufer, *Chem. Rev*. **87** (1987), 901.
28. N. J. Birch, *Metal Ions Biol. Syst.* **14** (1982),257.
29. S. Avissar *et al*., *Nature* **331** (1988), 440.
30. M. C. Espanol and D. Mota de Freitas, *Inorg. Chem*. **26** (1987), 4356.
31. P. F. Worley *et al*., *Science* **239** (1988), 1428.
32. B. M. Sutton, in Reference 159, p. 355.
33. K. C. Dash and H. Schmidbauer, *Metal Ions Biol. Syst.* **14** (1982), 179.
34. M. J. Cleare and J. D. Hoeschele, *Bioinorg. Chem.* **2** (1973), 187.
35. B. Rosenberg *et al*., *Nature* **222** (1969), 385.
36. P. Köpf-Maier and H. Köpf, *Chem. Rev.* **87** (1987), 1137.
37. P. Köpf-Maier and H. Köpf, *Struct. Bonding* **70** (1988), 105.
38. J. H. Toney, C. P. Brock, and T. J. Marks, *J. Am. Chem. Soc.* **108** (1986), 7263.
39. S. J. Bemers-Price and P. J. Sadler, in Reference 41, p. 527.
40. Reference 1, vol. 11, 1980.
41. M. Nicolini, ed., *Platinum and Other Metal Coordination Compounds in Cancer Chemotherapy*, Nijhoff, 1988.
42. Reference 8, p. 316.
43. Reference 4, p. 60.
44. C. C. Hinckley *et aI.*, in Reference 159, p. 421.
45. D. D. Perrin and H. Stiinzi, *Metal Ions Biol. Syst.* **14** (1982), 207.
46. C. Hill, M. Weeks, and R. F. Sehinazi, *J. Med. Chem.* **33** (1990), 2767.
47. B. Rosenberg, *Metal Ions in Biol.* **1** (1980), 1.
48. S. J. Lippard, *Science* **218** (1982), 1075.
49. B. Rosenberg, *Metal Ions Biol. Syst*. **11** (1980), 127.
50. J. M. Paseoe and J. J. Roberts, *Biochem. Pharmacol*. **23** (1974), 1345.
51. J. K. Barton and S. J. Lippard, *Metal Ions in Biol.* **1** (1980), 31.
52. P. J. Loehrer and L. H. Einhorn, *Ann. Intern. Med*. **100** (1984), 704.
53. R. F. Boreh, in Reference 41, p. 216.
54. L. R. Kelland *et al*., *Cancer Res*. **52** (1992), 822.
55. M. E. Howe-Grant and S. J. Lippard, *Metal Ions Biol. Syst.* **11** (1980), 63.
56. R. Faggiani *et al*., *J. Am. Chem. Soc*. **99** (1977), 777.
57. R. Faggiani *et al*., *Inorg. Chem*. **16** (1977), 1192.
58. T. G. Appleton, 1. R. Hall, and S. F. Ralph, in Reference 41, p. 634.
59. M. C. Lim and R. B. Martin, *J. Inorg. Nucl. Chem.* **38** (1976), 1911.
60. S. K. Mauldin *et al*., *Cancer Res*. **48** (1988), 5136.
61. W. I. Sundquist *et al*., *Inorg. Chem*. **26** (1987), 1524.
62. H. C. Harder and B. Rosenberg, *Int. J. Cancer* **6** (1970), 207.
63. J. H. Howle and G. R. Gale, *Biochem. Pharmacol*. **19** (1970), 2757.
64. S. Reslova, *Chem.-Biol. Interact*. **4** (1971), 66.
65. S. Reslova-Vasilukova, in T. A. Connors and J. J. Roberts, eds., *Recent Results in Cancer Research*, Springer, 1974, p. 105.
66. J. J. Roberts and A. J. Thomson, *Prog. Nucl. Acids Res. Mol. Biol*. **22** (1979), 71.
67. D. P. Bancroft, C. A. Lepre, and S. J. Lippard, *J. Am. Chem. Soc*. **112** (1990), 6860.
68. J.-P. Macquet, J.-L. Butour, and N. P. Johnson, in Reference 159, p. 75.
69. N. P. Johnson *et al*., *J. Am. Chem. Soc.* **107** (1985), 6376.
70. R. B. Ciccarelli, unpublished results.
71. J. C. Caradonna and S. J. Lippard, *Inorg. C*hem. **27** (1988), 1454.
72. K. Inagaki and Y. Kidani, *J. Inorg. Biochem.* **11** (1979), 39.
73. B. K. Teo *et al*., *J. Am. Chem. Soc.* **100** (1978), 3225.
74. H. M. Ushay, Ph.D. Dissertation, Columbia University, 1984.
75. A. B. Robins and M. O. Leach, *Cancer Treat. Rep*. **67** (1983), 245.
76. P. Bedford *et al*., *Cancer Res*. **48** (1988), 3019.

77. W. Bauer *et al.*, *Biochemistry* **17** (1978), 1060.
78. J. Filipski *et al.*, *Science* **204** (1979), 181.
79. K. M. Comess, C. E. Costello, and S. J. Lippard, *Biochemistry* **29** (1990), 2102.
80. W. A. Rembers, in *Antineoplastic Agents*, Wiley, 1984; p. 83.
81. S. E. Sherman and S. J. Lippard, *Chem. Rev.* **87** (1987), 1153.
82. J.-P. Macquet and T. Theophanides, *Bioinorg. Chem.* **5** (1975), 59.
83. D. M. L. Goodgame *et al.*, *Biochim. Biophys. Acta* **378** (1975), 153.
84. L. A. Zwelling *et al.*, *Cancer Res.* **38** (1978), 1762.
85. R. B. Ciccarelli *et al.*, *Biochemistry* **24** (1985), 7533.
86. S. J. Lippard and J. D. Hoeschele, *Proc. Natl. Acad. Sci. USA* **76** (1979), 6091.
87. G. L. Cohen *et al.*, *Science* **203** (1979), 1014.
88. S. J. Lippard, *Acc. Chem. Res.* **11** (1978), 211.
89. M. Howe-Grant *et al.*, *Biochemistry* **15** (1976), 4339.
90. J.-L. Butour and J.-P. Macquet, *Eur. J. Biochemistry* **78** (1977), 455.
91. J.-P Macquet and J.-L. Butour, *Biochimie* **60** (1978), 901.
92. S. F. Bellon and S. J. Lippard, *Biophys. Chem.* **35** (1990), 179.
93. J. A. Rice *et aI.*, *Proc. Natl. Acad. Sci. USA* **85** (1988), 4158.
94. H.-M. Wu and D. M. Crothers, *Nature* **308** (1984), 509.
95. S. F. Bellon, J. H. Coleman, and S. J. Lippard, *Biochemistry* **30** (1991), 8026.
96. W. Heiger-Bernays, J. M. Essigmann, and S. J. Lippard, *Biochemistry* **29** (1990), 8461.
97. J. J. Roberts *et al.*, in Reference 41, p. 16.
98. M. F. Pera, C. J. Rawlings, and J. J. Roberts, *Chem.-Biol. Interact.* **37** (1981), 245.
99. A. M. J. Fichtinger-Schepman *et al.*, in Reference 41, p. 32.
100. D. J. Beck *et al.*, *Nucleic Acids Res.* **13** (1985), 7395.
101. J. D. Page *et al.*, *Biochemistry* **29** (1990), 1016.
102. G. A. Curt, N. J. Clendeninn, and B. A. Chabner, *Cancer Treat. Rep.* **68** (1984), 87.
103. W. H. DeJong *et al.*, *Cancer Res.* **43** (1983), 4927.
104. A. Eastman and N. Schulte, *Biochemistry* **27** (1988), 4730.
105. A. Eastman *et al.*, in Reference 41, p. 178.
106. V. M. Richon, N. Schulte, and A. Eastman, *Cancer Res.* **47** (1987), 2056.
107. B. A. Donahue *et al.*, *Biochemistry* **29** (1990), 5872.
108. P. J. Stone, A. D. Kelman, and F. M. Sinex, *J. Mol. Biol.* **104** (1976), 793.
109. P. J. Stone, A. D. Kelman, and F. M. Sinex, *Nature* **251** (1974), 736.
110. H. M. Ushay, T. D. Tullius, and S. J. Lippard, *Biochemistry* **20** (1981), 3744.
111. T. D. Tullius and S. J. Lippard, *J. Am. Chem. Soc.* **103** (1981), 4620.
112. B. Royer-Pokora, L. K. Gordon, and W. A. Haseltine, *Nucleic Acids Res.* **9** (1981), 4595.
113. M. C. Poirier *et al.*, *Proc. Natl. Acad. Sci USA* **79** (1982), 6443.
114. S. J. Lippard *et al.*, *Biochemistry* **22** (1983), 5165.
115. E. Reed *et al.*, *J. Clin. Invest.* **77** (1986), 545.
116. M. C. Poirier *et al.*, *Environ. Health Persp.* **62** (1985), 49.
117. W. L Sundquist, S. J. Lippard, and B. D. Stollar, *Proc. Natl. Acad. Sci. USA* **84** (1987), 8225.
118. A. Eastman, *Biochemistry* **25** (1986), 3912.
119. A. M. J. Fichtinger-Schepman *et al.*, *Biochemistry* **24** (1985), 707.
120. A. M. J. Fichtinger-Schepman *et al.*, *Chem.-Biol. Interact.* **55** (1975), 275.
121. A. C. M. Plooyetal., *Carcinogenesis* **6** (1985), 561.
122. A. M. J. Fichtinger-Schepman *et al.*, *Cancer Res.* 47 (1987), 3000.
123. J. C. Dewan, *J. Am. Chem. Soc.* **106** (1984), 7239.
124. T. W. Hambly, *J. Chem. Soc. Chem. Comm.* (1988), 221.
125. J. H. J. den Hartog *et al.*, *J. Biomol. Struct. Dynam.* **2** (1985), 1137.
126. B. van Hemelryck *et al.*, *Biochem. Biophys. Res. Comm.* **138** (1986), 758.

127. L. S. Hollis *et al.*, in Reference 41, p. 538.
128. R. M. Wing *et al.*, *EMBO* **3** (1984), 1201.
129. J. R. Rubin, M. Sabat, and M. Sundaralingam, *Nucleic Acids Res.* **11** (1983), 6571.
130. S. E. Sherman *et al.*, *Science* **230** (1985), 412.
131. G. Admiraal *et al.*, *J. Am. Chem. Soc.* **109** (1987), 592.
132. S. F. Bellon, T. Takahara, and S. J. Lippard, unpublished results.
133. J. Kozelka *et al.*, *Biopolymers* **26** (1987), 1245.
134. B. Lippert, Prog, Inorg. Chem. 37 (1989), 1.
135. A. L. Pinto and S. J. Lippard, *Proc. Natl. Acad. Sci. USA* **82** (1985), 4616.
136. C. A. Lepre, K. G. Strothkamp, and S. J. Lippard, *Biochemistry* **26** (1987), 5651.
137. D. Gibson and S. J. Lippard, *Inorg. Chem.* **26** (1987), 2275.
138. J. L. van der Veer *et al.*, *J. Am. Chem. Soc.* **108** (1986), 3860.
139. C. A. Lepre *et al.*, unpublished results.
140. W. Saenger, *Principles of Nucleic Acid Structure*, Springer, 1984.
141. B. Malfoy, B. Hartman, and M. Leng, *Nucleic Acids Res.* **9** (1981), 5659.
142. T. D. Tullius and S. J. Lippard, *Proc. Natl. Acad. Sci. USA* **79** (1982), 3489.
143. B. E. Bowler and S. J. Lippard, *Biochemistry* **25** (1986), 3031.
144. B. E. Bowler, Ph.D. Dissertation, Massachusetts Institute of Technology, 1987.
145. J.-M Malinge, A. Schwartz, and M. Leng, *Nucleic Acids Res.* **15** (1987), 1779.
146. W. I. Sundquist *et al.*, *J. Am. Chem. Soc.* **112** (1990), 1590.
147. W. I. Sundquist *et al.*, *J. Am. Chem. Soc.* **110** (1988),8559.
148. D. P. Bancroft *et al.*, *J. Am. Chem. Soc.*, in press.
149. K. M. Comess, *Biochemistry* **25** (1992), 3975.
150. S. L. Bruhn, J. H. Toney, and S. J. Lippard, *Prog. Inorg. Chem.* **38** (1990), 477.
151. A. Sancar and G. B. Sancar, *Annu. Rev. Biochem.* **57** (1988), 29.
152. J. H. Toney *et al.*, *Proc. Natl. Acad. Sci. USA* **86** (1990), 8328; S. L. Bruhn *et al.*, *Proc. Natl. Acad. Sci. USA* **89** (1992), 2307; P. M. Pil and S. J. Lippard, *Science* **256** (1992), 234.
153. S. J. Brown, P. J. Kellett, and S. J. Lippard, *Science* **261** (1993), 603.
154. L. J. Naser *et al.*, *Biochemistry* **27** (1988), 4357.
155. S. E. Sherman *et al.*, *J. Am. Chem. Soc.* **107** (1988), 7368.
156. E. Rotondo *et al.*, *Tumori* **69** (1983), 31.
157. V. Brabec, O. Vrana, and V. Kleinwachter, *Studia Biophys.* **114** (1986), 199.
158. G. E. Plum and V. A. Bloomfield, *Biopolymers* **27** (1988), 1045.
159. J. K. Barton, *Chem. Eng. News* **66** (Sept. 26, 1988), 30.
160. S. J. Lippard, *Platinum, Gold. and Other Metal Chemotherapeutic Agents*, American Chemical Socicty, 1983.
161. W. I. Sundquist and S. J. Lippard, *Coord. Chem. Rev.* **100** (1990), 293.
162. I am grateful to the Alexander von Humboldt Foundation for a U.S. Senior Scientist Award, Massachusetts Institute of Technology for sabbatical leave time, and Prof. Drs. W. Herrmann and K. Wieghardt for their kind hospitality, all of which were essential for the preparation of the first draft of this chapter during the spring of 1988. I very much appreciate help from the following individuals: A. Davison, for providing Figure 9.2, and D. L. Bancroft, S. F. Bellon, S. L. Bruhn, J. N. Burstyn, K. M. Comess, G. B. Jameson, C. A. Lepre, and J. T. Toney for commenting critically on the manuscript. I also thank M. Mason for typing the first draft.

Contributors and Attributions

- Stephen J. Lippard (Massachusetts Institute of Technology, Department of Chemistry)

Thumbnail: Cisplatin, $PtCl_2(NH_3)_2$ A platinum atom with four ligands. (Public Domain; Benjah-bmm27).

9.6: Metals in Medicine is shared under a CC BY-NC-SA 4.0 license and was authored, remixed, and/or curated by LibreTexts.

9.6.1: Metal Deficiency and Disease

Essential Metals

Four main group (Na, K, Mg, and Ca) and ten transition (V, Cr, Mn, Fe, Co, Ni, Cu, Zn, Mo, and Cd) metals are currently known or thought to be required for normal biological functions in humans. Table 9.1 lists these elements, their relative abundances, and the medical consequences of insufficient quantities where known. The nutritional requirements for selected members of the essential metals are discussed in the following sections.

Table 9.1 - Essential metals and medical consequences resulting from their deficiency.[a]

a) Data taken from E.-i. Ochiai, *Bioinorganic Chemistry*, Allyn & Bacon, 1977, p. 6

Metal	Abundance	Abundance	Diseases Resulting from Metal Deficiency
	Sea Water mg/1 (ppm)	Earth's Crust mg/1 (ppm)	
Na	1.05×10^{4}	2.83×10^{4}	
K	380	2.59×10^{4}	
M-	1.35×10^{4}	2.09×10^{4}	
Ca	400	3.63×10^{4}	bone deterioration
V	2×10^{-3}	135	
Cr	5×10^{-3}	100	glucose tolerance (?)
Mn	2×10^{-5}	950	
Fe	1×10^{-2}	5.00×10^{4}	anemia
Co	1×10^{-4}	25	anemia
Ni	2×10^{-4}	75	
Cu	3×10^{-3}	55	brain disease, anemia, heart disease
Zn	1×10^{-2}	70	growth retardation, skin changes
Mo	1×10^{-2}	1.5	
Cd	1.1×10^{-4}	0.2	

Anemia and Iron[2]

Anemia results from insufficient oxygen supply, often because of a decrease in hemoglobin (Hb) blood levels. Approximately 65 to 70 percent of total body iron resides in Hb. In the U.S., many foods, especially those derived from flour, are enriched in iron. In third-world countries, however, scarcity of dietary iron is a major contributor to anemia. This information illustrates one important fact about disease that results from metal deficiency, namely, the need for an adequate supply of essential metals in food. A related aspect, one of greater interest for bioinorganic chemistry, is the requirement that metals be adequately absorbed by cells, appropriately stored, and ultimately inserted into the proper environment to carry out the requisite biological function. For iron, these tasks, among others, are performed by specific iron-chelating agents, the storage protein ferritin and the transport protein transferrin, the bioinorganic chemistry of which is extensively discussed in Chapter 1.

Another cause of anemia exists in individuals who have a mutant variety of hemoglobin, HbS, in which valine has been substituted for glutamic acid in the sixth position of the β subunits.[3] Interestingly, extensive studies have shown that this phenomenon, which

leads to sickling of the red blood cells, does not result from failure of the protein to bind heme or from changes in the O_2 binding constant of the iron atom. Rather, deoxy HbS polymerizes into soluble, ordered fibrous structures that lower the ability of blood to carry oxygen effectively to the tissues. These results illustrate the importance of structural features remote from the metal-binding domain in determining the functional characteristics of a metalloprotein.

Causes and Consequences of Zinc Deficiency[4-6]

The average adult contains ~ 2 g of zinc and requires a daily intake of 15 to 20 mg, only half of which is absorbed, to maintain this level. Although food in many technologically advanced societies contains sufficient zinc to afford this balance, zinc deficiencies occur in certain populations where there is either an unbalanced diet or food that inhibits zinc absorption. An especially interesting example of the latter phenomenon is found in certain villages in the Middle East where phytates, organic phosphates present in unleavened bread, chelate zinc ion and render it inaccessible. Zinc deficiency produces growth retardation, testicular atrophy, skin lesions, poor appetite, and loss of body hair. Little is known about the biochemical events that give rise to these varied consequences, although the three most affected enzymes are alkaline phosphatase, carboxypeptidase, and thymidine kinase. About 30 percent of zinc in adults occurs in skin and bones, which are also likely to be affected by an insufficient supply of the element. Zinc deficiency is readily reversed by dietary supplements such as $ZnSO_4$, but high doses (>200 mg) cannot be given without inducing secondary effects of copper, iron, and calcium deficiency.

Copper Deficiency[7]

More copper is found in the brain and heart than in any other tissue except for liver, where it is stored as copper thionein and released as ceruloplasmin or in the form of a complex with serum albumin. The high metabolic rate of the heart and brain requires relatively large amounts of copper metalloenzymes including tyrosinase, cytochrome c oxidase, dopamine-β-hydroxylase, pyridoxal-requiring monamine oxidases, and Cu-Zn superoxide dismutase. Copper deficiency, which can occur for reasons analogous to those discussed above for Fe and Zn, leads to brain disease in infants, anemia (since cytochrome oxidase is required for blood formation), and heart disease. Few details are known about the molecular basis for copper uptake from foods.

Summary

From the above anecdotal cases, for which similar examples may be found for the other metals in Table 9.1, the biological consequences of metal deficiency are seen to result from a breakdown in one or more of the following steps: adequate supply in ingestible form in foodstuffs; absorption and circulation in the body; uptake into cells; insertion into critical proteins and enzymes requiring the element; adequate storage to supply needed metal in case of stress; and an appropriate mechanism to trigger release of the needed element under such circumstances. Only for iron, and to a lesser extent copper and zinc, is there a reasonably satisfying picture of the molecular processes involved in this chain of events. The elucidation of the detailed mechanisms of these phenomena, for example, the insertion of iron into ferritin, remains an exciting challenge for the bioinorganic chemist (see Chapter 1).

9.6.1: Metal Deficiency and Disease is shared under a CC BY-NC-SA 4.0 license and was authored, remixed, and/or curated by LibreTexts.

9.6.2: Toxic Effects of Metals

Two Classes of Toxic Metal Compounds

As intimated in the previous section, the presence of excess quantities of an essential metal can be as deleterious as insufficient amounts. This situation can arise from accidental ingestion of the element or from metabolic disorders leading to the incapacitation of normal biochemical mechanisms that control uptake and distribution phenomena. These possibilities constitute one major class of metal toxicity. The other broad class results from entry of nonessential metals into the cell through food, skin absorption, or respiration. The toxicities associated with this latter class have received much recent attention because of the public health risks of chemical and radioisotopic environmental pollutants.

In this section, we survey examples of both categories, and discuss ways in which bioinorganic chemistry can contribute to the removal of toxic metals and restoration of normal function. One way involves chelation therapy, in which metal-specific chelating agents are administered as drugs to complex and facilitate excretion of the unwanted excess element. The use of desferrioxamine to treat iron poisoning is one example of this approach. A second role of bioinorganic chemistry is to identify fundamental biological mechanisms that regulate metal detoxification, and to apply the principles that emerge to help control the toxic effects of metal ions in the environment. Recent studies of mercury resistance and detoxification in bacteria provide an elegant example of the way in which biochemistry and molecular biology can be used to elucidate events at the molecular level. This work, which has uncovered the existence of metalloregulatory proteins, is described in some detail in Section III.F below. It represents a benchmark by which other investigations into the mechanisms of metal-detoxification phenomena may be evaluated.

Copper Overload and Wilson's Disease[8]

Wilson's disease results from a genetically inherited metabolic defect in which copper can no longer be tolerated at normal levels. The clinical manifestations are liver disease, neurological damage, and brown or green (Kayser-Fleischer) rings in the cornea of the eyes. Patients suffering from Wilson's disease have low levels of the copper-storage protein ceruloplasmin; the gene and gene products responsible for the altered metabolism have not yet been identified. Chelation therapy, using $K_2Ca(EDTA)$, the Ca^{2+} ion being added to replenish body calcium stores depleted by EDTA coordination, 2,3-dimercaptopropan-1-ol (BAL, British Anti-Lewisite), or d-penicillamine to remove excess copper, causes the symptoms to disappear. The sulfhydryl groups of the latter two compounds presumably effect removal of copper as Cu(I) thiolate complexes. Wilson's disease offers an excellent opportunity for modem methodologies to isolate and clone the gene responsible for this altered Cu metabolism, ultimately providing a rational basis for treatment.

Iron Toxicity[9]

Chelation therapy is also used to treat iron overload. Acute iron poisoning, such as that resulting from accidental ingestion of $FeSO_4$ tablets, results in corrosion of the gastrointestinal tract. Chronic iron poisoning, or hemochromatosis, arises from digestion of excess iron usually supplied by vessels used for cooking. A classic case of the latter is siderosis induced in members of the Bantu tribe in South Africa, who consume large quantities of beer brewed in iron pots and who suffer from deposits of iron in liver, kidney, and heart, causing failure of these organs. The chelating agent of choice for iron toxicity is the siderophore desferrioxamine, a polypeptide having a very high affinity for Fe(III) but not for other metals. Ferrioxamine chelates occur naturally in bacteria as iron-transport agents. Attempts to mimic and improve upon the natural systems to provide better ligands for chelation therapy constitutes an active area of bioinorganic research (see Chapter 1).

Toxic Effects of Other Essential Metals[10,11]

When present in concentrations above their normal cellular levels, most of the other metals listed in Table 9.1 are toxic. Calcium levels in the body are controlled by vitamin D and parathyroid hormones. Failure to regulate Ca^{2+} leads to calcification of tissue, the formation of stones and cataracts, a complex process about which little is understood (see Chapter 3). Chronic manganese poisoning, which can occur following ingestion of metal-oxide dust, e.g., among miners in Chile, produces neurological symptoms similar to Parkinson's disease. Neuron damage has been demonstrated. Although Zn toxicity is rare, it can lead to deficiencies in other essential metals, notably calcium, iron, and copper. Cobalt poisoning leads to gastrointestinal distress and heart failure. Metal poisoning by those elements has been treated by chelating agents, most frequently CaNaiEDTA), but the selectivity offered by the

ferrioxamine class of ligands available for iron has not even been approached. Fortunately, there are few cases involving these metals.

Plutonium: A Consequence of the Nuclear Age[12]

Some of the chelating agents developed to treat iron toxicity have found application as therapeutics for plutonium poisoning. Diethylenetriaminepentaacetic acid (DTPA) salts and siderophores are especially effective. Some improvement over the naturally occurring chelates has been made by tailoring the ligand to encapsulate completely the eight-coordinate Pu(IV) center. Although few individuals have been affected, ingestion of ^{239}Pu, for example, as small particles of PuO_2, at nuclear-reactor sites can have dire consequences. ^{239}Pu emits high energy ex particles, leading to malignancies of bone, liver, lung and lymph nodes, to which tissues it is transported by transferrin. With a maximum tolerated dose of only 1.5 μg, plutonium is among the most toxic metals known. We turn now to other, more classic examples of such industrial pollutants.

Mercuy Toxicity[13] and Bacterial Resistance[14-17]

Mercury is released into the environment as Hg(II) ions through weathering of its most common ore, HgS, red cinnabar. Organomercurials of general formula RHgX used in agriculture have also entered the environment as toxic waste. Both RHgX and HgX_2 compounds bind avidly to sulfhydryl groups in proteins, which can lead to neurological disease and kidney failure. Metallothionein is a favored protein target, which may help to limit mercury toxicity. A highly publicized case occurred in 1953 at Minimata, Japan, where 52 people died after eating mercury-contaminated fish and crustaceans near a factory waste outlet. The volatile, elemental form of mercury, Hg(0), is reportedly nontoxic, but its conversion to alkylmercury compounds by anaerobic microorganisms utilizing a vitamin B-12 biosynthetic pathway constitutes a serious health hazard.

Because of the high affinity of mercury for sulfur-donor ligands, mercury poisoning is treated by BAL; N-acetylpenicillamine has also been proposed. Recently, a very interesting natural detoxification system has been discovered in bacteria resistant to mercury; this system, when fully elucidated, might provide important strategies for treating heavy-metal poisoning in humans.

Presumably under environmental pressure, bacteria have developed mechanisms of resistance to HgX_2 and RHgX compounds in which mercury is recycled back to Hg(0). At least five gene products are involved in the bacterial mercury-resistance mechanism. MerT and MerP mediate the specific uptake of mercury compounds. MerB, organomercury lyase, and MerA, mercuric reductase, catalyze two of the reactions, given in Equations (9.1) and (9.2). Plasmids encoding the genes for these two proteins have been isolated. A typical arrangement of genes in the *mer* operon

$$RHgX + H^+ + X^- \xrightarrow[lyase]{organomercury} HgX_2 + RH \tag{9.1}$$

$$Hg(SR)_2 + NADPH + H^+ \xrightarrow[reductase]{mercuric} Hg(0) + NADP^+ + 2RSH \tag{9.2}$$

region of these plasmids is shown in Figure 9.1. The most thoroughly studied gene product is MerR, a metalloregulatory protein that controls transcription of the *mer* genes. In the absence of Hg(II) the MerR protein binds to DNA as a repressor, preventing transcription of the *merT, P, A*, and *B* genes (Figure 9.1) and negatively autoregulating its own synthesis. When Hg(II) is present, transcription of these genes is turned on. Interestingly, the MerR protein remains bound to the same site on DNA whether acting as an activator in the presence of Hg(II) or as a repressor in its absence. Random and site-specific mutagenesis studies implicate several cysteine residues in the carboxyl terminal region of the protein as candidates for the mercury-binding site.

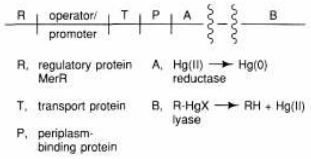
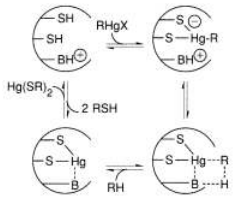


Figure 1, Reference 14).

Organomercury lyase, encoded by the *merB* gene, achieves the remarkable enzymatic step of breaking Hg-C bonds (Equation 9.1). It is a 22-kDa protein with no metals or cofactors. Two cysteine-sulfhydryl groups on the protein have been postulated to effect this chemistry, as depicted in Equation (9.3). Stereochemical studies of the Hg-C bond cleavage revealed retention of configuration, indicating that cleavage of the Hg-C bond probably does not proceed by a radical pathway. A novel concerted S_E2 mechanism has

been suggested. The enzyme turnover numbers, ranging from 1 min^{-1} for CH_3HgCl to 240 min^{-1} for butenylmercuric chloride, although slow, are ~10^5-10^8-fold faster than the nonenzymatic rate.



Mercuric ion reductase, the FAD-containing *merA* gene product, has several pairs of conserved cysteines. From site-specific mutagenesis studies, cysteine residues in the sequence 134-Thr-Cys-Val-Asn-Val-Gly-Cys-140 are known to comprise a redox-active disulfide group; in addition, a redox-inactive pair of cysteines near the carboxyl terminus is also required for the selective reduction of Hg(II). Exactly how the enzyme achieves the chemistry shown in Equation (9.2) is currently uncertain, but the redox activities of the flavin and disulfide/ thiol centers are undoubtedly involved. This enzyme serves both to detoxify mercury supplied directly from the environment as Hg(II) salts and to complete clearance of Hg^{2+} generated by the MerB protein from RHgX compounds. Clearly, Nature has invented a remarkable system to detoxify mercury in this fascinating class of Hg-resistant bacteria.

Cadmium and Lead Toxicity[18]

Gastrointestinal, neurological, and kidney toxicity are among the symptoms experienced by acute or chronic exposure to these heavy metals. The use of unleaded gasoline and the removal of lead-containing pigments from paint have substantially diminished the quantity of this element released to the environment each year. Cadmium sources include alkaline batteries, pigments, and plating. Lead poisoning can be treated by chelation therapy using $CaNa_2$(EDTA) (acute) or penicillamine (chronic). Although both Cd(II) and Pb(II) bind to sulfhydryl groups in thionein, we have little information at the molecular level on the mechanisms by which these elements induce toxicity.

Metals as Carcinogens[19,20]

Although most metal ions have been reported to be carcinogenic, the three most effective cancer-causing metals are Ni, Cr, and, to a lesser extent, Cd. Nickel subsulfide, Ni_2S_3, found in many nickel-containing ores, has been extensively studied and shown to be carcinogenic in humans and other animals. In short-term bioassays including mutagenesis, enhanced infidelity of gene replication *in vitro* and altered bacterial DNA repair were observed. Chromium is most carcinogenic as chromate ion (CrO_4^{2-}), which enters cells by the sulfate uptake pathway and is ultimately reduced to Cr(III) via a Cr(V)-glutathione intermediate species. The latter complex binds to DNA to produce a kinetically inert and potentially damaging lesion. Despite the fact that much information is available about metal-DNA interactions, molecular mechanisms of metal-induced carcinogenesis have not been elucidated. Two aspects of the problem are tumor initiation and tumor development, which are likely to involve different pathways. As new methods become available for studying the molecular events responsible for cancer (oncogenesis), it should be possible for bioinorganic chemists to unravel details of how metals act as carcinogens and as mutagens. Since cancer has genetic origins, metal/nucleic-acid chemistry is likely to be prominent in such mechanisms. As discussed later, metal-DNA interactions are an important aspect of the antitumor drug mechanism of *cis*-$[Pt(NH_3)_2Cl_2]$.

Summary

Toxicity can arise from excessive quantities of either an essential metal, possibly the result of a metabolic deficiency, or a nonessential metal. Both acute and chronic exposure can be treated by chelation therapy, in which hard-soft acid-base relationships are useful in the choice of chelating agent. Since chelates can also remove essential metals not present in toxic amounts, ligands with high specificity are greatly desired. The design and synthesis of such ligands for chelation therapy remains an important objective for the medicinal bioinorganic chemist. Until recently, studies of the toxic effects of metals and their removal, sometimes categorized under "environmental chemistry," have been empirical, with little insight at the molecular level. Application of the new tools of molecular biology to these problems has the potential to change this situation, as illustrated by rapid progress made in cloning the genes and studying the gene products of the mercury-resistance phenotype in bacteria. The discovery of such resistance

phenomena in mammalian cells, and even the remote prospect of transferring Hg-resistant genes from bacteria to humans, are exciting possibilities for the future.

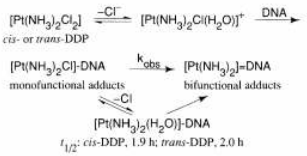
9.6.2: Toxic Effects of Metals is shared under a CC BY-NC-SA 4.0 license and was authored, remixed, and/or curated by LibreTexts.

9.6.3: Aspects of Platinum Binding to DNA

Given that DNA is a major target of platinum binding in cells, it is incumbent upon the bioinorganic chemist to investigate the nature of these interactions and their biological consequences. Of all the ligands studied in coordination chemistry, DNA is surely among the most complex. In the ensuing discussion, we first present experiments that delineate the chemical steps involved in *cis*- and *trans*-DDP binding to DNA as well as the chemical consequences of the adducts formed. We next describe the physical changes in the double helix that accompany platinum binding, and then we discuss the biological consequences that attend the platination of DNA. Subsequent sections describe the major adducts formed, in other words the regiospecificity of the drug, the three-dimensional structures of the adducts, and the way in which different structures within DNA can modulate platinum binding. Finally, we consider the response of the cell to Pt-DNA adducts, including studies with site-specifically modified DNA, and speculate about how this chemistry might relate to the antitumor drug mechanism.

a. Kinetics of Platinum Binding to DNA

The binding of *cis*- and *trans*-DDP to DNA has been studied[67] by ^{195}Pt NMR spectroscopy with the use of isotopically enriched ^{195}Pt, which has a nuclear spin I = $\frac{1}{2}$. The DNA used in this experiment was obtained from chicken red blood cell chromosomes that had been enzymatically degraded to relatively small pieces ranging from 20 to 60 base pairs in length (molecular-weight range 13 to 30 kDa). Since the ^{195}Pt chemical shifts are very sensitive to chemical environment, this NMR study provided important details about the kinetics and mechanism of platinum binding to the biopolymer. The rate-determining step in platination of the DNA is loss of chloride ion (Equation 9.5) to form the monoaqua complex, which rapidly coordinates to a nitrogen donor on the nucleic acid. The identification of the coordinating atom as nitrogen was possible because the ^{195}Pt chemical shift is characteristic of species having one chloride and three nitrogen ligands bound to Pt(II).[67] The spectroscopic changes that accompany the formation of the family of monofunctional adducts are shown in Figure 9.8. Subsequent hydrolysis of the second chloride ion leads to the formation of a second bond with DNA. This sequence of events affords bifunctional adducts and is similarly accompanied by discrete ^{195}Pt spectral changes (Figure 9.8). From the ^{195}Pt chemical-shift range of the final products, it was apparent that the *cis*-$\{Pt(NH_3)_2\}^{2+}$ moiety is bound primarily to two nitrogen donors on the nucleic acid. This chemistry is summarized in Equation (9.10), together with the half-lives for the mono-functional adducts. The half-lives were calculated from a kinetic analysis of the time-dependence of the ^{195}Pt spectral changes. As can be seen, the rates of closure of mono- to bifunctional adducts for the two isomers are quite similar, suggesting that their different biological properties are not a consequence of the kinetics of binding to DNA.



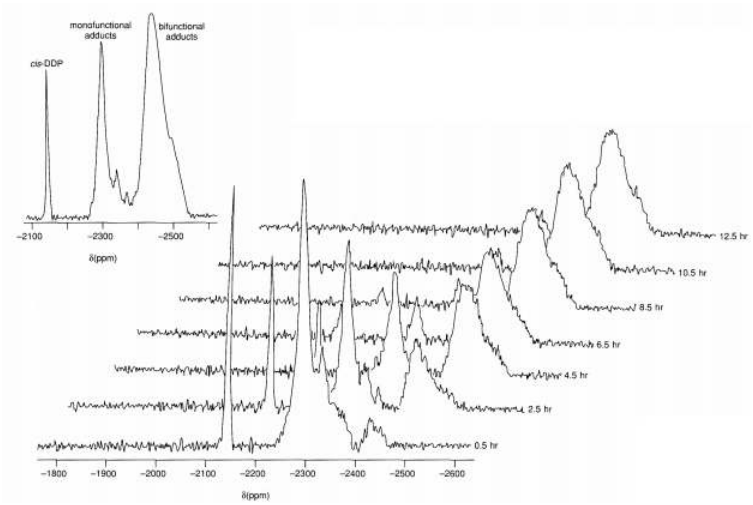


Figure 9.8 - Time course of the reaction between double-stranded chicken erythrocyte DNA and cis-$[Pt(NH_3)_2(H_2O)Cl]^+$ at a D/N = 0.07, in 3 mM NaCl and 1 mM NaH_2PO_4, 37 °C, pH 6.5. Each spectrum consists of 200,000 transients. The inset shows the sum of the individual spectra (reproduced by permission from Reference 67).

The next logical question to address is what donor atoms on DNA are coordinating to platinum in the mono- and bifunctional adducts. This important issue is discussed in considerable detail in Sections V.D.4 and V.D.5. As will be shown, the N7 atoms of the purine bases adenine and guanine are the principal binding sites. Alkylation of DNA at these positions facilitates depurination. Platinum binding to N7 atoms of purines (Figure 9.9), however, stabilizes the glycosidic (N9-C1') linkage.[68-70] Presumably the positive charge is better distributed over the platinum atom and its ligands in the adduct than over a purine alkylated at N7. On the other hand, platinum binding to N7 of guanine does perturb the charge distribution in the purine ring, as evidenced by the lowering of the pK_a of N1 by ≈ 2 units from its value in the unplatinated nucleotide (usually from $pK_a \approx 10$ to $pK_a \approx 8$).[71,72] This effect has been used to assign platinum binding sites in DNA fragments, as discussed below.

https://chem.libretexts.org/@go/page/484855

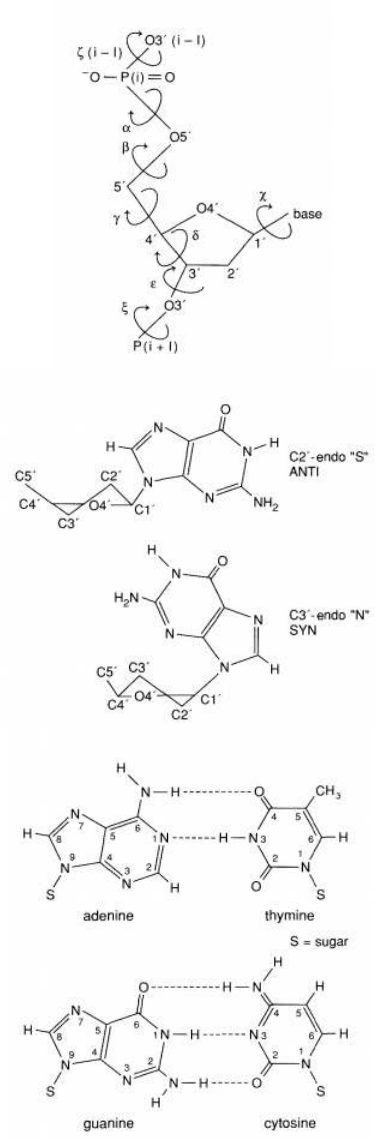


Figure 9.9 - Structural components of DNA. The left panel shows a schematic of the DNA backbone, including the deoxyribose ring numbering scheme and torsion angles. The center panel gives the two main classes of sugar pucker and base orientations. The right panel gives the bases in their Watson-Crick, A-T, and G-C pairs and the base numbering scheme, viewed down the helix axis, with the major grooves pointing toward the top of the figure and the minor grooves toward the bottom.

What are the chemical changes at the platinum center when *cis*-DDP binds to DNA? Both chloride ions are lost from the coordination sphere, as already indicated. Platinum EXAFS studies of calf-thymus DNA modified with *cis*-DDP revealed no chlorine backscattering features characteristic of Pt-CI bonds.[73] The spectra were consistent with the presence of four Pt-N/O linkages, since the technique is unable to distinguish between the two low-Z elements oxygen and nitrogen. Various studies reveal that, under most circumstances, the NH_3 ligands are not lost from DNA upon the binding of platinum ammine halides. For example, when ^{14}C-Iabeled *cis*-[$Pt(NH_2CH_3)_2Cl_2$] was allowed to bind to T7 (47 percent GC content) or *M. luteus* (73 percent GC content) DNA, no loss of radiolabel was found to accompany platinum binding.[74] *In vivo*, however, loss of amine ligands has been observed. Injection of ^{195m}Pt and ^{14}C doubly labeled [$Pt(en)CI_2$] into tumor-bearing mice resulted in unequal distribution of the two labels in various biochemical fractions, but there is no reason to believe that this result is relevant to the antitumor mechanism.[75] Metabolic inactivation of the drug could occur in a variety of ways unrelated to anticancer activity. The best evidence that ammine loss does not occur at the critical biological target of cisplatin is the finding, by using antibodies specific for *cis*-$\{Pt(NH_3)_2\}^{2+}$ nucleotide complexes (see Section V.D.4.c), that DNA, extracted from cells in culture or from human cancer patients treated with *cis*-DDP and subsequently degraded, contains intact Pt-NH_3 Iinkages.[76]

Once bonds are made between Pt and its targets on DNA, they are relatively inert kinetically. Platinum-DNA complexes can be subjected to various physical methods of separation and purification, including gel electrophoresis, ethanol precipitation, centrifugation, and chromatography, as well as to enzymatic and even chemical degradation procedures that digest the DNA, without releasing the platinum. Platinum can be removed, however, either by use of cyanide ion, to form the very stable ($K \sim 10^{41}$) $[Pt(CN)_4]^{2-}$ complex, or by excess thiourea.[77,78] These properties have proved to be extremely valuable in facilitating localization and characterization of the major *cis*- and *trans*-DDP binding sites on DNA.

Although Pt-DNA linkages are, generally speaking, kinetically inert, sometimes a particular adduct will rearrange into a more stable linkage isomer. One interesting example is the product of the reaction of *trans*-DDP with the dodecanucleotide 5'-d(TCTACGCGTTCT).[79] Initially the platinum coordinates to the two guanosine residues, forming a *trans*-$[Pt(NH_3)_2\{d(GCG)\}]$ 1,3-intrastrand crosslink. This complex rearranges to a more stable trans-$[Pt(NH_3)_2\{d(CGCG)\}]$ 1,4-intrastrand crosslink with a half-life of 129 h at 30 °C or 3.6 h at 62 °C. In this rearrangement product the platinum is coordinated to a cytosine and a guanosine residue.

As just described, the binding of bifunctional platinum complexes to DNA proceeds in a stepwise fashion. The second step is sufficiently slow (a few hours), however, that various reagents such as NH_3, nucleobases, and low concentrations of thiourea can coordinate to the fourth site and trap the monoadducts. Generally speaking, however, given sufficient time both *cis*- and *trans*-DDP will bind DNA in a bifunctional manner. As such, they bear some resemblance to organic alkylating agents, such as the nitrogen mustards, which have been employed as anticancer agents.[80]

b. Crosslinking Reactions of Platinum Complexes

There are three broad classes of DNA adducts that can be made by bifunctional platinum complexes. As illustrated for *cis*-DDP in Figure 9.10, they are DNA-protein crosslinks, interstrand DNA-DNA crosslinks, and intrastrand crosslinks,[81] A fourth possibility for platinum complexes is bidentate chelate ring formation utilizing two donor atoms on a nucleotide. For many years, a favored such postulated mode of binding was chelation by the N7-O6 positions of the guanine base (Figure 9.9), since this structure could be formed only by *cis*- and not by *trans*-DDP.[82,83]

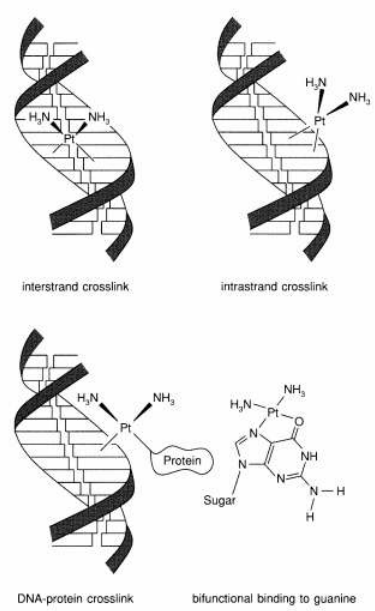


Figure 9.10 - Possible bifunctional binding modes of cis-DDP with DNA (reproduced by permission from Reference 81).

Such a structure has never been observed for *cis*-DDP binding to DNA, however. DNA-protein and interstrand crosslinks formed by platinum complexes have been the focus of many attempts to explain cytotoxicity and antitumor behavior.[84] The technique of alkaline elution, in which crosslinked DNA-DNA strands or DNA-protein molecules bind to filter paper following denaturation under basic conditions, sensitively and easily reveals such adducts. *trans*-DDP forms such adducts more rapidly than the *cis* isomer, perhaps because of its faster chloride-ion hydrolysis rates (see above) and a more favorable geometry, but they also seem to be repaired more rapidly in cells. As will be shown, interstrand and DNA-protein crosslinks are a small minority of adducts formed by

cisplatin, and their contribution to the cytotoxic and anticancer properties of the drug remains to be established. In studies of SV40 replication *in vivo*, DNA-protein crosslinking by *cis*- and *trans*-DDP was shown not to be correlated with the inhibition of DNA replication.[85]

What proteins form crosslinks to DNA? One possibility is the histones that make up the spools around which DNA is wound when packaged into chromatin in the nucleus. Studies[86] of *cis*- and *trans*-DDP binding to nucleosome core particles (each particle made up of eight histone proteins; around each particle is wound a 146-bp piece of DNA in a shallow superhelix of 1.75 turns) revealed the DNA binding to be little affected by the protein core. Both DNA-protein and specific histone crosslinked species were observed; from the latter it was suggested that DDP complexes might be useful crosslinking probes of biological structures. Other proteins likely to form crosslinks to DNA in the presence of platinum complexes are DNA-processing enzymes, or enzymes requiring a DNA template for normal function. In the *in vivo* SV40 study, for example, T antigen was one of the proteins found to be crosslinked to SV40 DNA by cisplatin.[85] Other nuclear proteins such as the high-mobility group (HMG) class are also crosslinked to DNA in the presence of *cis*-DDP. In all cases so far, DNA-protein crosslinking has occurred when platinum was added to cells. There is as yet no evidence that transfection of platinated DNA into cells results in such crosslinking or that crosslinks form during *in vitro* enzymatic digestions of platinated DNAs.

c. Physical Effects of Platinum-DNA Binding

(i). Unwinding, Shortening, and Bending of the Double Helix

Early studies of *cis*- and *trans*-DDP binding to DNA employed closed and nicked circular plasmids.[87] As was described in more detail in Chapter 8, closed circular DNAs are topologically constrained such that any change in the number of helical turns must result in an equal and opposite number of superhelical turns. Any reagent that unwinds the double helix reduces the number of helical turns. Consider, for example, a stretch of DNA that is 360 base pairs (bp) long. Normal B-DNA has ≈ 10.5 bp per turn or a helical winding angle of ≈ 34.3° per bp. Suppose the DNA is unwound, so that there are now 12 bp per turn or a winding angle of ≈ 30°. Instead of 34.3 helical turns (360 ÷ 10.5), the DNA now has only 30 (360 ÷ 12). If this DNA molecule were in the form of a covalently closed circle, the helical unwinding of -4.3 turns would be accompanied by a superhelical winding of +4.3 turns.

Planar organic dyes such as ethidium bromide (EtdBr) and inorganic complexes such as $[Pt(terpy)(HET)]^+$ (Figure 9.11) bind to DNA by intercalation, inserting between the base pairs and unwinding the double helix by ~ 26° per molecule bound (Figure 9.12).[88] This unwinding can be measured by monitoring changes in the superhelicity of closed circular DNA. This kind of DNA is subjected to certain topological constraints that lead to the formation of supercoils and superhelical winding that dramatically alter the hydrodynamic properties of the DNA. Either gel electrophoresis or analytical ultracentrifugation can be used to measure this phenomenon. The platinum complexes *cis*- and *trans*-DDP also produce changes in the superhelix density when bound to closed circular DNA.[87] As shown in Figure 9.13, increasing concentrations of platinum bound per nucleotide on the DNA first retard its mobility and then increase its mobility through the gel. These interesting alterations in gel mobility occur because the negatively coiled superhelix unwinds first into an open, or untwisted, form and then into a positively supercoiled form. The conformational changes, which are depicted in Figure 9.14, are directly proportional to the drug-per-nucleotide, or $(D/N)_b$, ratio. In addition to superhelical winding, both platinum complexes increase the mobility of nicked circular DNA in the gels (Figure 9.13). Nicked DNA has one or more breaks in the sugar-phosphate backbone, which relieve the topological constraint and prohibit the DNA from twisting into superhelical structures.

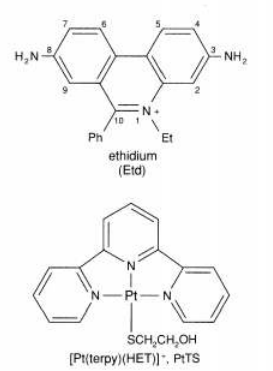


Figure 9.11 - Organic (top) and inorganic (bottom) intercalators.

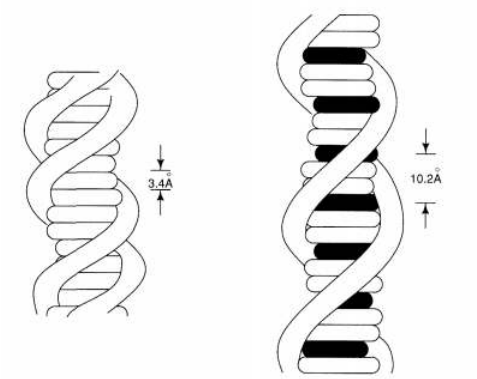


Figure 9.12 - Schematic representation of double-stranded DNA without (left) and with (shaded area, right) a bound intercalator (reproduced with permission from Reference 51).

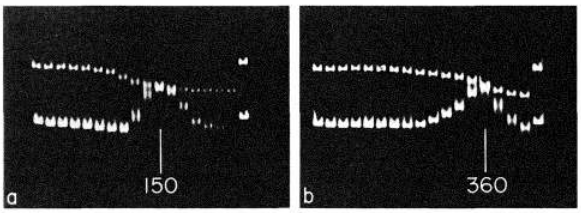


Figure 9.13 - Electrophoresis in 1 percent agarose gels of nicked and closed circular PSMI DNA incubated with (a) cis- and (b) trans-$[Pt(NH_3)_2Cl_2]$ as function of time. After electrophoresis, gels were stained with ethidium bromide. Reproduced with permission from Reference 51.

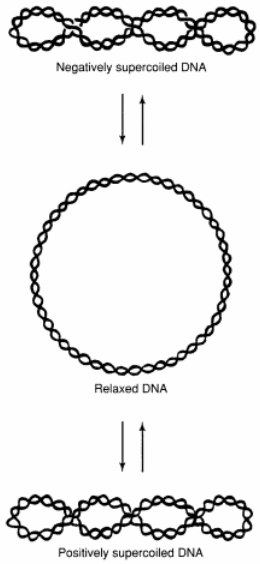


Figure 9.14 - Topological forms of closed circular DNA.

What could be the cause of these physical changes in the DNA structure upon *cis*- or *trans*-DDP binding? Intercalation can be excluded, not only because the compounds do not have the aromatic character normally associated with intercalators (Figure 9.11), but also through studies of the manner by which these and other platinum complexes inhibit the intercalative binding of EtdBr to DNA.[89,90] Platinum metallointercalators such as $[Pt(terpy)(HET)]^+$ are competitive inhibitors of EtdBr binding, as measured by fluorescence Scatchard plots, whereas the non-intercalators *cis*- and *trans*-DDP are not. Moreover, intercalation tends to lengthen and stiffen the double helix, whereas the mobility changes of nicked circular DNAs upon binding of *cis*- or *trans*-DDP were shown by electron microscopy experiments to arise from a pronounced shortening of the DNA with increased Pt binding.

One manner by which *cis*- or *trans*-DDP might produce these physical alterations in DNA structure is by kinking the double helix at or near the binding site. Such an effect could be produced by the bidentate attachment of platinum; the monofunctional $[Pt(dien)Cl]^+$ complex does not have these pronounced effects on DNA secondary structure.[91] Recently, it has been demonstrated that *cis*-DDP binding to DNA does indeed produce a pronounced bend in the helix axis.[92,93] The proof employed a gel-electrophoretic method of analysis that had previously been used to study DNA bending at naturally occurring specific sequences called A-tracts, consisting of five or six adenosine nucleosides in a row followed by about the same number of thymidine residues.[94] When these $d(A_5T_5)_2$ sequences are positioned in the center of a DNA restriction fragment of, say, 150 bp, the mobility of the DNA through polyacrylamide electrophoresis gels is greatly retarded compared to that of a similar DNA fragment where the A-tract is at the end. For the former fragment, the bent molecules presumably cannot snake their way through the pores of the polyacrylamide as well as the molecules whose bends are at the ends and have little effect on the linear structure. It was further shown that A-tracts bend the duplex toward the minor groove of the DNA. Moreover, in a DNA containing multiple A-tracts, the bends must be separated by integral numbers of helical turns (~ 10.5 bp) or else the effect will cancel and the gel mobility will be that of normal DNA of similar length. This latter phenomenon has been referred to as phasing.

With this background information in mind, we can now discuss the experiments with *cis*-DDP that demonstrated bending.[92,93] By methods described in Section V.D.8, a 22-bp oligonucleotide (22-mer) containing self-complementary overhanging ends ("sticky ends") was synthesized with a single *cis*-diammineplatinum(II) moiety linking adjacent guanosine residues (Figure 9.15A). A 22-mer was chosen since it has approximately two helical turns, accounting for some platinum-induced unwinding, and will thus have phased bends when polymerized. This platinated DNA was then labeled with ^{32}P and treated with the enzyme DNA ligase, which seals the ends, producing oligomers of the 22-mer having lengths 22, 44, 66, 88, 110, etc., bp. In these oligomers, the platinum atoms are spaced apart approximately by integral numbers of helical turns. As shown in Figure 9.15, studies of this family of oligomers by gel electrophoresis revealed a pronounced retardation compared to the mobility of unplatinated DNA oligomers of comparable size (line P22 in Figure 9.15B). The plots in this figure show the relative mobilities (R_L) of the different length multimers, compared to a control in which the top strand is not platinated, as a function of the length in base pairs. From the resulting curves may be extracted the extent of cooperative bending. When oligomers of a platinated DNA fragment in which the

metal atoms were spaced apart by 27 bp were examined, their relative mobilities were found to be nearly the same as unplatinated control molecules (line P27 in Figure 9.15B). These experiments unequivocally established that platinum kinks the double helix. As with A-tract-induced bends, the platinum atoms must be phased in order to induce cooperative bending. Comparison of the magnitudes of the gel mobility changes made it evident that *cis*-$\{Pt(NH_3)_2\}^{2+}$ binding produces a bend comparable to that of two A-tracts, ≈ 34°.

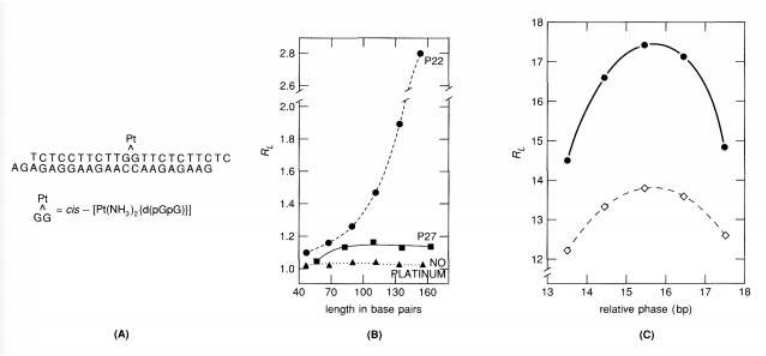


Figure 9.15 - Experiment to demonstrate that cis-$[Pt(NH_3)_2\{d(pGpG)\}]$ intrastrand crosslinks bend duplex DNA by ≈ 34°. Panel A shows the platinated 22-mer sequence, panel B the effect of platination on the gel-electrophoresis mobility of the 22-mer (P22) and a control 27-mer (P27) oligomers, and panel C the mobility of copolymerized DNAs containing cis-DDP and A-tract induced bends (●), 128-bp Pt + A-tract DNA; ♢ , 96-bp Pt + A-tract DNA) that maximize at approximately halfintegral helical turns corresponding to their phasing. For more detail consult Reference 93.

In a related series of experiments,[93] the platinated 22-mer was copolymerized with various A-tract-containing Il-mers to produce ladders of oligomers in which the phasing of Pt with respect to the center of the A-tract was varied, but the Pt atoms were always in phase. The results of these studies showed that maximum gel-mobility retardation occurred when the Pt and A-tract center were spaced apart by half-integral numbers of helical turns (Figure 9.15C). Since A-tracts bend the DNA into the minor groove, this result implies that platinum bends the DNA into the major groove. Only when phased by n/2 (n = integer) turns will copolymers of species situated alternatively in the major and minor grooves of DNA exhibit such cooperative bending. It will be shown later that helix bending of *cis*-DDP-DNA adducts into the major groove is in accord with their known structures.

The ability to prepare site-specifically platinated oligonucleotides (see Section V.D.8) has provided a means for measuring the extent to which *cis*-DDP produces local unwinding of the double helix.[95] When the platinum atoms are positioned with respect to one another, or phased, by exactly integral numbers of helical turns, the retardation of the DNA multimers in the gel is maximized. This phenomenon is illustrated in Figure 9.16, where the R_L values are plotted as a function of the interplatinum spacing for oligonucleotides containing the *cis*-$\{Pt(NH_3)_2d(GpG)\}$ intrastrand crosslink. When the resulting curve was analyzed, the maximum was found to occur at 21.38 bp. Since normal B-DNA has a helical repeat of 10.5 bp, one can compute the effect of platination from the expression [(21.38 - 2(10.5)] bp = 0.38 bp. From the fact that one helical turn of DNA comprises 360° and 10.5 bp, the unwinding of the DNA double helix due to the presence of a single *cis*-$\{Pt(NH_3)_2d(GpG)\}$ intrastrand crosslink can be calculated as

$$\left(\frac{0.38}{10.5}\right) \times 360 = 13^{o}. \qquad (9.6.3.1)$$

Similar studies of DNA platinated with *trans*-DDP have been carried out. In these, oligonucleotides containing the 1,3-*trans*-{Pt(NH3hd(GpNpG)} intrastrand crosslink were examined. The electrophoresis gels of polymerized 15-mers and 22-mers containing this adduct showed cooperative bending. This result indicates that bends at the sites of platination by *trans*-DDP are not phase sensitive, and has been interpreted to imply the formation of a "hinge joint" at these positions.[92,95] The directed bends and local unwinding of DNA produced by cisplatin could be an important structural element that triggers a response by cellular proteins. This subject is discussed in greater detail in Section V.D.7.d.

d. Biological Consequences of Platinum-DNA Binding

(i). Inhibition of Replication

Binding of *cis*-DDP to DNA inhibits replication both *in vivo* and *in vitro*, as shown by a variety of assays. Inhibition of replication of SV40 viral DNA in African green monkey cells as a function of the concentration of added *cis*-DDP is shown in Figure 9.17.

When SV40 virus infects monkey cells, it does not integrate its DNA into the genome of the host. Instead, it forms its own chromosomes in the cell nucleus. These so-called mini-chromosomes consist of ≈ 20 nucleosomes, fundamental chromosome building blocks. SV40 has its own life cycle, using virally encoded and cellular proteins to replicate and, ultimately, reassemble virus particles before lysing the cell and departing to infect neighboring cells.

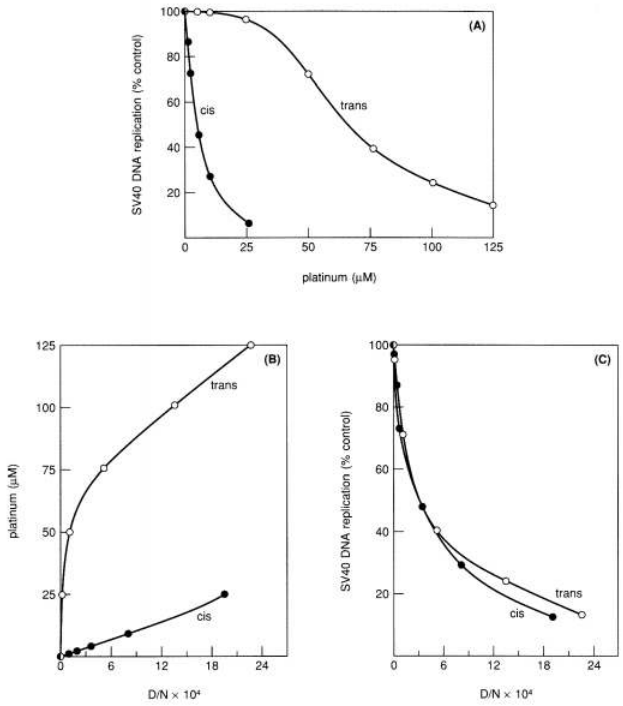


Figure 9.17 - SV40 DNA replication in CV-1 cells as a function of platinum concentration in the medium (panel A) or D/N (panel C). In panel B, DIN is plotted as a function of platinum concentration in the medium. SV40-infected cells were treated with cis-DDP (●) *or trans-DDP* (o) *at the indicated concentrations for 40 h. SV40 DNA replication relative to control (untreated) cells was measured by incorporation of [^{3}H]thymidine, added after the first 24 h of platinum treatment, and Pt in isolated SV40 chromosomes was measured by AAS. The data shown are from a representative experiment. Experiments were carried out in quadruplicate. Reproduced by permission from Reference 85.*

In the experiment shown in Figure 9.17, the SV40-infected cells were treated with cisplatin. After 24 h, [^{3}H]thymidine was added and, after 24 more hours, the cells were harvested, and SV40 DNA was isolated; the amount of DNA synthesis was recorded by comparing incorporated radiolabel with results from control experiments where no platinum was present. The data show that, when 25 μM platinum was present, SV40 DNA replication was reduced to about 5 percent of control. Quantitation reveals that, at ≈ 2 platinum atoms bound per thousand nucleotides (drug-per-nucleotide, or $(D/N)_b$, = 0.002), synthesis is only 10 percent that of control.

Recently, a related series of experiments has been carried out that can monitor DNA synthesis from templates platinated *in vitro*.[96] In this work, DNA plasmids containing the SV40 origin of replication are added to cellular extracts prepared from human kidney cells previously infected with adenovirus. In the presence of large T antigen, a virally encoded protein required for replication, SV40 DNA is synthesized from the plasmid templates. Synthesis can be conveniently monitored by [^{32}P]dATP incorporation. At a $(D/N)_b$ ratio of only 1.7 x 10^{-3}, DNA synthesis is about 5 percent of control, in agreement with the results of the *in vivo* study.

The binding of *cis*-DDP to DNA has also been measured for normal and tumor cells implanted in nude mice and in cells obtained from the ascites fluid of patients with ovarian carcinoma 24 h after their last dose.[97] The data for mouse bone marrow and a human pancreatic tumor xenograft show that, at a dose of 10 mg/kg, (D/Nh platinum binding levels of 3.3 x 10^{-6} and 1.82 x 10^{-6} reduce survival to 20 and 10 percent of control, respectively. These ratios are in good accord with platinum levels required to inhibit DNA synthesis in mammalian cells, as revealed by various studies, but substantially less than that needed for replication inhibition in the SV40 experiments described above. The difference can be readily explained, illustrating an important point. The SV40 genome, like most other DNAs of viral or plasmid origin, consists of only 15,000 nucleotides whereas the nuclear DNA of mammals has about 10^9 nucleotides. Thus, $(D/N)_b$ levels of ~ 10^{-6} would leave 99 out of 100 SV40 DNA molecules with no platinum at all, and

replication would hardly be affected. For the mammalian genome, $(D/N)_b$ values of 10^{-6} place 10^3 platinum atoms on each DNA genome, sufficient to inhibit replication and reduce cell survival. Platinum-DNA binding levels of this magnitude are found for ovarian ascites cells taken from patients receiving cisplatin chemotherapy.[97]

(ii). Mutagenesis and Repair

Apart from inhibition of DNA synthesis, what are the other biological consequences of cisplatin binding to DNA? One such consequence is mutagenesis, in which a normal base in the sequence is replaced by a different base. This phenomenon has been demonstrated for *cis*-DDP-treated cells in a variety of studies. What brings about such mutagenesis? There are several possibilities. One is that errors are introduced in DNA strands during attempts of the replication apparatus to synthesize past a platinum lesion. Another is that the platinum-damaged DNA is recognized by cellular repair systems that, in attempting to eliminate the platinated stretch of DNA, incorporate one or more incorrect nucleotides. Platinum-induced mutagenesis can lead to deleterious long-term health problems in patients treated with cisplatin. It is therefore important to understand the mechanism by which cellular DNA becomes mutated following platination, and to devise strategies for minimizing or eliminating this mutagenesis.

The foregoing considerations bring up another biological consequence of *cis*-DDP binding, namely, DNA repair. Removal of platinum from DNA by cellular repair mechanisms has been demonstrated by several groups. For example, in studying cis-DDP-treated human fibroblast cells in culture, it was found that the amount of bound platinum per nucleotide decreased according to first-order kinetics, from $(D/N)_b$ of 2.3×10^{-5} to 3.3×10^{-6} over a six-day period. Since Pt-DNA adducts are stable with respect to dissociation from DNA under physiological conditions (see above discussion), loss of platinum was attributed to DNA repair.[98]

How does the cell remove platinum from DNA? One mechanism is by a process known as excision repair, whereby the sugar-phosphate backbone on the platinated strand is hydrolyzed ("nicked") on either side of the damage and the remaining, unplatinated strand is used as a template for new DNA synthesis. The platinated oligonucleotide is displaced and the resulting gap filled in. In support of this picture is the fact that, in xeroderma pigmentosum (XP) human fibroblast cells, known to be deficient in excision repair, there is very little removal of platinum during post-treatment incubation.[99] Recent studies of *in vitro* repair of cisplatin-DNA adducts by a defined enzyme system, the ABC excision nuclease of *E. coli*, have provided some details at the molecular level about the process.[100,101] [^{32}P]-Labeled double-stranded DNA fragments containing $\{Pt(NH_3)_2\}^{2+}$ or $\{Pt(en)\}^{2+}$ adducts at random or defined sites were incubated with the enzyme. Cleavage of the platinated strand occurred at the 8th phosphodiester bond 5', and the 4th phosphodiester bond 3', to the GG or AG intrastrand crosslink. Further details about the identification and construction of such specific crosslinks will be given later in this chapter.

(iii). Drug Resistance

Another biological consequence of DNA-platinum interactions, probably related to the repair phenomenon, is resistance. Resistance of a cell to a chemotherapeutic agent, which can be inherent or acquired, is a phenotypical ability of the cell to tolerate doses of a drug that would be toxic to normal, or parent, cells.[102] Resistance is often acquired by prolonged exposure of cells in culture to the drug or, in patients, to repeated doses of drug therapy. There is not yet any direct proof that platinum-DNA interactions are responsible for acquired resistance to cisplatin. Studies of sensitive and resistant tumors in rats have shown, however, that after intravenous injection of 10 mg/kg of the drug, the platinum levels were the same after an hour, but after 24 hours a larger proportion of adducts had been removed in the resistant cells.[103] Similar results have been found for studies of Pt-DNA adducts in cultured L1210 cells of varying levels of resistance to cisplatin where, in the 18 h following a 6-hour incubation with the drug, the resistant cells had up to fourfold more platinum removed than the sensitive cells.[104]

Experiments have also been carried out showing that *cis*-DDP binding to DNA inhibits transcription, the formation of RNA from a gene, and that this phenomenon is less efficiently reversed for parent versus resistant L1210 cells in culture.[105] The assay involves transfection (the process whereby free or viral DNA or RNA is taken into a cell) of pRSVcat plasmid DNA into L1210 cells. The plasmid contains the bacterial *cat* gene in a position that permits its expression in mammalian cells. The *cat* gene encodes the enzyme chloroamphenicol acyltransferase (CAT), an activity readily measured following lysis of the cells. Transfection of the *cis*-DDP-damaged plasmid into resistant L1210 cells showed that up to eight times the amount of platinum was required in the resistant versus sensitive cells to produce a mean lethal hit (63 percent reduction in activity). This result is consistent with greater repair of platinum-DNA adducts in the resistant cells.

These results should not be construed to mean that DNA repair is the only mechanism of cisplatin resistance. There is evidence that relative amounts of glutathione are increased in cisplatin-resistant cells.[106] Glutathione presumably uses its thiol moiety to

coordinate platinum and diminish the amount that can bind to DNA. Reduced influx or increased efflux of a drug constitutes additional mechanisms by which cells become resistant. Further studies are required to ascertain which of these possibilities is most important for the cisplatin resistance phenomenon.

The discovery that cells can become resistant to cisplatin by repairing DNA lesions suggests a way to explain the selectivity of the drug for certain tumor tissue, and even the selective cytotoxicity of the drug for tumor versus normal cells of the same tissue. Tumor cells that cannot repair platinum-DNA adducts would be most affected by *cis*-DDP. This idea forms one of the central hypotheses about the molecular mechanism of action of *cis*-DDP, details of which can be probed by bioinorganic chemists. Specifically, it is important to inquire what DNA adducts formed by *cis*-DDP are both cytotoxic and repairable, what enzymes are responsible for such repair in mammalian cells, by what mechanisms these enzymes operate, and how this knowledge can be used to design better metal-based antitumor drugs and chemotherapeutic protocols.

(iv). DNA-protein Interactions

Most of the phenomena discussed in this section, inhibition of replication, DNA repair, drug resistance, and mutagenesis, probably involve interaction of a protein or group of proteins with platinated DNA. These interactions are clearly important in determining the biological consequences of DNA templates containing bound platinum. Very recent experiments have uncovered the existence of proteins from a variety of mammalian sources that bind specifically to DNA platinated with *cis*- but not *trans*-DDP.[107] Identifying the nature and function of these factors may provide important clues about the mechanisms of antitumor activity, drug resistance, or repair. Study of protein-DNA-drug interactions is an essential feature of the bioinorganic chemistry of platinum chemotherapeutic agents.

9.6.3: Aspects of Platinum Binding to DNA is shared under a CC BY-NC-SA 4.0 license and was authored, remixed, and/or curated by LibreTexts.

9.6.4: Survey of Metals Used for Diagnosis and Chemotherapy

Radiodiagnostic Agents[21,22]

Metal complexes having radioactive nuclei find many applications in medicine, such as in organ, and tissue imaging, Early detection of cancer, for example, by selective and imaging of the tumor using a radioactive metal compound can facilitate surgical removal or chemotherapeutic treatment before the disease reaches an advanced stage. radioisotopes used for diagnostic purposes be emit low-energy γ and no α or β particles. Table 9.2 lists the radionuclides most commonly employed for purpose in nuclear medicine. Among these, ^{99m}Tc is perhaps the most desirable,[23] for it gives off a 140-keV γ ray that is detected scintillation cameras and produces clear images. radionuclide is prepared from an alumina column loaded with $^{99}MoO_4^{2-}$, which decays to form $^{99m}TcO_4^-$, which in turn may be selectively eluted from the column with saline owing to its lower charge. treatment with a reducing agent in the presence of the appropriate ligands produces radiopharmaceuticals with desired water stability, and properties. Such complexes may be injected at concentrations of 10^{-6}-10^{-8} M. For example, isocyanide complexes such as $[Tc(CNR)_6]^+$= t-Bu, $CH_2CO_2Bu^t$, etc.) have been found to be taken up selectively into heart tissue and thus have the potential to be used as heart-imaging agents. Figure 9.2 displays bone as imaged a ^{99m}Tc bone agent. The dark correspond to surface areas of metabolic which can be used to diagnose or disease. One goal of research in this field is to images of myocardial infarcts or clogged arteries for physicians who can watch the patient's heart on a video surgery. Although chemical details responsible for the selective tissue of Tc isocyanide, and other complexes are largely synthetic modifications are and have many new compounds for evaluation.

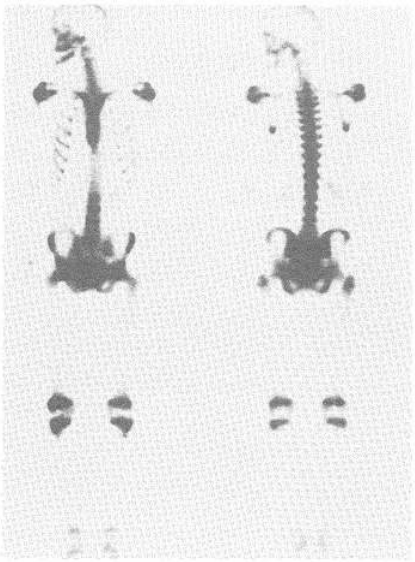


Figure 9.2 - Human skeleton (bone) imaged with ^{99m}Tc. Both anterior (left) and posterior (right) views are shown.

Table 9.2 - Radionuclides most commonly employed in diagnostic nuclear medicine.[a]

a) Data are from Table of the Isotopes in D. R. Lide, ed., *CRC Handbook of Chemistry and Physics*, CRC Press, 71 st ed., 1990-91, pp. 11-33 ff.

Radionuclide	Half-Life	Energy (keV)
^{57}Co	271 d	836
^{67}Ga	78 h	1,001
^{99m}Tc	6 h	140
^{111}In	67 h	172, 247
^{113m}In	104 m	392
^{123}I	13 h	1,230
^{169}Yb	32 d	207
^{197}Hg	64 h	159
^{201}Tl	72 h	135, 167

Among the few known to be absorbed selectively tumor cells is the antitumor antibiotic bleomycin (BLM),[24,25] the structure of which is portrayed in Figure 9.3. binds most radioactive metal ions, but the $^{57}Co(III)$ complex has the best tumor-to-blood ratio. Unfortunately, the long ^{57}Co (Table 9.2) has limited its clinical utility. Attempts to prepare ^{99m}Tc complexes of BLM with selective uptake properties approaching that of the cobalt have not yet been successful, although the target molecule would be a most valuable radiodiagnostic agent. One imaginative solution[26] to this problem was achieved by covalent attachment of an EDTA moiety to the terminal thiazole ring of BLM (Figure 9.3). The resulting Co(III) BLM-EDTA molecule was radiolabeled with $^{111}In^{3+}$ and found to be useful for diagnosis of cancer in humans. Also used for tumor imaging are ^{99m}Tc and ^{67}Ga citrate complexes, the latter being the agent of choice for many applications. Again, there is little known at the molecular level about the mechanism of tumor-cell specificity

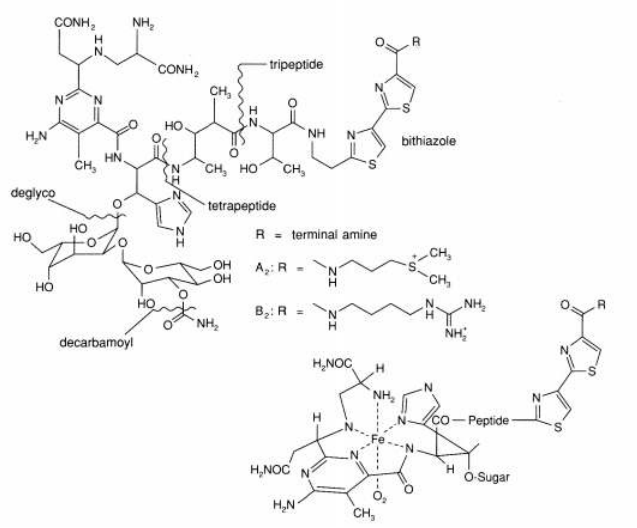


Figure 9.3 - Structure of bleomycin and its proposed iron complex (reproduced by permission from Reference 25).

An alternative approach to radionuclide-based tumor-imaging agents for diagnosis of disease is to modify, with metal chelating agents, antibodies raised against a biological substance, such as a tumor-cell antigen, hormone, or other target. Antibodies are proteins that are synthesized by specialized cells of the immune system in response to an external stimulant, or antigen. The high specificity and affinity of antibodies for the antigen can be used to target the antibody to a particular biological site, such as a site on the membrane of a particular cell type. Chelating agents are now routinely attached to antibodies and used to bind radioactive metal ions. The resulting radionuclide-labeled products are currently under extensive study in diagnostic medicine.[26]

Magnetic Resonance Imaging (MRI)[27]

Nuclear magnetic resonance (NMR) spectroscopy can be used to image specific tissues of biological specimens because of differences in the relaxation times of water proton resonances, usually brought about by paramagnetic metal ions. An early, pioneering example was the demonstration that Mn(lI) salts localize in normal heart-muscle tissue in dogs rather than in regions affected by blocked coronary arteries. Since the paramagnetism of the d^5 Mn(lI) ions alters the relaxation rate of nearby water protons, the normal and diseased tissue could be distinguished. Of the various metal ions surveyed in attempts to provide clinically useful NMR images in humans, Gd(III), Fe(III) , and Mn(lI) were found to give the best proton-relaxation enhancements. The gadolinium complex $[Gd(DTPA)(H_2O)]^{2-}$,an agent currently used in the clinic, has been successfully employed to image brain tumors. Ferric chloride improves gastrointestinal tract images in humans and, as already mentioned, manganous salts can be used for heart imaging. NMR imaging methodologies have advanced to the stage where increases as small as 10 to 20 percent in T_1^{-1}, the inverse nuclear-spin relaxation time, can be detected. As with radionuclide labeling, the complexes must be soluble and stable in biological fluids and relatively nontoxic, and are of greatest value when able to target a specific tissue. Even more important than targeting, however, is that proton relaxivity be maximally enhanced, an objective that depends not only upon the local binding constant but also upon large magnetic moments, long electron-spin relaxation (T_{le}) values, access to and the residence lifetime in the inner and outer coordination spheres by water molecules, and the rotational correlation time of the complex at its binding site. An obvious advantage of paramagnetic NMR over radioisotopic imaging agents is that there is no possibility of radiation damage; on the other hand, the need for 10-100 μM concentrations at the site of imaging is a distinct drawback. Both methods are likely to continue to be used in the future, and both will benefit from the design of new stable chelates that are selectively absorbed by the tissue to be diagnosed.

Lithium and Mental Health[28-31]

One in every 1,000 people in the United States currently receives lithium, as Li_2CO_3, for the treatment and prophylaxis of manic-depressive behavior. Doses of 250 mg to 2 g per day are administered in order to maintain a 0.5 to 2.0 mM concentration window, outside of which the drug is either toxic or ineffective. The detailed molecular mechanism by which Li^+ ion brings about its remarkable chemotherapeutic effects is largely unknown, but there are various theories. One theory proposes that lithium binds to inositol phosphates, inhibiting their breakdown to inositol, and so reducing inositol-containing phospholipids. A consequence of this chain of events would be disruption of the neurotransmission pathway based on inositol 1,4,5-triphosphate and 1,2-diacylglycerol, reducing neuronal communication, which is most likely hyperactivated in the manic state. This theory does not account for the antidepressive action of the drug, however. An alternative explanation is that lithium inhibits cyclic adenosine monophosphate (AMP) formation, again interfering with neurotransmission by intercepting this key intracellular signaling molecule. Recent experiments indicate that lithium affects the activation of G-proteins, a class of guanosine triphosphate (GTP)-binding proteins involved in information transduction. Possibly these effects result from displacement by Li^+ of Mg^{2+} from GTP and/or from protein-binding sites normally required for activation. Use of ^{7}Li NMR spectroscopy to study lithium transport in human erythrocytes suggests that it might be possible to apply this method to unravel details of the bioinorganic chemistry of lithium associated with the management of manic depression.

Gold and Rheumatoid Arthritis[23,32,33]

Gold compounds have been used in medicine for centuries, an application known as chrysotherapy. Since 1940, however, complexes of gold have been used most successfully to treat arthritic disorders in humans and other animals. Au(I) compounds are currently the only class of pharmaceuticals known to halt the progression of rheumatoid arthritis.

Until recently, gold compounds used to treat arthritis were painfully administered as intramuscular injections. Included were colloidal gold metal, colloidal gold sulfides, $Na_3[Au(S_2O_3)_2]$ (Sanocrysin), gold thiomalate and its sodium and calcium salts (Myochrisin), and polymeric gold thioglucose (Solganol, approved by the FDA). It was discovered, however, that triethylphosphinegold(l) tetra-O-acetylthioglucose (auranofin, Figure 9.4, approved by the FDA) was equally effective against rheumatoid arthritis and could be orally administered. The availability of this compound has sparked many studies of its biodistribution, stability, and possible metabolism that lead to antiarthritic activity. The mode of action of antiarthritic gold drugs is largely unknown, but it may involve binding of Au(I) to protein thiol groups, a process that inhibits the formation of disulfide bonds, and could lead to denaturation and subsequent formation of macroglobulins.

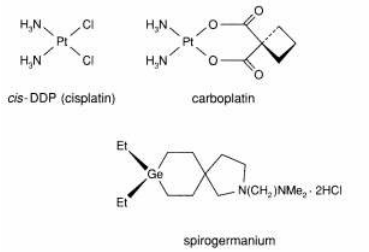


Figure 9.4 - Structures and trivial names of metal-based antitumor drugs.

Anticancer Drugs

1. Platinum Ammine Halides[34,35]

The discovery that *cis*-diamminedichloroplatinum(Il), *cis*-DDP or cisplatin (Figure 9.4), has anticancer activity in mice, and its subsequent clinical success in the treatment of genitourinary and head and neck tumors in humans, constitutes the most impressive contribution to the use of metals in medicine. Given in combination chemotherapy as an intravenous injection together with large amounts of saline solution to limit kidney toxicity, cisplatin treatment results in long-term (>5 yr) survival for more than 90 percent of testicular cancer patients. In a typical course, ~ 5 mg/kg body weight of the drug is administered once a week for four weeks. Extensive studies of platinum ammine halide analogues led to a series of empirical rules governing their chemotherapeutic potential. Specifically, it was concluded that active compounds should:

1. be neutral, presumably to facilitate passive diffusion into cells;
2. have two leaving groups in a *cis* configuration;
3. contain nonleaving groups with poor trans-Iabilizing ability, similar to that of NH_3 or organic amines;
4. have leaving groups with a "window of lability" centered on chloride.

These early structure-activity relationships have had to be modified somewhat, however, since chelating dicarboxylate ligands such as 1,1-dicarboxylatocyclobutane can replace the two chloride ions, and since cationic complexes with only one labile ligand, specifically, *cis*-$[Pt(NH_3)_2CI(4\text{-}X\text{-}py)]^+$, where X = H, Br, CH_3, etc., showed activity in some tumor screens. The two compounds shown in Figure 9.4, cisplatin and carboplatin (Figure 9.4), were the first to be approved for clinical use. Of particular interest to the bioinorganic chemist is that complexes having a *trans* disposition of leaving groups are inactive *in vivo*. This difference suggests the presence of a specific cellular receptor that, when identified, should facilitate the design of new, metal-based anticancer drugs. Present evidence strongly points to DNA as being the relevant cellular target molecule. Section V of this chapter expands on this topic in considerable detail.

2. Metallocenes and Their Halides: Ti, V, Fe[36,37]

Several compounds in this category, including $[(C_5H_5)_2TiX_2]$ (X = CI, Br, O_2CCl_3), $[(C_5H_5)_2VCl_2]$, $[(C_5H_5)_2NbCl_2]$, $[(C_5H_5)_2MoCl_2]$, and $[(C_5H_5)_2Fe]^+$ salts, exhibit significant activity against experimental animal tumors. Higher quantities (200 mg/kg) of these compounds than of *cis*-DDP can be tolerated with fewer toxic side effects, but their failure in two mouse leukemia screens commonly used to predict the success of platinum anticancer agents appears to have delayed their introduction into human clinical trials. Studies of Ehrlich ascites tumor cells treated with $[(C_5H_5)_2VCl_2]$ *in vitro* revealed selective inhibition of incorporation of radiolabeled thymidine, versus uridine or leucine, indicating that the complex blocks DNA replication. Unlike cisplatin, however, metallocene halides undergo rapid hydrolysis reactions in aqueous media, forming oxobridged and aqua complexes that may have a higher affinity for phosphate oxygen atoms than the heterocyclic nitrogen atoms of the bases in DNA.[38] Exactly how the ferrocenium ion might bind to DNA is even more obscure, although partial metallointercalation and groove binding are more likely than covalent attachment of the chemically unmodified cation. From the limited information available, metallocenes and their halides appear to behave fundamentally differently from platinum antitumor compounds. As a class, they provide a promising new opportunity to expand the scope of metal complexes used in cancer chemotherapy.

3. Gold and Other Metal Phosphines[39]

Following the successful entry of the soluble gold-phosphine complex auranofin (Figure 9.4) into the metal-based pharmaceuticals industry, several gold-phosphine complexes were examined for possible anticancer activity. Although auranofin itself was active in only a small fraction of the mouse tumor models tested, biological activity approaching that of cisplatin was discovered for many

analogues, most notably the diphosphine bridged complex [ClAu($PPh_2CH_2CH_2$ PPh_2)AuCI]. Attempts to replace the phosphine with As or S donor ligands, to increase or decrease the length of the 2-carbon bridge, or to replace the phenyl with alkyl groups all led to diminished activity. Most noteworthy is that the diphosphine ligands themselves have activity very similar to that of their gold complexes, and that Ag(I) and Cu(I) analogues are also effective. These results strongly imply that the phosphine ligands are the chemical agents responsible for the anticancer properties of these compounds. Coordination to a metal presumably serves to protect phosphines against oxidation to the phosphine oxides, which independent investigations have proved to be ineffective. A possible role for the metal in the cytotoxicity of the compounds cannot be ruled out, however.

4. Other Main Group and Transition-metal Compounds[36,40,41]

Several main group metal complexes exhibit anticancer activity. Gallium(III) nitrate is active against human lymphomas, but with dose-limiting side effects on the kidneys and gastrointestinal tract. Tin complexes of general formula $R_2L_2SnX_2$, where R = alkyl or phenyl, L_2 = py_2, bpy, or phen, and X_2 = two *cis*-oriented halide or pseudohalide leaving groups, are active against the mouse P388 leukemia tumor. The *cis* disposition of the leaving groups suggests a possible mechanism analogous to that of cisplatin (see below). Organo-gennanium compounds are also active, notably the derivative spirogermanium shown in Figure 9.4. Nothing is known about the mechanism of action of any of these compounds.

Following the discovery of activity for cisplatin, several thousand platinum and nearly 100 other transition-metal complexes have been screened in various tumor model systems in the hope of achieving better activity against a broader range of tumors. Among the classes of nonplatinum compounds showing some activity are ruthenium complexes *cis*-[$RuCl_2(DMSO)_4$], [$Ru(NH_3)_5$(Asc)] (CF_3SO_3), where Asc is ascorbate dianion, and *fac*-[$Ru(NH_3)_2Cl_4$] , all of which are believed to bind to DNA; binuclear rhodium complexes [$Rh_2(O_2CR)_4L_2$]; octahedral Pd(IV) complexes such as *cis*-[$Pd(NH_3)_2CI_4$]; and such miscellaneous molecules as the iron(II) complex of 2-formylpyridine thiosemicarbazone, the site of action of which is thought to be ribonucleotide reductase. These examples illustrate the broad scope encompassed by this field, which has a potential for developing fundamental infonnation about metal-biomolecule interactions as well as novel anticancer drugs. Much remains to be explored.

Miscellaneous Metals in Medicine

Numerous other anecdotal and some fairly elaborate studies have been reported for metal complexes as medicinal agents. The use of zinc applied topically to promote the healing of wounds dates back to around 1500 B.C., and silver is now commonly applied to prevent infection in bum patients.[42,43] Osmium carbohydrate polymers have been reported to have antiarthritic activity.[44] Transition-metal complexes have a long history of use as antibacterial and antiviral agents; for example, Zn^{2+} is used to treat herpes, possibly by inhibiting the viral DNA polymerase.[45] Early transition-metal (e.g., tungsten) polyoxoanions have been employed to treat AIDS patients.[46] Numerous reports have appeared detailing the anti-inflammatory, antiulcer, and analgesic activities of copper carboxylate complexes.[7] As in the previous section, these reports and others like them require more serious attention from bioinorganic chemists to elucidate the molecular events responsible for such a fascinating menu of biologically active metal complexes.

Summary and Prospectus

The clinical successes of platinum anticancer and gold antiarthritic drugs have changed the attitudes of many who doubted that heavy-metal compounds, notorious for their deleterious effects on human health, would ever playa serious role in chemotherapy. Indeed, we have seen that Hg^{2+}, Pb^{2+}, and Cd^{2+} are toxic elements. Even essential metals can be highly toxic if present in excess, either because of chronic or acute poisoning or because of metabolic defects that deregulate their control in the cell. An important common theme running throughout this discussion is selectivity. For a drug to be effective, it must be selectively toxic to diseased tissue while leaving nonnal tissue alone; or it must selectively kill harmful microorganisms at levels where it fails to deplete helpful ones. For a chelating agent to be useful in the toxic effects of metals, it must bind as selectively as possible to the deleterious ion while coordinating only weakly, if all, to others. For a diagnostic metal complex to be it must be taken up (or excluded) selectively from diseased cells relative to normal ones, or to one tissue type versus another. Rarely has such selectivity been designed in advance of the discovery of a useful metal-based pharmaceutical, although spectacular advances in biology, such as monoclonal antibodies, may be hastening the day when such an objective be common. Interestingly, the successes of such unlikely as *cis*-[$Pt(NH_3)_2Cl_2$] and [(Et_3P)Au(OAc_4-thioglucose)] in chemotherapy were driven by the personal involvement of individuals like B. Rosenberg for the former and B. Sutton for the latter. Like Hollywood producers, these men mustered every conceivable resource

to promote the compounds for testing, introduction into human clinical trials, and eventually approval by the FDA. Such zeal requires years, usually more than a decade, of sustained personal effort, and may be the reason why other metal complexes, such as those mentioned above, have not had the impact of a cisplatin or an auranofin. On average, only one of 7,000 such compounds makes it from the laboratory bench to the patient, at an average cost of 250 million dollars and a time interval of 13 years.

Another component of the evolving field of metals in medicine, however, is that, once a has proved its in the clinic, how does it work? This question is deceptively for coordination chemistry *in vivo*, and the of cells to respond to unnatural external stimuli such as metal complexes, are matters about which we are beginning to learn. As progress is made in this latter area, it should become possible to design drugs in a rational way to achieve the required selectivity.

The remainder of this chapter focuses on a case study where some progress in unraveling the molecular mechanism of a metal-based drug, cisplatin being made. If nothing else, this discussion will elucidate strategic guidelines that may be employed to attack similar questions about other chemotherapeutic metal compounds discussed earlier in this section. Unfortunately, there is very little information available about the molecular mechanisms of these other complexes. At this transition in our discussion, we move from general considerations to a specific, analysis. The reader must here take time to become familiar with the biological aspects of the new material.

9.6.4: Survey of Metals Used for Diagnosis and Chemotherapy is shared under a CC BY-NC-SA 4.0 license and was authored, remixed, and/or curated by LibreTexts.

9.6.5: Platinum Anticancer Drugs- A Case Study

History of the Discovery[47]

cis-[Pt(NH3hCh], a molecule known since the mid-19th century, has been a subject of considerable importance in the of inorganic stereochemistry and substitution reaction kinetics.[48] Its biological was discovered by accident. In the mid-1960s, biophysicist Barnett Rosenberg, at Michigan State University, was studying the effects of electric fields on the growth of *Escherichia coli* cells in culture. They had hypothesized that, during cell division, the orientation of the mitotic be affected by local electric which they hoped to perturb. Instead, they observed growth without cell division, the result being elongated, spaghetti-like bacterial filaments approaching 1 cm in length. After much detective work, they realized that small amounts of platinum from the electrodes used to apply the electric fields had reacted with NH_4CI in their buffer to produce various platinum ammine halide compounds. Two of these, *cis*-$[Pt(NH_3)_2Cl_2]$ and *cis*-$[Pt(NH_3)_2CI_4]$, were capable of inducing filamentous growth in the absence of any electric field. Since chemicals that produce filamentation in bacteria had been known to exhibit antitumor activity, Rosenberg was eager to have his platinum compounds tested. Unable to convince existing agencies like the National Cancer Institute (who to their credit later spearheaded the development of cisplatin) that a heavy-metal complex could actually be beneficial to animals, the Michigan State group set up their own animal-tumor screens. The results were nothing short of spectacular. Injection of *cis*-DDP directly into the abdominal cavity of mice into which a solid Sarcoma-180 tumor had been implanted led within a few days to a blackening (necrosis), reduction in size, and eventual disappearance of the tumor (Figure 9.5). The cured mouse enjoyed a normal lifespan. From these and other animal studies, physicians became convinced that administering platinum compounds to cancer patients might be worthwile, and a new field involving bioinorganic chemistry and cancer chemotherapy was born. The drug, marketed as Platinol with the generic name cisplatin, received FDA approval in 1979 and is today one of the leading anticancer agents.

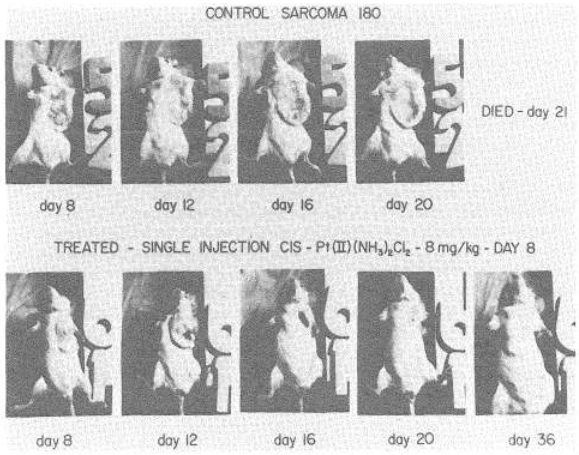


Figure 9.5 - Photographic demonstration of the dramatic ability of cisplatin to cure a Sarcoma-180murine tumor (reproduced by permission from Reference 47).

Principles that Underlie Drug Development

1. Strategic Considerations

There are two general routes to the development of inorganic complexes, and indeed most chemical compounds, as drugs. One, illustrated by cisplatin, arises from an empirical observation of biological activity followed by attempts to optimize the efficacy through investigations of structure-activity relationships (SAR). The goals are to minimize toxicity, to develop cell culture and animal screens for testing related compounds, and ultimately to elucidate the molecular mechanism. Knowledge of the molecular mechanism might evenlead to a rational strategy for designing better drugs.

The second general approach to drug design begins with known biochemistry. For example, ribonucleotide reductase is required in the first committed step in the biosynthesis of DNA, the conversion of ribo- to deoxyribonucleoside dir)hclsphat.es. The mammalian enzyme contains a binuclear non-heme iron center required for activity. Compounds that would selectively inhibit this enzyme by destroying this center are potentially useful as antiviral or antitumor agents. Another example is the enzyme reverse Iranscriptase, encoded by the HIV (AIDS) virus and required for its integration into the genome of the host cell. Compounds like

3'-azidothymidine (AZT) are accepted by the enzyme as substrates but, when added to the growing DNA chain, cannot be linked to the next nucleotide. Chain termination therefore occurs and the replication process becomes permanently interrupted. Attempts to find organic molecules or inorganic complexes that are more effective chain terminators than AZT constitute a rational strategy for developing new anti-AIDS drugs.

In the remainder of this chapter we describe research that has evolved following the discovery of biological activity for cisplatin. Although the initial breakthrough was serendipitous, subsequent studies have revealed many aspects of the molecular mechanism. From this known biochemistry we may one day be in a position to design more effective anticancer drugs and therapies based upon the fundamental bioinorganic chemistry of cisplatin.

2. Pre-clinical and Clinical Trials[49]

Predicting the chemotherapeutic potential of an inorganic compound such as *cis*-DDP prior to its introduction into human cancer patients is an important objective. Compounds are most easily tested for their cytotoxic effects on bacterial or mammalian cells in culture. Shown in Figure 9.6 are results for the survival of cultured L1210 cells in the presence of increasing amounts of *cis*- or *trans*-DDP.[50,51] The data reveal the markedly greater toxicity of the *cis* isomer, which is a much better anticancer agent than its stereoisomer. Unfortunately, no single assay has yet been found that can predict the chemotherapeutic potential of platinum compounds in humans. The best that can be obtained are results relative to those for *cis*-DDP, in which case toxicity at low dose is usually scored positive.

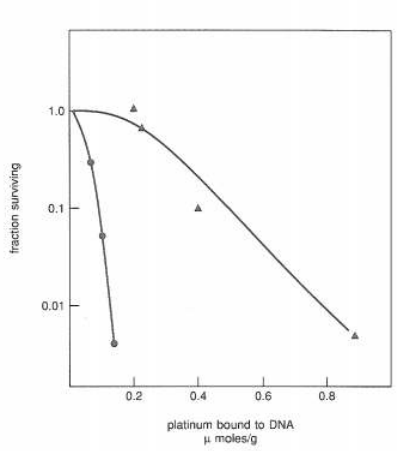


Figure 9.6 - Differential toxicity of cis- (●) and trans-DDP (▲) on HeLa cells growing in culture (reproduced by permission from Reference 51).

The next level of testing, often employed directly without first examining cell-culture results, involves animal (usually mammals, excluding human) screens.[49] Among the most popular measures of the chemotherapeutic activity of platinum compounds has been their ability to prolong the survival of mice bearing the L1210 or P388 leukemia. A suspension of cells is inoculated intraperitoneally (i.p., in the abdominal cavity), producing a leukemia that eventually progresses to the generalized disease. In one commonly used protocol, platinum compounds are dissolved in physiological saline (0.85 percent NaCl) or sterile H_2O and injected i.p. 24 h, 5, 9, and 13 days after inoculation of the leukemia cells. Several indices of antitumor activity and toxicity have been defined. The percent I.L.S., or increased lifespan measures the mean survival of treated versus control animals that were given no platinum drug. A related index is the median survival, percent T/C (Test/Control), which is 100 + percent I.L.S. The LD_{50} value measures toxicity as mean lethal dose,the amount of drug (usually in mg/kg body weight) required to kill half the animals. Potency is defined by lD_{90}, the inhibiting dose at which 90 percent of the tumor cells are killed. From these values, a therapeutic index (TI) = LD_{50}/lD_{90} is sometimes defined, which should be substantially greater than one. Typical values for *cis*-DDP are 85 percent I.L.S. at 8 mg/kg for the L1210 tumor, 13.0 mg/kg LD_{50}, and 1.6 mg/kg lD_{90} resulting in a TI of 8.1.

In addition to being tested in mice, cisplatin and related compounds have been screened in other mammals, specifically dogs and monkeys, mainly to look for possible dose-limiting side effects. Severe vomiting, once thought to be an insurmountable obstacle, was monitored by using ferrets. None of the animal screens can substitute for the ultimate test, however, which is human clinical trials. In 1972, such trials were initiated using terminally ill cancer patients. It was determined that intravenous (i.v.) injection,

rather than i.p. or oral administration, was the preferred method for giving the drug. Further details of the clinical development of cisplatin are discussed in a later section.

From the animal screens emerged the set of structure-activity relationships enumerated earlier (Section IV.E.1). Both cisplatin and carboplatin conform to these rules, and to date no compounds with demonstrably better antitumor activity have been tested in humans. The decision to move an experimental drug into the clinic is a difficult one, however, and it may be that molecules such as cis- $[Pt(NH_3)_2(4\text{-Br-py})Cl]Cl$ (see Section V.D.7.c) would be effective for tumors that are refractive to cisplatin chemotherapy. In any case, the foregoing chain of events, from studying the effects of a compound on cells in culture through animal screens and eventually to humans, constitutes the principal route for introducing a new anticancer drug. The process can take more than a decade.

3. Mechanism of Action Atudies

Once a class of compounds has been identified as biologically active, studies to elucidate the molecular mechanism of action can be undertaken. A first step is to identify the major cellular target or targets responsible for the chemotherapeutic properties of the drug. These investigations must also focus on chemical transformations that might take place in the solutions being administered and in the biological fluids that transport the drug to its ultimate target site. The next major step is to characterize the adduct or family of adducts made with the biological target molecule. The structure and kinetic lifetime of these adducts need to be investigated. Once this information is in hand, the effect of the adducts on the structure, stability, and function of the biological target molecule must be studied. Here many powerful new methodologies of modern molecular biology, genetics, and immunology can be brought to bear on the problem. The ultimate goals are to translate the molecular events elucidated into a realistic mechanism for how the drug molecule brings about its toxic effects selectively at the sites responsible for the disease and to use this information to design even better drugs.

Having progressed this far, we next need to bridge the gap between fundamental knowledge gained in studies of the mechanism of action and the SAR gleaned through pre-clinical and clinical trials. Whether such a happy situation can be reached for cisplatin remains to be seen, but there are encouraging signs, as we hope to demonstrate in the following discussion.

Clinical Picture for Cisplatin and Carboplatin[49,52]

1. Responsive Tumors and Combination Chemotherapy

It was an early observation that the best responses to cisplatin occurred in patients with genitourinary tumors. For testicular cancer, once a leading cause of death for males of age 20-40, cisplatin cures nearly all patients with stage A (testes alone) or B (metastasis or retroperitoneal lymph nodes) carcinomas. Platinum is usually given in combination with other drugs, commonly vinblastine and bleomycin for testicular cancer. This combination chemotherapy, as it is known, has several objectives. Some tumors have a natural or acquired resistance to one class of drugs and, by applying several, it is hoped that an effective reduction in tumor mass can be achieved. In addition, various drugs are known to affect different phases of the cell cycle, so several are applied simultaneously to allow for this possibility. Finally, synergism, where the response is greater than expected from simple additive effects, can occur, although it is rare. In addition to testicular cancer, platinum chemotherapy has produced responses in patients with ovarian carcinomas (>90 percent), head and neck cancers, non-small-cell lung cancer, and cervical cancer. Cisplatin is also effective when combined with radiation therapy.

2. Dose-limiting Problems; Toxicology

An early and quite worrisome adverse side effect of cisplatin was kidney toxicity. This problem, not commonly encountered with the older cancer drugs, nearly prevented its widespread use and eventual FDA approval. The major breakthrough here was made by E. Cvitkovic, who, while working at Sloan-Kettering Memorial Hospital in New York, administered large quantities of water by intravenous injection to patients, together with an osmotic diuretic agent such as D-mannitol. The rationale was that such hydration could ameliorate kidney toxicity by flushing out the heavy-metal complex. This simple idea worked, and the dose of the platinum compound could be increased threefold without accompanying nephrotoxicity. Hydration therapy is now commonly employed when cisplatin is administered. Among the other toxic effects encountered in cisplatin chemotherapy are nausea and vomiting, but this problem has also been controlled by use of antiemetic agents. Patients have also been known to experience bone-marrow suppression, a ringing in the ears, and occasional allergic reactions.

More recently, attempts have been made to extend cisplatin treatment to other broad classes of tumors by raising the dose above the ~5 mg/kg body weight levels given by i.v. injection every few weeks. Direct injection into the peritoneal cavity has been employed for refractory ovarian tumors. These more aggressive therapeutic protocols have been frustrated by drug resistance, a phenomenon by which cells learn to tolerate a toxic agent and for which many mechanisms exist, and by the return of the usual cisplatin side effects, most notably kidney toxicity and neurotoxicity. In order to combat toxic effects to the kidneys, chemoprotector drugs have been introduced. Based on the known affinity of platinum(II) complexes for sulfur-donor ligands, sodium diethyldithiocarbamate (DDTC) has been given both to experimental animals and to humans by i.v. infusion over about an hour following cisplatin administration.[53] DDTC inhibits many of the toxic side effects, particularly to the kidneys and bone marrow, without itself producing long-term side effects or apparently inhibiting the antitumor properties of *cis*-DDP. Similar efforts have been made to reduce the toxic effects of cisplatin with other sulfur-containing compounds including thiosulfate and the naturally occurring biomolecules glutathione, cysteine, and methionine. The relative amounts of the latter three molecules can be controlled by drugs that affect their normal cellular concentrations.

Another approach to reducing cisplatin toxicity is to develop new classes of platinum drugs or different routes of their administration. Carboplatin (Figure 9.4) is one result of these efforts. The bidentate chelating dicarboxylate leaving group in carboplatin presumably retards the rates of reactions leading to toxicity, but does not adversely interfere with the chemistry required for antitumor activity. Recently, promising platinum compounds for oral administration have been developed.[54] In Pt(IV) complexes of the kind *cis*, *trans*, *cis*-$[Pt(NH_3)(C_6H_{11}NH_2)\bullet(O_2CCH_3)_2Cl_2]$, where $C_6H_{11}NH_2$ is cyclohexylamine, have been found to be effective in preclinical screens. The greater kinetic inertness of these complexes apparently renders them sufficiently stable to the chemically harsh environment of the gastrointestinal tract. Once absorbed into the bloodstream, these compounds are metabolized to the Pt(II) analogues, *cis*-$[Pt(NH_3)(C_6H_{11}NH_2)Cl_2]$, which are presumed to be the active form of the drug. The Pt(IV) compound has recently entered clinical trials.

Although impressive inroads have been made in the management of human tumors by platinum chemotherapy, the fact remains that, apart from testicular and to a lesser extent ovarian cancer, the median survival times are measured in months. Clearly, there is much room for improvement.

3. Pharmacology[49,52]

Solutions of cisplatin are usually given in physiological saline (NaCl), since hydrolysis reactions occur that can modify the nature of the compound and its reactions *in vivo* (see below). Cisplatin is rapidly cleared from the plasma after injection, 70-90 percent of the platinum being removed within the first 15 minutes. It has been found that more than half the platinum binds to serum proteins and is excreted. Most of the platinum exits the body via the urine within a few days. These results account for the use of multiple-dose chemotherapy at intervals of several weeks. Animal studies employing *cis*-DDP labeled with ^{195m}Pt, a 99 keV γ-emitter with a 4.1-day half-life, reveal retention half-times in various tissues of 8.4 (kidney), 6.0 (ileum), 4.1 (liver), 2.8 (tumor), and 1.9 (serum) days following a single dose. Platinum distributes widely to all tissue, with kidney, uterus, liver, and skin having the most, and muscles, testes, and brain the least amount of the compound. There is no evidence for selective uptake into normal versus tumor cells.

9.6.5: Platinum Anticancer Drugs- A Case Study is shared under a CC BY-NC-SA 4.0 license and was authored, remixed, and/or curated by LibreTexts.

9.6.6: Mapping the Major Adducts of cis- and trans-DDP on DNA; Sequence Specificity

As we have seen, the antitumor activity of cisplatin is most likely the result of its DNA-binding properties. But what are the adducts? The human genome has more than a billion nucleotides. Does platinum recognize any special regions of the DNA or any particular sequences? In other words, is binding simply random or is there at least a regioselectivity? In this section, we discuss the best strategies for answering these questions, strategies that evolved in pursuit of learning how *cis*-DDP binds to DNA. We also illustrate their power in elucidating the DNA-binding properties of other metal complexes of interest to bioinorganic chemists.

a. Early Strategic Approaches

The first experiments to imply the sequence preferences of *cis*-DDP binding to DNA employed synthetic polymers.[108,109] Specifically, the buoyant density of poly(dG)•poly(dC), poly(dG•dC), and their *cis*-DDP adducts was studied in the analytical ultracentrifuge. The greatest shift in buoyant density was seen for the platinum adducts of poly(dG)•poly(dC), from which it was concluded that platinum forms an intrastrand crosslink between two neighboring guanosine nucleosides on the same strand. This interpretation was suggested by the known preference of metal ions, and especially platinum, for binding at the N7 position on the guanine base (Figure 9.9), information available from model studies of metal-nucleobase chemistry. Although other interpretations of the buoyant-density shift were possible, especially since the amount of platinum bound was not quantitated, the conclusion proved to be correct, as confirmed by later investigations. Interestingly, *trans*-DDP did not selectively increase the buoyant density of poly(dG)•poly(dC).

Following these initial experiments, the regioselectivity of *cis*-DDP binding was investigated by studying the inhibition of enzymatic digestion of platinated DNA. For example, the platinum complex inhibits the cleavage of DNA by restriction enzymes that recognize specific sequences and cut both strands of the double helix.[110] The resulting fragments are readily identified on electrophoresis gels. One such restriction enzyme is Bam HI. As shown by the arrows in Scheme (9.11), Bam HI cleaves a six-bp palindromic sequence at the phosphodiester bonds between two guanosine nucleosides. Formation of an intrastrand crosslink between the two adjacent guanosine nucleosides inhibits digestion by the enzyme. Another method, termed exonuclease mapping, involves digestion of the strands of duplex DNA from its 3'-ends.[111,112] When the enzyme encounters a bound platinum atom, it is unable to proceed further. Analysis of the digestion products by gel electrophoresis reveals the presence of discrete bands caused by the inhibition of digestion by bound platinum at specific sequences. Results from experiments of this kind were the most definitive at this time in demonstrating the profound regioselectivity of cisplatin for adjacent guanosines, and strongly supported the earlier conclusion that the drug was making an intrastrand d(GpG) crosslink.



Figure 9.18. Platinum is first bound to a single-stranded DNA template, in this example from bacteriophage M13mp18, to which is next annealed a short, complementary oligonucleotide termed a "primer" for DNA synthesis. Addition of the large (Klenow) fragment of *E. coli* DNA polymerase I and deoxynucleoside triphosphates, one of which bears a ^{32}P label, [α-^{32}P]dATP, initiates replication. When the enzyme encounters a platinum adduct, the chain is terminated. By running out the newly synthesized DNA strands on a sequencing gel, the sites of platinum binding can be detected by comparing the positions of the radiolabeled fragments with those obtained from sequencing ladders. The results of this procedure, which has been termed "replication mapping," confirmed that *cis*-DDP binds selectively to $(dG)_n$ ($n \geq 2$) sequences. In addition, they showed that *trans*-DDP blocks replication, in a much less regioselective manner, in the vicinity of sequences of the kind d(GpNpG), where N is an intervening nucleotide. These data afforded the first clear insight into the sequence preferences for *trans*-DDP on DNA. A control experiment run with DNA platinated by the monofunctional complex $[Pt(dien)CI]^+$ gave the interesting result that DNA synthesis was virtually unaffected.

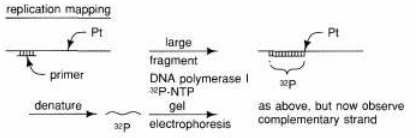


Figure 9.18 - Diagram illustrating the replication mapping experiment. To a single-stranded, platinated template is annealed a short primer for DNA synthesis using DNA polymerase I (Klenow fragment) and radiolabeled nucleotides. Sites of platinum binding are revealed as bands on gel electrophoresis where chain termination occurs (see text for details).

In yet another approach to the problem, DNA containing *cis*- or *trans*-DDP adducts was electrostatically coupled to bovine serum albumin, to enhance its antigenicity, and injected into rabbits.[113,114] The resulting antisera and antibodies were then studied for their ability to recognize and bind specifically to platinated DNAs having defined sequences, such as poly(dG)•poly(dC) and poly[d(GC)]•poly[d(GC)].

From experiments of this kind, the major *cis*-DDP adduct recognized by the antibody was found to be *cis*-[$Pt(NH_3)_2${d(GpG)}], in accord with the findings of the enzymatic mapping experiments. Unplatinated DNA was not recognized, nor was DNA platinated with *trans*-DDP. On the other hand, the antibody recognized DNA platinated with antitumor-active compounds [$Pt(en)Cl_2$] and [Pt(DACH)(CP)], where DACH = 1,2-diaminocyclohexane and CP = 4-carboxyphthalate. This result revealed that the antibody recognized the structural change in DNA that accompanies formation of d(GpG) intrastrand crosslinks, irrespective of the diamine ligand in the coordination sphere of the platinum atom. The antibody is also capable of distinguishing adducts formed by active versus inactive platinum complexes. Most importantly, DNA isolated from the cells of mice bearing the L1210 tumor five hours after cisplatin injection, was recognized.[113,115] Subsequent studies[116] revealed that these antibodies could detect cisplatin-DNA adducts formed in the white blood cells of patients receiving platinum chemotherapy. Thus, the antibody work linked the regiospecificity of platination chemistry *in vitro* with that occurring *in vivo* and in a clinically relevant manner.

Additional studies with monoclonal antibodies generated using DNA platinated with *cis*- or *trans*-DDP further confirmed and extended these results.[117] This later work indicated that intrastrand crosslinked d(ApG) and d(GpG) sequences possess a common structural determinant produced by *cis*-DDP platination, and that carboplatin is also capable of inducing the same DNA structure. For *trans*-DDP-platinated DNA, a monoclonal antibody was obtained that appeared to have the intrastrand d(GpTpG) adduct as its major recognition site. In all these studies, the primary structural determinant appears to be DNA duplex opposite the site of platination, since fairly major stereochemical changes could be made in the amine ligands with no appreciable effect on antibody binding.

b. Degradation, Chromatographic Separation, and Quantitation of DNA Adducts

Experiments in which DNA platinated with *cis*-DDP is degraded to chromatographically separable, well-defined adducts have been invaluable in revealing the spectrum of products formed. In a typical experiment, platinated DNA is digested with DNAse I, nuclease P1, and alkaline phosphatase. These enzymatic digestions degrade DNA into nucleosides that can be readily separated by high-performance liquid chromatography (HPLC). Detection of the adducts can be accomplished by the UV absorption of the nucleoside bases at 260 nm or, for platinum complexes containing a radioactively labeled ligand such as [^{14}C]ethylenediamine,[118] by monitoring counts. In addition to peaks corresponding to dA, dC, dG, and dT, the chromatographic trace contains additional peaks corresponding to specific platinum nucleobase adducts such as *cis*-[$Pt(NH_3)_2(dG)_2$]. The precise nature of these adducts was established by comparison with chemically synthesized compounds structurally characterized by NMR spectroscopy.[118-121] An alternative method for identifying the adducts employed antibodies raised against specific platinum-nucleobase complexes.[122]

This approach has revealed the relative amounts of various adducts formed by a variety of platinum complexes; selected results are summarized in Table 9.4. Usually, for cisplatin, the relative amounts of the various adducts formed varies according to the series *cis*-[$Pt(NH_3)_2${d(pGpG)}] > *cis*-[$Pt(NH_3)_2${d(pApG)}] > *cis*-[$Pt(NH_3)_2${d(GMP)}$_2$] > monofunctional adducts. Only when the total incubation time was short, less than an hour, were the monofunctional adducts more prevalent, as expected from the kinetic studies of *cis*-DDP binding to DNA discussed previously. It is noteworthy that no d(pGpA) adducts were detected. This result, which is consistent with information obtained by enzymatic mapping, can be understood on stereochemical grounds.[123] If the guanosine nucleoside N7 position is the most-preferred binding site on DNA, closure to make an N7,N7 intrastrand crosslink between two adjacent purine nucleotides is more feasible in the 5' direction along the helix backbone (N7•••N7 distance of ≈ 3 Å) than in the 3' direction (N7•••N7 distance ≈ 5 Å). In addition, molecular-mechanics modeling studies[124] indicate that a highly unfavorable steric

clash occurs between the 6-amino group of the 3'-adenosine residue in a d(pGpA) crosslink and the platinum ammine ligand, whereas in the platinated d(pApG) sequence, the 6-oxo group forms a stabilizing hydrogen bond to this ligand. A 28 kJ mol^{-1} preference of *cis*-DDP for binding d(pApG) over d(pGpA) was calculated.

Table 9.4 - Geometric features of the platinum coordination spheres of *cis*- [$Pt(NH_3)_2${d(pGpG)}].

a) Bond distances are in Angstroms and angles are in degrees.

b) Conventions used for assigning Base/Base and Base/PtN4 dihedral angles can be found in J. D. Orbell, L. G. Marzilli, and T. J. Kistenmacher, *J. Am. Chem. Soc.* **103** (l981), 5126. The numbers in square brackets refer to the corresponding N(ammine)•••O6 distance, in Å (see text).

Bond Distances and Angles[a]	Molecule 1	Molecule 2	Molecule 3	Molecule 4
Pt-N1	2.03(2)	2.01(2)	2.08(2)	2.08(2)
Pt-N2	2.03(3)	2.09(2)	2.04(3)	2.06(3)
Pt-N7A	2.01(2)	2.02(2)	1.91(3)	1.93(3)
Pt-N7B	2.05(2)	1.95(3)	2.00(3)	2.06(3)
N7A-Pt-N1	88.6(9)	90.3(9)	91.0(1)	88.4(9)
N7A-Pt-N2	179(1)	173.3(8)	178(1)	177(1)
N7A-Pt-N7B	89.1(9)	90.0(1)	85(1)	89(1)
N1-Pt-N2	92(9)	90.8(9)	91(1)	93(1)
qN1-Pt-N7B	176.5(9)	179.0(1)	173(1)	175(1)
N2-Pt-N7B	90.3(9)	89.0(1)	93(1)	89(1)

Dihedral Angles[b] Molecule	3'-Gua/5'-Gua	5'-Gua/PtN_4	3'-Gua/PtN_4
1	76.2(5)	110.6(5) [3.30(3)]	86.1(5)
2	81.0(5)	110.8(5) [3.49(3)]	95.5(5)
3	86.8(6)	81.0(6)	58.0(6) [3.11(4)]
4	80.6(5)	76.6(6)	59.6(6) [3.18(4)]

There are two likely sources of *cis*-[$Pt(NH_3)_2${d(GMP)}$_2$] in the spectrum of adducts. This species could arise from long-range intrastrand crosslinks, where the two coordinated guanosines are separated by one or more nucleotides. In support of this possibility is the fact that digestion of chemically synthesized *cis*-[$Pt(NH_3)_2${d(GpNpG)}], where N = C or A, led to *cis*-[$Pt(NH_3)_2${d(Gua)}-{d(GMP)}] and mononucleotides.[118,119,121] The other source of this product is interstrand crosslinked DNA, known to occur from the alkaline elution studies.

As indicated in Table 9.4, in all the experiments there was platinum that was unaccounted for in the quantitation procedures, which employed either antibodies, platinum atomic absorption spectroscopy, or a radiolabeled ethylenediamine ligand. Some of this material was assigned to oligonucleotides having high platinum content, resistant to enzymatic degradation.

Two important points emerge from the quantitation of adducts by this method. One is that intrastrand d(GpG) and d(ApG) crosslinks constitute the major adducts (>90 percent of total platination) made by cisplatin on DNA *in vivo*. Because they were identified by an antibody specific for their structures, no chemical change brought about by cellular metabolism has occurred. Secondly, the preponderance of these adducts far exceeds the frequency of adjacent guanosine or guanosine/adenosine nucleosides in DNA. This latter result implies a kinetic preference for, or recognition of, d(pGpG)- and d(pApG)-containing sequences by cisplatin.

c. Postscript: A Comment on Methodologies

With few exceptions, none of the experimental studies described in this section could have been carried out in 1969, when Rosenberg first demonstrated the anticancer activity of *cis*-DDP. The techniques of DNA sequencing, monoclonal antibody formation, oligonucleotide synthesis, HPLC, FPLC, and many of the higher resolution gel electrophoresis methodologies employed were the result of later developments driven by rapid advances in the fields of molecular biology and immunology. Future progress in elucidating the molecular mechanisms of action of cisplatin and other inorganic pharmaceuticals will no doubt benefit from new technological discoveries and inventions of this kind yet to come.

9.6.6: Mapping the Major Adducts of cis- and trans-DDP on DNA; Sequence Specificity is shared under a CC BY-NC-SA 4.0 license and was authored, remixed, and/or curated by LibreTexts.

9.6.7: Structure of Platinum-DNA Complexes

a. NMR Studies of Platinated Oligonucleotides

Once the major spectrum of adducts formed by *cis*- and *trans*-DDP with DNA began to emerge, it was of immediate interest to learn to what positions on the nucleobases the platinum atom was coordinated. Proton NMR spectroscopy soon proved to be an invaluable tool for obtaining this information.[71,125,126] Several ribo- and deoxyribooligonucleotides containing GG, AG, or GNG sequences were synthesized, and allowed to react with *cis*-DDP or its hydrolysis products, and the resulting complexes were purified by chromatography. All GG-containing oligomers formed intrastrand crosslinks with the $\{Pt(NH_3)_2\}^{2+}$ moiety coordinated to the N7 atoms. This structure was deduced from several criteria. Most frequently studied were the nonexchangeable base protons H8 and H2 of adenine, H6 of thymine, H8 of guanine, and H5 and H6 of cytosine (Figure 9.9). Coordination of platinum to N7 of guanine causes a downfield shift of the H8 proton resonance. More importantly, however, it also lowers the pK_a of the N1 proton by ~ 2 units, because platination adds positive charge to the base. Thus, titration of the platinated oligonucleotide over a pH range, and comparison of the results to those obtained for the unplatinated oligomer, reveals a difference in the midpoint of the transition in chemical shift of the H8 proton by 2 pH units if coordination occurs at N7. This effect is illustrated in Figure 9. 19 for the adduct *cis*- $[Pt(NH_3)_2\{d(ApGpGpCpCpT)\}N7\text{-}G(2),N7\text{-}G(3)]$, where the pK_a of N1 is seen to shift from ~ 10 to ~ 8 upon platination.[71] The pH titration in this example also reveals the pH-dependent chemical shift of the cytosine ^1H resonances at a pH of ~ 4.5, corresponding to protonation of the N3 atoms. The protonation of adenine N7 (pK_a ~ 4) is also frequently observed in these studies. These results conclusively demonstrate platinum coordination at N7 of the two guanosine nucleosides.

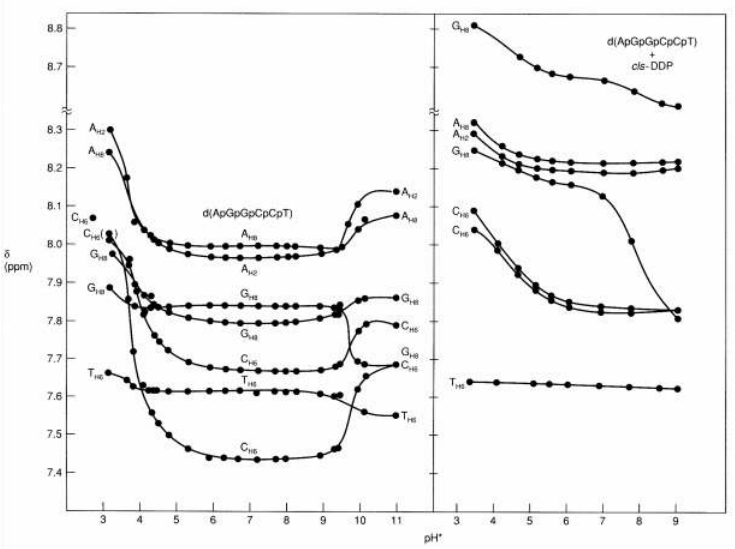


Figure 9.19 - Chemical shift (***δ***) vs. pH* of the nonexchangeable base protons of D_2O solutions of $[d(ApGpGpCpCpT)]_2$ (3.5 mM, 35 °C) and its cis-DDP adduct (2.5 mM, 70 °C). The pyrimidine resonances of the latter sample show no chemical shift changes with temperature over the range 35 < T < 70 °C while the purine resonances show a slight temperature-dependent chemical shift change of up to 0.1 ppm. Tetramethylammonium chloride was used as the internal standard (***δ*** 3.180). Reproduced by permission from J. C. Caradonna, S. J. Lippard, M. J. Gait, and M. Singh, J. Am. Chem. Soc. **104** (1982), 5793.

Although several of the oligonucleotides studied have self-complementary sequences, such that they can form a double helix when unplatinated, in no such case was a duplex observed for their platinated forms. The presence of the platinum-induced crosslink presumably decreases the stability of the doublestranded form of the oligonucleotide. Another interesting result is that all intrastrand $\{Pt(NH_3)_2\}^{2+}$ adducts of d(GpG) or d(ApG) have an altered deoxyribosesugar ring conformation. In normal, unplatinated form, these single-stranded or duplex oligonucleotides have a C2'-endo sugar pucker (Figure 9.9). Upon platination, the 5'-nucleotide switches to C3'-endo. This change is readily monitored by the ring proton-coupling constants $J_{H1'\text{-}H2'}$ and $J_{H1'\text{-}H2''}$. These protons constitute an ABX spin system such that the sum, $\Sigma^3J = {}^3J_{1'2'} + {}^3J_{1'2'}$, is most easily measured as the separation between the outermost peaks in the multiplet. For the C2'-endo conformation, a pseudotriplet occurs with Σ^3J = 13.6 Hz, and for C3'-endo, Σ^3J = 7.5 Hz. The 3'-guanosines in the adducts show greater conformational flexibility, having ~ 70 to 80 percent C2'-endo sugar puckers, depending upon the temperature.

Another conformational feature that could be deduced from ^{1}H NMR studies of all *cis*-DDP-platinated oligonucleotides containing an embedded d(GpG) sequence is that both guanosine nucleosides retain the anti orientation of the base around the C1'-N9 glycosidic linkage (Figure 9.9). This result was deduced from the lack of a pronounced nuclear Overhauser effect (NOE) between H8 and the H1' protons, such as would occur in the syn conformation. An NOE between H8 resonances on the two coordinated nucleosides was observed for adducts of d(ApTpGpG) and d(CpGpG), indicating that the two bases are in a head-to-head orientation with respect to the platinum coordination plane. In other words, both O6 atoms lie on the same side of that plane. Two oligonucleotides containing *cis*-[$Pt(NH_3)_2$(ApG)] adducts have been examined; their structural properties closely resemble those of the (GpG) adducts, with platinum coordinated to N7 of both purine bases.

In order to study double-stranded DNAs platinated on one strand, it was necessary to adopt a special strategy. First, the desired oligonucleotide is synthesized. It is preferable that the DNA strands not be self-complementary, since the affinity of such an oligomer for itself is so much greater than that for its platinated form that the desired, singly platinated duplex will not form. After the platinated single strand is synthesized and purified, the complementary strand is added. Several duplex oligonucleotide-containing *cis*-[$Pt(NH_3)_2${d(pGpG)}]-embedded adducts prepared in this manner have been studied by ^{1}H NMR spectroscopy. With the use of two-dimensional and temperature-dependent techniques, both the nonexchangeable base and sugar protons as well as the exchangeable (guanine N1 and thymine N3) N-H (imino) proton resonances were examined. The last are useful, since they give some measure of the extent to which the double helix remains intact. When not base-paired to their complements in the other strand, these protons exchange more rapidly with solvent (water) protons, leading at moderate exchange rates to broadening of the resonances and, at high exchange rates ($>10^{7}$ s^{-1}), disappearance of the signals. Several interesting results were obtained in these studies. In all of them, platination of the d(GpG) sequence brought about the same C2'-endo → C3'-endo sugar-ring pucker switch for the 5'-guanosine as seen in the single-stranded adducts. Head-to-head, anti conformations were also observed. At low temperatures, below the melting transition temperature, above which the duplex becomes single-stranded, the imino proton resonances were observed. This result was interpreted to mean that normal, Watson-Crick base pairs can still exist between the *cis*-DDP d(GpG) adduct and the d(CpC) sequence on the complementary strand. In the case of [d(TpCpTpCpG*pG*pTpCpTpC)]•[d(GpApGpApCpCpGpApGpA)], where the asterisks refer to the sites of platination, the imino proton resonances were assigned with the assistance of NOE experiments.[125] Temperature-dependent studies showed that, in the range - 4° < T < 46 °C, the imino resonances of the coordinated guanosine nucleosides broadened first with increasing temperature. Apparently the base pairs of the intrastrand crosslinked, platinated duplex DNA are disrupted, or "melted," outward from the point of platination as well as from the ends. Since the amino hydrogen atoms involved in base pairing were not observed in this study, a completely definitive structural analysis was not possible. Nevertheless, the authors proposed that the duplex would be kinked by an angle of ~ 60° at the *cis*-DDP binding site in order to preserve full duplex character.

Another useful NMR nucleus for monitoring *cis*-DDP-DNA interactions is ^{195}Pt, which is 34 percent abundant with I = $\frac{1}{2}$. When used in conjunction with ^{15}N (I = $\frac{1}{2}$) enriched NH_3 ligands, ^{195}Pt NMR resonances provide a powerful means for characterizing complexes in solution. The ^{195}Pt and ^{15}N chemical shifts are both sensitive to the ligand trans to the NH_3 group, as is the ^{195}Pt-^{15}N coupling constant.[127] ^{195}Pt NMR studies of *cis*-DDP binding have been carried out using nucleobases, small oligonucleotides, and even double-stranded fragments of 20 to 40 bp in length, as previously described (Section V.D.l). The major contribution of this method is to show whether platinum coordinates to a nitrogen or an oxygen donor atom on the DNA, since the ^{195}Pt chemical shift is sensitive to this difference in ligation.

b. X-ray Structural Studies

In recent years several oligonucleotide duplexes have been crystallized and characterized by x-ray diffraction methods. The probability of forming suitable single crystals of DNA fragments is disappointingly low, however, with only 1 in 10 such attempts being successful. Correspondingly, it has been difficult to crystallize platinated oligonucleotides. An alternative approach has been to soak nucleic-acid crystals of known structure with the platinum reagent in the hope of forming an isomorphous derivative, the structure of which could be obtained by using the changes in phases from the native material. In attempts to characterize a *cis*-DDP nucleic acid adduct, crystals of $tRNA^{Phe}$ and the self-complementary dodecamer d(CpGpCpGpApApTpTpCpGpCpG) were soaked with cisplatin solutions in the hope of obtaining useful metric information.[123,128,129] These efforts have thus far failed to produce a high-resolution structure, although they confirm the predilection for platinum to coordinate to the N7 position of purine rings. Addition of *cis*-DDP tends to disorder the crystal, with platinum going to several sites of partial occupancy.

A more fruitful approach has been to crystallize a purified oligonucleotide containing the coordinated *cis*-$\{Pt(NH_3)_2\}^{2+}$ moiety. The first x-ray structure to be deciphered through such a strategy was that of *cis*-$[Pt(NH_3)_2\{d(pGpG)\}]$.[130] This compound crystallizes with water solvent and glycine buffer molecules in the lattice. The crystals were grown at pH 3.8, where the terminal phosphate is monoprotonated in order to provide a neutral complex of diminished solubility. Two crystalline forms have been obtained, and both structures solved, one to 0.94 Å resolution. The latter contains four crystallographically independent molecules, which, although complicating the structure solution, afforded four independent views of the major adduct formed by *cis*-DDP with DNA. The four molecules form an aggregate, held together by hydrogen bonding and intermolecular base-base stacking interactions (Figure 9.20). There are two conformationally distinct classes that comprise molecules 1 and 2, and molecules 3 and 4; within each class, the molecules are related by an approximate C_2 symmetry axis.

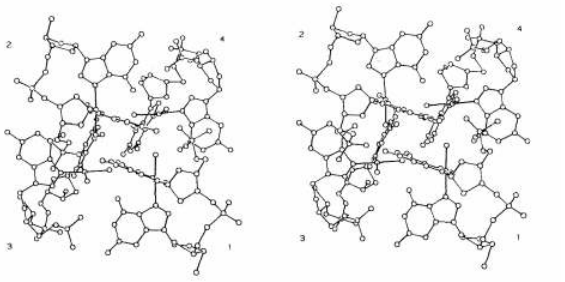


Figure 9.20 - Stereoview of aggregate of four cis-$[Pt(NH_3)_2\{d(pGpG)\}]$ molecules (reproduced by permission from Reference 130).

The molecular structure of molecule 1 is displayed in Figure 9.21; geometric information about all four molecules is contained in Table 9.4. As expected from the NMR studies, platinum coordinates to N7 atoms of the guanine bases, which are completely destacked (dihedral angles range from 76.2 to 86.7°), to form a square-planar geometry. The bases have a head-to-head configuration and conformational angles χ (Table 9.4 and Figure 9.9) that fall in the anti range. The sugar puckers of the 5'-deoxyribose rings for all four molecules have a C3'-endo conformation, and some of the 3'-sugar carbon atoms exhibit large thermal parameters suggestive of a less well-ordered structure. These results further demonstrate the similarity of the structure as detected in the solid state by x-ray diffraction and in the solution state by NMR spectroscopy.

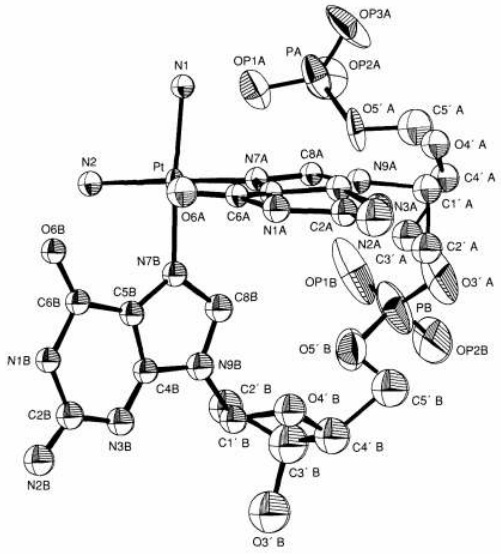


Figure 9.21 Molecular structure of cis-$[Pt(NH_3)_2d(pGpG)\}]$.

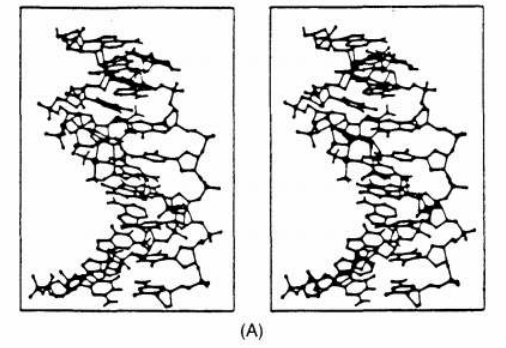
An interesting additional feature of the *cis*-$[Pt(NH_3)_2\{d(pGpG)\}]$ crystal structure is a hydrogen bonding interaction between an ammine ligand and the oxygen atom of the terminal phosphate group (OP1A•••N1, Figure 9.21). This intramolecular hydrogen bond is prominent in three of the four molecules in the asymmetric unit. Although the relevance of this hydrogen bonding interaction to the solution structure and molecular mechanism of cisplatin is presently unknown, it is interesting to note that the antitumor activity of platinum amine halide complexes is reduced when protons on coordinated NH_3 are replaced by alkyl groups.[34]

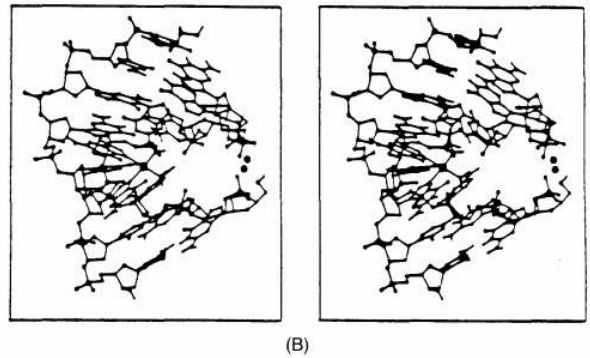
A second *cis*-DDP-oligonucleotide adduct characterized by x-ray crystallography is the neutral molecule *cis*-[$Pt(NH_3)_2${d(CpGpG)}].[131] Here again, there are several (three) molecules in the asymmetric unit. Although determined at lower resolution, the structure is similar in most respects to that of *cis*-[$Pt(NH_3)_2${d(pGpG)}] except for the presence of some weak NH_3•••O6(guanosine) intramolecular hydrogen bonding interactions and a few unusual sugar-phosphate backbone torsional angles. Also, no NH_3(H)••• phosphate(O) hydrogen bonds were observed.

From the foregoing discussion, it is apparent that adequate x-ray structure information is available for the *cis*-$\{Pt(NH_3)_2\}^{2+}$/d(pGpG) intrastrand crosslink. What is needed now are structures of the minor adducts and, most importantly, of adducts in double-stranded DNA. Very recently, dodecanucleotide duplexes containing *cis*-$\{Pt(NH_3)_2\}^{2+}$/d(pGpG) adducts have been crystallized, the structures of which are currently being investigated.[132]

c. Molecular Mechanics Calculations on Platinated Duplexes

As a supplement to x-ray structural information on double-stranded oligonucleotides containing an embedded *cis*-[$Pt(NH_3)_2${d(pGpG)}] adduct, several models have been constructed by using a molecular mechanics approach.[133] In this work, a set of coordinates was first obtained by amalgamation of structural information about standard double-helical DNAs and the platinated d(pGpG) fragment. Various starting structures were assumed, both linear and bent. The models were then refined according to various charge and stereochemical constraints built into the calculation. The results, which can reveal only what is feasible and not necessarily what actually happens, for both linear and bent structures are depicted in Figure 9.22 for two of the duplex sequences studied. In the linear model, the 5'-coordinated guanosine is rotated out of the stack, and its hydrogen bonding to the cytosine on the complementary strand is seriously disrupted. The imino N-H group is still involved in H-bonding, however; so this structure is not inconsistent with the NMR results. Two classes of kinked platinated duplex structures were encountered, with bending angles of 61 and 50°. In one of these, all Watson-Crick hydrogen bonds remain intact. These kinked structures are supported most strongly by the gel-electrophoresis experiments discussed in Section V.D.3.b.v.


(A)


(B)

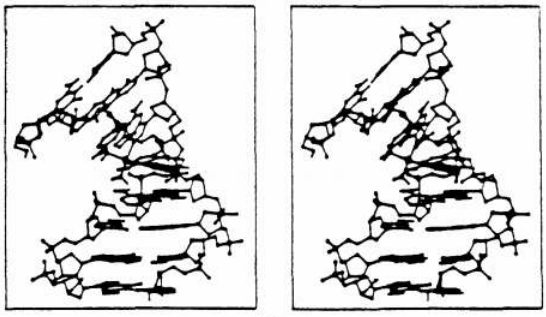


Figure 9.22 - (A) Stereoscopic view of the unkinked, platinated model of duplex d(TpCpTpCpG*pG*pTpCpTpC) from molecular-mechanics calculations. Counter ions used to stabilize the negative charge of the phosphates are not shown. (B) Stereoscopic view of the "high-salt" kinked, platinated model of duplex d(GpGpCpCpG*pG*pCpC) from molecular-mechanics calculations. Counter-ions are not depicted, with the exception of the bridging ion. (C) Stereoscopic view of the "low-salt" kinked, platinated model of duplex d(GpGpCpCpG*pG*pCpC). Counter-ions are not depicted. Reproduced with permission from Reference 133.

Molecular mechanics and the related molecular dynamics calculations are a potentially valuable tool for the bioinorganic chemist interested in how metal complexes might perturb the structures of biopolymers. Analysis of the results for cisplatin-DNA binding reveals that, compared with the sum of all contributions from the biopolymer, the Pt-DNA interactions constitute a small part of the overall energy. For the most accurate results, it is important to know the charge distributions on the metal and its ligands as well as the effects of solvent interactions. Much work needs to be done in these areas before the results of molecular mechanics and dynamics calculations can be used reliably to predict or analyze structures. At present, however, they are far superior to examination of space-filling molecular models, for example, and produce quantitatively revealing structural diagrams.

d. Platinum-Nucleobase Model Complexes

Several studies have been carried out of the *cis*-diammineplatinum(II) moiety coordinated to nucleobases in which the N9 (purine) or N3 (pyrimidine) positions either have been alkylated, to simulate the glycosidic linkages, or in which the actual nucleotide (AMP, dGMP, etc.) is employed.[134] These investigations are in many respects analogous to the synthesis and characterization by bioinorganic chemists of model complexes for the active site of a metalloenzyme. Their purpose is to simplify the problem, revealing kinetic, thennodynamic, and structural preferences of the primary building blocks involved in the metallodrug-biopolymer interaction, without the profound stereochemical constraints of the latter. Early studies of *cis*- and *trans*-DDP adducts with nucleobases (i) revealed the kinetic preferences for platinum binding to GMP and AMP, (ii) mapped out the preferred sites of platination (N7 of A and G; N1 of A; N3 of C; no N7-O6 chelate; no ribose or deoxyribose binding; only rare binding to phosphate oxygen atoms), (iii) demonstrated that Pt-N7 binding to G lowered the pK_a of N1-H by ~ 2 units, and (iv) led to the discovery of interesting new classes of coordination complexes such as the *cis*-diammineplatinum pyrimidine blues and metal-metal bonded diplatinum(III) complexes.

Attempts to model the intrastrand d(GpG) crosslink with nucleobases have met with only moderate success. Usually the O6 atoms of the two guanosine rings are on opposite sides of the platinum coordination plane ("head-to-tail" isomer). Only for *cis*-$[Pt(NH_3)_2(9\text{-EtG})_2]^{2+}$ was the correct isomer obtained. Nucleobase complexes of the *cis*-diammineplatinum(II) moiety have been valuable for testing the controversial proposal of N7,O6 chelate formation, which to date has not been observed. Several interesting discoveries of metal-nucleobase chemistry are that metal binding can stabilize rare tautomers, for example, the 4-imino, 2-oxo form of cytosine, through N4 binding, that coordination of platinum often produces unusual base pairing, and that metal migration from one donor site to another on an isolated nucleobase can occur. These model studies will continue to provide valuable insights into the possible chemistry of platinum antitumor drugs with DNA.

e. trans-DDP-DNA Adducts

Because *trans*-DDP is biologically inactive, it has received less attention than the *cis* isomer. Nevertheless, knowledge of its binding to DNA is important to have as a reference point for mechanistic comparison with the active compounds. Shortly after replication mapping experiments established that *trans*-DDP binds preferentially to d(GpNpG) and d(ApNpG) sequences,[135] several synthetic oligonucleotides containing such sequences were prepared and used to investigate reactions with the *trans* isomer.[136-138] Kinetic studies of *trans*-DDP with d(GpCpG) and d(ApGpGpCpCpT) revealed the presence of, presumably

monofunctional, intermediates that closed to form both intra- and interstrand products. In the reaction with d(GpCpG), the 1,3-intrastrand G-G chelate accounted for 70 percent of the product, and 21 percent of the remaining material was unreacted oligonucleotide. Proton NMR studies of purified *trans*-[$Pt(NH_3)_2${d(GpCpG)}] as well as the d(GpTpG) analog established platinum binding to N7 positions of the two trans guanosine nucleosides. As with the *cis*-[$Pt(NH_3)_2${d(pGpG)}] adducts, the 5'-guanosine residue no longer retained the normal B-DNA type conformation; instead, the sugar ring pucker switched to C3'-endo. A fairly detailed ^1H NMR characterization of *trans*- [$Pt(NH_3)_2${d(ApGpGpCpCpT)-N7-A(1),N7-G(3)}] revealed very similar features. This example nicely illustrates the different stereoselectivity of *cis*- and *trans*-DDP binding to DNA. The *cis* isomer forms exclusively an intrastrand d(GpG) crosslink, whereas the *trans* isomer makes a 1,3-d(A*pGpG*) adduct. A schematic depiction of the *trans*-$\{Pt(NH_3)_2\}^{2+}$ adduct is shown in Figure 9.23. As can be seen, the two purine rings enclose a large, 23-membered ring, the central guanosine residue is "bulged out," and the 5'-residue has a C3'-endo sugar pucker. This structure may be compared with that of *cis*-[$Pt(NH_3)_2${d(pGpG)}] (Figure 9.21), where the platinum is part of a smaller, 17-membered ring. Both space-filling model building studies and molecular mechanics calculations reveal that it would be stereochemically very unfavorable for the *trans*-$\{Pt(NH_3)_2\}^{2+}$ fragment to replace the *cis* analogue in an intrastrand crosslinked d(GpG) structure of the kind shown in Figure 9.21. Thus, for bidentate adducts, it seems clear that the important difference between *cis*- and *trans*-DDP binding to single-stranded DNA is revealed by the structures shown in Figures 9.21 and 9.23, respectively.

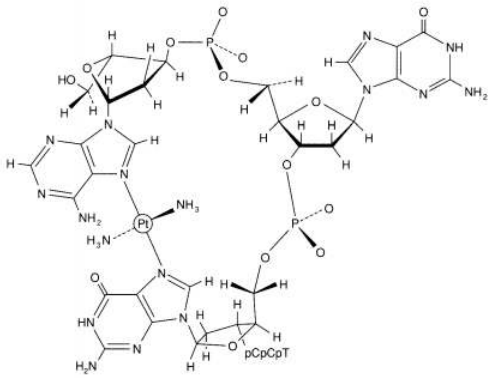


Figure 9.23 - Structure of the intrastrand 1,3-d(A*pGpG*) crosslink formed in the reaction of trans-DDP with d(ApGpGpCpCpT). Reproduced by permission from Reference 136.

Information about *trans*-DDP binding to double-stranded DNA is scanty, but very recent studies indicate that the *trans*-[$Pt(NH_3)_2${d(GpApG)-N7-G(1),N7-G(3)}] intrastrand crosslinked fragment can be embedded in duplex dodecamers.[139] Interestingly, for one sequence the melting temperature (T_M) of this duplex is not reduced over that of the unplatinated DNA fragment, in contrast to results for *cis*-DDP intrastrand d(GpG) adducts. This intriguing result, which agrees with earlier T_M studies of DNA platinated by *trans*-DDP, does not yet have a structural rationale. It is possibly relevant to the processing of bifunctional *trans*-DDP-DNA adducts *in vivo*.

f. Effects of Platination on DNA Structure

It is valuable to summarize at this stage all that has been learned concerning the changes in DNA structure that occur upon *cis*- or *trans*-DDP binding. *cis*-DDP intrastrand crosslinks result in unstacking of neighboring bases and a switch in the sugar pucker of the 5'-nucleoside from C2'-endo, the standard B-DNA conformation, to C3'-endo, a conformation encountered in A-DNA. These various forms of DNA have already been introduced in the previous chapter. Watson-Crick base pairing, although weakened, is probably maintained. Evidence that base pairing is altered comes from studies with antinucleoside antibodies that bind appreciably better to DNA platinated with *cis*-DDP than to unmodified DNA. These antibodies recognize the nucleobases much better in platinated than in unplatinated DNA, presumably because platination disrupts the double helix. Additional support for base-pair disruption comes from gradient gel-denaturation experiments using sitespecifically platinated DNA (see Section V.D.8.b). Intrastrand crosslinking by *cis*-DDP also bends the helix by about 34° and unwinds the duplex by 13°. When *trans*-DDP forms 1,3-intrastrand crosslinks, the nucleotides situated between the platinated residues may be bulged out; consistent with this picture is the fact that they present an especially good target for antinucleoside antibodies. In 1,3-intrastrand d(GpNpG) or d(ApNpG) adducts, the 5'-nucleoside sugar pucker is altered to C3 I-endo. Intrastrand crosslink formation by *trans*-DDP also leads to DNA bending,

but the platinum serves as the locus for a hinge joint and not for cooperative bending. These different effects of platination on DNA structure brought about by the two isomers are likely to be related to their different biological activities.

9.6.7: Structure of Platinum-DNA Complexes is shared under a CC BY-NC-SA 4.0 license and was authored, remixed, and/or curated by LibreTexts.

9.6.8: Site-specifically Platinated DNA 154

a. The Problem

Much of the information obtained about the mechanism of action of cisplatin has been derived from experiments where Pt-DNA binding has occurred *in vivo* or *in vitro*, with the use of random-sequence DNA having all available targets for the drug. In these studies, platination is controlled by the inorganic chemistry of *cis*-DDP in the medium and the accessibility of target sites on the DNA, as already discussed in considerable detail. As such, this situation best represents drug action as it actually occurs in the tumor cell. On the other hand, the resultant spectrum of DNA adducts makes it difficult, if not impossible, to understand the structural and functional consequences of any specific adduct. In order to address this problem, a methodology has been developed in which a single platinum adduct is built into a unique position in the genome. This approach is powerful and has the potential to be extended to the study of many other metal-based drugs. In this section, we discuss the strategy used to construct such site-specifically platinated DNA molecules and the information obtained thus far from their study. Some uses have already been discussed.

b. Synthesis and Characterization

Figure 9.29 displays the map of a genome constructed by insertion of platinated or unplatinated dodecanucleotide duplexes d(pTpCpTpApGpGpCpCpTpTpCpT)•d(pApGpApApGpGpCpCpTpApGpA) into DNA from bacteriophage M13mp18. This genome was constructed in the following manner.[154] Double-stranded DNA from M13mp18 was first digested with Hinc II, a restriction enzyme that recognizes a unique six-base-pair sequence in the DNA and cleaves the double helix there, leaving a blunt-ended (no overhanging bases) cleavage site. The unplatinated dodecamer duplex was next ligated into the Hinc II site, and the DNA amplified *in vivo*. The dodecamer can insert into the genome in two different orientations, the desired one of which, termed M13-12A-Stu I, was identified by DNA sequencing. The presence of the insert in the new DNA was checked by its sensitivity to the restriction enzyme Stu I, which cleaves at the d(AGGCCT) sequence uniquely situated in the dodecamer insert, and the absence of cleavage by Hinc II the site for which was destroyed. Next, Hinc II-linearized M13mp18 replicative form (RF) DNA was allowed to form a heteroduplex with excess viral DNA (which has only the + strand in the presence of the denaturant formamide which was dialyzed away during the experiment. The resulting circular DNA has a gap in the minus strand into which the platinated d(TCTAG*G*CCTTCT) was ligated (Figure 9.30). The latter material was prepared by the methods described in Section V.D.5.a and characterized by ^{1}H NMR spectroscopy. The resulting site-specifically platinated DNA contains a single *cis*-[$Pt(NH_3)_2${d(pGpG)}] intrastrand crosslink built into a unique position. The methodology is general, and has been used to create other known platinum-DNA adducts site-specifically in M13mp18.

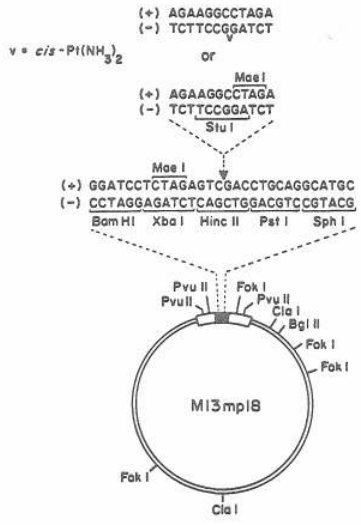


Figure 9.29 - Map of the genome created by insertion of cis-DDP platinated or unplatinated d(TpCpTpApGpGpCpCpTpTpCpT)-d(ApGpApApGpGpCpCpTpApGpA) into the Hinc II restriction site of bacteriophage M13mp18 DNA.

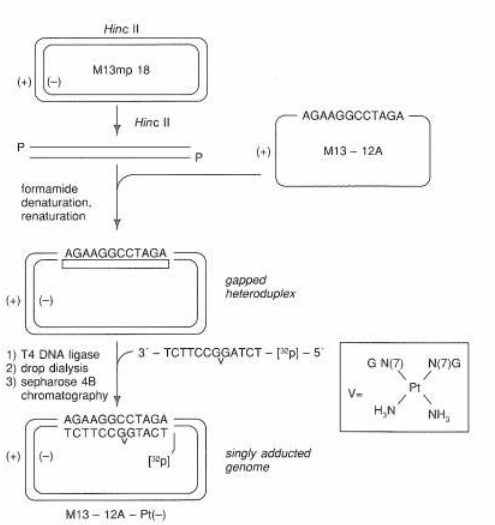


Figure 9.30 - Scheme for constructing site-specifically platinated genomes via gapped heteroduplex synthesis (reproduced by permission from Reference 154).

The chemical properties of the platinated DNA, termed M13-12A-Pt(-)-Stu I, were investigated by enzymatic, digestion and gel electrophoresis experiments. Platinum completely inhibits cleavage of the DNA by Stu I, as expected from the earlier restriction enzyme mapping studies. In addition, the *cis*- [$Pt(NH_3)_2${d(pGpG)}] and *cis*-[$Pt(NH_3)_2${d(pApG)}] intrastrand crosslinks were found to inhibit a variety of DNA polymerases, with only a small amount of bypass of the platinum lesion.[149] These results indicate that the most abundant adducts of cisplatin on DNA are able to block replication efficiently.

c. Biological Properties

When M13-12A-Pt(-)-Stu I DNA was introduced into *E. coli* cells by transformation, DNA synthesis was uninterrupted, because the cell can both repair the damage and use the unmodified (+) strand for synthesis. Consequently, a slightly different strategy was used to construct single-stranded M13-12A-Pt(+)-Stu I DNA, the details of which are available elsewhere.[154] This platinated template, in which the damage can neither be repaired nor bypassed by known mechanisms *in vivo*, was then transformed into *E. coli* cells co-plated with GW5100 cells. Under these conditions, viral DNA replication is detected by the expression of the *β*-galactosidase gene, which, in the presence of appropriate reagents in the medium, leads to formation of blue plaques on a clear background. The results clearly indicate that many fewer plaques appear when M13-12A-Pt(+) is introduced into the cells than when M13-12A-u(+) was employed, where u stands for unmodified DNA. In three repeats of this experiment, survival of DNA containing only a single *cis*-[Pt(NH3h{d(pGpG)}] crosslink was only 11 ± 1 percent.

These data provide unambiguous proof that the most frequent DNA adduct formed by cisplatin is toxic, capable of inhibiting replication when only a single such lesion is present on a natural DNA template of 7,167 nucleotides. The fact that as many as 10 percent of the transformed cells can bypass or repair the lesion is also of interest, and parallels the results found *in vitro*. In related work, it was found that the *cis*-[$Pt(NH_3)_2${d(pGpG)}] intrastrand crosslink is not very mutagenic, but that *cis*-[$Pt(NH_3)_2${d(pApG)}] intrastrand adducts are considerably more so. This finding is important, since mutations could lead to long-term secondary tumor production in patients treated with cisplatin. The methodology affords a way to screen new compounds that one would like to be equally effective at inhibiting replication but less mutagenic. In addition, by using repairdeficient mutant cell lines, as well as cisplatin resistant cells, one can study the effects of varying the properties of the host cells. Incorporation of site-specifically platinated DNA sequences into appropriate shuttle vectors will also facilitate investigation of toxicity, repair, and resistance in mammalian cells.

d. Prospectus

The foregoing discussion illustrates the power of site-specifically platinated DNAs as a probe of the molecular mechanism of the drug. We recall that similar strategies were employed to obtain uniquely modified DNA in the bending[92,93] and unwinding[95] experiments discussed previously. In principle, this technique can be applied to examine other aspects of the molecular mechanism of other metallochemotherapeutic agents. The requirements are a synthetic route to the uniquely modified genome, for which both

the inorganic coordination chemistry and molecular biology must be amenable, an adduct stable to the biological conditions for DNA synthesis, and a method (usually genetic) for scoring the biological effects being investigated. Site-specifically platinated DNAs allow the bioinorganic chemist to have maximal control over the genetics and should continue to provide valuable information about the molecular mechanism of action of cisplatin.

9.6.8: Site-specifically Platinated DNA [154] is shared under a CC BY-NC-SA 4.0 license and was authored, remixed, and/or curated by LibreTexts.

9.6.9: Bioinorganic Chemistry of Platinum Anticancer Drugs- How Might They Work?

The material in this section constitutes the major portion of this chapter. One important goal of the discussion is to illustrate, by means of an in-depth analysis of a single case history, the questions that must be addressed to elucidate the molecular mechanism of an inorganic pharmaceutical. Another is to introduce the techniques that are required to answer these questions, at least for the chosen case. The inorganic chemist reading this material with little or no biological background may find the experience challenging, although an attempt has been made to explain unfamiliar terms as much as possible. It is strongly advised that material in Chapter 8 be read before this section. Toward the end of this section, the results obtained are used to speculate about a molecular mechanism to account for the biological activity of the drug. Experiments directed toward evaluating the various hypotheses are delineated. Once the mechanism or mechanisms are known, it should be possible to design new and better antitumor drugs which, if successful, would be the ultimate proof of the validity of the hypotheses. This topic is discussed in the next and final section of the chapter. Such an analysis could, in principle, be applied to probe the molecular mechanisms of the other metals used in medicine described previously. In fact, it is hoped that the approach will prove valuable to students and researchers in these other areas, where much less information is currently available at the molecular level.

The material in this section has been organized in the following manner. First we discuss the relevant inorganic chemistry of platinum complexes in biological media. Next we summarize the evidence that DNA is a major target of cisplatin in the cancer cell, responsible for its antitumor activity. The chemical, physical, and biological consequences of damaging DNA by the drug are then described, followed by a presentation of the methodologies used to map its binding sites on DNA. The detailed structures of the DNA adducts of both active and inactive platinum complexes are then discussed, together with the way in which the tertiary structure of the double helix can modulate these structures. Finally, the response of cellular proteins to cisplatin-damaged DNA is presented, leading eventually to hypotheses about how tumor cells are selectively destroyed by the drug. Together these events constitute our knowledge of the' 'molecular mechanism," at least as it is currently understood.

1. Reactions of *cis*-DDP and Related Compounds in Aqueous, Biological, and Other Media

cis-Diamminedichloroplatinum(II) is a square-planar d^8 complex. As such, it belongs to a class of compounds extensively investigated by coordination chemists.[55] Typically, such compounds are relatively inert kinetically, do not usually expand their coordination numbers, and undergo ligand substitution reactions by two independent pathways with the rate law as given by Equation (9.4). The rate constants k_1 and k_2 correspond to first-order (solvent-assisted) and second-order (bimolecular) pathways;

$$Rate = (k_1 + k_2[Y])[complex] \tag{9.4}$$

[Y] is the concentration of the incoming ligand. Usually, $k_1 << k_2$ by several orders of magnitude. In biological fluids, however, the concentration of a potential target molecule could be ~10^{-6} M, in which case $k_1 \simeq k_2[Y]$. Substitution of ligands in *cis*-DDP, required for binding to a cellular target molecule, is therefore likely to proceed by the solvent-assisted pathway. Such a pathway is assumed in the ensuing discussion.

For the hydrolysis of the first chloride ion from *cis*- or *trans*-DDP,

$$[Pt(NH_3)_2Cl_2] + H_2O \rightleftharpoons [Pt(NH_3)_2Cl(OH_2)]^+ + Cl^- \tag{9.5}$$

the k_1 values at 25 °C are 2.5 x 10^{-5} and 9.8 x 10^{-5} s^{-1}, respectively.[55] These hydrolyzed complexes can undergo further equilibrium reactions, summarized by Equations (9.6) to (9.9).

$$[Pt(NH_3)_2Cl(OH_2)]^+ \rightleftharpoons [Pt(NH_3)_2Cl(OH)] + H^+ \tag{9.6}$$

$$[Pt(NH_3)_2Cl(OH_2)]^+ + H_2O \rightleftharpoons [Pt(NH_3)_2(OH_2)_2]^{2+} + Cl^- \tag{9.7}$$

$$[Pt(NH_3)_2(OH_2)_2]^{2+} \rightleftharpoons [Pt(NH_3)_2(OH_2)(OH)]^+ + H^+ \tag{9.8}$$

$$[Pt(NH_3)_2(OH_2)(OH)]^+ \rightleftharpoons [Pt(NH_3)_2(OH)_2] + H^+ \tag{9.9}$$

The formation of dimers such as $[Pt(NH_3)_2(OH)]_2^{2+}$ and higher oligomers can also occur,[56,57] but such reactions are unlikely to be important at the low platinum concentrations encountered in biological media, Reactions (9.5) to (9.9), which depend on pH and the chloride-ion concentrations, have been followed by ^{195}Pt (I = $\frac{1}{2}$, 34.4 percent abundance) and ^{15}N (using enriched compounds)

NMR spectroscopy. The latter method has revealed for the *cis*-diammine complexes pK_a values of 6.70 ± 0.10 at 25 °C for Reaction (9.6) and of 5.95 ± 0.1 and 7.85 ± 0.1 at 5 °C for Reactions (9.8) and (9.9), respectively.[58]

The effects of pH and Cl^- ion concentration on the species distribution of platinum compounds have been used to fashion the following plausible argument for the chemistry of *cis*-DDP *in vivo*.[59] With the use of thermodynamic data for the ethylenediamine (en) analogue $[Pt(en)Cl_2]$ the relative concentrations of hydrolyzed species at pH 7.4 were estimated (see Table 9.3) for blood plasma and cytoplasm (Figure 9.7). The higher chloride ion concentration in plasma preserves the complex as the neutral molecule cis-DDP, which passively diffuses across cell membranes. The lower intracellular chloride ion concentration facilitates hydrolysis reactions such as Equations (9.5) to (9.9), thereby activating the drug for binding to its biological target molecules. There is, of course, a reasonable probability that *cis*-DDP and species derived from it will encounter small molecules and macromolecules *in vivo* that divert it from this route to the target. We have already seen such cases; cisplatin binds to serum proteins, and there is good evidence that intracellular thiols react with the drug.[60] Glutathione, for example, is present in millimolar concentrations in cells. How, one might ask, does cisplatin swim through such a sea of sulfur donors to find its target in the tumor cell? Is it possible that a modified form of the drug, in which a Pt-CI bond has been displaced by thiolate to fonn a Pt-S bond, is the actual species responsible for its activity? Although these questions have not yet been satisfactorily answered, there is reason to believe that such reactions are not directly involved in the molecular mechanism of action. As evident from structure-activity relationship studies, the most active compounds have two labile ligands in *cis* positions. If Pt-S bonds were required, then compounds already having such linkages would be expected to exhibit activity and they do not. Rather, it seems most likely that the antitumor activity of cisplatin results from surviving species of the kind written in Equations (9.5) to (9.9) that find their way to the target molecule, and that the induced toxicity must arise from a significantly disruptive structural consequence of drug binding. Since only *cis* complexes are active, it is reasonable for the coordination chemist to infer that the stereochemistry of this interaction is of fundamental importance.

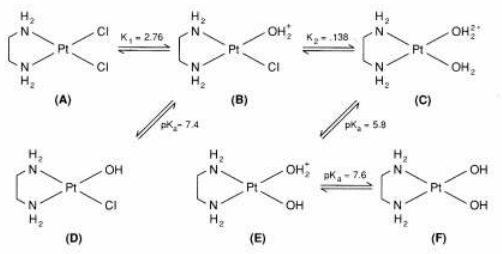


Figure 9.7 - Hydrolysis reactions of antitumor platinum complexes and an estimate of the species present in plasma and cytoplasm (reproduced by permission from Reference 51).

Table 9.3 - Distribution of various adducts formed between *cis*-DDP or $[^3H][Pt(en)Cl_2]$[a] and DNA *in vitro* and *in vivo*.[118-122]

a) A radiolabeled analogue of *cis*-DDP, [^{3}H]dichloroethylenediamineplatinum(II).

b) A_2 represents either $(NH_3)_2$ or ethylenediamine.

c) By difference.

d) Percentage of adducts based on total amount of platinum eluted from the separation column.

e) Percentage of adducts based on total amount of radioactivity eluted from the separation column.

f) Not given.

g) Chinese hamster ovary cells treated with 83 μM *cis*-DDP.

h) Results from ELISA.

i) Results from AAS. Where the signal was too weak for reliable quantitation, the maximal amount possible is given. Adapted from Table 1 in Reference 81.

D/N Ratio	Total Incubation Time	Adducts Formed			Mono-functional Adducts	Remaining Platinum[c]
		cis-[PtA_2{d(pGpGl}][b]	*cis*-[PtA_2{d(pApG}][b]	*cis*-[PtA_2{d(GMP)}$_2$][b]		
In vitro						
0.055[c]	5 h (50 °C)	47-50%	23-28%	8-10%	2-3%	10%
0.022[d]	5 h (50 °C)	60-65%	20%	~4%	~2%	9-14%
0.01[e]	16 h (37 °C)	62%	21%	7%	—	10%
[ef]	30 m (37 °C)	36%	3%	8%	40%	13%
[ef]	2 h (37 °C)	54%	9%	9%	14%	14%
[ef]	3 h (37 °C)	57%	15%	9%	4%	15%
In vivo						
[dg]	1 h (37 °C)	35.9 ± 4.7%[h]	<34%[i]	3.1 ± 1.6%[h]	38.5%[i]	~22%
[dg]	25 h (37 °C)	46.6 ± 6.8%[h]	<48%[i]	3.0 ± 0.9%[h]	<14.5%[i]	~50%

Reactions of platinum compounds with components in media used to dissolve them can give and undoubtedly have given rise to misleading results, both in fundamental mechanistic work and in screening studies. A particularly noteworthy example is dimethylsulfoxide (DMSO), which even recently has been used to dissolve platinum compounds, presumably owing to their greater solubility in DMSO compared to water. As demonstrated by ^{195}Pt NMR spectroscopy, both *cis*- and *trans*-DDP react rapidly ($t_{1/2}$ = 60 and 8 min at 37 °C, respectively) to form $[Pt(NH_3)_2CI(DMSO)]^+$ complexes with chemical and biological reactivity different from those of the parent ammine halides.[61]

2. Evidence that DNA is the Target

Two early sets of experiments pointed to interactions of cisplatin with DNA, rather than the many other possible cellular receptors, as an essential target responsible for cytotoxicity and antitumor properties.[62,63] Monitoring the uptake of radiolabeled precursors for synthesizing DNA, RNA, and proteins, showed that [^{3}H]thymidine incorporation was most affected by therapeutic levels of cisplatin for both cells in culture and Ehrlich ascites cells in mice. Since independent studies showed that *cis*-DDP binding to DNA polymerase does not alter its ability to synthesize DNA, it was concluded that platination of the template and not the enzyme was responsible for the inhibition of replication.

In a second kind of experiment demonstrating that DNA is a target of cisplatin, hydrolyzed forms of the drug in low concentrations were added to a strain of *E. coli* K12 cells containing a sex-specific factor F.[64,65] After free platinum was removed, these F^+ cells were conjugated with a strain of *E. coli* K12 cells lacking this factor that had previously been infected with lambda bacteriophage. Addition of *cis*-DDP, but not *trans*-DDP, directly to the latter infected F^- cells had been shown in a separate study to accelerate cell lysis. Conjugation with the platinum-treated F^+ cells produced the same effect, strongly suggesting that Pt had been transferred from the F^+ to the F^- cells. Since only DNA is passed between the F^+ and F^- strains, it was concluded that Pt was attached to the DNA and that this modification was essential for the observed lysis of the cell. Further studies showed a good correlation between cell lysis by platinum compounds and their antitumor properties.

Various other observations are consistent with the notion that platinum binding to DNA in the cell is an event of biological consequence.[66] The filamentous bacterial growth observed in the original Rosenberg experiment is one such piece of evidence, since other known DNA-damaging agents, for example, alkylating drugs and x-irradiation, also elicit this response. Another is the greater sensitivity toward *cis*-DDP of cells deficient in their ability to repair DNA. Finally, quantitation of the amount of platinum bound to DNA, RNA, and proteins revealed that, although more Pt was bound to RNA per gram biomolecule, much more Pt was on the DNA when expressed as a per-molecule basis. In the absence of any selective interaction of Pt with a specific molecule, only

one out of every 1,500 protein molecules (average M.W. ~60 kDa) in a cell will contain a single bound platinum atom, whereas hundreds or thousands of Pt atoms are coordinated to DNA (M.W. ~10^{11}). If the replication apparatus cannot bypass these lesions, then cell division will not occur, and tumor growth is inhibited.

Although these and other results all point to DNA as an important cellular target of cisplatin, most likely responsible for its anticancer activity, this information does not explain why tumor cells are more affected by *cis*-DDP than non-tumor cells of the same tissue. Moreover, why is *trans*-DDP, which also enters cells, binds DNA, and inhibits replication, albeit at much higher doses (see discussion below), not an active anticancer drug? What causes cisplatin to kill cells and not merely to arrest tumor growth? The latter can be explained by DNA synthesis inhibition, but not necessarily the former. Very recent studies have begun to address these questions using powerful new methodologies of molecular and cell biology, as described in subsequent sections of this chapter. The results, although preliminary, continue to point to DNA as the most important cellular target of cisplatin.

9.6.9: Bioinorganic Chemistry of Platinum Anticancer Drugs- How Might They Work? is shared under a CC BY-NC-SA 4.0 license and was authored, remixed, and/or curated by LibreTexts.

9.6.10: Bioinorganic Chemistry of Platinum Anticancer Drugs; How Might They Work? (Part 2)

6. Effects of DNA Structure on Platinum Binding

a. A-, B-, and Z-DNA[140]

As discussed in more detail in Chapter 8, double-helical DNA can adopt different polymorphic forms depending on the conditions in solution or polycrystalline fiber. Even within a given DNA molecule, there can be sequence-dependent local secondary and tertiary structural differences that constitute important signals for cellular DNA binding and processing molecules. An example already discussed is the recognition of palindromic sequences by type II restriction endonucleases. As shown in Figure 9.24, three such DNA polymorphs are the right-handed A- and B- and the left-handed Z-forms. Most commonly encountered in solution is B-DNA, characterized by well-classified major and minor grooves designated by arrows in Figure 9.24. The targets of platinum binding, guanine N7 atoms, are situated in the major groove.

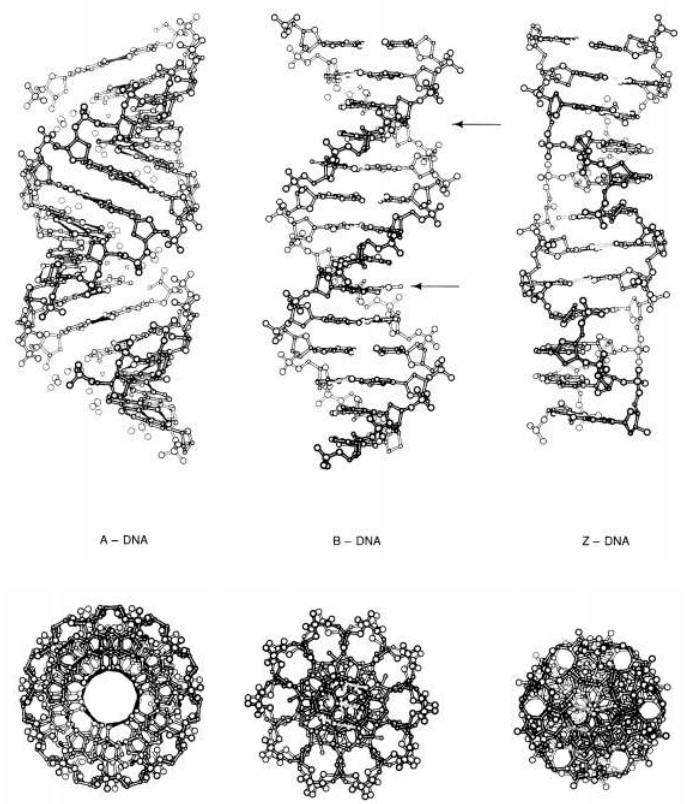


Figure 9.24 - Representations of side (above) and top (below) views of three major classes of double-stranded DNA. For B-DNA, arrows near the top and bottom of the helix designate the minor and major grooves, respectively. Reproduced with permission from Reference 140.

To what extent do sequence-dependent local structural modulations affect platinum binding? Although no general answer to this question can be given, there are several interesting anecdotal pieces of information worth mentioning. Z-DNA, a form favored by alternating purine-pyrimidine sequences such as in poly d(GC), does not constitute a particularly good target for *cis*-DDP binding. For one thing, it lacks the preferred d(GpG) or d(ApG) sequences. The monofunctional $[Pt(dien)Cl]^{+}$ complex, however, facilitates the B-DNA → Z-DNA conformational transition, as demonstrated by circular dichroism and ^{31}P NMR spectroscopic data.[141] In Z-DNA, the guanosine nucleoside adopts the syn conformation (Figure 9.9), which is presumably favored by placing a bulky $\{Pt(dien)\}^{2+}$ moiety on N7. Moreover, the local charge density on DNA is greater in Z- than B-DNA, owing to the closer proximity of the phosphate groups, and the former is presumably stabilized by the +2 charge on the platinum complex.

b. Effects of Local Sequence and of Free and Linked Intercalators on Platinum Binding

Of more interest perhaps to anticancer drug-DNA interactions is the fact that some d(GpG), d(ApG), and even d(GpA) targets for *cis*-DDP binding are very sensitive to the sequences in which they are embedded. This phenomenon was first discovered during exonuclease III mapping studies of cisplatin binding to a 165-bp restriction fragment from pBR322 DNA.[142] Although *cis*-DDP binding stops the enzyme at G_3, G_5, and GAGGGAG sequences, at a $(D/N)_b$ ratio of 0.05 there is little evidence for coordination to an apparently favored G_6CG_2 sequence (Figure. 9.25, lane 8). When platination was carried out in the presence of the DNA intercalator EtdBr (Figure 9.11), however, the G_6CG_2 sequence became a Pt binding site (Figure 9.25, lanes 9-12). A more extensive exonuclease III mapping study of this phenomenon suggested that d(CGG)-containing sequences in general are less well platinated by *cis*-DDP.[143,144] Moreover, only EtdBr, and not other acridine or phenanthridinium type intercalators, was able to promote an enzyme-detectable *cis*-DDP binding to these sequences. A suggested explanation for these results is that local d(purCGG) sequences might have an A-DNA-type structure (Figure 9.24) in which the major groove is narrow, inhibiting access of platinum to N7 of guanosine nucleosides. In the presence of the intercalator EtdBr, the local DNA structure might be altered in such a manner as to permit binding.[143,144]

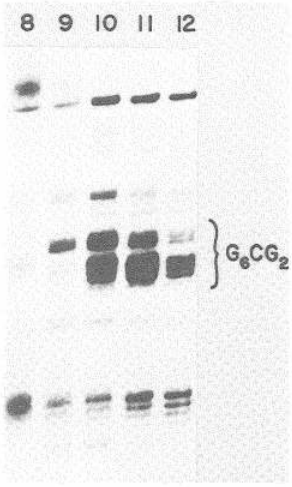


Figure 9.25 - Autoradiograph of Exo III mapping results for cis-DDP binding to a 165-bp DNA restriction fragment. The Pt/nucleotide ratio is 0.05. Lanes 8-12 contain DNA platinated in the presence of 0, 0.012, 0.057, 0.12, and 0.23 Etd/nucleotide, respectively. For more details, see Reference 142.

In accord with this interpretation, and further to delineate a possible reason why acridines and deaminated ethidium cations do not promote cisplatin binding to d(purCGG) sequences, NMR studies were performed that revealed the mean residence time of EtdBr on DNA to be 6 to 21 times longer than that of any of the other intercalators examined.[144] Thus, for these latter intercalators, the local DNA structure presumably can relax back to one unfavored for cisplatin binding before it can diffuse to the site. Moreover, when acridine orange (AO), one of the five intercalators studied that does not promote cisplatin binding to excluded sites, was covalently attached to dichloroethylenediamineplatinum(ll) (Figure 9.26) via a hexamethylene linker chain, the resulting AO-Pt molecule was able to bind to all d(CpGpG) sites, as determined by exonuclease III mapping. In the tethered molecule, the high local concentration near the intercalator binding site facilitates attachment of the $\{Pt(en)\}^{2+}$ moiety to DNA before the acridine orange fragment can diffuse away and the structure can relax to reform the excluded site.

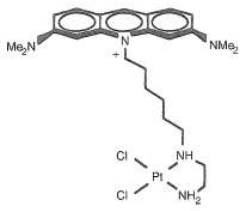


Figure 9.26 - Structure of AO-Pt in which the $\{Pt(en)C_{12}\}$ moiety is linked by a hexamethylene chain to acridine orange.

Subsequently, the excluded site phenomenon was found for *cis*-DDP binding, as assayed by the 3'-5'-exonuclease activity of T4 DNA polymerase.[145] Enzyme stopping sites were observed at all d(GpG) sequences, but only weakly when at a d(GTGGTC) site.

Similarly, d(ApG) was not modltled when embedded in pyGAGCpy and pyGAGCA sequences. Although most d(GpA) sequences were not platinated, as detected by T4 mapping, a few were. These results further underscore the importance of local sequence modulation of cisbinding to DNA.

c. DNA-Promoted Reaction Chemistry

In the EtdBr-enhanced binding of *cis*-DDP to DNA, a small fraction (< 5 percent) of the intercalator is strongly bound and can be dialyzed out only very slowly.[145] The detailed structure of this DNA-cisplatin-EtdBr ternary complex has been established, and involves *cis*-$\{Pt(NH_3)_2\}^{2+}$ binding to the exocyclic amino groups of ethidium as well as to donor sites on DNA.[146] This assignment was proved by synthesizing *cis*- $[Pt(NH_3)_2CEtd)CI]^{2+}$ complexes in dimethylformamide solution and then allowing them to react with DNA. The optical spectra of the resulting adducts were identical to that of the ternary complex. The reaction of *cis*-DDP, and DNA to form the ternary complex is promoted by the favorable orientation of the exocyclic amino group of intercalated Etd with respect to the coordination plane of bound to the double helix. The N-8 exocyclic amino group of ethidium, bound intercalatively at a site adjacent to a purine N-7 coordinated *cis*-$\{Pt(NH_3)_2CI\}^{+}$ moiety, is positioned above the platinum atom in a structure resembling the transition state for a square-planar substitution reaction. The structure of this transition state has been modeled in a molecular mechanics calculation (Figure 9.27 See color plate section, page C-16.),[147] and evidence has been obtained that indicates selective binding of platinum to the Etd N-8 amino position.[148]

Since cisplatin is usually administered in combination chemotherapy with other drugs, many of which contain intercalating functionalities, strong covalent, DNA-promoted interactions between drug molecules at a target site must be considered as possibly relevant to the molecular mechanism of action. In such a situation, there must be a strong binding preference for both drug molecules for the same target sequences, since on probability grounds alone it is unlikely that both would migrate to the same site by random diffusion at the low concentrations found *in vivo*.

d. Effects of DNA Function on Platinum Binding

Although there is yet little known about this topic for cisplatin, it is worth pointing out that other DNA-targeted drugs, such as bifunctional alkylating agents, bind preferentially to actively transcribed genes. It is therefore possible that platinum exhibits such preferences, for example, to single-stranded DNA at or beyond the transcription fork, compared to duplex DNA in chromatin structures. Or, perhaps, it too binds selectively to actively transcribed DNA. Investigation of these possibilities seems worthwhile.

7. Speculations About the Molecular Mechanism

a. Is There a Single Mechanism?

Most investigators now agree that DNA is the cytotoxic target of cisplatin. We have seen that the drug inhibits DNA replication by binding to the template and halting the processive action of DNA polymerase. Less well-studied is the inhibition of transcription by platinum-DNA adducts, but recent evidence clearly indicates that they can do so. Studies of the effects of platinum on cells growing in culture reveal that DNA replication and cell growth can continue without cell division in the presence of low levels (1 μ g/mL) of *cis*-DDP cells are arrested at the G2 phase, the stage of cell growth just preceding division.[105] G2 arrest was reversible, but at higher cisplatin levels (8 μg/mL), cell death occurred. These observations led to the speculation that, perhaps, post-replication DNA repair can handle the toxicity associated with a platinum-damaged template, at least for DNA synthesis, but that there is no known pathway by which transcription can circumvent Pt-DNA lesions. Possibly, inhibition of transcription is ultimately a more lethal event than inhibition of replication. This idea is inconsistent with the well-established fact that thymidine incorporation into DNA is more affected by low levels of cisplatin than is uridine incorporation into RNA. Might there be more than one biochemical pathway by which cisplatin manifests its anticancer activity? Further work is necessary to address this intriguing question.

b. Is There a "Critical Lesion"?

We now have an excellent understanding of the major DNA adducts made by *cis*-DDP, their structures, and the corresponding DNA distortions. Information about adducts made by the inactive *trans* isomer, though not as complete, is also substantial. During the period when this knowledge was being accumulated, it was of interest to learn whether a "critical lesion," a specific DNA adduct with a unique molecular structure might be responsible for the antitumor activity of the drug. At present, it appears that all bidentate adducts made by *cis*- and *trans*-DDP can inhibit replication, although they may not be equally efficient at doing so.[149]

Even monofunctional adducts of the kind formed by *cis*-$[Pt(NH_3)_2(4\text{-Br-py})Cl]^+$ can block replication.[96] Thus, it be better to think about the concept of "critical lesion" in a functional sense, where the rates of adduct formation, removal, and enzyme inhibition together determine which family of adducts will exhibit antitumor activity and which will not. Here the biochemistry of the host cell will also be an important determinant. Clearly, more studies are required to delineate these possibilities.

c. Replication and Repair in the Tumor Cell[150]

If the anticancer activity of cisplatin arises from damaged DNA templates, then the drug could be selectively toxic to cancer versus normal cells of the same tissue if repair of DNA damage occurred more efficiently in the latter. The best way to study this phenomenon would be to measure the platinum-DNA levels and list the spetrum of adducts formed in tumor versus normal biopsy tissue obtained from patients undergoing cisplatin chemotherapy. As described previously, methodologies are now reaching the point where such experiments can be carried out in order to test the key hypotheses about the mechanism of action of cisplatin. In addition, powerful new methods have recently been developed to screen for DNA bmdlnlg proteins. If one could identify proteins that bind selectively to *cis*-DDP-platinated DNA and determine function, further insights into cellular replication and repair phenomena would be forthcoming. Such cellular factors that bind selectively to DNA containing cisplatin adducts have, in fact, recently been discovered.[107] The experiments that led to this finding and their possible implications for the molecular mechanism of cisplatin are described in the next section.

d. Structure-Specific (or Damage) Recognition Proteins[150]

If selective repair of platinum-DNA adducts in cells of different origin is an integral part of the anticancer mechanism of *cis*-DDP, then it is important to identify the cullular factors associated this phenomenon. In bacteria, *cis*-DDP adducts on DNA are removed by excision repair, a process in which the lesion is first identified and then excised by the uvrABC excinuclease system.[151] In this process, the uvrA protein first binds to the adducted DNA. Subsequently, the uvrB and C proteins excise the damaged strand, which additional cellular proteins rebuild by copying the genetic information from the remaining strand.

The repair of *cis*-DDP intrastrand crosslinks in mammalian cells is much less well understood. Under the assumption that an analogue of the uvrA protein might exist in such cells, experiments were carried out to try to isolate and clone the gene for such a protein. In particular, the mobility of platinated DNA restriction fragments of defined length was found to be substantially retarded in electrophoresis gels following incubation extracts from human HeLa cells.[107] This gel-mobility shift was attributed to the binding of factors termed "damage recognition proteins" (or DRPs). Subsequent studies with site-specifically platinated oligonucleotides (see V.D.8) revealed that the cisplatin DRP binds specifically to DNA containing the intrastrand *cis*-$[Pt(NH_3)_2\{d(pGpG)\}]$ or *cis*-$[Pt(NH_3)_2\{d(pApG)\}]$ crosslink. In parallel work, the gene encoding for a DRP was cloned[152] and used to demonstrate the occurrence of such a in nearly all eukaryotic cells. Since binding of the DRP to platinated DNA is not specific for the ammine ligands opposite the crosslinked nucleobases, the interaction is thougllt to involve recognition of local changes in the twist and bending of the double helix. Figure 9.28 depicts one possible structure for the complex formed between *cis*-DDP platinated DNA and a DRP. More recently, the cloned proteins were found to contain a high mobility group (HMG) protein box, and even HMG 1 itself binds to cisplatin-modified DNA.[152] The class of proteins was renamed "structure-specific recognition proteins" (SSRPs).

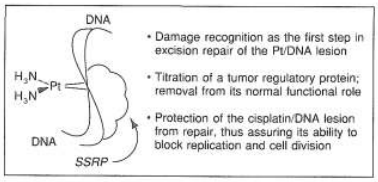


Figure 9.28 - Model depicting the binding of an SSRP to cisplatin-damaged DNA and several hypotheses for its role in the molecular mechanism.

The discovery of SSRPs that bind specifically to cisplatin-modified DNA raises several questions that are the subjects of current study. The first is to determine whether the proteins are an integral component in the mechanism of action of the drug. Although it has not yet been possible to induce the proteins by treating cells with cisplatin, nor have elevated or suppressed levels been found in platinum-resistant cells, deletion of an SSRP gene in yeast has re(~enltlv afforded a mutant strain less sensitive to cisplatin than wild-type cells.[153] This result links a yeast SSRP with cellular sensitization to the drug. Such a protein could contribute to the molecular mechanism in one of several ways (Figure 9.28). It might be the analogue of uvrA, which, as mentioned above,

recognizes damage and signals the cell to perform excision repair. If so, then one would like to depress the levels of the protein in cancer cells to make them more sensitive to the drug. A second possibility is that the true role of the SSRP is to serve as a tumor-cell activator, and that cisplatin lesions titrate it away from its functionally active sites on the DNA. Alternatively, binding of the protein could protect cisplatin adducts from repair, preserving their lethality at the time of cell division and leading to the arrest of tumor growth. This last hypothesis would require more of the SSRP in cells sensitive to the drug. Studies are currently in progress to delineate these three and other hypotheses, and to learn whether the discovery of the SSRPs has heralded the final chapter in the quest for the molecular mechanism of cisplatin or merely been an entertaining sidelight.

e. Drug Resistance: What Do We Know?[150]

Perhaps the most serious problem for successful chemotherapy of tumors is drug resistance.[102] In most tumors there exists a subpopulation of cells that are naturally resistant to a given drug; as the sensitive cells are killed, these refractory clones take over. In addition, resistance can be acquired by tumor cells following repeated application of the drug. Attempts to identify mechanisms responsible for cisplatin resistance have therefore been the subjects of considerable research activity. Other DNA-damaging agents sometimes amplify genes as a mechanism of drug resistance. An example is the multidrug resistance phenomenon, in which a gene encoded for a P-glycoprotein is amplified in cells resistant to agents such as daunomycin. This protein is believed to increase efflux of the drug through the cell membrane by an ATP-dependent, energy-driven pump. There is currently an intensive search underway to see whether the cisplatin resistance phenomenon has a genetic origin. If a cisplatin resistance gene could be cloned and its phenotype identified, a powerful new avenue would be opened to overcome drug resistance.

9.6.10: Bioinorganic Chemistry of Platinum Anticancer Drugs; How Might They Work? (Part 2) is shared under a CC BY-NC-SA 4.0 license and was authored, remixed, and/or curated by LibreTexts.

9.6.11: Design of New Inorganic Anticancer Drugs

1. Objectives

Although chemotherapy has made significant contributions to cancer treatment, the effect of cisplatin on testicular cancer being a showcase example, early detection and surgical removal of all neoplastic tissue still remain the preferred means of combating most forms of the disease. What steps need to be taken to devise better chemotherapeutic agents? One answer is to understand the biochemical mechanisms that underlie the transformation of normal into neoplastic cells and to attack the disease on the basis of that knowledge. The value of this approach is indisputable, but it need not be the only one. We have seen that *cis*-$[Pt(NH_3)_2Cl_2]$, a simple third-row transition-metal complex containing no carbon atoms, can contribute significantly to cancer chemotherapy. This example alone should lead us to search for improved inorganic drugs based on the evolving knowledge of the mechanism of action of *cis*-DDP. What then should our objectives be? Three answers are immediately apparent. First, we need to find compounds that are active against resistant cells. Such compounds are termed "second-generation" platinum drugs, and are the focus of much activity in the pharmaceutical industry. Their development will be facilitated by understanding the fundamental biochemistry of cisplatin drug resistance, designing complexes to circumvent the cellular resistance mechanisms. Second, there needs to be an improved spectrum of activity, to be provided by the so-called "third-generation" compounds. The major cancers of the colon, breast, and lung are not effectively diminished by cisplatin chemotherapy. Finally, cisplatin toxicity is often dose-limiting, and there is a need for agents with a greater chemotherapeutic index-to-toxicity ratio. Some of these objectives may ultimately be met by modifying the mode of delivery of cisplatin, for example, by encapsulating the drug in a tumor-seeking liposome or attaching it to a tissue-specific monoclonal antibody. A major step in alternative delivery has recently been taken with the development of a class of oral platinum complexes that have just entered clinical trials.[54] These complexes are platinum(IV) cycloalkylamine species of the kind *cis*, *trans*, *cis*-$[Pt(NH_3)(C_6H_5NH_2)(O_2CCH_3)_2Cl_2]$. The prospects are reasonably good that new platinum and other metal anticancer drugs can be designed in a bioinorganic chemical approach to the problem.

2. Strategies for Drug Development

a. Can We Build on Our Knowledge About Cisplatin?

If we consider what is known about the molecular mechanism of cisplatin, what properties are desirable in the design of new metal complexes for testing? The molecules should be reasonably stable kinetrically and soluble in biological fluids, cross the cell membrane, bind covalently to DNA, and inhibit gene function. As described previously in this section of the chapter, powerful methods are now available to screen compounds for these properties in a relatively short time. But there are additional factors required for metallodrug anticancer activity, above and beyond these criteria; *trans*-DDP, after all, has all five of the above properties and is not active. Probably one should add to the list the requirement that the complex have two substitutionally labile *cis* sites for intrastrand crosslinking of adjacent DNA nucleotides; such a criterion would, of course, rule out molecules like *trans*-DDP. Recall, however, that *cis*-$[Pt(NH_3)_2(4\text{-X-py})Cl]^+$ complexes (X = Br, Me) are active. These cations have the five properties listed above, but, as far as is currently known, bind only monofunctionally to DNA. The pyridine ring moiety of a covalently attached platinum atom could possibly intercalate into a neighboring interbase pair site on the DNA, making a pseudointrastrand crosslinked adduct structurally similar to the *cis*-DDP-d(pGpG) structure. Further information is required about these active, monofunctional cations before any firm conclusions can be drawn. Nevertheless, it is useful to remember that if the requirement of two substitutionally labile *cis* ligands had been rigorously followed, this new class of monofunctional platinum complexes would not have been discovered.

Another rationale for designing new platinum or other metal antitumor drugs could emerge with a better understanding of the SSRPs in the mechanism of action of cisplatin. For example, if they serve to protect cisplatin lesions on DNA from repair, one would want to design complexes that form adducts that bind even more strongly to the purified protein. The strength of this binding interaction, having been a serendipitous discovery, surely cannot have been maximized. A tighter SSRP-platinated DNA complex would require the use of less platinum, and thus afford lower toxicities.

b. Is Platinum Uniquely Suited?

Given the above criteria, platinum is the only metal to be chosen for further drug development? The answer to this question is "probably not" but a few points need to be kept in mind. Given the assumption that the geometry of the *cis*-$[Pt(NH_3)_2\{d(GpG)\}]$

intrastrand crosslink was important for the antitumor activity of cisplatin, computer graphics methods were employed to probe the stereochemical consequences of modifying this structure.[155] Addition of axial chloride or water ligands in fifth and sixth coordination positions to form pseudo-octahedral adducts, for example, introduces several steric clashes with the guanosine O6 atoms. An octahedral complex, for example *cis*,*cis*,*cis*-$[Pt(NH_3)_2Cl_2(OH)_2]$, bifunctionally coordinated to DNA either would not form an intrastrand d(GpG) crosslink or would form an adduct structurally different from that made by *cis*-DDP. This octahedral complex Pt(IV), known as "tetraplatin" in the pharmaceutical industry, is active, but is believed to be reduced *in vivo* to platinum(II) before coordinating to DNA.[156,157] These considerations might imply that the best strategy for inorganic drug development would be to employ square-planar d^8 complexes. Clearly there are as yet no definitive answers. Nevertheless, the criteria derived from the mechanism of action studies of cisplatin represent an excellent starting point for designing new antitumor metallodrugs.

c. How Important are Amine Ligands?

Here again, the answer is not unequivocal, but amines (including NH_3) are probably ideally suited ligands for covalent DNA-binding metal complexes. Even completely inert complexes such as $[Co(NH_3)_6]^{3+}$ show sequence and DNA polymorph binding preferences,[158] suggesting that the N-H bonds orient toward the phosphate and heterocyclic nitrogen atoms in the major groove, forming hydrogen-bonding interactions. This chemistry is analogous to the binding and recognition of organic amines and polyamines, such as spermine and spermidine, by nucleic acids. Apart from amines, hydrophobic groove-binding and/or intercalating ligands such as o-phenanthroline and its derivatives should be considered. Molecules such as $[Rh(DIP)_3]^{3+}$, where DIP = 4,7-diphenyl-1,10penanthroline, bind to DNA and have proved to be useful structural probes (Chapter 8). Recent work has shown that $[Rh(DIP)_2Cl_2]^+$ binds preferentially to d(GpG) sequences, like cisplatin, although its antitumor properties have not yet been investigated.[159]

3. Second and Third-generation Platinum Anticancer Drugs

Improvements over cisplatin have been made, most notably the molecule carboplatin (Figure 9.4), which is less nephrotoxic and has been reported to be effective in some patients where cisplatin chemotherapy has failed. These properties come solely from the dicarboxylate leaving group, which is kinetically more inert to substitution. Studies with monoclonal antibodies have shown the DNA adducts of carboplatin to be identical with those formed by *cis*-DDP.[117]Other platinum compounds that have undergone clinical trials are close analogues of *cis*-$[PtA_2X_2]$, or tetraplatin, *cis*,*cis*,*cis*-$[PtA_2X_2Y_2]$, that obey the classic structure-activity relationships. The activity of cationic triamines, *cis*-$[Pt(NH_3)_2LCI]CI$, where L is pyridine, a substituted pyridine, pyrimidine, or purine, against S180 ascites and L1210 tumors in mice opens a new vista of possible structures to be tried. The intercalator-linked complex AO-Pt (Figure 9.26) has also been found to show activity in the S180 ascites system, suggesting a further class of complexes that could be studied. The oral compounds, *cis*,*trans*,*cis*-$[Pt(NH_3)(C_6H_5NH_2)(O_2CCH_3)_2Cl_2]$, survive the digestive tract, are taken across the gastrointestinal mucosa, and metabolize to *cis*-$[Pt(NH_3)(C_6H_5NH_2)Cl_2]$, a cisplatin analogue.[54] As such they are effective pro-drugs that could become the major platinum agent in clinical use. Until these recent advances, there was a general impression that, by chance, the best compound discovered was the first one, cisplatin. There is now sufficient reason to expect that innovative experimentation will lead to improved drugs, bearing in mind the comment made earlier (Section IV.G.) that sustained individual effort for up to a decade can be required to move a compound from the laboratory bench into the clinic.

4. Nonplatinum Antitumor Metal Complexes

a. Soft Metals

As mentioned in Section IV.E., some compounds of Pd(II), Au(I), Rh(II), and Ru(II or III) have been screened for antitumor activity, but much more work needs to be done in this arena. The higher metal-ligand exchange rates of Pd(II), ~10^5 faster than those of Pt(Il), make these complexes potentially more toxic, as some preliminary animal studies have shown. By use of chelating or organometallic complexes, however, this problem might be avoided. The properties of Ru, Rh, and to a lesser extent Au amine and polypyridine complexes would seem to make them attractive candidates, and indeed there appears to be renewed interest in these molecules.[160] Inorganic chemists interested in pursuing drug development with these metals need to forge alliances with biological colleagues equipped to do the necessary animal screening and to develop in-house expertise for cell culture and related biochemical work. The techniques are not all that difficult and it is actually fun to undertake studies of the biological consequences of metallodrug chemistry.

b. Metallocenes and Metallocene Dihalides[36-37]

Although complexes such as $[(C_5H_5)_2TiCl_2]$ are superficially analogous to *cis*-DDP, in being potentially bifunctional DNA crosslinking agents, their hydrolytic reactions are sufficiently different to cast doubt on the value of this comparison. The fact that antitumor activity has been found for this very different class of inorganic compound, however, suggests that perhaps bioinorganic chemists have explored only a very small sample of possible metallodrugs.

9.6.11: Design of New Inorganic Anticancer Drugs is shared under a CC BY-NC-SA 4.0 license and was authored, remixed, and/or curated by LibreTexts.

9.7: Electron Transfer

Overview

Metalloproteins containing a single type of redox cofactor can be divided into two general classes: electron carriers and proteins involved in the transport or activation of small molecules. Some of the factors that seem to be characteristic of electron-transfer proteins (these proteins are sometimes called "electron transferases") are: (a) possession of a suitable cofactor to act as an electron sink (metal center with multiple stable oxidation states); (b) placement of the cofactor close enough to the protein surface to allow electrons to move in and out; (c) existence of a hydrophobic shell adjacent to, but not always entirely surrounding, the cofactor; (d) small structural changes accompanying electron transfer; and (e) an architecture that permits slight expansion or contraction in preferred directions upon electron transfer.

Metalloproteins that function as electron transferases typically place their metal coordination sites in a hydrophobic environment and may provide hydrogen bonds (in addition to ligands) to assist in stabilizing both the oxidized and the reduced forms of the cofactor. Metal-ligand bonds remain intact upon electron transfer to minimize inner-sphere reorganization energy. Many of the complex multisite metalloenzymes (e.g., cytochrome c oxidase, xanthine oxidase, the nitrogenase FeMo protein) contain redox centers that function as intramolecular electron transferases, shuttling electrons to/from other metal centers that bind exogenous ligands during enzymatic turnover.

There are three classes of metal containing electron transferases, each of which contains many members that exhibit important structural differences: blue copper proteins, iron-sulfur proteins, and cytochromes.

Blue Copper Proteins

Blue copper proteins were first isolated from bacteria in the 1950s and from plant tissues in the early 1960s. The intense blue color of these proteins is due to a strong absorption band at a wavelength of about 600 nm. Although simple Cu^{2+} complexes, such as $[Cu(H_2O)_6]^{2+}$ and $[Cu(NH_3)_4]^{2+}$, are also blue due to an absorption band at 600 nm, the intensity of the absorption band is about 100 times less than that of a blue copper protein. Moreover, the reduction potential for the Cu^{2+}/Cu^{+} couple in a blue copper protein is usually +0.3 to +0.5 V, considerably more positive than that of the aqueous Cu^{2+}/Cu^{+} couple (+0.15 V).

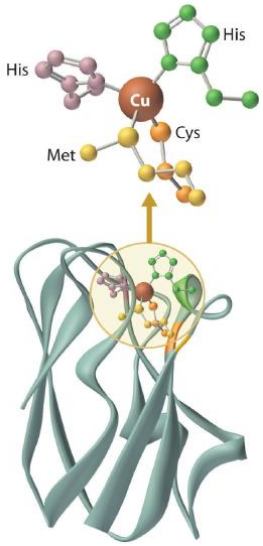


Figure **9.7.1**: A Blue Copper Protein. In both the oxidized and reduced forms of a blue copper protein, the copper is coordinated by four ligands (two histidine imidazole nitrogen atoms, a cysteine thiolate sulfur, and a thioether sulfur of a methionine) in a roughly tetrahedral arrangement.

The copper center in blue copper proteins has a distorted tetrahedral structure, in which the copper is bound to four amino acid side chains (Figure **9.7.3**). Although the most common structures for four-coordinate Cu^{2+} and Cu^{+} complexes are square planar and tetrahedral, respectively, the structures of the oxidized (Cu^{2+}) and reduced (Cu^{+}) forms of the protein are essentially identical. Thus

the protein forces the Cu^{2+} ion to adopt a higher-energy structure that is more suitable for Cu^{+}, which makes the Cu^{2+} form easier to reduce and raises its reduction potential.

Moreover, by forcing the oxidized and reduced forms of the metal complex to have essentially the same structure, the protein ensures that electron transfer to and from the copper site is rapid because only minimal structural reorganization of the metal center is required. Kinetics studies on simple metal complexes have shown that electron-transfer reactions tend to be slow when the structures of the oxidized and reduced forms of a metal complex are very different, and fast when they are similar. You will see that other metal centers used for biological electron-transfer reactions are also set up for minimal structural reorganization after electron transfer, which ensures the rapid transfer of electrons.

The blue copper proteins are characterized by intense S(Cys) → Cu chargetransfer absorption near 600 nm, an axial EPR spectrum displaying an unusually small hyperfine coupling constant, and a relatively high reduction potential.[4,8-10] With few exceptions (e.g., photosynthetic organisms), their precise roles in bacterial and plant physiology remain obscure. X-ray structures of several blue copper proteins indicate that the geometry of the copper site is approximately trigonal planar, as illustrated by the *Alcaligenes denitrificans* azurin structure (Figure 6.5).[11,12] In all these proteins, three ligands (one Cys, two His) bind tightly to the copper in a trigonal arrangement. Differences in interactions between the copper center and the axially disposed ligands may significantly contribute to variations in reduction potential that are observed[12] for the blue copper electron transferases. For example, $E^{\circ\prime}$ = 276 mV for *A. denitrificans* azurin, whereas that of *P. vulgaris* plastocyanin is 360 mV. In *A. denitrificans* azurin, the Cu-S(Met) bond is 0.2 Å longer than in poplar plastocyanin, and there is a carbonyl oxygen 3.1 Å from the copper center, compared with 3.8 Å in plastocyanin. These differences in bond lengths are expected to stabilize Cu^{II} in azurin to a greater extent than in plastocyanin, and result in a lower $E^{\circ\prime}$ value for azurin.

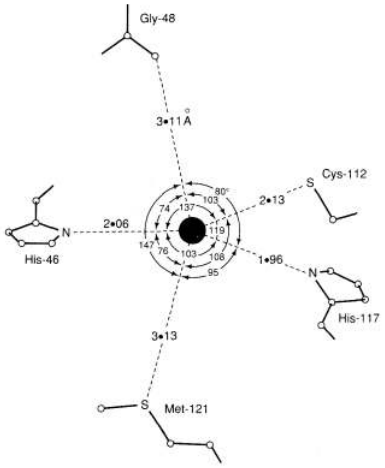


Figure 6.5 - Structure of the blue copper center in azurin.[11]

Iron Sulfur Proteins

Although all known bacteria, plants, and animals use iron–sulfur proteins to transfer electrons, the existence of these proteins was not recognized until the late 1950s. Iron–sulfur proteins transfer electrons over a wide range of reduction potentials, and their iron content can range from 1 to more than 12 Fe atoms per protein molecule. In addition, most iron–sulfur proteins contain stoichiometric amounts of sulfide (S^{2-}).

These properties are due to the presence of four different kinds of iron–sulfur units, which contain one, two, three, or four iron atoms per Fe–S complex (Figure **9.7.5**). In all cases, the Fe^{2+} and Fe^{3+} ions are coordinated to four sulfur ligands in a tetrahedral environment. Due to tetrahedral coordination by weak-field sulfur ligands, the iron is high spin in both the Fe^{3+} and Fe^{2+} oxidation states, which results in similar structures for the oxidized and reduced forms of the Fe–S complexes. Consequently, only small structural changes occur after oxidation or reduction of the Fe–S center, which results in rapid electron transfer.

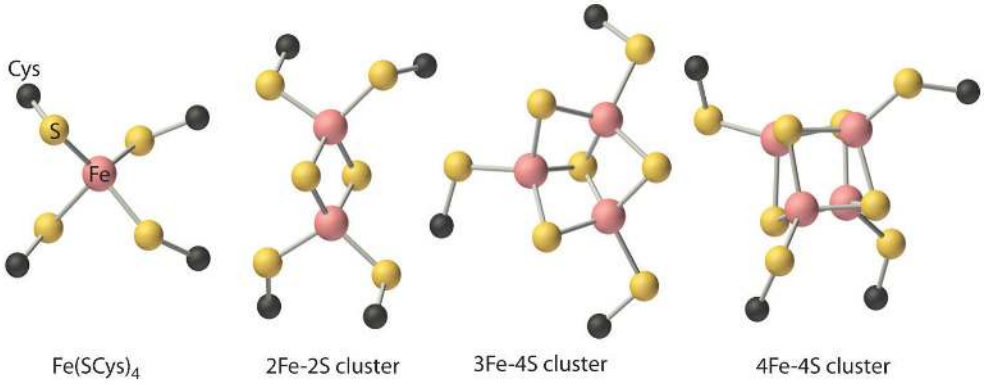


Figure **9.7.5**: Fe–S Centers in Proteins: Four kinds of iron–sulfur centers, containing one, two, three, and four iron atoms, respectively, are known in electron-transfer proteins. Although they differ in the number of sulfur atoms provided by cysteine thiolates versus sulfide, in all cases the iron is coordinated to four sulfur ligands in a roughly tetrahedral environment.

The iron-sulfur proteins play important roles[13,14] as electron carriers in virtually all living organisms, and participate in plant photosynthesis, nitrogen fixation, steroid metabolism, and oxidative phosphorylation, as well as many other processes (Chapter 7). The optical spectra of all iron-sulfur proteins are very broad and almost featureless, due to numerous overlapping charge-transfer transitions that impart red-brown-black colors to these proteins. On the other hand, the EPR spectra of iron-sulfur clusters are quite distinctive, and they are of great value in the study of the redox chemistry of these proteins.

The simplest iron-sulfur proteins, known as rubredoxins, are primarily found in anaerobic bacteria, where their function is unknown. Rubredoxins are small proteins (6 kDa) and contain iron ligated to four Cys sulfurs in a distorted tetrahedral arrangement. The $E^{\circ\prime}$ value for the $Fe^{III/II}$ couple in water is 770 mV; that of *C. pasteurianum* rubredoxin is -57 mV. The reduction potentials of iron-sulfur proteins are typically quite negative, indicating a stabilization of the oxidized form of the redox couple as a result of negatively charged sulfur ligands.

The [2Fe-2S] ferredoxins (10-20 kDa) are found in plant chloroplasts and mammalian tissue. The structure of *Spirulina platensis* ferredoxin[15] confirmed earlier suggestions, based on EPR and Mössbauer studies, that the iron atoms are present in a spin-coupled [2Fe-2S] cluster structure. One-electron reduction ($E^{\circ\prime}$ ~ -420 mV) of the protein results in a mixed-valence dimer (Equation 6.3):

$$[Fe_2S_2(SR)_4]^{2-} \underset{-e^-}{\overset{+e^-}{\rightleftharpoons}} [Fe_2S_2(SR)_4]^{3-} \tag{6.3}$$

$$Fd_{ox} \qquad Fd_{red} \tag{9.7.1}$$

$$2Fe(III) \qquad Fe(II) + Fe(III) \tag{9.7.2}$$

The additional electron in Fd_{red} is associated with only one of the iron sites, resulting in a so-called trapped-valence structure.[16] The $[Fe_2S_2(SR)_4]^{4-}$ cluster oxidation state, containing two ferrous ions, can be produced *in vitro* when strong reductants are used.

Four-iron clusters [4Fe-4S] are found in many strains of bacteria. In most of these bacterial iron-sulfur proteins, also termed ferredoxins, two such clusters are present in the protein. These proteins have reduction potentials in the -400 mV range and are rather small (6-10 kDa). Each of the clusters contains four iron centers and four sulfides at alternate comers of a distorted cube. Each iron is coordinated to three sulfides and one cysteine thiolate. The irons are strongly exchange-coupled, and the [4Fe-4S] cluster in bacterial ferredoxins is paramagnetic when reduced by one electron. The so-called "high-potential ironsulfur proteins" (HiPIPs) are found in photosynthetic bacteria, and exhibit anomalously high (~350 mV) reduction potentials. The *C. vinosum* HiPIP (10 kDa) structure demonstrates that HiPIPs are distinct from the [4Fe-4S] ferredoxins, and that the reduced HiPIP cluster structure is significantly distorted, as is also observed for the structure of the oxidized *P. aerogenes* ferredoxin. In addition, oxidized HiPIP is paramagnetic, whereas the reduced protein is EPR-silent.

This bewildering set of experimental observations can be rationalized in terms of a "three-state" hypothesis (i.e., $[4Fe\text{-}4S(SR)_4]^{n-}$ clusters exist in three physiological oxidation states).[17] This hypothesis nicely explains the differences in magnetic behavior and redox properties observed for these iron-sulfur proteins (Equation 6.4):

$$[4Fe-4S(SR)_4]^{-} \underset{-e^-}{\overset{+e^-}{\rightleftharpoons}} [4Fe-4S(SR)_4]^{2-} \underset{-e^-}{\overset{+e^-}{\rightleftharpoons}} [4Fe-4S(SR)_4]^{3-} \tag{6.4}$$

$$HiPIP_{ox} \qquad HiPIP_{red} \qquad Ferredoxin_{red} \tag{9.7.3}$$

$$Ferredoxing_{ox} \tag{9.7.4}$$

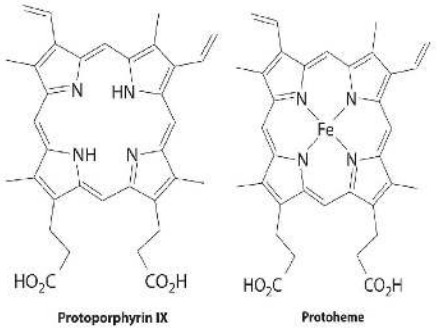
The bacterial ferredoxins and HiPIPs all possess tetracubane clusters containing thiolate ligands, yet the former utilize the -2/-3 cluster redox couple, whereas the latter utilize the -1/-2 cluster redox couple.

The protein environment thus exerts a powerful influence over the cluster reduction potentials. This observation applies to *all* classes of electron transferases—the factors that are critical determinants of cofactor reduction potentials are poorly understood at present but are thought[18] to include the low dielectric constants of protein interiors (~4 for proteins vs. ~78 for H_2O), electrostatic effects due to nearby charged amino-acid residues, hydrogen bonding, and geometric constraints imposed by the protein.

Cytochromes

The cytochromes (from the Greek cytos, meaning “cell”, and chroma, meaning “color”) were first identified in the 1920s by spectroscopic studies of cell extracts. Based on the wavelength of the maximum absorption in the visible spectrum, they were classified as cytochromes a (with the longest wavelength), cytochromes b (intermediate wavelength), and cytochromes c (shortest wavelength). It quickly became apparent that there was a correlation between their spectroscopic properties and other physical properties. For examples, cytochromes c are generally small, soluble proteins with a reduction potential of about +0.25 V, whereas cytochromes b are larger, less-soluble proteins with reduction potentials of about 0 V.

All cytochromes contain iron, and the iron atom in all cytochromes is coordinated by a planar array of four nitrogen atoms provided by a cyclic tetradentate ligand called a porphyrin. The iron–porphyrin unit is called a heme group. The structures of a typical porphyrin (protoporphyrin IX) and its iron complex (protoheme) are shown here. In addition to the four nitrogen atoms of the porphyrin, the iron in a cytochrome is usually bonded to two additional ligands provided by the protein, as shown in Figure **9.7.4**.



A cytochrome. Shown here is protoporphyrin IX and its iron complex, protoheme.

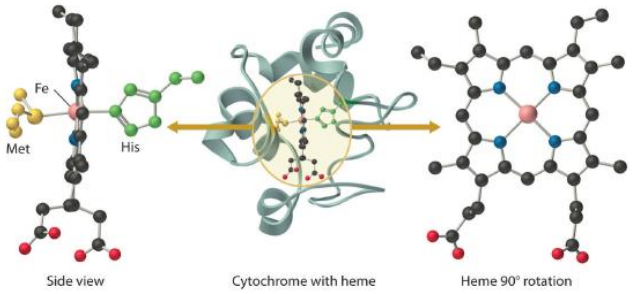


Figure **9.7.4**: A Cytochrome c. In a cytochrome c, the heme iron is coordinated to the nitrogen atom of a histidine imidazole and the sulfur atom of a methionine thioether, in addition to the four nitrogen atoms provided by the porphyrin.

In contrast to the blue copper proteins, two electron configurations are possible for both the oxidized and reduced forms of a cytochrome, and this has significant structural consequences. Thus Fe^{2+} is d^6 and can be either high spin (with four unpaired electrons) or low spin (with no unpaired electrons). Similarly, Fe^{3+} is d^5 and can also be high spin (with five unpaired electrons) or

low spin (with one unpaired electron). In low-spin heme complexes, both the Fe^{2+} and the Fe^{3+} ions are small enough to fit into the "hole" in the center of the porphyrin; hence the iron atom lies almost exactly in the plane of the four porphyrin nitrogen atoms in both cases. Because cytochromes b and c are low spin in both their oxidized and reduced forms, the structures of the oxidized and reduced cytochromes are essentially identical. Hence minimal structural changes occur after oxidation or reduction, which makes electron transfer to or from the heme very rapid.

> *Electron transfer reactions occur most rapidly when minimal structural changes occur during oxidation or reduction*

As a class, the cytochromes[19-22] are the most thoroughly characterized of the electron transferases. By definition, a cytochrome contains one or more heme cofactors. These proteins were among the first to be identified in cellular extracts because of their distinctive optical properties, particularly an intense absorption in the 410-430 nm region (called the Soret band). Cytochromes are typically classified on the basis of heme type. Figure 6.6 displays the three most commonly encountered types of heme: heme a possesses a long phytyl "tail" and is found in cytochrome c oxidase; heme b is found in b-type cytochromes and globins; heme c is covalently bound to c-type cytochromes via two thioether linkages. Cytochrome nomenclature presents a real challenge! Some cytochromes are designated according to the historical order of discovery, e.g., cytochrome c_2 in bacterial photosynthesis. Others are designated according to the λ_{max} of the α band in the absorption spectrum of the reduced protein (e.g., cytochrome c_{551}).

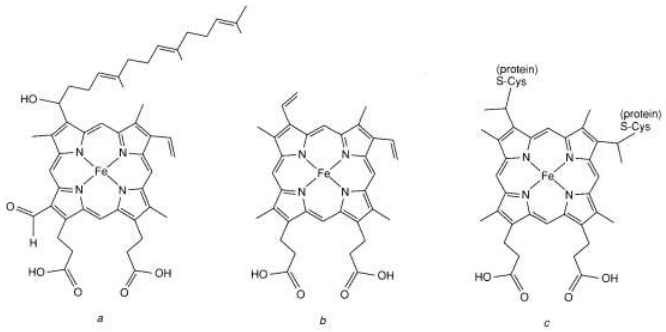


Figure 6.6 - Structures of hemes a, b, and c.

Cytochromes c are widespread in nature. Ambler[23] divided these electron carriers into three classes on structural grounds. The Class I cytochromes c contain axial His and Met ligands, with the heme located near the N-terrninus of the protein. These proteins are globular, as indicated by the ribbon drawing of tuna cytochrome c (Figure 6.7). X-ray structures of Class I cytochromes c from a variety of eukaryotes and prokaryotes clearly show an evolutionarily conserved "cytochrome fold," with the edge of the heme solvent-exposed. The reduction potentials of these cytochromes are quite positive (200 to 320 mV). Mammalian cytochrome c, because of its distinctive role in the mitochondrial electron-transfer chain, will be discussed later.

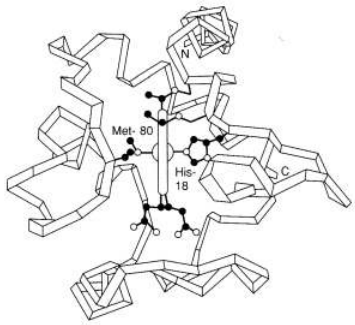


Figure 6. - Structure of tuna cytochrome c.

Class II cytochromes c ($E^{\circ\prime}$ ~ -100 mV) are found in photosynthetic bacteria, where they serve an unknown function. Unlike their Class I cousins, these c-type cytochromes are high-spin: the iron is five-coordinate, with an axial His ligand. These proteins, generally referred to as cytochromes c' , are four-α-helix bundles (Figure 6.8). The vacant axial coordination site is buried in the protein interior.

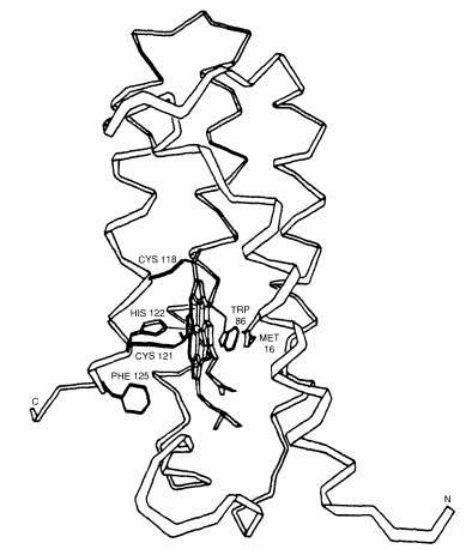


Figure 6.8 - Structure of cytochrome c'.

Finally, Class III cytochromes c, also called cytochromes c_3, contain four hemes, each ligated by two axial histidines. These proteins are found in a restricted class of sulfate-reducing bacteria and may be associated with the cytoplasmic membrane. The low molecular weights of cytochromes c_3 (~14. 7 kDa) require that the four hemes be much more exposed to the solvent than the hemes of other cytochromes (see Figure 6.9), which may be in part responsible for their unusually negative (-200 to -350 mV) reduction potentials. These proteins possess many aromatic residues and short heme-heme distances, two properties that could be responsible for their anomalously large solid-state electrical conductivity.[24]

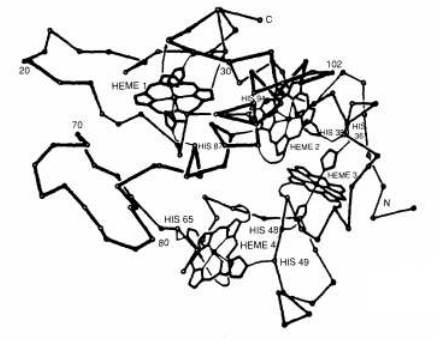


Figure 6.9 - Structure of cytochrome c_3.

9.7: Electron Transfer is shared under a CC BY-NC-SA 4.0 license and was authored, remixed, and/or curated by LibreTexts.

CHAPTER OVERVIEW

10: Special Topics

10.1: f-Block Metals- Lanthanides and Actinides

10.1.1: Introduction

10.1.2: f-Orbitals and Oxidation States

10.1.3: Atoms and Ion Sizes

10.1.3A: The Lanthanoid Contraction

10.1.3B: Coordination Numbers

10.1.4: Spectroscopic and Magnetic Properties

10.1.4A: Electronic Spectra and Magnetic Moments - Lanthanoids

10.1.4B: Luminescence of Lanthanoid Complexes

10.1.4C: Electronic Spectra and Magnetic Moments - Actinoids

10.1.5: Sources of the Lanthanoids and Actinoids

10.1.5A: Occurrence and Separation of the Lanthanoids

10.1.5B: The Actinoids

10.1.6: Lanthanoid Metals

10.1.7: Inorganic Compounds and Coordination Complexes of the Lanthanoids

10.1.7A: Halides

10.1.7B: Hydroxides and Oxides

10.1.7C: Complexes of Ln(III)

10.1.8: Organometallic Complexes of the Lanthanoids

10.1.8A: \(\sigma\)-Bonded Complexes

10.1.8B: Cyclopentadienyl Complexes

10.1.8C: Bis(arene) Derivatives

10.1.8D: Complexes Containing the \(\eta^8\)-cyclooctatetraenyl Ligand

10.1.9: The Actinoid Metals

10.1.10: Inorganic Compounds and Coordination Complexes of Thorium, Uranium, and Plutonium

10.1.10A: Thorium

10.1.10B: Uranium

10.1.10C: Plutonium

10.1.11: Organometallic Complexes of Thorium and Uranium

10.1.11A: (\sigma\)-Bonded Complexes

10.1.11B: Cyclopentadienyl Derivatives

10.1.11C: Complexes Containing the \(\eta^8\)-cyclooctatetraenyl Ligand

10.2: Physical Inorganic Techniques

10.2.1: Electronic Spectroscopy

10.2.1A: UV-VIS Absorption Spectroscopy

10.2.1B: Types of Absorption

10.2.1C: Absorbance and the Beer-Lambert Law

10.2.1D: Emission Spectroscopy

10.2.2: Nuclear Magnetic Resonance (NMR) Spectroscopy

10.2.3: Electron Paramagnetic Resonance (EPR) Spectroscopy
10.2.3A: What is EPR Spectroscopy?
10.2.3B: The Zeeman Electronic Effect
10.2.3C: EPR Spectra
10.2.4: Mossbauer Spectroscopy
10.2.4A: The Technique of Mossbauer Spectroscopy
10.2.4B: What Can Isomer Shift Data Tell Us?
10.2.5: Structure Determination - Diffraction Methods
10.2.5A: X-Ray Diffraction (XRD)
10.2.5B: Single Crystal X-Ray Diffraction
10.2.5C: Powder X-Ray Diffraction
10.2.5D: Single Crystal Neutron Diffraction
10.2.5E: Electron Diffraction
10.2.5F: Low-Energy Electron Diffraction (LEED)
10.2.5G: Structural Databases
10.2.6: Photoelectron Spectroscopy (PES, UPS, XPS, ESCA)
10.2.7: Mass Spectrometry
10.2.7A: Electron Ionization (EI)
10.2.7B: Fast Atom Bombardment (FAB)
10.2.7C: Matrix-Assisted Laser Desorption Ionization Time-of-Flight (MALDI-TOF)
10.2.7D: Electrospray Ionization (ESI)
10.3: Fluxional Behavior
10.3.1: Determination of Energetics of Fluxional Molecules by NMR

10: Special Topics is shared under a CC BY-NC-SA 4.0 license and was authored, remixed, and/or curated by LibreTexts.

SECTION OVERVIEW

10.1: f-Block Metals- Lanthanides and Actinides

Topic hierarchy

10.1.1: Introduction

10.1.2: f-Orbitals and Oxidation States

10.1.3: Atoms and Ion Sizes

- 10.1.3A: The Lanthanoid Contraction
- 10.1.3B: Coordination Numbers

10.1.4: Spectroscopic and Magnetic Properties

- 10.1.4A: Electronic Spectra and Magnetic Moments - Lanthanoids
- 10.1.4B: Luminescence of Lanthanoid Complexes
- 10.1.4C: Electronic Spectra and Magnetic Moments - Actinoids

10.1.5: Sources of the Lanthanoids and Actinoids

- 10.1.5A: Occurrence and Separation of the Lanthanoids
- 10.1.5B: The Actinoids

10.1.6: Lanthanoid Metals

10.1.7: Inorganic Compounds and Coordination Complexes of the Lanthanoids

- 10.1.7A: Halides
- 10.1.7B: Hydroxides and Oxides
- 10.1.7C: Complexes of Ln(III)

10.1.8: Organometallic Complexes of the Lanthanoids

- 10.1.8A: \(\sigma\)-Bonded Complexes
- 10.1.8B: Cyclopentadienyl Complexes
- 10.1.8C: Bis(arene) Derivatives
- 10.1.8D: Complexes Containing the \(\eta^8\)-cyclooctatetraenyl Ligand

10.1.9: The Actinoid Metals

10.1.10: Inorganic Compounds and Coordination Complexes of Thorium, Uranium, and Plutonium

- 10.1.10A: Thorium
- 10.1.10B: Uranium
- 10.1.10C: Plutonium

10.1.11: Organometallic Complexes of Thorium and Uranium

10.1.11A: (\sigma\)-Bonded Complexes
10.1.11B: Cyclopentadienyl Derivatives
10.1.11C: Complexes Containing the \(\eta^8\)-cyclooctatetraenyl Ligand

---

10.1: f-Block Metals- Lanthanides and Actinides is shared under a CC BY-NC-SA 4.0 license and was authored, remixed, and/or curated by LibreTexts.

10.1.1: Introduction

10.1.1: Introduction is shared under a CC BY-NC-SA 4.0 license and was authored, remixed, and/or curated by LibreTexts.

10.1.2: f-Orbitals and Oxidation States

10.1.2: f-Orbitals and Oxidation States is shared under a CC BY-NC-SA 4.0 license and was authored, remixed, and/or curated by LibreTexts.

10.1.3: Atoms and Ion Sizes

10.1.3: Atoms and Ion Sizes is shared under a CC BY-NC-SA 4.0 license and was authored, remixed, and/or curated by LibreTexts.

10.1.3A: The Lanthanoid Contraction

10.1.3A: The Lanthanoid Contraction is shared under a CC BY-NC-SA 4.0 license and was authored, remixed, and/or curated by LibreTexts.

10.1.3B: Coordination Numbers

10.1.3B: Coordination Numbers is shared under a CC BY-NC-SA 4.0 license and was authored, remixed, and/or curated by LibreTexts.

10.1.4: Spectroscopic and Magnetic Properties

10.1.4: Spectroscopic and Magnetic Properties is shared under a CC BY-NC-SA 4.0 license and was authored, remixed, and/or curated by LibreTexts.

10.1.4A: Electronic Spectra and Magnetic Moments - Lanthanoids

10.1.4A: Electronic Spectra and Magnetic Moments - Lanthanoids is shared under a CC BY-NC-SA 4.0 license and was authored, remixed, and/or curated by LibreTexts.

10.1.4B: Luminescence of Lanthanoid Complexes

10.1.4B: Luminescence of Lanthanoid Complexes is shared under a CC BY-NC-SA 4.0 license and was authored, remixed, and/or curated by LibreTexts.

10.1.4C: Electronic Spectra and Magnetic Moments - Actinoids

10.1.4C: Electronic Spectra and Magnetic Moments - Actinoids is shared under a CC BY-NC-SA 4.0 license and was authored, remixed, and/or curated by LibreTexts.

10.1.5: Sources of the Lanthanoids and Actinoids

10.1.5: Sources of the Lanthanoids and Actinoids is shared under a CC BY-NC-SA 4.0 license and was authored, remixed, and/or curated by LibreTexts.

10.1.5A: Occurrence and Separation of the Lanthanoids

10.1.5A: Occurrence and Separation of the Lanthanoids is shared under a CC BY-NC-SA 4.0 license and was authored, remixed, and/or curated by LibreTexts.

10.1.5B: The Actinoids

10.1.5B: The Actinoids is shared under a CC BY-NC-SA 4.0 license and was authored, remixed, and/or curated by LibreTexts.

10.1.6: Lanthanoid Metals

10.1.6: Lanthanoid Metals is shared under a CC BY-NC-SA 4.0 license and was authored, remixed, and/or curated by LibreTexts.

10.1.7: Inorganic Compounds and Coordination Complexes of the Lanthanoids

10.1.7: Inorganic Compounds and Coordination Complexes of the Lanthanoids is shared under a CC BY-NC-SA 4.0 license and was authored, remixed, and/or curated by LibreTexts.

10.1.7A: Halides

10.1.7A: Halides is shared under a CC BY-NC-SA 4.0 license and was authored, remixed, and/or curated by LibreTexts.

10.1.7B: Hydroxides and Oxides

10.1.7B: Hydroxides and Oxides is shared under a CC BY-NC-SA 4.0 license and was authored, remixed, and/or curated by LibreTexts.

10.1.7C: Complexes of Ln(III)

10.1.7C: Complexes of Ln(III) is shared under a CC BY-NC-SA 4.0 license and was authored, remixed, and/or curated by LibreTexts.

10.1.8: Organometallic Complexes of the Lanthanoids

10.1.8: Organometallic Complexes of the Lanthanoids is shared under a CC BY-NC-SA 4.0 license and was authored, remixed, and/or curated by LibreTexts.

10.1.8A: σ -Bonded Complexes

10.1.8A: σ-Bonded Complexes is shared under a CC BY-NC-SA 4.0 license and was authored, remixed, and/or curated by LibreTexts.

10.1.8B: Cyclopentadienyl Complexes

10.1.8B: Cyclopentadienyl Complexes is shared under a CC BY-NC-SA 4.0 license and was authored, remixed, and/or curated by LibreTexts.

10.1.8C: Bis(arene) Derivatives

10.1.8C: Bis(arene) Derivatives is shared under a CC BY-NC-SA 4.0 license and was authored, remixed, and/or curated by LibreTexts.

10.1.8D: Complexes Containing the η 8 -cyclooctatetraenyl Ligand

10.1.8D: Complexes Containing the η^8-cyclooctatetraenyl Ligand is shared under a CC BY-NC-SA 4.0 license and was authored, remixed, and/or curated by LibreTexts.

10.1.9: The Actinoid Metals

10.1.9: The Actinoid Metals is shared under a CC BY-NC-SA 4.0 license and was authored, remixed, and/or curated by LibreTexts.

10.1.10: Inorganic Compounds and Coordination Complexes of Thorium, Uranium, and Plutonium

10.1.10: Inorganic Compounds and Coordination Complexes of Thorium, Uranium, and Plutonium is shared under a CC BY-NC-SA 4.0 license and was authored, remixed, and/or curated by LibreTexts.

10.1.10A: Thorium

10.1.10A: Thorium is shared under a CC BY-NC-SA 4.0 license and was authored, remixed, and/or curated by LibreTexts.

10.1.10B: Uranium

10.1.10B: Uranium is shared under a CC BY-NC-SA 4.0 license and was authored, remixed, and/or curated by LibreTexts.

10.1.10C: Plutonium

10.1.10C: Plutonium is shared under a CC BY-NC-SA 4.0 license and was authored, remixed, and/or curated by LibreTexts.

10.1.11: Organometallic Complexes of Thorium and Uranium

10.1.11: Organometallic Complexes of Thorium and Uranium is shared under a CC BY-NC-SA 4.0 license and was authored, remixed, and/or curated by LibreTexts.

10.1.11A: (\sigma\)-Bonded Complexes

10.1.11A: (\sigma\)-Bonded Complexes is shared under a CC BY-NC-SA 4.0 license and was authored, remixed, and/or curated by LibreTexts.

10.1.11B: Cyclopentadienyl Derivatives

10.1.11B: Cyclopentadienyl Derivatives is shared under a CC BY-NC-SA 4.0 license and was authored, remixed, and/or curated by LibreTexts.

10.1.11C: Complexes Containing the η 8 -cyclooctatetraenyl Ligand

10.1.11C: Complexes Containing the η^8-cyclooctatetraenyl Ligand is shared under a CC BY-NC-SA 4.0 license and was authored, remixed, and/or curated by LibreTexts.

10.2: Physical Inorganic Techniques

10.2: Physical Inorganic Techniques is shared under a CC BY-NC-SA 4.0 license and was authored, remixed, and/or curated by LibreTexts.

SECTION OVERVIEW

10.2.1: Electronic Spectroscopy

Topic hierarchy

10.2.1A: UV-VIS Absorption Spectroscopy

10.2.1B: Types of Absorption

10.2.1C: Absorbance and the Beer-Lambert Law

10.2.1D: Emission Spectroscopy

10.2.1: Electronic Spectroscopy is shared under a CC BY-NC-SA 4.0 license and was authored, remixed, and/or curated by LibreTexts.

10.2.1A: UV-VIS Absorption Spectroscopy

10.2.1A: UV-VIS Absorption Spectroscopy is shared under a CC BY-NC-SA 4.0 license and was authored, remixed, and/or curated by LibreTexts.

10.2.1B: Types of Absorption

10.2.1B: Types of Absorption is shared under a CC BY-NC-SA 4.0 license and was authored, remixed, and/or curated by LibreTexts.

10.2.1C: Absorbance and the Beer-Lambert Law

10.2.1C: Absorbance and the Beer-Lambert Law is shared under a CC BY-NC-SA 4.0 license and was authored, remixed, and/or curated by LibreTexts.

10.2.1D: Emission Spectroscopy

10.2.1D: Emission Spectroscopy is shared under a CC BY-NC-SA 4.0 license and was authored, remixed, and/or curated by LibreTexts.

SECTION OVERVIEW

10.2.2: Nuclear Magnetic Resonance (NMR) Spectroscopy

Topic hierarchy

10.2.2: Nuclear Magnetic Resonance (NMR) Spectroscopy is shared under a CC BY-NC-SA 4.0 license and was authored, remixed, and/or curated by LibreTexts.

SECTION OVERVIEW

10.2.3: Electron Paramagnetic Resonance (EPR) Spectroscopy

Topic hierarchy

10.2.3A: What is EPR Spectroscopy?

10.2.3B: The Zeeman Electronic Effect

10.2.3C: EPR Spectra

10.2.3: Electron Paramagnetic Resonance (EPR) Spectroscopy is shared under a CC BY-NC-SA 4.0 license and was authored, remixed, and/or curated by LibreTexts.

10.2.3A: What is EPR Spectroscopy?

10.2.3A: What is EPR Spectroscopy? is shared under a CC BY-NC-SA 4.0 license and was authored, remixed, and/or curated by LibreTexts.

10.2.3B: The Zeeman Electronic Effect

Magnetism results from the circular motion of charged particles. This property is demonstrated on a macroscopic scale by making an electromagnet from a coil of wire and a battery. Electrons moving through the coil produce a magnetic field (Figure **10.2.3*B*.1**), which can be thought of as originating from a magnetic dipole or a bar magnet.

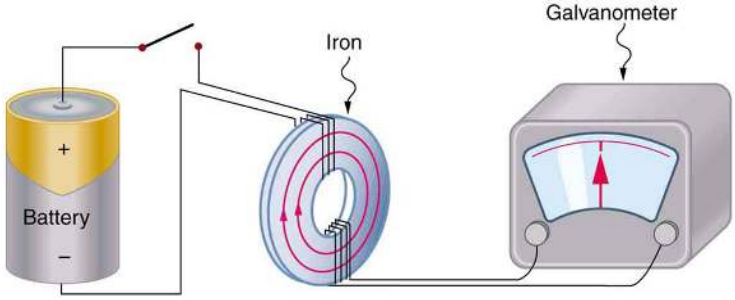


Figure **10.2.3*B*.1**: Faraday's apparatus for demonstrating that a magnetic field can produce a current. A change in the field produced by the top coil induces an emf and, hence, a current in the bottom coil. When the switch is opened and closed, the galvanometer registers currents in opposite directions. No current flows through the galvanometer when the switch remains closed or open. (CC BY 3.0; OpenStax).

> *Magnetism results from the circular motion of charged particles.*

Electrons in atoms also are moving charges with angular momentum so they too produce a magnetic dipole, which is why some materials are magnetic. A magnetic dipole interacts with an applied magnetic field, and the energy of this interaction is given by the scalar product of the magnetic dipole moment, and the magnetic field, $\vec{B}$.

$$E_B = -\vec{\mu}_m \cdot \vec{B} \tag{10.2.3B.1}$$

Magnets are acted on by forces and torques when placed within an external applied magnetic field (Figure **10.2.3*B*.2**). In a uniform external field, a magnet experiences no net force, but a net torque. The torque tries to align the magnetic moment ($\vec{\mu}_m$ of the magnet with the external field $\vec{B}$. The magnetic moment of a magnet points from its south pole to its north pole.

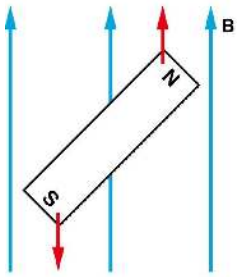


Figure **10.2.3*B*.2**: A magnet will feel a force to realign in an external field, i.e., go from a higher energy to a lower energy. The energy of this system is determined by Equation 10.2.3B.1 and classical can vary since the angle between $\vec{\mu}_m$ and $\vec{B}$ can vary continuously from 0 (low energy) to 180° (high energy).

In a non-uniform magnetic field a current loop, and therefore a magnet, experiences a net force, which tries to pull an aligned dipole into regions where the magnitude of the magnetic field is larger and push an anti-aligned dipole into regions where magnitude the magnetic field is smaller.

Quantum Effects

As expected, the quantum picture is different. Pieter Zeeman was one of the first to observe the splittings of spectral lines in a magnetic field caused by this interaction. Consequently, such splittings are known as the **Zeeman effect**. Let's now use our current knowledge to predict what the Zeeman effect for the 2p to 1s transition in hydrogen would look like, and then compare this prediction with a more complete theory. To understand the Zeeman effect, which uses a magnetic field to remove the degeneracy of different angular momentum states, we need to examine how an electron in a hydrogen atom interacts with an external magnetic

field, $\vec{B}$. Since magnetism results from the circular motion of charged particles, we should look for a relationship between the angular momentum $\vec{L}$ and the magnetic dipole moment $\vec{\mu}_m$.

The relationship between the magnetic dipole moment $\vec{\mu}_m$ (also referred to simply as the magnetic moment) and the angular momentum $\vec{L}$ of a particle with mass m and charge q is given by

$$\vec{\mu}_m = \frac{q}{2m}\vec{L} \tag{10.2.3B.2}$$

For an electron, this equation becomes

$$\vec{\mu}_m = -\frac{e}{2m_e}\vec{L} \tag{10.2.3B.3}$$

where the specific charge and mass of the electron have been substituted for q and m. The magnetic moment for the electron is a vector pointing in the direction opposite to $\vec{L}$, both of which classically are perpendicular to the plane of the rotational motion.

Exercise 10.2.3B.1

Will an electron in the ground state of hydrogen have a magnetic moment? Why or why not?

The relationship between the angular momentum of a particle and its magnetic moment is commonly expressed as a ratio, called the gyromagnetic ratio, γ. Gyro is Greek for turn so gyromagnetic simply relates turning (angular momentum) to magnetism. Now you also know why the Greek sandwiches made with meat cut from a spit turning over a fire are called gyros.

$$\gamma = \frac{\mu_m}{L} = \frac{q}{2m} \tag{10.2.3B.4}$$

In the specific case of an electron,

$$\gamma_e = -\frac{e}{2m_e} \tag{10.2.3B.5}$$

Exercise 10.2.3B.2

Calculate the magnitude of the gyromagnetic ratio for an electron.

To determine the energy of a hydrogen atom in a magnetic field we need to include the operator form of the hydrogen atom Hamiltonian. The Hamiltonian always consists of all the energy terms that are relevant to the problem at hand.

$$\hat{H} = \hat{H}^0 + \hat{H}_m \tag{10.2.3B.6}$$

where $\hat{H}^0$ is the Hamiltonian operator in the absence of the field and $\hat{H}_m$ is written using the operator forms of Equations 10.2.3B.1 and 10.2.3B.3),

$$\hat{H}_m = -\hat{\mu}\cdot\vec{B} = \frac{e}{2m_e}\hat{L}\cdot B \tag{10.2.3B.7}$$

The scalar product

$$\hat{L}\cdot\vec{B} = \hat{L}_x B_x + \hat{L}_y B_y + \hat{L}_z B_z \tag{10.2.3B.8}$$

simplifies if the z-axis is defined as the direction of the external field because then B_x and B_y are automatically 0, and Equation 10.2.3B.6 becomes

$$\hat{H} = \hat{H}^0 + \frac{eB_z}{2m_e}\hat{L}_z \tag{10.2.3B.9}$$

where B_z is the magnitude of the magnetic field, which is along the z-axis.

We now can ask, “What is the effect of a magnetic field on the energy of the hydrogen atom orbitals?” To answer this question, we will not solve the Schrödinger equation again; we simply calculate the expectation value of the energy, $\langle E\rangle$, using the existing hydrogen atom wavefunctions and the new Hamiltonian operator.

$$\langle E \rangle = \left\langle \hat{H}^0 \right\rangle + \frac{eB_z}{2m_e} \left\langle \hat{L}_z \right\rangle \tag{10.2.3B.10}$$

where

$$\left\langle \hat{H}^0 \right\rangle = \int \psi^*_{n,l,m_l} \hat{H}^0 \psi_{n,l,m_l} d\tau = E_n \tag{10.2.3B.11}$$

and

$$\left\langle \hat{L}_z \right\rangle = \int \psi^*_{n,l,m_l} \hat{L}_z \psi_{n,l,m_l} d\tau = m_l \hbar \tag{10.2.3B.12}$$

Exercise 10.2.3*B*.3

Show that the expectation value $\left\langle \hat{L}_z \right\rangle = m_l \hbar$.

The expectation value approach provides an exact result in this case because the hydrogen atom wavefunctions are eigenfunctions of both $\hat{H}^0$ and $\hat{L}_z$. If the wavefunctions were not eigenfunctions of the operator associated with the magnetic field, then this approach would provide a first-order estimate of the energy. First and higher order estimates of the energy are part of a general approach to developing approximate solutions to the Schrödinger equation. This approach, called perturbation theory, is discussed in the next chapter.

The expectation value calculated for the total energy in this case is the sum of the energy in the absence of the field, E_n, plus the Zeeman energy, $\frac{e\hbar B_z m_l}{2m_e}$

$$\langle E \rangle = E_n + \frac{e\hbar B_z m_l}{2m_e} \tag{10.2.3B.13}$$

$$= E_n + \mu_B B_z m_l \tag{10.2.3B.14}$$

The factor

$$\frac{e\hbar}{2m_e} = -\gamma_e \hbar = \mu_B \tag{10.2.3B.15}$$

defines the constant μ_B, called the **Bohr magneton**, which is taken to be the fundamental magnetic moment. It has units of 9.2732×10^{-21} erg/Gauss or 9.2732×10^{-24} Joule/Tesla. This factor will help you to relate magnetic fields, measured in Gauss or Tesla, to energies, measured in ergs or Joules, for any particle with a charge and mass the same as an electron.

Equation 10.2.3B.14 shows that the m_l quantum number degeneracy of the hydrogen atom is removed by the magnetic field. For example, the three states ψ_{211}, ψ_{21-1}, and ψ_{210}, which are degenerate in zero field, have different energies in a magnetic field, as shown in Figure 10.2.3*B*.3.

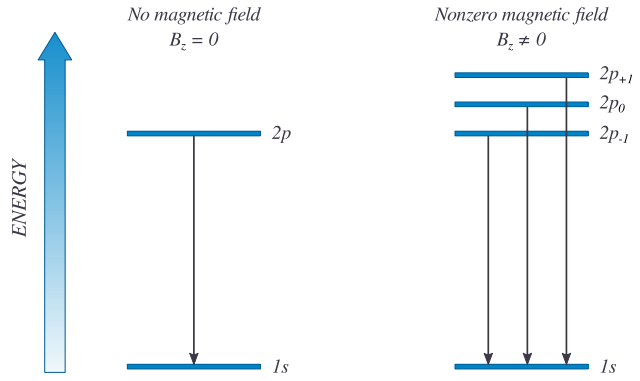


Figure 10.2.3*B*.3: The Zeeman effect. Emission when an electron switches from a 2p orbital to a 1s orbital occurs at only one energy in the absence of a magnetic field, but can occur at three different energies in the presence of a magnetic field.

The $m_l = 0$ state, for which the component of angular momentum and hence also the magnetic moment in the external field direction is zero, experiences no interaction with the magnetic field. The $m_l = +1$ state, for which the angular momentum in the z-direction is +ħ and the magnetic moment is in the opposite direction, against the field, experiences a raising of energy in the presence of a field. Maintaining the magnetic dipole against the external field direction is like holding a small bar magnet with its poles aligned exactly opposite to the poles of a large magnet (Figure **10.2.3*B*.5**). It is a higher energy situation than when the magnetic moments are aligned with each other.

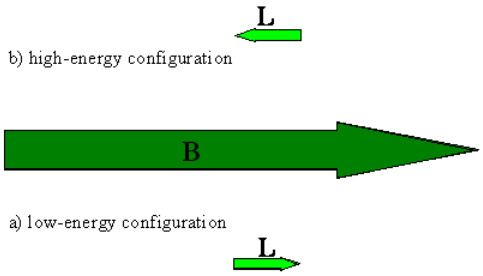


Figure **10.2.3*B*.4**: The effect of an external magnetic field (***B***) on the energy of a magnetic dipole (***L***) oriented a) with and b) against the applied magnetic field.

Exercise 10.2.3*B*.4

Carry out the steps going from Equation 10.2.3B.10 to Equation 10.2.3B.14.

Exercise 10.2.3*B*.5

Consider the effect of changing the magnetic field on the magnitude of the Zeeman splitting. Sketch a diagram where the magnetic field strength is on the x-axis and the energy of the three 2p orbitals is on the y-axis to show the trend in splitting magnitudes with increasing magnetic field. Be quantitative, calculate and plot the exact numerical values using a software package of your choice.

Exercise 10.2.3*B*.6

Based on your calculations in Exercise **10.2.3*B*.2** sketch a luminescence spectrum for the hydrogen atom in the n = 2 level in a magnetic field of 1 Tesla. Provide the numerical value for each of the transition energies. Use cm^{-1} or electron volts for the energy units.

10.2.3B: The Zeeman Electronic Effect is shared under a CC BY-NC-SA 4.0 license and was authored, remixed, and/or curated by LibreTexts.

- **8.4: Magnetic Properties and the Zeeman Effect** by David M. Hanson, Erica Harvey, Robert Sweeney, Theresa Julia Zielinski is licensed CC BY-NC-SA 4.0. Original source: https://web.archive.org/web/20200619182410/http://www.chemeddl.org.

10.2.3C: EPR Spectra

10.2.3C: EPR Spectra is shared under a CC BY-NC-SA 4.0 license and was authored, remixed, and/or curated by LibreTexts.

SECTION OVERVIEW

10.2.4: Mossbauer Spectroscopy

Topic hierarchy

10.2.4A: The Technique of Mossbauer Spectroscopy

10.2.4B: What Can Isomer Shift Data Tell Us?

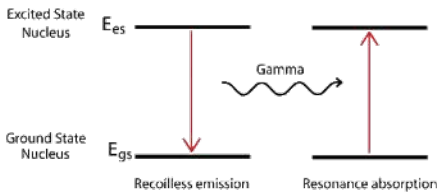
10.2.4: Mossbauer Spectroscopy is shared under a CC BY-NC-SA 4.0 license and was authored, remixed, and/or curated by LibreTexts.

10.2.4A: The Technique of Mossbauer Spectroscopy

Mössbauer spectroscopy is a versatile technique used to study nuclear structure with the absorption and re-emission of gamma rays, part of the electromagnetic spectrum. The technique uses a combination of the Mössbauer effect and Doppler shifts to probe the hyperfine transitions between the excited and ground states of the nucleus. Mössbauer spectroscopy requires the use of solids or crystals which have a probability to absorb the photon in a recoilless manner, many isotopes exhibit Mössbauer characteristics but the most commonly studied isotope is ^{57}Fe.

Introduction

Rudolf L. Mössbauer became a physics student at Technical University in Munich at the age of 20. After passing his intermediate exams Mössbauer began working on his thesis and doctorate work in 1955, while working as an assistant lecturer at Institute for Mathematics. In 1958 at the age of 28 Mössbauer graduated, and also showed experimental evidence for recoilless resonant absorption in the nucleus, later to be called the Mössbauer Effect. In 1961 Mössbauer was awarded the Nobel Prize in physics and, under the urging of Richard Feynman, accepted the position of Professor of Physics at the California Institute of Technology.



Mössbauer Effect

The recoil energy associated with absorption or emission of a photon can be described by the conservation of momentum. In it we find that the recoil energy depends inversely on the mass of the system. For a gas the mass of the single nucleus is small compared to a solid. The solid or crystal absorbs the energy as phonons, quantized vibration states of the solid, but there is a probability that no phonons are created and the whole lattice acts as the mass, resulting in a recoilless emission of the gamma ray. The new radiation is at the proper energy to excite the next ground state nucleus. The probability of recoilless events increases with decreasing transition energy.

$$P_R = P_\gamma$$

$$P_\gamma^2 = P_\gamma^2$$

$$2ME_R = \frac{E_\gamma^2}{c^2}$$

$$E_R = \frac{E_\gamma^2}{2Mc^2}$$

Doppler Effect

The Doppler shift describes the change in frequency due to a moving source and a moving observer. f is the frequency measured at the observer, v is the velocity of the wave so for our case this is the speed of light c, v_r is the velocity of the observer, v_s is the velocity of the source which is positive when heading away from the observer, and f_0 is the initial frequency.

$$f = \left(\frac{v + v_r}{v + v_s}\right) f_0$$

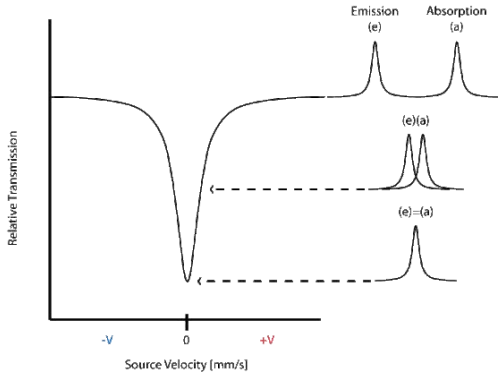
$$f = \left(\frac{c}{c + v_s}\right) f_0$$

In the case where the source is moving toward a stationary observer the perceived frequency is higher. For the opposite situation where the source travels away from the observer frequencies recorded at the observer will be of lower compared to the initial wave. The energy of a photon is related to the product of Planck's constant and the frequency of the electromagnetic radiation. Thus for

increasing frequencies the corresponding energy also increase, and the same is true in the reverse case where frequencies decrease and therefore energy decreases.

$$E = \frac{hc}{\lambda} = h\nu$$

The energy differences between hyperfine states are minimal (fractions of an eV) and the energy variation is achieved by the moving the source toward and away from the sample in an oscillating manner, commonly at a velocity of a few mm/s. The transmittance is then plotted against the velocity of the source and a peak is seen at the energy corresponding to the resonance energy.

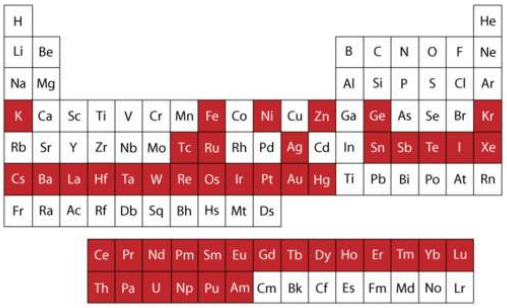


In the above spectrum the emission and absorption are both estimated by the Lorentzian distribution.

Mössbauer Isotopes

By far the most common isotopes studied using Mössbauer spectroscopy is ^{57}Fe, but many other isotopes have also displayed a Mössbauer spectrum. Two criteria for functionality are

1. The excited state is of very low energy, resulting in a small change in energy between ground and excited state. This is because gamma rays at higher energy are not absorbed in a recoil free manner, meaning resonance only occurs for gamma rays of low energy.
2. The resolution of Mössbauer spectroscopy depends upon the lifetime of the excited state. The longer the excited state lasts the better the image.



Both conditions are met by ^{57}Fe and it is thus used extensively in Mössbauer spectroscopy. In the figure to the right the red colored boxes of the periodic table of elements indicate all elements that have isotopes visible using the Mössbauer technique.

Hyperfine Interactions

Mössbauer spectroscopy allows the researcher to probe structural elements of the nucleus in several ways, termed isomer shift, quadrupole interactions, and magnetic splitting. These are each explained by the following sections as individual graphs, but in practice Mössbauer spectrum are likely to contain a combination of all effects.

Isomer Shift

An isomeric shift occurs when non identical atoms play the role of source and absorber, thus the radius of the source, R_s, is different that of the absorber, R_a, and the same holds that the electron density of each species is different. The Coulombic interactions affects the ground and excited state differently leading to a energy difference that is not the same for the two species. This is best illustrated with the equation:

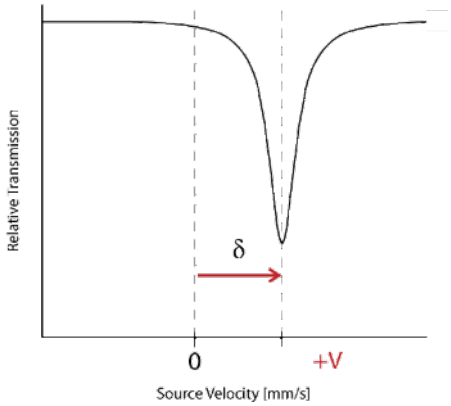
$$R_A \neq R_S$$

$$\rho_S \neq \rho_S$$

$$E_A \neq E_S$$

$$\delta = E_A - E_S = \frac{2}{3} nZe^2(\rho_A - \rho_S)(R_{es}^2 - R_{gs}^2)$$

Where delta represents the change in energy necessary to excite the absorber, which is seen as a shift from the Doppler speed 0 to V_1. The isomer shift depends directly on the s-electrons and can be influenced by the shielding p, d, f electrons. From the measured delta shift there is information about the valance state of the absorbing atom



The energy level diagram for δ shift shows the change in source velocity due to different sources used. The shift may be either positive or negative.

Quadrupole Interaction

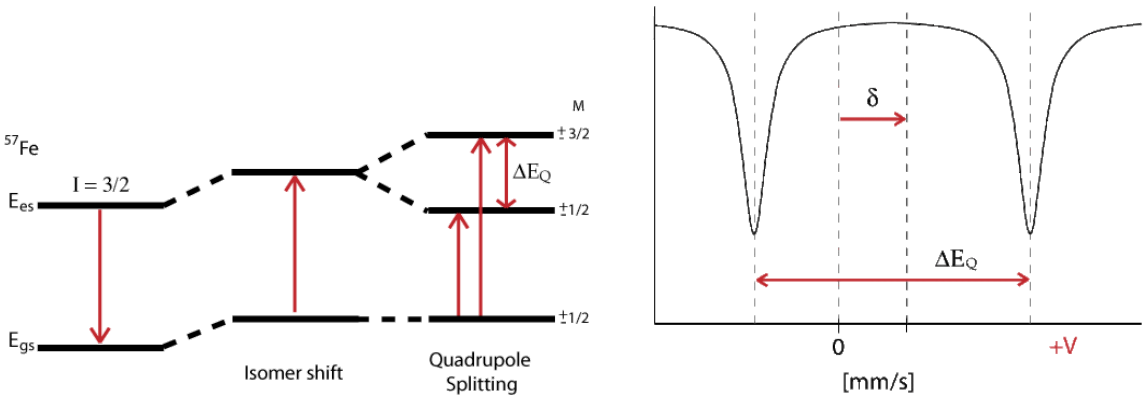
The Hamiltonian for quadrupole interaction using ^{57}Fe nuclear excited state is given by

$$H_Q = \frac{eQV_{ZZ}}{12}[3I_Z^2 - I(I+1) + \eta(I_X^2 - I_y^2)]$$

where the nuclear excited states are split into two degenerate doublets in the absence of magnetic interactions. For the asymmetry parameter $\eta = 0$ doublets are labeled with magnetic quantum numbers $m_{es} = \pm 3/2$ and $m_{es} = \pm 1/2$, where the $m_{es} = \pm 3/2$ doublet has the higher energy. The energy difference between the doublets is thus

$$\Delta EQ = \frac{eQV_{zz}}{2}\sqrt{1 + \frac{\eta^2}{3}}$$

The energy diagram and corresponding spectrum can be seen as



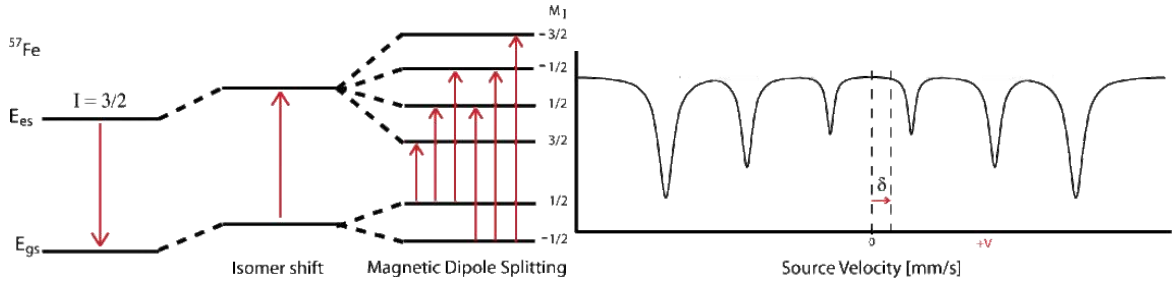
Magnetic Splitting

Magnetic splitting of seen in Mössbauer spectroscopy can be seen because the nuclear spin moment undergoes dipolar interactions with the magnetic field

$$E(m_I) = -g_n \beta_n B_{eff} m_I \tag{14}$$

https://chem.libretexts.org/@go/page/488708

where g_n is the nuclear g-factor and β_n is the nuclear magneton. In the absence of quadrupole interactions the Hamiltonian splits into equally spaced energy levels of



The allowed gamma stimulated transitions of nuclear excitation follows the magnetic dipole transition selection rule:

$$\Delta I = 1$$

and

$$\Delta m_I = 0, \pm 1$$

where m_I is the magnetic quantum number and the direction of β defines the nuclear quantization axis. If we assume g and A are *isotropic* (direction independent) where $g_x = g_y = g_z$ and B is actually a combination of the applied and internal magnetic fields:

$$H = g\beta S \cdot B + AS \cdot I - g_n\beta_n B \cdot I$$

The electronic Zeeman term is far larger then the nuclear Zeeman term, meaning the electronic term dominates the equation so S is approximated by $\langle S \rangle$ and

$$\langle S_z \rangle = m_s = \pm \frac{1}{2}$$

and

$$\langle S_x \rangle = \langle S_y \rangle \approx 0$$

$$H_n = A\langle S \rangle \cdot I - g_n\beta_n B \cdot I$$

Pulling out a $-g_n\beta_n$ followed by I leaves

$$H_n = -g_n\beta_n \left(-\frac{A\langle S \rangle}{g_n\beta_n} + B \right) I$$

Substituting the internal magnetic field with

$$B_{int} = -\frac{A\langle S \rangle}{g_n\beta_n}$$

results in a combined magnetic field term involving both the applied magnetic field and the internal magnetic field

$$H_n = -g_n\beta_n(B_{int} + B) \cdot I$$

which is simplified by using the effective magnetic field B_{eff}

$$H_n = -g_n\beta_n B_{eff} \cdot I$$

References

1. Gütlich, P. , Link, R. , & Trautwein, A. (1978). *Mössbauer spectroscopy and transition metal chemistry*. Inorganic chemistry concepts, v. 3. Berlin: Springer-Verlag.
2. G J Long and F Grandjean (1993) *Mössbauer Spectroscopy Applied to Magnetism and Materials*. New York. , Science Vol. 1,, eds.
3. Lawrence Que, J. , Ed. (2000). *Physical Methods in Bioinorganic Chemistry*. Sausalito, CA, University Science Books.
4. Filatov, M. (2007). "On the calculation of Mössbauer isomer shift. " The Journal of Chemical Physics 127(8): 8.

5. Introduction to mossbauer spectroscopy. 2013]. Available from http://www. rsc. org/Membership/Networking/InterestGroups/MossbauerSpect/part2. asp.
6. Bubek, Moritz, and Dennis Rettinger. 2004. Mossbauer-effekt.
7. Haskins, J. R. 1965. Advanced mossbauer-effect experiments. American Journal of Physics: 646.
8. Kistner, O. C. , and A. W. Sunyar. 1960. Evidence for quadrupole interaction of Fe57m, and influence of chemical binding on nuclear gamma-ray energy. Physical Review Letters 4 (8): 412.
9. Preston, R. S. , S. S. Hanna, and J. Heberle. 1962. Mössbauer effect in metallic iron. Physical Review 128 (5): 2207.

Problems

1. The magnetic splitting of $m_I = 0$ intensity of transition is related to $sin^2(\theta)$ of the angle between the incoming gamma ray and the effective magnetic field. When is the intensity of transition at max?
2. Why is it important for the sample to be in solid or crystalline state?
3. What case will result in a delta shift of 0. 00 mm/s?
4. Why is the Doppler effect important to Mössbauer spectroscopy?
5. Why are both the emission and absorption distributions the same? (both estimated with Lorentzian functions)

10.2.4A: The Technique of Mossbauer Spectroscopy is shared under a CC BY-NC-SA 4.0 license and was authored, remixed, and/or curated by LibreTexts.

- **Mössbauer Spectroscopy** by Kevin MacDow is licensed CC BY 4.0.

10.2.4B: What Can Isomer Shift Data Tell Us?

Among the drawbacks of the technique are the limited number of gamma ray sources and the requirement that samples be solid in order to eliminate the recoil of the nucleus. Mössbauer spectroscopy is unique in its sensitivity to subtle changes in the chemical environment of the nucleus including oxidation state changes, the effect of different ligands on a particular atom, and the magnetic environment of the sample.

As an analytical tool Mössbauer spectroscopy has been especially useful in the field of geology for identifying the composition of iron-containing specimens including meteors and moon rocks. In situ data collection of Mössbauer spectra has also been carried out on iron rich rocks on Mars.[10]

In another application, Mössbauer spectroscopy is used to characterize phase transformations in iron catalysts, e.g., those used for Fischer–Tropsch synthesis. While initially consisting of hematite (Fe_2O_3), these catalysts transform into a mixture of magnetite (Fe_3O_4) and several iron carbides. The formation of carbides appears to improve catalytic activity, however it can also lead to the mechanical break-up and attrition of the catalyst particles, which can cause difficulties in the final separation of catalyst from reaction products.[11]

Mössbauer spectroscopy has also been used to determine the relative concentration change in the oxidation state of antimony (Sb) during the selective oxidation of olefins. During calcination all the Sb ions in an antimony-containing tin dioxide catalyst transform into the +5 oxidation state. Following the catalytic reaction, almost all Sb ions revert from the +5 to the +3 oxidation state. A significant change in the chemical environment surrounding the antimony nucleus occurs during the oxidation state change which can easily be monitored as an isomer shift in the Mössbauer spectrum.[12]

This technique has also been used to observe the second-order transverse Doppler effect predicted by the theory of relativity, because of very high energy resolution.[13]

Contributors and Attributions

- Wikipedia

10.2.4B: What Can Isomer Shift Data Tell Us? is shared under a CC BY-NC-SA 4.0 license and was authored, remixed, and/or curated by LibreTexts.

- **4.10B: What Can Isomer Shift Data Tell Us?** is licensed CC BY-NC-SA 4.0.

SECTION OVERVIEW

10.2.5: Structure Determination - Diffraction Methods

Topic hierarchy

10.2.5A: X-Ray Diffraction (XRD)

10.2.5B: Single Crystal X-Ray Diffraction

10.2.5C: Powder X-Ray Diffraction

10.2.5D: Single Crystal Neutron Diffraction

10.2.5E: Electron Diffraction

10.2.5F: Low-Energy Electron Diffraction (LEED)

10.2.5G: Structural Databases

10.2.5: Structure Determination - Diffraction Methods is shared under a CC BY-NC-SA 4.0 license and was authored, remixed, and/or curated by LibreTexts.

10.2.5A: X-Ray Diffraction (XRD)

10.2.5A: X-Ray Diffraction (XRD) is shared under a CC BY-NC-SA 4.0 license and was authored, remixed, and/or curated by LibreTexts.

10.2.5B: Single Crystal X-Ray Diffraction

10.2.5B: Single Crystal X-Ray Diffraction is shared under a CC BY-NC-SA 4.0 license and was authored, remixed, and/or curated by LibreTexts.

10.2.5C: Powder X-Ray Diffraction

10.2.5C: Powder X-Ray Diffraction is shared under a CC BY-NC-SA 4.0 license and was authored, remixed, and/or curated by LibreTexts.

10.2.5D: Single Crystal Neutron Diffraction

10.2.5D: Single Crystal Neutron Diffraction is shared under a CC BY-NC-SA 4.0 license and was authored, remixed, and/or curated by LibreTexts.

10.2.5E: Electron Diffraction

10.2.5E: Electron Diffraction is shared under a CC BY-NC-SA 4.0 license and was authored, remixed, and/or curated by LibreTexts.

10.2.5F: Low-Energy Electron Diffraction (LEED)

10.2.5F: Low-Energy Electron Diffraction (LEED) is shared under a CC BY-NC-SA 4.0 license and was authored, remixed, and/or curated by LibreTexts.

10.2.5G: Structural Databases

10.2.5G: Structural Databases is shared under a CC BY-NC-SA 4.0 license and was authored, remixed, and/or curated by LibreTexts.

10.2.6: Photoelectron Spectroscopy (PES, UPS, XPS, ESCA)

Learning Objectives

- Demonstrate how photoelectron spectroscopy can be used to resolve the absolute energies of molecular orbitals.

Photoelectron spectroscopy (PES) utilizes photo-ionization and analysis of the kinetic energy distribution of the emitted photoelectrons to study the composition and electronic state of the surface region of a sample.

- **X-ray Photoelectron Spectroscopy** (XPS) uses soft x-rays (with a photon energy of 200-2000 eV) to examine electrons in *core*-levels.
- **Ultraviolet Photoelectron Spectroscopy** (UPS) using vacuum UV radiation (with a photon energy of 10-45 eV) to examine electrons in *valence* levels.

Both photoelectron spectroscopies are based upon a single photon in/electron out process. The energy of a photon of all types of electromagnetic radiation is given by the Planck–Einstein relation:

$$E = h\nu \tag{10.2.6.1}$$

where h is Planck constant and ν is the frequency (Hz) of the radiation. UPS is a powerful technique to exam molecular electron structure since we are interested in the molecular orbitals from polyatomic molecules (especially the valence orbitals) and is the topic of this page.

Photoelectron spectroscopy uses monochromatic sources of radiation (i.e. photons of fixed energy). In UPS the photon interacts with valence levels of the molecule or solid, leading to ionization by removal of one of these valence electrons. The kinetic energy distribution of the emitted photoelectrons (i.e. the number of emitted photoelectrons as a function of their kinetic energy) can be measured using any appropriate electron energy analyzer and a photoelectron spectrum can thus be recorded.

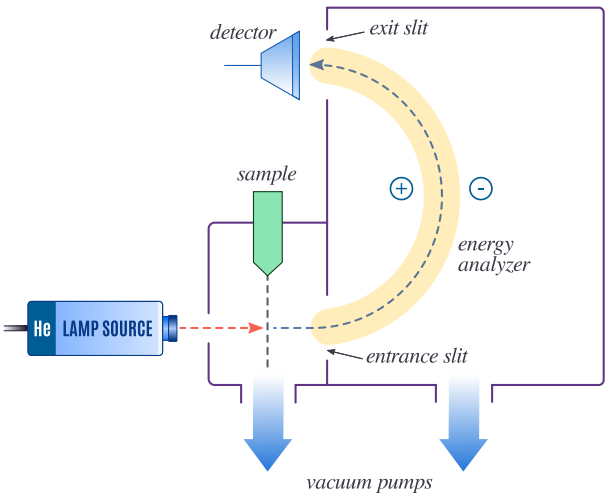


Figure 10.4.1: Diagram of a basic, typical PES instrument used in UPS, where the radiation source is an UV light source. When the sample is irradiated, the released photoelectrons pass through the lens system which slows them down before they enter the energy analyzer. The analyzer shown is a spherical deflection analyzer which the photoelectrons pass through before they are collected at the collector slit. (CC BY 4.0; Ümit Kaya via LibreTexts)

The process of photoionization can be considered in several ways. One way is to look at the overall process for a species A:

$$A + \text{photon} \rightarrow A^+ + e^- \tag{10.2.6.2}$$

Conservation of energy then requires that (after using Equation 10.2.6.1):

$$E(A) + h\nu = E(A^+) + E(e^-) \tag{10.2.6.3}$$

Since the free electron's energy is present solely as kinetic energy (KE) (i.e., there is no internal energy in a free electron)

$$E(e^-) = KE$$

Equation 10.2.6.3 can then be rearranged to give the following expression for the KE of the photoelectron:

$$KE = h\nu - [E(A^+) - E(A)] \tag{10.2.6.4}$$

The final term in brackets represents the difference in energy between the ionized and neutral species and is generally called the **vertical ionization energy** (IE) of the ejected electron; this then leads to the following commonly quoted equations:

$$KE = h\nu - IE \tag{10.2.6.5}$$

or

$$IE = h\nu - KE \tag{10.2.6.6}$$

The vertical ionization energy is a direct measure of the energy required to just remove the electron concerned from its initial level to the vacuum level (i.e., a free electron). Photoelectron spectroscopy measures the relative energies of the ground and excited positive ion states that are obtained by removal of single electrons from the neutral molecule.

Note

Equation 10.2.6.5 may look familiar to you as it the same equation Einstein used to describe the photoelectric effect except the vertical ionization energy (IE) is substituted for workfunction Φ. Both vertical ionization energy and workfunctions are metrics for the binding energy of an electron in the sample.

At a fundamental level, ionization energies are well-defined thermodynamic quantities related to the heats of protonation, oxidation/reduction chemistry, and ionic and covalent bond energies. Ionization energies are closely related to the concepts of electronegativity, electron-richness, and the general reactivity of molecules. The energies and other characteristic features of the ionization bands observed in photoelectron spectroscopy provide some of the molecular orbitals detailed and specific quantitative information regarding the electronic structure and bonding in molecules.

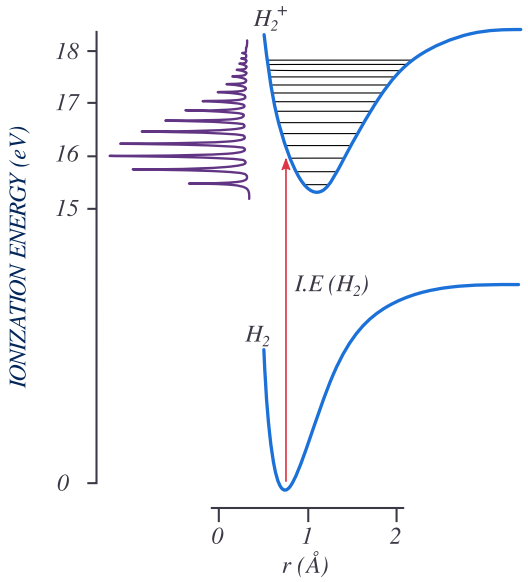


Figure 10.4.2: Vertical ionization process for molecular hydrogen. (CC BY 4.0; Ümit Kaya via LibreTexts)

Ionization is explicitly defined in terms of transitions between the ground state of a molecule and ion states as shown in Equation 10.2.6.6 and as illustrated in the Figure 10.4.2. Nonetheless, the information obtained from photoelectron spectroscopy is typically discussed in terms of the electronic structure and bonding in the ground states of neutral molecules, with ionization of electrons

occurring from bonding molecular orbitals, lone pairs, antibonding molecular orbitals, or atomic cores. These descriptions reflect the relationship of ionization energies to the molecular orbital model of electronic structure.

Ionization energies are directly related to the energies of molecular orbitals by Koopmans' theorem, which states that the negative of the eigenvalue of an occupied orbital from a Hartree-Fock calculation is equal to the *vertical ionization energy* to the ion state formed by removal of an electron from that orbital (Figure 10.4.3), provided the distributions of the remaining electrons do not change (i.e., frozen).

$$I_j = -\epsilon_j \tag{10.2.6.7}$$

There are many limitations to Koopmans' theorem, but in a first order approximation each ionization of a molecule can be considered as removal of an electron from an individual orbital. The ionization energies can then be considered as measures of orbital stabilities, and shifts can be interpreted in terms of orbital stabilizations or destabilizations due to electron distributions and bonding. Koopmans' theorem is implicated whenever an orbital picture is involved, but is not necessary when the focus is on the total electronic states of the positive ions.

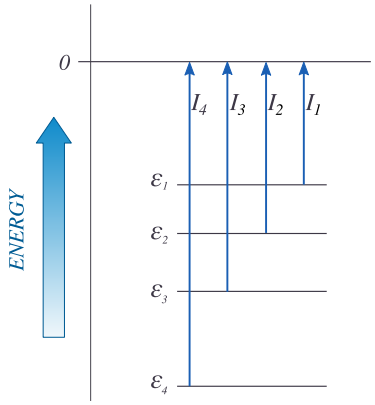


Figure 10.4.3: Within Koopmans' Theorem, the energies of the orbitals ϵ have an attractively simple physical interpretation: they give the amount of energy necessary to remove (ionize) the electron out of the molecular orbital, which corresponds to the negative of the experimentally observable ionization potential (I). (CC BY 4.0; Ümit Kaya via LibreTexts)

Koopmans' Theorem

Koopmans' theorem argues that the negative of the eigenvalue of an occupied orbital from a Hartree-Fock calculation is equal to the vertical ionization energy to the ion state formed by removal of an electron from that orbital.

Several different ionization energies can be defined, depending on the degree of vibrational excitation of the cations. In general, the following two types of ionization energies are considered (Figure 10.4.4):

- Adiabatic ionization energy corresponds to the ionization energy associated with this transition

  $$M(X, v''=0) + h\nu \rightarrow M^+(x, v'=0) + e^-$$

  Adiabatic ionization energy that is, the minimum energy required to eject an electron from a molecule in its ground vibrational state and transform it into a cation in the lowest vibrational level of an electronic state x of the cation.
- Vertical ionization energy corresponds to the ionization energy associated with this transition

  $$M(X, v''=0) + h\nu \rightarrow M^+(x, v'=n) + e^-$$

  where, the value n of the vibrational quantum number v' corresponds to the vibrational level whose wavefunction gives the largest overlap with the v" = 0 wavefunction. This is the most probable transition and usually corresponds to the vertical transition where the internuclear separations of the ionic state are similar to those of the ground state.

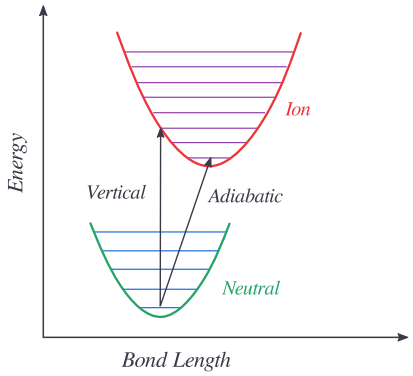


Figure 10.4.4: Difference between vertical and adiabatic ionization energies for a simple harmonic oscillator system. (CC BY 4.0; Ümit Kaya via LibreTexts)

The geometry of an ion may be different from the neutral molecule. The measured ionzation energy in a PES experiment can refer to the vertical ionization energy, in which case the ion is in the same geometry as the neutral, or to the adiabatic ionzaiton energy, in which case the ion is in its lowest energy, relaxed geometry (mostly the former though). This is illustrated in the Figure 10.4.4. For a diatomic the only geometry change possible is the bond length. The figure shows an ion with a slightly longer bond length than the neutral. The harmonic potential energy surfaces are shown in green (neutral) and red (ion) with vibrational energy levels. The vertical ionzation energy is **always greater** than the adiabatic ionzation energy.

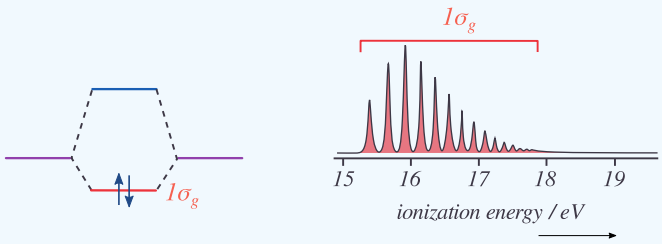
Differing Ionization Energies

You have been exposed to three metrics of ionization energies already, which are similar, but with distinct differences:

- The *ionization energy* (also called *adiabatic ionization energy*) is the lowest energy required to effect the removal of an electron from a molecule or atom, and corresponds to the transition from the lowest electronic, vibrational and rotational level of the isolated molecule to the lowest electronic, vibrational and rotational level of the isolated ion.
- The *binding energy* (also called *vertical ionization energy*) is the energy change corresponding to an ionization reaction leading to formation of the ion in a configuration which is the same as that of the equilibrium geometry of the ground state neutral molecule.
- The *workfunction* is the minimum energy needed to remove an electron from a (bulk) solid to a point in the vacuum.

Example 10.4.1: Molecular Hydrogen

As you remember, the molecular orbital description of molecular hydrogen involves two $|1s\rangle$ atomic orbitals generating a bonding $1\sigma_g$ and antibonding $2\sigma_u^*$ molecular orbitals. The two electrons that are responsible for the H_2 bond are occupied in the $1\sigma_g$.



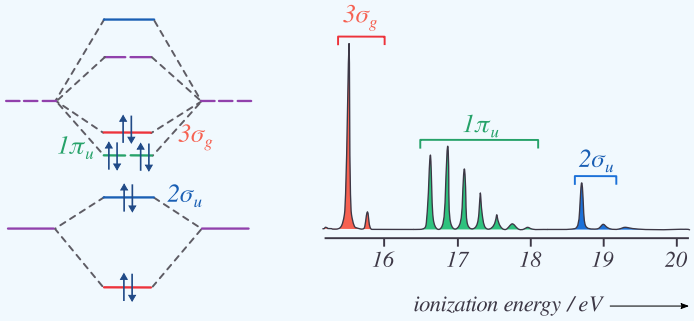
MO diagram and PES spectrum of H_2. (CC BY 4.0; Ümit Kaya via LibreTexts)

The PES spectrum has a single band that corresponds to the ionization of a $1\sigma_g$ electron. The multiple peaks are due to electrons ejecting from a range of stimulated vibrational energy levels. When extensive vibrational structure is resolved in a

PES molecular orbital, then the removal of an electron from that molecular orbital induces a significant change in the bonding (in this case an increase in the bond length since the bond order has been reduced).

Example 10.4.2: Molecular Nitrogen

Diatomic nitrogen is more complex than hydrogen since multiple molecular orbitals are occupied. Four molecular orbitals are occupied (the two $1\pi_u$ orbitals are both occupied). The UV photoelectron spectrum of N_2, has three bands corresponding to $3\sigma_g$, $1\pi_u$ and $2\sigma_u$ occupied molecular orbitals. Both $3\sigma_g$ and $2\sigma_u$ are weakly bonding and antibonding. The $1\sigma_g$ orbital is not resolved in this spectrum since the incident light $h\nu$ used did not have sufficient energy to ionize electrons in that deeply stabilized molecular orbital.



MO diagram and PES spectrum of N_2. (CC BY 4.0; Ümit Kaya via LibreTexts)

Note that extensive vibrational structure for the $1\pi_u$ band indicates that the removal of an electron from this molecular orbital causes a significant change in the bonding.

Hydrogen Chloride

The molecular energy level diagram for HCl is reproduced in Figure 10.4.5

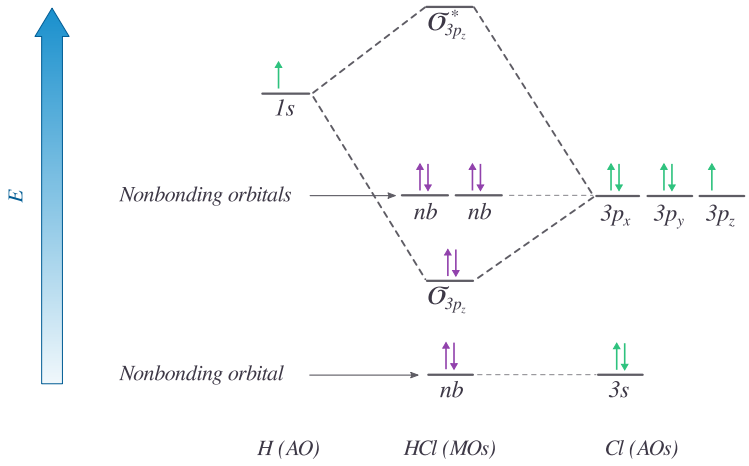


Figure 10.4.5: Molecular Orbital Energy-Level Diagram for HCl. The hydrogen 1s atomic orbital interacts molecular orbitals strongly with the $3p_z$ orbital on chlorine, producing a bonding/antibonding pair of molecular orbitals. The other electrons on Cl are best viewed as nonbonding. As a result, only the bonding σ orbital is occupied by electrons, giving a bond order of 1. (CC BY 4.0; Ümit Kaya via LibreTexts)

Important aspects of molecular orbital diagram in Figure 10.4.5:

- The H 1*s* energy lies well above the Cl 2*s* and 2*p* atomic orbitals;
- The valence electron configuration can be written $3\sigma^2 1\pi^4$;

- The H 1*s* orbital contributes only to the σ molecular orbitals, as does one of the Cl 2*p* orbitals (hence the lines in Figure 10.4.5 connecting these atomic orbitals and the 3σ and 4σ molecular orbitals);
- The remaining Cl 2*p* orbitals (ie those perpendicular to the bond axis) are unaffected by bonding, and these form the 1π molecular orbitals;
- The 1π orbitals are nonbonding - they are not affected energetically by the interaction between the atoms, and are hence neither bonding nor antibonding;
- The 3σ orbital is weakly bonding, and largely Cl 2*p*;
- The 3σ* orbital is antibonding, and primarily of H 1*s* character;

Figure 10.4.6 shows the analogous MO diagram and photoelectron spectrum for **HCl**. The spectrum has two bands corresponding to non-bonding 1*p* (or 1π) molecular orbitals (with negligible vibrational structure) and the 3*s* bonding molecular orbital (vibrational structure).

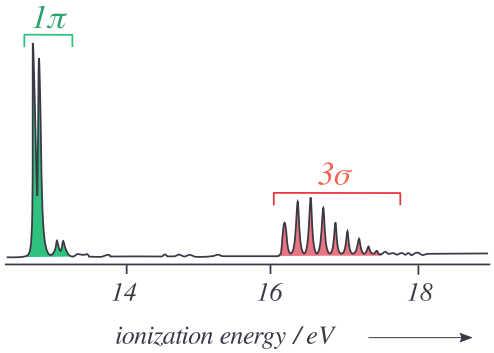


Figure 10.4.6: Photoelectron spectrum **HCl**. (CC BY 4.0; Ümit Kaya via LibreTexts)

The higher energy (more stabilized) core molecular orbitals are not observed since the incident photon energy $h\nu$ is below their ionization energies.

Water

In the simplified valence bond theory perspective of the water molecule, the oxygen atom form four sp^3 hybrid orbitals. Two of these are occupied by the two lone pairs on the oxygen atom, while the other two are used for bonding. Within the molecular orbital picture, the electronic configuration of the H_2O^+ molecule is $(1a_1)^2(2a_1)^2(1b_2)^2(3a_1)^2(1b_1)^2$ where the symbols a_1, b_2 and b_1 are orbital labels based on molecular symmetry that will be discussed later (Figure 10.4.7). Within Koopmans' theorem:

- The energy of the $1b_1$ HOMO corresponds to the ionization energy to form the H_2O^+ ion in its ground state $(1a_1)^2(2a_1)^2(1b_2)^2(3a_1)^2(1b_1)^1$.
- The energy of the second-highest molecular orbitals $3a_1$ refers to the ion in the excited state $(1a_1)^2(2a_1)^2(1b_2)^2(3a_1)^1(1b_1)^2$.

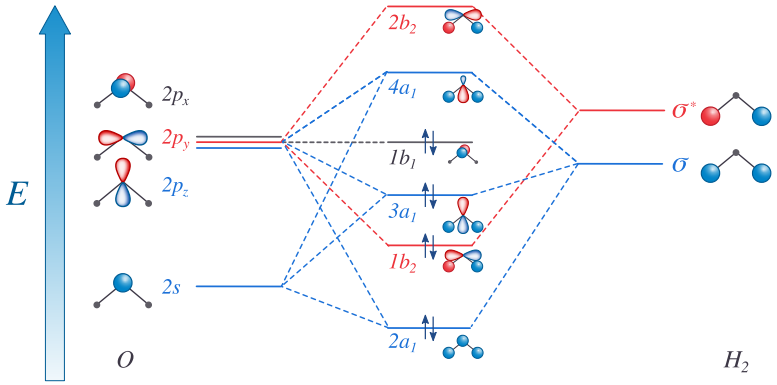


Figure 10.4.7: MO diagram for water. (CC BY 4.0; Ümit Kaya via LibreTexts)

The Hartree–Fock orbital energies (with sign changed) of these orbitals are tabulated below and compared to the experimental ionization energies.

Molecular orbital	Hartree–Fock orbital Energies (eV)	Experimental Ionization Energies (eV)
$2a_1$	36.7	32.2
$1b_2$	19.5	18.5
$3a_1$	15.9	14.7
$1b_1$	13.8	12.6

As explained above, the deviations between orbital energy and ionization energy is small and due to the effects of orbital relaxation as well as differences in electron correlation energy between the molecular and the various ionized states.

The molecular orbital perspective has the lone pair in different orbitals (one in a non-bonding orbital ($1b_1$ and one in the bonding orbitals). We tern to the photoelectron spectroscopy to help identify which theory is more accurate (i.e., describes reality better). The photoelectron spectrum of water in Figure 10.4.6 can be interpreted as having three major peaks with some fine structure arises from vibrational energy changes. The light source used in this experiment is not sufficiently energetic to ionize electrons from the lowest lying molecular orbitals.

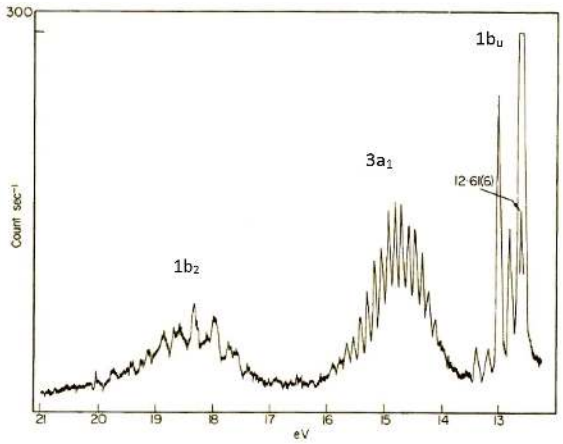


Figure 10.4.8: Photoelectron spectrum of water. Note the energy axes is flipped compared to other spectra on this page. This spectrum does not go to high enough energy to show the deep $2a_1$ molecular orbital.

If water was formed two identical O-H bonds and two lone pairs on the oxygen atom line valence bond theory predicts, then the PES in Figure 10.4.8 would have two (degenerate) peaks, one for the two bonds and one for the two lone pairs. The photoelectron spectrum clearly shows three peaks in the positions expected for the molecular orbitals in Figure 10.4.8.

If the molecular orbitals in Figure 10.4.7 represent the real electronic structure, how do we view the bonding? These molecular orbitals are delocalized and bare little relationship to the familiar 2-center bonds used in valence bond theory. For example, the $2a_1$ $1b_1$ and $3a_1$ molecular orbitals all have contributions from all three atoms, they are really 3-centered molecular orbitals. The bonds however can be thought of as representing a build up of the total electron density which loosely put is a total of all the orbital contributions. Despite this, we keep the ideas of hybridization and 2-center bonds because they are useful NOT because they represent reality

Summary

A photoelecton spectrum can show the relative energies of occupied molecular orbitals by ionization. (i.e. ejection of an electron). A photoelectron spectrum can also be used to determine energy spacing between vibrational levels of a given electronic state. Each orbital energy band has a structure showing ionization to different vibrational levels.

10.2.6: Photoelectron Spectroscopy (PES, UPS, XPS, ESCA) is shared under a CC BY-NC-SA 4.0 license and was authored, remixed, and/or curated by LibreTexts.

- **10.4: Photoelectron Spectroscopy** by Roger Nix is licensed CC BY 4.0.

SECTION OVERVIEW

10.2.7: Mass Spectrometry

Topic hierarchy

10.2.7A: Electron Ionization (EI)

10.2.7B: Fast Atom Bombardment (FAB)

10.2.7C: Matrix-Assisted Laser Desorption Ionization Time-of-Flight (MALDI-TOF)

10.2.7D: Electrospray Ionization (ESI)

10.2.7: Mass Spectrometry is shared under a CC BY-NC-SA 4.0 license and was authored, remixed, and/or curated by LibreTexts.

10.2.7A: Electron Ionization (EI)

10.2.7A: Electron Ionization (EI) is shared under a CC BY-NC-SA 4.0 license and was authored, remixed, and/or curated by LibreTexts.

10.2.7B: Fast Atom Bombardment (FAB)

10.2.7B: Fast Atom Bombardment (FAB) is shared under a CC BY-NC-SA 4.0 license and was authored, remixed, and/or curated by LibreTexts.

10.2.7C: Matrix-Assisted Laser Desorption Ionization Time-of-Flight (MALDI-TOF)

10.2.7C: Matrix-Assisted Laser Desorption Ionization Time-of-Flight (MALDI-TOF) is shared under a CC BY-NC-SA 4.0 license and was authored, remixed, and/or curated by LibreTexts.

10.2.7D: Electrospray Ionization (ESI)

10.2.7D: Electrospray Ionization (ESI) is shared under a CC BY-NC-SA 4.0 license and was authored, remixed, and/or curated by LibreTexts.

10.3: Fluxional Behavior

10.3: Fluxional Behavior is shared under a CC BY-NC-SA 4.0 license and was authored, remixed, and/or curated by LibreTexts.

10.3.1: Determination of Energetics of Fluxional Molecules by NMR

Introduction to Fluxionality

It does not take an extensive knowledge of chemistry to understand that as-drawn chemical structures do not give an entirely correct picture of molecules. Unlike drawings, molecules are not stationary objects in solution, the gas phase, or even in the solid state. Bonds can rotate, bend, and stretch, and the molecule can even undergo conformational changes. Rotation, bending, and stretching do not typically interfere with characterization techniques, but conformational changes occasionally complicate analyses, especially nuclear magnetic resonance (NMR).

For the present discussion, a fluxional molecule can be defined as one that undergoes an intramolecular reversible interchange between two or more conformations. Fluxionality is specified as intramolecular to differentiate from ligand exchange and complexation mechanisms, intermolecular processes. An irreversible interchange is more of a chemical reaction than a form of fluxionality. Most of the following examples alternate between two conformations, but more complex fluxionality is possible. Additionally, this module will focus on inorganic compounds. In this module, examples of fluxional molecules, NMR procedures, calculations of energetics of fluxional molecules, and the limitations of the approach will be covered.

Examples of Fluxionality

Bailar Twist

Octahedral trischelate complexes are susceptible to Bailar twists, in which the complex distorts into a trigonal prismatic intermediate before reverting to its original octahedral geometry. If the chelates are not symmetric, a Δ enantiomer will be inverted to a Λ enantiomer. For example not how in Figure **10.3.1.1** with the GaL_3 complex of 2,3-dihydroxy-N,N‘-diisopropylterephthalamide (Figure **10.3.1.2** he end product has the chelate ligands spiraling the opposite direction around the metal center.

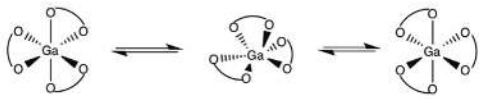


Figure **10.3.1.1** Bailar twist of a gallium catchetol *tris*-chelate complex. Adapted from B. Kersting, J. R. Telford, M. Meyer, and K. N. Raymond, *J. Am. Chem. Soc.*, 1996, 118, 5712.

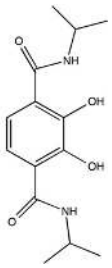


Figure **10.3.1.2** Substituted catchetol ligand 2,3-dihydroxy-N,N‘-diisopropylterephthalamide. Adapted from Kersting, B., Telford, J.R., Meyer, M., Raymond, K.N.; *J. Am. Chem. Soc.*, 1996, 118, 5712.

Berry Psuedorotation

D_{3h} compounds can also experience fluxionality in the form of a Berry pseudorotation (depicted in Figure **10.3.1.3**), in which the complex distorts into a C_{4v} intermediate and returns to trigonal bipyrimidal geometry, exchanging two equatorial and axial groups . Phosphorous pentafluoride is one of the simplest examples of this effect. In its ^{19}FNMR, only one peak representing five fluorines is present at 266 ppm, even at low temperatures. This is due to interconversion faster than the NMR timescale.



Figure **10.3.1.3** Berry pseudorotation of phosphorus pentafluoride.

Sandwich and Half-sandwich Complexes

Perhaps one of the best examples of fluxional metal complexes is $(\pi^5\text{-}C_5H_5)Fe(CO)_2(\pi^1\text{-}C_5H_5)$ (Figure **10.3.1.4**. Not only does it have a rotating η^5 cyclopentadienyl ring, it also has an alternating η^1 cyclopentadienyl ring (Cp). This can be seen in its NMR spectra in Figure **10.3.1.5**. The signal for five protons corresponds to the metallocene Cp ring (5.6 ppm). Notice how the peak remains a sharp singlet despite the large temperature sampling range of the spectra. Another noteworthy aspect is how the multiplets corresponding to the other Cp ring broaden and eventually condense into one sharp singlet.



Figure **10.3.1.4** Structure of $(\pi^5\text{-}C_5H_5)Fe(CO)_2(\pi^1\text{-}C_5H_5)$. Reprinted with permission from M. J. Bennett Jr., F. A. Cotton, A. Davison, J. W. Faller, S. J. Lippard, and S. M. Morehouse, *J. Am. Chem. Soc.*, 1966, **88**, 4371. Copyright: American Chemical Society (1966).

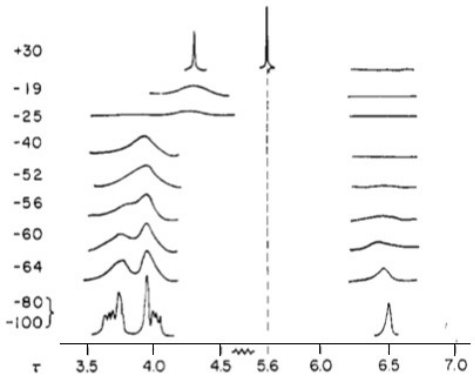


Figure **10.3.1.5** Variable temperature NMR spectra of $(\pi^5\text{-}C_5H_5)Fe(CO)_2(\pi^1\text{-}C_5H_5)$. Reprinted with permission from M. J. Bennett Jr., F. A. Cotton, A. Davison, J. W. Faller, S. J. Lippard, and S. M. Morehouse, *J. Am. Chem. Soc.*, 1966, **88**, 4371. Copyright: American Chemical Society (1966).

An Example Procedure

ample preparation is essentially the same for routine NMR. The compound of interest will need to be dissolved in an NMR compatible solvent ($CDCl_3$ is a common example) and transferred into an NMR tube. Approximately 600 µL of solution is needed with only micrograms of compound. Compounds should be at least 99 % pure in order to ease peak assignments and analysis. Because each spectrometer has its own protocol for shimming and optimization, having the supervision of a trained specialist is strongly advised. Additionally, using an NMR with temperature control is essential. The basic goal of this experiment is to find three temperatures: slow interchange, fast interchange, and coalescence. Thus many spectra will be needed to be obtained at different temperatures in order to determine the energetics of the fluctuation.

The process will be much swifter if the lower temperature range (in which the fluctuation is much slower than the spectrometer timescale) is known. A spectra should be taken in this range. Spectra at higher temperatures should be taken, preferably in regular increments (for instance, 10 K), until the peaks of interest condense into a sharp single at higher temperature. A spectrum at the coalescence temperature should also be taken in case of publishing a manuscript. This procedure should then be repeated in reverse; that is, spectra should be taken from high temperature to low temperature. This ensures that no thermal reaction has taken place and that no hysteresis is observed. With the data (spectra) in hand, the energetics can now be determined.

Calculation of Energetics

For intramolecular processes that exchange two chemically equivalent nuclei, the function of the difference in their resonance frequencies ($\Delta\nu$) and rate of exchange (k) is the NMR spectrum. Slow interchange occurs when $\Delta\nu >> k$, and two separate peaks are observed. When $\Delta\nu << k$, fast interchange is said to occur, and one sharp peak is observed. At intermediate temperatures, the peaks are broadened and overlap one another. When they completely merge into one peak, the coalescence temperature, T_c is said

to be reached. In the case of coalescence of an equal doublet (for instance, one proton exchanging with one proton), coalescences occurs when $\Delta v_0 t = 1.4142/(2\pi)$, where Δv_0 is the difference in chemical shift at low interchange and where t is defined by 10.3.1.1, where t_a and t_b are the respective lifetimes of species a and b. This condition only occurs when $t_a = t_b$, and as a result, k = ½ t.

$$\frac{1}{t} = \frac{1}{t_a} + \frac{1}{t_b} \tag{10.3.1.1}$$

For reference, the exact lineshape function (assuming two equivalent groups being exchanged) is given by the Bloch Equation, 10.3.1.2, where g is the intensity at frequency *v*,and where K is a normalization constant.

$$g(v) = \frac{Kt(v_a + v_b)^2}{[0.5(v_a + v_b) - u]^2 + 4\pi^2 t^2 (v_a - v)^2 (v_b - v)^2} \tag{10.3.1.2}$$

Low Temperatures to Coalescence Temperature

At low temperature (slow exchange), the spectrum has two peaks and $\Delta v >> t$. As a result, 10.3.1.3 reduces to 10.3.1.4, where T_{2a} is the spin-spin relaxation time. The linewidth of the peak for species a is defined by 10.3.1.5.

$$g(v)_a = g(v)_b = \frac{KT_{2a}}{1 + T_{2a}^2 (v_a - v)^2} \tag{10.3.1.3}$$

$$(\Delta v_a)_{1/2} = \frac{1}{\pi}\left(\frac{1}{T_{2a}} + \frac{1}{t_a}\right) \tag{10.3.1.4}$$

Because the spin-spin relaxation time is difficult to determine, especially in inhomogeneous environments, rate constants at higher temperatures but before coalescence are preferable and more reliable.

The rate constant k can then be determined by comparing the linewidth of a peak with no exchange (low temp) with the linewidth of the peak with little exchange using, 10.3.1.5, where subscript *e* refers to the peak in the slightly higher temperature spectrum and subscript *0* refers to the peak in the no exchange spectrum.

$$k = \frac{\pi}{\sqrt{2}}[(\Delta v_e)_{1/2} - (\Delta v_0)_{1/2}] \tag{10.3.1.5}$$

Additionally, k can be determined from the difference in frequency (chemical shift) using 10.3.1.6, where $\Delta v_0$is the chemical shift difference in Hz at the no exchange temperature and Δv_e is the chemical shift difference at the exchange temperature.

$$k = \frac{\pi}{\sqrt{2}}(\Delta v_0^2 - \Delta v_e^2) \tag{10.3.1.6}$$

The intensity ratio method, 10.3.1.7, can be used to determine the rate constant for spectra whose peaks have begun to merge, where r is the ratio between the maximum intensity and the minimum intensity, of the merging peaks, I_{max}/I_{min}.

$$k = \frac{\pi}{\sqrt{2}}(r + (r^2 - r)^{1/2})^{-1/2} \tag{10.3.1.7}$$

Additionally, k can be determined from the difference in frequency (chemical shift) using 10.3.1.8, where $\Delta v_0$is the chemical shift difference in Hz at the no exchange temperature and Δv_e is the chemical shift difference at the exchange temperature.

$$k = \frac{\pi}{\sqrt{2}}(\Delta v_0^2 - \Delta v_e^2) \tag{10.3.1.8}$$

The intensity ratio method, 10.3.1.9 can be used to determine the rate constant for spectra whose peaks have begun to merge, where r is the ratio between the maximum intensity and the minimum intensity, of the merging peaks, I_{max}/I_{min}

$$k = \frac{\pi}{\sqrt{2}}(r + (r^2 - r)^{1/2})^{-1/2} \tag{10.3.1.9}$$

As mentioned earlier, the coalescence temperature, T_c is the temperature at which the two peaks corresponding to the interchanging groups merge into one broad peak and 10.3.1.10 may be used to calculate the rate at coalescence.

$$k = \frac{\pi \Delta v_0}{\sqrt{2}} \tag{10.3.1.10}$$

Higher Temperatures

Beyond the coalescence temperature, interchange is so rapid (k >> t) that the spectrometer registers the two groups as equivalent and as one peak. At temperatures greater than that of coalescence, the lineshape equation reduces to 10.3.1.11.

$$g(v) = \frac{KT_2}{[1 + \pi T_2(v_a + v_b + 2v)^2]} \tag{10.3.1.11}$$

As mentioned earlier, determination of T_2 is very time consuming and often unreliable due to inhomogeneity of the sample and of the magnetic field. The following approximation (10.3.1.12) applies to spectra whose signal has not completely fallen (in their coalescence).

$$k = \frac{0.5\pi\Delta v^2}{(\Delta v_e)_{1/2} - (\Delta v_0)_{1/2}} \tag{10.3.1.12}$$

Now that the rate constants have been extracted from the spectra, energetic parameters may now be calculated. For a rough measure of the activation parameters, only the spectra at no exchange and coalescence are needed. The coalescence temperature is determined from the NMR experiment, and the rate of exchange at coalescence is given by 10.3.1.10. The activation parameters can then be determined from the Eyring equation (10.3.1.13), where k_B is the Boltzmann constant, and where $\Delta H^{\ddagger} - T\Delta S^{\ddagger} = \Delta G^{\ddagger}$.

$$ln(\frac{k}{t}) = \frac{\Delta H^{\ddagger}}{RT} - \frac{\Delta S^{\ddagger}}{R} + ln(\frac{k_B}{h}) \tag{10.3.1.13}$$

For more accurate calculations of the energetics, the rates at different temperatures need to be obtained. A plot of ln(k/T) versus 1/T (where T is the temperature at which the spectrum was taken) will yield $\Delta H^{\ddagger}$, $\Delta S^{\ddagger}$, and $\Delta G^{\ddagger}$. For a pictorial representation of these concepts, see Figure **10.3.1.6**.

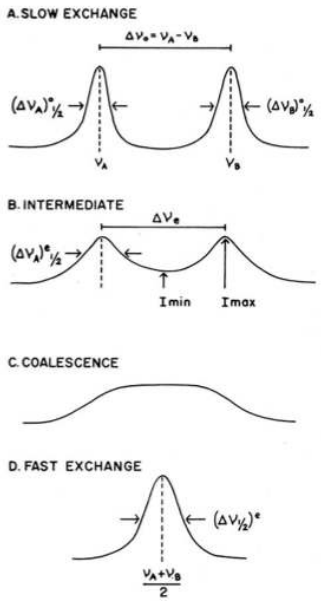


Figure **10.3.1.6** Simulated NMR temperature domains of fluxional molecules. Reprinted with permission from F. P. Gasparro and N. H. Kolodny, *J. Chem. Ed.*, 1977, 4, 258. Copyright: American Chemical Society (1977).

Diverse Populations

For unequal doublets (for instance, two protons exchanging with one proton), a different treatment is needed. The difference in population can be defined through 10.3.1.14, where P_i is the concentration (integration) of species i and $X = 2\pi\Delta vt$ (counts per second). Values for Δvt are given in Figure **10.3.1.7**.

$$\Delta P = P_a - P_b = [\frac{X^2 - 2}{3}]^{3/2}(\frac{1}{X}) \tag{10.3.1.14}$$

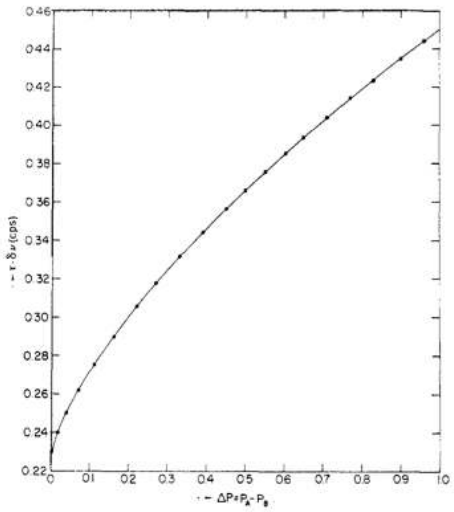


Figure **10.3.1.7** Plot of Δ*v*t versus ΔP. Reprinted with permission from H. Shanan-Atidi and K. H. Bar-Eli, *J. Phys. Chem.*, 1970, **74**, 961. Copyright: American Chemical Society (1970).

The rates of conversion for the two species, k_a and k_b, follow $k_aP_a = k_bP_b$ (equilibrium), and because $k_a = 1/t_a$and $k_b = 1/t_b$, the rate constant follows 10.3.1.15.

$$k_i = \frac{1}{2t}(1 - \Delta P) \tag{10.3.1.15}$$

From Erying's expressions, the Gibbs free activation energy for each species can be obtained through 10.3.1.16 and 10.3.1.17.

$$\Delta G_a^{\ddagger} = RT_c\, ln(\frac{kT_c}{h\pi\Delta v_0} \times \frac{X}{1 - \Delta P_a}) \tag{10.3.1.16}$$

$$\Delta G_b^{\ddagger} = RT_c\, ln(\frac{kT_c}{h\pi\Delta v_0} \times \frac{X}{1 - \Delta P_b}) \tag{10.3.1.17}$$

Taking the difference of 10.3.1.16 and 10.3.1.17 gives the difference in energy between species a and b (10.3.1.18).

$$\Delta G^{\ddagger} = RT_c ln(\frac{P_a}{P_b} = RT_c ln(\frac{1+P}{1-P}) \tag{10.3.1.18}$$

Converting constants will yield the following activation energies in calories per mole (10.3.1.19 and 10.3.1.20).

$$\Delta G_a^{\ddagger} = 4.57T_c[10.62\ +\ log(\frac{X}{2p(1-\Delta P)}) +\ log(T_c/\Delta v)] \tag{10.3.1.19}$$

$$\Delta G_b^{\ddagger} = 4.57T_c[10.62\ +\ log(\frac{X}{2p(1-\Delta P)}) +\ log(T_c/\Delta v)] \tag{10.3.1.20}$$

To obtain the free energys of activation, values of log (X/(2π(1 + ΔP))) need to be plotted against ΔP (values T_c and Δ*v0* are predetermined).

This unequal doublet energetics approximation only gives $\Delta G^{\ddagger}$ at one temperature, and a more rigorous theoretical treatment is needed to give information about $\Delta S^{\ddagger}$ and $\Delta H^{\ddagger}$.

Example of Determination of Energetic Parameters

Normally ligands such as dipyrido(2,3-a;3′,2′-j)phenazine (dpop') are tridentate when complexed to transition metal centers. However, dpop' binds to rhenium in a bidentate manner, with the outer nitrogens alternating in being coordinated and uncoordinated. See Figure **10.3.1.8**for the structure of $Re(CO)_3$(dpop')Cl. This fluxionality results in the exchange of the aromatic protons on the dpop' ligand, which can be observed via ^{1}HNMR. Because of the complex nature of the coalescence of doublets, the rate constants at different temperatures were determined via computer simulation (DNMR3, a plugin of Topspin). These spectra are shown in Figure **10.3.1.8**.

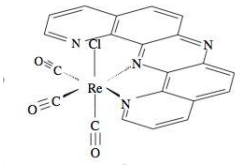


Figure **10.3.1.8** The structure of $Re(CO)_3$(dpop')Cl. Reprinted with permission from K. D. Zimmera, R. Shoemakerb, and R. R. Ruminski, *Inorg. Chim. Acta.*, 2006, **5**, 1478. Copyright: Elsevier (2006).

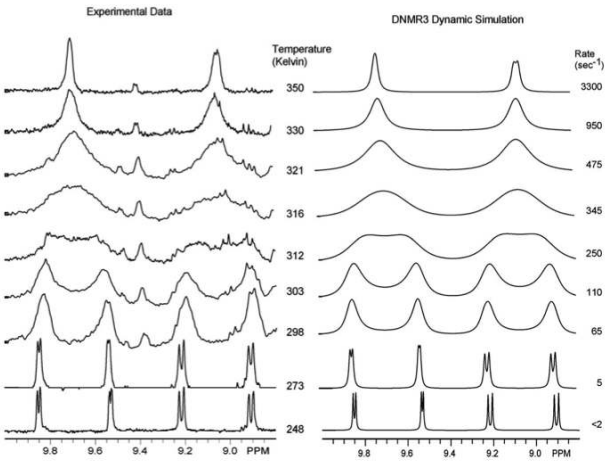


Figure **10.3.1.9** experimental and simulated ^{1}HNMR spectra for $Re(CO)_3$(dpop')Cl. Reprinted with permission from K. D. Zimmera, R. Shoemakerb, and R. R. Ruminski, *Inorg. Chim. Acta.*, 2006, **5**, 1478. Copyright: Elsevier (2006).

The activation parameters can then be obtained by plotting ln(k/T) versus 1/T (see Figure **10.3.1.9** for the Eyring plot). $\Delta S^{\ddagger}$ can be extracted from the y-intercept, and $\Delta H^{\ddagger}$ can be obtained through the slope of the plot. For this example, $\Delta H^{\ddagger}$, $\Delta S^{\ddagger}$ and $\Delta G^{\ddagger}$. were determined to be 64.9 kJ/mol, 7.88 J/mol, and 62.4 kJ/mol.

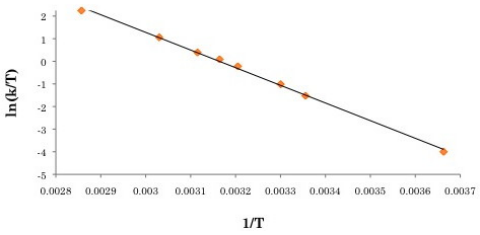


Figure **10.3.1.10** Eyring plot of ln(k/T) versus 1/T for $Re(CO)_3$(dpop')Cl. Adapted from K. D. Zimmera, R. Shoemakerb, and R. R. Ruminski, *Inorg. Chim. Acta*, 2006, **5**, 1478. Copyright: Elsevier (2006).

Limitations to the Approach

Though NMR is a powerful technique for determining the energetics of fluxional molecules, it does have one major limitation. If the fluctuation is too rapid for the NMR timescale (< 1 ms) or if the conformational change is too slow meaning the coalescence temperature is not observed, the energetics cannot be calculated. In other words, spectra at coalescence and at no exchange need to be observable. One is also limited by the capabilities of the available spectrometer. The energetics of very fast fluxionality (metallocenes, PF_5, etc) and very slow fluxionality may not be determinable. Also note that this method does not prove any fluxionality or any mechanism thereof; it only gives a value for the activation energy of the process. As a side note, sometimes the coalescence of NMR peaks is not due to fluxionality, but rather temperature-dependent chemical shifts.

This page titled 10.3.1: Determination of Energetics of Fluxional Molecules by NMR is shared under a CC BY-NC-SA 4.0 license and was authored, remixed, and/or curated by Pavan M. V. Raja & Andrew R. Barron (OpenStax CNX) via source content that was edited to the style and standards of the LibreTexts platform.

- **6.2: Determination of Energetics of Fluxional Molecules by NMR** by Pavan M. V. Raja & Andrew R. Barron is licensed CC BY 4.0. Original source: http://cnx.org/contents/ba27839d-5042-4a40-afcf-c0e6e39fb45425.2.

Index

A

A values
5.3: Ligand Substitution Mechanisms
acidity
3.3: Acidity of the Hexaaqua Ions
active site
9.2: Introduction to Amino Acids and Proteins
alkene
6.5.1: Linear π Systems
Alkyl Complexes
6.6.1: Metal Alkyls
amino acids
9.2: Introduction to Amino Acids and Proteins
ammonia ligands
5.1: Thermodynamic Stability of Metal Complexes
analogous complexes
5.1: Thermodynamic Stability of Metal Complexes
arene
6.5.1: Linear π Systems
aromatic
6.5.1: Linear π Systems
aromatic ligands
6.5.1: Linear π Systems
Associative Substitution
5.3: Ligand Substitution Mechanisms
atomic term symbols
4.2: Quantum Numbers of Multielectron Atoms
Aufbau principle
1.2.2.3: Aufbau Principle

B

back strain
3.6.3.2.7: Bulky groups weaken the strength of Lewis acids and bases because they introduce steric strain into the resulting acid-base adduct.
bent
1.5.2: Valence Shell Electron-Pair Repulsion
beta elimination
6.6.1: Metal Alkyls
beta elmination
6.6.1: Metal Alkyls
7.2.4: β-Elimination Reactions
bidentate
3.6.2: Nomenclature and Ligands
birefringence
8.14: Structures Related to NaCl and NiAs
block diagonal
2.3.2: Representations of Point Groups
Bohr Atom
1.3: Rutherford's Atom
Bohr model
1.3: Rutherford's Atom
bond angle
1.5.2: Valence Shell Electron-Pair Repulsion
Bragg equation
8.9: X-ray Crystallography
bridging ligand
3.6.2: Nomenclature and Ligands

C

carbene
6.6.2: Carbenes
carbenes
6.6.2: Carbenes
character (matrix)
2.3.2: Representations of Point Groups
character table
2.3.3: Character Tables
charge transfer band
3.6.3.2.3: The electronic spectra of charge transfer complexes illustrate the impact of frontier orbital interactions on the electronic structure of Lewis acid-base adducts
Chelate complexes
5.1: Thermodynamic Stability of Metal Complexes
chelate effect
5.1: Thermodynamic Stability of Metal Complexes
Chelation
5.1: Thermodynamic Stability of Metal Complexes
CO Insertions
7.2.1: Introduction to Insertion
7.2.2: CO Insertions (Alkyl Migration)
complex ion
3.2: Lewis Acids and Bases
3.3: Acidity of the Hexaaqua Ions
3.6: Coordination Chemistry- Structure and Isomers
compression
3.7.6: Jahn-Teller Distortions
conservative forces
1.3: Rutherford's Atom
coordinate covalent bond
3.2: Lewis Acids and Bases
coordination complex
3.6: Coordination Chemistry- Structure and Isomers
coordination number
3.6.4: Coordination Numbers and Structures
correlation diagrams
4.3.2: Correlation Diagrams
Coulombic force
1.3: Rutherford's Atom
Crabtree
6.5.3: Odd-numbered π Systems
crystal field orbitals
6.5.1: Linear π Systems
crystal field splitting
3.7.1: Crystal Field Theory
3.7.2: Crystal Field Stabilization Energy
3.7.3: Factors That Affect Crystal Field Splitting
crystal field stabilization energy
3.7.2: Crystal Field Stabilization Energy
5.2: Trends in Kinetic Lability
crystal field theory
3.7.1: Crystal Field Theory
3.7.2: Crystal Field Stabilization Energy
cyclopentadienyl ligands
6.5.3: Odd-numbered π Systems
cyclopropanations
6.6.2: Carbenes

D

dative
6.5.1: Linear π Systems
dative actor ligands
6.5.1: Linear π Systems
dearomatization
6.5.1: Linear π Systems
decomposition
6.6.1: Metal Alkyls
deinsertion
7.2.1: Introduction to Insertion
7.2.2: CO Insertions (Alkyl Migration)
diamagnetic
3.7.1: Crystal Field Theory
diastereomeric
6.5.1: Linear π Systems
dipole moment
1.5.2: Valence Shell Electron-Pair Repulsion
1.5.3: Molecular Polarity
dissociation constant
3.2: Lewis Acids and Bases
Drago and Wayland's EC Model
3.5: Quantitative Measures of Hardness and Softness
3.6.3.3.2: Quantitative Measures of Hardness, Softness, and Acid-Base Interactions from a Hard Soft Acid-Base Principle Perspective Involve Orbital Energies and/or Apportioning Acid-Base Bonding in Terms of Electrostatic and Covalent Factors

E

ECW model
3.6.3.3.2: Quantitative Measures of Hardness, Softness, and Acid-Base Interactions from a Hard Soft Acid-Base Principle Perspective Involve Orbital Energies and/or Apportioning Acid-Base Bonding in Terms of Electrostatic and Covalent Factors
effective nuclear charge
1.2.2.4: Shielding
electronegativity (Mulliken)
3.5: Quantitative Measures of Hardness and Softness
3.6.3.3.2: Quantitative Measures of Hardness, Softness, and Acid-Base Interactions from a Hard Soft Acid-Base Principle Perspective Involve Orbital Energies and/or Apportioning Acid-Base Bonding in Terms of Electrostatic and Covalent Factors
Electronic Configurations
3.7.6: Jahn-Teller Distortions
electrophile
3.6.3.2: Lewis Concept and Frontier Orbitals
electrophilic attack
6.5.1: Linear π Systems
6.6.1: Metal Alkyls
elimination
7.2.1: Introduction to Insertion
7.2.2: CO Insertions (Alkyl Migration)
elongation
3.7.6: Jahn-Teller Distortions
enzymes
9.2: Introduction to Amino Acids and Proteins
ethylenediamine ligands
5.1: Thermodynamic Stability of Metal Complexes

F

Fischer carbenes
- 6.6.2: Carbenes

fluorite (structure)
- 8.15: Tetrahedral Structures

formal charge
- 1.5.1.3: Formal Charge

formation constant
- 3.2: Lewis Acids and Bases

front strain
- 3.6.3.2.7: Bulky groups weaken the strength of Lewis acids and bases because they introduce steric strain into the resulting acid-base adduct.

frontier orbitals
- 3.6.3.2.1: The frontier orbital approach considers Lewis acid-base reactions in terms of the donation of electrons from the base's highest occupied orbital into the acid's lowest unoccupied orbital.

frustrated Lewis pair
- 3.6.3.2.8: Frustrated Lewis pair chemistry uses Lewis acid and base sites within a molecule that are sterically restricted from forming an adduct with each other.

frustrated Lewis pair chemistry
- 3.6.3.2.8: Frustrated Lewis pair chemistry uses Lewis acid and base sites within a molecule that are sterically restricted from forming an adduct with each other.

H

halogen bond
- 3.6.3.2.6: Lewis base strength may also be estimated by measuring structural or energy changes upon formation of a Lewis acid-base complex, as illustrated by efforts to spectroscopically assess the strengths of halogen bonds

Hapticity
- 3.6.2: Nomenclature and Ligands

Heck reaction
- 6.5.1: Linear π Systems

Hexaaqua Ions
- 3.3: Acidity of the Hexaaqua Ions

high spin
- 3.7.1: Crystal Field Theory
- 3.7.2: Crystal Field Stabilization Energy
- 3.7.3: Factors That Affect Crystal Field Splitting
- 3.7.6: Jahn-Teller Distortions

hybrid orbital
- 1.5.6: Hybrid Atomic Orbitals

hybridization
- 1.5.6: Hybrid Atomic Orbitals

hydration
- 3.7.2: Crystal Field Stabilization Energy

Hydricity
- 6.4.3: Hydrides and Dihydrogen Complexes

hydride complexes
- 6.4.3: Hydrides and Dihydrogen Complexes

Hydrocyanation
- 7.1.3: Reductive Elimination

hydrogen bonding
- 1.5.4: Hydrogen Bonding

hypervalency
- 1.5.1: Lewis Electron-Dot Diagrams

hypovalency
- 1.5.1: Lewis Electron-Dot Diagrams

I

inert complex
- 5.2: Trends in Kinetic Lability

inner coordination sphere
- 3.6: Coordination Chemistry- Structure and Isomers

Insertions
- 7.2.3: Migratory Insertion-1,2-Insertions

Interchange
- 5.3: Ligand Substitution Mechanisms

intermediate
- 5.2: Trends in Kinetic Lability

ionic radius
- 3.3: Acidity of the Hexaaqua Ions

K

Kapustinskii equation
- 8.23: Kapustinskii Equation

Kulinkovich cyclopropanation
- 6.5.1: Linear π Systems

L

labile complex
- 5.2: Trends in Kinetic Lability

Lancashire
- 3.7.6: Jahn-Teller Distortions

Lewis acid
- 3.2: Lewis Acids and Bases

Lewis base
- 3.2: Lewis Acids and Bases

ligand
- 3.2: Lewis Acids and Bases
- 3.6: Coordination Chemistry- Structure and Isomers
- 6.6.2: Carbenes

ligand field theory
- 3.7.4: Ligand Field Theory

ligand substitution
- 5.3: Ligand Substitution Mechanisms
- 6.5.1: Linear π Systems
- 7.1.1: Ligand Dissociation and Substitution

ligands
- 3.6.2: Nomenclature and Ligands
- 7.1.3: Reductive Elimination

linear
- 1.5.2: Valence Shell Electron-Pair Repulsion

low spin
- 3.7.1: Crystal Field Theory
- 3.7.2: Crystal Field Stabilization Energy
- 3.7.3: Factors That Affect Crystal Field Splitting
- 3.7.6: Jahn-Teller Distortions

M

Marcus Theory
- 5.7.1: Outer Sphere Electron Transfer

metal alkyl complexes
- 7.2.4: β-Elimination Reactions

Metal carbenes
- 6.6.2: Carbenes

metal complexes
- 5.1: Thermodynamic Stability of Metal Complexes

metal hydrides
- 6.4.3: Hydrides and Dihydrogen Complexes

metallacyclopropane
- 6.5.1: Linear π Systems

methylene
- 6.6.2: Carbenes

microscopic reversibility
- 7.1.3: Reductive Elimination

microstates
- 4.2: Quantum Numbers of Multielectron Atoms

Migratory insertion
- 6.4.3: Hydrides and Dihydrogen Complexes
- 6.6.1: Metal Alkyls
- 7.2.1: Introduction to Insertion
- 7.2.2: CO Insertions (Alkyl Migration)
- 7.2.3: Migratory Insertion-1,2-Insertions

miller indicies
- 8.10: Miller Indices (hkl)

monodentate
- 3.6.2: Nomenclature and Ligands
- 5.1: Thermodynamic Stability of Metal Complexes

monodentate ligands
- 5.1: Thermodynamic Stability of Metal Complexes

N

node
- 1.5.5: Valence Bond Theory

Nomenclature of Inorganic Compounds
- 3.6.2: Nomenclature and Ligands

nucleophile
- 3.6.3.2: Lewis Concept and Frontier Orbitals

nucleophilic aromatic substitution
- 6.5.1: Linear π Systems

nucleophilic attack
- 6.6.1: Metal Alkyls

O

octahedral
- 1.5.2: Valence Shell Electron-Pair Repulsion
- 3.7.1: Crystal Field Theory

Octahedral Complexes
- 3.6.4: Coordination Numbers and Structures

Octahedral Preference
- 3.7.2: Crystal Field Stabilization Energy

Octahedral Site Preference Energy
- 3.7.2: Crystal Field Stabilization Energy

olefin metathesis
- 6.6.2: Carbenes

olefin polymerization
- 6.5.1: Linear π Systems

orbital mixing
- 1.6.3.2: Orbital Mixing

organic chemistry
- 6.4.3: Hydrides and Dihydrogen Complexes
- 7.2.4: β-Elimination Reactions

organometallic chemistry
- 6.4.3: Hydrides and Dihydrogen Complexes

outer coordination sphere
- 3.6: Coordination Chemistry- Structure and Isomers

Outer Sphere Electron Transfer
- 5.7.1: Outer Sphere Electron Transfer

overlap
- 1.5.5: Valence Bond Theory

Oxidative addition
- 6.4.3: Hydrides and Dihydrogen Complexes
- 6.6.1: Metal Alkyls
- 7.1.2: Oxidative Addition
- 7.1.3: Reductive Elimination

oxidative ligation
7.1.2: Oxidative Addition
oxidative ligations
6.4.3: Hydrides and Dihydrogen Complexes

P

paramagnetic
3.7.1: Crystal Field Theory
Particle in a box
1.2.2.1: Particle in a Box
Pearson's absolute hardness
3.5: Quantitative Measures of Hardness and Softness
3.6.3.3.2: Quantitative Measures of Hardness, Softness, and Acid-Base Interactions from a Hard Soft Acid-Base Principle Perspective Involve Orbital Energies and/or Apportioning Acid-Base Bonding in Terms of Electrostatic and Covalent Factors
penetration
1.2.2.4: Shielding
Peptide bond
9.2: Introduction to Amino Acids and Proteins
philosopher's stone
1.1.3: History of Inorganic Chemistry
pi acceptor
3.7.4: Ligand Field Theory
pi bond
1.5.5: Valence Bond Theory
pi donor
3.7.4: Ligand Field Theory
pi system
6.5.1: Linear π Systems
6.5.3: Odd-numbered π Systems
pi systems
6.5.1: Linear π Systems
6.5.3: Odd-numbered π Systems
proteins
9.2: Introduction to Amino Acids and Proteins

R

radius
3.3: Acidity of the Hexaaqua Ions
reaction coordinate diagram
5.2: Trends in Kinetic Lability
Reactivity Trends
7.2.1: Introduction to Insertion
7.2.2: CO Insertions (Alkyl Migration)
7.2.3: Migratory Insertion-1,2-Insertions
Reductive elimination
6.6.1: Metal Alkyls
7.1.2: Oxidative Addition
7.1.3: Reductive Elimination
resonance
1.5.1.1: Resonance
resonance structures
1.5.1.1: Resonance
ring slippage
6.5.1: Linear π Systems
rotation axis
2.3.2: Representations of Point Groups

S

SALC
2.5.2: Carbon Dioxide
seesaw
1.5.2: Valence Shell Electron-Pair Repulsion
shielding
1.2.2.4: Shielding
Shrock carbenes
6.6.2: Carbenes
sigma bond
1.5.5: Valence Bond Theory
sigma donor
3.7.4: Ligand Field Theory
site selectivity
6.5.1: Linear π Systems
sp hybrid orbital
1.5.6: Hybrid Atomic Orbitals
sp2 hybrid orbital
1.5.6: Hybrid Atomic Orbitals
sp3 hybrid orbital
1.5.6: Hybrid Atomic Orbitals
sp3d hybrid orbital
1.5.6: Hybrid Atomic Orbitals
sp3d2 hybrid orbital
1.5.6: Hybrid Atomic Orbitals
spectator
6.5.1: Linear π Systems
spectrochemical series
3.7.3: Factors That Affect Crystal Field Splitting
spin pairing energy
3.7.1: Crystal Field Theory
3.7.2: Crystal Field Stabilization Energy
square planar
3.7.1: Crystal Field Theory
square pyramidal
1.5.2: Valence Shell Electron-Pair Repulsion
Stephan's phosphinoborane
3.6.3.2.8: Frustrated Lewis pair chemistry uses Lewis acid and base sites within a molecule that are sterically restricted from forming an adduct with each other.
stereochemistry
7.2.1: Introduction to Insertion
7.2.2: CO Insertions (Alkyl Migration)
7.2.3: Migratory Insertion-1,2-Insertions
stereoselectivity
6.5.1: Linear π Systems
stereospecific
7.2.4: β-Elimination Reactions
strong field
3.7.4: Ligand Field Theory
substitution reactions
6.5.3: Odd-numbered π Systems
substitutions
5.3: Ligand Substitution Mechanisms
7.1.1: Ligand Dissociation and Substitution
substrate
9.2: Introduction to Amino Acids and Proteins
symmetry elements
2.1: Symmetry Elements and Operations
symmetry operation
2.3.2: Representations of Point Groups
symmetry operations
2.1: Symmetry Elements and Operations

T

tetrahedral
1.5.2: Valence Shell Electron-Pair Repulsion
3.7.1: Crystal Field Theory
Tetrahedral Complexes
3.6.4: Coordination Numbers and Structures
thermodynamically
5.1: Thermodynamic Stability of Metal Complexes
thermodynamically stable
5.1: Thermodynamic Stability of Metal Complexes
trans effect
5.5: The Trans Effect Observation
transition state
5.2: Trends in Kinetic Lability
transmetalation
6.6.1: Metal Alkyls
tridentate
3.6.2: Nomenclature and Ligands
trigonal bipyramidal
1.5.2: Valence Shell Electron-Pair Repulsion
trigonal planar
1.5.2: Valence Shell Electron-Pair Repulsion
trigonal pyramidal
1.5.2: Valence Shell Electron-Pair Repulsion
trimethylenediamine
5.1: Thermodynamic Stability of Metal Complexes

U

unsaturated ligands
7.2.1: Introduction to Insertion
7.2.2: CO Insertions (Alkyl Migration)
Usanovich acids
3.6.3.2: Lewis Concept and Frontier Orbitals
Usanovich bases
3.6.3.2: Lewis Concept and Frontier Orbitals

V

valence bond theory
1.5.5: Valence Bond Theory
valence shell electron pair repulsion theory
1.5.2: Valence Shell Electron-Pair Repulsion
vinylidenes
6.6.2: Carbenes
VSEPR
1.5.2: Valence Shell Electron-Pair Repulsion

W

Wacker oxidation
6.5.1: Linear π Systems
weak field
3.7.4: Ligand Field Theory
Wittig reaction
6.6.2: Carbenes

Glossary

Sample Word 1 | Sample Definition 1

Detailed Licensing

Overview

Title: CHM 321: Inorganic Chemistry

Webpages: 304

Applicable Restrictions: Noncommercial

All licenses found:

- CC BY-NC-SA 4.0: 99.3% (302 pages)
- Undeclared: 0.7% (2 pages)

By Page

- CHM 321: Inorganic Chemistry - *CC BY-NC-SA 4.0*
  - Front Matter - *CC BY-NC-SA 4.0*
    - TitlePage - *CC BY-NC-SA 4.0*
    - InfoPage - *CC BY-NC-SA 4.0*
    - Table of Contents - *Undeclared*
    - Licensing - *CC BY-NC-SA 4.0*
  - 1: Atomic Structure, Molecular Structure, and Bonding - *CC BY-NC-SA 4.0*
    - 1.1: Introduction to Inorganic Chemistry - *CC BY-NC-SA 4.0*
      - 1.1.1: What is Inorganic Chemistry? - *CC BY-NC-SA 4.0*
      - 1.1.2: Inorganic vs Organic Chemistry - *CC BY-NC-SA 4.0*
      - 1.1.3: History of Inorganic Chemistry - *CC BY-NC-SA 4.0*
    - 1.2: Atomic Structure - *CC BY-NC-SA 4.0*
      - 1.2.1: Historical Development of Atomic Theory - *CC BY-NC-SA 4.0*
        - 1.2.1.1: The Periodic Table - *CC BY-NC-SA 4.0*
        - 1.2.1.2: Discovery of Subatomic Particles and the Bohr Atom - *CC BY-NC-SA 4.0*
      - 1.2.2: The Schrödinger equation, particle in a box, and atomic wavefunctions - *CC BY-NC-SA 4.0*
        - 1.2.2.1: Particle in a Box - *CC BY-NC-SA 4.0*
        - 1.2.2.2: Quantum Numbers and Atomic Wave Functions - *CC BY-NC-SA 4.0*
        - 1.2.2.3: Aufbau Principle - *CC BY-NC-SA 4.0*
        - 1.2.2.4: Shielding - *CC BY-NC-SA 4.0*
      - 1.2.3: Periodic Properties of Atoms - *CC BY-NC-SA 4.0*
        - 1.2.3.1: Ionization energy - *CC BY-NC-SA 4.0*
        - 1.2.3.2: Electron Affinity - *CC BY-NC-SA 4.0*
        - 1.2.3.3: Covalent and Ionic Radii - *CC BY-NC-SA 4.0*
    - 1.3: Rutherford's Atom - *CC BY-NC-SA 4.0*
    - 1.4: Bohr's Atom - *CC BY-NC-SA 4.0*
    - 1.5: Simple Bonding Theory - *CC BY-NC-SA 4.0*
      - 1.5.1: Lewis Electron-Dot Diagrams - *CC BY-NC-SA 4.0*
        - 1.5.1.1: Resonance - *CC BY-NC-SA 4.0*
        - 1.5.1.2: Breaking the octet rule with higher electron counts (hypervalent atoms) - *CC BY-NC-SA 4.0*
        - 1.5.1.3: Formal Charge - *CC BY-NC-SA 4.0*
        - 1.5.1.4: Lewis fails to predict unusual cases-Boron and Beryllium - *CC BY-NC-SA 4.0*
      - 1.5.2: Valence Shell Electron-Pair Repulsion - *CC BY-NC-SA 4.0*
        - 1.5.2.1: Lone Pair Repulsion - *CC BY-NC-SA 4.0*
        - 1.5.2.2: Multiple Bonds - *CC BY-NC-SA 4.0*
        - 1.5.2.3: Electronegativity and Atomic Size Effects - *CC BY-NC-SA 4.0*
      - 1.5.3: Molecular Polarity - *CC BY-NC-SA 4.0*
      - 1.5.4: Hydrogen Bonding - *CC BY-NC-SA 4.0*
      - 1.5.5: Valence Bond Theory - *CC BY-NC-SA 4.0*
      - 1.5.6: Hybrid Atomic Orbitals - *CC BY-NC-SA 4.0*
    - 1.6: Molecular Orbital Theory - *CC BY-NC-SA 4.0*
      - 1.6.1: Prelude to Molecular Orbital Theory - *CC BY-NC-SA 4.0*
      - 1.6.2: Formation of Molecular Orbitals from Atomic Orbitals - *CC BY-NC-SA 4.0*
        - 1.6.2.1: Molecular Orbitals from s Orbitals - *CC BY-NC-SA 4.0*
        - 1.6.2.2: Molecular Orbitals from p Orbitals - *CC BY-NC-SA 4.0*

        - 1.6.2.3: Molecular orbitals from d orbitals - *CC BY-NC-SA 4.0*
        - 1.6.2.4: Nonbonding Orbitals and Other Factors - *CC BY-NC-SA 4.0*
      - 1.6.3: Homonuclear Diatomic Molecules - *CC BY-NC-SA 4.0*
        - 1.6.3.1: Molecular Orbitals - *CC BY-NC-SA 4.0*
        - 1.6.3.2: Orbital Mixing - *CC BY-NC-SA 4.0*
        - 1.6.3.3: Diatomic Molecules of the First and Second Periods - *CC BY-NC-SA 4.0*
        - 1.6.3.4: Photoelectron Spectroscopy - *CC BY-NC-SA 4.0*
      - 1.6.4: Heteronuclear Diatomic Molecules - *CC BY-NC-SA 4.0*
        - 1.6.4.1: Polar bonds - *CC BY-NC-SA 4.0*
        - 1.6.4.2: Ionic Compounds and Molecular Orbitals - *CC BY-NC-SA 4.0*
  - 2: Molecular Symmetry and Group Theory - *CC BY-NC-SA 4.0*
    - 2.1: Symmetry Elements and Operations - *CC BY-NC-SA 4.0*
    - 2.2: Point Groups - *CC BY-NC-SA 4.0*
      - 2.2.1: Groups of Low and High Symmetry - *CC BY-NC-SA 4.0*
      - 2.2.2: Other Groups - *CC BY-NC-SA 4.0*
    - 2.3: Properties and Representations of Groups - *CC BY-NC-SA 4.0*
      - 2.3.1: Matrices - *CC BY-NC-SA 4.0*
      - 2.3.2: Representations of Point Groups - *CC BY-NC-SA 4.0*
      - 2.3.3: Character Tables - *CC BY-NC-SA 4.0*
    - 2.4: Examples and Applications of Symmetry - *CC BY-NC-SA 4.0*
      - 2.4.1: Molecular Vibrations - *CC BY-NC-SA 4.0*
      - 2.4.2: Chirality - *CC BY-NC-SA 4.0*
    - 2.5: Generating SALCs for Polyatomic Molecules - *CC BY-NC-SA 4.0*
      - 2.5.1: Bifluoride anion - *CC BY-NC-SA 4.0*
      - 2.5.2: Carbon Dioxide - *CC BY-NC-SA 4.0*
      - 2.5.3: H_2O - *CC BY-NC-SA 4.0*
      - 2.5.4: NH_3 - *CC BY-NC-SA 4.0*
      - 2.5.5: CO_2 (Revisted with Projection Operators) - *CC BY-NC-SA 4.0*
      - 2.5.6: BF_3 - *CC BY-NC-SA 4.0*
  - 3: Acid-Base Chemistry and an Introduction to Coordination Compounds - *CC BY-NC-SA 4.0*
    - 3.1: Bronsted-Lowry acids and bases - *CC BY-NC-SA 4.0*
    - 3.2: Lewis Acids and Bases - *CC BY-NC-SA 4.0*
    - 3.3: Acidity of the Hexaaqua Ions - *CC BY-NC-SA 4.0*
    - 3.4: Hard/Soft Acids and Bases - *CC BY-NC-SA 4.0*
    - 3.5: Quantitative Measures of Hardness and Softness - *CC BY-NC-SA 4.0*
    - 3.6: Coordination Chemistry- Structure and Isomers - *CC BY-NC-SA 4.0*
      - 3.6.1: History - *CC BY-NC-SA 4.0*
      - 3.6.2: Nomenclature and Ligands - *CC BY-NC-SA 4.0*
      - 3.6.3: Acid-Base and Donor-Acceptor Chemistry - *CC BY-NC-SA 4.0*
        - 3.6.3.1: Acid-Base Models as Organizing Concepts - *CC BY-NC-SA 4.0*
        - 3.6.3.2: Lewis Concept and Frontier Orbitals - *CC BY-NC-SA 4.0*
          - 3.6.3.2.1: The frontier orbital approach considers Lewis acid-base reactions in terms of the donation of electrons from the base's highest occupied orbital into the acid's lowest unoccupied orbital. - *CC BY-NC-SA 4.0*
          - 3.6.3.2.2: All other things being equal, electron withdrawing groups tend to make Lewis acids stronger and bases weaker while electron donating groups tend to make Lewis bases stronger and acids weaker - *CC BY-NC-SA 4.0*
          - 3.6.3.2.3: The electronic spectra of charge transfer complexes illustrate the impact of frontier orbital interactions on the electronic structure of Lewis acid-base adducts - *CC BY-NC-SA 4.0*
          - 3.6.3.2.4: Substances' solution phase Lewis basicity towards a given acid may be estimated using the enthalpy change for dissociation of its adduct with a reference acid of similar hardness. - *CC BY-NC-SA 4.0*
          - 3.6.3.2.5: In the boron trifluoride affinity scale, the enthalpy change on formation of an adduct between the base and boron trifluoride is taken as a measure of Lewis basicity. - *CC BY-NC-SA 4.0*
          - 3.6.3.2.6: Lewis base strength may also be estimated by measuring structural or energy changes upon formation of a Lewis

acid-base complex, as illustrated by efforts to spectroscopically assess the strengths of halogen bonds - *CC BY-NC-SA 4.0*
- 3.6.3.2.7: Bulky groups weaken the strength of Lewis acids and bases because they introduce steric strain into the resulting acid-base adduct. - *CC BY-NC-SA 4.0*
- 3.6.3.2.8: Frustrated Lewis pair chemistry uses Lewis acid and base sites within a molecule that are sterically restricted from forming an adduct with each other. - *CC BY-NC-SA 4.0*

- 3.6.3.3: Hard and Soft Acids and Bases - *CC BY-NC-SA 4.0*
  - 3.6.3.3.1: Hard-Hard and Soft-Soft preferences may be explained and quantified in terms of electrostatic and covalent and electronic stabilization on the stability of Lewis acid-base adducts - *CC BY-NC-SA 4.0*
  - 3.6.3.3.2: Quantitative Measures of Hardness, Softness, and Acid-Base Interactions from a Hard Soft Acid-Base Principle Perspective Involve Orbital Energies and/or Apportioning Acid-Base Bonding in Terms of Electrostatic and Covalent Factors - *CC BY-NC-SA 4.0*
  - 3.6.3.4: Problems - *CC BY-NC-SA 4.0*
- 3.6.4: Coordination Numbers and Structures - *CC BY-NC-SA 4.0*
- 3.6.5: Isomerism - *CC BY-NC-SA 4.0*

- 3.7: Coordination Chemistry- Bonding - *CC BY-NC-SA 4.0*
  - 3.7.1: Crystal Field Theory - *CC BY-NC-SA 4.0*
  - 3.7.2: Crystal Field Stabilization Energy - *CC BY-NC-SA 4.0*
  - 3.7.3: Factors That Affect Crystal Field Splitting - *CC BY-NC-SA 4.0*
  - 3.7.4: Ligand Field Theory - *CC BY-NC-SA 4.0*
  - 3.7.5: Metal-Metal Bonds - *CC BY-NC-SA 4.0*
    - 3.7.5.1: Metal-Metal Multiple Bonds - *CC BY-NC-SA 4.0*
  - 3.7.6: Jahn-Teller Distortions - *CC BY-NC-SA 4.0*

- 4: Electronic Structure and Spectra of d-Metal Complexes - *CC BY-NC-SA 4.0*
  - 4.1: Absorption of Light - *CC BY-NC-SA 4.0*
    - 4.1.1: Beer-Lambert Absorption Law - *CC BY-NC-SA 4.0*
  - 4.2: Quantum Numbers of Multielectron Atoms - *CC BY-NC-SA 4.0*
    - 4.2.1: Finding Microstates and Term Symbols - *CC BY-NC-SA 4.0*
    - 4.2.2: Spin-Orbit Coupling - *CC BY-NC-SA 4.0*
  - 4.3: Electronic Spectra of Coordination Compounds - *CC BY-NC-SA 4.0*
    - 4.3.1: Symmetry labels for split terms - *CC BY-NC-SA 4.0*
    - 4.3.2: Correlation Diagrams - *CC BY-NC-SA 4.0*
    - 4.3.3: Tanabe-Sugano Diagrams - *CC BY-NC-SA 4.0*
    - 4.3.4: Applications of Tanabe-Sugano Diagrams - *CC BY-NC-SA 4.0*
    - 4.3.5: Tetrahedral Complexes - *CC BY-NC-SA 4.0*
    - 4.3.6: Selection Rules - *CC BY-NC-SA 4.0*
    - 4.3.7: Charge-Transfer Spectra - *CC BY-NC-SA 4.0*
    - 4.3.8: Applications of Charge-Transfer - *CC BY-NC-SA 4.0*
- 5: Reactions of d-Metal Complexes - *CC BY-NC-SA 4.0*
  - 5.1: Thermodynamic Stability of Metal Complexes - *CC BY-NC-SA 4.0*
  - 5.2: Trends in Kinetic Lability - *CC BY-NC-SA 4.0*
  - 5.3: Ligand Substitution Mechanisms - *CC BY-NC-SA 4.0*
  - 5.4: Substitutions in Square Planar Complexes - *CC BY-NC-SA 4.0*
    - 5.4.1: Kinetics and Stereochemistry of Square Planar Reactions - *CC BY-NC-SA 4.0*
    - 5.4.2: Evidence for Associative Reactions - *CC BY-NC-SA 4.0*
  - 5.5: The Trans Effect Observation - *CC BY-NC-SA 4.0*
  - 5.6: The Trans Effect Explanation - *CC BY-NC-SA 4.0*
  - 5.7: Redox Mechanisms - *CC BY-NC-SA 4.0*
    - 5.7.1: Outer Sphere Electron Transfer - *CC BY-NC-SA 4.0*
    - 5.7.2: Inner Sphere Electron Transfer - *CC BY-NC-SA 4.0*
- 6: Organometallic Chemistry - *CC BY-NC-SA 4.0*
  - 6.1: Introduction to Organometallic Chemistry - *CC BY-NC-SA 4.0*
  - 6.2: Nomenclature, Ligands, and Classification - *CC BY-NC-SA 4.0*

- 6.3: Electron Counting in Organometallic Complexes - *CC BY-NC-SA 4.0*
  - 6.3.1: The 18 Electron Rule - *CC BY-NC-SA 4.0*
  - 6.3.2: Simplifying the Organometallic Complex by Deconstruction - *CC BY-NC-SA 4.0*
- 6.4: Survey of Organometallic Ligands - *CC BY-NC-SA 4.0*
  - 6.4.1: Carbon Monoxide (Carbonyl Complexes) - *CC BY-NC-SA 4.0*
  - 6.4.2: Ligands similar to CO - *CC BY-NC-SA 4.0*
  - 6.4.3: Hydrides and Dihydrogen Complexes - *CC BY-NC-SA 4.0*
- 6.5: Bonding between Metal Atoms and Organic Pi Systems - *CC BY-NC-SA 4.0*
  - 6.5.1: Linear π Systems - *CC BY-NC-SA 4.0*
  - 6.5.2: Cyclic π systems - *CC BY-NC-SA 4.0*
  - 6.5.3: Odd-numbered π Systems - *CC BY-NC-SA 4.0*
  - 6.5.4: Fullerene Complexes - *CC BY-NC-SA 4.0*
- 6.6: Metal-Carbon Bonds - *CC BY-NC-SA 4.0*
  - 6.6.1: Metal Alkyls - *CC BY-NC-SA 4.0*
  - 6.6.2: Carbenes - *CC BY-NC-SA 4.0*
  - 6.6.3: Carbyne (Alkylidyne) Complexes - *CC BY-NC-SA 4.0*
  - 6.6.4: Carbido and Cumulene Complexes - *CC BY-NC-SA 4.0*
  - 6.6.5: Carbon Wires- Polyyne and Polyene Bridges - *CC BY-NC-SA 4.0*
- 6.7: Characterization of Organometallic Complexes - *CC BY-NC-SA 4.0*

○ 7: Organometallic Reactions and Catalysis - *CC BY-NC-SA 4.0*

- 7.1: Reactions Involving Gain or Loss of Ligands - *CC BY-NC-SA 4.0*
  - 7.1.1: Ligand Dissociation and Substitution - *CC BY-NC-SA 4.0*
  - 7.1.2: Oxidative Addition - *CC BY-NC-SA 4.0*
  - 7.1.3: Reductive Elimination - *CC BY-NC-SA 4.0*
  - 7.1.4: Sigma Bond Metathasis - *CC BY-NC-SA 4.0*
  - 7.1.5: Application of Pincer Ligands - *CC BY-NC-SA 4.0*
- 7.2: Reactions Invloving Modification of Unsaturated Ligands - *CC BY-NC-SA 4.0*
  - 7.2.1: Introduction to Insertion - *CC BY-NC-SA 4.0*
  - 7.2.2: CO Insertions (Alkyl Migration) - *CC BY-NC-SA 4.0*
  - 7.2.3: Migratory Insertion-1,2-Insertions - *CC BY-NC-SA 4.0*
  - 7.2.4: β-Elimination Reactions - *CC BY-NC-SA 4.0*
  - 7.2.5: Abstraction and Addition - *CC BY-NC-SA 4.0*
- 7.3: Organometallic Catalysts - *CC BY-NC-SA 4.0*
  - 7.3.1: Catalytic Deuteration - *CC BY-NC-SA 4.0*
  - 7.3.2: Hydroformylation - *CC BY-NC-SA 4.0*
  - 7.3.3: Monsanto Acetic Acid Process - *CC BY-NC-SA 4.0*
  - 7.3.4: Wacker (Smidt) Process - *CC BY-NC-SA 4.0*
  - 7.3.5: Hydrogenation by Wilkinson's Catalyst - *CC BY-NC-SA 4.0*
  - 7.3.6: Olefin Metathesis - *CC BY-NC-SA 4.0*
- 7.4: Heterogeneous Catalysts - *CC BY-NC-SA 4.0*
  - 7.4.1: Ziegler-Natta Polymerizations - *CC BY-NC-SA 4.0*
  - 7.4.2: Water-Gas Shift Reaction - *CC BY-NC-SA 4.0*
- 7.5: Problems - *CC BY-NC-SA 4.0*
  - 7.5.1: Concept Review Questions Chapter 12 - *CC BY-NC-SA 4.0*
  - 7.5.2: Homework Problems Chapter 12 - *CC BY-NC-SA 4.0*

○ 8: Solid State Chemistry - *CC BY-NC-SA 4.0*

- 8.1: Prelude to Metals and Alloys - *CC BY-NC-SA 4.0*
- 8.2: Unit Cells and Crystal Structures - *CC BY-NC-SA 4.0*
- 8.3: Crystal Structures of Metals - *CC BY-NC-SA 4.0*
- 8.4: Conduction in Metals - *CC BY-NC-SA 4.0*
- 8.5: Atomic Orbitals and Magnetism - *CC BY-NC-SA 4.0*
- 8.6: Ferro-, Ferri- and Antiferromagnetism - *CC BY-NC-SA 4.0*
- 8.7: Hard and Soft Magnets - *CC BY-NC-SA 4.0*
- 8.8: Defects in Metallic Crystals - *CC BY-NC-SA 4.0*
- 8.9: X-ray Crystallography - *CC BY-NC-SA 4.0*
- 8.10: Miller Indices (hkl) - *CC BY-NC-SA 4.0*
- 8.11: Powder X-ray Diffraction - *CC BY-NC-SA 4.0*
- 8.12: Prelude to Ionic and Covalent Solids - Structures - *CC BY-NC-SA 4.0*
- 8.13: Close-packing and Interstitial Sites - *CC BY-NC-SA 4.0*
- 8.14: Structures Related to NaCl and NiAs - *CC BY-NC-SA 4.0*
- 8.15: Tetrahedral Structures - *CC BY-NC-SA 4.0*
- 8.16: Layered Structures and Intercalation Reactions - *CC BY-NC-SA 4.0*

- 8.17: Ionic Radii and Radius Ratios - *CC BY-NC-SA 4.0*
- 8.18: Structure Maps - *CC BY-NC-SA 4.0*
- 8.19: Energetics of Crystalline Solids- The Ionic Model - *CC BY-NC-SA 4.0*
- 8.20: Born-Haber Cycles for NaCl and Silver Halides - *CC BY-NC-SA 4.0*
- 8.21: Lattice Energies and Solubility - *CC BY-NC-SA 4.0*
- 8.22: Spinel, Perovskite, and Rutile Structures - *CC BY-NC-SA 4.0*
- 8.23: Kapustinskii Equation - *CC BY-NC-SA 4.0*
- 8.24: New Page - *CC BY-NC-SA 4.0*

9: Bioinorganic Chemistry - *CC BY-NC-SA 4.0*

- 9.1: Biological Significance of Iron, Zinc, Copper, Molybdenum, Cobalt, Chromium, Vanadium, and Nickel - *CC BY-NC-SA 4.0*
- 9.2: Introduction to Amino Acids and Proteins - *CC BY-NC-SA 4.0*
- 9.3: Overview of Hemoglobin and Myoglobin - *CC BY-NC-SA 4.0*
  - 9.3.1: Myoglobin, Hemoglobin, and their Ligands - *CC BY-NC-SA 4.0*
  - 9.3.2: Oxygen Transport by the Proteins Myoglobin and Hemoglobin - *CC BY-NC-SA 4.0*
- 9.4: Ferrodoxins, Hydrogenases, and Nitrogenases - Metal-Sulfide Proteins - *CC BY-NC-SA 4.0*
  - 9.4.1: Iron-sulfur Proteins and Models - *CC BY-NC-SA 4.0*
  - 9.4.2: Iron-sulfur Proteins and Models (Part 2) - *CC BY-NC-SA 4.0*
  - 9.4.3: Iron-sulfur Proteins and Models (Part 3) - *CC BY-NC-SA 4.0*
  - 9.4.4: Iron-sulfur Proteins and Models (Part 4) - *CC BY-NC-SA 4.0*
- 9.5: The Reaction Pathways of Zinc Enzymes and Related Biological Catalysts - *CC BY-NC-SA 4.0*
  - 9.5.1: About Carbonic Anhydrase - *CC BY-NC-SA 4.0*
  - 9.5.2: Catalytic Mechanism - *CC BY-NC-SA 4.0*
  - 9.5.3: Metal Substitution - *CC BY-NC-SA 4.0*
- 9.6: Metals in Medicine - *CC BY-NC-SA 4.0*
  - 9.6.1: Metal Deficiency and Disease - *CC BY-NC-SA 4.0*
  - 9.6.2: Toxic Effects of Metals - *CC BY-NC-SA 4.0*
  - 9.6.3: Aspects of Platinum Binding to DNA - *CC BY-NC-SA 4.0*
  - 9.6.4: Survey of Metals Used for Diagnosis and Chemotherapy - *CC BY-NC-SA 4.0*
  - 9.6.5: Platinum Anticancer Drugs- A Case Study - *CC BY-NC-SA 4.0*
  - 9.6.6: Mapping the Major Adducts of cis- and trans-DDP on DNA; Sequence Specificity - *CC BY-NC-SA 4.0*
  - 9.6.7: Structure of Platinum-DNA Complexes - *CC BY-NC-SA 4.0*
  - 9.6.8: Site-specifically Platinated DNA \ (\;^{154}\) - *CC BY-NC-SA 4.0*
  - 9.6.9: Bioinorganic Chemistry of Platinum Anticancer Drugs- How Might They Work? - *CC BY-NC-SA 4.0*
  - 9.6.10: Bioinorganic Chemistry of Platinum Anticancer Drugs; How Might They Work? (Part 2) - *CC BY-NC-SA 4.0*
  - 9.6.11: Design of New Inorganic Anticancer Drugs - *CC BY-NC-SA 4.0*
- 9.7: Electron Transfer - *CC BY-NC-SA 4.0*

10: Special Topics - *CC BY-NC-SA 4.0*

- 10.1: f-Block Metals- Lanthanides and Actinides - *CC BY-NC-SA 4.0*
  - 10.1.1: Introduction - *CC BY-NC-SA 4.0*
  - 10.1.2: f-Orbitals and Oxidation States - *CC BY-NC-SA 4.0*
  - 10.1.3: Atoms and Ion Sizes - *CC BY-NC-SA 4.0*
    - 10.1.3A: The Lanthanoid Contraction - *CC BY-NC-SA 4.0*
    - 10.1.3B: Coordination Numbers - *CC BY-NC-SA 4.0*
  - 10.1.4: Spectroscopic and Magnetic Properties - *CC BY-NC-SA 4.0*
    - 10.1.4A: Electronic Spectra and Magnetic Moments - Lanthanoids - *CC BY-NC-SA 4.0*
    - 10.1.4B: Luminescence of Lanthanoid Complexes - *CC BY-NC-SA 4.0*
    - 10.1.4C: Electronic Spectra and Magnetic Moments - Actinoids - *CC BY-NC-SA 4.0*
  - 10.1.5: Sources of the Lanthanoids and Actinoids - *CC BY-NC-SA 4.0*
    - 10.1.5A: Occurrence and Separation of the Lanthanoids - *CC BY-NC-SA 4.0*
    - 10.1.5B: The Actinoids - *CC BY-NC-SA 4.0*
  - 10.1.6: Lanthanoid Metals - *CC BY-NC-SA 4.0*
  - 10.1.7: Inorganic Compounds and Coordination Complexes of the Lanthanoids - *CC BY-NC-SA 4.0*

- 10.1.7A: Halides - *CC BY-NC-SA 4.0*
- 10.1.7B: Hydroxides and Oxides - *CC BY-NC-SA 4.0*
- 10.1.7C: Complexes of Ln(III) - *CC BY-NC-SA 4.0*
- 10.1.8: Organometallic Complexes of the Lanthanoids - *CC BY-NC-SA 4.0*
  - 10.1.8A: \(\sigma\)-Bonded Complexes - *CC BY-NC-SA 4.0*
  - 10.1.8B: Cyclopentadienyl Complexes - *CC BY-NC-SA 4.0*
  - 10.1.8C: Bis(arene) Derivatives - *CC BY-NC-SA 4.0*
  - 10.1.8D: Complexes Containing the \(\eta^8\)-cyclooctatetraenyl Ligand - *CC BY-NC-SA 4.0*
- 10.1.9: The Actinoid Metals - *CC BY-NC-SA 4.0*
- 10.1.10: Inorganic Compounds and Coordination Complexes of Thorium, Uranium, and Plutonium - *CC BY-NC-SA 4.0*
  - 10.1.10A: Thorium - *CC BY-NC-SA 4.0*
  - 10.1.10B: Uranium - *CC BY-NC-SA 4.0*
  - 10.1.10C: Plutonium - *CC BY-NC-SA 4.0*
- 10.1.11: Organometallic Complexes of Thorium and Uranium - *CC BY-NC-SA 4.0*
  - 10.1.11A: (\sigma\)-Bonded Complexes - *CC BY-NC-SA 4.0*
  - 10.1.11B: Cyclopentadienyl Derivatives - *CC BY-NC-SA 4.0*
  - 10.1.11C: Complexes Containing the \(\eta^8\)-cyclooctatetraenyl Ligand - *CC BY-NC-SA 4.0*
- 10.2: Physical Inorganic Techniques - *CC BY-NC-SA 4.0*
  - 10.2.1: Electronic Spectroscopy - *CC BY-NC-SA 4.0*
    - 10.2.1A: UV-VIS Absorption Spectroscopy - *CC BY-NC-SA 4.0*
    - 10.2.1B: Types of Absorption - *CC BY-NC-SA 4.0*
    - 10.2.1C: Absorbance and the Beer-Lambert Law - *CC BY-NC-SA 4.0*
    - 10.2.1D: Emission Spectroscopy - *CC BY-NC-SA 4.0*
  - 10.2.2: Nuclear Magnetic Resonance (NMR) Spectroscopy - *CC BY-NC-SA 4.0*
  - 10.2.3: Electron Paramagnetic Resonance (EPR) Spectroscopy - *CC BY-NC-SA 4.0*
    - 10.2.3A: What is EPR Spectroscopy? - *CC BY-NC-SA 4.0*
    - 10.2.3B: The Zeeman Electronic Effect - *CC BY-NC-SA 4.0*
    - 10.2.3C: EPR Spectra - *CC BY-NC-SA 4.0*
  - 10.2.4: Mossbauer Spectroscopy - *CC BY-NC-SA 4.0*
    - 10.2.4A: The Technique of Mossbauer Spectroscopy - *CC BY-NC-SA 4.0*
    - 10.2.4B: What Can Isomer Shift Data Tell Us? - *CC BY-NC-SA 4.0*
  - 10.2.5: Structure Determination - Diffraction Methods - *CC BY-NC-SA 4.0*
    - 10.2.5A: X-Ray Diffraction (XRD) - *CC BY-NC-SA 4.0*
    - 10.2.5B: Single Crystal X-Ray Diffraction - *CC BY-NC-SA 4.0*
    - 10.2.5C: Powder X-Ray Diffraction - *CC BY-NC-SA 4.0*
    - 10.2.5D: Single Crystal Neutron Diffraction - *CC BY-NC-SA 4.0*
    - 10.2.5E: Electron Diffraction - *CC BY-NC-SA 4.0*
    - 10.2.5F: Low-Energy Electron Diffraction (LEED) - *CC BY-NC-SA 4.0*
    - 10.2.5G: Structural Databases - *CC BY-NC-SA 4.0*
  - 10.2.6: Photoelectron Spectroscopy (PES, UPS, XPS, ESCA) - *CC BY-NC-SA 4.0*
  - 10.2.7: Mass Spectrometry - *CC BY-NC-SA 4.0*
    - 10.2.7A: Electron Ionization (EI) - *CC BY-NC-SA 4.0*
    - 10.2.7B: Fast Atom Bombardment (FAB) - *CC BY-NC-SA 4.0*
    - 10.2.7C: Matrix-Assisted Laser Desorption Ionization Time-of-Flight (MALDI-TOF) - *CC BY-NC-SA 4.0*
    - 10.2.7D: Electrospray Ionization (ESI) - *CC BY-NC-SA 4.0*
- 10.3: Fluxional Behavior - *CC BY-NC-SA 4.0*
  - 10.3.1: Determination of Energetics of Fluxional Molecules by NMR - *CC BY-NC-SA 4.0*

- Back Matter - *CC BY-NC-SA 4.0*
  - Index - *CC BY-NC-SA 4.0*
  - Glossary - *CC BY-NC-SA 4.0*
  - Detailed Licensing - *CC BY-NC-SA 4.0*
  - Detailed Licensing - *Undeclared*

https://chem.libretexts.org/@go/page/484648

Detailed Licensing

Overview

Title: CHM 321: Inorganic Chemistry

Webpages: 304

Applicable Restrictions: Noncommercial

All licenses found:

- CC BY-NC-SA 4.0: 99.3% (302 pages)
- Undeclared: 0.7% (2 pages)

By Page

- CHM 321: Inorganic Chemistry - *CC BY-NC-SA 4.0*
  - Front Matter - *CC BY-NC-SA 4.0*
    - TitlePage - *CC BY-NC-SA 4.0*
    - InfoPage - *CC BY-NC-SA 4.0*
    - Table of Contents - *Undeclared*
    - Licensing - *CC BY-NC-SA 4.0*
  - 1: Atomic Structure, Molecular Structure, and Bonding - *CC BY-NC-SA 4.0*
    - 1.1: Introduction to Inorganic Chemistry - *CC BY-NC-SA 4.0*
      - 1.1.1: What is Inorganic Chemistry? - *CC BY-NC-SA 4.0*
      - 1.1.2: Inorganic vs Organic Chemistry - *CC BY-NC-SA 4.0*
      - 1.1.3: History of Inorganic Chemistry - *CC BY-NC-SA 4.0*
    - 1.2: Atomic Structure - *CC BY-NC-SA 4.0*
      - 1.2.1: Historical Development of Atomic Theory - *CC BY-NC-SA 4.0*
        - 1.2.1.1: The Periodic Table - *CC BY-NC-SA 4.0*
        - 1.2.1.2: Discovery of Subatomic Particles and the Bohr Atom - *CC BY-NC-SA 4.0*
      - 1.2.2: The Schrödinger equation, particle in a box, and atomic wavefunctions - *CC BY-NC-SA 4.0*
        - 1.2.2.1: Particle in a Box - *CC BY-NC-SA 4.0*
        - 1.2.2.2: Quantum Numbers and Atomic Wave Functions - *CC BY-NC-SA 4.0*
        - 1.2.2.3: Aufbau Principle - *CC BY-NC-SA 4.0*
        - 1.2.2.4: Shielding - *CC BY-NC-SA 4.0*
      - 1.2.3: Periodic Properties of Atoms - *CC BY-NC-SA 4.0*
        - 1.2.3.1: Ionization energy - *CC BY-NC-SA 4.0*
        - 1.2.3.2: Electron Affinity - *CC BY-NC-SA 4.0*
        - 1.2.3.3: Covalent and Ionic Radii - *CC BY-NC-SA 4.0*
    - 1.3: Rutherford's Atom - *CC BY-NC-SA 4.0*
    - 1.4: Bohr's Atom - *CC BY-NC-SA 4.0*
    - 1.5: Simple Bonding Theory - *CC BY-NC-SA 4.0*
      - 1.5.1: Lewis Electron-Dot Diagrams - *CC BY-NC-SA 4.0*
        - 1.5.1.1: Resonance - *CC BY-NC-SA 4.0*
        - 1.5.1.2: Breaking the octet rule with higher electron counts (hypervalent atoms) - *CC BY-NC-SA 4.0*
        - 1.5.1.3: Formal Charge - *CC BY-NC-SA 4.0*
        - 1.5.1.4: Lewis fails to predict unusual cases-Boron and Beryllium - *CC BY-NC-SA 4.0*
      - 1.5.2: Valence Shell Electron-Pair Repulsion - *CC BY-NC-SA 4.0*
        - 1.5.2.1: Lone Pair Repulsion - *CC BY-NC-SA 4.0*
        - 1.5.2.2: Multiple Bonds - *CC BY-NC-SA 4.0*
        - 1.5.2.3: Electronegativity and Atomic Size Effects - *CC BY-NC-SA 4.0*
      - 1.5.3: Molecular Polarity - *CC BY-NC-SA 4.0*
      - 1.5.4: Hydrogen Bonding - *CC BY-NC-SA 4.0*
      - 1.5.5: Valence Bond Theory - *CC BY-NC-SA 4.0*
      - 1.5.6: Hybrid Atomic Orbitals - *CC BY-NC-SA 4.0*
    - 1.6: Molecular Orbital Theory - *CC BY-NC-SA 4.0*
      - 1.6.1: Prelude to Molecular Orbital Theory - *CC BY-NC-SA 4.0*
      - 1.6.2: Formation of Molecular Orbitals from Atomic Orbitals - *CC BY-NC-SA 4.0*
        - 1.6.2.1: Molecular Orbitals from s Orbitals - *CC BY-NC-SA 4.0*
        - 1.6.2.2: Molecular Orbitals from p Orbitals - *CC BY-NC-SA 4.0*

- 1.6.2.3: Molecular orbitals from d orbitals - *CC BY-NC-SA 4.0*
- 1.6.2.4: Nonbonding Orbitals and Other Factors - *CC BY-NC-SA 4.0*
- 1.6.3: Homonuclear Diatomic Molecules - *CC BY-NC-SA 4.0*
- 1.6.3.1: Molecular Orbitals - *CC BY-NC-SA 4.0*
- 1.6.3.2: Orbital Mixing - *CC BY-NC-SA 4.0*
- 1.6.3.3: Diatomic Molecules of the First and Second Periods - *CC BY-NC-SA 4.0*
- 1.6.3.4: Photoelectron Spectroscopy - *CC BY-NC-SA 4.0*
- 1.6.4: Heteronuclear Diatomic Molecules - *CC BY-NC-SA 4.0*
- 1.6.4.1: Polar bonds - *CC BY-NC-SA 4.0*
- 1.6.4.2: Ionic Compounds and Molecular Orbitals - *CC BY-NC-SA 4.0*

2: Molecular Symmetry and Group Theory - *CC BY-NC-SA 4.0*

- 2.1: Symmetry Elements and Operations - *CC BY-NC-SA 4.0*
- 2.2: Point Groups - *CC BY-NC-SA 4.0*
- 2.2.1: Groups of Low and High Symmetry - *CC BY-NC-SA 4.0*
- 2.2.2: Other Groups - *CC BY-NC-SA 4.0*
- 2.3: Properties and Representations of Groups - *CC BY-NC-SA 4.0*
- 2.3.1: Matrices - *CC BY-NC-SA 4.0*
- 2.3.2: Representations of Point Groups - *CC BY-NC-SA 4.0*
- 2.3.3: Character Tables - *CC BY-NC-SA 4.0*
- 2.4: Examples and Applications of Symmetry - *CC BY-NC-SA 4.0*
- 2.4.1: Molecular Vibrations - *CC BY-NC-SA 4.0*
- 2.4.2: Chirality - *CC BY-NC-SA 4.0*
- 2.5: Generating SALCs for Polyatomic Molecules - *CC BY-NC-SA 4.0*
- 2.5.1: Bifluoride anion - *CC BY-NC-SA 4.0*
- 2.5.2: Carbon Dioxide - *CC BY-NC-SA 4.0*
- 2.5.3: H_2O - *CC BY-NC-SA 4.0*
- 2.5.4: NH_3 - *CC BY-NC-SA 4.0*
- 2.5.5: CO_2 (Revisted with Projection Operators) - *CC BY-NC-SA 4.0*
- 2.5.6: BF_3 - *CC BY-NC-SA 4.0*

3: Acid-Base Chemistry and an Introduction to Coordination Compounds - *CC BY-NC-SA 4.0*

- 3.1: Bronsted-Lowry acids and bases - *CC BY-NC-SA 4.0*
- 3.2: Lewis Acids and Bases - *CC BY-NC-SA 4.0*
- 3.3: Acidity of the Hexaaqua Ions - *CC BY-NC-SA 4.0*
- 3.4: Hard/Soft Acids and Bases - *CC BY-NC-SA 4.0*
- 3.5: Quantitative Measures of Hardness and Softness - *CC BY-NC-SA 4.0*
- 3.6: Coordination Chemistry- Structure and Isomers - *CC BY-NC-SA 4.0*
- 3.6.1: History - *CC BY-NC-SA 4.0*
- 3.6.2: Nomenclature and Ligands - *CC BY-NC-SA 4.0*
- 3.6.3: Acid-Base and Donor-Acceptor Chemistry - *CC BY-NC-SA 4.0*
- 3.6.3.1: Acid-Base Models as Organizing Concepts - *CC BY-NC-SA 4.0*
- 3.6.3.2: Lewis Concept and Frontier Orbitals - *CC BY-NC-SA 4.0*
- 3.6.3.2.1: The frontier orbital approach considers Lewis acid-base reactions in terms of the donation of electrons from the base's highest occupied orbital into the acid's lowest unoccupied orbital. - *CC BY-NC-SA 4.0*
- 3.6.3.2.2: All other things being equal, electron withdrawing groups tend to make Lewis acids stronger and bases weaker while electron donating groups tend to make Lewis bases stronger and acids weaker - *CC BY-NC-SA 4.0*
- 3.6.3.2.3: The electronic spectra of charge transfer complexes illustrate the impact of frontier orbital interactions on the electronic structure of Lewis acid-base adducts - *CC BY-NC-SA 4.0*
- 3.6.3.2.4: Substances' solution phase Lewis basicity towards a given acid may be estimated using the enthalpy change for dissociation of its adduct with a reference acid of similar hardness. - *CC BY-NC-SA 4.0*
- 3.6.3.2.5: In the boron trifluoride affinity scale, the enthalpy change on formation of an adduct between the base and boron trifluoride is taken as a measure of Lewis basicity. - *CC BY-NC-SA 4.0*
- 3.6.3.2.6: Lewis base strength may also be estimated by measuring structural or energy changes upon formation of a Lewis

acid-base complex, as illustrated by efforts to spectroscopically assess the strengths of halogen bonds - *CC BY-NC-SA 4.0*
- 3.6.3.2.7: Bulky groups weaken the strength of Lewis acids and bases because they introduce steric strain into the resulting acid-base adduct. - *CC BY-NC-SA 4.0*
- 3.6.3.2.8: Frustrated Lewis pair chemistry uses Lewis acid and base sites within a molecule that are sterically restricted from forming an adduct with each other. - *CC BY-NC-SA 4.0*

- 3.6.3.3: Hard and Soft Acids and Bases - *CC BY-NC-SA 4.0*
  - 3.6.3.3.1: Hard-Hard and Soft-Soft preferences may be explained and quantified in terms of electrostatic and covalent and electronic stabilization on the stability of Lewis acid-base adducts - *CC BY-NC-SA 4.0*
  - 3.6.3.3.2: Quantitative Measures of Hardness, Softness, and Acid-Base Interactions from a Hard Soft Acid-Base Principle Perspective Involve Orbital Energies and/or Apportioning Acid-Base Bonding in Terms of Electrostatic and Covalent Factors - *CC BY-NC-SA 4.0*
  - 3.6.3.4: Problems - *CC BY-NC-SA 4.0*
- 3.6.4: Coordination Numbers and Structures - *CC BY-NC-SA 4.0*
- 3.6.5: Isomerism - *CC BY-NC-SA 4.0*

- 3.7: Coordination Chemistry- Bonding - *CC BY-NC-SA 4.0*
  - 3.7.1: Crystal Field Theory - *CC BY-NC-SA 4.0*
  - 3.7.2: Crystal Field Stabilization Energy - *CC BY-NC-SA 4.0*
  - 3.7.3: Factors That Affect Crystal Field Splitting - *CC BY-NC-SA 4.0*
  - 3.7.4: Ligand Field Theory - *CC BY-NC-SA 4.0*
  - 3.7.5: Metal-Metal Bonds - *CC BY-NC-SA 4.0*
    - 3.7.5.1: Metal-Metal Multiple Bonds - *CC BY-NC-SA 4.0*
  - 3.7.6: Jahn-Teller Distortions - *CC BY-NC-SA 4.0*

- 4: Electronic Structure and Spectra of d-Metal Complexes - *CC BY-NC-SA 4.0*
  - 4.1: Absorption of Light - *CC BY-NC-SA 4.0*
    - 4.1.1: Beer-Lambert Absorption Law - *CC BY-NC-SA 4.0*
  - 4.2: Quantum Numbers of Multielectron Atoms - *CC BY-NC-SA 4.0*
    - 4.2.1: Finding Microstates and Term Symbols - *CC BY-NC-SA 4.0*
    - 4.2.2: Spin-Orbit Coupling - *CC BY-NC-SA 4.0*
  - 4.3: Electronic Spectra of Coordination Compounds - *CC BY-NC-SA 4.0*
    - 4.3.1: Symmetry labels for split terms - *CC BY-NC-SA 4.0*
    - 4.3.2: Correlation Diagrams - *CC BY-NC-SA 4.0*
    - 4.3.3: Tanabe-Sugano Diagrams - *CC BY-NC-SA 4.0*
    - 4.3.4: Applications of Tanabe-Sugano Diagrams - *CC BY-NC-SA 4.0*
    - 4.3.5: Tetrahedral Complexes - *CC BY-NC-SA 4.0*
    - 4.3.6: Selection Rules - *CC BY-NC-SA 4.0*
    - 4.3.7: Charge-Transfer Spectra - *CC BY-NC-SA 4.0*
    - 4.3.8: Applications of Charge-Transfer - *CC BY-NC-SA 4.0*
- 5: Reactions of d-Metal Complexes - *CC BY-NC-SA 4.0*
  - 5.1: Thermodynamic Stability of Metal Complexes - *CC BY-NC-SA 4.0*
  - 5.2: Trends in Kinetic Lability - *CC BY-NC-SA 4.0*
  - 5.3: Ligand Substitution Mechanisms - *CC BY-NC-SA 4.0*
  - 5.4: Substitutions in Square Planar Complexes - *CC BY-NC-SA 4.0*
    - 5.4.1: Kinetics and Stereochemistry of Square Planar Reactions - *CC BY-NC-SA 4.0*
    - 5.4.2: Evidence for Associative Reactions - *CC BY-NC-SA 4.0*
  - 5.5: The Trans Effect Observation - *CC BY-NC-SA 4.0*
  - 5.6: The Trans Effect Explanation - *CC BY-NC-SA 4.0*
  - 5.7: Redox Mechanisms - *CC BY-NC-SA 4.0*
    - 5.7.1: Outer Sphere Electron Transfer - *CC BY-NC-SA 4.0*
    - 5.7.2: Inner Sphere Electron Transfer - *CC BY-NC-SA 4.0*
- 6: Organometallic Chemistry - *CC BY-NC-SA 4.0*
  - 6.1: Introduction to Organometallic Chemistry - *CC BY-NC-SA 4.0*
  - 6.2: Nomenclature, Ligands, and Classification - *CC BY-NC-SA 4.0*

- 6.3: Electron Counting in Organometallic Complexes - *CC BY-NC-SA 4.0*
  - 6.3.1: The 18 Electron Rule - *CC BY-NC-SA 4.0*
  - 6.3.2: Simplifying the Organometallic Complex by Deconstruction - *CC BY-NC-SA 4.0*
- 6.4: Survey of Organometallic Ligands - *CC BY-NC-SA 4.0*
  - 6.4.1: Carbon Monoxide (Carbonyl Complexes) - *CC BY-NC-SA 4.0*
  - 6.4.2: Ligands similar to CO - *CC BY-NC-SA 4.0*
  - 6.4.3: Hydrides and Dihydrogen Complexes - *CC BY-NC-SA 4.0*
- 6.5: Bonding between Metal Atoms and Organic Pi Systems - *CC BY-NC-SA 4.0*
  - 6.5.1: Linear π Systems - *CC BY-NC-SA 4.0*
  - 6.5.2: Cyclic π systems - *CC BY-NC-SA 4.0*
  - 6.5.3: Odd-numbered π Systems - *CC BY-NC-SA 4.0*
  - 6.5.4: Fullerene Complexes - *CC BY-NC-SA 4.0*
- 6.6: Metal-Carbon Bonds - *CC BY-NC-SA 4.0*
  - 6.6.1: Metal Alkyls - *CC BY-NC-SA 4.0*
  - 6.6.2: Carbenes - *CC BY-NC-SA 4.0*
  - 6.6.3: Carbyne (Alkylidyne) Complexes - *CC BY-NC-SA 4.0*
  - 6.6.4: Carbido and Cumulene Complexes - *CC BY-NC-SA 4.0*
  - 6.6.5: Carbon Wires- Polyyne and Polyene Bridges - *CC BY-NC-SA 4.0*
- 6.7: Characterization of Organometallic Complexes - *CC BY-NC-SA 4.0*

7: Organometallic Reactions and Catalysis - *CC BY-NC-SA 4.0*

- 7.1: Reactions Involving Gain or Loss of Ligands - *CC BY-NC-SA 4.0*
  - 7.1.1: Ligand Dissociation and Substitution - *CC BY-NC-SA 4.0*
  - 7.1.2: Oxidative Addition - *CC BY-NC-SA 4.0*
  - 7.1.3: Reductive Elimination - *CC BY-NC-SA 4.0*
  - 7.1.4: Sigma Bond Metathasis - *CC BY-NC-SA 4.0*
  - 7.1.5: Application of Pincer Ligands - *CC BY-NC-SA 4.0*
- 7.2: Reactions Invloving Modification of Unsaturated Ligands - *CC BY-NC-SA 4.0*
  - 7.2.1: Introduction to Insertion - *CC BY-NC-SA 4.0*
  - 7.2.2: CO Insertions (Alkyl Migration) - *CC BY-NC-SA 4.0*
  - 7.2.3: Migratory Insertion-1,2-Insertions - *CC BY-NC-SA 4.0*
  - 7.2.4: β-Elimination Reactions - *CC BY-NC-SA 4.0*
  - 7.2.5: Abstraction and Addition - *CC BY-NC-SA 4.0*
- 7.3: Organometallic Catalysts - *CC BY-NC-SA 4.0*
  - 7.3.1: Catalytic Deuteration - *CC BY-NC-SA 4.0*
  - 7.3.2: Hydroformylation - *CC BY-NC-SA 4.0*
  - 7.3.3: Monsanto Acetic Acid Process - *CC BY-NC-SA 4.0*
  - 7.3.4: Wacker (Smidt) Process - *CC BY-NC-SA 4.0*
  - 7.3.5: Hydrogenation by Wilkinson's Catalyst - *CC BY-NC-SA 4.0*
  - 7.3.6: Olefin Metathesis - *CC BY-NC-SA 4.0*
- 7.4: Heterogeneous Catalysts - *CC BY-NC-SA 4.0*
  - 7.4.1: Ziegler-Natta Polymerizations - *CC BY-NC-SA 4.0*
  - 7.4.2: Water-Gas Shift Reaction - *CC BY-NC-SA 4.0*
- 7.5: Problems - *CC BY-NC-SA 4.0*
  - 7.5.1: Concept Review Questions Chapter 12 - *CC BY-NC-SA 4.0*
  - 7.5.2: Homework Problems Chapter 12 - *CC BY-NC-SA 4.0*

8: Solid State Chemistry - *CC BY-NC-SA 4.0*

- 8.1: Prelude to Metals and Alloys - *CC BY-NC-SA 4.0*
- 8.2: Unit Cells and Crystal Structures - *CC BY-NC-SA 4.0*
- 8.3: Crystal Structures of Metals - *CC BY-NC-SA 4.0*
- 8.4: Conduction in Metals - *CC BY-NC-SA 4.0*
- 8.5: Atomic Orbitals and Magnetism - *CC BY-NC-SA 4.0*
- 8.6: Ferro-, Ferri- and Antiferromagnetism - *CC BY-NC-SA 4.0*
- 8.7: Hard and Soft Magnets - *CC BY-NC-SA 4.0*
- 8.8: Defects in Metallic Crystals - *CC BY-NC-SA 4.0*
- 8.9: X-ray Crystallography - *CC BY-NC-SA 4.0*
- 8.10: Miller Indices (hkl) - *CC BY-NC-SA 4.0*
- 8.11: Powder X-ray Diffraction - *CC BY-NC-SA 4.0*
- 8.12: Prelude to Ionic and Covalent Solids - Structures - *CC BY-NC-SA 4.0*
- 8.13: Close-packing and Interstitial Sites - *CC BY-NC-SA 4.0*
- 8.14: Structures Related to NaCl and NiAs - *CC BY-NC-SA 4.0*
- 8.15: Tetrahedral Structures - *CC BY-NC-SA 4.0*
- 8.16: Layered Structures and Intercalation Reactions - *CC BY-NC-SA 4.0*

- 8.17: Ionic Radii and Radius Ratios - *CC BY-NC-SA 4.0*
- 8.18: Structure Maps - *CC BY-NC-SA 4.0*
- 8.19: Energetics of Crystalline Solids- The Ionic Model - *CC BY-NC-SA 4.0*
- 8.20: Born-Haber Cycles for NaCl and Silver Halides - *CC BY-NC-SA 4.0*
- 8.21: Lattice Energies and Solubility - *CC BY-NC-SA 4.0*
- 8.22: Spinel, Perovskite, and Rutile Structures - *CC BY-NC-SA 4.0*
- 8.23: Kapustinskii Equation - *CC BY-NC-SA 4.0*
- 8.24: New Page - *CC BY-NC-SA 4.0*

9: Bioinorganic Chemistry - *CC BY-NC-SA 4.0*

- 9.1: Biological Significance of Iron, Zinc, Copper, Molybdenum, Cobalt, Chromium, Vanadium, and Nickel - *CC BY-NC-SA 4.0*
- 9.2: Introduction to Amino Acids and Proteins - *CC BY-NC-SA 4.0*
- 9.3: Overview of Hemoglobin and Myoglobin - *CC BY-NC-SA 4.0*
  - 9.3.1: Myoglobin, Hemoglobin, and their Ligands - *CC BY-NC-SA 4.0*
  - 9.3.2: Oxygen Transport by the Proteins Myoglobin and Hemoglobin - *CC BY-NC-SA 4.0*
- 9.4: Ferrodoxins, Hydrogenases, and Nitrogenases - Metal-Sulfide Proteins - *CC BY-NC-SA 4.0*
  - 9.4.1: Iron-sulfur Proteins and Models - *CC BY-NC-SA 4.0*
  - 9.4.2: Iron-sulfur Proteins and Models (Part 2) - *CC BY-NC-SA 4.0*
  - 9.4.3: Iron-sulfur Proteins and Models (Part 3) - *CC BY-NC-SA 4.0*
  - 9.4.4: Iron-sulfur Proteins and Models (Part 4) - *CC BY-NC-SA 4.0*
- 9.5: The Reaction Pathways of Zinc Enzymes and Related Biological Catalysts - *CC BY-NC-SA 4.0*
  - 9.5.1: About Carbonic Anhydrase - *CC BY-NC-SA 4.0*
  - 9.5.2: Catalytic Mechanism - *CC BY-NC-SA 4.0*
  - 9.5.3: Metal Substitution - *CC BY-NC-SA 4.0*
- 9.6: Metals in Medicine - *CC BY-NC-SA 4.0*
  - 9.6.1: Metal Deficiency and Disease - *CC BY-NC-SA 4.0*
  - 9.6.2: Toxic Effects of Metals - *CC BY-NC-SA 4.0*
  - 9.6.3: Aspects of Platinum Binding to DNA - *CC BY-NC-SA 4.0*
  - 9.6.4: Survey of Metals Used for Diagnosis and Chemotherapy - *CC BY-NC-SA 4.0*
  - 9.6.5: Platinum Anticancer Drugs- A Case Study - *CC BY-NC-SA 4.0*
  - 9.6.6: Mapping the Major Adducts of cis- and trans-DDP on DNA; Sequence Specificity - *CC BY-NC-SA 4.0*
  - 9.6.7: Structure of Platinum-DNA Complexes - *CC BY-NC-SA 4.0*
  - 9.6.8: Site-specifically Platinated DNA \(\;^{154}\) - *CC BY-NC-SA 4.0*
  - 9.6.9: Bioinorganic Chemistry of Platinum Anticancer Drugs- How Might They Work? - *CC BY-NC-SA 4.0*
  - 9.6.10: Bioinorganic Chemistry of Platinum Anticancer Drugs; How Might They Work? (Part 2) - *CC BY-NC-SA 4.0*
  - 9.6.11: Design of New Inorganic Anticancer Drugs - *CC BY-NC-SA 4.0*
- 9.7: Electron Transfer - *CC BY-NC-SA 4.0*

10: Special Topics - *CC BY-NC-SA 4.0*

- 10.1: f-Block Metals- Lanthanides and Actinides - *CC BY-NC-SA 4.0*
  - 10.1.1: Introduction - *CC BY-NC-SA 4.0*
  - 10.1.2: f-Orbitals and Oxidation States - *CC BY-NC-SA 4.0*
  - 10.1.3: Atoms and Ion Sizes - *CC BY-NC-SA 4.0*
    - 10.1.3A: The Lanthanoid Contraction - *CC BY-NC-SA 4.0*
    - 10.1.3B: Coordination Numbers - *CC BY-NC-SA 4.0*
  - 10.1.4: Spectroscopic and Magnetic Properties - *CC BY-NC-SA 4.0*
    - 10.1.4A: Electronic Spectra and Magnetic Moments - Lanthanoids - *CC BY-NC-SA 4.0*
    - 10.1.4B: Luminescence of Lanthanoid Complexes - *CC BY-NC-SA 4.0*
    - 10.1.4C: Electronic Spectra and Magnetic Moments - Actinoids - *CC BY-NC-SA 4.0*
  - 10.1.5: Sources of the Lanthanoids and Actinoids - *CC BY-NC-SA 4.0*
    - 10.1.5A: Occurrence and Separation of the Lanthanoids - *CC BY-NC-SA 4.0*
    - 10.1.5B: The Actinoids - *CC BY-NC-SA 4.0*
  - 10.1.6: Lanthanoid Metals - *CC BY-NC-SA 4.0*
  - 10.1.7: Inorganic Compounds and Coordination Complexes of the Lanthanoids - *CC BY-NC-SA 4.0*

- 10.1.7A: Halides - *CC BY-NC-SA 4.0*
- 10.1.7B: Hydroxides and Oxides - *CC BY-NC-SA 4.0*
- 10.1.7C: Complexes of Ln(III) - *CC BY-NC-SA 4.0*
- 10.1.8: Organometallic Complexes of the Lanthanoids - *CC BY-NC-SA 4.0*
  - 10.1.8A: \(\sigma\)-Bonded Complexes - *CC BY-NC-SA 4.0*
  - 10.1.8B: Cyclopentadienyl Complexes - *CC BY-NC-SA 4.0*
  - 10.1.8C: Bis(arene) Derivatives - *CC BY-NC-SA 4.0*
  - 10.1.8D: Complexes Containing the \(\eta^8\)-cyclooctatetraenyl Ligand - *CC BY-NC-SA 4.0*
- 10.1.9: The Actinoid Metals - *CC BY-NC-SA 4.0*
- 10.1.10: Inorganic Compounds and Coordination Complexes of Thorium, Uranium, and Plutonium - *CC BY-NC-SA 4.0*
  - 10.1.10A: Thorium - *CC BY-NC-SA 4.0*
  - 10.1.10B: Uranium - *CC BY-NC-SA 4.0*
  - 10.1.10C: Plutonium - *CC BY-NC-SA 4.0*
- 10.1.11: Organometallic Complexes of Thorium and Uranium - *CC BY-NC-SA 4.0*
  - 10.1.11A: (\sigma\)-Bonded Complexes - *CC BY-NC-SA 4.0*
  - 10.1.11B: Cyclopentadienyl Derivatives - *CC BY-NC-SA 4.0*
  - 10.1.11C: Complexes Containing the \(\eta^8\)-cyclooctatetraenyl Ligand - *CC BY-NC-SA 4.0*

- 10.2: Physical Inorganic Techniques - *CC BY-NC-SA 4.0*
  - 10.2.1: Electronic Spectroscopy - *CC BY-NC-SA 4.0*
    - 10.2.1A: UV-VIS Absorption Spectroscopy - *CC BY-NC-SA 4.0*
    - 10.2.1B: Types of Absorption - *CC BY-NC-SA 4.0*
    - 10.2.1C: Absorbance and the Beer-Lambert Law - *CC BY-NC-SA 4.0*
    - 10.2.1D: Emission Spectroscopy - *CC BY-NC-SA 4.0*
  - 10.2.2: Nuclear Magnetic Resonance (NMR) Spectroscopy - *CC BY-NC-SA 4.0*
  - 10.2.3: Electron Paramagnetic Resonance (EPR) Spectroscopy - *CC BY-NC-SA 4.0*
    - 10.2.3A: What is EPR Spectroscopy? - *CC BY-NC-SA 4.0*
    - 10.2.3B: The Zeeman Electronic Effect - *CC BY-NC-SA 4.0*
    - 10.2.3C: EPR Spectra - *CC BY-NC-SA 4.0*
  - 10.2.4: Mossbauer Spectroscopy - *CC BY-NC-SA 4.0*
    - 10.2.4A: The Technique of Mossbauer Spectroscopy - *CC BY-NC-SA 4.0*
    - 10.2.4B: What Can Isomer Shift Data Tell Us? - *CC BY-NC-SA 4.0*
  - 10.2.5: Structure Determination - Diffraction Methods - *CC BY-NC-SA 4.0*
    - 10.2.5A: X-Ray Diffraction (XRD) - *CC BY-NC-SA 4.0*
    - 10.2.5B: Single Crystal X-Ray Diffraction - *CC BY-NC-SA 4.0*
    - 10.2.5C: Powder X-Ray Diffraction - *CC BY-NC-SA 4.0*
    - 10.2.5D: Single Crystal Neutron Diffraction - *CC BY-NC-SA 4.0*
    - 10.2.5E: Electron Diffraction - *CC BY-NC-SA 4.0*
    - 10.2.5F: Low-Energy Electron Diffraction (LEED) - *CC BY-NC-SA 4.0*
    - 10.2.5G: Structural Databases - *CC BY-NC-SA 4.0*
  - 10.2.6: Photoelectron Spectroscopy (PES, UPS, XPS, ESCA) - *CC BY-NC-SA 4.0*
  - 10.2.7: Mass Spectrometry - *CC BY-NC-SA 4.0*
    - 10.2.7A: Electron Ionization (EI) - *CC BY-NC-SA 4.0*
    - 10.2.7B: Fast Atom Bombardment (FAB) - *CC BY-NC-SA 4.0*
    - 10.2.7C: Matrix-Assisted Laser Desorption Ionization Time-of-Flight (MALDI-TOF) - *CC BY-NC-SA 4.0*
    - 10.2.7D: Electrospray Ionization (ESI) - *CC BY-NC-SA 4.0*
- 10.3: Fluxional Behavior - *CC BY-NC-SA 4.0*
  - 10.3.1: Determination of Energetics of Fluxional Molecules by NMR - *CC BY-NC-SA 4.0*

- Back Matter - *CC BY-NC-SA 4.0*
  - Index - *CC BY-NC-SA 4.0*
  - Glossary - *CC BY-NC-SA 4.0*
  - Detailed Licensing - *CC BY-NC-SA 4.0*
  - Detailed Licensing - *Undeclared*